Lecture Notes in Civil Engineering

Kaustubh Dasgupta · T. K. Sudheesh ·
K. I. Praseeda · G. Unni Kartha ·
P. E. Kavitha · S. Jawahar Saud *Editors*

Proceedings of SECON 2020

Structural Engineering and Construction Management

Springer

Lecture Notes in Civil Engineering

Volume 97

Series Editors

Marco di Prisco, Politecnico di Milano, Milano, Italy

Sheng-Hong Chen, School of Water Resources and Hydropower Engineering, Wuhan University, Wuhan, China

Ioannis Vayas, Institute of Steel Structures, National Technical University of Athens, Athens, Greece

Sanjay Kumar Shukla, School of Engineering, Edith Cowan University, Joondalup, WA, Australia

Anuj Sharma, Iowa State University, Ames, IA, USA

Nagesh Kumar, Department of Civil Engineering, Indian Institute of Science Bangalore, Bengaluru, Karnataka, India

Chien Ming Wang, School of Civil Engineering, The University of Queensland, Brisbane, QLD, Australia

Lecture Notes in Civil Engineering (LNCE) publishes the latest developments in Civil Engineering - quickly, informally and in top quality. Though original research reported in proceedings and post-proceedings represents the core of LNCE, edited volumes of exceptionally high quality and interest may also be considered for publication. Volumes published in LNCE embrace all aspects and subfields of, as well as new challenges in, Civil Engineering. Topics in the series include:

- Construction and Structural Mechanics
- Building Materials
- Concrete, Steel and Timber Structures
- Geotechnical Engineering
- Earthquake Engineering
- Coastal Engineering
- Ocean and Offshore Engineering; Ships and Floating Structures
- Hydraulics, Hydrology and Water Resources Engineering
- Environmental Engineering and Sustainability
- Structural Health and Monitoring
- Surveying and Geographical Information Systems
- Indoor Environments
- Transportation and Traffic
- Risk Analysis
- Safety and Security

To submit a proposal or request further information, please contact the appropriate Springer Editor:

– Mr. Pierpaolo Riva at pierpaolo.riva@springer.com (Europe and Americas);
– Ms. Swati Meherishi at swati.meherishi@springer.com (Asia - except China, and Australia, New Zealand);
– Dr. Mengchu Huang at mengchu.huang@springer.com (China).

All books in the series now indexed by Scopus and EI Compendex database!

More information about this series at http://www.springer.com/series/15087

Kaustubh Dasgupta · T. K. Sudheesh ·
K. I. Praseeda · G. Unni Kartha ·
P. E. Kavitha · S. Jawahar Saud
Editors

Proceedings of SECON 2020

Structural Engineering and Construction Management

Springer

Editors
Kaustubh Dasgupta
Department of Civil Engineering
Indian Institute of Technology Guwahati
Guwahati, Assam, India

K. I. Praseeda
Department of Civil Engineering
NSS College of Engineering
Akathethara, Kerala, India

P. E. Kavitha
Department of Civil Engineering
Federal Institute of Science and Technology (FISAT)
Angamaly, Kerala, India

T. K. Sudheesh
Department of Civil Engineering
Indian Institute of Technology Palakkad
Palakkad, Kerala, India

G. Unni Kartha
Department of Civil Engineering
Federal Institute of Science and Technology (FISAT)
Angamaly, Kerala, India

S. Jawahar Saud
Department of Civil Engineering
Federal Institute of Science and Technology (FISAT)
Angamaly, Kerala, India

ISSN 2366-2557 ISSN 2366-2565 (electronic)
Lecture Notes in Civil Engineering
ISBN 978-3-030-55114-8 ISBN 978-3-030-55115-5 (eBook)
https://doi.org/10.1007/978-3-030-55115-5

© Springer Nature Switzerland AG 2021
This work is subject to copyright. All rights are reserved by the Publisher, whether the whole or part of the material is concerned, specifically the rights of translation, reprinting, reuse of illustrations, recitation, broadcasting, reproduction on microfilms or in any other physical way, and transmission or information storage and retrieval, electronic adaptation, computer software, or by similar or dissimilar methodology now known or hereafter developed.
The use of general descriptive names, registered names, trademarks, service marks, etc. in this publication does not imply, even in the absence of a specific statement, that such names are exempt from the relevant protective laws and regulations and therefore free for general use.
The publisher, the authors and the editors are safe to assume that the advice and information in this book are believed to be true and accurate at the date of publication. Neither the publisher nor the authors or the editors give a warranty, expressed or implied, with respect to the material contained herein or for any errors or omissions that may have been made. The publisher remains neutral with regard to jurisdictional claims in published maps and institutional affiliations.

This Springer imprint is published by the registered company Springer Nature Switzerland AG
The registered company address is: Gewerbestrasse 11, 6330 Cham, Switzerland

Preface

Construction, maintenance, rehabilitation and demolition are the four phases in the life cycle of a structure. Development and implementation of eco-friendly and cost-effective practices in every phase of this life cycle is the key to creating a sustainable future of the planet. The focus of the first International Conference on Structural Engineering and Construction Management (SECON 2020) was "Innovative Practices in Construction, Rehabilitation and Demolition of Structures" as its main theme and intended to become a platform for researchers to discuss the current directions in research and development in this broad domain.

This proceedings comprises the papers presented at SECON 2020 as book chapters in lecture notes in civil engineering published by Springer. This is the fourth edition and the first international edition of SECON series of conferences organised by Federal Institute of Science and Technology (FISAT), Angamaly, Kerala, India. SECON series of conference has always enjoyed good acceptance and excellent participation from researchers from all across the country. There was an overwhelming response to SECON 2020 also but the pandemic forced the organisers to host the event online, over two days, in the month of May on 14th and 15th. The hard hours put in by the organisers had a grand outcome—SECON 2020 became the first international conference to be hosted completely online in India. The conference was successful in providing a platform for research scholars, students, academicians and practicing engineers for meaningful exchange of ideas and deliberations at an international level. The papers presented spread across current and future technologies, experimental investigations and research findings in the areas related to the conference themes and were presented in 20 parallel sessions spread over the span of two days. We believe that the deliberations of the conference helped us achieve the purpose of dissemination and passing on the innovative methodologies and practices in place globally.

This two-day International Conference on Structural Engineering and Construction Management (SECON 2020) had extensive support and participation from across the world, with papers from two international universities, 25 national institutions and four R&D divisions of industries. More than 300 abstracts were screened and double blind reviewed to shortlist 85 papers for presentation.

The quality of the papers presented, almost 70% rejection rate are indicators of the standard the conference was able to accomplish.

On behalf of the organising committee, I express sincere thanks to Ms. Anitha P., Chairman, Governing Body—FISAT, Dr. George Issac, Principal and Dr. K. S. M. Panicker, Director (Academics), whose constant guidance helped us to organise the conference. I would like to express my gratitude to each and every advisory committee members, reviewers, session chairs and the contributors of research for their constant support and efforts at making the conference a grand success. I extend my sincere gratitude to Prof. Ir. Serge Vandemeulebroecke and Prof. Ir. lic. Bart Van Zegboreck for their valuable time and input as the international advisory committee and keynote speakers. Their diligence and enthusiasm to be part of the event helped overcome the challenges of time zones at the peak of the pandemic. The conference also had support from industry, professional organisations both at national and international levels. I would like to place on record the heartfelt thanks to PARADIGM, ASCE Student Chapter, IEI Kochi Local Centre, ICI Student Chapter and ISTE-FISAT chapter for the unrelenting support for the conduct of the conference.

I extend my whole hearted thanks to Dr. Unni Kartha G., General Convenor, SECON 2020 and Head of Department, Department of Civil Engineering, Mr. Jawahar Saud S., Co-Convenor, SECON 2020 and Ms. Rinu J. Achison, Treasurer, SECON 2020, for their constant encouragement and reason of keen interest in the various stages of the planning and execution of the event. I also take this opportunity to thank all our management committee members and executive committee of PTA who have shown great belief in us and urged us towards excellence for the growth of the institute and the students.

Last but not least, I would like to thank the entire team of faculty members, non-teaching staff and student volunteers for the untiring support for the smooth conduct of the event. This conference would not have been possible without the incredible help and support of all our colleagues and scholars of the department. Wishing you all very best and looking forward to the next edition of the event.

Angamaly, India

Dr. P. E. Kavitha
Convenor, SECON 2020

Contents

Performance Evaluation on the Properties of Metakaolin—Fly Ash Based Self Compacting Concrete 1
K. Aswani and C. A. Abin Thomas

Studies on Inclusion of Polypropylene (PP) Geo-fabric in Concrete 11
K. S. Sreekeshava, A. S. Arunkumar, Manish S. Dharek, and Prashanth Sunagar

Dual-Pipe Damper with Bracing System for Seismic Retrofitting 23
V. Bincy and S. Usha

Experimental Studies on Performance of Geo-synthetic Strengthened Brick Masonry Infill 31
K. S. Sreekeshava and A. S. Arunkumar

Assessment of Governance Gaps in Landslide Risk Reduction—A Case Study from Kattippara Panchayath, Kozhikode District 43
K. Sreerekha and S. Jawahar Saud

Evaluation of Progressive Collapse Resistance of Steel Moment Resisting Frames 57
Anjaly James and Asha Joseph

Structural Performance of GFRP Deck Strengthened with Light Weight Ultra-High Strength Concrete 69
K. Teena John, P. E. Kavitha, and R. Renjith

Effect of Combination of Mineral Admixtures on the Properties of Self Compacting Concrete 79
Reya Grace Jacob and K. N. Resmi

Evaluation of Sustainable SMA Mix Prepared Using Recycled Concrete Aggregates 87
A. A. Ruksana, P. S. Sethulakshmi, Mariya Thomas, Midhun Joby, and Sharon Jacob

Investigation on Performance of Fly Ash Based Self Compacting Concrete with Metakaolin and Quarry Dust 101
Elizabeth Jose and Anju Paul

Feasibility Study of Plastic Granules and Alccofine in Fly Ash Based Self-Compacting Concrete 111
Fiona Alias and Tellma John

Effect of Magnetized Water with Coconut Fibre Reinforced Concrete 121
C. Nived, M. Sherin Babu, P. Adithya Das, Noble M. Babu, and P. E. Kavitha

Seismic Performance of Oblique Columns in High Rise Building 131
Nikha Santhosh and Gayathri Krishna Kumar

Experimental Investigation on the Performance of Self Compacting Concrete Using Copper Slag 141
Ajana Prince and M. Preethi

Development of Metakaolin and Flyash Based Geopolymer Concrete at Ambient Temperature Curing 151
S. Anjana Chandran and B. R. Beena

Seismic Evaluation of High Rise Buildings Using Hybrid Configuration of Grid Systems 159
K. N. Vaisakh and Neeraja Nair

Sustainability Assessment of Terracotta Tile Waste Based Geopolymer Building Block 169
S. Usha, Deepa G. Nair, and Subha Vishnudas

Study on Structural Performance of Non-prismatic Girders with Double Corrugated Stiffened Steel and Composite Webs 179
M. Saranya Radhakrishnan and P. Binu

Structural Performance of Multi-sectional CFST Columns with Double Corrugated Plate 189
P. A. Azna and Ranjan Abraham

Experimental Study of Seismic Response Reduction Effects on Multi Storey Frames with Particle Damper 205
N. Athulya Vijay and K. P. Saji

Control Effectiveness of Wing with Elevon of a Typical Reusable Launch Vehicle 213
Nyle Nazar, P. Ashok Gandhi, S. Rajendran, and Manju George

Analytical Study on Dynamic Behaviour of Bolted Beam Column Steel Connections with Reduced Beam Sections 225
Deepa P. Antoo and Asha Joseph

Experimental Study of Self-cleaning Concrete by Using Various Photocatalysts 241
Geethu Benny and Gayathri Krishna Kumar

Thermo Structural Optimisation Study on Slim Floor Beam with Hollow Core Slabs 251
Athul Deepak Krishna and Neeraja Nair

Study of Geo-polymer Concrete with Replacement of Fine Aggregate Using Bottom Ash 261
Sweety Viswanath and Nincy Jose

Effect of Waste Carpet Fibres and Palm Oil Fuel Ash on Self Compacting Concrete 271
Minnu P. Alias and Tellma John

Elemental Approach to Design a Worker Profile as a Selection Tool in Last Planner System© 281
C. Mrinal Raja, Vinay Mathews, and Grace Mary Abraham

Development of Optimum Mix for Laterite Soil Brick by Adding Clam Shell Powder and Metakaolin 297
Devika Sudhakaran and Emy Poulose

Analytical Assessment on the Behaviour of Conical Shell Foundation 307
T. Lamya and M. K. Sheeja

Experimental Investigation on Packing Density of Concrete Using Wet Packing Method 317
Mariya Jacob and K. N. Resmi

Influence of Alkali Resistant Glass Fiber on the Reduction of Plastic Shrinkage Cracking of Self Compacting Concrete 325
Anju George and C. A. Abin Thomas

Development of Bricks Using Plastic Wastes 335
Gouri S. Kumar and S. Sreerath

Stabilization of Lateritic Soil Using Natural Fibres 345
B Krishnendu and Anjana Bhasi

Clogging Resistant Pervious Block 353
M. V. Akshara and M. Preethi

Analytical Study of Timber-Concrete Composite (TCC) Beam Using Different Interlocking Joints 365
K. S. Sandra and P. R. Reshmi

Analytical Study of GFRG Laminated Beam with Internally and Externally Strengthened with Cold Formed Steel 373
Meera Haridas and Chippy M. Rajan

Shear Strengthening of Concrete Block Masonry Walls Under In-Plane Diagonal Loading Using Fibers 389
P. Akhil kumar and S. Unnikrishnan

Structural Performance of Innovative Multi Cellular Corrugated Steel Column (MCCSC) 401
Agnes Davis Thuluvath and Reshma Prasad

Study of Fly Ash Based Light Weight Concrete with Plastic Waste Aggregate as a Partial Replacement of Coarse Aggregate 413
Thasni Kaseem and S. Sreerath

Modified Magnetized Water Concrete Using Nanosilica 421
Punya Lal and P. E. Kavitha

Optimisation of Multistoried Building Using Outrigger System 433
Jeslin C. Johnson and Reshma Prasad

Seismic Vulnerability Assessment of City Regions Based on Building Typology 443
Dharsana Satish, E. Lalith Prakash, and K. B. Anand

Development of Reinforced Concrete Beam with Plastic Balls in Neutral Axis 453
Milu Reji and V. V. Anu

Progressive Collapse Analysis of RC Buildings Using Linear Static and Non-linear Static Method 461
A. Salman and K. I. Praseeda

Effect of Magnetized Water on the Mechanical Properties of Fly Ash Based Self Compacting Concrete 471
P. P. Magida Ruby and R. Vasudev

Effect of Immersion Time on the Mechanical Properties of Glass Fibre Reinforced Concrete with Glass Powder Immersed in Water 481
K. Sana and Anju Paul

Assessment of Fraction Effects on Flow Characteristic of Cement Mortar Using Natural and Manufactured Sand 491
Chintan Vohra and Parth Thaker

A Comparative Investigation on the Utilization of Marble Dust and Granite Dust in the Cement Mortar Against the Sulphate Resistance 523
PL. Meyyappan and M. Jemimah Carmichael

An Effective Replacement of Granite and Marble Powder on Cement Mortar Subjected to Chloride Ion Penetration Test 533
PL. Meyyappan and M. Jemimah Carmichael

An Experimental and Analytical Investigation on the Characteristics of Light Weight Concrete Using Waste Burnt Ash and Pumice Stones 543
PL. Meyyappan, M. Pallikonda Rajasekaran, and R. Sathya Soroopan

Applications of Functionally Graded Materials in Structural Engineering—A Review 553
S. L. Akshaya, Amar Prakash, and J. Bharati Raj

Efficient Utilization of Recycled Concrete Aggregates for Structural Applications—An Experimental Study 567
Jagan Sivamani, T. R. Neelakantan, P. Saravana Kumar, C. Mugesh Kanna, H. Vignesh Harish, and M. R. Akash

Evaluation of Strength and Diffusion Capability of High Volume Fly Ash Based Engineered Cementitious Composites Incorporating Powder Scrap Rubber 581
Abhishank Kumar, Shashi Kant Sharma, and Davinder Singh

A Probabilistic Approach for Predicting the Fatigue Life of Concrete 593
D. R. Renju and Keerthy M. Simon

Convergence Study of Reinforced Concrete Beam-Column Joints Under Impact Loads 601
Jhuma Debnath and Hrishikesh Sharma

Evaluation of Cementitious Mixes for Printing 611
M. Vishruthi, S. Raghavendra, Y. Ravi Teja, and K. B. Anand

Review of Performance of Existing Vertical Irregularity Indicators for Steel Framed Buildings 625
Brij M. Shah, Robin Davis, C. G. Nandakumar, and Pradip Sarkar

Modelling the Rheological Properties of Fly Ash Incorporated Superplasticized Cement Paste at Different Temperature Using Multilayer Perceptrons in Tensorflow 635
Rogin C. Robert, Nelvin Mani Kuriakose, K. Gopikrishnan, Dhanya Sathyan, and C. B. Rajesh

Study on Shear Strength of Corrugated Webs with Artificial Corrosion Pits 647
M. V. Rahul and V. I. Beena

Collapse and Buckling Behavior of Octagonal Concrete Filled Steel Column Connected to a Beam Under Cyclic Loading 657
Silia Mary Silbi and Sajan Jose

Comparative Study on Effect of Different Mineral Admixtures on Plastic Fiber Reinforced Concrete 667
K. S. Somiya and Vidya Jose

Shear Behavior of Joints in Precast Prestressed Concrete Segments-A Finite Element Study 679
Sheela J. George, A. K. Farvaze Ahmed, S. Maheswaran, and Mathews M. Paul

Structural Performance of Innovative Lean Duplex Stainless Steel Built-Up Columns Under Various Loading 691
M. S. Hima and Samithamol Salim

Blended Cement Using Calcined Clay and Limestone for Sustainable Development—A Review 701
Ranjan Abraham, T. R. Neelakantan, Ramesh Babu Chokkalingam, and Elson John

Seismic Performance Improvement Techniques for Infill Frames—A Review 711
A. Athira Nair and Keerthy M. Simon

Analysis of the Concrete Filled Steel Tubes with Diagonal Ribs 719
K. P. Ansa and S. Keerthi

Seismic Pounding Between Adjacent RC Buildings with Asymmetric Alignment 735
P. Ambili, V. N. Krishnachandran, and Katta Venkataramana

Performance Characteristics of Self-cured Recycled Aggregate Concrete with SCM's 745
Lakshmi Thotakura, Sankar Kumar Reddy Pullalacheruvu, Ganesh Babu Kodeboyina, and V. Krishna Rao Mupparisetty

Experimental Investigation on Hydrophobic Concrete 755
Ahallya Raveendran and Jiji Antony

Study of the Behavior of Air Entrained Concrete Containing Mineral Admixtures with the Addition of Coal Bottom Ash 765
Shashi Kant Sharma, Kanish Kapoor, Sandeep Singh, and K. P. Marisala Chaitanya

Investigation on the Effect of Steel Fibers in Self Curing Concrete 779
Annamol Sunny and Elba Helen George

Effect of Communication Patterns in Safety Performance of Construction Workers 789
Reshma Geordy, M. B. Sridhar, and J. Sudhakumar

Development of Pavement Quality SCC Having High Early Strength Under Site Conditions 803
Shashi Kant Sharma, Kanish Kapoor, Dadi Rambabu, and Mohit Kumar

Hybrid Model Based on PPP and EPC Contracts 819
Rahul Rajasekharan and Shibi Varghese

AHP Model for Performance Improvement in LSGD Projects 835
Ammu David and Shibi Varghese

Prevention of Flutter Instability in Control Surface of a Test Vehicle Through Parametric Studies 851
Bilpriya, S. Rajendran, P. Ashok Gandhi, and Manju George

Experimental Investigations on Using Distributed Fiber Sensing for Monitoring Pipelines 865
Shika George, B. Arun Sundaram, and Mathews M. Paul

Performance Assesment of GGBS and Rice Husk Ash Based Geopolymer Concrete 875
Maria Eldho, V. Srinivasan, and Sarah Anil

Analysis of Strains in Brick Masonry Prism Using ABAQUS 883
Agnus A. Mathew, S. Saibabu, Vimal Mohan, and Deepa Varkey

Machine Learning Approach to Failure Mode Prediction of Reinforced Concrete Infilled Frames 899
J. Ashish Manoj, A. Asiya, Dasari Navya, G. Ganesh Kumar, and P. Robin Davis

Punching Shear Strengthening of Flat Slabs with External Bonded CFRP on Grooves (EBROG) 909
Jijo P. George and Roshini T. Mohan

Study on Performance of Concrete Made with Copper Slag and Mineral Admixtures 917
E. Lalith Prakash, Prakash Chinnayan, K. Siva Kavinesh, Ambrish Adithiya, G. Sarath Sanjeev, Sriram Gnanaprakasam, and Gautham Sukumar

Effect of Size and Shape of Concrete Column Elements Exposed to High Temperature 929
Y. K. Guruprasad

Diagrid Structural System for Tilted Steel Buildings 939
Archana Joy Eluvathingal and G. Unni Kartha

Investigation on the Suitability of Jarofix as a Fine Aggregate Replacement in Concrete Building Blocks 949
Robert V. Thomas and Deepa G. Nair

Performance Evaluation on the Properties of Metakaolin—Fly Ash Based Self Compacting Concrete

K. Aswani and C. A. Abin Thomas

Abstract Self-compacting concrete (SCC) is concrete which is proportioned in such a way that it is compacted by its weight assuring complete filling of formwork even when access is hindered by narrow gaps between reinforcing bars. The rheology properties were determined by the test as filling ability, passing ability, and segregation resistance. Strength properties were determined by compressive, split tensile, flexural strength. The successful utilization of fly ash and metakaolin in SCC mixes not only lower the cost of SCC but also provide a solution to the disposal and environmental problems connected with these materials.

Keywords Self-compacting concrete · Flyash · Metakaolin

1 Introduction

Self-compacting concrete can be defined as fresh concrete that flows under its weight and does not require external vibration to undergo compaction. Self-compacting concrete has been used in bridges and even on pre-cast sections. SCC is ideal to be used in the following applications such as drilled shafts, columns, earth retaining systems, areas with a high concentration of rebar and pipes/conduits.

In the journal of J. M. Khatib studied properties such as workability, compressive strength, ultrasonic pulse velocity (V), absorption and shrinkage and the results indicate that high volume FA can be used in SCC to produce high strength and low shrinkage. Replacing 40% of PC with FA resulted in the strength of more than 65 N/mm^{2}at 56 days [1, 2]. In the journal of Rahmat Mandanoust, S. Yasin Mousavi studied the fresh and hardened properties of self-compacting concrete containing metakaolin (MK) and the result shows that 10% MK can be considered as a suitable replacement regarding the economic efficiency, fresh and hardened properties of MK concrete [3, 4]. In the journal of P Dinakar, S N Manu evaluated the self

K. Aswani (✉) · C. A. Abin Thomas
Department of Civil Engineering, Federal Institute of Science and Technology (FISAT), Ernakulam 68377, India
e-mail: aswanik23101994@gmail.com

© Springer Nature Switzerland AG 2021

K. Dasgupta et al. (eds.), *Proceedings of SECON 2020*,
Lecture Notes in Civil Engineering 97,
https://doi.org/10.1007/978-3-030-55115-5_1

compactability and strength characteristics and the results indicate that high strength SCC of about 120 MPa is obtained [5, 6]. In this journal V. Kannan, K. Ganesh studied about the durability properties of self-compacting concrete (SCC) containing rice husk ash, Metakaolin (MK) and a combination of MK and RHA were studied and the result showed that SCC blended with RHA and a combination of RHA and MK showed a considerable improvement in durability than unblended SCC [7]. In this paper Frank Cassagnabere investigate the compressive strength of cement-based materials at both early (1 day) and later (28 days) ages under steam curing conditions and the results showed that metakaolin (MK) is a very promising solution at a clinker replacement rate of 12.5–25% by mass [8].

This paper studied the replacement of cement using metakaolin and flyash undergoing various tests in fresh and hardened properties.

2 Experimental Investigations

Cement

OPC of grade 53 conforming IS 4031: part2,3 is used. Physical properties of cement are given in Table 1.

Fine Aggregate

The fine aggregate used is Msand as per IS specifications IS 2386-Part3. Physical properties of fine aggregate are tabulated on Table 2 and gradation curve are given in Fig. 1.

Table 1 Physical properties of cement

S. No.	Properties	Value	Limits
1	Specific gravity	3.13	3.10–3.25
2	Standard consistency	30%	26–33%
3	Initial setting time	73 min	Not less than 30 min
4	Fineness	5.8%	Should not exceed 10%

Table 2 Physical properties of fine aggregate

S. No.	Properties	M-Sand	Limits
1	Specific gravity	2.74	2.5–2.9
2	Water absorption	1.30%	0.3–2.5%
3	Fineness modulus	2.86	2–3.5

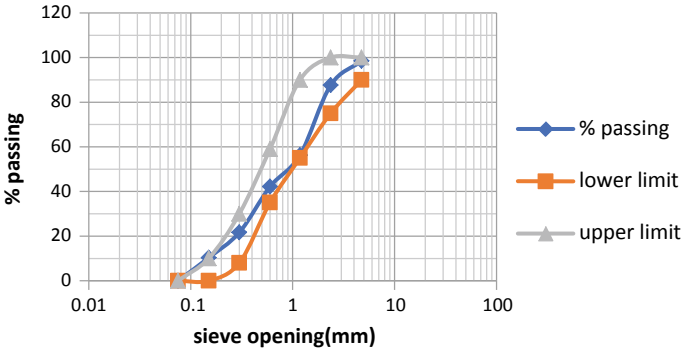

Fig. 1 Gradation curve of FA

Table 3 Physical properties of coarse aggregate

S. No.	Properties	Coarse aggregate	Limits
1	Specific gravity	2.69	2.5–3
2	Water absorption	0.93%	0.1–2%

Coarse Aggregate

The maximum coarse aggregate size used was 12.5 mm. Tests on coarse aggregate are done conforming to IS 2386-1963 (Part 3). Physical properties of coarse aggregate are given in Table 3.

Flyash and Metakaolin

Class F flyash used based on IS 3812:1981. The chemical properties of flyash and metakaolin are tabulated in Table 4.

Polycarboxylate Ether Superplasticizer

Remix HP 20 is poly-carboxylate ether-based superplasticizers (PCEs) which allow a water reduction up to 30%.

Table 4 chemical properties of FA and MK

Parameters	FA (%)	MK
SiO_2	63.8	52
Al_2O_3	21.29	40
Fe_2O_3	0.39	3.6

Table 5 Trial mix design of fly ash

Trial no.	w/b ratio	Binder (C + FA)	Fine aggregate (kg/m^3)	Coarse aggregate (kg/m^3)	Superplasticizer	Slump (mm)
1	0.38	448	1250	698	3.58	632
2	0.40	425	1288	610	3.40	655
3	0.42	405	1200	647	3.24	695
4	0.43	395	1212	650	3.16	650
5	0.45	378	1263	662	3.024	644

Table 6 Trial mix design of metakaolin

Trial no.	w/b ratio	Binder (C + MK)	Fine aggregate (kg/m^3)	Coarse aggregate (kg/m^3)	Superplasticizer	Slump (mm)
1	0.40	425	1288	620	3.4	680
2	0.42	405	1200	654	3.24	700
3	0.43	395	1212	659	3.16	685

3 Mix Design

The mix composition is chosen to satisfy all performance criteria for the concrete in both the fresh and hardened states. Trial mix design of flyash and metakaolin are given in Tables 5 and 6. water is taken as 170 kg/m^3

In the above trials we get good result of slump flow at a w/b ratio of 0.42.

So combined replacement of MK and FA taken at a w/b ratio of 0.42.

4 Test Procedures

4.1 Casting and Curing of Specimen

The following mould was used to cast the concrete specimens for various studied as per IS: 516-1956

- 150 * 150 * 150 mm moulds were used to cast cubes to determine the compressive strength of concrete.
- 150 * 300 mm moulds were used to cast cylinders to determine split tensile strength and modulus of elasticity of concrete.
- 100 * 100 * 500 mm moulds were used to cast beams to determine flexural strength in concrete.

Table 7 List of tests on SCC

Characteristic property	Test method	Measured unit
Filling ability	Slump flow (mm)	Total spread
Cohesiveness	T500	Flow time
Viscosity	V funnel	Flow time
Passing ability	L box	Flow time

Fig. 2 Slump flow

The specimens in their mould were covered and kept at room temperature for 24hrs. These were then kept submerged in water for curing they remained in the tank until for testing after 7 and 28 days.

4.2 Fresh Properties of SCC

A wide range of test methods have been developed to measure and asses the fresh properties of SCC, Table 7 lists the most common tests conducted on SCC. All the test is conducted based on IS 10262: 2019. Figures 2, 3 and 4 shows the slump test, L box test, and V funnel test.

4.3 Properties of Hardened Concrete

To determine the mechanical properties, the test specimens were removed from the water bath and surface water was removed using a dry cloth, immediately before testing. This was to ensure that the test specimens were tested at a saturated—surface

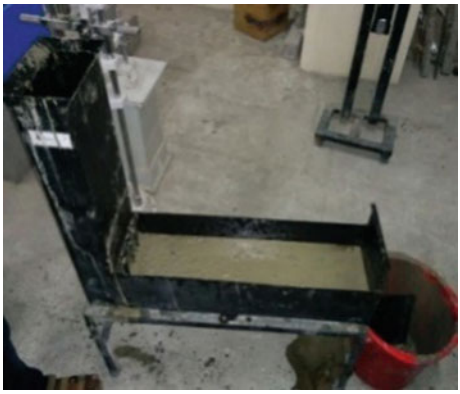

Fig. 3 L box test

Fig. 4 V Funnel test

dry condition (SSD) conditions. All the tests were conducted based on IS. Various tests to be carried out on hard concrete are:

- Compressive strength
- Split tensile
- Flexural strength.

Figures 5, 6 and 7 shows the compressive strength, tensile strength, flexural strength of SCC.

Fig. 5 Compressive strength

Fig. 6 Tensile strength

Fig. 7 Flexural strength

5 Result and Discussion

5.1 Properties of Fresh Concrete

The higher the slump flow value, the greater is its ability to fill formwork under its weight. A minimum slump value of 660 mm and maximum slump value of mm750 is recommended by guideline as per IS Code IS 10262: 2019. A tolerance of ±50 mm is accepted. A minimum T500 flow of 2 s. Table 8 shows slump flow and T500 values. The test result satisfies the minimum requirement.

Viscosity can be assessed by the V Funnel flow time as per IS 1199(Part 6). The viscosity is divided into two classes that is V1 and V2. V1 has the good filling ability even with congested reinforcement. V2 class viscosity is more likely to exhibit a thixotropic effect, which helps to improve segregation resistance. For V1 class, time taken to pass the concrete from V Funnel shall be ≤8 s and V2 class between 8 sans 25 s. L box test is performed to check passing ability. The minimum ratio for the test is taken as 0.8. Test conducted the three optimized samples of MK replacing 10% of cement, FA replacing 30% of cement and a combination of MK and FA at 15% and 25%. The test result satisfies the IS 10262.2019. The obtained values are tabulated in Table 9.

Table 8 Slump flow test

Mix	Slump flow (mm)	T_{500} slump flow (sec)
MK5	680	4.2
MK10	698	4.3
MK15	705	4.5
MK20	690	4.8
FA10	670	4.5
FA20	684	4.6
FA30	695	4.7
FA40	680	4.8
MK5 FA35	688	4.5
MK10 FA 30	692	4.6
MK15 FA25	708	4.6
MK20 FA20	710	4.7
MK25 FA 20	690	4.8

Table 9 L box and V funnel test

Mix	L Box	V Funnel
MK 10	0.95	7.1
FA 30	0.92	7.51
MK15 FA25	0.98	7.94

Table 10 Compressive strength

Mix	Compressive strength at 7th day (MPa)	Compressive strength at 28th day (MPa)
MK 5	28.96	37.59
MK 10	29.43	40.15
MK 15	28.75	37.48
MK 20	27.64	36.27
FA 10	28.39	35.40
FA 20	28.97	36.64
FA 30	29.14	38.08
FA 40	28.15	36.04
MK5 FA35	27.4	35.07
MK10 FA 30	28.5	36.47
MK15 FA25	30.4	42.04
MK20 FA20	29.8	39.4
MK25 FA 20	27.2	35.4

Table 11 Splitting tensile strength and flexural strength

Mix		Splitting tensile strength (N/mm^2) at 28 day	Flexural strength (N/mm^2) at 28 day
MK 10		4.51	4.85
FA 30		4.58	4.90
MK15 FA25		4.98	5.2

5.2 Properties on Hardened Concrete

Cube specimen were tested after 7 and 28 days of curing. The failure load was noted for each mix three cubes were tested and the average value is reported. The obtained values of compressive strength at the 7th and 28th day are given in Table 10.

Split Tensile Strength and Flexural Strength were conducted on the three optimized samples of MK replacing 10% of cement, FA replacing 30% of cement and a combination of MK and FA at 15 and 25%. The test result was given in Table 11.

6 Conclusion

- The inclusion of MK and FA can improve the fresh and hardened properties because both the mineral admixtures contain a high amount of alumina and silica. This helps to the production of excess C–S–H gel and result in increasing compressive strength, splitting tensile strength and flexural strength.

- The successful utilization of fly ash and metakaolin in SCC mixes not only lower the cost of SCC but also provide a solution to the disposal and environmental problems connected with these materials.

References

1. Mahalingam B, Nagamanib K, Kannan LS, Haneefaa KM, Bahurudeend A (2016) Assessment of hardened characteristics of raw fly ash blended self-compacting concrete. Perspect Sci 8:709–711
2. Khatib JM (2008) Performance of self-compacting concrete containing fly ash. Constr Build Mater 22:1963–1971
3. Abouhussien AA, Assem AA (2015) Hassan optimizing the durability and service life of self-consolidating concrete containing metakaolin using statistical analysis. Constr Build Mater 76:297–306
4. Madandoust R, Yasin Mousavi S (2012) Fresh and hardened properties of self-compacting concrete containing metakaolin. Constr Build Mater 35:752–760
5. Vejmelkova E, Koppert M, Grzeszczyk S, Skalin B, Černý R (2011) Properties of self-compacting concrete mixtures containing metakaolin and blast furnace slag. Constr Build Mater 25:1325–1331
6. Dinakar P, Manu SN (2014) Concrete mix design for high strength self-compacting concrete using metakaolin. Constr Build Mater 60:661–668
7. Kannan V, Ganesan K (2014) Chloride and chemical resistance of self compacting concrete containing rice husk ash and metakaolin. Constr Build Mater 51:225–234
8. Cassagnabère F, Mouret M, Escadeillas G, Broilliard P, Bertrand A (2010) Metakaolin, a solution for the precast industry to limit the clinker content in concrete: mechanical aspects. Constr Build Mater 24:1109–1118

Studies on Inclusion of Polypropylene (PP) Geo-fabric in Concrete

K. S. Sreekeshava, A. S. Arunkumar, Manish S. Dharek, and Prashanth Sunagar

Abstract The concrete is a composite material made by proper proportions of fine aggregates, course aggregates along with proper water to cement ratio. This composite in hard state very strong in compression and having ability to take more gravity loads. Concrete members are weak in tension hence commonly steel is adopted as reinforcement in all over the world. Several researchers tried to enhance the tensile reinforcement by various alternative materials and also successfully showed the importance of various fibres and alloy materials in concrete. The materials used for enhancing tensile strength must possess good bond strength, thermal resistance, corrosion resistance and recyclable. In this present paper, an experimental work has been conducted to know the behaviour of polypropylene (PP) Geo-fabric as partial replacement for reinforcement in concrete for non-importance small scale structural members. Different tests like compression, split tensile, flexure tests have been conducted with the presence of PP Geo-fabric and results shown better performance compared with normal conventional test specimens.

Keywords Geo-fabrics · Reinforcement · Polypropylene · Construction · Brittle failure · GI wires

K. S. Sreekeshava (✉)
Department of Civil Engineering, Jyothy Institute of Technology, Bengaluru, affiliated to Visvesvaraya Technological University, Belagavi, India
e-mail: sreekeshava.ks@jyothyit.ac.in

A. S. Arunkumar
Department of Civil Engineering, BMS College of Engineering, Bengaluru, affiliated to Visvesvaraya Technological University, Belagavi, India

M. S. Dharek
Department of Civil Engineering, BMS Institute of Technology and Management, Bengaluru, affiliated to Visvesvaraya Technological University, Belagavi, India

P. Sunagar
Department of Civil Engineering, Ramaiah Institute of Technology, Bengaluru, affiliated to Visvesvaraya Technological University, Belagavi, India

© Springer Nature Switzerland AG 2021

K. Dasgupta et al. (eds.), *Proceedings of SECON 2020*,
Lecture Notes in Civil Engineering 97,
https://doi.org/10.1007/978-3-030-55115-5_2

1 Introduction

Beams are one dimensional horizontal structural members predominantly subjected to transverse loads and negligible axial loads. These are mainly designed to resist shear and flexural loads. The reinforcement plays a major role to resist against different failures but transverse reinforcements are provided to resist against shear failure and longitudinal reinforcements are provided to resist flexure failure of beams [1, 2]. In general, the shear failure is controlled by providing closed transverse stirrups and flexure failure are controlled by providing tensile and compression reinforcements along longitudinal directions. Production of steel affects the environment adversely by emitting CO_2 to environment and also steel having certain drawbacks when it is used as a construction material similar to concrete [3]. Proper care should be taken by providing sufficient cover to protect steel from corrosion.

The hardened concrete exhibits better compressive strength and week tensile strength. The reinforcement acts like better skeletal support in structural members [4, 5]. But in case of non-structural importance small scale structures steel reinforcement would be economical, in such cases the alternative for steel reinforcement become essential. In case of non-structural significance works the only focus is to provide nominal safe minimum reinforcement to improve the ductility of the members. In recent past several researchers focusing on this intent to replace steel partially or fully by proper alternative reinforcing material. The Geo-fabrics are used as alternative to reinforcement in small scale non-structural importance works because of its better interlocking behavior with cement concrete and imparts better tensile strength [6, 7].

Geo-fabrics are usually made of synthetic polymers such as polypropylene, polyesters, polyethylene and polyamides, varying polymers and manufacturing process results in array of geotextiles suitable for a variety of civil construction applications. Basically these Geo-fabrics are classified as Uniaxial, Bi-axial and Tri-axial Geo-fabrics represented in Fig. 1 [8–10].

Recently the importance of Geo-fabrics is explored by several researchers in the application of concrete works [1, 9]. Geo-fabrics reinforcement provides better alternative solution for small scale structural works. The prime objective of this study

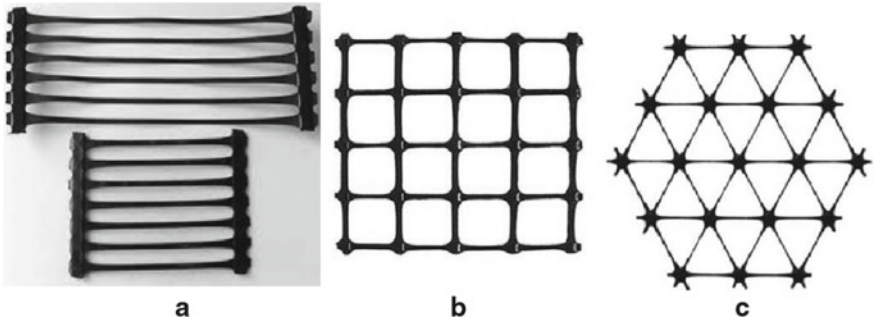

Fig. 1 **a** Uniaxial geo-fabric; **b** biaxial geo-fabric; **c** tri-axial geo-fabric

is to investigate the flexural behavior of polypropylene (PP) Biaxial Geo-fabrics with and without reinforcement.

2 Experimental Sequences

2.1 Basic Material Characterisation

The tests specimens were casted using different materials. Behavior of individual material plays a significant role in the strength and durability of structural members. In this experimental work an ordinary Portland cement of 53 grade and coarse aggregate pertaining sieve size less than 20 mm were considered. Fine aggregates are locally available having less than 4.75 mm size was considered as per code of practice. The 3 and 2 mm Galvanized iron (GI) wires were used as reinforcements because, the alternative reinforcement Polypropylene (PP) Geo-fabrics are 2 mm thick Bi-axial grids hence for the compatibility of replacement GI wires were considered. Experimental tests were conducted on materials and results were tabulated in Tables 1, 2 and 3.

Table 1 Properties of cement

Experiment name	Relevant code of practice	Test results	Permissible value as per code
Fineness	IS 269	7.2%	Maximum 10%
Normal consistency	IS 4031-part 4	31%	26–33%
Soundness	IS 4031-part 3	6.8 mm	<10 mm
Specific gravity	IS 2720-part 3	3.16	3.12–3.19
Initial setting time	IS 4031	38 min	Minimum 30 min
Final setting time	IS 4031	290 min	Maximum 600 min

Table 2 Properties of Coarse aggregate

Experiment name	Relevant code of practice	Test results	Permissible value as per code
Specific gravity	IS 2386	2.7	2.5–0.3.2
Water absorption	IS 2386	1.3%	<2%
Flakiness index	IS 2386	22%	<30%
Elongation index	IS 2386	20%	<30%
Aggregate crushing test	IS 2386	19%	<30%
Aggregate impact test	IS 2386	16%	<24%
Los Angeles abrasion test	IS 2386	21%	<30%

Table 3 Properties of manufacturing sand (M-sand)

Experiment name	Relevant code of practice	Test results	Permissible value as per code
Specific gravity	IS 2730-Part 3	Bulk G = 2.64	2.53–2.69
		Apparent G = 2.56	
Water absorption	IS 2386-Part 3	1.3%	<2%

The GI wires and PP Geo-fabrics were tested in digital strain controlled universal testing machine (UTM). The experimental setups are shown in Fig. 2 and results are tabulated in Table 4.

Fig. 2 Tensile testing in universal testing machine

Table 4 Properties of reinforcements

Material	Ultimate load (N)	Ultimate tensile strength (MPa)	Breaking load (N)	Breaking stress (MPa)	Young's modulus (MPa)
3 mm Ø GI wire	2600	352	1560	256	1.8×10^6
2 mm Ø GI wire	2104	334	1375	228	1.68×10^6
2 mm thick Bi-axial PP Geo-fabric	1926	206	976	193	1.9×10^6

2.2 Experimental Investigation

2.2.1 Experimental Investigation on Cement Mortar

Mortar is a composite mixture and used to protect the reinforcements in structures. The experimental investigations were performed on 1:6 proportion cement sand mortar with water cement ratio equal to 0.6 which was arrived based on mini flow table test conducted on mortar. Sometimes mortar used as a binding material for masonry units as well as for wallets to protect it from environment and also to give better view from architectural point of view. In this present study PP Geo-fabrics are used as reinforcements so it is required to check the performance with mortar. Hence, the flexural strength and Tensile strength of 1:6 mortars with and without PP Geo-fabrics are evaluated in this section. The flexural strength test is conducted as per ASTM D7264/D7264M-07 code of practice. As per code the PP Geo-fabrics are sandwiched between 12 mm thick mortar and minimum 5 numbers of specimens were considered having each specimen gauge length of 90 mm and tested under 25kN digital universal testing machine [11]. The test specimens were shown in Fig. 3 and results of test after 28 days aging were tabulated in Table 5.

The Tension tests are carried with and without PP Geo-fabrics in 1:6 cement sand mortar. The mortar samples were having dimensions 200 × 600 × 25 mm prepared and test conducted in accordance with AC434.13 guidelines. Experimental setups along with specimen are shown in Fig. 4 and results after 28 days of aging have been tabulated in Table 6.

Fig. 3 Mortar laminates for flexure test

Table 5 Flexure test on mortar

Type of specimen	Flexural strength (MPa)	Flexural modulus (MPa)
Conventional 1:6 mortar	3.96	2185
PP geo-fabrics laminated 1:6 mortar	4.28	2896

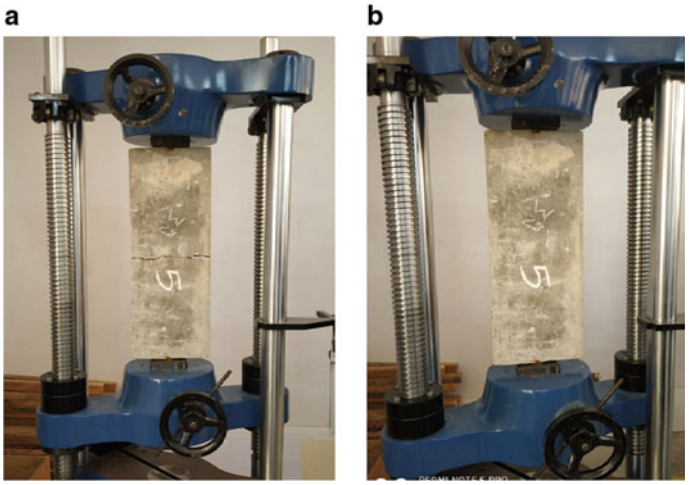

Fig. 4 **a** Tension test on mortar before test; **b** specimen after test

Table 6 Tension test on mortar

Type of specimen	Ultimate load (N)	Tensile strength (MPa)
Conventional 1:6 mortar	8100	1.62
PP geo-fabrics laminated 1:6 mortar	12,140	2.43

2.2.2 Experimental Investigation on Concrete

The designed mix proportion of 1:1:2 is used for concrete specimen casting. The mix proportions were designed in accordance with IS 10262:2019 and ordinary Portland cement of grade 53 with water cement ratio of 0.5 is used for specimen casting. The compression, split tensile strength, Flexure tests were conducted by testing cubes, cylinders and prisms respectively. Specimens were reinforced with PP Geo-fabrics depends on normal conventional specimens failure and plastic hinge formation zones [12]. Test specimens were shown in Fig. 5 and the average five specimens results are represented with the help of graphical representation shown in Fig. 6.

2.2.3 Experimental Investigation on Beam Specimen

Beams are one dimensional structural members having larger length compared to cross sectional area. In this present study 150 × 150 × 700 mm size beams were considered with different reinforcement configurations and the test is carried in accordance with IS: 516-1959. The PP Geo-fabrics were reinforced with two types of reinforcements. In both two types of reinforcements shear reinforcements were replaced

Fig. 5 Specimens used for testing

Fig. 6 **a** Compressive strength; **b** split tensile strength; **c** flexural strength

a

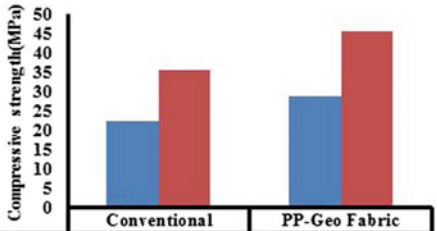

	Conventional	PP-Geo Fabric
Compressive strength 7 Days	22.5	28.9
Compressive strength 28 Days	35.5	45.6

b

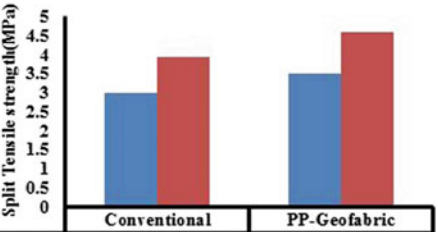

	Conventional	PP-Geofabric
Split Tensile strength 7 Days	2.98	3.51
Split Tensile strength 28 Days	3.92	4.59

c

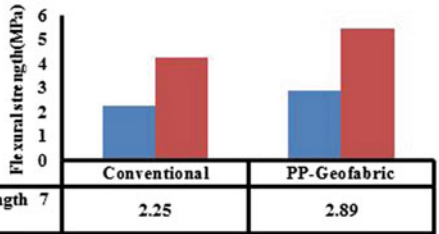

	Conventional	PP-Geofabric
Flexural strength 7 Days	2.25	2.89
Flexural strength 28 Days	4.26	5.48

Table 7 Details of beam specimen

Description of beam	Longitudinal reinforcement		Transverse reinforcement	
	Top (mm)	Bottom (mm)	Size (mm)	Spacing (mm)
Plain cement concrete	–	–	–	–
GI reinforced beam	2–3Ø	2–3Ø	2Ø	25
PP Geo-fabric reinforced Facing	2–3Ø	2–3Ø	2 mm thick PP Geo-fabrics connected to four faces	
PP Geo-fabric reinforced Facing	2–3Ø	2-3Ø	2 mm thick PP Geo-fabrics wrapped to main reinforcement	

by PP Geo-fabrics completely by two different methods. In first type shear reinforcement is completely replaced by PP Geo-fabric on face of the beam and in second type of beam PP Geo-fabrics are completely wrapped all around main reinforcement. Different configurations were considered in this present study is tabulated in Table 7 and different types of reinforcement materials used to cast the specimens shown in Fig. 7.

In all combinations each type of three numbers of beams are considered for the study. After casting all the specimens are cured with water for 28 days before the test. The test on beams subjected to four-point loading and the load applied at the rate of 67 N/s on all varieties of Beams. Test specimens and experimental setup shown in Fig. 8 and test results are tabulated in Table 8.

Failure patterns of different types of beams are presented in Fig. 9 and it shows the importance of reinforcement compared with plain cement concrete beams. The PP Geo-fabric by wrapping showed the better resistant to failure and to control the

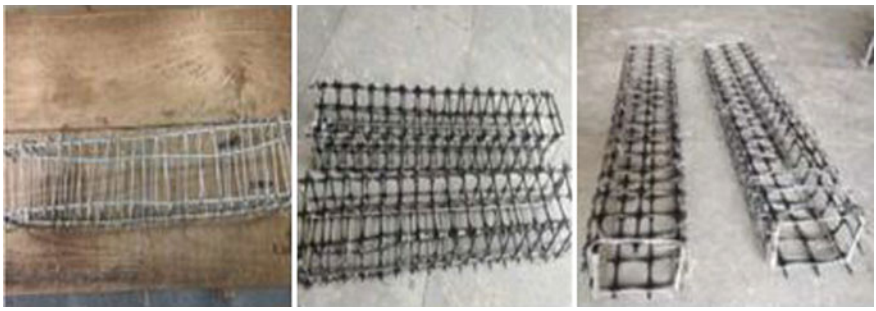

Fig. 7 **a** GI Wire reinforcement; **b** PP geo-fabrics face reinforcement; **c** PP geo-fabrics wrapped to main reinforcement

Fig. 8 **a** Beam specimens; **b** four point bending

Table 8 Comparison of beam results

Type of beam	Ultimate stress (MPa)	Ultimate load (kN)	Mode of failure	Cost per beam specimen (₹)
Plain cement concrete beam	3.9	22.05	Brittle	70
GI reinforced concrete beam	5.10	30.01	Ductile	185
PP geo-fabric facing reinforced concrete beam	4.92	27.8	Ductile	140
PP geo-fabric reinforced by wrapping	4.89	26.8	Ductile	140

cracks compared to all other type of specimens. The PP Geo-fabrics helps to control the shear cracks by better aggregate interlocking mechanism.

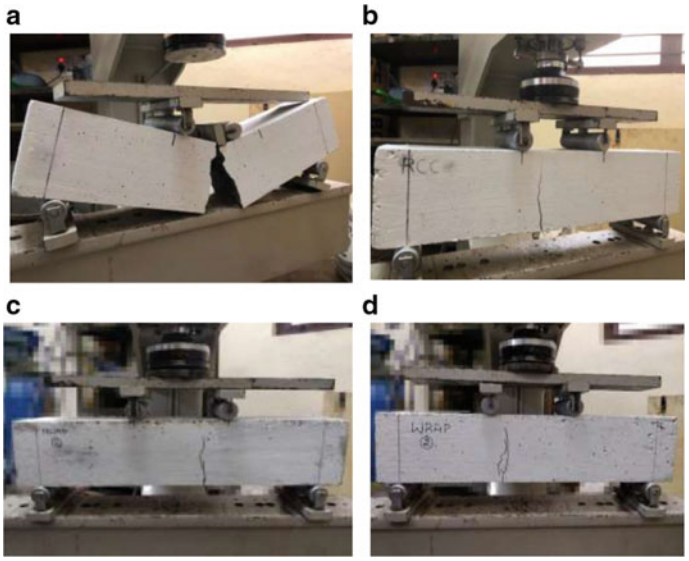

Fig. 9 **a** Failure pattern of plain concrete beam; **b** GI reinforcement; **c** PP geo-fabric wrapping; **d** PP geo-fabric facing

3 Conclusion

The following conclusions were observed in this experimental investigation.

1. The cement mortar tests showed that significant enhancement in strength of PP Geo-fabric reinforcement was observed which was due to better interlocking behaviour and improved bond strength compared with un-reinforced specimens.
2. Basic Concrete element like cubes and cylinders with PP Geo-fabrics showed 1.5–2 times greater strength compare with conventional specimens in both compression and tension. This clearly indicates the improvement in the mechanical properties due to inclusion of PP Geo-fabrics in concrete.
3. Ultimate load of RCC beam when subjected to flexure test was 30.01 kN. The ductile mode of failure was observed in the beams. In Geo-wrap reinforced beams 85% of the flexural strength of GI-RCC beams was obtained by replacing the shear reinforcement of RCC section with Geo-grid in the form of a wrap.
4. In Geo-fabric facing reinforced beams 80% of the actual flexural strength of GI-RCC beam was achieved and about 90% of the actual flexural strength of PP Geo-fabric wrapping beam was achieved. This implies that the Geo-facing reinforced beams are not feasible as the strength obtained is less than the wrapped beam. The advantage of the Geo-fabric facing reinforced beams is that it prevents the beam from undergoing brittle mode of failure. The crack width of PP Geo-fabric reinforced beams is comparatively less than all other types of Beams considered in this study.

Acknowledgements Authors would like to acknowledge Visvesvaraya Technological University TEQIP CELL, Belagavi, (Ref: VTU/TEQIP 3/2019/321) for providing financial assistance to conduct this experimental work under Research competitive funding scheme.

References

1. Sreekeshava KS, Arun KAS (2018) Experimental studies on response of biaxial geo-grid proportioned cement concrete. i-Manager's J Civ Eng 8(2):15. https://doi.org/10.26634/jce.8.2.14550
2. Perkins S (1999) Mechanical response of geosynthetic-reinforced flexible pavements. Geosynth Int 6(5):347–382. https://doi.org/10.1680/gein.6.0157
3. Dharek MS, Sunagar P, Bhanu Tej KV, Naveen SU (2019) Fresh and hardened properties of self-consolidating concrete incorporating alumina silicates. In: Das B, Neithalath N (eds) Sustainable construction and building materials. Lecture Notes in Civil Engineering, vol 25. Springer, Singapore
4. Duan L, Wang F-M, Chen W-F (1989) Flexural rigidity of reinforced concrete members. ACI Struct J 86(4):419–427. https://doi.org/10.14359/9228
5. Tak-Bun DL (2006) Flexural ductility improvement of FRP-reinforced concrete members. https://doi.org/10.5353/th_b3890775
6. Hughes BP, Watson AJ (1978) Compressive strength and ultimate strain of concrete under impact loading. Mag Concr Res 30(105):189–199. https://doi.org/10.1680/macr.1978.30.105.189
7. Meski FE, Chehab GR (2014) Flexural behavior of concrete beams reinforced with different types of geogrids. J Mater Civ Eng 26(8):04014038. https://doi.org/10.1061/(asce)mt.1943-5533.0000920
8. Sobhan K, Tandon V (2008) Mitigating reflection cracking in asphalt overlays using geosynthetic reinforcements. Road Mater Pavement Design 9(3):367–388. https://doi.org/10.3166/rmpd.9.367-388
9. Sivakamasundari S, Daniel AJ, Kumar A (2017) Study on flexural behavior of steel fiber RC beams confined with biaxial geo-grid. Procedia Eng 173:1431–1438. https://doi.org/10.1016/j.proeng.2016.12.206
10. Shukla SK (2002) A text book of geosynthetics and their applications. Thomson Thelfold Publications, London. ISBN: 0727731173
11. Sreekeshava KS, Arunkumar AS, Ravishankar BV (2020) Experimental studies on brick masonry elements with geo-fabric bed joint reinforcement. Advances in sustainable construction materials lecture notes in civil engineering, pp 33–41. https://doi.org/10.1007/978-981-15-3361-7_3
12. Sreekeshava KS, Arunkumar AS, Ravishankar BV (2020) Experimental studies on polyester geo-fabric strengthened masonry elements. Lecture notes in civil engineering advances in computer methods and geomechanics, pp 727–736. https://doi.org/10.1007/978-981-15-0886-8_58

Dual-Pipe Damper with Bracing System for Seismic Retrofitting

V. Bincy and S. Usha

Abstract Dual-Pipe Damper (DPD) is a metallic yielding device for the passive earthquake energy dissipation. It consists of two welded pipes, which is positioned to take shear. DPD works in flexural form, on the basis of plastic-deformation of steel materials. According to previous researchers, multistory frames equipped with DPD exhibit a stable hysteresis loop with excellent energy absorption capacity under dynamic non-linear time—history analysis. Present study investigates the lateral resisting capacity of DPD by pushover analysis and to find out the best dimensions of DPD for buildings conforming to IS 800:2007. From this study, the optimum frame equipped with DPD is identified which can be utilized for a better seismic retrofitting.

Keywords Seismic retrofitting techniques · Dual-Pipe Damper · Metallic Yield Dampers · Parametric study · Pushover analysis

1 Introduction

"Natural disasters are less natural than you think" [1]. Disasters hardly kill human but structures do it. Nature remains full of hazards, but only some of them wreak disaster [1]. It is human-built structures, not the shaking ground, that kill when an earthquake strikes [1]. Major portion of India is prone to earthquake and the rate of loss of lives is considerably high. Hence the scope of retrofitting techniques is increasing day by day. Seismic retrofitting techniques are those techniques which make a structure more resistant to seismic activity during earthquake still they are not preventive measures. Recent studies are being conducted to improve the effectiveness of dampers. Dampers are the mechanical devices to dissipate kinetic energy of seismic

V. Bincy (✉) · S. Usha
Department of Civil Engineering, Sree Narayana Gurukulam College of Engineering, Ernakulam, Kerala, India
e-mail: bincyveena1995@gmail.com

S. Usha
e-mail: ushaushus11@rediffmail.com

© Springer Nature Switzerland AG 2021

K. Dasgupta et al. (eds.), *Proceedings of SECON 2020*,
Lecture Notes in Civil Engineering 97,
https://doi.org/10.1007/978-3-030-55115-5_3

waves penetrating through a building and metallic dampers are those which dissipate energy by deforming their original shape. Many researches on metallic dampers are being conducted to improve the performance and at the same time to evolve a best model which shows greater energy dissipation [2–5]. Dual-Pipe Damper (DPD) is a metallic yielding device for the passive control of structures, introduced recently. It consists of two horizontal pipes welded together which are efficiently connected to the building frame. It has been proved that DPDs are effective in reducing the seismic performance of multi-storey structures, specifically up to ten storey buildings [6]. Study on Dual-Pipe Dampers exhibit good seismic retrofitting. In the earlier studies, the size of the pipes in DPD is pretty small, intended for laboratory experiments. When it comes to practical cases, these sizes may not enough for effective and efficient seismic retrofitting. The present study investigates how the variation in dimensions of pipes in DPD affect the seismic performance of a building frame and to find out the effective DPD model suitable for the building frame conforming to IS 800:2007; code for general construction in steel.

2 Summary of Literature Survey

Several experimental and analytical investigations were conducted on structures to explore the limitations and advantages of usage of metallic dampers in structures, the seismic performance of structures during earthquake with and without seismic retrofitting techniques, different bracing systems to produce maximum seismic retrofitting property etc. Hence, review on the previous works will give sufficient information for the present study.

A well-known passive energy dissipation device, Metallic Yield Damper (MYD) provides a new way to resist the imposed loads to structural elements. Its effectiveness and low cost are now well recognized and extensively tested in the past [4]. Comparative study was conducted among the available well-known metallic dampers such as Pipe Damper (PD), Dual-Pipe Damper (DPD), Infilled-Pipe Dampers (IPD), Triangular-plate Added Damping and Stiffness (TADAS), Slit Damper (SD), Shear Panel Damper (SPD), Honeycomb Damper (HD), Cast Steel Yielding Brace (CSYB), Double Function Metallic Damper X-Shaped (DFDMX) and Box-Shaped Slit Damper using important parameters [4]. Dual-Pipe Damper (DPD) is a recently proposed metallic yield damper, which shows comparatively high energy dissipation through yielding [4]. It is a passive energy dissipating device and the energy dissipation is in the form of plastic deformation. The total energy dissipation value of DPD (49.2 kJ) is the second largest among all the metallic dampers [7]. Light in weight, cost effectiveness, easy degree of installation and a medium degree of replaceability are its advantages [4, 7]. In a steel building frame installed with DPD, the inelastic energy absorbed by the main frames decreases quickly by increasing the DPD yield strength. Hence the most important design parameters of DPD are stiffness, strength and yield displacement [7]. When we consider the case of design of steel building frames, it is suggested to follow IS 800:2007. In codal method

of design, the column and beam sections for steel building frames are selected by choosing the plastic moment capacity ratio for buildings situated on medium soil of various seismic zones of India, supports are taken as fixed support. The grade of steel suggested by authors was RSJ 300 and 345 MPa [8]. The authors identified the main drawback of DPD is that, they are less effective in reducing the seismic performance of a twenty storey building than a five and ten storey building due to the higher natural period and overall bending mode of the taller buildings [7].

Extensive studies are being conducted to improve the performance and to evolve new patterns of metallic dampers for effective seismic performance. In the present study, Dual-Pipe Damper (DPD) with building frame conforming to IS 800:2007 is analyzed to check its suitability.

3 Numerical Analysis

In order to verify the accuracy of a numerical model using finite element software, numerical analysis from a journal is reciprocated using its model dimensions and other input parameters. The details from Journal [4] were opted for the validation of mathematical model using the finite element software ANSYS 16.1. The model named as M1L25 was taken for the validation purpose. The specimen has an outside pipe diameter of 140 mm and thickness of 5.1 mm. The length of pipes in DPD is 25 mm. Modulus of elasticity from the journal is 203 GPa. After proper modeling and meshing of M1L25, the model is provided cyclic load, following the loading protocol in the journal. The maximum displacement and force corresponding to maximum displacement obtained from the validation are 30.01 mm and 56.63 kN respectively. Also the maximum displacement and the force due to maximum displacement observed from the journal are 30 mm and 59 kN respectively. The percentage error obtained is less than 5%.

Parametric study on Dual-Pipe Damper (DPD) using pushover analysis to find the best model applicable to building frame conforming to IS 800:2007 is aimed in this study.

3.1 Modeling of Dual-Pipe Damper (DPD) with Building Frame

Numerical modeling of the DPD base model was performed by the finite element software ANSYS 16.1 WORKBENCH. The model's material property was assigned in the engineering data section of the ANSYS software. The engineering data section of the software consists of pre-assigned values for each material. The material properties given for the model is shown in Table 1.

Table 1 Material properties of base model

Material	Steel
Yield strength	345 MPa
Modulus of elasticity	2×10^{11} Pa
Poisson's ratio	0.3
Density	7850 kg/m^3

Table 2 Specifications of building frame

Building frame	Plan dimension	Storey height (m)	Column size	Beam size
IS III-8	L = 5@4 m; B = 7@4 m	5	ISWB 450	ISMB 400

The model consists of a building frame equipped with DPD and a V bracing system. The building is considered as residential building frame. The length of the plan is varied in X direction and breadth of the plan in Y direction. The storey height is varied through Z direction [8]. The specifications of building frame chosen for modeling are given in the Table 2 [8]. The building is having fixed support situated on medium soil of various seismic zones of India [8]. The nomenclature of building starting as Indian Standards (IS), plan and number of storey in building [8]. The DPD consists of two horizontal pipes connected together [4]. A rigid plate is provided below the pipes for the proper connection and load transfer. The V-bracing system is provided to support DPD in the model, which has a minimum section of 100 × 100 mm.

Each model in the present study is named according to its dimension of the pipes in the DPD model. For example, DPD 300-15-25 is a model having diameter of pipe 300 mm, thickness of the pipe 15 mm and length of the pipe 25 mm.

3.2 Support and Loading for DPD Base Model

Displacement is given at the top of the model in the Z direction. Figure 1 shows the loading protocol that is the variation of displacement given to the model. Figure 2 shows the model created for the analysis with fixed support at the bottom of the base model.

Fig. 1 Loading protocol

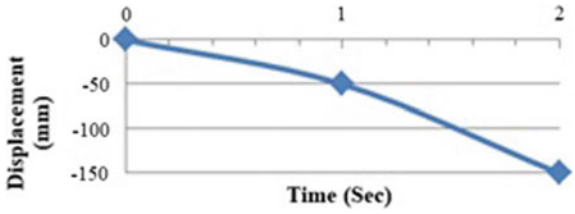

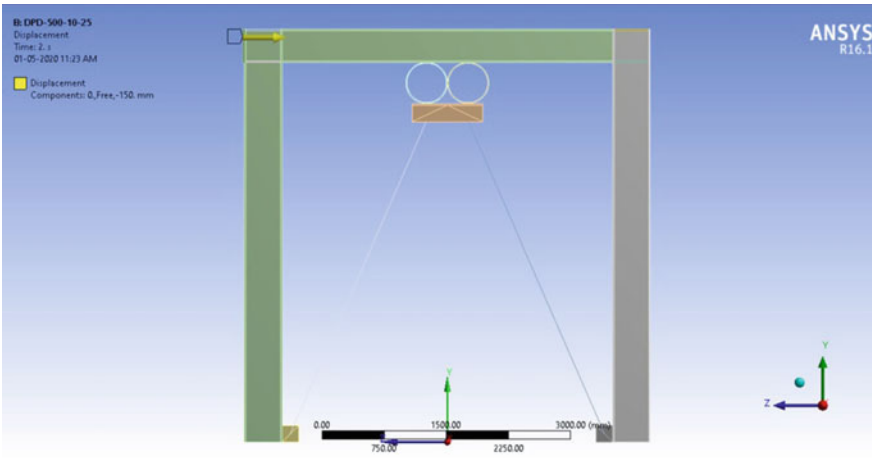

Fig. 2 Model created for the analysis

3.3 Parametric Studies on DPD Model

Parametric study using push over analysis was conducted on the DPD models. Three parameters were varied accordingly to find out the best model suitable for the building frame conforming to IS 800:2007. The parameters varied are diameter (500, 400, 300 and 200 mm), thickness (10, 15 and 20 mm) and length (25, 50 and 75 mm) of the pipes in DPD. The length and thickness of pipes in the DPD models are selected according to the suggestions made by previous studies. The minimum length of pipes in DPD provided was 25 mm [4]. Varying three parameters at a time is tiresome. Hence the study is divided into two different steps. In the first step, the value of one of the parameters is fixed and the other two parameters are varied. In the second step, the parameter which stands fixed in the first step is varied for the optimized models from first step. This approach seems to be effective and efficient. In the present study, the length of pipes of DPD is set to 25 mm and the study was done by varying the diameter and thickness of the pipes in DPD. The diameter of the pipes DPD was varied as 500, 400, 300 and 200 mm. For each diameter of DPD, the thickness was varied as 10, 15 and 20 mm. The corresponding models created are DPD 500-10-25, DPD 500-15-25, DPD 500-20-25, DPD 400-10-25, DPD 400-15-25, DPD 400-20-25, DPD 300-10-25, DPD 300-15-25, DPD 300-20-25, DPD 200-10-25, DPD 200-15-25 and DPD 200-20-25. In the second step, some of the models which show better performance (specifically, the models show ultimate load carrying capacity) from the first step were selected and subjected to further variation of length of pipes in DPD as 50 and 75 mm. Here, the model DPD 500-10-25 is one of the optimum models obtained from the first step. Hence, the length of pipes in the model DPD 500-10-25 is changed from 25 to 50 mm and then to 75 mm and these models (DPD 500-10-50 and DPD 500-10-75) are tested. Similarly, all the optimum

models from the first step were taken to the second step of parametric study. From the parametric study, the best model applicable for the building frame conforming to IS 800:2007 are found out. The effect of variation in dimensions of pipes of DPD in the performance of building frame is also figured out.

4 Results and Discussion

From the parametric study of the model, it is observed that the thickness of the pipes in DPD model affects the performance. The models with a thickness of 15 mm is effective than 10 mm but all the models with a thickness of pipes in DPD as 20 mm, exhibited a quick failure without taking much load as compared to the other models. Hence such models with a thickness of pipes in DPD were rejected from further study. When we consider the case of diameter of pipes in DPD, the models with a diameter of 200 mm showed an unpredictable behavior and it has been concluded that such models are not suitable for practical purposes. For the models tested, as the diameter of pipes in DPD increases, it showed an increasing load carrying capacity. But load carrying capacity itself cannot be taken as a measure of better performance. The better performance of a model can be defined by considering the ultimate load and the corresponding deflection, yield load and the corresponding deflection, yield stiffness and ductility. Ductility is the capacity of a material to deform permanently in response to stress [9]. Most common steels, for example, are quite ductile and hence can accommodate local stress concentrations [9]. The ultimate load, ultimate deflection, yield load and yield deflection of each model can be obtained from the finite element software itself. The Yield stiffness and Ductility of each model were found out using the following equations:

$$Yield\ stiffness = \frac{Yield\ load}{Yield\ deflection}$$

$$Ductility = \frac{Ultimate\ deflection}{Yield\ deflection}$$

Table 3 shows the test results of different models. DPD models with ductility above 30 were selected to find the best model. Four models which show ductility above 30 are DPD 200-10-25, DPD 200-15-25, DPD 500-15-75 and DPD 300-15-75. The highest load carrying capacity (742.5kN) of the model is observed with DPD 300-15-75, whereas highest ductility model (DPD 200-10-25) exhibit low load carrying capacity (518.4kN). Model DPD 200-15-25 also show low load carrying capacity. Considering ultimate load capacity and ductility together, DPD 300-15-75 exhibit the best performance among the other models. Hence DPD 300-15-75 was selected for the application in building frames conforming to IS 800:2007.

Table 3 Test results of different models

Specimen	Ultimate load (kN)	Ultimate deflection (mm)	Yield load (kN)	Yield deflection (mm)	Yield stiffness (kN/mm)	Ductility
Frame only	471.0	246.6	224.8	24.5	9.2	10.1
DPD 500-10-25	507.0	109.2	60.7	6.8	8.9	16.0
DPD 500-15-25	536.1	110.6	48.1	4.5	10.8	24.8
DPD 500-15-50	624.6	140.9	84.2	6.6	12.8	21.4
DPD 500-15-75	705.9	215.8	93.4	6.5	14.4	33.3
DPD 400-10-25	499.9	88.6	43.9	4.5	9.7	19.6
DPD 400-15-25	530.2	89.8	56.3	4.4	12.8	20.5
DPD 400-15-50	612.2	91.3	67.5	4.3	15.78	21.3
DPD 400-15-75	719.9	143.4	1.1E+02	6.3E+00	18.0	22.7
DPD 300-10-25	493.5	102.6	50.0	4.4	11.3	23.1
DPD 300-15-25	535.5	80.9	73.2	4.2	17.4	19.3
DPD 300-15-50	637.9	76.5	87.5	4.2	20.9	18.3
DPD 300-15-75	742.5	131.5	95.1	4.3	22.0	30.4
DPD 200-10-25	518.4	207.0	36.1	2.1	17.2	98.8
DPD 200-15-25	531.8	91.2	48.4	2.5	19.4	36.5
DPD 200-15-50	442.2	30.4	106.4	4.9	21.6	6.2
DPD 200-15-75	583.1	36.0	166.8	4.9	33.8	7.3

5 Conclusion

DPD models with different diameters (500, 400, 300 and 200 mm) were studied by varying thickness (10, 15 and 20 mm) and length (25, 50 and 75 mm) to select the best model applicable for the building frame conforming to IS specification. The model with 300 mm diameter, 75 mm length and 15 mm thickness (DPD 300-15-75) shows

comparatively better results in Push-over analysis. This model can be selected for implementing in the selected building frame which conforms to IS 800:2007. This damper model is suitable for further investigations with the selected building frame.

References

1. Sapiens, https://www.sapiens.org/culture/natural-disaster-less-natural-than-you-think/
2. Aghlara R, Tahir MM, Adnan AB (2018) Experimental study of pipe-fuse dampers for passive energy dissipation in structures. J Constr Steel Res 148
3. Mahyari SL, Riahi HT, Hashemi M (2019) Investigating the analytical and experimental performance of a pure torsional yielding damper. J Constr Steel Res 161(2019):385–399
4. Maleki S, Mahjoubi S (2013) Dual-pipe damper. J Constr Steel Res 85
5. Shi J-X, Kozono S, Shimoda M, Takino M, Wada D, Liu Y (2019) Non-parametric shape design optimization of elastic-plastic shear panel dampers under cyclic loading. Eng Struct 189(2019):48–61
6. Mahjoubi S, Maleki S (2016) Seismic performance evaluation and design of steel structures equipped with dual-pipe dampers. J Constr Steel Res 122
7. Aglara R, Tahir MM (2017) A passive metallic damper with replaceable steel bar components for earthquake protection of structures. Eng Struct 159
8. Rami Reddy V, Krishna V (2018) Comparative study in performance of steel buildings in various seismic zones of India. Int J Civ Eng Technol
9. Encyclopaedia Britannica, https://www.britannica.com/technology/materials-testing/Measures-of-ductility

Experimental Studies on Performance of Geo-synthetic Strengthened Brick Masonry Infill

K. S. Sreekeshava and A. S. Arunkumar

Abstract The behaviors of masonry infill under the action of sudden disasters are highly unpredictable. Infill is very strong and behaves better under the action of gravity loads because of its strong nature under compression but it shows versatile behavior under shear. In any kinds of high rise buildings infill actions are ignored in design but contribution of infill under lateral loads are highly significant. The infill contributes to strength and stiffness of frames under lateral forces and also the interfaces between frame and infill are fails because of its weak bond. Several researchers studied the significance of strengthening of masonry infill and stated that significance of strengthening under flexure and shear. In this present paper an experimental work has been presented on two different types of Geo-synthetics strengthened to brick masonry infill and results are compared with unreinforced conventional masonry infill elements. The results shown the better performance in load carrying capacity and also in flexure and shear compared with conventional specimens.

Keywords Shear · Flexure · Reinforcement · Stiffness · Masonry infill · Wallets · Shear

1 Introduction

The Brick masonry is used as an infill across all over the world. Masonry behaviors under disasters are highly unpredictable and also cause severe problems to structural elements. Several researchers have been stated the importance of infill and also proposed the different techniques to overcome the effects on infill under disasters.

K. S. Sreekeshava (✉)
Department of Civil Engineering, Jyothy Institute of Technology, Bengaluru, affiliated to Visvesvaraya Technological University, Belagavi, India
e-mail: sreekeshava.ks@jyothyit.ac.in

A. S. Arunkumar
Department of Civil Engineering, BMS College of Engineering, Bengaluru, affiliated to Visvesvaraya Technological University, Belagavi, India

© Springer Nature Switzerland AG 2021

K. Dasgupta et al. (eds.), *Proceedings of SECON 2020*,
Lecture Notes in Civil Engineering 97,
https://doi.org/10.1007/978-3-030-55115-5_4

Major observations stated that the infill is mainly failed due to the insufficient ability to resist under shear and flexure [1, 2].

Masonry is composite material made of masonry unit and cement: sand mortar. The south Indian bricks are very soft and having low compressive strength compared to Northern part of India [3]. In this part of brick masonry possess low modulus of elasticity and also brick unit are soft compared to cement: sand mortar [4].

The infill is very strong under axial compressive loads and also fails suddenly under small amount of lateral loads because of its brittle nature. Several researchers were focused on strengthening the infill by a different reinforcing technique which includes the fiber reinforced polymer technique. In this technique the polymers are applied on the surface of infill and subjected to validate with various tests. The tests result showed the importance of polymer reinforcing in infill and also faced the drawback to apply on wet surfaces of infill [5].

To encounter this drawback a new technique has been developed by researchers which can be easily applied on wet surfaces and showed the better performance in all aspects. The composite system can be developed with the help of cementitious matrix so called as fabric reinforced cementitious matrix (FRCM) technique [6].

The Geo-synthetics are polymeric materials widely used in civil engineering applications includes Geotechnical and highway pavements. These materials possess high tensile strength, recyclable, corrosive resistant and fire resistant. Because of its high ductility and tensile strength used as a reinforcing material in many infrastructure projects. The interlocking behavior of Geo-synthetics helps to enhance the bonding between materials hence recommended to use as reinforcing material between two composite units [7].

2 Experimental Sequence

2.1 Basic Materials Characterisation

The materials like Cement, manufactured sand, portable water, table moulded bricks and Geo-synthetics (Polyester and Polypropylene type) were used in this present study. The ordinary Portland cement of 53 grade is conform to BIS specification IS: 12269-2013 [8] and Manufactured sand were conform to IS: 383-2016 used for specimen fabrication [9]. Locally available table moulded bricks are used as infill material along with 1:5 cement:sand mortar. The Polyester and Polypropylene types of Geo-synthetics are used for strengthening masonry infill elements like prisms and wallets. The basic materials characterizations are listed in Tables 1, 2, 3 and 4.

The Polyester and Polypropylene two types of Geo-synthetics were tested under 25 kN digital strain controlled universal testing machine to know the mechanical properties. The Geo-synthetics used in this study is shown in Fig. 1.

Table 1 Properties of cement

Experiment name	Test results	Permissible value as per code (IS: 12269-2013)
Fineness (%)	7.1	Maximum 10
Normal consistency (%)	30	26–33
Soundness (mm)	6.6	<10
Specific gravity	3.10	3.12–3.19
Initial setting time (min)	36	Minimum 30
Final setting time (min)	295	Maximum 600

Table 2 Properties of manufacturing sand (M-sand)

Experiment name	Test results	Permissible value as per code (IS: 383-2016)
Specific gravity	Bulk G = 2.65	2.53–2.69
	Apparent G = 2.55	
Water absorption (%)	1.2	<2

Table 3 Properties of table moulded brick

Dimension (mm)	Water absorption (%)	Modulus of rupture (Mpa)	Compressive strength (Mpa)	Weight density (kN/m^3)
212 × 102 × 75	13.50	1.21	3.9	13.60

Table 4 Properties of geo-synthetics

Geo-fabric	Ultimate load (N)	Ultimate tensile strength (Mpa)	Breaking load (N)	Breaking stress (Mpa)	Young's modulus (Mpa)	Cost/m^2 (Rs.)
Polyester	920	135	880	120	1.16×10^6	70
Polypropylene	1026	153	996	146	1.89×10^6	75

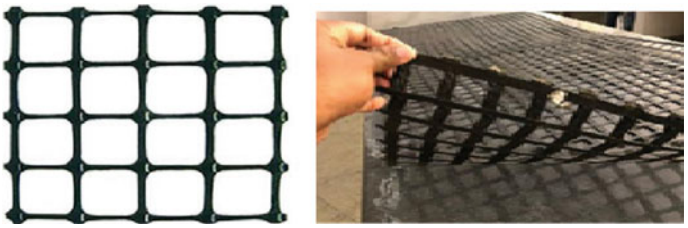

(a) Polypropylene (b) Polyester

Fig. 1 Geo-synthetics used in this present study

2.2 Experimental Studies on Masonry Mortar

The constructions of infill with weak mortar are generally adopted across southern part of India. In this present context a mortar ratio of 1:5 (Cement:sand) is used for masonry elements fabrication. To know the bonding behavior of Geo-synthetic along with mortar can be studied with the help of flexure and tension test. The experimental investigations were performed on cement:sand mortar with water cement ratio 0.6. Mortar is a composite mixture and used to protect the reinforcements in structures. Sometimes mortar used as a binding material for masonry units as well as for wallets to protect it from environment and also to give better view from architectural point of view. In this present study PP Geo-fabrics are used as reinforcements so it is required to check the performance with mortar. Hence, the flexural strength and Tensile strength of 1:5 mortars with and without Geo-synthetics are evaluated in this section. The flexural strength test is conducted as per ASTMD7264/D7264M-07 code of practice [10]. As per code the Geo-synthetics are laminated between 12 mm thick mortar and minimum 5 numbers of specimens were considered having each specimen gauge length of 90 mm and tested under 25 kN digital universal testing machine. The test specimens were shown in Fig. 2 and results of test after 28 days aging were tabulated in Table 5.

The Tension tests are carried with and without Geo-synthetics in 1:5 cement sand mortar. The mortar coupons were having dimensions 200 × 600 × 25 mm prepared and test conducted in accordance with AC434.13 guidelines [10]. Experimental setups along with specimen shown in Fig. 3 and results after 28 days of aging were tabulated in Table 6.

Fig. 2 Mortar laminates for flexure test

Table 5 Flexure test results

Type of specimen along with 1:5 mortar	Flexural strength (MPa)	Flexural modulus (MPa)
Conventional specimen	3.96	2185
Polyester geo-synthetic	4.28	2896
Polypropylene geo-synthetic	4.86	3025

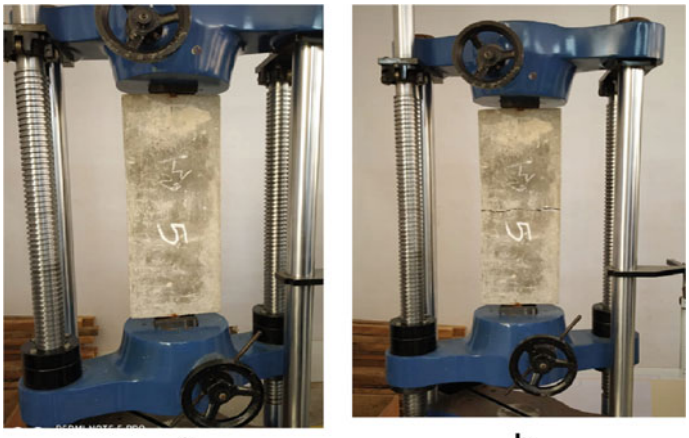

Fig. 3 **a** Tension test on mortar before test; **b** specimen after test

Table 6 Tension test results

Type of specimen along with 1:5 mortar	Ultimate load (N)	Tensile strength (MPa)
Conventional	8100	1.62
Polyester geo-synthetic	12,140	2.43
Polypropylene geo-synthetic	14,156	2.96

2.3 Experimental Studies on Masonry Prisms

2.3.1 Compressive Strength of Masonry Prisms

The compressive strength is the important factor to decide the strength of masonry infill. The test is carried out in accordance with ASTM C 1314-03b test method. Prisms were built using four masonry units with 12 mm thick 1:5 mortars. All masonry units are laid in stack bond position with aspect ratio of 3.52 and tested after 21 days of full age curing. The two types of Geo-synthetics are applied on prisms in two ways. The strengthening using geo-synthetics can be done by placing on face of the prism and also at each bed joints with the help of mortar. The test specimens were shown in Fig. 4 and test results are tabulated in Table 7.

2.3.2 Flexural Strength of Masonry Prisms

The masonry prisms in flexure can be checked in accordance with EN 1052-2:1999 standard code of practice. Stack bonded prisms were placed horizontally and equal concentrated loads are applied at the span third points. The flexural strength for prism

Fig. 4 Masonry prisms

is given in Eq. 1.

$$f_x = \frac{3F_{i\max}(l_1 - l_2)}{2bt_u^2}\text{Mpa} \tag{1}$$

where

f_x Flexural strength of masonry Prism (Mpa)
F_{imax} Maximum breaking load (N)
b height or width of the specimen perpendicular to the direction of the span (mm)
t_u Width of masonry unit (mm)
l_1 Center to Center distance between the supports (mm)
l_2 Center to Center distance between equal concentrated loads (mm).

The masonry flexural strength helps to estimate the effect of resistance due to lateral forces on the masonry infill. The testing specimens are similar to compressive strength test were shown in Fig. 5. The results showed the importance of Geo-synthetic reinforced on face of the masonry infill and experimental results are tabulated in Table 8.

2.4 Experimental Studies on Masonry Wallets

2.4.1 Load Bearing Capacity of Masonry Wallets

The actual behavior of masonry infill is obtained by conducting load bearing capacity test on wallets in accordance with EN 772-1 standards specifications. The specimens were 600 × 600 × 230 mm in dimension and cured for 28 days in ambient environment with the help of gunny bags. Two types of geo-synthetics with two differently strengthened techniques and also unreinforced conventional wallets were considered for the experimentation. The tests conducted under 2000 kN loading frame and under axial loads displacement are captured with the help of digital strain gauges.

Table 7 Masonry prisms compressive strength test results

S. No.	Specimen type	Description	Number of specimens	Breaking load (N)	Compressive strength (Mpa)	Correction factor	Corrected compressive strength (Mpa)
01	PC1	Conventional prism	03	55,020	2.62	1.11	2.87
02	PC2	Polypropylene geo-synthetic strengthened on face of prism	03	67,226	3.2	1.11	3.52
03	PC3	Polyester geo-synthetic strengthened on face of Prism	03	59,824	2.84	1.11	3.13
04	PC4	Polypropylene geo-synthetic strengthened at bed joint of prism	03	65,276	3.10	1.11	3.41
05	PC5	Polyester geo-synthetic strengthened at bed joint of Prism	03	62,482	2.97	1.11	3.27

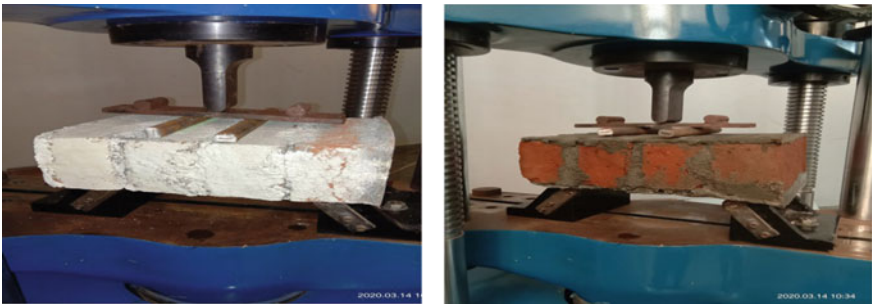

Fig. 5 Masonry prisms under flexure

Table 8 Masonry prisms flexure test results

S. No.	Specimen type	Description	Number of specimens	Breaking load F_{imax} (N)	Flexural strength f_x (Mpa)
01	PF1	Conventional prism	05	4010	0.42
02	PF2	Polypropylene geo-synthetic strengthened on face of prism	05	11,600	1.25
03	PF3	Polyester geo-synthetic strengthened on face of prism	05	7100	0.76
04	PF4	Polypropylene geo-synthetic strengthened at bed joint of prism	05	4600	0.49
05	PF5	Polyester geo-synthetic strengthened at bed joint of prism	05	4300	0.46

Fig. 6 Masonry bearing capacity test

Table 9 Masonry bearing capacity test results

S. No.	Specimen type	Description	Number of specimens	Breaking load (kN)	Modulus of elasticity (Mpa)
01	CWB1	Conventional wallet	03	210	1560
02	PWB2	Polypropylene geo-synthetic strengthened on face of wallet	03	245	2345
03	PWB3	Polyester geo-synthetic strengthened on face of wallet	03	227	2135
04	PWB4	Polypropylene geo-synthetic strengthened at bed joint of Wallet	03	240	4260
05	PWB5	Polyester geo-synthetic strengthened at bed joint of wallet	03	255	5026

The specimens are shown in Fig. 6 and experimental results are represented in Table 9.

2.4.2 Shear Capacity of Masonry Wallets

The shear capacity of wallets under in-plane loads plays a major role in prediction of failure mechanism of masonry. The specimens were 600 × 600 × 230 mm in dimension and cured for 28 days in ambient environment with the help of gunny bags. In-fills are very weak in shear because of its brittleness and composite action between mortar-masonry units. The shear capacity of wallets estimated with strengthened and un-strengthened wallets of same category specimens of load bearing test in accordance with EN 1052-3 codal standard specifications. The specimens with testing arrangements are shown in Fig. 7 and results are tabulated in Table 10.

The specimen after shear strength test shows the behavior of infill under the action of in-plane loads. The conventional specimen failed sudden and brittle fracture occurred while conducting the test. The specimens strengthened by polyester and polypropylene in both type of strengthening technique bed joint as well as face of wallets performed better compared to un-strengthened wallets. The specimens after testing are presented in Fig. 8.

Table 10 Masonry shear strength test results

S. No.	Specimen type	Description	Number of specimens	Breaking load (kN)	Shear stress (Mpa)
01	CWS1	Conventional wallet	03	255	0.91
02	PWS2	Polypropylene geo-synthetic strengthened on face of wallet	03	295	1.05
03	PWS3	Polyester geo-synthetic strengthened on face of wallet	03	280	0.98
04	PWS4	Polypropylene geo-synthetic strengthened at bed joint of Wallet	03	310	1.14
05	PWS5	Polyester geo-synthetic strengthened at bed joint of wallet	03	345	1.48

Fig. 7 Masonry Shear strength test

2.4.3 Cost Comparison Analysis

The cost comparison analysis plays a significant role for the adaptation of work under practical circumstances. In present study two types of geo-synthetics has been used as an additional reinforcing materials in conventional specimens. The cost analysis has been done by considering conventional and Geo-synthetic reinforcing wallets of one cubic meter. The results are tabulated in Table 11.

Table 11 Cost analysis

Description	Approximate cost for one cubic meter of concrete (Rs.)	Total cost required to geo-synthetic for one cubic meter (Rs.)	Total cost (Rs.)
Conventional specimen	6000–6500	Nil	6000–6500
Polyester geo-synthetic	6000–6500	1200	7200–7700
Polypropylene geo-synthetic	6000–6500	960	6960–7460

(A) Un-Strengthened (B) Face strengthened (C) Bed-joint Strengthened

Fig. 8 Masonry wallets after shear strength test

3 Conclusion

From the experimental observations on brick masonry elements strengthened with two types of Geo-synthetics in two different ways and also on un-strengthened masonry the following conclusions were made.

1. The materials characteristics showed the importance of Geo-synthetics by its high tensile property and ductility.
2. The mortar test showed the enhancement of 10–15% in both polyester and polypropylene Geo-synthetic compared with unstrengthen mortar in both flexure as well as in tensile strength test.
3. Compressive strength on masonry prisms showed the importance of face strengthening technique by both the types of Geo-synthetics. The bed joint strengthening showed 10–15% of enhancement and faces strengthening by 15–20% compared with unstrengthen conventional specimens.
4. Flexural strength test on prisms showed the significance of face strengthening technique by both types of Geo-synthetics. The face strengthened specimens showed 65–70% of enhancement compared with conventional as well as bed joint strengthened specimens.
5. Test on wallets shows the realistic behavior of infill under compression and shear. In both the tests the Geo-synthetics strengthened specimens showed better performance compared with conventional specimens.

Geo-synthetics are recyclable, thermal resistant, and non-corrosive and possess good tensile properties with composites like masonry and concrete. Hence Geo-synthetics are recommended to adopt in larger scale to avoid the brittle fracture of masonry structure.

Acknowledgements Authors would like to acknowledge Visvesvaraya Technological University TEQIP CELL, Belagavi, (Ref: VTU/TEQIP 3/2019/321) for providing financial assistance to conduct this experimental work under Research competitive funding scheme.

References

1. Sreekeshava KS, Arunkumar AS, Ravishankar BV (2020) Experimental studies on polyester geo-fabric strengthened masonry elements. Lecture notes in civil engineering advances in computer methods and geomechanics, pp 727–736. https://doi.org/10.1007/978-981-15-0886-8_58
2. Sreekeshava KS, Arunkumar AS, Ravishankar BV (2020) Experimental studies on brick masonry elements with geo-fabric bed joint reinforcement. Advances in sustainable construction materials lecture notes in civil engineering, pp 33–41. https://doi.org/10.1007/978-981-15-3361-7_3
3. Sarangapani G, Reddy BVV, Jagadish KS (2005) Brick-mortar bond and masonry compressive strength. J Mater Civ Eng 17(2):229–237. https://doi.org/10.1061/(asce)0899-1561(2005)17:2(229)
4. Sreekeshava KS, Arunkumar AS (2019) Effect of polypropylene (PP) geo-fabric reinforcement in brick masonry under axial loads. Int J Recent Technol Eng Regular Issue 8(3):369–373. https://doi.org/10.35940/ijrte.c4181.098319
5. Sagar SL, Singhal V, Rai DC, Gudur P (2016) Diagonal shear and out of plane flexural strength of fabric reinforced cementitious matrix-strengthened masonry wallets. J Compos Const. https://doi.org/10.1061/(ASCE)CC.1943-5614.0000796
6. Sadak H, Lissel S (2013) Seismic performance of masonry walls with GFRP and geogrid Bed joint reinforcement. Constr Build Mater 41(2013):977–989
7. Sreekeshava KS, Arunkumar AS (2018) Experimental studies on response of biaxial geo-grid proportioned cement concrete. i-Manager's J Civ Eng 8(2):15. https://doi.org/10.26634/jce.8.2.14550
8. BIS (Bureau of Indian Standards) (2013) Indian standard code of practice for structural use of unreinforced masonry, IS 12269, New Delhi, India
9. BIS (Bureau of Indian Standards) (2016) Indian standard code of practice for structural use of unreinforced masonry, IS 383, New Delhi, India
10. ASTM (2015) Standard test methods for diagonal tension (shear) in masonry assemblages. ASTM 7264/D7264M-07, West Conshohocken, PA
11. ASTM (2011) Standard test methods for diagonal tension (shear) in masonry assemblages. AC.434

Assessment of Governance Gaps in Landslide Risk Reduction—A Case Study from Kattippara Panchayath, Kozhikode District

K. Sreerekha and S. Jawahar Saud

Abstract Landslides are hazards which frequently occur and affect the life of human, animals and damage properties. Kattippara Panchayath is a highly landslide prone area in which landslides had occurred in different locations and public have been asked to stay away from this area. Currently there are no effective strategies to reduce the risks of landslides. A Geographic Information System has proved to be a useful tool for analysing and managing landslide related data. Landslide susceptibility map of the study area is prepared using Arc GIS software by combining some of the critical factors like land use pattern, geology, geomorphology etc. It can be used for assessing the risks of landslides, for developing early warning systems and mitigation plans. This paper seeks to identify the existing governance gaps in the study area, to ascertain the status of existing risk reduction measures available, the constraints associated with such measures, and thereby to suggest suitable measures to fill the identified gaps. This paper concludes with a synthesis of governance gaps and opportunities to reduce the risk of such disasters.

Keywords Landslide · Risk · Risk reduction · Landslide susceptibility map

1 Introduction

Landslides are major natural hazards which frequently occur and affect the life of human and animals, damage properties. Different phenomena cause landslides, including intense or prolonged rainfall, earthquakes, and a variety of human activities [1]. Landslides constitute a major natural hazard in India which accounts for considerable loss of life and damage to communication routes, human settlements, agricultural fields and forest lands [2]. The Western Ghats of Kerala are highly fragile

K. Sreerekha (✉) · S. Jawahar Saud
Department of Civil Engineering, Federal Institute of Science and Technology, Ernakulam 683577, India
e-mail: sreerekhaclt@gmail.com

S. Jawahar Saud
e-mail: jawahar405@gmail.com

© Springer Nature Switzerland AG 2021

K. Dasgupta et al. (eds.), *Proceedings of SECON 2020*,
Lecture Notes in Civil Engineering 97,
https://doi.org/10.1007/978-3-030-55115-5_5

and are under repeated threats of landslides. Kozhikode is the worst affected district with respect to the number of landslide incidences, casualties and property loss [3]. Landslide can happen unexpectedly and in most cases it become worse due to lack of proper governance. Governance is cited as the most recommended landslide disaster risk reduction component [4]. As governance, in general, refers to the processes of decision-making and implementation, risk governance applies the principles of good or sound identification, assessment, management and communication of risks. Governance is a crucial point for proper planning and implementation; it would require bringing together engineering, environmental and communities in a joint effort [5]. The analysis and management of landslide related data can be made easier with the help of Geographic Information System (GIS). Landslide susceptibility map of the study area can be prepared using Arc GIS software by combining some of the critical factors like land use pattern, geology, geomorphology etc. It can be used for assessing the risks of landslides, for developing early warning systems and mitigation plans [6]. The main objectives of this works are established (1) to identify the governance gaps in landslide risk reduction activities in the study area (a) to generate landslide vulnerability zonation map using remote sensing and GIS techniques (2) to understand the status of existing risk reduction measures in the study area (3) to identify the governance gaps related to landslide risk reduction in the study area.

Many areas of Kerala are prone to frequent landslides in the past because of intense rainfall. These landslides, year after year bring about untold misery to human settlements apart from causing devastating damages to transportation and communication network [7]. This work gives the detailed analysis of accessible data from the study area which helps in creating awareness among people about the current visible risks, and to identify the existing gaps in landslide risk reduction.

2 Selection of Study Area

Kattippara is a panchayth (Latitude 11° 47′ 08″ and Longitude 75° 92′ 13″) in Kozhikode district, Kerala. It is a village with a lot of hilly areas. As the name indicates, it is famous for hard rocks which we can find everywhere in this village. Kattippara Panchayath is a highly landslide prone and unstable area. The major source of income in this village is agriculture. Majority of the population depend on the agriculture crops such as rubber, coconut, ginger, pepper etc. A very minority only depend on business and govt. jobs. Kattippara has a generally cool humid climate with a very hot season extending from March to May. The average annual rainfall is more than 3500 mm and it is the highest rain fall in this region. According to 2011 Census report, the population in the study area was 30,123 and the population density was 1400/km^2. On 14 June 2018 a major landslide in the form of debris flow along with mudslips erupted in 8 different locations of Kattippara Panchayth. 14 persons were killed and many others injured, 14 houses were totally washed out, 20 houses were partially damaged and transportation systems as well as communication systems were badly affected by the landslide. The triggering factor for this landslide

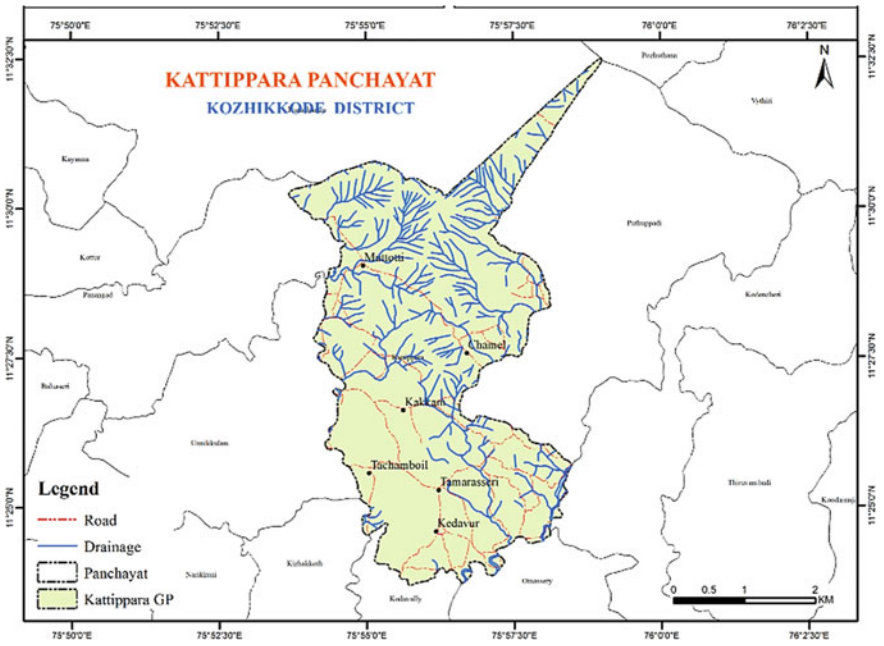

Fig. 1 Base map of the study area. *Source* GSI

was the action of quarrying and intense rainfall. Still people are residing in this area and currently there are no effective strategies to reduce the risks of landslide. The base map of the study area is shown in Fig. 1.

2.1 Data Collection

The data collections were carried out in two stages, one through developing the landside hazard zonation map and another one was the administration of questionnaire survey. Based on the past and landslide in the study area different survey techniques were used for data collection directly from the affected victims, local bodies, respective authorities of disaster prone areas etc.

2.1.1 Questionnaire Preparation

Two types of questionnaires are prepared, one for authorities and other for residents of Kattippara Panchayth. While preparing the questionnaire both open ended as well as closed ended questions were used. Three point likert scale questions were used in the survey. Questions were generated in such a way to collect the maximum data

considering people knowledge, experiences, thoughts, and their role during disaster, to identify the governance gaps and to generate the hazard zonation map etc. Total 600 responses were collected from the community survey. The responses of questionnaire survey were then analysed using SPSS software.

2.1.2 Collection of Different Maps for Generating Landslide Susceptibility Map

Landslide zonation is commonly shown on maps, which display the spatial distribution of classes (Landslide Zonation). Landslide zonation refers to "The division of the land in homogeneous areas or domains and their ranking according to degrees of actual/potential hazard caused by mass movement" [8]. For the preparation of landslide hazard zonation map different maps are collected they are Slope map, Soil map, Land use and land cover map, Geomorphology map, Geology map, Drainage density map, Relief map. After collecting all these maps then it is overlaid in Arc GIS software to get the final landside hazard zonation map.

3 Results

3.1 Analysis of Questionnaire Survey

The statistical method of analysis was carried out using Statistical Package for Social Science (SPSS) [9]. Since for developing an effective Disaster management plan for an area, a proper study regarding the risk factors, capacity of the exposed community etc. should be determined. Total 600 responses were collected from the study area. The following figures show the personal details of the respondents (Figs. 2, 3 and 4).

From these figures it is clear that most of the respondents are male (51%). Most of the respondents fall in the age category 30–55 (39%) and more than 55 (39%). Figure 4 compares the educational qualification of the people. From this figure it is clear that majority of the people have school level education, nearly 12% of the

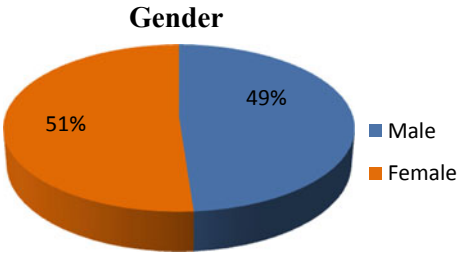

Fig. 2 Gender of respondents

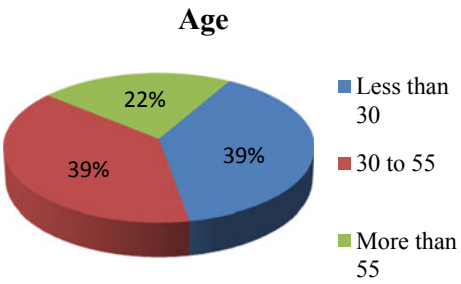

Fig. 3 Age of respondents

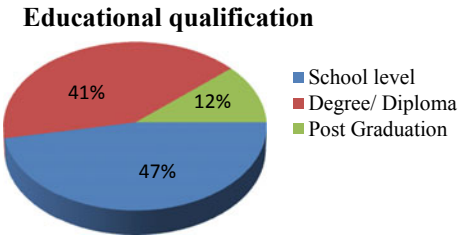

Fig. 4 Educational qualifications of respondents

respondents have post-graduation. So it says that lack of education plays a role in their poor awareness level about the risks of land slides.

3.2 Analysis of Questionnaire Using Chi Square Test

The chi-square test for independence, also called Pearson's chi-square test or the chi-square test of association, is used to discover if there is a relationship between two categorical variables [10]. In this study different question was taken as parameters and the relation between these parameters are found. The following figures show the relation between different parameters.

3.2.1 Age and Preparedness of People

Age and preparedness of people was tested to examine the influence of age on preparedness [11]. The results of Fig. 5, shows that people with age more than 55 are least prepared to face a disaster comparing with other two groups. This is may be due to lack of proper awareness programs from the authorities.

The evidences from the graph show that training programs and awareness sessions should be strengthened. It's very essential that young people have to be well trained to face a disaster because they can do a range of roles including response, recovery effort, and protection of others. So these training programs should be conducted by the role players for improving the preparedness and overall reliance of the people.

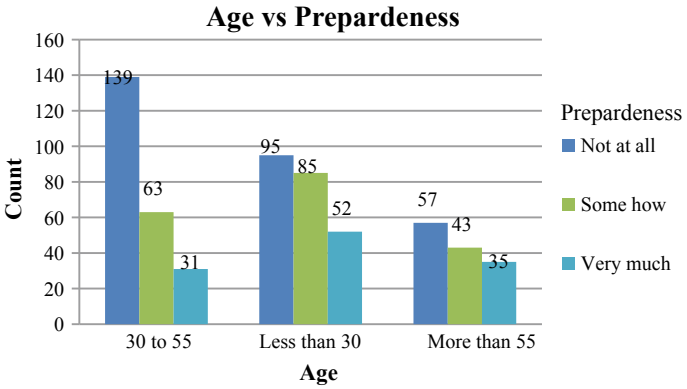

Fig. 5 Age versus preparedness of people

3.2.2 Frequency and Warning System

Both the frequency and the impact of landslide have been increasing for the past decades in the study area. When the frequency of landslides in the study area was tested against the status of warning systems it clearly depicts the warning system is not enough to tackle the slides. Landslides occur in the area 0–5 slides per year, but the early warning systems are not in place to provide warnings which leads to more risk to the community. From Fig. 6, a largest portion of respondents address the need for an early warning system. The successful implementation of early warning system can save lives to a greater extend [12]. In this study area landslide monitoring and dissemination of warning information remains a complex process where technical and communications skill should work closely together to overcome this constrain.

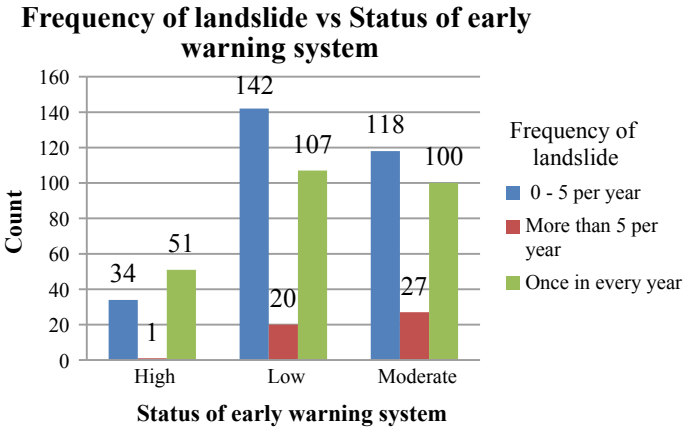

Fig. 6 Frequency versus warning system

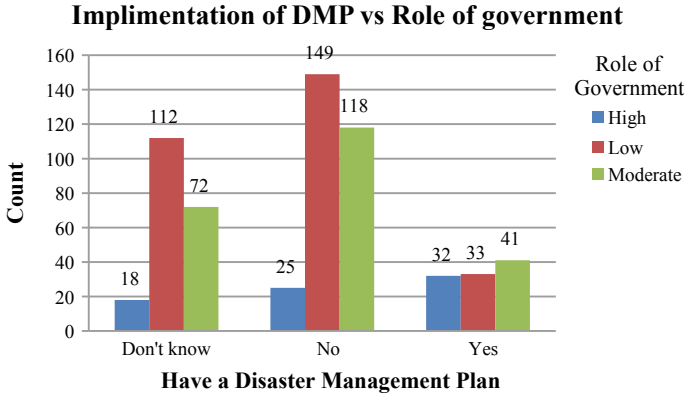

Fig. 7 Implementation of DMP versus role of government

3.2.3 Implementation of Disaster Management Plan and Role of Government

This test examines the implementation of disaster management plan (DMP) against role of government. Result of Fig. 7, shows that there is no effective disaster management plan in place to tackle the landslide and most of the people don't even know about DMP it clearly indicates the lack of awareness among people. This reminds that there is huge governance gap in generating enough awareness in people.

This shows the need of experts in the field of disaster management for proper planning and implementation of a DMP. It was found that a considerable portion of people in this area was neither accustomed nor comfortable with the regular conduct of mock drill exercises which are a prerequisite for the implementation of preparedness activities. This is a challenging thing that needs to be overcome to have a robust preparedness structure in this area.

3.2.4 Role of Government in Landslide Risk Reduction Activities and Relocation Programs in Risk Zones

When the role of government in landslide risk reduction (LRR) activities and relocation programs in risk zones tested the result of this examined parameters shows that (Fig. 8) there is no relocation programs in the place to protect the element at risk. People still resides in the vulnerable zones. They should be relocated to a safer place before a future landslide. Proper relocation programs should be taken in high risk zones.

From the survey it was clear that planned relocation programs in this area for the benefit of people at risk was not undertaken by the authorities. Lack of sufficient fund was the major reason behind this. Planned relocation programs should be carried out

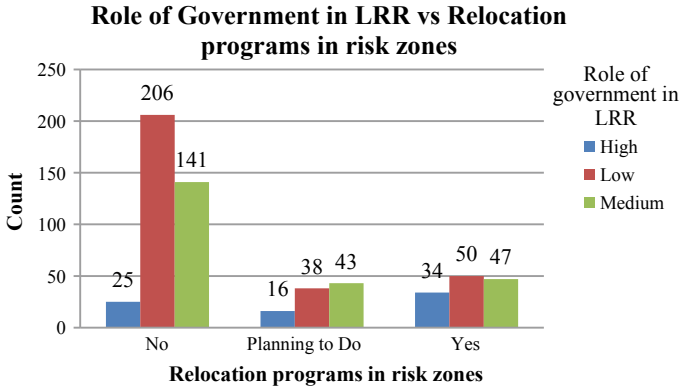

Fig. 8 Role of government in (LRR) versus relocation programs in risk zones

at individual, household or community level with in a right based frame work to ensure the safety of the people at risk.

3.3 Generation of Landslide Hazard Zonation Map

Better understanding of landslide prone areas will help people to live in harmony with the nature [13]. Since this study area is highly susceptible to landslides, preparation of landslide hazard zonation map (LHZM) is very important. This map will give the areas that are prone to landslides and the safe areas, which in-turn will help the administrators for planning and future development activities [14]. Generation of the LHZM with the help of Geographic Information System (GIS) environment could give better results and yield actual ground like scenarios for landslide hazard mapping [15]. The landslide hazard zonation map of the study area created using Arc GIS software is shown in Fig. 9. This map is generated by overlaying different maps one over other in Arc GIS software. The different maps used are Slope map, Soil map, Land use and land cover map, Geomorphology map, Geology map, Drainage density map, Relief map.

The incident landslides in Kattippara Panchayth are deep-seated landslides, which can be explained by the higher quantities of monsoon rainfall and illegal action of quarries in this area. The intensity of landslides is observed to have increased in the last 10 years. The occurrence of landslide was accelerated by anthropogenic disturbances such as deforestation, terracing and cultivation of crops lacking capability to add root cohesion in steep slopes. Invariably, in most of the failed slopes, natural drainage was blocked or modified without adequate provision for surface drainage. Unplanned developmental activities like conversion of agricultural land for the construction of buildings, road cuttings, cut and fill structures and withdrawal of toe support have also seen to increase the risk to the community from landslides.

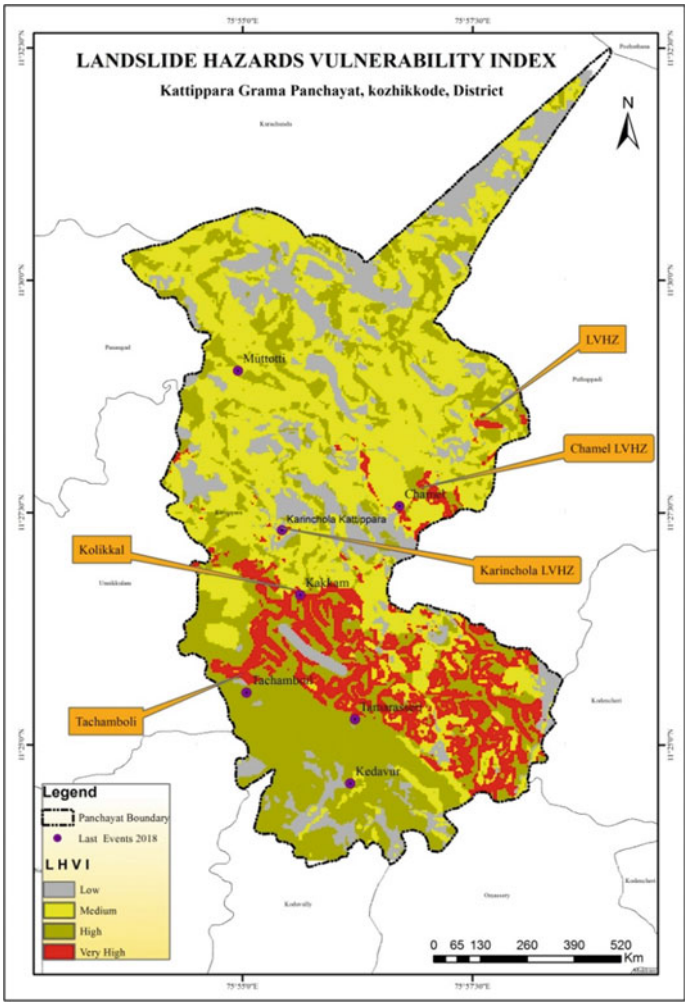

Fig. 9 Landslide hazard zonation map of the study area

The mapping of different parameters was done which influence in the occurrence of landslide. The resulting map shows High risk landslide prone areas of the study area. The landslide susceptibility map was validated by using landslide incidence points of the study area, and most of the incident points fall on the very high risk zone in the landslide susceptibility map.

Area in square Kilo meter and percentage of land involved in each risk zone is given in Table 1.

Most of the areas in Kattippara Panchayth fall in very high risk zone, high risk zone, and moderately risk zone shown in red, green and yellow colour respectively.

Table 1 Area and percentage of land included in risk zones

LHZ class	Area (km^2)	Percentage
Low	12.0	16.5
Medium	29.4	40.3
High	22.9	32.0
Very high	7.9	11.0

4 Discussions

Landslide is a natural disaster which causes severe damage to the life and the properties [16]. From the analysis of the questionnaire survey with the help of statistical methods and using different maps such as Slope map, Soil map, Land use and land cover map, Geomorphology map, Geology map, Drainage density map, Relief map etc. [17], LHZM was generated. Generation of LHZM using GIS techniques helped to find out the governance gaps in the study area. From the LHZM, it was estimated that the study area has highly unstable zones and are vulnerable to landslide activities [18]. The risk zones identified through the interaction with respondents during the survey correspond to the same risk zones of the landslide risk zone map. From this study it was observed that Remote Sensing and GIS technique can be effectively used in the preparation of hazardous zonation maps. The results confirm that the proposed LHZM will help planners and engineers to reduce losses of life and properties through prevention and mitigation measurements.

The results from the analysis show the existence of governance gaps. Most of the people were not sufficiently aware of the risks of landslides. The results of the questionnaire survey show the lack of awareness among the community. Public Awareness and Education Program for Landslide risk management were not periodically conducted by the local authorities of the study area. Similarly before any community action can be taken, residents needed some knowledge of the landslide. So this is the responsibility of the local government, no such activities or initiatives are taken from the side of local government in the study area. Residents were not taught about what is a slope, types of landslides, factor of landslides, triggers of landslides and key concepts on retaining walls and geological aspects and through seminars and public talks, the public will get a briefing of landslide.

As urban development invades the hilly areas, slope security is important to watch for signs of landslide [19]. Man-made structures after converting the natural slopes are becoming more and more prevalent in this area and they are not monitored which need to be routinely checked. Another major finding was maintenance or regular control over the physical condition of the house; it is simple to do, yet often neglected. Proper maintenance can make the difference between safety and disaster [20, 21]. In some cases the slope land was owned by private parties and the local authority will contact the landlord. In some cases, they may not respond and may be notified of the action. Lack of coordination among different authorities was identified as a major governance gap. The various authorities should coordinate and work hand in hand

with addressing the risk of landslides. It was found that, there are no prerequisites at the house hold level, such as Family Emergency Plan, to determine what everyone will do in the event of a home emergency. Through this study it is understood that people have never participated in a mock drill or community based disaster risk education programs. There are no mock drills or activities in this area run by the Authorities. Role of disaster management focal persons and disaster management committee members to prioritize, plan and implement measures to reduce human and material losses from potential landslides are trivial in this area. Based on the analysis of the data it is found that the conditions of drainage systems are very poor in this area, drainage systems have clogged and damaged. This should be corrected by the respective authorities along with the active participation of the community. Similarly there are areas in this Panchayath which have been identified for the provision of retaining wall but they have not been implemented by the authorities. It is evident that there is a need for greater fund allocation by the government for implementing preparedness activities at the grassroots level which is most important and missing factor in this area.

5 Conclusions

Landslides are one of the major disasters which affect 15% of landmass [22]. It leads to destruction of life and property [23]. Kattippara Panchayath is the most affected region in Kozhikode district during the past landslides. The triggering factors for landslide in this area are the illegal action of quarrying, the improper land use pattern and intense rainfall. The results of this work can be used to evaluate the consequences of land use change on landslide vulnerability and risk. The risk of landslide in this area can be reduced to a great extend with help of proper planning and the implementation of different landslide mitigation strategies such as provision of retaining wall, provision of efficient drainage system, implementation of early warning system, and development of awareness among community through mock drills, training programs etc. with the help of respective authorities. Lack of proper governance is identified as one of the major issue in the study area which should be bridged with possible mitigation strategies. The Landslide hazard zonation map of the study area was generated with the help of GIS techniques and this map identified the risk zones in the study area. The landslide hazard zonation map was validated by using landslide incidence points of the study area which were identified through the administration of the community survey. The generated LHZM shows that change in land-use pattern was a major triggering factor in the occurrence of landslide. The lands which were used for agricultural purposes have turned into construction work, and road work. From the analysis of data it was very clear that there are no enough measures or plans to deal with a future landslide. Lack of coordination among the authorities and that with the community in planning, prioritizing and implementing the risk reduction plans as well as illegal action off quarries were found to be a major issue in the study area. Involvement of communities in all the

phases of landslide disaster plays a crucial role in sustainable risk reduction. Lack of proper disaster management plan and training at different levels of people are one of the main gaps identified from this study, so all these indicates the need of such training activities, remedial measures, and the implementation of a proper disaster management plan. The need for coordination at the local level, inadequate early warning systems and a slow response time are also very important constraints for implementing preparedness plan in this area. The goal of the study was to identify the governance gaps and from the analysis of collected data such gaps are identified and explained. If sufficient data are available, the methodology used in this work can be used for evaluating landslide risk reduction activities in another vulnerable zone. The LHZM of such areas can be generated for developing and implementing suitable risk reduction strategies.

References

1. Kaya H, Cavu A, Baha S, Calık E, Disaster management and disaster preparedness: examples of practices in California and Turkey, pp 36–47
2. Government HA, Disaster Management Ministry of Home Affairs
3. Ninu Krishnan MV, Pratheesh P, Rejith PG, Vijith H (2015) Determining the suitability of two different statistical techniques in shallow landslide initiation susceptibility assessment in the western ghats. Environ Res Eng Manage 70(4):27–39
4. Trias APL, Lassa J, Surjan A (2019) Connecting the actors, discovering the ties: exploring disaster risk governance network in Asia and the Pacific. Int J Disaster Risk Reduct 33:217–228
5. Pardeshi SD, Autade SE, Pardeshi SS (2013) Landslide hazard assessment: recent trends and techniques, pp 1–11
6. Sachithanandan J (2015) Identification of potential landslide vulnerable zones of Wayanad district, Kerala using remote sensing and GIS identification of potential landslide vulnerable zones of Wayanad district, Kerala using remote sensing and GIS dissertation submitted to in, Sept 2015
7. Kuriakose SL, Muraleedharan C (2009) History of landslide susceptibility and a chorology of landslide-prone areas in the Western Ghats of Kerala, India, pp 1553–1568. https://doi.org/10.1007/s00254-008-1431-9
8. Fell R, Corominas J, Bonnard C, Cascini L, Leroi E, Savage WZ (2008) Guidelines for landslide susceptibility, hazard and risk zoning for land use planning. Eng Geol 102(3–4):85–98
9. Arkkelin D (2014) Using SPSS to understand research and data analysis
10. Rana R, Singhal R (2015) Chi-Square test and its application in hypothesis testing. J Pract Cardiovasc Sci 1(1):69–71. https://doi.org/10.4103/2395-5414.157577
11. Sulal NL, Archana KG (2019) Note on post disaster studies for landslides occurred in June 2018 at Idukki District, Kerala, June 2018, pp 1–24
12. "Geo-Frontiers 2011 © ASCE 2011 3706," pp 3706–3715, 2011
13. Sandholz S, Lange W, Nehren U (2018) Governing green change: ecosystem-based measures for reducing landslide risk in Rio de Janeiro. Int J Disaster Risk Reduct 32(June 2017):75–86
14. Raveendran S (2015) Landslide hazard zonation and vulnerability assessment of western ghats—a case study in Devikulam Taluk of Idukki District, Kerala. 5(6):185–190
15. Anbalagan R, Singh B (1996) Landslide hazard and risk assessment mapping of mountainous terrains—a case study from Kumaun Himalaya, India. Eng Geol 43(4):237–246. https://doi.org/10.1016/S0013-7952(96)00033-6
16. Choi KY, Cheung RWM (2013) Journal of rock mechanics and geotechnical landslide disaster prevention and mitigation through works in Hong Kong. Integr Med Res 5(5):354–365

17. Dai FC, Lee CF, Ngai YY (2002) Landslide risk assessment and management: an overview. Eng Geol 64(1):65–87
18. Boulanger RW, Khosravifar A (2012) GeoCongress 2012 © ASCE 2012 3199, GeoCongress 2012, no 303, pp 3199–3208
19. Yin Y (2011) Recent catastrophic landslides and mitigation in China. J Rock Mech Geotech Eng 3(1):10–18. https://doi.org/10.3724/sp.j.1235.2011.00010
20. Anderson MG, Holcombe E, Blake JR, Ghesquire F, Holm-Nielsen N, Fisseha T (2011) Reducing landslide risk in communities: evidence from the Eastern Caribbean. Appl Geography 31(2):590–599
21. Beckenstein M (1971) System management, pp 354–356. https://doi.org/10.2307/j.ctvbd8hx9.6
22. Huang R, Li W (2011) Formation, distribution and risk control of landslides in China. J Rock Mech Geotech Eng 3(2):97–116
23. Pilgrim NK (1999) Landslides, risk and decision-making in Kinnaur district: bridging the gap between science and public opinion. Disasters 23(1):45–65. https://doi.org/10.1111/1467-7717.00104

Evaluation of Progressive Collapse Resistance of Steel Moment Resisting Frames

Anjaly James and Asha Joseph

Abstract Structural safety has always been an important factor for the design of civil engineering projects. One of the mechanisms of structural failure that has gathered increased attention over the past few decades is referred to as progressive collapse. Progressive collapse is the spread of an initial local damage from element to element, resulting eventually in the collapse of an entire structure. The potential cause that can trigger progressive collapse are categorized as: aircraft impact, design/construction error, fire, gas explosions, accidental overload, hazardous materials, vehicular collision, bomb explosions, etc. The aim of this study is to investigate the performance of 15 storeyed geometrically regular and irregular buildings with steel frame system to progressive collapse. Alternate path method based on dynamic analysis is performed based on Indian standard codes. According to alternate path method, the structure is designed such that if one component fails, alternate paths are available for the load and a general collapse does not occur. The response of the building to progressive collapse was studied in detail using structural software for building analysis and design, ETABS.

Keywords Progressive collapse · Time history analysis · Steel building · ETABS

1 Introduction

Many buildings are designed today with various geometries for serviceability, aesthetical or economical reasons. There are buildings which suffered significant and unexpected damages due to their irregularities and in that way, irregularities could be an evident parameter regarding progressive collapse resistance. Normal loads are usually considered directly or indirectly in the design process through existing codes

A. James (✉) · A. Joseph
Federal Institute of Science and Technology, Angamaly, Ernakulam, India
e-mail: anjalyjamesthengola@gmail.com

A. Joseph
e-mail: ashameledath@gmail.com

© Springer Nature Switzerland AG 2021

K. Dasgupta et al. (eds.), *Proceedings of SECON 2020*,
Lecture Notes in Civil Engineering 97,
https://doi.org/10.1007/978-3-030-55115-5_6

and standards, while abnormal loads are rarely considered in design practices which may have probability to lead to a progressive collapse. A progressive collapse is defined as a partial or total failure of a structure that mostly occurs when a structure loses a primary component like column during any hazard event [1]. During such a hazard, the primary load carrying member of the structure, columns may get overloaded when the gravity loads is transmitted to the adjoining columns in the structure. As these hazards have low probability of occurrence, they are not considered in the structural design [2]. Progressive collapse is a dynamic process wherein a collapsing system continually seeks alternate load paths in order to survive. Among many different approaches to design structures to resist progressive collapse, the guidelines generally recommend the alternate path method. In this approach, the structure is designed such that if one component fails, alternate paths are available for the loads to transfer and a general collapse does not occur. Alternate path method consists in designing the structure so that stresses can be redistributed following the loss of a vertical bearing member. This approach has the benefit of simplicity and directness. The existence of alternate load paths, ranges from static linear analysis through static nonlinear analysis, to dynamic linear or nonlinear analyses [3]. This alternate load path approach was selected as the preferred one by several standards, such as General Services Administration (GSA) and the Department of Defence (DoD). Both organizations have issued guidelines that specify fully detailed computational procedures.

From the history, there are several events of progressive collapse like Ronan Point Building, London (1968) the loss of support at the 18th floor caused the floors above to collapse, the Murrah Federal Office Building (1995) in Oklahoma City was destroyed by a bomb [4]. Also, in recent years, the 8 storey Rana Plaza commercial office complex in Savar, Bangladesh (2013), suffered a collapse and the Plasco Building, a high-rise building in Iran (2017), caught fire and collapsed. Clear conceptual step-by-step descriptions of various procedures for progressive collapse analysis by Marjanishvili et al. (2006) using commercially available structural analysis software, such as SAP2000, demonstrates that dynamic analysis procedures not only yield more accurate results, but are also easy to perform for progressive collapse determination [5]. Gerasimidis et al. (2012) studied on the response of irregular steel frames in case of initial damage, expressed by the total removal of their columns, one in turn leading to useful conclusions regarding the influence of such a property in their resistance to disproportionate collapse [6]. The conclusions arrived from the study of Stewart (2016) were, the progressive collapse cost premium of 1–4% of building cost is a reasonable and conservative basis for cost-benefit assessment. These costs seem reasonable, as design measures are less costly than retrofit measures [7]. Also, the cost-benefit analysis of UFC and GSA design provisions to mitigate against progressive collapse showed that these measures only become cost-effective when the threat likelihood is a very high 1 in 1000 per building per year.

2 Analysis Procedure

Alternate path method based on dynamic procedure is used in this study according to GSA guidelines using ETABS 2017 software. For progressive collapse analysis, GSA mandates several loss scenarios; however, only one element removal is required at a time. Analysis is carried out as threat-independent, meaning that the cause of element failure is not considered. The sole relevant fact is that the element is suddenly unable to carry load.

The dynamic method of analysis deals with the application of ground motions to any structure in order to evaluate the response of the building at each increment of time. The loads acting on a structure at the time of an earthquake is necessarily dynamic. In order to perform a time history analysis, a real time acceleration time data of an earthquake has to be considered. Here, time history analysis is performed considering the earthquake data of El Centro earthquake occurred in 1940 at Mexico.

According to GSA guidelines for a structure under study it is required to remove the columns at the middle of the short side, at the middle of the long side and at the corner of the building as shown in Fig. 1.

For progressive collapse analysis, the following load combinations shall be applied after the removal of load carrying members [3].

For linear and nonlinear dynamic analysis: DL + 0.25 LL, where DL = Dead Load and LL = Live Load.

2.1 Applied Loads for Analysis

A live load of 4 kN/m^2 is applied as per IS: 875 (part 2): 1987 and the dead load is software assigned. Lateral loads are applied as wind load in X direction and wind load in Y direction as per IS: 875 (part 3): 1987 [8]. Seismic loads are applied as

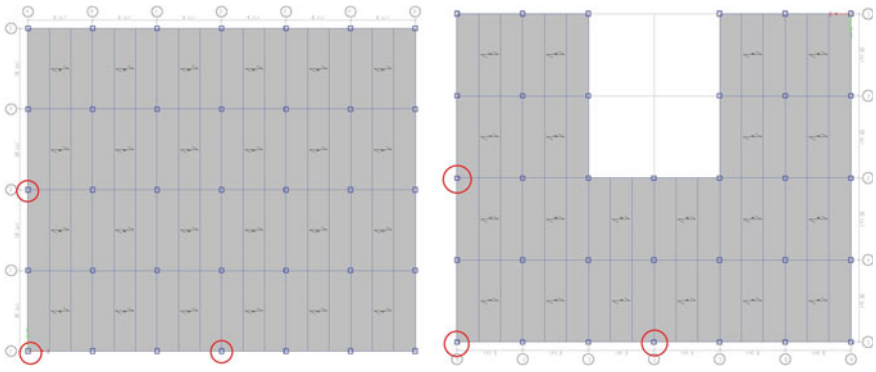

Fig. 1 Column removal locations recommended by GSA for a regular and irregular structure

seismic load in X direction and seismic load in Y direction as per IS 1893: 2002 (part 1). Seismic loads are applied as per moderate seismic zone and high seismic zone [9]. For dynamic analysis procedure, Load = DL + 0.25LL [3] is applied as an increased gravity load as per GSA guidelines 2013.

2.2 Acceptance Criteria

Acceptance criteria for the structural components shall be determined as Demand Capacity Ratio**.** Demand-to-capacity ratios (DCR) for moment is defined as the ratio of the maximum moment demand Mmax of the beam or column calculated from dynamic analysis to its expected ultimate moment capacity Mp, which is calculated as the product of plastic section modulus and yield strength [3]. According to the acceptance criteria from GSA guidelines the calculated value of DCR for columns should be less than unity in order to resist progressive collapse.

2.3 Methodology Adopted

In order to study the influence of plan irregularity in progressive collapse resistance, a buildings having regular and irregular plan are chosen. The 3D models of regular and irregular structure is prepared using ETABS 2017 and the analysis is carried out for the load combinations as per the design codes for Steel to be safe against seismic loading corresponding to Zone V. The axial forces acting on a column element is computed before eliminating any member. These forces are then applied as upward point loads at the location of column removal to stimulate the instantaneous column removal. This corresponds to the initial case where the column is at place and functioning at its full capacity. A ramp function is defined to simulate the abrupt removal of the column element after a certain time has elapsed so that the upward point loads is suddenly removed. The time interval for ramping down the column forces shall not exceed one tenth of the period associated with the structure. Linear dynamic analysis using time-history analysis is performed. The results based on DCR for columns, axial force near the removed member and vertical displacement are evaluated for typical and atypical structure to arrive at conclusions.

3 Model Description

The structures were modelled using beam and column elements of 15 storey steel frame building, with six bays in the longitudinal direction and four in the transverse direction for a regular structure. The irregular structure is modelled as a C-shaped structure with similar dimensions. Here the geometry of irregularity is considered

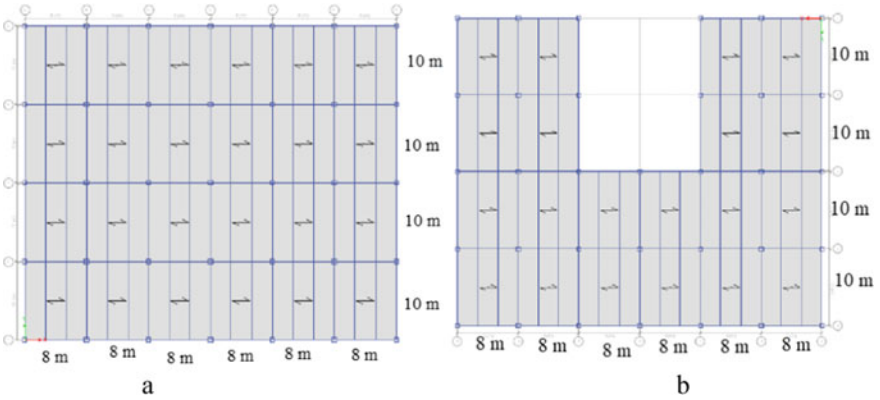

Fig. 2 Plan of **a** regular building and **b** irregular building

in plan. The plan of the basic models for regular and irregular structures are shown in Fig. 2. The longitudinal direction has a uniform column spacing of 8 m, while on the four-bay side columns are spaced every 10 m. Main girders are ISMB 550. Floor-to-floor height for every story is 3.3 m. 550 × 550 × 30 box columns span throughout the height and ISMB 450 grade secondary beams are used [10]. The floor diaphragms are constructed of composite metal deck with slab thickness of 90 mm. The modulus of elasticity and yield strength of the steel material is taken as 2×10^5 MPa and 250 MPa respectively. Analysis and design are done by using the software product of computers and structures, Inc (CSI), called ETABS 2017 as one of the powerful finite element computer programs. 3D view of the models are as shown in Fig. 3.

4 Results and Discussions

Alternate path method based on dynamic procedure is used in this study according to GSA guidelines. DCR value, axial force near the removed column and vertical displacement etc. are identified and tabulated.

4.1 Demand-to-Capacity Ratios (DCR)

Demand-to-capacity ratios (DCR) were calculated for each frame member, and the building response was evaluated by comparing the calculated DCR values based on the recommendations of GSA guidelines [3].

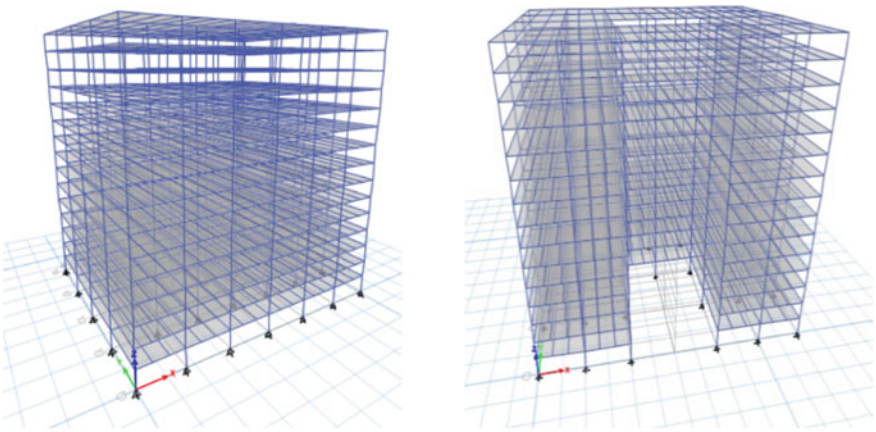

Fig. 3. 3D view of basic models for **a** regular building and **b** irregular building

$$\mathrm{DCR} = \frac{\mathrm{Mmax}}{\mathrm{Mp}} \tag{1}$$

$$\mathrm{Mp} = \mathrm{Fy} \times \mathrm{Z_x} \tag{2}$$

where Fy = 250 MPa and $Z_x = 2359.80\ \mathrm{cm}^3$

$= 250 \times 2359.80 = 589.95$ kN m.

The permissible value for DCR of column is 1. The values of DCR exceeding the permissible limits are considered as failed. The obtained DCR values for all column removal scenarios as per GSA guidelines 2013 for typical and atypical structures are pictorially plotted as above. Figures 4, 5 and 6 shows the DCR values for column removal scenarios of regular structures and Figs. 7, 8 and 9 shows the DCR values for column removal scenarios of irregular structures.

It shows that for a regular structure under various column removal conditions, the structure is able to resist progressive collapse since it has got a DCR less than unity. But for the irregular structure DCR values when the corner column is removed shows much greater than unity. This shows that the irregular structure undergoes progressive collapse when the corner column is removed. Also, the calculated DCR values seems to be greater for a corner column removal scenario, showing that corner column is the critical element. While comparing the DCR value calculated for corner column removal scenario—the most critical case, the DCR of irregular structure is more than twice of regular structure. From this it can be concluded that, regular structures are able to withstand the progressive collapse whereas the irregular structures fail to resist them.

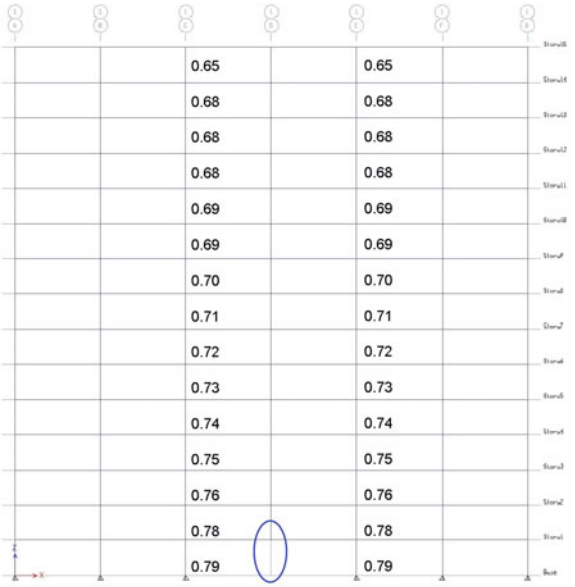

Fig. 4 DCR for long side middle column removal scenario—regular structure

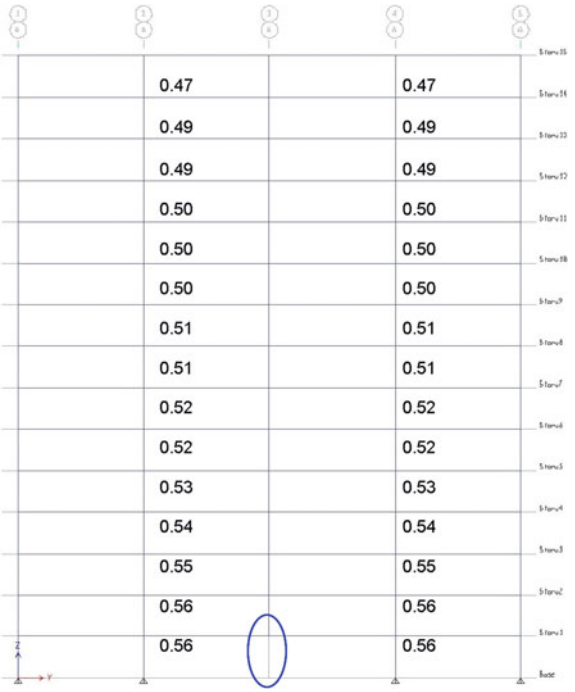

Fig. 5 DCR for short side middle column removal scenario—regular structure

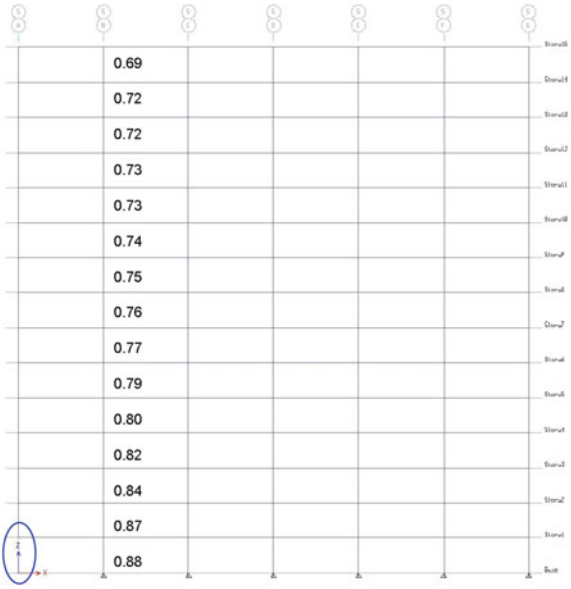

Fig. 6 DCR for corner column removal scenario—regular structure

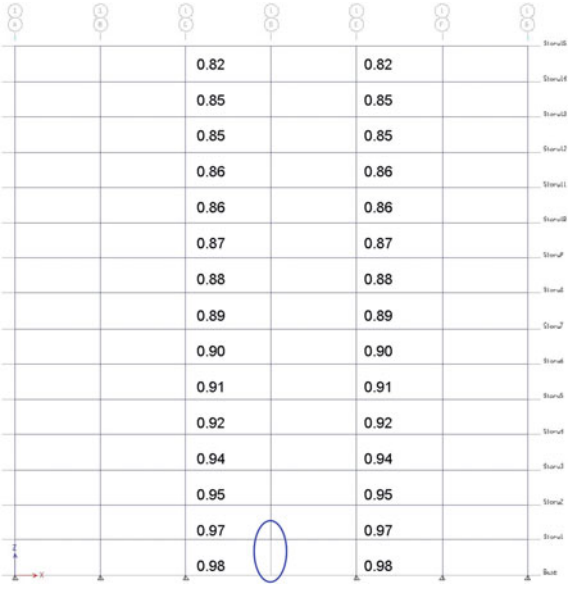

Fig. 7 DCR for long side middle column removal scenario—irregular structure

4.2 Axial Forces

The axial forces developed in the columns can be identified for studying the pattern of redistribution of loads. Also, this redistribution of loads shows the direction of

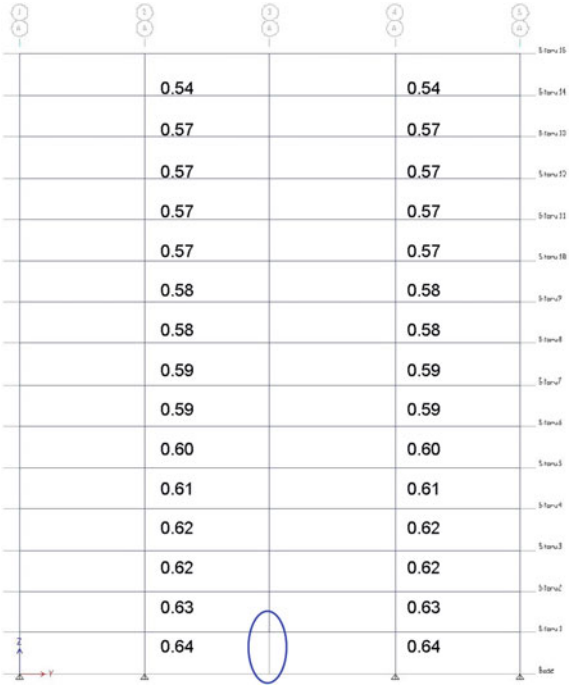

Fig. 8 DCR for short side middle column removal scenario—irregular structure

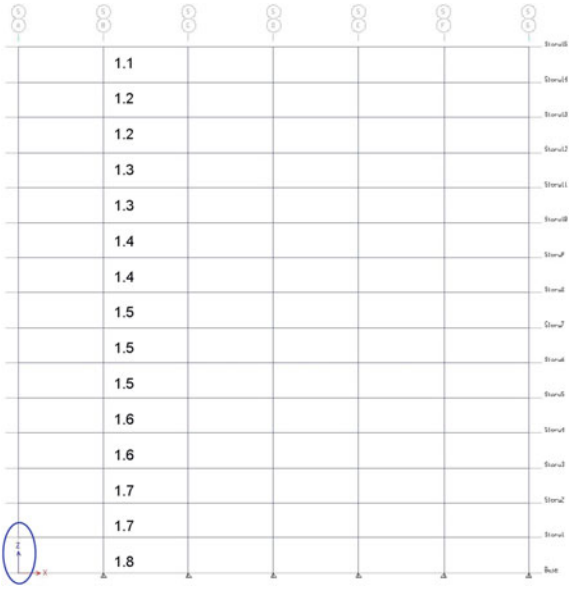

Fig. 9 DCR for corner column removal scenario—irregular structure

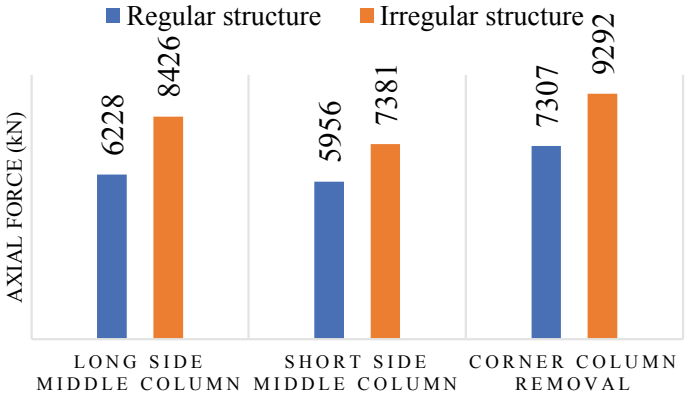

Fig. 10 Axial force near the removed column

progressive collapse. From the axial force diagrams, it can be drawn that axial force near the removed column is more in case of corner columns. For a regular structure, the maximum value of 7307 kN is obtained in the case of a column lost in the corner location which was relatively higher than the axial force near the middle column loss scenario of long side and short side. But for a irregular structure, the maximum value of 9292 kN is obtained in the case of a column lost in the corner location which was relatively higher than the axial force near the middle column loss scenario of long side and short side.

The values of axial force of irregular structure seems to be 27% more than a regular structure. For the regular structure where columns are safe, the obtained axial loads are less than maximum axial load capacity. The magnitude of axial force is more when the building is an irregular structure than for a regular structure, and is depicted in Fig. 10. It is also observed that the column adjacent to the removed column underwent higher force than other columns, which implied the redistribution of forces from the removed column to the nearest columns.

4.3 Vertical Displacement

The maximum displacement of the structure is shown in Fig. 11. For a regular structure, the maximum value of 10 mm is obtained in the case of a column lost in the corner location which was relatively higher than the displacement for a middle column loss scenario of long side and short side. For the irregular structure, the maximum value of 15 mm is obtained in the case of a column lost in the corner location, higher than the displacement for a middle column loss scenario of long side and short side. There is an increase of 50% in vertical displacements for irregular buildings over a regular building under the progressive collapse mechanism.

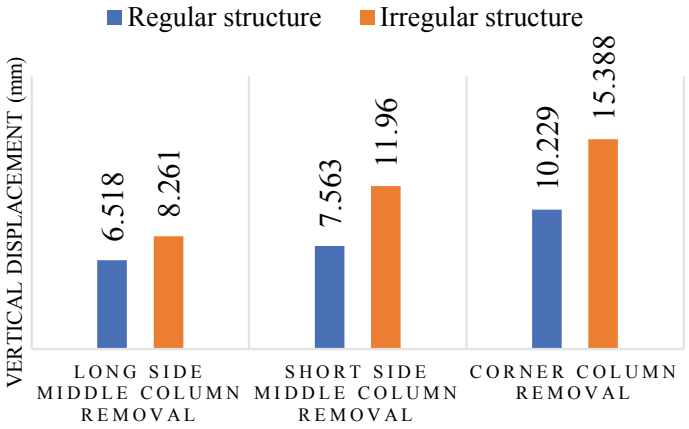

Fig. 11 Maximum vertical displacement of regular and irregular buildings

From the results it can be concluded that a column lost in the corner region of a building is the most critical than middle column lose scenarios and also the displacements will be minimum for a regular structure. And based on this study the best practical advice to reduce the potential of progressive collapse is to consider a regular geometry to the structures. The typical structures possess inherent ability to resist progressive collapse than atypical structures.

5 Conclusions

Based on the limited study of progressive collapse in a G + 15 storey regular and irregular steel structures, following conclusions are drawn:

- By comparing parameters such as DCR values, axial forces and vertical displacements, it can be concluded that corner column removal condition in base is more critical in a building, both for regular and irregular buildings.
- The DCR values, axial forces and the vertical displacements irregular building are higher than regular building, for all scenarios considered.
- The regular structure is not severely damaged under progressive collapse. But the irregular structure undergoes progressive collapse when the corner column is removed. The DCR of irregular structure is more than twice of regular structure under critical element removal scenario. Then it will be safe to avoid irregular geometry for the structures, to resist the progressive collapse.
- By removing a column, a great force is imposed to its adjacent column which shows progressive collapse direction. Also, the values of axial force of irregular building seems to be 27% more than a regular building.

- Maximum displacements obtained from the analysis show a higher value for irregular buildings. There is an increase of 50% in vertical displacements for irregular buildings under progressive collapse analysis compared to regular buildings.

References

1. Mahmoud YM, Hassam MM, Mourad SA, Sayed HS (2018) Assessment of progressive collapse of steel structures under seismic loads. Alexandria Eng J 57:3825–3839
2. Kim J, Kim T (2008) Assessment of progressive resisting capacity of steel moment frames. J Constr Steel Res 65(1):169–179
3. GSA (2013) Progressive collapse analysis and design guidelines for new federal office buildings and major modernization projects. The US General Services Administration
4. Marchand Walter KA, Farid Alfawakhiri P (2004) Blast and progressive collapse. Facts for Steel Buildings, American Institute of Steel Construction, Inc.
5. Marjanishvili S, Agnew E (2006) Comparison of various procedures for progressive collapse analysis. J Perform Constr Facil ASCE
6. Gerasimidis S, Bisbos CD, Baniotopolus CC (2012) Vertical geometric irregularity assessment of steel frames on robustness and disproportionate collapse. J Constr Steel Res 74:76–89
7. Stewart MG (2016) Risk of progressive collapse of buildings from terrorist attacks: are the benefits of protection worth the cost? J Perform Constr Facil ASCE 31:04016093
8. IS 1893 (2002) Criteria for earthquake resistant design of structures. Bureau of Indian Standards
9. IS 875 (1988) Code of practice for design loads for buildings and structures. Bureau of Indian Standards
10. IS 800 (2007) General construction on steel: code of practice. Bureau of Indian Standards

Structural Performance of GFRP Deck Strengthened with Light Weight Ultra-High Strength Concrete

K. Teena John, P. E. Kavitha, and R. Renjith

Abstract This paper presents the numerical investigations carried out on pultruded prototype glass fibre reinforced polymer (GFRP) composite bridge deck panels under static loading. To carry out the analysis decks with four different core shapes having almost same cross sectional area and weight were taken. The loading was applied with a patch of size 580 mm × 230 mm by displacement controlled method until failure. To understand the behavior of the deck, loading was applied at the center of the deck. Based on these observations trapezoidal section is to be found more beneficial in terms of load carrying capacity and secant stiffness. Strengthening of the GFRP deck with trapezoidal core shape were done by filling alternate cores with light weight ultra-high strength concrete with steel reinforcement on the top portion at a spacing of 100 mm and 150 mm respectively. Based on the load carrying capacity and the deflection limit the optimum configuration is taken and their load carrying capacity is compared with the same model without strengthening.

Keywords Glass fibre reinforced polymer · Bridge deck panel · Static loading · Deflection · Sustainability · Steel reinforced (SR) · Un reinforced (UR)

1 Introduction

The bridge decks needs maximum maintenance because of corrosion and deterioration [1]. Conventional materials and technologies which were suitable for bridge deck applications shows lack in durability and fatigue for demanding applications

K. Teena John (✉) · P. E. Kavitha
Department of Civil Engineering, FISAT, Angamaly, Kerala 683577, India
e-mail: teenajohn95@gmail.com

P. E. Kavitha
e-mail: kavithapurakat@gmail.com

R. Renjith
Department of Mechanical Engineering, FISAT, Angamaly, Kerala 683577, India
e-mail: renjith499@gmail.com

© Springer Nature Switzerland AG 2021

K. Dasgupta et al. (eds.), *Proceedings of SECON 2020*,
Lecture Notes in Civil Engineering 97,
https://doi.org/10.1007/978-3-030-55115-5_7

[2, 3]. Life cycle analysis estimates indirect costs to the user due to traffic delays and lost productivity more than the direct cost of repair. In recent years, high-performance fibre-reinforced polymer (FRP) composite materials have been identified as a good alternative for rehabilitating deteriorated bridges. One of the most promising applications for this high-performance material is bridge decking. GFRP decks manufactured with pultrusion having more fiber volume comparing with other techniques [4, 5]. Important applications of FRP decks include replacement of under-strength decks in existing bridges, and the provision of temporary running surfaces. Due to low elastic modulus of GFRP materials, GFRP-reinforced sections exhibit higher deformation characteristics when compared to equivalent reinforced steel sections [6].

2 Literature Review

The energy consumption of various materials was studied, and it can be noted that FRP decks consume very lower energy as they generally contain glass fibers. This reveals that a substantial saving in energy consumption when the bridge superstructure is made of glass fiber polymer materials [7].

Kim et al. [8] studied the design, analysis and fabrication of a reusable pultruded GFRP (Glass fiber reinforced polymer) deck panel that can be used to furnish roadway surface. E-Glass fibers and polyester resin are taken as fiber and matrix respectively for the pulrusion process of GFRP deck panel. ABAQUS with a four node shell element (SR4) was used for the analysis. In this study the deflection limit proposed by EUROCOMP was assumed to reduce the vibration of the deck panel under live load. Two patch load cases were taken namely load case 1 and load case 2. Load case 1 means truck is passing in the girder direction and load case 2 on the other hand; the truck is passing in the direction that is orthogonal to the girder. From the results it is clear that Load case 1 is more critical than load case 2. Deflection limit is the critical design parameter of GFRP deck panel [8]. Kim et al. [9] conducted the design, analysis of hybridized GFRP deck panel. Hybridization increases the elastic modulus and stiffness of a GFRP flexural member. For this two decks are taken named as deck A and deck B. For the Deck-A type, the top and bottom flanges are reinforced with uniformly spaced steel wires. For the Deck-B type, the webs are reinforced with a flat steel plate and the width of the steel plate was assumed to be 130 mm. Structural performance of the hybrid deck profiles was compared on the basis of FE analysis and, the flexural stiffness of the hybrid deck panel (the Deck-A type) is about 114% greater than that of the non-hybrid deck panel. The deck type A was found to be more beneficial compared to deck type B in terms of flexural stiffness [9]. Kim et al. [10] compared the static load performance of the GFRP deck panel reinforced with steel wires and unreinforced deck panels. At the design load level, the flexural stiffness of the steel reinforced GFRP panels was approximately 12.3% greater than that of the unreinforced GFRP panels. The ultimate load carrying capacity of the Series SR specimens was approximately 28% less than that of the

Series UR specimens. This may be due to the geometrical deviation of steel wires in the alignment of fibers and mats which disturbs the orientation of fibers [10].

Wang et al. [11] developed Ultra-lightweight cement composite (ULCC). The studied cenosphere is a by-product composed by spherical particles with diameter ranging from 30 to 300 μm, consisted of approximately 9.5% of organic matter. It contains steel fibres, ordinary Portland cement, water, silica fume, chemical admixtures and cenospheres. Application of ULCC reduces self-weight around 36–52%, densities ranging from 1250 to 1550 kg/m^3 and high compressive strength more than 60 MPa [11].

3 Research Gap

From the viewed literatures it is clear that the hybridization method which used to increase the flexural stiffness and elastic modulus of the GFRP deck, leads to the reduction in the load carrying capacity. So this study tries to improve the flexural stiffness of the deck with increase in the load carrying capacity.

4 Strengthening of GFRP Deck with Optimum Configuration

The entire numerical study is done with the help of FEA by using ANSYS 16.1.

4.1 Materials

1. **GFRP**

In fabricating the deck profile E-glass fiber roving (8800 TEX), continuous strand mat (CSM), biaxial glass fiber fabric (BGF) with ply angles of 0°/90°, quadriaxial glass fiber fabric (QGF) with ply angles of 0°/+45°/90°/−45°, and unsaturated polyester resin was employed. The properties taken for modelling the GFRP deck is taken from [10] is shown in Table 1.

2. **Light weight ultra-high strength concrete**

The cenospheres are hollow alumino-silicate spheres with particle sizes ranging from 10 to 300 mm. The density of cenosphere used in this paper was 820 kg/m^3. Considering the low water-to-binder ratio, the super plasticizer was used to achieve good workability. Straight steel fiber with a diameter of 0.16 mm and a length of 13 mm with an aspect ratio 81.3 was used to improve the tensile strength of the ULCC [11]. Figure 1 shows some of the key components of ULCC.

Table 1 Properties of GFRP composite [10]

S. No.	Properties	Flange	Web
1	Elastic modulus (GPa) (E_{11})	26.9	28.7
	(E_{22})	13	13.2
2	Shear modulus (GPa) (G_{12})	3.1	5.3
3	Yield strength (MPa)	405.3	422.3
4	Poisson's ratio ν_{12}	0.21	0.31
5	Mass density (kg/m^3)	1900	1900

Fig. 1 Rectangular shape [9]

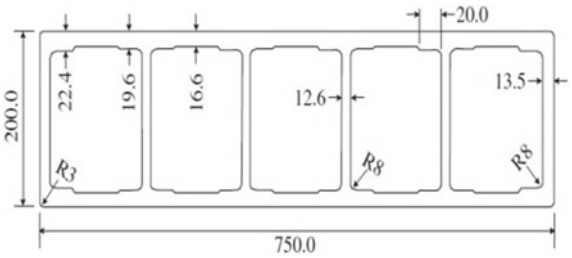

Table 2 Properties of ULCC [11]

S. No.	Properties	
1	Compressive strength (MPa)	48.03
2	Elastic modulus (GPa)	10.79
3	Tensile strength (MPa)	2.03
4	Density (kg/m^3)	1250

The property taken for modelling the ULCC is taken from [11] is shown in Table 2.

4.2 Determination of Best Deck Shape

Deck with a rectangular core shape from [9] was taken as the base model. With reference to this base model three other shapes are modelled which includes rhombus shape, semi elliptical shape and trapezoidal shape respectively. These three models having almost same cross sectional area and self-weight as that of the base model. Area and self-weight of each model was found from ANSYS and moment of inertia is calculated from AUTOCAD by using the command mass properties. The geometry details regarding the models are given in Table 3.

These three different core shaped decks are given below. Figure 1 shows the base model (rectangular shape). These decks are modelled in AUTOCAD 2016. Figures 2, 3, 4 show rhombus, semi elliptical and trapezoidal core shaped decks respectively.

Table 3 Geometric details of models

S. No.	Core shape	Area (mm^2)	Self-weight (kg)	Moment of inertia (mm^4)
1	Rectangular	39812.4	189.1	49×10^7
2	Rhombus	39516.4	187.1	44×10^7
3	Semi elliptical	40564.4	192.68	50×10^7
4	Trapezoid	39686.8	188.51	54.6×10^7

Fig. 2 Rhombus shape

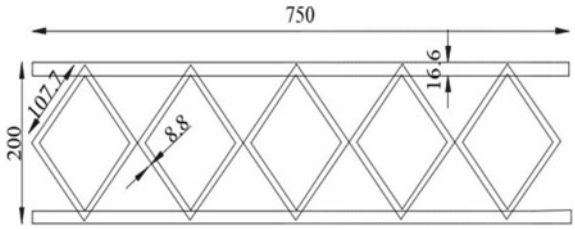

Fig. 3 Semielliptical shape

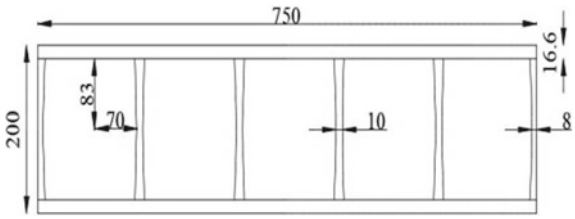

Fig. 4 Trapezoidal shape

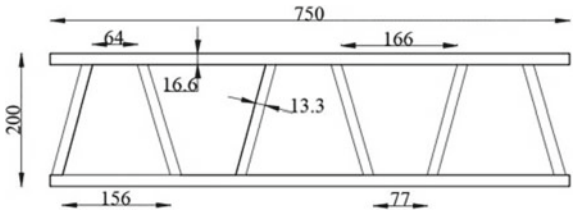

These decks are modelled in ANSYS 16.1 using various sketching tools. Material properties were assigned to webs and flanges of GFRP members of the deck.

4.2.1 Loading and Boundary Conditions

Test set up of the finite element model is shown in Fig. 5. The left and right side of the deck are simply supported by means of a steel plate fixed on both sides of the deck with a spacing of 155 mm. For determining the structural behavior of different deck configurations in GFRP, static structural analysis is to be performed. Loading

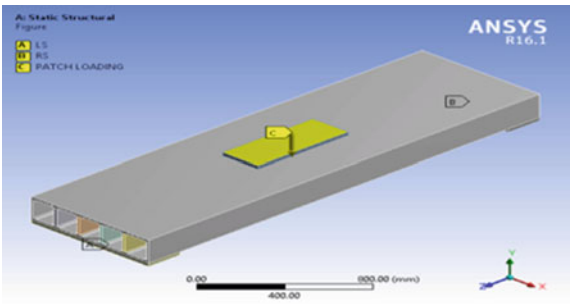

Fig. 5 Test set up

was applied using patch loading (patch of size 580 mm × 230 mm) by displacement controlled method until failure.

4.2.2 Results and Discussion

Table 4 lists the initial failure load (ultimate load), the center displacement measured at the initial failure and design load level (122.3 kN), and the estimated secant stiffness of the specimens when the patch load was placed at the center of the deck. The standard design truck load specified in [10] was used as a design live load; and the self-weight of the deck panel was considered to be a dead load. Thus, the design live load is a rear wheel load of a standard design truck. The deflection limit recommended by EUROCOMP 1996 ranges from span/150 to span/400. Although a deflection limit of span/400 was assumed to reduce the vibration of the deck panel under a live load. Note that the central deflection of the deck panel due to the self-weight of the deck and the live load was used to check the deflection limit.

Figure 6 shows the load versus centre displacement graph for each deck shapes when the patch load was placed at the centre of the deck. From the analysis it is clear that the ultimate load carrying capacity is more in the case of trapezoidal section compared with the rectangular (base model), rhombus and semi elliptical sections. The load carrying capacity is least in the case of rectangular section. The load carrying

Table 4 Summary of analysis results

S. No.	Core shape	Ultimate load (kN)	Centre displacement (mm)		Secant stiffness at design load (kN/mm)
			At ultimate load	At design load	
1	Rectangular	553.25	34.378	6.22	19.66
2	Rhombus	573.3	32.217	6.33	19.32
3	Semi elliptical	597.44	24.748	6.06	20.18
4	Trapezoid	599.17	28.048	5.632	21.72

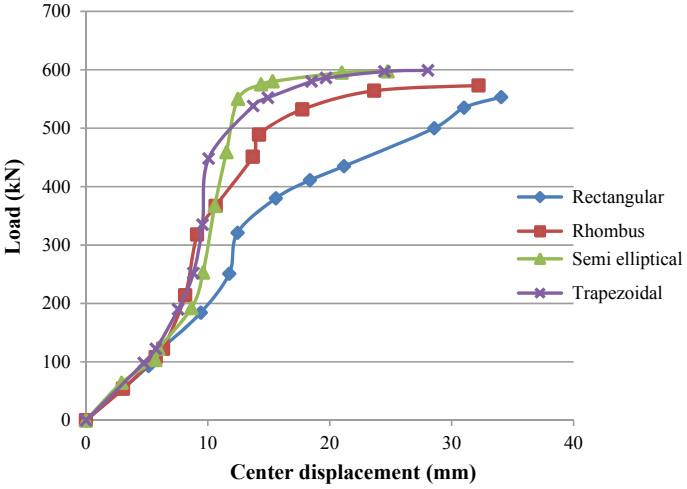

Fig. 6 Load displacement curve

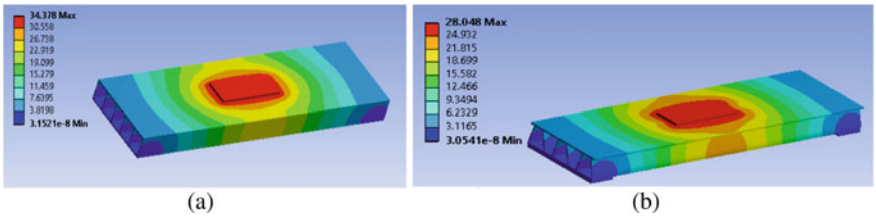

Fig. 7 Deformed shape

capacity of rhombus, semi elliptical and trapezoidal sections was increased to 3.62, 7.98 and 8.3% comparing with the base model.

Figure 7a, b show the deformed shape of the rectangular, trapezoidal sections respectively.

4.3 Strengthening of GFRP Deck

The strengthening was done on the trapezoidal section which is the best section among other three. Two deck specimens were taken for strengthening. One specimen was reinforced with Fe 500 steel bars of diameter 6 mm at a spacing of 100 mm (GF100) and other specimen at a spacing of 150 mm (GF150) with a 50 mm thick ULCC above the GFRP flange. Then ULCC is filled along the alternate cores of the deck and the top portion of the flange by a thickness of 50 mm thus by making a composite concrete GFRP deck. Same loading conditions and arrangements were

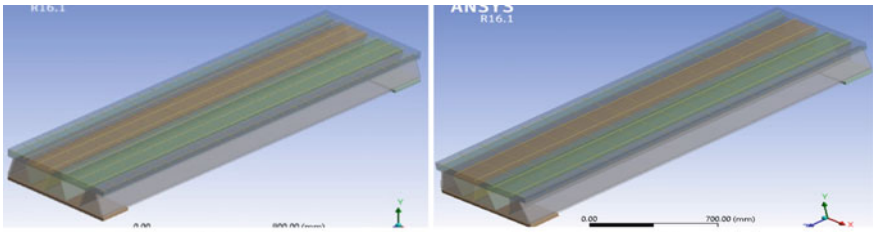

Fig. 8 Steel reinforcement

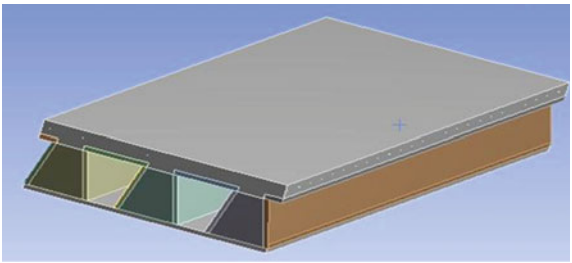

Fig. 9 Deck filling with ULCC and steel reinforcement

used as in the previous analysis by placing the patch loading at the centre of the deck by displacement controlled method until failure. Figure 8a, b shows the steel reinforcement of diameter 6 mm in the form of a mesh with a spacing of 100 mm and 150 mm respectively. Figure 9 shows the deck after filling the cores with ULCC.

4.3.1 Results and Discussion

Table 5 lists the initial failure load (ultimate load), the center measured at the initial failure and design load level (122.3 kN) and the estimated secant stiffness of the Specimens. Specimen name GF 100 and GF 150 shows the deck strengthened with ULCC with a steel reinforcement spacing of 100 mm and 150 mm respectively. Figure 10 shows the load displacement curve of various specimens. A comparison is

Table 5 Summary of test results

S. No.	Specimen ID	Ultimate load (kN)	Center displacement (mm)		Secant stiffness at design load (kN/mm)
			At ultimate load	At design load	
1	GF 100	721.42	23.585	4.912	24.89
2	GF 150	699	25.144	5.13	23.84
3	GF w/o concrete	599.17	28.048	5.632	21.72

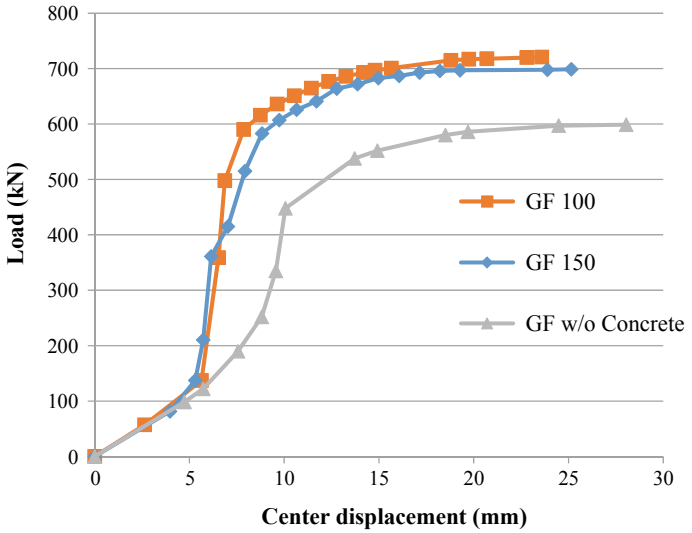

Fig. 10 Load displacement curve

also done with trapezoidal section without strengthening. The load carrying capacity of strengthened section with a steel reinforcement of 100 mm, 150 mm were greater than of about 20.40, 16.61% comparing with the section without strengthening. The deflection limit at the design live load level is safe for the sections with strengthening comparing with the section without strengthening.

5 Conclusions

To determine static load performance of GFRP deck with different core shapes this a patch loading of size 580 mm × 230 mm is placed at the centre of the deck. The results of these analysis showed that the deck with trapezoidal core shape performed better comparing with the others in terms of more load carrying capacity and secant stiffness at the design live load level (122.3 kN). The ultimate load carrying capacity of the trapezoidal section at centre of the deck was 8.3% more comparing with the base model (i.e. rectangular shape). The center displacement of the rectangular, rhombus, semi elliptical and trapezoidal sections were 13.6, 15.6, 10.68 and 2.86% greater than the deflection limit. Secant stiffness of the semi elliptical and trapezoidal sections were 2.64, 10.46% greater comparing with the base model. Secant stiffness of the rhombus section is considerably getting reduced by 1.82% compared to the base model. This shape study reveals that moment of inertia and elastic modulus are the one of the governing factors for predicting the performance of deck with different core shapes. By understanding the moment of inertia of decks with different core shapes alone, it is not possible to predict section with more load carrying capacity,

since GFRP exhibits orthotropic elasticity. Although moderately complex shapes of a deck profile can be efficiently pultruded nowadays, rectangular and trapezoidal shapes are widely used for the cross sectional shapes. Therefore the trapezoidal section was found to be more effective comparing with the others.

But the deflection limit of trapezoidal section was 2.86% more than with the allowable limit. To overcome this, hybridization of the trapezoidal section is to be carried out with the use of light weight ultra-high strength concrete by filling in alternate cores and above the top of the flange in 50 mm thick. Steel reinforcement is provided on the top of the flange with suitable spacing along with this.

The static analysis on the centre of the modified concrete GFRP composite bridge deck was performed by placing patch loading at the centre of the deck. This proposed method of strengthening increased the load carrying capacity of the deck specimen up to 20.4 and 16.61% and secant stiffness also increased up to 14.59 and 9.76% for specimens GF100, GF150 comparing with the deck without strengthening (GF W/o concrete). The deflection limit at the design live load level is safe for the sections with strengthening comparing with the section without strengthening. Although the performance of the proposed GFRP deck panel was evaluated by means of FE analysis, the short term and long term performances of the panel must be validated experimentally.

References

1. Xin H, Mosallam AS, Liu Y, Wang C, He J (2018) Experimental and numerical investigation on assessing local bearing behavior of a pultruded GFRP bridge deck. Compos Struct 204:712–730
2. Stankiewicz B (2012) Composite GFRP deck for bridge structures. Procedia Eng 40:423–427
3. Li Y-F, Meda H, Chen W (2018) The design and analysis of internally stiffened GFRP tubular decks—a sustainable solution. Sustainability 10(12):4538
4. Larco C, Pahonie R, Edu I (2015) The effects of fibre volume fraction on a glass-epoxy composite material. INCAS Bull 7(3):113
5. Chen ZF, Wan LL, Lee S, Ng M, Tang JM, Liu M, Lee L (2008) Evaluation of CFRP, GFRP and BFRP material systems for the strengthening of RC slabs. J Reinf Plast Compos 27(12):1233–1243
6. Zhang Y, Mosallam A, Liu Y, Sun Y, Xin H, He J (2019) Assessment of flexural behavior of pultruded GFRP laminates for bridge deck applications. Adv Mater Sci Eng
7. Muthuraj MP, Nithyapriya K (2017) Experimental studies on multicellular GFRP bridge deck panels under static and fatigue loading. Sādhanā 42(12):2171–2181
8. Kim H-Y, Lee S-Y (2009) A pultruded GFRP deck panel for temporary structures. Compos Struct 91:20–30
9. Kim H-Y, Lee S-Y (2012) A steel reinforced hybrid GFRP deck panel for temporary bridges. Constr Build Mater 34:192–200
10. Kim H-Y, Lee S-Y (2019) Static and fatigue load performance of a pultruded GFRP deck panel reinforced with steel wires. Compos Struct 207:166–175
11. Wang J-Y, Gao XL, Yan JB (2018) Developments and mechanical behaviors of steel fiber reinforced ultra-light weight cement composite with different densities. Constr Build Mater 171:643–653

Effect of Combination of Mineral Admixtures on the Properties of Self Compacting Concrete

Reya Grace Jacob and K. N. Resmi

Abstract Self-compacting concrete abbreviated as SCC is a recently developed concept in which the ingredients of the concrete mix are proportioned in such a way that the concrete is compacted by its own weight without or little vibration, assuring complete filling of formwork even when access is hindered by narrow gaps between reinforcing bars. Cement is the most important constituent material, since it binds the aggregates and resists the atmospheric action. Manufacturing of cement emits about 0.8 ton of CO_2 in atmosphere for every ton of cement manufacture. The utilization of supplementary cementing materials as natural pozzolans like dolomite powder, fly ash, GGBS etc. in concrete production is one of the solutions to reduce the cement content. This paper deals with the fresh and hardened properties of self compacting concretes made with combination of GGBS and dolomite, GGBS and fly ash as cement replacement in different amounts. The trial mixes are formed based on IS 10262: 2019. The workability properties of the mixes are evaluated by workability testes such as slump flow test, V-funnel test, L-box test. The hardened properties of the concrete are evaluated by compressive strength, flexural strength and tensile strength. The successful utilisation of fly ash, GGBS and dolomite powder in SCC mixes would not only lower the cost of SCC, but could also provide a solution to the disposal and environmental problems connected with these materials.

Keywords Self compacting concrete · Ground granulated blast furnace slag · Dolomite powder · Fly ash

R. G. Jacob (✉) · K. N. Resmi
Department of Civil Engineering, Federal Institute of Science and Technology, Ernakulam 68377, India
e-mail: reya1795@gmail.com

K. N. Resmi
e-mail: reshmikn@gmail.com

© Springer Nature Switzerland AG 2021

K. Dasgupta et al. (eds.), *Proceedings of SECON 2020*,
Lecture Notes in Civil Engineering 97,
https://doi.org/10.1007/978-3-030-55115-5_8

1 Introduction

Concrete is the basic civil engineering material used in most of the civil engineering structures. The recent development in the field of concrete technology represents a great step toward manufacturing of concrete. Self-compacting concrete abbreviated as SCC is a recently developed concept in which the ingredients of the concrete mix are proportioned in such a way that the concrete is compacted by its own weight without or little vibration, assuring complete filling of formwork even when access is hindered by narrow gaps between reinforcing bars. The main property that defines SCC is high workability in attaining compaction and specified hardened properties [1].

Cement, fine aggregate, coarse aggregate, mineral admixtures, chemical admixtures and water are the constituents of concrete. Cement is the most important constituent material, since it binds the aggregates and resists the atmospheric action. Manufacturing of cement emits about 0.8 ton of CO_2 in atmosphere for every ton of cement manufacture [2]. The utilization of supplementary cementing materials as natural pozzolans like dolomite powder, rice husk ash, fly ash, egg shell powder, silica fume, metakaolin etc. in concrete production is one of the solutions to reduce the cement content [3].

Dolomite is a carbonate material composed of calcium magnesium carbonate $CaMg(CO_3)_2$. Its use improves properties such as weathering action, reduces shrinkage, fissure development and water absorption. By the proper usage of dolomite powder, the objective of cost reduction of construction can be obtained. We found the cost of dolomite is very cheap than cement and it is easily available locally [4]. Fly ash or flue ash, also known as pulverized fuel ash is a coal combustion product that is composed of the particulates (fine particles of burned fuel) that are driven out of coal-fired boilers together with the flue gases. Depending upon the source and composition of the coal being burned, the components of fly ash vary considerably, but all fly ash includes substantial amounts of silicon dioxide (SiO_2) (both amorphous and crystalline), aluminium oxide (Al_2O_3) and calcium oxide (CaO), the main mineral compounds in coal-bearing rock strata. Ground Granulated Blast furnace Slag (GGBS) is a by product from the blast furnaces used to make iron. GGBS is used to make durable concrete structures in combination with ordinary Portland cement and/or other pozzolanic materials. Concrete made with GGBS cement sets more slowly than concrete made with ordinary Portland cement, depending on the amount of GGBS in the cementitious material, but also continues to gain strength over a longer period in production conditions [5]. This results in lower heat of hydration and lower temperature rises, and makes avoiding cold joints easier, but may also affect construction schedules where quick setting is required.

Table 1 Chemical composition of GGBS

Characteristics	Test result
Specific gravity	2.85
Magnesia. Content (%)	7.73
Sulphide sulphur (%)	0.50
Sulphite content (%)	0.38
Manganese content (%)	0.12
Chloride content (%)	0.009
Moisture content (%)	0.10

Table 2 Chemical composition of fly ash and dolomite powder

Parameters tested	Fly ash	Dolomite powder (%)
Calcium oxide (CaO)	0.44%	33.27
Magnesium Oxide (MgO)	–	7.96
Silicon Dioxide (SiO_2)	63.8%	40.50
Aluminium Oxide (Al_2O_3)	1.29%	0.55
Ferric oxides (Fe_2O_3)	0.39	0.18

2 Experimental Program

2.1 Materials

Ordinary Portland Cement of 53 grade was used in the investigation. Ground granulated blast furnace slag (GGBS), fly ash and dolomite powder are used as supplementary cementitious material and their chemical compositions are given in Tables 1 and 2. Crushed granite angular aggregate from a local source, having a maximum size of 12.5 mm, was used as coarse aggregate and M-Sand used as fine aggregate.

2.2 Mix Proportions

For the study M25 grade concrete is designed as per IS 10262: 2019. Water binder ratio of 0.43 and 0.4% of admixture is adopted for all the mixes. The objective of the project is to study the (a) effect of GGBS and dolomite powder on the properties of SCC and (b) effect of GGBS and fly ash on the properties of SCC. To obtain the first objective five mixes with different proportions of GGBS and dolomite powder were prepared and tested. The designation of specimens with GGBS and dolomite is presented in Table 3.

To obtain the second objective five mixes with different proportions of GGBS and fly ash were prepared and tested. The designation of specimens with GGBS and fly ash is given in Table 4.

Table 3 Designation of specimen with GGBS and dolomite powder

Mix ID	Proportion of binder materials
D0	Cement 60% + GGBS 40% + DP 0%
D5	Cement 60% + GGBS 35% + DP 5%
D10	Cement 60% + GGBS 30% + DP 10%
D15	Cement 60% + GGBS 25% + DP 15%
D20	Cement 60% + GGBS 20% + DP 20%

Table 4 Designation of specimen with GGBS and fly ash

Mix ID	Proportion of binder materials
F0	Cement 60% + GGBS 40% + FA 0%
F10	Cement 60% + GGBS 30% + FA 10%
F20	Cement 60% + GGBS 20% + FA 20%
F30	Cement 60% + GGBS 10% + FA 30%
F40	Cement 60% + GGBS 0% + FA 40%

2.3 Testing of Specimen

The workability properties of the mixes were evaluated by slump flow test and the hardened properties were evaluated by compressive strength, flexural strength and tensile strength tests. Concrete cubes of size 150 × 150 × 150 mm, concrete cylinder of size 150 mm × 300 mm and concrete beams of 100 × 100 × 500 mm were prepared for compressive strength, split tensile strength and flexural strength test respectively.

3 Results and Discussion

3.1 Effect of GGBS and Dolomite Powder on SCC

3.1.1 Fresh Properties

The slump values were recorded as soon the concrete was mixed. The results of slump flow test for each mix are shown in Table 5. As per IS: 10262—2019 the acceptance range for slump flow and T_{50} slump flow of class SF2 is 660–750 mm and 2–5 s respectively. The slump flow test results obtained here is within this range.

3.1.2 Hardened Properties

Compressive strength, split tensile strength and flexural strength test results at different ages are given in Tables 6 and 7. It is observed that compressive strength

Table 5 Slump flow test results of SCC with GGBS and dolomite powder

S. No.	Mix ID	Flow diameter (mm)	T_{50} slump flow (s)
1	Control mix	674	4.5
2	D0	686	3.5
3	D5	684	3.6
4	D10	678	4
5	D15	676	4.1
6	D20	671	4.3

Table 6 Compressive strength of SCC with GGBS and dolomite powder

S. No.	Mix ID	7 day compressive strength (MPa)	28 day compressive strength (MPa)
1	Control mix	24.34	32.65
2	D0	26.52	33.78
3	D5	27.43	37.32
4	D10	28.46	38.87
5	D15	26.12	35.56
6	D20	24.85	34.92

Table 7 Tensile and flexural strength of SCC with GGBS and dolomite powder

S. No.	Mix ID	28 day tensile strength (MPa)	28 day flexural strength (MPa)
1	Control mix	2.57	5.9
2	D0	3.19	6.29
3	D5	3.21	6.31
4	D10	3.57	6.45
5	D15	3.33	6.39
6	D20	2.9	6.36

increases from 26.52 to 28.46 MPa at 7 days and 33.78 to 38.87 MPa at 28 days with the increase in dolomite powder content from 0 to 10%. SCC mix with 30% of GGBS and 10% of dolomite powder obtained maximum tensile strength and flexural strength of 3.57 MPa and 6.45 MPa respectively.

Table 8 Slump flow test results of SCC with GGBS and fly ash

S. No.	Mix ID	Flow diameter (mm)	T_{50} slump flow (sec)
1	Control Mix	674	4.5
2	F0	686	3.5
3	F10	680	3.9
4	F20	675	4.2
5	F30	670	4.5
6	F40	667	4.8

Table 9 Compressive strength of SCC with GGBS and fly ash

S. No.	Mix ID	7 day compressive strength (MPa)	28 day compressive strength (MPa)
1	Control mix	24.34	32.65
2	F0	26.52	33.78
3	F10	26.98	35.87
4	F20	28.12	38.62
5	F30	25.42	37.24
6	F40	25.04	34.08

3.2 Effect of GGBS and Fly Ash on SCC

3.2.1 Fresh Properties

The results of slump flow test for each mix are shown in Table 8. The slump flow test results obtained here is within the acceptance range specified in IS: 10262—2019 for SCC.

3.2.2 Hardened Properties

Compressive strength, split tensile strength and flexural strength test results at different ages are given in Tables 9 and 10. It is observed that compressive strength, tensile strength, flexural strength increases with the increase in fly ash content upto 20%. SCC mix which incorporates of powder material comprising of 60% ordinary Portland cement, 20% GGBS and 20% fly ash obtains high strength.

4 Conclusions

On the basis of the results obtained, the following conclusions have been drawn:

Table 10 Tensile and flexural Strength of SCC with GGBS and fly ash

S. No.	Mix ID	28 day tensile strength (MPa)	28 day flexural strength (MPa)
1	Control mix	2.57	5.9
2	F0	3.19	6.29
3	F10	3.52	6.33
4	F20	3.68	6.52
5	F30	3.31	6.46
6	F40	3.05	6.36

- Dolomite powder and GGBS can be used partially to enhance the strength properties of concrete which makes the mix economical than conventional concrete.
- All the mixes with GGBS and dolomite powder show acceptable fresh properties.
- Mix with 30% of GGBS and 10% of dolomite powder obtained maximum compressive, tensile and flexural strength.
- It is possible to manufacture self-compacting concrete using GGBS and fly ash with acceptable fresh and hardened properties.
- All the mixes with GGBS and fly ash show acceptable fresh properties.
- Maximum strength is obtained for mix with 20% of GGBS and 20% of fly ash.

References

1. Barbhuiya S (2011) Effects of fly ash and dolomite powder on the properties of self-compacting concrete. Constr Build Mater 25(8):3301–3305
2. Preethi G, Prince G (2015) Effect of replacement of cement with dolomite powder on the mechanical properties of concrete. Int J Innov Sci Eng Technol 2(4):1083–1088
3. Jelčić Rukavina M, Gabrijel I, Bjegović D (2015) Modifications of dolomite-based self-compacting concrete properties using mineral additives. Tehnički vjesnik 22(1):233–240
4. Deepa Balakrishnan S, Paulose KC (2013) Workability and strength characteristics of self compacting concrete containing fly ash and dolomite powder. Am J Eng Res 2:43–47
5. Kuruba Anil P, Chowdary L (2017) Study on strength properties of self compacting concrete using GGBS and lime stone powder as mineral admixtures. Int J Innov Res Sci Eng Technol 6(3)

Evaluation of Sustainable SMA Mix Prepared Using Recycled Concrete Aggregates

A. A. Ruksana, P. S. Sethulakshmi, Mariya Thomas, Midhun Joby, and Sharon Jacob

Abstract The disposal of Construction and Demolition (C&D) waste generated in the cities has become a serious environmental problem nowadays. The use of Recycled Concrete Aggregates (RCA) obtained from this C&D waste can reduce the amount of virgin aggregates for pavement construction. In this study, the recycled concrete aggregates are used in the manufacture of Stone Matrix Asphalt (SMA) mix. The fine and coarse aggregates in SMA mixes are partially replaced by RCA. The Marshall and volumetric properties of the SMA mixes containing RCA are evaluated and compared with the conventional SMA mix. The use of these SMA mixes prepared with RCA reduces the volume of natural resources consumed and solves the disposal problem of the C&D waste. This study thus actually paves a sustainable way for the asphalt pavement industry.

Keywords Construction and demolition (c&d) waste · Stone matrix asphalt (SMA) · Sustainability · Recycled concrete aggregates (RCA)

A. A. Ruksana (✉) · P. S. Sethulakshmi · M. Thomas · M. Joby · S. Jacob
Department of Civil Engineering, Federal Institute of Science and Technology (FISAT), Ernakulam 683577, India
e-mail: ruksanaabdulkareem@gmail.com

P. S. Sethulakshmi
e-mail: sethupurakkattu@gmail.com

M. Thomas
e-mail: mariyaarackal1998@gmail.com

M. Joby
e-mail: midhunjoby77@gmail.com

S. Jacob
e-mail: sharonjacob1611@gmail.com

© Springer Nature Switzerland AG 2021

K. Dasgupta et al. (eds.), *Proceedings of SECON 2020*,
Lecture Notes in Civil Engineering 97,
https://doi.org/10.1007/978-3-030-55115-5_9

1 Introduction

Road networks play a crucial role in the economic and social development of a country. The spurt in the growth of traffic and overloading of vehicles decreases the life span of roads laid with conventional bituminous mixes. This also leads to the reduction in the riding quality due to premature failure of the flexible pavements. It is observed that Stone Matrix Asphalt mixture (SMA) is an ideal mixture for long lasting highways. SMA is a gap graded aggregate-asphalt hot mixture with 70–80% coarse aggregate, 8–12% filler, 6.0–7.0% binder and normally 0.3% fibre. SMA provides excellent resistance to rutting due to slow, heavy and high volume traffic, and resistance to deformation at high pavement temperatures. Environmental, economic and technical problems have led to increasing attention being paid to the subject of recycling solid waste materials in the construction of road infrastructure.

Studies were carried by Giri et al. [1] on the use waste materials such as recycled concrete aggregates (RCA) and waste polyethylene from milk packaging (WPMP) in bituminous mixes. RCA was pre-treated with bituminous emulsion (PRCA) to reduce its water absorption. The performance of the different bituminous mixes was found out in terms of Marshall test parameters. Bituminous mixes containing PRCA and WPMP produce good results compared with conventional aggregate mixes. El-Badawy et al. [2] reviewed the current status of using recycled materials in pavement construction worldwide and the gained benefits in terms of economic savings, environmental impact, and sustainability. A study was conducted by Dalhat et al. [3] on the effect of using combined form of recycled plastic waste (RPW) as a mineral aggregate supplement in a dense-graded hot mix asphalt (HMA). The results showed that combined RPW as an aggregate supplement has advantages over the use of normal aggregates.

This study aims to partially replace the natural aggregates in SMA mixtures through laboratory studies, and compares the test results with mixtures containing natural aggregate. For this purpose, Marshall Stability test were conducted on samples with and without RCA in SMA mix. Using of the RCA decrease areas required for disposal by removing the increase of waste concrete. It results in decreasing of the consumption of energy from aggregate production and transportation.

2 Materials

2.1 Aggregates

Aggregates were collected from a local supplier. Coarse aggregates of 20 mm down (Aggregate 1) and 10 mm down (Aggregate 2) and quarry dust were used. The physical properties of the aggregates such as the Aggregate Impact Value, Aggregate Crushing value, Water Absorption, Flakiness Index, Elongation Index and Specific Gravity were determined and they satisfied all the physical requirements specified

Fig. 1 Coir fiber used during experimentation process

by IRC: SP: 79-2008**.** The aggregates were sieved to meet the physical requirements specified by IRC: SP: 79-2008 [4].

2.2 Bitumen

VG-30 bitumen was collected from a local supplier. Tests such as Softening Point, Ductility, Penetration and Specific Gravity were conducted and its physical properties were satisfied as per the requirements specified by IS 73: 2013 [5].

2.3 Stabilizer Used-Coir Fibre

As coconut fibre contains certain amount of cellulose, this will result in better interlock between the aggregates and thereby improving the strength and reducing the possibility of drain down during transport and paving. Panda et al. [6] has suggested a 0.3% coconut fibre addition in the SMA mixes which brings significant improvement in the engineering properties of SMA mixes (Fig. 1).

2.4 Recycled Concrete Aggregates (RCA)

Construction and Demolition (C&D) waste were collected from Maradu flat demolition site. Steel reinforcement were removed. The RCA used in this investigation for SMA mixes satisfied all the physical requirements specified by IRC: SP: 79-2008. Rondon-Quintana et al. [7] studied the use of blast furnace slag aggregate in hot-mix asphalt. Here, virgin aggregates are partially replaced with RCA. C&D waste

Fig. 2 C&D Waste in Maradu Site

Fig. 3 RCA

collected from the demolition site is shown in Fig. 2 and the prepared RCA is shown in Fig. 3.

3 Methodology

3.1 Aggregate Proportioning by Rothfutch Method

Two types of mixtures were prepared in this study. Mix I consisted of virgin aggregates (CSA) and it was used as a control mix. Mix II was prepared with a combination of RCA and CSA. The sieve analysis of Mix I and Mix II were conducted and the

grain size distribution curves for both the mixes were plotted. The obtained gradations of Mix I and II should be within the desired limits set by IRC: SP: 79-2008. The mixes were then prepared in the obtained aggregate proportions.

3.2 Marshall Method of Mix Design

The aggregates and quarry dust (total weight equal to 1200 gm) and coir fibre (0.3% of total weight of aggregates) were proportioned and mixed for Mix I. The cylindrical specimens were prepared in the laboratory following the Marshall mix design procedure. First sieving is done for coarse and fine aggregates. Sampling of coarse and fine aggregates is carried out for 13 mm SMA composition as specified by IRC: SP: 79-2008. Total sample weight is 1200 gm including filler and binder. Aggregates were heated to a temperature of 120–140 °C and bitumen was heated to a temperature of 130 °C. The bitumen was added in required quantities i.e., 5, 5.5, 6, 6.5 and 7%. It is then mixed with bitumen and is compacted with a hammer with a falling weight of 4.54 kg falling from a height of 40 cm, by giving 50 blows on each side for compaction. The sample is allowed to dry for the next 24 h and then it is taken out of the mould with the help of sample ejector. Its weight in air, water, radii, thickness and height is calculated. Before conducting the Marshall test, each of the samples was kept in hot water bath for 30 min at 60 °C. Two samples each of 5.5, 6, 6.5 and 7% bitumen were prepared respectively for bituminous course and Marshall Test was carried out to calculate their stability.

Similarly, the aggregates, quarry dust and RCA (total weight equal to 1200 gm) and coir fibre (0.3% of total weight of aggregates) were proportioned and mixed. Two samples each of 5.5, 6, 6.5 and 7% bitumen were prepared respectively for Mix II and Marshall Test was carried out (Fig. 4).

3.2.1 Marshall Test

The samples are removed from the hot water bath and supposed to undergo Marshall Test. It is kept under testing machine and loaded at constant rate of deformation of 5 mm per minute till failure. The test head with the specimen is placed in position in the loading machine and the base-plate of the loading machine is raised until the top of the test head is in contact with the bottom of the proving ring or load cell. The deformation measuring dial gauge or flow meter is now placed in position and adjusted to read zero. The load is applied through the Marshall test setup maintaining a constant deformation rate of 51 mm per minute. The load and deformation readings are closely observed. The maximum load at failure (in kN) and the corresponding deformation (or flow) readings (in mm) are noted. The Marshall test apparatus is shown in Fig. 5. The samples are placed in the hot water bath 30 minutes before the test (Fig. 6).

The Marshall Stability value is computed using the calibrated equation as:

Fig. 4 Sampling, Mixing, Pouring and Compaction of Mix II

Marshall Stability (kN) = (0.0249x-0.5549), where x is the number of divisions in proving ring.

The corrected Marshall Stability value of each specimen is determined by applying the appropriate correction factor.

3.2.2 Calculations

Theoretical Specific gravity, Bulk density, Volumetric properties (% of air voids (V_v), % volume of bitumen (V_b), % of voids in mineral aggregate (VMA) and % of voids filled with bitumen (VFB)) and Optimum Bitumen Content (OBC) were determined. Based on the Marshall tests performed above, and the values computed, the following graphs were plotted:

- Corrected Marshall Stability versus Bitumen Content
- Flow versus Bitumen Content
- Unit Weight or Bulk Density (G_m) versus Bitumen Content
- Percent Air Voids in the total mix (V_v) versus Bitumen Content

Fig. 5 Marshall test apparatus

Fig. 6 Placing of the samples in the water bath

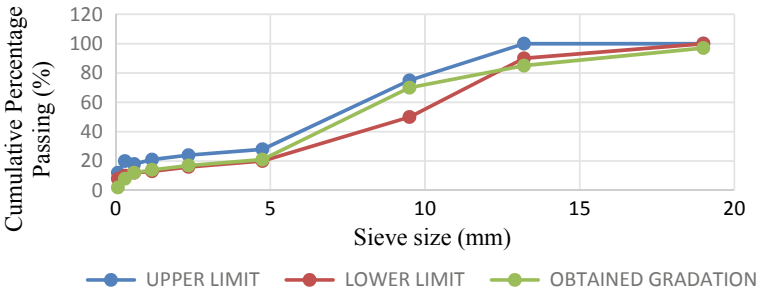

Fig. 7 Conventional SMA gradation curve

The optimum bitumen content (OBC) for the mix design is taken as the bitumen content corresponding to the median of the design limits of Percent Air Voids in the total mix (4%).

4 Results and Discussions

4.1 Aggregate Mix Proportioning

4.1.1 Conventional SMA Mix

From the sieve analysis performed on Aggregates 1(A), Aggregate 2(B) and quarry dust(C), the grain size distribution curve was plotted and the mix proportions were determined by Rothfutch method. The percentage of aggregates A, B and C in total mix were obtained as given below:

$$\text{A} = 20\%, \quad \text{B} = 64\% \quad \text{and} \quad \text{C} = 16\%.$$

The gradation curve for Mix I is within the limits specified in IRC: SP: 79-2008 and is shown in Fig. 7.

4.1.2 Modified SMA Mix

From the sieve analysis performed on 20 mm down CA(A), 20 mm down RCA(B), 10 mm down FA(C) and quarry dust(D), the grain size distribution curve was plotted and the mix proportions were determined by Rothfutch method. The percentage of aggregates A, B, C and D in total mix were obtained as given below:

$$\text{A} = 8\%, \quad \text{B} = 13\%, \quad \text{C} = 61.5\% \quad \text{and} \quad \text{D} = 17.5\%.$$

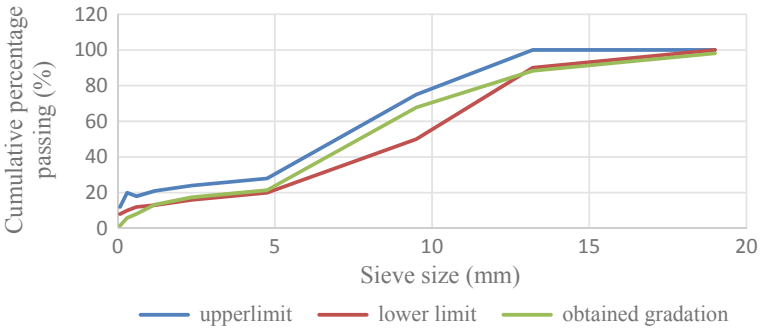

Fig. 8 Modified SMA gradation curve

The gradation curve for Mix II is within the limits specified in IRC: SP: 79-2008 and is shown in Fig. 8.

4.2 Determination of Optimum Bitumen Content (OBC)

4.2.1 Conventional SMA Mix

By plotting Air Voids versus Bitumen content (Fig. 9) graph, the optimum bitumen content for conventional SMA mix was determined. The bitumen content corresponding to 4% air voids is taken as optimum bitumen content and the OBC is 6%. By plotting Stability versus Bitumen content, Flow versus Bitumen content and

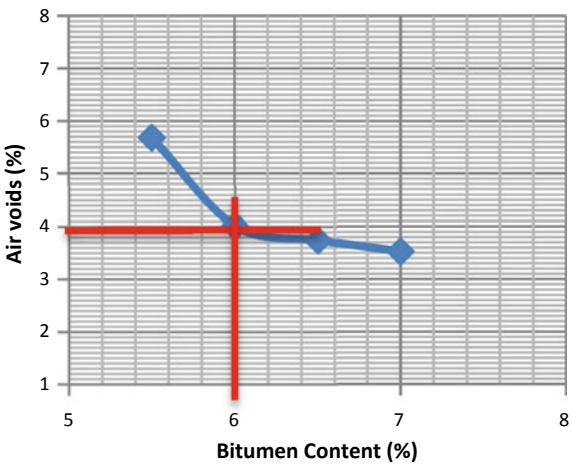

Fig. 9 Air voids versus bitumen content graph for Mix I

Table 1 Marshall and volumetric properties of conventional mix

Bitumen content (%)	Marshall stability (kN)	Flow (mm)	Density (g/cc)	V_v (%)	VMA (%)	Marshall quotient (kN/mm)
5.5	10.166	3.22	2.399	5.683	18.026	3.158
6	12.361	3.45	2.425	4.018	17.565	3.583
6.5	11.956	3.575	2.416	3.745	18.301	3.346
7	10.03	4.35	2.406	3.529	19.067	2.306

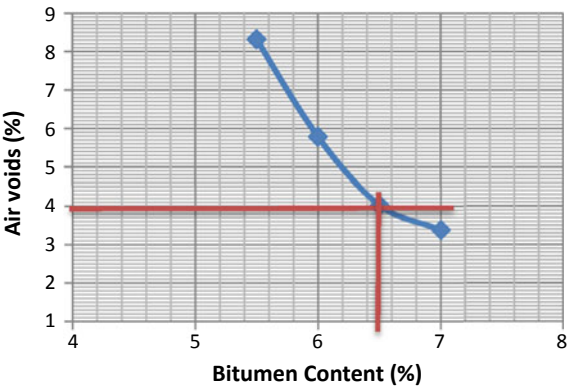

Fig. 10 Air voids versus bitumen content graph for Mix II

Density versus Bitumen content graphs, the Marshall and other volumetric properties were found for the evaluating the performance of the mix. The data presented in Table 1 is based on an average value of two specimens.

4.2.2 Modified SMA Mix

By plotting Air Voids versus Bitumen content (Fig. 10) graph, the optimum bitumen content for modified SMA mix was determined. The obtained OBC is 6.5%. Stability versus Bitumen content, Flow versus Bitumen content and Density versus Bitumen content graphs were plotted to find the Marshall and other volumetric properties. The data presented in Table 2 is based on an average value of two specimens.

4.3 Comparison of Conventional and Modified SMA Mix

The comparison of the prepared Conventional and Modified SMA mixes are shown in Fig. 11.

Table 2 Marshall and volumetric properties of modified mix

Bitumen content (%)	Marshall stability (kN)	Flow (mm)	Density (g/cc)	V_v (%)	VMA (%)	Marshall quotient (kN/mm)
5.5	11.095	3	2.094	8.39	19.095	3.699
6	13.284	3.175	2.14	5.788	17.748	4.184
6.5	13.581	3.35	2.171	4.027	17.018	4.055
7	11.771	4.225	2.168	3.382	17.407	2.786

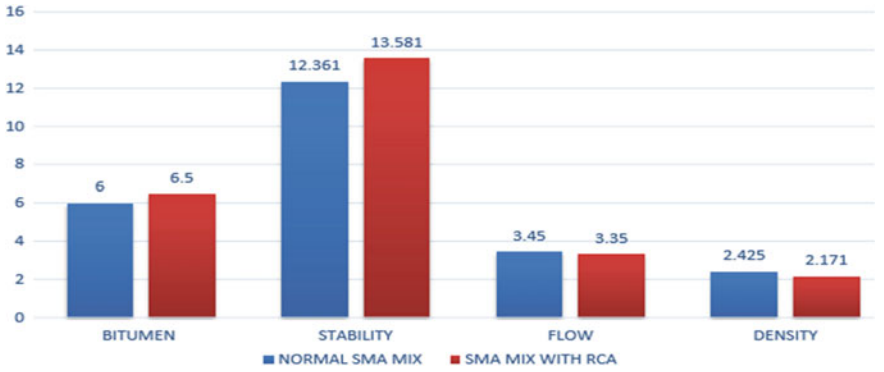

Fig. 11 Comparison of conventional and modified SMA mix

Following conclusions were obtained after the comparison of the conventional and modified SMA mixes:

- **Marshall Stability**

SMA mix with RCA shows better stability value when compared with the reference mix. Due to the interlock of aggregates, the stability has increased by 9.87%.

- **Flow value**

Flow value increases with increase in bitumen content. Generally increase is slow, but later with increase in bitumen content flow value increases. The flow value of SMA mix with RCA has decreased by 2.9%.

- **Air voids**

Since recycled aggregates are porous they absorb more asphalt compared to virgin aggregates leaving less quantity of asphalt binder to fill up the volume of voids. As a result, air voids increase with the level of RA addition in the mix.

- **Voids in mineral aggregate**

VMA in mixes made of RCA is higher than the reference mixes which are made of the natural aggregates. As the recycled aggregates are more porous than natural aggregates, they require more asphalt binder to fill in the pores.

- **Density**

The density of the reference mix is higher than the RCA mix as it require more asphalt to achieve density similar to a mix made with natural aggregates. The density value has decreased by 10.47%.

- **Optimum Binder Content**

The presence of the residual cement mortar on the RCA particles results in the formation of a more porous surface texture of RCA, when compared with virgin aggregates. This explains the reason of the higher bitumen absorption of RCA.

5 Conclusion

The primary objective of the study is to evaluate the use of recycled concrete aggregates (RCA) in SMA mixes. Thus the incorporation of RCA in SMA mixes resulted in its increased stability and bitumen content and decreased flow and density.

RCA is a sustainable alternative to natural aggregates. In this study, around 60% of natural aggregates were replaced by RCA. This reduced the cost of production by around 17%. Thus the incorporation of RCA in pavement mixes preserves the natural resources and reduces the C&D waste disposal problems. However, the use of RCA increased the OBC. This is due to the higher bitumen absorption by the porous cement mortar present on RCA. Hence further studies should be carried out on methods to reduce the bitumen consumption and produce sustainable pavement mixes with improved performance.

References

1. Giri JP, Panda M, Sahoo UC (2018) Performance of bituminous mixes containing treated recycled concrete aggregates and modified by waste polyethylene. J Mater Civ Eng ASCE 30:899–910
2. El-Badawy SM, Gabr AR, Abd El-Hakim RT (2019) Recycled materials and by-products for pavement construction. In: Handbook of ecomaterials. Springer
3. Dalhat MA, Al-Abdul Wahhab HI, Al-Adham K (2019) Recycled plastic waste asphalt concrete via mineral aggregate substitution and binder modification. J Mater Civ Eng ASCE 31:1261–1271
4. IRC: SP: 79 (2008) Tentative specifications for stone matrix asphalt. Indian Road Congress

5. IS 73 (2013) Paving bitumen specification. Bureau of Indian Standards, India
6. Panda M, Suchismita A, Giri JP (2018) Utilization of ripe coconut fiber in stone matrix asphalt mixes. Int J Transp Sci Technol 2:289–302
7. Rondón-Quintana HA, Ruge-Cárdenas JC, Farias MM (2018) Behaviour of hot-mix asphalt containing blast furnace slag as aggregate: evaluation by mass and volume substitution. J Mater Civ Eng ASCE 31:364–374

Investigation on Performance of Fly Ash Based Self Compacting Concrete with Metakaolin and Quarry Dust

Elizabeth Jose and Anju Paul

Abstract Self-compacting concrete is a fresh concrete that flows under its own weight and does not require external vibration to undergo compaction. It is used in the construction where, it is hard to use vibrators for consolidation of concrete. The acute shortage and high price of river sand led to the enormous usage of M sand in construction. Use of quarry dust as a fine aggregate is a good alternative to M sand and a better remedy to the disposal of quarry dust. Quarry dust is a by-product from the crushing process during quarrying activities. Large scale of cement production causes the discharge of high amount of carbon dioxide resulting in global warming. This can be reduced by the use of metakaolin, as a partial replacement for cement contributing to higher workability, long term strength and to make concrete more economically available. In this study an attempt is made to study on the M40 equivalent fly ash based self-compacting concrete is partially replacing cement with metakaolin by 10, 15 and 20% of weight of cement and the fine aggregate is partially replacing with quarry dust by 20, 25, 30 and 35% of weight of fine aggregate and in order to evaluate the strength parameters, they are compared with M40 equivalent fly ash based self-compacting concrete.

Keywords Self-compacting concrete · Metakaolin · Quarry dust

1 Introduction

Self-compacting concrete (SCC) is a concrete which can be placed and compacted under its self weight without vibration effort. It has high workability that it can flow under its own weight [1]. SCC mixes usually contain superplasticizer, high content of fines and/or viscosity modifying additive (VMA). The use of superplasticizer maintains the fluidity, the fine content provides stability of the mix resulting in resistance against bleeding and segregation [2]. Self-compacting concrete is a recent development in the construction industry. The utilization of SCC started growing

E. Jose (✉) · A. Paul
Toc H Institute Science and Technology, Arakkunnam, India
e-mail: elizabethjose043@gmail.com

© Springer Nature Switzerland AG 2021

K. Dasgupta et al. (eds.), *Proceedings of SECON 2020*,
Lecture Notes in Civil Engineering 97,
https://doi.org/10.1007/978-3-030-55115-5_10

rapidly, EFNARC, making use of broad practical experience of all members of Europe federation with SCC, has drawn up specification and guidelines to provide a frame work for design and use of high quality SCC during 2001 [3].

Various types of pozzolanic materials that improve cement properties have been used in cement industry for a long time such as Metakaolin (MK). It possesses a high reactivity with calcium hydroxide having the ability to accelerate cement hydration. Metakaolin reacts with the calcium hydroxide during the hydration process of OPC to form the calcium silicate hydrate (C-S-H) gel [4, 5]. The scarcity of good quality natural river sand due to depletion of resources and restriction due to environmental consideration has made concrete manufactures to look for suitable alternative fine aggregate. One such alternative is Quarry Dust (QD), it is generally considered as a waste material after the extraction and processing of rocks can be used as a replacement for fine aggregate [6–8]. The experimental program is designed to investigate the strength of fly ash based self-compacting concrete by replacement of cement with metakaolin at 10, 15 and 20% by weight of cement and replacement of fine aggregate with quarry dust at 20, 25, 30 and 35% by weight of fine aggregate. The slump flow test, T50 test and J ring test were conducted for all mixes to know the fresh property of self-compacting concrete. Compressive strength, Flexural strength and Split tensile strength test was conducted at 7 and 28 days and the values are compared with the values of fly ash based self-compacting concrete.

2 Objectives

The main objective of this investigation is:

- To establish M40 equivalent Fly ash based Self-Compacting Concrete based on strength parameters.
- To evaluate the optimum percentage of Metakaolin in Fly Ash based SCC, the metakaolin is partially replaced at 10, 15 and 20% of weight of cement.
- To evaluate the optimum percentage of Quarry Dust with optimum percentage of Metakaolin in Fly Ash based SCC, the quarry dust is partially replaced at 20, 25, 30 and 35% of weight of FA.
- To analyse the fresh and hardened properties of Fly Ash based SCC with optimum percentage of Metakaolin and Quarry Dust.

3 Materials and Properties

The different material tests used in this investigation and test results of the materials are illustrated in Table 1.

The sieve analysis was done for the gradation of aggregate. From that study the fine aggregate and quarry dust are in zone 2, these can be used for the concrete works. The water absorption is also conducted for coarse aggregate (not greater than 2%)

Table 1 Material properties

Materials	Tests	Test results	Reference code
Cement	Fineness	5%	IS 4031-1988 Part-IV (Reaffirmed 2009)
	Consistency	32%	IS 4031-1988 Part-XI (Reaffirmed 2009)
	Initial setting time	45 min	IS 4031-1988 Part-V (Reaffirmed 2009)
	Specific gravity	3.15	IS 4031-1988 Part-IV (Reaffirmed 2009)
Fine aggregate	Specific gravity	2.68	IS 2386-1963 Part-III (Reaffirmed 2016)
	Water absorption	2.24%	IS 2386-1963 Part III (Reaffirmed 2016)
Coarse aggregate	Specific gravity	2.72	IS 2386-1963 Part-III (Reaffirmed 2016)
	Water absorption	0.354%	IS 2386-1963 Part III (Reaffirmed 2016)
Quarry dust	Specific gravity	2.57	
Fly ash	Specific gravity	2.3	
Metakaolin	Specific gravity	2.6	

and fine aggregate (between 0.3 and 2.5%) and the results are in specified limits, shown in Table 1. Based on these material properties the mix design is carried out.

3.1 Mix Design

The mix designs were carried out for concrete grade 40 MPa based on European Federation for Specialist Construction Chemicals and Concrete Systems (EFNARC) guidelines [9] and IS 10262: 2009 [10] (Table 2).

Table 2 Mix design of specimen with varying percentage of fly ash, metakaolin and quarry dust

Notation	Cement (kg/m^3)	Fly ash (kg/m^3)	Fine aggregate (kg/m^3)	Coarse aggregate (kg/m^3)	QD (kg/m^3)	MK (kg/m^3)	SP (l/m^3)	Water (l/m^3)
F30 (CM)	413	177	848	765	0	0	3.54	200
F30MK10	354	177	848	765	0	59	3.54	200
F30MK15	324.5	177	848	765	0	88.5	3.54	200
F30MK20	295	177	848	765	0	118	3.54	200
F30MK15QD20	324.5	177	679	765	169	88.5	3.54	200
F30MK15QD25	324.5	177	636	765	212	88.5	3.54	200
F30MK15QD30	324.5	177	594	765	254	88.5	3.54	200
F30MK15QD35	324.5	177	551	765	297	88.5	3.54	200

Table 3 Workability results

Mixes	Slump flow (mm)	J-ring (mm)	Passing ability (mm)	T50 slump flow (s)	Remarks (as per ASTM 1621/C 1621 M)
F30 (CM)	681	672	9	2.5	No visible blocking since passing ability values are between 0–25 mm
F30MK10	670	662	8	3	
F30MK15	690	681	9	2.5	
F30MK20	675	667	8	2.8	
F30MK15QD20	715	706	9	2.5	
F30MK15QD25	705	695	10	2.6	
F30MK15QD30	690	682	8	2.9	
F30MK15QD35	674	665	9	3.5	

4 Results and Discussions

4.1 Fresh Properties

The main characteristics of Self-Compacting Concrete are the properties in the fresh state. Several test methods have been developed in attempts to characterize the properties of Self-Compacting Concrete. In this study three properties are used to evaluate the fresh properties of Self-Compacting Concrete, shown in Table 3. F30 represents the SCC containing fly at 30%. F30MK10, F30MK15 and F30MK20 represents the SCC containing MK at 10%, 15% and 20% respectively. F30MK15QD20, F30MK15QD25, F30MK15QD30 and F30MK15QD35 represents the SCC containing QD at 20%, 25%, 30% and 35% respectively. Fresh property tests are done and the fresh properties of SCC satisfies the requirements of EFNARC guidelines.

4.2 Hardened Properties

The properties of hardened SCC were measured in terms of Compressive Strength, Split Tensile Strength test and Flexural Strength Test confirming to IS 516: 1959.

Compressive strength test was conducted on 150 mm × 150 mm × 150 mm concrete cubes as per IS 516: 1959 (reaffirmed 2018) in digital compression testing machine. Compressive strength test was conducted after 7 days and 28 days of curing. The compressive strength of fly ash based self-compacting concrete cubes by varying the percentage of metakaolin and quarry dust is given in Table 4 and Fig. 1. After 28 days of curing the SCC with 15% metakaolin gives the maximum compressive strength, the value is 57.8 N/mm^2 at 28 days. This mix gives 17.4% increase in

Table 4 Compressive strength of self-compacting concrete with different mix

Notation	Compressive strength (N/mm^2)	
	7 days	28 days
F30 (CM)	**36.45**	**49.23**
F30MK10	44.8	57.1
F30MK15	**45.21**	**57.8**
F30MK20	44.01	56.2
F30MK15QD20	35.8	48.2
F30MK15QD25	**37.8**	**50.3**
F30MK15QD30	39.2	52.31
F30MK15QD35	35.9	48.5

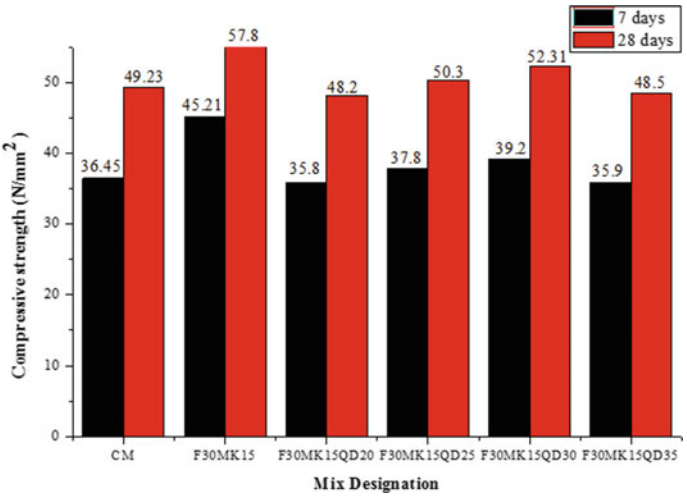

Fig. 1 Variation of compressive strength with optimum percentage of fly ash, metakaolin and varying percentage of quarry dust

strength at 28 days when correlated to control mix. The reasons for improve the compressive strength of SCC is metakaolin reacts with the calcium hydroxide during the hydration process of OPC to form the calcium silicate hydrate (C-S-H) gel and it enhance strength parameters. The compressive strength for 25% QD is 50.3 N/mm^2. This mix gives 14.91% decrease in strength when compared to F30MK15 and 2.17% increase in strength at 28 days when correlated to control mix. The reasons of the improvement in strength is the higher amount of finer particles in the quarry dust act like fillers by filling the voids between cement paste and aggregate and thus increases the strength.

Split tensile strength test was conducted as per IS: 5816: 1999 (reaffirmed 2018) in digital compression test in machine. Split tensile strength test was conducted after 7 and 28 days of curing. The effects of metakaolin in fly ash based self-compacting

Table 5 Split tensile strength of fly ash based self-compacting concrete with varying percentage of metakaolin

Notation	Split tensile strength (N/mm^2)	
	7 days	28 days
CM	**2.8**	**3.9**
F30MK10	3.3	4.2
F30MK15	**3.6**	**4.4**
F30MK20	3.1	4.1
F30MK15QD20	2.9	4
F30MK15QD25	**3.1**	**4.1**
F30MK15QD30	3.3	4.2
F30MK15QD35	2.8	3.9

concrete on the tensile strength are shown in Table 5. The tensile strength value of SCC increases with increase in percentage of cement replacement with metakaolin upto a percentage of 15%. The split tensile strength gain maximum at 15% replacement of cement with metakaolin. The effects of metakaolin and quarry dust in fly ash based self-compacting concrete on the tensile strength are shown in Table 5 and Fig. 2. The split tensile strength is obtained as 4.1 N/mm^2 for 25% replacement.

This mix gives 7.31% decrease in strength when compared to F30MK15 and 5.12% increase in strength at 28 days when correlated to control mix.

Flexural strength test was conducted as per IS 516: 1959 (Reaffirmed 2018) in Universal testing machine. Flexural strength test was conducted after 28 days of curing. The effects of metakaolin in fly ash based self-compacting concrete on the flexural strength are shown in Table 6. The maximum flexural strength is 6.2 N/mm^2 for 15% replacement of metakaolin. The effects of metakaolin and quarry dust in fly

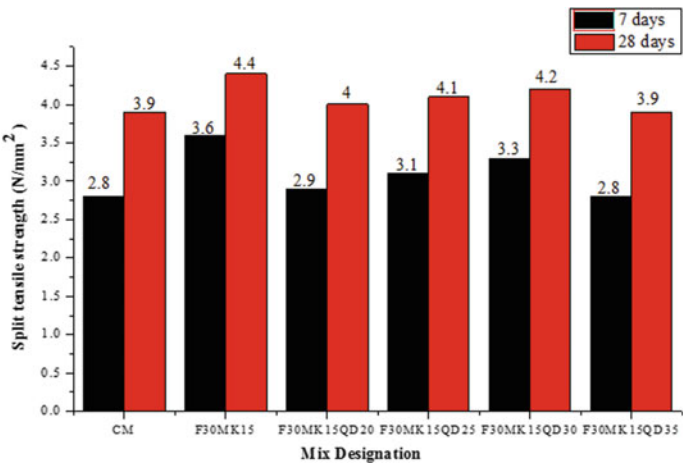

Fig. 2 Split tensile strength of fly ash based self-compacting concrete with optimum percentage of metakaolin and varying percentage of quarry dust

Table 6 Flexural strength of fly ash based self-compacting concrete with varying percentage of metakaolin

Notation	Flexural strength (N/mm^2)
	28 days
CM	**5.4**
F30MK10	5.9
F30MK15	**6.2**
F30MK20	5.5
F30MK15QD20	5.5
F30MK15QD25	**5.7**
F30MK15QD30	5.9
F30MK15QD35	5.3

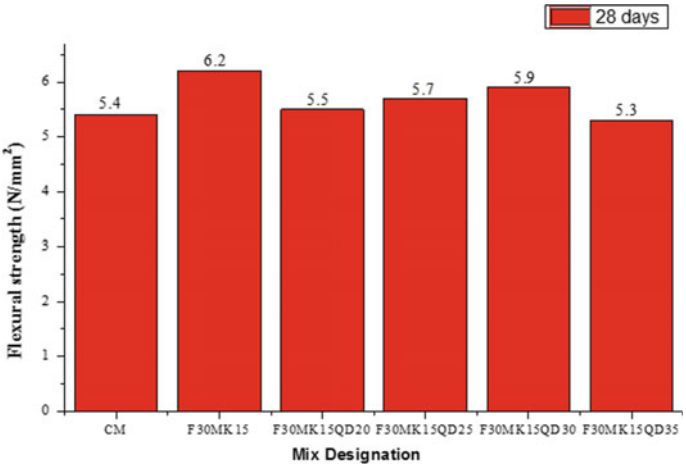

Fig. 3 Flexural strength of fly ash based self-compacting concrete with optimum percentage of metakaolin and varying percentage of quarry dust

ash based self-compacting concrete on the flexural strength are shown in Table 6 and Fig. 3. The flexural strength is 5.7 N/mm^2 for 25% replacement of fine aggregate by quarry dust. This mix gives 8.77% decrease in strength compared with F30MK15 and 5.5% increase in strength at 28 days when correlated to control mix.

5 Conclusions

Based on the experimental investigation, the following conclusions were drawn.

- Mix proportion of SCC is derived with various test conforming to the requirements of Self compacting concrete conforming to the acceptance criteria of SCC and

EFNARC guidelines. Fresh property tests of all the mixes are done and the fresh properties of SCC satisfies the requirements of EFNARC guidelines.

- The control mix can be adopted as F30 based on strength parameters.
- In fly ash based SCC with 15% MK compared with control mix, the compressive strength increased about 17.4% (49.23–57.8 N/mm^2), split tensile strength increased about 12.82% (3.9–4.4 N/mm^2) and the flexural strength is increased about 14.1% (5.4–6.2 N/mm^2) at 28 days.
- Also the fresh properties of SCC with 15% MK satisfies the requirements of EFNARC guidelines.
- The optimum amount of metakaolin was obtained as 15% in terms of compressive strength, split tensile strength and flexural strength. Beyond the optimum replacement level, the strength was reduced, but greater than the control mix.
- The reasons for improve the strength parameters of SCC is metakaolin reacts with the calcium hydroxide during the hydration process of OPC to form the calcium silicate hydrate (C-S-H) gel and it enhance strength parameters.
- In fly ash based SCC with 15% MK and 25% QD is compared with F30MK15, the compressive strength decreased about 14.91% (57.8–50.3 N/mm^2), split tensile strength decreased about 7.31% (4.4–4.1 N/mm^2) and the flexural strength is decreased about 8.77% (6.2–5.7 N/mm^2) at 28 days.
- In fly ash based SCC with 15% MK and 25% QD is compared with control mix, the compressive strength increased about 2.17% (49.23–50.3 N/mm^2), split tensile strength increased about 5.12% (3.9–4.1 N/mm^2) and the flexural strength is increased about 5.5% (5.4–5.7 N/mm^2) at 28 days.
- The optimum amount of quarry dust was obtained as 25% and these values are less than the optimum percentage of metakaolin mix, but greater than control mix.
- The main reason of the improvement in strength parameters is the higher amount of finer particles in the concrete mix, these finer particles of quarry dust act like fillers by filling the voids between cement paste and aggregate and thus strengthen the concrete specimen.
- The use of quarry dust as a replacement for fine aggregate is environmentally helpful and it reduce the construction cost. So the quarry dust is an alternative material for replacing fine aggregate for manufacturing of concrete.
- So it can be concluded that, the fly ash based self-compacting concrete with 15% replacement of metakaolin in cement and 25% replacement of quarry dust in fine aggregate shows greater strength and workability than the control mix. It can be effectively used where compaction is very difficult due to the presence of heavy reinforcements like beams, columns and for structural members with typical architectural requirements.

References

1. Madandoust R, Yasin SM (2015) Fresh and hardened properties of self-compacting concrete containing Metakaolin. J Constr Build Mater 35:752–760
2. Johnsirani SK, Jagannathan AD, Kumar DR (2013) Experimental investigation on self compacting concrete using quarry dust. Int J Sci Res Publ 3:1–5
3. Balamurugan GD, Anish V (2013) Self-compacting concrete with quarry dust as partial replacement for fine aggregate and fly ash for cement with fibre reinforcement. Int Res J Eng Technol 04:1167–1174
4. Gill SA, Siddique R (2018) Strength and micro-structural properties of self-compacting concrete containing metakaolin and rice husk ash. J Constr Build Mater 2:323–332
5. Kannan V (2018) Strength and durability performance of self compacting concrete containing self-combusted rice husk ash and Metakaolin. J Constr Build Mater 160:169–179
6. Chaudhary S, Gupta T, Kothari S, Siddique S, Ravi K (2017) Influence of stone processing dust on mechanical, durability and sustainability of concrete. J Constr Build Mater 223:918–927
7. Rai B, Kumar S, Satish K (2016) Effect of quarry waste on self-compacting concrete containing binary cementitious blends of fly ash and cement. J Adv Mater Sci Eng 1:1–11
8. Rambabu C, Srileela P (2017) Study on partial replacement of fine aggregate by quarry rock fly ash. Int J Eng Res Technol 6:46–53
9. EFNARC (2002) Specification and guidelines for self-compacting concrete, www.efnarce.org
10. IS 10262 (2009) Indian standard concrete mix proportioning- guidelines (First revision). Bureau of Indian standards, New Delhi

Feasibility Study of Plastic Granules and Alccofine in Fly Ash Based Self-Compacting Concrete

Fiona Alias and Tellma John

Abstract Self-compacting concrete (SCC) is a fluidic concrete mix which does not require tamping or vibration and gains its fluid property from high proportion of fine aggregate, super plasticizers and viscosity enhancing admixtures. High amount of cement and chemical admixtures used in SCC reduces its wide scale usage. Alccofine can be used as a better substitute to cement due to its cementitious properties. The work aims at the possibility of recycling waste plastic granules (polyethylene terephthalate (PET) used in the plastic bag production) as a fine aggregate instead of sand in the manufacturing of the self-compacting concrete. Cement is partially replaced with alccofine at 8, 10 and 12% by weight of cement and the optimum percentage of alccofine was obtained. To the mix with optimum percentage of alccofine, the fine aggregate is substituted with the plastic granules at dosages 5, 10, 15 and 20% proportions by the volume of the fine aggregate. The fresh and hardened properties of M40 equivalent fly ash based self-compacting concrete were compared and evaluated.

Keywords Self-compacting concrete · Alccofine · Plastic granules

1 Introduction

Self-compacting concrete (SCC) is a highly flowable type of concrete that spreads into the form without the need for mechanical vibration. Self-compacting concrete is a non-segregating concrete that is placed by means of its own weight.

Supplementary cementitious materials (SCM) are finely ground solid materials that are used to replace a portion of the cement in a concrete mixture [1]. Alccofine is a specially processed product based on slag of high glass content with high reactivity obtained through the process of controlled granulation [2–6].

F. Alias (✉) · T. John
Toc H Institute of Science and Technology, Ernakulam, India
e-mail: fionaaliasnarekattu@gmail.com

© Springer Nature Switzerland AG 2021

K. Dasgupta et al. (eds.), *Proceedings of SECON 2020*,
Lecture Notes in Civil Engineering 97,
https://doi.org/10.1007/978-3-030-55115-5_11

Now- a-days due to constant sand mining the natural sand is depleting at an alarming rate. Scarcity of good quality river sand due to depletion of resources and restriction due to environmental consideration has made concrete manufactures to look for suitable alternative to fine aggregate. The replacement of fine aggregate in the mixture with low cost, recycled plastic granules (PG) which reduces the dead load of the structure, overall cost, in turn reduces the pollution.

The experimental program is designed to investigate the strength of fly ash based self-compacting concrete by replacing cement with alccofine at ratios of 8, 10 and 12% by weight of cement and replacing fine aggregate with plastic granules at 5, 10, 15 and 20% by volume of fine aggregate. The experimental program is aimed to study the workability and strength parameters. Slump flow test, T50 slump flow test and J-ring test were conducted for all mixes to ascertain the fresh property of self-compacting concrete. Compressive strength, Flexural strength, and Split tensile strength test was conducted at 7 and 28 days and the values were obtained.

2 Objectives

The main objectives of this investigation are given below:

- To establish M40 equivalent fly ash based Self-compacting concrete based on strength parameters.
- To establish the optimum percentage of alccofine in the fly ash based SCC, the alccofine is partially replacing the cement in the ratios 8, 10 and 12% by weight of cement in the fly ash based SCC based on strength parameters.
- To evaluate the optimum percentage of Plastic Granules (replacing fine aggregate by volume in the order of 5, 10, 15 and 20%) in the SCC mix with optimum percentage of alccofine.
- To analyse fresh and hardened properties of fly ash based SCC with optimum percentage of alccofine and plastic granules.

3 Materials and Properties

The different materials used in this investigation and their physical properties are illustrated in Table 1.

3.1 Mix Design

There is no standard method for SCC mix design and many academic institutions, admixture, ready-mixed, pre cast and contracting companies have developed their own mix proportioning methods. Several methods exist for the mix design of SCC.

Table 1 Material properties

Materials	Properties	Test results	Reference code
Cement	Specific gravity	3.15	IS 4031-1988 Part-IV (Reaffirmed 2009)
	Fineness	5%	IS 4031-1988 Part-IV (Reaffirmed 2009)
	Consistency	32%	IS 4031-1988 Part-XI (Reaffirmed 2009)
	Initial setting time	45 min	IS 4031-1988 Part-V (Reaffirmed in 2009)
Fine aggregate	Specific gravity	2.72	IS 2386-1963 Part-III (Reaffirmed 2016)
	Water absorption	2.54%	IS 2386-1963 Part-III (Reaffirmed 2016)
Coarse aggregate	Specific gravity	2.67	IS 2386-1963 Part-III (Reaffirmed 2016)
	Water absorption	0.335%	IS 2386-1963 Part-III (Reaffirmed 2016)
Alccofine	Specific gravity	2.9	
	Fineness	>12,000 (cm^2/gm)	
Fly ash	Specific gravity	2.3	
Plastic granules	Specific gravity	1.31	

The mix designs were carried out for concrete grade 40 MPa based on European Federation for Specialist Construction Chemicals and Concrete Systems (EFNARC) guidelines [7] and the details are given in Table 2.

Table 2 Mix design of specimen with varying percentage of fly ash, alccofine and plastic granules

Mix	Cement (kg/m^3)	Fly ash (kg/m^3)	Alccofine (kg/m^3)	Fine aggregate (kg/m^3)	Plastic granules (kg/m^3)	Coarse aggregate (kg/m^3)	SP (l/m^3)	Water (l/m^3)
F30	413	177	0	865	0	753	3.54	200
F30AC8	365.8	177	47.2	865	0	753	3.54	200
F30AC10	354	177	59	865	0	753	3.54	200
F30AC12	342.2	177	70.8	865	0	753	3.54	200
F30AC10PG5	324.5	177	59	839.62	25.38	753	3.54	200
F30AC10PG10	324.5	177	59	814.24	50.76	753	3.54	200
F30AC10PG15	324.5	177	59	788.86	76.14	753	3.54	200
F30AC10PG20	324.5	177	59	763.5	101.52	753	3.54	200

4 Results and Discussion

4.1 Fresh Properties

To determine the fresh properties of SCC, various tests were performed like slump flow, T50 slump flow test time and J-ring test. All these tests were carried out to check passing ability, viscosity/flowability and filling ability self-compacting concrete. All the equipment for various tests confirms to dimension as given by EFNARC. The flow values of different mix proportions are listed in Table 3 in which SCC is the normal self-compacting concrete, F28, F30 and F32 represents the self-compacting concrete containing fly ash at 28%, 30% and 32% respectively. F30AC8, F30AC10 and F30AC12 represents the fly ash based self-compacting concrete with alccofine at 8%, 10% and 12% respectively. And F30AC10PG5, F30AC10PG10, F30AC10PG15 and F30AC10PG20 represents the fly ash-alccofine based self-compacting concrete with plastic granules at 5%, 10%, 15% and 20% respectively.

The slump flow test were conducted for finding the filling ability. For self-compacting concrete with plastic granules, slump flow diameter values varies between 707 and 719 mm, which were determined as the average of two measured diameter of flowed concrete. As per EFNARC [7] test results of self-compacting concrete with plastic granules as fine aggregate can be categorized as SF2, which is suitable for many normal applications such as walls and columns.

T50 slump flow test were conducted for finding the viscosity or flowability of the self-compacting concrete mixes. From Table 3, it can be see that by increasing the plastic granules content decreases the slump flow time. It was determined that all self-compacting concrete mixtures were in the boundaries of the VS2 viscosity specified by EFNARC [7].

J-ring test was conducted for finding the passing ability of SCC mixes. The results of J-ring test are given in Table 3.

Table 3 Workability results

Mixes	T50 slump flow (s)	Slump flow (mm)	J-ring (mm)	Passing ability (mm)	Remarks (as per ASTM 1621/C 1621M)
F30 (CM)	2.5	680	671	9	No visible blocking since passing ability values are between 0 and 25 mm
F30AC8	2.2	703	693	10	
F30AC10	1.9	720	711	9	
F30AC12	2.1	716	706	10	
F30AC10PG5	2.8	707	698	9	
F30AC10PG10	2.6	711	701	10	
F30AC10PG15	2.3	716	708	8	
F30AC10PG20	2.2	719	710	9	

4.2 Hardened Properties

The hardened properties of SCC were measured in terms of Compressive Strength, Split Tensile Strength test and Flexural Strength Test confirming to IS 516:1959 (Reaffirmed 2004), IS: 5816: 1999 (Reaffirmed 2004) and IS 516: 1959 (reaffirmed 2004) respectively.

The 7th and 28th day compressive strength of mixtures is given in Table 4. The optimum percentage of fly ash is found to be 30% and it is taken as the control mix. After 28 days of curing the SCC with 10% alccofine gives the maximum compressive strength. This is due to high pozzolanic nature and unique chemical composition of alccofine [8–10]. Then the compressive strength of self-compacting concrete cubes made with optimum percentage of fly ash, alccofine and varying percentage of plastic granules is tested (Fig. 1) and the range of compressive strength values in this work were about 48.31–41.8 MPa. Decrease in compressive strength was observed as plastic granule content is increased in comparison with the control mix and the mix with fly ash and alccofine without plastic granules. This may be because the plastic granule has lesser density when compared with natural aggregate [11].

Table 4 Compression test results

S. No.	Mix	Compressive strength (N/mm^2)	
		7 days	28 days
1	F30 (CM)	36.56	48.5
2	F30AC8	42.3	51.2
3	F30AC10	45.5	56.6
4	F30AC12	44.6	52.8
5	F30AC10PG5	36.23	48.31
6	F30AC10PG10	34.55	46.21
7	F30AC10PG15	33.36	44.54
8	F30AC10PG20	32.2	41.8

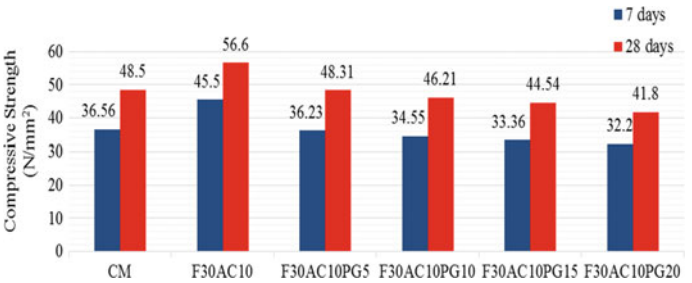

Fig. 1 Variation of compressive strength with optimum percentage of fly ash, alccofine and varying percentage of plastic granules

Split tensile strength test was conducted after 7 and 28 days of mixtures and the tensile strength value of SCC increases with increase in percentage of cement replacement with alccofine upto a percentage of 10%. The tensile strength increases a maximum of 4.86 N/mm^2 for 10% alccofine content and as the alccofine content exceeds the value of 12%, the split tensile strength decreases to 4.35 N/mm^2. The range of split tensile strength values in fly ash-alccofine based SCC with varing percentage of plastic granules were about 3.9–3.4 MPa (Fig. 2). Decrease in split tensile strength was observed as plastic granule content is increased in comparison with the control mix and the mix with fly ash and alccofine without plastic granules. This may due to the poor adhesive strength between the surface of the plastic granules and the cement paste [12–14] (Table 5).

Flexural strength test was conducted after 28 days and the maximum flexural strength is 6.34 N/mm^2 for 10% replacement of alccofine. The range of flexural strength values for fly ash-alccofine based SCC with varying percentage of plastic granules were about 5.32–4.73 MPa (Fig. 3). Decrease in flexural strength was observed as plastic granule content is increased in comparison with the control mix and the mix with fly ash and alccofine without plastic granules. This may due to the low resistance of the plastic granules [12] (Table 6).

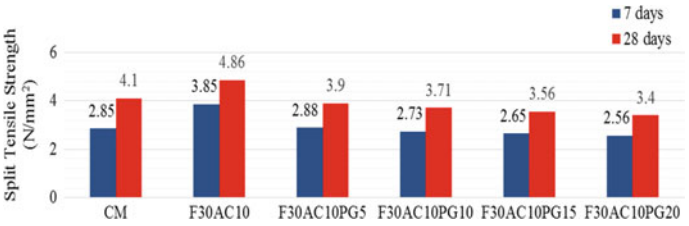

Fig. 2 Split tensile strength of fly ash based self-compacting concrete with optimum percentage of alccofine and varying percentage of plastic granules

Table 5 Split tensile test results

S. No	Mix	Split tensile strength (N/mm^2)	
		7 days	28 days
1	CM	2.85	4.1
2	F30AC8	3.3	4.65
3	F30AC10	3.85	4.86
4	F30AC12	3.45	4.35
5	F30AC10PG5	2.88	3.9
6	F30AC10PG10	2.73	3.71
7	F30AC10PG15	2.65	3.56
8	F30AC10PG20	2.56	3.4

Table 6 Flexural strength results

S. No	Mix	Flexural strength (N/mm^2) (28 days)
1	CM	5.36
2	F30AC8	5.64
3	F30AC10	6.34
4	F30AC12	5.82
5	F30AC10PG5	5.32
6	F30AC10PG10	5.1
7	F30AC10PG15	4.89
8	F30AC10PG20	4.73

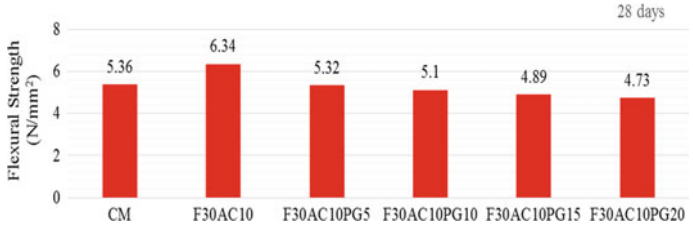

Fig. 3 Flexural strength of fly ash based self-compacting concrete with optimum percentage of alccofine and varying percentage of plastic granules

5 Conclusions

This work intended to analyse the mechanical properties of fly ash based Self-compacting concrete prepared with partial replacement of cement with alccofine and partial replacement of fine aggregate with plastic granules. Based on the results of presented work, the following main concluding remarks are made:

- The utilization of Fly ash as a partial replacement of cement increases the workability of concrete and also reduces the construction cost with efficient utilization of industrial waste.
- The compressive strength, split tensile strength and flexural strength increases with the replacement of fly ash for cement at 30%, so it was adopted as the control mix (optimum percentage of fly ash).
- The result of the fresh-state properties of fly ash based and fly ash-alccofine based SCC fulfilled the workability parameters.
- The optimum amount of alccofine was obtained as 10% in terms of strength parameters. 10% replacement of cement with alccofine showed an increase of 16.7% in compressive strength, 18.29% in split tensile strength and 18.28% in flexural strength compared with control mix. It was due to optimized size, ultra-fine nature (finer than other hydraulic materials), unique chemical composition and high glass content in alccofine.

- Slump flow test results of self-compacting concrete with plastic granules as fine aggregate were categorized as SF2, which is suitable for many normal applications such as walls and columns.
- Test result of T50 slump flow test shows self-compacting concrete with plastic granules mixtures were in the boundaries of the VS2 viscosity.
- The addition of 5% plastic granules into the alccofine-fly ash based SCC decreased the compressive strength by 0.39%, split tensile strength by 5.12% and flexural strength by 0.75% in comparison with control mix.
- Decrease in compressive strength, split tensile strength and flexural strength were observed as plastic granule content increased in comparison with control mix and the mix with fly ash-alccofine based SCC without plastic granules. This may be because the plastic granule has lesser density when compared with natural aggregate and also due to the poor adhesive strength between the surface of the plastic granules and the cement paste.
- So, it can be concluded that, the fly ash based SCC with 10% alccofine and 5% plastic granules gives better strength than the target strength. So it can be effectively replaced with fine aggregate.

References

1. Bernal AS, Juengera GCM, Snellings R (2019) Supplementary cementitious materials: new sources, characterization, and performance insights. Cem Concr Res 122:257–273
2. Gogal A, Sharma D, Sharma S (2016) Utilization of waste foundry slag and alccofine for developing high strength concrete. Int J Electrochem Sci 3190–3205
3. Jamnu MA, Upadhyay SP (2014) Effect on compressive strength of high performance concrete incorporating alccofine and fly ash. Int J Innovative Res Sci Eng Technol 3(2):124–128
4. Jawahar JG, Sashidhar C, Venkata KB (2019) Investigation on ternary blended self compacting concrete using fly ash and alccofine. Int J Recent Technol Eng 7(5S2):447–451
5. Mathur A, Mathur M (2018) Performance of concrete by partial replacement of alccofine – 1203. Int J Eng Res Technol 6(11):1–5
6. Mini KM, Mohan A (2018) Strength and durability studies of SCC incorporating silica fume and ultra-fine GGBS. J Constr Build Mater 171:919–928
7. EFNARC (2002) Specification and guidelines for self-compacting concrete. www.efnarce.org
8. Aggarwal P, Aggarwal Y, Khatana SR (2015) Effect of alccofine on fresh and hardened properties of self compacting concrete. In: National conference on technological innovations for sustainable infrastructure, pp 13–14
9. Anto J, Baby B (2017) Study of properties of self compacting concrete with micro steel fibers and alccofine. Int Res J Adv Eng Sci 2(2):83–87
10. Kala FT, Kavitha S (2016) Evaluation of strength behavior of self-compacting concrete using alccofine and GGBS as partial replacement of cement. Indian J Sci Technol 9(22)
11. Hama MS, Hilal NN (2016) Fresh properties of self-compacting concrete with plastic waste as partial replacement of sand. Int J Sustain Built Environ 6:299–308
12. Aboutaleb D, Maallem M, Safi B, Saidi M (2013) The use of plastic waste as fine aggregate in the self-compacting mortars: effect on physical and mechanical properties. J Constr Build Mater 43:436–442
13. Daraei A, Faraj RH, Sherwani AFH (2019) Mechanical, fracture and durability properties of self-compacting high strength concrete containing recycled polypropylene plastic particles. J Build Eng 25:100808

14. Milehsara DS, Nik SA, Omran LO, Sadrmomtazi1 A (2015) The combined effects of waste PET particles and pozzolanic materials on the properties of self-compacting concrete. J Cleaner Prod 1–17
15. Al-Hadithia AI, Moslehb WK, Noamana AT (2019) Mechanical properties and impact behavior of PET fiber reinforced self-compacting concrete (SCC). Compos Struct 224:1–12

Effect of Magnetized Water with Coconut Fibre Reinforced Concrete

C. Nived, M. Sherin Babu, P. Adithya Das, Noble M. Babu, and P. E. Kavitha

Abstract Sustainability is a wide accepted concept in modern construction scenario. Even though the construction industry is revolutionizing in a significant manner in terms of both equipment and materials used, the cost of construction has skyrocketed along with the deteriorative impact on environment. This resulted in the adoption of a more balanced approach with the environment which lead to the adoption of natural coconut fibre for the strength enhancement in concrete. Coconut fibre is available in abundance, which makes it quite viable as a reinforcement material in concrete. Significant changes in constituents and properties of concrete were initiated and Engineers started using coconut fibre as supplementary materials in concrete, often with adequate considerations. Through research and tests the change in properties of concrete when normal water is replaced by magnetic water is observed. The magnetized water helps in increasing the compressive strength in concrete and the problem of shrinkage crack formation due to the higher heat of hydration is eliminated by the addition of coconut fibre [1]. Addition of Coconut fibre helps in increasing the flexural strength of concrete. The magnetized water contributes to higher strength characteristics of the concrete and fibre being natural in origin is ecologically sustainable and can bring down the global carbon footprint quite effectively.

C. Nived (✉) · M. Sherin Babu · P. Adithya Das · N. M. Babu · P. E. Kavitha
Department of Civil Engineering, Federal Institute of Science and Technology (FISAT), Ernakulam 683577, India
e-mail: cnived02@gmail.com

M. Sherin Babu
e-mail: sherinmukkungal@gmail.com

P. Adithya Das
e-mail: padithyadas@outlook.com

N. M. Babu
e-mail: noblebabu588@gmail.com

P. E. Kavitha
e-mail: kavithapurakat@gmail.com

© Springer Nature Switzerland AG 2021

K. Dasgupta et al. (eds.), *Proceedings of SECON 2020*,
Lecture Notes in Civil Engineering 97,
https://doi.org/10.1007/978-3-030-55115-5_12

Keywords Magnetized water · Coconut fibre · Sustainability · Reinforcement material · Compressive strength · Flexural strength

1 Introduction

Concrete is most widely used man-made construction material in the world. Recent studies show variation strength of concrete with type of water used. The construction industry is revolutionizing in two major ways. One way is the development of construction techniques, such as using automated tools in construction. The other is the advancement in high-performance construction materials, such as the introduction of high strength concrete. Among these high-performance materials, fibre reinforced concrete (FRC) is gradually gaining acceptance from civil engineers. In recent years, research and development of fibers and matrix materials and fabrication process related to construction industry have grown rapidly. Their advantages over other construction materials are their high tensile strength to weight ratio, ability to be molded into various shapes and potential resistance to environmental conditions, resulting in potentially low maintenance cost. These properties make FRC composite a good alternative for innovative construction. They are also non-abrasive in nature, cheap and easily available. Research work is being carried out to find the possibility of coconut-fibre as a vertical reinforcement in mortar-free interlocking structures. This is believed to be a cost-effective solution to earthquake-resistant housing. This study aims to investigate the effect of using magnetized water on concrete reinforced with processed coconut fibre. The objective is to compare the engineering properties of magnetized water concrete and concrete with ordinary tap water.

2 Constituent Materials

The constituent materials used are cement, coarse aggregates, fine aggregates, magnetized water, and coconut fiber.

Cement used was OPC 53 grade Dalmia cement. Tests were conducted to make sure that the cement was up to the Indian standard of specification. The Specific gravity of Cement was found out to be 3.19. Fineness modulus was 6% and the initial setting time of cement mortar was 42 min.

M-sand was used as fine aggregate. Tests were conducted and the results obtained are mentioned bellow: Specific gravity: 2.5, Fineness modulus: 2.7, Water absorption: 1.10% and conforming to grading zone-II (Fig. 1).

Coarse aggregate of 20 mm nominal size were used and the specific gravity was found out to be 2.71. The water absorption was 0.6%. The results of tests were acceptable and the materials were proven to meet the required standards.

The admixture used is Viscosity modifying admixture (VMA). Coconut fibre was processed and combined before adding.

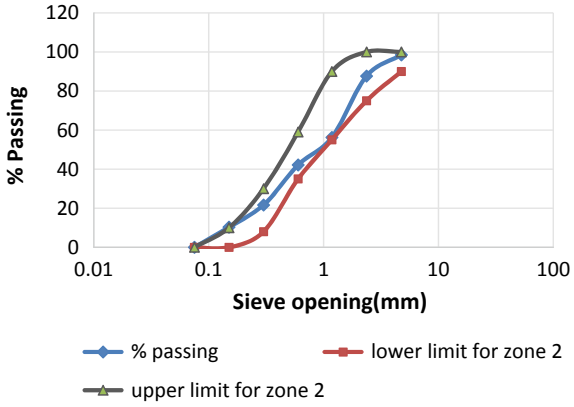

Fig. 1 Particle distribution curve for fine aggregate

2.1 Magnetized Water

For magnetizing water it is circulated through a magnetic field of 1 T. The effect of magnetizing is influenced by the time of exposure [2]. Water is magnetized for 24 h, 48 h, 72 h and 96 h. The magnetic field can break down these water clusters and reduce the bond angle and hence increase solubility [3]. The magnetized water shows greater value for pH. In other words pH value indicates whether the water is magnetized or not.

PermagN-406 is for magnetizing water at constant magnetic field. The set up consist of a motor, pumps for circulating water and a magnetizer (Fig. 2). The exposure time for magnetizing was 24 h, 48 h, 72 h and 96 h [4].

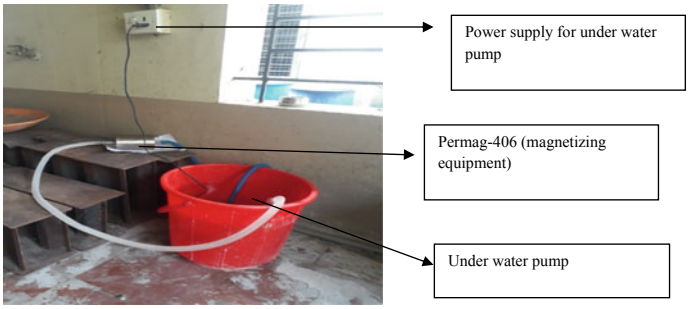

Fig. 2 Magnetization setup

2.2 Coconut Fibre (Fig. 3)

The advantages of coconut fibre are its low cost, reasonable specific strength, low density, ease of availability, enhanced energy recovery, biodegradability and its ability to be recycled in nature in a carbon neutral manner [5].

3 Test on Material Properties

On Magnetized Water:

PH and Hardness test: Increase in pH value will change the nature of water from acidic to basic which decreases the corrosion rate (Fig. 4) [6]. Hardness decreases with magnetization which shows induction of magnetic flux in water changes the property of hardness (Fig. 5) [7].

Fig. 3 Processed and combed coconut fibre

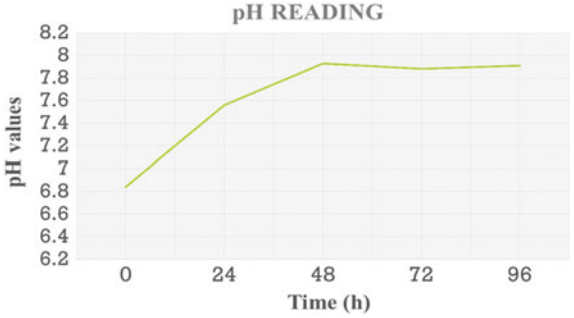

Fig. 4 Variation of pH value with duration of applied magnetic flux

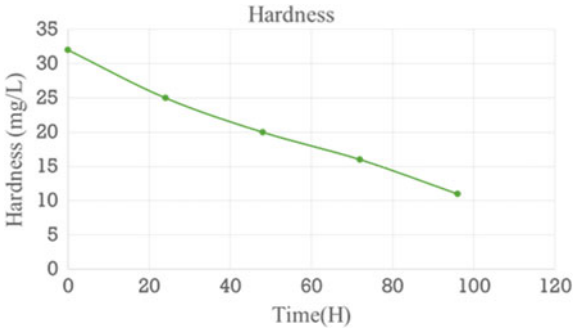

Fig. 5 Variation of hardness with duration of applied magnetic flux

On Coconut Fibre:

Water absorption test: Obtained water absorption is 111.76%.

Workability: Good workability of 18.75% is obtained for magnetized concrete mix with coconut fibre when comparing to normal water concrete with coconut fibre.

4 Test Procedure

Tests on cement, coarse aggregate and fine aggregate are conducted to ensure that they meet quality standards. Water is magnetised and tested using the pH meter.

Mix design used as per IS 10262:2019 [8] is of M 20 grade, cement grade: 53, size of aggregate: 20 mm, W/C: 0.45 (by experience) using viscosity modifying admixture as chemical admixture. Trial and error method is adopted to arrive at the suitable normal concrete mix. Hence arrived at different mix proportions, Trial mix 1 = 1:3.7:2.04:0.45, Trial mix 2 = 1:3.23:1.76:0.4, Trial mix 3 = 1:2.95:1.62:0.4 the strength of which is tabulated below (Table 1).

From the obtained values it is evident that trial mix 3 has greater strength and good workability than the other two mixes hence arrived at trial mix 3.

Compressive strength of cubes (M20 grade)are tested with specimens made with magnetized water with varying magnetising time (0 h, 24 h, 48 h, 72 h, 96 h). The optimum time for magnetisation is obtained. Concrete mix is made with varying

Table 1 Compressive strength of trial mix done in concrete cubes (Fig. 6)

Mix	7th day strength (MPa)	28th day strength	Slump
Trail mix 1	16.07	17.00	Shear slump (65 mm)
Trail mix 2	19.29	21.64	Shear slump (78 mm)
Trail mix 3	20.89	29.71	True slump (98 mm)

Fig. 6 Cubes for testing

coconut fibre content (3%, 5%, and 7%) and tests are conducted. Sustainable concrete mix is obtained.

5 Result and Discussions

5.1 Effect of Magnetized Water on Concrete

The compressive strength of cube specimens is obtained from compression testing machine. Instead of normal water the water is magnetized for 24 hrs, 48 hrs, 72 hrs and 96 hours for casting cubes to get desirable result (Fig. 7). The compressive strength of magnetized concrete is tabulated below

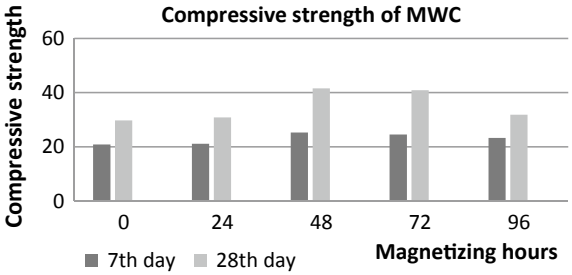

Fig. 7 Compressive strength versus magnetization hours

Table 2 Increase in strength of 7th and 28th day of MWC (cube test)

Magnetization (h)	pH of water	7th day compressive strength (MPa)	Increase in strength (%)	28th day compressive strength (MPa)	Increase in strength (%)
0	6.84	20.89	–	29.71	–
24	7.56	21.12	1.11	30.87	3.90
48	7.93	25.29	21.06	41.60	40.02
72	7.82	24.51	17.33	40.90	37.66
96	7.43	23.31	11.58	31.83	7.14

Table 3 28th day flexural strength on magnetized water concrete

Specimen No.	Flexural strength	Average
1	3.4	3.53
2	3.8	
3	3.8	

5.2 Effect of Magnetized Water Without Coconut Fibre

Flexural strength test after 28 days of curing was performed on 3 beams of magnetized water concrete. The results are tabulated below

5.3 Effect of Magnetized Water Concrete with Coconut Fibre

Trial mix 1 and trial mix 2 gave shear slump of 65 mm and 78 mm respectively (Table 1), which are not within the range. Hence were rejected. In trial mix 3 mix proportion obtained is1:1.61:2.95:0.4, slump obtained is 98 mm using 3.96 mL admixture, which is in the required range. The 28th day Strength obtained is 29.71 MPa. Hence it is accepted. PermagN-406 is used as the magnetizer. Increased strength of 21.06% and 40.02% were obtained in 48 h and after there is a decrease of 3.01% and 2.36% in 7th and 28th day's compressive strength respectively (Table 2). For 2.5 cm fiber [9] Optimum flexural strength is obtained for 5% of coconut fibre (Table 4; Fig. 8).

6 Conclusions

The following conclusions are derived based on the present study;

- It is observed that magnetization of water from zero to 96 h increased pH from 6.84 to 7.91. Hence it is inferred that the process of magnetization causes an

Table 4 28th day flexural strength of 48 h magnetized water concrete (coconut fibre induced)

Length	Percentage of coconut fibre (%)	Specimen No.	28th day flexural strength	Average
2.5 cm	3	1	4.20	4.26
		2	4.40	
		3	4.20	
	5	1	5.80	5.73
		2	5.80	
		3	5.60	
	7	1	4.40	4.53
		2	4.60	
		3	4.60	

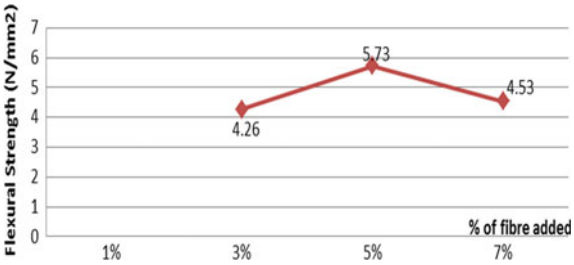

Fig. 8 Graph showing variation of flexural strength with % fibre added

increase in pH value of water making the water more basic in nature and is highly recommended in concreting.

- It is also observed that the slump of concrete mix increased from 98 to 100 mm when magnetized water is used instead of ordinary water. Hence magnetized water is recommended in concrete to improve the workability of concrete.
- Coconut fibre, a sustainable addition to improve the flexural strength of concrete has been selected for the present investigation and its disadvantage of excessive water absorption of 11.5% is overcome by using saturated surface dry coconut fibre instead of dry fibre.
- A commonly observed disadvantage of fibre reinforced concrete is its reduced workability [10]. In the present study the slump value of 80 mm is increase to 85 mm. Thus the disadvantage of fibre reinforced concrete is overcome in the present study by the incorporation of magnetic water.
- Studies on strength characteristics showed that Increased strength of 21.06% and 40.02% were obtained in 48 h magnetization and after there is a decrease of 3.01% and 2.36% in 7th and 28th day's compressive strength respectively (Table 4).
- Based on the studies it is evident that coconut fibre reinforced shows an increased compressive strength and flexural strength (Fig. 8) compared to ordinary concrete

and its disadvantage of low workability can be overcome by the use of magnetized water.

References

1. Sher Mohammed, Rima Das (2011) Strength of concrete with added natural substitutes, World Journal of Engineering (WJE). Department of civil engineering NIT, Agarthala
2. Bharath S, Subraja S, Arun Kumar P (2016) Influence of magnetized water on concrete by replacing cement partially with copper slag. JCPS 9(4)
3. Holysz L, Szczes A, Chibowski (2007) Effects of a static magnetic field on water and electrolyte solutions. J Colloid Interface Sci
4. Su N, Wu Y-H, Mar C-Y (2000) Effect of magnetic water on the engineering properties of concrete containing granulated blast-furnace slag. Cem Concr Res 30
5. Aditya Tom (2015) Coconut Fibre Reinforced Concrete. [Online] 64,1–100. Available: https://www.researchgate.net/publication/275407239_Coconut_Fibre_Reinforced_Concrete
6. Hamza bem amor, Anish Elaoud1, Mahmoud Hayzn (2018) Does magnetic field effect water pH, Asian Res J Agric Art 8(1):39196
7. Banejad H, Abdosalehi E (2009) The effect of magnetic field on water hardness reducing. In: Thirteenth international water technology conference, vol 29
8. IWTC Indian standard recommended guidelines for concrete mix design, IS 10262-2019, Bureau of Indian standards, New Delhi
9. Srinidhi P, Gokulapriya K, Parthiban P (2019) Experimental study on strength enhancement of concrete by using magnetic water and coconut fiber. Int Res J Eng Technol (IRJET) 06(04). e-ISSN: 2395-0056
10. Shivkumar GL, Vasudevan AK (2009) Strength and stiffness response of coir fiber-reinforced tropical soil. J Mater Civ Eng 20(9)

Seismic Performance of Oblique Columns in High Rise Building

Nikha Santhosh and Gayathri Krishna Kumar

Abstract Nowadays various construction techniques are adopted in order to increase the seismic performance of the building. The latest technology of "weak beam and strong column" is given more importance and hence the columns in a seismic resistant structure play a vital role in assessing the overall strength of the building against the effect of seismic forces. Oblique Column is the column, which neither parallel nor at right angles to a specified line, means they are slanted or rotated at an angle. In this paper, seismic performance of Y shaped oblique column in symmetrical and asymmetrical high rise building was studied using Etabs 2016 software and was compared with conventional column building. Space utilisation achieved by adopting Y shaped column was also studied. Optimum angle of inclination of Y was investigated. Parameters like maximum displacement, storey drift, time period of high rise building with Y shaped were studied by performing time history analysis and compared with conventional column building.

Keywords Oblique column · Y shaped column · Etabs · Time history analysis

1 Introduction

The level of high-rise buildings is an important indicator of technological strength. With the continued development and progress of economy, technology and material in recent years, pretty a few countries are conceived to design and built more and higher buildings [1]. Due to the large population and small per capita area, the needs of high-rise buildings become much more urgent. By the various architectural

N. Santhosh (✉) · G. K. Kumar
Federal Institute of Science and Technology, Angamaly, Ernakulam, India
e-mail: nikhasanthosh9@gmail.com

G. K. Kumar
e-mail: gaya3krishnakumar92@gmail.com

© Springer Nature Switzerland AG 2021

K. Dasgupta et al. (eds.), *Proceedings of SECON 2020*,
Lecture Notes in Civil Engineering 97,
https://doi.org/10.1007/978-3-030-55115-5_13

features and style, more and more complex high rise buildings are appearing. High rise structures can be one that by virtue of height is affected by lateral forces due to wind or earthquake or sometimes both [2].

In any type of structure, the basic purpose of all kinds of structural systems is to transfer gravity loads effectively. Dead loads, live load and snow load are the most common loads resulting from the effect of gravity. Other than these vertical loads, buildings are also subjected to lateral loads caused by wind, blasting or earthquake. Because of lateral loads, high stresses in structure or sway movement or vibration can occur [3]. Therefore, structure should have sufficient strength against vertical loads together with adequate stiffness to resist lateral forces. Conventional seismic design attempts to make buildings that do not collapse under strong earthquake shaking, but may sustain damage to non-structural elements and to some structural members in the building. This may render the building non-functional after the earthquake, which may be problematic in some structures, like hospitals, which need to remain functional in the aftermath of the earthquake [3, 4]. The latest technology of "weak beam and strong column" is given more importance and hence the columns in a seismic resistant structure play a vital role in assessing the overall strength of the building against the effect of seismic forces [5, 6]. The use of oblique columns instead of normal columns is an innovative technique to increase the seismic resistance of high rise building [1, 5, 6].

A vertical structural member subjected to axial compression in the majority with some or no moment is termed as a column. The Oblique Column is the column, which neither parallel nor at right angles to a specified line, means they are slanted or rotated at an angle [2, 7–9]. In recent years, many buildings are constructed in irregular structure system with inclined columns. Inclined columns are originated from the category of structural framing members gravity load loaded columns and can be applied to both rigid as well as braced frames [5]. In this paper, the seismic performance and space utility that can be achieved by adopting Y shaped oblique columns was studied.

2 Methodology Adopted

A 3D model is created using Etabs 2016 with conventional column. Design check is carried out for each model to determine the maximum span length that the column can carrying safely. All columns are replaced by Y shaped column by providing inclined members, in the failure models. Space utilisation acquired by using Y columns and amount of concrete required is estimated. Non-linear dynamic analysis using time history analysis is performed to study the seismic behaviour of structure with Y columns. The results based on the parameters, maximum storey displacement, storey drift and time period are evaluated to arrive at conclusions. The time history function data entered for analysis process was that of El Centro California.

3 Modeling of Structure

G + 14 storey building of plan dimension 34 m × 16 m is modelled. Storey height is taken as 3 m. All beams are of the size 300 mm × 450 mm and column size is mm 300 mm × 800 mm. M30 grade concrete and Fe 500 steel is used for the structural members. Slab thickness is considered as 125 mm. Models having same building layout with different column spacing is modelled with conventional to determine the maximum span length that can be provided between the normal columns safely. Table 1 shows the various models created to determine the maximum span length that can be provided between the normal columns and to estimate the reduction in the number of column when Y column is used.

Columns are modified into Y shape, where the normal columns fail by providing two symmetrical inclined members on either side of the column. Inclined members are provided at a slope of 1V: 2H. Figures 1 and 2 shows the plan view of all the models with rectangular and Y column respectively.

To study the seismic behaviour of building with Y column, models with various angle of inclination with respect to the vertical axis at two different depth from the ceiling is created. Table 2 shows the various model created for the analysis.

3.1 Loading

A live load of 4 kN/m^2 is applied as per IS: 875 (Part II) 1987 and the dead load is software assigned. Lateral loads are applied as seismic load in X and Y direction as per IS 1893 (Part 1 2002). The design earthquake load is computed based on the zone factor of 0.24, medium soil, importance factor of 1 and the response reduction factor of 5. The support conditions are assumed as fixed.

Table 1 Models

Model ID	Type of column	No. of bays in X direction	Length of longer span
MR1	Rectangular	7 (Unequal spacing)	6
MR2	Rectangular	6 (Equal spacing)	6
MR3	Rectangular	5 (Unequal spacing)	8
MY1	Y	5	8
MR4	Rectangular	5	10
MY2	Y	5	10

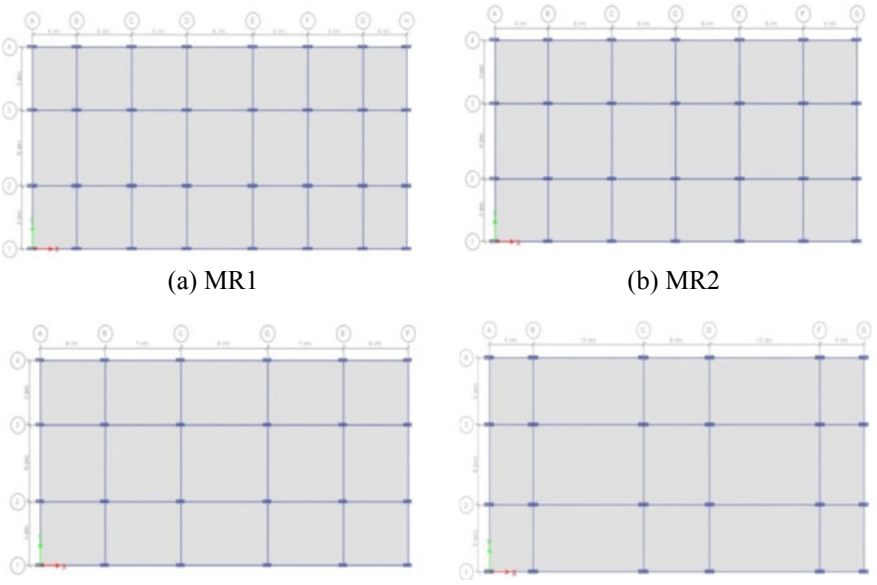

(a) MR1 (b) MR2

(c) MR3 (d) MR4

Fig. 1 Plan view of models with rectangular columns

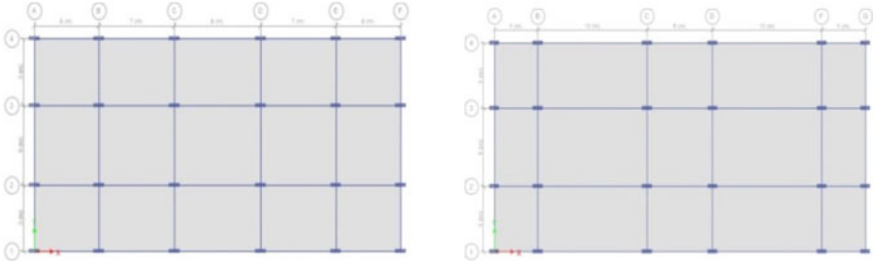

(a) MY1 (b) MY2

Fig. 2 Plan view of models with Y columns

4 Analysis and Discussion

To estimate the reduction in the number of columns, design check is carried out in Etabs. Seismic behaviour of models with Y shaped columns is studied by conducting time history analysis.

Table 2 Y column models

Model Id	Angle of inclination (°)	Depth of inclination (m)
AY10	10	1
AY20	20	
AY30	30	
AY40	40	
AY45	45	
AY50	50	
AY55	55	
AY60	60	
BY10	10	
BY20	20	
BY30	30	1.5
BY40	40	
BY45	45	
BY50	50	

4.1 Design Check Results

Design check was performed in all the modelled structures. Overstressed beam and failure of columns were identified using the design check process which will be indicated in red colour and pink colour indicates that all members passed the design check. In MR1, MR2 all the rectangular column and beam members pass the design check. So the members provided are sufficient to carry the loads safely. In MR3 and MR4 members in the longer span undergo failure. Maximum spacing that can be provided between the normal columns is found as 6 m.

In models MR3 and MR4 all the columns, except the corner columns are replaced by Y shaped columns. Figure 3 shows the plan view design check results of model MY1 and MY2.

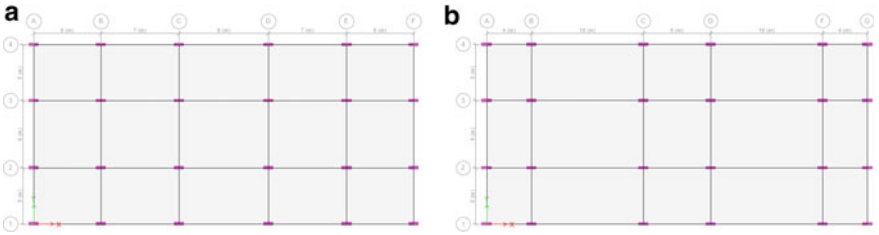

Fig. 3 **a** Design check of model MY1. **b** Design check of model MY2

Table 3 Comparison of rectangular and Y shaped columns

	Normal columns	Y shaped columns	Percentage change (%)
No. of columns	32	24	25
Column free space area	428.8 m^2	472 m^2	10.07
Quantity of concrete	1861.25 m^3	1937.614 m^3	4.06

And it is seen that all the members passed the design check (indicated by pink colour). So the members provided are sufficient to carry the loads safely. Table 3 shows the comparison between rectangular and Y shaped columns.

Comparing the model MR1 and MY2, in which the beam column layout remains the same, 32 numbers of rectangular columns, can be replaced by 24 Y columns of same cross section. The reduction in the number of columns increases the column free space, thereby increase the floor utility. Quantity of concrete required for the whole structure was also determined.

4.2 Seismic Analysis Results

Maximum storey displacement, storey drifts and time period are determined by using time history analysis, at different angle of inclination of Y column and at two different depths. Figures 4 and 5 shows the maximum storey displacement obtained along longer direction at a depth of 1 m and 1.5 m respectively.

Maximum displacement obtained for the base model (MR1) is 23.16 mm. Maximum displacement is found to be minimum at an inclination of 50° and 40° when depth is 1 m and 1.5 m respectively.

Storey drift of the base model is obtained as 0.000626. Storey drift goes on decreasing up to 50° and 40° inclination in two cases. Beyond this, there is a slight increase in the drift values. Figures 6 and 7 shows the storey drift obtained for the models at two different depths.

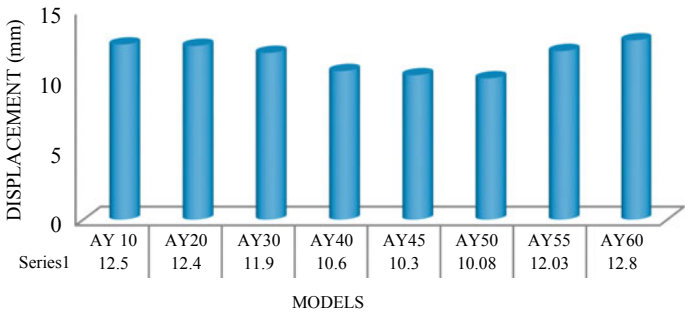

Fig. 4 Maximum storey displacement for models at an inclination depth of 1 m

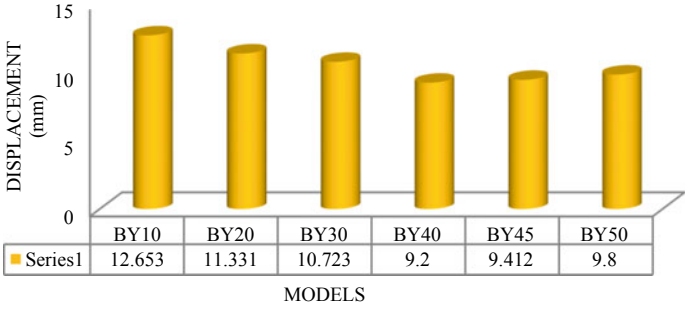

Fig. 5 . Maximum storey displacement for models at an inclination depth of 1.5 m

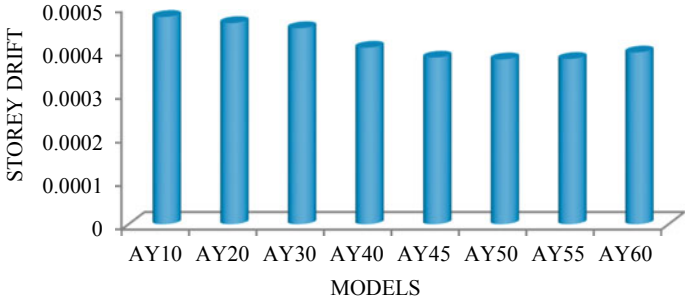

Fig. 6 Storey drift for models at an inclination depth of 1 m

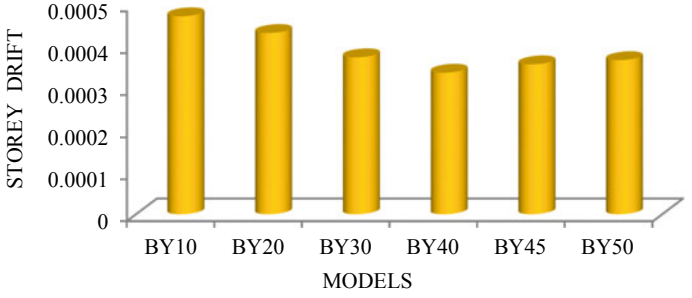

Fig. 7 Storey drift for models at an inclination depth of 1.5 m

Time period of the base model is obtained as 2.18 s. At 50° inclination time period is obtained as 1.635 s and on further increase in the angle of inclination time period goes on increasing for the models having depth 1 m. When the depth of inclination is 1.5 m, time period obtained as 1.419 s for 40° inclination.

While comparing the three parameters, optimum angle of inclination is obtained as 50° and 40° for a depth of 1 m and 1.5 m respectively. Among the two models,

Table 4 Comparison of the seismic performance of optimum Y models and normal column

	Normal column	Y columns	
		A	B
Max. storey displacement (mm)	23.16	10.08	9.2
Storey drift	0.000626	0.000379	0.000337
Time period (sec)	2.18	1.635	1.419

Y column provided at a depth of 1.5 m with an angle of inclination 40° gives better seismic performance. Table 4 shows the seismic performance comparison of optimum models.

5 Conclusions

Based on the limited study of the seismic performance of oblique column in G + 14 storey building, following conclusions can be drawn:

- By adopting Y shaped column the number of normal columns can be reduced by 25%. Hence, floor area can be increased by 10%, but there is a 4% increase in the quantity of concrete.
- Seismic resistance of the structure can be increased by replacing normal columns with Y shaped columns.
- Y columns provided at a depth of 1 m shows better performance when the angle of inclination is 50° and for columns provided at a depth of 1.5 m better performance is shown at an angle of 40°.
- Among the two optimum models, y column provide at 1.5 m depth and at an inclination of 40° show better seismic performance. There is decrease of 60.27% in maximum displacement, 46.16% in storey drift and time period get reduced by 31%.

References

1. Hua K, Yang Y (2012) Study on high-rise structure with oblique columns by ETABS, SAP2000, MIDAS/GEN and SATWE. Procedia Eng 31:474–480
2. Jaiswal M, Prusty SD (2017) A Comparative analysis on zigzag structure with varia tion in inclination angle of column subject to lateral load. In: The international conference on composite materials and structures. Indian Institute of Technology, Hyderabad
3. Bagheri B, Firoozabad ES (2012) Comparative study of the static and dynamic analysis of multi-storey irregular building. Int J Civ Environ Eng 6(11)
4. Todorovska MI (1999) Base isolation by a soft first story with inclined columns. J Eng Mech 125(4):448–457
5. Rouzmehr F, Saleh Jalali R (2014) Response of buildings with inclined first-story columns to near-fault ground motion. J Rehabil Civ Eng 2–1:19–34
6. Reddy KN (2017) A study on multi-storeyed building with oblique columns by using ETABS. Int J Innovative Res Sci Eng Technol 6
7. Radha BP, Vijaya GS (2018) Seismic analysis of RCC structure with inclined additional columns at corner columns. Int J Civ Eng Technol (IJCIET) 9(6)
8. Abhilash AS, Keerthi Gowda BS (2016) A comparative study of multi-storey RC structures with Y-shaped columns. In: International conference on trends and recent advances in civil engineering, TRACE 2016
9. Narayanan V, Aiswarya S (2017) Effect of oblique column and viscous damper on podium structure using Etabs. Int Res J Eng Technol (IRJET) 04(05)

Experimental Investigation on the Performance of Self Compacting Concrete Using Copper Slag

Ajana Prince and M. Preethi

Abstract Copper manufacturing industry produces bulk quantity of copper slag as an industrial by-product. Its management and disposal is a major challenge for the environment, thus an urgent need for its potential alternative is recommended. The intent of the current work was to design self-compacting concrete mixes incorporating copper slag as fine aggregate replacement. Self-compacting concrete is a highly flowable type of concrete that spreads into the form and compact without the need for external vibration. Self-compacting concrete was developed as per IS 10262:2019 using copper slag as fine aggregates with partial and full replacement of sand. Five different SCC mixes with 0% as control mix, 10%, 20%, 30%, 40% and 50% of copper slag substituting sand were cast and tested for both fresh and mechanical properties. The results obtained indicates that the flowability and passing ability of SCC mixes enhanced as the content of copper slag increased. Compressive strength and split tensile strength were also increased as the content of copper slag enhanced. A substitution of up to 40% copper slag as a sand replacement yielded compressive strength of about 41.23 MPa.

Keywords SCC · Copper slag · Flyash · Fine aggregate

1 Introduction

Self-compacting is the newest innovating category of high performance concrete characterized for its unique quality to flow and compact by itself under its own weight in highly dense reinforcement without any application of external or internal vibration. The use of relatively high content of binder as well as high dosages of chemicals admixtures as compared to conventional concrete will enhances fluidity

A. Prince (✉) · M. Preethi
Department of Civil Engineering, Federal Institute of Science and Technology (FISAT), Ernakulam 683577, India
e-mail: ajanaprince24@gmail.com

M. Preethi
e-mail: preethiml83@gmail.com

© Springer Nature Switzerland AG 2021

K. Dasgupta et al. (eds.), *Proceedings of SECON 2020*,
Lecture Notes in Civil Engineering 97,
https://doi.org/10.1007/978-3-030-55115-5_14

and maintains its stability without segregation and bleeding [1]. Aggregates perform significant character in enhancing the strength and workability of concrete, as it occupies about 60–70% volume in the concrete matrix. Incorporating huge volume of aggregates in construction possibly will lead to scarcity of aggregates and also cause an interruption for a sustainable environment. To eliminate such environmental obstacles and to overcome the inadequacy of aggregates, either supplementary materials or waste by-products generated from industries can be utilised as aggregates. Copper slag is one such industrial by-product obtained in bulk quantity during matte smelting and refining process of copper metal. In India, nearly 2.4 million tons of copper slag was produced in every year, which shared about 3.5% of world's copper slag [2]. The main objective of this study was to investigate the effect of using copper slag as a partial replacement for sand in self-compacting concrete. The study includes the following tasks:

- Evaluate the effect of copper slag replacement on the fresh properties of concrete
- Investigate the effect of copper slag replacement as a fine aggregate on the compressive, tensile and flexural strength of concrete mixes.

2 Materials Used

Ordinary Portland cement of grade 53 conforming IS 8112-1989 and class F flyash con-forming to IS 3812: 1981 is used as cementitious materials. The flyash used is in dry dense form. It is gray to brown in colour. Physical properties and chemical composition and of flyash are given in Table 1. The fine aggregate used are M-Sand having a specific gravity of 2.75 and copper slag with a specific gravity of 3.5 and both of them have comparable gradations, which satisfy grading limit, zone 2 as per IS 383:1970. Copper slag is a by-product material produced from the process of manufacturing copper and its chemical compositions are given in Table 2. The water absorption of copper slag is 0.38% which is very much less when compared to that of M-sand with 1.31%. Figure 1 shows the particle size distribution curve of M-Sand and copper slag. Coarse aggregates of maximum 12.5 mm size were used in SCC mixes. Poly-carboxylate ether-based superplasticizers in liquid form having a specific gravity of about 1.10 is used at a dosage of 0.3–0.8% by weight of cementitious materials to improve workability.

Table 1 Physical properties and chemical composition of flyash

Physical properties		Chemical composition	% of chemical component
Specific gravity	2.2	SiO_2	63.8
Specific surface area	649.9 m^2/kg	Al_2O_3	21.29
Average particle size	22.2 μm	CaO	2.9
Form	Powder	Fe_2O_3	0.39

Table 2 Chemical composition of copper slag

Chemical composition	% of chemical component
FeO	45
SiO_2	28
Al_2O_3	2
CaO	1.5
MgO	1

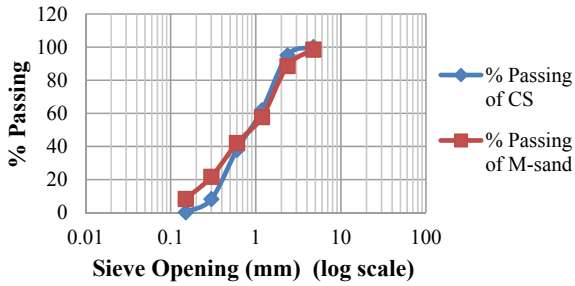

Fig. 1 Particle size distribution curve for fine aggregate

3 Mixture Proportions

M30 control mix was developed according to IS 10262:2019 by trial and error method. Percentage of flyash is fixed same for all mix which is 25%. Class F fly ash is known to control the destructive alkali aggregate reaction when used to replace 15–30% of portland cement and also due to the increased pozzolanic action it mainly helps in the development of strength [3]. Then six concrete mixes were prepared including control mix by partially replacing M-Sand with different proportion of copper slag ranging from 0 to 50% at an increment of 10%. Mix with 10% copper slag was designated as CS10 where CS stands for copper slag. In the same way, other mixes were designated with change in the percentage of CS. The mix proportions of all concrete mixes are shown in Table 3. The quantities of CS and sand were varied by equivalent volume method.

4 Results and Discussions

4.1 Fresh Properties

The fresh properties were performed in order to assess the flowability, passing ability, and the viscosity of SCC; which are the key principals of designing SCC. From the results, it was inferred that there was improvement in workability values on

Table 3 Mix proportions of different SCC mixes

Mix	CS0	CS10	CS20	CS30	CS40	CS50
Free water-binder ratio	0.42	0.42	0.42	0.42	0.42	0.42
Cement (kg/m^3)	320	320	320	320	320	320
Flyash (kg/m^3)	110	110	110	110	110	110
Water (kg/m^3)	180	180	180	180	180	180
M-sand (kg/m^3)	1000	900	800	700	600	500
Copper slag (%)	0	10	20	30	40	50
Copper slag (kg/m^3)	0	127	254.5	382	509	636.5
Coarse aggregate (kg/m^3)	765	765	765	765	765	765
Superplasticizer (kg/m^3)	3.44	3.44	3.44	3.44	3.44	3.44

addition of copper slag. All the mixes were in good accordance with the classifications prescribed in the IS code.

4.1.1 Slump Flow and T50

Slump flow diameters in the range of 668–688 mm were observed for all SCC mixes and were categorized under the slump flow class SF2. The slump flow obtained for 40% copper slag is shown in Fig. 2 and the variations are shown in Fig. 3. From Table 4, the slump flow value augmented as content of copper slag increased; and reached 688 mm for the mix incorporating 50% copper slag. The increment in slump flow diameter was owed to the smooth, glassy texture and low water absorption characteristic of copper slag that increased the flow ability of SCC mixes [2]. The time taken by SCC mixes to reach 500 mm diameter is marked as T50 and the results indicates that T50 time varied from 3.5 to 2.4 s and all mixes were in the class VS2

Fig. 2 Slump flow of SCC mix

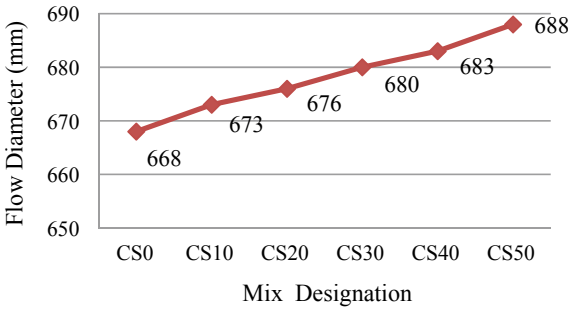

Fig. 3 Slump flow for different mixes

Table 4 Test results of different mixes

Mixes	Slump flow (mm)	T50 (s)	Strength (MPa)			
			$(f_{cu})^a$	$(f_{cu})^b$	$(f_t)^b$	$(f_{cr})^b$
CS0	668	3.5	25.12	36.79	3.12	5.27
CS10	673	3.3	26.31	37.54	3.47	5.63
CS20	676	3.2	28.16	39.69	3.79	5.94
CS30	680	2.9	29.8	40.99	4.18	6.31
CS40	683	2.7	30.52	41.23	4.13	6.34
CS50	688	2.4	29.27	39.42	3.86	6.17

f_{cu} = cube compressive strength, f_t = tensile strength, f_{cr} = flexural strength
[a]Cured at 7 days
[b]Cured at 28 days

on the basis of viscosity. The T50 time decreased as there was increase in copper slag content which is shown in Table 4. This could be due to the low water absorption characteristic of copper slag grains [4].

4.1.2 V-Funnel

It was inferred from the Table 5 that, the time taken to empty the funnel was maximum for the concrete mix having 0% copper slag. It decreased with the increasing content of copper slag. All the mixes were under the viscosity class V1. As shown in Fig. 4, the V-funnel time decreased from 7.5 to 5.8 s as the amount of copper slag increased

Table 5 V-funnel test and L-box test of SCC mixes

S. No.	Mix	L box ratio	V funnel time (s)
1	CS0	0.84	7.5
2	CS40	0.91	5.8

Fig. 4 V funnel time

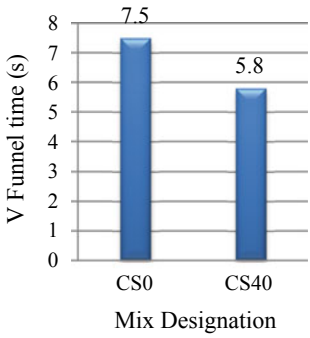

Fig. 5 L box ratio

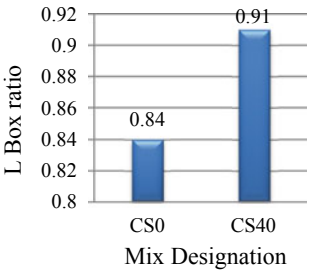

from 0% to optimum content of 40% [5]. The set up for the V-funnel test was shown in Fig. 6.

4.1.3 L-Box

The L-box test determined the passing ability of SCC mix which enables the flow through tight openings and congested reinforcements [6]. It can be noticed from Fig. 5 that blocking ratio ranged from 0.84 to 0.91 for SCC mixes containing 0% to optimum content of 40% copper slag. The results are shown in Table 5. The apparatus for the L-box test was shown in Fig. 7.

4.2 Strength Properties

4.2.1 Compressive Strength

Compressive strength tests were carried out on cubic specimens of size 150 mm × 150 mm × 150 mm after 7 and 28 days of curing. Table 4 shows that the compressive strength of control concrete was found to be 36.79 MPa at 28-day curing period.

Fig. 6 V funnel apparatus for SCC mix

Fig. 7 L box test for SCC mix

Maximum enhancement in strength of about 12% was observed for SCC incorporating 40% copper slag compared to control concrete at 28 days curing. This strength gain was mainly due to the sharp edges of slag particles, it helps in improving cohesion of the concrete matrix [7]. However, an insignificant reduction in strength of about 4.6% was observed beyond 40% copper slag replacement. The excessive free water content in the concrete mixes with high copper slag content causes the particles of the constituents to separate and leaves pores in the hardened concrete which

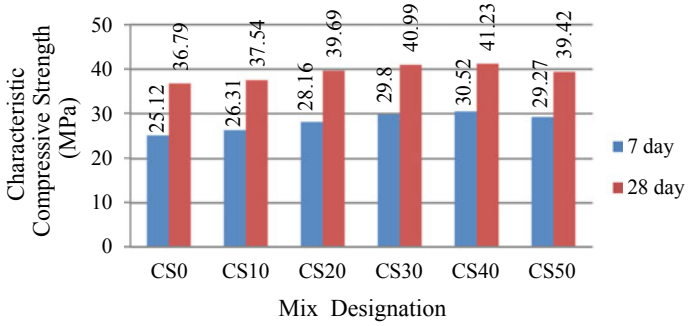

Fig. 8 Characteristic compressive strength of concrete mixes

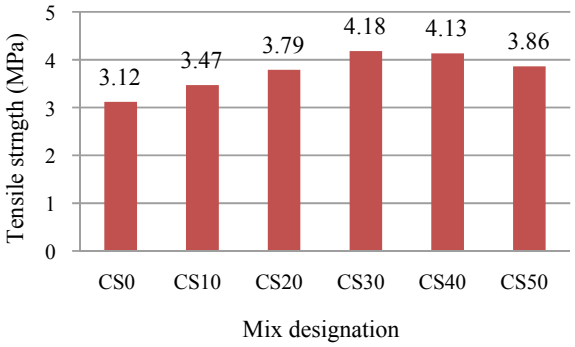

Fig. 9 Tensile strength of concrete mix

consequently causes reduction in the concrete strength [8]. Figure 8 represents the variation in compressive strength for different mixes.

4.2.2 Splitting Tensile Strength

Test were carried out on cylinder specimens of size 150 mm × 300 mm. Utilization of copper slag in SCC mixes increased split tensile strength up to 30% replacement at 28 day curing as presented in Table 6 [8]. The strength augmented from 3.12 to 4.18 MPa for SCC mix from 0 to 30% copper slag. After 30% replacement the strength decreased to 4.13 MPa and is shown in Fig. 9.

4.2.3 Flexural Strength

The 28 day flexural strength values for concrete are presented in Table 6. The tests were done in beam specimen of size 100 mm × 100 mm × 500 mm. Utilization of

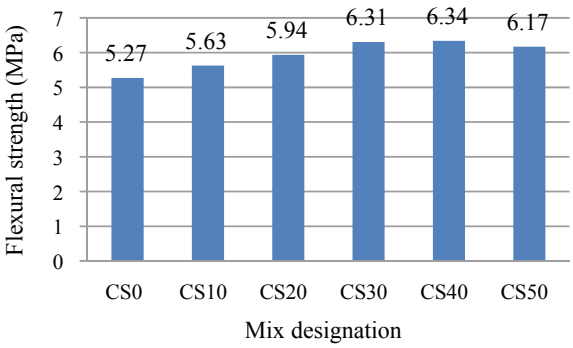

Fig. 10 Flexural strength of concrete mix

copper slag in SCC mixes increased flexural strength to 6.34 MPa at 40% replacement and then decreased to 6.17 MPa after 40% replacement and is shown in Fig. 10.

5 Conclusion

Copper slag is a non-hazardous material. For the same water cement ratio and fixed quantity of superplasticizer, SCC mixes could be designed resulting increased strength results. The incorporation of copper slag in SCC mixes as fine aggregate replacement escalated the fresh properties. Slump flow values, V funnel times and L-box ratio of all mixes were in the class of SF2 and VF1 respectively. Following conclusion can be drawn based on the research conducted.

1. The glassy texture and the low water absorption characteristic of copper slag grains led to improved fresh properties of SCC mixes.
2. The compressive strength and flexural strength of concrete was highest for 40% copper slag and a decline in strength was noticed beyond 40%. The decrease in strength was due to the increase in free water content on higher replacement
3. Split tensile strength augmented in SCC mixes incorporating copper slag up to 30% substitution. The strength enhancement owed to the angular edges of copper slag grains that led to the improvement in the cohesion of concrete matrix.
4. Therefore, it is recommended that up to 40% of copper slag can be used as a replacement for fine aggregates in order to obtain a concrete with good strength requirements based on compressive strength results.

References

1. Khatib JM (2008) Performance of self-compacting concrete containing fly ash. Constr Build Mater 22:1963–1971
2. Al-Jabri KS, Al-Saidy AH, Taha R (2011) Effect of copper slag as a fine aggregate on the properties of cement mortars and concrete. Constr Build Mater 25:933–938
3. Mohamad OA, Najm OF (2016) Compressive strength and stability of sustainable self-consolidating concrete containing fly ash, silica fume, and GGBS. Int J Environ Res 1–16
4. Al-Jabri KS, Hisada M, Al-Oraimi SK, Al-Saidy AH (2009) Copper slag as sand replacement for high performance concrete. Cem Concr Compos 31:483–488
5. Zhao H, Sun W, Wu X, Gao B (2015) The properties of the self-compacting concrete with fly ash and ground granulated blast furnace slag mineral admixtures. J Clean Prod 95:66–74
6. Uysal M, Sumer M (2011) Performance of self-compacting concrete containing different mineral admixtures. Constr Build Mater 25:4112–4120
7. Wu W, Zhang W, Ma G (2010) Optimum content of copper slag as a fine aggregate in high strength concrete. Mater Des 31:2878–2883
8. Vijayaraghavan J, Belin Jude A, Thivya J (2017) Effect of copper slag, iron slag and recycled concrete aggregate on the mechanical properties of concrete. Resour Policy 53:219–225

Development of Metakaolin and Flyash Based Geopolymer Concrete at Ambient Temperature Curing

S. Anjana Chandran and B. R. Beena

Abstract Concrete is the one of the most widely used construction material. Portland cement is the main ingredient for making concrete. The cement industry is responsible for about 5% of total CO_2 emission worldwide, which is the main cause of global warming. In order to reduce CO_2 emission, an ecofriendly construction material called geopolymer concrete was developed as a substitute for cement. Geopolymer concrete is a type of concrete which is produced by the chemical reaction of inorganic molecules. The aim of the study is to develop a geopolymer concrete using metakaolin and fly ash as binder material. Different proportion of metakaolin and fly ash were prepared by varying the proportion of activator to binder ratio from 0.6 to 1.0. The performance of different mixes were compared using mechanical properties like compressive strength, flexural strength and split tensile strength. Sodium hydroxide solution with 12 M concentration and sodium silicate solution were used as activator in a proportion of 2:5. The coarse aggregate consisted of graded gravel with a maximum size of 12.5 mm and fine aggregates was M sand. From the present study geopolymer concrete of compressive strength 32.21 N/mm^2 was developed. The optimized mix was obtained with the activator to binder ratio 0.9 as well as 60:40 proportion of metakaolin and fly ash.

Keywords Geopolymer · Metakaolin · Fly ash · Activator to binder ratio · NaOH · Na_2SiO_3

S. Anjana Chandran (✉) · B. R. Beena
Department of Civil Engineering, Federal Institute of Science and Technology (FISAT), Ernakulum 683577, India
e-mail: anjanachandran.1996@gmail.com

B. R. Beena
e-mail: beenabr@gmail.com

© Springer Nature Switzerland AG 2021

K. Dasgupta et al. (eds.), *Proceedings of SECON 2020*,
Lecture Notes in Civil Engineering 97,
https://doi.org/10.1007/978-3-030-55115-5_15

1 Introduction

Nowadays, the necessity of using environmental friendly construction materials which supports the concepts of sustainable development is one of the main environmental concerns in the construction industry. The production of Ordinary Portland Cement (OPC) is one of the main cause of global warming. For producing one tonne of cement requires about two tonnes of raw materials (shale and limestone) and it releases about 0.87 tonne of CO_2, about 3 kg of Nitrogen Oxide (NO_x), an air contaminant that contributes to ground level smog and 0.4 kg of PM10 (Particulate matter of size 10 μm), an air borne particulate matter that is harmful to the respiratory tract when inhaled. The global release of CO_2 from all sources is estimated at 23 billion tonnes a year and the portland cement production accounts for about 7% of total CO_2 emissions. But, the use of concrete and cement-based composites, as the most widely used construction materials, are still inevitable in the future. Thus, the use of supplementary cementitious materials such as fly ash, metakaolin, rice husk ash and slag or finding alternative cement-less binders to OPC are essential. Development of geopolymer as an alternative cement-less binder to OPC was one of the significant breakthrough in the field of concrete technology in the twentieth century. The term geopolymer concrete was initially introduced by Davidovits. Geopolymer is synthesised from materials of geological origin such as metakaolin or industrial by-products such as fly ash and slag etc. They are rich in silica and alumina with high alkaline activators. Manufacture of fly ash based geopolymer have at least 80% less CO_2 emission and approximately 60% less embodied energy compared to production of OPC.

Over the last few decades, extensive researches and developments on geopolymer technology have been undertaken worldwide with hopes to promote the geopolymer concrete as an ultimate sustainable construction material for the future. From the studies it is pointed out that the rate of polymer formation is influenced by many parameters like, curing temperature, water content, fly ash/metakaolin ratio, alkali concentration, initial solids content, silicate and aluminate ratio, pH and the type of activators used [1–3] and mechanical properties of the geopolymers are greatly dependent on the concentration of NaOH solution. The strength of the geopolymer increase along with the increase of NaOH concentration within 4–12 mol/l [1] also pozzolanic reactions are accelerated by increase in curing temperature and time up to a limit [4, 5]. Geopolymer with Si/Al $\geq$ 3 showed worse chemical stability in air than those with Si/Al $\leq$ 2.5 [6]. In the present study, metakaolin and fly ash based geopolymer with activator to binder ratio between 0.6 and 1.0 was developed and optimized, to make geopolymer concrete with a view towards application as a construction material. Fly ash is a solid waste while kaolin is a non-renewable (although abundant) natural clay resource. Metakaolin is highly reactive due to its fine size and amorphous nature [2].

Table 1 Chemical composition of fly ash

Constituents	SiO_2	Al_2O_3	CaO	Fe_2O_3
Mass %	63.8	21.29	0.44	0.39

Table 2 Chemical composition of metakaolin

Constituents	SiO_2	Al_2O_3	Fe_2O_3	TiO_2	CaO	MgO	Na_2O	K_2O	Loss on ignition
Mass %	52.0	40.0	3.60	2.65	1.09	0.03	0.10	0.03	1.00

2 Experimental Investigations

2.1 Materials

The primary aluminosilicate source material used in preparing geopolymer specimens were metakaolin and fly ash blend. Commercially produced metakaolin with an average particle size of 1.86 μm and low calcium fly ash with an average particle size of 22.2 μm were collected from a local supplier. The specific gravity of fly ash and metakaolin was found to be 2.3 and 2.6 respectively. Chemical compositions of fly ash and metakaolin are employed were shown in Tables 1 and 2.

Sodium hydroxide (NaOH) and sodium silicate solution (Na_2SiO_3) were used as alkali activators. NaOH pellets as well as Na_2SiO_3 gel used were procured from the local supplier. Sodium hydroxide pellets having 98% purity and sodium silicate solution with composition of 15.9% Na_2O, 31.4% SiO_2 and 52.7% H_2O were used for alkali activation, with specific gravity 1.6. Here M sand with specific gravity 2.75, fineness modulus 2.785 and water absorption 1.27% was used as fine aggregate at saturated surface dry condition. Crushed angular coarse aggregate from a local source, having a maximum size of 12.5 mm, was used for the present study having specific gravity 2.79 and water absorption 0.60%. The test for aggregates conducted as per IS 2386-1963 (part 3).

2.2 Mixture Proportions

Initially the ratio between Na_2SiO_3 and NaOH was kept constant as 2.5 for all the mixes. Then mix design was by varying the activator- binder ratios ranging from 0.6 to 1.0, by keeping NaOH molarity constant at 12 M (480 g of NaOH pellets dissolved in 1 L distilled water) and metakaolin to fly ash proportion as 60 and 40%. The material quantity of various mixes were shown in Table 3. Once the optimum proportion of activator to binder was obtained, effect of binder proportion was studied by varying the proportion of metakaolin to fly ash by 20–80, 40–60, 60–40 and 80–20. There by the proportion of Si/Al got modified as shown in Table 4.

Table 3 Mix proportion

Material	Quantity (kg/m^3)				
	Mix 1	Mix 2	Mix 3	Mix 4	Mix 5
Activator to Binder ratio (A/B)	0.6	0.7	0.8	0.9	1
Fly ash	138	129.8	122.66	116.21	110.4
Metakaolin	207	194.8	183.99	174.31	165.6
Coarse aggregate	1304	1304	1304	1304	1304
Fine aggregate	554	554	554	554	554
NaOH	59.14	64.94	70.09	74.7	78.85
Na_2SiO_3	147.86	162.36	175.24	186.77	197.15

Table 4 Variation of Si/Al ratio of mixes

Mix name	GP1	GP2	GP3	GP4
% Metakaolin	20	40	60	80
Si/Al	2.45	2.10	1.80	1.5

The polymerization process is a relatively quick chemical reaction involving alkaline liquids and Si-Al minerals. The end product is a three-dimensional polymeric ring structure comprising of Si–O–Al-bonds [7]. So the Si/Al ratio is an essential parameter to check the properties of geopolymer.

2.3 Specimen Preparation

The geopolymeric precursor and alkaline silicate solution were mixed by hand for 10 min before being cast into cubic moulds. The dimensions of the geopolymer cubic specimens prepared were 150 mm × 150 mm × 150 mm. The samples were then vibrated to release any residual air bubbles. Subsequently, the moulded samples were sealed with a film and transferred to an air-tight container to prevent moisture loss.

Geopolymers used in this study were produced under ambient conditions (room temperature and atmospheric pressure) to ensure cost effectiveness and ease of production in practical applications. Three samples of each batch were prepared and average strength values were recorded. Similarly for split tensile test concrete cylinders of size 150 mm diameter and 300 mm height and flexural test specimens of size 100 × 100 × 500 mm were cast. M25 grade OPC concrete specimens with water cement ratio 0.4 were also cast in the same mould and vibrated on a shake table. It used for comparison purposes. Water curing had done for cement concrete mixes.

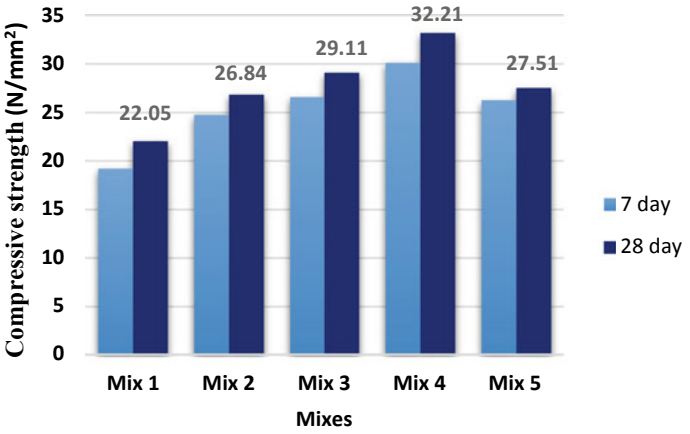

Fig. 1 Variation of compressive strength with different A/B ratio

3 Results and Discussion

3.1 Effect of Activator Binder Ratio on Geopolymer Concrete

Figure 1 showed the compressive strength of synthetic geopolymer concrete by changing activator to binder (A/B) ratio. With the increase of A/B ratio up to 0.9 compressive strength increases then decreases. To study the effect of activator to binder ratio on the compressive strength, 5 mixes were prepared by varying activator to binder ratio from 0.6 to 1.0 and maximum compressive strength of 32.21 N/mm^2 observed for Mix 4 with activator to binder ratio 0.9.

Geopolymeric material is readily workable even at a very low liquid/solid ratio (below 0.4) but for metakaolin based geopolymer more liquid is required than fly ash based one, due to its large surface area and very fine particle size. Also high activator content enhances the dissolution of raw materials and increases the solubility of silicates and aluminates which resulted in high strength. So up to a limit strength properties increases with increase in A/B ratio. Then (After A/B ratio 0.9) strength decreases due to decrease in binder content in geopolymer concrete.

3.2 Development of Geopolymer Concrete with Optimum Metakaolin-Fly Ash Proportion

Clay and metakaolin are the most widely used raw materials for the production of geopolymers. However, fly ash is also used in the production of geopolymers. During the geopolymerisation process, fly ash reacted with the alkaline solution and causes the formation of cementitious material. In many cases, fly ash cannot complete

dissolution before the final hardening due to the low reactivity and slow setting of the fly ash [8]. During the geopolymerisation process, metakaolin powder partially or completely dissolved in the alkaline solution and forms tetrahedral aluminosilicate units. Which accelerates the polymerization process [9].

The effect of metakaolin and fly ash content on compressive strength of geopolymers at ambient temperature curing is as shown in Fig. 2. The effect of variation in the proportion of binder, metakaolin and fly ash was studied. In this case all other parameter is fixed and only the two binder proportion are varied (20%, 40%, 60%, and 80%). With the increase of metakaolin content the strength of concrete increases. It is because fly ash particles in geopolymers are poorly dissolved during reaction process achieved by alkaline activation at ambient temperature, leading to high porosity and in turn low strength in high fly ash contained geopolymers. However, in the case of metakaolin and fly ash based geopolymer concrete with high metakaolin substitution, the microstructure appears denser, which enhances the mechanical strength of the mixtures. Metakaolin has high reactivity, amorphous nature and very fine particle size when compared with fly ash. Here maximum strength is obtained in a specimen with 60% metakaolin and 40% fly ash content as binder material.

Normal OPC M25 concrete mix was cast for comparative purpose. Because the optimum compressive strength of geopolymer is in the range of characteristic strength of M25 mix. The flexure test and split tensile strength of the optimum geopolymer mix and normal concrete were varied as shown in Fig. 3.

The flexural and tensile strength of geopolymer concrete is less than that of normal M25. It may improve by incorporating fibers in geopolymer concrete.

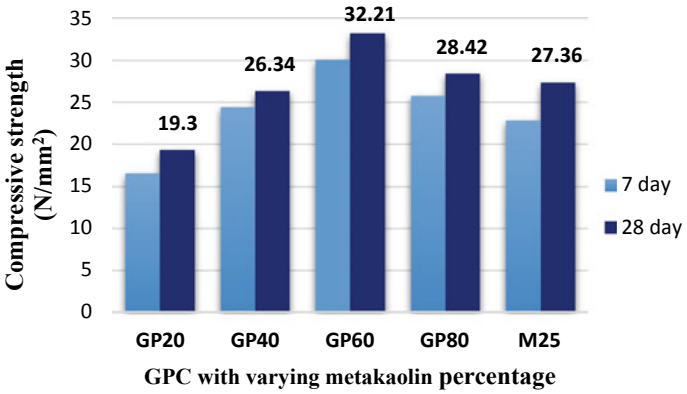

Fig. 2 Variation of compressive strength with different MK percentage

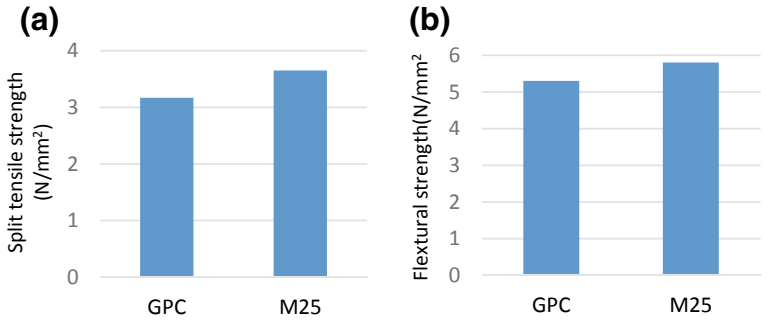

Fig. 3 Test result of **a** split tensile strength and **b** flexural strength

4 Conclusion

In the present study, attempts were made to investigate the effect of activator to binder (A/B) ratio and metakaolin fly ash ratio on the synthesis of geopolymer concrete. From the study, it had been observed that compressive strength increased with the increase in the A/B ratio till 0.9 and then decrease. Geopolymer with 60% metakaolin and 40% fly ash showed high compressive strength. With increase of metakaolin content Si/Al ratio decreases, geopolymer with Si/Al ratio 1.80 showed high strength properties. The compressive strength of GPC increases with increase in metakaolin percentage up to 60% it is due to its chemical composition, particle size and large surface area. So, this study showed that 60% metakaolin substitution with 0.9 activator to binder ratio having 12 M concentration of NaOH provided a better geopolymerization and significantly improved the compressive strength. But the flexural and tensile strength of geopolymer concrete was less than normal conventional concrete.

References

1. Li W, Yan F (2005) Synthesis and mechanical properties of metakaolinite-based geopolymer. Colloids Surf A Physicochem Eng Aspects 268(1–3):1–6
2. Kong D, Sanjayan JG, Sagoe-Crentsil K (2007) Comparative performance of geopolymers made with metakaolin and fly ash after exposure to elevated temperatures. Cem Concr Res 37(12):1583–1589
3. Zhang HY, Kodur V, Qi SL, Cao L, Wua B (2014) Development of metakaolin–fly ash based geopolymers for fire resistance applications. Constr Build Mater 55:38–45
4. Görhan G, Aslaner R, Şinik O (2016) The effect of curing on the properties of metakaolin and fly ash-based geopolymer paste. Compos B Eng 97:329–335
5. Al-Shathr BS, Al-Attar TS (2016) Effect of curing system on metakaolin based geopolymer concrete. J Babylon Univ Eng Sci 24(3)
6. He P, Wang M, Fu S, Jia D, Yan S (2016) Effects of Si/Al ratio on the structure and properties of metakaolin based geopolymer. Ceram Int 42(13):14416–14422

7. Chen L, Wang Z, Wang Y, Feng J (2016) Preparation and properties of alkali activated metakaolin-based geopolymer. Materials 9(9):767
8. Zhang Z, HaoWanga YZ, Reid A, Provis JL, Bullena F (2014) Using fly ash to partially substitute metakaolin in geopolymer synthesis. Appl Clay Sci 88–89(2014):194–201
9. Pavithra P, Srinivasula Reddy M, Dinakar P, Hanumantha Rao B, Satpathy BK, Mohanty AN (2016) Effect of the Na2SiO3/NaOH ratio and NaOH molarity on the synthesis of fly ash-based geopolymer mortar. In: Geo-Chicago. ASCE, pp 336–341

Seismic Evaluation of High Rise Buildings Using Hybrid Configuration of Grid Systems

K. N. Vaisakh and Neeraja Nair

Abstract The developments in construction techniques, materials, structural systems and analytical methods for analysis opened the door for the growth of high rise buildings. The lateral resistance of such a structure is offered by interior structural systems or exterior structural systems. Recently, grid systems are adopted in tall buildings due to its structural efficiency, superiority in aesthetic appeal and flexibility in architectural planning. Diagrids and hexagrids contain diamond shaped modules and hexagons respectively, throughout exterior of structure and they don't have any external vertical columns. The behaviour of high rise buildings using combination of grid systems has not been explored. This study focuses on the structural performance of high rise steel buildings for various combinations of grid systems. In this study ETABS V16 software was used for modelling and analysis of a 36 storey building with regular floor plan. Models were created using combinations of diagrid and hexagrid systems with optimum diagonal angle and module density. Time history analysis of these models were carried out to examine their seismic performance. The combinations with better performance were determined Combined grid system is a viable option when governed by overall weight and cost.

Keywords Diagrid · Hexagrid · Octagrid · Time history analysis · ETABS

K. N. Vaisakh (✉) · N. Nair
Federal Institute of Science and Technology, Angamaly, Ernakulam, India
e-mail: kvaisakhn@gmail.com

N. Nair
e-mail: neeraja15@gmail.com

© Springer Nature Switzerland AG 2021

K. Dasgupta et al. (eds.), *Proceedings of SECON 2020*,
Lecture Notes in Civil Engineering 97,
https://doi.org/10.1007/978-3-030-55115-5_16

1 Introduction

1.1 General

Construction of multi-storey building is rapidly increasing throughout the world due to the rapid growth of urban population and limitation of available land. Lateral loading due to wind or earthquake are the governing factors in the design of high rise buildings along with the action of gravitational loading. In order to resist the lateral loads, either interior or exterior structural systems are employed.

In the diagrid structures, the vertical columns from the periphery of the structure are eliminated and it consists of diamond shaped modules. A triangulated configuration is formed in the diagrid structural systems because of the modules and due to this, diagrids are able to carry gravity and lateral loads and distribute them in a very uniform and regular pattern [1].

The hexagrid consists of multiple hexagonal grids at the exterior perimeter surfaces of building. The hexagrid system is a particular form of belt trusses mixed tubular system and resists lateral loads acting in tension or compression. Similarly, octagrid contain several octagons arranged at the exterior of the structure. Module density of a hexagrid or octagrid denotes the number of hexagon or octagon modules around the periphery [2].

1.2 Research Significance

Construction of multi-storey building is rapidly increasing throughout the world due to efficient structural systems, advances in construction technology and shortage of urban land available for construction. As the height of structure increases, the influence of lateral loads increases and requires lateral load resisting structures to resist them. The grid system is widely used for recent tall buildings due to the structural efficiency and aesthetic potential. The employment of Diagrid, Hexagrid or Octagrid structural systems in a building give rise to various advantages like reduction of interior columns giving large column free spaces.

This paper focuses on the performance of hybrid combination of the grid systems and to find the structural system that exhibits least top storey displacement and drift. It also aims to introduce a new aspect in architectural way and improving the structural stability of high rise buildings. A 36 storey building with a regular floor plan is used to compare the structural weight and material cost of all building models to determine the most economical option among the models.

2 Modelling and Analysis

2.1 Analysis Technique

In this paper the focus is given to seismic analysis. Seismic analysis of all models is done using ETABS 2016 software. Time history analysis is a step by step process of analysing the dynamic response of a structure to a specified loading that may vary with time. The time history function data entered for analysis process was that of El Centro Earthquake (Imperial Valley earthquake) which occurred in 1940 at southern California. It had a moment magnitude of 6.9 and a maximum perceived intensity of X (Extreme) on the Mercalli intensity scale. Comparison of results for all models is done in terms of maximum top storey displacement, storey drift, base shear and structural steel weight. The better model is determined by comparing the results.

2.2 Building Configuration

The 36 storey building is having 36 m × 36 in plan dimension and each storey height is 3.6 m. The design dead load and live load on floor slab are 3.75 kN/m^2 and 2.5 kN/m^2 respectively. Member sizes were taken as given in the journal Jani and Patel [3]. The design earthquake load is computed based on the zone factor of 0.16, medium soil, importance factor of 1 and response reduction factor of 5 (IS: 1893 (Part-I), 2016). The grade of steel and concrete used is Fe250 and M25 respectively. The thickness of slab is taken as 120 mm. The support conditions are assumed as hinged [3] (Figs. 1, 2 and Table 1).

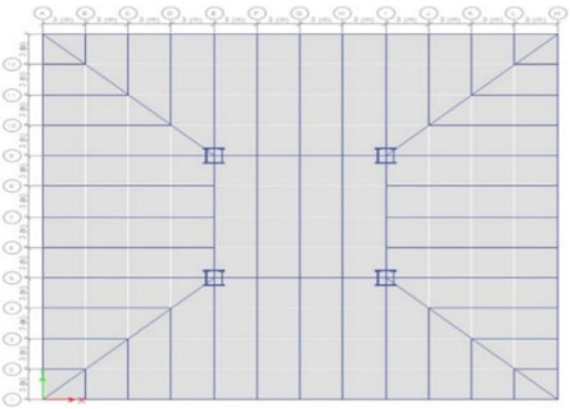

Fig. 1 Typical floor plan

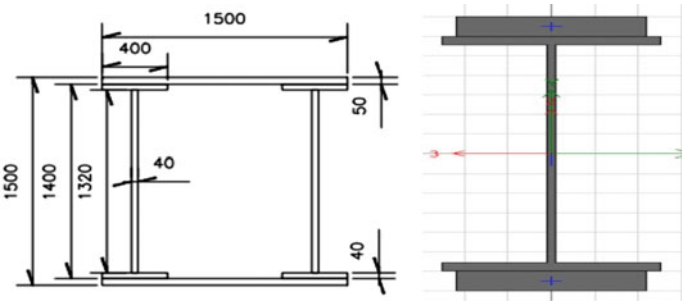

Fig. 2 **a** Interior column [1], **b** ISWB600 with top and bottom plate of 220 mm × 50 mm

Table 1 Typical member sizes [1]

Exterior columns	Interior columns	Beams
375 mm pipe sections with 12 mm thick (from 19 to 36th storey)	1500 mm × 1500 mm	ISMB550
450 mm pipe sections with 25 mm thickness (from 1st to 18th storey)		ISWB600 with top and bottom plate of 220 mm × 50 mm

2.3 Models Analysed

The various models analysed are (i) Diagrid with 6 storey modules [DIA] [1], (ii) Hexagrid with 4 storey modules [HEX] [4], (iii) Octagrid with 3 storey modules [OCT] [5], (iv) Diagrid from 1st to 18th storey and Hexagrid from 19 to 36th storey [DIA-HEX], (v) Hexagrid from 1st to 18th storey and Diagrid from 19 to 36th storey [HEX-DIA], (vi) Diagrid and Hexagrid on perpendicular sides [PS-DH], (vii) Diagrid and Octagrid on perpendicular sides [PS-DO], (viii) Hexagrid and Octagrid on perpendicular sides [PS-HO] (Figs. 3 and 4).

3 Results and Discussions

3.1 Storey Displacement

As per IS 1893 (Part 1): 2016, permissible maximum storey displacement = 0.004H = 0.0004 * 129.6 = 0.5184 m, where H is the height of the building. The values of storey displacement of all the models for load cases of Earthquake in x and y-direction are found to be within the limit (Figs. 5 and 6).

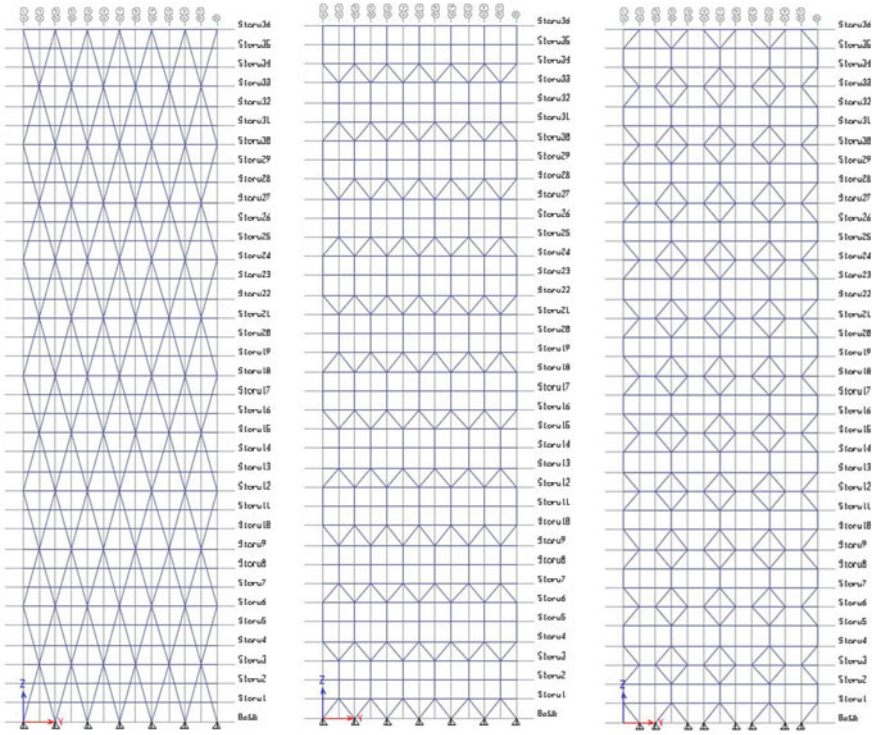

Fig. 3 Elevation of **a** diagrid model with 6 storey modules, **b** hexagrid model with 4 storey modules, **c** octagrid model with 3 storey modules

3.2 Storey Drift

The permissible inter-storey drift as per IS 13 (Part 1): 2016, is 0.004 h = 0.004 × 3.6 = 0.0144 where h is the storey height of the structure. All models satisfy the storey drift condition (Figs. 7 and 8).

3.3 Base Shear

The base shear is highest for diagrid structure and lowest for octagrid structure. The base shear of the combination models lies between these two values (Figs. 9 and 10).

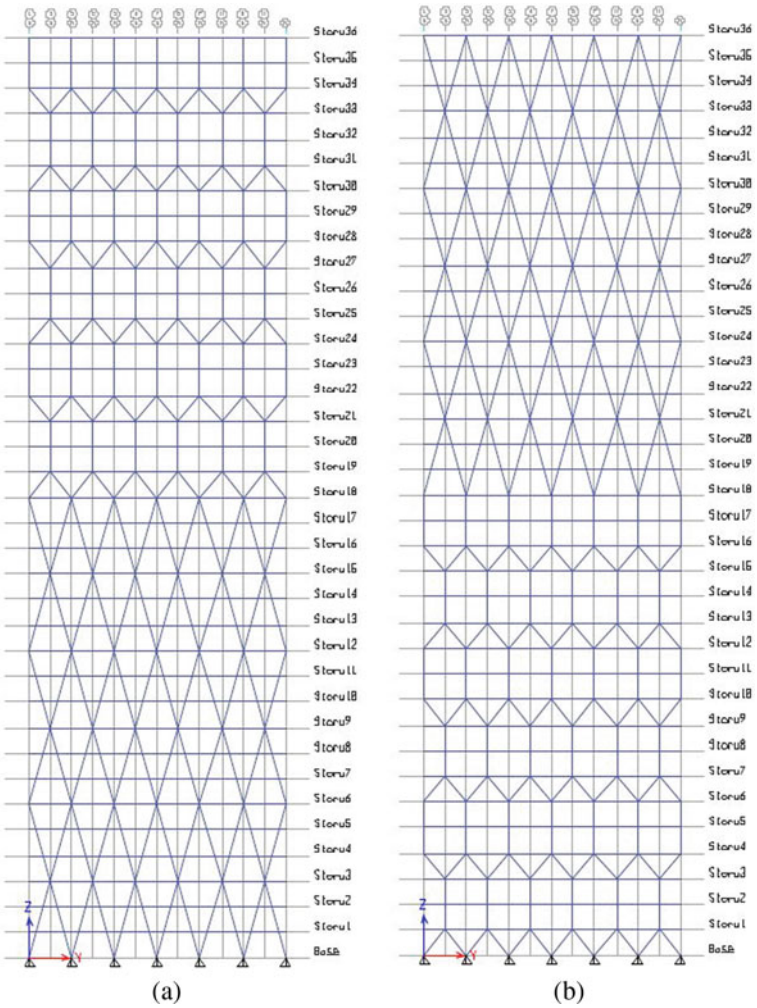

Fig. 4 Elevation of **a** DIA-HEX, **b** HEX-DIA

3.4 Structural Weight

Structural steel weight is comparatively less for octagrids and more for diagrids (Fig. 11).

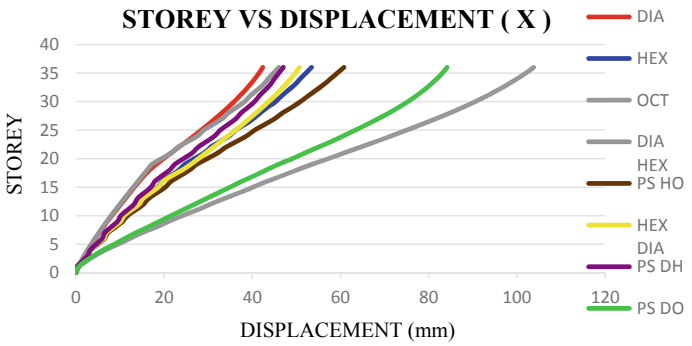

Fig. 5 Maximum storey displacement of various models in x-direction

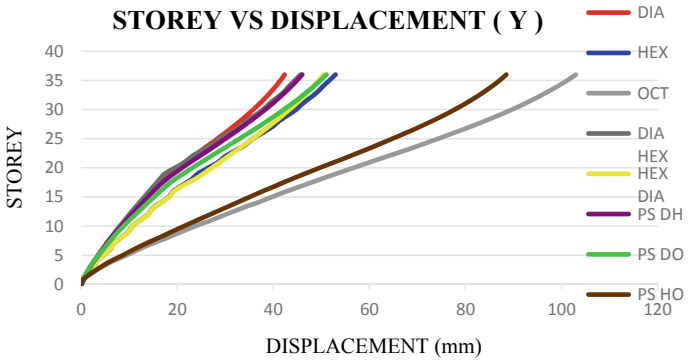

Fig. 6 Maximum storey displacement of various models in y-direction

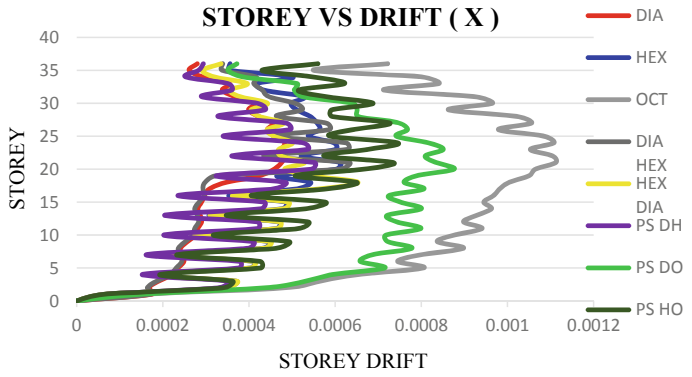

Fig. 7 Maximum storey drift of various models in x-direction

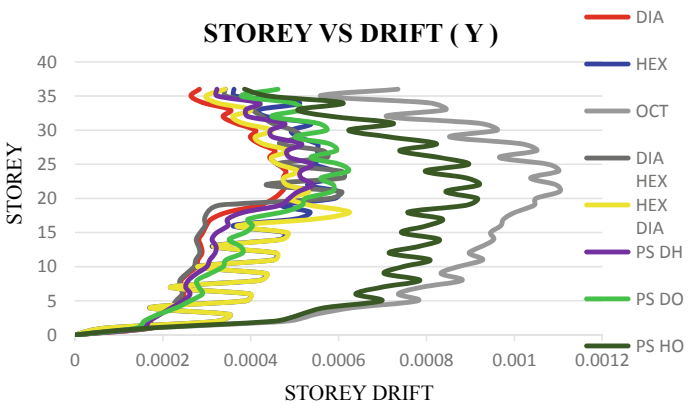

Fig. 8 Maximum storey drift of various models in y-direction

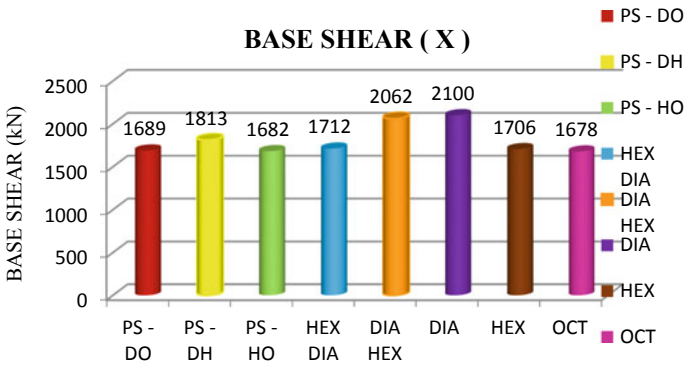

Fig. 9 Base shear of various models in x-direction

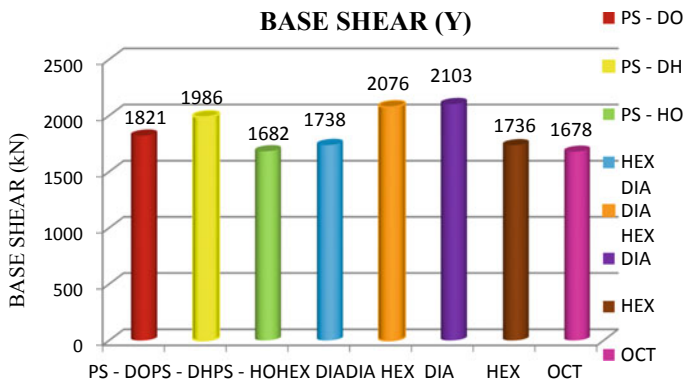

Fig. 10 Base shear of various models in y-direction

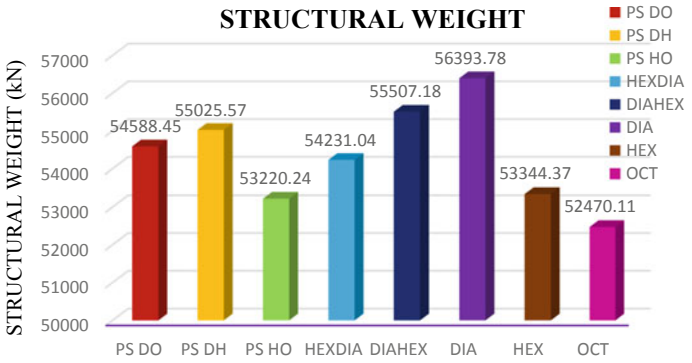

Fig. 11 Structural weight for various models

Table 2 Comparison of various parameters considered

Model	Linear static analysis					
	Maximum displacement (mm)		Max drift		Base shear (kN)	
	X	Y	X	Y	X	Y
DIA	42.35	42.32	0.000484	0.00048	2100	2103
HEX	53.43	52.94	0.000612	0.000601	1706	1736
OCT	103.78	102.98	0.001112	0.001103	1678	1678
DIA HEX	46.03	45.67	0.000633	0.00061	2062	2076
HEX DIA	50.72	50.44	0.000653	0.000625	1712	1738
PS DH	47.03	45.99	0.000552	0.000541	1813	1986
PS DO	84.15	51.04	0.000876	0.000622	1689	1821
PS HO	60.77	88.47	0.000745	0.00092	1682	1682

3.5 Comparison of Results

See Table 2.

4 Conclusions

Among the three grid systems, diagrid system have higher seismic resistance and octagrid have the least. For octagrid structures the displacement reduces by about 40–50% by combining it with hexagrid and diagrid respectively. Hexagrid structures also shows reduction in displacement when used in combination with diagrid. Considering the different combinations of the grid system, combination involving diagrid and hexagrid have better seismic performance. The DIAHEX, HEXDIA and

PS DH combinations have better seismic resistance compared to other models. The performance of octagrid can be improved by combining it with hexagrid or diagrid. There is considerable reduction in the quantity of steel used for the various combinations when compared to diagrid structures and hence there is reduction in the material cost.

References

1. Jani KD, Patel PV (2013) Design of diagrid structural system for high rise steel buildings as per indian standards. In: ASCE structures congress, 2013
2. Raghu Prasad BK, Kavya AJ (2014) Comparative performance of octagrid and hexagrid lateral load resisting systems for tall building structure. Int J Eng Res Appl 4(11):74–80. ISSN : 2248-9622
3. Jani KD, Patel PV (2013) Analysis and design of diagrid structural system for high rise steel buildings. Procedia Eng 51:92–100
4. Montuori GM, Mele E, Brandonisio G, De Luca A (2014) Geometrical patterns for diagrid buildings: exploring alternative design strategies from the structural point of view. Eng Struct 71:112–127
5. Isaac PL, Ipe BA (2017) Comparative study of performance of high rise buildings with diagrid, hexagrid and octagrid systems under dynamic loading. Int Res J Eng Technol 04(05)

Sustainability Assessment of Terracotta Tile Waste Based Geopolymer Building Block

S. Usha, Deepa G. Nair, and Subha Vishnudas

Abstract Cement concrete blocks are one of the popular masonry units used in construction. The conventional binder, cement cause heavy impact on environment due to its high utilization of natural resources and emission of CO_2 during production. To overcome this issue an attempt has been made to develop geopolymer binder from terracotta tile waste as alternative to cement and its application in concrete blocks. In this paper sustainability evaluation of terracotta tile waste based geopolymer concrete block (GCB) over cement concrete block (CCB) has been evaluated through a modified frame work by considering four aspects of sustainability. Socio-cultural factor with three sub criteria (acceptance, awareness and decentralized production), economic factor with four sub criteria (infrastructure, unskilled labour, accessibility to material and material efficiency), technological factor with two sub criteria (strength and durability), environmental factor with three sub criteria (energy efficiency, waste management, and feasibility for reuse or renewability) of GCB and CCB were evaluated. Quantitative evaluation of four sub criteria under technological and environmental sustainability were discussed in detail using results of experimental research conducted as per the standards and calculated amount of embodied energy and CO_2 emission of both the blocks, which reveals that GCB is more sustainable than CCB. However GCB being in the infancy stage, remaining eight sub criteria under socio-cultural, economic and environmental factors were qualitatively analyzed using available information. The overall result indicates that GCB is more sustainable than CCB.

Keywords Sustainability · Geopolymer · Tile waste

S. Usha (✉)
Department of Civil Engineering, Sree Narayana Gurukulam College of Engineering, Kochi, India
e-mail: ushaushus11@rediffmail.com

D. G. Nair · S. Vishnudas
Division of Civil Engineering, School of Engineering, CUSAT, Kochi, India

© Springer Nature Switzerland AG 2021

K. Dasgupta et al. (eds.), *Proceedings of SECON 2020*,
Lecture Notes in Civil Engineering 97,
https://doi.org/10.1007/978-3-030-55115-5_17

1 Introduction

Fundamental objective of sustainable approach is environmental protection. A product is defined as a sustainable one, if minimum environmental impact is developed during its life cycle. To assess the sustainability of a product, step by step evaluation from cradle to grave has to be done. Important areas are selection of materials and design processes for sustainable products [1].

According to Brundtland sustainable development is defined as "development that meets the needs of the present without compromising the ability of future generations to meet their own needs" [2]. For the civil engineering community, the concept of sustainable development involves the use of high performance materials produced at a reasonable cost and with the lowest possible environmental impact [3]. Practically full sustainability achievement is not possible [1], that means for any material, it is impossible to be perfectly sustainable [4].

Geopolymer technology points towards the sustainable and environmental friendly approaches which minimizes energy requirements and CO_2 emissions by using industrial wastes and by products. Geopolymers are alkali activated aluminosilicate materials with alkaline silicate solution at ambient or slightly elevated temperatures.

Sustainable construction was conceptualized as combination of four aspects of sustainability such as socio-cultural, economic, technological and environmental sustainability. The above conceptual frame work for sustainable affordable construction was framed by, giving equal importance to all sustainable factors [5].

Manufacture of materials and products, its handling and usage in construction and site related activities cause environment pollution [6]. Higher the embodied energy, higher will be the embodied carbon and higher will be the impact on global warming [7]. CO_2 emissions during the production of cement and concrete are the major pollution inducers in construction industry. Carbon dioxide equivalent emissions generated by geopolymer concrete were found less than that of OPC based concrete [8, 9]. Enhancement in the utilization of local materials for energy reduction, promotion in recycling of energy-intensive materials, encouragement in energy-efficient designs and technologies, sustainable utilization of natural resources and reduction in pollution creating materials for achieving sustainable construction [10, 11].

Present study aims to analyse the sustainability of terracotta tile waste based geopolymer concrete blocks with respect to cement concrete blocks. Terracotta tile wastes generated during manufacture of roof tiles and demolition of old tiled roof houses in Kerala, India are used for the study. The feasibility study on geopolymer binder from tile waste has been done [12] and using that geopolymer binder, GCB was produced as an alternative to CCB.

2 Frame Work for Sustainability Assessment

A modified conceptual framework (Fig. 1), is used to evaluate the suitability of GCB by comparing it with conventional CCB of same mix proportion. Through this framework, sustainable material can be achieved by fulfilling the various criteria mentioned under the four factors of sustainability (socio-cultural factors, economic factors, technological factors and environmental factors) with equal significance.

As per the frame work, acceptance, awareness and decentralized production under socio-cultural factor, economic factor with infrastructure, unskilled labour, accessibility to material and material efficiency, technological factor (strength and durability), energy efficiency, waste management, and feasibility for reuse or renewability under environmental factor of GCB and CCB were evaluated.

2.1 Limitations Adopted in Evaluation

Main difference involved in the production of GCB and CCB are in manufacturing processes of binder used in both the blocks. Since transportation effect of materials to lab is approximately similar for both the blocks, it is not taken into account.

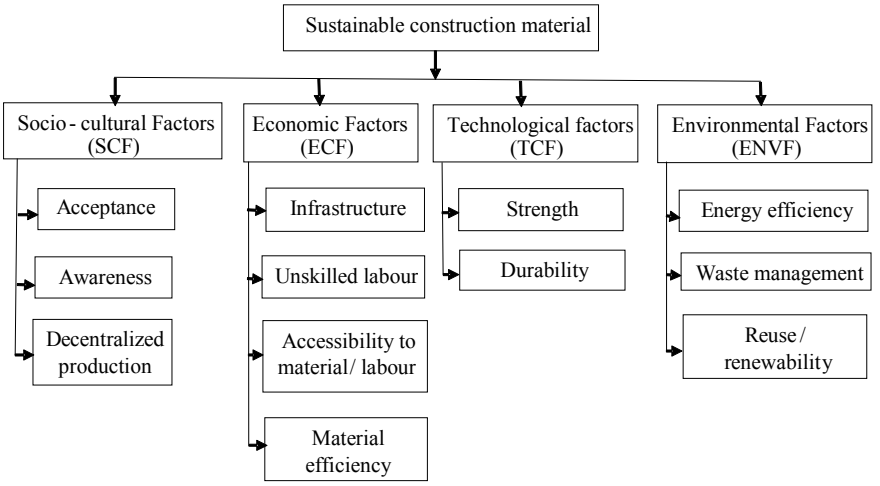

Fig. 1 Modified conceptual framework for sustainability analysis of a construction material

2.2 *Data Used for the Assessment of CO_2 Emission and Embodied Energy*

Energy utilization and CO_2 emission contribution in each step of the block production process are considered for calculation. According to Jagadish et al., embodied energy and CO_2 emission of a product can be arrived by multiplying the conversion factor with the corresponding ingredient quantity [13]. Conversion factors for embodied energy of each material consumed are taken from referred journals [13, 14] for the impact assessment. CO_2 emission factor is adopted from journal publication of Turner and Collins [8]. As per Davidovits, corrections for the concentration of NaOH and sodium silicate are applied in Tables 3 and 4. Percentage concentration is multiplied with quantity to arrive the correct quantity [15].

3 Sustainability Assessment of Geopolymer Concrete Block

Geopolymer concrete blocks and cement concrete blocks of size 300 mm × 200 mm × 150 mm with binder (geopolymer/cement), fine aggregate and coarse aggregate in 1:3:6 mix proportions were cast as per standards. GCBs were cured at room temperature, whereas CCBs were water cured. Geopolymer binder for the present study was prepared from terracotta tile waste powder and alkali activator, with alkali activator to binder ratio as 0.6, sodium silicate to sodium hydroxide solution ratio as 1 and sodium hydroxide molarity as 8 M.

Sustainability analysis of GCB was carried out by considering the four factors of sustainability in detail as per the frame work (Fig. 1). For each factors GCB and CCB are compared. Quantitative analysis of technological factor with two sub criteria (strength and durability) and environmental factor with two sub criteria (energy efficiency and waste management) were done in detail using results of experimental research conducted as per IS: 2185 Part1 (2005) [16] and calculated amount of embodied energy and CO_2 emission of both the blocks. Since the production of geopolymer blocks are in research stage, remaining eight sub criteria under socio-cultural, economic and environmental factors were qualitatively analyzed by comparing both the blocks.

3.1 *Technological Factors (TCF)*

Strength and durability are the basic criteria for technological sustainability.

Strength: Compressive strength and block density are considered as basic requirement for strength characteristics. Compressive strength and density tests were conducted for GCB and CCB as per IS: 2185 Part1 (2005). The results obtained are tabulated in Table 1. The compressive strength and bulk density of the geopolymer

Table 1 Comparison of the properties between geopolymer and cement concrete blocks

Strength criteria	Cement block	Geopolymer block	Value as per IS: 2185 Part1 (2005)	Remarks
Compressive strength	9.5 N/mm^2	5.6 N/mm^2	≥5 N/mm^2	Attained the strength as per IS [16]
Block density	2055.3 kg/m^3	2047.0 kg/m^3	≥1800 kg/m^3	

blocks are strong enough to meet the requirements as per the code provision and par with cement concrete block. As per the code, both the blocks could be used as load bearing unit [16].

Durability: Durability refers to the property of a material that can resist any unacceptable deterioration over a certain period. Water absorption and resistance to aggressive environments are measures of durability.

Test for water absorption as per IS: 2185 Part1 (2005) was conducted for both the blocks. Acid resistance and sulphate resistance of the blocks were tested by immersing in 3% concentration solutions of H_2SO_4 and sodium sulphate for 168 days. The residual strength after immersion in the aggressive environments is found as % of initial strength. The results are compared and shown in Table 2.

The percentage of water absorption for both the blocks satisfies the required specification of IS: 2185 (Part)-2005. Superior performance of GCB over CCB against acid and sulphate resistance can be confirmed from the results presented in Table 2. Hence better durability performance can be evaluated with GCB.

Above discussion shows that the technological sustainability of proposed geopolymer concrete block is over cement concrete block.

3.2 Environmental Factors (ENVF)

Discussion on environmental sustainability of geopolymer concrete block and cement concrete block are based on the three criteria such as energy efficiency, waste management, and the feasibility for reuse or renewability.

Energy efficiency: Energy efficiency is evaluated based on embodied energy. Embodied energy of each ingredient used for the manufacture of block is calculated by multiplying quantity and energy factor of the corresponding ingredient. Embodied energy of one block is arrived by adding the embodied energy of each ingredient. The detailed calculation of embodied energy of one block is given in Table 3. Since geopolymer concrete block production is in research stage, the embodied energy of one block is calculated without considering the energy for transportation of materials to the laboratory.

Embodied energy of cement block is high due to the presence of energy intensive cement. From the above table embodied energy of GCB is 5.15 MJ/block and that of CCB is 15.17 MJ/block. Embodied energy of GCB is 66% lower than that of CCB and hence verifying the better efficiency of GCB over CCB.

Table 2 Comparison of durability criteria between CCB and GCB

Durability criteria	Cement block	Geopolymer block	Remarks
%Water absorption	4.61%	5.98%	≤10% (IS: 2185)
Long term resistance to H_2SO_4 acid (168 days) as residual strength	24.87% of initial compressive strength	71.29% of initial compressive strength	Geopolymer block is better than cement block
Long term resistance to sodium sulphate (168 days) as residual strength	69.37% of initial compressive strength	73.31% of initial compressive strength	Geopolymer block is better than cement block

Table 3 Embodied energy calculation for one building block

Material	Quantity (kg)	Correction coefficient as per [15]	Embodied energy at source (MJ/kg)	References	Total energy for one block	
					Cement block	Geopolymer block
Coarse aggregate	13.97	–	0.10	[14]	1.40	1.40
Fine aggregate	6.98	–	0.02	[14]	0.14	0.14
Cement	2.33	–	5.85	[13]	13.63	–
Tile powder	2.33	–	0.31		–	0.72
NaOH	0.17	0.97	4.98	[14]	–	0.82
Na_2SiO_3	0.7	0.55	5.37	[14]	–	2.07
	Total energy for one block				15.17 MJ	5.15 MJ

Waste management: This criteria refers to the pollution of environment due to the application of the proposed technology/production of material from cradle to grave. Air pollution can be taken as a measure to assess this criteria. It is measured in terms of CO_2 emission during the manufacture of blocks. CO_2 emission of each ingredient used for the manufacture of block is calculated by multiplying quantity and emission factor of the corresponding ingredient. CO_2 emission of one block is arrived by adding the CO_2 emission of each ingredient. Calculations were done based on the production of one block in the laboratory and presented in Table 4.

Table 4 CO_2 emission calculation for one building block

Material	Quantity (kg)	Correction coefficient as per [15]	CO_2 emission/kg production (kg) [8]	Total CO_2 emission for one block (kg)	
				Cement block	Geopolymer block
Coarse aggregate	13.97	–	0.04	0.56	0.56
Fine aggregate	6.98	–	0.01	0.07	0.07
Cement	2.33	–	0.82	1.91	–
Tile powder	2.33	–	0.02	–	0.05
NaOH	0.17	0.97	1.91	–	0.31
Na_2SiO_3	0.7	0.55	1.22	–	0.47
	Total CO_2 emission for one block (kg)			2.54	1.46

The CO_2 emission during the production of cement block is 2.54 kg/block and that of GCB is 1.46 kg/block, i.e. 42.5% lower than that of CCB. Hence air pollution caused by GCB is less compared to CCB during production.

Reusability or Renewability of the material/technology: Reusability of geopolymer block is as comparable to that of the cement block.

Above discussion verifies the environment sustainability of proposed geopolymer concrete block over cement concrete block with respect to all the criteria.

3.3 Socio-cultural Factors (SCF)

Criteria's adopted for socio-cultural sustainability are acceptance, awareness and decentralized production by the above frame work. A comparative study of both the building blocks with respect to each of these criteria is presented.

Acceptance: Colour, texture, surface finish and dimensional stability are the basic features other than strength, durability and affordability that decide the acceptability of a building block among different stake holders. The uniform brick red colour, good texture, smooth surface finish and good dimensional stability of the geopolymer blocks (Fig. 2b) over the conventional concrete blocks (Fig. 2a) can be expected as the positive features for superior acceptance.

Awareness: Awareness on any innovative material/product is a basic criterion for socio-cultural sustainability. As these building blocks are not yet in practice, this criterion can be met by ensuring proper measures for publicity.

Decentralized production: GCB can be manufactured in the similar manner as that of CCBs. This ensures the easy availability of these proposed blocks similar to that of CCBs.

With respect to the above discussion, the socio-cultural sustainability of GCB can be said as comparable to that of CCB.

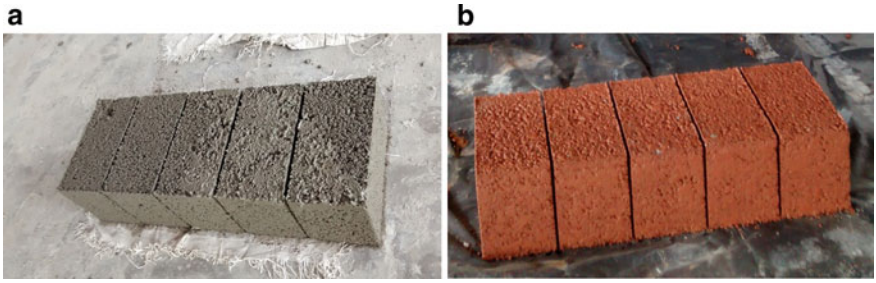

Fig. 2 **a** Cement concrete blocks, **b** geopolymer concrete blocks

3.4 Economic Factors (ECF)

Economic Factors are assessed by different criteria such as infrastructure, unskilled labour, accessibility to material and material efficiency. A comparative discussion of both the building blocks with respect to each of these criteria is presented here.

Infrastructure: The infrastructure facilities required for the manufacture of both the blocks are same as that of cement concrete block.

Accessibility to material and unskilled labour: Accessibility of raw materials and labour required for the production of both the blocks are comparable. Cement in the cement concrete block is replaced by terracotta tile waste and alkaline activator in the proposed geopolymer concrete block. The damaged/faulty tiles remain as the waste material from tile factories and used tiles from dismantled traditional houses in Kerala justifies the accessibility of the raw materials for the production of the new binder and hence ensuring the affordability of geopolymer block.

Material efficiency: Comparison of geopolymer block and cement concrete block with respect to this criterion justify the superiority of GCB over CCB as it utilizes waste materials.

Even though geopolymer concrete block is comparable with respect to cement concrete block under various criteria of economic sustainability discussed above, affordability of these blocks can be verified only after commercial production.

4 Conclusion

The sustainability assessment of GCB was evaluated with four factors (socio-cultural, economic, technological and environmental factors) of modified frame work. Quantitative analysis was done with two sub criteria each of technological and environmental sustainability by comparing the experimental results of GCB with that of CCB. The following conclusions are summarized based on the quantitative analysis of technological and environmental sustainability.

- The performance of GCB is better than CCB under technological sustainability.
- In environmental sustainability analysis, embodied energy of GCB is 66% lower than that of CCB, which is a measure of energy efficiency. CO_2 emission, during the production of GCB is 42.5% lower than that of CCB. The reduction of air pollution in terms of CO_2 and energy saving during production can be achieved by GCB compared to CCB.

With respect to socio cultural and economic sustainability, terracotta tile waste based geopolymer blocks show a comparable expected result with conventional building blocks, as it is only in the research stage.

The overall analysis reveals that geopolymer concrete blocks are more sustainable than cement concrete blocks.

References

1. Lennart L, Ljungberg (2007) Materials selection and design for development of sustainable products. Mater Des 28(2):466–479
2. WCED (1987) Our common future, world commission on environment and development. Oxford University Press, New York
3. Bilodeau A, Malhotra VM (2000) High-volume fly ash system: concrete solution for sustainable development. ACI Mater J 97(1):41–48
4. Pimsiri T (2007) Green buildings: defining sustainable construction materials in Thailand. Master of Architecture thesis. Iowa State University, Ames
5. Nair DG (2006). Sustainable-affordable housing for the poor in Kerala. PhD thesis, Delft University Technology
6. Sabnis A, Mysore P, Anant S (2015) Construction materials-embodied energy footprint-global warming; interaction. Structural Engineers World Congress, Conference Paper, October, Singapore
7. Rehan and Ahmed (2012) Construction and the environment, report of environmental control directorate. Public Commission for the Protection of Marine Resources, Environment & Wildlife, Kingdom of Bahrain
8. Turner LK, Collins FG (2013) Carbon dioxide equivalent (CO2-e) emissions: a comparison between geopolymer and OPC cement concrete. Constr Build Mater 43:125–130
9. Petrillo A, Cioffi R, Ferone C, Colangelo F, Borrelli C (2016) Eco-sustainable geopolymer concrete blocks production process. Agric Agr Sci Proc 8:408–418
10. Shams S, Sadrul Islam AKM, Arafat A (2010) Bhuiyan, sustainable construction: a step towards reducing CO_2 emission. In: The 1st built environment development symposium: real estate and housing sustainability, Dammam, 25–27 Oct
11. Shams S, Sadrul Islam AKM (2010) Sustainable construction and approaches for greener homes. https://doi.org/10.1109/ICDRET.2009.5454230. Source: IEEE Xplore, Conference paper
12. Usha S, Nair DG, Vishnudas S (2016) Feasibility study of geopolymer binder from terracotta roof tile waste. Procedia Technol 25:186–193
13. Jagadish KS, Venkatarama Reddy BV, Nanjunda Rao KS (2014) Alternative building materials and technologies. New Age International (P) Limited Publishers, New Delhi
14. Ostwal T, Manojkumar V, Chitawadagi (2014) Experimental investigations on strength, durability, sustainability and economic characteristics of geopolymer concrete blocks. Int J Res Eng Technol 3(6):115–122
15. Davidovits, J. (2015) False values on CO_2 emission for geopolymer cement/concrete published in scientific papers. Technical paper #24. Geopolymer Institute Library. www.geopolymer.org
16. IS: 2185 (Part1)-2005. Concrete masonry units—specification, part 1 hollow and solid concrete blocks. Bureau of Indian Standards, New Delhi, India

Study on Structural Performance of Non-prismatic Girders with Double Corrugated Stiffened Steel and Composite Webs

M. Saranya Radhakrishnan and P. Binu

Abstract There are some impediments to the effective use of conventional flat web steel girders such as poor web stability and low buckling strength. To overcome these kinds of problems, the idea of using steel corrugated webs to bridge girders has been introduced to get enhanced web stability and buckling strength. The existing studies on bridge girders with steel corrugated webs are focused on single corrugated web girders. According to previous researches, large forces generated on the girders result in buckling of single corrugated web. This paper focuses on Double corrugated web girders. The Double corrugated web girders can be strengthen either by providing stiffeners along with the corrugated web or by making the web as a composite one. This paper consists of buckling investigations on Double Corrugated Stiffened Steel Web Non-prismatic girders (DCSSWG) consist of two stiffened corrugated steel webs with steel flat flanges and also on Double Corrugated Composite Web Non-prismatic girders (DCCWG) having Ultra-Lightweight Cement Composite fill (ULCC) in the space between two corrugated steel webs. Buckling performance of Non-prismatic girders with Double Corrugated Stiffened Steel Webs and Double Corrugated Composite Webs having different tapered ratios are investigated using ANSYS 16.1 software. The results obtained from the study have shown that Non prismatic girders with Double Corrugated Composite Webs show more buckling strength as compared to Double Corrugated Stiffened Steel Webs for the same tapered ratio.

Keywords Tapered ratio · Non-prismatic girder · Corrugated web

M. Saranya Radhakrishnan (✉) · P. Binu
Department of Civil Engineering, Sree Narayana Gurukulam College of Engineering, Ernakulam, Kerala, India
e-mail: saranyavjec@gmail.com

© Springer Nature Switzerland AG 2021

K. Dasgupta et al. (eds.), *Proceedings of SECON 2020*,
Lecture Notes in Civil Engineering 97,
https://doi.org/10.1007/978-3-030-55115-5_18

1 Introduction

The corrugated steel web plates have a lot of favorable properties and recently it is used for many structural engineering applications, especially in the field of bridges. Bridge girders with corrugated webs have a number of advantages such as more out-of plane stiffness, higher buckling resistance and shear capacity, excellent strength and web stability than that of conventional flat web girders. Some examples of bridges provided with corrugated steel web girders are the Maupré Bridge constructed in France and the Hondani Bridge constructed in Japan. According to previous researches, large forces generated on the girders result in buckling of single corrugated steel webs. For improving its strength and web stability, Double corrugated webs can be provided. The present study focuses on Double corrugated web girders. The purpose of this paper is to obtain numerical modelling results on Single and Dual linearly tapered girders (Non-prismatic girders) with Double corrugated webs. A tapered girder is wider at one end than the other, giving a tapered appearance to the member and the term Tapered ratio is the ratio between maximum web height to minimum web height of tapered girders (Non-prismatic girders). The objectives of this paper are to investigate buckling performance of Single Non-prismatic girders with Double Corrugated Stiffened Steel Webs and Double Corrugated Composite Webs for different tapered ratios and also to investigate buckling performance on Dual Non-prismatic girders with Double Corrugated Stiffened Steel Webs and Double Corrugated Composite Webs for different tapered ratios of corrugated web.

2 Literature Review

Kovesdi and Dunai [1] conducted investigations on prismatic single corrugated web girders and patch load resistance was determined. It was showed that loading length, flat flange thickness and also girder span have a significant effect on patch loading resistance and buckling strength of girders. Kovesdi et al. [2] investigated Interacting stability behavior of steel I-girders with single corrugated steel webs. The results showed that interacting stability depended more on ratio of flange to corrugated web patch loading resistance of prismatic steel I-girders. Hassanein and Kharoob [3] conducted study on the single corrugated steel webs of tapered bridge girders. From the study, the increase in shear strength was found to be linear with the web thickness increment of the linearly tapered corrugated steel webs. Zevallos et al. [4] presented a study on shear performance of tapered web panels of the linearly tapered bridge girders with single corrugated steel webs. It was observed that web thickness of girders has a greater influence on their shear behaviour. Wang et al. [5] conducted study on prismatic steel I-girders with single corrugated webs for various stiffener arrangements. From the study it can be observed that strength and stability of corrugated web with vertical stiffeners was more than that of horizontal stiffeners.

Other studies [6–11] show that, a lot of parameters related to geometry (such as thickness of web and flanges, fold height-to-width aspect ratio of corrugated web, the fold width-to-thickness ratio of web, span, web corrugation angle, flange inclination angle etc.) and loading conditions (including position of the applied load [parallel, inclined fold or corner area], loading length etc.) affect behaviour of trapezoidal corrugated web girders. According to previous researches and studies large forces on the girders result in buckling failure of single corrugated webs. To strengthen it, Double corrugated web girders can be provided.

3 Numerical Study on Non-prismatic Girders

The geometric details of the corrugated web for all models considered for this study are shown in Fig. 1. For numerical study both Single (Fig. 2) and Dual (Fig. 3) Non-prismatic girders are considered. For Single Non-prismatic girders, three kinds of models were made using shell 181 elements. First one is Single Non-prismatic girder with Double Corrugated Web (DCWG), where additional stiffeners or members were not provided. Second one is Single Non-prismatic girder with Double Corrugated Stiffened Steel Web (DCSSW) and third one is Single Non-prismatic girder with Double Corrugated Composite Webs (DCCWG). Each model consists of steel flat flanges and steel corrugated webs, connected by normal welding. In case of DCSSW, additional stiffeners having same thickness of corrugated webs were provided in between the two corrugated webs as shown in Fig. 4. In case of DCCW, an extra material Ultra-Lightweight Cement Composite (ULCC) fill was provided in space between two corrugated steel webs instead of stiffeners. For Dual Non-prismatic girders, two kinds of models were made using shell 181 elements, one is with DCSSW and another one is with DCCW. Both Single and Dual girders are simply supported and 4 points loading was applied. The Properties of steel corrugated web for all models are shown in Table 1. ULCC is characterized by low density <1500 kg/m^3 and high compressive strength >60 MPa. The properties of ULCC for composite webs are given in Table 2 (Figs. 2, 3 and 4).

The length of Single and Dual Non-prismatic girders was adopted as 4500 mm and 9000 mm respectively, Thickness of flat flange is 20 mm and for corrugated web is 6 mm, Width of flange is 300 mm and height of corrugated web for each

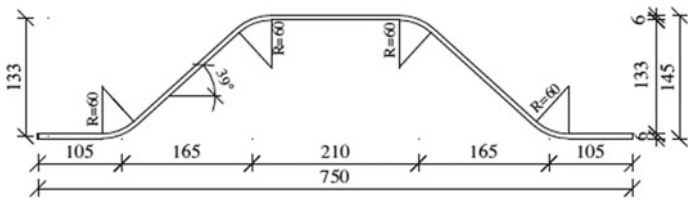

Fig. 1 The geometric details of corrugated steel web [1]

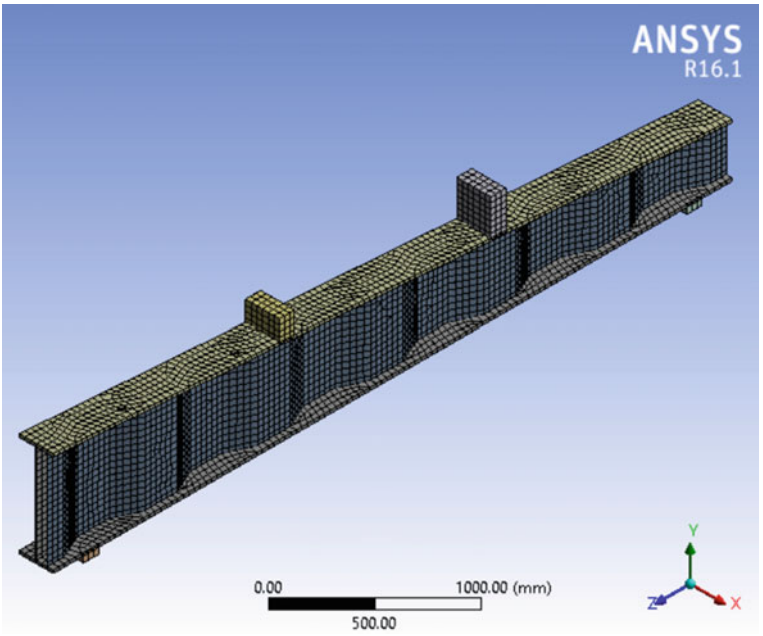

Fig. 2 Single non-prismatic girder

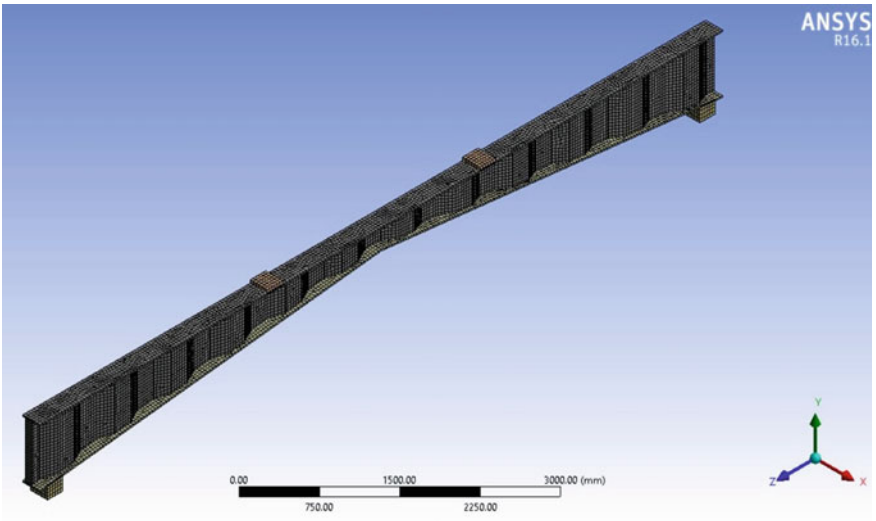

Fig. 3 Dual non-prismatic girder

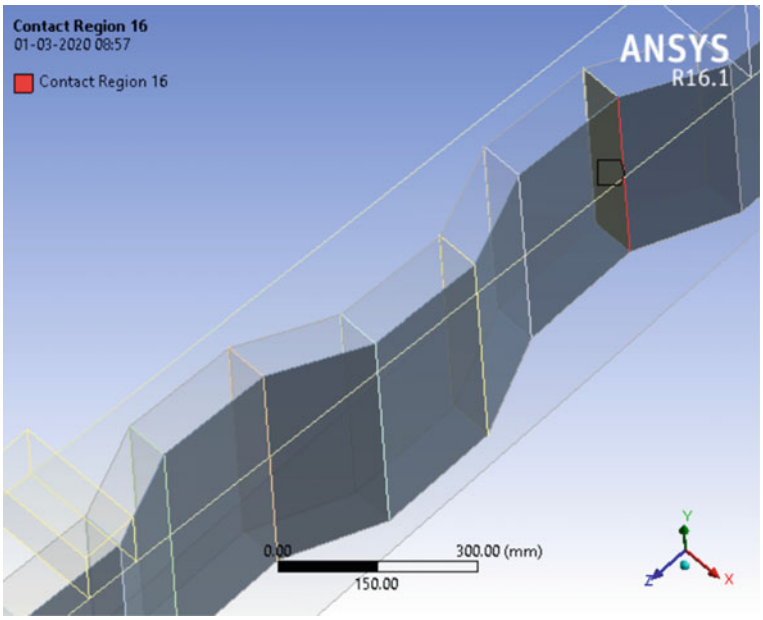

Fig. 4 Double corrugated stiffened steel web

Table 1 Material properties of corrugated web

Properties	Values
Modulus of elasticity	2×10^5 N/mm^2
Poisson's ratio	0.3
Density	7850 kg/m^3
Yield strength	379 MPa

Table 2 Material properties of ULCC for composite web

Properties	Values
Modulus of elasticity of ULCC	10.62 GPa
Poisson's ratio of ULCC	0.15
Density of ULCC	1250 kg/m^3

model is adopted as in Table 3 for different tapered ratios of web. The performance of Non-Prismatic girders was investigated under different tapered ratios of web. The average height of corrugated web for each model is about 500 mm. Tapered ratios of 1.5, 2, 3, and 4 was adopted for this numerical study of Single Non-prismatic girders and for Dual Non-prismatic girders tapered ratios of 2, 3 and 4 was adopted.

Table 3 Tapered ratios for girders

Tapered ratio of web (h_1/h_2)	Height of web h_1 (mm)	Height of web h_2 (mm)
1.5	600	400
2	670	335
3	750	250
4	800	200

4 Results and Discussion

4.1 Load-Deflection Curve for Single Non-prismatic Girders

The Ultimate load and total deformation of each specimens was obtained from ANSYS 16.1. WORKBENCH. Each specimen was failed by local buckling of corrugated web. Figures 5, 6 and 7 show combined Load-Deflection curve for single Non-prismatic girders with Double Corrugated Web (DCWG), Single Non-prismatic girders with Double Corrugated Stiffened Steel Web (DCSSWG) and Single Non-prismatic girders with Double Corrugated Composite Web (DCCWG) respectively obtained for different tapered ratios of corrugated web.

From the obtained results, it can be observed that Single Non-prismatic girders with Double Corrugated Composite Web (DCCWG) show high load carrying capacity and better strength as compared to Single Non prismatic girders with Double Corrugated Stiffened Steel Web (DCSSWG) for the same tapered ratio. Figure 8 shows the final results for Single Non-prismatic girders.

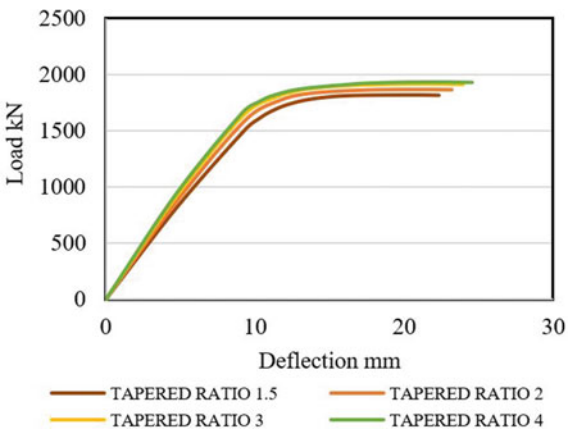

Fig. 5 Load-deflection curve for single non prismatic girders with double corrugated web (DCWG) for different tapered ratios

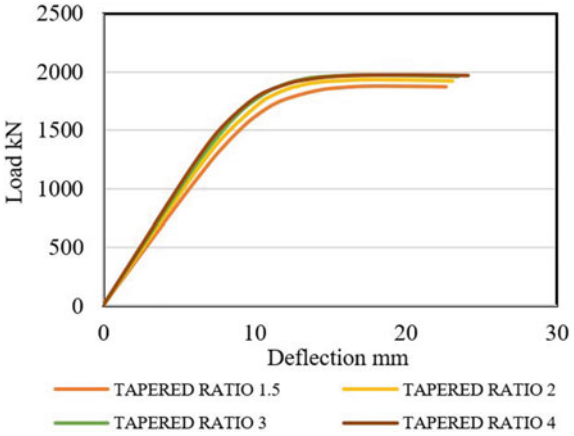

Fig. 6 Load–deflection curve for single non prismatic girders with double corrugated stiffened steel web (DCSSWG) for different tapered ratios

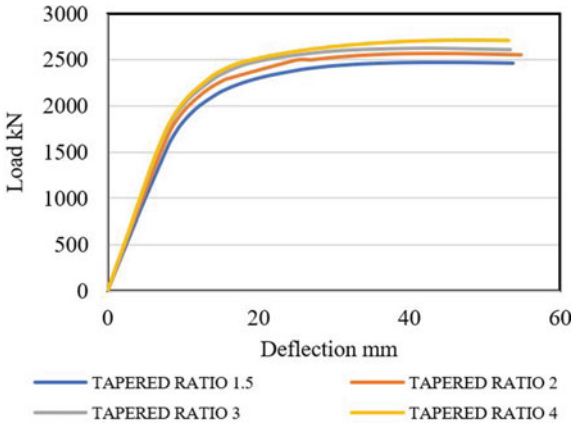

Fig. 7 Load–deflection curve for single non prismatic girders with double corrugated composite web (DCCWG) for different tapered ratios

4.2 Load-Deflection Curve for Dual Non-prismatic Girders

The Ultimate load and total deformation of each specimens was obtained from ANSYS 16.1. WORKBENCH. Each specimen was failed by local buckling of corrugated web. Figures 9 and 10 show combined Load-Deflection curve for Dual Non prismatic girders with DCSSW and Dual Non prismatic girders with DCCW respectively, obtained for different tapered ratios of corrugated web.

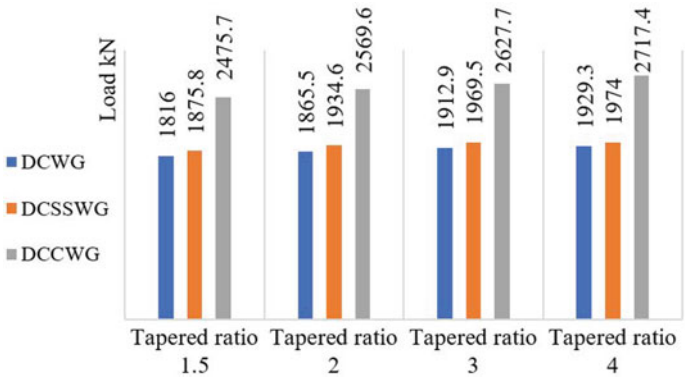

Fig. 8 Load carrying capacity obtained for single non-prismatic girders

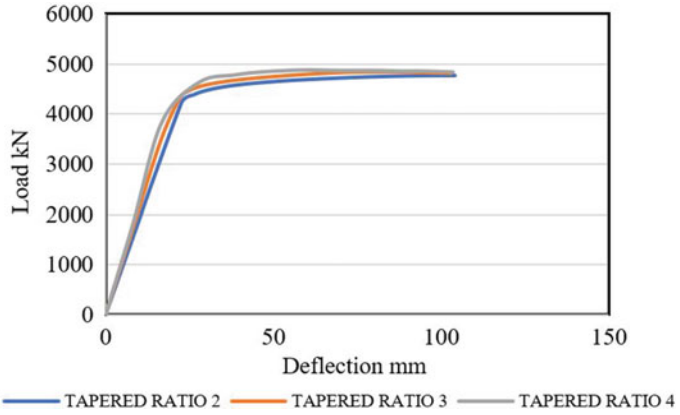

Fig. 9 Load-deflection curve for dual non prismatic girders with double corrugated stiffened steel web [DCSSWG] for different tapered ratios

From the obtained results, it can be observed that Dual Non-prismatic girders with Double Corrugated Composite Web (DCCWG) show high load carrying capacity and better strength as compared to Dual Non prismatic girders with Double Corrugated Stiffened Steel Web (DCSSWG) for the same tapered ratio. Figure 11 shows the final results for Dual Non-prismatic girders.

5 Conclusions

The Single and Dual Non prismatic girders with Double corrugated web can be strengthen in two ways. One way is to provide Double corrugated steel web with

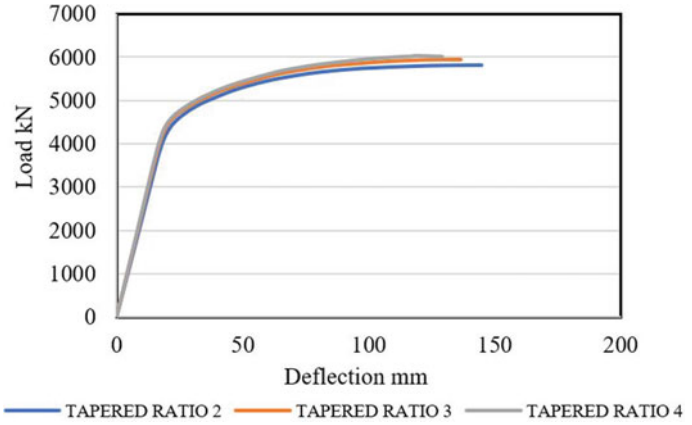

Fig. 10 Load-deflection curve for dual non prismatic girders with double corrugated composite web [DCCWG] for different tapered ratios

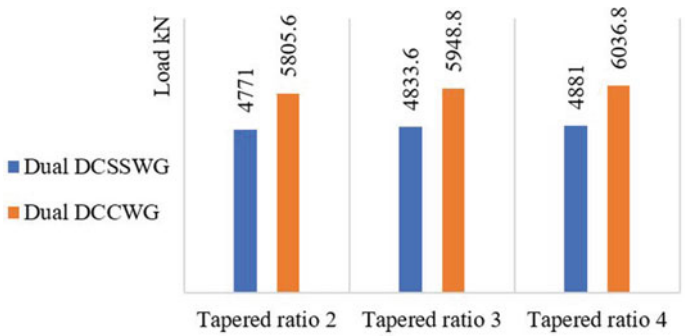

Fig. 11 Load carrying capacity obtained for dual non prismatic girders

stiffeners. Another way is to provide Ultra Lightweight Cement Composite fill along with Double corrugated steel webs. From the results obtained from this paper, it can be concluded as follows;

- The load carrying capacity and buckling strength of Non-prismatic girders with Double corrugated web is affected by tapered ratio of web, in case of both Single and Dual girders. In all cases load-carrying capacity is gradually improved as per the increase in tapered ratio of corrugated web.
- The strength and load carrying capacity of Single and Dual Non-prismatic girders with Double corrugated web can be improved by means of providing stiffeners or by making the web as composite one by providing ULCC fill.
- Both Single and Dual Non prismatic girders with Double corrugated composite web exhibit more buckling strength and the rate of improvement of strength is excellent for composite web than that of stiffened steel web.

References

1. Kovesdi B, Dunai L (2011) Determination of the patch loading resistance of girders with corrugated webs using nonlinear finite element analysis. Comput Struct 89
2. Kovesdi B, Dunai L, Kuhlmann U (2012) Interacting stability behaviour of steel I-girders with corrugated webs. Thin-Walled Struct 61:132–144
3. Hassanein MF, Kharoob OF (2014) Shear buckling behavior of tapered bridge girders with steel corrugated webs. Eng Struct 74:157–169
4. Zevallos E, Hassanein MF, Real E, Mirambell E (2016) Shear evaluation of tapered bridge girder panels with steel corrugated webs near the supports of continuous bridges. Eng Struct 113:149–159
5. Wang S, He J, Liu Y (2019) Shear behavior of steel I—girder with stiffened corrugated web. Part I: experimental study. Thin-Walled Struct 140:248–262
6. Nie J-G, Zhu Li, Tao M-X, Tang L (2013) Shear strength of trapezoidal corrugated steel webs. J Constr Steel Res 85:105–115
7. Guo T, Sause R (2014) Analysis of local elastic shear buckling of trapezoidal corrugated steel webs. J Constr Steel Res 102:59–71
8. Jáger B, Dunai L, Kövesdi B (2017) Flange buckling behavior of girders with corrugated web. Part I: experimental study. Thin-Walled Struct 118:181–195
9. Leblouba M, Barakat S, Altoubat S, Junaid TM, Maalej M (2017) Normalized shear strength of trapezoidal corrugated steel webs. J Constr Steel Res 136:75–90
10. Leblouba M, Barakat S, Al-Saadon Z (2018) Shear behavior of corrugated web panels and sensitivity analysis. J Constr Steel Res 151:94–107
11. Wang Z-Y, Li X et al (2018) Shear response of trapezoidal profiled webs in girders with concrete-filled RHS flanges. Eng Struct 174:212–228

Structural Performance of Multi-sectional CFST Columns with Double Corrugated Plate

P. A. Azna and Ranjan Abraham

Abstract Single concrete filled steel tube (CFST) members are widely used in building structures and bridges due to their high strength, ductility, toughness, fire resistance[1], energy absorption capacity, fast track construction and low cost, which is due to the composite action between steel tube and core concrete. This study examines structural performance of composite columns comprising of concrete filled steel tubes connected with double corrugated plate. T-shape, C-shape and Z-shaped sections are selected for this study. Non-linear finite element (FE) model was developed using ANSYS 16.1 to study structural performance of these special shaped CFST columns (SCFST). SCFST columns were analysed under axial compression, eccentric and lateral loads. Failure pattern, buckling capacity, strength and stiffness of specimens were investigated.

Keywords SCFST columns · Finite element analysis (FEA) · Double corrugated plate · Eccentricity · Buckling analysis

1 Introduction

Single concrete filled steel tube (CFST) members are widely used in building structures and bridges due to their high strength, ductility, toughness, fast track construction and low-cost, which is due to the composite action between steel tube and its core concrete [2]. Moreover, shuttering is not required during construction, which reduces construction cost and time. These advantages have been widely exploited and led to the extensive use of concrete filled tubular structures [3, 4]. To further

P. A. Azna (✉) · R. Abraham
Department of Civil Engineering, Ilahia College of Engineering and Technology, Mulavoor P.O., Muvattupuzha, Ernakulam, Kerala 686673, India
e-mail: aznapa786@gmail.com

R. Abraham
e-mail: ranjanabraham@icet.ac.in

© Springer Nature Switzerland AG 2021

K. Dasgupta et al. (eds.), *Proceedings of SECON 2020*,
Lecture Notes in Civil Engineering 97,
https://doi.org/10.1007/978-3-030-55115-5_19

the development of CFST columns and to promote application of CFST columns in building structures, many scholars have proposed special shaped CFST columns, such as multiple cell special shaped CFST columns [5], special shaped columns fabricated using concrete filled steel tubes [6] and special shaped concrete-filled steel tube columns [7].

Studies have shown that constraining effect of special shaped CFST columns is largely concentrated at their corners and this effect decreases rapidly outside the corner. Material strengths of the steel and concrete are not used to their full advantage in column, since constraining effect of steel plate in middle section of column on core concrete is negligible [3]. To address this issue, many scholars have attempted to optimize various special-shaped CFST columns. Zhang et al. [3] proposed L-shaped column comprising concrete filled steel tube connected by double vertical steel plate filled with concrete (LCFST-D). Xu [8] proposed multi-cell shaped CFST column connected by steel linking plates. It has been shown that special-shaped columns comprising CFST connected by single vertical steel plates cannot meet the requirements of high-rise steel housing construction in terms of bearing capacity and welding transverse stiffeners, complicating their application in rapid industrial construction processes.

In this study, structural performance of T-shape, C-shape and Z-shaped columns comprising concrete filled steel tubes connected with double corrugated plate is assessed. A finite element (FE) model was developed using ANSYS 16.1 to understand structural performance of these special shaped CFST columns (SCFST). Columns were analyzed under axial compression, eccentric and lateral loads. Column limbs were provided with concrete filled steel tubes primarily for withstanding compressive forces. Built-up section offered greater stiffness and were proved to be more advantageous in situations of large load eccentricity and/or high slenderness ratio, as it consisted of multiple column limbs. CFST columns with plate connections have been widely used in large-span structures and bridges. Plate connected CFST members could be used as such, as they could be embedded in walls of buildings.

2 Finite Element Modelling

2.1 General

Finite element model was developed using SOLID186 element of ANSYS 16.1 to investigate structural behaviour of SCFST columns. SOLID186 is a higher order 3D 20-node solid element exhibiting quadratic displacement behavior, defined by 20 nodes having three degrees of freedom per node (translations in the nodal x, y and z-directions) ie, UX, UY, UZ.

2.2 Geometry

SCFST column connected with double corrugated plate were adopted for Finite Element Analysis. Sectional dimensions of mono-steel tubes were 100 × 100 × 5.75 mm. Length of column was 3000 mm. Vertical steel plates were provided with a width of 140 mm and thickness of 6 mm. Geometry of T-shape, C-shape and Z-shaped CFST column connected with double corrugated plate in finite Element modelling are shown in Figs. 1 and 2. Mechanical properties of mono-steel tube and vertical steel plate are shown in Table 1. Multilinear isotropic hardening was used to reproduce plastic behavior of materials. Weight of finite element models were kept constant in all cases. Stress–strain curve for steel and concrete are shown in Figs. 3 and 4 respectively.

Figure 5 Boundary conditions of SCFST column with double corrugated plate connection. To stimulate real conditions, SCFST column was analyzed with both ends constrained in X, Y, and Z displacement directions. In addition, rotation about

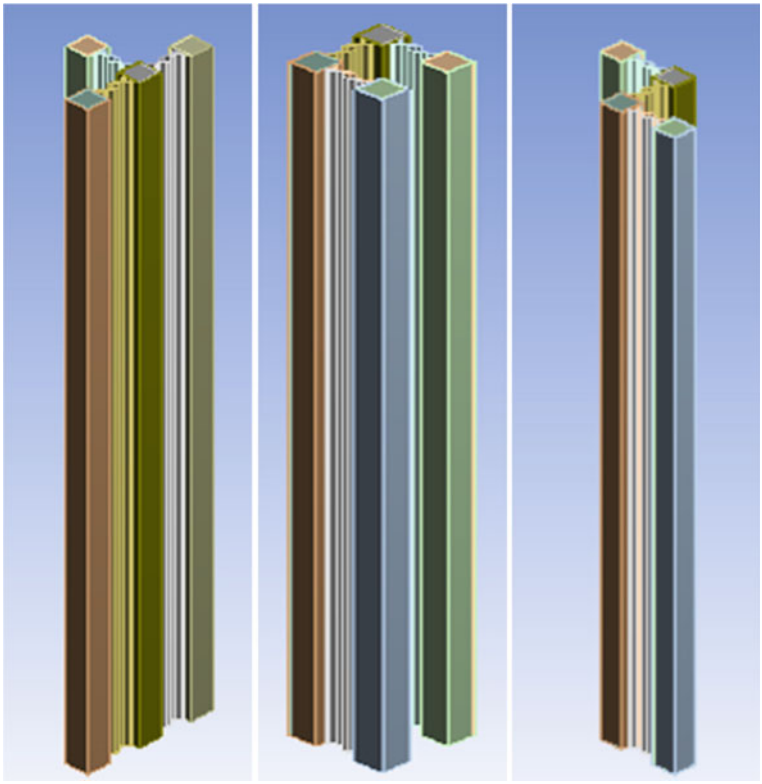

Fig. 1 Geometry of T-shape, C-shape and Z-shaped CFST columns connected with corrugated plate

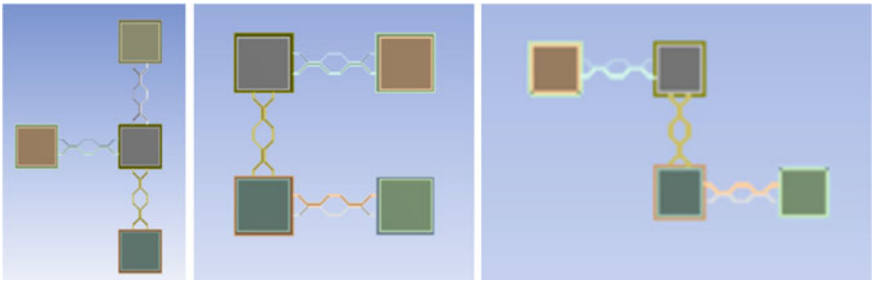

Fig. 2 Top view of T-shape, C-shape and Z-shaped CFST columns connected with corrugated plate

Table 1 Mechanical properties (as in journal [3])

Material	Size or thickness (mm)	f_y (MPa)	E_s (MPa)	Poisson's ratio (μ)
Steel tube	100 × 100 × 5.75	380	2.01×10^5	0.3
Corrugated plate	140 × 6	368	1.76×10^5	0.3
Concrete	$f_c = 32.4$ N/mm^2			0.15

f_y = yield strength of steel, E_s = modulus of elasticity of steel, f_c = compressive strength of concrete

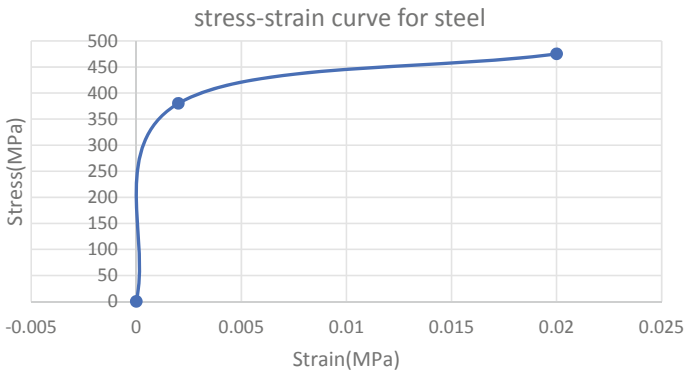

Fig. 3 Stress–strain curve for steel

Y-axis was also constrained and load was applied in one direction. FE contains 3 DOF per node for the model, but support condition is given as remote displacement and it represented in UX, UY, UZ and ROT X, ROT Y, ROT Z. As the support condition is pinned, rotation about y axis was constrained.

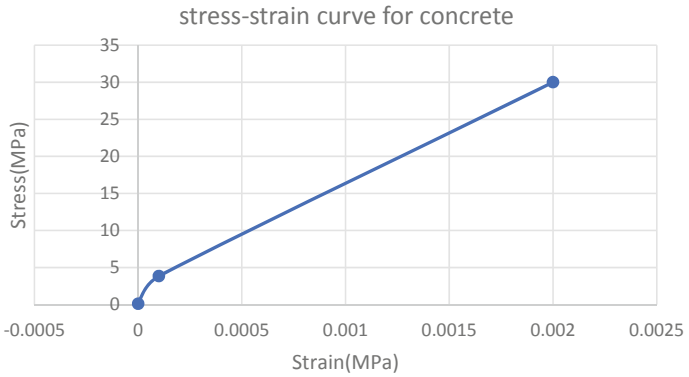

Fig. 4 Stress–strain curve for concrete

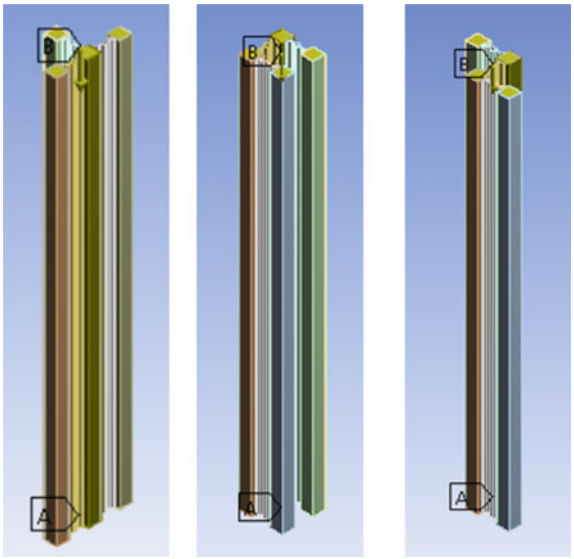

a) T-shape b) C-shape c) Z-shape

Fig. 5 Boundary conditions of SCFST columns

2.3 Analytical Results

2.3.1 Axial Compression

Columns were axially loaded. Displacement controlled force was given in the analysis. Figure 6 shows comparison of load–displacement curve obtained from finite element model. From load–displacement curve it was observed that, Z-shaped

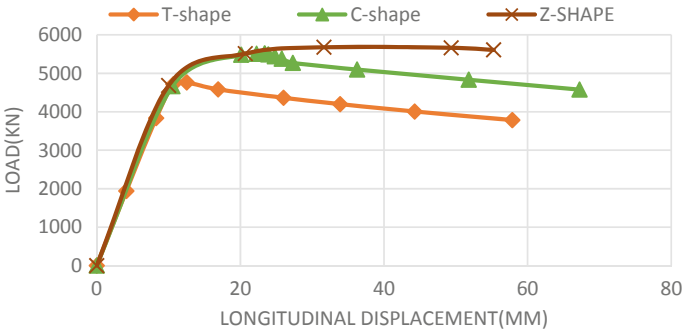

Fig. 6 Comparison of load–displacement curves of specimens

column showed better performance than C-shape and T-shaped column in axial compression. Figure 7 represents stress distribution along entire specimen under axial loading. T-shape and C-shaped column showed complete global buckling towards outside. Global buckling was the major failure mode. Damage occurred mainly in middle part of columns. For Z-shaped column, corner CFST tubes underwent local limb buckling indicating that it resisted lateral deformation and offered better loading performance compared to others.

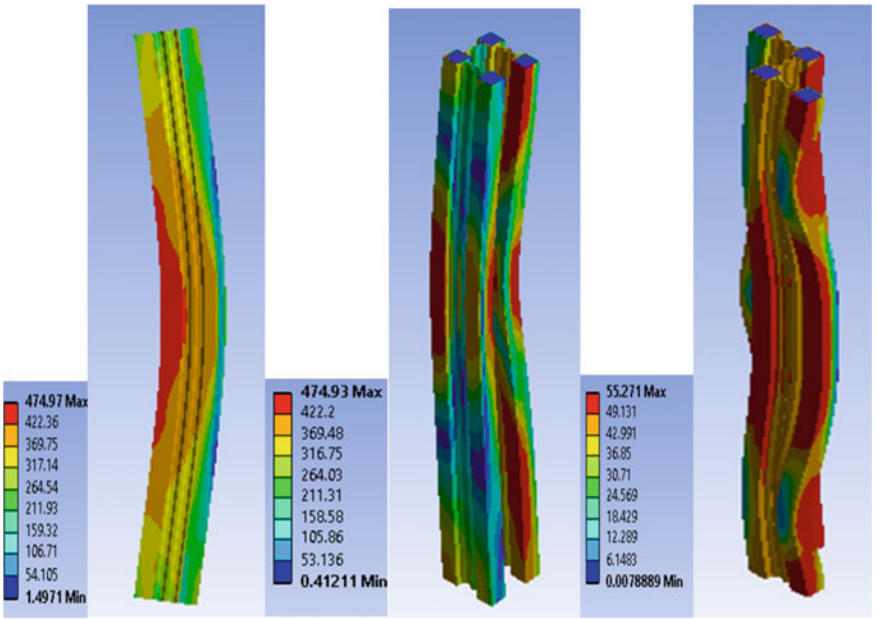

Fig. 7 Von-mises stress diagram of typical failures of specimen

2.3.2 Eccentric Loading

Specimens were analysed for different eccentric loading in both directions. Centroid of composite areas was determined and eccentric loading is given at points of 25% and 50% eccentricity from the CG point. Figures 8 and 9 represents load–displacement comparison of specimens at 25% eccentricity in x and z direction respectively. Table 2 shows the values of eccentricities taken for analysis.

Figure 10 represents variation of ultimate load due to 25% and 50% eccentricity in both X and Z direction. As eccentricity increased, ultimate load reduced. T-shaped column showed better performance under eccentric loading in both directions. Due to asymmetrical shapes, eccentric loading performance in Z-direction was more for C-shape and Z-shaped columns than in X-direction. T-shaped column showed better eccentric performance in X-direction than Z-direction. Figure 11 shows stress variation of specimens and it reveals that each of the specimen largely exhibited global buckling of steel tube towards outside.

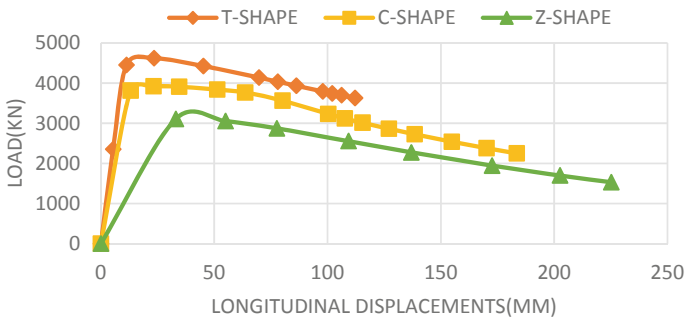

Fig. 8 Comparison of load–displacement curves at an eccentricity of 25% in X-direction

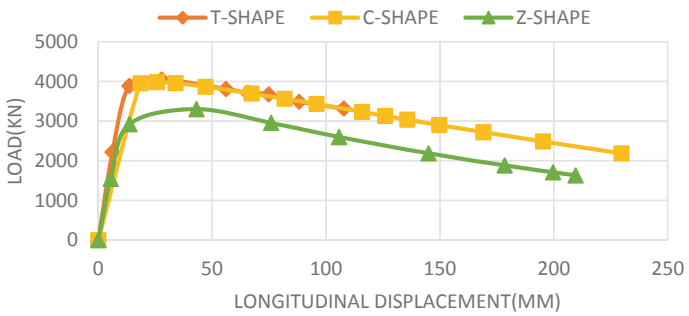

Fig. 9 Comparison of load–displacement curves at an eccentricity of 25% in Z-direction

Table 2 Values of eccentricities taken in both directions

Column type	X-axis		Z-axis	
	25%	50%	25%	50%
T-shape	27.204	54.407	72.5	145
C-shape	42.5	85	42.5	85
Z-shape	72.5	145	42.2	85

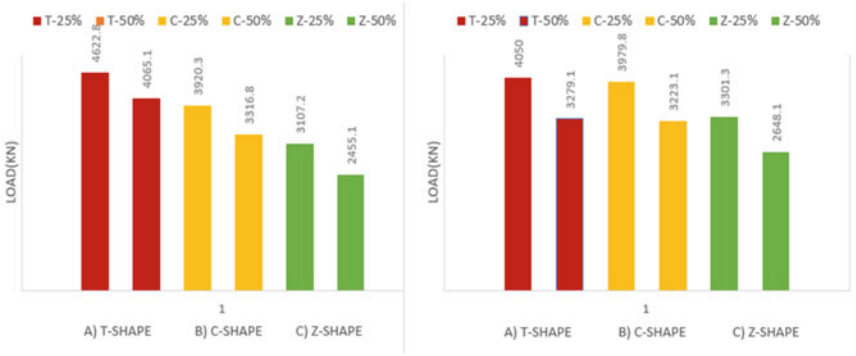

a) X-direction b) Z-direction

Fig. 10 Comparison of ultimate load at different eccentricity

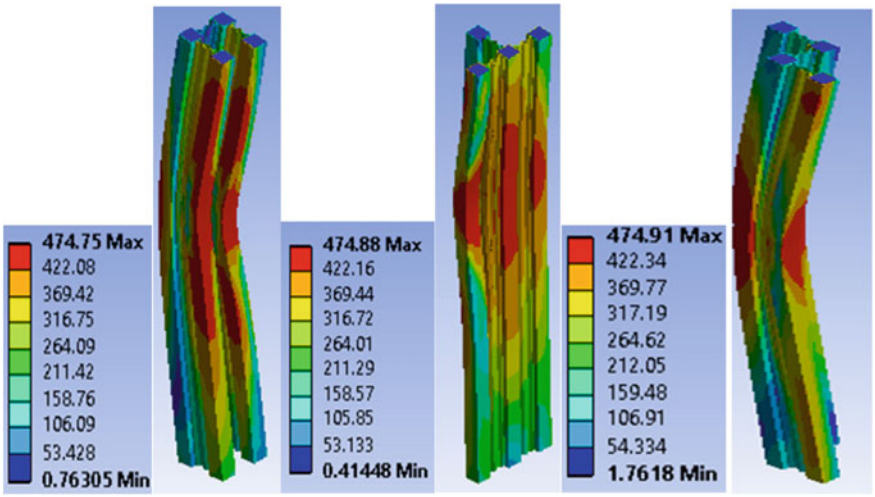

a) C-shape b) T-shape d) Z=shape

Fig. 11 Von-mises stress diagram of typical failures of specimen

2.3.3 Lateral Loading

Lateral loading is very important in zones of high seismic risk. Lateral loading is achieved by making bottom support fixed and top support free. Based on analysis results, Z-shaped column showed better performance under lateral loading due to stability of its shape rather than ordinary shaped columns. C-shaped column showed more deflection in both x and z direction which means that it has more ductility compared to other ones. Figure 12 represents comparison of lateral load–displacement curves in both x and z direction for each specimen. Deflection was observed to be more for C-shaped column reveals that it is more ductile compared to others.

Z-shaped column showed better performance in both axial and lateral loading conditions and mono columns functioned well together under loading. Table 3 shows results for varying slenderness ratio. Slenderness ratio is checked to show the variation in ultimate strength. As slenderness ratio increased, strength, stiffness and ultimate load decreased and the specimen experienced large deflection. Figure 13 shows variation of ultimate strength due to increase in slenderness ratio under axial loading condition.

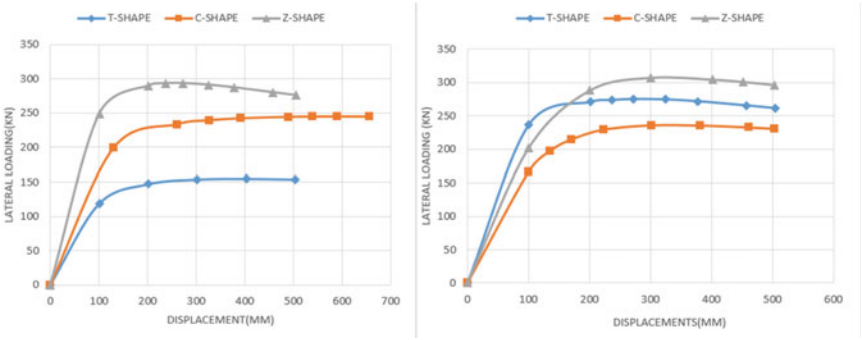

a) Lateral load in x-direction b) lateral load in z-direction

Fig. 12 Comparison of lateral load–displacement curves in x and z-direction

Table 3 Finite element analysis results for varying slenderness ratio

Column type	Size of column (mm)	Length (mm)	Slenderness ratio	Ultimate load (kN)
Z1	100 × 100 × 5.75	2000	16.37	6140
Z2	100 × 100 × 5.75	2500	20.46	6074
Z3	100 × 100 × 5.75	3000	24.55	5678

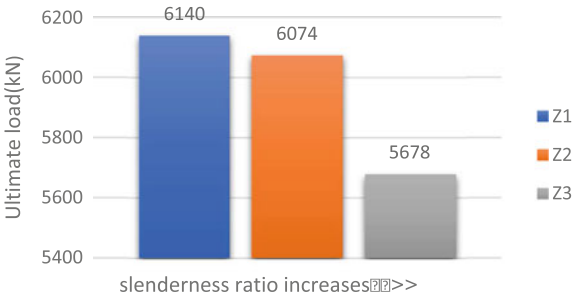

Fig. 13 Variation of strength due to increase in slenderness ratio

2.3.4 Comparison with Hollow Steel Tube Column Under Axial Loading

T-shape, C-shape and Z-shaped hollow steel tubes connected with double corrugated plate were analysed under axial loading for comparing their structural performance with SCFST columns. Figure 14 shows the geometry of hollow steel columns. Figure 16 shows comparison in ultimate strength for SCFST and hollow steel tube columns. Special shaped CFST columns offered better performance than hollow steel tube columns, due to composite action between steel tube and its core concrete. Internal filling with concrete increased load carrying capacity of column and effectively delayed buckling of column due to greater stiffness. Table 4 shows comparison

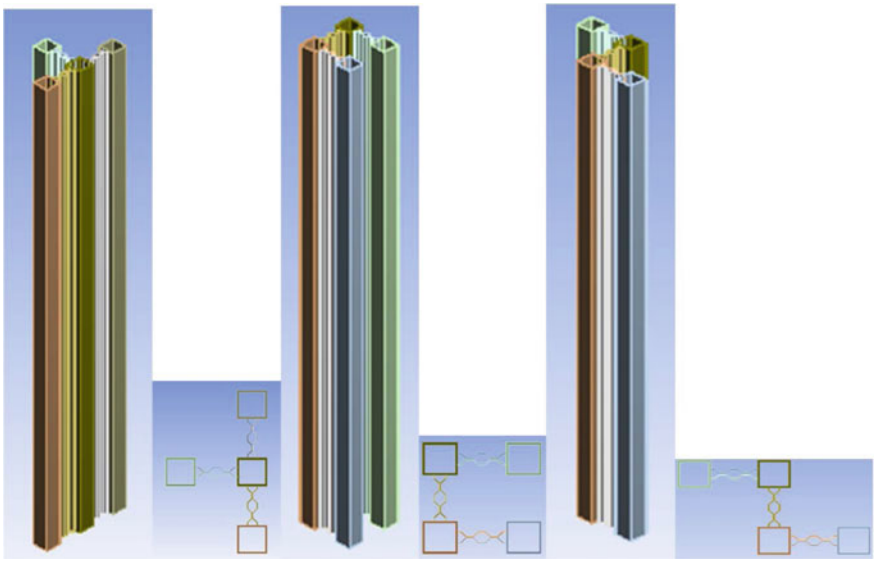

Fig. 14 Geometry of T-shape, C-shape, Z-shape hollow steel tube columns

Table 4 Comparison of load–deflection values

Column type	SCFST		Hollow steel tube	
	Deflection (mm)	Max load (kN)	Deflection (mm)	Max load (kN)
T-shape	12.533	4762.1	16.344	3767.7
C-shape	23.38	5519.5	48.638	5027.6
Z-shape	31.631	5678	46.017	5019.3

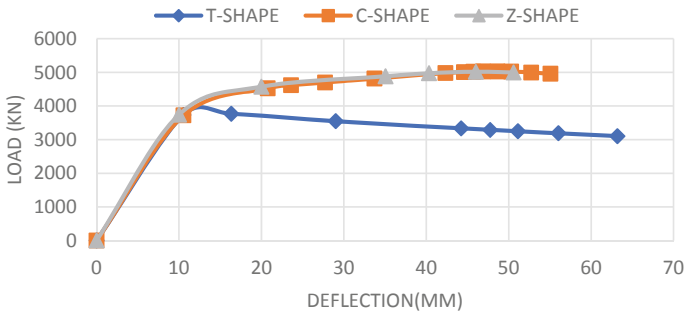

Fig. 15 Comparison of load–displacement curves of specimens

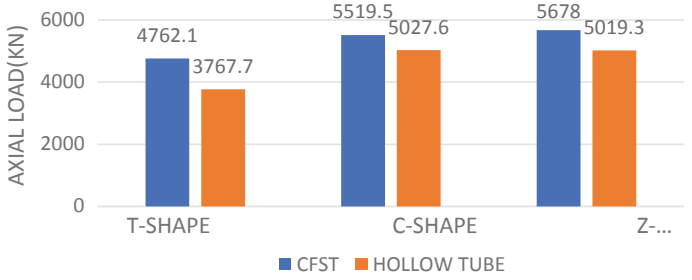

Fig. 16 Comparison of strength for SCFST and hollow steel tubes

of load–deflection values. And Fig. 15 shows the comparison of load–displacement curves.

3 Validation of an LCFST-D Column

The performance of L-shaped columns under axial compression were evaluated by Zhang et al. [3] in the paper—"*Performance of L-shaped columns comprising concrete-filled steel tubes Under axial compression*". L-shaped CFST column connected by double-vertical steel plate (LCFST-D column) is validated with the data

available in this paper. Finite-element results are compared to the experimental results available from the paper. Table5 describes the mechanical properties of specimen validated. Figure 17 shows the geometry of LCFST-D column.

The boundary conditions of specimens were set to be same as in the test specified in journal. Coupling points were specified at the centroid of top of the column to form rigid surfaces. Top of the column was constrained in the X and Z displacement directions. Rotation about the X-axis, Y-axis and Z-axis was constrained. Bottom of the column was constrained in the three (X, Y, and Z) displacement directions; in addition, rotation about Y-axis was constrained [3].

Table 5 Mechanical properties of LCFST-D column

Material	Size or thickness (mm)	Length (mm)	f_y (MPa)	E_s (MPa)	Poisson's ratio (μ)
Steel tube	100 × 100 × 5.75	2000	380	2.01×10^5	0.3
Steel plate	100 × 5.75	2000	368	1.76×10^5	0.3
Concrete	$f_c = 32.4$ N/mm^2				0.15

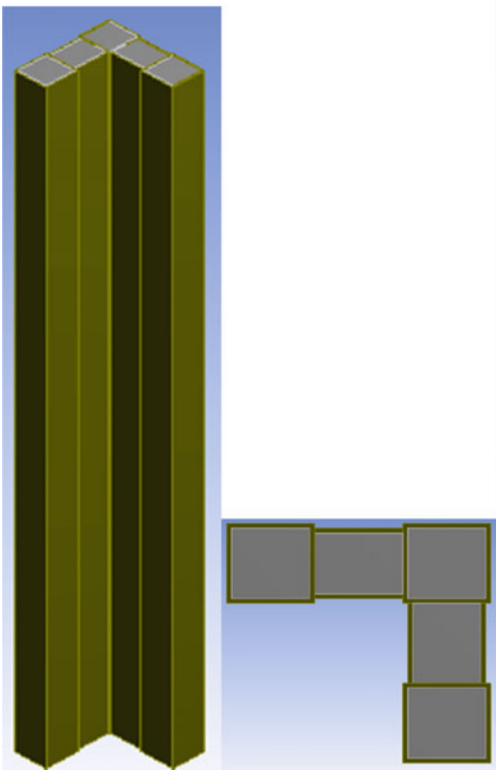

Fig. 17 Geometry of LCFST-D column

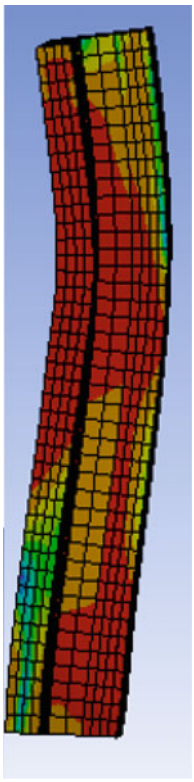

Fig. 18 von-mises stress diagram of failure column

The failure model of finite element simulation was similar to the actual failure model, as shown in Fig. 18. It shows a global buckling behavior. This similarity indicates that finite element model can be used to simulate actual failure. Maximum deformation value from the experimental result obtained is 22.01 mm and total deformation obtained from the finite Element Analysis is 22.25 mm. Figure 19 shows the load–deflection curve of column analyzed. Ultimate load of LCFST-D column analyzed through validation is 4921 kN. The ultimate load of the specimen is about 4603.57 kN from the experimental results and 4958 kN from the finite element results that explained in the journal [3]. Table 6 shows the comparison of results. The percentage of difference in the ultimate load is 6.89% which is within limits.

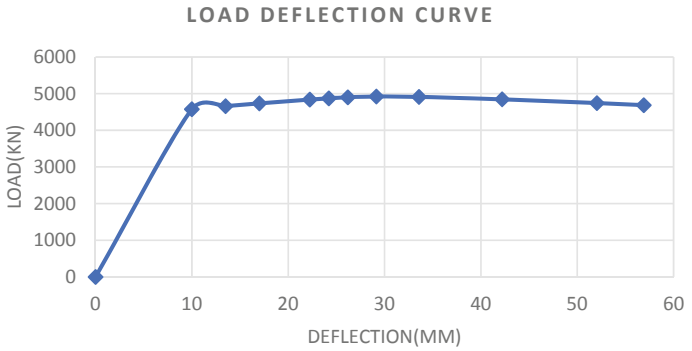

Fig. 19 Load–deflection curve of LCFST-D column

Table 6 Comparison of results

	Ultimate load (kN)	% of error
Experimental	4603.57	6.895138
FEA (validated)	4921	
Journal FEA	4958	

4 Conclusions

Structural performance of SCFST columns under various loading conditions was investigated. Based on results, following conclusions are drawn:

- Global buckling was the major failure mode and damage occurred mainly in middle part of columns and stress was concentrated on outer mono tubes.
- T-shape and C-shaped columns exhibited global buckling of steel tube and vertical corrugated plate towards outside.
- Local limb buckling occurred for Z-shaped column under axial loading and it had less lateral deformation. Local buckling occurred only for end CFST tubes and clear local buckling occurred at top and bottom of corner CFST tube.
- Z-shaped CFST column showed better performance under axial and lateral loads and T-shaped column showed better performance under eccentric load.
- C-shaped column showed more deflection in both x and z direction under lateral loading which means that it has more ductility compared to other ones.
- Slenderness ratio significantly influenced bearing capacity. Ultimate bearing capacity and stiffness of column reduced as slenderness ratio increased.
- SCFST columns showed greater load carrying capacity and stiffness compared to hollow steel tube column.

References

1. Han L-H, Song T-Y, Zhou K, Cui Z-Q (2018) Fire performance of CFST triple-limb laced columns. J Struct Eng
2. Yang Y-F, Liu M, Fu F (2018) Experimental and numerical investigation on the performance of three-legged CFST latticed columns under lateral cyclic loadings. J Thin-Walled Struct 132:176–194
3. Zhang W, Chen Z, Xiong Q (2018) Performance of L-shaped columns comprising concrete filled steel tubes under axial compression. J Constr Steel Res 145:573–590
4. Huang Z, Jiang L-Z, Frank Chen Y, Luo Y, Zhou W-B (2018) Experimental study on the seismic performance of concrete filled steel tubular laced columns. J Steel Compos Struct 26(6):719–731
5. Yang Y, Yang H, Zhang S (2010) Compressive behaviour of T-shaped concrete filled steel tubular columns. Int J Steel Struct 10(4):419–430
6. Chen Z, Bin R, Fafitis AS (2009) Axial compression stability of a crisscross section column composed of concrete-filled square steel tubes. J Mech Mater Struct 4(10)
7. Tao Z, Wang ZB, Yu Q (2013) Finite element modelling of concrete filled steel-stub columns under axial compression. J Constr Steel Res 89(5):121–131
8. Xu M, Zhoua T, Chena Z, Li Y, Bisby L (2016) Experimental study of slender LCFST columns connected by steel linking plates. J Constr Steel Res 127:231–241

Experimental Study of Seismic Response Reduction Effects on Multi Storey Frames with Particle Damper

N. Athulya Vijay and K. P. Saji

Abstract Particle damper (PD), an innovative type of passive vibration control system, is a developing concept in the current period. This type of damper consists of small particles that are placed in the cavity of the primary structure which is likely subjected to vibration. The energy dissipation mechanism occurs due to the inelastic collision of particles present in the damping cavity and friction between particles. Compared to other passive vibration control methods, particle damper can be effectively introduced into structure without significant modification of primary structure. This study is mainly intended to the experimental investigations on the behaviour of particle damper under varying parameters. Parametric study investigates the efficiency of particle dampers in mitigating dynamic responses of MDOF structures. This study focuses on the performance of particle damper by using different types of particles and their combinations. Types of particles used in this study are metallic (steel balls) and viscoelastic polymer (silicone rubber balls).

Keywords Particle damper · Passive vibration control · Shake table

1 Introduction

The construction of high-rise buildings has increasing demand all over the world, especially in the developing countries. The main challenge faced by these high-rise building is the control of structural vibration during a seismic event. To ensure the safety and comfort of occupants it is necessary to control this structural vibration. Particle damper is an innovative type of passive vibration control system, which is developing in the present stage. Particle damping technology is a form of an auxiliary-mass type vibration damper. This type of damper consists of small particles

N. Athulya Vijay (✉) · K. P. Saji
Civil Engineering Department, Government College of Engineering, Kannur, India
e-mail: athulyavijaydeepam@gmail.com

K. P. Saji
e-mail: kpsaji@gcek.ac.in

© Springer Nature Switzerland AG 2021

K. Dasgupta et al. (eds.), *Proceedings of SECON 2020*,
Lecture Notes in Civil Engineering 97,
https://doi.org/10.1007/978-3-030-55115-5_20

placed in the cavity of the primary structure which is likely to be subjected to vibration. Compared to other passive vibration control methods, particle damper can be effectively introduced without significant modification of primary structure. Due to simplicity, moderate cost, good durability, and temperature insensitivity, importance of particle damper is drastically increasing in present stage.

The idea of particle damping is originated from the concept of impact damper. The impact damper consists of a mass which moves between the walls of the container. This impact process results in high noise and considerable amount of impact forces. The concept of impact damper is popular since 1937. Instead of using single mass, Masri and Ibrahim [1] conducted an analytical investigation of the steady-state motion of a two-particle, single-container impact damper which was attached to a sinusoidally excited primary system. His results showed that vibration reduction is about twice for particle damper than single impact damper of equivalent mass. From 1985 onwards researchers are more focused on particle damper. Arki et al. [2] studied the vibration reduction effect of impact damper consisting of a bed of granular materials moving in container fixed to primary vibrating system. The response of the system depends on mass ratio, clearance, exciting force and frequency ratio. Even for a small mass ratio, better performance of the system could be achieved by suitably fixing the clearance of the container.

In the case of multi-unit particle damper, as the cavity size increases the number of collision between particles reduces, so the effectiveness of damping reduces. Hence it is found that by increasing the unit member with decreasing the radius of cavity better damping performance can be achieved [3–7].

In 2010, Lu et al. [8] numerically studied the damping performance of vertical and horizontal particle dampers attached to single degree of freedom system (SDOF) and multi degree of freedom systems (MDOF) under free vibration, stationary random excitation as well as non-stationary random excitation, with single component or multi-component. They studied the behaviour of particle damper by using the concept of Effective Momentum Exchange and the amount of internal energy dissipation due to impact and friction.

Multi-unit multi particle damper is known as Multi-unit particle damper. Properly designed multi-unit particle dampers can achieve good vibration attenuation with small addition of mass [9].

The damping characteristics of particle damper under horizontal-vertical excitation are comparable to that of particle damper under vertical excitation only. Even though in horizontal-vertical excitation, due to the incorporation of horizontal motion in addition to vertical motion, specific damping capacity is significantly improved. Improvement in specific damping capacity is due to the oblique impact between particles [10].

The damping performance of particle damper is stable and efficient. Comparative study of damping performance of particle damper with other types of dampers such as tuned mass damper and tuned liquid damper were carried out [11–13]. Their result shows that particle damper reduces the seismic response better than tuned mass

damper and tuned liquid damper. Because, in the case of particle damper, friction between the particles and impact between particles and between particles and its container cause energy dissipation, in addition to the energy dissipation by tuning frequency.

Particle damper is a new passive control method applied to civil engineering, structures and the technology is in a developing stage. Most of the studies with particle dampers are mainly focused on SDOF systems or other structures such as cantilevers and stiffened plates, whereas investigations on MDOF structure with particle dampers are very rare. The present study is on a MDOF structure with particle dampers and the experiment is carried out on a horizontal shake table apparatus.

2 Experimental Study

2.1 Shake Table Test on Three Storied Frame

The present study is mainly focused on the behavior of three storied frame with particle damper. The frame is made of four Aluminum columns of total height of 1200 mm with each floor having a height of 400 mm. The aluminum column used is of thickness 3 mm. The horizontal excitation given to the base of a three storied aluminium base frame was studied on the shake table. The experimental set up is as shown in Fig. 1. Frequency-displacement graph of base frame are as shown in Fig. 2. From graph it is clear that max displacement occurred at the third floor and minimum occurred at first floor. The max displacement was 110.931 mm for a frequency of 2.41172 Hz. Hence the natural frequency of the base frame is taken as 2.41172 Hz. Displacements at each floor level are measured. The input frequency is varied from zero to the first and second natural frequencies.

2.2 Base Frame with Particle Damper

Particles used in this study are metallic (steel balls) and viscoelastic polymer (silicone rubber balls) and with 8 mm diameter. The ratio of weight of damper to weight of structure is known as mass ratio. The mass ratio used in this study is 5 and 3%. The experimental setup with damper is shown Fig. 3.

2.2.1 With Steel Ball

Shake table test was conducted on a three storied aluminium base frame with steel particle damper. Damper was placed in each storey level and the responses were taken. Figure 4 represents the frequency displacement graph of top floor with particle

Fig. 1 Experimental setup

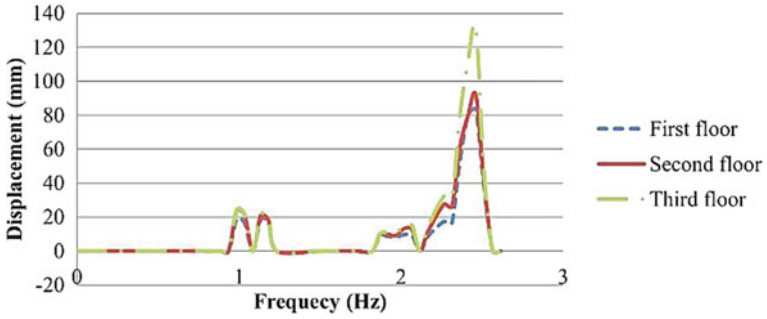

Fig. 2 Frequency displacement graph of frame without damper

Fig. 3 Experimental setup with damper at third floor

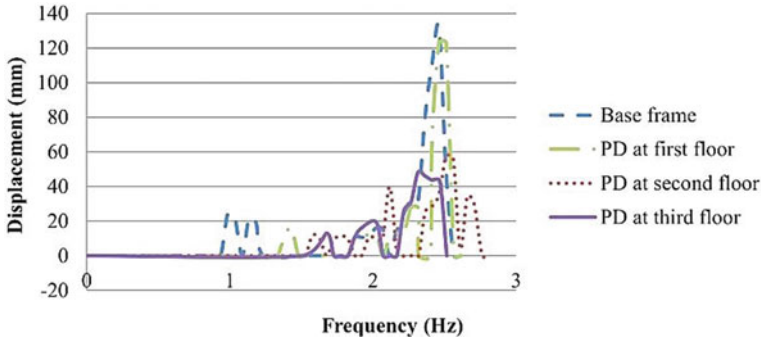

Fig. 4 Frequency displacement graph of top floor with steel ball (mass ratio 5%)

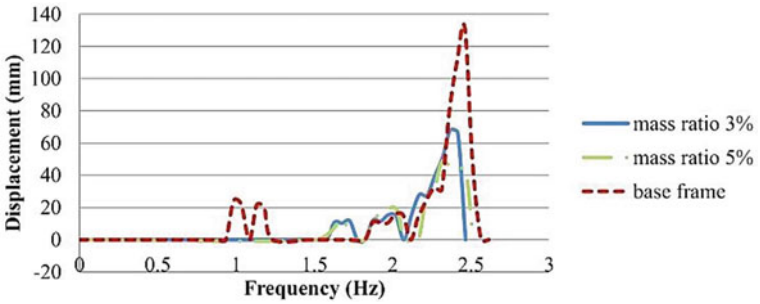

Fig. 5 Frequency displacement graph of top floor with steel ball

damper at each storey level with mass ratio 5%. When the particle damper at top storey level, the maximum top storey displacement of base frame with particle damper is reduced by 63.4% (in first mode of vibration) compared to base frame without damper. The maximum top storey displacement of base frame with particle damper is reduced by 55.94% compared to base frame without damper, when the particle damper at second storey level. And for particle damper at first storey level the maximum top storey displacement of base frame with particle damper is reduced by 5.97% compared to base frame without damper.

Figure 5 represents the frequency displacement graph of particle damper at top storey level with mass ratio 5% and 3%. From the results the maximum top storey displacement of particle damper with 5% mass ratio is reduced by 41.57% compared to particle damper with 3% mass ratio.

2.2.2 With Silicone Rubber Ball

Shake table test was conducted on a three storied aluminium base frame with silicone rubber particle damper. Damper was placed in each storey level and the responses were taken. Figure 6 represents the frequency displacement graph of top floor with particle damper at each storey level with mass ratio 3%. When the particle damper at top storey level, the maximum top storey displacement of base frame with particle damper is reduced by 41.1% compared to base frame without damper. The maximum top storey displacement of base frame with particle damper is reduced by 29.1% compared to base frame without damper, when the particle damper at second storey level. And for particle damper at first storey level the maximum top storey displacement of base frame with particle damper is reduced by 17.34% compared to base frame without damper.

Figure 7 represents the frequency displacement graph of particle damper (steel ball, silicone rubber ball) at top storey level with mass ratio 3%. The reduction in maximum top storey displacement of steel ball particle damper and silicone rubber ball particle damper are comparable.

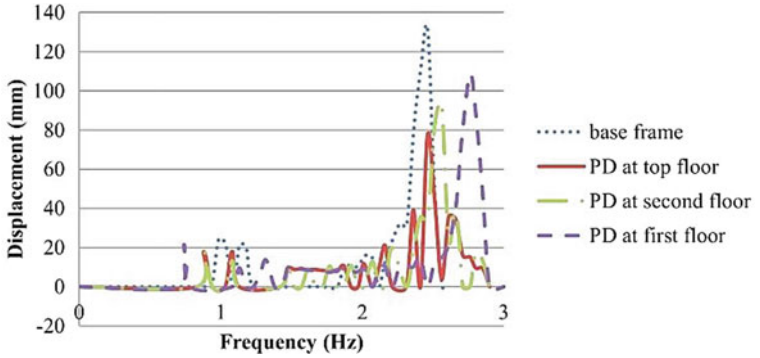

Fig. 6 Frequency displacement graph of top floor with silicone rubber ball (mass ratio 3%)

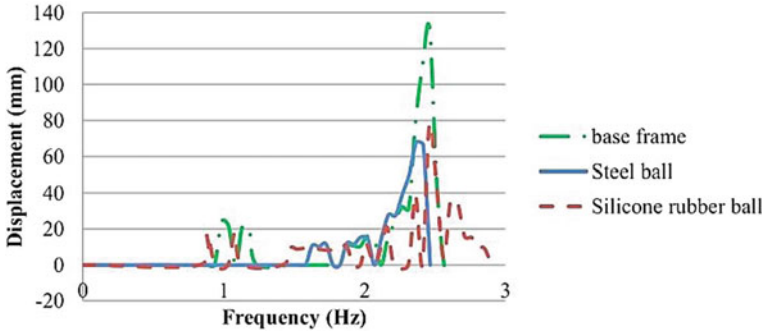

Fig. 7 Frequency displacement graph of top floor (mass ratio 3%)

3 Conclusions

This study is mainly intended to the experimental investigations on the behaviour of particle damper under varying parameters. Parametric study investigates the efficiency of particle dampers in mitigating dynamic responses of MDOF structures, and the following conclusions can be drawn from this investigation.

- From the results obtained, it has been found that particle damper can effectively control the vibration of MDOF structures.
- Metallic particles can effectively reduce vibration of the MDOF structure. In the first mode of vibration, the top storey displacement is reduced by 63.4% for base frame with 5% steel particles on the top floor of the frame.
- As mass ratio increases the damping performance increases. From the results the maximum top storey displacement of particle damper with 5% mass ratio is reduced by 41.57% compared to particle damper with 3% mass ratio.

- Viscoelastic polymers also can effectively reduce vibration of the MDOF structure. Silicone rubber ball can effectively reduce the top storey displacement about 41.1%, with mass ratio 3%
- At mass ratio 3%, the reduction in maximum top storey displacement of steel ball particle damper and silicone rubber ball particle damper are comparable.
- The given experimental set up allows only the measurement horizontal displacement of each floor with varying support displacement frequency. More insight could have been developed had there been a time history data.

References

1. Masri SF, Ibrahim AM (1967) Response of the impact damper to stationary random excitation. J Acoust Soc Am 53:200–211
2. Arki Y, Yokomichi I, Inoue J (1985) Impact damper with granular materials. Jpn Soc Mech Eng 28(241):1466–1471
3. Popplewell N, Semerc Gil SE (1989) Performance of the bean bag impact damper for a sinusoidal external force. J Sound Vib 133(2):193–223
4. Cempel C, Lotz G (1993) Efficiency of vibrational energy dissipations by moving shots. J Struct Eng 119(9):2642–2652
5. Saeki M (2005) Analytical study of multi-particle damping. J Sound Vib 281:1133–1144
6. Trigui M, Foltete E, Abbes MS, Fakhfakh T, Bouhaddi N, Haddar M (2009) An experimental study of a multi-particle impact damper. Mech Eng Sci 223(9):2029
7. M. Gharib, S. Ghani (2013) Free vibration analysis of linear particle chain impact damper. J Sound Vib 332:6254–6264
8. Lu Z, Lu X, Masri SF (2010) Studies of the performance of particle dampers under dynamic loads. J Sound Vib 329:5415–5433
9. Lu Z, Lu X, Lu W, Masri SF (2012) Shaking table test of the effects of multi-unit particle dampers attached to an MDOF system under earthquake excitation. Earthq Eng Struct Dyn 41:987–1000
10. Wang YR, Liu B, Tian AM, Tang W (2016) Experimental and numerical investigations on the performance of particle dampers attached to a primary structure undergoing free vibration in the horizontal and vertical directions. J Sound Vib 371:35–55
11. Lu Z, Chen X, Zhou Y (2017) An equivalent method for optimization of particle tuned mass damper based on experimental parametric study. J Sound Vib 419:571–584
12. Lu Z, Huang B, Wang Z, Zhou Y (2018) Experimental comparison of dynamic behavior of structures with a particle damper and a tuned mass damper. J Struct Eng 144(12):04018211
13. Fu B, Jiang H, Wu T (2019) Comparative studies of vibration control effects between structures with particle dampers and tuned liquid dampers using substructure shake table testing methods. Soil Dyn Earthq Eng 121:421–435

Control Effectiveness of Wing with Elevon of a Typical Reusable Launch Vehicle

Nyle Nazar, P. Ashok Gandhi, S. Rajendran, and Manju George

Abstract Modern aircraft structures uses more lightweight materials such as composites for their design. This makes the aeroelastic study an extremely important aspect of aircraft design. By having more light weight control surfaces, the control effectiveness study becomes vital in today's scenario. Control effectiveness is the ability of a control surface such as an aileron or a rudder to produce aerodynamic forces and moments to change the airplane orientation and manoeuvre it along the intended flight path. This paper presents the static aeroelastic analysis of a typical reusable launch vehicle focusing on control effectiveness of elevon. A Reusable Launch Vehicle (RLV) is the space analogy of an aircraft. Ideally it takes off vertically on the back of a dispensable rocket and then glides back down like an aircraft. MSC PATRAN and MSC NASTRAN were the software's used for Finite Element Modeling and Analysis. The main aim of the analysis is to compute the control effectiveness of launch vehicle along its trajectory to determine whether it is efficient to control the vehicle. The objectives of this work are, to study the control surface effectiveness of elevon by carrying out static aeroelastic analysis using NASTRAN inbuilt aerodynamics, for a typical Reusable Launch Vehicle (RLV).

Keywords Static aeroelasticity · Control effectiveness · Typical reusable launch vehicle · Finite element modeling

Nomenclature

Xcp Center of Pressure (m)
Xcg Center of Mass (m)

N. Nazar (✉) · M. George
Department of Civil Engineering, Mar Baselios Institute of Technology and Science, Nellimattom, India
e-mail: nylenazar1@gmail.com

P. A. Gandhi · S. Rajendran
STR, VSSC, ISRO, Thiruvananthapuram, India

© Springer Nature Switzerland AG 2021

K. Dasgupta et al. (eds.), *Proceedings of SECON 2020*,
Lecture Notes in Civil Engineering 97,
https://doi.org/10.1007/978-3-030-55115-5_21

Q Dynamic pressure (Pa)
Qdiv Divergence dynamic pressure (Pa)
E Young's Modulus (N/m^2)
I Area moment of inertia (m^4)

1 Introduction

Aeroelasticity is the interaction between aerodynamics, inertia and elastic forces. The flexibility of modern airplane structures is fundamentally responsible for various types of aeroelastic problems. These problems would not exist if the airplane structures were perfectly rigid. Structural stability itself may not be objectionable; however aeroelastic phenomena arise when structural deformations induce additional aerodynamic forces. Static aeroelasticity is the analysis which deals with the static or steady-state response of an elastic body to fluid flow. In an airplane, two significant static aeroelastic effects may occur Divergence and Control reversal. The phenomenon in which, elastic twist of a wing suddenly becomes infinite and causing the wing to fail is called Divergence. Control reversal is a phenomenon occurring in control surfaces and wing, in which these surfaces reverse their usual functionality, that is the rolling direction associated with a given aileron moment is reversed. Divergence occurs when a lifting surface deflects under aerodynamic load to increase the applied load, or move the load so that the twisting effect on the structure is increased. The increased load deflects the structure further, which eventually brings the structure to the point of divergence. Control surface reversal is the loss or reversal of the expected response of a control surface, due to the deformation of the main lifting surface (wing). Aircraft are designed to avoid aeroelastic failures such as divergence and control reversal and critical dynamic instabilities such as flutter which is the uncontained vibration that can lead to the destruction of an aircraft. Control effectiveness is the ability of a control surface such as an aileron or a rudder to produce aerodynamic forces and moments to control airplane orientation and maneuver along a flight path. This paper focuses on computing the control effectiveness of a typical reusable launch vehicle and how the control effectiveness is sensitive to off-nominal conditions. In rockets, aerodynamic stability is often provided by fins, by keeping the centre of pressure (Xcp) at aft of the centre of gravity (Xcg).

Aerodynamic and Inertia forces bend the rocket due to its Elasticity, which changes the angle of attack along the length. Due to deflection, the aerodynamic force increases in the forward region and decreases in the aft ward region, thus moving Xcp forward. The inertia forces also change accordingly due to acceleration. Fin divergence is also a static aero elastic failure caused due to instability. The changed load distribution along the length bends the rocket, which causes further change in loads. The changed load distribution moves the centre of pressure forward towards centre of gravity. If the centre of pressure coincides with centre of gravity, the rocket will become unstable which is called the divergence. The operational speed

(or dynamic pressure) of the rocket must be below the divergence speed (or dynamic pressure) by a factor of 2. Observance of the criterion $\frac{Q}{Q_{\text{div}}} \leq \frac{1}{2}$ provides a twofold advantage. In addition to maintaining a margin for providing for the uncertainties in the aeroelastic parameters, it also limits the aeroelastic magnification of external loading.

2 Literature Review

As $\frac{Q}{Q_{\text{div}}}$ becomes large and instability is approached, the effects of externally applied loads are magnified in a sense similar to the resonant or near resonant response of vibrating system [1–3]. Aeroelastic phenomena in modern high-speed aircraft have profound effect upon the design of structural members and also upon mass distribution, lifting surface plan forms and control system design [4]. The reduction of weight ratio in the wing structure improves the efficiency and performance of an aircraft wing [5]. Amongst all the aircraft parts, reduction in the weight of the wing has got higher importance [6]. Generally, an aircraft wing structures are designed using pure aluminum material. Divergence is a disastrous phenomenon where the aerodynamic moments due to elastic deformations overpower the restoring moments of the structure [7]. At the critical divergence speed, no statically stable equilibrium condition exists [8]. Many previous studies have been conducted on the aeroelastic analysis of wings [9–11]. In the present work, control effectiveness of wing with elevon of a typical reusable launch vehicle is estimated, thereby to assess the structural and stability problems.

3 Modelling

Reusable Launch Vehicle (RLV) is a winged vehicle that will take off like a rocket and glide back to land like a plane. A reusable launch vehicle is a space launch system intended to allow for recovery of all or part of the system for later reuse. The configuration of RLV is similar to that of an aircraft with the complexity of both launch vehicle and aircraft. During its landing phase, RLV is intended to land on a runway similar to aircraft. Small wings provide manoeuvrability support during landing. Out of all parts of an aircraft, the wing plays a major role in getting high performance. Reusable Launch Vehicle technologies are developed to achieve low-cost access to space. RLV consists of a fuselage (body), a nose cap, double delta wings and twin vertical tails. It also consists of symmetrically placed active control surfaces called Elevons and Rudders. The structure was modeled in MSC PATRAN and was analyzed in MSC NASTRAN. MSC PATRAN and MSC NASTRAN were the finite element tools used for the dynamic and aeroelastic analysis of RLV. Once the geometry of the structure was created, finite element discretization was done followed by meshing. CQUAD4, CTRIA3 and CBEAM elements were used to represent the

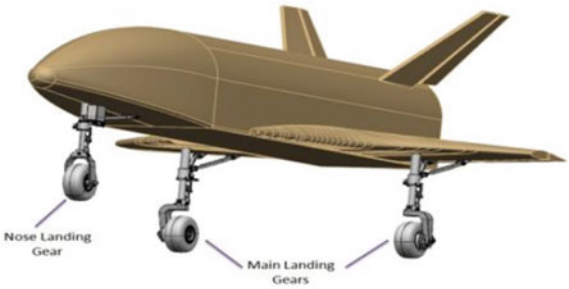

Fig. 1 CADD model of a typical reusable launch vehicle

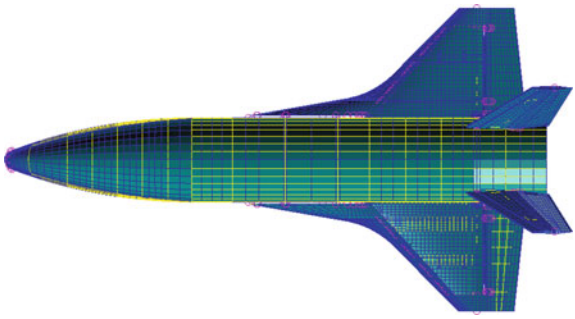

Fig. 2 Finite Element model of a typical reusable launch vehicle

individual components. Figure 1 shows the CADD model of RLV for descent phase and Fig. 2 shows a finite element model of a typical reusable launch vehicle.

4 Analysis

The analysis which deals with the static or steady state response of an elastic body to a fluid flow (typically stability) is termed as static aeroelasticity. In a typical reusable launch vehicle, wing is the lifting surface and the elevon is used as the control surface. If the deflection of the wing and elevon is so much, sometimes the intended purpose of control surface may be completely nullified. A condition occurring during the flight, at a speed called control reversal speed, the function of control system will be totally reversed. Then the control structure effectiveness will be lost. This has to be theoretically analyzed. Figure 3 shows the descent trajectory details of RLV.

For carrying out static aeroelastic analysis, it is important to generate the aerodynamic force acting on the vehicle accurately. MSC/NASTRAN has inbuilt aerodynamics which generates this aerodynamic force. MSC/NASTRAN uses plate theories such as Doublet Lattice Method for subsonic Mach number, ZONA51 for transonic & low supersonic Mach numbers and Piston theory for high supersonic Mach numbers to generate the aerodynamic force within NASTRAN. To utilize the NASTRAN

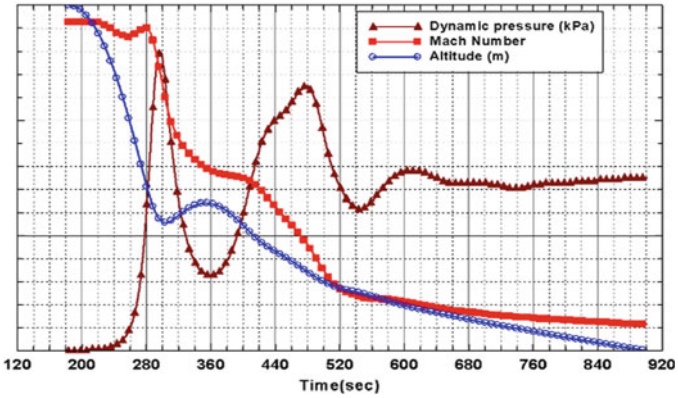

Fig. 3 Descent trajectory of RLV

inbuilt aerodynamics, aero mesh is generated for wing and elevon alone as our focus is to find the elevon effectiveness including interference from wing. Two-way biased aerodynamic mesh is generated to capture the leading edge and trailing edge aerodynamics as shown in Fig. 4. Infinite plate splining theory is used to couple the structure mesh and aerodynamic mesh for transfer of forces.

Control effectiveness of reusable launch vehicle as such designed (here in referred as Original case) is carried out for various Mach numbers. The control effectiveness

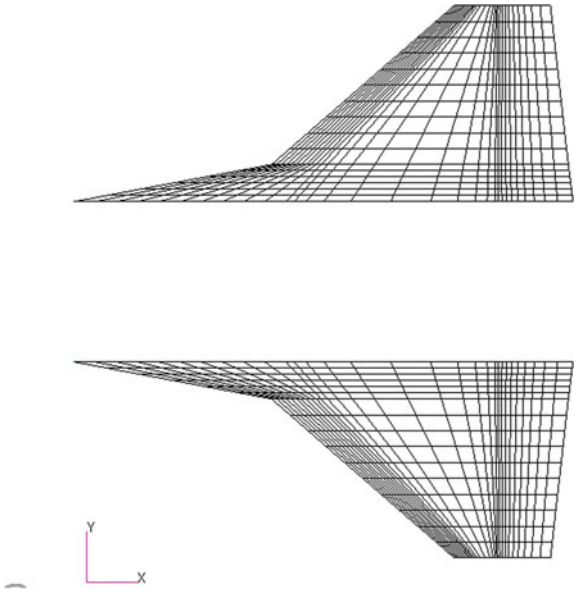

Fig. 4 Aerodynamic mesh for Wing and elevon of typical RLV

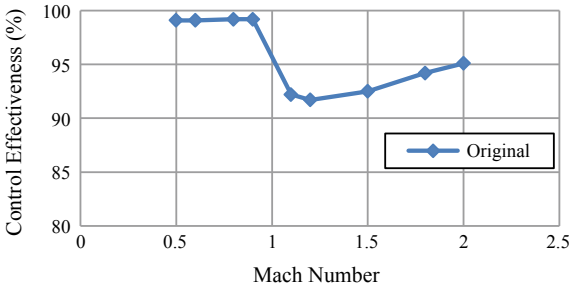

Fig. 5 Control effectiveness versus mach number curve for original configuration

of a control surface is calculated in terms of percentage (%) as follows

$$Control\ effectiveness(\%) = \frac{Flexible\ force}{Rigidy\ body\ Force} * 100$$

Figure 5 shows the control effectiveness curve at various Mach numbers of original configuration.

5 Results and Discussions

Static aeroelastic analysis was carried out on the RLV with aerodynamics applied on wing and elevon. Steady level flight conditions were considered. The vehicle is supported at C.G for PITCH and PLUNGE and rest of the DOF are arrested. Several off-nominal studies were carried out to ascertain the effect of various parameters such as dynamic pressure, flexural rigidity (EI) and material change on control effectiveness. The reason for choosing the above parameters is that they are the most probable and influential parameters in affecting the control effectiveness, when a scaled up version of RLV configuration is designed. Since the mission requirement may vary for the scaled up version, the trajectory may be slightly difference and hence the dynamic pressure. While scaling up it is also estimated that the flexural rigidity (EI) may reduce upto 16% and a different material option may be chosen to avoid dynamic aeroelastic phenomena like flutter.

Control effectiveness is generally calculated as the ratio of flexible force to rigid force as percentage. From NASTRAN output the control effectiveness is calculated as the ratio of Elastic unrestrained aerodynamic coefficient to Rigid splined trim variable aerodynamic coefficient, as given in Fig. 6.

TRIM VARIABLE	COEFFICIENT	RIGID		ELASTIC		INERTIAL	
		UNSPLINED	SPLINED	RESTRAINED	UNRESTRAINED	RESTRAINED	UNRESTRAINED
ELEV1	CX	4.287313E-18	4.287313E-18	1.483405E-18	4.269086E-18	0.000000E+00	-3.966095E-02
	CY	-4.316419E-19	-4.316419E-19	-2.023885E-18	-4.118522E-19	0.000000E+00	-1.027023E-08
	CZ	2.318815E-01	2.318815E-01	5.872159E-02	2.298013E-01	0.000000E+00	2.298013E-01
	CMX	7.163783E-02	7.163783E-02	7.067206E-02	7.066256E-02	0.000000E+00	2.030992E-04
	CMY	-1.056267E-01	-1.056267E-01	-6.518432E-02	-1.048237E-01	0.000000E+00	-1.048237E-01
	CMZ	-1.429804E-18	-1.429804E-18	-2.091367E-18	-1.411739E-18	0.000000E+00	3.291372E-05
ELEV2	CX	7.411001E-18	7.411001E-18	4.554912E-18	7.342414E-18	0.000000E+00	-3.963553E-02
	CY	2.485924E-18	2.485924E-18	8.257084E-19	2.438794E-18	0.000000E+00	-1.026771E-08
	CZ	2.318812E-01	2.318812E-01	5.858850E-02	2.297799E-01	0.000000E+00	2.297799E-01
	CMX	-7.163779E-02	-7.163779E-02	-7.056992E-02	-7.057940E-02	0.000000E+00	2.030929E-04
	CMY	-1.056265E-01	-1.056265E-01	-6.508433E-02	-1.047495E-01	0.000000E+00	-1.047496E-01
	CMZ	3.149733E-18	3.149733E-18	2.431645E-18	3.111716E-18	0.000000E+00	3.289262E-05

MARCH 11, 2020 MSC Nastran 6/10/16 PAGE 29

Fig. 6 Results obtained from f06 file for Original configuration

5.1 Effect of Dynamic Pressure

Unlike aircraft, RLV has a particular descent trajectory through which it glides back to runway. But during it descent, off nominal trajectory cases can occur depending on various parameters such as variation in thrust, mass, aero data and also due to deviation in the flight path. So to study the effect of dynamic pressure on control effectiveness, the dynamic pressure is increased to 1.5 times and 2.0 times. 1.5Q stands for 1.5 times the dynamic pressure (Q) and so on. Comparison curve is shown in Fig. 7. From the figure it is observed the control effectiveness dips down to 84% when the dynamic pressure is doubled. It is seen that as the dynamic pressure increases the control effectiveness come down. The values of divergence dynamic pressures are arrived by carrying out a separate static aeroelastic analysis of RLV. The operational speed of the rocket must be below the divergence speed by a factor of 2and hence half the value of divergence dynamic pressure is taken as the maximum allowable dynamic pressure. The results along with nominal values are shown in Fig. 8. Divergence analysis of the RLV revealed that the maximum off-nominal dynamic pressure can be allowed twice the value of operating dynamic pressure in subsonic regime, so up to 2Q is considered for the control effectiveness studies.

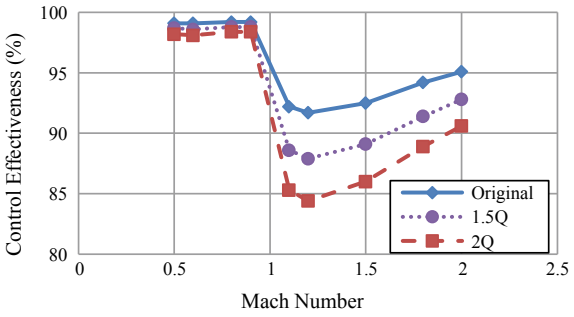

Fig. 7 Control effectiveness versus mach number curve for original, 1.5Q and 2Q

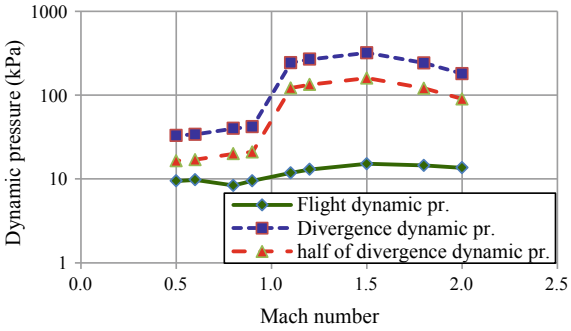

Fig. 8 Divergence dynamic pressure curve

5.2 *Effect of Flexural Rigidity*

Usually before RLV is successfully configured, a scaled down version will be initially flown and by analyzing the flight parameters, scaled up version of the same RLV will be subsequently flown. If we assume that the same design is used and the structure is just scaled up, then the effect of scaling up can be studied by reducing the flexural rigidity (EI) of the structure. Further EI reduction is possible by optimization of the structure using advanced thermal protection system. RLV configuration has a thermal protection to reduce the thermal effects while re-entering. The thermal protection generally used is silica tiles. Because of silica tiles, the structure has a stringent requirement for keeping the displacement minimum. Higher displacement will lead to crack in the silica tile, leading to the failure of the mission. So the structure is designed to meet this displacement. So the thickness of the structures is generally in the higher side, when compared to stress in the structure to meet the displacement requirement. In future the thermal protection may be replaced with an advanced protection system then the structure can be really optimized to get a weight reduction. But this optimization may lead to thickness reduction and hence EI reduction.

Herein two cases are studied by reducing the flexural rigidity by 20 and 40%. The comparison of control effectiveness of scaled up configuration with ORIGINAL configuration is shown in Fig. 9. As seen from the figure, the effect of EI is not worse than the effect of dynamic pressure. So scaling up the RLV with the same design thickness will not be detrimental.

5.3 *Effect of Material Change*

A typical Reusable Launch Vehicle is originally composed of various materials such as leading edge is made up of steel, wing is aluminum and elevon is titanium. For the easiness of manufacturing, sometimes it is required to use same material for main lifting surfaces namely wing leading edge, wing and elevon. A study is carried out by

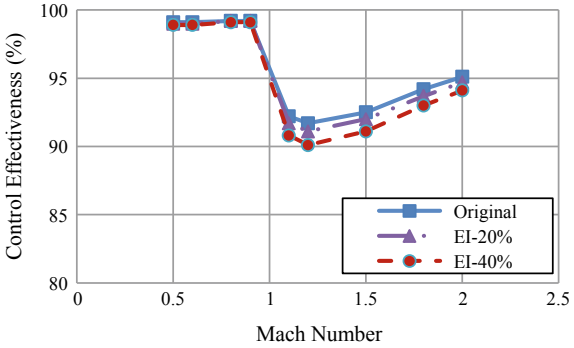

Fig. 9 The comparison of flexural rigidity curves with Original

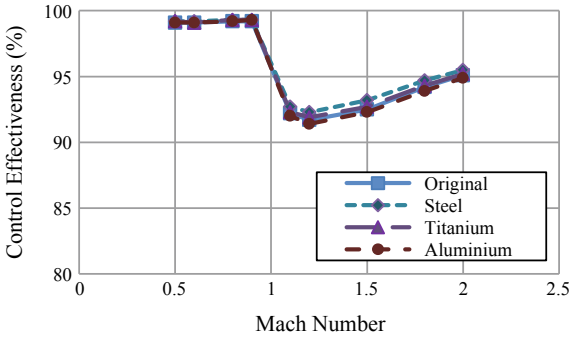

Fig. 10 Control effectiveness versus mach number curve for various materials

changing wing Leading edge, wing and elevon to a single material. Here the assumption made is that all these structures will have the same Original mass irrespective of material change. This assumption is made just to see the effect of EI due to material change. Figure 10 shows the effect of material change on control effectiveness and it is seen that the material change does not affect control effectiveness to a greater extent as dynamic pressure.

5.4 Different Combinations of Off-Nominal Cases

The static aeroelastic analysis of RLV is carried out for the combination of off-nominal cases described in the previous section to ascertain the effect on control effectiveness. Various combinations of material, dynamic pressure and flexural rigidity are studied as given below:

- TITANIUM + 1.5Q
- STEEL + 1.5 Q
- ALUMINIUM + 1.5Q
- TITANIUM + 2Q
- STEEL + 2Q
- ALUMINIUM + 2Q
- EI-20% + 1.5Q
- EI-20% + 2Q
- EI-40% + 1.5Q
- EI-40% + 2Q

For the first case, the material of control surfaces is changed into Titanium and the dynamic pressure is increased by 1.5 times. EI-20% means, flexural rigidity is reduced by 20%. Similarly it is done for other cases also. Figures 11 and 12 shown is the comparison curve for various combinations. As seen from these figures, Effect of material change with the combination of dynamic pressure, (with the assumption that overall mass does not change with material change), steel material seems to give a better control effectiveness when compared to other materials. Figures 13

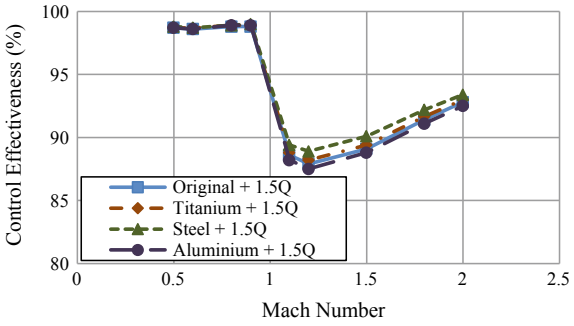

Fig. 11 Control effectiveness versus mach number curve for original and various combinations

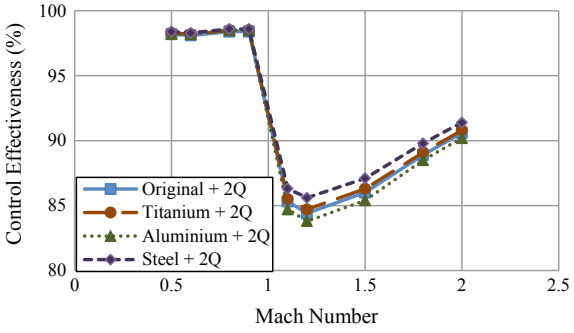

Fig. 12 Control effectiveness versus mach number curve for various combinations of 2Q

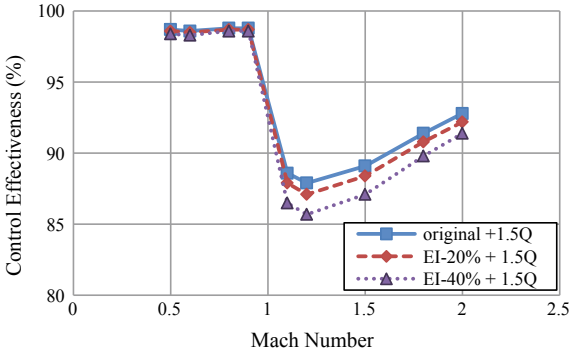

Fig. 13 Control effectiveness versus mach number curve for various combinations of EI & 1.5Q

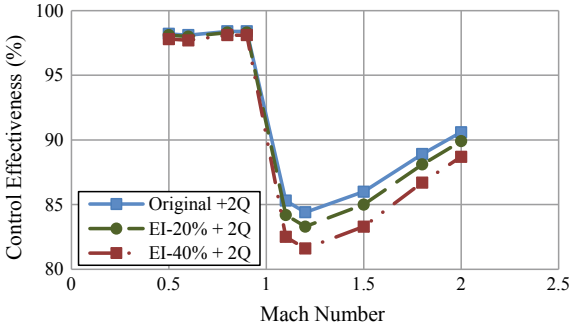

Fig. 14 Control effectiveness versus mach number curve for various combinations of EI & 2Q

and 14 show the effect of scaling up the size (flexural rigidity reduction) with the combination of dynamic pressure. The control effectiveness is very much reduced to 82%, for higher dynamic pressure and EI reduced to 40%. As observed in Sects. 5.1, 5.2 and 5.3, the increase in the dynamic pressure has the maximum effect on the control effectiveness.

6 Conclusion

Static aeroelastic analysis of Reusable Launch vehicle (RLV) was carried out at steady level flight condition for various Mach numbers to ascertain the control effectiveness of the elevon. Divergence analysis of the RLV revealed that the maximum off-nominal dynamic pressure can be allowed twice the value of operating dynamic pressure in subsonic regime. Analyses were carried out with 1.5 times and 2.0 times the nominal dynamic pressure, along with the Flexural rigidity (EI) reduction to take care of scaling up, and Material change for manufacturing easiness. From the

results of various analyses, it is found that the increase in dynamic pressure has more significant effect in reducing the control effectiveness, compared to Material change or reduction in flexural rigidity. The increase in dynamic pressure brings down the control effectiveness by 7%, whereas EI reduction up to 40% brings down the control effectiveness by 1.5% and material change brings down the control effectiveness by less than 1%. For different combination of off nominal cases, increase in dynamic pressure by 2 times and reduction in EI by 40% together brings down the control effectiveness by 10%.

Acknowledgements The authors would like to acknowledge, the scientists from VSSC, ISRO and ADA who have initially guided us in successfully carrying out the static aeroelastic analysis and divergence analysis for RLV. We would also like to acknowledge MSC NASTRAN technical support people for guiding us in the software side. We would like to express our sincere gratitude to the above without their initial support this paper wouldn't have seen the light.

References

1. Alley Jr VL, Harper Gerringer A (1967) An analysis of aeroelastic divergence in unguided launch vehicles. NASA Technical Note, NASA TN D–3281
2. Thompson WT, Dahleh MD (2011) Theory of vibrations with applications. University of California, vol 5
3. Petyt M (2003) Introduction to finite element vibration analysis. Institute of Sound and Vibration Research, vol 7
4. Bisplinghoff RL, Ashley H, Halfman RL (1996) Aeroelasticity. Dover Publications
5. Praveen R, Surendar E, Shyam Kumar K (2018) Design, static structural and modal analysis of aircraft wing NACA 4412 using ANSYS workbench 14.5. Int J Eng Sci Invent (IJESI), 61–71
6. Katon M, Rahman NA, Manap N (2017) Theoretical and finite element method of static structural analysis at wing segment. ARPN J Eng Appl Sci, 4491–4493
7. Fung YC (2003) An introduction to the theory of aeroelasticity. University of California, vol. 3
8. Sruthi K, Lakshmana Kishore T, Komaleswara Rao M (2017) Design and structural analysis of an aircraft wing by using aluminium silicon carbide composite materials. IJEDR 5, 949–959
9. Lee I, Miura H, Chargin MK (1992) Static aeroelastic analysis for generic configuration. J Aircraft
10. Xie C, Wang L, Yang C, Li Y (2013) Static aeroelastic analysis of very flexible wings based on non-planar vortex lattice method. Chin J Aeronaut
11. Lina Q, Zhou Z, Chi Z (2019) Static aeroelastic characteristics of grid structure wing. IEEE Aerosp Conf

Analytical Study on Dynamic Behaviour of Bolted Beam Column Steel Connections with Reduced Beam Sections

Deepa P. Antoo and Asha Joseph

Abstract Recent earthquakes highlighted that, conventional steel moment frame (SMF) shows brittle failure due to the seismic actions. Greater damages are due to the stress concentration at the interface of beam and column. A number of improved beam to column connection design strategies have been proposed. Reduced beam section (RBS) connection was introduced as a safety approach to reduce stress concentration at the panel zone. RBS promote the formation of plastic hinges within the reduced beam section of the beam at a specific distance from column face. The finite element analysis of steel beam-column connection arrangement was carried out for studying the strength behavior of beam column joint. In this paper cyclic analysis of bolted steel beam-column connections with RBS were using finite element analysis software ANSYS 16.1. The cyclic behavior of bolted beam column joints with and without RBS techniques are investigated. Cyclic behavior of variable configuration of reduced beam sections was also examined. From the analysis, it is observed that the specimen with RBS dissipates more energy than the conventional moment connection. Connection region remained in the elastic area due to plastic hinge formation in the RBS zone. The applied RBS geometry protects the connection and its components (endplate, column flange, bolts, welds) from failure. To investigate the effectiveness of RBS in inclined beams, 3D finite analysis is performed on the frame with a slope of 10°, 20°, 30° from the orthogonal.

Keywords Bolted beam column connection · Reduced beam section · Finite element model · Cyclic loading · Dynamic behavior

D. P. Antoo (✉) · A. Joseph
Federal Institute of Science and Technology, Angamaly, Ernakulam, India
e-mail: deepapantoo1996@gmail.com

A. Joseph
e-mail: ashameledath@gmail.com

© Springer Nature Switzerland AG 2021

K. Dasgupta et al. (eds.), *Proceedings of SECON 2020*,
Lecture Notes in Civil Engineering 97,
https://doi.org/10.1007/978-3-030-55115-5_22

1 Introduction

Steel moment resisting frames are widely used as seismic load resisting systems of buildings in high seismic regions. The connections of moment resisting frames have superior ductility and energy dissipation capacity due to the inelastic behavior of the beams and panel zone. Some moment connections have poor seismic performance. New moment connections were developed after the 1994 Northridge earthquake and 1995 Kobe earthquake. Reduced beam section with Bolted web (RBS-B) moment connections was one of the newly developed connections [1]. RBS-B connections limit the amount of moment demand transferred to the face of the column, and promote the formation of internal plastic hinges within the reduced beam section of the beam by trimming the beam flange width at a specific distance from the column face [2]. Extended end plate moment connections can be designed to be suitable for use in seismic force resisting moment frames [3]. During earthquake, the reduced section plays an important role as a structural fuse and dissipate the seismic energy by forming a plastic hinge through yielding and buckling of the beam. Since the steel behaves in a stable and ductile manner and the plastic hinge is also limited to the intended location, the brittle failure in connection can be avoided [4].

Various shape cutouts are possible (constant, tapered or radius cut) to reduce the cross-sectional area. RBS moment-resisting connection improves the ductility of steel member [5, 6]. Improved ductility characteristics and cost effectiveness makes RBS preferable in seismic region [7]. Typical geometry for the design of radius cut RBS are shown in Fig. 1.

AISC 358 provides a number of prequalified connections for seismic applications in special and intermediate steel moment frames. The design standard was developed assuming that beams frame orthogonally into a column in both the elevation and plan of the frame. In real-life construction, however the beam can be skewed in plan or sloped in elevation (Fig. 2). While these prequalified connections may be applicable when the slope angle does not deviate too much from orthogonal, it is not clear if these connections can be applied to cases when the angle is large [9]. The objective of this study was to investigate the cyclic behavior of bolted beam column joints with and without RBS techniques and also to analyze the dynamic behavior of variable configuration of reduced beam sections with slope angles (10°, 20°, 30°).

2 Finite Element Modeling

2.1 Formulation of the Model

Two specimens were studied, designated as, connection without RBS as ‘WRBS’ and with RBS as ‘RBS with circular cut’. RBS connection was designed based on specifications given as per AISC and FEMA guidelines.

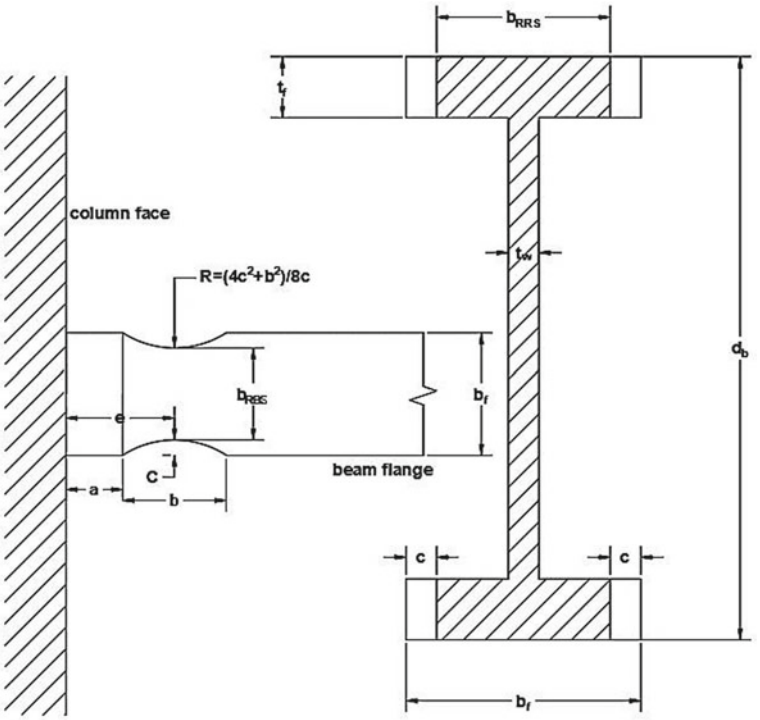

Fig. 1 Typical geometry of the radius cut RBS [8]

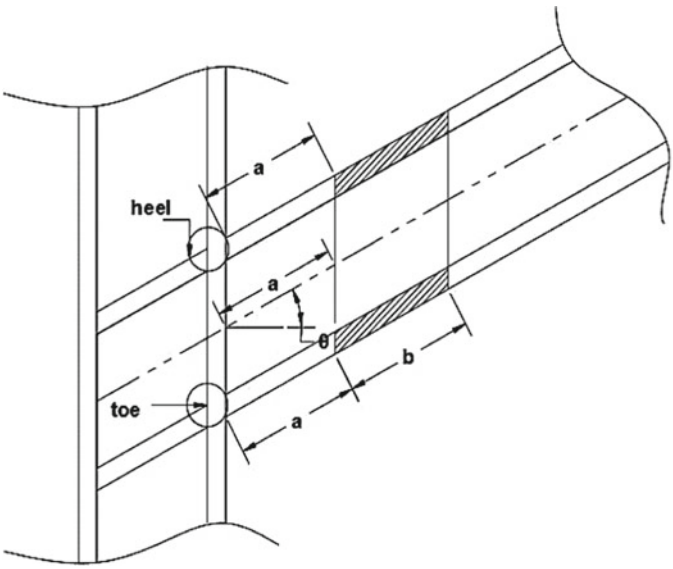

Fig. 2 Sloped RBS moment connection [10]

A beam to column bolted connection is modeled with an extended endplate, where the cross-sections were HE 300B and HE 160A for the column and the beam respectively. The total height of the column is 1797 mm and the beam span is 1000 mm. Double web plates of 12 mm thickness and continuity stiffeners equal to the beam flange thickness were assembled to the column, strengthening the panel zone. Web plates of 400 × 208 × 12 mm, continuity plates 262 × 100 × 10 mm, extended end plates 250 × 310 × 20 mm and 8 mm end plate welds were provided. Also M20, 10.9 grade bolts were used in the connections.

2.2 *Loading Protocol and Boundary Conditions*

The finite element modeling and analysis of present study is carried out using ANSYS 16.1 Workbench. Boundary conditions of the finite element model is shown in Fig. 3. The top and bottom of the column are provided with fixed boundary conditions thereby restricting the translations and rotations in x, y and z directions. For determining the cyclic behavior of different configurations in RBS, cyclic loading was applied at the beam tip. This loading protocol was developed to obtain the behavior of beam column moment connections. The details of loading sequence for AISC loading protocol is presented in Table 1.

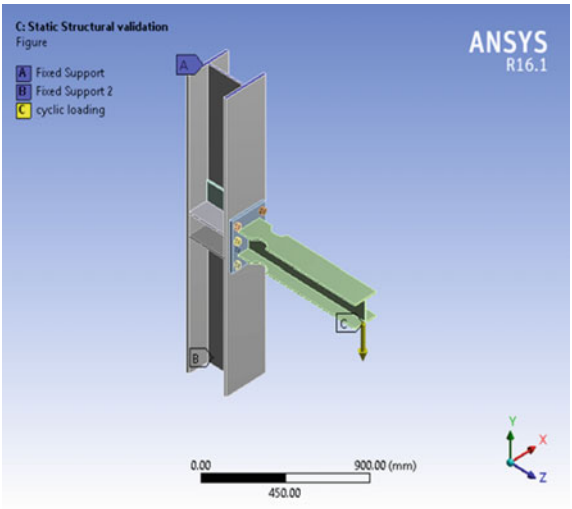

Fig. 3 Boundary conditions

Table 1 AISC 2002 loading schedule

Load step	Peak deformation, δ_y	Number of cycles
1	±0.375	6
2	±0.50	2
3	±0.75	2
4	±1.00	4
5	±1.50	2
6	±2.00	2
7	±3.00	2
8	±4.00	2

2.3 Geometric Modelling of Specimen

The study aims to analyze the cyclic behavior of bolted beam column joints with and without RBS techniques (Figs. 4 and 5). RBS with circular cut outs are made near the column face in the flanges of the beam. The modeling include the modeling of beam, column, extended endplate, double web plates, continuity stiffeners and

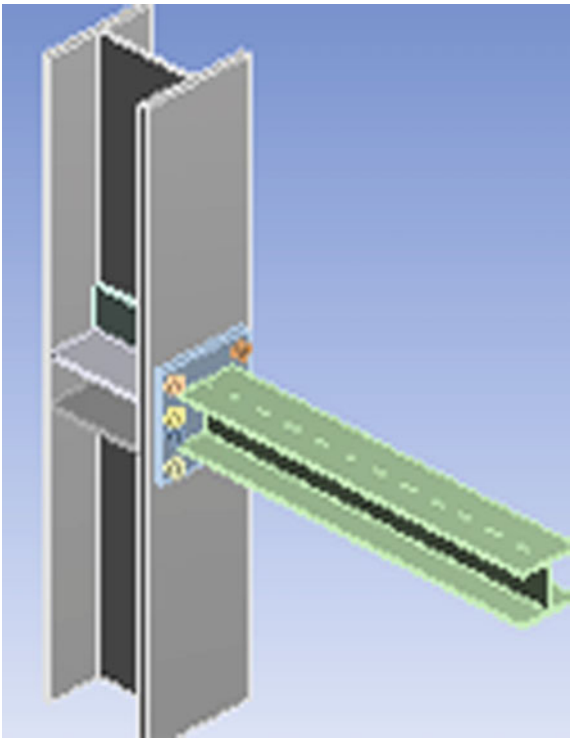

Fig. 4 FE model without RBS

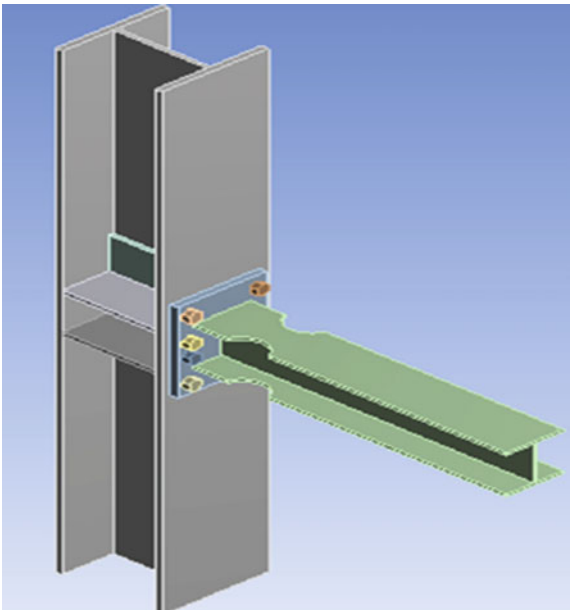

Fig. 5 RBS with circular cut

Table 2 Dimensions of RBS with circular cut

Distance of the beginning of the RBS from column face, a (mm)	Area of RBS (mm^2)	Length of the RBS, b (mm)	Depth of the flange cut, c (mm)	Radius of the cuts in both top and bottom flanges at the RBS, r (mm)
96	3321.7	114	40	60.61

reduced sections of beam. The geometry is defined for the configurations as shown in Table 2.

Element SOLID 186 was used for the 3-D finite element modelling. Bilinear isotropic hardening was used for modelling the materials. The mechanical properties of steel sections of beam and column are: modulus of elasticity $-2x10^5$ MPa, poisons ratio -0.3 and yield strength for beam -430 MPa.

Frictionless contact is provided between column to extended end plate connections. Frictional contact is provided between extended end plate to bolt, column to bolt connections and also in the column to nut connections. Bonded contacts are provided between column to web plates, column to continuity plates, bolt to nut, web plate to continuity plate, and also in extended end plate to beam.

2.4 Geometric Modelling of Inclined Beams

To investigate the effectiveness of RBS in inclined beams, 3D finite element models are developed with a slope angle in the elevation of the frame with a slope of 10, 20, 30 degrees from the orthogonal (Figs. 6, 7 and 8). Cyclic responses of these inclined beams with RBS were examined.

3 Effect of RBS on Cyclic Response

The parameters such as stress distribution, load carrying capacity, deformation and energy absorption are studied. The location of plastic hinge is identified in each configuration. According to the capacity design concept, the formation of plastic hinge should be away from the column face [11]. The cyclic behavior of bolted beam column joint with and without RBS techniques are studied by applying a cyclic loading at the tip end of the beam. AISC loading protocol given in Table 1 was used for this purpose. Load versus deformation curve is plotted to obtain the energy dissipation. The response parameters to cyclic loading such as deformation, stress,

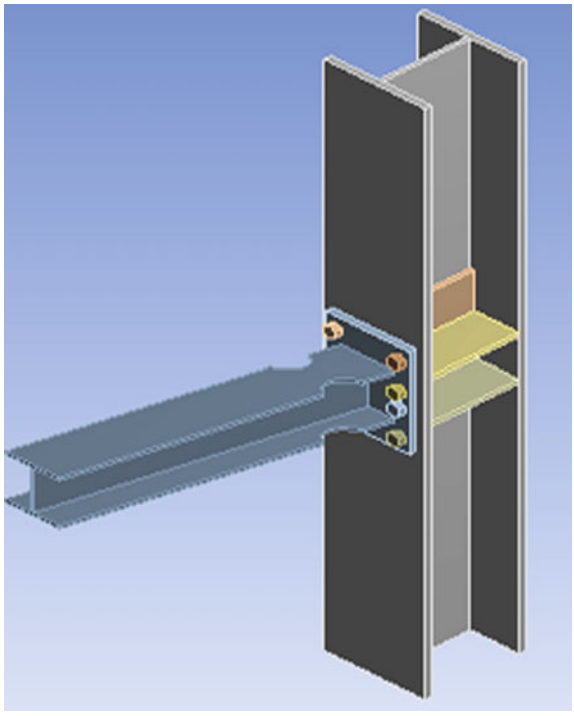

Fig. 6 10° Beam inclination

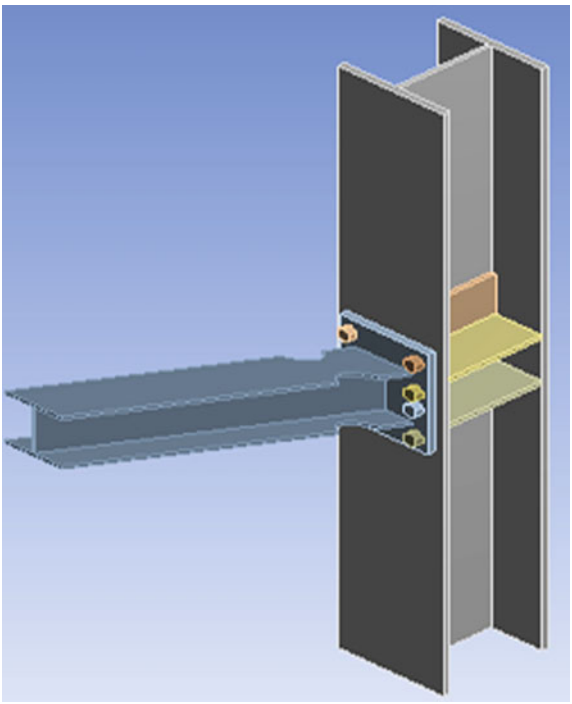

Fig. 7 20° Beam inclination

load carrying capacity and energy dissipation are tabulated in Table 3 for beams with and without RBS.

3.1 Stress Distribution

The structure is analyzed after the application of the cyclic loading at the free end of the beam. The stress distribution for each configuration is noted and is given in Table 3. The maximum stress in column and beam for both configurations is compared. By providing circular cut, the stress in column is reduced by 7.9% and plastic hinge location is shifted to reduced beam section. Hence it is recommended that RBS with circular cut gives better performance.

3.1.1 Beam Column Joint Without RBS

By performing the cyclic analysis, it is found that the major stress is concentrated at the column face, which is not recommended for the seismic performance. The stress distribution for beam column joint without RBS is shown in Fig. 9.

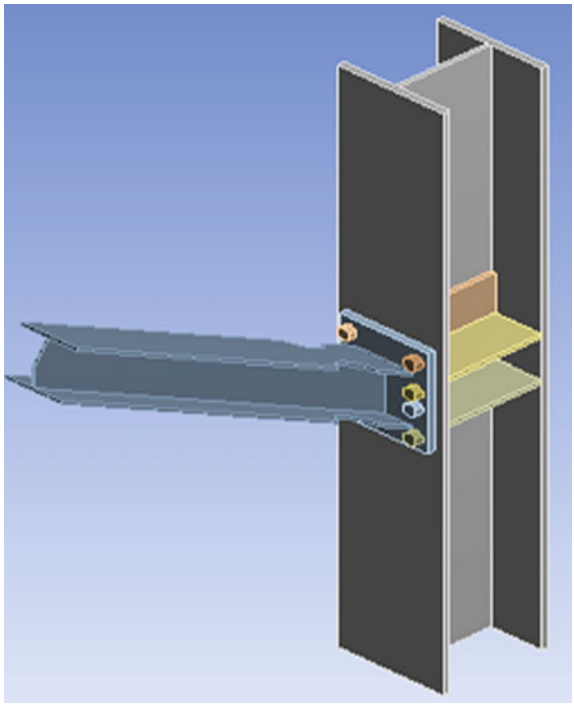

Fig. 8 30° Beam inclination

Table 3 Analysis response for beams with and without RBS

Cross section	Yield load (kN)	Ultimate load (kN)	Max column stress (MPa)	Maxbeam stress (MPa)	Yield deformation (mm)	Ultimate deformation (mm)	Energy dissipation (kJ)
Without RBS	30.657	99.864	521.71	460.93	7.5	60	13.975
Circular	28.102	72.667	480.46	555.36	7.5	60	18.901

3.1.2 RBS with Circular Cut

Under the cyclic loading, maximum stress of 555.36 MPa is occurred at the reduced beam section and 480.46 MPa at the column. Stress of 881.07 MPa is found to occur in the bolt. For this configuration, the plastic hinge position is changed from the column face to the RBS region. The stress distribution for the reduced beam section with circular cut is shown in Fig. 10.

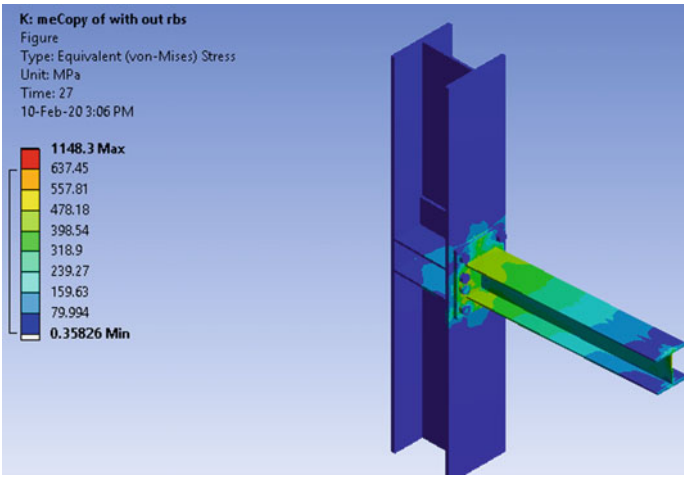

Fig. 9 Stress distribution of beam column joint without RBS

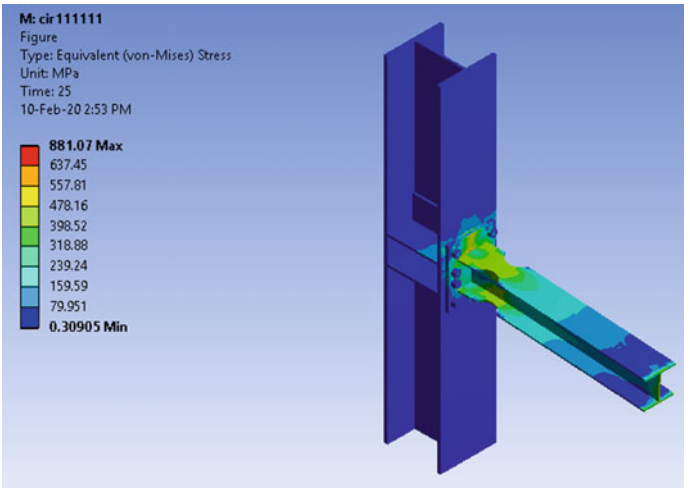

Fig. 10 Stress distribution of RBS with circular cut

3.2 Hysteretic Energy Dissipation

Load v/s deformation curve is plotted for the selected configuration. Area under the hysteresis curve gives the energy dissipation values [12]. The energy dissipation of RBS with circular cut, is 18.901 kJ, which is 35.24% higher than conventional connection. The curves obtained for different configurations are shown in Figs. 11 and 12. The energy dissipation corresponding to each model is given in Table 3.

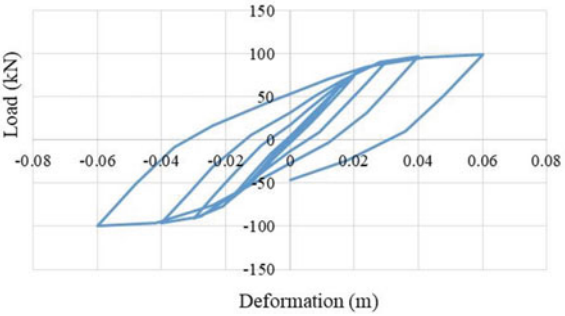

Fig. 11 Hysteresis curve for beam column joint without RBS

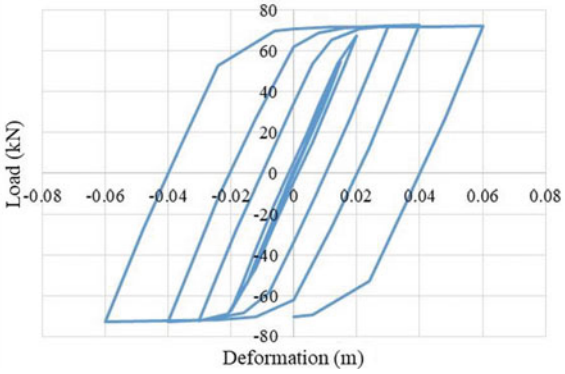

Fig.12 Hysteresis curve for RBS with circular cut

4 Effect of Inclination of Beams on Cyclic Behavior

Study is conducted to evaluate the effect of beam slope angle along with different design factors on the cyclic response of Reduced Beam Section (RBS) moment connections. Based on AISC-358, in sloped RBS connections, a small deviation from orthogonal does not change the performance of RBS connection significantly. However, for greater slope angles, e.g. 28° [8], adjustments should be made to avoid the adverse impact of slope angle, such as fracture at beam flange welds and increased strain demands at the heel location. RBS connections with smaller beam slope angle experience lower strain demands and less potential for fracture [8]. The response parameters to cyclic loading such as deformation, stress, load carrying capacity and energy dissipation are tabulated in Table 4 for variable alignment of beams.

4.1 Stress Distribution

After the application of cyclic loading at free end of the beam, it is found that in all cases (beam inclinations 10°, 20°, 30°), the plastic hinge zone have shifted to a

Table 4 Analysis response for variable alignment of beams

Inclination angles	Yield load (kN)	Ultimate load (kN)	Max column stress (MPa)	Max beam stress (MPa)	Yield deformation (mm)	Ultimate deformation (mm)	Energy dissipation (kJ)
10°	27.902	74.653	508.79	554.81	7.5	60	18.722
20°	27.597	75.615	464.1	537.45	7.5	60	18.535
30°	27.128	76.244	517.4	508.22	7.07	56.415	17.202

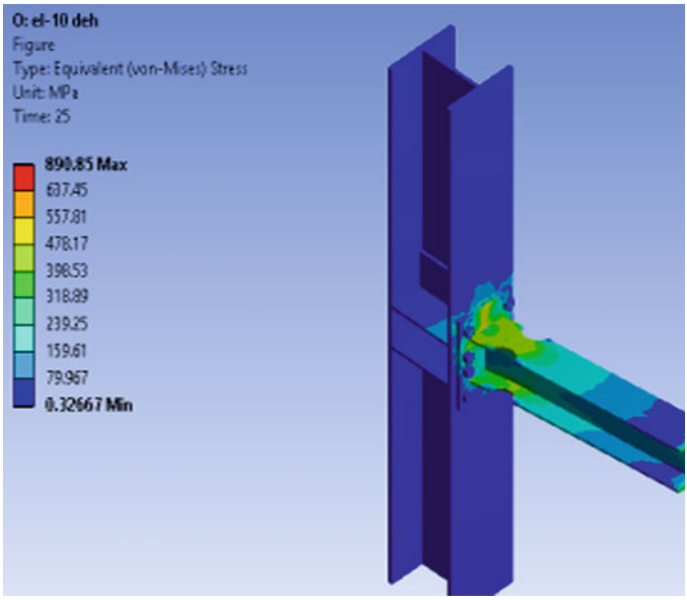

Fig. 13 RBS with slope angle 10°

distance away from the beam to column interface. i.e. to the RBS. Model with 20° slope angle shows, a maximum stress of 537.45 MPa at the RBS and 464.1 MPa at the column. Stress of 884.94 MPa is found to occur in the bolt which is less than that of RBS with 30° slope angle. The stress distribution for each configuration is noted in Table 4. The stress distribution of RBS with variable slope angles (10°, 20°, 30°) are shown in Figs. 13, 14 and 15.

4.2 Energy Dissipation Capacity

The energy dissipation capacity through yielding and buckling of the beam can be defined by the area within the hysteresis loop. The curves obtained for RBS with

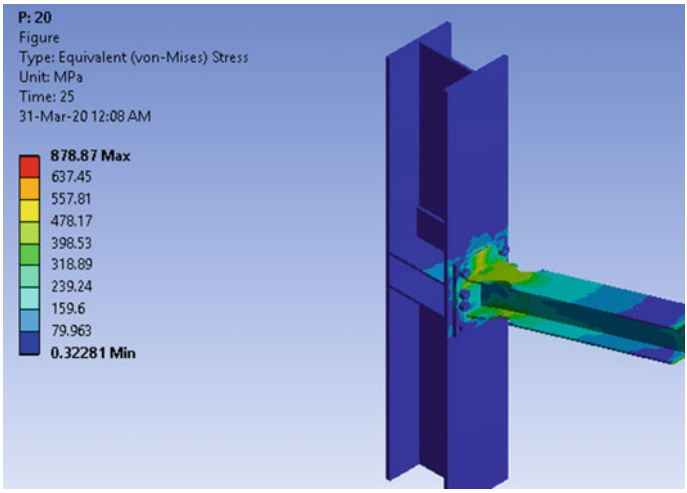

Fig. 14 RBS with slope angle 20°

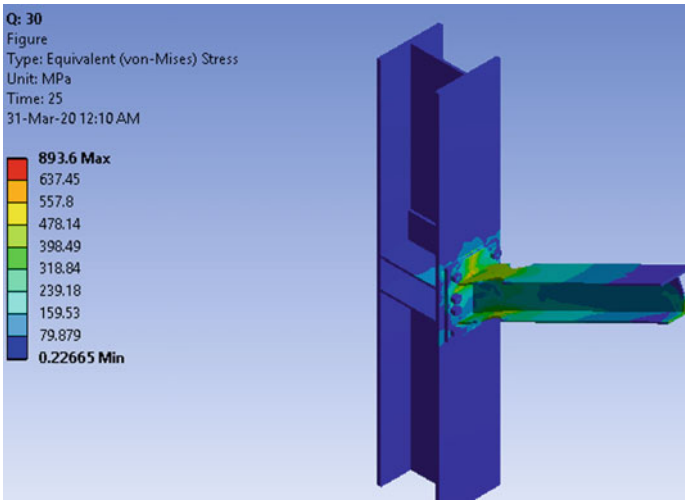

Fig. 15 RBS with slope angle 30°

slope angles (10°, 20°, 30°) are shown in Figs. 16, 17 and 18. The energy dissipation corresponding to each angle is given in Table 4.

The ultimate load carrying capacity for 20° inclination is higher than 10°. Hysteresis energy dissipation capacity decreases as slope angle increases. The models with slope angles 10° and 20° shows hysteresis energy dissipation capacity higher than 30° inclination (17.202 kJ). Increase in hysteresis energy dissipation capacity

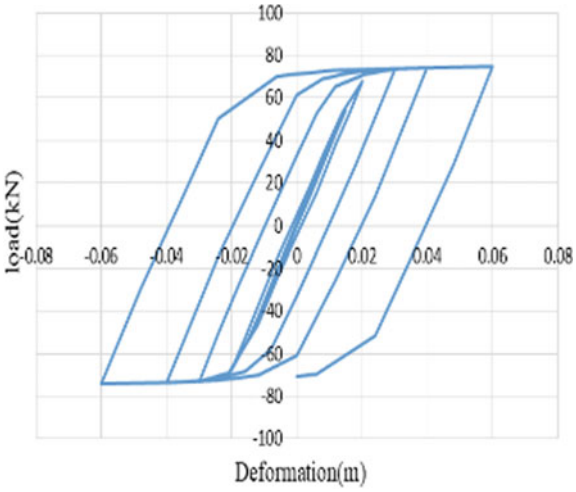

Fig. 16 Hysteresis curve for RBS with slope angle 10°

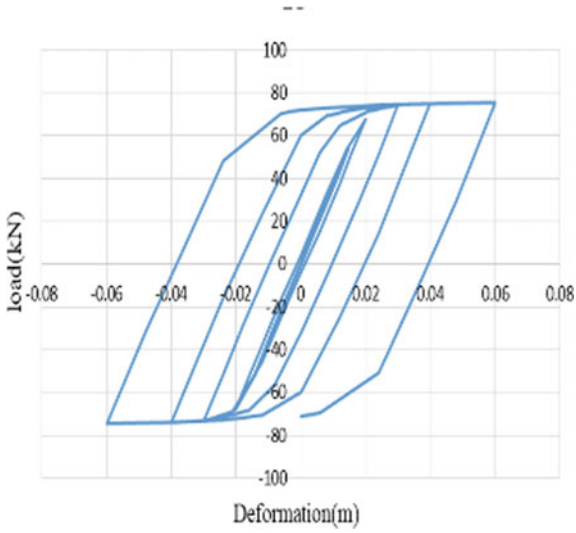

Fig. 17 Hysteresis curve for RBS with slope angle 20°

by 7.749% was observed in 20° slope angle when compared to RBS having 30° slope angle.

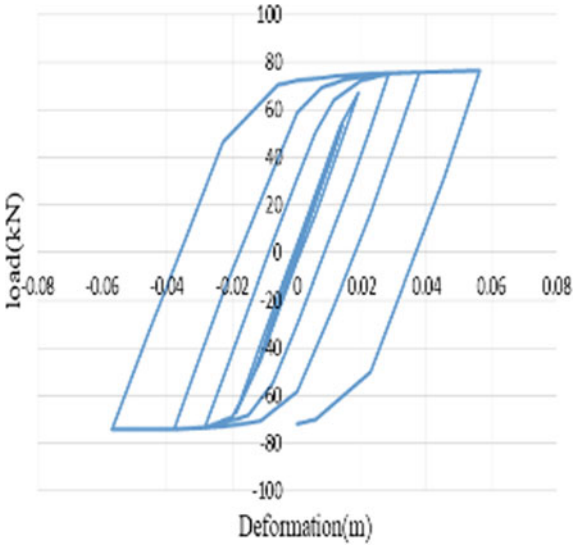

Fig. 18 Hysteresis curve for RBS with slope angle 30°

5 Conclusions

Connections should be designed to be stronger, mobilizing the stresses to a desired location along the length of the beam away from the connection assembly, creating the "weak beam-strong column" mechanism.

The concluding remarks obtained from the comparison of cyclic behavior of bolted beam column joints with and without RBS techniques are highlighted here:

- By adopting reduced beam section the plastic hinge location is shifted from the column face to the RBS region.
- The column stress in circular configuration was reduced by 7.9% on comparing with the conventional moment connection and it has a load carrying capacity of 72.667 kN.
- Increase in energy dissipation by 35.24% was observed in circular cut when compared with conventional connection.

The effect of RBS in inclined beams under cyclic loading is also studied in this paper. Sloped beam column connection with three different angles (10°, 20°, 30°) were analyzed and the major findings are summarized as follows:

- From the study considering the stress concentration on column, deformation and energy dissipation, the beams with inclination of 20° gives better results.
- Models with a slope angle of 10° and 20° showed ultimate deformation upto 60 mm where as the model with a beam slope angle of 30° can withstand only upto 56.415 mm.
- For RBS having 20° slope angle, the column stress is reduced by 10.3% when compared to 30° beam inclination.

- Increase in hysteresis energy dissipation capacity by 7.749% was observed in 20° slope angle when compared to RBS having 30° slope angle.
- The ultimate load carrying capacity for 20° inclination is higher than 10°.
- RBS connections with larger slope angles have greater potential for fracture and high strain demands.
- Ultimate deformation, hysteresis energy dissipation capacity decreases as slope angle increases.

References

1. Han SW, Moon K-H, Hwang S-H, Stojadinovic B (2012) Rotation capacities of reduced beam section with bolted web (RBS-B) connections. J Constr Steel Res 70:256–263
2. Swati AK, Gaurang V (2014) Study of steel moment connection with and without reduced beam section. Case Stud Struct Eng 1:26–31
3. Sumner EA, Murray TM (2002) Behavior of extended end-plate moment connections subject to cyclic loading. J Struct Eng 128(4):501–508
4. Hong J-K (2019) Sloped RBS moment connections at roof floor subjected to cyclic loading: Analytical investigation. Int J Steel Struct 19(1):329–339
5. Christos, Dimitra T (2018) Reduced beam section (RBS) moment connections-analytical investigation using finite element method. Civ Eng J 4(6):1240–1253
6. Rahnavard R, Hassanipour A, Siahpolo N (2015) Analytical study on new types of reduced beam section moment connections affecting cyclic behavior. Case Stud Struct Eng 3:33–51
7. Kulkarni RB, Vaghe VM (2014) Experimental study of bolted connections using light gauge channel sections and packing plates at the joints. Int J Adv Struct Eng (IJASE) 6(4):105–119
8. Lee C-H, Jeon S-W, Kim J-H, Uang C-M (2005) Effects of panel zone strength and beam web connection method on seismic performance of reduced beam section steel moment connections. J Struct Eng 131(12):1854–1865
9. Mohammadi NM, Moradi S (2020) Effects of design factors on the cyclic response of sloped RBS moment connections. Eng Struct 207(2020):110228
10. Kim D-W, Ball SC, Sim H-B, Uang C-M (2016) Evaluation of sloped RBS moment connections. J Struct Eng 142(6):04016013
11. Sophianopoulos DS, Deri AE (2019) Steel beam-to-column RBS connections: FEM analysis under cyclic loading. World J Mech 9:17–28
12. Sofias CE, Kalfas CN, Pachoumis DT (2014) Experimental and FEM analysis of reduced beam section moment endplate connections under cyclic loading. Eng Struct 59:320–329

Experimental Study of Self-cleaning Concrete by Using Various Photocatalysts

Geethu Benny and Gayathri Krishna Kumar

Abstract A construction material that removes pollutants from the air as it keeps its surface clean. This new astonishing concrete that not only keeps itself clean but also removes pollutants from the air is called Self-Cleaning Concrete. Self-cleaning concrete is a technique to reduce the air contaminants such as NO_x, SO_2, CO_2 and VOC'S from vehicular traffic on streets, any industrial activity and the urban environment. In this paper a study has been carried out on the compressive strength of self-cleaning concrete by introducing the photocatalytic materials such as titania (TiO_2), zinc oxide (ZnO), aluminium oxide (Al_2O_3). Self-cleaning property of the photocatalytic concrete is studied by using RhB (Rhodamine dye) discolouration under UV light, a standard test for self-cleaning cementitious materials. The properties of self-cleaning concrete is then compared with the that of M25 grade normal concrete and the results are studied.

Keywords Self-cleaning concrete · TiO_2 · ZnO · Al_2O_3 · Rhodamine dye · Compressive strength

1 Introduction

Buildings are exposed to many organic contaminants. From bird residue to diesel fumes, all urban buildings are constantly exposed to organic material that makes their surfaces appear dirty. Yet there's another kind of organic material constantly bombarding buildings that is harder to see: NO_x (nitrogen oxides). NO_x is the primary component of smog which not only makes buildings dirty, but also threatens the quality of the air we breathe. To overcome this, Photocatalytic materials such as

G. Benny (✉) · G. K. Kumar
Department of Civil Engineering, Federal Institute of Science and Technology (FISAT), Ernakulam 683577, India
e-mail: geethubenny.edatt@gmail.com

G. K. Kumar
e-mail: gaya3krishnakumar92@gmail.com

© Springer Nature Switzerland AG 2021

K. Dasgupta et al. (eds.), *Proceedings of SECON 2020*,
Lecture Notes in Civil Engineering 97,
https://doi.org/10.1007/978-3-030-55115-5_23

titania (TiO_2), zinc oxide (ZnO), Alumina (Al_2O_3) is added to the concrete thus self-cleaning properties can be determined. A construction material removes pollutants from the air as it keeps its surface clean. This new astonishing concrete that not only keeps itself clean but also removes pollutants from the air is called Self Cleaning Concrete. The key to such properties are photocatalytic components that use the energy from ultraviolet rays to oxidize most organic and some inorganic compounds [1]. This accelerates the process of natural oxidation and faster pollutant decomposition. Air pollutants that would normally result in discoloration of exposed surfaces are removed from the atmosphere by the components, and their residues are washed off by rain [1, 2].

2 Objectives of the Study

The objectives of the experimental research work include;

- To access the cleaning capacity of concrete using TiO_2, ZnO, Al_2O_3.
- To study compressive strength, decolourization using RhB dye.
- To compare the compressive strength and decolourization of concrete cubes made from TiO_2, ZnO, Al_2O_3.
- To compare the properties of self-cleaning concrete with that of normal M25 grade concrete.

3 Scope

- Concrete faces the problem of tending to become dirty when exposed to polluted area. This can be reduced by using self-cleaning capability of concrete by using TiO_2, ZnO, Al_2O_3.

4 Experimental Work

4.1 Materials Used

4.1.1 Cement

Ordinary Portland cement (OPC)-53 grades confirming to IS: 12269–1987 was used. The properties are given in Table 1.

Table 1 Properties of cement

Fineness modulus	Specific gravity	Initial setting time
6%	3.17	42 min

Table 2 Properties of fine aggregate

Specific gravity	Grade
2.75	Zone II

Table 3 Properties of coarse aggregate

Specific gravity	Grade
2.83	Well graded

Table 4 Physical properties of titanium dioxide

Average particle size	Purity	Specific gravity
35 nm	99%	1.4

4.1.2 Fine Aggregate

Fine aggregate used for the experimental study was manufactured sand. The physical properties of fine aggregate are given in Table 2.

4.1.3 Coarse Aggregate

Coarse aggregate used in this experiment are of 20 mm nominal size. The physical properties of coarse aggregate are given in Table 3.

4.1.4 Titanium Dioxide

Titanium dioxide is a chemical compound, also known as titania, is the naturally occurring oxide of titanium, chemical formula TiO_2. Table 4 shows the physical properties of titanium dioxide.

4.1.5 Zinc Oxide

Zinc oxide is an inorganic compound with the formula ZnO. ZnO is a white powder that is insoluble in water. Table 5 shows the properties of zinc oxide.

Table 5 Physical properties of zinc oxide

Average particle size	Purity	Specific gravity
55 nm	99%	5.6

Table 6 Physical properties of aluminium oxide

Average particle size	Purity	Specific gravity
55 nm	99%	3.9

4.1.6 Aluminium Oxide

Aluminium oxide is a chemical compound of aluminium and oxygen with the chemical formula Al_2O_3. It is commonly called alumina. Table 6 shows the properties of aluminium oxide.

4.1.7 Rhodamine B

It is a chemical compound and a dye. It is often used as a tracer dye within water to determine the rate and direction of flow and transport. Rhoda mine dyes are used extensively in biotechnology applications.

4.2 Mix Proportion

M25 grade mix design was carried out with reference to IS code-10262: 2009 [1]. A ploy-carboxylate ether based superplasticiser is used at a dosage of 0.3% by weight of cement to improve the workability. Trial and error method is adopted to arrive at the suitable normal concrete mix. Hence arrived at a mix proportion which is tabulated in Table 7

Hence the mix proportion adopted is 1:1.77:3.24.

Table 7 Mix proportion

Cement (kg)	Fine aggregate (kg/m^3)	Coarse aggregate (kg/m^3)	Chemical admixture (kg/m^3)	Water (kg/m^3)
390	693.2	1264	1.17	169.5

4.3 Methodology

- The properties of the raw materials such as cement, fine aggregate, coarse aggregate which are used for the investigation is studied. All the experiments that are done to determine the characteristics of the materials are carried out as per Indian Standards.
- All the materials for casting concrete were taken and were mixed using hand mixing under desirable conditions and they are allowed for casting in the prefabricated moulds [3].
- In the mix TiO_2, ZnO, Al_2O_3 were added in varying percentages such as 0.5%, 1%, 1.5% of weight of cement and self-cleaning concrete is made.
- Specimens were demoulded 24 h after casting and are cured in water until the testing age [4].
- The compressive strength of concrete cubes of size 150 × 150 × 150 mm were tested at 7 days and 28 days to obtain optimum of TiO_2, ZnO, Al_2O_3.
- Self-cleaning action of concrete is studied on cubes with the help of RhB solution. After one day of curing, the concrete cubes are dipped into RhB solution. Then the cubes are taken out and exposed to direct sunlight to observe the self-cleaning action. Photographs are taken at different intervals and the self-cleaning action is observed.

4.4 Results and Discussions

4.4.1 Estimation of Optimum Percentage of Photocatalysts

Concrete cubes were casted with varying percentages of TiO_2, ZnO, Al_2O_3. 3 cubes were prepared for each mix and compressive strength test was conducted after 7 days and 28 days appropriate curing. Based on the results optimum percentage of different photocatalysts were determined.

The results indicated that the compressive strength of concrete produced by adding photocatalytic (TiO_2, ZnO, Al_2O_3) nano-particles show higher value at 1% which is greater than the value for control mix. This may be due to the fact that 1% of these nano-particles will fill all the pores of concrete thus imparts a dense micro structure to concrete [5, 6]. After 1% of TiO_2, ZnO, Al_2O_3 the compressive strength decreases this may be due to excess amount of these photocatalysts covers the cement particles which disrupt the water cement reaction and hence the strength decreases on further increment. Therefore the optimum percentage is found to be 1–1.5%. Figures 1, 2 and 3 depicts the variation of average compressive strength for varying percentages of TiO_2, ZnO, Al_2O_3 respectively.

Figure 4 depicts the graph between average compressive strength v/s optimum dosage of TiO_2, ZnO, Al_2O_3.

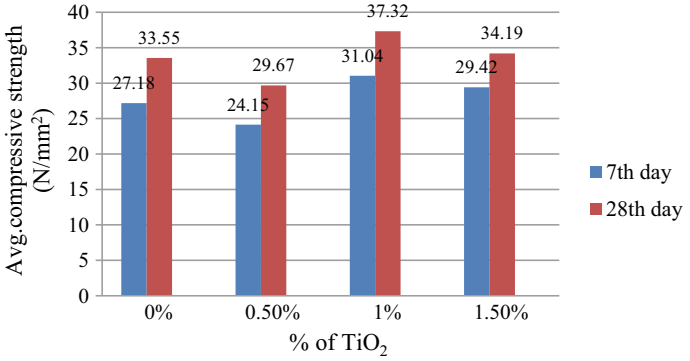

Fig. 1 Average compressive strength versus % of TiO_2

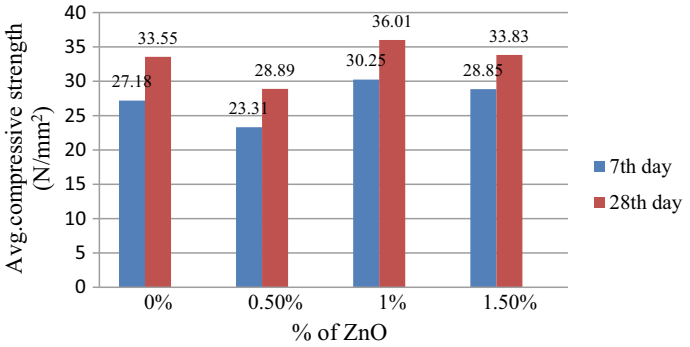

Fig. 2 Average compressive strength versus % of ZnO

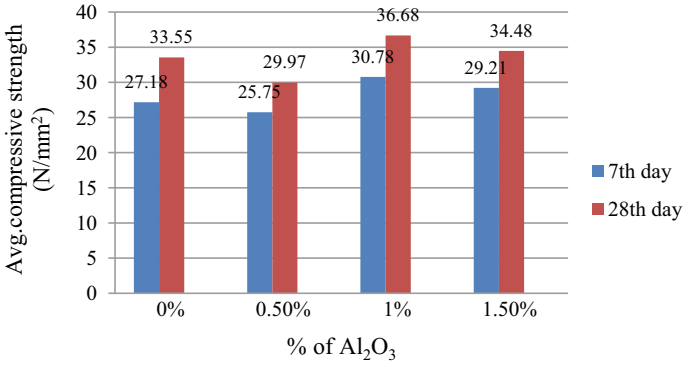

Fig. 3 Average compressive strength versus % of Al_2O_3

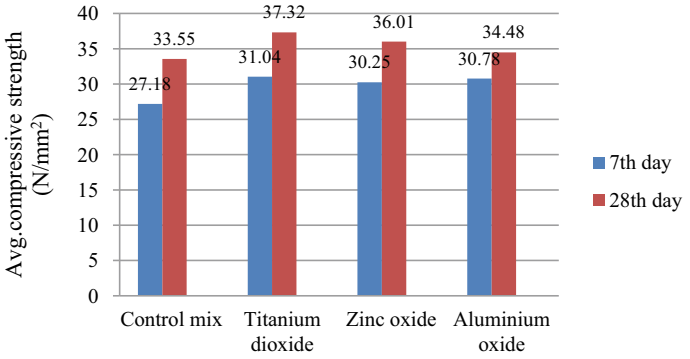

Fig. 4 Average compressive strength versus optimum dosage of TiO_2, ZnO, Al_2O_3

4.4.2 Decolourization Test

Concrete cubes were casted with 1% of TiO_2, ZnO, Al_2O_3. In this test the concrete containing photocatalysts have been evaluated based on decolourization under sun light, (a standard test for self-cleaning cementitious materials). After one day of curing, on the surface of the casted concrete cubes 1 ml of Rhodamine dye is dropped on each cube sample and placed under direct sunlight and the photographs are taken at different intervals and the self-cleaning action is observed [7]. Figure 5, 6, 7 shows the results recorded at different intervals.

The results indicated from the Rhodamine decolourization test is that the cube sample made with 1% TiO_2 shows a better cleaning action compared to that of Al_2O_3, ZnO and control mix (CM). Therefore self-cleaning action of the concrete cubes made with photocatalysts can be compared as; $TiO_2 > Al_2O_3 > ZnO \geq CM$.

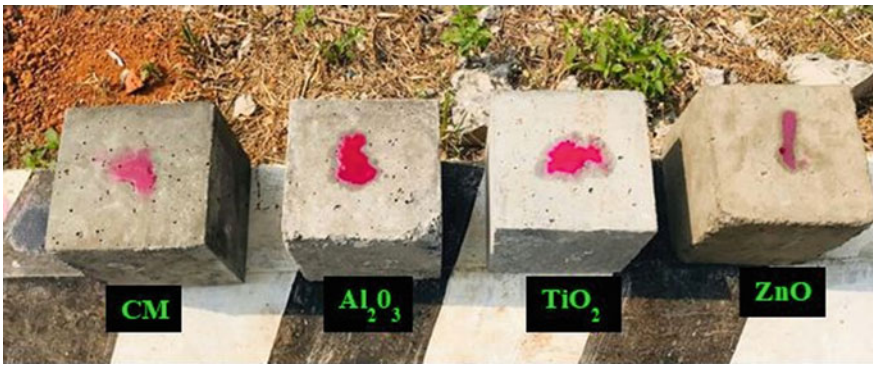

Fig. 5 Sample cubes placed under sunlight

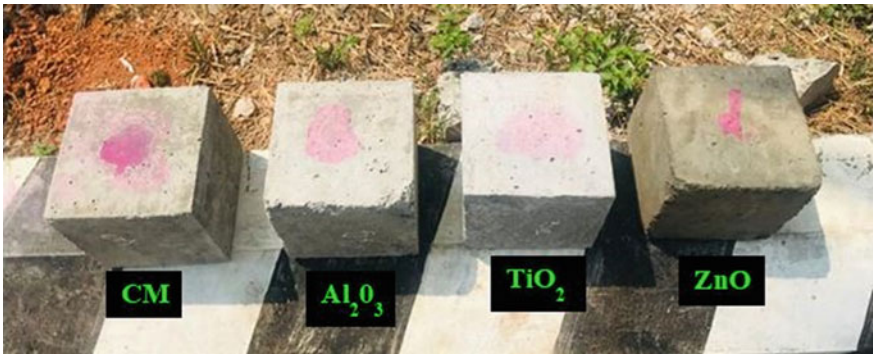

Fig. 6 After 2 h under sunlight

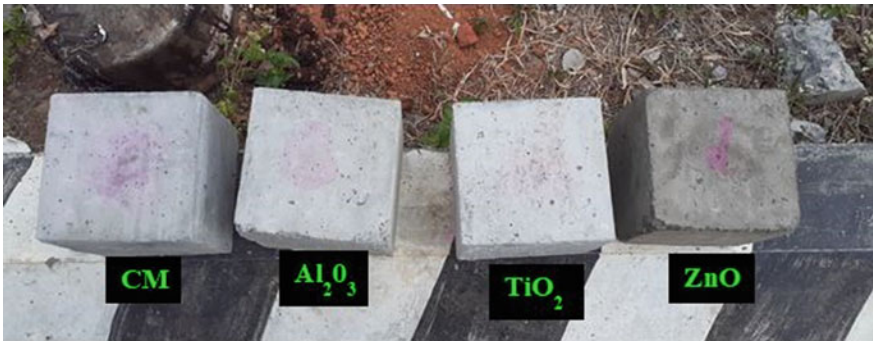

Fig. 7 After 5 h under sunlight

5 Conclusions

- Adding 0.5%, 1%, 1.5% of TiO_2, ZnO, Al_2O_3, it is observed that 1% of addition gives higher compressive strength than the control mix.
- The increase in strength is may be due to nanoparticles act as a protective material to improve the density of concrete that decreases the porosity of concrete significantly.
- The results indicated from the Rhodamine decolourization test is that the cube sample made with 1% TiO_2 shows a better cleaning action compared to that of Al_2O_3, ZnO and control mix (CM).

References

1. Antony J, Kannan SU (2018) Study on the properties of self cleaning concrete using titanium dioxide. J Trend Sci Res Dev 2:248–253
2. Dhanabal M, Sakthivel R, Arun T (2018) Experimental study of photocatalytic concrete using titanium dioxide. J Innov Res Sci Technol 4(11)
3. Feng D, Xie N, Gong C, Leng Z, Xiao H, Lui H, Shi X (2013) Study on the properties of self-cleaning concrete using titanium dioxide. Indus Eng Chem Res 52:11575–11582
4. Abdul Hafiz SB, Prakash KB (2017) An experimental investigation on the effect of nano-TiO_2 particles on the properties of concrete. J Eng Technol 4:2621–2626
5. Raj A (2019) Behaviour of self-cleaning concrete by using various photocatalysts. Int Res J Eng Technol 06(05)
6. Pathak A, Tiwari A (2017) Effect of zinc oxide nanoparticle on compressive strength and durability of concrete. J Res Appl Sci Eng Technol 5:445–500
7. Vignesh T, Sumathi A, Saravana Raja Mohan K (2018) Study on self-cleaning concrete using nano-liquid TiO_2. Int J Eng Technol 7(3.12):860–863

Thermo Structural Optimisation Study on Slim Floor Beam with Hollow Core Slabs

Athul Deepak Krishna and Neeraja Nair

Abstract Slim-floor beams are a novel typology of steel beams where the steel profile is fully embedded within the concrete floor depth. Slim-floor beams are a well-known and cost-effective solution that permits a significant reduction of floor thickness, and are increasingly used in industrial and commercial buildings. While the use of this system is increasing in the construction practice, the available investigations on its thermal performance are still scarce. Therefore, this paper focuses on analyzing the fire behaviour of slim-floor beams with hollow-core slabs as a flooring system and improving its fire-resistance. A finite element model was developed through ANSYS 16.1 and the thermal performance of different type of composite beam configuration and steel plate thickness was studied by conducting transient thermal analysis. Also, structural analysis of the following models using these material sections for SFB were conducted and its structural behaviour was studied. The conclusions suggest that the thermal performance of SFB configuration can be improved by using innovative solutions, advanced materials or external protection.

Keywords Slim floor beam · Hollow core slab · Thermal performance · ANSYS

1 Introduction

One of the most common typologies of steel–concrete composite beam used in practice is the so-called slim-floor beam [1]. The main characteristic of this typology is that the whole height of the beam remains embedded within the floor depth. Taking advantage of this reduced height, slim-floor beams offer several improved performances such as the total floor thickness reduction and the provision of clear under-floor space for the easy installation of technical equipment.

A. D. Krishna (✉) · N. Nair
Federal Institute of Science and Technology, Angamaly, Ernakulam, India
e-mail: athuldeepakkrishna@gmail.com

N. Nair
e-mail: neeraja15@gmail.com

© Springer Nature Switzerland AG 2021

K. Dasgupta et al. (eds.), *Proceedings of SECON 2020*,
Lecture Notes in Civil Engineering 97,
https://doi.org/10.1007/978-3-030-55115-5_24

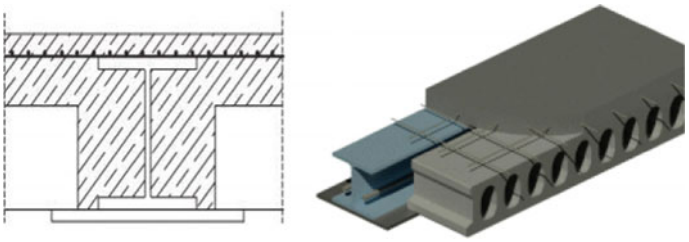

Fig. 1 Slim floor beam with hollow core slab

Slim-floor beams can be used combined with different floor elements, such as profiled steel deck or precast concrete slabs. One of the most interesting typology is obtained from combining the slim-floor beam with precast hollow core slabs, which provides additional benefits as the fast erection and the structural efficiency for longer spans shown in Fig. 1.

Due to the fact that the steel beam is totally embedded within the concrete floor, the fire behaviour of slim floor beams is remarkable [2]. Being exposed to fire only from their lower flange, in contrast with other types of composite beams not fully embedded within the concrete floor, slim-floor beams can achieve higher fire resistance times.

2 FEM of Slim Floor Beam with Hollow Core Slab

2.1 Geometry

This research is focused on the development of an advanced Finite Element Model for the evaluation of slim-floor composite beams, mainly of SFB typology, combined with precast hollow core slab floors supported by the bottom steel plate and welded to the lower flange of the beam.A finite element thermal model for simulating nonlinear heat transfer analysis was developed through ANSYS 16.1 and the thermal performance of different type of composite beam configuration, types of thermal resistant concrete, and steel plate thickness was studied by conducting transient thermal analysis. Also, structural analysis of the following models using these material sections for SFB were conducted and its structural behaviour was studied.

Particularly, for the analysis of the slim-floor in fire, two finite element models were needed: a thermal model and a mechanical model. Thermal model was for conducting the transient thermal analysis to find their thermal performance and mechanical model was for conducting the static structural analysis for finding their structural performance. All model parts were meshed using three dimensional eight-noded heat transfer solid elements. A maximum finite element size of 20 mm was employed for meshing all concrete parts and size of 5 mm was used for steel elements (Fig. 2; Table 1).

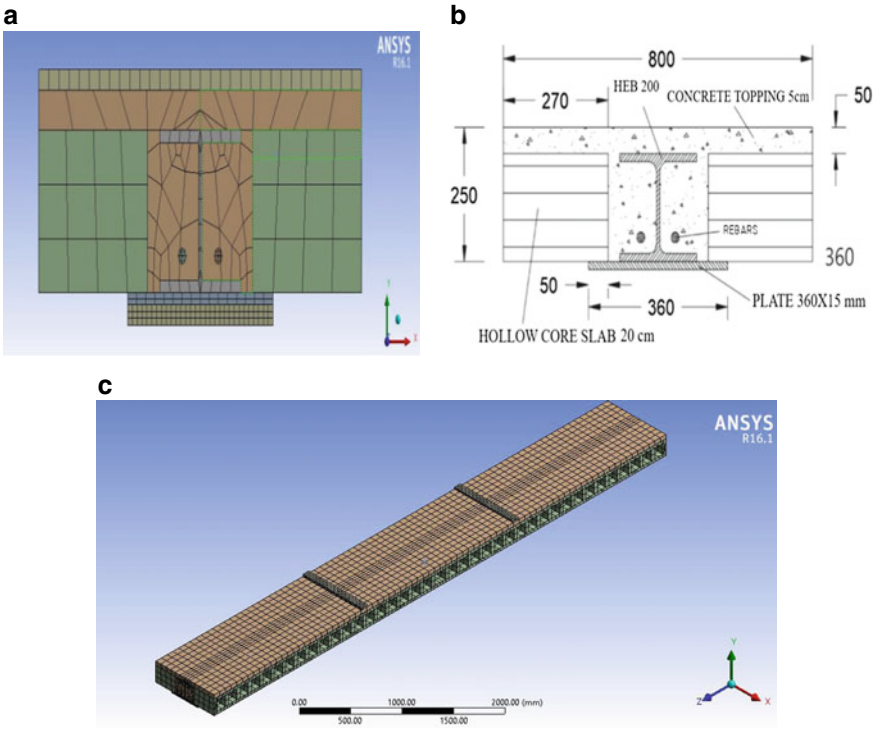

Fig. 2 **a** Mesh view of numerical model, **b** CAD drawing, **c** 3D View of SFB with HCS model

Table 1 The sizes of validated slim floor beam with hollow core slab [1]

Parameters	Size
Length	3200 mm
I Section	HEB 200
Base plate	360 × 15 mm
Rebars	2Ø20 mm bar
Concrete topping	50 mm
Hollow core slab	200 mm
Width of web	42 mm
Width of hole	115 mm
Height of hole	130 mm

2.2 Material Specification and Engineering Properties

The objective of the parametric study is to assess the influence of the below mentioned parameters over the fire behaviour of slim-floor beams. The list of parameters

Table 2 Parametric study

Parameter	Different material cases
I Beam material type	GFRP [3]
Base plate	Stainless Steel [4]
Bottom plate thickness	5 mm, 10 mm, 15 mm

Table 3 Thermal properties of various materials used

Material	Density (kg/m^3)	Thermal conductivity (W/mK)	Specific heat (J/kgK)
Structural steel [1]	7850	60.5	434
GFRP [3]	1870	0.35	640
Stainless steel [4]	7750	15.1	480

studied is shown in Table 2 and the thermal properties of various materials used is shown in Table 3.

2.3 Analysis

A sequentially coupled thermal-stress analysis was used to conduct the numerical simulation, thus two different models were needed: a heat transfer model and a mechanical model. The analysis was performed by first conducting a pure heat transfer analysis for computing the temperature field and afterwards a stress/deformation analysis for calculating the structural response. The slim-floor cross-section was only exposed to fire from its lower surface, matching with the electrical furnace setup and real fire exposure conditions of slim-floor beams in practical situations. The values recommended in EN 1991-1-2 were adopted for the governing parameters of the heat transfer problem. The thermal analysis is done by using transient thermal analysis.

3 Comparison of the Thermal Performance

During transient thermal analysis, the SFB configuration was exposed to standard fire ISO-834 model [1]. In order to evaluate the thermal behaviour of each specimen, based on journals [5], six thermocouples positions are located in the cross section of finite element model. They are TC1, TC2, TC3, TC4, TC5 and TC6. But out of these six locations; three locations are taken for thermal performance comparison. They

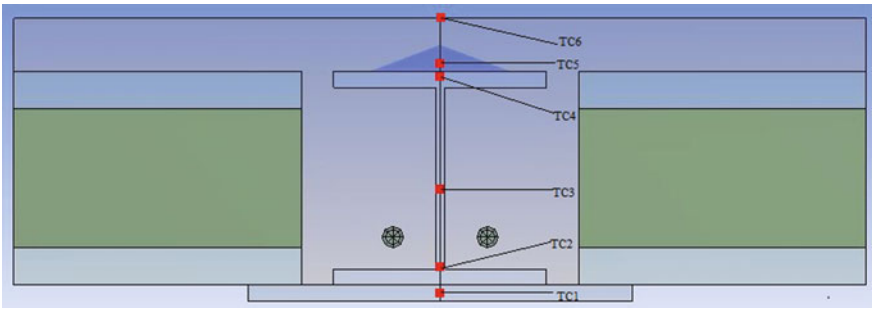

Fig. 3 Six Thermocouple location in SFB with HCS

are TC1 placed at the middle part of the base plate, TC3 was placed at the middle of the I beam and TC6 was placed at the top of the slim floor beam shown in Fig. 3.

After conducting the thermal analysis then the static structural analysis was carried out. The SFB model was roller supported at the both ends. Loading plates were provided at L/3 distance of the total span length shown in Fig. 2c. The structural analysis was carried out by displacement control method. And maximum load carrying capacity was found by plotting load displacement graph.

3.1 Effect of Structural Steel

After transient thermal analysis the maximum temperature recorded in various thermocouple locations were recorded. The maximum temperature recorded in SFB using structural steel in embedded I beam and base plate was 769 °C at TC1, 560 °C at TC4 and 167.7 °C at top surface. This shows the temperature distribution of structural steel material. The temperature curve for slim floor beam with hollow core slab using structural steel material section in the embedded I beam section and base plate is shown in Fig. 4.

The structural response for slim floor is presented in terms of the total load carrying capacity obtained from the FE modeling. For comparison purposes the load values are taken, after the static analysis the maximum load it can carry is 341.432 kN for structural steel.

3.2 Effect of GFRP

In this thermal analysis the SFB with HCS is analysed by changing the structural steel section by GFRP section was carried out. After the thermal analysis the temperature curve for slim floor beam with hollow core slab using GFRP material section is shown in Fig. 5.

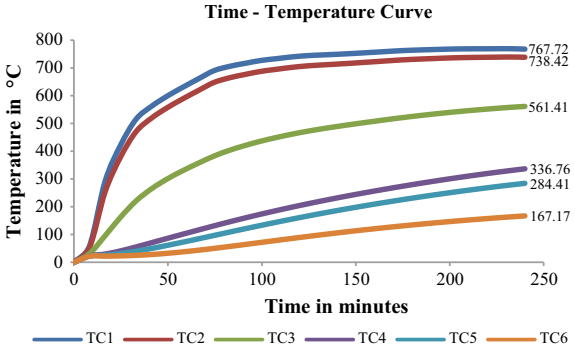

Fig. 4 The temperature curve of SFB with HCS using structural steel material section

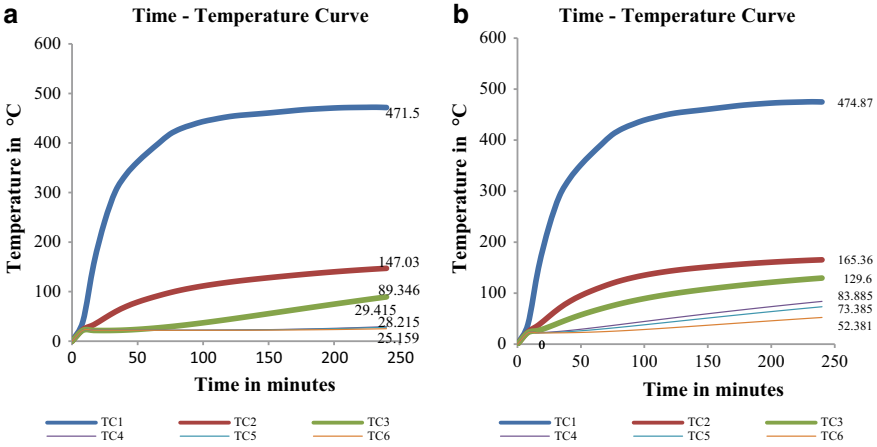

Fig. 5 The temperature curve of SFB with HCS using GFRP material section **a** in the embedded I beam section and base plate **b** in base plate only

The maximum temperature recorded in SFB using GFRP in embedded I beam and base plate was 471.5 °C at TC1, 89.35 °C at TC3 and 25.16 °C at top surface TC6. And in case of GFRP in base plate only, the maximum temperature recorded was 474.87 °C at TC1, 129.6 °C at TC3 and 52.38 °C at TC6. This decrease in temperature in SFB with HCS is due to the change in the thermal properties of GFRP. This shows that GFRP material section has good thermal performance compared to structural steel material. After the static analysis the maximum load the GFRP that can carry in two cases are 272.4 kN and 320.84 kN. Thus the maximum load the GFRP material section that can carry in both cases are low when compared to structural steel material section. But it has good thermal properties than structural steel material section.

3.3 *Effect of Stainless Steel*

In this thermal analysis, the SFB with HCS is analysed by changing the structural steel section by stainless steel section was carried out. After the thermal analysis the temperature curve for slim floor beam with hollow core slab using stainless steel section is shown in Fig. 6.

The maximum temperature was recorded in various thermocouple locations. The maximum temperature recorded in SFB using stainless steel in embedded I beam and base plate was 741.28 °C at TC1, 425.32 °C at TC3 and 77.635 °C at top surface TC6. And in case of stainless steel in base plate only, the maximum temperature recorded was 739.23 °C at TC1, 517.8 °C at TC3 and 156.24 °C at TC6. This decrease in temperature in SFB with HCS is due to the change in the thermal properties of stainless steel. This shows that stainless steel material section has good thermal performance compared to structural steel material. After the static analysis the maximum load the stainless steel that can carry in two cases are 242.724 kN and 341.1 kN. Thus the maximum load the stainless steel material sections that can carry in both cases are low when compared to steel material section. But it has good thermal properties than steel material section.

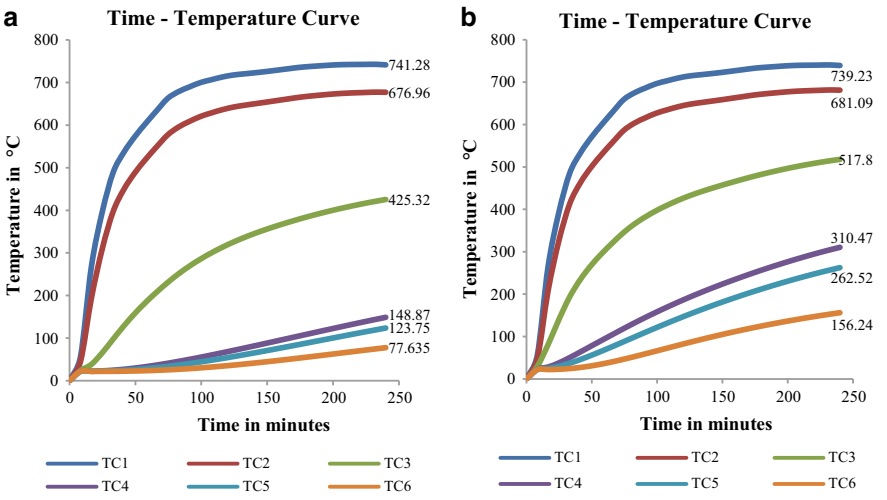

Fig. 6 The temperature curve of SFB with HCS using stainless steel material section **a** in the embedded I beam section and base plate, **b** in base plate only

Table 4 Maximum temperature at thermocouple location

S. No.	Material	Thickness (mm)	TC1 (°C)	TC3 (°C)	TC6 (°C)
1	Structural steel	15	769	560	167.7
2	Stainless steel	15	739	517.8	156.75
3	Structural steel	5	775.2	569.35	170.53
4	Stainless steel	5	764.5	552.35	166.28

3.4 Effect of Bottom Plate Thickness

In this thermal analysis, the SFB with HCS is analysed by changing the depth of bottom plate. And also the property of the structural steel and stainless steel was applied to the varying bottom plate thickness simultaneously.

Table 4 shows the maximum temperature recorded in various thermocouple locations. From the result it can be observed that reducing the bottom plate thickness of SFB using stainless steel leads to a decrease in temperature between 1.4 and 3.9%. As far as stainless steel material is concerned its material cost is high compared to structural steel. By comparing the above tabulated result and cost of each material it can concluded that the base plate of thickness 15 mm can be replaced by base plate of 5 mm thickness having material property of stainless steel. Here we can reduce material required for base plate and also use of stainless steel material will have better strength retention at elevated temperatures.

4 Conclusion

Based on parametric studies conducted, the influence of the different parameters over slim-floor configuration, the following conclusion can be drawn:

- Hence by use of thermal resistant material like GFRP the temperature can be reduced by a percentage of 38–77% in different locations of SFB model when compared to structural steel model. This shows good thermal performance than structural steel.
- By use of stainless steel, the temperature can be reduced by a percentage of 3–8% in different locations of SFB model when compared to structural steel model. Hence a better fire performance.
- But in case of their structural performance, the maximum load carrying capacities obtained are 320.84 and 341.1 for GFRP and stainless steel respectively. Hence they have considerably low loading carrying capacity than structural steel.

- The effect of the bottom steel plate thickness was studied. It may also be regarded as good alternatives to applying external protection by means of using stainless steel base plate of small thickness, with the related cost and material savings. Apart from a better fire performance, it also provides improved durability and an aesthetic finishing to the ceiling.

References

1. Kim HJ, Kim HY, Park SY (2011) An experimental study on fire resistance of slim floor beam. Appl Mech Mater, 752–757
2. Aguado JV, Albero V, Espinos A, Hospitaler A, Romero ML (2016) A 3D finite element model for predicting the fire behavior of hollow-core slabs. Eng Struct 108:12–27
3. Berardi U, Dembsey N (2015) Thermal and fire characteristics of FRP composites for architectural applications. Polymers 7(11):2276–2289
4. Leroy G, Insausti A, Ng KT, Ashraf M (2010) Elevated temperature material properties of stainless steel alloys. J Constr Steel Res 66(5):634–647
5. Albero V, Espinós A, Serra E, Romero ML, Hospitaler A (2018) Numerical study on the flexural behaviour of slim-floor beams with hollow core slabs at elevated temperature. Eng Struct 180:561–573

Study of Geo-polymer Concrete with Replacement of Fine Aggregate Using Bottom Ash

Sweety Viswanath and Nincy Jose

Abstract Current cement production across the globe is 4.0 billion tonnes per annum and growing at 4% annually and it have a huge effect on the global warming. This calls for the development and use of alternative binder materials which will have less carbon footprint on environment. The sustainable alternatives to conventional cement can be developed by utilizing the cementitious properties of industrial byproducts like flyash, bottomash and GGBS. Flyash and GGBS are used as binder material 50% each. Bottomash is used for the replacement of fine aggregate. NaOH, Na_2SiO_3 were used as alkaline activators. Casting and curing of geopolymer concrete (GPC) is done under ambient temperature. This paper was aimed at examining the fly ash-ggbs based GPC along with replacing the fine aggregate using bottomash. Study deals with investigating the influence of varying molarity of NaOH viz., (8 M, 10 M, 12 M, 14 M, 16 M) and to examine the influence of varying bottom ash content (25–100%) on the mechanical properties of geopolymer concrete. Also to establish relative performance of GPCs with respect to OPCs.

Keywords Flyash · GGBS · Bottomash · Geopolymer concrete · Alkaline activator · Ambient temperature

1 Introduction

Cement production across the globe is 4.0 billion tonnes per annum and growing at 4% annually and extreme energy is required to produce it. This is having huge effect on the global warming. Barely an option left out with except mitigating the emission of green houses to a great extent. This calls for major attention of researchers for development and use of alternative binder materials, which will have less carbon

S. Viswanath (✉) · N. Jose
Department of Civil Engineering, Federal Institute of Science and Technology (FISAT), Ernakulam 68377, India
e-mail: sweety.viswanath@gmail.com

N. Jose
e-mail: nincyjose12@gmail.com

© Springer Nature Switzerland AG 2021

K. Dasgupta et al. (eds.), *Proceedings of SECON 2020*,
Lecture Notes in Civil Engineering 97,
https://doi.org/10.1007/978-3-030-55115-5_25

footprint on environment. Efforts have, therefore, been made to reduce the use of portland cement by introducing other supplementary cementitious materials (SCM). In view of this, there is a need to develop sustainable alternatives to conventional cement utilizing the cementitious properties of industrial byproducts such as fly ash, ground granulated blast furnace slag. These materials are byproducts from industrial processes and thus require less energy to produce compared to PC production. The production of geopolymers takes place through the geopolymerization process. Geopolymer cement, high-alkali–poly (siliate-siloxo) cement, results from an inorganic polycondensation reaction, and so called geopolymerisation yielding three dimensional zeolitic frameworks.

Better compressive strength noticed in increase in NaOH molarity [1]. GPC's cured at the ambient temperature do not undergo exothermic processes to the extent that are experienced by conventional OPC's [2]. Compressive strength of coal ash based GPC's increases with decrease in liquid to binder ratio [2]. Curing temperature and method of curing influences the compressive strength of the specimen [3]. No mix design code is available, so it is needed to review on the results which had come out upto till date work done [3]. Super plasticizer retards the early setting property and improved the workability of flyash- GGBS based GPC's [4]. Strength of GPC improves with the addition of SP. However, SP dosage higher than 0.5% of total binder content lead to significant reduction in strength of the mixes. Low (8 M) and high (14 M) concentration of alkali solution result in similar pattern of strength in GPC mixes [4]. Slag as a part of flyash binder is effective to accelerate setting time of GPC in ambient condition [5]. Compressive strength of ambient cured concrete increases as the age of concrete increases [5].

The present study aims to develop GPC cured under ambient temperature by using sodium hydroxide and sodium silicate as alkaline activators. Flyash and GGBS are used as binder material. Coal bottom ashes (BAs) is replaced as filler material. Compressive strength of fly ash-slag based geopolymer concrete was determined after 7 days and 28 days of curing with an alkaline liquid to binder ratios of 0.6. First objective is to optimize the concentration of NaOH and then bottomash used as replacement at interval of 0, 25, 50, 75 and 100%. Then the study is further extended to 40 and 60% of replacement. The experimental program was aimed to study the effect on mechanical properties like compressive strength, flexural strength and split tensile strength.

Table 1 Characteristics of flyash

Components	Results
Ferric oxide	0.39%
Aluminium oxide	21.29%
Silicon dioxide	63.8%
Calcium oxide	0.44%
Magnesium oxide	0.41%
Loss of ignition	< 1%
Particle size	22.2 μm

Table 2 Characteristics of GGBS

Characteristics	Test results
$CaO + MgO + SiO_2$	76.03
Magnesia content	7.73
Chloride content	0.009
Sulphite content	0.38
Fineness (m/kg)	390
Specific gravity	2.85
Particle size (cumulative %)	97.10 μm

2 Preparation of GPC Cubes

2.1 Materials

2.1.1 Flyash

For geopolymer concrete siliceous pulverized low calcium fly ash is obtained from Thrippunithara, Ernakulam, India, having a specific gravity of 2.3 (Table 1).

2.1.2 Ground Granulated Blast Furnace Slag (GGBS)

GGBS of specific gravity 2.85 obtained from the Asstra Chemicals, Chennai, India; were used as the source material (Table 2).

2.1.3 Bottomash and Aggregates

Bottom ash is obtained from Essar and Co, Bangalore of specific gravity 2.34 and water absorption 2.4%. Coarse aggregate used were locally available crushed angular granite metal of 12 mm size having the specific gravity of 2.88 and for fine aggregate

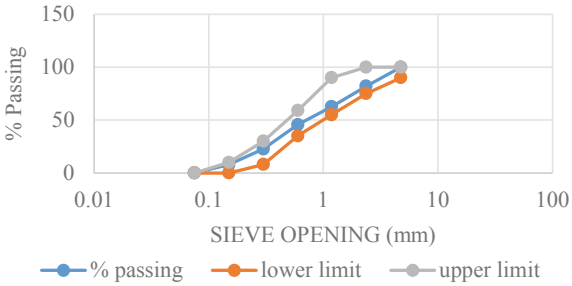

Fig. 1 Particle size distribution of bottomash

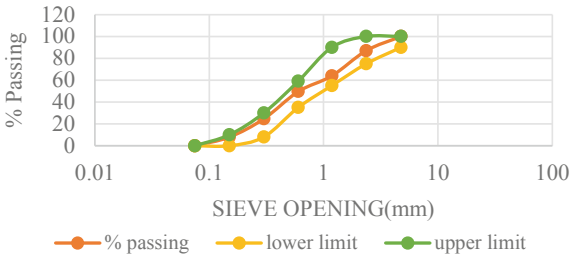

Fig. 2 Particle size distribution of Msand

Table 3 Characteristics of bottomash and aggregates

Property	Bottomash	Fine aggregate	Coarse aggregate
Specific gravity	2.34	2.747	2.88
Water absorption (%)	2.4	1.4	0.3
Fineness modulus	2.6%	2.83	

manufactured sand which is also locally available having the specific gravity of 2.75 were used. Aggregates falls into zone II as per IS383: 1970 (Figs. 1 and 2; Table 3).

2.1.4 Alkaline Activators

97% purity sodium hydroxide (NaOH) pellets and sodium silicate (Na_2SiO_3) with 28.13% Na_2O, 28.13% SiO_2, and 40.74% H_2O were used. For the NaOH solution, NaOH pellets were mixed with distilled water and stirred until all the pellets were completely dissolved. The solution was then left for a minimum of 10 h before use.

2.2 Mix Design

Once the dry mix of aggregates and the binder materials is prepared, alkaline activator is poured to it and thoroughly mixed to ensure complete reaction. Alkaline activator was prepared one day prior to the casting of the specimen. The mixture was placed in the mould 150 mm cube and vibrated for two minutes for proper compaction. The specimens along with mould were covered with polythene sheet to avoid moisture evaporation during ambient temperature.

Curing was done at room temperature. Experiments were done by varying parameter NaOH concentration 8 M, 10 M, 12 M, 14 M and 16 M and studying the effect of replacement of bottomash as fine aggregate. Sodium silicate to sodium hydroxide ratio fixed as 2.5. Alkaline to binder ratio is fixed as 0.6. Flyash and GGBS are taken in the ratio 50:50. Assume that normal density aggregates in SSD condition are to be used and the unit weight of concrete is 2400 kg/m^3.

Take the mass of combined aggregates as 77% of the mass of concrete.

For all mixes the mix ratio obtained is 1:1.875:3.482.

Thus; Coarrse Aggregate = 1201.2 kg/m^3
Fine aggregate = 646.8 kg/m^3
Mass of Alkaline liquid = 207 kg/m^3
Alkaline liquid to Binder ratio = 0.6
Mass of Binder material = 345 kg/m^3
Ratio of sodium silicate solution to sodium hydroxide solution = 2.5.

2.3 Casting of Cubes

The conventional method used in the making of normal concrete is adopted to prepare geo-polymer concrete. First, the fly ash, GGBS, coarse aggregate and fine aggregate mixed in dry condition for 3–4 min and then the alkaline solution which is a combination of sodium hydroxide solution and sodium silicate solution added to the dry mix. The mixing is done about 6–8 min for proper bonding of all the materials. After the mixing, the cubes are casted by giving proper compaction.

The sizes of the cubes used are of size 150 mm × 150 mm × 150 mm. Compressive strength of fly ash based geopolymer concrete was determined after 7 days and 28 days of curing under ambient temperature with an alkaline liquid to binder ratios of 0.6. The experiment was conducted to investigate the strength properties of geopolymer concrete. Bottomash used as replacement at interval of 0, 25, 50, 75, 100%. Then the study was further extended to 40 and 60% of replacement. The experimental program was aimed to study the effect of bottomash content on mechanical properties like compressive strength (Fig. 3).

Fig. 3 Casting of cubes

3 Experimental Study

3.1 Compressive Strength

Initially the concentration of NaOH is varied from 8 to 16 M and compressive strength is tested for 7th and 28th day to optimise the NaOH concentration. The compressive strength of geopolymer mixes at 7th and 28th day is shown in Table 4 (Fig. 4).

Compressive strength increases with the increase in concentration of NaOH in alkaline activator. Alkaline activator with high molarity (8–14 M) increases the formation of alumino silicates and geo-polymeric gel, thereby increasing the strength However, the higher alkaline content (16 M) in the geopolymers promoted greater

Table 4 Compressive strength for varying NaOH concentration

NaOH concentration (M)	7th day compressive strength (MPa)	28th day compressive strength (MPa)
8	21.33	24.08
10	22.8	25.44
12	25.96	29.27
14	28.24	33.36
16	24.32	26.62

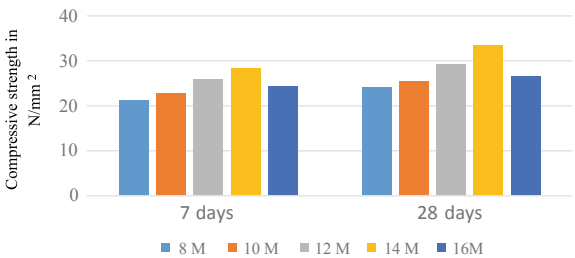

Fig. 4 Compressive strength of 7 and 28 days

Table 5 Compressive strength for varying percentage of bottomash replacement

% of Bottomash replacement	7th day compressive strength (MPa)	28th day compressive strength (MPa)
25	23.11	25.39
40	24.03	26.77
50	27.05	29.94
60	30.46	34.53
75	24.20	26.58
100	21.39	22.96

solid dissolution but excess hydroxide ion concentration caused aluminosilicate gel precipitation in the early stages, hindering further geopolymerization and decreasing strength. Thus NaOH concentration for further study is taken as 14 M.

After the optimisation of NaOH concentration, the replacement of fine aggregate using Bottom ash is carried out. Viz., 25, 50, 75, 100% and then 40 and 60% is also done to assure the exact range of value in which the strength tis the maximum. The compressive strength of those GPC mixes are as in Table 5 (Fig. 5).

It is found that 60% of replacement results in higher compressive strength. Slight increase in the strength is due to the pozzolanic reaction of bottomash. Water absorption for bottomash is slightly more than that of fine aggregate MSand thus strength decreases with the increase in percentage of bottomash.

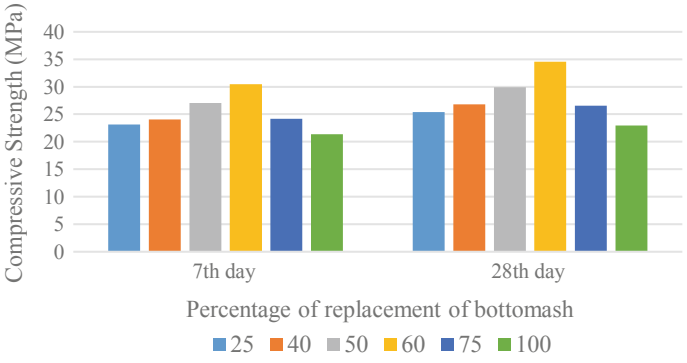

Fig. 5 Graphical representation of compressive strength for varying bottom ash replacement

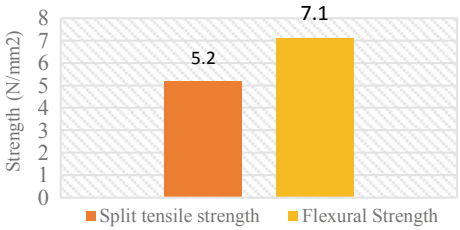

Figure 6 Graphical representation of split tensile strength and flexural strength

3.2 Split Tensile Strength

Splitting tensile strength test was conducted on cylindrical specimens of 150 mm diameter and 300 mm height at 28 days in accordance with IS specifications and procedures.

3.3 Flexural Strength

Flexural tests were conducted on beam of size 100 × 100 × 500 mm subjected to two point loading at 28 days in accordance with IS specifications and procedures.

For geopolymer concrete specimens with 14 M NaOH concentration and 60% replacement of fine aggregate by bottomash has following results (Fig. 6).

4 Conclusion

Compressive strength increases with the increase in concentration of NaOH in alkaline activator. Alkaline activator with high molarity (8–14 M) increases the formation of alumino silicates and geo-polymeric gel, thereby increasing the strength However, the higher alkaline content (16 M) in the geopolymers promoted greater solid dissolution but excess hydroxide ion concentration caused aluminosilicate gel precipitation in the early stages, hindering further geopolymerization and decreasing strength [6]. Thus NaOH concentration for further study is taken as 14 M. Compressive strength increases with the bottomash replacement as fine aggregate upto 60% afterwards it decreases. It is found that 60% of replacement results in higher compressive strength. Slight increase in the strength is due to the pozzolanic reaction of bottomash. Water absorption for bottomash is slightly more than that of fine aggregate MSand thus strength decreases with the increase in percentage of bottomash [7]. Even though the strength development is less for bottom ash concrete, it can be equated to lower grade of normal concrete and making utilization of waste material justifies the concrete mix-development. Bottom ash used as fine aggregates replacement enables the large utilization of waste product.

References

1. Pavithra P, Srinivasa Reddy M et al (2016) Effect of the Na2SiO3/NaOH ratio and NaOH molarity on the synthesis of flyash- based geopolymer mortar. Geo Chicago, ASCE
2. Xie T, Ozbakkaloglu T (2015) Behavior of low calcium fly and bottom ash-based geopolymer concrete cured at ambient temperature. Ceram Int J 41:5945–5958
3. Dibyendu Adak and Saroj Mandal, "Strength and Durability Performance of Flyash Based Process modified Geopolymer concrete", Journal of Materials in Civil Engineering, Vol.31, Issue 9- September 2019, ASCE
4. Manjunath GS, Radhakrishna, Giridhar C, Jadhav M (2011) Compressive strength deelopment in ambient cured geopolymer mortar. Int J Earth Sci Eng 04(06) ISSN 0974-5904
5. Tran Viet Hung; Dao Van Dong; Nguyen Ngoc Long and Ta Duy Hien. "Study on the Mechnaical Properties of the Flyash Geopolymer Concrete", International Journal of Civil Engineering and Technology, Vol. 8, Issue 3, March 2017, IAEME
6. Topark-Ngarm P, Chindaprasirt P, Sata V (2015) Setting time, strength, and bond of high-calcium flyash geopolymer concrete. J Mater Civ Eng ASCE 27(7)
7. Chotetanorm C, Chindaprasirt P, Sata V, Rukzon S, Sathonsaowaphak A (2013) High-calcium bottom ash geopolymer: sorptivity, pore size, and resistance to sodium sulfate attack. J Mater Civ Eng ASCE 25(1)

Effect of Waste Carpet Fibres and Palm Oil Fuel Ash on Self Compacting Concrete

Minnu P. Alias and Tellma John

Abstract Self-compacting concrete (SCC) is a flowing concrete that does not require vibration and should not be vibrated. Palm oil fuel ash (POFA) is a by-product obtained during the burning of waste materials such as palm kernel shell, palm oil fiber, and palm oil husk. It can be utilized to partially replace cement in a concrete mix considering its good pozzolanic properties and high performance in the development of strength of concrete. This work highlights the scope of finding the properties of M40 equivalent (considering structural applications) fly ash based self compacting fiber reinforced concrete in cooperating waste carpet polypropylene fibers and palm oil fuel ash. Cement is replaced with palm oil Fuel Ash at 10, 20, and 30% by weight of cement and optimum percentage of palm oil fuel Ash is found. In the self compacting Concrete mix having optimum percentage of palm oil fuel Ash, Polypropylene carpet fiber fractions at 0.25, 0.5, 0.75, 1% by volume of concrete are incorporated and the optimum percentage of addition of waste carpet fibers is found by testing the mechanical properties. The fresh and hardened properties of the M40 equivalent fly ash based self compacting fiber reinforced mix with optimum palm oil fuel ash and optimum waste carpet fibers were compared and evaluated.

Keywords Self-compacting concrete · Palm oil fuel ash · Waste carpet fibers

1 Introduction

Self-compacting concrete (SCC) is characterized by its ability to consolidate under its own weight without any means of compaction or vibration. SCC has the ability to spread smoothly in congested reinforced elements due to its flowability and use of small size aggregates. Sustainability considerations in concrete industry have led to the development of new green concrete by utilization of waste fibrous materials. The advantages of recycling include reducing environment pollution, reducing land filling and disposal of wastes and preserving natural resources. Introducing fibers into the

M. P. Alias (✉) · T. John
Toc H Institute of Science and Technology, Ernakulam, India
e-mail: minnualias@gmail.com

© Springer Nature Switzerland AG 2021

K. Dasgupta et al. (eds.), *Proceedings of SECON 2020*,
Lecture Notes in Civil Engineering 97,
https://doi.org/10.1007/978-3-030-55115-5_26

concrete matrix can improve its properties, and enable the utilization of high strength concrete, while maintaining a ductile behaviour. Self-compaction encourages the application of macro-fiber reinforcement in concrete, mitigating concerns regarding reduced workability [1].

The experimental program is intended to investigate the strength of fly ash based self-compacting concrete by replacement of cement with palm oil fuel ash at 10, 20, 30, and 40% by weight of cement and addition of Organic waste carpet fibers at 0.25, 0.5, 0.75 and 1% by weight of concrete. The experimental program is aimed to study the workability and strength parameters. The slump flow test, T50 test and J ring test were conducted for all mixes to know the fresh property of self-compacting concrete. Compressive strength, Flexural strength and Split tensile strength test was conducted at 7 and 28 days and the values are compared with the values of fly ash based self-compacting concrete.

1.1 Objectives

The main objectives of this investigation are

- To establish Fly Ash based Self Compacting concrete Equivalent to M40 grade.
- To evaluate the optimum percentage of palm oil Fuel Ash by partial replacement of cement in the ratios of 10, 20, 30 and 40% by weight of the cement in the mix with optimum percentage of fly ash based on strength parameters.
- To evaluate the optimum percentage of waste carpet fibers partially replaced (0.25, 0.5, 0.75 and 1%) by volume of concrete with optimum percentage of Palm Oil Fuel Ash based on strength parameters.
- To analyse the durability properties of Fly Ash based SCC with optimum percentage of Palm Oil Fuel Ash and Waste Carpet Fibers.
- To analyse and compare the results obtained with Fly Ash based Self-Compacting Concrete.

2 Materials and Properties

The properties of various materials used in this investigation and their physical properties are given in Table 1 [2].

3 Mix Design

There is no standard method for SCC mix design and many academic institutions, admixture, ready-mixed, pre cast and contracting companies have developed their own mix proportioning methods. Several methods exist for the mix design of SCC.

Table 1 Material properties

Materials	Properties	Test results	Reference code
Cement	Fineness	5%	IS 4031-1988 Part-IV (Reaffirmed 2009)
	Consistency	32%	IS 4031-1988 Part-XI (Reaffirmed 2009)
	Initial setting time	45 min	IS 4031-1988 Part-V (Reaffirmed 2009)
	Specific gravity	3.15	IS 4031-1988 Part-IV (Reaffirmed 2009)
Fine aggregate	Specific gravity	2.68	IS 2386-1963 Part-III (Reaffirmed 2016)
Coarse aggregate	Specific gravity	2.72	IS 2386-1963 Part-III (Reaffirmed 2016)
Palm oil fuel ash	Specific gravity	2.23	
Fly ash	Specific gravity	2.3	
Waste carpet fibers	Density	964 kg/m^3	
	Aspect ratio	44	

Table 2 Mix design of specimen with varying percentage of fly ash

Notation	Cement (kg/m^3)	Fly ash (kg/m^3)	Fine aggregate (kg/m^3)	Coarse aggregate (kg/m^3)	SP (l/m^3)	Water (l/m^3)
F28	425	165	848	765	3.54	200
F30 (CM)	413	177	848	765	3.54	200
F32	401	189	848	765	3.54	200

The mix designs were carried out for concrete grade 40 MPa based on European Federation for Specialist Construction Chemicals and Concrete Systems [3] guidelines and the details of the mix design [4] are given in Table 2.

4 Results and Discussions

4.1 Fresh Properties

The main characteristics of Self-Compacting Concrete are the properties in the fresh state. To determine the fresh properties of SCC, various tests were performed like slump flow, T50 slump flow test time and J-ring test. All the equipment for various tests confirms to dimension as given by EFNARC. In this study three properties are used to evaluate the fresh properties of Self - Compacting Concrete, shown in Table 3. F28, F30 & F32 represents the SCC containing fly at 28%, 30% and 32% respectively. F30POA10, F30POA20 & F30POA30, F30POA40 represents the SCC containing Palm Oil Fuel Ash at 10%, 20%, 30% and 40% respectively [5]. F30POA20CP.25, F30POA20CP.5, F30POA20CP.75, F30POA20CP1 represents the SCC containing

Table 3 Workability results

Mixes	Slump flow (mm)	T50 slump flow (sec)	J–Ring (mm)	Passability (mm)
F30(CM)	681	3.3	672	9
F30POA10	678	3.5	668	10
F30POA20	700	3.4	680	20
F30POA30	690	4	670	20
F30POA40	670	4.6	640	30
F30POA20CP.25	660	3.3	657	3
F30POA20CP.5	640	4.5	634	6
F30POA20CP.75	628	5.2	519	9
F30POA20CP1	619	7.3	604	15

Carpet waste fibers at 0.25%, 0.5%, 0.75% & 1% respectively [5]. Fresh property tests results satisfies the requirements of EFNARC guidelines.

The slump flow test were conducted for finding the filling ability. The Spread diameter decreases as the percentage content of Carpet Fiber increases. For self-compacting concrete with Fibers, slump flow diameter values varies between 600 and 750 mm [1].

T50 slump flow test were conducted for finding the viscosity or flowability of the self-compacting concrete mixes. From Table 3, it can be see that by increasing the Carpet fiber content the flowing ability gets reduced.

J-ring test was conducted for finding the passing ability of SCC mixes [6]. Passing ability gets decreased as the Carpet fiber volume increases The results of shows that fiber volume fractions at 0.25% gives maximum workability [7].

4.2 Hardened Properties

The compressive strength of self-compacting concrete cubes made with varying percentage of Fly Ash is tested after 7 and 28 days and the results are shown in Table 4 and Fig. 1. After 28 days of curing the SCC with 30% fly ash gives the maximum compressive strength. The compressive strength of self-compacting concrete cubes made with optimum percentage of fly ash and varying percentage of Palm Oil Fuel Ash is tested after 7 and 28 days. After 28 days of curing the SCC with 20% palm oil fuel ash gives the maximum compressive strength due to the pozzolanic activity of POFA [8]. The compressive strength of self-compacting concrete cubes with optimum percentage of fly ash, palm oil fuel ash and varying percentage of waste carpet fibers are tested after 7 and 28 days. After 28 days of curing the maximum compressive strength is 51.7 N/mm^2, for 0.25% replacement of Carpet fibers. At higher percentages of carpet fibers compressive strength was decreased compared to

Table 4 Compression test results

Notation	Compressive strength (N/mm^2)	
	7 days	28 days
F30 (CM)	37.35	50.23
F30POA10	35.9	50.48
F30POA20	36.3	51.73
F30POA30	30.7	49.34
F30POA40	30	47.96
F30POA20CP.25	38.217	51.7
F30POA20CP.5	35.91	51.3
F30POA20CP.75	34.65	49.35
F30POA20CP1	34.1	48.2

Fig. 1 Testing of compressive strength

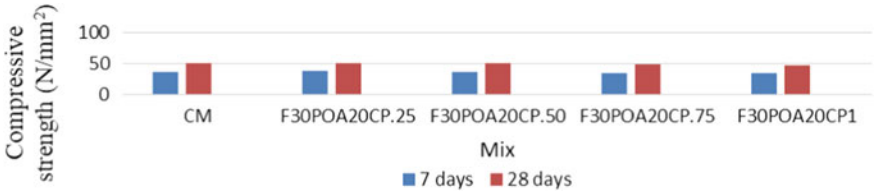

Fig. 2 Variation of compressive strength with optimum percentage of fly ash, palm oil fuel ash and varying percentage of carpet fibers

Table 5 Split tensile strength results

Notation	Split tensile strength (N/mm^2)	
	7 days	28 days
CM	2.98	4.01
F30POA10	3.11	4.03
F30POA20	3.12	4.13
F30POA30	2.86	3.84
F30POA40	2.77	3.72
F30POA20CP0.25	3.03	4.32
F30POA20CP0.50	3.1	4.42
F30POA20CP0.75	3.15	4.45
F30POA20CP1	3.04	4.34

control mix, due to its high absorbance characteristic of carpet fibers which reduced the amount of water in SCC mixture (Fig. 2; Tables 5 and 6).

Split tensile strength test was conducted in digital compression test in machine. The effects of Palm Oil Fuel Ash in fly ash based self-compacting concrete on the tensile strength are studied. The tensile strength value of SCC increases with increase

Table 6 Flexural strength test results

Notation	28 days
CM	5.5
F30POA10	5.32
F30POA20	5.4
F30POA30	5.26
F30POA40	5.1
F30POA20CP0.25	5.31
F30POA20CP0.50	5.51
F30POA20CP0.75	5.78
F30POA20CP1	5.68

in percentage of cement replacement with palm oil fuel Ash upto 20%. The tensile strength increases to a maximum of 4.13 N/mm^2 for 20% palm oil fuel ash content. The effects of Carpet fibers in fly ash based self-compacting concrete with optimum percentage of palm oil fuel ash on the tensile strength are studied. An increase in tensile strength by 4% was observed when Carpet fiber content was 0.75% for curing period of 28 days. The tensile strength increases to a maximum of 4.45 N/mm^2 for 0.75% carpet fiber reinforced self compacting concrete mix (Figs. 3 and 4).

Fig. 3 Testing of split tensile strength

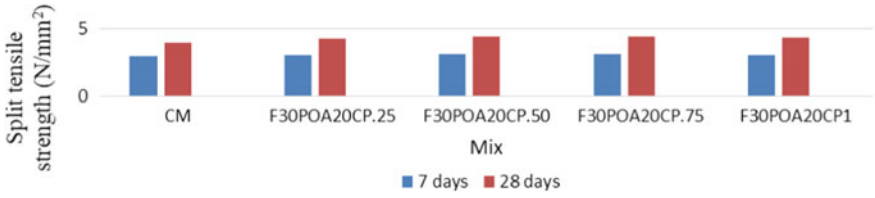

Fig. 4 Split tensile strength of fly ash based self–compacting concrete with optimum percentage of Palm Oil Fuel Ash and varying percentage of carpet fibres

Flexural strength test was conducted as per IS 516:1959 (Reaffirmed 2018) in Universal testing machine. Flexural strength test was conducted after 7 and 28 days of curing. The effects of Palm Oil Fuel Ash in fly ash based self–compacting concrete on the flexural strength are studied. The maximum flexural strength is 4.13 N/mm^2 for 20% replacement of Palm Oil Fuel Ash. The effects of Waste Carpet fibers in fly ash based self-compacting concrete with optimum percentage of palm oil fuel ash on the flexural strength are studied. The maximum flexural strength is 4.45 N/mm^2 for 0.75% replacement of waste carpet fibers (Figs. 5 and 6).

Fig. 5 Testing of flexural strength

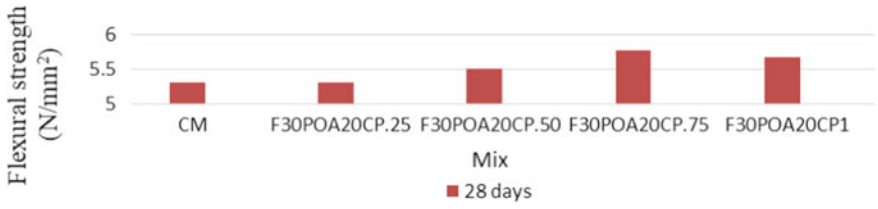

Fig. 6 Flexural strength of fly ash based self-compacting concrete with optimum percentage of palm oil fuel ash and varying percentage of carpet waste fibers

5 Conclusions

- Fresh properties of SCC are tested and it satisfies the requirements of EFNARC guidelines.
- The maximum compressive strength of fly ash based SCC with 20% POFA mix is 51.73 N/mm^2, split tensile strength is 4.13 N/mm^2 and the flexural strength is 5.4 N/mm^2, which are greater than the control mix. The optimum amount of palm oil fuel ash was obtained as 20% in terms of compressive strength, split tensile strength and flexural strength.
- The Addition of Waste Carpet Fibers into the concrete mix containg optimum percentage of fly ash and palm oil fuel ash increased the compressive strength upto an optimum of 0.25%. Polypropylene Carpet fibers did not influence the compressive strength of SCC.
- Presence of Carpet fibers at varying percentage volume, increased the tensile strength by 4% and flexural strength by 10%.
- The use of Palm Oil fuel ash as a replacement for fine aggregate is environmentally helpful and it helps in reducing the construction cost. So Palm Oil Fuel Ash is an alternative material for replacing Cement for manufacturing of concrete.
- So it can be concluded that, the fly ash based self-compacting concrete with 20% replacement of palm oil fuel ash and 0.25% replacement of waste carpet fibers shows better strength and workability than the control mix.

References

1. Abdullahi O, Douba A, Farrag S, Yehia S (2016) Mechanical and durability evaluation of fiber-reinforced self-compacting concrete. J Constr and Build Mater 121:120–133
2. IS 2386:1963 Methods of tests for aggregate of concrete. Bureau of Indian Standards, New Delhi
3. EFNARC (2002) Specification and guidelines for self-compacting concrete. www.efnarce.org
4. IS 10262:2009 Indian standard concrete mix proportioning- guidelines (First revision). Bureau of Indian Standards, New Delhi
5. Awal ASMA, Mohammad Hosseini H (2016) Green concrete production incorporating waste carpet fiber and palm oil fuel ash. J Clean Product 137:157–166
6. ASTM C1621 C1621M:2017 standard method for passing ability of self consolidating concrete by jring
7. Ghanbarpour S, Hosseinpour I, Mazaheripour H, Mirmoradi HS (2011) The effect of polypropylene fibers on the properties of fresh and hardened lightweight self-compacting concrete. J Constr Build Mater 25:351–358
8. Alnahhal FM, Alsubari B, Ibrahim Z, Jumaat ZM, Shafigh P (2018) Properties of eco-friendly self-compacting concrete containing modified treated palm oil fuel ash. J Constr Build Mater 158:742–754
9. Johari MAM, Tayeh AB, Yusuf MO, Zeyad AM (2017) Pozzolanic reactivity of ultrafine palm oil fuel ash waste on strength and durability performances of high strength concrete. J Clean Product 144:511–522
10. Kumar TS, Sahan AH, Skariah B (2017) Sustainable concrete containing palm oil fuel ash as a supplementary cementitious material—a review. Renew Sustain Energy Rev 80:550–561

Elemental Approach to Design a Worker Profile as a Selection Tool in Last Planner System©

C. Mrinal Raja, Vinay Mathews, and Grace Mary Abraham

Abstract Pull planning is an approach where the schedule is worked in reverse order. In pull planning, the final decisions are taken by the Project Manager. This decision making involves a chain of correspondence from Construction Manager to Project Engineer to Site Engineer and finally to the Foreman. Transfer of workers from one site to another is also one among the decisions that are taken by a Project Manager. To select a worker, a manager shall desire certain attributes depending on the requirement for the transfer. However, the cascading chain of correspondence results in a biased decision. Thus, selection of a suitable worker to transfer is an issue. In this paper, a set of construction labour selection attributes are identified based on expert interviews. The attributes identified are Skill, Regular attendance, Responsibility, Health, Safety at work, Discipline, Technical Soundness, Daily wage rate, Language and Previous accident history. These identified attributes are then quantitatively analysed using questionnaire survey and literature reviews. They are then given weightage based on the study. Selection attributes can be collectively called a Worker Profile. This worker profile can be introduced to reduce the gap between the Manager and a foreman. However, the benefits of this worker profile in the pull planning process need to be evaluated in real-life cases.

Keywords Pull planning · Selection attribute · Worker profile · Worker assessment

1 Introduction

In the Last Planner System (LPS), projects are considered as production systems. Thus for productivity, LPS ensures that for an activity to occur, all the prerequisites are available. To manage, this production system has two controls: Production Unit

C. M. Raja (✉)
Department of Civil Engineering, M.Tech SECM, Amal Jyothi College of Engineering, Kerala, India
e-mail: mrinalrajac@ce.ajce.in

V. Mathews · G. M. Abraham
Amal Jyothi College of Engineering, Kerala, India

© Springer Nature Switzerland AG 2021

K. Dasgupta et al. (eds.), *Proceedings of SECON 2020*,
Lecture Notes in Civil Engineering 97,
https://doi.org/10.1007/978-3-030-55115-5_27

control and Workflow control [1]. In LPS, the Planning engineer thinks and plans as the last planner and finds the requirements at the stage of execution. During the planning process, seven workflows occur such as people, information, equipment, materials, prior work, safe external conditions and safe space. Recent trends show that contracting companies have started implementing lean techniques for work execution. Of several lean techniques, Last Planner System (LPS) developed by Ballard has gained more desirability due to its collaborative pull planning approach and Percent Plan Complete metrics those allow to measure the deviations. Not only in LPS but also other planning systems, to properly allocate and select a worker there is no proper worker selection tool in this stage of planning. The supervisor has to decide based on past experiences.

2 Literature Review

Labour productivity is a concept spread over all industries. With regard to Construction labour productivity (CLP), the information about the performance of people is scarce in the construction industry.

- Many companies do not have a formal process for tracking and collecting actual progress. The contractors prefer a method which requires less time, dedication and involvement [2].
- The data available are not collected in a uniform manner. Also increase in cost due to collecting data in paper-based systems [3].
- The level of skills of hired craftsmen being supplied needs to be taken into consideration, which affects project's cost performance [4].
- Commercial availability of any stochastic system which can estimate activity productivity [5].

Thus a stochastic system, which can bring in reliable data is needed for the industry. Such a system that will instil less human effort, cost and time-saving features in real-time. Designing a procedure adoptable by the contracting company is the demand of the industry.

3 Objective

This is not a concept that replaces labour productivity but is a systematic methodology to enhance data collection, analysis and manifest. Thus a worker profile has its prospects into the industry where productivity is often estimated based on the requirement or unprincipled techniques. Although this sounds to be like a catchy commercial phrase, it never explains better than this, "Therefore the right people at the right jobs at the right time get the work done efficiently".

The concept put forth in this paper shall be specific to the construction industry. The industry requires a procedure or methodologies that will consume less cost and time which can provide easy, reliable data. This paper is idealising a reputation or worker profile incorporating desirable attributes which will reflect the efficiency and competence of the particular worker at hand.

4 Methodology

The research problem is to develop a tool that shall be reliable, universal, trackable, cost-effective and less time-consuming. This research suggests a worker profile (WP) that will resolve the research problem. So, to design a WP, it should have elements that will help create the characteristics of a worker. These attributes which will help establish a reputation of that worker are to be defined. The attributes are adopted from factors that affect CLP because the improvement in these factors shall improve CLP. Questionnaire surveys and expert interviews were used to find the relevance of CLP and the desirable attributes of a worker. The survey specifications design has undergone five general stages in the development and completion of a survey as documented by Blair et al. [6]. The survey was conducted on an online survey platform, surveymonkey.com. The platform was selected since the survey could be sent via social networks (such as WhatsApp, Telegram, E-mail, etc.). Once attributes are identified, they are weighed on a survey consensus. Based on the weights, the attributes are aligned in the profile. To make the evaluation measurable and controllable, control parameters are defined with the help of literature. Few controls are assisted with further sub-controls. Every control and sub-control shall be measured on a scale from 0 to 5. This results as the Worker Profile, where all the attributes are given scores.

To assess a worker, the Worker Profile sheet was used realtime and was also the same time-period was recorded using a mobile camera (iPhone 7+) and tripod. Using the recorded video, the worker was again assessed by different evaluators, later on during improvements in the WP.

4.1 Factors Affecting Construction Labour Productivity (CLP)

Extensive study has already been conducted by Rojas and Aramvareekul [7]. A critical review conducted by Yi and Chan [8] gives deeper insights into the factors affecting and challenges at different levels of work front (industry, project and task). A more specific study on the factors affecting masonry CLP in the Indian construction industry has been done by Karthik [9]. All these factors affect labour and eventually affects the CLP. Increasing productivity is a collective effort thus the variables

(factors) when optimised helps improve productivity. A universal concern [3] to incorporate those factors at the site and help create reliable data can be tracked and collected [4] as required. For WP, the basic attributes are shaped by the factors affecting CLP. WP tries to understand the implications of all the factor towards a worker perspective. Thus desirable attributes were identified from these factors. Thus a system which is stochastic [5], which can bring in reliable data is needed for the industry. Such a system that will instil less human effort, cost and time saving [4] features in real-time. Designing a procedure adoptable by the contracting company is the current demand of the industry.

To understand the awareness within construction professionals, a questionnaire survey was conducted. This survey marks the relevance of a CLP and the insights from the survey portrays that CLP is a necessity which is to be collected regularly. CLP is profoundly known from work (68%) than academics (28%), thus CLP estimation is implemented at the site. 49% uses own/personalised methods which proves that there is no universal method used to estimate CLP in our construction industry. 70% of participants have reported back that the method is either complicated or difficult to perform and agrees to CLP has to be used to evaluate a worker.

4.2 Desirable Attributes of a Worker

In a computer game, there exists a gamer/avatar profile, contentious data is exhibited. Such data can be used to compare between like-trades or like-skilled tradesmen. The profile idealization was required since worker allocation/reallocation happens every now and then. In order to result in a worker profile, desirable attributes were to be found. With the help of factors that affect CLP, attributes were identified which nominally resonate to the construction sites. They were Skill, Regular attendance, Health, Safety at work, Responsibility, Discipline, Technical soundness, Daily wage rate, Language and Previous accident (Table 1).

To find the Relative Importance Index (RII), an online survey among construction industry professionals, such as engineers, managers, timekeepers, safety officers, consultants, helped in moulding a few numbers of qualities. The most weighted quality was Skill and the least was previous accident history. With these characteristics, the worker profile shall be idealised from the RII in Table 2. This survey received a 47% response rate.

4.3 Metaphysical Trade Classification

Based on abstract reasoning, activities have been divided into trades that label workers as mason, helper, steel fitter, carpenter, welder, electrician, etc. therefore for each trade, a worker profile integration has to be done to effectively monitor the performance of a worker at the site. The WP provides data in similarity with a curriculum

Table 1 Factors affecting masonry labour productivity in building construction in India Karthik [4]

Categories	Description of factors
Work Force	Lack of skill and experience of workers, Lack of empowerment, high workforce absenteeism/turnover, physical performance and fatigue, low labour morale/commitment, poor relation among workers, low amount of pay, little or no financial rewards, lack of labour recognition program, payment delay
Management team	Bad leadership skill, poor relation between workers and superintendent, lack of labour surveillance, lack of periodic meeting with labour, poor or no supervision method, incompetent supervisors, incomplete/revise drawings, inspection delay, variations/change orders during execution, method of construction
Working condition	Working 7 days per week, frequency of working overtime, poor work planning, unrealistic scheduling, labour interface and congestion, design complexity, accidents, unsafe working conditions, inadequate safety plan, working at heights
Material and equipment	Material shortages, unsuitable material locations, equipment and tool shortages, poor condition of tools and equipment
Unforeseen and unfamiliar factors	Rework, use of information and communication technologies, weather conditions, stringent inspection

Table 2 Qualities of a worker—results from online questionnaire survey (source Online survey)

	Attribute	RII
1	Responsibility	0.944
2	Regular attendance	0.944
3	Skill	0.933
4	Health	0.922
5	Safety at work	0.900
6	Discipline	0.889
7	Technical soundness	0.844
8	Daily wage rate	0.767
9	Language	0.767
10	Previous Accident	0.633

vitae, or most similarly like a gamer profile. Change in trade or promotion in designation is possible with the help of WP. From site observations, there are mason related works such as blockwork, plastering, tilework, concreting and repair works. As an inception stage, the blockwork mason is chosen and WP is designed accordingly. Henceforth, the worker mentioned will be a blockwork mason.

4.4 Identifying Activities

So what are the tasks and related activities that a mason does at the site? The need to identify activities is a necessity before proceeding to any more procedure of idealizing the worker profile. For more in-depth analysis requires Work sampling, which considers cycle time instead of accumulating the number of productive work carried out by the worker. An ergonomic nature is provided with the help of adopting features such as the task is divided into activities that represent each motion of the worker and the time is recorded to each activity [10]. Thus the total time taken by the worker to complete a work within a period is his/her productivity.

4.5 Categorizing Productive Works

In work sampling, activities are identified as (1) Productive work (2) Semi-productive work and (3) Non-productive work. Not only productive but also other two categories add up to the overall productivity. These semi and non-productive activities support productive activities to complete a task. WP adopt the productive classification of activity. The worker does activities such as Mixing mortar, Placing mortar, Lifting brick, Positioning brick, Levelling, Verticality, Pointing to complete a task by the end of the day.

4.6 Worker Profile for a Blockwork Mason

Microsoft Excel is simply selected as a platform for the profile because of its wide acceptance among analysts and timekeepers. Creation of a mobile application and enabling its cloud computing capabilities are the future scope of this research.

5 Controls

The desirable attributes have been identified in the previous chapter. The WP has been designed according to the weights received for the attributes from the survey. While in practice, it was found out that, the attributes were not evaluated to its true essence. Judging must be based on factors or criteria that bring in the final picture of that attribute. Henceforth, we call these criteria which help define the attribute as ‘Controls’.

5.1 Skill

Skill is an attribute that has more importance. This attribute relates more to the productivity of the worker. The state of the insights and techniques of Taylor's in modern management proves to be still valid. Hence on an ergonomic methodology of activity sampling, each activity in a task is recorded. The total time is taken for the worker to out the quantity of final. The mason performs those identified activities mentioned earlier. Each of these acts consumes time and all of them are repetitive acts and are not done as a continuous cycle of activities.

In the evaluation using a worker profile, the total time is recorded and the average time for each activity is calculated. This includes idle time as well. Thus the observer shall evaluate the quality control showcased by the mason on a scale of 5, along with the time taken to complete the recorded amount of work. For the study, 8 h were noted to be the daily hours of work in construction sites.

$$\text{CLP} = \text{Q}/\text{T}_\text{s}\text{m}^3/\text{manhours/day}$$

where,

Q is the Quantity of work done during the time of evaluation.
T_s is the total time taken for observation.

Depending upon the type of block/brick used the productivity of a mason varies from 0.33 to 0.72 m^3/manhours/day according to Delhi Analysis of Rates. A worker spends up to 8 manhours/day. Hence the CLP estimated in Skill, rates the worker between a score between 0 and 5. This evaluation must be done multiple times on various days in a week to get more reliable data.

5.2 Regular Attendance

Regular attendance is an attribute that is the second most valued attribute of a worker as identified from the survey. The reason why this is most desirable is that the less turnover of workers to site reduces the overall productivity of the project. Hence this attribute directly addresses one among many factors that affect CLP, Absenteeism. Absenteeism is classified into the workforce-related factors and has an RII of 0.79 among other factors affecting CLP of a mason. This data is to be fed by the timekeeping team of the construction site into the WP.

5.3 Responsibility

Responsibility is an attribute that defines a person of his/her leadership, motivation and work management skills. Leadership in construction can be classified into

Transformational, Transactional, Full Range and other four types of leadership styles. Accordingly, sub-controls are provided such that a characteristic description of these styles are measurable in real-life. Motivation has a direct impact on worker performance because of its effects or influences are managed by external factors. This evaluation has its basic understanding from the work of Siriwardana and Ruwanpura [11], whose conceptual model was the evaluation of a workgroup. In motivation, Vroom's expectancy theory is adopted. Based on which, the three variables, thus sub-controls are Expectancy, Instrumentality and Valence. Work management is the responsibility of the worker as well as management. This control can be evaluated using sub-controls such as site management, material management and work planning. These sub-controls shall be evaluated on a scale of 1–5.

5.4 Health

Health attribute considers controls such as Sick leave intensity, repetition of sickness and medical condition if any. Physical performance and fatigue are important when a worker is studied for CLP. So it is one among several factors that affect CLP. Although evaluation of one's physical strength without any interruption of the ongoing work is not possible. Thus a direct observational parameter is not collected for this attribute. The available data from timekeepers, safety and administration are used.

5.5 Safety at Work

Most of the studies, discuss on unsafe acts and unsafe behaviours. 98% of all accidents caused in construction-site are due to unsafe behaviours than unsafe acts whose contribution is 85% [12]. Behaviour is more evident than an attitude. Anyone can have a safe attitude towards work, but while practising them, workers tend to compromise due to simple distractions or unavailability of resources. Thus behaviour is far more effective than attitude. Incentives to nurture safe behaviour could be expensive or applicable to short periods of time. Hence, in WP, Health is controlled by two controls, one being Safe Behaviours and the other Safe Acts, all having equal weightage. These sub-controls rated on a scale of 0–5 shall impart a mentality of cooperation. The workers get a notice period or a track record of their unsafe acts and at the same time encouragement for the safe procedures.

5.6 Discipline

Fair but firm discipline attribute a good work environment. Discipline is often added to the responsibilities of a supervisor. It depends on the supervisor how disciplined

his/her team is. It is important to note that often workers are entrusted with the task and are updated by the end of the day. Enforcement of the supervisor increases the discipline but this can result in demotivation. Thus ample amount of appreciation must be given to workers also which maintain the discipline of a site. Punitive action will only instigate rebellion from the worker. Thus inclusion of Discipline in WP gives the labour a buffer period for the worker to improve himself in regard to his code of conduct and etiquettes within the workplace. Hence, the Discipline is controlled by Misbehaviour, Inappropriate dressing, Duty cuts, Disciplinary actions and Attitude. Attitude is again sub-classified into Work, Safety, Co-worker and Management. Each of the control and sub-control shall be rated upon a scale of 0–5.

5.7 Technical Soundness

Technical soundness is an attribute which is looked upon once the above attributes are well and profoundly good. A workers' technical soundness can be evaluated based on controls such as Experience, Training, Inspection assistance and Certification. In Karthik and Rao [9] study suggests that lack of skill and experience of a worker has the highest importance in CLP with an RII of 0.83. Experience of a masonry worker is categorised into 0 years (apprentice), 1 year (novice), 3 years or above (novice) and more than 5 years (journeymen). With years of experience, the mason finds balance with proficiency, productivity, and ergonomic safety. An apprentice works in safety to achieve proficiency and productivity but does not achieve the productivity and safety levels of journeymen [13]. The score shall be in between 1 and 5. Certification is another way how workers can qualitatively be assessed. In a construction site, a mason may be desired of having certifications related to specific equipment, IRATA, aerial lift training, cradle operator, crane rigger, etc.

Each certification shall provide scores for a worker in WP. Inspection assistance is the control that determines the performance of a worker while facing an inspection at the site. Inspections are very important in projects to confirm the authority of approval and coherence of work with the technical drawing.

5.8 Daily Wage Rate

In India, SOR is taken as the reference for materials and wages. In Delhi Analysis of Rates (DAR Vol. 1), the daily wage of a brick mason ranges between ₹481 and ₹500, for expected productivity of 0.44–0.47 m^3 of work. Figure 3 shows the various quantity of work done by a mason per day. Actual rates in site for a brick mason ranges between ₹800 and ₹1100 for a quantity of 1.5–2.0 m^3. For a worker to understand his stance amongst other workers, this can be evident from the wage he draws. This attribute in a WP helps in selecting a mason for a specific cost code in a project also (Figs. 1 and 2).

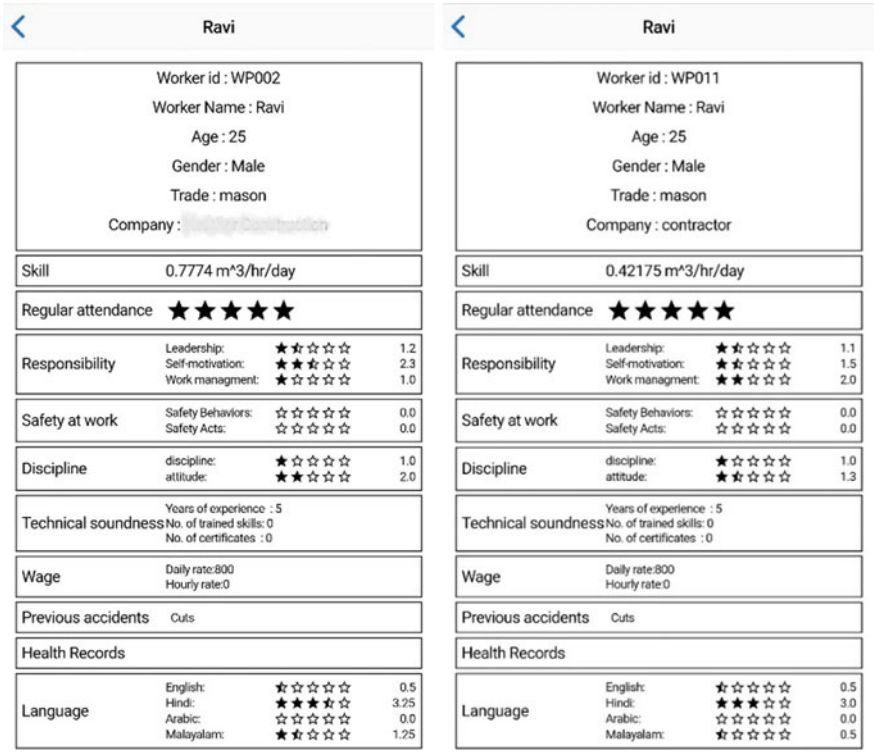

Fig. 1 Worker profile from "WorPro" of worker 1—evaluator 1 (left)—evaluator 2 (right)

5.9 Language

According to the International Migrant Stock 2019 report (released by the Population Division of the United Nations Department of Economic and Social Affairs), India is the top source of international migrants with 17.5 million international migrants, constituting 6.4% of world's total migrant population. Empirical support was found that foreign language skill positively and significantly associates with individual task performance. Knowing multiple languages helps the mason to communicate with people of various native origin and effective in his performance. Speaking the same language helps in building trust and to understand better.

Language attribute evaluates the capacity of the worker to Write, Read, Listen, and Speak. Although a worker primarily needs to listen (understand) and speak a language, which is important than other sub-controls, all are given equal importance. The ability of a worker to read and write, and let him get promoted or better incentives. The scoring pattern will be on a scale between 0 and 5.

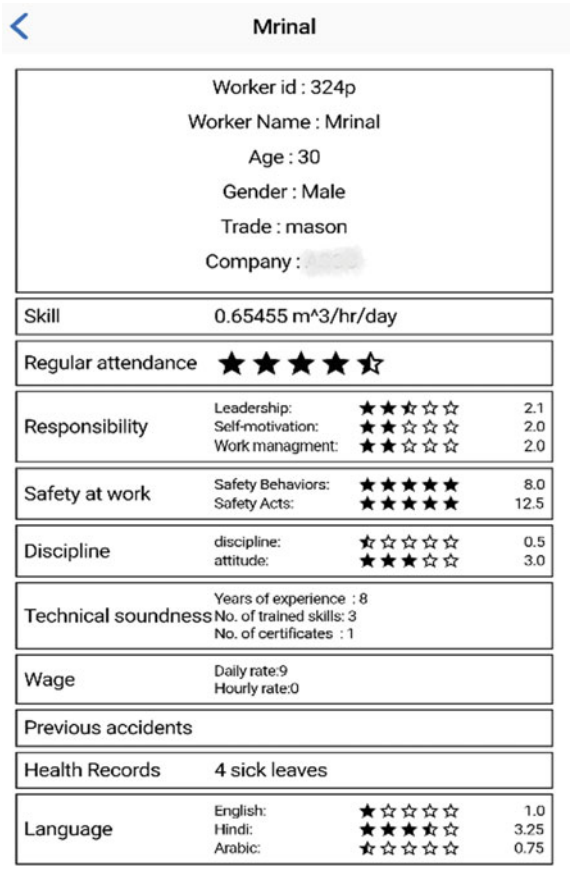

Fig. 2 Sample worker profile from "WorPro"

5.10 Previous Accident

Similar to Health, this attribute gathers information from the timekeeping, safety and administration departments. This attribute gains a position in WP since we know how an accident interrupts the workflow in a construction site. Workers with previous accident history must be noted and supervised. The risk of occupational accidents, human injuries is reportedly high in the construction industry which have not only influenced safety and health but also on economics as well. Compensation and rate of cure expenses follow them. The accidents shall be marked as Death, Maim, Burn, Fracture, Hernia, Strains, Crush or Cuts and Perforation [14]. This attribute provides a score as well as orients the worker to the safety department for further counselling or training processes.

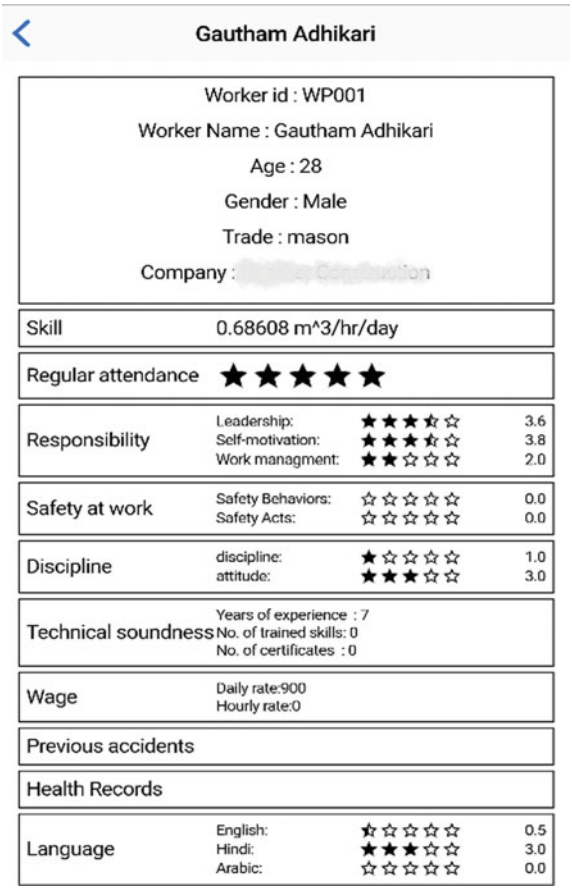

Fig. 3 WP from "WorPro" of worker 2

6 Results and Discussions

This study examined the role of CLP in the construction industry. The results show that CLP is a known fact and can be used to evaluate a worker regularly. The complication of estimating CLP was rated above 60% in the survey. It also suggested the lack of reliable, universal, systematic, trackable, less complex and less time-consuming methods to assess CLP. Responses up to 49% justified the use of own/personalised method for assessment. Nowadays, CLP has paramount importance in the construction sector and is a deciding factor in workflow study.

Managers have always shown a selective practice among skilled workers. Thus, certain attributes are desired from workers for the manager to select. Such attributes were identified from technical interviews and literature review which were weighed using a survey. A WP resulted from these attributes. Put into practice, the WP displayed flaws. The rating system was not able to establish controllability and measurability of attributes. Hence, the WP was then categorised as attributes, controls

ID no.	MASON						Date			Method	WrkSamp/FieldRatg/SminRatg
							Time			Skill	Block/Tile/Plaster/Concreting/Repair
	Name										
	Age									Location	
	Sex									Contractor	
										Last evaluated on	
	ATTRIBUTE	*	*	*	*	*	Quality control			Quantity of work	Remarks
1	Skill	mixing mortar	placing mortar	lifting brick	positioning brick	idle time	Levelling	Verticality	painting	cu.m / length	
		total	total	total	total	total	total	total	total	Total time	
2	Regular attendance										
3	Responsibility	Leadership		Self-motivation		Work management					Score between 0 and 5
		Transformational	Commitment	Expectancy	in-group relationships	site management					
			Role Model		equality	material arrangement					
			Clarity in vision		group affiliation	work planning					
			Communication								
		Transactional	Training & coaching others	instrumentality	better performance						
			Delegation								
			problem-solving strategies								
			Improvisation	Valence	Self appreciation						
			Goal achievement/work completion								
		Full Range	All of the above								
4	Health	Sick leave (50%)	Repetition of sickness (25%)	Medical condition (25%)							Score between 0 and 5
5	Safety at work	Safe Behaviours(eg)		Safe Acts(eg)							Score between 0 and 5
		PPE		Co-worker safety							
		Safety Helmet		Safe working							
		Safety shoes		Improper use of plant /equipment							
		Safety gloves		Careless storage of tool							
		Safety Jackets (reflectors)		working at heights							
		ear defenders		careless use of electronic gadgets							
		eye protectors									
		respirators									
		Housekeeping									
6	Discipline	Misbehaviour	Inappropriate dressing	Duty cuts	Disciplinary actions	Attitude					Score between 0 and 5
						work					
						safety					
						co-worker					
						management					
7	Technical soundness	experience	training	certification	inspection assistance						Score between 0 and 5
		more than 5yrs	Equipment training		drawing to site						
		3yrs or above	Safety training								
		1 year or above	Skill updating								
		less than 1 year	No training								
8	Daily wage rate		/hr or /day	No. of hours / day							Score between 0 and 5
9	Language	L1	L2	L3	L4						Score between 0 and 5
10	Previous accident										Score between 0 and 5

Fig. 4 Worker profile sheet for a worker

and sub-controls. Attribute and control assure controllability of the parameter that helps in projecting the characteristics of the worker. Whereas the latter ensure measurability. The sub-controls are reliable parlance used in the construction personnel community. Thus controls and sub-controls were defined. Most of the controls are rated on a scale of 0–5, whereas some attributes are given a score based on merit. Hence, the Worker Profile sheet is designed shown in Fig. 4.

The Worker Profile helped to compare workers based on the attributes as shown in Figs. 1 and 3. This helps a manager or a planning engineer whilst workflow allocation to select workers based on their specific requirement.

A worker was evaluated by multiple evaluators, and this showed that the attributes resulted in different rating. To get a standard evaluation technique, the evaluators need to perform Inter-Observer Reliability tests (IOR). Such an IOR test is also being developed as part of the study.

The evaluation process can be a tedious task in a WP sheet since work sampling techniques are used. WP must be updated multiple times to get better information and also evaluated by more than one evaluator to ensure a standard assessment. Generating the data is now known but the method of using pen and paper is excruciating. Thus, an application was also developed in an android platform that helps the evaluator to register scores and comments with the tap of his/her finger. The mobile application named "WorPro" is not made available in the Google Play Store but is in its Beta version with testing ongoing. A sample WP is shown in Fig. 2. This mobile app offers a future scope of inducing mobile camera-based diagnosing tools that can

partially automate the evaluation. WP is also envisaged as a benchmark evaluator for workers in a company which has specific benchmark scores for attributes in an apprentice worker.

Break of chain of command, is one important scenario which has to be effectively resolved. The WP is an assessment tool and also helps in a direct comparison between workers. WP helps a PM to overcome the biased decision from the cascading chain of correspondence down the line. WP helps a planning engineer to allocate the workers, specific to the project requirement. However, the mobilisation decision of resources rests with the PM. Instead of overriding the interests of the subordinating line of command, the accomplished and competent PM possess the ability to make informed, timely and effective project decisions. Hence, the PM shall device a decision making technique which can combine both objective fact based analysis and subjective human-centric input [15]. This enables the PM to compose outcomes that potentially satisfy the practical and emotional project related needs of stakeholders.

7 Conclusion

The most used planning tool and a lean construction technique practised in most of the structured construction firms is the Last Planner System (LPS). The amount of workflow occurring during the planning process is immense and one among those workflows is people. Finding the right people with the right skill sets is an exigency. Such a task is still relied upon the last planners, instead of a Planning Engineer or a responsible Project Manager. Thus WP in this planning process helps to recommend the right people for the required task. Then the PM may raise requisition for the release of a particular worker if in case he/she is engaged in another project or within the PM's project but need to expedite the work or replace, if necessary. The question of breaking the chain of command rests upon the PM unless he/she wishes to do so.

On the other hand, WP is an amalgamation of information regarding a worker that is available to the management and planning personnel to be used for the best of projects' performance. Pull planning, a forefront concept is used in LPS for planning, with the aid of WP gets to plan the worker required for a project in advance and submit requests for induction or transfer. In this modern era, major computing possibilities are brought in for various productivity related and other studies as well. WP is now developed into an Android app (Beta version) "WorPro". This expands the possibilities of reliable, universal, simple, less time consuming, an adoptable and real-time trackable tool for data coding, collection, data file construction, analysis and a final report in the form of a Worker Profile.

References

1. Ballard HG (2000) The last planner system of production control. Cambridge University Press, Cambridge
2. Motwani J, Kumar A, Novakoski M (1995) Measuring construction productivity: a practical approach. Work Study 44(8):18–20
3. Song L, Abourizk SM (2008) Measuring and modeling labor productivity using historical data. J Constr Eng Manage 134:786–794
4. Karimi H, Taylor TRB, Dadi GB, Goodrum PM, Srinivasan C (2018) Impact of skilled labor availability on construction project cost performance. J Constr Eng Manage 144(7):04018057
5. Gelisen G, Griffis FHB (2014) Automated productivity-based schedule animation: simulation-based approach to time-cost trade-off analysis. J Constr Eng Manage 140(4):1–10
6. Blair J, Czaja RF, Blair EA (2013) Designing surveys. SAGE Publications
7. Rojas EM, Aramvareekul P (2003) Is construction labor productivity really declining? J Const Eng Manage 129(1):41–46
8. Yi W, Chan PCA (2014) Critical review of labor productivity research in construction journals. J Manage Eng 30(2):214–225
9. Karthik D, Kameswara Rao CB (2019) Identifying the significant factors affecting the masonry labour productivity in building construction projects in India. Int J Constr Manage, 1–9 (Taylor & Francis)
10. Kart L, Sylvie N, Tiphaine L (2018) Development of the ergonomic activity sampling (EAS) method to analyse video-documented work processes with activity sampling. Ergon Int J 2(7)
11. Siriwardana CSA, Ruwanpura JY (2012) A conceptual model to develop a worker performance measurement tool to improve construction productivity. In: Construction research congress 2012, proceedings of the 2012 construction research congress 179–188
12. Choudhry RM (2014) Behavior-based safety on construction sites: a case study. Accident Anal Prevent Elsevier Ltd 70:14–23
13. Alwasel A, Abdel-Rahman EM, Haas CT, Lee S (2017) Experience, productivity, and musculoskeletal injury among masonry workers. J Constr Eng Manage 143(6):05017003
14. Soltanzadeh A, Mohammadfam I, Moghimbeigi A, Akbarzadeh M (2016) Analysis of occupational accidents induced human injuries: a case study in construction industries and sites. J Civ Eng Constr Technol 7(1):1–7
15. Cohen CB (2005) Project management decision making: blending analysis and intuition. Paper presented at PMI® Global Congress 2005—Latin America, Panama City, Panama. Newtown Square, PA: Project Management Institute

Development of Optimum Mix for Laterite Soil Brick by Adding Clam Shell Powder and Metakaolin

Devika Sudhakaran and Emy Poulose

Abstract Brick is a widely accepted building material used from ancient civilization to this era. The fields of brick manufacture have been undergone tremendous changes through several decades. Use of cement and lime in the soil for production of brick may stabilize the soil and thereby improve the strength and durability properties of bricks. On the other hand the use of such materials results in high energy consumption and production of CO_2. Therefore making the brick environmental friendly and cost effective, the addition of metakaolin and clam shell powder, instead of cement can be done. This research shows the development of an optimum mix for laterite soil brick by adding metakaolin-clamshell powder (MK-CSP), an artificial pozzolana and waste material respectively. The hydration process of metakaolin, which containing high silica and alumina content react with the calcite present in clam shell powder that containing calcium carbonate result in the formation of calcium aluminate and calcium silicate hydrate at the time of hydration [1]. These cementicious compounds densify the loose clam shell powder paste. The effect of addition of various quanties (2.5% and 2.5%, 5% and 5%, 5% and 10%, 10% and 5%, 5% and 15%.10% and 10%, 15% and 5%) of metakaolin and clam shell powder respectively by weight of laterite soil on mechanical, physical and durability properties of brick were established.

Keywords Metakaolin · Clamshell powder · Laterite soil · Physical properties · Mechanical properties · Durability

1 Introduction

Brick is an essential building material used in all over the world from the very beginning. India is the second largest producer of bricks in the world. From ancient period human beings started the construction of various structures with locally available materials and with the growing experiences of them, there were changes in the material used in all the field of constructions. Changes also occurred in brick

D. Sudhakaran (✉) · E. Poulose
Toc H Institute of Science and Technology, Ernakulam, India
e-mail: devikavaishnavam97@gmail.com

© Springer Nature Switzerland AG 2021

K. Dasgupta et al. (eds.), *Proceedings of SECON 2020*,
Lecture Notes in Civil Engineering 97,
https://doi.org/10.1007/978-3-030-55115-5_28

production, the method of production and the combination of material used were changing continuously. Clay bricks were a common scenario in the construction. Along with the various circumstances, modifications of ordinary clay bricks also came into existence. The use of fertile agricultural land for making clay bricks also created problems in the field of cultivation; it could in turn affect the brick industry. Therefore researchers focused to replace the clay bricks partially or fully with other types of soil [2] and also with the addition of different waste materials from industries, some supplementary cementitions materials [2–5] like fly ash/GGBS/used brick powder; even fibers were incorporated for the production of bricks.

Clamshell powder is a waste material obtained from the processing of clam meat. Use of this powder in the production of brick could help to reduce the accumulation of clam shell powder waste in the environment. This shell powder has the potential to be used as a cementitions material in concrete, as its chemical composition is almost similar to Portland cement and the main component in the clam shell powder is calcium carbonate. The pozzolanic material used for the production of brick in this study is metakaoline, which is formed when the mineral kaolin is heated to a temperature between 600–800 ºC.

This work is carried out for developing an optimum mix of clam shell power and metakaolin to produce laterite soil brick. The present study focused on the suitability of using this waste product in laterite soil brick to improve the strength parameters. Laterite soil is used to produce bricks in this study instead of clay. This soil is naturally available from the earth.

2 Experimental Methodology

The experimental program is designed for developing an optimum mix for laterite soil brick by adding clam shell powder and metakaolin in 2.5 and 2.5%, 5 and 5%, 5 and 10%, 10 and 5%, 5 and 15%, 10 and 10%, 15 and 5%, by weight of soil. The experimental program is aims to study the flow parameters, optimum moisture content and maximum dry density, unconfined compressive strength of soil mixed with the above percentages of CSP and MK. Bricks were prepared with the same combinations of additives on the soil and the compressive strength, water absorption, linear shrinkage, apparent porosity, efflorescence, bulk density and initial rate of absorption values of bricks were also evaluated. From the test results optimum mix combination of additives with soil was identified.

2.1 Materials and Properties

The different materials used in this investigation and their physical properties are illustrated in Table 1.

Table 1 Material properties

Materials	Properties		Test results	Reference code
Laterite soil	Specific gravity		2.7	IS 2720 (Part III): 2006 [6]
	Optimum moisture content (%)		21.20	IS 2720 (Part VII):2006
	Dry density (kg/m^3)		1.64	
	Atterberg's limits (%)	Liquid limit	41	IS 2720 (Part V): 2006
		Plastic limit	18.48	
		Plasticity index	23	
	Particle size distribution	Silt size articles (%)	60	IS 220 (Part IV): 2006 [7]
		Clay size particles (%)	40	
Metakaolin	Specific gravity		2.8	
Clam shell powder	Specific gravity		2.1	

2.2 Combined Effects of CSP and MK on Laterite Soil

In this experimental investigation, effects of addition of seven different combinations in 2.5 and 2.5%, 5 and 5%, 5 and 10%, 10 and 5%, 5 and 15%0.10% and 10%, 15 and 5% of CSP and MK on laterite soil and without additive was found out. The Atterberg limits, Optimum moisture content, dry density and unconfined compressive strength were found out for all of the above combinations. The Atterberg limits of mixture is important in determining whether the combination has enough plasticity index to be used for the preparation of bricks as per IS 2117:1991 (range of plasticity index shall be 15–25). The optimum moisture content was determined to find the quantity of water required to produce a mixture of maximum dry density.

2.2.1 Atterberg Limits

Atterberg limits are the water content at which soil changes from one state to another, Atterberg limits for each mix were conducted [8]. Determination of atterberg limits is important in preparation of bricks, it helps in determining whether the soil has enough plasticity to be used as bricks. Atterberg limits in 2.5 and 2.5%, 5 and 5%, 5 and 10%, 10 and 5%, 5 and 15%, 10 and 10%, 15 and 5% of CSP and MK mixed with soil is shown in Table 2. Due to the plastic and cohesive nature of Metakaolin and clam shell powder, that binds each other and with soil when mixed with water, the liquid limit and plasticity index was increased as expected. The plastic limit might be decreased due to the increased amount of clay content contributed by MK, which requires less water for the mix to reach plastic limit.

Table 2 Effect of CSP and MK on Atterberg limits of laterite soil

MK (%)	CSP (%)	Laterite soil (%)	Liquid limit (%)	Plastic limit (%)	Plasticity index (%)
0	0	100	41	18.48	23
2.5	2.5	95	46.2	30	16.2
5	5	90	48	28.8	19.2
5	10	85	49.44	28.1	21.34
10	5	85	52	26.5	25.5
5	15	80	53	25.2	27.8
10	10	80	54.5	24.48	30.02
15	5	80	55.2	23.8	31.4

Table 3 Effect of CSP and MK on OMC and maximum dry density of soil

MK (%)	CSP (%)	Laterite soil (%)	OMC (%)	Dry density (g/cc)
0	0	100	21.20	1.64
2.5	2.5	95	22.15	1.58
5	5	90	25.12	1.55
5	10	85	26.45	1.51
10	5	85	28.64	1.43
5	15	80	31.45	1.35
10	10	80	32.12	1.38
15	5	80	34.25	1.34

2.2.2 Optimum Moisture Content (OMC) and Dry Density

The optimum moisture content of soil is the water content at which a maximum dry unit weight can be achieved after a given compaction effort. In this study, the optimum moisture content for varying proportions is determined to find the quantity of water to be added for the production of bricks. The test was carried out to determine the maximum dry density and optimum moisture content of 2.5 and 2.5%, 5 and 5%, 5 and 10%, 10 and 5%, 5 and 15%, 10 and 10%, 15 and 5% of CSP and MK mixed with soil is shown in Table 3. It was found that maximum dry density decreased with increase in CSP and MK addition. Maximum dry density with minimum moisture content means minimum shrinkage, minimum voids, and increase in strength of soil. The pozzolanic reaction of MK and CSP with soil increases the OMC.

2.2.3 Unconfined Compressive Strength (UCS)

The unconfined compressive strength is defined as the compressive stress at which an unconfined cylindrical specimen of soil will fail in a simple compression test. The

Table 4 Effect of CSP and MK on unconfined compressive strength of soil

MK (%)	CSP (%)	Laterite soil (%)	UCS (kg/cm^2)
0	0	100	0.16
2.5	2.5	95	0.18
5	5	90	0.20
5	10	85	0.21
10	5	85	0.23
10	10	80	0.25
5	15	80	0.28
15	5	80	0.33

unconfined compressive strength of soil mixed with in 2.5 and 2.5%, 5 and 5%, 5 and 10%, 10 and 5%, 5 and 15%, 10 and 10%, 15 and 5% of CSP and MK was found. The mixture was prepared at optimum moisture content. The UCS of various mixtures is shown in Table 4. It was observed that the UCS value of mixtures increases with the increase in amount of additives in soil indicates that the cohesion of lateritic soil increases due to addition of MK and CSP.

2.2.4 Preparation and Testing of Bricks

Bricks were hand moulded and are burnt in the electric oven. Raw materials are mixed manually by varying the proportion of metakaolin and clam shell powder and laterite soil. The mix proportion used for the preparation of bricks is shown in Table 5. The mixture was prepared with the predetermined optimum moisture content. Water content is an important factor affecting the quality of the bricks. Mould size was selected as 190 × 90 × 90 mm which is the size of burnt bricks as per IS 2691:1988. The bricks are air dried until it is left with less moisture after which the bricks are dries in oven at 110 °C for 24 h. Bricks are then taken out and cooled. Various tests

Table 5 Mix design for the preparation of bricks

Mix designation	MK (%)	CSP (%)	Laterite soil (%)
B0	0	0	100
B1	2.5	2.5	95
B2	5	5	90
B3	5	10	85
B4	10	5	85
B5	5	15	80
B6	10	10	80
B7	15	5	80

Table 6 Compressive strength values for bricks

Mix code (%)	Compressive strength (Mpa)
B0	3.2
B1	3.54
B2	3.76
B3	3.86
B4	3.82
B5	4.11
B6	4.32
B7	4.68

were conducted to check the quality of bricks. The manufactured bricks were tested for its physical and durability properties. According to Indian standard code the tests for bricks include compressive strength, efflorescence and water absorption, it was conducted as per IS 3495 (Part I-III) and hence ASTM standards were used to find out initial rate of absorption, bulk density. Initial rate of absorption was conducted as per ASTM C67 and bulk density was conducted as per ASTM C20 (2010).

3 Results and Discussion

3.1 Compressive Strength

The compressive strength test was conducted according to IS 3495 (Part I): 1992 [9]. The compressive strength values of all the bricks prepared with the different mixes were depicted in Table 6. The values show that the compressive strength increased with increase in percentage of additives on soil. It was found that all the bricks satisfied the minimum compressive strength requirement as per IS 1077:1992, as per IS 1077:1992 the minimum value of compressive strength required is 3.5 Mpa.

The compressive strength value of these bricks mainly depends on the pozzolanic reaction between MK and CSP with the soil particles. Compressive strength of brick increases with the addition of MK and CSP was due to the improvement in the soil properties by the action of these stabilizers (Fig. 1).

3.2 Water Absorption of Bricks

The water absorption was determined according to IS 3495 (Part II): 1992. The result of water absorption with increase in percentage of additives on soil is shown in Table 7. The variation of water absorption with increase in percentage of additives is shown in Fig. 2. Water absorption of the bricks mainly depends on the porosity. Increase

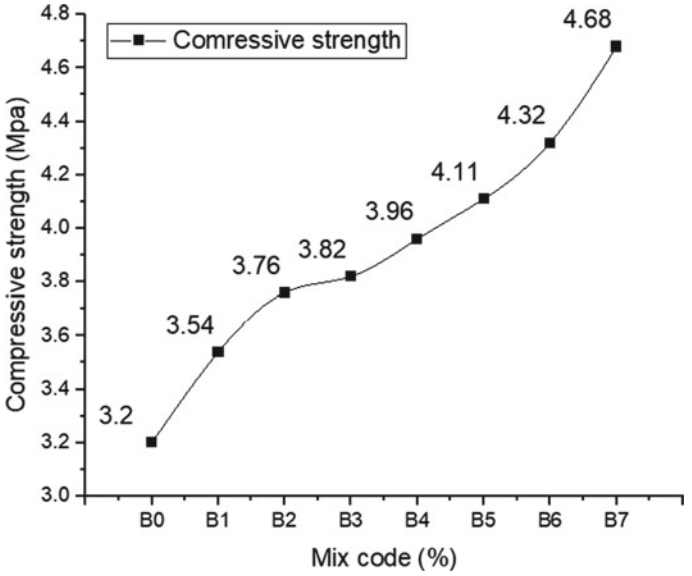

Fig. 1 Variation of compressive strength with different percentage of MK and CSP

Table 7 Water absorption test results

Mix code (%)	Water absorption (%)
B0	9.0
B1	9.8
B2	10.2
B3	11.6
B4	12.0
B5	15.4
B6	16.3
B7	18.6

in porosity due to the escape of heat during the hydration process of the stabilizers during mixing increases the value of water absorption.

3.3 Efflorescence of Bricks

To know the presence of soluble salts in a brick, the efflorescence test was conducted according to IS 3495 (Part II): 1992. It was found that all the bricks were showing "slight" efflorescence because the additives involved in the preparation of brick

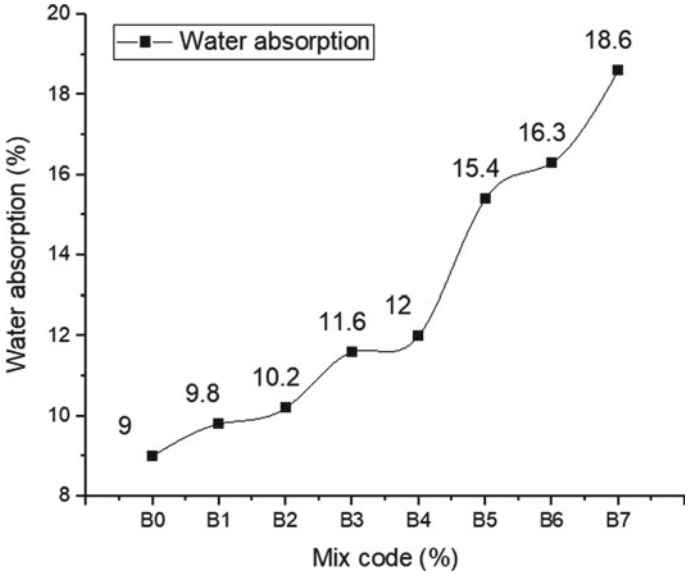

Fig. 2 Variation of water absorption with different percentage of MK and CSP

includes some amount of alkaline salts. Therefore the bricks are in range that does not affect the aesthetics of the building.

3.4 Initial Rate of Absorption (IRA)

Initial rate of absorption was conducted as per ASTM C67, it is important to find the initial rate of absorption to assist in mortar section. The observed values are given in the Table 8.

Table 8 IRA test results

Mix code (%)	IRA (g/cm^2/min)
B0	0.15
B1	0.18
B2	0.3
B3	0.42
B4	0.45
B5	0.56
B6	0.59
B7	0.68

Table 9 Bulk density test results

Mix code (%)	Bulk density (g/cc)
B0	1.92
B1	1.83
B2	1.65
B3	1.52
B4	1.45
B5	1.42
B6	1.39
B7	1.31

3.5 Bulk Density

Bulk density of brick is defined as the dry weight of brick per unit volume of brick. High bulk density is an indication of less pore size. Table 9 shows the values of bulk density of bricks.

The bulk density of bricks mainly depends on the method of manufacturing and the method of burning of bricks. It is observed that with the increase in the amount of additives, light weight bricks can be made.

4 Conclusions

In this work, the effect of adding various percentages of MK and CSP on properties of laterite soil was investigated for developing an optimum mix of MK and CSP with laterite soil brick. The following main concluding remarks are made based on various experiments:

- The variation of compressive strength, water absorption, efflorescence, bulk density and initial rate of absorption of bricks made by adding laterite soil with 0%, 2.5% and 2.5%, 5% and 5%, 5% and 10%, 10% and 5%, 5% and 15%, 10% and 10%, 15% and 5% of MK and CSP by weight of laterite soil and without the additives was found out.
- It was found that the compressive strength values of all the bricks made with the above combinations were above 3.5 N/mm^2, which is the minimum compressive strength requirement as per IS 3620:1979.
- Compressive strength of brick increases with the addition of MK and CSP was due to the improvement in the soil properties by the pozzolanic action of these stabilizers.
- It was found that the water absorption of bricks till 10% MK and 5% CSP with soil was within the permissible limit as per IS 3620:1979 [10]. Rest of the combinations has values more than 12%.

- All the bricks showed slight efflorescence. The bulk density decreased with increase in addition of MK and CSP; hence light weight bricks were produced. From the results, it was found that bricks produced by adding 10% MK and 5% CSP with laterite soil can be used for construction.

References

1. Aguilar S, Francisco AS, Olivares H (2010) Assessment of phase formation in lime-based mortars with added metakaolin, Portland cement and sepiolite, for grouting of historic masonry. J Cem Concr Res 40:66–76
2. Eva N, Rovnanikova P (2016) Effect of slag and calcium carbonate addition on the development of geopolymer from indurated laterite. Constr Build Mater 120:530–539
3. Arjun D, Malhotra SK (1990) Lime-stabilized red mud. J Mater Struct Constr 23:252–255
4. Daniel M, Heath A, Walker P (2019) Use of metakaolin with stabilised extruded earth masonry units. Construct Build Mater 78:172
5. Bal H, Jannot Y, Quenette N, Chenu A, Gaye S (2012) Water content dependence of the porosity, density and thermal capacity of laterite based bricks with millet waste additive. Construct Build Mater, 144–150
6. IS 2720 (Part–3): 1980 (Reaffirmed 2002); Method of test for soils, Determination of specific gravity. Bureau of Indian Standards, New Delhi
7. IS 2720 (Part–5): 1985 (Reaffirmed 2006); Method of test for soils, Grain size analysis. Bureau of Indian Standards, New Delhi, 28
8. IS 2720 (Part–4): 1985 (Reaffirmed 2006); Method of test for soils, Determination of liquid and plastic limit. Bureau of Indian Standards, New Delhi
9. IS 3495 (Part I–III): 1992 (Reaffirmed 2002); Indian standard methods of tests of burnt clay building bricks. Bureau of Indian Standards, New Delhi
10. IS 3620:1979**:** Specification for laterite stone block for masonry. Bureau of Indian Standards, New Delhi

Analytical Assessment on the Behaviour of Conical Shell Foundation

T. Lamya and M. K. Sheeja

Abstract Shell foundations have been used as an economic alternative to the conventional flat shallow foundations, in situations where heavy loads are to be transferred to weaker soil. Among the shells which have come into wider use in foundation, is the conical shell. The frustum of cone is probably the simplest form in which a shell can be used as foundations. This paper aims to study about a different foundation shape that reduces the foundation cost by reducing the required amount of concrete and reinforcing steel bars. Also, to achieve lower soil stresses by changing the foundation shape which will result in reduced settlements and foundation stresses. Analytical studies are performed on circular flat foundation and conical shell foundation using finite element software ANSYS 19.0 and their performances such as ultimate load carrying capacity and soil settlement characteristics have been compared.

Keywords Shell foundations · Shallow foundations · Conical shell foundation · Finite element software · Ultimate load carrying capacity · Soil settlement characteristics

1 Introduction

The essential requirement of a foundation is its ability to transfer the load from the superstructure to the subsoil in such a way that the induced stresses doesn't exceed the allowable bearing capacity of the soil nor cause excessive settlement. Shell foundation has been considered the best shallow foundation for transferring heavy load to weak soils in situations where conventional shallow foundations undergoes excessive settlement. In cases where heavy load is to be transferred to weaker soils with lower bearing capacity, if flexural members like slab and beam are used, the bending moment and shear in them will be large, which will result in an increased section size. Shells, which act mostly in tension or compression will be more efficient and

T. Lamya (✉) · M. K. Sheeja
AISAT, Kochi, India
e-mail: lamya.shakir@gmail.com

© Springer Nature Switzerland AG 2021

K. Dasgupta et al. (eds.), *Proceedings of SECON 2020*,
Lecture Notes in Civil Engineering 97,
https://doi.org/10.1007/978-3-030-55115-5_29

economical in such situations. The amount of material required for a shell foundation to carry a load will be much less than that required for the flexural members. Even though the material cost is lesser, the labour cost involved in the formation of shell foundation will be larger than that is required for the flat foundations. So, in situations where material to labour cost ratio is high, shell foundation can be considered as the best option. Different types of shells used in civil engineering practice are domes, hyperbolic shells, cylindrical shells, paraboloidal shells, and conoids. Although, due to the constructional easiness and various other factors, cone and hyperbolic paraboloids are the two shape of shells that is commonly adopted for practical purposes. The bureau of Indian standards has also published IS 9456 (1980) Code of practice for design and construction of conical and hyperbolic paraboloid type of shell foundations.

1.1 Scope of Using Shells in Foundations

The plain structural elements like beam and slab, which resists their transverse loads, along with self-weight, in flexure, while the non-planar structural elements like shells resist their transverse load in the form of membrane compression, membrane tension, or membrane shear.

Concrete is highly efficient in compression and slightly efficient in tension, with a moderate efficiency in bending. So, if the flexural element like slab or beam is replaced with shell element, then the applied load creates a membrane compression. And the effect of this membrane compression will be of low magnitude when compared to the effect of the same applied load on plain structural element. This ultimately results in a section with reduced thickness, which makes the construction cost effective.

1.2 Objectives

The objective of this study is to determine the ultimate load carrying capacity of conical shell foundation and circular flat foundation of same thickness and to compare their results.

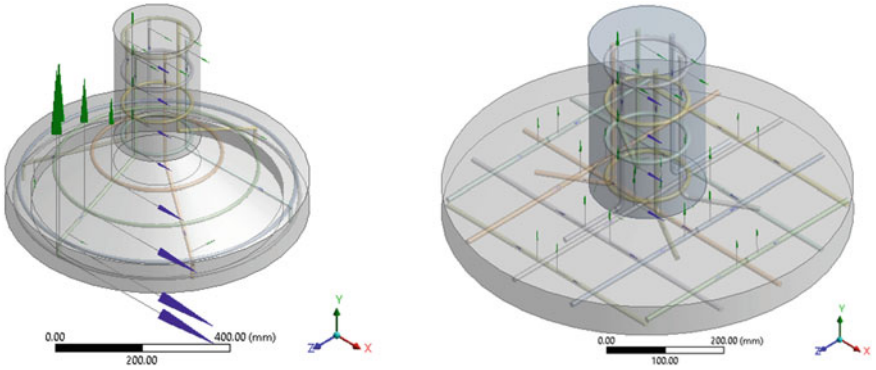

Fig. 1 **a** Finite element model of reinforced conical shell foundation. **b** Finite element model of reinforced circular flat foundation

2 Details of Shell and Soil

2.1 Geometry of Foundation and Soil

The dimensions of the conical shell foundation used for this study is obtained by designing using membrane theory according to IS 9456:1980. Conical shell foundation of diameter 700 mm, thickness 60 mm and ratio of rise to radius 0.5 is chosen. The dimensions for flat circular foundation such as the diameter and thickness are taken similar to the conical shell so that their performances can be compared (Fig. 1).

The dimension of soil block is fixed as per load distribution pattern. The dimension of soil thus considered is 1.75 m × 1.75 m, which is greater than twice the dimension of the foundation and the depth of the soil block considered is 1.45 m from the bottom of the shell, which is also greater than the minimum depth required for a foundation.

2.2 Properties of Concrete, Soil, and Reinforcement

Concrete is defined with linear isotropic property in which Von-mises failure criterion is considered. The material properties of footing are indicated in Table 1. The sand soil mass is modelled as an elastoplastic material using the Mohr–Coulomb plasticity model. The properties of the medium dense sand considered are enlisted in Table 2.

Table 1 Properties of foundation materials

S. No.	Properties	Concrete	Reinforcement bars
1	Modulus of elasticity, E_c (kN/m^2)	2.236×10^7	2×10^8
2	Poisson's ratio, υ	0.15	0.3
3	Density (kN/m^3)	22	7850
4	Tensile yield strength (Mpa)	2	250
5	Compressive yield strength (Mpa)	20	250
6	Tensile ultimate strength (Mpa)	5	460
7	Compressive ultimate strength (Mpa)	41	0

Table 2 Properties of soil

Sl. No:	Soil properties	Values
1	Modulus of elasticity, E_c (kN/m^2)	25×10^3
2	Poisson's ratio, υ	0.3
3	Density (kg/m^3)	1673
4	Cohesion (kN/m^2)	5
5	Angle of internal friction	33^o
6	Dilatancy angle	3^o

3 Finite Element Modelling

This work studies the performance of conical shell foundation and circular flat foundation under static loading using Finite Element Methods (FEM). The conical shell foundation is designed based to the Membrane theory (IS 9456:1980). The investigation is conducted using the FEM Software ANSYS WORKBENCH version 19.

3.1 Concrete Element Type

In ANSYS WORKBENCH the concrete element model used for analysis is SOLID 186 which is higher order element having 20 nodes.

3.2 Contacts Provided

Contact between two elements is provided in order to act as a single unit. The area between the inverted conical shell foundation and soil is made as bonded contact.

The contact between the reinforcement bars and concrete is also made as bonded contact with target as concrete and contact as rebars.

3.3 Meshing

A suitable mesh size with maximum element quality and minimum skewness is selected. Tetrahedral meshing method is used for flat circular foundation and hexa-dominant meshing method is used for conical shell foundation. Figures of the meshed model is shown (Fig. 2).

4 Static Structural Analysis

In this study, static structural analysis was conducted. A static analysis calculates the effects of steady state loading condition of the structure. Various incremental loads were considered as vertical column loading in order to determine the ultimate load carrying capacity. Since the shape of foundation is the governing factor, ultimate load carrying capacity is determined on the basis of the strain value of concrete. As the load is increased, the equivalent elastic strain value also increases, and the load corresponding to the maximum equivalent elastic strain (as 0.002 for footing) is considered as the ultimate load carrying capacity.

In the soil model, the boundary conditions are provided in such a way as to produce a similar condition in the actual case. The four sides are provided with remote displacement by fixing the axis perpendicular to the corresponding face,

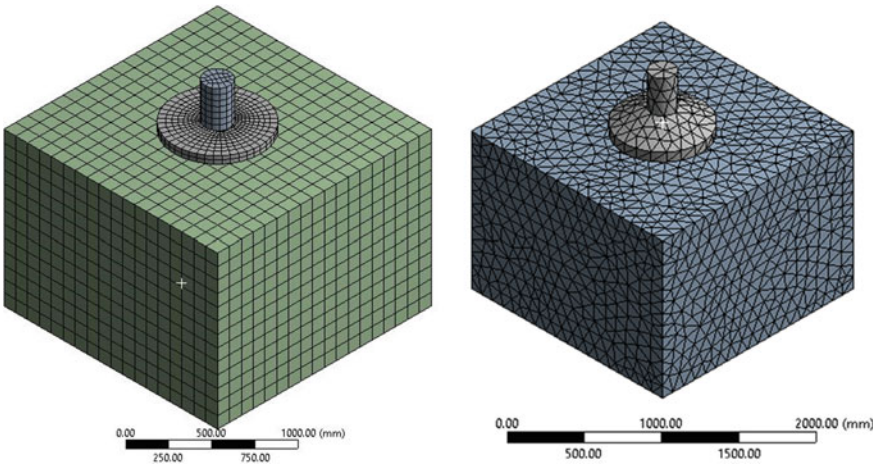

Fig. 2 **a** FEM mesh of circular flat foundation. **b** FEM mesh of conical shell foundation

which indicates that each face restricts the lateral movement. Although, the movement of the bottom face is fixed in both directions. Figure 3 shows the boundary condition of both the numerical models.

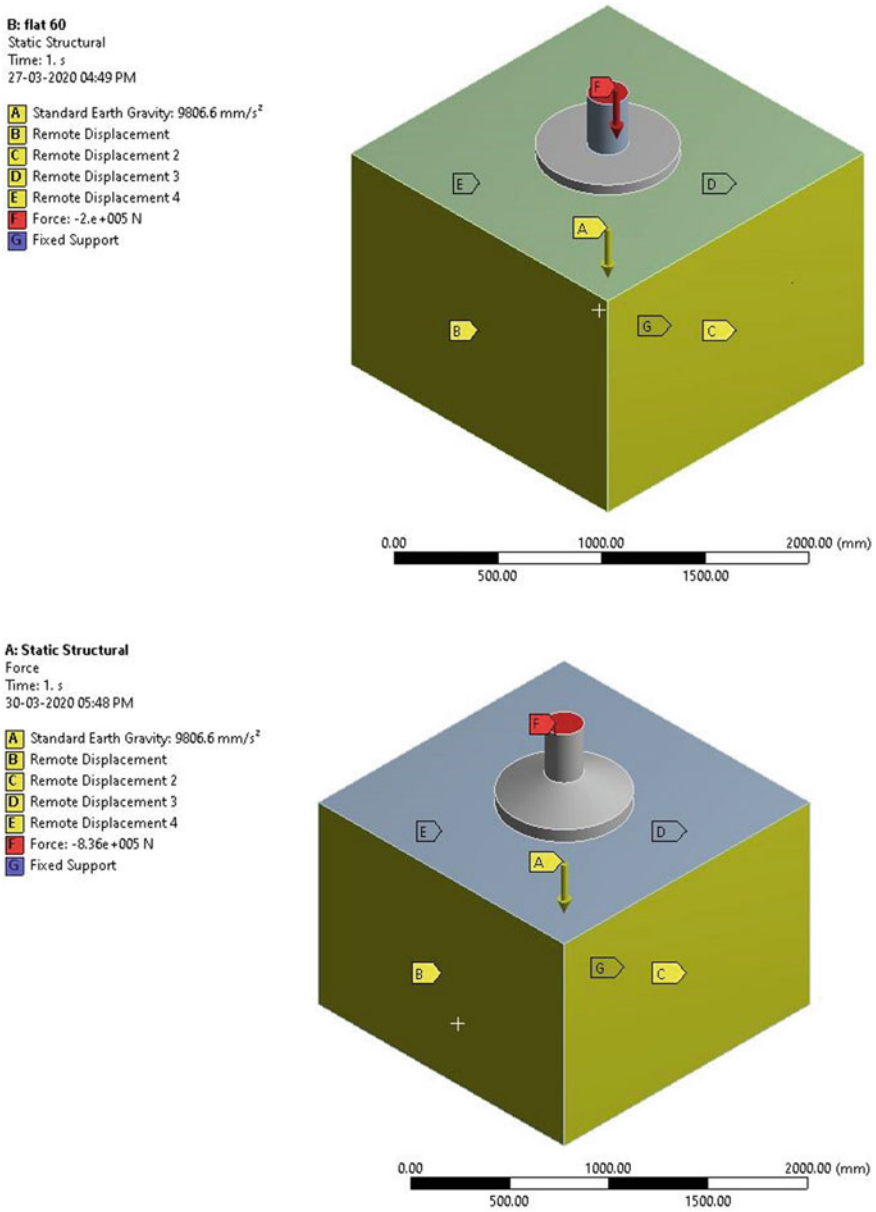

Fig. 3 **a** BCs for circular flat foundation. **b** BCs for conical shell foundation

5 Results and Discussion

The structural behaviours such ultimate load carrying capacity and soil settlement characteristics of conical shell foundation and flat circular foundation were compared. The conical shell showed much better behaviour when compared to flat ones.

5.1 Ultimate Load Carrying Capacity

In this study, as the effect of shape of the foundation on various characteristics is the main focus, the ultimate load carrying capacity is analysed based on the equivalent elastic strain value of concrete, unlike the soil shear failure in general case. The load applied at which the equivalent elastic strain value of concrete exceeds 0.002 is considered as the ultimate load carrying capacity (Fig. 4).

The conical shell foundation showed a maximum equivalent elastic strain value at a vertical column load of 780 kN and the circular flat foundation showed a maximum equivalent elastic strain value at a vertical column load of 250 kN. This indicates that the conical shell foundation has the capacity to carry a load more than 3 times that of its flat counter part.

5.2 Settlement Results

The conical shell foundation at its ultimate load of 780 kN settles 33.872 mm whereas the flat circular foundation at its ultimate load of 250 kN settles 33.465 mm. This indicates that the flat circular foundation settles at more faster rate than conical shell foundation. Figures shows settlement details obtained from the analysis (Fig. 5).

6 Conclusion

The static performances of the conical shell foundation is compared with the flat circular foundation by static analysis using ANSYS software. However, the results obtained from this study cannot be generalized since they are relevant only for the specific data provided in the analysis. The results of the present study show that the load carrying capacity of conical shell foundation is 3 times more than that of its flat counterpart. Settlement of conical shell foundation is at a lower rate when compared to its flat counterpart. Therefore, conical shell foundation can be considered as better alternative to flat foundation where heavy load is to be transferred to weaker soil.

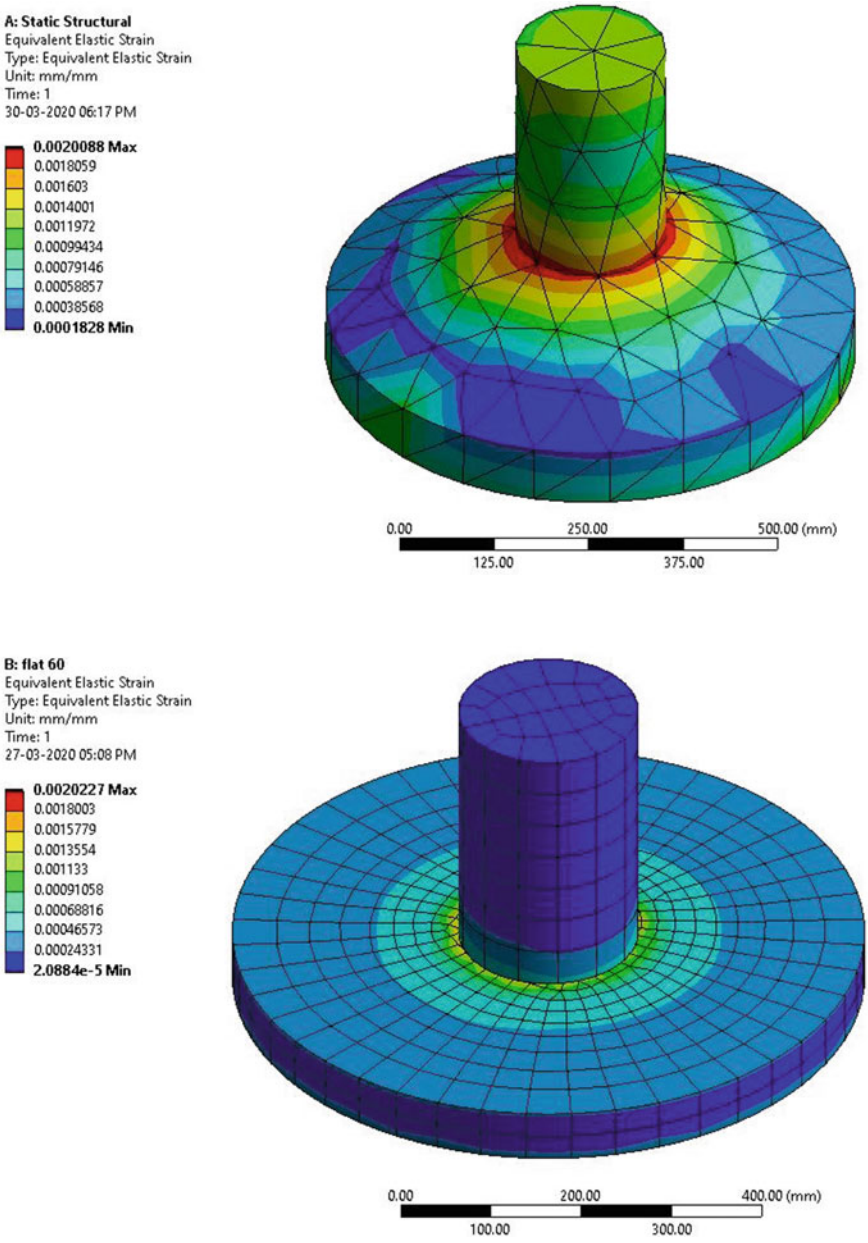

Fig. 4 Elastic strain shading contours corresponding to the ultimate loads

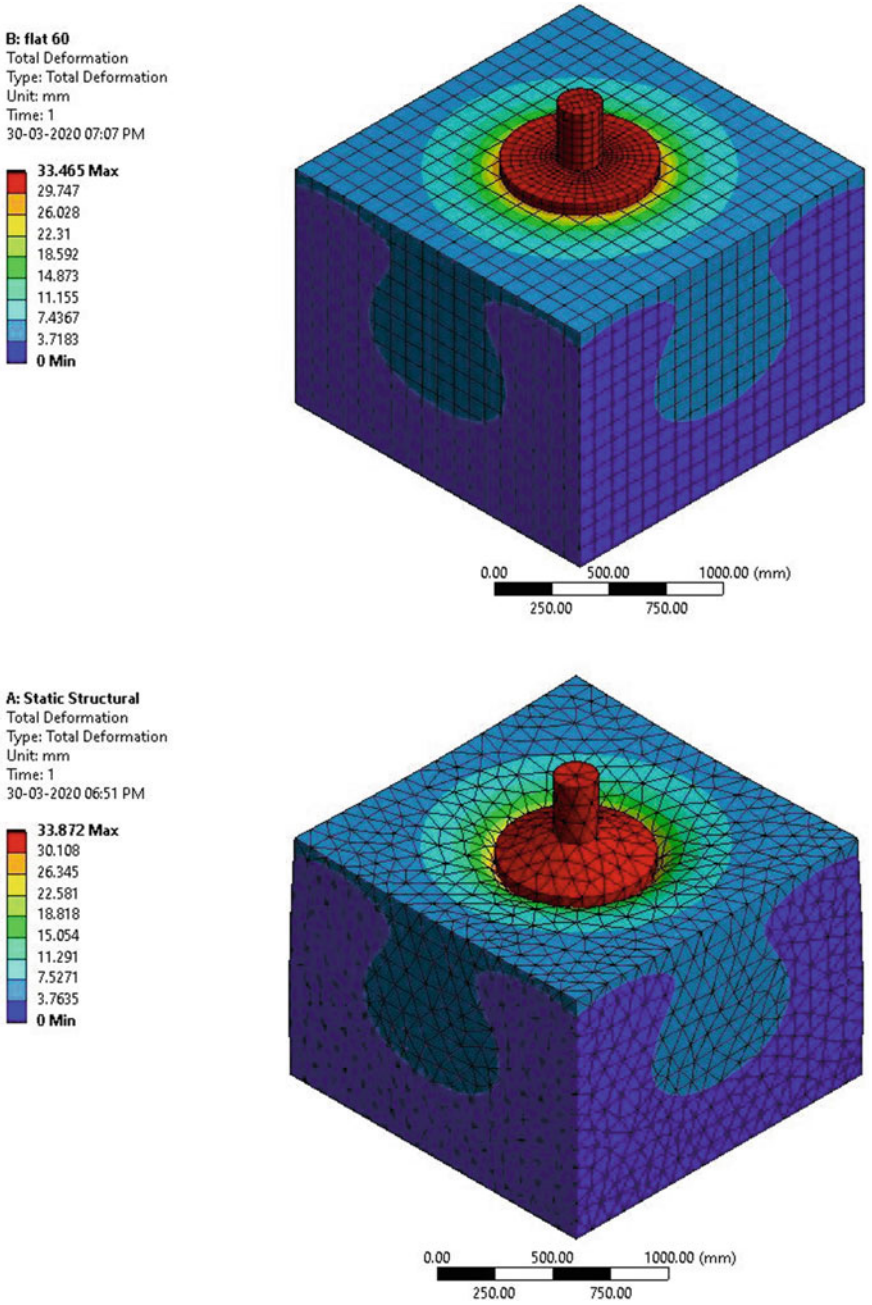

Fig. 5 Settlement shading contours corresponding to the ultimate loads

References

1. Abdel-Rahman MM, Hanna AM (1988) Ultimate bearing capacity of triangular shell strip footing on sand. J Geotech Eng ASCE 116(2):1851–1863
2. Al-azzawi AA (2013) A study of the behaviour of shell footings using finite element analysis. Eng Technol J Part (A) 31(19):90–102
3. Azzam WR, Nazr AM (2014) Bearing capacity of shell strip footing on reinforced sand. J Adv Res, 1–11
4. Chehol ET (2009) A study on the design and advantage of conical type shell foundation using analytical and FEM. Addis Ababa University
5. Esmaili D, Hataf N (2008) Experimental and numerical investigation of ultimate load capacity of shell foundation on reinforced and unreinforced sand. Iran J Sci Technol 32(B5):491–500
6. Esmaili D, Hataf N (2013) Determination of ultimate load capacity of conical and pyramidal shell foundations using dimensional analysis. Int J Adv Eng Technol 37(C+):423–435
7. Fattah et al. (2015) Experimental and theoretical study on bearing capacity of conical shell foundations composed of reactive powder concrete. Acta, 312
8. Huat BBK, Mohammed TA (2006) Finite element study using FE code (PLAXIS) on the geotechnical behaviour of shell footings. J Comput Sci 2(1):104–108 (USA, NY)
9. Huat BBK, Mohammed TA, Abdullah AA (2007) Numerical and field study on triangular shell footing for low rise building. Int J Eng Technol 1(4):194–204
10. IS: 9456 (1980) Indian standard code of practice for design and construction of conical and hyperbolic paraboloidal types of shell foundation. Bureau of Indian Standards, New Delhi
11. Kurian NP (2006) Shell foundations: geometry, analysis, design and construction. Alpha Science International Limited

Experimental Investigation on Packing Density of Concrete Using Wet Packing Method

Mariya Jacob and K. N. Resmi

Abstract Packing of the particles has great impact on the performance of concrete. When only the ordinary Portland cement was used in concrete, the voids content tends to be large. To overcome this problem, supplementary cementitious materials finer than OPC is added to fill into the voids so as to improve the packing density. In this study wet packing method is used to evaluate the packing density of concrete containing supplementary cementitious material as Metakaolin. This paper deals with the packing density and the strength characteristics of concrete developed by varying the metakaolin content from 0 to 20% by volume. There is an optimum percentage for the replacement of cement with Metakaolin. The results show better positive results while comparing with the normal concrete.

Keywords Packing density · Wet packing method · Metakaolin · Compressive strength

1 Introduction

Concrete is a multiphase material consisting of coarse aggregate, fine aggregate, binding material, and water [7]. To improve the strength and durability of concrete it is essential to lower the w/c ratio. But it is necessary to provide the concrete mix with certain workability. If only OPC is used as cementitious material it becomes difficult to lower the w/c ratio because the water added must be sufficient to fill up the voids of the cementitious materials to avoid entrapped air. When OPC was only used as cementitious material in concrete the void content becomes quite large. Also, the incorporation of high binder content can result in higher w/c demand and creates greater risk of thermal and shrinkage cracking. To overcome this issue,

M. Jacob (✉) · K. N. Resmi
Department of Civil Engineering, Federal Institute of Science and Technology (FISAT), Ernakulam 68377, India
e-mail: mariyajacob96@gmail.com

K. N. Resmi
e-mail: reshmikn@gmail.com

© Springer Nature Switzerland AG 2021

K. Dasgupta et al. (eds.), *Proceedings of SECON 2020*,
Lecture Notes in Civil Engineering 97,
https://doi.org/10.1007/978-3-030-55115-5_30

supplementary cementitious materials finer than OPC, such fly ash, silica fume, metakaolin etc. can be added to fill into the voids. Thus, it will improve the packing density of cementitious materials. Packing density is the ratio of solid volume to bulk volume [5, 6]. By optimising the entire particle system, it is seen that the medium size particles are just enough to fill up the voids between larger size particles and the smaller size particles are just enough to fill up the voids between medium size particles and so on. Thus, packing density of the entire particle system gets maximized and thus it will increase the strength, durability and dimensional stability of the concrete.

Theoretical packing models such as Aim model, the Toufar model and the Modified Toufar model etc. and computer Simulations were developed for the study of packing of particles [3]. Packing density of concrete have rarely been directly measured. Dry packing methods has several problems as (a) it is quite sensitive to the compaction applied (b) it does not include the possible effects of water and admixtures (c) the agglomeration and loose packing of the finer particles seriously affects the measured packing density[6, 8]. To resolve the above stated problems, researchers developed wet packing method and measures the packing density of concrete under wet condition.

2 Materials

The materials used for the study were ordinary portland cement, Fine aggregate (M-sand), coarse aggregate, metakaolin and super plasticiser.

2.1 Cement

Ordinary portland cement of Grade 53 with commercial name “Sharjah cement” was collected and its physical properties was tested according to IS 4031:1991-Part 2. The results are shown in Table 1.

Table 1 Properties of cement

Physical properties	Values
Fineness of cement (%)	8
Specific gravity	3.174
Standard consistency (%)	32
Initial setting time	85 min

Table 2 Properties of fine aggregate

Properties of fine aggregate	Values
Sand type	M-sand
Grade	Zone II
Specific gravity	2.75
Water absorption (%)	1.4
Fineness modulus	2.8

Table 3 Properties of coarse aggregate

Properties of coarse aggregate	Values
Specific gravity	2.79
Water absorption (%)	0.3

2.2 Fine Aggregate

M-sand was collected and its material properties was found according to IS 2386:2016-Part 3. The results are shown in Table 2.

2.3 Coarse Aggregate

The 20 mm nominal size well graded aggregate was used in the study. They were collected and tested according to IS 2386:2016-part 3 and the results are shown in Table 3.

2.4 Mineral Admixture

Metakaolin was the mineral admixture used for the study. The chemical composition and physical properties of metakaolin is shown in Tables 4 and 5 respectively.

Table 4 Chemical composition of Metakaolin

Chemical	Mass (%)
SiO_2	52
Al_2O_3	40
Fe_2O_3	3.6
TiO_2	2.65
CaO	1.09

Table 5 Physical properties of Metakaolin

Physical properties of Metakaolin	Values
Appearance	Off-white
Specific gravity	2.6
Specific surface area (m^2/g)	19.5
Average particle size (μm)	1.86

2.5 Superplasticiser

A poly carboxylate ether based superplasticiser with specific gravity 1.1 is used at a dosage of 0.3% by weight of cement so as to improve the workability.

3 Experimental Programme

The experimental program consists of packing density and compressive strength properties.

3.1 Packing Density Test

Test method employed in the work was the same as the wet packing method suggested by the Author Kwan [6]. It involves the following steps as first the concrete mix was mixed thoroughly at desired w/c ratio. Then the mix was filled into the container in 3 layers and after filling each layer vibration was applied at constant rate. Finally, the bulk density of the mix was found and from that solid concentration was found. In order to determine the wet packing density, it is necessary to find out the solid concentrations at different w/c ratios to cover the optimum w/c ratio. The initial W/C ratio opted was 0.3. The Super plasticiser was added at a constant dosage of 0.3%. Vibration was provided at a constant rate of 10 s for each layer. The content of the metakaolin was varied from 0 to 20% by volume and the packing density test was conducted.

The solid concentration 'Ø' and voids ratio 'u' can be thus determined as:

$$\text{Solid concentration, } \emptyset = \frac{V_s}{V}$$

where,

V_s Solid volume of the particles (Determined from the W/C ratio and the weight of the mixture).

V Bulk volume of mixture (i.e. Volume of container).

$$Voidratio, u = \frac{1 - \emptyset}{\emptyset}$$

Plotting the solid concentration and voids ratio against the w/c ratio, the maximum solid concentration (i.e. wet packing denisity) and minimum voids ratio can be determined.

3.2 Compressive Strength Test

Compressive strength test was conducted according to IS 516-2000. Metakaolin was varied from 0 to 20% by volume and the compressive strength test results was found for 7 day and 28 day. The samples were designated as MK0, MK5, MK10, MK15, MK20.

4 Results and Discussions

4.1 Packing Density

The wet packing density test was conducted. A typical example of variations of the solid concentration with the w/c ratio obtained during the wet packing density test of a typical concrete mix sample with 0% metakaolin content is given in Fig. 1. From fig it was observed that the solid concentration increases, reaches a maximum and then decreases. The increase in the solid concentration is due to that as the w/c ratio increased, water films get merged, and additional water will be filled into the voids to reduce air interlock. As a result, the solid concentration will be increased. The

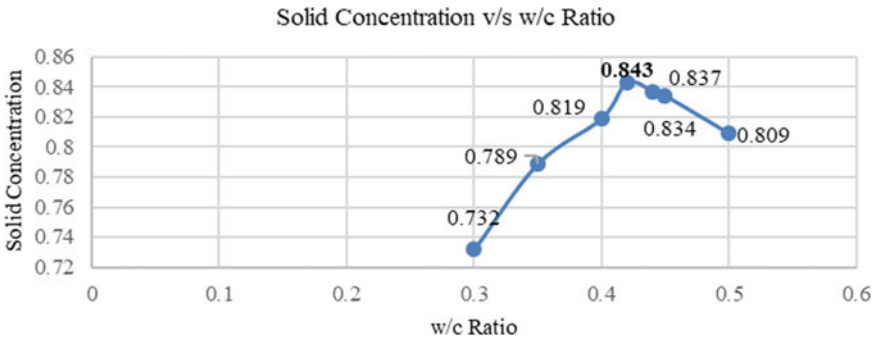

Fig. 1 Solid concentration of concrete mix (0% metakaolin) versus W/C ratio

decrease in the solid concentration is due to that the water added became more than enough to fill up the voids and the solid particles will be dispersed in the water in the form of a suspension, causing the solid concentration to decrease [6].

At w/c ratio lower than the saturation state, the water added is not enough to fill up the voids. So, the air will be entrapped and thus it forms water bridges between the particles. This causes the solid concentration to decrease as the w/c ratio decreases. When the w/c ratio becomes higher than saturation state, a suspension is formed, and the particles will be dispersed in the water. This causes the solid concentration to decrease as the w/c ratio increases. Hence, there is an optimum w/c ratio at which the particles are most closely packed, the voids will be minimum and the solid concentration reaches its maximum value. Therefore, this maximum solid concentration so achieved will be taken as the wet packing density [6].

Packing density results of each mixes are given in Table 6. Results shows that 10% replacement of metakaolin shows the maximum packing density. But even at 15 and 20% replacement the packing density was higher than the 0% replacement mix. The results show that inclusion of the supplementary cementitious materials finer than OPC can be added to fill into the voids to improve the packing density of concrete. From Fig. 2 it was observed that there is an optimum level of replacement for the improving the packing density. The incorporation of high content of fine particles can lead to an increase in the inter particle distance due to the loosening effect of the

Table 6 Packing density results of the various mixes

Replacement % with cement	Solid concentration	Void ratio
0% (M25)	0.843	0.186
5%	0.844	0.185
10%	0.856	0.168
15%	0.852	0.174
20%	0.848	0.179

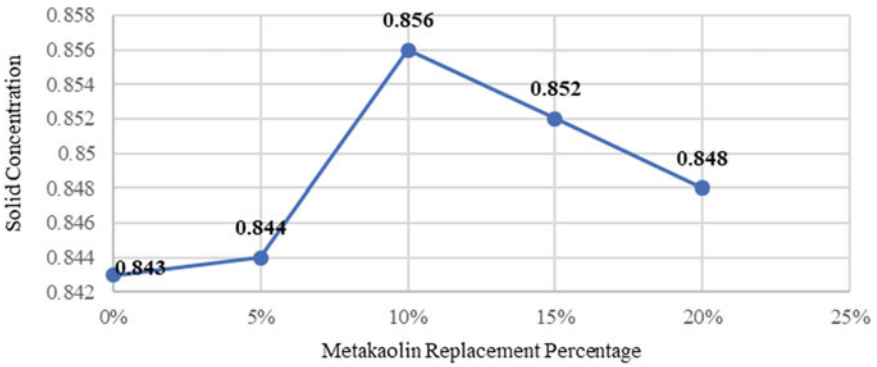

Fig. 2 Solid concentration results of various mixes

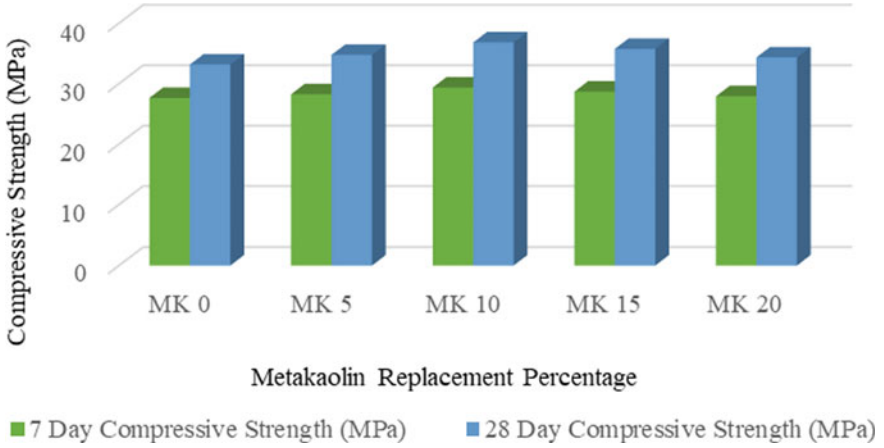

Fig. 3 Compressive strength results of the concrete samples

fine particles. The use of excessive fine particles can push the coarse particles apart and results in lower packing density [4]. At the optimum level thus, the void ratio was reduced 10%.

4.2 Compressive Strength

Compressive strength test results are shown in Fig. 3. Based on the results, the optimum content was determined as 10% and beyond that it decreases. The improvement in the strength is due to the reaction of metakaolin with CH crystals so to create the secondary C-S-H. It contains high amounts of alumina and silica. Metakaolin is finer than OPC and is capable of getting into the smaller voids to increase overall packing [2]. The reduction in strength after 10% of replacement is explained as the result of a clinker dilution effect and due to the high surface area of metakaolin [1].

5 Conclusions

The following conclusions are observed from the experimental study.

- Blending of OPC with supplementary cementitious materials finer than OPC, can be added to fill into the voids so as to improve the packing density.
- Metakaolin increases the packing density of the concrete mixes.
- The packing density of concrete mixes increases with increase in the percentage of metakaolin up to 10% replacement of cement. Beyond the optimum content the packing density of the concrete tends to be decreased.

- At the optimum percentage it was observed that 10% of the void ratio was reduced.
- Metakaolin concrete increases the compressive strength. The strength of the concrete mixes increases with the increase in the metakaolin content up to 10% replacement of the cement. Beyond the optimum content the compressive strength tends to be decreased.
- So, it is clear that the packing density is directly related to the compressive strength.

References

1. Dinakar P, Sahoo PK, Sriram G (2013) Effect of metakaolin content on the properties of high strength concrete. Int J Concr Struct Mater 7(3):215–223
2. Johari MM, Brooks JJ, Kabir S, Rivard P (2011) Influence of supplementary cementitious materials on engineering properties of high strength concrete. Constr Build Mater 25(5):2639–2648
3. Jones MR, Zheng L, Newlands MD (2002) Comparison of particle packing models for proportioning concrete constituents for minimum voids ratio. Mater Struct 35(5):301–309
4. Kwan AKH, Wong HHC (2008) Packing density of cementitious materials: part 2—packing and flow of OPC + PFA + CSF. Mater Struct 41(4):773
5. Kwan AKH, Li LG, Fung WWS (2012) Wet packing of blended fine and coarse aggregate. Mater Struct 45(6):817–828
6. Li LG, Kwan AKH (2014) Packing density of concrete mix under dry and wet conditions. Powder Technol 253:514–521
7. Wong HHC, Albert KHK (2005) Packing density: a key concept for mix design of high-performance concrete. In: Proceedings of the materials science and technology in engineering conference, HKIE materials division, Hong Kong, pp 1–15
8. Wong HHC, Albert KHK (2008) Packing density of cementitious materials: part 1—measurement using a wet packing method. Mater Struct 41(4):689–701

Influence of Alkali Resistant Glass Fiber on the Reduction of Plastic Shrinkage Cracking of Self Compacting Concrete

Anju George and C. A. Abin Thomas

Abstract Plastic shrinkage cracking has become one of the serious problems in concrete elements especially in structures with large surface area/volume ratios and affect the durability of the structure. This paper quantifies the effectiveness of fly ash and alkali resistant (AR) glass fibre on cracking of plastic self compacting concrete. The aim of this experimental work was to study the plastic shrinkage evolution in fly ash based self compacting concrete (SCC) and to examine the effectiveness of alkali glass fibre in SCC to reduce shrinkage cracks. The test was carried out in the mould based on ASTM C1579. At early ages compressive strength of the SCC mixes was similar to that of the reference mix and the maximum strength was observed for 25% replacement by fly ash and is considered as the reference mix. Alkali resistant glass fibres of 12 mm length were added to reference mix of SCC at different dosages of volume fractions of 0.1, 0.2 and 0.3% and the shrinkage test were conducted. The plastic shrinkage test results of Ordinary concrete, reference SCC and SCC mix with various dosages of glass fibre were compared. The SCC mix with AR glass fibre of Volume fraction of 0.2% was found out to be most effective.

Keywords Plastic concrete · Self compacting concrete · Shrinkage crack · Shrinkage · Fly ash · AR glass fibre

1 Introduction

Cracks accelerate the ingress of harmful fluids, impairing the durability of reinforced concrete structures. The earliest crack formation can occur right after concrete placement and compaction, i.e., before initial setting when concrete has lost its fluidity but has not yet achieved any appreciable cohesion [1]. Shrinkage is primarily responsible

A. George (✉) · C. A. Abin Thomas
Department of Civil Engineering, Federal Institute of Science and Technology (FISAT), Ernakulam 68377, India
e-mail: ajgeorgeanju9@gmail.com

C. A. Abin Thomas
e-mail: abinabraham80@gmail.com

© Springer Nature Switzerland AG 2021

K. Dasgupta et al. (eds.), *Proceedings of SECON 2020*,
Lecture Notes in Civil Engineering 97,
https://doi.org/10.1007/978-3-030-55115-5_31

for such failures. Hence a main focus of maintaining a durable structure is based on its shrinkage properties.

Plastic shrinkage may cause early age cracking on the young concrete surface before the setting. This mechanical phenomenon occurs due to rapid and excessive moisture loss, mainly in form of water evaporation. If the evaporation rate is higher than the bleeding rate, the thin water layer that commonly covers the surface of the fresh concrete disappears. The developed shrinkage leads to tensile strain accumulation at the concrete surface. If the tensile strain exceeds the very low early age tensile strain capacity, the young concrete may start to crack [2]. Plastic shrinkage is greater for higher rate of evaporation of water which in turn depends on the air temperature, the concrete temperature, the relative humidity of the air, and wind speed [3]. Since the proportion of aggregate and cement in SCC are relatively low and high, respectively, these factors tend to promote a higher shrinkage of SCC compared to normal concrete [4].

In an experimental investigation carried out by Philippe Turcry et al. [2] examine the plastic shrinkage cracking of self-consolidating concrete (SCC). Five SCC mixtures with compressive strengths were compared to five ordinary concrete (OC) mixtures. For restrained plastic tests, the authors used a mould very similar to ASTM C 1579 mould. Restrained shrinkage tests reveal that SCC tend to have less wider cracks than OC. It shows that SCC could be more vulnerable to shrinkage cracking, especially during setting.

Mirza and Soroushian [5] studied the effect of AR glass fibre on crack and temperature resistance of light weight concrete; they found that inclusion of glass fibre (GF) reduces the crack width and negative effect caused due to temperature. They stated that GF improves the serviceability and durability characteristics of concrete.

The effect of Alkali-resistant (AR) glass fibre (0, 0.03, 0.06 and 0.1%) reinforcement on durability of concrete as explained by Rao et al. [6] found that maximum improvement in durability of concrete was achieved with different percentages of glass fibres at 0.1% for all the grades of concrete. This study focuses on investigating and quantifying the effectiveness of using fly ash on reducing early shrinkage in self compacting concrete and the effect of alkali resistant glass fibre on plastic shrinkage of concrete.

2 Experimental Investigation

2.1 Materials

Ordinary Portland cement (OPC) of 53-grade (IS: 12269, 1987) and commercially available flyash were used as a powder material. The specific gravity of cement is 3.17 with an initial setting time of 92 min and final setting time of 412 min [7]. A poly- carboxylate ether based superplasticiser with a specific gravity of 1.1 is used at a dosage of 0.3–0.8% by weight of cement to improve workability.

Table 1 Physical and chemical properties of fly ash

Physical properties		Chemical compositions	
Specific gravity	2.2	SiO_2	63.8%
Specific surface area	649.9 m^2/kg	Al_2O_3	21.29%
Average particle size	22.2 μm	CaO	2.9%
Form	Powder	Fe_2O_3	0.39%

The fly ash is used as a mineral admixture in this study. It is in dry dense form conforming to IS 3812: 1981. It is gray to brown in colour. Physical and chemical properties of fly ash are presented in Table 1. Cem-FIL Alkali resistant glass fibre with modulus of elasticity 72 GPa, filament diameter 14 μm, length 12 mm, tensile strength 1700 MPa and specific gravity as 2.68 g/cm^3 was used in this work. As per IS 383:1970 the grading for fine aggregate and different zones are provided and the fine aggregate used is manufacture sand belongs to zone 2. Course aggregate used is of 12 mm nominal size.

2.2 Mix Proportion of Normal and SCC Mix

Initially normal M30 mix and control SCC mix was prepared. The fibre reinforced SCC mix was prepared by adding 0.1–0.3% volume fractions (VF) of glass fibre to the optimised SCC. Control mix of characteristic compressive strength 30 N/mm^2 is developed. The mix proportion was done in accordance with IS 10262: 2019 guidelines. Mix proportions with varying fly ash percentage and VF of glass fibre is tabulated in Table 2.

2.3 Assessment of Rheological Properties of the Mix

To ensure the rheological properties of SCC flow ability, passing ability and segregation resistance tests were performed on control SCC and Glass fibre SCC (GFSCC) mixes according to IS 10262:2019 guidelines. Slump flow and T500 slump flow time tests for filling ability, V-funnel test for the viscosity and segregation resistance, L-box test to assess the flow of concrete and passing ability where performed to study the workability of the mix. In case of the normal M30 mix, slump test is performed to determine the workability of the mix.

Table 2 Mix proportions of various mixes

Mix designation	W/P	Fly ash (kg/m^3)	Cement (kg/m^3)	FA (kg/m^3)	CA (kg/m^3)	Water (kg/m^3)	S.P (kg/m^3)	GF (%)	g/m^3
Mn	0.4	–	396	840	1046	178.8	1.584	–	–
M_{F20}	0.43	81.397	325	1200	631	175	3.256	–	–
M_{F25}	0.43	101.741	305.238	1200	631	175	3.256	–	–
M_{F30}	0.43	122.1	284.9	1200	631	175	3.256	–	–
M_{F35}	0.43	98.851	264.54	1200	631	175	3.256	–	–
Mop0.1	0.43	101.741	305.238	1200	631	175	3.256	0.1	373.1
Mop0.2	0.43	101.741	305.238	1200	631	175	3.256	0.2	746.3
Mop0.3	0.43	101.741	305.238	1200	631	175	3.256	0.3	1119.9

Fig. 1 Plastic shrinkage mould

2.4 Plastic Shrinkage Tests

The concrete mixes were poured into the plastic shrinkage mold without any external vibration or compaction. Figure 1 shows the mould for plastic shrinkage measurement is designed and fabricated based on ASTM C1579. Plastic shrinkage is measured using a steel mould of 600 × 200 × 100 mm size with three stress risers [8]. The central riser is with a height of 63.5 mm which is used to provide maximum stress concentration on the central area and promote cracking. The other two risers of height 32 mm each are use to provide restrain in concrete. 10 bolts of 5 mm diameter are provided at both ends to increase the restrain as shown in Fig. 1. The mould was made of cast iron and transparent acrylic sheet is provided on one side to make the crack visible along the depth of mould [1, 9, 10]. During the test the time of occurrence of the initial centre line crack, propagation time of the crack on the concrete surface and the crack width was recorded. The test was conducted in wind condition at 4.5 m/s air flow condition. The temperature and humidity was, respectively, in the range of 26–35 °C and 50–70%.

2.5 Compressive Strength

To determine compressive strength three cubes of size 150 × 150 × 150 mm were casted and tested for each mix. The compressive strength test was performed according to IS: 516, 1959.

Table 3 Rheological properties of the SCC mix

Mix designation	Slump flow (mm)	T_{500} t (s)	V funnel t (s)	L box (H2/H1)
M_{F25}	678	3.7	6.5	0.9
Mop0.1	675	3.95	6.9	0.9
Mop0.2	670	4.12	7.8	0.86
Mop0.3	662	4.5	10	0.82

3 Experimental Results and Discussions

3.1 Rheological Properties of the Mix

For the ordinary concrete sump test is performed and a slump of 100 mm was obtained. The mix falls to a medium workable category (75–100 mm) as per IS 456:2000. The SCC mixes developed satisfied the SF2 category. Addition of glass fibres did not improve the workability and higher dosages tend to reduce the workability of the mix. Table 3 shows the rheological properties of the mix.

3.2 Compressive Strength

The optimum replacement percentage of fly ash to be used is found to be 25% the weight of cement is observed from Fig. 2. As the percentage of fly ash increased, the 7 day strength reduced for the concrete mixes. The 28 day strength of SCC mixes was nearly the same of the same normal mix (Mn) [11, 12]. Since the pozzolonic reactions of supplementary cementitious materials are slow and depend on the calcium hydroxide availability, the strength gain takes longer time for fly ash incorporated concrete mixes [13].

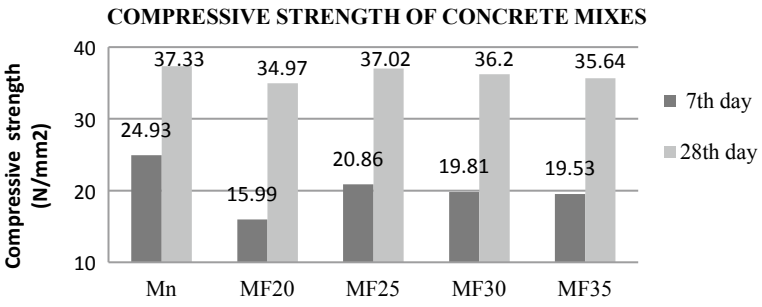

Fig. 2 Compressive strength of concrete mixes with various percentage of fly ash

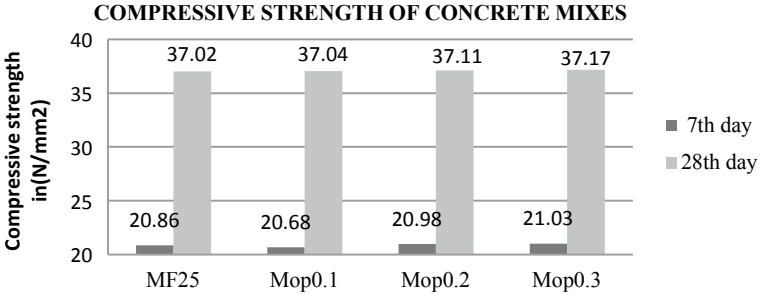

Fig. 3 Compressive strength of concrete mixes with various VF of glass fibre

The low amount of glass fibre incorporated as shown in Fig. 3 cannot be considered as reinforcement and the mechanical behaviour was similar for mixtures with and without fibres. Since all the mixes with fibre show similar strength, the fibre added only act as a local reinforcement [14].

3.3 Plastic Shrinkage

The time of occurrence of the initial centre line crack and the time of propagation of crack indicates the plastic shrinkage behaviour of the concrete.

The time of propagation of crack is taken as the time difference between the time of occurrence of center line full length crack and centre line initial crack. The full length crack of the specimen of concrete formed in mould during testing is shown in Fig. 4. The crack development is observed with the naked eyes. Time of occurrence of centre line initial crack and time for crack propagation of SCC mix with fly ash alone, SCC with glass fibre and that of normal M30 mix is tabulated in Table 5.

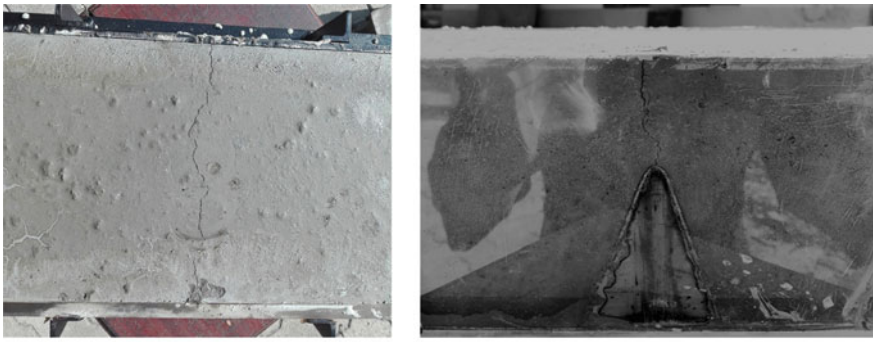

Fig. 4 **a** Top view and **b** side view of full length crack evolution in specimen

Table 5 Plastic shrinkage behaviour of various concrete mixes

Specimen	Volume fraction of AR-GF (%)	Time for initial crack (min)	Time for full length crack (min)	Time for crack propagation (min)	Crack width (mm)
Mn	0.0	94	127	33	0.4
Mop	0.0	154	188	34	0.5
Mop0.1	0.1	195	240	45	0.1
Mop0.2	0.2	210	–	–	0.08
Mop0.3	0.3	213	–	–	0.08

'–' indicates that the full length crack has not been developed till the final setting time. The observation for cracks is terminated on reaching the final setting time

Table 5 shows that the mix of normal M30 concrete without fly ash showed a faster initial centerline crack where as the mix of SCC with fly ash alone showed delayed initial centre line crack but the crack propagation was fast [3, 15]. The plastic shrinkage test performed in the windy condition revealed that SCC tends to have less cracking than OC. Because of its fluid consistency, SCC is thought to have a greater strain capacity than OC in fresh state. It also indicates the lower bleeding rate of SCC than OC.

Based on the compressive strength of various mixes with varying percentage of fly ash content, the mix with 25% replacement is considered as the optimum mix for SCC and this mix is opted as reference mix for testing shrinkage with various volume fractions of Alkali Resistant glass fibre.

With this mix as the reference mix, various volume fractions of 0.1, 0.2 and 0.3% of AR glass fibre were conducted as shown in Fig. 5. It can be observed that compared to the reference mix the time taken by glass fibre incorporated SCC to develop initial crack is more. It can also be observed that the propagation of crack also took more

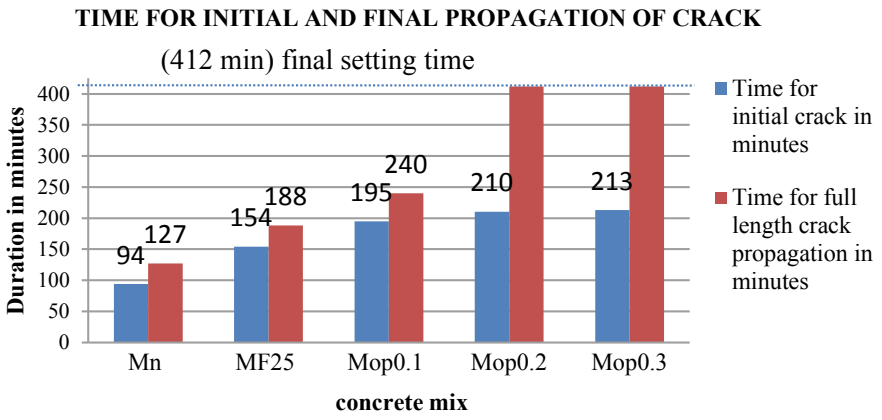

Fig. 5 Time for initial and final propagation of crack

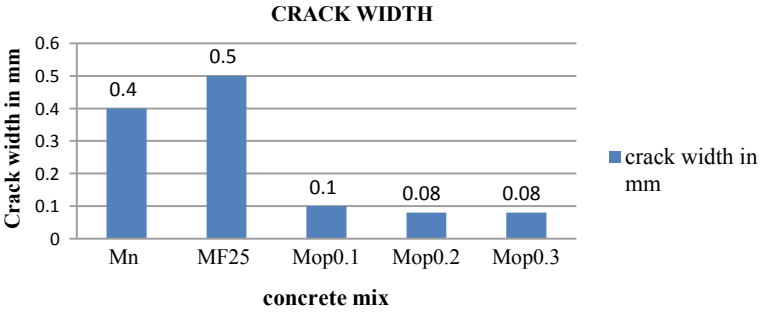

Fig. 6 Crack width of different mixes

time. The width of the crack considerably reduces compared to the reference mix. At higher dosages the duration for crack development also increases.

The time taken for 0.2 and 0.3% GF are at the same range. It was also observed that a full length crack was not developed at 0.2 and 0.3% GF. Independently to the type or amount of glass fibre, the inclusion of glass fibre produced a similar reduction of maximum crack length. In all the mixtures studied; the inclusion of AR-glass fibres reduced the cracked area and the maximum crack length. Larger amounts of fibre did not show an increase of cracking control efficiency [16]. The delayed crack occurrence can be inferred as a positive effect of supplementary cementitious materials and AR glass fibre on the plastic shrinkage of concrete.

The crack width is measured with the help of a hand held microscope. It can be observed that the crack width considerably reduces when AR glass fibre is incorporated. Figure 6 shows the crack width of different mixes. When considering Mop 0.2 and Mop 0.3 they both show the same crack width. Therefore, there is not a linear relationship between fibre amount and cracking control efficiency. Hence percentage around 0.2% can be considered as optimum for the crack control. The orientation of crack fibre can also play an important role in crack reduction. The fibres that align perpendicular to the crack can arrest the crack from further propagation. The results of maximum cracking time pointed out that low amount of the AR-glass fibres studied can control cracking due to plastic shrinkage at early ages, acting as a local reinforcement when concrete cracks [14].

4 Conclusions

In this paper, the effect of using fly ash and alkali resistant glass fibre on controlling the plastic shrinkage cracks in SCC are studied. Plastic shrinkage tests were conducted on normal M30 mix (Mn), SCC mixes with 25 % fly ash alone (Mop) and SCC mix with varying VF of Glass fibres (0.1%, 0.2% and 0.3%). From the experimental investigation it can be concluded that, the delay on the beginning of plastic shrinkage registered in SCC samples, with regard to standard concrete, pointed to a delay of

SCC bleeding. SCC with fly ash alone showed delayed initial centre line crack but the crack propagation was fast. Fibre added acted as a local reinforcement and reduced the plastic shrinkage, i.e.; the maximum crack length and crack width was considerably reduced. There is not a linear relationship between fibre amount and cracking control efficiency and a volume fraction of 0.2% is considered as the optimum dosage. Adding more volume of GF in concrete reduces the workability of SCC and had no significant effect on the compressive strength.

References

1. Sayahi F, Emborg M, Hedlund H (2017) Plastic shrinkage cracking in concrete—influence of test methods. In: 2nd international RILEM/COST conference on early age cracking and serviceability in cement-based materials and structures—EAC2 12–14 September 2017, ULB-VUB, Brussels, Belgium
2. Turcry P, Loukili A (2006) Evaluation of plastic shrinkage cracking of self-consolidating concrete. ACI Mater J 103-M30:272–279
3. Brooks J (2015) "Shrinkage of concrete". Concrete and masonry movements 22(6):137–185. https://doi.org/10.1016/B978-0-12-801525-4.00006-6
4. Kristiawan SA, Taib M, Aditya M (2015) Effect of high volume fly ash on shrinkage of self-compacting concrete. Procedia Eng 125(2015):705–712
5. Mirza FA, Soroushian P (2002) Effects of alkali-resistant glass fibre inforcement on crack and temperature resistance of lightweight concrete. Cem Concr Compos 24:223–227
6. Rao PS, Mouli KC, Sekhar TS (2012) Durability studies on glass fibre reinforced concrete. J Civ Eng Sci 1:37–42
7. IS: 4031-(1996) Method of physical tests for hydraulic cement—specification. Bureau of Indian Standards, New Delhi (March)
8. Arya EK, James JS, John E (2020) Study on the effectiveness of shrinkage reducing admixtures on plastic shrinkage of concrete. In: Proceedings of SECON'19. SECON 2019. Lecture Notes in Civil Engineering, vol 46. Springer, Cham
9. Combrinch R, Ateyl L, Boshoff WP (2018) Interaction between settlement and shrinkage cracking in plastic concrete. Constr Build Mater 185:1–11
10. Combrinck R, Boshoff WP (2013) Typical plastic shrinkage cracking behaviour of concrete. Magaz. Concr. Res. 65(8):486–493
11. Haque MN, Kayali O (1998) Properties of high strength concrete using fine fly ash. Cem Concr Res 28:1445–1452
12. McCarthy MJ, Dhir RK (1999) Towards maximising the use of fly ash as a binder. Fuel 78:121–132
13. Zhao Y, Gong J, Zhao S (2017) Experimental study on shrinkage of HPC containing fly ash and ground granulated blast-furnace slag. Constr Build Mater 155(2017):145–153
14. Barluenga G, Hernandez-Olivares F (2007) Cracking control of concretes modified with short AR-glass fibres at early age. Experimental results on standard concrete and SCC. Cem Concr Res 37:1624–1638
15. Altoubat S, Junaid MT, Leblouba M, Badran D (2017) Effectiveness of fly ash on the restrained shrinkage cracking resistance of self-compacting concrete. Cement and Concr Compos 79:9e20
16. Sivakumar VR, Kavitha OR, Prince Arulraj G, Srisanthi VG (2017) An experimental study on combined effects of glass fibre and Metakaolin on the rheological, mechanical, and durability properties of self-compacting concrete. Appl Clay Sci 0169–1317

Development of Bricks Using Plastic Wastes

Gouri S. Kumar and S. Sreerath

Abstract Modern world is facing a serious situation of waste management, especially plastic waste. There has been a considerable imbalance between the availability of conventional building materials and their demand in the recent past. On the other hand various type of sands such as foundry sand are abundantly available and the disposal of waste plastics (Poly Ethylene Terephthalate, Poly Propylene etc.) is a biggest challenge, as repeated recycling of PET bottles pose a potential danger of being transformed to a carcinogenic material and only a small proportion of PET bottles are being recycled. In the present study, the effectiveness of PET bottles on manufacturing of bricks is analyzed and properties of plastic-soil bricks are assessed. PET bottles are melted and into this molten plastic mix, sand is added in various proportions. Plastic-soil bricks using M sand and as well as foundry sand are manufactured. Various standard tests on bricks are conducted as per IS 3495 (Parts 1–4) such as compressive strength test, water absorption test, efflorescence test, hardness test, soundness test, impact test, thermal resistance test, prism Test. Through the results obtained from the standard tests, the optimum percentage of plastic is estimated. It is studied that plastic-soil bricks show excellent behavior when compared to conventional burnt clay bricks.

Keywords Waste management · PET · Foundry sand

1 Introduction

Plastic is one of the recent engineering materials which have many good characteristics which include versatility, lightness, hardness, resistance to chemicals, water and impact. It consists of a wide range of synthetic or semi-synthetic organic compounds

G. S. Kumar (✉) · S. Sreerath
Department of Civil Engineering, Federal Institute of Science and Technology (FISAT), Ernakulam 683577, India
e-mail: gouriskumar96@gmail.com

S. Sreerath
e-mail: iamsreerath@gmail.com

© Springer Nature Switzerland AG 2021

K. Dasgupta et al. (eds.), *Proceedings of SECON 2020*,
Lecture Notes in Civil Engineering 97,
https://doi.org/10.1007/978-3-030-55115-5_32

that are malleable and can be molded into different solid objects. Plastic can be made to different shapes when they are heated. Solid waste management, especially the huge quantity of waste plastics has become one of the major environmental concerns nowadays. Plastic is one of the daily increasing useful as well as a hazardous material. At the time of need, plastic is found to be very useful but after its use, it is simply thrown away and thus creating all kinds of hazards. They are non-biodegradable and can remain on earth for 4500 years without degradation. In India approximately 40 million tons of the municipal solid waste is generated annually, with evaluated increasing at a rate of 1.5–2% every year [1]. Accumulation of such wastes can result into hazardous effects to both human and plant life. Hence these plastics are to be effectively utilized. Today it is impossible for any vital sector to work efficiently without usage of plastic starting from agriculture to industries [2]. Thus we cannot prohibit the use of plastic. So reusability of plastic should be the better option [3]. Waste foundry sand is a byproduct from the production of both ferrous and nonferrous metal castings. It is high quality silica sand. Disposal of this is a big problem thus reusing it for construction is better option [4]. The idea of plastic-soil brick is observed to be feasible through various studies. Compressive strength of plastic-soil bricks of specific proportions are shown to be higher than conventional bricks and water absorption of these bricks are observed to be negligible [2, 5]. It is also studied that plastic-soil bricks are far more economical than conventional bricks [4]. The present research is performed to study the properties of bricks manufactured by mixing sand and Poly Ethylene Terephthalate (PET) bottles. This study is mainly focused on obtaining information regarding the suitability of such plastic-soil bricks for use in construction industry.

2 Experimental Investigation

2.1 Methodology

Materials used are PET bottles, sand and bitumen. A mould of size 20 × 10 × 10 cm is prepared. The plastic bottles are turned into molten form by using stones and firewood. The drum is placed over the above setup and then the plastic bottles are added to the drum one by one and the sand is added to it when it turns into hot liquid according to various proportions as shown in Table 1. The sand added is mixed thoroughly using rod and trowel before it hardens. At the final stage bitumen is added in the range of 2% by weight of sand in molten form to the plastic-soil mix. These mixtures are then poured into the brick mould and they are compacted using steel rod and surface is finished using trowel. The brick can be easily demoulded by just lifting the wooden mould after 30 min (Fig. 1) [6, 7].

Table 1 Proportion of plastic, sand and bitumen

Plastic-soil ratio	Plastic (g)	Sand (g)	Bitumen (2% by weight of soil in g)
1:2	1620	3240	64.8
1:3	1080	3240	64.8
1:4	810	3240	64.8
1:5	648	3240	64.8
1:6	540	3240	64.8

Fig. 1 **a** Cleaning and shredding of PET bottles. **b** Melting of plastic. **c** Addition and mixing of sand and bitumen. **d** Compaction of brick using steel rod. **e** Prepared brick

2.2 Mix Proportion

Various proportions of plastic, soil and bitumen used are shown.

After the preparation of brick specimens 24 h of air cooling was adopted. Various tests adopted for this study are Compressive strength test, Water absorption test, Prism test, Efflorescence test, Hardness test, Soundness test, Impact test and Thermal resistance test. For each tests 3 samples were used and the average was taken as the final result.

Table 2 Average compressive strength of plastic-M sand bricks of ratio 1:4

Days of water curing	Average compressive strength (N/mm^2)
3 days	11.20
7 days	11.65
28 days	11.83
24 h of air cooling	11.74

3 Results and Discussions

3.1 Effect of Water Curing on Strength of Plastic-Soil Bricks

To study the effect of water curing on the compressive strength of plastic-soil bricks, compressive strength test was conducted for plastic-M sand brick of ratio 1:4 after 3, 7 and 28 days of water curing and also after 24 h of air cooling.

Table 2 shows that there is not much effect of water cooling on compressive strength of plastic-soil bricks. So 24 h of air cooling is adopted.

3.2 Compressive Strength

The average compressive strength of various proportions of plastic-soil bricks is shown in Table 3. Based on the results obtained it is clear that plastic-soil bricks of ratio 1:4 with 2% bitumen have higher compressive strength compared to burnt clay bricks. It shows that as the plastic content increases, the compressive strength increases up to a certain limit and then decreases. This may be due to the decrease in adhesive strength between plastic and sand. It seems that bonding between plastic particles and sand is weak after certain limit as the increase in plastic content might

Table 3 Compressive strength of Plastic-M-sand bricks and Plastic-Foundry sand bricks

Sample	Bitumen (% by weight of M-sand)	Average compressive strength (Plastic-M sand) (N/mm^2)	Average compressive strength (Plastic-foundry sand) (N/mm^2)
1:2	2	7.83	6.88
1:3	2	8.5	7.9
1:4	2	11.74	9.99
1:5	2	10.06	8.11
1:6	2	8.08	7.10
Normal burnt clay bricks		8.85	8.85

Table 4 Water absorption of plastic-M sand bricks and Plastic-Foundry sand bricks

Sample	Bitumen (% by weight of foundry sand)	Water absorption (%)–Plastic-M sand bricks	Water absorption (%)–Plastic-foundry sand bricks
1:2	2	2.5	1.42
1:3	2	2.09	1.26
1:4	2	1.16	0.71
1:5	2	1.53	1.02
1:6	2	2.63	1.54
Normal burnt clay bricks		13.01	13.01

have caused the brick to be much flexible, which in turn reduces its compressive strength. The compressive strength of plastic-soil bricks using M sand is higher than the compressive strength of plastic-soil bricks using foundry sand. However foundry sand bricks are having compressive strength greater than that of normal burnt clay bricks so they are a cheaper alternative to plastic-M sand bricks since foundry sand is abundantly available waste sand.

3.3 Water Absorption

Water absorption for different ratios of plastic-soil bricks were determined and are shown in Table 4. From table it is clear that water absorption value is least for plastic-soil brick of ratio 1:4 with 2% of bitumen in both M sand bricks and foundry sand bricks compared to normal burnt clay bricks. The percentage reduction of water absorption compared to burnt clay bricks in plastic-M sand brick is 92.4% and in plastic-foundry sand brick is 95.3%. So water absorption test showed excellent performance of plastic-soil bricks.

3.4 Prism Test

Prism test was done for mortar ratio 1:3 for Plastic-M-sand bricks and Plastic-Foundry sand bricks of ratios 1:4 with 2% bitumen and it was compared with that of the burnt clay bricks. The Compressive strength test results of Plastic-soil bricks and normal burnt clay bricks masonry prisms are tabulated in Table 5. The masonry prisms shown in Fig. 2 consists of 3 bricks stacked with a mortar thickness of 12 mm. Therefore the total height of prism will be above 30 cm. The h/t ratio of the prism is 3.1 which indicate the requirement of correction factor as per IS: 1905-1987.

Table 5 Compressive strength of masonry prisms

Mix designation	Compressive strength (N/mm^2)
PM3 masonry prism	11.5
PF3 masonry prism	9.7
Normal burnt clay brick masonry prism	7.2

Fig. 2 Masonry prism of plastic-M-sand bricks, Plastic-Foundry sand bricks and normal burnt clay bricks

It is observed that the compressive strength of plastic-M-sand masonry prism and Plastic-foundry sand masonry prism is greater than that of burnt clay brick masonry prism. Hence, plastic-soil bricks can be used as a substitute for burnt clay bricks for the construction of walls [8].

3.5 Efflorescence Test

The efflorescence test showed an excellent performance on the plastic-soil bricks. There was no formation of grey or white layer on the brick surface. From this test we can conclude that no traces of alkalis were presented in this plastic-soil brick whereas the burnt clay bricks showed a slight deposit of alkali on the brick surface [2].

3.6 Hardness Test

In this test, a scratch was made on brick surfaces. This test was carried out for all proportion of bricks. While the scratch was made with the help of a finger nail on

the bricks, no impression was left on the sand brick surface whereas the burnt clay bricks showed a light impression on the brick surface [9].

3.7 Soundness Test

In this test, two bricks from same proportion were taken and they were struck with each other. The bricks were not broken and a clear ringing sound was produced same as that of burnt clay bricks. So the bricks are good [2].

3.8 Impact Test

In this test, the bricks were made to drop from a height of 1 m on one of its corner. If the bricks are broken, it indicates low impact value and not acceptable for construction work. The plastic-soil bricks were not broken or shattered and it indicates the brick are of good quality [2].

3.9 Thermal Resistance Test

The Plastic-M sand bricks and Plastic-Foundry sand bricks of ratio 1:4 with 2% bitumen were kept in the oven at 100 °C for 24 h and then the compressive strength for the bricks were determined [2]. The compressive strength of the plastic-M sand brick was found to be 10.5 N/mm^2. The compressive strength of the plastic-foundry sand brick was found to be 8.9 N/mm^2. The compressive strength of burnt clay bricks after thermal resistance test was found to be 8.11 N/mm^2. Hence both the bricks show the same reduction in compressive strength which is about 10% [10].

4 Cost Analysis

4.1 Labour Cost

Labours required	
(1) Head mason	1/10
(2) Mazdoor	1/3
(3) Bristi	1/2

(continued)

(continued)

Labours required	
Head mason rate	₹471/day
Labour rate	₹377/day
One labour can manufacture	300 bricks [4]
So, labour cost per unit bricks	1367/900 = ₹1.5/brick

4.2 Transportation Cost

M-Sand

Density of M-Sand	1788.07 kg/m^3
Volume of truck	14.5 m^3
Rate for 1 trip of truck	₹4000
Cost of transport of M-sand	4000/25927.02 = ₹0.15/kg
M-sand required for 1 brick	3.240 kg
Cost of transport of M-sand	0.15 × 3.240 ₹0.486/brick

Foundry sand

Density of foundry sand	2590 kg/m^3
Volume of truck	14.5 m^3
Rate for 1 trip of truck	₹4000
Cost of transport of foundry sand	4000/37555 = ₹0.1/kg = 0.1 × 1.68 = ₹0.16/brick
Foundry-sand required for 1 brick	3.240 kg
Cost of transport of foundry-sand	0.1 × 3.240 ₹0.324/brick

Bitumen

Rate of Bitumen	₹20/kg
Bitumen Required for 1 Brick	0.064 kg
Cost of Bitumen	20 × 0.064 = ₹1.28/brick

PET bottles

Quantity of PET bottles filled in a truck	3000 kg
Cost of transport of PET bottles	4000/3000 = ₹1.3/kg
PET bottles required for 1 brick	1.620 kg
Cost of transport of PET bottles	1.3 × 1.620 = ₹2.1/brick

Firewood Cost

Rate of firewood	₹5000/tones
Firewood required	0.2 tones per 1000 bricks
Cost of firewood for 1000 bricks	5000 × 0.2 = ₹1000
Cost of firewood	1000/1000 = ₹1/brick

4.3 Total Cost of Bricks

Cost of M sand brick	1.5 + 0.486 +1.28 + 2.1 + 1 = ₹6.36/brick
Cost of foundry sand brick	1.5 + 0.324 +1.28 + 2.1 + 1 = ₹6.2/brick
Cost of burnt clay brick of same size	₹8/brick

5 Conclusions

Plastic-soil bricks possess more advantages than burnt clay bricks and it is cost effective. The efficient usage of waste plastic has resulted in effective usage of plastic waste and thereby can solve the problem of safe disposal of plastics.

- Brick made with 1:4 ratio of Plastic to M-sand gives a compressive strength of 11.74 N/mm^2 and that of plastic-foundry sand is 9.99 N/mm^2, which is greater than normal burnt clay bricks. It can be used as a permanent structure in the construction of walls.
- The water absorption for the brick is almost negligible. There was less amount of water absorption for all the ratios of plastic-soil bricks and is least for ratio 1:4. Water absorption of plastic-soil brick is 98.2% less than burnt clay bricks.
- The compressive strength of masonry prism made of plastic-M-sand bricks and masonry prism made of plastic-foundry sand bricks were found to be more than compressive strength of conventional brick masonry prism. Hence, plastic-soil

bricks can be used as a substitute for burnt clay bricks for the construction of walls.

- We know that the cost of burnt clay brick is ₹8/brick. Cost of plastic-soil brick is around ₹6/brick. So it is economical than burnt clay bricks [4].
- The efflorescence test showed an excellent performance on the plastic-soil bricks as there were no traces of alkalis present. Thermal Resistance test was satisfactory as both the bricks showed the same reduction in compressive strength.

References

1. Thirugnanasambantham N, Tharun Kumar P, Sujithra R, Selvaraman R, Bharathi P (2017) Manufacturing and testing of plastic sand bricks. Int J Sci Eng Res (IJ0SER) 5(4)
2. Aiswaria K, Abdulla K (2018) Manufacturing and experimental investigation of bricks with plastic and M-Sand. Int J Innovat Res Sci Eng Technol 7(6)
3. Singh L, Boss Singh P, Thokchom S (2017) Manufacturing bricks from sand and waste plastics. In: National conference on innovations in science and technology (NCIST-17), 5(3)
4. Manjarekar AS, Ravi D. Gulpatil, Patil VP, Nikam RS, Jeur CM (2017) Utilization of plastic waste in foundry sand bricks. Int J Res Appl Sci Eng Technol (IJRASET) 5(3)
5. Keerti MN, Patel J, Soragavi N, Biradar S, Yashwanta R (2016) Plastic-soil bricks. IJSRD—Int J Sci Res Dev 4(8)
6. Sahu MK, Singh L (2017) Critical review on types of bricks type 14: plastic sand bricks. Int J Mech Product Eng 5(11)
7. Mahajan P, Girase D, Lokhande AR (2018) Plastic-soil bricks substituting traditional bricks. Int J Res Appl Sci Eng Technol (IJRASET) 6(1)
8. Thaickavil NN, Thomas J (2018) Behaviour and strength assessment of masonry prisms. Case Stud Construct Mater pp 23–38
9. Dinesh S, Dinesh A, Kirubakaran K (2016) Utilization of waste plastic in manufacturing of bricks and paver blocks. Int J Appl Eng Res 11(3)
10. Miruthula G, Kokila L, BalaMurugan G (2016) Experimental investigation on plastic-soil bricks. Int J Eng Sci Comput 6(4)

Stabilization of Lateritic Soil Using Natural Fibres

B Krishnendu and Anjana Bhasi

Abstract Numerous ground improvement techniques have been used to stabilize marginal soils to make it more feasible for construction purposes. Soil reinforcement using natural fibres is increasingly preferred as they are sustainable, readily available and inexpensive. This study aims at improving the engineering properties of lateritic soil using the natural coir fibres as reinforcement material. Laboratory tests such as UCS test and direct shear test have been carried out to evaluate the effect of various fibre parameters such as fibre content and fibre length on the engineering properties of soil. Results showed significant improvement in the strength characteristics of lateritic soil after the addition of coir fibres. Optimum fibre parameters that contributed to the enhanced performance of soil were also identified.

Keywords Lateritic soil · Coir fibres · UCS test

1 Introduction

Lands used for construction purpose should be such that the structure constructed over it should not undergo excessive settlement or any kind of damages. Various techniques have been used to improve the properties of weak soils to enable them to withstand the different loading conditions. Reinforcement using fibres, geosynthetics, different ground improvement techniques, soil nailing etc. are some of the techniques.

Vidal [1] first introduced the concept of using reinforcements for improving the properties of soil. Reinforcing soil using natural fibres is carried out from ancient times. Compared to geosynthetics, soil—fibre mix is easy to prepare, and chances of development of potential weak planes are less. Coir, jute, palm etc. are some of the widely used natural fibres.

B. Krishnendu (✉) · A. Bhasi
Department of Civil Engineering, National Institute of Technology Calicut, Calicut, Kerala 673601, India
e-mail: krishnendu993@gmail.com

A. Bhasi
e-mail: anjanabhasi@nitc.ac.in

© Springer Nature Switzerland AG 2021

K. Dasgupta et al. (eds.), *Proceedings of SECON 2020*,
Lecture Notes in Civil Engineering 97,
https://doi.org/10.1007/978-3-030-55115-5_33

Prabakar and Sridhar [2] studied the effect of randomly distributed sisal fibre on the strength behaviour of c-ϕ soils by conducting various laboratory tests. It was observed that cohesion increased with an increase in fibre content up to a certain value, beyond which cohesion reduced, and angle of internal friction showed non-linear variation. Sivakumar et al. [3] conducted triaxial tests on coir fibre reinforced expansive soil and concluded that deviator stress increased with increase in fibre content and diameter. The increase in fibre content also increased cohesion and angle of internal friction of the composite soil. Jamellodin et al. [4] studied the effect of oil palm fibre on the strength behaviour of soil by conducting compaction and triaxial compression tests at varying fibre contents. The study concluded that increase in fibre content increased the cohesion up to a particular value of fibre content, beyond which it decreased. Angle of internal friction showed little variations at different fibre contents. Wang et al. [5] conducted laboratory tests to assess the strength improvement of expansive soil treated with jute fibres and concluded that jute fibres are effective in improving the strength parameters of expansive soil. It was observed that certain fibre parameters significantly influenced the strength improvement. These parameters were found to be fibre content, fibre length and fibre orientation.

This study focuses on improving the engineering properties of lateritic soil using natural coir fibres. The current work also assesses the strength improvement and the optimum fibre parameters that contribute to it.

2 Materials and Methods

2.1 Soil

Lateritic soil was collected from Vallithode, near Iritty in Kannur district of Kerala. This area is frequently prone to landslides. Index and engineering properties of soil were tested based on SP 36 (Part 1)—1987 of the Indian Standard (IS) specifications. Properties of the soil are listed in Table 1.

2.2 Fibres

Coir fibres were supplied by Go Green products. Figure 1 shows the coir fibres used as reinforcement. Properties of the coir fibres are listed in Table 2. Fibres were cut into three different lengths, namely 10, 20 and 30 mm (Fig. 1a–c).

Table 1 Properties of lateritic soil

Properties	Value
Specific gravity	2.7
Liquid limit (%)	46.45
Plastic limit (%)	27.05
Shrinkage limit (%)	15.7
Plasticity index	19.4
Optimum moisture content (%)	20.7
Maximum dry density (g/cm^3)	1.615
Unconfined compressive strength (kPa)	152.55
Cohesion (kPa)	76.27

Fig. 1 Coir fibres: **a** 10 mm; **b** 20 mm; **c** 30 mm

Table 2 Physical properties of coir fibres

Property	Value
Diameter (mm)	0.25
Density (g/cm^3)	0.71

2.3 Tests on Soil Mixed with Fibres

2.3.1 Determination of OMC and MDD

Soil-fibre mixes were prepared at three different fibre contents (0.3, 0.6 and 0.9%) and three different fibre lengths (10, 20 and 30 mm). Light compaction tests were carried out on all nine soil fibre mixes as per IS 2720: Part 7, to find out the optimum moisture content and maximum dry density in each case. Fibres were randomly mixed with dry soil thoroughly, and then the required amount of water was added.

Soil was again mixed properly. Soil fibre mix was filled into the mould in three layers, and each layer was tamped 25 times using a hammer of 2.6 kg weight and 310 mm height of fall.

2.3.2 Unconfined Compression Test

Specimens for unconfined compression test were prepared using the optimum moisture content and maximum dry density values obtained from the compaction test. Cylindrical samples of 3.8 cm diameter and 7.6 cm height were prepared. The rate of applied strain was 1.5 mm/min.

2.3.3 Direct Shear Test

Direct shear tests were conducted on all different soil fibre mixes to find out the effect of fibre content and fibre length on angle of internal friction of soil. Samples were prepared at optimum moisture content and maximum dry density.

3 Results and Discussion

3.1 Variation of OMC and MDD

As shown in Table 3, optimum moisture content and maximum dry density showed considerable variation with different fibre content and length.

Table 3 OMC and MDD for different soil samples

Soil	OMC (%)	MDD (g/cm^3)
Plain soil	20.7	1.615
Soil + 0.3% 10 mm fibre	21.5	1.605
Soil + 0.6% 10 mm fibre	21.9	1.59
Soil + 0.9% 10 mm fibre	22.2	1.585
Soil + 0.3% 20 mm fibre	21.8	1.595
Soil + 0.6% 20 mm fibre	22	1.58
Soil + 0.9% 20 mm fibre	22.3	1.57
Soil + 0.3% 30 mm fibre	22.1	1.57
Soil + 0.6% 30 mm fibre	22.2	1.565
Soil + 0.9% 30 mm fibre	23.6	1.555

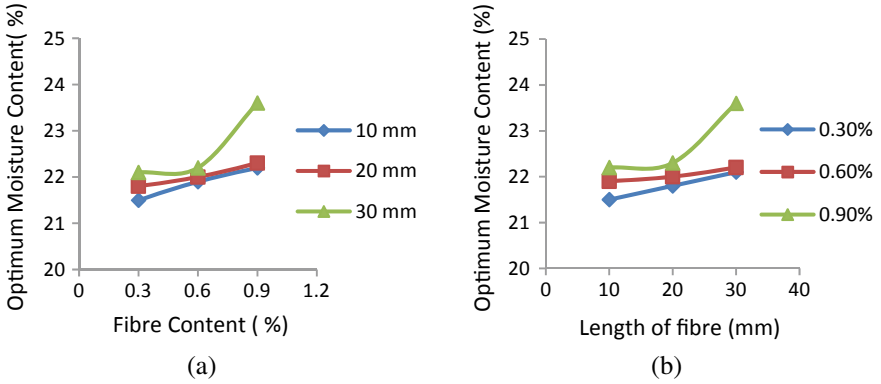

Fig. 2 Variation of OMC with **a** fibre content and **b** fibre length

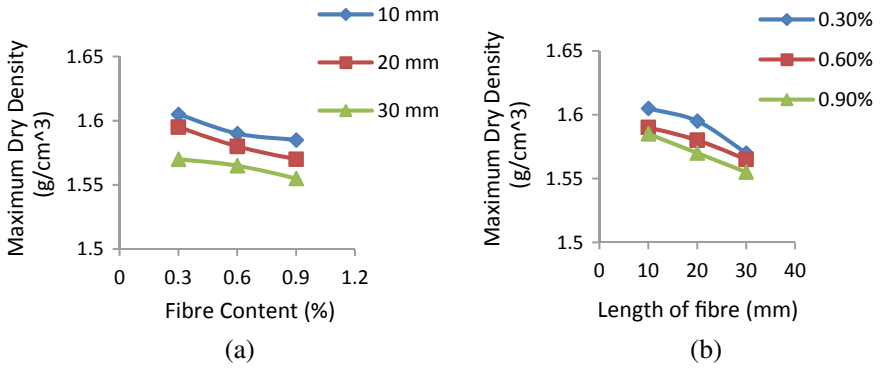

Fig. 3 Variation of MDD with **a** fibre content and **b** fibre length

It was observed that the addition of coir fibres increased the optimum moisture content. This increase in moisture content is due to the absorption of water by the fibres. Figure 2 shows the variation of OMC with different fibre content and length.

Maximum dry density decreased with increase in fibre content and length. This decrease can be attributed to the replacement of soil particles by lightweight fibres. Figure 3 shows the variation of maximum dry density with different fibre contents and lengths.

3.2 Effect of Fibre Content and Fibre Length on UCS Value

Soil mixed with 10 mm long fibres showed higher unconfined compressive strength (UCS) and cohesion compared to plain soil for a fibre content of 0.3 and 0.6% whereas the values did not show much variation for 0.9%. For soil samples mixed

with 20 mm long fibres, UCS value increased only for 0.6% fibre content. For 0.3% fibre content, strength values did not show much variation, and for 0.9%, it was lower than that of plain soil. For soil samples mixed with 30 mm long fibres, UCS value increased for only 0.6%. For 0.3 and 0.9%, the values were lower as compared to plain soil. For all three fibre lengths, maximum UCS values were obtained for 0.6%. Among the three different lengths, the maximum strength value was obtained for soil mixed with 10 mm long fibres. Higher fibre content results in higher replacement of soil particles by fibres. Kinking of fibres is also likely to occur at higher length and content. This lead to fibres forming lumps or bundles inside the soil matrix and not getting properly and uniformly mixed. These can be reasons for the reduction in strength of soil samples mixed with longer fibres at higher contents. Figures 4 and 5 shows variation of unconfined compressive strength and cohesion for various soil—fibre mixes.

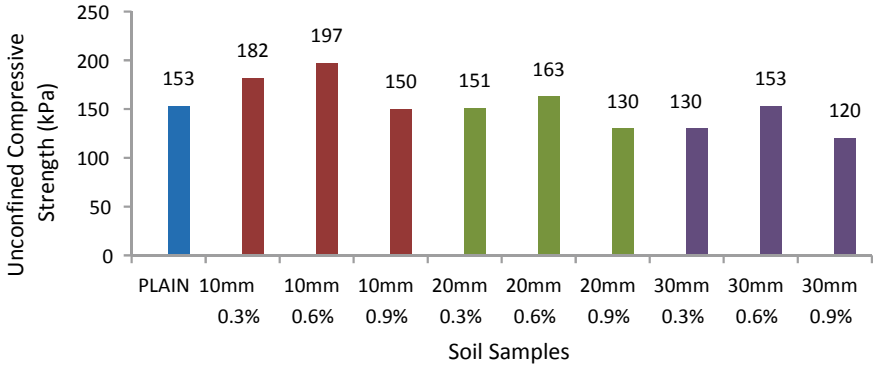

Fig. 4 Variation of unconfined compressive strength

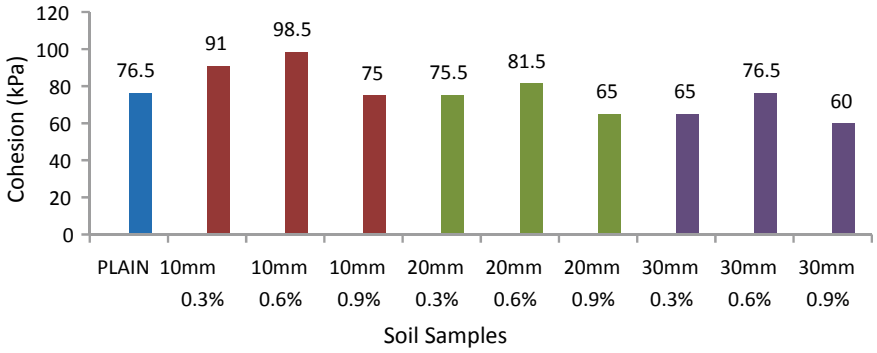

Fig. 5 Variation of cohesion

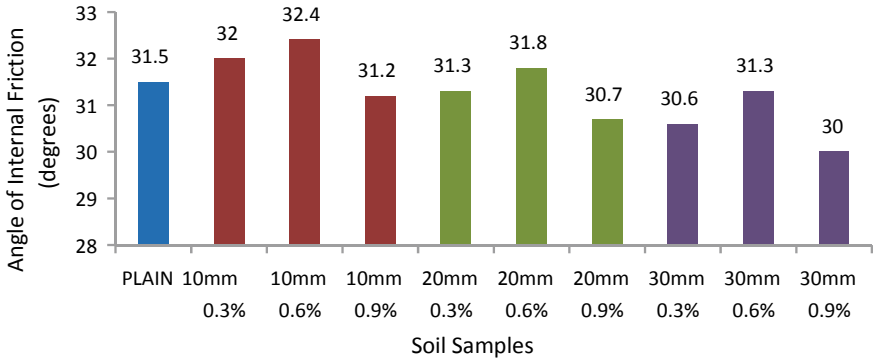

Fig. 6 Variation of angle of internal friction

3.3 Effect of Fibre Content and Fibre Length on Angle of Internal Friction

Angle of internal friction did not show much variation with increase in fibre content or fibre length. The maximum friction angle value obtained was 32.4° for soil mixed with 10 mm long fibres at 0.6% by weight of soil. The values obtained for all soil-fibre mixes were between 30° and 32.4°. For a particular fibre length (say 10 mm), angle of internal friction increased till 0.6% beyond which the value reduced. This same trend was observed for 20 and 30 mm long fibres also. The variation of the angle of internal friction is shown in Fig. 6.

4 Conclusions

The major conclusions that can be drawn from the current study are as follows:

- Lateritic soil reinforced with coir fibres showed good improvement in engineering properties.
- Fibre parameters such as length and content had a significant influence in improving the properties of lateritic soil. Maximum improvement was observed for soil sample reinforced with 10 mm long coir fibres at 0.6% by weight of soil.
- Addition of coir fibres resulted in an increase in the unconfined compressive strength and cohesion of soil, whereas the angle of internal friction showed near-zero variation.

References

1. Vidal H (1969) The principle of reinforced earth. Highway Res Rec 282:1–16
2. Prabakar J, Sridhar RS (2002) Effect of random inclusion of sisal fibre on strength behaviour of soil. Constr Build Mater 16(2):123–131
3. Sivakumar Babu GL, Vasudevan AK (2008) Strength and stiffness response of coir fibre reinforced tropical soil. J Mater Civ Eng 20(9):571–577
4. Jamellodin Z, Talib ZA, Kolop R, Md Noor N (2010) The effect of oil palm fibre on strength behaviour of soil. In: Proceedings of the 3rd SANREM conference
5. Wang Y-X, Guo P-P, Ren W-X, Yuan B-X (2017) Laboratory investigation on strength characteristics of expansive soil treated with jute fiber reinforcement. Int J Geomech 17(11):52–63

Clogging Resistant Pervious Block

M. V. Akshara and M. Preethi

Abstract In recent years, Pervious Concrete (PC) has been increasingly promoted as an effective sustainable drainage system to mitigate surface flooding in urban areas. However, the pore structure of PC can become clogged by sediment particles and its ability to drain storm-water runoff gradually decreases. Therefore an alternative to PC, which is resistant to clogging, should be developed. This Clogging Resistant Pervious pavement block (CRP) was prepared by introducing straight pore channels of varying numbers into mortar for obtaining different porosity. Flexible pipes were introduced to 1:2 mortar mixes for developing straight pore channels in the mortar cubes. Mortar cubes of porosity starting from 1 to 6% were casted. Optimum porosity was determined by permeability test using falling head permeability apparatus and compression test. Optimum porosity was obtained at 4% porosity for CRP. This innovative system will help alleviate urban flooding and contribute towards a more sustainable urbanization.

Keywords Clogging · PC · Porosity · Permeability

1 Introduction

The impervious nature of the conventional pavement systems has resulted in flash floods. In recent years, PC has been increasingly promoted to mitigate surface flooding. PC is a popular type of permeable pavement as it has the ability to transport large volumes of water through the porous structure of the material. However, the pore structure of PC can become clogged. Therefore, it is important to develop Clogging Resistant Pervious pavement block. One approach is to engineer a pore structure that is uniform and has low tortuosity. The overall aim of this study was

M. V. Akshara (✉) · M. Preethi
Department of Civil Engineering, Federal Institute of Science and Technology (FISAT), Ernakulam 683577, India
e-mail: akshara.mv2912@gmail.com

M. Preethi
e-mail: preethiml83@gmail.com

© Springer Nature Switzerland AG 2021

K. Dasgupta et al. (eds.), *Proceedings of SECON 2020*,
Lecture Notes in Civil Engineering 97,
https://doi.org/10.1007/978-3-030-55115-5_34

the development of a new permeable pavement system as an alternative to PC which is more durable, less prone to clogging and does not require frequent maintenance [1–5].

2 Objectives of the Study

1. Developing permeable pavement as an alternative to PC with low tortuosity pore structure that is not only resistant to clogging, but also has high permeability and strength.
2. Determine the permeability and strength characteristics of Clogging Resistant Pervious pavement block and compare it with PC and pavement block (PB).

3 Literature Review

Alalea Kia, Hong S. Wong, Christopher R. Cheeseman studied clogging potential for permeable concrete.

This paper reports on different clogging test methods used to determine the performance of permeable concrete. It involves applying flowing water containing sand and/or clay in cycles through the sample and measuring the change in flow rate. When simultaneously exposed to sand and clay all samples were showing reduction in permeability. This was due to the adhering of flocculated clay to surface of sand particles and this caused increased clogging.

Alalea Kia, Hong S. Wong, Christopher R. Cheeseman studied clogging in permeable concrete.

This paper reviews the clogging mechanism in permeable concrete. Permeable concrete requires regular maintenance by vacuum sweeping and pressure washing, but the effectiveness and viability of these methods was questionable. In this paper it is concluded that the greater potential for clogging in permeable concrete was related to the tortuosity of the connected porosity.

Alalea Kia, Hong S. Wong, Christopher R. Cheeseman defined clogging potential for permeable concrete.

This paper compares a set of laboratory prepared permeable concretes with close packed glass spheres and aggregate particles of varying size and commercial permeable concretes. They are exposed to different clogging methods to understand this clogging phenomenon. It involves applying flowing water containing sand and/or clay in cycles through the sample and measuring the change in permeability. All samples showed greater permeability reductions when exposed to sand and clay simultaneously. Based on measuring the initial permeability decay, half-life cycle and number of cycles to full clogging these were the three methods used to define clogging potential.

Alalea Kia, Hong S. Wong, Christopher R. Cheeseman prepared a paper on control of clogging in conventional permeable concrete and development a new high strength clogging resistant permeable concrete pavement.

In this study, a new type of permeable concrete that can be poured on-site to form a low tortuosity microstructure that is not only resistant to clogging, but also has high permeability and strength is developed. This newly developed permeable concrete was prepared by introducing straight pore channels of varying size and number into self-compacting mortar. Samples with porosity ranging from 11 to 32% were tested. In all cases, permeability and compressive strength were substantially higher than conventional permeable concrete.

4 Experimental

4.1 Sample Preparation

CRP are made by using 1:2 mortar mix of Zone II fine aggregates at a w/c ratio of 0.4 with porosity (P) ranging from 1 to 6%. For developing pores in CRP, plastic tubes of dia 6 mm were introduced into mortar in varying number according to the porosity. Plastic tubes were held in place by using specially prepared mould in which steel rods are welded at the base plate. Cylindrical specimens and cubes with target porosity ranging from 1 to 6% P were made. Optimum porosity was decided by testing permeability and compressive strength [2–5] (Fig. 1).

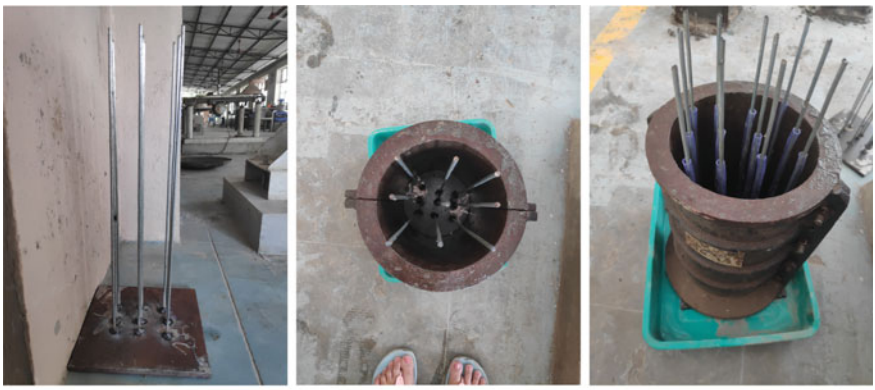

Fig. 1 Mould prepared by welding steel rods on base plate

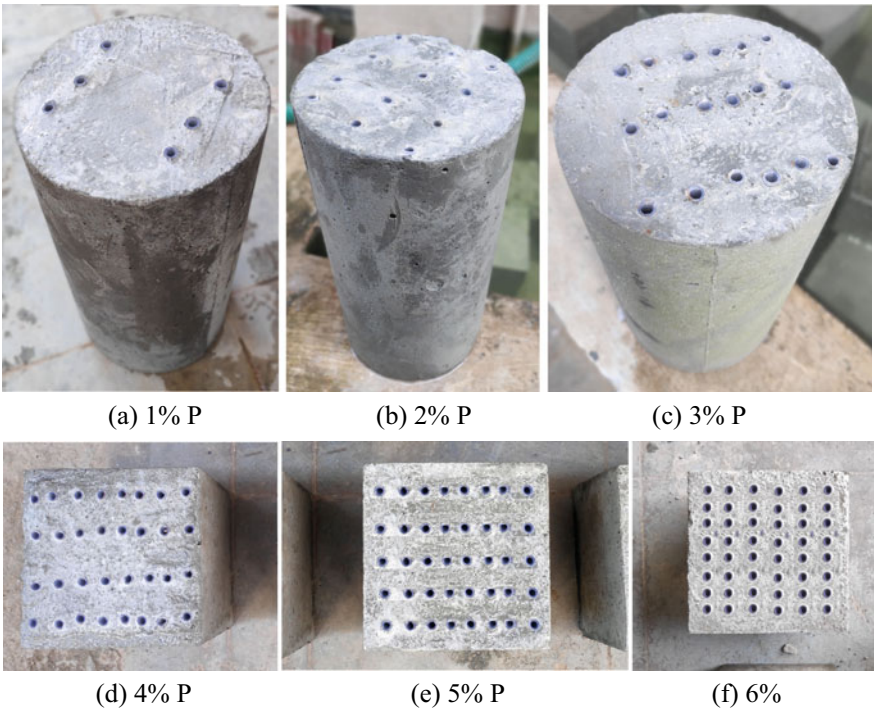

(a) 1% P (b) 2% P (c) 3% P

(d) 4% P (e) 5% P (f) 6%

Fig. 2 CRP samples containing straight pore channels (plastic tubes) of varying number in self-compacting mortar to achieve porosity ranging from 1 to 6%

4.2 Porosity

Porosity (Ø) of CRP was calculated from by the equation:

$$\emptyset = \left[\frac{(V_p \times n)}{V_c} \right] \times 100$$

where V_p is the volume of each pore (plastic tube), n is the number of pores and Vc is the volume of the cylindrical sample (m^3) [1] (Fig. 2; Table 1).

4.3 Permeability

A falling head permeability setup was used to measure permeability. The test was conducted as per ACI 522R 10 (Fig. 3).

For each sample, permeability (k, cm/s) was determined as per Darcy's law:

Table 1 Mix compositions of CRP

Mix	Porosity (%)	No of tubes
CRP 1	1	6
CRP 2	2	12
CRP 3	3	18
CRP 4	4	25
CRP 5	5	30
CRP 6	6	38

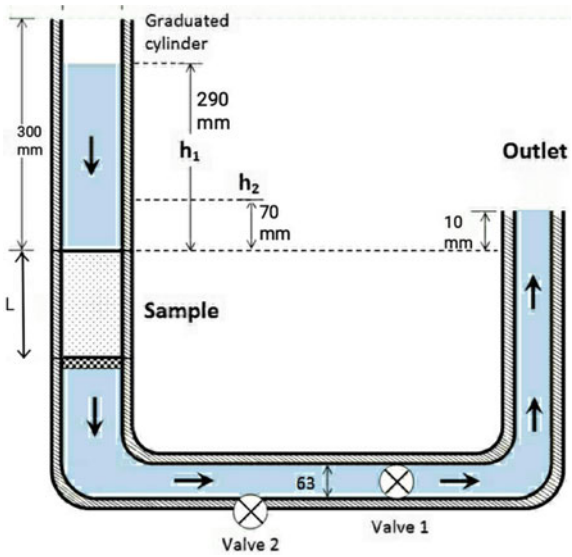

Fig. 3 Falling head permeability cell

$$k = \frac{2.303 \times a \times L \times \log\left(\frac{h1}{h2}\right)}{A \times t}$$

K is the permeability coefficient, (cm/s), t is the time, (s), a is the cross-sectional area of the specimen, (cm^2), A is the cross-sectional area of the calibrated cylinder, (cm^2), h_1 and h_2 are the initial water head and final water head, (cm), L is the length of the specimen, (cm) [1, 6].

Table 2 Permeability values obtained for CRP with varying percentage of porosity

PC mix	Specimen	Time, t (s)	Permeability, k (cm/s)	Average permeability(cm/s)
CRP 1	1	1093.57	0.039	0.045
	2	947.76	0.045	
	3	820.17	0.052	
CRP 2	1	656.14	0.065	0.074
	2	520.11	0.082	
	3	561.17	0.076	
CRP 3	1	380.79	0.112	0.112
	2	325.56	0.131	
	3	448.93	0.095	
CRP 4	1	191.25	0.223	0.226
	2	194.74	0.219	
	3	180.71	0.236	
CRP 5	1	94.56	0.451	0.457
	2	92.11	0.463	
	3	93.12	0.458	
CRP 6	1	61.90	0.689	0.688
	2	65.21	0.654	
	3	59.15	0.721	

5 Results and Discussion

5.1 Permeability

As per ACI 522R-10 permeability of PC varies from 0.14 to 1.22 cm/s this is taken as required permeability for CRP since it is developed as an alternative to PC (Table 2).

Here the permeability value of both 4, 5 and 6% comes in the range.

5.2 Compressive Strength

As expected the compressive strength was inversely proportional to porosity (Fig. 4).

As per ACI 522R-10 the compressive strength of PC is between 2.8 and 28 MPa and compressive strength of all CRP samples comes in this range [6, 7].

CRP with 4, 5 and 6% P satisfies the permeability range and all CRP satisfies the compressive strength range also considering that compressive strength is inversely proportional to the porosity CRP samples with maximum compressive strength and

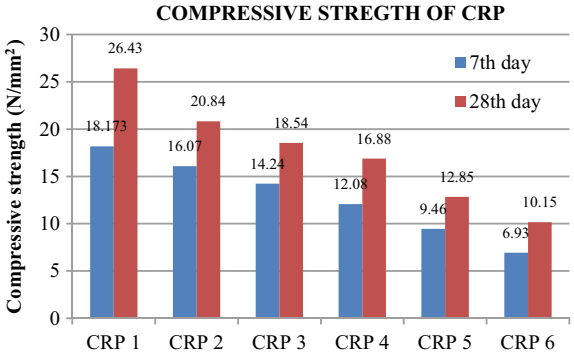

Fig. 4 Compressive strength of CRP after 7th and 28th day of curing

that comes in the permeability range should be taken as optimum percentage porosity. Therefore 4% P CRP was taken as optimum.

6 Preparing PC for Comparison

Since CRP is developed as an alternative to PC they should be compared in order to make sure that CRP is more favorable than PC. For comparing, the percentage porosity of both should be equal but according to ACI 522R 10 the range of porosity for PC was 15–30%. Therefore a PC mix was developed by assuming the porosity as 16% which satisfies the permeability range of PC and then the porosity of mix were reduced by replacing coarse aggregate with fine aggregate till the porosity becomes 4%. Percentage of voids where determined by standard proctor hammer [8] (Tables 3, 4).

At 25% replacement of coarse aggregate with fine aggregate the porosity of PC was obtained as 4%. Therefore it was taken for comparison.

Table 3 PC mix proportion

Sl. No	Mix	% of fines	Cement (kg)	Coarse aggregates (kg)	Fine aggregates (kg)	Water (kg)
1	PC1	0	411.51	1478.7	0	141
2	PC2	5	411.51	1404.77	73.93	141
3	PC3	10	411.51	1330.83	147.87	141
4	PC4	15	411.51	1256.9	221.80	141
5	PC5	20	411.51	1182.96	295.74	141
6	PC6	25	411.51	1109.025	369.67	141

Table 4 Percentage of voids in PC mixes with varying percentage of fine aggregates

Sl. No.	PC mix	Theoretical density, T (kg/m^3)	Experimental density, D (kg/m^3)	Percentage of voids (%)
1	PC1	2504.23	2109.77	15.75
2	PC2	2502.11	2161.23	13.62
3	PC3	2500	2202.40	11.904
4	PC4	2497.25	2284.73	8.51
5	PC5	2498.73	2332.76	6.64
6	PC6	2490.29	2380.76	4.39

Table 5 Permeability values obtained for PC with 4% of porosity

PC mix	Specimen	Time, t (s	Permeability, k (cm/s)	Average permeability (cm/s)
PC	1	2030.91	0.021	0.017
	2	2665.57	0.016	
	3	2843.28	0.015	

6.1 Permeability

See Table 5.

6.2 Compressive Strength

See Table 6.

7 Comparison of Parameters

In this investigation CRP was compared with PC of same porosity and with pavement blocks (PB). Pavement blocks were purchased from manufacturing shops (Figs. 5 and 6).

Table 6 Compressive strength of PC with 4% porosity after 7th and 28th day of curing

PC	7th day compressive Strength (MPa)	28th day compressive Strength (MPa)
	8.90	10.36

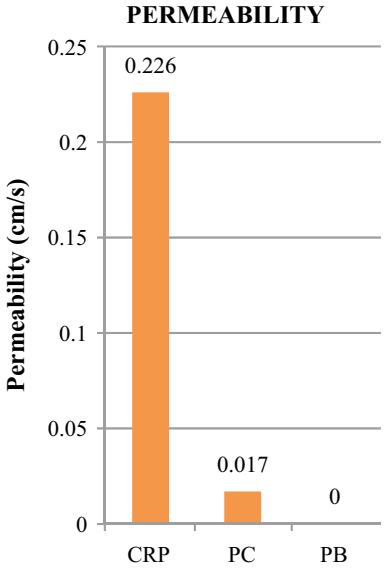

Fig. 5 Permeability of CRP,PC, PB

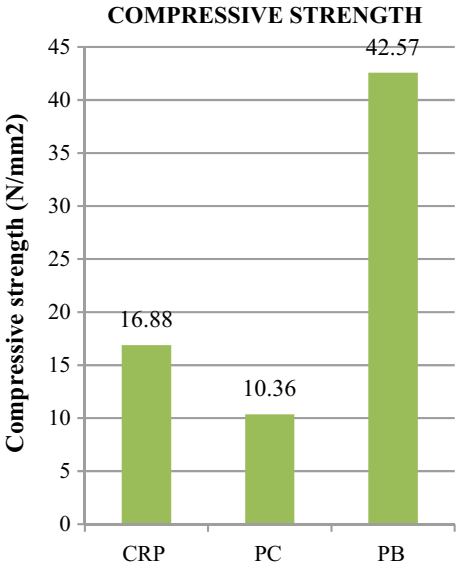

Fig. 6 Compressive strength of CRP, PC, PB

7.1 Permeability and Compressive Strength

The permeability of CRP was about 1229.41% greater than that of PC at equal porosity. Therefore it can be concluded that for similar porosities, the permeability's of CRP are about an order of magnitude larger than that of PC samples. The compressive strength of CRP was about 62.93% greater than that of PC at equal porosity. Therefore it can be concluded that for similar porosities, compressive strength of CRP are much larger than that of PC samples. Compressive strength of PB was 152.19% greater than that of CRP but it was zero permeable.

8 Field Test for CRP and PC

Field test was conducted by embedding one cylinder from both CRP and PC in the parking lot of my college. The specimens were embedded in the ground such that at least one wheel load passes over the specimens. After 30 days, the specimens were taken out and permeability was calculated.

Sample	Permeability before field test (cm/s)	Permeability after field test (cm/s)
CRP	0.226	0.0226
PC	0.017	0.009

From field test it was observed that there was no change in the permeability for CRP, but there is a significant reduction in permeability of PC. This shows that at equal porosity the CRP specimen remained without clogging and PC specimen clogged after 30 days field test.

9 Conclusion

- At equivalent porosity, the permeability of CRP was 1229.41% greater than conventional PC. This was due to the difference in pore structure of PC. The pores in PC have a complex structure with variable cross-sections and random interconnectivity. Due to its high permeability CRP will greatly enhance the ability of engineers and urban planners to mitigate against urban flooding and in the long term will allow the design and deployment of a new generation of flood resistant infrastructure.
- At equivalent porosity, the compressive strength of CRP was 62.93% greater than that of conventional PC. This was due to the higher cement paste content, the porosity distribution and the lack of coarse aggregate in CRP. Whereas the compressive strength of pavement block was 152.19% greater than that of CRP but it was zero permeable.

- Since CRP has greater compressive strength than PC it can be laid in the pavements with lesser thickness than the thickness required for PC to achieve the same strength. This will result in a reduction of the overall consumption of materials and time.
- After 30 days field test it was observed that the CRP specimen remained without clogging and PC specimen was clogged. This shows that CRP specimens doesn't undergo clogging as rapidly as PC specimens therefore it doesn't require frequent maintenance as that of PC. Since the maintenance of such pavements is quiet costly CRP becomes more economical.
- CRP can be engineered with low porosity (4%) to achieve high compressive strength (16.88 MPa) and high permeability (0.226 cm/s), but does not clog after field test. The development of a high-strength Clogging Resistant Pervious pavement will reduce the need for time consuming and expensive maintenance, a significant advantage over conventional permeable pavements, which will reduce the long-term operational cost of the system. CRP can be cast on-site to achieve uniform pore structure. It retains high porosity and permeability for storm-water to infiltrate throughout, while having high compressive strength suitable for use in lightly loaded pavements.
- From the above points it can be concluded that CRP is a better and more economical alternative to PC.

References

1. Kia A, Wong HS, Cheeseman CR (2019) High-strength clogging resistant permeable pavement. Int J Pavement Eng
2. Kia A, Wong HS, Cheeseman CR (2017) Clogging in permeable concrete: a review. J Env Manage
3. Kia A, Wong HS, Cheeseman CR (2018) Defining clogging potential for permeable concrete. J. Environ Manage
4. Kia A, Wong HS, Cheeseman CR (2018) Control of clogging in conventional permeable concrete and development of a new high strength clogging resistant permeable concrete pavement. J. Environ Manage
5. Kia A, Wong HS, Cheeseman CR (2017) Clogging potential of permeable concrete. J Environ Manage
6. ACI 522R 10 (2010) Report on PC. American Concrete Institute
7. ASTM C39 Standard test method for compressive strength of cylindrical concrete specimen
8. ASTM C1688 Standard test method for density and void content of freshly mixed PC. American Society for Testing and Materials

Analytical Study of Timber-Concrete Composite (TCC) Beam Using Different Interlocking Joints

K. S. Sandra and P. R. Reshmi

Abstract Timber Concrete Composite (TCC) beam is a structural technique widely used for strength and stiffness upgrading of new and existing timber floors, bridges, buildings etc. The main reason for this development is the advantages it offers in terms of higher stiffness, lighter weight, and cost effective compared to RC beams. A TCC beam comprises a concrete slab connected to a timber beam by means of shear connectors. The shear connectors resist the shear and plays a critical role in TCC beam by connecting and introducing a composite action between the upper concrete slab and lower timber beam. Hence to ensure and improve this composite action, a better connection of timber and concrete along with shear connectors is necessary. In this study, a new connection system is introduced in the form of interlockings between timber and concrete. The behavior of TCC beam with interlockings of types rectangular and dovetail joints is analysed using ANSYS 16.1 and the best connection system is selected based upon the load deflection behavior, the relative slip between concrete and timber as well as direct stress on shear connectors of TCC beam. Further TCC beam under longitudinal non-prismatic condition is also studied with the best connection system. From the results obtained it was concluded that TCC beam with dovetail joint of tenon angle 60° is the best joint. Also TCC beam under non prismatic condition with central rise 50 mm showed better performance in terms of load carrying capacity and deflection.

Keywords Shear connectors · Composite action · Slip

K. S. Sandra (✉) · P. R. Reshmi
Department of Civil Engineering, Sree Narayana Gurukulam College of Engineering, Ernakulam, Kerala, India
e-mail: sandraks5991@gmail.com

P. R. Reshmi
e-mail: reshmipr555@gmail.com

© Springer Nature Switzerland AG 2021

K. Dasgupta et al. (eds.), *Proceedings of SECON 2020*,
Lecture Notes in Civil Engineering 97,
https://doi.org/10.1007/978-3-030-55115-5_35

1 Introduction

Composite construction technology are becoming more popular in construction industries nowadays with the introduction of newer construction materials and technical know-how of integrating different materials for achieving desired engineering properties. Timber Concrete Composite (TCC) beam is one such composite construction technology which utilises the complimentary properties of both concrete and timber. The concrete slab, which has high compressive strength, resists the compressive force and the timber web which has good tensile resistance, resists the tensile force [1]. The concrete slab and the timber beam are connected by shear connectors that transfer the shear force between the two materials. The shear connectors play the most important role in a TCC beam by connecting and inducing slab to beam composite action. Hence a proper connection of shear connectors with timber and concrete is necessary to enhance this composite action.

Different types of connection system has been introduced. Zhang et al. [1], studied the use of a new connection system in the form of a hardwood layer in a prefabricated timber–concrete composite (TCC) beam. The hardwood layer was glued to the top of a timber web to reinforce a dowel type connection. From the study it was found that using this hardwood layer between timber and concrete can enhance the composite action and can increase the slip modulus of shear connectors. Yeoh et al. [2] conducted an experimental tests of notched and plate connectors for LVL-Concrete composite beams. From this study, a 300 mm long rectangular reinforced notch connection was selected as the best connection due to the high strength and slip modulus, while a 2×333 mm toothed metal plate connection appeared to be the most practical and labor cost effective since it does not involve any notching. Also it was found that none of the notched connections exhibited a brittle failure due to the use of a lag screw, whereas a brittle failure was observed in the toothed metal plate connection characterized by tearing of the plate. Khorsandnia et al. [3] studied performance of TCC beam with fasteners such as normal wood screws (NS), SFS Intec screws (SFS) and bird-mouth notch coach screw (BM). It was found that NS had a quite brittle behavior and SFS showed low ductility after the peak load. A fairly ductile response was seen in BM before the failure point and hence BM was suggested when more ductile behavior is needed. From Auclair et al. [4] study, a new elongated composite connector was developed for timber concrete composite structure. The stiffness and strength of the connection depends on the external and internal diameters of the connector and it was found that the elongated connector diameters control the deflection and the structural ductility.

In this study TCC beam with new connection system in the form of interlocking of types dovetail joints (with tenon angle 45° and 60°) and rectangular joints (with tenon angle 90°) between timber and concrete of TCC beam have been modelled using ANSYS 16.1 software and are compared with each other. Further TCC beam under longitudinal non prismatic condition is also modelled with the best connection system and the performance is studied.

2 Numerical Study of TCC Beam with Interlocking Joints

The analytical study includes the development of finite element models to evaluate the performance of a TCC beam with interlocking joints of types dovetail joint and rectangular joint. The model includes a 6000 mm long TCC beam with concrete slab of 800 mm width and 60 mm depth. The timber used for the study was LVL (Laminated Veneer Lumber) of 400 mm depth and 126 mm width. The shear connectors used were M20 × 240 mm arranged in a single row. The spacing of shear connectors were selected as per Zhang et al. [1]. The beam is simply supported by two roller supports. Steel mesh of 8 mm diameter is incorporated in concrete slab to prevent cracking. The material properties assigned to the model are presented in Table 1. TCC beam is developed with dovetail joint of tenon angle (45° and 60°) and rectangular joints with tenon angle 90°. A schematic view of the model is shown in Fig. 1. The dimensions of dovetail and rectangular joint are shown in Table 2. Figure 2 presents the cross sectional view of TCC beam with interlocking joints.

Further the TCC beam is modelled under non prismatic condition with the best joint selected. Non prismatic TCC beam is developed by choosing the central rise (V1) of timber beam as 50, 100 and 150 mm and dimension of concrete slab taken as same as that of prismatic TCC beam. A longitudinal view of non prismatic TCC beam is shown in Fig. 3. Performance of prismatic and non prismatic TCC beam is evaluated in terms of load carrying capacity, relative slip between timber and concrete and direct stress on shear connectors.

Table 1 Material properties

Materials	Modulus of elasticity (MPa)	Yield strength (MPa)	Poisons ratio
Concrete	2.7×10^4	4.17	0.15
Timber	1.35×10^4	49	0.2
Shear connectors	2×10^5	250	0.3

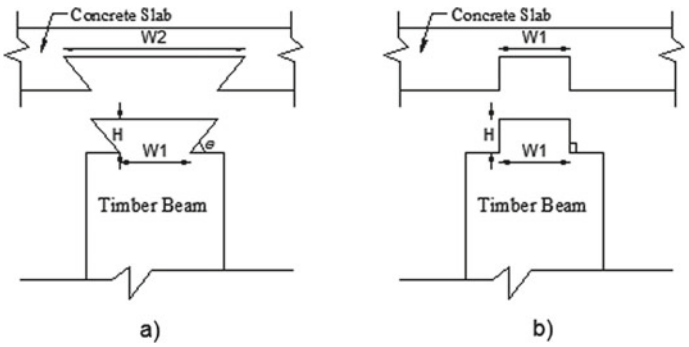

Fig. 1 Schematic view of the model drawn in AutoCAD **a)** Dovetail joint **b)** Rectangular joint

Table 2 Dimensions of joints

Types of interlocking	Neck width W1 (mm)	Head width W2 (mm)	Neck length H (mm)	Tenon angle ϴ
Dovetail joint	75	85	10	45°and 60°
Rectangular joint	75	75	10	90°

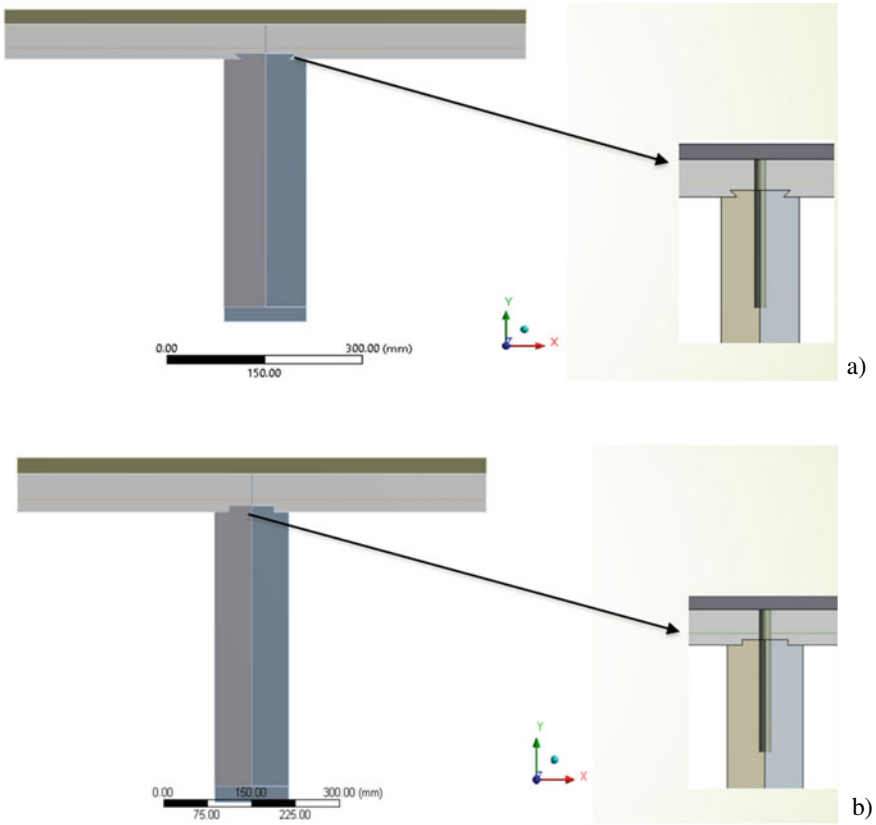

Fig. 2 TCC beam with interlocking joints **a)** Dovetail joint **b)** Rectangular joint

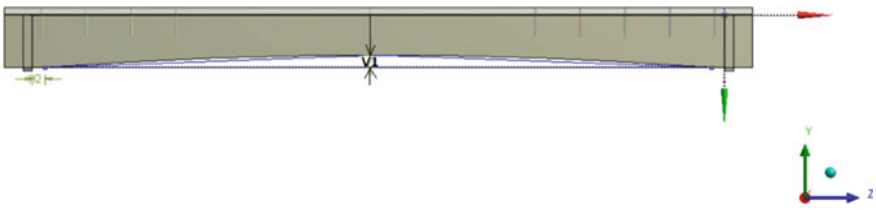

Fig. 3 Longitudinal view of non prismatic TCC beam (where V1 = central rise)

3 Results and Discussion

The results of numerical analysis such as load carrying capacity, deflection, relative slip between timber and concrete as well as the direct stress on shear connectors are shown in Table 3. The load versus deflection graph is shown in Fig. 4. It can be concluded that TCC beam with interlocking joints showed better performance compared to TCC beam without joints in terms of load carrying capacity and direct stress on shear connectors. Presence of interlocking joints induced a better composite action thus reducing the direct stress on shear connectors. Load carrying capacity of TCC beam with dovetail joint of tenon angle 60° was found to be 337.34 kN with a maximum deflection value of 84.62 mm shown in Fig. 5. TCC beam with dovetail joint with tenon angle 60° showed a 18.4% increase in load carrying capacity compared to beam without joints. A minor difference in values was obtained between dovetail joint as well as rectangular joint. However load carrying capacity for tenon angle 60° was found higher compared to the other. Hence dovetail joint with tenon angle 60° was selected as the best joint. An increase in relative slip as well as direct stress value was observed for dovetail joint with tenon angle 60°. This can be attributed to the fact that as the load carrying capacity increased, the relative slip

Table 3 Comparison of results Of TCC beam with joints

Types of interlocking	Tenon angle ϴ	Ultimate load (kN)	Maximum deflection (mm)	Maximum slip (mm)	Direct stress on connectors (MPa)
No joint	–	284.93	81.11	7.70	187.18
Dovetail joint	45°	333.65	84.29	7.02	97.96
Dovetail joint	60°	337.34	84.62	8.06	100.89
Rectangular joint	90°	328.62	84.50	8.03	98.82

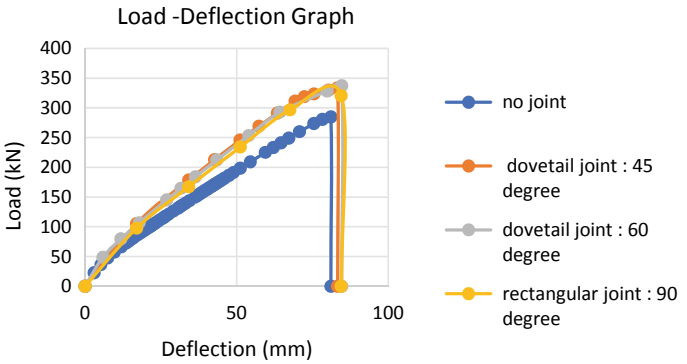

Fig. 4 Load-deflection graph of TCC beam

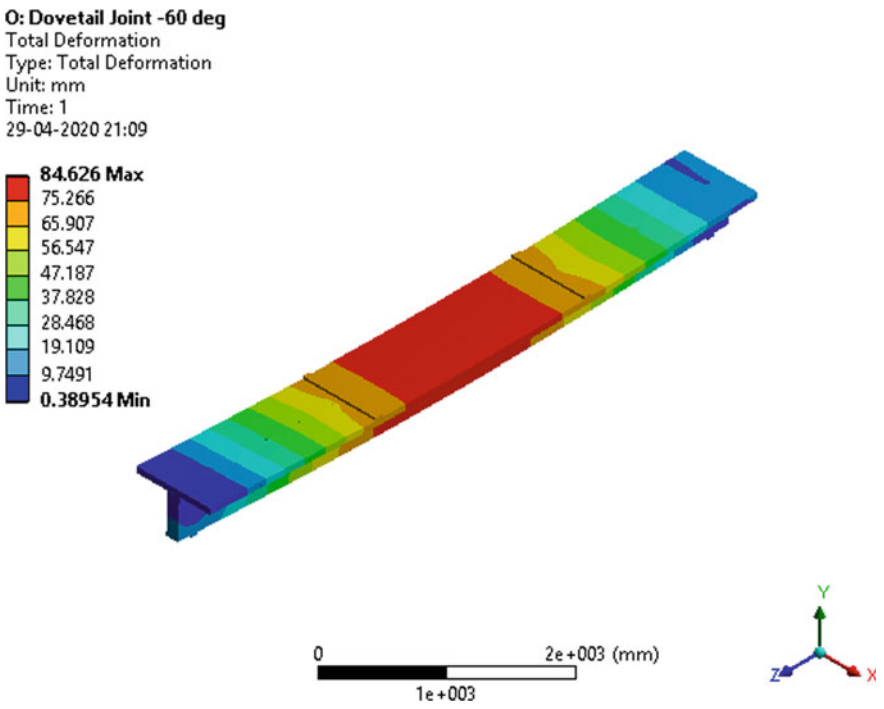

Fig. 5 Total deformation of TCC beam with dovetail joint of tenon angle 60° (Max = 84.62 mm)

between timber and concrete as well as the direct stress on shear connectors also increased.

Further the results obtained from the numerical analysis of TCC beam under non prismatic condition using dovetail joint with tenon angle 60°showed that non prismatic TCC beam with central rise 50 mm showed better performance compared to non prismatic TCC beam with central rise 100 and 150 mm. The results obtained are presented in Table 4. From the graph shown in Fig. 6 beam with central rise 50 mm have a higher load carrying capacity of 265.52 kN with a lower deflection value of 86.87 mm shown in Fig. 7. As the central rise was increased, depth of cross

Table 4 Comparison of results of non prismatic TCC beam

Central rise V1 (mm)	Tenon angle of joint θ	Ultimate load (kN)	Maximum deflection (mm)	Maximum slip (mm)	Direct Stress on connectors (MPa)
50	60°	265.52	86.87	7.50	97.17
100	60°	202.46	88.57	6.24	95.65
150	60°	147.39	89.761	5.64	84.74

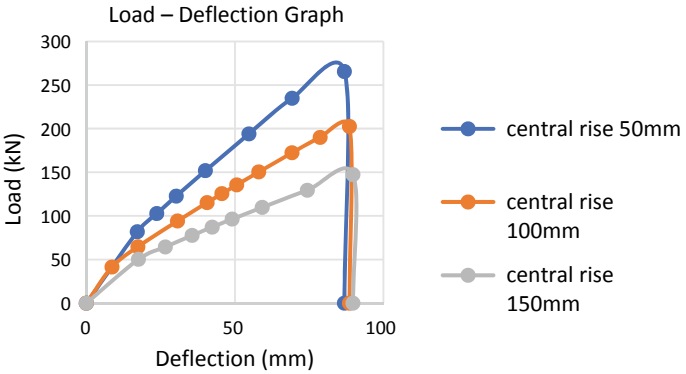

Fig. 6 Load-deflection graph of non prismatic TCC beam

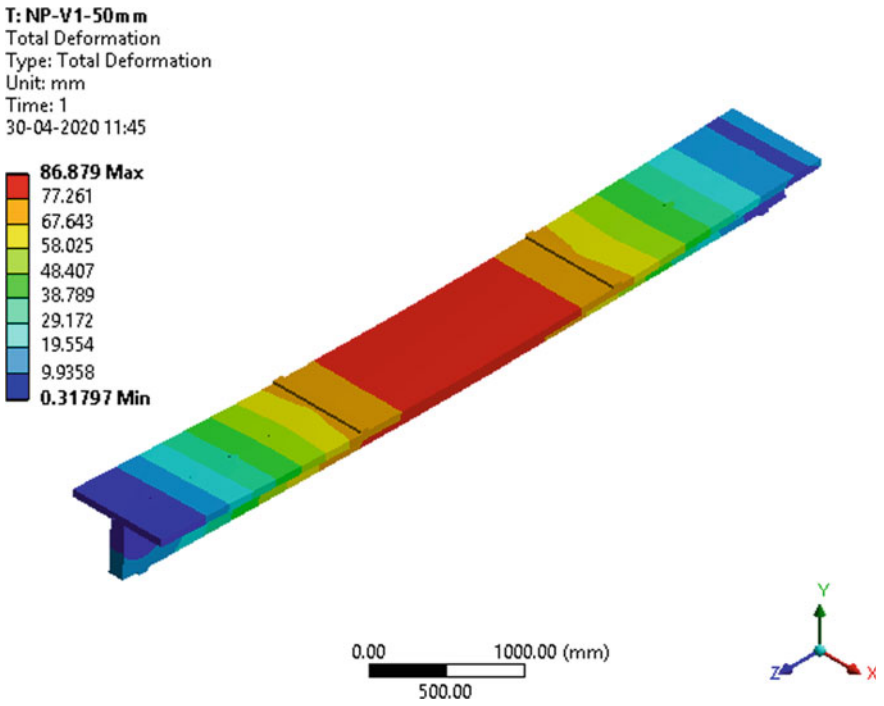

Fig. 7 Total deformation of non prismatic TCC beam with central rise 50 mm (Max = 86.87 mm)

section of beam decreased thus resulting in large deflection in beams with central rise 100 mm and 150 mm.

4 Conclusions

In the present study, new connection system were introduced in the form of interlockings between timber and concrete. TCC beam with interlocking of types dovetail joint with 2 tenon angles 45° and 60° and rectangular joint with tenon angle 90° were studied. Further TCC beam under non prismatic condition were also studied with the best interlocking joint selected. The results are summarized as follows;

- TCC beam with interlocking joints showed better performance compared to beam without joints. Presence of interlocking joints induced a better composite action, thus increasing the load carrying capacity and reducing the direct stress on shear connectors.
- A minor difference in values were obtained for both the joints. Since TCC beam with dovetail joint of tenon angle 60° showed higher load carrying capacity with a value of 337.34 kN. Hence it was selected as the best joint.
- TCC beam under non prismatic condition was modelled with the best joint selected. Non prismatic TCC beam with central rise 50 mm showed better performance with a higher load carrying capacity of 265.52 kN and lower deflection 86.87 mm but with higher slip value 7.50 mm and direct stress value of 97.17 MPa.

References

1. Zhang Y, Raftery GM, Quenneville P (2019) Experimental and analytical investigations of a timber–concrete composite beam using a hardwood interface layer. J Struct Eng 145(7):04019052
2. Yeoh D, Fragiacomo M, De Franceschiand M, Buchanan AH (2011) Experimental tests of notched and plate connectors for LVL-concrete composite beams. J Struct Eng 137(2):261–269
3. Khorsandnia N, Valipourand HR, Crews K (2012) Experimental and analytical investigation of short-term behaviour of LVL–concrete composite connections and beams. Elsevier 37:229–238
4. Auclair SC, Sorelli L, Salenivich A (2016) A new composite connector for timber-concrete composite structures. Elsevier 112:84–92

Analytical Study of GFRG Laminated Beam with Internally and Externally Strengthened with Cold Formed Steel

Meera Haridas and Chippy M. Rajan

Abstract An alternative structure for RC beam is a challenging factor in the field of structural engineering. Various studies had been conducted to introduce a cost-effective light weight structure which can replace RC structure. Studies on Glass Fiber Reinforced Gypsum (GFRG) panel sandwitched with Cold Formed Steel (CFS) is one such recent alternative technique to RC structure. In this paper, a GFRG laminated beam developed and strengthened by encasing Cold Formed Steel (CFS) internally and externally is analyzing using ANSYS 16.1 Software for evaluating flexural behaviour of developed beam. It is expected that this combined arrangement of GFRG panel and CFS will provide a cost-effective, light weight and load bearing structure with substantial strength to replace RC.

Keywords GFRG laminates · GFRG · Cold formed steel · Alternate for RC beam

1 Introduction

An alternative for concrete is a challenging factor in this engineering field. Various studies had conducted to introduce light weight concrete structures which will have the strength equal to normal RC structures. But in future the production cost and material cost will get increased and inversely affect the total construction of the structural field. So an introduction of sandwich beams had evolved with various material sandwiched and forms a composite beam. Composite beam is constructed to increase stiffness or strength or to reduce cost. Sandwich structures offer significant weight savings in many structural applications due to their high stiffness and bending strength to weight ratios. This led to the development of cold-formed steel structures (CFS) which is then sandwiched with concrete and light weight concrete for reduction of weight.

M. Haridas (✉) · C. M. Rajan
Sree Narayana Gurukulam College of Engineering, Kadayiruppu, Kolenchery, Ernakulam, Kerala, India
e-mail: meeraharidas22@gmail.com

© Springer Nature Switzerland AG 2021

K. Dasgupta et al. (eds.), *Proceedings of SECON 2020*,
Lecture Notes in Civil Engineering 97,
https://doi.org/10.1007/978-3-030-55115-5_36

Cold-formed steel (CFS) is the type of steel fabricated by the cold forming process. Cold-formed steel structural members have been used for housing for many years [1]. In recent years CFS elements are used more and more as primary load bearing structures in pallet racks, industrial buildings and residential houses. Several studies have conducted using CFS for the construction of beam by encasing partially or fully in the RC beam.

In thinking of reduced weight, different materials are used with this CFS [2]. As an alternative material for concrete, Glass fiber reinforced gypsum can be used. Panels are a composite of materials consisting of gypsum plaster and glass fibers [3]. These glass fibers provide strength to the panels. This material is used in residential, commercial, and industrial building due to its ease with construction and sufficient strength characteristics. In recent years there are building that constructed with this gypsum panel [4]. A new method of using GFRG laminates for making the beam is to be introduced and effects are to be investigated.

The purpose of this paper is to obtain a numerical result on the flexural behaviour of GFRG Laminated encased with CFS externally and internally using the software ANSYS 16.1. The objective of this study include: (1) To study flexural behaviour of GFRG laminates with various laminate thickness and aspect ratio, (2) To study the effect on strengthening of laminated beam with externally and internally Encased cold formed steel (CFS).

2 Numerical Study

The Finite Element Analysis (FEA) is the simulation of any given physical phenomenon using the numerical technique called Finite Element Method (FEM). GFRG Laminated beam were modelled using 20 nodded beam 186 elements. Beam 186 is suitable for analyzing slender to moderately stubby/thick BEAM structures. The element supports plasticity, hyperelasticity, creep, stress stiffening, large deflection, and large strain capabilities.

The structural performance of GFRG Laminated beams were done under varying aspect ratio and thickness by keeping the weight of all beam as the same. Two point loading was provided for the analysis. Three models of GFRG laminated beam with laminate thickness 10, 13, and 15 mm and with 2.5, 1.4, and 1.1 aspect ratio. The depth of each beam are 150, 110, and 100 mm (Table 1). Epoxy and screws of circular cross section are used for the tightening process. The analysis requires input data for

Table 1 Laminated beams used for the modelling

Laminate thickness (mm)	Total thickness (mm)	Depth (mm)	Aspect ratio
10	60	150	2.5
13	78	115	1.4
15	90	100	1.1

Table 2 Material properties of model

Element type	Material property
Solid 186	Young's modulus = 1.3×10^7 PSI
	Poisson ratio = 0.2
	Density = 1680 kg/m^3

material properties are as show in Table 2. Figures 1, 2 and 3 shows the front view of GFRG Laminated beam with various thickness and aspect ratio. The specimen with laminate thickness 10 mm and aspect ratio 2.5 is used for further analysis as it shows better property than compared to others. Figures 4, 5, 6 and 7 shows the laminated beam with different CFS encasement.

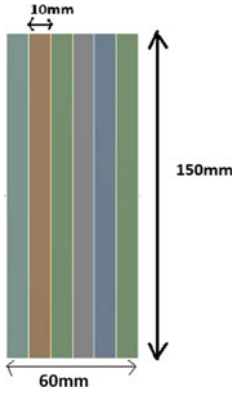

Fig. 1 Modeled view of GFRG laminated beam with thickness 10 mm and aspect ratio 2.5

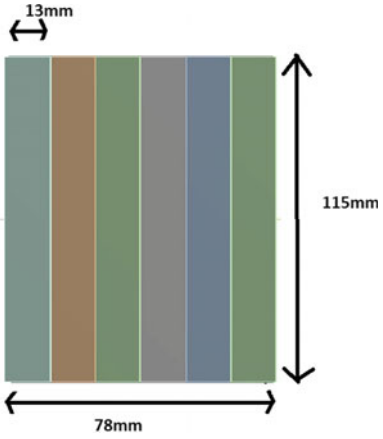

Fig. 2 Modeled view of GFRG laminated beam with thickness 13 mm and aspect ratio 1.4

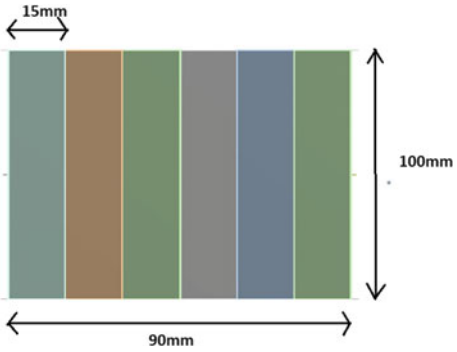

Fig. 3 Modeled view of GFRG laminated beam with thickness 15 mm and aspect ratio 1.1

Fig. 4 Modeled view of GFRG laminated beam with aspect ratio 2.5 strengthened externally with CFS (C section)

3 Results and Discussion

3.1 Flexural Study of Laminated Beam Without CFS Encasement

From Table 3 it is observed that beam with laminate thickness 10 mm and aspect ratio 2.5 have good load carrying capacity compared to other beams. Beam with laminate thickness 15 mm and aspect ratio 1.1 shows minimum load carrying capacity with ultimate load of 33.062 kN. The variation in deformation between beams of aspect ratio 1.1 and 1.4 are very small. Deformation refers to the change in size or shape of an object. Comparing the three beams the large deformation is shown by the beam with laminate thickness 13 mm of about 22.387. From the graph it is clearer that beam

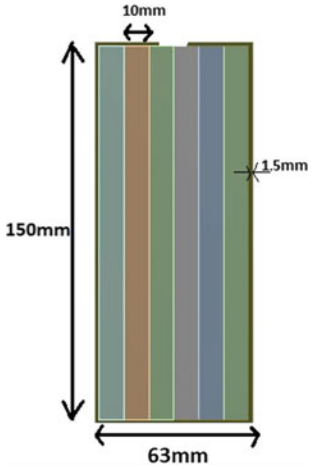

Fig. 5 Modeled view of GFRG laminated beam with aspect ratio 2.5 strengthened externally with CFS (U section)

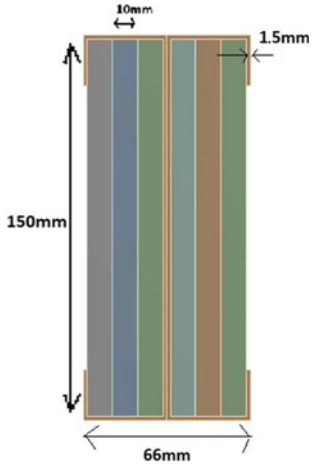

Fig. 6 Modeled view of GFRG laminated beam with aspect ratio 2.5 strengthened internally with CFS (I section)

with aspect ratio 2.5 can carry a max load of 50.698 kN with a minimum deflection of 12.331 mm, which can be taken as the beam for the further study. Figures 8, 9, 10 and 11 shows the deformed beams with different aspect ratio.

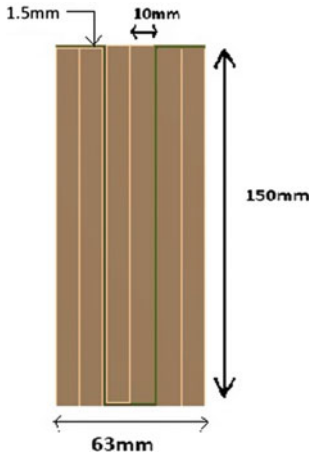

Fig. 7 Modeled view of GFRG laminated beam with aspect ratio 2.5 strengthened internally with CFS (HAT section)

Table 3 Ultimate load and deflection of beams

Aspect ratio 1.1		Aspect ratio 1.4		Aspect ratio 2.5	
Load	Deflection	Load	Deflection	Load	Deflection
0	0	0	0	0	0
28.559	5.7995	33.636	5.8411	47.673	5.8201
31.83	12.07	38.442	12.11	50.698	12.331
33.062	22.032	38.443	22.387	50.668	12.968
32.808	32.342	37.855	32.946	50.666	13.003

3.2 Flexural Study on GFRG Laminated Beams with CFS Encased Externally with C and U Section

The flexural study is conducted on all laminate thickness only with c section. Out of the best is used for the further strengthening process. C section is encased externally. Figures 4 and 5 shows the front view of base model and two point loading is provided. Figures 12 and 13 shows the total deformation of each beam for the externally encased beams with CFS. Both C and U shows better performance (Tables 4 and 5; Fig. 14).

From the above graph shown the ultimate load of the beam is obtained as 121.031 kN and with a deflection of 11.377 mm. This value is slightly less than strengthened with C section with an ultimate load of 123.928 kN &deflection 11.083 mm. In externally strengthening process both can be used. But strengthening process using C section is better than the other one by 2%.

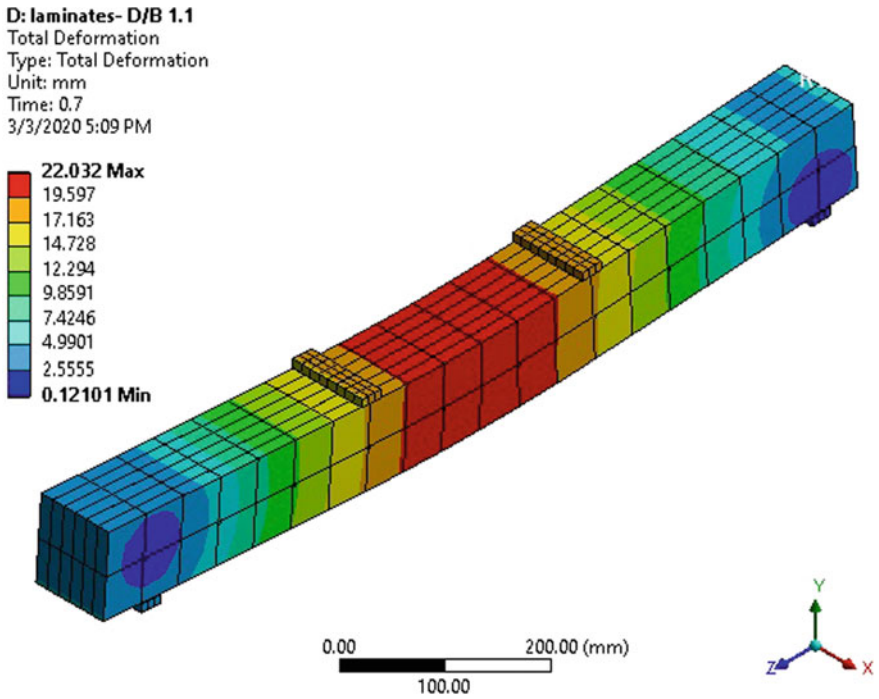

Fig. 8 Total deformation of GFRG laminated beam with thickness 15 mm and aspect ratio 1.1

3.3 Flexural Study on GFRG Laminated Beams with CFS Encased Internally with I and Hat Section

From the above internally strengthened beam with I section and Hat section, I section shows the better result than the Hat section. But while checking the deflection of both Hat section shows better result. I section shows the ultimate load of 142.526 kN and deflection of 12.046 mm and Hat section shows the ultimate load of 107.038 kN and deflection of 8.5654 mm. From the result we could conclude that I section is effective (Tables 6 and 7; Figs. 15, 16, 17 and 18).

From the load deflection it is clearly shown that the internally strengthened I section shows the better result with ultimate load 142.526 kN and deflection of 12.046. In comparing externally encased bean using C section and U section, both are effective in load carrying. They have only a minute difference in their deflection corresponding to their ultimate load. In comparing the internally strengthened beam using I and Hat section, I section is more effective.

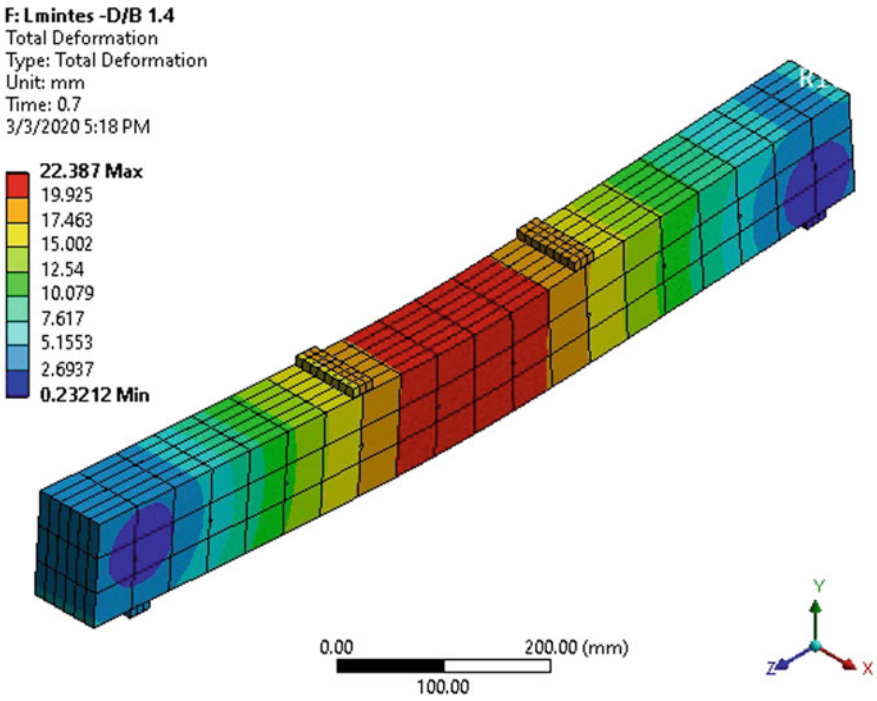

Fig. 9 Total deformation of GFRG laminated beam with thickness 13 mm and aspect ratio 1.4

3.4 Comparison of Ultimate Load and Deflection of D/B = 2.5 Without CFS and Internally Strengthened with CFS

See Table 8.

3.5 Comparison of Ultimate Load and Deflection of D/B = 2.5 Without CFS and Externally Strengthened with CFS

See Table 9.

4 Conclusion

In the present study analysis of all beam with and without CFS were studied. From the analysis it is clear that GFRG laminated beam with CFS encasement shows

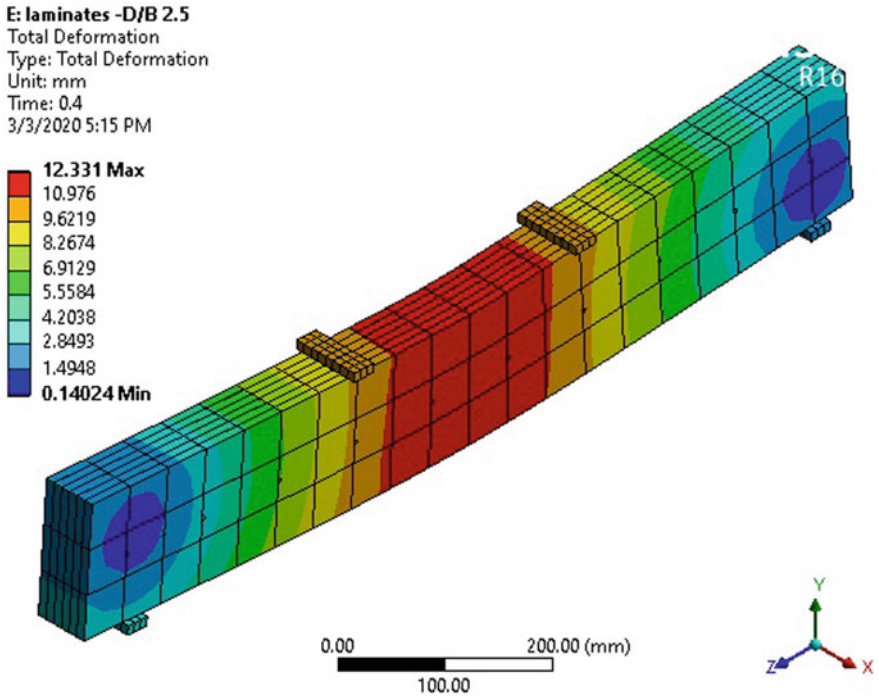

Fig. 10 Total deformation of GFRG laminated beam with thickness 10 mm and aspect ratio 2.5

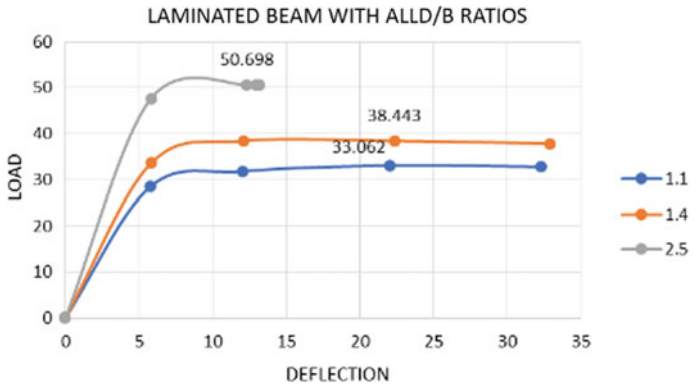

Fig. 11 Load deflection graph of GFRG laminated beam with all D/B ratios

improved strength characteristics. The strength enhancement study was done using C, U, I, &HAT sections of Cold Formed Steel.

- In comparing externally encased beam using C section and U section, both are effective in load carrying with a difference of 2% in load carrying capacity.

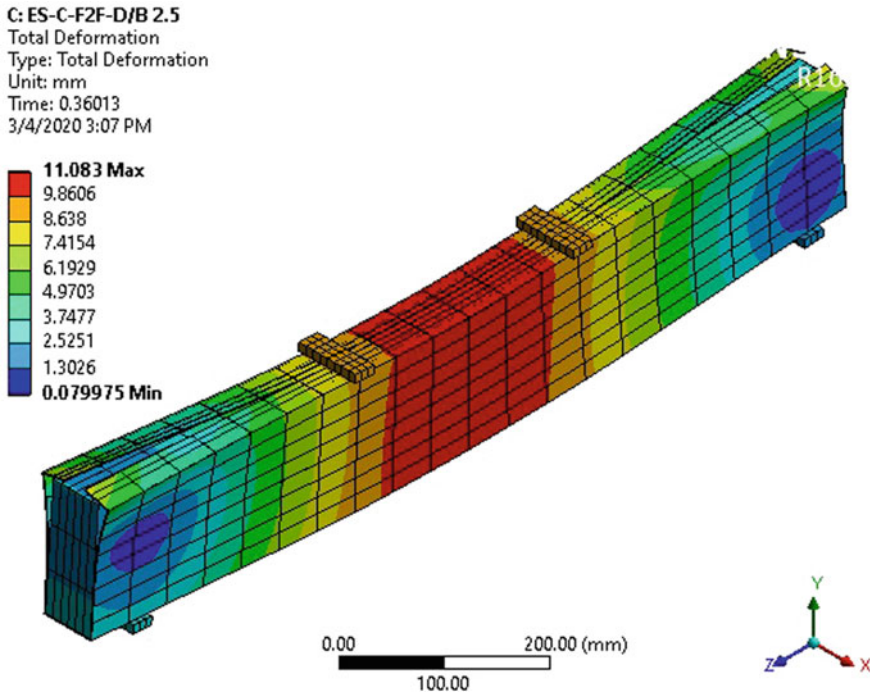

Fig. 12 Total deformation of GFRG laminated beam with thickness 10 mm and aspect ratio 2.5 strengthened externally with CFS (C Section)

- In comparing the internally strengthened beam using I and Hat section, I section is more effective in load carrying with an increase of 25%.
- In comparing all sections I section shows improved load carrying capacity with 25% than HAT section, 15% than U section, and 13% than C section.
- In the comparison with laminated beam and with strengthened beam with different sections of CFS, a greater increase (approximately 2 to 3 times) in strength was recognized.

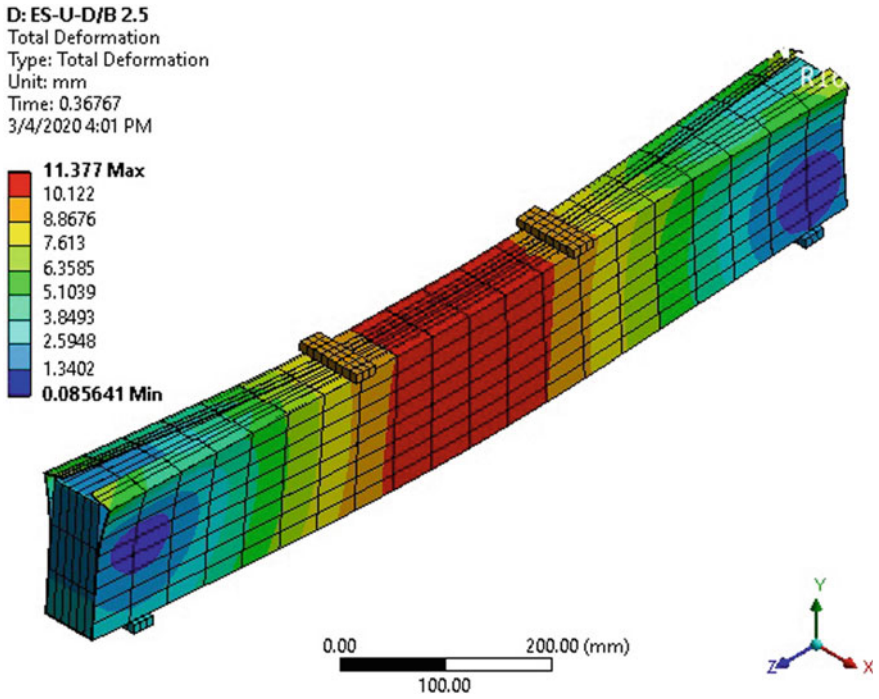

Fig. 13 Total deformation of GFRG laminated beam with thickness 10 mm and aspect ratio 2.5 strengthened externally with CFS (U Section)

Table 4 Ultimate load and deflection of strengthened beams with CFS with C section

Laminate thickness	Total thickness	Depth	Aspect ratio	Ultimate load (Kn)	Deflection (Mm)
10 mm	60	150	2.5	123.928	11.083
13 mm	78	115	1.4	90.156	11.556
15 mm	90	100	1.1	81.285	17.167

Table 5 Ultimate load and deflection of strengthened beams with CFS with C and U section

U section		C section	
Load	Deflection	Load	Deflection
0	0	0	0
117.738	6.968	120.58	7.0475
118.489	7.135	122.378	7.9186
119.072	7.2851	123.57	9.3661
119.794	7.99	123.916	10.165
120.701	9.3209	123.928	11.083
121.031	11.377	123.828	12.014
120.705	13.466	123.717	12.724

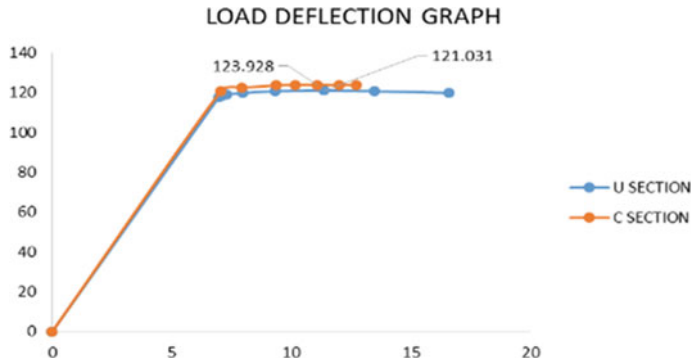

Fig. 14 Load deflection graph of C and U section

Table 6 Ultimate load and deflection of strengthened beams with CFS with I & HAT section

I section		Hat section	
Load	Deflection	Load	Deflection
0	0	0	0
115.157	2.9787	62.751	1.982
133.483	4.3356	97.868	4.0589
139.487	5.8651	101.16	4.6234
141.833	8.2921	104.158	5.1893
142.526	12.046	105.692	6.0758
141.425	15.872	106.517	7.0079
141.311	16.224	107.038	8.5654
141.289	16.347	106.265	10.463

Table 7 Ultimate load and deflection of strengthened beams

Strengthening	Section	Ultimateload (kn)	Deflection (mm)
Externally encased	C	123.928	11.083
	U	121.031	11.377
Internally encased	I	142.526	12.046
	HAT	107.038	8.5654

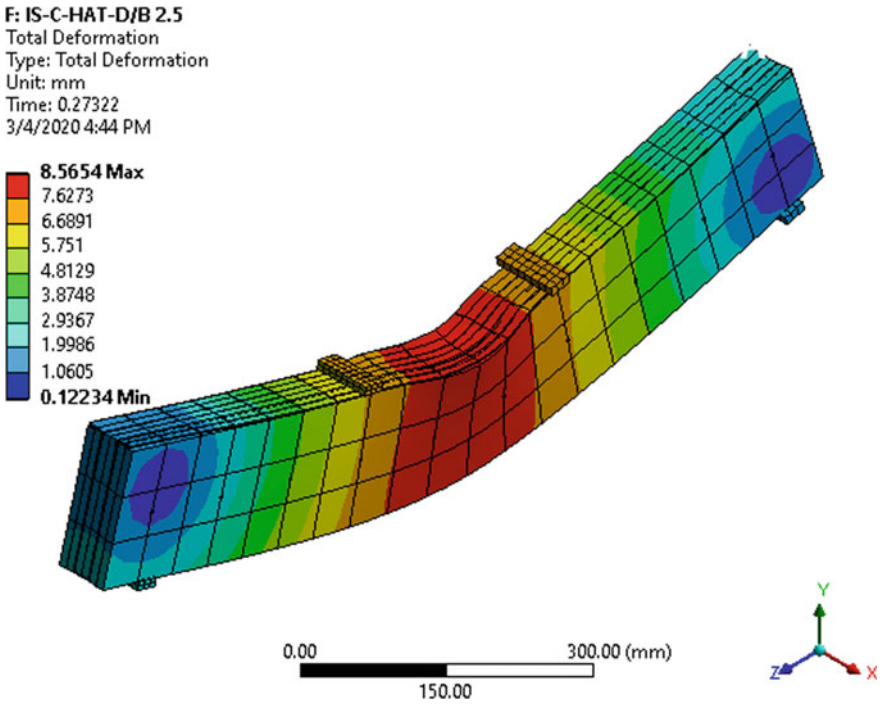

Fig. 15 Total deformation of GFRG laminated beam with thickness 10 mm and aspect ratio 2.5 strengthened externally with CFS (HAT Section)

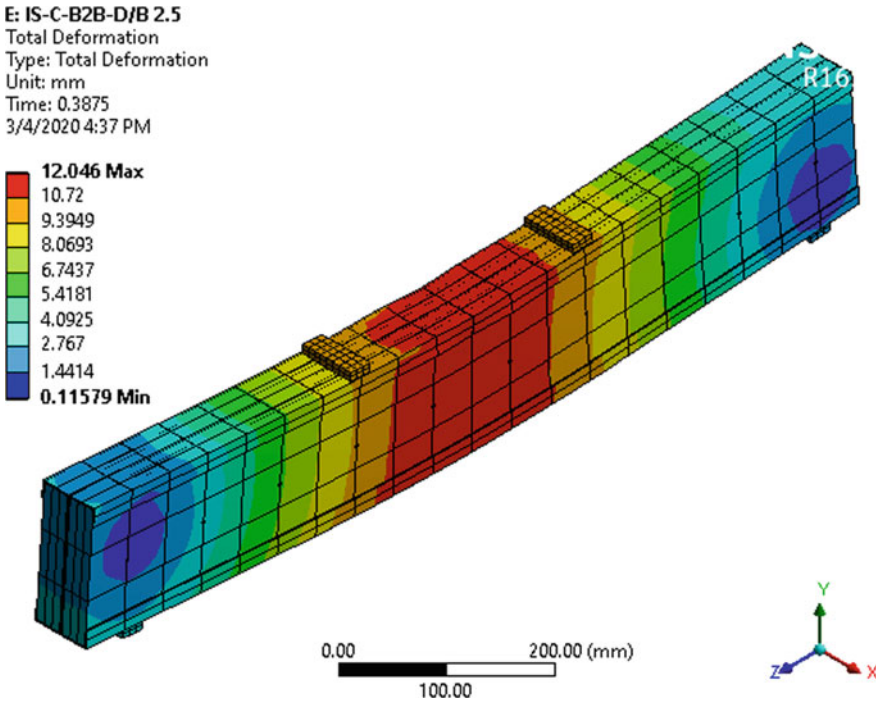

Fig. 16 Total deformation of GFRG laminated beam with thickness 10 mm and aspect ratio 2.5 strengthened externally with CFS (I section)

Fig. 17 Load deflection graph of I and HAT section

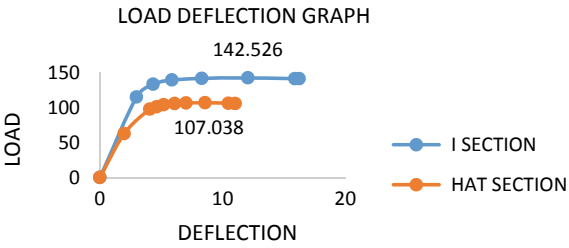

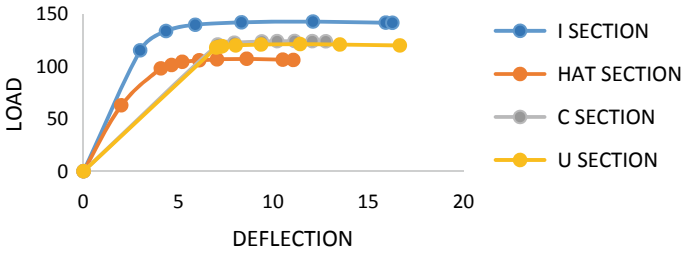

Fig. 18 Load deflection graph of all section

Table 8 Ultimate load and deflection of without and internally strengthened beams

Section	Ultimate load (kN)	Deflection (mm)
Without CFS	50.698	12.331
I section	142.526	12.046
Hat section	107.038	8.5654

Table 9 Ultimate load and deflection of without and internally strengthened beams

Section	Ultimate load (kN)	Deflection (mm)
Without CFS	50.698	12.331
C section	123.928	11.083
U section	121.031	11.377

References

1. Youssef Kamal A, Khalil1a NN (2017) Cold-formed steel U-section encased in simple support reinforced concrete beam. J. Mech Civil Eng ISSN: 2456-1479
2. Hegyi P., Dunai L (2016) Experimental investigations on ultra-lightweight-concrete encased cold-formed steel structures part II: stability behaviour of elements subjected to compression. Thin-Walled Struct 101(2016):100–108
3. Fenga R (2019) Seismic performance of cold-formed steel framed shearwalls with steel sheathing and gypsum board. Thin-Walled Struct 143(2019):10
4. Selvaraj S (2018) Studies on cold-formed steel stud panels with gypsum sheathing subjected to out-of-plane bending. J Struct. Eng ©ASCE, ISSN: 0733-9445

Shear Strengthening of Concrete Block Masonry Walls Under In-Plane Diagonal Loading Using Fibers

P. Akhil kumar and S. Unnikrishnan

Abstract Unreinforced masonry wall (URM) is a traditional method and are widely used all around India. URM can be commonly found in reinforced concrete structures in many earthquake prone countries. Masonry walls are more vulnerable during earthquakes. URM structures are not naturally stable and can generally increase the lateral strength and stiffness of the structural system and thus improve the structural performance up to a certain range of seismic load. Hence, it is essential to find solutions to strengthen URM walls. The present study aims at investigating the in-plane shear behavior of solid concrete block masonry wall and masonry strengthened with GFRP mesh and polypropylene fiber (PP) externally bounded as a reinforcing material. The tests are conducted to determine the optimum percentage of polypropylene fiber. An experimental study is carried out involving a series of masonry walls made of concrete blocks are prepared and are reinforced with GFRP and PP fiber. The wallettes are subjected to diagonal axial compression test according to ASTM E 519-02. The main focus of the study is to investigate the strength characteristics of masonry wall and to know the practical applications of this technique. The strengthening effect caused by the concrete block masonry on in-plane shear behavior including failure modes, shear strength, modulus of rigidity and ductility are investigated. The walls are subjected to in-plane diagonal tensile (shear) test. The shear strength parameters are studied and the application of fibers for strengthening of masonry walls is observed.

Keywords In-plane diagonal · Masonry · Ductility

P. Akhil kumar (✉) · S. Unnikrishnan
Sree Buddha College of Engineering, Pattoor, Alappuzha, India
e-mail: akhilcivil1995@gmail.com

S. Unnikrishnan
e-mail: unnisubhash89@gmail.com

© Springer Nature Switzerland AG 2021

K. Dasgupta et al. (eds.), *Proceedings of SECON 2020*,
Lecture Notes in Civil Engineering 97,
https://doi.org/10.1007/978-3-030-55115-5_37

1 Introduction

Masonry walls are the most commonly used type of constructions throughout the world and it is the part of any building where more durable and reliable. The word masonry refers to anything constructed by masons using materials such as stones, tiles, bricks, concrete blocks etc. Brick is the commonly used type of masonry. Nowadays, concrete block masonry is rapidly gaining in popularity as a comparable material. However, the durability and strength of masonry wall constructions depends on the type and quality of material used and the workmanship [1].

Masonry buildings may be defined as the construction of individual building units bonded together with mortar. The individual units may be stones, bricks, precast blocks or solid concrete blocks. Masonry buildings are constructed as massive structures and hence large enough to attract horizontal forces during earthquakes. A number of the world's greatest earthquakes occurred in India in the last century. The occurrence of recent earthquakes in India and in different parts of the world results in losses, especially human lives that have highlighted the structural inadequacy of buildings to carry seismic loads. Severity of ground shaking, at a given location during seismic may be minor, moderate or strong.

Unreinforced masonry walls (URM) are the most common and widely used as a building technique all over the world. It is the traditional type of construction technique available in the existing world. The term unreinforced refers to the absence of tensile resisting elements, such as the steel reinforcing bars found in modern reinforced concrete structures. Tensile resisting elements are crucial inorder to resist lateral forces such as forces that develop during earthquakes. Unreinforced masonry wall is more vulnerable to earthquake. In many developed and developing countries masonry construction is the common practice due to its cost effectiveness and easy construction method. The design philosophies of these masonry buildings are focused on gravity loading and many URM structures are potentially earthquake vulnerable. Due to the existence of a large number of buildings constructed by unreinforced masonry brick walls, reconstruction is not the most appropriate and practical solution [2].

When the ground shakes due to earthquake or seismic acceleration, an unreinforced masonry wall can fail in two ways i.e. either in-plane or out-of-plane in the direction depending on the direction of seismic loads. To improve the seismic resistance of a structure, the main objective is to strengthen the in-plane response of structural walls. There are several techniques to strengthen the masonry walls such as textile reinforced mortar (TRM) used to strengthen brick masonry, fiber reinforced polymers (FRP), shotcreting, application of steel elements, bed- joint reinforcement, post tensioning techniques, using ferrocement etc. [3, 4]. Another suitable technique is to overlay the walls with fibers which is light weight and can be easily applied. By using fibers, there will be no additional wastage of time for construction and low cost. In this method, different fibers and fabrics are placed on the surface of the masonry wall incorporated with plaster coating. Strengthening of unreinforced masonry wall using steel rods, ferrocement etc. are widely used. In this study, an experimental

investigation has been carried out to strengthen the unreinforced masonry walls using GFRP mesh and polypropylene fiber (PP). These fibers are locally available fibers and have advantages such as high tensile strength and resistance to deformation and superior for micro cracking behavior. Here the investigation is carried out in masonry wall using GFRP fabric/mesh and PP fiber with 1:4 and 1:1 mortar mixes. GFRP fabric is a strengthening material which is coated with alkali resistant latex. This reinforcement grids are highly protective against temperature and have an excellent strength and resistant to alkali [5]. These fabrics can prevent the frequently occurring tensions in ceilings and walls. Similarly, PP fiber can reduce the damage of occurring micro-cracks. Few studies are available for strengthening of URM walls with fibers but a considerable number of researches have been conducted in reinforced concrete structures with fibers. The present study aims to evaluate and analyze the strength characteristics of URM solid concrete block walls strengthened by fibers.

Although from the previous studies collected the valuable information regarding the importance of using alkali resistant glass reinforced fiber polymer (AR-GFRP) and polypropylene fiber. Some parameters such as its effects on failure modes, efficiency in strengthening masonry walls are need to be more investigated. The main objective of this paper presents an experimental program where URM walls are externally reinforced with AR- GFRP and PP subjected to in-plane diagonal loading according to ASTM E519-02 and also to determine the optimum percentage of fibers. The in-plane shear behavior of URM walls including ductility, failure modes, and effect of fibers, shear strength and modulus of rigidity are investigated.

2 Materials

Various laboratory test were carried out to find out the physical properties of cement, fine aggregate and solid concrete blocks as per IS recommendation. Here the cement used is ordinary Portland cement (OPC) 53 grade conforming to IS: 12269-1987 and M sand is taken as fine aggregate passing through 4.75 mm sieve is taken for the study. Here, M sand conforming to Zone II was used. Solid concrete blocks of size 300 mm $\times$ 200 mm $\times$ 150 mm which is locally available is chosen for the casting masonry panels. Solid concrete blocks of grade C was chosen for the study and conforms to IS: 2185(part 1)–2005. GFRP mesh is a strengthening material which is coated with alkali resistant (AR) latex is used for strengthening of URM walls. Polypropylene fiber is also used in this study to determine the optimum percentage and for strengthening of masonry walls.

Table 1 Details of masonry wall testing configurations

Specimen	Size (m)	No. of samples	Condition of walls
CB-N	0.66 × 0.66 × 0.23	3	Unreinforced wall
CB-F	0.66 × 0.66 × 0.23	3	Reinforced wall with GFRP
CB-P	0.66 × 0.66 × 0.23	3	Reinforced wall with PP

3 Experimental Investigation

3.1 Test Specimens

The experimental works were carried out on hardened concrete to find out the optimum percentage of fibers required and to take the normal mix ratio for the study and to study the in-plane shear behavior of masonry panels under in-plane diagonal tensile loading. For that mortar cube test was done. Mortar cubes of size 75 mm × 75 mm × 75 mm were prepared and cast. Common mix ratio of normal mortar used in masonry works is 1:3, 1:4 and 1:6 of cement to sand ratio and 1:1 ratio is taken for mortar mix having fibers. For each series 6 cubes were cast and the optimum percentage is evaluated by compressive strength tests.

The experimental investigations were performed on three set of URM walls of size 660 mm × 660 mm × 230 mm. The masonry panels were built using solid concrete block units and normal mortar that were tested under in-plane diagonal tensile (shear) test method as per specification conforms to ASTM E519-02. All the specimens are designed as laboratory specimens that represent a section of masonry wall that are nominally similar to that of adopted in actual building construction. One plain specimen was taken as reference wall. Second set of masonry panels were constructed and externally strengthened with AR- Glass Fiber mesh on two faces. Next set of masonry panels were constructed and externally strengthened with PP fiber. Table 1 indicates the details of masonry wall testing configurations and Fig. 1 shows the schematic diagram of masonry wall.

3.2 Construction Process

Before the construction of URM walls, firstly the surface of the solid concrete blocks is to be wet to prevent the absorption of water from the mortar mix. To cast the concrete block masonry panel, the first layer of blocks was laid over 10 mm thick horizontal layer of mortar mix. Masonry panels were built using solid concrete blocks having nominal dimensions of 300 mm × 200 mm × 150 mm. The blocks are placed over the mortar composed of Ordinary Portland cement and sand in the proportion 1:4 with a w/c ratio of 0.5. Different layers are placed and the joints are filled with mortar with thickness of bed and head joints of 10 mm as shown in Fig. 2. For strengthening

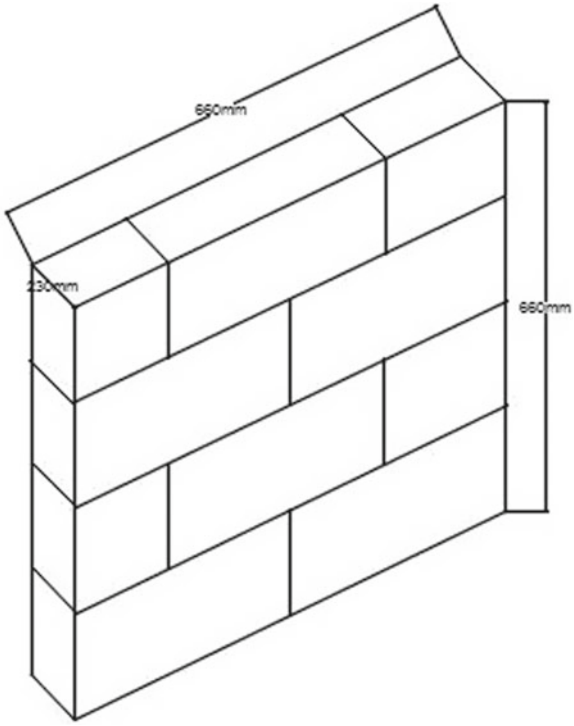

Fig. 1 Schematic diagram of masonry wall

of URM walls using GFRP mesh/fabrics, firstly the masonry surface should be dirt free of dust and other loose materials. The first layer of mortar mix was overlaid after wetting the wall surface. The GFRP mesh was placed on the face of the walls and embedded into the mortar. The second layer of mortar is applied over the wall. For strengthening of URM walls using PP fiber, as mentioned above firstly the masonry faces should be cleaned. Then, the layer of mortar mix with 1:1 ratio and optimum percentage of PP fiber is mixed and plastered over the masonry wall with thickness of 15 mm. Once the total thickness of plaster was applied, the plaster surface was hand trowelled so that excess mortar can be strike off to achieve a uniform thickness. After the construction and plastering of masonry wall panels with and without fibers, curing is carried for 14 days using sand bags placed over it.

3.3 Test Setup and Testing Procedure

The test setup is adopted as per ASTM E519-02 standards for determining the in-plane diagonal tensile (shear) strength of masonry panels. It consists of a loading frame, two loading shoes which are made up of steel, a hydraulic jack and three

Fig. 2 Casting of concrete block masonry panel

LVDT's. Masonry wall is scaled down and is placed diagonally supported by two loading shoes one placed at the top corner and other at the bottom corner of the masonry wall. The force was transferred to the walls by means of these loading shoes. A constant and uniform compression load is placed over the in-plane bed joint of the masonry wall. By loading the masonry assemblage, causes compression along one diagonal in loading frame thus causing a diagonal tension failure with the specimen splitting apart parallel to the direction of load. This modified test method was adopted to measure the in-site in-plane responses of concrete block sections more accurately than other available methods. The applied loads were recorded using a load cell which is placed on top corner of the wall above the loading shoe. Two LVDT"s are fixed on the face of the walls, one oriented along the compression side (vertical) and other placed in the tension side (horizontal) of the walls, inorder to measure the shortening and elongation of the walls in two different directions. Another LVDT was fixed on the top of the wall to measure the applied displacement. These LVDT"s was connected to a data acquisition system inorder to read the loads and displacements. The test setup of in-plane diagonal loading is shown in Fig. 3.

Fig. 3 Setup of in-plane diagonal loading

4 Results and Discussion

4.1 Mortar Cubes

Two different types of mortar mix were prepared. One with normal mortar mix and the other with mortar mix based on the percentage of fibers added in the mix which includes cement, fine aggregate, and fiber. The fibers include polypropylene fiber and GFRP mesh was used. These fibers except GFRP were taken to determine its optimum percentage to be taken. GFRP mesh and PP fiber were used for strengthening of masonry walls. Mortar cubes of 1:4 and 1:1 ratios were prepared in 75 mm × 75 mm × 75 mm and tested for compressive strength of mortar cubes by testing in compression testing machine.

Different percentage of fibers such as 0.5, 1, 1.5, 2% have been used to find out the optimum value. From the test results, it can be concluded that the 28 day compressive strength of mortar cubes with polypropylene fiber was obtained as 31.64 N/mm^2. With these different percentages of fiber higher percent of improvement is noticed with 1.5% of PP fiber, further experiments are carried out with this percentage of

fiber. The presence of particular amount of fibers in the matrix was the reason for increase in compressive strength.

4.2 Test on Masonry Panels

The experimental investigations were conducted on 3 samples of specimens of solid concrete block panels. The first set of specimen consists of unreinforced concrete block masonry panel (CB-N), the next set of sample consists of reinforce concrete block masonry panel strengthened with GFRP mesh (CB-F), and the other set of sample strengthened using PP fiber (CB-P). The behavior of masonry walls is highly non-linear. Inorder to find out the behavior of masonry walls, the actual behavior is idealized with the hysteresis curve [3, 6]. Bilinear idealization is recommended by all the codal provisions to assess the performance of the existing structures. In this study, the ultimate shear strength and ductility is evaluated for masonry wallettes applied with GFRP fabric and PP fiber. It is obtained by ensuring that areas below actual and bilinear hysteresis curve were equal. An equivalent bilinear hysteresis curve was defined for all reinforced walls with reference to Fig. 4.

The calculations of shear stress and shear strain are formulated using the equations:

$$\text{Shear Stress S} = \frac{0.707P}{A}$$

where

S Shear stress on net area, MPa
P Applied load, N
A Net area of the specimen, mm^2, calculated as follows:

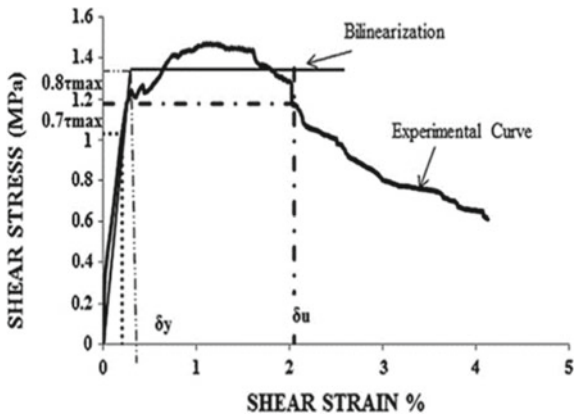

Fig. 4 Bilinear idealization curve

$$A = \frac{(W + h)tn}{2}$$

where

w Width of specimen, mm,
h Height of specimen, mm
t Total thickness of specimen, mm
n Percent of the gross area of the unit that is solid, expressed as a decimal

1. Shear Strain, $\gamma = \frac{\Delta \mathbf{V} + \Delta \mathbf{H}}{g}$
where

γ Shearing strain, or mm/mm
$\Delta \mathbf{V}$ Vertical shortening, mm
$\Delta \mathbf{H}$ Horizontal extension, mm
g Vertical gage length, mm

2. Modulus of Rigidity $G = \frac{\mathbf{S}}{\gamma}$
where

G Modulus of rigidity, MPa

In masonry panels without fiber, cracks were firstly developed along the diagonal followed by sliding shear failure at a load of 122 kN for the specimen. For masonry panel strengthened using GFRP and polypropylene fibers behaves like a composite material during the application of load and failure occurs along the diagonal. Sliding shear failure is not predominant in strengthened walls. The solid concrete block panel strengthened using fibers prevents the panels from direct sliding failure by holding the blocks together. The failure pattern of strengthened specimen is shown in Fig. 5. The shear stress-strain values are obtained by load and deflection along horizontal and vertical direction and plotted on a graph showing shear strain along X-axis and shear stress along Y-axis.

Using bilinear idealization can be find out the values of ductility corresponding to 0.7 T_{max} and 0.8 T_{max} and corresponding values of modulus of rigidity as per ASTM E519-02. Figures 6, 7 and 8 indicates the shear stress-strain curve based on the experimental test data. Table 2 shows the experimental results of ductility for concrete block specimen under in-plane diagonal test.

Based on the values obtained from shear stress and strain, various parameters such as modulus of rigidity and ductility were evaluated with the help of bilinear idealization curve. The details from the experimental investigation, values are calculated as per specification of ASTM E519-02. The solid concrete block panels with and without fibers are studied based on the parameter and conclusion is arrived. During testing the advantage is that it behaves like a composite material and shows the importance of using fiber in strengthening masonry walls. From the figure mentioned above, it can be seen that the masonry wall strengthened using fibers behaves initially a linearly elastic manner and then reduced as the failure begins.

Fig. 5 Failure pattern of strengthened specimen

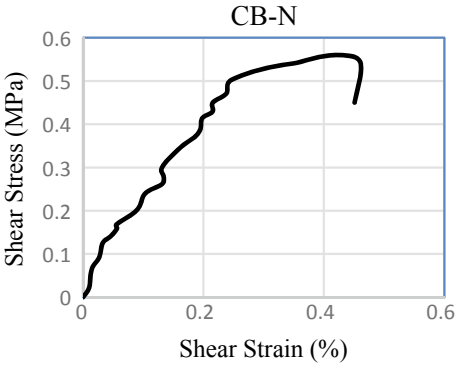

Fig. 6 Unreinforced block specimen curve

5 Conclusions

The masonry structures are very brittle and weak in lateral resistances. It is required to control failure and collapse during earthquakes. Hence, there comes the importance of strengthening the existing masonry structures against lateral loads. The main

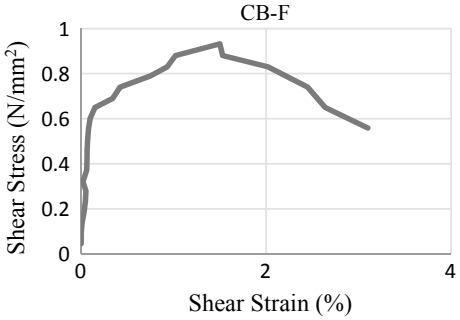

Fig. 7 Concrete block specimen curve with GFRP fiber

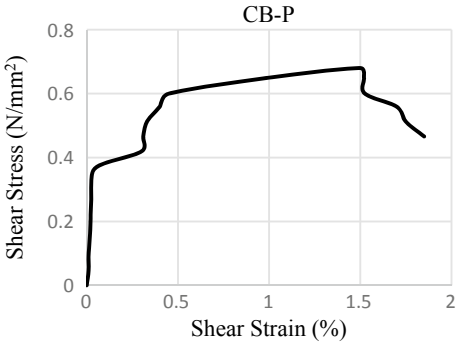

Fig. 8 Concrete block specimen curve with PP with fiber

Table 2 Experimental results of specimens under in-plane diagonal test

Panel	P_{max} (kN)	τ_{max} (N/mm^2)	τ/τ_o	d_y (%)	d_u (%)	$\mu \frac{du}{dy}$	G (MPa)
CB-N	121	0.55	–	–	–	–	13.75
CB-G	199	0.926	1.68	0.41	2.35	5.73	61.73
CB-P	148	0.69	1.25	0.45	1.67	3.71	69

P_{max}—maximum load applied, τ_{max}—maximum shear stress, d_y—yield drift, d_u—ultimate drift corresponding to 0.8 τ_{max}, μ—ductility of specimen; G—Modulus of rigidity

focus of the study is on the adaptability of fiber on lateral strengthening of masonry panels. Two different fibers were used which include GFRP mesh and PP fiber. The conclusions that are obtained from the experimental study are presented below:

- The study is conducted to find out the solution to strengthen the existing load bearing masonry structures made of solid concrete blocks locally available in the locality. For unreinforced concrete block specimen (CB-N), since it is very brittle the failure was sudden and did not have the efficiency to carry sliding-shear failure and diagonal failure. Also the failure has been occurred through debonding of bed joints. For reinforced concrete block specimens, it confines the best efficiency having the possibility of carrying shear behaviour. The failure initiated along the

bottom crushing followed by diagonal cracking in a ductile manner. Reinforced masonry panels carry higher stress and provide ductility thereby carrying more energy than that of unreinforced concrete block masonry panels.

- GFRP mesh and PP fibers were used for strengthening the concrete block masonry walls and the proposed method of strengthening confines the masonry behaves like a composite material with increased properties. The fibers hold the concrete block masonry structures thereby increases the resistance to failure.
- Shear strength of specimen is increased up to 20% by the application of fiber on concrete block masonry panels.
- After strengthening of URM specimen, the ductility ratio 3–5 times than that of unstrengthened concrete block masonry panel.
- It shows a significant increase in shear strength and ductility. This technique is more effective and shown more diagonal load carrying capacity.
- The technique is more effective by the application of GFRP mesh in masonry panel and shows more diagonal load carrying capacity of almost 2 times that of normal concrete block masonry panel.

Acknowledgements The authors gratefully would like to thank and acknowledge the Kerala State Council for Science, Technology and Environment (KSCSTE) for granding the funding for the work and also acknowledge the teachers, management and the principal of Sree Buddha College of Engineering, Pattoor for their kind support.

References

1. Yardim Y, Lalaj O (2016) Shear strengthening of unreinforced masonry wall with different fiber reinforced mortar jacketing. J Construct Build Mater 102:149–154 (Elsevier)
2. Lin Y, Wotherspoon L, Ingham JM (2014) In-plane strengthening of unreinforced masonry wallettes using ECC shotcrete. J Struct Eng 13:33–42 (Elsevier)
3. Shabdin M, Zargaran M, Attari NKA (2018) Experimental diagonal tension (shear) test of Un-Reinforced Masonry (URM) walls strengthened with textile reinforced mortar (TRM) J Construct Build Mater 164:704–715 (Elsevier)
4. Ashraf M et al (2012) Seismic behavior of unreinforced and confined brick masonry walls before and after ferrocement overlay retrofitting. Int J Architectural Heritage 6:665–688
5. El-Diasity M, Okail H et al (2015) Structural performance of confined masonry walls retrofitted using ferrocement and GFRP under in-plane cyclic loading. J Struct 94:54–69 (Elsevier)
6. Marcari G et al (2007) In-plane shear performance of masonry panels strengthened with FRP. Composites: part B engineering 38:887–901 (Elsevier)

Structural Performance of Innovative Multi Cellular Corrugated Steel Column (MCCSC)

Agnes Davis Thuluvath and Reshma Prasad

Abstract The extensive use of thin-walled steel structural systems in the building and construction industry is mostly indebted for their high strength to weight ratio attributes and remarkable fabrication versatility. Corrugated plates which falls in this category, also have a wide range of application in various engineering fields. They are lightweight, economical, and have much higher load carrying capacities than flat plates. The corrugation shape provides continuous stiffening which permits the use of thinner plates. Fabrication costs for elements with corrugated panels are normally lower. A corrugated column is a hollow column constructed by welding together four corrugated panels. Multi Cellular Corrugated Steel Column (MCCSC) is a kind of hollow column where Multi Cellular stiffeners are provided inside hollow column. Three different types of Single Skin Corrugated (SSC) columns with different stiffener configurations (diamond, plus and cross shapes) were chosen. Stiffeners increases the load carrying capacity as well as the buckling capacity of the column. Double Skin Corrugated (DSC) columns with square and circular core at the center to which stiffeners are welded is also developed. In this paper the behavior of MCCSC subjected to axial and eccentric loading is studied using ANSYS Workbench 16.1 software and it was found that column with diamond shaped stiffener showed best performance in both SSC and DSC columns.

Keywords Single skin corrugated steel column · Double skin corrugated steel column · Multi Cellular corrugated steel column (MCCSC) · Axial loading · Eccentric loading

A. D. Thuluvath (✉) · R. Prasad
Federal Institute of Science and Technology, Angamaly, Ernakulam, India
e-mail: agnesdavisthulu@gmail.com

R. Prasad
e-mail: reshma.prasad1@gmail.com

© Springer Nature Switzerland AG 2021

K. Dasgupta et al. (eds.), *Proceedings of SECON 2020*,
Lecture Notes in Civil Engineering 97,
https://doi.org/10.1007/978-3-030-55115-5_38

1 Introduction

Nowadays almost all industries are redirecting their strategic plans to developing environmentally friendly products and building and construction industry is not an exemption. Structural elements made from steel alloys are yet the most common ones. They give greater flexibility and higher strength-to-weight ratio than conventional sections. This enhances efficiency and reduces cost [1]. Among these sections, Hollow Structural Sections (HSS) are most reliable one. Hollow sections as steel profiles are not only in competition with concrete, but also, may substitute for other steel profiles due to their superiority with regard to strength and stability [2]. Corrugated hollow sections create lightweight and visually attractive structures that benefit communities and environments. The corrugation shape provides continuous stiffening which permits the use of thinner plates [3].

The use of fabricated hollow sections from corrugated plates was introduced by Nassirnia et al. [1] for the first time. The idea was further developed by implementing concrete-filled double skin columns and combining with ultra-high strength steel tubes [4–7]. Studies were conducted by researchers on the performance of corrugated steel columns under uniaxial loading. Thus, optimum profile geometry for corrugations was concluded with trapezoidal as best ones [8]. Investigating different corrugation parameters demonstrates that higher angle of inclination and corrugation height enhance column strength. So critical local buckling of corrugated columns can be effectively enhanced [9, 10].

Usually corrugated hollow square column is fabricated by welding four corrugated plates [1]. The use of stiffeners of different shapes (diamond, plus and cross) inside SSC column is expected to enhance column strength. Remodeling SSC as DSC column with two types (square and circular) of cores and incorporating stiffeners is further expected to enhance column strength. Thus, in this study, a theoretical analysis was performed to predict the structural behavior (load carrying capacity and deformation) of corrugated column subjected to axial and eccentric loads by using ANSYS Workbench 16.1.

2 Test Programme

In order to converge at the required objective finite element analysis was done on various SSC steel column and DSC steel column using ANSYS Workbench 16.1 software to check the maximum axial and eccentric load carrying capacity.

Table 1 Material properties used for validation

Material	Density (kg/m^3)	Elastic modulus (MPa)	Poison's ratio	Fy (MPa)
Steel plates	7850	210,000	0.3	250

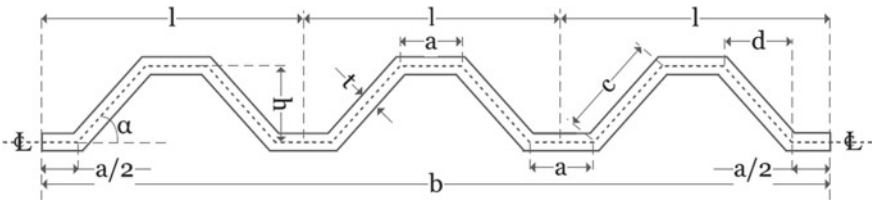

Fig. 1 Trapezoidal corrugated plate cross-section and dimension notation (*Source* Mohammad Nassirnia et al. [1])

2.1 Material Properties

The specimens used are homogeneous in nature as it has only steel. Fe250 steel was chosen for the analysis. Engineering properties of the specimens were chosen purely on the basis of experimental results from journal 'Innovative hollow corrugated column' by Nassirnia et al. [1]. Table 1 shows summary of material properties used for modeling in ANSYS Workbench 16.1.

2.2 Specimen Description

The paper presents an analytical study on the effects of stiffeners on a corrugated steel column under axial and eccentric loading. A total number of 10 corrugated steel columns were analyzed. All the corrugated steel column specimens are of 1000 mm long and different configurations of stiffener plates are provided. Figure 1 shows cross section of corrugated plate and details of model is shown in Table 2.

2.3 Methodology

Three types of single skin corrugated steel columns are developed with diamond, plus and cross shaped stiffener configurations. Six types of double skin corrugated steel columns of square and circular core are developed with diamond, plus and cross shaped stiffener configurations. Cross section is modeled in x-y plane. For all models, the boundary conditions adopted are the same. Both axial loading and eccentric loading is done. Bottom support is fixed, while loads are applied at the top face of the column. Axial loads are applied as displacements. Maximum displacements

Table 2 Specimen identification

Parameters	Dimensions
Inclination angle (α)	45°
Width of corrugation (a)	20 mm
Height of corrugation (h)	15 mm
Thickness of corrugation (t)	3 mm
Length of corrugation (l)	70 mm
Depth of corrugation (d)	15 mm
Total length of column (L)	1000 mm
Width-Breadth dimensions of SSC	210 mm × 210 mm
Width-Breadth dimensions of Square core in DSC	117 mm × 117 mm
Diameter of circular core in DSC	167 mm

provided for the proposed model is 20 mm along z-direction. The boundary condition at bottom of columns are assumed to be clamped. In eccentric loading, eccentricity is provided at half distance from center of column in x-direction and load is applied along z-direction. End results will give the maximum axial load it can carry. The major parameter set was the shape of stiffeners on which the strength mainly depends on and secondary parameter being shape of inner cores in DSC. Results were compared with SSC and DSC models and best configuration in terms of maximum load carrying capacity was obtained.

3 Modeling and Analysis

SSC and DSC models are modeled separately. Initially all the engineering data of steel were fed as input values and geometry was created. SOLID 186 element is used for modeling. All models are of 1000 mm length. Mesh size of 10 mm was chosen such that a better convergence was obtained with the experimental results. Under static structural, load and support were created and assigned in terms of displacement. Force reaction and total deformation were chosen as output variables based on which performance of specimens are compared in terms of maximum load carrying capacity. Loading is varied, based on which analysis was performed. Variations were made on corrugated hollow steel columns by providing stiffeners of different shapes. 3 mm thickness is adopted for connecting stiffeners and outer corrugated panels. Figure 2 shows various single skin model with different stiffeners.

Double skin corrugated steel column consists of a hollow square and circular flat steel core inside the single hollow steel column. Both square and circular cores are modeled so that it has equal volume. The core is connected to outer skin by different types of stiffeners. Various DSC models with square and circular cores is shown in

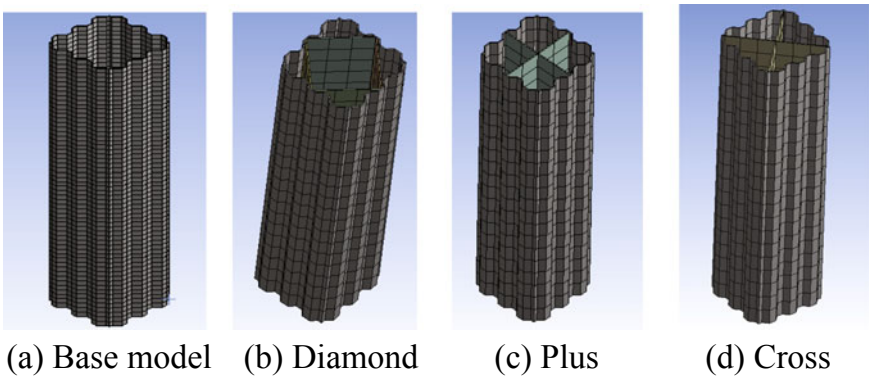

Fig. 2 SSC models with different stiffener patterns

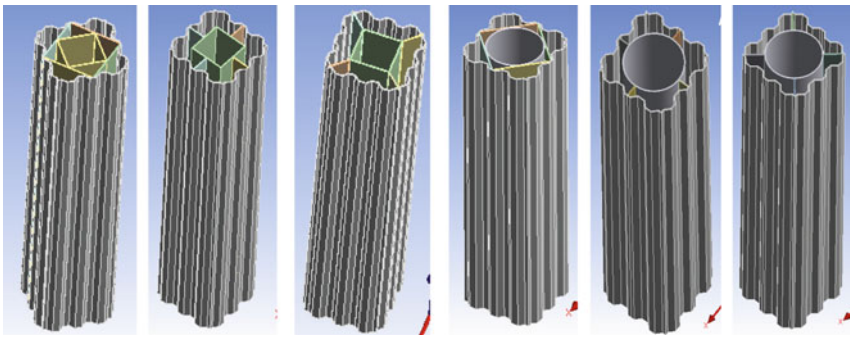

Fig. 3 Models of square and circular cores with different stiffeners

Fig. 3. Models are subjected to axial and eccentric loading. Developing such DSC models increases load carrying and buckling capacity compared to SSC models.

4 Results and Discussions

Strength to weight ratios of all the columns with stiffeners are evaluated. Failure patterns obtained for all types of corrugated steel columns in case of both axial and eccentric loading are analyzed. Comparison of force reaction with corresponding deformations are done. Load—deformation curves are plotted for SSC and DSC models under both cases of loading. Figures 4 and 5 indicates deformation patterns of diamond, plus and cross models under axial and eccentric loading of SSC models. Force reaction and deformation obtained from the analysis are compared. Graphs are

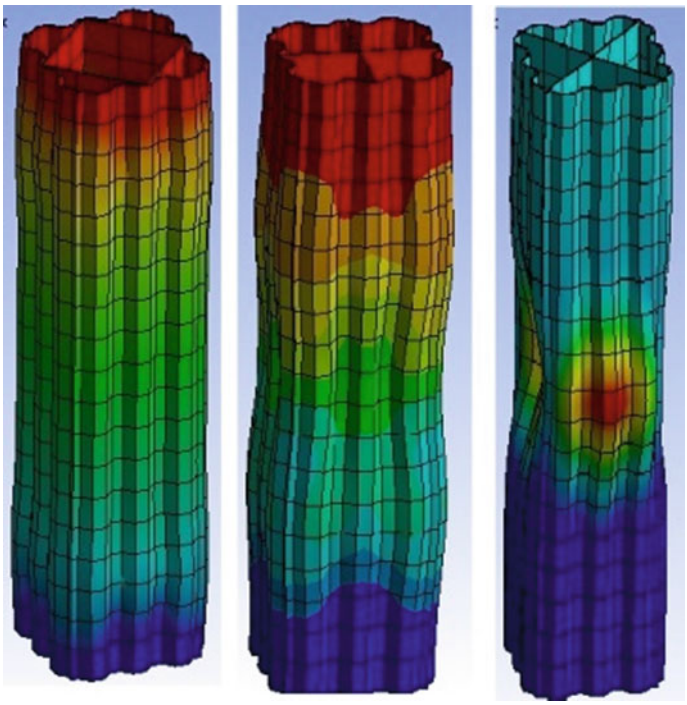

Fig. 4 Deformation under axial loading

plotted between loads and deformations for SSC models under both axial (AL) and eccentric (EL) loading separately and are shown in Fig. 6 and 7 respectively.

DSC models with square core and circular core with diamond, plus and cross stiffeners subjected to axial and eccentric loading is shown in Figs. 8 and 9 respectively. Under axial loads all models under goes global buckling while under eccentric loads local buckling is appeared to be happen due to localized compression of steel member.

Graphs showing load-deformation curve are indicated in Figs. 10 and 11.

By comparing analytical results plotted in graphs the maximum loading carrying capacities and corresponding deformations for each model along with strength to weight ratios of models with stiffeners are tabulated. It is observed that both SSC and DSC models with same types of stiffener for same behavior. Tables 3 and 4 shows considerable increase in load carrying capacity of SSC and DSC columns when different types of stiffeners are used. Variations are noted under axial and eccentric loading.

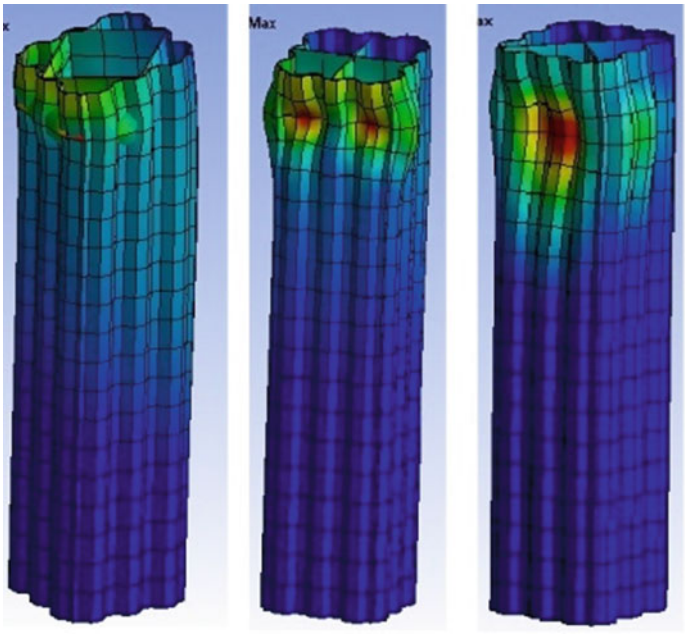

Fig. 5 Deformation under eccentric loading

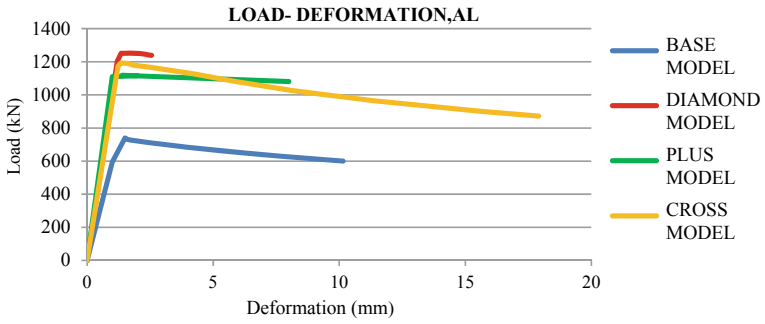

Fig. 6 Load deformation axial loading

5 Conclusions

In this paper, an analytical study on hollow corrugated steel columns under axial and eccentric loading is performed by using ANSYS Workbench 16.1. Based on the results obtained by various corrugated models, it is found out that strength to weight ratio for SSC models for all columns with different stiffener pattern is obtained around 6.67 under axial loading and around 4.67 under eccentric loading. Strength to weight ratio for DSC models under axial loading for both square and circular core

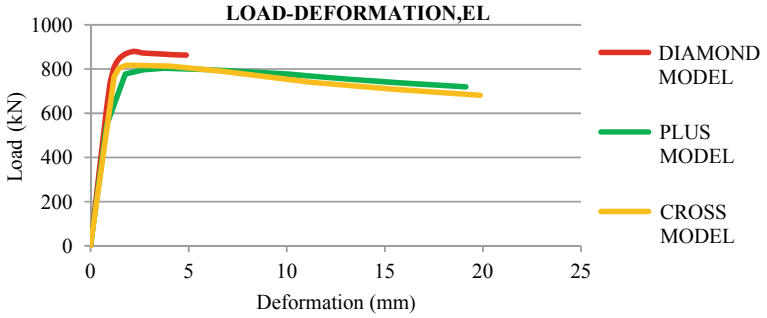

Fig. 7 Load deformation eccentric loading

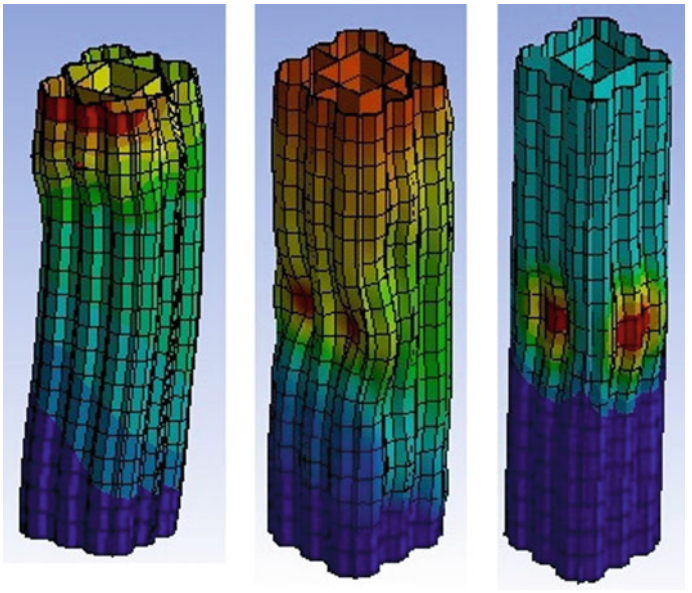

Fig. 8 Deformation under AL

is found around 5.6 and similarly, under eccentric loading it is found around 4. Since models with stiffener under same types of loading have almost similar strength to weight ratio values, the difference is negligible.

SSC with diamond shaped stiffener have 65% increase in load carrying capacity than the column without stiffeners under axial loading. It is also observed that compared to other stiffeners, there is 11% increase in load carrying capacity. Under eccentric loading, load carrying capacity is increased by 68% than the column without stiffeners and 9% increase for columns with other stiffeners.

Similarly, DSC of square core with diamond stiffener have 28% increase in load carrying capacity than the SSC with diamond stiffener under axial loading and 23%

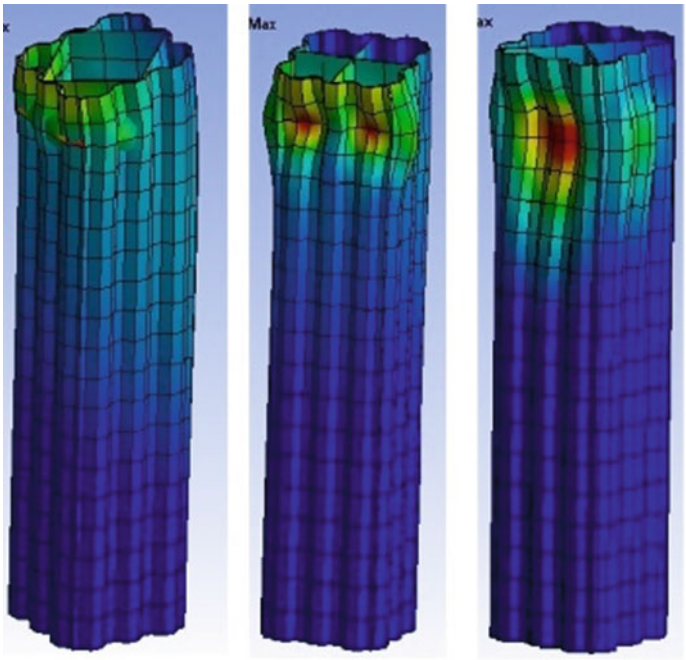

Fig. 9 Deformation under EL

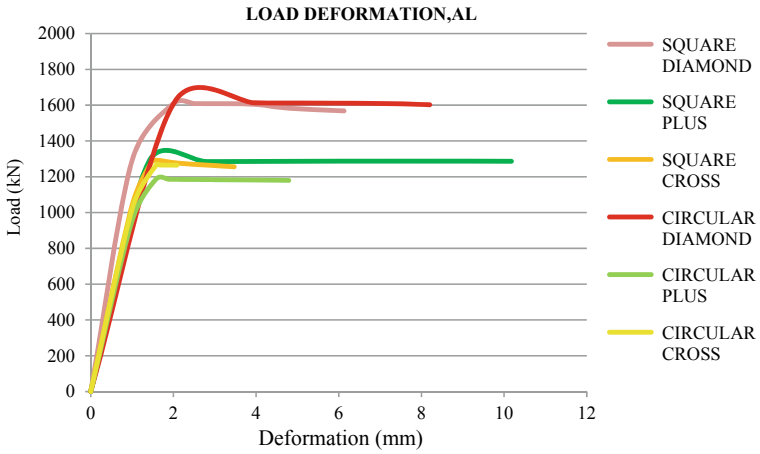

Fig. 10 Load-deformations under axial loading

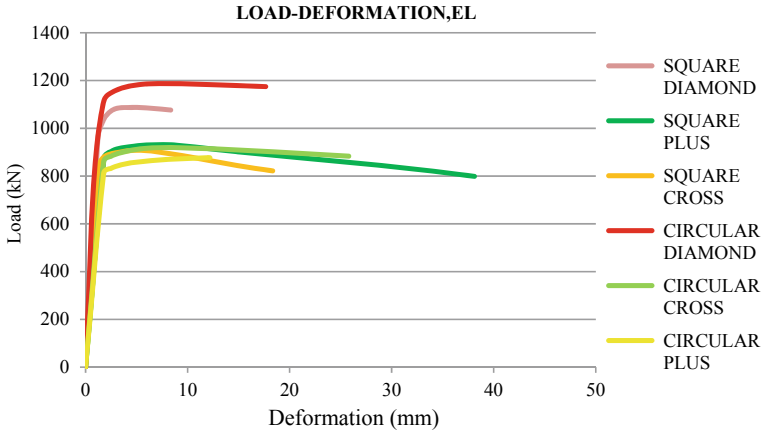

Fig. 11 Load-deformation under eccentric loading

Table 3 Maximum loads and deformations under axial and eccentric loading (SSC)

SSC models	Axial loading			Eccentric loading		
	Load (kN)	Deformation (mm)	Strength to wt ratio	Load (kN)	Deformation (mm)	Strength to wt ratio
Base model	758.36	1.5	–	523.7	3.17	–
Diamond model	1252	1.6	6.5	879.96	2.19	4.5
Plus model	1118	14	6.8	803.96	3.75	4.8
Cross model	1192	1.4	6.7	817.78	1.84	4.6

increase under eccentric loading. DSC of circular with diamond stiffener have 28% increase in load carrying capacity than SSC with same stiffener pattern under axial loading and 34.8% increase under eccentric loading. Thus, it is concluded that the corrugated column with diamond shaped stiffener shows the best structural performance under both axial and eccentric loading. It is mainly due to peculiarity of diamond shape and column with diamond shape stiffener is chosen as the best model.

Table 4 Maximum loads and deformations under axial and eccentric loading (DSC)

DSC models	Axial loading			Eccentric loading		
	Load (kN)	Deformation (mm)	Strength to wt ratio	Load (kN)	Deformation (mm)	Strength to wt ratio
Square diamond	1608.7	2.5048	5.4	1086.9	5.3179	3.8
Square cross	1292.9	1.5153	5.6	897.91	3.0576	4.1
Square plus	1287.3	8.05	5.8	931.15	8.1614	4.2
Circular diamond	1612.1	4.0006	5.4	1186.8	6.5155	3.8
Circular cross	1265.7	1.5853	5.6	919.35	8.1101	4.1
Circular plus	1186.8	1.5814	5.8	877.23	11.958	4.2

References

1. Nassirnia M, Heidarpour A, Zhao X-L, Minkkinen J (2015) Innovative hollow corrugated columns: a fundamental study. Eng Struct 94:43–53
2. Javidan F, Heidarpour A, Zhao X-L, Minkkinen J (2015) Performance of innovative fabricated long hollow columns under axial compression. J Construct Steel Res 106:99–109
3. Farahi M, Heidarpour A, Zhao X-L, Al-Mahaidi R (2016) Compressive behaviour of concrete-filled double-skin sections consisting of corrugated plates. Eng Struct 111:467–477
4. Farhana S, Johnson J (2019) Combined effect of with and without corrugated concrete filled double skin tubular sections subjected to axial, Biaxial, and Lateral Loading
5. Farahi M, Heidarpour A, Zhao X-L, Al-Mahaidi R (2016) Parametric study on the static compressive behaviour of concrete-filled double-skin sections consisting of corrugated plates. Thin-walled Struct 107:526–542
6. Javidan F, Heidarpour A, Zhao X-L, Minkkinen J (2016) Application of high strength and ultra-high strength steel tubes in long hybrid compressive members: experimental and numerical investigation. Thin-Walled Struct 102:273–285
7. Zhou F, Young B (2019) Experimental investigation of concrete-filled single-skin and double-skin steel oval hollow section stub columns. Thin-Walled Struct 140:157–167
8. Nassirnia M, Heidarpour A, Zhao X-L (2017) Experimental behaviour corrugated columns under lateral impact loading. Procedia Eng 173:383–390
9. Nassirnia M, Heidarpour A, Zhao X-L, Minkkinen J (2016) Innovative hollow columns comprising corrugated plates and ultra high-strength steel tubes. Thin-Walled Struct 101:14–25
10. Nassirnia M, Heidarpour A, Zhao X-L (2017) A benchmark analytical approach for evaluating ultimate compressive strength of hollow corrugated stub columns. Thin-Walled Struct 117:127–139

Study of Fly Ash Based Light Weight Concrete with Plastic Waste Aggregate as a Partial Replacement of Coarse Aggregate

Thasni Kaseem and S. Sreerath

Abstract In concrete industry there has been increasing trend towards use of recycled aggregate to save lot of natural resources and to provide lightweight concrete (LWC). Compared with conventional concrete, LWC can considerably cut back the dead load of structural elements. The low biodegradability of plastic and the presence in massive quantities of waste plastic negatively impact the environment. This study focuses on the development of light weight concrete using waste materials as a part of waste management. This study presents the mechanical properties of concrete by using waste plastic as a partial replacement of coarse aggregate in various proportions of 5, 10, 15, 20% and by replacing cement with 10, 20, 30% of fly ash. The low densified composite material was much lighter than that of the conventional light weight concrete. To offset the reduction of strength due to the less densified structure, the addition of mineral admixture was proposed. The investigation using fly ash has showed an improvement in the compressive strength.

Keywords Compressive strength · light weight concrete · Fly ash · Plastic aggregate · Density

1 Introduction

Lightweight concrete has extreme importance to the construction industry. The specialties of lightweight concrete are its less density and thermal conductivity. So its benefits are that there is a reduction of dead load, quicker building rates in construction and lesser transport and handling costs. Lightweight material suitable for a wide range of purposes such as panels, block production, floor and roof screeds, wall

T. Kaseem (✉) · S. Sreerath
Department of Civil Engineering, Federal Institute of Science and Technology (FISAT), Ernakulam 683577, India
e-mail: thathuthasnis123@gmail.com

S. Sreerath
e-mail: iamsreerath@gmail.com

© Springer Nature Switzerland AG 2021

K. Dasgupta et al. (eds.), *Proceedings of SECON 2020*,
Lecture Notes in Civil Engineering 97,
https://doi.org/10.1007/978-3-030-55115-5_39

casting, complete house casting, sound barrier walls, floating homes, void infill, slope protection, outdoor furniture and many more applications [1].

Normal weight concrete a density in the range of 2240–2400 kg/m^3. Lightweight concrete (LWC) has a density of less than 2000 kg/m^3 is referred as structural LWC. Introducing various types of lighter aggregates into the matrix is a suitable way to lower a concrete density. The crushed stone and sand are the components that are commonly replaced with lightweight aggregate (LWA) to develop LWC. When light weight concrete is used for the structure to replace normal concrete, the weight of the structure is reduced by 20–40%. This is an efficient way to deduce dead load of the structure [2].

Disposal of waste plastic around the world is a major challenge which society is facing today. Worldwide plastic production in 1950 was 1.7 Mt. By 2012, this had increased by approximately 170 times to 288 Mt. For solving the spoilage of large amount of plastic materials and to meet the increasing need for aggregates, reuse of plastic in concrete is considered as the feasible application for light weight concrete [3].

Fly ash is a by-product of the combustion of pulverised coal and is a pozzolanic material. When it is combined with Portland cement and water, it produces a product similar to that formed by cement hydration and having a denser microstructure make it less permeable. The fly ash replacement level as 15 - 25% is recommended for high strength concrete, while it can be used as more than 50% of total binder for concrete [4].

This study focuses on the utilization of plastic aggregate to develop the light weight concrete and fly ash is used to improve strength of the concrete.

2 Materials used

2.1 Cement

Ordinary Portland cement (OPC)-53 grades confirming to IS: 4031-1991 part 2 was used (sharjah cement). Physical properties of cement shown in Table 1.

Table 1 Physical properties of cement

Fineness	Specific gravity	Initial setting time	Consistency
5.8%	3.16	42 min	32%

Table 2 Properties of fine aggregate

Fineness modulus	Specific gravity	Water absorption
2.83	2.75	1.31%

Table 3 Properties of Coarse aggregates

Specific gravity	Water absorption
2.78	0.93%

2.2 Fine Aggregate

M sand is used as fine aggregate conforming to grading zone-II. IS 2386-2016(part 3) (Table 2)

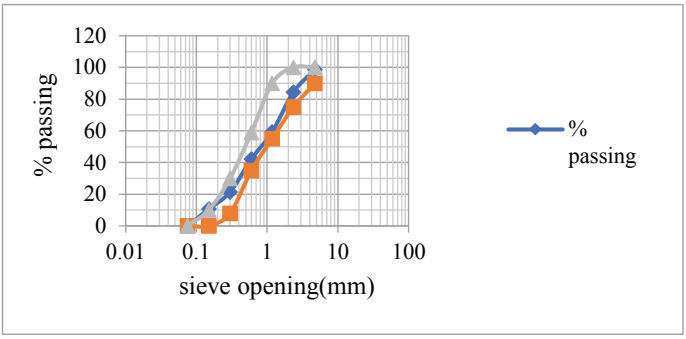

From the gradation curve, fine aggregate is confirming to grading zone II.

2.3 Coarse Aggregate

The coarse aggregate used in this work was of 10 mm nominal size (Table 3).

2.4 Plastic Waste Aggregate

Waste plastic materials such as broken plastic bottle, bucket, basket and thin container made by Low Density Polyethylene (LDPE) had been collected, shredded and washed (Fig. 1; Table 4).

Fig. 1 Plastic aggregates

Table 4 Properties of plastic aggregates

Specific gravity	Water absorption
0.9	0.02%

2.5 Fly Ash

See Table 5.

3 Mix proportion

M25 grade mix design was carried out with reference to IS code - 10262:2009 [5]. The mix proportion was given in Table 6.

M25 mix was casted in cubes and cured for 28 days. The results of compressive strength and slump were shown in Table 7.

Table 5 Properties of fly ash

Specific gravity	Particle size	Surface area
2.2	22.2 μm	649.9 m^2/kg

Table 6 Mix proportion of control mix

Mix	Cement (kg)	Fine aggregate (kg/m^3)	Coarse aggregate (kg/m^3)	Chemical admixture (kg/m^3)	Water (L)
Control mix	386	720.96	1223.98	3.06	154.8

Table 7 Compressive strength of control mix

Mix	7th day strength (MPa)	28th day strength (MPa)	Slump (mm)
Control mix	21.81	28.26	True slump (100)

4 Result and Discussion

The result obtained from Compressive tests conducted on concrete on various percentage of plastics and fly ash are discussed below.

4.1 Optimisation of Plastic

4.1.1 Compressive Strength

The concrete cubes of size 150 mm × 150 mm × 150 mm were casted in a mould by replacing coarse aggregate with 5, 10, 15 and 20% plastic aggregate and kept for 28 days [6]. The compressive strength is shown in Fig 2. The optimum value of compressive strength was obtained in 20% replacement of plastic aggregate (Table 8).

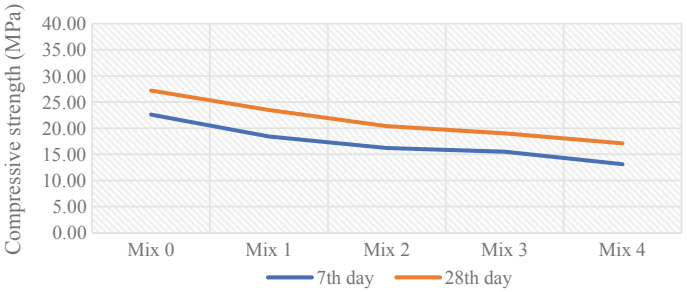

Fig. 2 Graph showing compressive strength of specimens

Table 8 Mix proportions

	% of plastic	Cement (kg/m^3)	Fine aggregate (kg/m^3)	Coarse aggregate (kg/m^3)	Chemical admixture (kg/m^3)	Water (L)
Mix 0	0	386	720.96	1223.98	3.06	154.8
Mix 1	5	386	720.96	1162.78	3.06	154.8
Mix 2	10	386	720.96	1101.58	3.06	154.8
Mix 3	15	386	720.96	1040.3	3.06	154.8
Mix 4	20	386	720.96	979.184	3.06	154.8

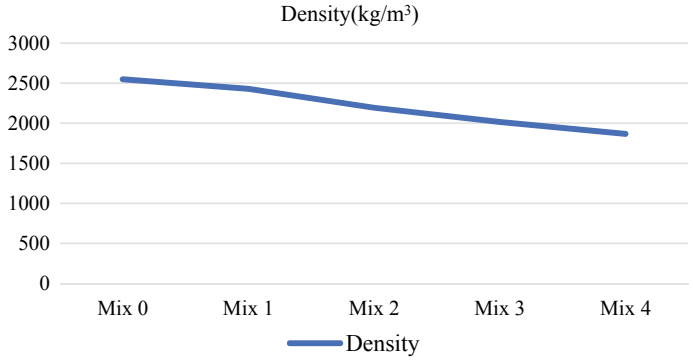

Fig. 3 Graph showing the density of mixes

The value of compressive strength for mixture decreased at increasing the content of waste plastic aggregate. It can be concluded that the ratio 20% of plastic gives the lowest density of 1866.66 kg/m^3 which confirmed to light weight concrete. These behaviours give us an idea about the percentage of replacement for added plastic must be controlled within the allowable compressive strength. Decrement in the strength is due to the lower specific gravity of the plastic and it has lack of bonding with matrix [3] (Fig. 3).

The density of concrete varies from 1866.66 to 2548.14 kg/m^3, indicating a saving in the self-weight. An increase in plastic weight percentage added to the mix led to a decrease in the values of densities for the prepared concrete due the low specific gravity of plastic [7].

4.2 Optimisation of Fly Ash

4.2.1 Compressive Strength

To offset the reduction of strength due to the less densified structure, the addition of fly ash was proposed. The cubes of size 150 mm × 150 mm × 150 mm were casted by replacing cement with 10, 20, 30 and 40% fly ash and cured for 28 days [8]. Compressive strength was recorded in Fig 4. The test was conducted to find the optimum mix of fly ash (Table 9).

The value of compressive strength for mixture increased at increasing the content of Fly ash and decreased at a specific point. It can be concluded that the 30% of fly ash gives the highest compressive strength of which confirmed to light weight concrete. These behaviours give us an idea about the percentage of replacement for added fly ash must be controlled to develop high strength. The increment in strength is due to the good pozzolanic action of fly ash [9] (Fig. 5).

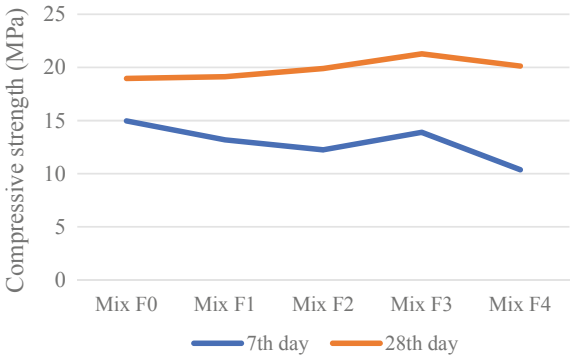

Fig. 4 Graph showing compressive strength of specimen

Table 9 Mix proportions

	% of Fly ash	Cement (kg/m^3)	Fine aggregate (kg/m^3)	Coarse aggregate (kg/m^3)	Chemical admixture (kg/m^3)	Water (L)
Mix 0	10	347.4	720.96	979.184	3.06	154.8
Mix F1	20	308.8	720.96	979.184	3.06	154.8
Mix F2	30	270.2	720.96	979.184	3.06	154.8
Mix F3	40	231.6	720.96	979.184	3.06	154.8

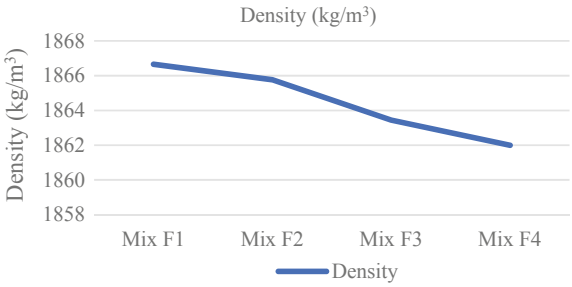

Fig. 5 Graph showing the density of mixes

5 Conclusions

- Lightweight concrete generally has a density of less than 2000 kg/m^3 and 20% of plastic gives the lowest density of 1866.66 kg/m^3 which confirmed to light weight concrete. The value of compressive is decreasing from 28.26 to 18.96 MPa.
- 20% plastic aggregate replacement decreases split tensile strength from 3.22 MPa to 2.21 MPa and flexural strength from 3.45 MPa to 2.57 MPa and it shows there is a decrement in the strength. As the results shows decrement in the strength properties, cement is partially replaced with fly ash.

- By the addition of fly ash up to 30% the compressive strength is increased to 21.28 MPa and increases split tensile strength from 2.21 to 2.53 MPa and flexural strength from 2.57 to 2.78 MPa.
- Replacement of cement with fly ash in a controlled dosage helps to enhance the strength parameters of the concrete. As the spoilage of waste plastic is one of the main hazard to our society, plastics can be utilised to develop low densified concrete structure.

References

1. Manindra Kumar S, Kirti C, Anil Kumar S (2013) Experimental study of light weight concrete using plastics. Arora 2(5)
2. Hameed AM, Abdul-Fatah Ahmed B (2018) Employment of plastic waste in the light weight concrete. Technologies and materials for renewable energy, Environ Sustain 2(4) (Elsevier)
3. Choi Y-W, Moon D-J, Chung J-S, Cho S-K (2004) Effects of waste PET bottles aggregate on the properties of concrete cement and concrete. Research 4(3) (Elsavier)
4. Mehmannavaz T, Sumadi SR, Bhutta MAR, Samadi M, Sajjadi SM (2013) Effect of waste materials in lightweight concrete. Australian J Basic Appl Sci 7(11):513–519
5. Panyakapo P, Panyakapo M (2008) Reuse of thermosetting plastic waste for lightweight concrete. Waste Manage 3(2):1581–1588
6. Alqahtani F, Ghataora, G, Khan MI, Dirar I, Kioul A, Al-Otaibi M (2015) Lightweight concrete containing recycled plastic aggregates. In: International conference on electromechanical control technology and transportation (ICECTT) 2(6)
7. Habib Md Z, Alom Md M, Hoque MdM (2017) Concrete production using recycled waste plastic as aggregate. J Civil Eng (IEB) 3(1)
8. Nadesan MS, Dinakar P (2010) Mix design and properties of fly ash waste lightweight aggregates in structural lightweight concrete. J Hazardous Mater 2(4) (Elsavier)
9. Kayali O, Zhu B (2005) Chloride induced reinforcement corrosion in lightweight aggregate high-strength fly ash. Concrete Construct Build Mater 19(4):327–336

Modified Magnetized Water Concrete Using Nanosilica

Punya Lal and P. E. Kavitha

Abstract It is expected that in the near future, the civil engineering community will have to produce structures in harmony with the concept of sustainable development through the use of high-performance materials with low environmental impact that are produced at a reasonable cost. Magnetic water concrete provides one route towards this objective. When water passes through a magnetic flux it is known as magnetized water. The magnetic effects changes the physical & chemical parameters of natural water, resulting in improvement of filtration properties and increase dissolving properties of water Su et al.(Cem Concr Res 30, 2000 [1]). One of the basic characteristics of magnetically treated water, which has major importance in concrete making, is its pertaining to colloidal particles allowing a more complete hydration process to occur and enhancing the mechanical strength of concrete. The magnet used to make the water magnetic is permag-N406 Bharath et al. (JCPS 9(4) 2016, [2]). The changes in properties of magnetized water such as pH value, hardness and evaporation rate were studied. The optimal value of magnetization is also carried to find out the maximum exposure time of water with the magnetic field. Study on compressive strength, split tensile strength, workability and plastic shrinkage of concrete were carried. Cement is also partial replaced with Nano silica by 5, 10, 15 and 20% for obtaining good characteristic strength.

Keywords Magnetization · Permag N-406 · Nanosilica · Workability · Shrinkage

P. Lal (✉) · P. E. Kavitha
Department of Civil Engineering, Federal Institute of Science and Technology (FISAT), Ernakulam 683577, India
e-mail: punyapyarilal@gmail.com

P. E. Kavitha
e-mail: kavithapurakat@gmail.com

© Springer Nature Switzerland AG 2021

K. Dasgupta et al. (eds.), *Proceedings of SECON 2020*,
Lecture Notes in Civil Engineering 97,
https://doi.org/10.1007/978-3-030-55115-5_40

1 Introduction

Water is a vital ingredient of concrete as it participates actively in the chemical reaction with cement. It oversees the hydration of cement, workability, microstructure, strength and overall durability of concrete. Magnetized water while mixing concrete will increase mechanical property and also higher workability for the same water cement ratio [3]. Magnetization increases negative ionic hydration, thus intensifying the damaging effect on the water crystal structure [4]. One of the basic characteristics of magnetically treated water, which has major importance in concrete making, is its pertaining to colloidal particles and solutions. In the mixing of water and cement, hydration reaction will first take place on the surface of the cement particles. A thin layer of hydration products is thus formed on the cement particles, which hinders further hydration of the cement particles, thus preventing the development of mechanical strength of the concrete. However, if magnetic water is used instead, water molecules can easily penetrate into the cement particles, allowing a more complete hydration process [5]. The objectives involved in this experimental research work are to study the variation of properties of water when it is subjected to a magnetic field at different hours of magnetization. To study the effect of magnetization hours on strength properties and to investigate on the mechanical properties of modified magnetized concrete using Nano silica (5, 10, 15 and 20%). To study the effect on workability of modified magnetized concrete using Nano silica and the plastic shrinkage behaviour of concrete.

2 Literature Review

Youkai Wang et al. investigated on the properties of water such as Boiling point, Specific heat, Evaporation amount. Concrete cube sample are prepared using water magnetized with 100, 200, 300, 400 mT Magnetic field. With the use of magnetized water there found a decreases in boiling point and specific heat, increases evaporation amount.

Nan su et al. water is treated water with different magnetic field intensity 0.2, 0.4 … 1.35 T. Optimum magnetization is obtained in the field range of 0.8–0.2 T. Studied effect of partial replacement of cement with ggbs together with magnetized water. Adding gbbs is found to increase the compressive strength of mortars increases up to 21%.

S. Bharath et al. Mix 1 consists of 100% Cement. Mix 2, Mix 3, Mix 4 and Mix 5 were replaced with 10%, 15%, 20% and 30% of copper slag respectively day compressive strength of MWC with 85% Cement + 15% Copper slag (85C + 15CS) as 27.53 MPa which was higher than 23.33 MPa that of control mix (TWC1).

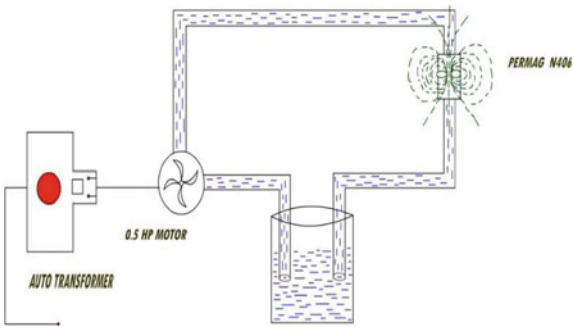

Fig. 1 Magnetizing set up

H. Wei et al. Water is treated at different magnetic field intensity. Early-age shrinkage cracking resistance of concrete mixed with magnetic water is improved than those mixed with tap water. Number of cracks and the maximum width of cracks decrease in comparison with that of normal concrete mixed with tap water.

3 Magnetization

In this process the water is circulated in the magnetic field of 9000 Gauss using the magnet, PERMAG N-406 to induce magnetic flux in the water. This Recirculated water is used for the casting of concrete specimens. The setup includes an autotransformer, 0.5 HP general purpose motor, PERMAG and pump connecting the tank and magnet. This controls the flow of water in the setup. The setup adopted for the magnetic treatment of water is shown in Fig. 1 'PERMAG' changes the physical state of the minerals, while maintaining their chemical state [2].

4 Materials Used

4.1 Materials

Ordinary Portland cement (OPC)-53 grades confirming to IS: 12269-1987 was used. Fineness modulus 6%, specific gravity 3.19 and with initial setting time 96 min. In the present investigations, M sand is used as fine aggregate and has a specific gravity of 2.5 and conforming to grading zone-II. Water absorption and fineness modulus 2.71 and 1.10% respectively. The coarse aggregate used in this work was of 20 mm nominal size. It has a specific gravity of 2.71 and water absorption 0.6%.

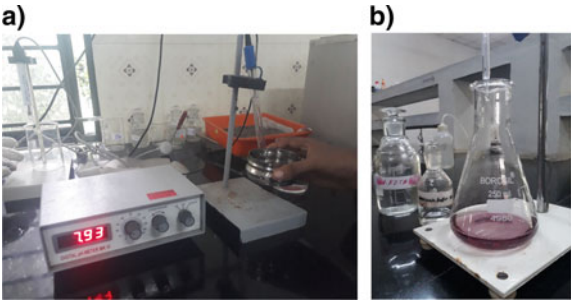

Fig. 2 **a** pH meter. **b** Hardness test

Table 1 Variation in properties of magnetized water

Magnetizing hours (h)	0	24	48	72	96
pH	6.84	7.56	7.93	7.86	7.91
Hardness	32	30	20	16	11

4.2 Magnetic Water

In the present study water is magnetized for 24, 48, 72 and 96 h [6] and studied on variation of pH using pH meter, and hardness (Fig. 2) of magnetized water by titration method. From Table 1 it is clear that the nature of water changes from acidic (6.84) to basic (7.91) since the pH value increase with magnetization this is due to the effect of magnetization on carbon dioxide hydration [7] and hard to soft water by separating Ca and Mg from water [8, 9] (Fig. 2).

4.3 Nano Silica

Silica fume can replace cement in quantities of 5–20%. The specific gravity of nanosilica was obtained as 2.17 (Table 2; Fig. 3).

Table 2 Composition of silica

CaO (%)	MgO (%)	SiO_2 (%)	Al_2O_3 (%)	Fe_2O_3 (%)
0.27	0.09	98.38	0.01	0.006

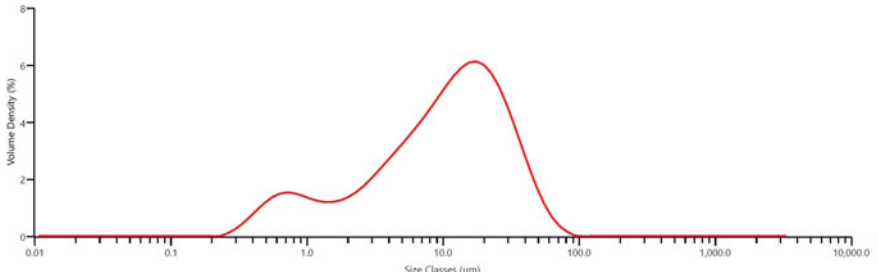

Fig. 3 Particle distribution curve of nanosilica

5 Mix Proportion

Trial mix 1 = 1: 3.7: 2.04: 0.45, Trial mx 2 = 1:1.76:3.23:0.4, Trial mix 3 = 1:2.95:1.62:0.4. M20 grade mix design was carried out with reference to IS code-10262:2019. Super plastizer used is auramix 200. Trial and error method is adopted to arrive at the suitable normal concrete mix. Hence arrived at different mix proportion the strength of which is tabulated below (Tables 3 and 4).

The strength of the three cubes where determined which is tabulated above. From the obtained values it is evident that the M_3 have greater strength and good workability than the other two mixes hence arrived at M_3.

Table 3 Mix proportion of trial mix

Mix (1 cube)	Cement(kg)	Fine aggregate (kg)	Coarse aggregate (kg)	Chemical admixture (mL)	Water (L)
M_1	330	673.49	1221.20	3.06	148.5
M_2	371	655.09	1199.61	3.3	148.5
M_3	396	638.17	1169.90	3.67	158.4

Table 4 Strength of trial mix

Mix	7th day strength (MPa)	28th day strength (MPa)	Slump
M_1	16.07	17.00	Shear slump (65)
M_2	19.29	21.64	Shear slump (70)
M_3	20.89	29.71	True slump (98)

6 Result and Discussion

6.1 Effect of Magnetization Hour on Compressive Strength

The compressive strength of cube specimens is obtained from compression testing machine. Instead of normal water the water is magnetized for 24, 48, 72 and 96 h for casting cubes to get desirable result. The compressive strength of magnetized concrete is tabulated below. This improvement is mainly due to the complete hydration achieved due to magnetization [10] (Table 5; Fig. 4).

It was concluded that subjecting the water to 48 h of magnetization has got desirable results. For further study mix with 48 h magnetized water is used and mineral admixture, nano silica were partially replaced in different percentages with cement 5, 10, 15 and 20%.

Table 5 Optimum magnetization

Magnetizing hours (h)	Compressive strength (MPa)	
	7th day	28th day
0	20.89	29.71
24	21.21	30.87
48	25.29	41.60
72	24.51	40.90
96	23.31	31.83

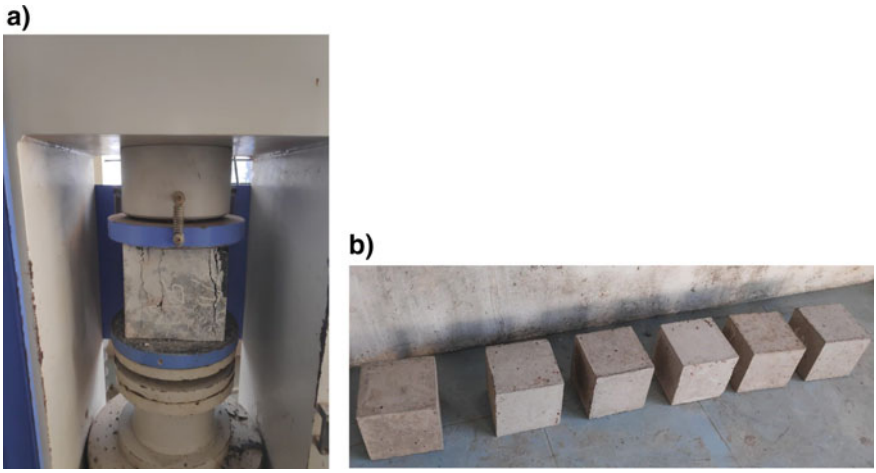

Fig. 4 **a** compressive test **b** Cube specimen

Table 6 Strength properties of magnetized concrete partially replaced with nanosilica

Magnetized mix with Nano silica (%)	Compressive strength (MPa)		Split tensile strength (MPa)	
	7th day	28th day	7th day	28th day
0	25.29	41.06	2.21	3.01
5	29.04	43.21	3.11	3.81
10	34.76	46.67	4.34	4.42
15	28.88	46.61	3.21	3.65
20	30.50	45.73	3.33	3.78

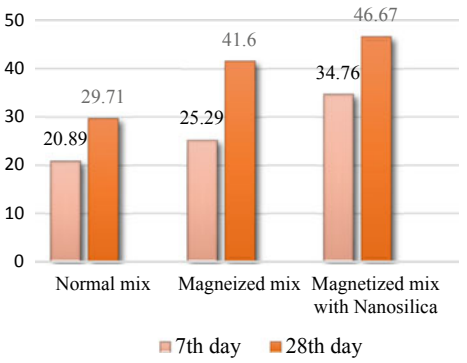

Fig. 5 Comparison of 7th day and 28th day compressive strength

6.2 *Effect of 48 h Magnetization on Mechanical Properties of Concrete Replaced with Nano Silica*

Strength properties of 48 h Magnetized concrete replaced with the admixture nanosilica are shown in Table 6. It is observed that mix with 48 h magnetized water with 10% nanosilica obtained maximum strength properties among all mixes. From this study it was also observed that, mix with magnetized water gives better strength properties than the mix with ordinary water. Nano-silica mixed cement can generate nano-crystals of C-S-H gel after hydration. Nano-crystals accommodate in the micro pores of the cement concrete, hence improving the permeability and strength of concrete [11] (Fig. 5).

6.3 *Effect of Magnetization on Workability of Concrete Re Placed with Nano Silica*

In the present study the cement is partially replaced with 10% nanosilica. One of the demerit of nanosilica is it make the concrete mix less workable [6]. So in the

Table 7 Workability of different mix

With nano silica	Without nano silica		
Normal mix (NWC NS)	Magnetized mix (MWC NS)	Normal mix (NWC)	Magnetized mix (MWC)
82 mm	121 mm	98 mm	100 mm

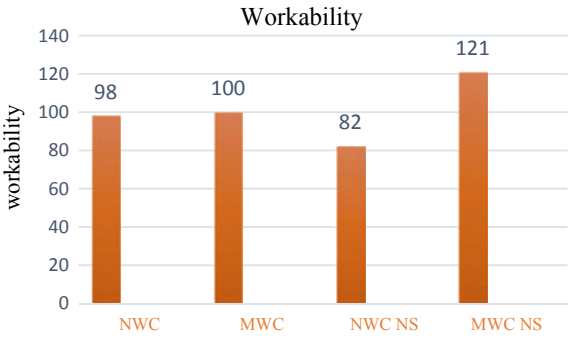

Fig. 6 Comparison of workability

present work the influence of nanosilica along with magnetized water is studied. And it is observed that. Nanosilica has a demerit of making concrete less workable when comparing with normal concrete without nanosilica. so more water need to be added into the mix. Using magnetized water in such mix can improve the workability of concrete even without adding more water into the mix due to the increase in solubility and viscosity [12] (Table 7; Figs. 6 and 7).

6.4 Effect of Magnetization on Plastic Shirnkage of Concrete Replaced with Nanosilica

Plastic shrinkages are by both water evaporation and cement hydration [13]. Normaly when nanosilica is used in a concrete mix it result in the shrinkage of mix due to its desire for higher water content for making the mix workable. The study shows that when magnetized water is used instead of normal water the rate of shrinkage is reduced this may be due to the influence of magnetization on surface tension and specific heat of water [14, 15] (Table 8; Figs. 8 and 9).

Fig. 7 Slump

Table 8 Plastic shrinkage behaviour of normal and magnetized concrete with nanosilica

Mix	Central line initial crack (Min)	Central line final crack (Min)	Time for crack propagation (Min)	Crack width (mm)
Normal mix with nano silica	56	75	19	4
Magnetized mix with nano silica	144	91	53	2

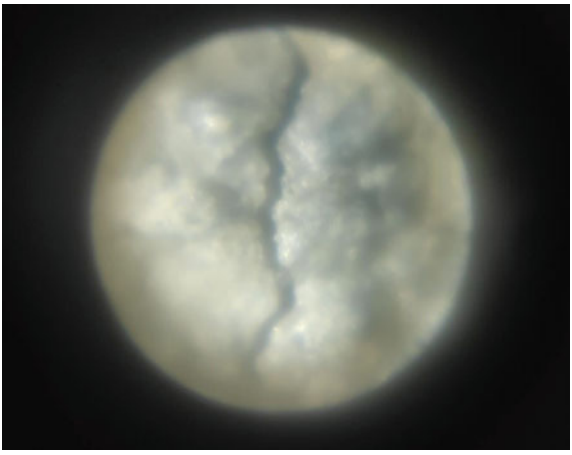

Fig. 8 Normal mix with 4 mm crack

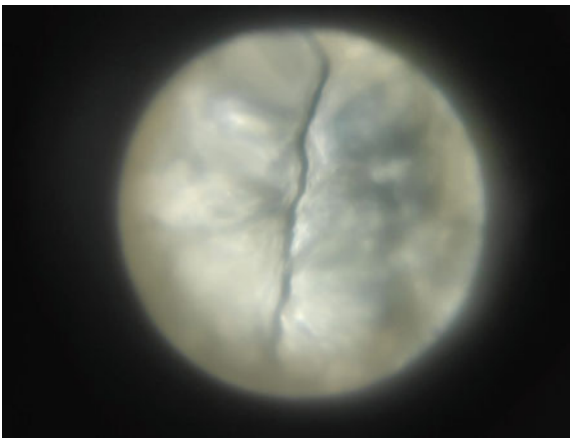

Fig. 9 Magnetized mix with 2 mm crack

7 Conclusion

- Arrived at three trial mixes. Among which 3rd mix (M_3) with mix proportion 1:2.95:1.62:0.4, has good strength and workability. hence it is accepted.
- The nature to water magnetized changes from acidic (6.84) to basic (7.93) and hard (30) to soft water (11).
- Increase strength of 19.74% and 55.74% is obtained for 48 h magnetization and after there is a decrease of 3.01% and 1.68% at 7th day and 28th day strength respectively. Hence the optimum magnetization is 48 h.
- The optimum nanosilica content is 10% of cement with an increase of 19.69% and 8% in compressive strength and 66.35% and 35.41% in split tensile strength for 7th and 28th day respectively.
- Increased workability of 47.56% is obtained for magnetized concrete mix with nanosilica when comparing to normal water concrete with nanosilica.
- Nanosilica has a demerit of making concrete less workable of about 16.46%. so more water need to be added into the mix using magnetized water in such mix can improve the workability of concrete by 23.46% even without adding more water into the mix.
- Plastic shrinkage can be reduced to a greater extent in magnetized water concrete with nano silica.
- Time for appearing initial crack is 144 min for magnetized mix and 56 min for normal mix with nanosilica and the width of crack obtained for normal and magnetized concrete mix with nanosilica is 4 mm and 2 mm respectively this may be due to the specific heat and lower surface tension of magnetized water.

References

1. Su N, Wu Y-H, Mar C-Y (2000) Effect of magnetic water on the engineering properties of concrete containing granulated blast-furnace slag. Cem Concr Res 30
2. Bharath S, Subraja S, Arun Kumar P (2016) Influence of magnetized water on concrete by replacing cement partially with copper slag. JCPS 9(4)
3. Soto-Bernal JJ, Gonzalez-Mota R, Rosales-Candelas I, Ortiz-Lozano JA (2011) Effects of static magnetic fields on the physical, mechanical, and microstructural properties of cement pastes. Adv Mater Sci Eng 4
4. Siva Konda Reddy B, Ghorpade VG, Sudarsana Rao H (2014) Influence of magnetic water on strength properties of concrete. Ind J Sci Technol 7(1)
5. Ramachandran H, Sruthi DK (2018) An experimental study on the use of magnetized water in concrete with M sand as fine aggregate. IOSR J Eng
6. Vinod kumar, Gopala Krishna Sastry KV (2017) Effect of magnetized water on the properties of concrete with different pozzloanic material. J Adv Res Dyn Control Syst 9
7. Bem Amor H, Elaoud A, Hayzn M (2018) Does magnetic field effect water pH. Asian Res. J. Agric. Article 8(1):39196
8. Holysz L, Szczes A, Chibowski E (2007) Effects of a static magnetic field on water and electrolyte solutions. J Colloid Interface Sci
9. Banejad H, Abdosalehi E (2009) The effect of magnetic field on water hardness reducing. Thirteenth International Water Technology Conference, IWTC
10. Afshin H, Gholizadeh M, Khorshidi N (2010) Improving mechanical properties of high strength concrete by magnetic water technology. Scientia Iranica, Trans A: Civil Eng 17
11. Nilli M, Ehsani A, Shabani K (2009) Influence of nano SiO_2 and micro silica on concrete performance. Bu-Ali Sina University Iran
12. Abdel-Magida TIM, Hamdanb RM, Abdelgade AAB (2017) Effect of magnetized water on workability and compressive strength of concrete. In: International conference on analytical models and new concepts in concrete and masonry structures AMCM
13. Wei H, Wanga Y, Luo J (2017) Influence of magnetic water on early-age shrinkage cracking of concrete. Constr Build Mater 147
14. Wang Y, Wei H, Li Z (2017) Effect of magnetic field on the physical properties of water. Results in Phys 8:262–267
15. Manjupriya T, Malathy R (2016) Experimental investigation on strength and shrinkage properties of concrete mixed with magnetically treated water. Int J Eng Adv Res Technol 2(3)

Optimisation of Multistoried Building Using Outrigger System

Jeslin C. Johnson and Reshma Prasad

Abstract The rapid developments of materials, construction technologies and structural systems have given rise to a significant increase of skyscrapers over the past decades. The reduction of the top drifts and base core overturning moments under lateral loads, such as earthquakes and wind loads, has drawn increasing attention in the structural design of super-tall buildings. Outrigger system is considered one of the most effective structural systems to improve the structural lateral stiffness and overall stability, which has been widely used in high-rise buildings. Optimum locations for Installations of outrigger systems can be found. Overall displacements and lateral drift can be reduced. Outrigger systems enhance the stiffness of high rise buildings by the introduction of stiff outriggers at different locations. The effect of outrigger in a setback building is studied. The loads considered are as per IS codes. An Etabs model of 45 storey building is considered for this study. Linear time history analysis has been adopted and data of El-Centro earthquake is used as an input. The different parameters considered are the storey displacement and storey drifts. Effect of adding outriggers to an asymmetrical building is considered.

Keywords Outrigger · Etabs · Time history analysis

1 Introduction

Increasing number of global human population leads to construction of tall buildings which have different types in terms of lateral resisting systems. Tall building has always been a vision of dreams and technical advancement leading to the progress of the world [1]. There has been a demonstrated competitiveness that exists in mankind to proclaim to have the tallest building in the world [2]. As buildings have gotten

J. C. Johnson (✉) · R. Prasad
Federal Institute of Science and Technology, Angamaly, Ernakulam, India
e-mail: cjeslinj@gmail.com

R. Prasad
e-mail: reshma.prasad1@gmail.com

© Springer Nature Switzerland AG 2021

K. Dasgupta et al. (eds.), *Proceedings of SECON 2020*,
Lecture Notes in Civil Engineering 97,
https://doi.org/10.1007/978-3-030-55115-5_41

taller and narrower, the structural engineer has been increasingly challenged to meet the imposed drift requirements while minimizing the architectural impact of the structure [3]. From the early moment frames to today's ultra-efficient mega-braced structures, the structural engineering profession has come a long way [4]. The major factor that affects the design of tall structures is its sensitivity to the horizontal load. The design of tall and slender structures is controlled by two governing factors, strength (material capacity), and stiffness (drift) produced by the action of lateral loading, such as wind and earthquake [5]. The overall geometry of a building often dictates which factor governs the overall design. As a building becomes taller and more slender, drift considerations become more significant. When an earthquake waves travel through the building, it is subjected to massive forces, acceleration and displacement that makes the building highly unstable and eventually it collapses [6]. Undoubtedly, the factor that governs the design for a tall and slender structure most of the times is not the fully stressed state but the drift of the building.

In this paper, best location of outrigger in an asymmetric building is investigated. Hence to make high rise asymmetrical buildings safe against lateral loads, outrigger structural system is used. Investigations were done on building with asymmetrical setback in one direction, to find the optimum outrigger location, to study the effect of dual outrigger and to evaluate the seismic performance of setback building with various outrigger configurations.

1.1 Outrigger in Buildings

Outriggers are rigid horizontal structures designed to improve building overturning stiffness and strength by connecting the building core or spine to distant columns [7]. This is a horizontal load resisting system [8]. Outriggers are horizontal members which connects the interior core of the structure to the outer most columns. Outrigger in a structure can vary from single to multiple according to the height and construction of the building [9]. For high rise buildings, particularly in seismic active zone or wind load dominant, this system can be chosen as an appropriate structure with this exterior columns are used effectively and overall deflection of the structure is reduced. This system helps in reducing the movement of the core when compared to the system with freely standing core without outriggers [10]. The restrain caused by the outrigger reduces the lateral drift at top. The stiffness of the structural system increases by 20–30% by introducing the outrigger structural system [4]. When horizontal loading acts on the building, the column restrained outriggers resist the rotation of the core, causing the lateral deflections and moments in the core to be smaller than if the free standing core alone resisted the loading.

2 Research Methodology

A 45 storey building with regular configuration and setback in one direction was modelled as bay frame with and without the outrigger structural system at various locations to evaluate the seismic performance of the structure. Plan dimension was 35 m × 35 m. Storey height is taken as 3.1 m. It has 7 bays in both longitudinal direction and transverse direction with an equal spacing of 5 m. Figure 1a and b depicts the 3D view of the base model of the 45 storey building and setback building respectively. Setback building has 12 stories with 7 bays, 11 stories with 5 bays and 22 stories with 3 bays respectively in both directions. Setback building is modelled by removing 110 frames from the regular building model. All beams are of the size 300 mm × 600 mm and M50 grade is used. Column size is 700 mm × 700 mm for stories 24 to 45. Column size of 900 mm × 1000 mm is used for storey 1–23. All columns are of M 60 grade concrete and Fe 415 steel is used. Slab thickness is considered as 150 mm. The size of shear wall is taken as 400 mm. A live load of 4 kN/m^2 is applied as per IS: 875 (Part II) 1987 and the dead load is self-weight and Floor finish of 1 kN/m^2. Lateral loads are applied as seismic load in X and Y direction as per IS 1893 (Part 1 2002). The design earthquake load is computed based on the zone factor of 0.36, hard soil, importance factor of 1 and the response reduction factor of 5 (IS: 1893 (Part-I), 2002). The support conditions are assumed as fixed. The columns were checked for load combinations of 1.5 (DL + LL) and was found safe. The property moment of inertia was modified for columns as 0.3. Time history analysis using El-Centro Earthquake data is carried out for all the models to determine the seismic performance.

Modelling was done using the Etabs 2016. Parameters like maximum storey displacement and maximum storey drift values were considered to compare the results. The regular building and asymmetrical building was analysed for the optimum

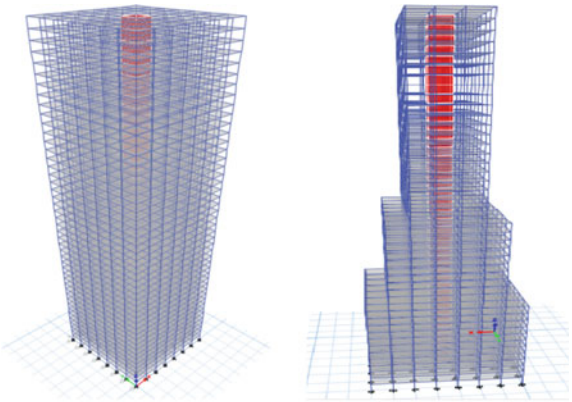

Fig. 1 Three dimensional view of **a** Regular building **b** Setback building

outrigger location. Then the efficiency of dual location is studied in asymmetrical building and then the performances of various outrigger configurations were studied.

3 Seismic Analysis Results

Seismic parameters like maximum displacement and storey drift was considered for analysis of building. Evaluation was done by comparing the seismic performance of building with and without outrigger system. Time history analysis using El-Centro Earthquake data is carried to determine the seismic performance of the models.

3.1 Regular Building

The regular building was analyzed for the optimum location of outrigger by placing X shaped outriggers at 0.2 H, 0.4 H, 0.6 H and 0.8 H height of the building. H indicates the height of the building. Hence the outriggers were placed at 9th, 18th, 27th and 36th storey of the building and are named as RB-0.2, RB-0.4, RB-0.6 and RB-0.8 respectively.

The variation of lateral displacement and drift is shown in Fig. 2. From Fig. 2a It was observed that when the outrigger was provided at 0.6 H location i.e., 27th floor, maximum top storey displacement control was by 34.75% and from Fig. 2b, it was observed that maximum top storey drift control was by 15.38%. Other studies conducted on the efficiency of regular building also obtained similar results [1]. Thus by providing outrigger at 0.6 H drift and displacement of the regular building has maximum control.

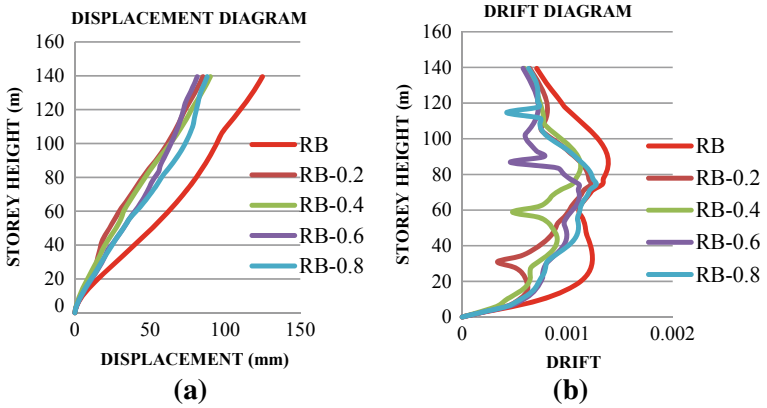

Fig. 2 Storey displacement and drift for regular building at various outrigger locations

3.2 Setback Building

The asymmetrical building was analyzed with the same outrigger locations as in the case of regular building to find the optimum location.

3.2.1 Optimal Location of Outrigger

SB denotes setback building. Following models as per Table 1 were investigated for the optimal location study.

Seismic analysis results on building with setback in one direction are detailed in this section. Figures 3 and 4 depict the lateral drift and displacement of setback building without outrigger and with outrigger at various locations. By providing outrigger drift and displacement was reduced as seen in figure. It was observed that by providing outrigger at 0.6 H i.e. at 27th floor, top storey drift was controlled to a maximum of 40.00 and 38.46% (Fig. 4) and top storey displacement was controlled by maximum of 43.53 and 43.99% (Fig. 3) in X and Y direction respectively.

Table 1 Models for optimum location study of SB

	Model ID	Remarks
Models for optimal location study	SB	No outrigger
	SB-0.2	Outrigger at 0.2 H
	SB-0.4	Outrigger at 0.4 H
	SB-0.6	Outrigger at 0.6 H
	SB-0.8	Outrigger at 0.8 H

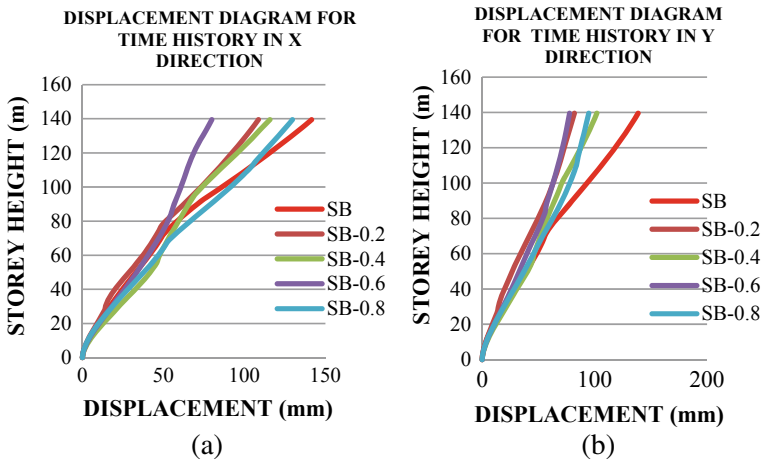

Fig. 3 Displacement for setback building with various outrigger locations in x and y direction

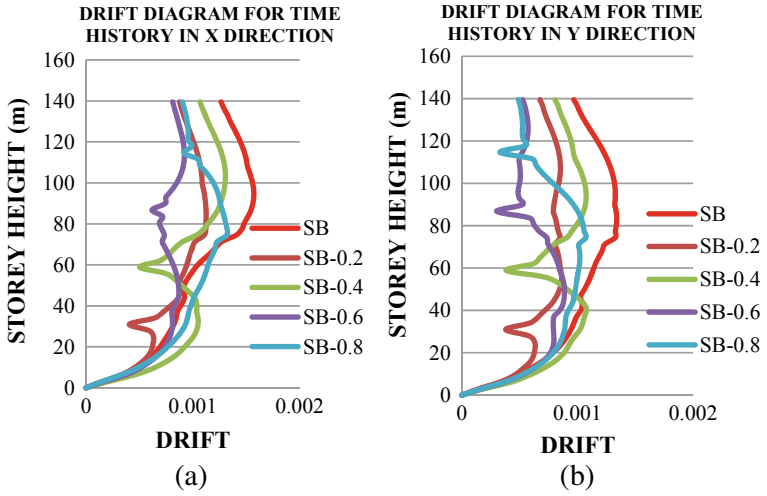

Fig. 4 Drift for setback building with various outrigger locations in x and y directions

It was also observed from the displacement graph that till 20 m, there is little variation between various models. There are no much variations in displacement until 80 m height for models with and without outrigger systems. The effects of outrigger in displacement control are clearly evident above 80 m, which is around 26th storey. There is stiffness change at 23rd and 24th storey and above that the storey layout remains the same. This above phenomenon observed may be due to this fact. From Fig. 4, It is clear that effective drift control is observed at locations were outriggers are provided. While checking the top storey displacement and drift the model with outrigger at 0.6 H location was found to be more effective.

3.2.2 Performance of Dual Outrigger

From the optimal location study in the previous section, the first location of the outrigger was found to be at 0.6 H and effect of dual outrigger was studied by varying the location of second outrigger. Models for dual location study are illustrated in Table 2.

The results from the time history analysis in X and Y directions are depicted in graphical form in Figs. 5 and 6. Figure 5 denotes the displacements and Fig. 6 denotes drift. All the models behave similarly till 20 m height as it is evident in Fig. 5. It was also observed that even though the model SB-2, exhibits good displacement control between 20 and 100 m height in x direction and between 20 and 80 m in y direction, the model SB-3 showed greater displacement control over rest height of building. While considering the top storey displacements in both directions model SB-3, showed maximum control. Hence SB-3 can be considered as the optimum model. On the other hand when the dual outrigger was provided in 0.8 H (SB-6),

Table 2 Models for dual location study

	Model id	Remarks
Models for dual location study	SB-1	Outrigger at 0.6 H
	SB-2	Outrigger at 0.6 H and 0.2 H
	SB-3	Outrigger at 0.6 H and 0.4 H
	SB-4	Outrigger at 0.6 H and 26th floor
	SB-5	Outrigger at 0.6 H and 28th floor
	SB-6	Outrigger at 0.6 H and 0.8 H

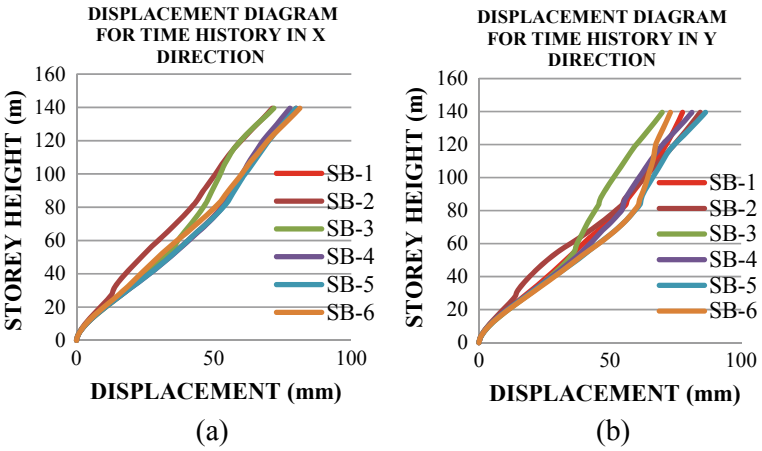

Fig. 5 Displacement for setback building with dual outrigger locations in x and y directions

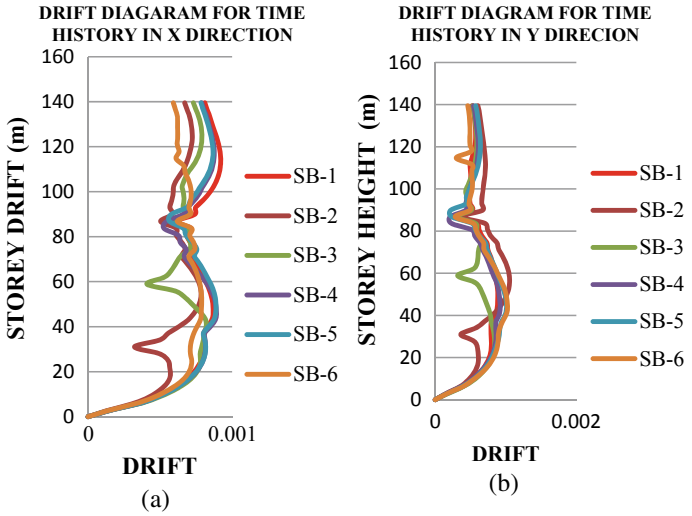

Fig. 6 Drift for setback building with dual outrigger locations in x and y directions

the top storey displacement was increased by 1.67% in x direction. In Y direction maximum increase was shown by SB-5 i.e., dual location of outrigger at 28th floor.

From Fig. 6, it can be summarized that maximum storey drift control is observed at locations were outriggers are provided. It was observed that by placing outrigger at 0.4 H location in addition to outrigger at 0.6 H (SB-3), top storey drift was controlled by a maximum value of 10.86 and 4.54% (Fig. 5) and top storey displacement was controlled by a maximum value of 10.16 and 9.99% (Fig. 6) in X and Y directions respectively. Hence it was concluded that the optimal dual outrigger locations in the asymmetrical building was 0.6 H and 0.4 H.

3.2.3 Configuration Study

Performances of asymmetric models with various configurations of outriggers were studied. All the models has their outrigger located at 0.6 H and 0.4 H. The various outrigger configurations considered were X shaped, X + X belt truss, X + V belt truss, V shape, V + V belt truss and V + X belt truss. Table 3 shows the model IDs and description.

The base model with no outrigger was also depicted in the displacement and drift diagrams for comparison. Figures 7a and 8a depicts the time history analysis of displacement and drift in x direction and Figs. 7b and 8b depicts the time history analysis of displacement and drift in y direction.

In building models with outriggers, displacement control is clearly visible from 50 m height, which is not visible in case of building without outriggers. Variation in storey drift has two inward curves indicating maximum control of drift at locations where outriggers are placed. It was observed from configuration study that the drift control and displacement is almost similar in all configurations in dual position. So it can be concluded that all the configurations have the same effect on the building.

Table 3 Models for configuration study

	Model id	Remarks
Models for configuration study	SB-A	X shape
	SB-B	X + X Belt truss
	SB-C	V shape
	SB-D	V + V Belt truss
	SB-E	X shape +V belt
	SB-F	V shape +X belt

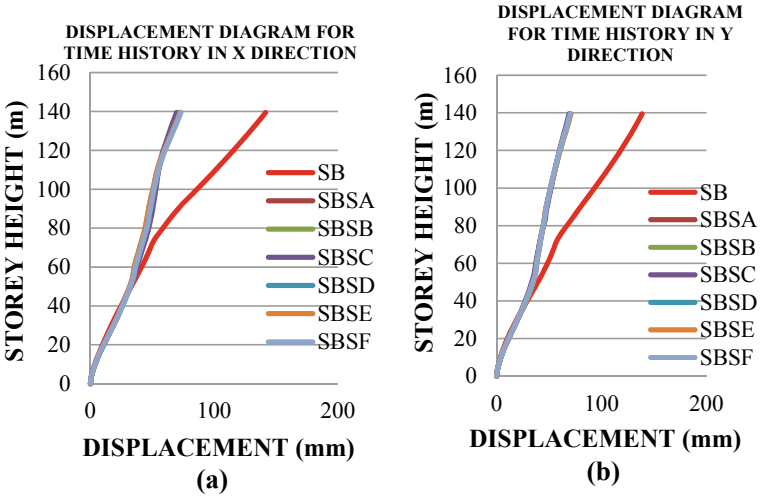

Fig. 7 Displacement for setback building with different outrigger shapes in x and y directions

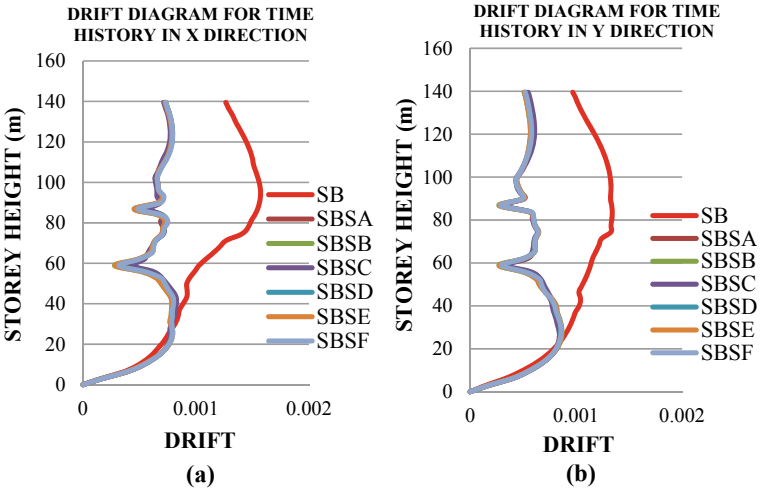

Fig. 8 Drift for setback building with different outrigger shapes in x and y directions

4 Conclusions

Based on the study of the seismic performance of multi-storied G + 44 storey building, following conclusions can be drawn:

- In regular symmetrical building, by providing outrigger at 0.6 H location, top storey drift was controlled by 15.38% and displacement by 34.75% in x and y

direction. Hence optimum location for outrigger in regular symmetric building was found as 0.6 H.

- In building with setback, by providing outrigger at 27th floor i.e., 0.6 H was found as optimum position. It was observed that top storey displacement was reduced to 43.53 and 43.99% in x and y direction. Top storey drift values were observed to be reduced by 10.86 and 4.54% in x and y directions respectively.
- From the analysis study of dual outrigger system it was concluded that by effective use of outrigger in 0.6 H and 0.4 H, the top storey drift was controlled by 10.16 and 9.99% and top storey displacement was controlled by 10.86 and 4.54% in x and y directions while comparing with building with single outrigger.
- Different configurations showed almost same behaviour in controlling the drift as well as displacement of the building. So all the outrigger configuration seemed to have same effect on the building model.

References

1. Kamath, K, Divya N, Rao AU (2012) A study on static and dynamic behavior of outrigger structural system for tall buildings. Bonfring Int J Ind Eng Manage Sci 2(4):15–20
2. Nanduri PMB, Kiran R, Suresh B, Ihtesham Hussain MD (2013) Optimum position of outrigger system for high-rise reinforced concrete buildings under wind and earthquake loadings. Am J Eng Res 2(8):76–89
3. Dsouza E, Dileep Kumar U (2017) A study of outrigger system in seismic response of tall structures by non-linear analysis. Int J Innovative Res Sci Eng Technol 6(8)
4. Balling RJ, Lee JS (2014) Simplified model for analysis and optimization of skyscrapers with outrigger and belt trusses. J Struct Eng 141(9):04014231
5. Shivacharan K, Chandrakala S, Karthik NM (2015) Optimum position of outrigger system for tall vertical irregularity structures. IOSR J Mech Civil Eng (IOSR-JMCE) e-ISSN 2278-1684
6. Masuda S, Rajhing G (2018) Comparative analysis of high rise building with outriggers and water tank in different zones. Int J Res Eng Technol 7(7). ISSN 2278-0882
7. Kim H-S, Lee H-L, Lim Y-J (2019) Multi-objective optimization of dual-purpose outriggers in tall buildings to reduce lateral displacement and differential axial shortening. Eng Struct 189:296–308
8. Kala A, Mangulkar M, Jain I (2017) The use of outrigger and belt truss system for high-rise RCC building. Int J Civil Eng Technol (IJCIET) 8:1125–1129
9. Samadi M, Jahan N (2019) Determining the effective level of outrigger in preventing collapse of tall buildings by IDA with an alternative damage measure. Eng Struct 191:104–116
10. Subramni T, Murali K (2018) Analytical Study of Tall Building with outtrigger system with respect to seismic and wind analysis using ETABS. Int J Eng Technol 7(3.10):77–82

Seismic Vulnerability Assessment of City Regions Based on Building Typology

Dharsana Satish, E. Lalith Prakash, and K. B. Anand

Abstract Over half of India's territory zone is prone to seismic tremors, and the Indian subcontinent has encountered many earthquakes in the past. This study focuses on the vulnerability assessment of buildings by Rapid Visual Screening (RVS) in selected regions of Tier II city of south India—Coimbatore. The building typologies present in various city regions (normally designated as Corporation wards) and potential seismic vulnerability of buildings in each city region (ward) is determined by RVS methodology. The RVS vulnerability scores obtained for all the wards included in this study are low, indicating that these city regions are potentially vulnerable with substantial to very heavy damages in the event of an earthquake. The outcome of the study is useful in preparing efficient earthquake policies at the local level. Further assessment and strengthening are recommended for the buildings in these selected wards with high seismic hazard.

Keywords Building typology · Rapid visual screening · Damage grades · Seismic vulnerability

1 Introduction

In the preceding 70 years, the country experienced 29 seismic events with a death toll of 51,915 and an economic loss of nearly 5297 million US Dollars according to the International disaster database. Over 75% of seismic tremor-related human setbacks are brought about by the failure of structures [1]. The general construction practices in India are greatly influenced by locally available materials, traditional construction practices, topography, etc. The application of Indian standard codes is not widely implemented in the construction of residential buildings [2]. This trend in residential building construction is a matter of concern in terms of seismic resistance.

D. Satish · E. Lalith Prakash (✉) · K. B. Anand
Department of Civil Engineering, Amrita School of Engineering, Amrita Vishwa Vidyapeetham, Coimbatore, India
e-mail: e_lalithprakash@cb.amrita.edu

© Springer Nature Switzerland AG 2021

K. Dasgupta et al. (eds.), *Proceedings of SECON 2020*,
Lecture Notes in Civil Engineering 97,
https://doi.org/10.1007/978-3-030-55115-5_42

The Federal Emergency Management Agency (FEMA) developed the Rapid Visual Screening (RVS) method [3] to determine the buildings that may be potentially hazardous under Maximum Considered Earthquake (MCE) at the site of the building. The procedure for Rapid Visual Screening was refined and used by Srikanth [4], Jain et al. [5], Pathak [6], Sarmah et al. [7], Chanu [8]. The RVS scheme can be implemented relatively quickly and inexpensively to determine potentially seismically hazardous buildings. The building score reflects the probability of collapse or partial collapse of the building during an earthquake. Hence this method is adopted for the study.

2 Details of Study Region

As per the 2014 annual Indian city survey, Coimbatore is the second largest city (details in Table 1) and urban agglomeration in the South Indian state of Tamil Nadu.

Coimbatore lies in the peninsular shield region and significant research was done on the seismic hazard and risk estimation. Future probable earthquake zones were located considering subsurface rupture phenomena and hazard values are estimated at rock level in the City of Coimbatore [9]. The seismic risk was assessed for the Coimbatore city by overlaying the land-use and deterministic seismic hazard map [10]. An Earthquake readiness index tool was developed for the Indian subcontinent and its reliability was tested and evaluated by conducting a field survey at the City of Coimbatore [11]. Therefore hazard and preparedness study is carried out in previous studies and there is a research gap where vulnerability of building types is not assessed for the study region.

As per Municipal city corporation delimitation 2011, following the Coimbatore City Municipal Corporation Act, 1981, the government of Tamil Nadu divides the City of Coimbatore into seventy-two territorial divisions (Fig. 1). The boundary data of each ward in the city were collected from Coimbatore City Corporation [12] and the study area was validated with GPS (global positioning system) coordinates.

As per Census 2011, around 85% of total buildings in Coimbatore City Corporation are residential buildings. Therefore the scope of the study is limited to the vulnerability assessment of typical corporation wards based on residential buildings.

Coimbatore city is placed in Seismic Zone III (pga 0.16 g) as per the latest release of IS 1983 [13]. The collision process of the Indian plate with the Eurasian plate is still underway at a rate of 45 mm/year inducing an anticlockwise rotation of the plate throughout southwest Peninsular India [14].

Table 1 Details of the study region

Latitude	Longitude	Area	Elevation	Population
10°10′–11°30′	76°50′–77°30′	105.5 km^2	432 from MSL	1.6 million

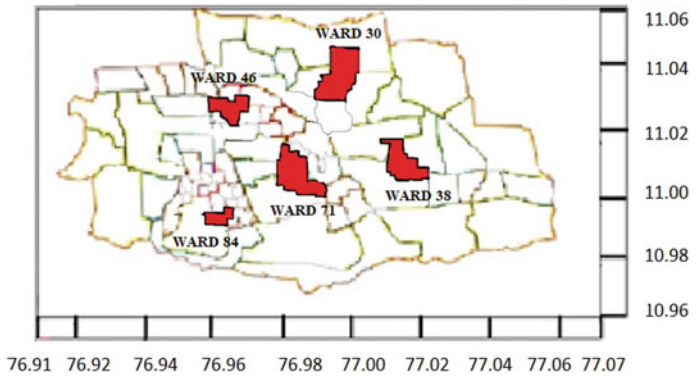

Fig. 1 Delimitation map of 72 territorial divisions with selected wards

3 Methodology

This study aims to determine the seismic vulnerability of residential buildings in the high seismic hazard zone at the city of Coimbatore through the rapid visual screening method and also to represent it as a ward-wise RVS vulnerability score. The methodology indicated in Fig. 2 is elaborated in subsequent sections.

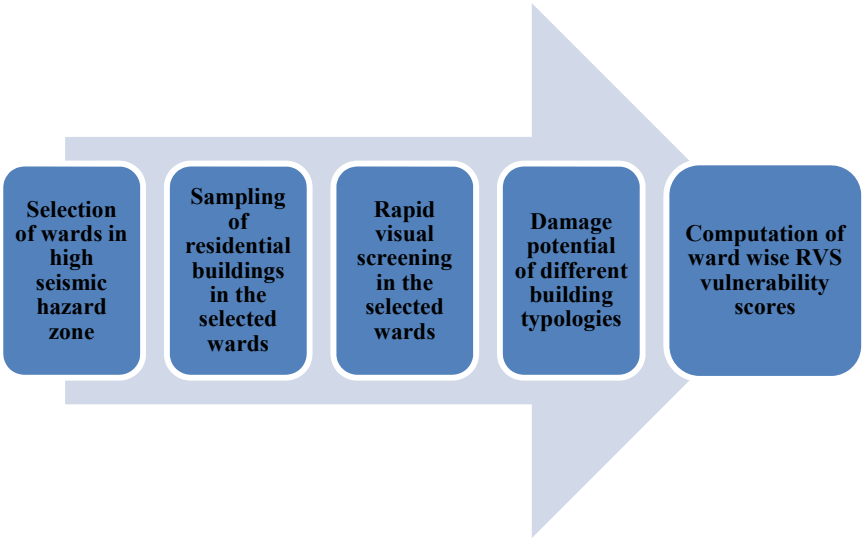

Fig. 2 Methodology of the Work

3.1 Selection of Wards

A hazard map for Coimbatore City Corporation by considering various factors, predominantly Peak Ground Acceleration, Amplification factor, Soil thickness, Shear wave velocity has been generated in an earlier study by Gopalakrishnan [15]. For the present study, five wards belonging to very high hazard zone alone were selected as a representative sample, for determining the seismic vulnerability of buildings on a much conservative side.

The above Deterministic seismic hazard map [15] has been developed using the formula:

$$\begin{aligned} DSM =& (PGAwDPGAr + DAFwDAFr + DSTwDSTr \\ &+ DSSwDSSr + DPFwDPFr + DPPwDPPr + DLLwDLLr \\ &+ DELwDELr + DDRwDDRr + DGGwDGGr) \Big/ \sum w \end{aligned} \tag{1}$$

PGA, AF, ST, SS, PF, PP, LL, EL, DR and GG represent Peak Ground Acceleration, Amplification factor, Soil thickness, Shear wave velocity, Predominant frequency, Population, Land use/Land cover, Elevation, Drainage & Geology and Geomorphology respectively. w and r represent assigned ranks and normalized weights for each factor.

3.2 Sampling

The number of residential buildings in each ward is obtained from the delimitation proposal of Coimbatore Corporation. Yamane [16] provided a simplified formula for determining the sample size.

For a confidence level of 95%, with 10% error:

$$n = N/\left(1 + N\left(e^2\right)\right) \tag{2}$$

where n, N and e represent the number of samples, total population and level of precision respectively.

The number of samples from each ward is computed from the above expression (Table 2). The rapid visual screening was carried out for the sample size of ninety nine in each of the selected wards.

Table 2 Sample size in the different selected wards

Ward number	Corporation zone	Number of residential buildings in the proposed ward	Sample size (95% CL, 10% Error)
30	North	4425	97
38	West	5015	98
46	Central	3960	98
71	West	3360	97
84	Central	3994	98

3.3 Rapid Visual Screening

For visual surveys, the buildings are categorised based on construction material, performance during the past earthquake, horizontal and vertical framing system, etc. The present study area predominantly consists of six model building types (as adapted from Prasad et al. 2009) and presented in Table 3.

Sinha [17] suggest a procedure for rapid visual screening of buildings to determine potential seismic vulnerability for all the four zones in India. Since Coimbatore fall under Seismic zone III, a refined RVS matrix was framed including adobe building type (Table 4) as per IS 1893(2016). Three vulnerability parameters are considered for determining the potential vulnerability of building, viz., soil type, vertical irregularity and plan irregularity.

Table 3 Predominant model building types in the study region

SL No	Label	Wall/framing type	Stories
1	Adobe	Rammed mud/stone masonry with lime or cement mortar	1–2
2	C1 L	Concrete moment-resisting frame	1–3
3	C1 M	Concrete moment-resisting frame	4–7
4	C2 M	Concrete shear wall	4–7
5	C3 L	RC frame with URM infills	1–3
6	URML	Burnt clay/concrete blocks with lime or cement mortar	1–2

Table 4 Matrix for calculation of RVS score

Scores	Building types					
	Adobe	C1 L	C1 M	C2 M	C3 L	URML
Base score (BS)	2.4	3	3.2	4	3.2	3
Vertical irregularity (VI)	−1.5	−2	−2	−2	−2	−1.5
Plan irregularity (PI)	−0.5	−0.5	−0.5	−0.5	−0.5	−0.5
Medium soil (S)	−0.4	−0.6	−0.6	−0.8	−0.6	−0.4

Table 5 Expected damage level as a function of the RVS score

RVS scores	Damage potential
S < 0.3	High probability of Grade 5 damage; Very high probability of Grade 4 damage
0.3 < S < 0.7	High probability of Grade 4 damage; Very high probability of Grade 3 damage
0.7 < S < 2.0	High probability of Grade 3 damage; Very high probability of Grade 2 damage
2.0 < S < 3.0	High probability of Grade 2 damage; Very high probability of Grade 1 damage
S > 3.0	Probability of Grade 1 damage

Source: Sinha et al. [17]

Base Score has been computed for each Building type based on available damage and loss estimation functions that reflects the estimated likelihood that building will collapse if the building is subjected to the maximum considered earthquake (MCE) ground motion similar to the work done by Sinha et al. [17]. The final scores are computed by deducing performance score, based on soil type, plan irregularities and vertical irregularities from the base score.

The vertical and plan irregularities in framed buildings are assessed as per 1893(Part 1) 2016 and that of Unreinforced Masonry structures (URML) is assessed as per methodology adopted by Dogangun [18]. The soil type of entire city belongs to stiff soil Type D as per NEHRP [15] and the same has been considered for the final score calculation.

Since the seismic vulnerability of the adobe is extreme, the vertical irregularity and plan irregularity is assumed to be present in all adobe buildings in Coimbatore city.

Final RVS Score of a building:

$$S = (BS + VI + PI + S) \tag{3}$$

The damage potential of buildings is determined based on the final RVS score (S). Table 5 represents the damage potential level of building as a function of the final score.

4 Results and Discussions

The visual survey, as well as the data accumulation of selected five wards shown in Fig. 3, viz., ward numbers 30, 38, 46, 71 and 84, was carried out. Final RVS scores for each of the 99 samples are computed based on building typology, presence of irregularities and soil type. The presence of both vertical and plan irregularity will contribute to the seismic vulnerability of the building. The results of RVS shows that both plan and vertical irregularities are present in more than 50% of buildings in almost all the wards (Table 6). The percentage of buildings without irregularity is almost less than 5% in all the wards. Buildings with plan irregularity alone in all

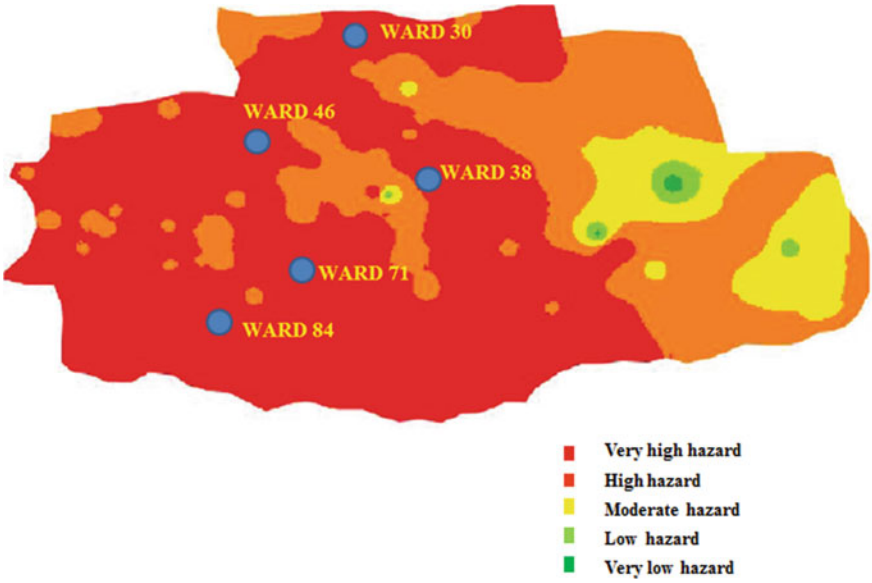

Fig. 3 Selected wards in the highest seismic hazard zones

Table 6 The percentage of buildings with irregularity across the samples in selected wards

Wards	Plan and vertical irregularity (%)	Plan irregularity (%)	Vertical irregularity (%)	Without irregularity (%)
Ward 30	62.62	4.04	27.27	6.06
Ward 38	57.57	5.05	31.31	5.05
Ward 46	68.68	1.01	27.27	3.03
Ward 71	31.31	4.04	58.58	6.06
Ward 84	53.53	1.01	41.41	4.04

the wards are lesser than 5% which indicates that construction practices in the city generally avoid irregularities in the plan. Vertical irregularity in buildings is greater than 30% in almost all the wards. In all the selected wards only a minor percentage of buildings are planned without any type of irregularity.

The RVS vulnerability score is estimated as the weighted average of RVS scores in each ward and is computed (Table 7) by accounting the number of buildings in each building typology as per the following equation.

$$\text{RVS Vulnerability score of a ward} = \frac{\sum No: \ of \ model \ building \ type \ \times \ Average \ scores \ of \ model \ building \ type}{Number \ of \ samples \ in \ ward} \tag{4}$$

Table 7 Computation matrix for RVS vulnerability score of each ward

Building type	Average RVS score	Number of buildings in each building typology corresponding to				
		Ward 30	Ward 38	Ward 46	Ward 71	Ward 84
Adobe	0	10	11	10	6	10
C1 L	0.876	10	4	8	11	15
C1 M	0.316	4	7	12	16	6
C2 M	0.921	8	7	4	16	6
C3 L	0.551	40	53	55	40	51
URML	0.761	16	17	10	16	5

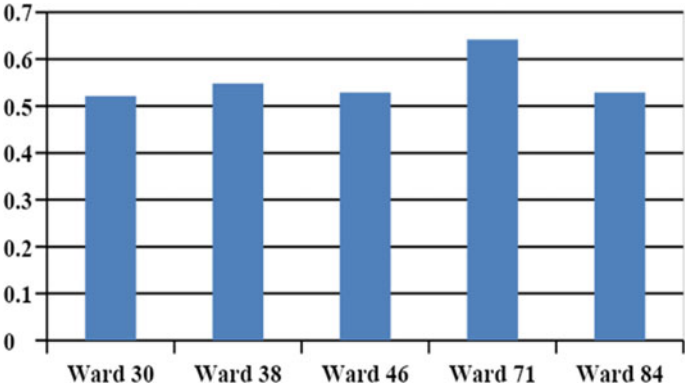

Fig. 4 RVS Vulnerability scores of the selected wards

The RVS vulnerability score for each of the selected wards is shown in Fig. 4. The wards with greater scores are least vulnerable and that of lesser scores are highly vulnerable to a seismic event. The RVS vulnerability scores of ward 71 are high due to the greater distribution of C2 M and C1 L buildings. The RVS vulnerability scores obtained for all the selected wards is less than 0.7, hence the selected wards are highly vulnerable to earthquake.

5 Conclusion

The rapid visual screening was performed in the city of Coimbatore to identify the seismic vulnerability of selected wards. Five representative wards belonging to very high hazard zone were selected with the help of available literature. Around a hundred residential buildings were surveyed in each of the selected wards. Six building typologies were predominantly distributed across the selected wards. More than 90% of the residential buildings are observed to have some form of irregularity

making them vulnerable to seismic damage. The RVS vulnerability scores of all wards range between 0.5 and 0.6, hence buildings in the selected wards are susceptible to heavy damage. Since the RVS vulnerability scores obtained for the selected wards is less than 0.7, the regions are potentially vulnerable to earthquake damages. A quick vulnerability assessment procedure for populated settlements has been illustrated through this case study for the city of Coimbatore.

References

1. Spence R, Coburn A (1992) Strengthening buildings of stone masonry to resist earthquakes. Meccanica 27(3):213–221
2. Prasad JSR, Singh Y, Kaynia AM, Lindholm C (2009) Socioeconomic clustering in seismic risk assessment of urban housing stock. Earthq Spectra 25(3):619–641
3. FEMA 154 (2002) Rapid visual screening of buildings for potential seismic hazards. Federal Emergency Management Agency, Washington, D.C.
4. Srikanth T et al (2010) Earthquake vulnerability assessment of existing buildings in Gandhidham and Adipur Cities Kachchh, Gujarat (India). Eur J Scient Res 41(3):336–353. ISSN 1450-216X
5. Jain SK et al (2010) A proposed rapid visual screening procedure for seismic evaluation of RC-Frame buildings in India. Earthquake Spectra 26(3):709–729
6. Pathak J (2008) Earthquake vulnerability assessment of Guwahati urban centre. In: The 14th world conference on earthquake engineering October 12–17, 2008, Beijing, China
7. Sarmah T (2018) Earthquake vulnerability assessment for RCC buildings of Guwahati City using rapid visual screening. Procedia Eng 212
8. Chanu NM et al (2018) A proposed rapid visual screening procedure for developing countries. Int J Geotechn Earthquake Eng 9(2)
9. Anbazhagan et al (2012) Seismic hazard map of Coimbatore using subsurface fault rupture. Natural Hazards February
10. Prakash EL, Kolathayar S, Ramkrishnan R (2018) Seismic risk assessment for Coimbatore integrating Seismic Hazard and Land Use. In: Geo shanghai international conference. Springer, Singapore, pp 117–124
11. Kolathyar S et al (2017) Development of earthquake readiness index tool to assess individual earthquake preparedness level. In: Urbanization challenges in emerging economies, ASCE India conference, New Delhi
12. Coimbatore corporation data on draft ward delimitation proposal, Government of Tamil Nadu (2017)
13. Bureau of Indian Standards (2016) IS: 1893–2016, Criteria for earthquake resistant design of structure. Bureau of Indian Standards, New Delhi
14. Biham R (2004) Earthquakes in India and the Himalaya: tectonics, geodesy and history. Ann Geophys 47(2/3)
15. Gopalakrishnan S (2012) Seismic hazard analysis for Coimbatore corporation using GIS. Ph.D thesis, Anna University
16. Yamane et al (1968) Elementary sampling theory. J Am Statistical Assoc 63(322). https://www.unfpa.org/publications/state-world-population-2007
17. Sinha R et al (2004) A national policy for seismic vulnerability assessment of buildings and procedure for rapid visual screening of buildings for potential seismic vulnerability

18. Dogangun (2008) Seismic performance of masonry buildings during recent Earthquakes in Turkey. In: The 14th world conference on earthquake engineering October 12–17, 2008, Beijing, China

Development of Reinforced Concrete Beam with Plastic Balls in Neutral Axis

Milu Reji and V. V. Anu

Abstract Concrete is one of the most widely used construction material. Its usage is twice that of steel, wood, plastics and aluminium combined. It provides superior fire resistance compared with wooden construction and gains strength over time. Structures made of concrete can have a long service life. The major drawback in concrete works is that the structures will be heavier. In case of RC beams the strength of concrete lying in and near the neutral axis is not fully utilized. So this unutilized concrete is replaced by light weight plastic balls. This is an alternative to reduce the use of concrete. Plastics offer great resistance against chemicals and solvents. The concrete just above the neutral axis is less stressed where as the concrete below neutral axis serves as a shear transmitting media. Plastic material offers a good bond between concrete layers. The stresses in beams are maximum at top and bottom where as, it is zero at the neutral axis. The cement content can also be decreased by saving the concrete which reduces the greenhouse gaseous emissions. So it is considered as eco-friendly. Specimens of solid RC beam, hollow RC beam and RC beam with plastic balls are casted, tested and made a comparison.

Keywords Reinforced concrete beams · Neutral axis · Plastic balls

1 Introduction

In this paper an attempt is being made to reduce weight and the cost of reinforced concrete structural member by replacing the concrete in and near the neutral axis. However, in RC beams strength of concrete lying in and near the neutral axis is not fully utilized. So this unutilized concrete is replaced by plastic balls.

Findings from previous studies are as follows. The flexural strength of RC hollow beams is almost the same when compared with the RC control beam. The deflection at the ultimate stage and yield stage of hollow beams with double openings are greater compared to hollow beams with single openings. Up to 17.5% removal of

M. Reji (✉) · V. V. Anu
Toc H Institute of Science and Technology, Arakkunnam, Ernakulum, India
e-mail: milususanreji@gmail.com

© Springer Nature Switzerland AG 2021

K. Dasgupta et al. (eds.), *Proceedings of SECON 2020*,
Lecture Notes in Civil Engineering 97,
https://doi.org/10.1007/978-3-030-55115-5_43

concrete at tension zone will not affect the flexural behaviour of the beams. Hollow beams are having greater ductility when compared to the control beam. Both beams failed by flexure failure. When comparing the moment of inertia of both beams, hollow beam has lower value. So hollow beam has more deflection [1]. In reinforced concrete beams, less stressed concrete near neutral axis can be replaced by bricks. With the help of stress block diagram in filled zone is obtained. Method of initial functions is used for the analysis of in filled reinforced concrete composite beams. The method of initial function (MIF) is an analytical method of elasticity theory. The results obtained by MIF are compared with those predicting by Finite Element Method (FEM) based software ANSYS, and it is observed that they are comparable [2]. Presence of voids in low stressed zone does not cause any significant strength reduction. For this work no extra time or labour is required. Economy and reduction of weight in beams depends on the percentage replacement of concrete. As the size of structure increase material usage get reduced These members can be used for sustainable and environment friendly construction work as it saves concrete which reduces the emission of carbon dioxide during the production of cement [3].

From the literature reviews, it is understood that in RC beams, less stressed concrete in and near neutral axis can be replaced by some light weight material. Several types of in filled materials like Brick, Expanded polystyrene sheet (EPS), LSRC (Lightweight Sandwich Reinforced Concrete) sections, Terracotta hollow blocks etc. had already done. Also an experiment was done with hollow beams. But it was observed that when the beams are kept hollow more moisture content will comes in contact and may results in chemical attack. And also they are not able to withstand the impact loads. Plastic wastes are among these wastes; their disposal has harmful effects on the environment due to their long biodegradation period, and therefore one of the logical methods for reduction of their negative effects is the application of these materials in other industries. To overcome this drawback an attempt has been made to investigate the effects of RC beam with plastic balls are kept in the place of concrete in neutral axis.

2 Materials

Cement is conventionally used as the primary binder for the production of concrete. There are alternative materials which can be used to reduce the environmental issues associated with cement production. In this paper Class F fly ash is used by 20% of binder content. M-sand was used as the fine aggregate confirming to Zone II by IS 383:1970. Coarse aggregate of nominal size 20 mm was used as per IS 383:1970 specifications. Various tests were conducted for cement fly ash and aggregates and recorded in Table 1. Super plasticizers, also known as high range water reducers, which are chemical admixtures used when a well-dispersed particle suspension is required. Here Master Glenium is used which is composed of synthetic polymers specially designed to allow considerable reduction of water while maintaining control on extend of set retardation. Properties of master glenium are recorded in Table 2.

Table 1 Test results

S. No.	Characteristics	Values obtained
1	Specific gravity of cement	3.15
2	Standard consistency of cement	32%
3	Initial setting time of cement	70 min
4	Fineness of cement	5%
5	Specific gravity of fly ash	2.6
6	Specific gravity of fine aggregates	2.7
7	Specific gravity of coarse aggregates	2.69

Table 2 Physical properties of Master Glenium

Aspect	Dark brown free flowing liquid
Relative density	1.24 ± 0.02 at 25 °C
pH	>6
Chloride ion content	<0.2%

Reinforced beams are kept as hollow with help of PVC pipes of diameters 30 mm, 40 mm and 50 mm. It has a specific gravity of 1400 ± 20 kg/m^3. Plastic balls of diameter 30 mm, 40 mm and 50 mm are also used for the replacement of concrete in neutral axis.

3 Mix Design

The process of selecting suitable ingredients of concrete and determining their relative amounts with the objective of producing a concrete of the required, strength, durability, and workability as economically as possible, is termed the concrete mix design. It was done as per IS 10262:2019 is in line with ACI 211. Cement, Fly ash, fine aggregate and coarse aggregate subjected to dry mixing for about 2 min and then required quantity of water is added. After mixing, determine the slump of fresh concrete. The concrete was then placed in mould with proper compaction. After 24 h demoulded the cubes and subjected to curing. The specimens were tested at 7 and 28 days from the day of casting. The mix proportion for control mix fly cement: fine aggregate: coarse aggregate was 1:2.03:3.59 and water cement ratio is 0.42.

4 Experimental Details

Reinforced concrete beam of size 150 × 250 × 900 mm was casted as control beam in a wooden mould. The reinforcement for the beam specimens was 2 nos. of 10 mm diameter at tension zone and 2 hanger bars of 10 mm diameter with a cross-sectional area of 314 mm^2. Shear reinforcement provided for the specimens are of 6 mm diameter stirrups at 125 mm spacing. Reinforced concrete beams with concrete replacement in neutral axis as hollow (30 mm, 40 mm and 50 mm diameter) and with plastic balls (30 mm, 40 mm and 50 mm diameter) has the same control beam specifications are casted and tested.

The depth of neutral axis is calculated by considering M40 grade concrete and Fe415 steel with an effective cover of 20 mm. For under-reinforced beams,

$$(x_u/d) = \left(0.87 f_y A_{st}\right) \Big/ \left(0.36 f_{ck} bd\right)$$
$$x_u = (0.87 \times 415 \times 157) \Big/ (0.36 \times 40 \times 150)$$
$$= 26.24\,\text{mm}$$

5 Results and Discussions

5.1 *Load Carrying Capacity*

It is defined as the maximum load that the beam can carry without reducing its level of performance. When comparing the load carrying capacity of two replaced beams with control beam, the hollow beam as lower load carrying capacity. That means that the deflection is more for hollow beams. Figure 1: shows the load carrying capacity and of control beam (CB), hollow beams (HB30, HB40, HB50) and beam with plastic balls (PB30, PB40, PB50).

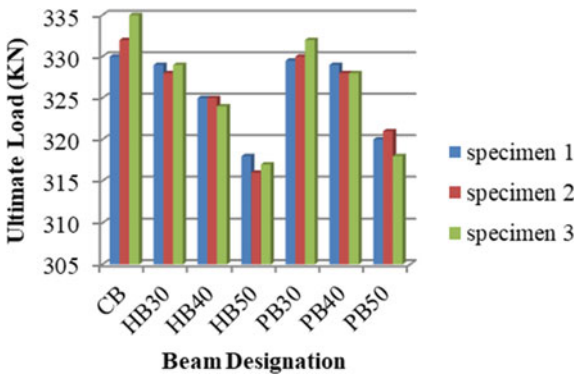

Fig. 1 Load carying capacity

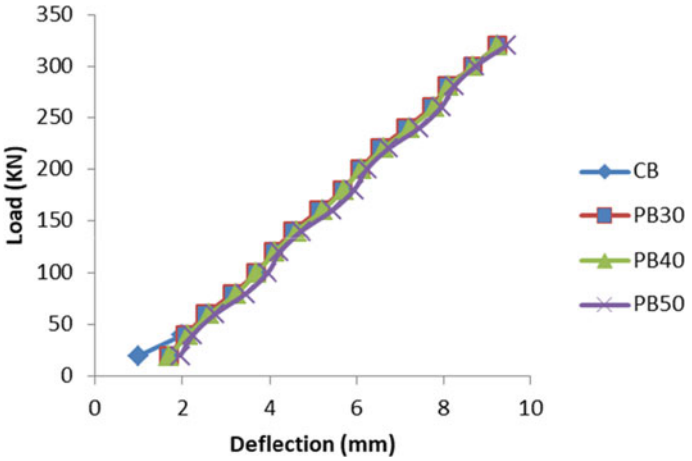

Fig. 2 Load versus deflection graph

Fig. 3 Load versus deflection graph

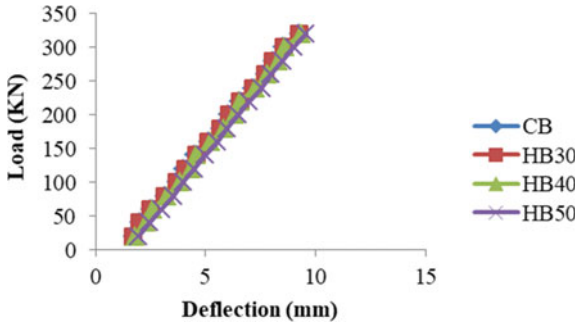

5.2 Load Versus Deflection Graph

As load increases deflection also increases which means that the relationship between load and deflection is linear. At a point the relation between the load and deflection became non linear and the structure became plastic. Figures 2 and 3 shows the load values and corresponding deflection.

5.3 Crack Pattern

From Figs. 1 and 2, it is clear that the deflection is less and the load carrying capacity of control beam s higher as compared to the beams with hollow neutral axis and the beams with plastic balls. It also found that the variation is comparable.

5.4 Concrete Saving

In case of construction concrete is one of the most essential components. While estimating quantity of concrete for particular structural work, normally 3–5% is considered as wastage. But wastage of concrete more than that. It can increase the cost of project and may affect project progress. So, it is necessary to control the concrete wastage. In RC beams strength of concrete lying in and near the neutral axis is not fully utilized. So this unutilized concrete can be removed. Volume reduction can be found by

In case of pipes,

$$\text{Percentage reduction} = [\text{V2}/\text{V1}] \times 100 = [1130.4/33750] \times 100 = 3.34\%$$

In case of balls,

$$\text{Percentage reduction} = [\text{V3}/\text{V1}] \times 100 = [770.27/33750] \times 100 = 2.28\%$$

For 0.9 m length about 3.34% concrete can be saved when it is kept as hollow and 2.28% concrete can be saved when the concrete in neutral axis is replaced by the plastic balls. If the size of structure increased the amount of concrete can also reduced. So in large scale construction works concrete can be saved more effectively.

5.5 Cost Reduction

For a project about 75% of cost will be consumed by the materials. When the amount of concrete has saved, the quantity of cement, fine aggregates, coarse aggregates and water get saved. When the use of materials get reduced it will linearly related to the cost of project. Thus the cost will get reduced. The material reduction will not much affect the load bearing capacity. Economy can be attained without causing any considerable strength variation for beam.

5.6 Self Weight Reduction

In RC beams strength of concrete lying in and near the neutral axis is not fully utilized. So this unutilized concrete can be removed. The unit weight of concrete is 25 kN/mm^2. By removing that unutilized concrete the self weight of the beam get reduced.

Weight of beam, W1 = 1.21 × 68.15 = 82.46 kg
Volume of pipe V2 = $\pi r^2 l$ = 3.14 × .82 × 35.43 = 71.22 cu.inches
V2 = 71.22/1728 = 0.041 cu.ft.
Weight of concrete saved W2 = 0.041 × 68.15 = 2.80 kg
Weight of hollow beam = 82.46–2.80 = 79.66 kg
Volume of ball V3 = 4/3[πr^3] = 4/3[3.14 × .83] = 2.133 cu.inches
For 90 cm beam 23 balls of 2 cm radius is required to replace the concrete in the place of neutral axis.
V3 = 23 × 2.133 = 49.066 cu.inches
V3 = 49.066/1728 = 0.028 kg
Weight of concrete saved W3 = 0.028 × 68.15 = 1.9082 kg ~ 2 kg
Weight of beam with plastic balls = = 82.46 − 2.80 = 80.46 kg

This reduction is for a beam of 0.9 m as the structure became larger the weight of reduction get increased.

6 Conclusions

In RC beams the concrete lying in and near the neutral axis is not fully utilized. So this unutilized concrete is replaced with PVC pipe and plastic balls. While comparing reinforced concrete beam, hollow beam and the beam with plastic ball their strength properties are comparable. Based on the experimental work, the following conclusions are obtained.

- Load carrying capacity of control beam, hollow beam and the beam with plastic balls are comparable. Load carrying capacity of control beam is 332 kN, hollow beam is 324 kN and beam with balls is 328 kN.
- In case of deflection, it is more for hollow beam as compared with control beam and beam with plastic ball. Crack will be first formed on hollow beam.
- One of the main advantages comes on decrease in the use of concrete. About 3.34% of concrete get reduced in case of hollow beam and 2.28% of concrete get reduced in the case of beam with plastic balls when compared to control beam.
- When the amount of concrete gets saved it will reduce the material cost which will cause cost reduction in overall project.
- Self weight reduction is another goal from this work. About 2.8 kg weight gets reduced for hollow beam and 2 kg weight get reduced for beam with plastic balls.

References

1. Ahmedb AFB, Hameeda MA (2019) Employment the plastic waste to produce the light weight concrete. Proceeding of Energy Engineering 157:30–38
2. Manalo A, Fam A, Thiru A, Fahid F (2018) Flexural and shear behaviour of layered sandwich beams. Const Build Mater 173:429–442
3. AlAjarmeh OS, Benmokrane B, Karunasena W, Manalo AC, Mendis P, Nguyen KTQ (2019) Compressive behavior of axially loaded circular hollow concrete columns reinforced with GFRP bars and spirals. Constr Build Mater 194:12–23

Progressive Collapse Analysis of RC Buildings Using Linear Static and Non-linear Static Method

A. Salman and K. I. Praseeda

Abstract Progressive collapse is one of the most devastating types of building failures, most often leading to costly damages and possible loss of life. To study the effect of failure of columns on the entire structure, 15 storey RC building is considered. The progressive collapse analysis and modelling of the building is done using SAP2000. Linear static and Non-linear static analysis is performed to understand progressive collapse. Comparing the results of linear static and non-linear static it is found that non-linear static procedure for progressive collapse analysis is the more effective method than linear static in which a primary load-bearing structural element is removed and the structural material is allowed to undergo non-linear behaviour.

Keywords Progressive collapse · Linear static · Non-linear dynamic · SAP2000

1 Introduction

Progressive collapse can be defined as a total collapse of a structure due to the spread of a local failure from element to element throughout the structure. It is also called disproportionate failure because the collapse does not follow the path of the original cause. Progressive collapse can be triggered by manmade or natural hazards. Fire, blast, earthquake and extreme loading conditions can lead to progressive collapse. Progressive collapse is a complicated process where the collapsing system should be able to redistribute the loads in order to prevent the loss of critical structural members and total collapse. The inability of the structural system to redistribute the collapse load is the major problem. After the local failure the structural members seeks an alternative load path for the redistribution and the absence of an alternative path leads to the entire collapse. Techniques which helps to provide an alternate path can resist progressive collapse also ductility, redundancy and continuity must be considered in design of beams, columns and frame connections to allow for potential redistribution of large loads and to prevent collapse.

A. Salman (✉) · K. I. Praseeda
Department of Civil Engineering, NSS College of Engineering, Palakkad, Kerala 678008, India
e-mail: iamsalman947@gmail.com

© Springer Nature Switzerland AG 2021

K. Dasgupta et al. (eds.), *Proceedings of SECON 2020*,
Lecture Notes in Civil Engineering 97,
https://doi.org/10.1007/978-3-030-55115-5_44

For the first time structural engineers faced this phenomenon in 1968 when the Ronan Point Tower was destroyed. It was due to a human error gas explosion that leads to precast concrete panels near the 18th floor causing the floors above to collapse and this event was like a thrust for further study of progressive collapse. Also extensive research was going on during the past years because of the increasing rate of victims resulting from terrorist attacks and natural disasters, some of the examples include the collapse of the World Trade Center (2001) due to terrorist attack and the bombing of the Murrah Federal Building (1995) in Oklahoma City. Traditionally the structural engineers focused on optimizing the most economic sections while meeting the code requirements. Thus most of the structures are designed to resist gravity loads and lateral loads which are resulting from wind and earthquakes. So the conventionally designed structures get collapse when an unexpected extreme load act on the structure. There are complex computer programs and simulation tools that can be used to model progressive collapse response of buildings. Any FEMA based software can be used to find the potential for progressive collapse in buildings. The guidelines for progressive collapse evaluation is issued by General Services Administration (GSA).

Generally, the analysis can be done in four ways Linear static, linear dynamic, non-linear static and non-linear dynamic.

2 Building Configuration

To study the effect of progressive collapse on the structure after removing column a G+ 15 storey RC building is considered. The structure designed for an importance factor of 1 as per IS 1893:2002. Bay size is taken as 6 m in X-direction and 4 m in Y-direction. Building size in plan is 36 × 24 m. base to plinth height is taken as 2 m, plinth to ground floor as 4 m, which is a hollow plinth, typical floor height as 3.5 m and 230 mm thick walls. The column and beam sizes are 800 × 800 mm and 300 × 600 mm respectively (Fig. 1).

3 Progressive Collapse Analysis

Linear static and Non-linear static analysis is used to analyse the potential of progressive collapse by considering certain loading criteria's and guidelines provided by GSA. The progressive collapse analysis is done using the structural analysis and design software SAP2000. Progressive collapse analysis is basically removing a critical column and analysing the capacity of the structure to withstand the above condition.

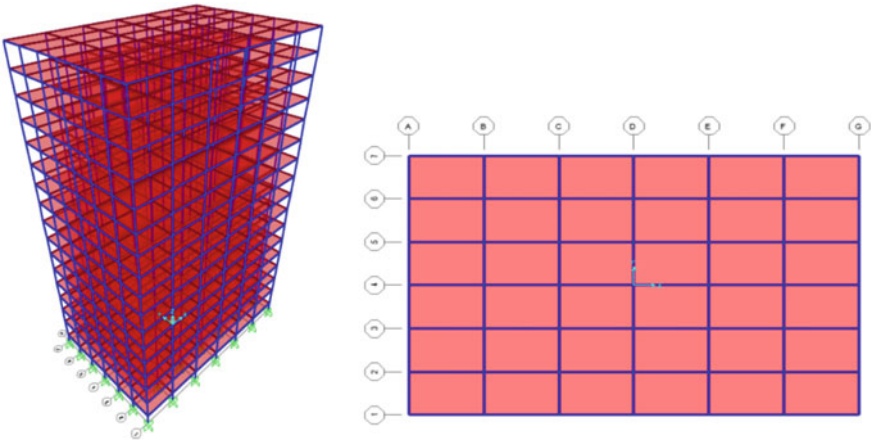

Fig. 1 3D model and typical floor plan of the considered RC building

3.1 Structure Loads and Design Data

Indian Standard codes are used for the designing and loading criteria with the guidelines of GSA. (IS-456, IS-875, IS-893-2002)

L.L at typical floor: 2 kN/m^2
L.L at roof: 1.5 kN/m^2
Floor finish: 1.0 kN/m^2
Wall load at typical floor: 13.685 kN/m^2
Parapet wall load at terrace: 4.6 kN/m^2
Concrete grade: M25
Steel grade: Fe 415
Seismic zone: 3
Zone factor: 0.16
Soil type: Type 2
Response reduction factor: 5

Along with above cases, load combinations are considered for design of structural elements as per IS 1893:2002.

4 Linear Static Analysis

Linear static method is the simplest analysis method of progressive collapse analysis which gives a vague idea about structure resistance against progressive collapse. As this method doesn't include dynamic behaviour, Dynamic Increase Factor (DIF) is used to represent the dynamic effect, the factor 2 in the loading criteria is the dynamic

increase factor. For the linear static progressive collapse analysis, the gravity load applied as per GSA guidelines is,

$$\text{Load} = 2\text{DL} + 0.5\text{LL}$$

where,

DL dead load.
LL live load.

Here, the column is removed from the location which is either corner column or central column one at a time (as per GSA) and perform the linear static analysis with the gravity load imposed and determine the demand for the specific column removal case and from the originally designed building section capacity of the members has to be determined. Then checkout the DCR (Demand to Capacity Ratio). If the DCR value exceeds the acceptance criteria the member considered as failed. Thus the DCR value helps to determine the potential for progressive collapse of building.

4.1 DCR Value Calculation

Demand to capacity ratio which is the ratio between the demand coming to the member after the column loss to the capacity of the member in the normal case

$$DCR = \frac{\text{Qud}}{Qce}$$

where,

Q_{ud} Acting force (Demand) determined in the component or moment.
Q_{ce} Expected ultimate capacity of the component (moment or forces).

The accepted criteria as per GSA for DCR value is.

DCR < 2 for typical structural configurations
DCR < 1.5 for irregular configurations.

4.2 Analysis

DCR value of beams for flexure are calculated from top to bottom stories at 2 locations i.e. at left and right side of the removed column.

From the DCR values obtained for flexure it is observed that the loss of central column makes the structure a bit vulnerable. The value of DCR ratio is high at the bottom and top storey. In top beams DCR greater than 2 subjected to progressive

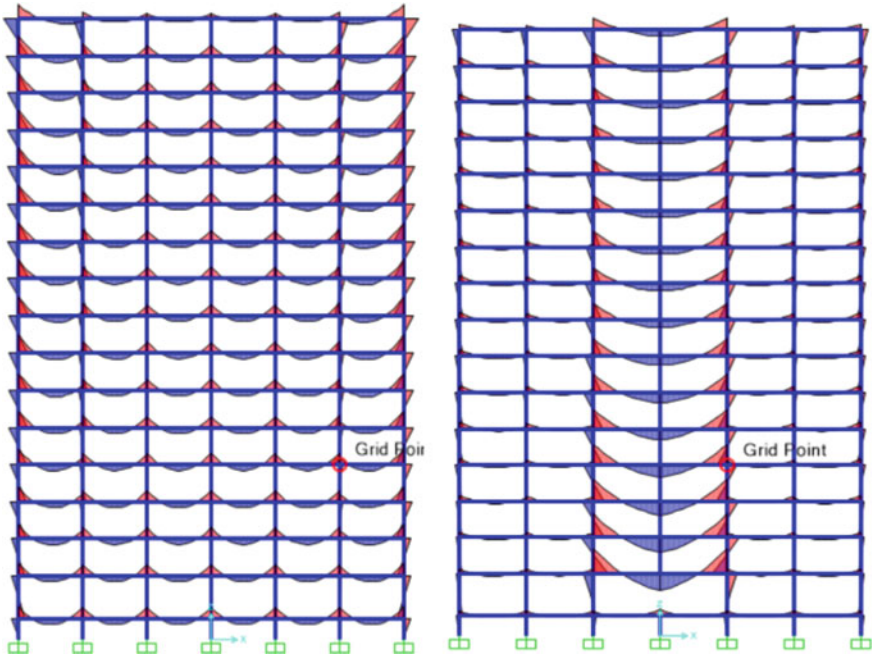

Fig. 2 BMD before and after central column removal case

collapse failure. This is because the beams at the top most level are having least amount of reinforcement. Therefore, the capacity of beams at top level are less. And in the bottom most level also the values are greater than 2 which shows the members adjacent to the removed column are experiencing higher stresses which makes the beams vulnerable (Fig. 2 and Table 1).

5 Non-linear Static Analysis

The Non-linear static analysis is either force controlled or deformation controlled. In force controlled analysis, load is applied step by step until maximum load is attained or structure collapse.

GSA guideline has provided following stepwise procedure for analysis.

Step1: Prepare the model, perform concrete design and determine the reinforcement

Step2: Define hinge properties for beams and columns. For default hinges SAP2000 uses Tables 5–6 of FEMA-356.

Step3: Define Non-linear case with GSA load combination, set required number of steps. Apply local distribution.

Table 1 DCR of beams for flexure in central column removal case

STOREY	DCR (RIGHT)	DCR (LEFT)
15	3.235	3.235
14	2.035	2.035
13	2.03	2.03
12	2.07	2.07
11	2.07	2.07
10	1.99	1.99
9	1.94	1.94
8	1.93	1.93
7	1.95	1.95
6	1.99	1.99
5	2.06	2.06
4	2.15	2.15
3	2.28	2.28
2	2.4	2.4
1	2.6	2.6
G	3.05	3.05

Step4: Create column loss scenario perform non-linear static analysis
Step5: Observe the hinge formation pattern.

For each degree of freedom there is a force displacement curve with values at five points A-B-C-D-E, and there are additional deformation measures at points IO (immediate occupancy), LS (life safety) and CP (collapse prevention) these are informational measures which gives yield value and plastic deformation (Figs. 3, 4 and 5).

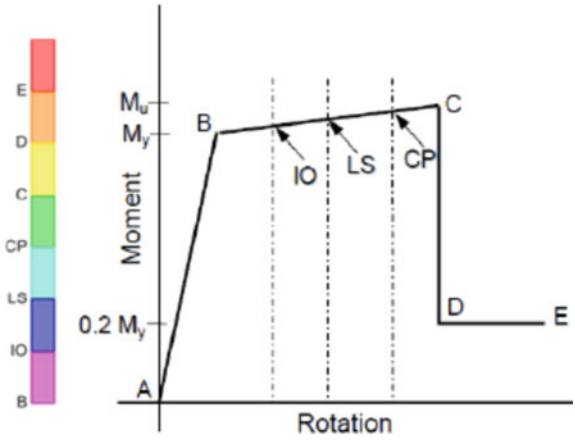

Fig. 3 Force–displacement curve. B—Yielding, C—Ultimate capacity for push over analysis, D—Residual strength. E—Total failure, IO—immediate occupancy, LS—life safety, CP—collapse prevention

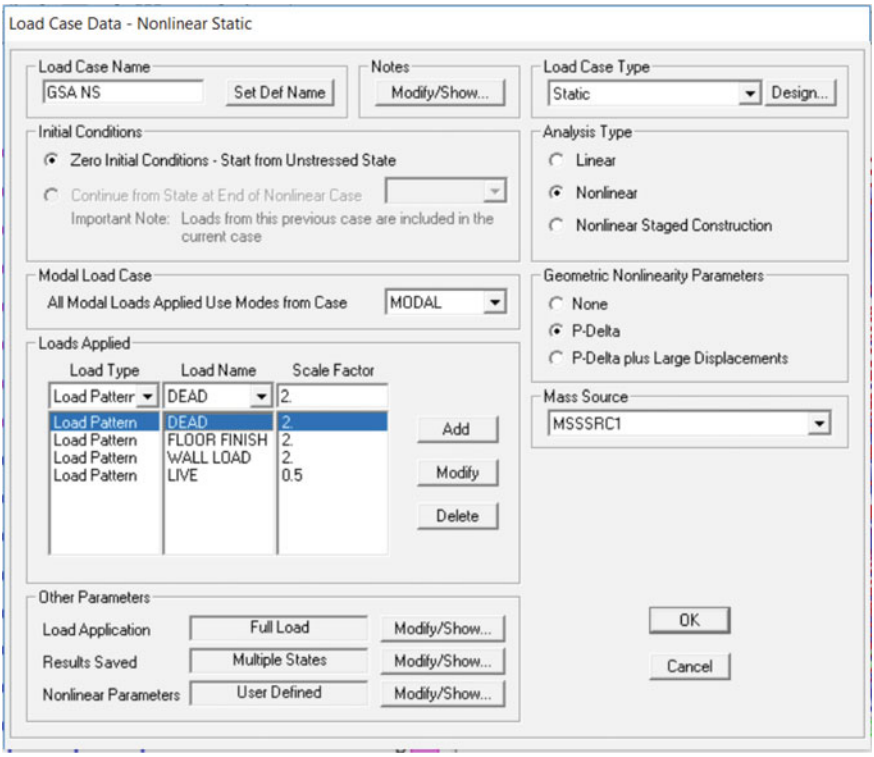

Fig. 4 Definition for non-linear case

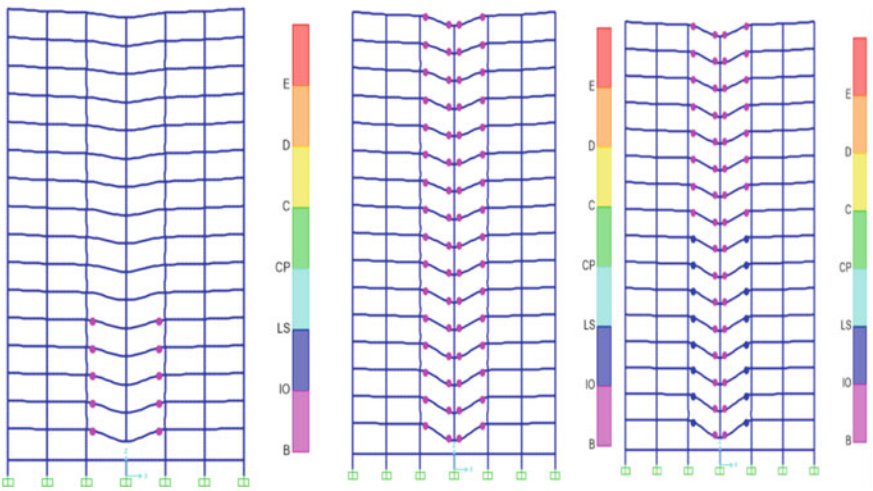

Fig. 5 Deformed shape and hinge formation of frame after central column removal case

The hinge started forming at the bottom stories from where the column is removed. And thereon, the hinges started propagating in the upward direction. The hinges reach Life safety level and are formed at the bottom storeys. The life safety level indicates there will not be any casualty due to progressive collapse, but cannot be used for further living.

6 Results and Discussion

In this paper linear static and non-linear static analysis is carried out for a G+ 15 storey RC building as per GSA guidelines. From the linear static progressive collapse analysis, it is found that bottom and top storeys are vulnerable to progressive collapse since its DCR ratio exceeds the value 2. The cases in which the linear static analysis showed that the structure is susceptible to progressive collapse, are found to be safe to resist progressive collapse in non-linear analysis method. But structure cannot be used for further living. Linear static analysis can only give a vague idea about the potential of progressive collapse, whereas non-linear static analysis helps to understand the hinge formations at yield and also helps to understand the moment redistribution.

7 Conclusion

Linear static is the simplest and least time taking method whereas non-linear static analysis will take more time and little bit complicated. But after the analysis it can been seen that the results of linear static analysis are not accurate because it does not consider the material and geometrical non-linearity, whereas non-linear static analysis includes the non-linearity which helps it to get a more accurate results. So even though the linear static analysis is less complicated and less time taking it is highly recommending to consider non-linear static analysis over linear static analysis for progressive collapse analysis.

References

1. Qian K, Weng YH, Li B (2019) Improving behavior of reinforced concrete frames to resist progressive collapse through steel bracings. J Struct Eng (United States) 145(2):1–17
2. Abdelwahed B (2019) A review on building progressive collapse, survey and discussion. Case Stud Constr Mater 11
3. Rahnavard R, Fard FFZ, Hosseini A, Suleiman M (2018) Nonlinear analysis on progressive collapse of tall steel composite buildings. Case Stud Constr Mater 8(March):359–379
4. Li L-L et al (2018) Analysis of robustness of steel frames against progressive collapse. J Constr Steel Res 143:264–278

5. Lim NS, Tan KH, Lee CK (2018) A simplified model for alternate load path assessment in RC structures. Eng Struct 171(October 2017):696–711
6. Delfian J (2018) Numerical assessment of the effect of progressive collapse phenomenon on the behavior of high-rise concrete structures. Soil Struct Interact J 3(1):1–11
7. Li Y, Lu X, Guan H, Ren P (2017) Numerical investigation of progressive collapse resistance of reinforced concrete frames subject to column removals from different stories. Adv Struct Eng 19(2):314–326
8. Patel Kevins J, Patel Thushar N (2017) Effects of irregularity on progressive collapse of RCC nuilding. Department of Civil Engineering, Sardar Vallabhai Patel Institute of Technology
9. Qian K, Li B, Ma JX (2017) Load-carrying mechanism to resist progressive collapse of RC buildings. J Struct Eng (United States) 141(2):1–14
10. Umesh Jamakhandi SB (2015) Design and analysis of blast load on structures
11. Yu J, Tan KH (2014) Special detailing techniques to improve structural resistance against progressive collapse. J Struct Eng (United States) 140(3):1–15
12. Byfield M, Mudalige W, Morison C, Stoddart E (2014) A review of Progressive Collapse research and regulations. Proc Inst Civ Eng Struct Build 167(8):447–456
13. Yu J, Tan KH (2013) Structural behavior of RC beam-column subassemblages under a middle column removal scenario. J Struct Eng (United States) 139(2):233–250
14. Qian K, Li B (2013) Strengthening and retrofitting of RC flat slabs to mitigate progressive collapse by externally bonded CFRP laminates. J Compos Constr 17(4):554–565
15. Cai JG, Xu YX, Zhuang LP, Feng J, Zhang J (2012) Comparison of various procedures for progressive collapse analysis of cable-stayed bridges. J Zhejiang Univ Sci A 13(5):323–334
16. Baciu C, Lupoae M (2012) Nonlinear analysis for a reinforced concrete frame structure under extreme loads. Constructii 13(1):51
17. Hadi MNS, Alrudaini TMS (2011) Preventing the progressive collapse of reinforced concrete buildings
18. Khandelwal K, El-Tawil S (2011) Pushdown resistance as a measure of robustness in progressive collapse analysis. Eng Struct 33(9):2653–2661
19. Kokot S, Anthoine A, Negro P, Solomos G (2010) Static and dynamic analysis of a reinforced concrete flat slab frame building for progressive collapse. JRC Scientific and Technical Reports JRC 62663; European Commission, Joint Research Centre
20. Kim J, Kim T (2009) Assessment of progressive collapse-resisting capacity of steel moment frames. J Constr Steel Res 65(1):169–179

Effect of Magnetized Water on the Mechanical Properties of Fly Ash Based Self Compacting Concrete

P. P. Magida Ruby and R. Vasudev

Abstract The water used in concrete plays a vital role in cement hydration, managing workability and durability of structure. The limited availability of drinking water raise the importance of optimizing use of drinking water in concrete construction. Magnetized water is prepared by passing normal water through a magnetic field of 0.6 T, 0.8 T, 1.0 T and 1.2 T. The magnetized water can be considered as an innovative technology to optimize the over usage of drinking water in construction. Magnetized water has a unique ability to break down the water clusters and thereby it enhance properties of concrete mix. The aim of this work is to investigate the effect of magnetized water (0.6 T, 0.8 T, 1.0 T and 1.2 T) on fly ash by weight of cement (fresh and hardened properties).

Keywords Fly ash · Hydration · Innovative technology · Magnetized water · Mechanical properties

1 Introduction

Self compacting concrete (SCC) was first developed in Japan, in the early nineties, under the stimulating leadership of Prof. Okamura. The main idea to develop self compacting concrete was to improve the labor conditions at the building site and in the factory (noise, dust, vibrations).The main reasons behind the popularity of self compacting concrete are the following, faster construction, reduction in site man power, better surface finish, easy placing, improved durability, greater freedom in design, thinner concrete sections, absence of vibration, reduced noise levels, safer working environment are the unique properties of self-compacting concrete, the remaining fresh and hardened properties are same as traditional concrete. It has been observed that performance wise SCC is more capable than conventional concrete

P. P. M. Ruby (✉) · R. Vasudev
Toc H Institute of Science and Technology, Eranakulm, India
e-mail: magidaruby@gmail.com

© Springer Nature Switzerland AG 2021

K. Dasgupta et al. (eds.), *Proceedings of SECON 2020*,
Lecture Notes in Civil Engineering 97,
https://doi.org/10.1007/978-3-030-55115-5_45

because of its fluidity. This can reach all possible corners of formwork, without giving any compaction efforts whereas in conventional concrete needs additional effort for its compaction.

Water consumption is rising as the population and human needs grow. Industrial sector comes in the second place with 20% water consumption. In concrete production practice there is more than one billion tonnes of water consumed each year. Water used in concrete production plays a vital role in the concrete mix, starting from governing the hydration process of cement, along with proper curing in order to reach the desired strength. This constraint along with the limited availability of drinking water across the planet raised the important issue of optimizing the use of water in concrete constructions. When water passes through a magnetic flux it is known as magnetized water. The level of magnetization is controlled by the method used and water purity. Using magnetized water has promising potentials in increasing the strength. Magnetized water shows better properties compared to normal water. The fly ash is a fine powder that is a by product of burning pulverized coal in electric generation power plants. Fly ash is a pozzolanic substance containing aluminous and siliceous material. Fly ash is a waste material, ad there by an effective waste disposal method can be proposed.

2 Objectives of the Work

- To establish M40 equivalent Fly ash based Self compacting concrete with trial mix (from 25%, 30% and 35% cement replacement by fly ash by weight of binder content along with Normal water).
- To develop magnetized water passing through a magnetic field of 0.6, 0.8, 1.0 and 1.2 T.
- To the measure the properties of magnetized water (different field magnetized water).
- To develop M 40 equivalent self compacting concrete with different field magnetized water (0.6, 0.8, 1.0 and 1.2 T) and cement replacement by the addition of fly ash (40% and 60% by weight of cement).
- To evaluate the optimum of magnetized water and fly ash in SCC based on strength properties.

3 Experimental Methodology

The experimental methodology is designed to investigate the effect of magnetized water on fly ash based self compacting concrete. In this proposed work the normal tap water is replaced by magnetized water (0.6 T, 0.8 T, 1.0 T and 1.2 T) and the cement is replaced by fly ash (30%, 40% and 60% to the weight of binder content).The experimental methodology aimed to study the fresh and hardened properties of concrete

mixes. Fresh properties are slump flow test and J ring test, the hardened properties are Compressive strength test and split tensile strength test.

3.1 Materials and Properties

The different materials used in the investigation are listed below and there physical properties are stated in Table 1.

1. Cement: 53 grade ordinary Portland cement confirming IS: 12269:1987 was used.
2. Fine aggregate: M sand with specific gravity 2.68,the fine aggregate conforming to zone II according to IS: 383-1970 was used.
3. Coarse aggregate: The coarse aggregate of size 12 mm and down, having specific gravity of 2.73.
4. Superplasticizer: To improve the workability of concrete Superplasticizer is used. It is an admixture of a new generation based on modified polycarboxylic ether.
5. Fly Ash: Class F fly ash is used for the experimental study. The chemical composition of fly ash is illustrated in Table 2.
6. Normal water: The pH Value of Normal tap water is 7.07.
7. Magnetized water: The pH Value of magnetized water (0.6 T, 0.8 T, 1.0 T and 1.2 T) are as follows 7.12, 7.29, 7.37, 7.48.
8. Magnets: Permanent Neyodinum earth magnets have been used (each magnet of 0.2 T), Shape of the magnets are round, Dimension of the magnet is 15 * 2 mm. The unit of magnetic felid is TESLA (T).
9. Steel wires.
10. Iron rod: Iron rod of length 48 cm and diameter 1 cm is opted.
11. PVC Pipe: Transparent color pvc pipe of dimension, diameter 0.5 cm and length 180 cm is opted.

Table 1 Material properties

Materials	Properties	Test results	Reference code
Cement	Specific Gravity	3.14	IS 4031-1988 Part-IV (Reaffirmed 2009)
	Fineness	5%	IS 4031-1988 Part-IV (Reaffirmed 2009)
	Consistency	32%	IS 4031-1988 Part-XI (Reaffirmed 2009)
	Initial setting time	60 min	IS 4031-1988 Part-V (Reaffirmed 2009)
Fine aggregate	Specific gravity	2.68	IS 2386-1963 Part-III (Reaffirmed 2009)
	Water absorption	2.60%	IS 2386-1963 Part-III (Reaffirmed 2009)
Coarse aggregate	Specific gravity	2.73	IS 2386-1963 Part-III (Reaffirmed 2009)
	Water absorption	0.358%	IS 2386-1963 Part-III (Reaffirmed 2016)
Fly ash	Specific gravity	2.6	

Table 2 Chemical composition of fly ash

No.	Parameters	Results (%)
1	SiO_2	46.80
2	Al_2O_3	23.70
3	Fe_2O_3	10.20
4	CaO	7.9
5	MgO	1.00
6	K_2O	0.77
7	SO_3	1.20
8	Loss on ignition	6.9

3.2 Preparation of Magnetized Water

Iron rod of dimension (length 48 cm and diameter 1.5 cm), In oder to prevent rusting of rod, the rod is painted. The rod is winded by wires and the permanent Neyodinum magnets are being placed over the iron rod (0.2 T single unit).Both the ends of iron rod is connected by pvc pipe, the ends of the pipes are connected to another set of beakers.

The beakers are kept in two heights (say H_1 and H_2), the water will flow from higher level to lower level. The beaker 1 is assigned to take up the normal water and beaker 2 is assigned to take up magnetized water. The water is assigned to pass through the experimental set up for about 24 h in oder to change the normal water to magnetized water. To ensure or check the water being magnetized check the pH value of the water. {Here water flows under the gravitational force (No external pumping system is used)} (Fig. 1).

3.3 Mix Design

The mix design were carried out for concrete grade 40 MPa based on European Federation for Specialist Construction chemicals and Concrete Systems (EFNARC) guidelines [6]. The details of mixes are given in Table 3. All the ingredients are first mixed in dry condition [6]. The water (normal water and magnetized water) and super plastizeres are added to the mix and thoroughly mixed together and hence the obtained mixed is subjected to check out the workability test [6]. SCC-O means control mix obtained from 25%, 30% and 35% cement replaced fly ash. 30% cement replacement by fly ash is opted as control mix, that is denoted as SCC-O.

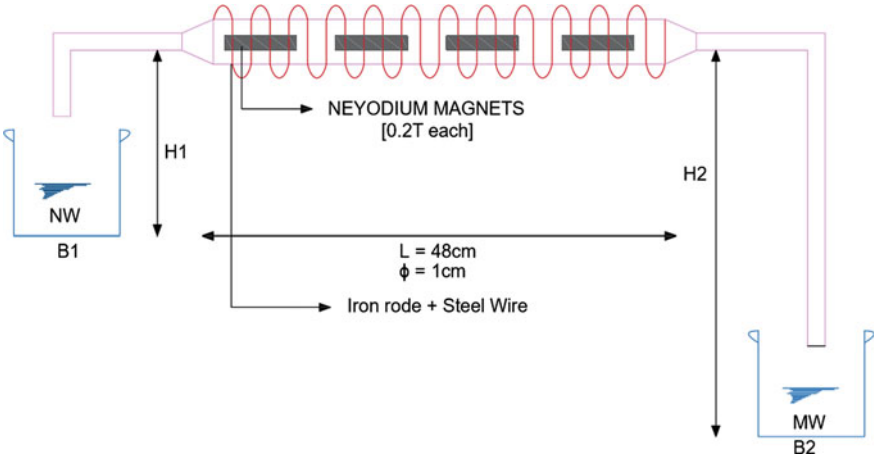

Fig. 1 Experimental set up used for preparation of magnetized water. Specifications are given below NW: Normal water, MW: Magnetized water, H_1: Height from B_1 to magnetizing unit, H_2: Height from B_2 to magnetizing unit, B_1: Beaker no 1, B_2: Beaker no 2

Table 3 Mix design

Material	Cement	Fly ash	Fine aggregate	Coarse aggregate	Water
Quantity (kg/m^3)	413	177	868.14	753	200
Ratio	1	0.428	2.102	1.82	0.40

4 Result and Discussion

4.1 Fresh Properties

The self compacting or self consolidating concrete shows certain properties during their fresh state. The mix design of SCC depends on the passing ability and flowing ability without any segregation [1, 4] (Table 4).

4.2 Hardened Properties

The Hardened properties of Fly ash (30%, 40% and 60%) based self compacting concrete with magnetized water (0.6 T, 0.8 T, 1.0 T and 1.2 T), were measured in terms of compressive strength test and split tensile strength test confirming to IS 516:1959 (Reaffirmed 2004) and IS:5816:1999 (Reaffirmed 2004) respectively. The compression test was conducted on 54 cubes of size 150 mm * 150 mm * 150 mm. 2000 kN Compression Testing Machine is used. The value at the failure point is

Table 4 Fresh properties of different SCC mixes

No.	Mix designation	T 50 slump flow (s)	Slump flow (mm)	J Ring (mm)	Passing ability (mm)
1	SCC-O	2.4	704	695	9
2	0.6 T FA 30 SCC	2.5	688	680	8
3	0.6 T FA 40 SCC	2.1	692	683	9
4	0.6 T FA 60 SCC	2.2	699	690	9
5	0.8 T FA 30 SCC	2.6	691	682	9
6	0.8 T FA 40 SCC	2.0	694	684	10
7	0.8 T FA 60 SCC	2.3	698	690	8
8	1.0 T FA 30 SCC	2.3	699	691	8
9	1.0 T FA 40 SCC	2.5	704	695	9
10	1.0 T FA 60 SCC	2.2	709	699	10
11	1.2 T FA 30 SCC	2.4	708	698	8
12	1.2 T FA 40 SCC	2.3	713	703	10
13	1.2 T FA 60 SCC	2.5	715	707	8

noted and strength is obtained by the relation between load and area. (Compressive strength = load/Area).

Control mix is obtained by replacement of cement by 30% Fly ash and along with normal water. Further the cement is replaced by various percentage of fly ash (30%, 40% and 60%) along with various type of magnetized water (0.6 T, 0.8 T, 1.0 T and 1.2 T). According to 7 day compressive strength test, when 60% of cement is replaced by fly ash along with various types of water the compressive strength is less compared to control mix [12, 14].

During 28 day compressive strength test, similar trend is shown when 60% cement is replaced by fly ash, i.e. compressive strength is decreasing. Optimum mix preferred here on the basis of compressive strength is 0.8 T at 40% FA replacement (category III). The increase in compressive strength can be due to fact that when the magnetic field is applied to water, the single water molecules will be get partly separated from the water molecule [5, 7, 9]. The number of this strong activity of this single water molecule will be increased which can greatly enhance the activity of magnetic water [8, 10, 11]. Therefore magnetic water molecules can easily enter the cement and fly ash grains and can make the hydration more completely. But in case of 60% cement replacement by FA, the strength is increasing but it doesn't shows a similar trend in increase in strength compared to 30% and 40% FA with different field water. Reason can be, the fly ash requires more time to form sodium alumino silicate hydrate (secondary compounds) gel to build up the mechanical property (Figs. 2 and 3) [13, 15].

Split tensile strength test is conducted on 39 cylinders of 150 m * 300 mm size, 2000 kN capacity. Compression Testing Machine is used to conduct test. The value at the failure point is noted. The formula used for calculation of split tensile strength

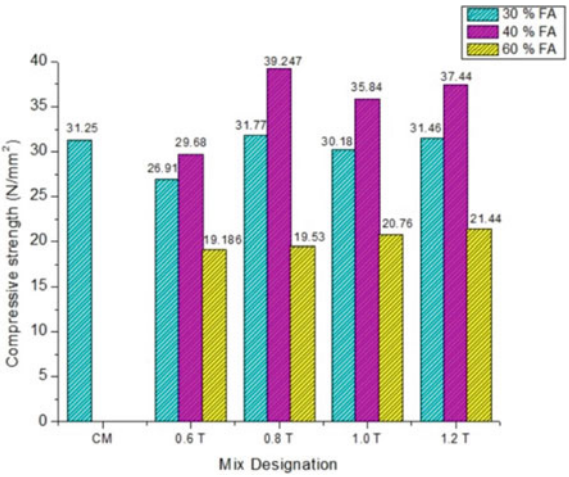

Fig. 2 7 day compressive strength test of control mix and various type of magnetized water along with fly ash based SCC

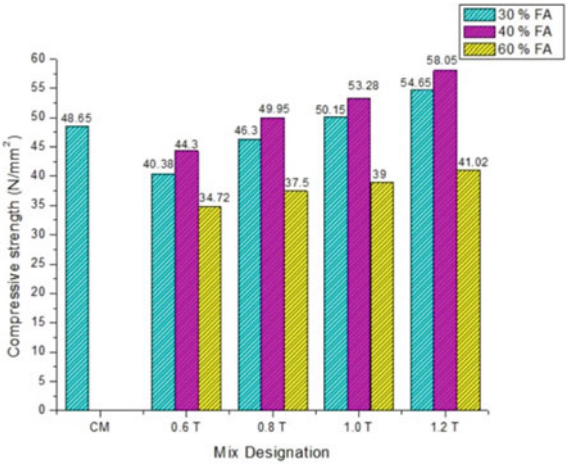

Fig. 3 28 day compressive strength test of control mix and various type of magnetized water along with fly ash based SCC

is 2P/(3.14 D * L) The 7 day and 28 day split tensile strength test results are shown in Figs. 4 and 5 [2, 3].

Optimum mix chosen out on the basis of split tensile strength is 0.8 T at 40% FA replacement (category III).The reason is similar as commented above in compressive strength [2, 3].

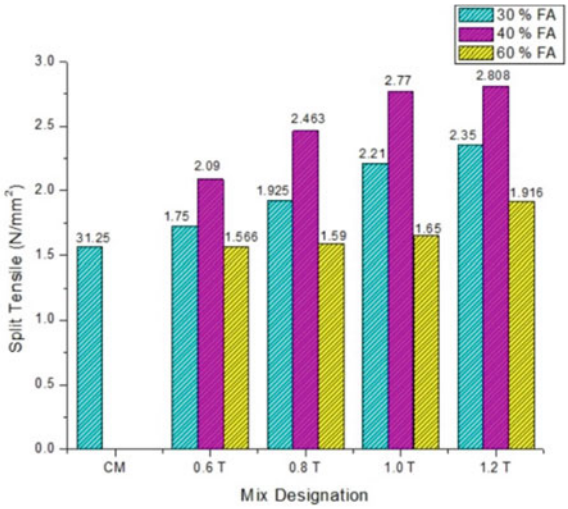

Fig. 4 7 day split tensile strength test of control mix and various type of magnetized water along with fly ash based SCC

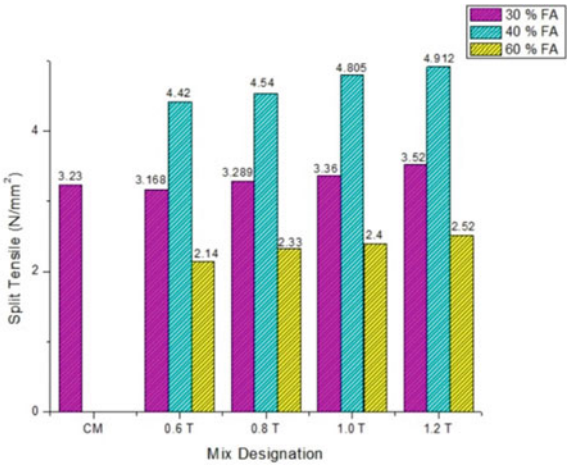

Fig. 5 28 day split tensile strength test of control mix and various type of magnetized water along with fly ash based SCC

5 Conclusions

The research finding over the investigation on the effect of magnetized water on the mechanical properties of fly ash based self compacting concrete is given as follows.

- Magnetized water improves the improves the workability properties of the specimen (Table 3, Remarks 'as per ASTM1621/C1621M): No visible blocking since passing ability values are between 0 and 25 mm').
- Magnetized water improves the cement hydration process. When the magnetic field is applied to water, the single water molecules will be get partly separated from the water molecule. The number of this strong activity of this single water molecule will be increased which can greatly enhance the activity of magnetic water. Therefore magnetic water molecules can easily enter the cement and fly ash grains and can make the hydration more completely.
- Increasing in compressive strength for 30% and 40% FA is noted out along with different categories of magnetized water (0.6 T, 0.8 T, 1.0 T and 1.2 T).
- When the cement is replaced by fly ash at 60% (To weight of cement) along with various categories of magnetized water (0.6 T, 0.8 T, 1.0 T and 1.2 T) the compressive strength is less than compared to control mix.
- Increasing in split tensile strength for 30% and 40% FA is noted out along with different categories of magnetized water (0.6 T, 0.8 T.1.0 T and 1.2 T).
- Similar result is shown in split tensile strength, when the cement is replaced by fly ash at 60% (To weight of cement) along with various categories of magnetized water (0.6 T, 0.8 T, 1.0 T and 1.0 T) the split strength is less than compared to control mix.
- Percentage of increase in compressive strength is about 6–14% (for 30% and 40% FA with various field MW).
- Percentage of increase in split tensile strength is about 4–12.8% (for 30% and 40% FA with various field MW).
- Percentage of increase in compressive strength and split tensile strength is about 2.4–8% and 2–6% (for 60% FA with different field water).

References

1. Abdalhmid MJ, Ashour AF, Sheehan T (2019) Long-term drying shrinkage of self-compacting concrete: experimental and analytical investigation. J Constr Build Mater 202:825–837
2. Abdelgader AAB, Hamdan RM, Magid TIMA, Omer MEA (2017) Effect of magnetized water on workability and compressive strength of concrete. In: Proceedings of international conference on analytical models and new concepts in concrete and masonry structures AMCM, vol 193, pp 494–500
3. Akinpelu AM, Muhammed ZF, Odeyemi OS, Olafusi SO (2019) Evaluation of splitting tensile and compressive strength relationship of self compacting concrete. J King Saud Univ Eng Sci 31:19–25
4. Brouwers HJH, Radix HJ (2005) Self Compacting concrete theoretical and experimental study. J Cement Concr Res 35:2116–2136
5. Chun XZ, Feng XP (2013) The magnetization of water arising from a magnetic-field and its applications in concrete industry. Int J Eng Res Appl 03(5):1541–1552
6. EFNARC (2002) Specification and guidelines for Self Compacting Concrete. www.efnarc.org
7. Esmaeilnezhad E, Choi HJ, Schaffie M, Gholizadeh M, Ranjbar M (2017) Characteristics and applications of magnetized water as a green technology. J Clean Prod 161:908–921

8. Gao K, Gong Z, Wang Y, Ou Y, Zhan J, Zhang B (2013) The effect of a static magnetic field on the hydrogen bonding in water using frictional experiments. J Mol Struct 1052:102–104
9. Gao H, Wang X, Wang Y, Yang Z, Yao X (2015) Analysis on properties of magnetised water and its application in sprayed concrete. J Mater Innov 19:215–218
10. Gao H, Wang Y, Yao X (2014) Analysis on microstructure of impermeability of magnetized water concrete. J Chem Pharm Res 06(7):189–199
11. Jose J, Roy N, Shine T (2018) Comparative experimental investigation on strength characteristics of concrete mixed with magnetized water. Int J Innov Res Sci Eng Technol 07(2):1566–1571
12. Luo J, Wang Y, Wei H (2017) Influence of magnetic water on early age shrinkage cracking of concrete. J Constr Build Mater 14:91–100
13. Magriotis MZ, Ramalho CT, Toledo EJL (2008) Influence of magnetic field on physical chemical properties of the liquid water: insights from experimental and theoretical models. J Mol Struct 888:409–415
14. Malathy R, Manjupriya T (2016) Experimental investigation on strength and shrinkage properties of concrete mixed with magnetically treated water. Int J Eng Adv Res Technol 02(3):46–50
15. Mar CY, Su N, Wu HY (2000) Effect of magnetic water on the engineering properties of concrete containing granulated blast furnace slag. J Cement Concr Res 30:599–605

Effect of Immersion Time on the Mechanical Properties of Glass Fibre Reinforced Concrete with Glass Powder Immersed in Water

K. Sana and Anju Paul

Abstract Production of cement causes environmental problems like global warming due to the release of carbon dioxide. Usage of cement can be reduced by partially replacing cement in concrete with a suitable material. This paper studies the effect of water immersed glass powder and glass fibre mechanical properties of concrete. Cement is partially replaced with 10, 15 and 20% of glass powder by weight of cement immersed in water at 1.5, 3, 4.5 and 6 h. Glass powder is added to the water required for the mix before adding it to the cement and aggregates. Then 0.25, 0.5, 0.75 and 1% glass fibre by weight of cement is incorporated in to the concrete containing optimum percentage of glass powder with optimum immersion time. Glass fibre having length of 6 mm and diameter 14 μm is used. Calcium and sodium ions are dissolved in presence of water from glass powder (Abo-Hasseira et al. in Constr Build Mater 206:674–682, 2019 [1]; Elaqra et al. in Constr Build Mater 203:75–82, 2019 [5]). Concentration of sodium ions decreases with immersion time as it bonds with silicon dioxide on the surface of glass powder particles (Abo-Hasseira et al. in Constr Build Mater 206:674–682, 2019 [1]). This paper discusses compressive strength, flexural strength and split tensile strength of concrete. Higher strength is obtained due to the packing filling effect of glass powder and pozzolanic reaction due to the free ions in water before mixing with the concrete.

Keywords Glass powder · Glass fibre · Mechanical properties · Immersion time · Pozzolanic property

K. Sana (✉) · A. Paul
Department of Civil Engineering, Toc H Institute of Science and Technology, Arakkunnam, Ernakulam, India
e-mail: sanathoufeek@gmail.com

A. Paul
e-mail: anjukpaul@gmail.com

© Springer Nature Switzerland AG 2021

K. Dasgupta et al. (eds.), *Proceedings of SECON 2020*,
Lecture Notes in Civil Engineering 97,
https://doi.org/10.1007/978-3-030-55115-5_46

1 Introduction

Sustainable construction is a method of creating structures with renewable and recyclable resources, reducing energy consumption, using waste materials etc. Sustainable concrete can be developed by replacing fine aggregate and coarse aggregate, using supplementary cementitious materials etc. Waste management is a big challenge in the present time. Indian glass industry produces huge amount of glass waste. Glass waste is difficult to dispose. Generally glass wastes are disposed on land which is not an economical solution. So the utilization of glass waste in concrete is done in many ways as cement replacement, fine aggregate replacement etc. As concrete is the most used construction material, huge quantity of cement is produced every year. Cement production causes emission of carbon dioxide which may cause environmental problems [2]. So even if a small quantity of cement production can be reduced, it will be very beneficial to the environment. Glass is mainly composed of silica. Use of milled waste glass in concrete as partial replacement of cement [6, 7] will be an important step towards the development of sustainable infrastructure systems. Glass in its powdered forms is expected to undergo pozzolanic reactions with cement hydrates, forming secondary Calcium Silicate Hydrate (C–S–H) [9, 10, 12]. Water immersed glass powder helps to form more C–S–H in concrete, due to the hydrolysis of glass powder in to free ions of SiO_2, CaO and Na_2O in the water [1, 5]. When glass powder is added to water more sodium ions are formed due to the higher mobility of sodium ions compared to calcium ions. But the concentration of sodium ions will decrease as a function of immersion time as it bonds with the silicon dioxide on the surface of glass powder particles [1, 5]. The double effect of the development of pozzolanic reaction due to the increase of the free ions in the water before mixing with the concrete and the packing filling effect of glass powder will cause early development of compressive strength [1, 5]. Usage of glass fibre in concrete improves compressive strength, tensile strength, ductility etc of concrete [3, 4, 11]. Glass fibre reinforced concrete has many advantages such as lightweight, fire resistant property etc. Incorporation of glass fibre and water immersed glass powder in concrete may enhance the properties of concrete in terms of strength and durability.

2 Experimental Programme

2.1 Materials

The materials used in this study are cement, glass powder (GP), fine aggregate, coarse aggregate, water, Super plasticizer and glass fibre (GF). Ordinary Portland cement of 53 grade conforming to IS 12269:1987 (reaffirmed 2013) is used. Fine aggregate used in this work is M-sand (manufactured sand) confirming to zone II of IS 383:1970 (reaffirmed 2016). Coarse aggregate used in this work is crushed

Table 1 Chemical composition of glass powder

Silica (SiO_2)	72.5
Alumina (Al_2O_3)	0.4
Iron oxide (Fe_2O_3)	0.2
Calcium oxide (CaO)	9.7
Magnesium oxide (MgO)	3.3
Sodium oxide (Na_2O)	13.7
Potassium oxide (K_2O)	0.1
Loss of ignition	0.36
Fineness percentage passing (sieve size)	80 (45 μm)
Unit weight (kg/m^3)	2579
Specific gravity	2.58

Table 2 Properties of glass fibre

Property	Value
Fibre length (mm)	6
Filament diameter (microns)	14
Loss on ignition (%)	1
Moisture (%)	0.9
Softening point (°C)	845
Specific gravity	2.68

stone with a maximum nominal aggregate size of 20 mm confirming to IS 383:1970 (reaffirmed 2016). Glass powder is made by crushing and milling process of glass containers, bottles, pieces of window glass etc. in to grounded form. Glass powder used in this work is collected from cloudtail India Private Limited, its chemical composition is given in Table 1. Glass fibre is a material consisting of numerous extremely fine fibres of glass. Glass fibre used in this study is collected from Buddha Building Technology, its properties are given in Table 2. Figures 1 and 2 show glass powder and glass fibre respectively. Super plasticizer used was Master glenium and potable water was used for both mixing and curing.

2.2 Mix Design

The mix design was done as per IS 10262:2019 [8]. The mix proportion with a water cement ratio of 0.41 is shown in Table 3.

Fig. 1 Glass powder

Fig. 2 Glass fibre

Table 3 Mix proportion

Mix designation	Cement (kg/m^3)	Fine aggregate (kg/m^3)	Coarse aggregate (kg/m^3)
M30	385	703	1192
	1	1.82	3.09

2.3 Preparation of Water Immersed Glass Powder Concrete (WGP) and Glass Fibre Reinforced Water Immersed Glass Powder Concrete (GFWGP)

Cement was partially replaced with 10, 15 and 20% glass powder by weight of cement. Glass powder was first immersed in water required for the mix for different immersion times of 1.5, 3, 4.5 and 6 h. Then the glass powder along with the mixing water was added to the concrete mix. Glass fibre was added to the water immersed glass powder concrete containing optimum glass powder content with optimum immersion time. Glass fibre was added in different percentages of 0.25, 0.5, 0.75 and 1% by weight of cement.

2.4 Results and Discussions

The results of compressive strength, split tensile strength and flexural strength of concrete specimens for water immersed glass powder concrete and glass fibre reinforced water immersed glass powder concrete are as follows.

2.4.1 Compressive Strength

Compressive strength test was conducted on 150 mm × 150 mm × 150 mm concrete cubes as per IS 516:1959 (reaffirmed 2018) in digital compression testing machine. Compressive strength test was conducted after 7 days and 28 days of curing. Compressive strengths of water immersed glass powder concrete mixes and glass fibre reinforced water immersed glass powder concrete mixes are shown in Figs. 3, 4 and 5 respectively.

Maximum 28 day compressive strength of 43.92 N/mm^2 was obtained for 10% glass powder content with an immersion time of 1.5 h but the optimum percentage of glass powder content was 15% with an immersion time of 4.5 h, having a 28 day compressive strength of 41.59 N/mm^2. WGP concrete mix containing 15% glass powder with an immersion time of 4.5 h is taken as the optimum WGP concrete as it replaces more cement comparing with 10% glass powder replacement and it showed an increase in compressive strength of 7.57% comparing with the control mix.

Compressive strength of GFWGP concrete increased up to 0.75% glass fibre addition. Maximum compressive strength of 43.85 N/mm^2 is obtained for 0.75% GF with a percentage increase of 13.4% and 5.43% compared to control mix and optimum mix of WGP concrete.

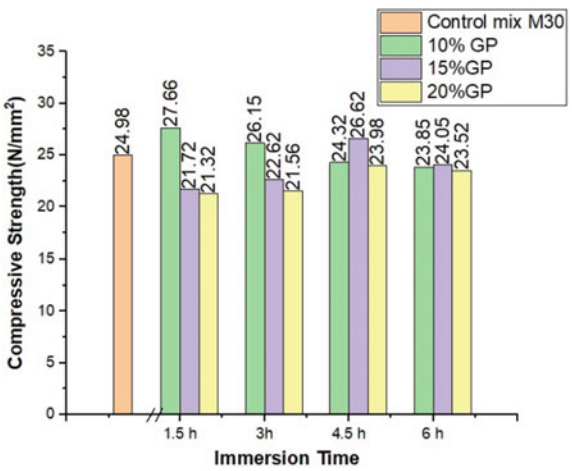

Fig. 3 7 day compressive strength of concrete mixes with different percentages of glass powder content at different immersion times

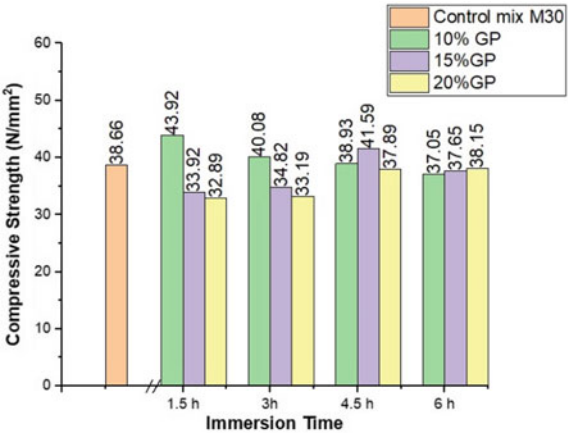

Fig. 4 28 day compressive strength of concrete mixes with different percentages of glass powder content at different immersion times

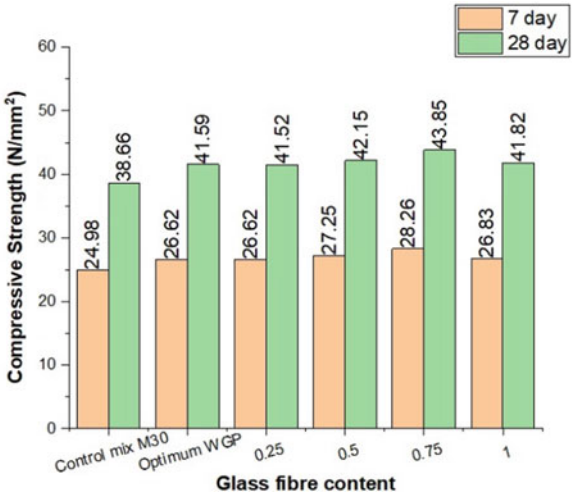

Fig. 5 Compressive strength of water immersed glass powder concrete with different percentage fibre reinforcement

When glass powder immersed in water SiO_2, CaO, Na_2O ions are dissolved in water. These ions will help to form more calcium silicate hydrate than portlandite in cement hydration. Progress of the pozzolanic reaction due to silica present in the undissolved glass powder and packing filling effect of glass powder that is densification of interfacial transition zone by smaller glass powder particles contributed strength to water immersed glass powder concrete mixes. The increase in strength parameters of glass fibre reinforced water immersed glass powder concrete mixes are due to bridging effect of glass fibre at the surface of cracks.

2.4.2 Split Tensile Strength

Split tensile strength test was conducted as per IS 5816:1999 (reaffirmed 2018) in digital compression testing machine. Split tensile strength test was conducted after 28 days of curing. Split tensile strengths of WGP concrete mixes and GFWGP concrete mixes are shown in Figs. 6, 7 and 8 respectively. A percentage decrease of 8.57% is observed for split tensile strength of optimum WGP mix compared to

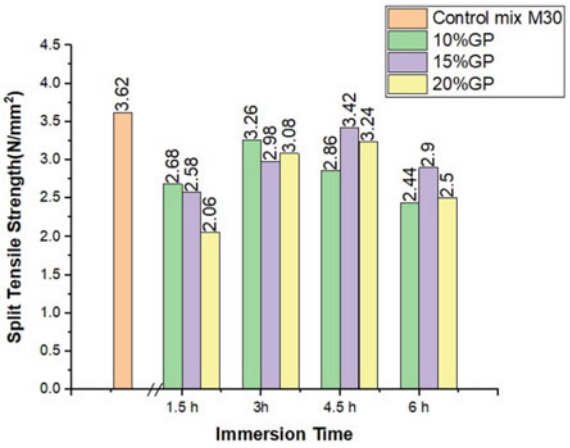

Fig. 6 28 day split tensile strength of concrete mixes with different percentages of glass powder content at different immersion times

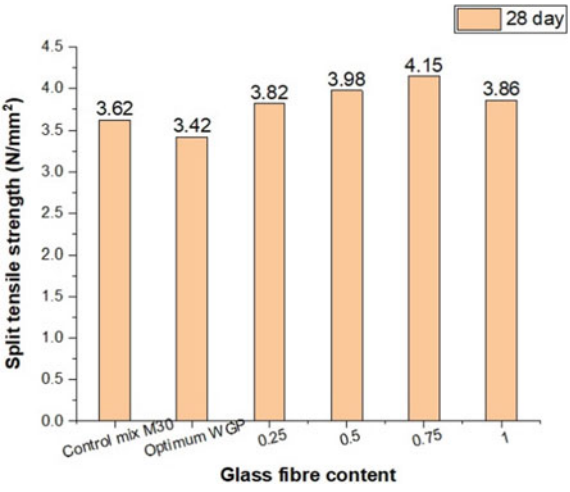

Fig. 7 Split tensile strength of water immersed glass powder concrete with different percentage fibre reinforcement

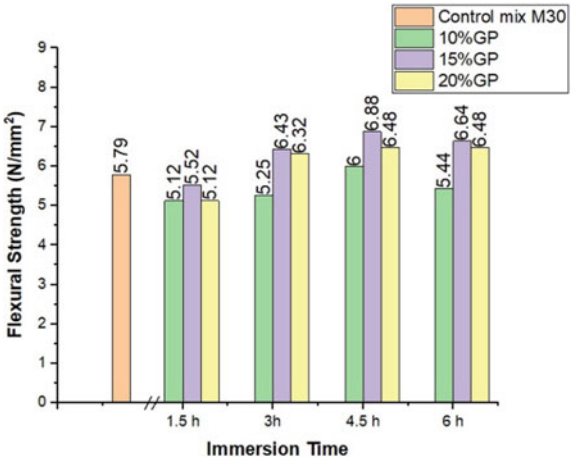

Fig. 8 28 day flexural strength of concrete mixes with different percentages of glass powder content at different immersion times

control mix. An increase in split tensile strength of 14.6% is obtained for GFWGP concrete containing 0.75% glass fibre content compared to control Mix.

2.4.3 Flexural Strength

Flexural strength test was conducted as per IS 516:1959 (Reaffirmed 2018) in Universal testing machine. Flexural strength test was conducted after 28 days of curing. Flexural strengths of water immersed glass powder concrete mixes and glass fibre reinforced water immersed glass powder concrete mixes are shown in Figs. 8 and 9 respectively. An increase in flexural strength of 18.88% is obtained for the optimum WGP mix compared to the control mix. An increase in flexural strength of 21.76% is obtained for GFWGP concrete containing 0.75% glass fibre content compared to control Mix.

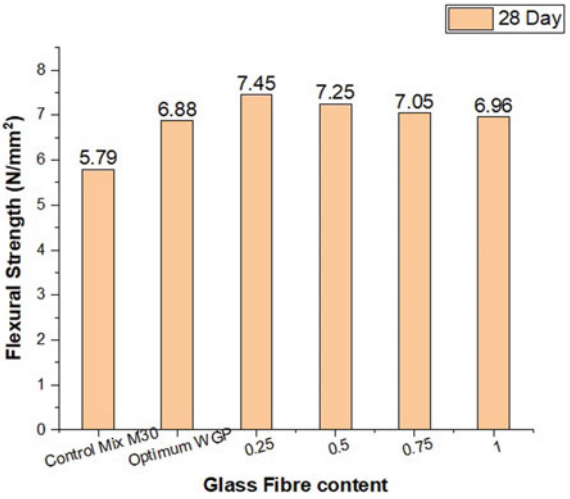

Fig. 9 Flexural strength of water immersed glass powder concrete with different percentages fibre reinforcement

3 Conclusion

In this study, an experimental investigation on the strength properties of water immersed glass powder concrete and glass fibre reinforced water immersed glass powder concrete was conducted. The following conclusions were made,

- An increase in compressive strength of 7.57% is obtained for the optimum mix of WGP Concrete containing 15% glass powder by weight of cement with an immersion time of 4.5 h.
- Optimum mix of WGP concrete showed a percentage decrease of 8.57 for split tensile strength compared to control mix.
- Maximum compressive strength of 43.85 N/mm^2 is obtained for 0.75% GF with a percentage increase of 13.4% and 5.43% compared to control mix (38.66 N/mm^2) and optimum mix (41.59 N/mm^2) of WGP concrete.
- An increase of 14.6% is obtained for split tensile strength of GFWGP concrete containing 0.75% GF (4.15 N/mm^2) compared to control Mix (3.62 N/mm^2).
- Flexural strength of GFWGP concrete 0.75% GF increased by 21.76% compared to control mix.
- Significant improvement in flexural strength is obtained for all GFWGP concrete mixes, but flexural strength decreased with increase in glass fibre content
- The increase in strength properties are due to the packing filling effect and pozzolanic reaction of glass powder and bridging effect of glass fibre.

References

1. Abo-Hasseira AB, Al-Afghany MA, Alwan MD, Elaqra HA, Elmasry IH, Tabasi AM (2019) Effect of immersion time of glass powder on mechanical properties of concrete contained glass powder as cement replacement. Constr Build Mater 206:674–682
2. Aboshama AY, Aliabdo AA (2016) Utilization of waste glass powder in the production of cement and concrete. Constr Build Mater 124:866–877
3. Akca AH, Akyuncu V, Chowdhury S, Kabay N, Kizilkanat AB (2015) Mechanical properties and fracture behaviour of basalt and glass fibre reinforced concrete: an experimental study. Constr Build Mater 100:218–224
4. Ali B, Qureshi LA (2019) Influence of glass fibres on mechanical and durability performance of concrete with recycled aggregates. Constr Build Mater 228:1–15
5. Elaqra HA, Haloub MAA, Rustom RN (2019) Effect of new mixing method of glass powder as cement replacement on mechanical behavior of concrete. Constr Build Mater 203:75–82
6. Elaqra H, Rustom R (2018) Effect of using glass powder as cement replacement on rheological and mechanical properties of cement paste. Constr Build Mater 179:326–335
7. Ghahremaninezhad A, Kamali M (2015) Effect of glass powders on the mechanical and durability properties of cementitious materials. Constr Build Mater 98:407–416
8. IS 10262:2019 Indian standard Concrete mix proportioning—guidelines (Second revision), Bureau of Indian standards, New Delhi
9. Islam GMS, Kazi N, Rahman MH (2017) Waste glass powder as partial replacement of cement for sustainable concrete practice. Int J Sustain Built Environ 6:37–44
10. Ismail SI, Naber NE, Rahma A (2017) Effect of glass powder on the compression strength and the workability of concrete. Cogent Eng 4:1–12
11. Kasagani H, Rao CBK (2018) Effect of graded fibers on stress strain behaviour of glass fiber reinforced concrete in tension. Constr Build Mater 183:592–604
12. Zheng K (2016) Pozzolanic reaction of glass powder and its role in controlling alkali-silica reaction. Cement Concr Compos 67:30–38

Assessment of Fraction Effects on Flow Characteristic of Cement Mortar Using Natural and Manufactured Sand

Chintan Vohra and Parth Thaker

Abstract The concrete's workability is divided into three phases namely coarse aggregate phase, mortar phase and cement paste phase. The coarse aggregate phase comprises of coarse aggregate and mortar phase. The mortar phase of concrete primarily comprises of binder, fine aggregate and water. The function of mortar phase is to impart workability to the concrete. Holistically, factors like water content, shape of aggregates and gradation of aggregates plays an important role in regulating the workability of mortar. However, there is no such methodology established from which one can predict the workability of concrete based on the texture and shape parameters of aggregates. To study the relation of above-mentioned factors on the workability, tests were carried out using uniformly graded and well graded Natural sand and Manufactured sand for assessment of shape parameters and workability. The shape parameters of fine aggregates were obtained through Digital Image Processing (DIP) method which was conducted on at least 600 individual particles from each grade of both samples. The workability of cement mortar for both the samples are tested at water-cement ratios (0.3, 0.35, 0.40, 0.45, 0.5) and cement-sand ratios (1:1, 1:2, 1:3, 1:4). Mini flow table test was used to check workability in terms of its average flow. From the experimental results a relationship is developed, which states that the average flow of zone sand is proportional to the weighted average of the product of the average flow of the mortar for a particular sieve class, at its corresponding W/C and C/S ratio, and proportion in the given sand sample. The proposed equation to predict the workability of cement mortar is validated using test results.

Keywords Workability · Digital image processing · Mini flow table test · Average flow diameter · Shape and size characteristics

C. Vohra (✉)
Contech Chemicals, Ahmedabad, Gujarat, India
e-mail: chintanvohra@gmail.com

P. Thaker
Fuji Silvertech Concrete Pvt. Ltd., Ahmedabad, Gujarat, India
e-mail: parththaker2003@gmail.com

© Springer Nature Switzerland AG 2021

K. Dasgupta et al. (eds.), *Proceedings of SECON 2020*,
Lecture Notes in Civil Engineering 97,
https://doi.org/10.1007/978-3-030-55115-5_47

Abbreviations

A_p	Area of particle outline
D_a	Diameter of a circle with an area equal to that of the particle outline
D_c	Diameter of smallest circumscribed circle
P_p	Perimeter of particle outline
P_a	Perimeter of a circle of the same area as particle outline
A_c	Area of the smallest circumscribing circle
D_{ins}	Diameter of the largest inscribed circle Perimeter,
P_{conv}	Perimeter of convex hull
Sn	Sieve class
NS	Natural sand
MS	Manufactured sand
W/C	Water-Cement ratio
C/S	Cement-Sand ratio
DIP	Digital Image Processing
DSLR	Digital Single-Lens Reflex Camera
IS	Indian Standard

1 Introduction

1.1 Background

Workability of concrete is a physical parameter which affects the strength and durability of concrete [1–3]. The placement method, space constraints and the size of aggregate are governing parameters for establishing a bracket in which workability of the mix is defined [4, 5]. The concrete is a three-phase system that primarily consists of a coarse aggregate phase, mortar phase, and cement phase. The workability of the concrete's field of influence lies in the mortar phase. The factors governing workability of mortar phase is shape and size of fine aggregates, cement to sand ratio and water cement ratio [6, 7]. The effect of cement and sand and water binder ratio on cement mortar can quantified by various fresh properties tests with suitable indicators for degree of workability in the mix, and in addition with assessing quantifiable rheological parameters [8–10]. However, only some research has been done on how the contribution of shape parameters of aggregate on the workability of mortar is affected [11, 12]. On visual inspection one can predict that the aggregates which are angular or has rough texture can reduce the workability of mortar as compared to the aggregates which are round and has smooth texture. However, at this time no research has been done regarding at what degree, various shape factors affect workability. Shape parameters not limited to angularity but other parameters like sphericity, roundness, texture, surface area, flakiness, elongation, and aspect ratio

are parameters contributes to define a shape of aggregate [13–18]. For this study tests are carried out with respect to shape parameters like angularity, roundness, sphericity, and aspect ratio considering them the primary shape factors. These are primary factors which not only impacts the workability of cement mortar but also affects the hardening properties of concrete [10, 18–22]. Research shows that crushed aggregates having a higher angular number increases tensile properties of concrete in the concrete compared to the ones with rounded aggregates [2, 24–27]. Similarly, the shape of the crushed stone aggregates significantly impacted the rutting resistance in asphalt mix concrete [28, 29].

Digital Image Processing (DIP) has its application in various disciplines such as medicine, meteorology, geology, material science, and manufacturing. In civil engineering DIP is used for studying the shape and size of aggregate particles, to identify fracture cracks on the cross section of hardened concrete, to map the cracks on asphalt surface [23, 30, 31]. There are various methods to carry out DIP depending upon the complexity of the element and the order of assessment of that element [4, 17, 32–34]. One of the techniques involves extracting 3-D quantitative parameters assessment using 2-D image information [34, 35]. Another method uses CT scan imaging techniques to identify the surface texture and shape factors of aggregate particles using vector projection method and aggregate shape parameters are drawn out from the scan [36–38]. The image processing measures the shape parameters of an element by converting the image into a binary image where each pixel is assigned 1 and 0 based on black and white in their respective block. The software processes the binary image, to output shape data from the aggregate projected pixels [40].

1.2 Need of Study

To study the shape parameters, influence on the workability of cement mortar one must have a clear understanding of the particle size distribution over the entire spectrum of the given sample of aggregates. The method of sieve analysis can be deemed inaccurate method for calculating the mean average size of aggregate as the relatively elongated aggregates tend to pass from the sieve, therefore, reporting error in the results. DIP on the other hand can simultaneously report all the shape parameters on a single run [34, 39, 41]. Particle size distribution can be carried out efficiently and quickly by processing the image of aggregate. In addition, gross surface area of the aggregate particles can be determined from the results obtained from DIP to understand the correlation between cement paste film thickness, water film thickness, and workability of cement mortar [41, 42]. This study can contribute in developing an empirical equation which can be used to predict the workability of the concrete mix which can help engineers to conduct relatively less trials compared to traditional methods of trial and error while designing a concrete mix [9, 43, 44]. This study can also help researchers with the role of shape factors in rheological properties of concrete. In addition to optimize workability of mortar, research has been carried out for optimizing water film thickness and paste film thickness. These parameters will

enable researchers to correlate the film thickness, shape effects to the workability of mortar [41, 44, 45]. The effect in mortar phase can be extended further from mortar phase to concrete phase. This will also help to understand rheological properties of concrete and Non-Newtonian characteristics, cement mortar exhibits at low water cement ratios. Study shows that the thickness of cement film and water film in the mortar phase has a significant effect on fluidity of concrete [46].

1.3 Purpose and Objectives

The purpose of this study is to compare the shape characteristics of the river sand and manufactured sand as given in Table 1 by using the method of DIP; and to measure the workability of cement mortar using individual fraction of sand and artificially zone sand at a range of different water-cement ratios and cement-sand ratios. The results of the shape characteristics and the workability will then be checked for degree of correlation. A probable methodology will be proposed which can help researchers to predict the workability of mortar or concrete from the results obtained from DIP.

Table 1 Shape characteristics definitions and schematic diagram [47]

Parameter	Definition	Figure	Significance
Sphericity	Da/Dc	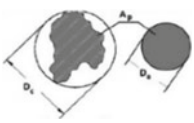	Sphericity is concerned only with the form of the grain i.e. how close its shape resembles to a sphere but not how round the boundaries of the particle are
Roundness	$(Pp)^2/4 \sqcap Ap$		Roundness is concerned with the degree of roundness of edges of any given surface of aggregates
Roughness/angularity	$(pconv/Pp)^2$		The angularity is the measure of the degree of sharpness on the surface of particle. Higher angularity number more will be the sharp edges
Aspect ratio	Major axis/minor axis	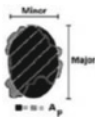	Aspect ratio is the ratio of dimension of major axis to minor axis

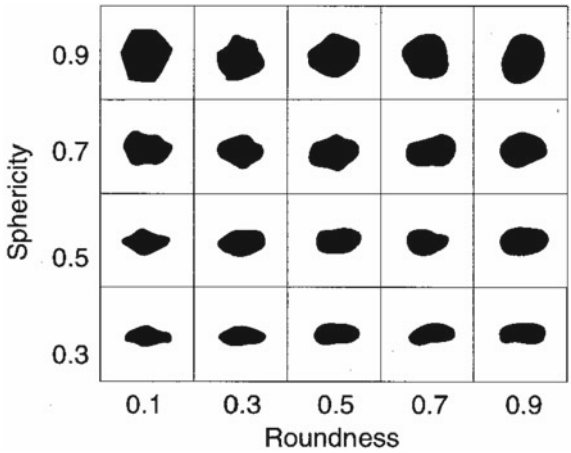

Fig. 1 Visual inspection of degree of roundness and sphericity in aggregates [2]

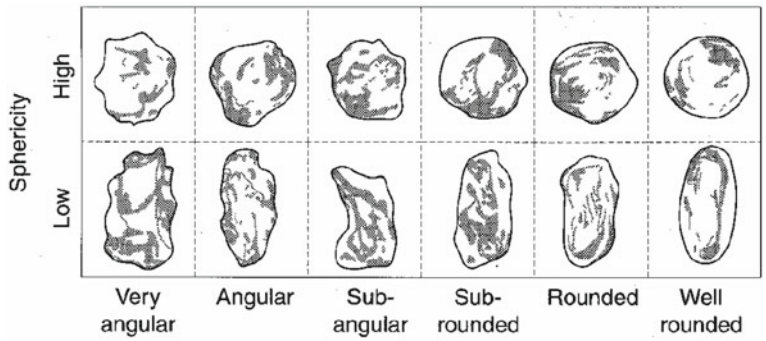

Fig. 2 Visual inspection for shape of aggregates [2]

The shape of aggregates can also be assessed visually and can be classified as angular or rounded. Figures 1 and 2 explains to assess the aggregates shape based on visual inspection and value of shape parameters.

2 Expermental Materials and Methodology

2.1 Materials

For the experiment, Ordinary Portland Cement of 53 grade was used as a binder. OPC-53 confirms the specifications provided in IS:269:2015 [48]. The tests of the physical properties were carried out as per IS:4031 and chemical analysis as per

Table 2 Size class of manufactured sand and river sand [52]

Size class	Sieve size range	
	Lower sieve size (Material retained on)	(Upper size sieve) (Material passing from)
S1	2.36 mm	4.75 mm
S2	1.18 mm	2.36 mm
S3	600 μm	1.18 mm
S4	300 μm	600 μm
S5	150 μm	300 μm

IS:4032 [49, 50]. Two tests were conducted to determine the void content within the aggregate and in loosely packed sand. The test is carried out in accordance with IS:2386 Part-3: 1963 (Reaffirmed 2016): specific gravity, density, voids, absorption, and bulking [51]. The fine aggregates were procured in different size classes. For testing, the workability of mortar using fine aggregates with blend of each sieve class, sand samples of different zones for natural sand and quarry sand, were prepared by artificially proportioning each sieve class to form sand samples of Zone-1, Zone-2 and Zone-3 each confirming to IS: 383: specifications for coarse and fine aggregate of concrete [52]. The proportion of sand from each sieve class is taken as the average of upper and lower limit the percentage passing from the sieve as given in Tables 2, 3 and 4 shows the proportion of each sieve class for different zones of sand given in Fig. 3.

The research was divided in two parts, the first part was to conduct Digital Image Processing of at least 600 aggregate particles from each sieve class were conducted, and after obtaining the shape parameters such as sphericity, roundness, angularity, and aspect ratio correlation analysis was carried out.

In second part of the test to check the workability of cement mortar; samples were prepared with different water cement ratios (W/C = 0.3, 0.35, 0.4, 0.45, 0.5), cement to sand ratios for individual class size, and artificially blended sand in ratios (C:A = 1:1, 1:2, 1:3, 1:4). The samples were tested on a modified mini flow table and average flow in millimeters was measured. The detail experimental program is shown in Table 5.

Table 3 Artificially zoned sand sample proportioning

Zone-1				Zone-2			Zone-3		
Sieve size	Average of percentage passing from IS:383: 2016 (A) (%)	Cumulative percentage particles retained (B) (%)	|B(n) − B(n − 1) (%)|	Average of percentage passing from IS:383: 2016 (A)	Cumulative percentage particles retained (B)	|B(n) - B(n-1)|	Average of Percentage Passing from IS:383: 2016 (A)	Cumulative Percentage particles retained (B)	|B(n) - B(n-1)|
10 mm	100.00	0.00	0.00	100.00	0.00	0.00	100.00	0.00	0.00
4.75 mm	95.00	5.00	5.00	95.00	5.00	5.00	95.00	5.00	5.00
2.36 mm	76.50	23.50	18.50	86.50	13.50	8.50	91.50	8.50	3.50
1.18 mm	48.00	52.00	28.50	70.50	29.50	16.00	76.41	23.59	15.09
600 μm	21.50	78.50	26.50	44.00	56.00	26.50	40.05	59.95	36.36
300 μm	5.00	95.00	16.50	8.00	92.00	36.00	9.00	91.00	31.05
150 μm	0.00	100.00	5.00	0.00	100.00	8.00	0.00	100.00	9.00

Table 4 Proportion of each sieve class for different zones of sand

Sieve class	Sieve size	Zone-1 (%)	Zone-2 (%)	Zone-3 (%)
S1	4.75–2.36 mm	5.00	5.00	5.00
S2	2.36–1.18 mm	18.50	8.50	3.50
S3	1.18–600 μm	28.50	16.00	15.09
S4	600–300 μm	26.50	26.50	36.36
S5	300–150 μm	21.50	44.00	40.05

Fig. 3 Different sieve class of natural sand sample

3 Experimental Programme and Results

3.1 Pilot Study

Pilot study is carried out to check the working range of DIP setup which can result with minimum error and measure the behavior of mortar for low and high workability. Various methods are available to check the workability of fresh cement mortar based on which different workability indicators are developed. It was observed that the DIP setup worked accurately for sieve class ranging from S1 to S4. The workability test is carried out using a modified mini flow table which has a base plate of diameter of 450 mm in order to measure the flow of high workable mix efficiently. An attempt was made to measure workability of mixes which had zero flow by using stress and strain indicators using geotechnical vane shear test in accordance with IS: 2720 (Part-30) laboratory vane shear test [52, 53], however, due to its low angular velocity, the sample started showing a stiffening effect before failure hence the readings were not accurate.

3.1.1 Digital Image Processing of Aggregates

To determine the operating range of the setup, particles of different sieve classes were placed on the tray and DIP was conducted and particles were analyzed. It was discovered that the accuracy was reduced for particles of a size range 300–150 μm. For example, if the particle size was smaller than 300 μm, a test was carried out by using a stereo zoom microscope. However, all the images acquired were difficult to analyze as it was difficult to differentiate between foreign particles,

Table 5 Experimental program

Test	Testing of sample	Sample type	Cement sand ratio	Water cement ratio
Mini flow table test for natural sand and manufactured sand	Testing of graded aggregates	4.75–2.36 mm (S1)	C:S = 1:1	W/C = 0.30 W/C = 0.35 W/C = 0.40 W/C = 0.45 W/C = 0.50
			C:S = 1:2	
			C:S = 1:3	
			C:S = 1:4	
		2.36–1.18 mm (S2)	C:S = 1:1	
			C:S = 1:2	
			C:S = 1:3	
			C:S = 1:4	
		1.18 mm–600 μm (S3)	C:S = 1:1	
			C:S = 1:2	
			C:S = 1:3	
			C:S = 1:4	
		600–300 μm (S4)	C:S = 1:1	
			C:S = 1:2	
			C:S = 1:3	
			C:S = 1:4	
		300–150 μm (S5)	C:S = 1:1	
			C:S = 1:2	
			C:S = 1:3	
			C:S = 1:4	
	Testing of fine aggregates constituting of each sieve class	Zone-1	C:S = 1:1	
			C:S = 1:2	
			C:S = 1:3	
			C:S = 1:4	
		Zone-2	C:S = 1:1	
			C:S = 1:2	
			C:S = 1:3	
			C:S = 1:4	
		Zone-3	C:S = 1:1	
			C:S = 1:2	
			C:S = 1:3	
			C:S = 1:4	

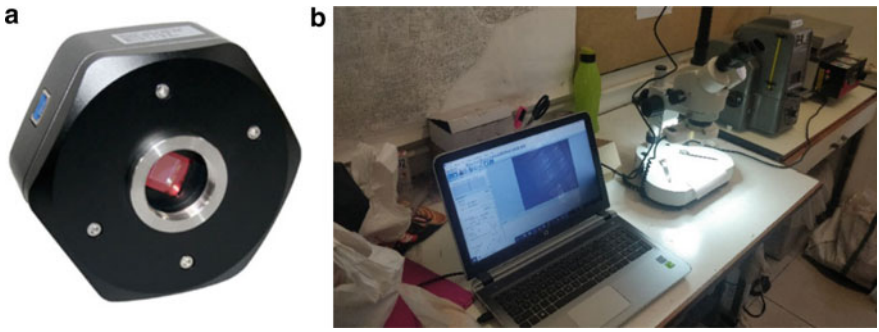

Fig. 4 **a** Microscope camera. **b** Setup of stereo microscope

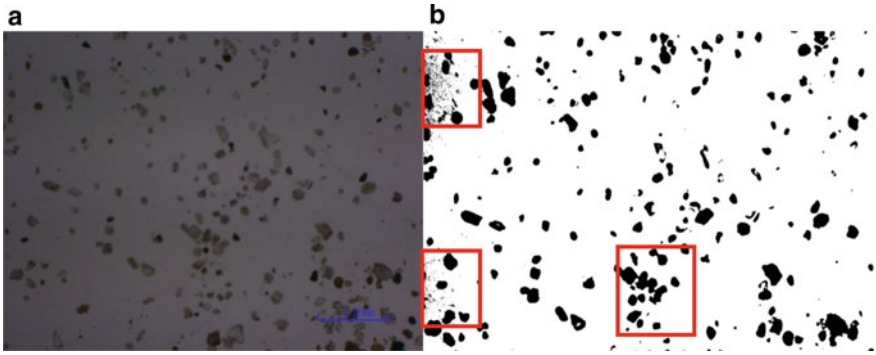

Fig. 5 **a** Image of Natural Sand acquired from microscope. **b** DIP image of the acquired image

cracks, and the actual aggregate particles. Moreover, manual separation of particles was difficult which resulted into clustered output which would output inaccurate reading. Therefore, the method was not adopted further. Figure 4 shows the setup of microscope, connected with Procam microscopic camera of 20 MP mounted over stereo microscope of Radical make (Fig. 5).

3.1.2 Workability of Mortar

The modified flow table test is performed to check the operating range, that is from harsh mix to flowable mix as shown in Fig. 6. Harsh mix is classified as the concrete mix in a fresh state which deforms or cracks on application of static or dynamic stress [55]; the mix resisted to flow on testing it on modified flow table test and generated cracks through the matrix on testing. To cover the spectrum of quantifying workability of harsh mix, geotechnical vane shear apparatus in accordance with IS:2720 (Part-30) laboratory vane shear test was used as illustrated in Fig. 7. Workability of harsh mixes can be defined as a two-point function of shear stress and strain. Higher the

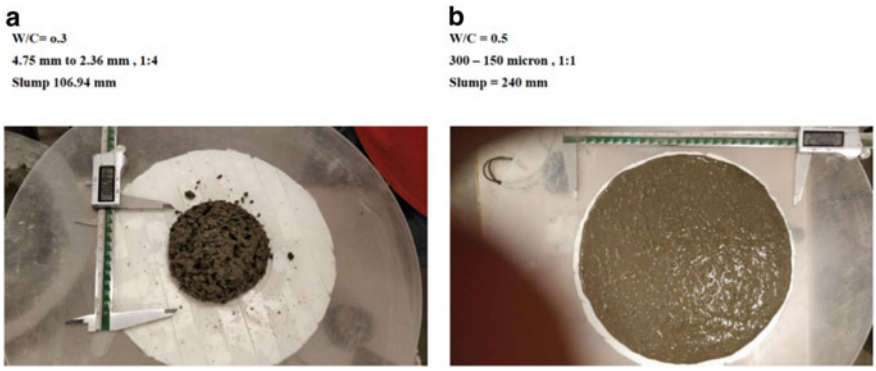

Fig. 6 Pilot-study—Flowability check. **a** Harsh mix. **b** Flowable mix

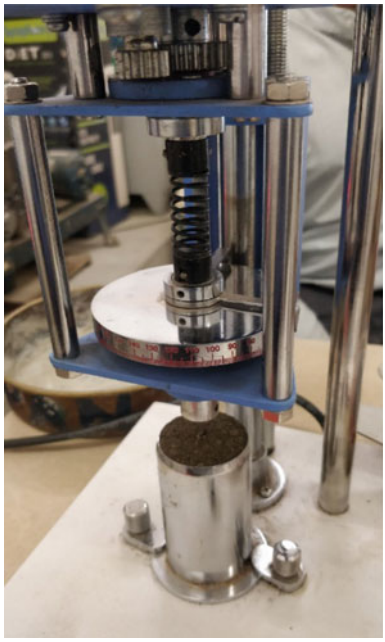

Fig. 7 Pilot study—Vane shear test for harsh mix

torque exerted to rotate the vane blades in the mix, harsher is the mix [54, 56]. It was observed that because of slow rotational speed of the vane shear apparatus the results obtained was inaccurate because of the stiffening effect in the cement mortar. Therefore, a single point mini flow table test was used to check the workability of cement mortar.

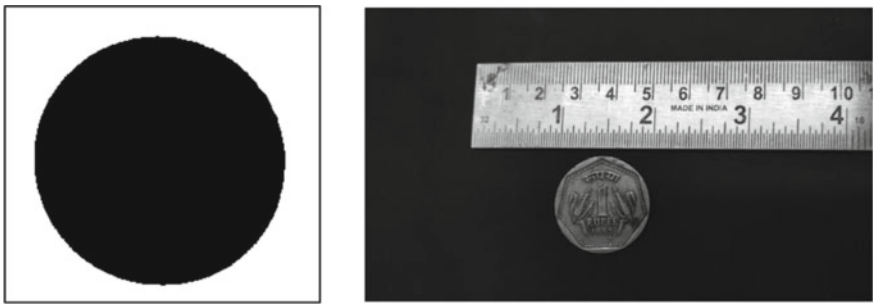

Fig. 8 Calibration of DIP setup using a uniform object

3.2 Experimental Program

3.2.1 Digital Image Processing Calibration

The DIP setup consists of a digital single-lens reflex (DSLR) camera, model no D5500, Nikon make equipped with a 35 mm lens was mounted over a tripod. The surface on which the aggregates samples were placed, were approximately 70 mm away from the camera lens, so that the device can focus on the samples clearly. For calibration, a uniform object like a coin is used for DIP as shown in Fig. 8. The error was $\pm 0.02\%$ and was obtained by comparing dimensions obtained digitally and manually with the help of Vernier calipers.

The river sand samples had lighter shades and less dark particles, they were kept above black paper which was painted with two coats of generic black spray paint, while the quarry sand samples were kept over the white background like A4 size 75 GSM printing paper. This enables the software to differentiate the sample from background efficiently and incurring less error.

3.2.2 Digital Image Processing

Every fine aggregate specimen of a different sieve class was clustered in a group of 100 and was placed in a grid pattern on the tray right below the camera's viewfinder near a metric scale for scaling of image. The captured image was then subjected to image correction; image was first converted to an 8-bit color toned image type thereafter; image threshold was calibrated in a way to minimize the background noise. The background noise was then removed by removing outliers. The edges of the image were corrected by eroding and dilating the edges of the particles. Afterwards, the conversion shape parameters were extracted out from the image. Figure 10 shows the actual image conversion to a 2 bit image over which the software run particle analysis (Fig. 9).

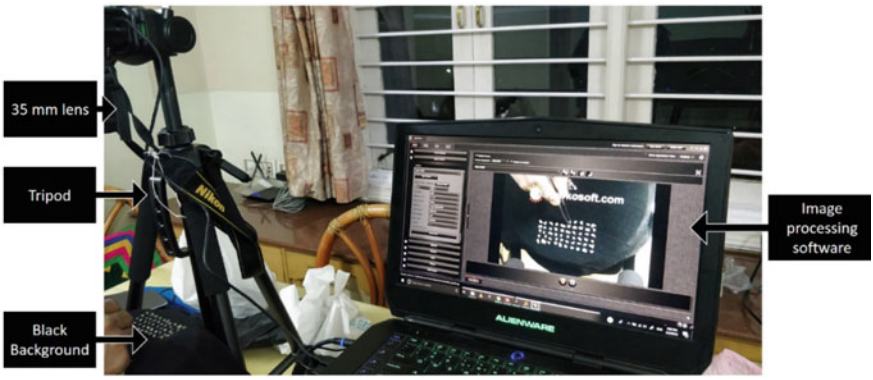

Fig. 9 Particle arrangement and image capturing process

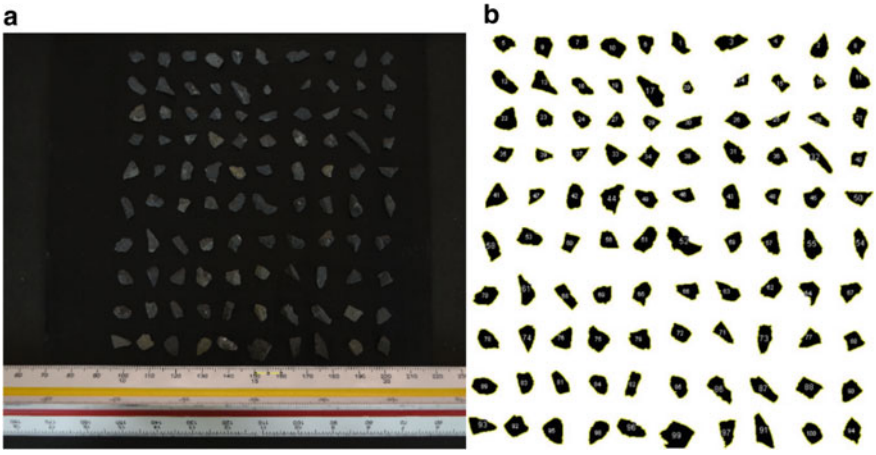

Fig. 10 **a** Captured image. **b** Final image for shape analysis

3.3 Workability of Mortar

The cement and aggregate samples were pre-packed in calculated proportion in a zip lock bags, then labeled with the mix proportion details, water cement ratio, aggregate type/zone of sand, and type of aggregates as shown in Fig. 11. The samples were then dry mixed in the digital Hobart mixing machine for 30 s. The required quantity of water was then added and mixed at low speed for 30 s and high speed for 2.5 min. The sample was then placed in mini flow table mould in two layers each compacted by providing 25 strokes using rubber tamping rod. The mold was then removed, and the table was allowed to drop 15 times from 25 mm height in a 2 s interval. The flow spread in millimeters was recorded using a digital Vernier caliper on pre-marked chord lines (Fig. 12 and Table 6).

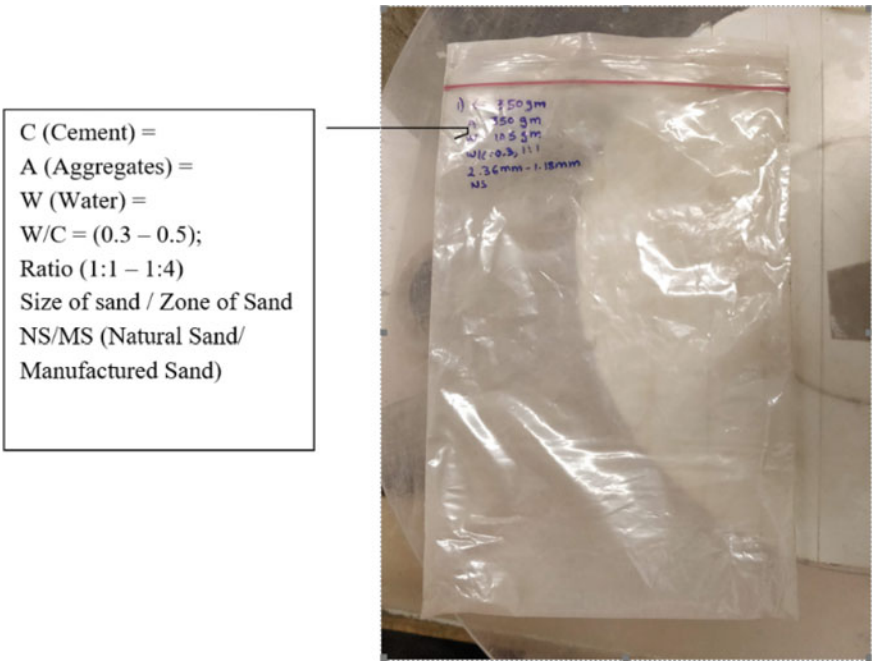

Fig. 11 Nomenclature for pre-packed bags

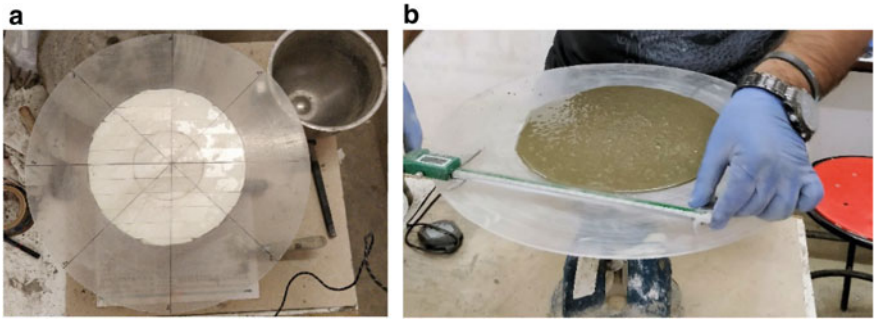

Fig. 12 **a** Flow Measurement mark. **b** Measurement of flow using Vernier calipers

Table 6 Batching details

Total sample weight = 600 g per batch		
Mix ratio	Cement (g)	Sand (g)
1:1	300	300
1:2	200	400
1:3	150	450
1:4	120	480

Table 7 Natural sand flow trend for different sieve class

Natural Sand Flow Trend (mm)															
W/C	0.3			0.35			0.4			0.45			0.5		
C:S	1:1	1:2	1:3	1:1	1:2	1:3	1:1	1:2	1:3	1:1	1:2	1:3	1:1	1:2	1:3
S1	100.61	0.00	0.00	115.48	0.00	0.00	145.73	101.22	0.00	199.15	106.85	0.00	230.49	115.21	0.00
S2	121.43	0.00	0.00	169.96	100.77	0.00	213.52	125.69	101.74	255.20	160.73	103.81	263.43	197.24	110.98
S3	110.39	0.00	0.00	166.78	100.35	0.00	207.97	107.00	0.00	245.99	118.75	0.00	254.54	184.69	0.00
S4	109.16	0.00	0.00	122.43	0.00	0.00	199.93	105.18	0.00	250.06	106.42	0.00	261.89	139.39	0.00
S5	100.43	0.00	0.00	100.55	0.00	0.00	115.74	0.00	0.00	142.96	100.62	0.00	155.88	103.44	0.00

3.4 Data Collection and Analysis

3.4.1 Shape Parameters of Aggregates Obtained from Digital Image Processing

There were 4–5% of aggregates particles whose mean dimension in X and Y direction was larger than the sieve size through which the particle passes. Hence, sieve analysis is not an accurate method for determining the mean particle size. Particles of S3, shows relatively higher voids as compared to other fractions in loose and compacted state as shown in Fig. 13.

Considering the given data, from Figs. 2 and 3, manufactured sand has a sub-angular and sub-rounded shape for the particles whose size lies between 4.75 mm and 600 μm. The aggregates whose size was smaller than 600 μm fall under the category of rounded aggregates. While Natural Sand is rounded or well rounded, Quarry sand possesses higher angularity as compared to Quarry sand, and natural aggregates are highly circular as compared to manufactured sand (Figs. 16 and 17).

A linear regression analysis is carried out and R^2 value is obtained to find best fit. To find out correlation between the shape parameters and void ratio, the regression analysis is performed. In case of natural sand, stronger relationship of various shape parameters and void ratio is observed, compared to manufactured sand as depicted in Figs. 18, 19, 20 and 21.

Sieve class having high angularity and aspect ratio, low packing efficiency is observed. Here natural sand shows better packing efficiency, resulting to relatively less voids as compared to manufactured sand. Aggregates which has high aspect

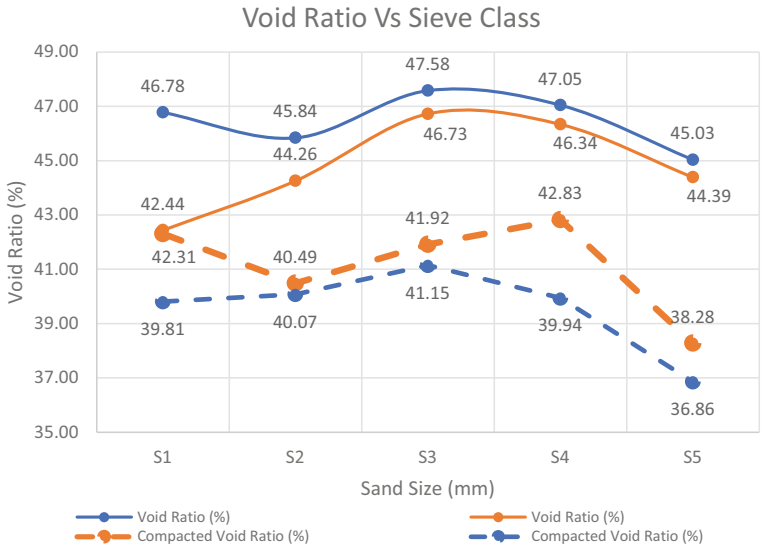

Fig. 13 Void ratio versus sieve class

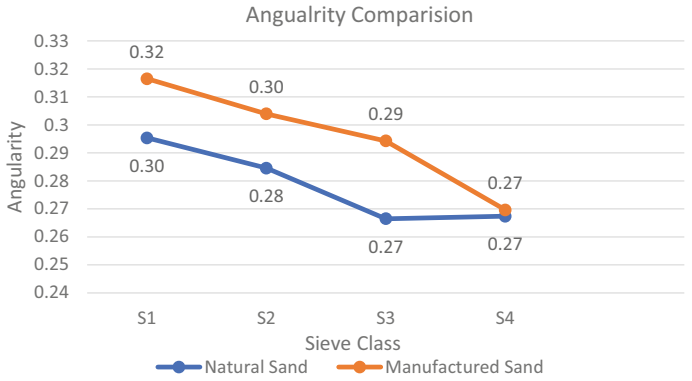

Fig. 14 Angularity versus sieve class

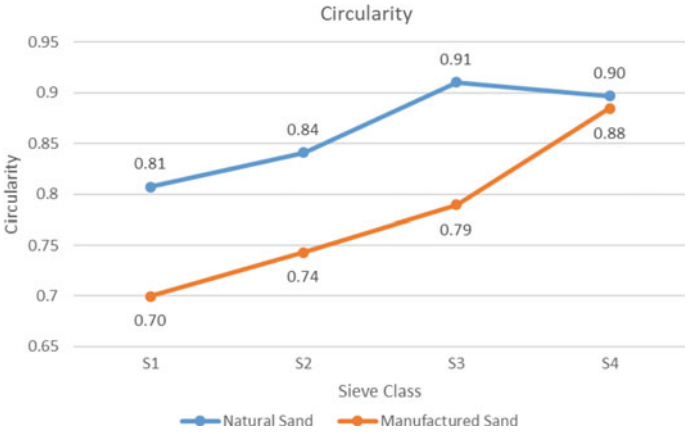

Fig. 15 Circularity versus sieve class

ratio i.e. major axis is relatively larger than minor axis and high angularity, such samples when stacked upon other similar aggregates particles forms pocket in between resulting it to have high void ratio. From Figs. 18 and 21 depicts void ratio decreases as the angularity number and aspect ratio decreases. However, from Fig. 13 it is observed that on compaction, the packing efficiency increases in case of manufactured sand as compared to natural sand. Figures 14 and 15 depicts that as the circularity number and roundness of the aggregate particles increase the void ratio increases.

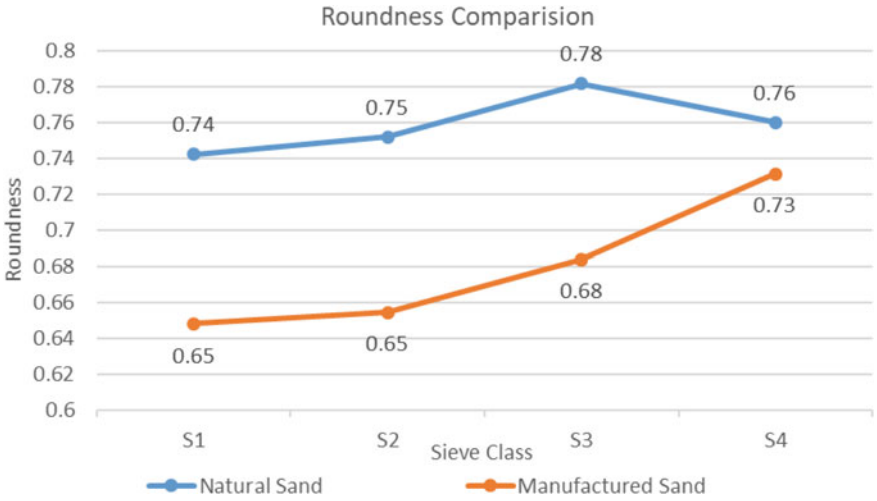

Fig. 16 Roundness versus sieve class

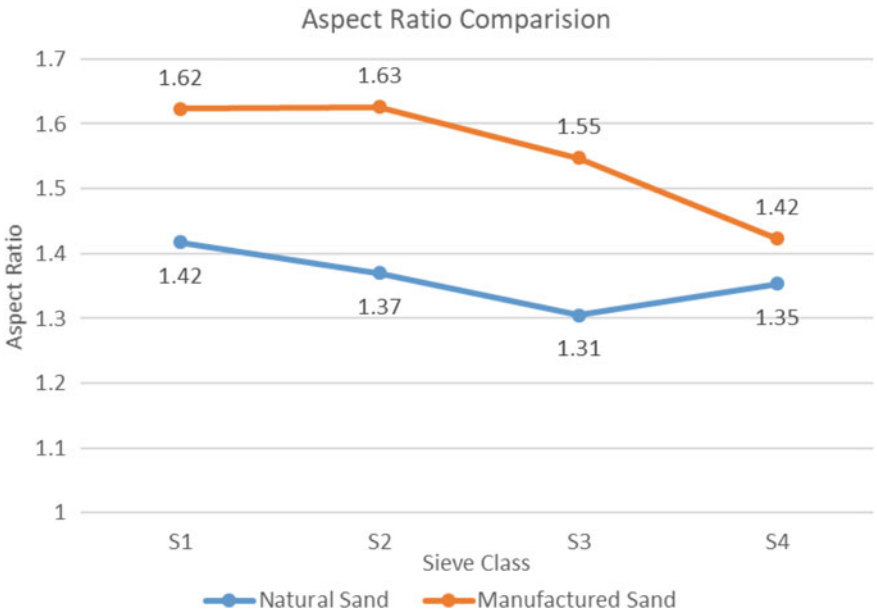

Fig. 17 Aspect ratio versus sieve class

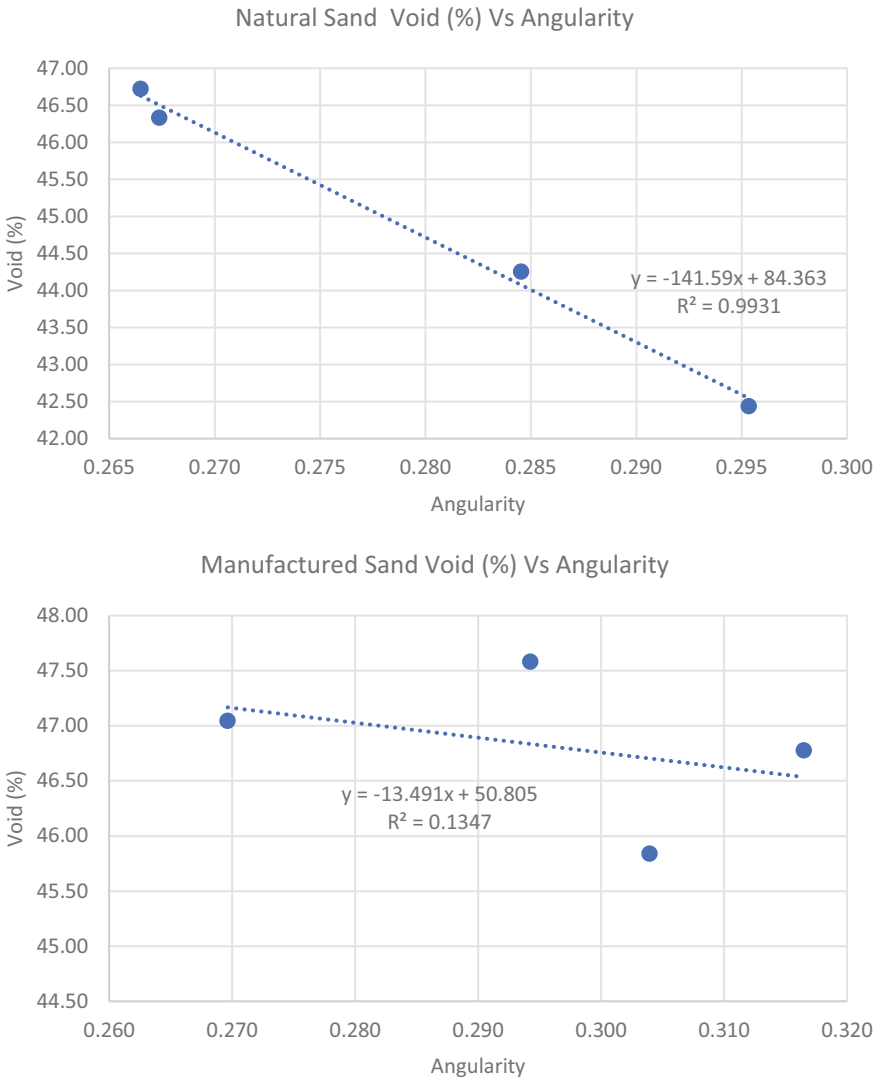

Fig. 18 Regression analysis of angularity for MS and RS

3.4.2 Workability of Cement Mortar

A total of 168 out of 380 samples were tested with the modified flow table test, and the remaining samples resulted to be harsh mixes. Following observations were made from the obtained results:

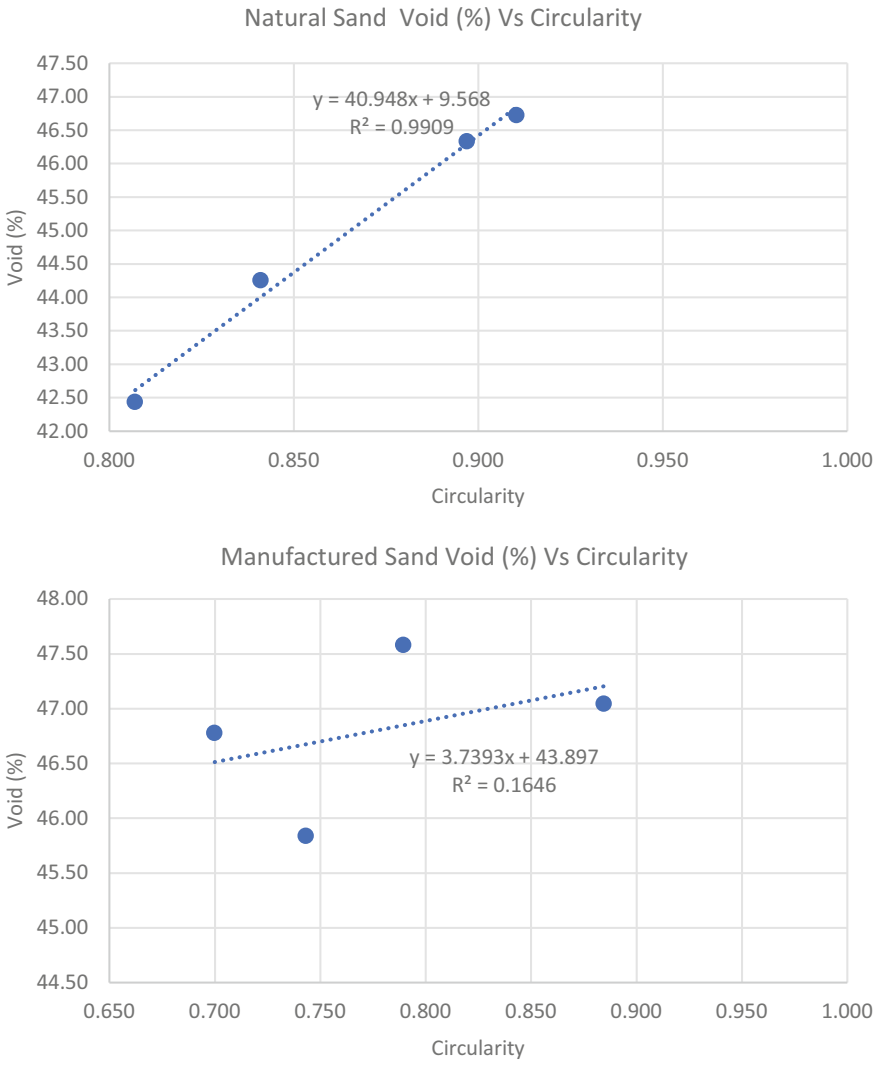

Fig. 19 Regression Analysis of Circularity for MS and RS

1. For the sieve class, natural sand shows lower workability compared to manufactured sand despite having relatively higher degree of roundness, low angularity index, and high spherical shape.
2. Visually it has been observed that, the cement mortar exhibits low workability, if the voids are not filled with adequate amount of cement paste.
3. The flowability of all in aggregates is higher than the flowability of mortar made from sieve class having similar water cement ratio and similar proportion.

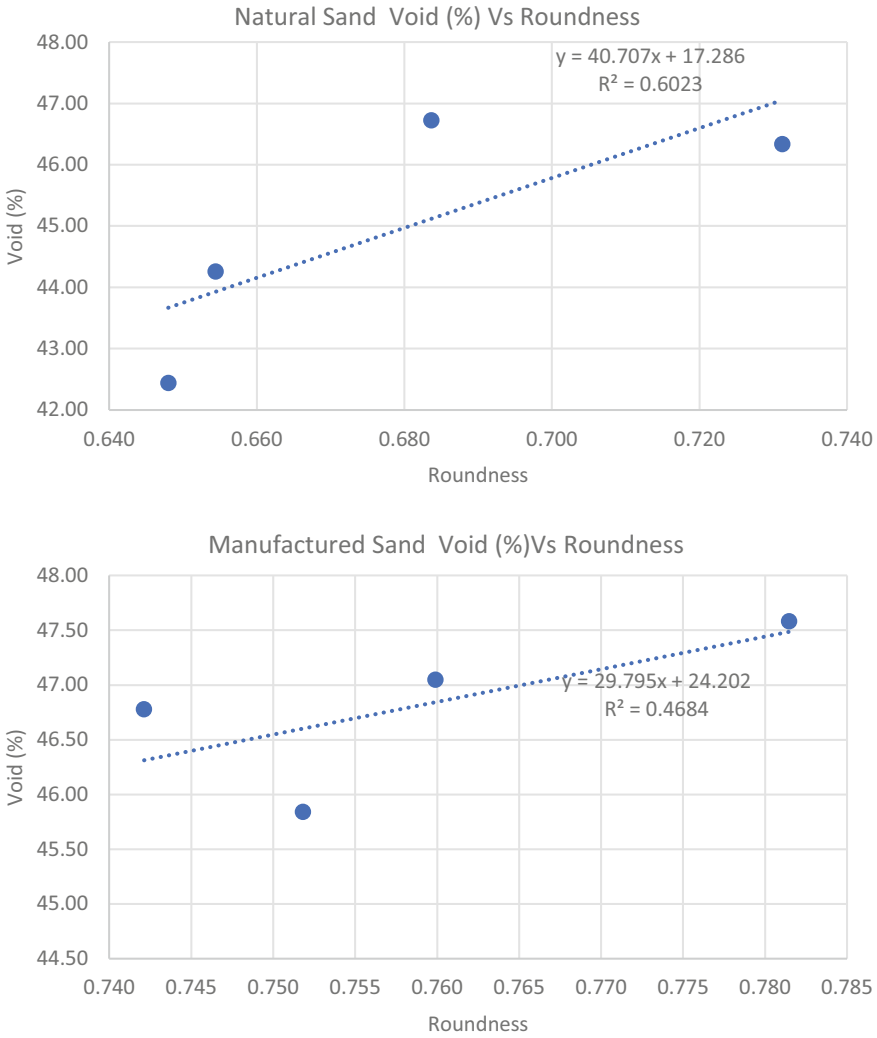

Fig. 20 Regression analysis of roundness for MS and RS

3.4.3 Results for Modified Flow Table Test

Figure 22 shows average flow diameter versus different sieve class for Natural and Manufactured sand. Tables 7 and 8 represent test results for different sieve class of natural and manufactured sand.

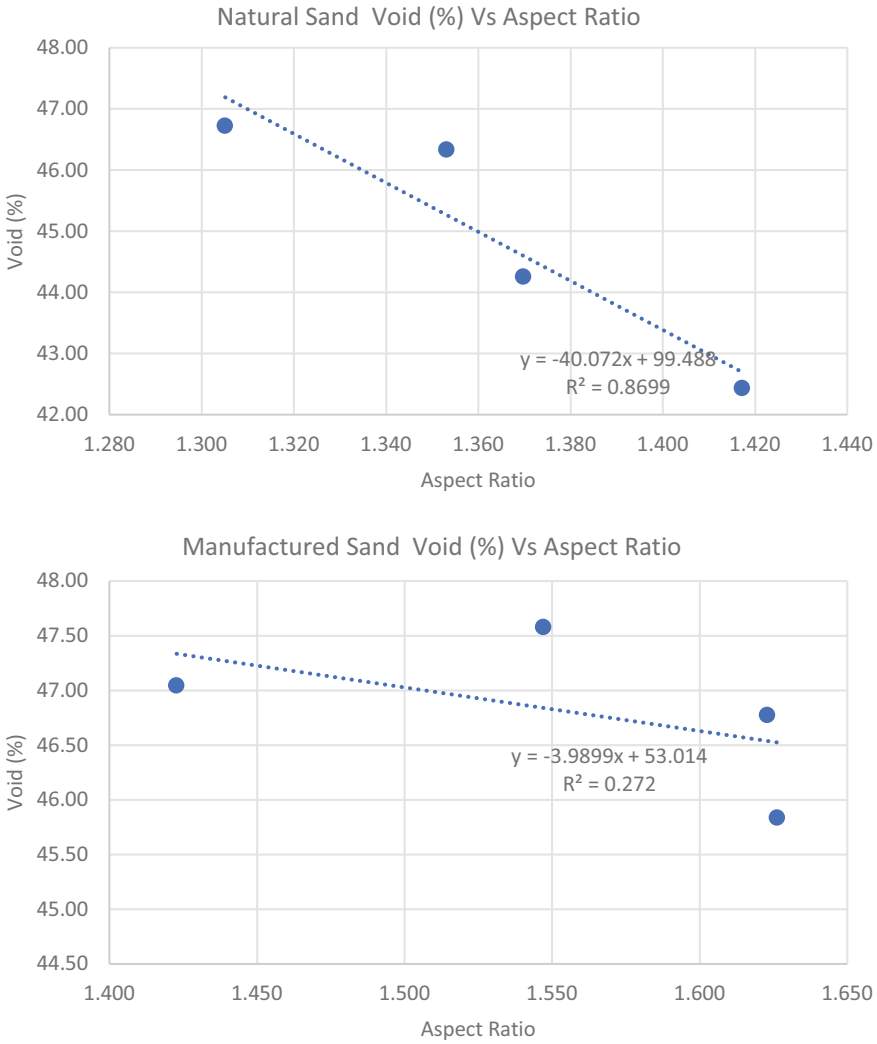

Fig. 21 Regression analysis of aspect ratio for MS and RS

3.4.4 Natural Sand and Manufactured Sand Flow Trend for Different Sieve Class

See Fig. 22 and Tables 7 and 8.

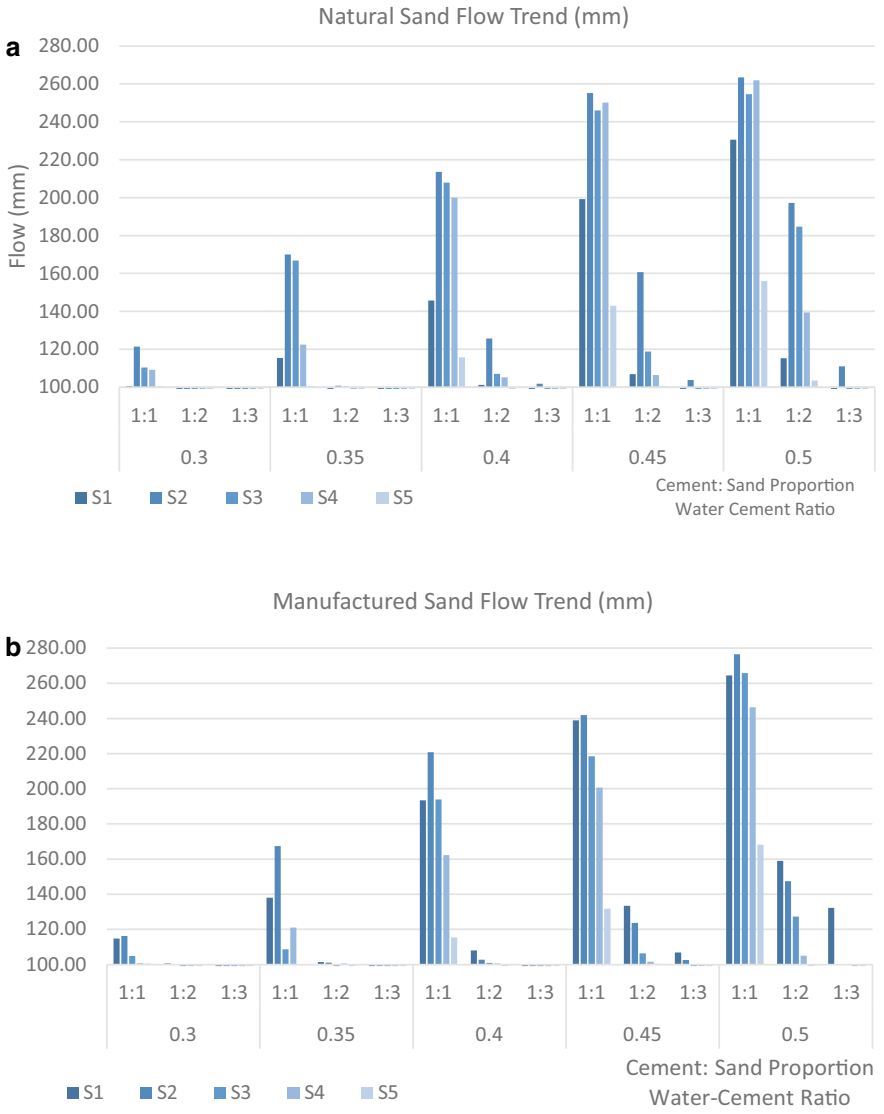

Fig. 22 **a** Natural Sand Flow trend for different sieve class. **b** Manufactured sand flow trend for different sieve class

3.4.5 Natural Sand and Manufactured Sand Flow Trend for Different Zones of Sand

Figure 23 shows average flow diameter versus different zones for Natural and Manufactured sand. Tables 9 and 10 represent test results for different zones of natural and manufactured sand.

Table 8 Manufactured Sand Flow trend for different sieve class

Manufactured Sand Flow Trend (mm)															
W/C	0.3			0.35			0.4			0.45			0.5		
C:S	1:1	1:2	1:3	1:1	1:2	1:3	1:1	1:2	1:3	1:1	1:2	1:3	1:1	1:2	1:3
S1	114.79	100.57	0.00	138.03	101.49	0.00	193.42	108.02	0.00	239.00	133.44	106.94	264.55	158.95	132.20
S2	116.29	100.29	0.00	167.32	101.12	0.00	220.89	102.71	0.00	241.87	123.76	102.54	276.62	147.49	
S3	104.87	0.00	0.00	108.62	0.00	0.00	193.95	100.87	0.00	218.42	106.43	0.00	265.77	127.32	
S4	100.77	0.00	0.00	121.04	100.56	0.00	162.24	100.63	0.00	200.66	101.55	0.00	246.44	104.98	0.00
S5	100.57	0.00	0.00	100.00	0.00	0.00	115.46	0.00	0.00	131.77	100.39	0.00	168.26	0.00	0.00

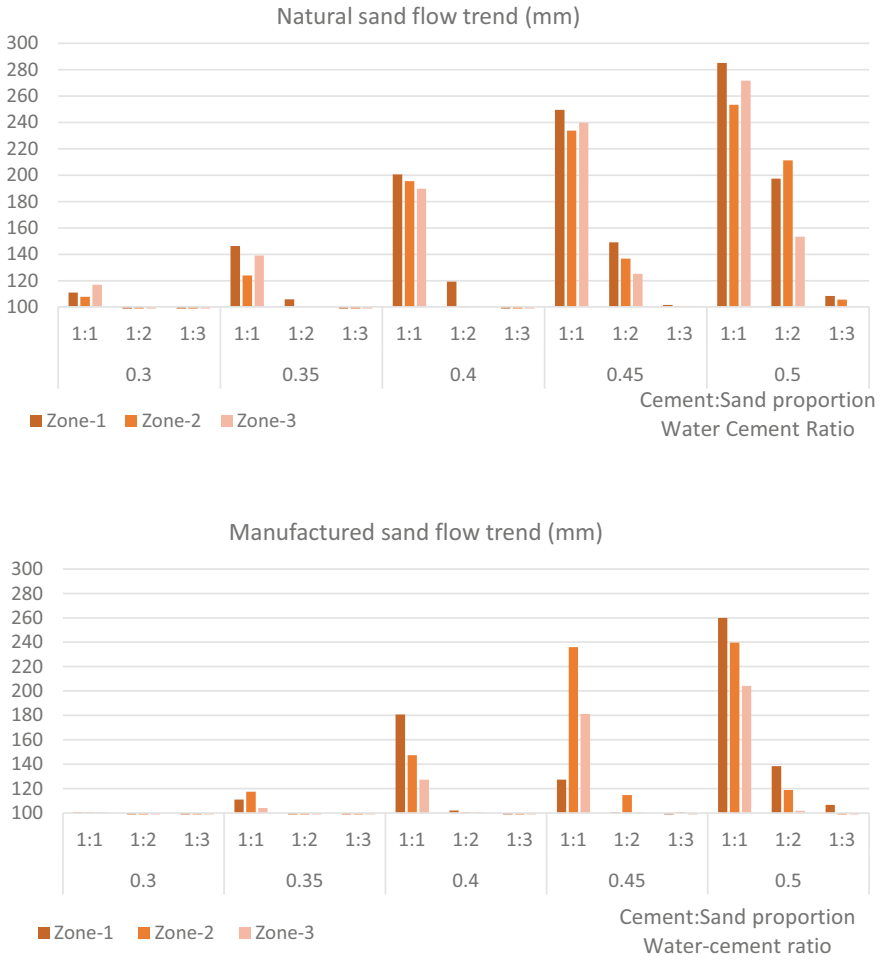

Fig. 23 **a** Natural Sand Flow trend for different zones of sand. **b** Manufactured sand flow trend for different zones of sand

Each sieve class when combined in certain proportions makes certain zone of fine aggregate. The workability of cement mortar, in terms of average flow is directly proportional to the proportion of sieve class in sand sample and weighted average of flow of cement mortar of each sieve class. To obtain the average flow in particular sieve class, the water cement ratio and cement sand ratio should be the same with the cement mortar utilizing the zone sand.

A relation is developed that is used to predict the flow of cement mortar using certain zone. The relation is stated as Eq. 1.

Average flow of cement mortar using zone sand

Table 9 Natural sand flow trend for different zones of sand

Natural sand flow trend for different zones of sand (mm)															
W/C	0.3			0.35			0.4			0.45			0.5		
C:S	1:1	1:2	1:3	1:1	1:2	1:3	1:1	1:2	1:3	1:1	1:2	1:3	1:1	1:2	1:3
Zone-1	110.91	0.00	0.00	146.41	105.82	0.00	200.68	119.35	0.00	249.47	149.00	101.62	285.21	197.39	108.38
Zone-2	107.74	0.00	0.00	123.92	100.59	0.00	195.42	100.68	0.00	233.74	136.78	100.56	253.33	211.15	105.71
Zone-3	116.86	0.00	0.00	139.07	100.36	0.00	189.81	100.68	0.00	239.67	125.30	100.80	271.62	153.31	100.63

Table 10 Manufactured sand flow trend for different zones of sand

Manufactured sand flow trend for different zones of sand (mm)															
W/C	0.3			0.35			0.4			0.45			0.5		
C:S	1:1	1:2	1:3	1:1	1:2	1:3	1:1	1:2	1:3	1:1	1:2	1:3	1:1	1:2	1:3
Zone-1	100.65	0.00	0.00	110.99	0.00	0.00	180.63	101.90	0.00	127.24	100.53	0.00	259.97	138.45	106.65
Zone-2	100.42	0.00	0.00	117.43	0.00	0.00	147.34	100.55	0.00	235.98	114.56	100.58	239.76	118.74	0.00
Zone-3	100.68	0.00	0.00	104.05	0.00	0.00	127.24	100.55	0.00	181.07	100.59	0.00	204.12	101.81	0.00

Table 11 Validation of net average flow using developed equation

Sieve class	Sieve size	Average flow (mm)	Percentage (%)	Average flow * percentage	Net average flow (mm)
S1	4.75–2.36 mm	115.48	5.00	5.77	123.59
S2	2.36–1.18 mm	169.96	8.5.00	14.45	
S3	1.18 mm–600 μm	166.78	16.00	26.68	
S4	600–300 μm	122.43	26.50	32.44	
S5	300–150 μm	100.55	44.00	44.24	

Table 12 Variation in predicted and actual flow for Zone-2 natural sand

Zone of sand	W/C ratio	Ratio	Actual average flow (mm)	Predicted average flow (mm)	Variation in %
Zone -2	0.35	1:1	123.92	123.59	0.27

$$= \frac{\sum_{i=1}^{n} (Proportion\ of\ sieve\ class\ in\ sand\ (\%) * Average\ \ flow\ in\ mm\ of\ sieve\ class\ \left(\frac{W}{C}, \frac{C}{S}\right)}{\sum Proportion\ of\ sieve\ class\ in\ sand} \tag{1}$$

where i = sieve class number.

The validation of developed equation is carried out using natural sand of Zone-2, W/C = 0.35 and C/S = 1:1.

Table 11 shows the sieve class, sieve size, average flow in mm which is taken from Table 7. It also has percentage weight taken from Table 3. The weighted average is calculated as per Table 11, to find the net average flow for artificially zone-2 natural sand.

Variation in predicted and actual flow of artificial zone-2 natural sand is summarized in Table 12. It has been observed that the variation in predicted and actual average flow is 0.27%. Therefore, developed relationship is validated.

Figure 24 Contribution to flow by each sieve class illustrates the contribution to the flow by each sieve class. Relationship has been checked for other results; the variation between actual and predicted average flow lies between 0 and 20%.

4 Conclusion

Some major findings which were observed during the testing and observation which came from results can be summarized as under.

1. Shape factors like angularity, roundness and circularity of aggregates, started to show similar characteristics as the particles get finer.
2. The natural sand gives higher roundness value than the Crushed aggregate.

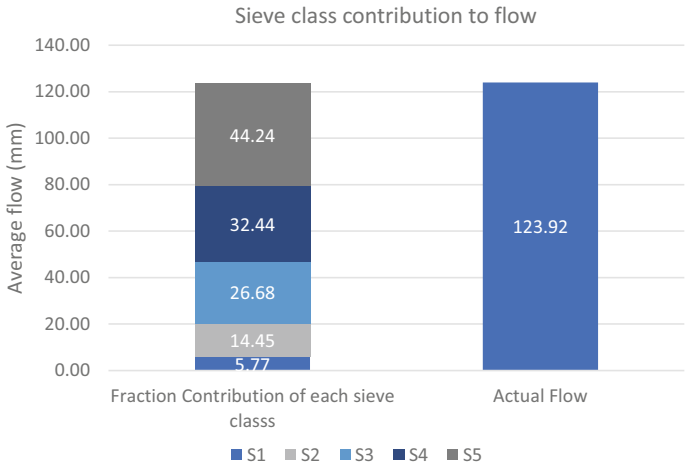

Fig. 24 Contribution to flow by each sieve class

3. Angularity is not the prime factor which can be used to determine the void ratio of the sand. Parameters like angularity, circularity, roundness and aspect ratio are also the variables for the function for determining void ratio in the sand sample.
4. A relationship is developed whose validation with the obtained data is shown with a variation margin of ±20% hence this relationship holds true.
   The net flow of sand of certain zone can be determined with Eq. 1.
   $$\frac{\sum_{i=1}^{n} Proportion\ of\ sieve\ class\ in\ sand\ (\%) * Average\ flow\ in\ mm\ of\ sieve\ class\ \left(\frac{W}{C}, \frac{C}{S}\right)}{\sum Proportion\ of\ sieve\ class\ \text{in sand}}$$
   Though the individual performance of each sieve class in natural sand mortar exhibited low workability than that of manufactured sand, natural sand exhibited higher degree of workability when the aggregates from each sieve class were combined.
5. DIP method is fast and accurate to determine the not only the size of aggregate but also various shape characteristic of the same.

Acknowledgements The material used in the tests were provided by **Contech Chemicals Pvt. Ltd**. The present work was carried out at CEPT Material Testing lab. The authors would like to thank Mr. Jagdish, Mr. Bikas Das and Ms. Rinkal Prajapati for providing support during testing and material handling in the lab. The authors are also grateful to Ms. Siddhee Kasudia for her generous help in editing and proof checking.

References

1. Pandya MD, Arora NK, Thaker P (2012) State of art paper: investigation of workability of cement paste, cement Mortar and concrete. Int J Adv Eng Res Stud II(I):16–23. E-ISSN 2249-8974
2. Ahn N, Fowler DW (2000) An experimental study on the guidelines for using higher contents of aggregate microfines in Portland cement concrete. Int Cent Aggregates Res, 435
3. Kotak S, Thaker P (2016) Assessment of water film thickness, Paste film thickness and the fresh properties of cement mortar. Int J Sci Technol Eng 2(12):407–412
4. Vohra C, Thaker P (2019) Optimization of cement mortar mix using digital image analysis: state of Art. GRD J (February), 198–203
5. Harini M, Shaalini G, Dhinakaran G (2011) Effect of size and type of fine aggregates on flowability of mortar. KSCE J Civ Eng 16(1):163–168
6. Nilsen UA, Monterio PJ (1993) Concrete: a three phase material, pp 147–151
7. Kar A, Ray I, Unnikrishnan A, Davalos JF (2013) Composite modeling to predict shrinkage of concretes containing supplementary cementitious materials from paste volumes. Constr Build Mater 43(April):139–155
8. Sathyan D, Balakrishnan AK, Mohandas SM (2018) Temperature influence on rheology of superplasticized pozzolana cement and modeling using RKS algorithm. J Mater Civ Eng 30(9):04018221
9. Popovics S (1980) Calculation of the water requirement of mortar and concrete. Matériaux Constr 13(5):343–352
10. Fabro F, Gava GP, Grigoli HB, Meneghetti LC (2011) Influence of fine aggregates particle shape in the concrete properties, vol 4, no 2, pp 191–201
11. Polat R, Yadollahi MM, Sagsoz AE, Arasan S (2013) The correlation between aggregate shape and compressive Strength of concrete: digital image processing approach. Int J Struct Civ Eng Res.ijscer.com 2(3):2319–6009
12. Jamkar SS, Rao CBK (2004) Index of aggregate particle shape and texture of coarse aggregate as a parameter for concrete mix proportioning. Cem Concr Res 34(11):2021–2027
13. Das A (2005) A revisit to aggregate shape parameters. Most, pp 1–5
14. Cavarretta I, Coop M, O'Sullivan C (2010) The influence of particle characteristics on the engineering behaviour of granular materials. Geotechnique 60(6):413–423
15. Aïssoun BM, Hwang SD, Khayat KH (2016) Influence of aggregate characteristics on workability of superworkable concrete. Mater Struct Constr 49(1–2):597–609
16. Quiroga PW, Fowler DW (2004) The effects of aggregates characteristics on the performance of Portland cement concrete the effects of aggregates characteristics on the performance of Portland cement concrete 6. Performing Organization Code
17. Al-rousan T, Masad E, Tutumluer E (2007) Evaluation of image analysis techniques for quantifying aggregate shape characteristics. Constr Build Mater 21:978–990. www.elsevier.com/locate/conbuildmat
18. Thaker P, Arora N (2019) Measurement of aggregate size and shape using image analysis. Lect Notes Civ Eng 46:739–747
19. Kwan AKH, Wong HHC (2008) Packing density of cementitious materials: Part 2-packing and flow of OPC + PFA + CSF. Mater Struct Constr 41(4):773–784
20. McCave IN, Syvitski JPM (1991) Principles and methods of geological particle size analysis. Princ Methods Appl Part Size Anal, 3–21
21. Polat R, Mohabbi Yadollahi M, Emre Sagsoz A, Arasan S (2013) The correlation between aggregate shape and compressive strength of concrete: digital image processing approach
22. Vangla P, Roy N, Mendu K, Latha GM (2015) Digital image analysis for the determination of size and shape parameters of sand grains. In: Golden Jubilee conference of the IGS Bangalore, Geo Innovations, 2014, no August 2015, pp 30–31
23. Rivas JA (2005) Three-dimensional digital image processing and reconstruction of granular particles

24. Li J, Zhang J, Qian G, Zheng J, Zhang Y (2019) Three-dimensional simulation of aggregate and asphalt mixture using parameterized shape and size gradation. J Mater Civ Eng 31(3):04019004
25. Lucas Júnior JLO, Babadopulos LFAL, Soares JB (2010) Aggregate–binder adhesiveness assessment and investigation of the influence of morphological and physico-chemical properties of mineral aggregates. Road Mater Pavement Des 0629:1–16
26. Faulkner GD (1911) Adhesive Strength of cement mortar. University of Illinois
27. Fang M, Park D, Singuranayo JL, Chen H, Li Y (2019) Aggregate gradation theory, design and its impact on asphalt pavement performance: a review. Int J Pavement Eng 20(12):1408–1424
28. Wu J, Wang L, Hou Y, Xiong H, Lu Y, Zhang L (2018) A digital image analysis of gravel aggregate using CT scanning technique. Int J Pavement Res Technol 11(2):160–167
29. Anochie-boateng JK, Africa S, Maina J (2015) Determination of aggregate morphological properties using laser and their effects on rutting of asphalt mixes, September
30. Balter S (1999) Digital image processing an algorithmic approach using MATLAB, vol 46, no 4
31. Kwan AKH, Mora CF, Chan HC (1999) Particle shape analysis of coarse aggregate using digital image processing. Cem Concr Res
32. Kumara GHAJJ, Hayano K, Ogiwara K (2012) Image analysis techniques on evaluation of particle size distribution of gravel. Int J GEOMATE 3:290–297
33. Thaker P, Arora NK (2015) Critical review of aggregate shape characteristic assessment techniques. In: UKIERI concrete congress—concrete research driving profit and sustainability, pp 1041–1054
34. Allen T (2003) Particle size analysis by image analysis. Powder Sampl Part Size Determ, no November, pp 142–207
35. Zhou B, Wang J, Wang H (2017) Three-dimensional sphericity, roundness and fractal dimension of sand particles. Géotechnique, 1–13
36. Kumara JJ, Hayano K, Kikuchi Y (2017) Evaluation of area- and volume-based gradations of sand-crushed stone mixture by 2D images. KSCE J Civ Eng 21(3):774–781
37. Erdoğan S (2016) Determination of aggregate shape properties using X-ray tomographic methods and the effect of shape on concrete rheology, no. October
38. Barksdale RD, Kemp MA, Sheffield WJ, Hubbard JL (1991) Measurement of aggregate shape, surface area, and roughness. Transp Res Rec 1301:107–116
39. Kwan AKH, Mora CF, Chan HC (1999) Particle shape analysis of coarse aggregate using digital image processing. Cem Concr Res 29(9):1403–1410
40. Thaker PK (2018) Estimation of superplasticizer dosage to achieve desired workability of cement mortar. Ph.D. Thesis, no September
41. ASTM D3398 (2006) Standard test method for index of aggregate particle shape and texture, vol 00, no. Reapproved 2006, pp 1–4
42. Li LG, Kwan AKH (2011) Mortar design based on water film thickness. Constr Build Mater 25(5):2381–2390
43. Panda RP, Das SS, Sahoo PK (2016) An empirical method for estimating surface area of aggregates in hot mix asphalt. J Traffic Transp Eng (English Ed) 3(2):127–136
44. Bouvet A, Ghorbel E, Bennacer R (2010) The mini-conical slump flow test: analysis and numerical study. Cem Concr Res 40(10):1517–1523
45. Kwan AKH, Fung WWS (2009) Packing density measurement and modelling of fine aggregate and mortar. Cem Concr Compos 31(6):349–357
46. Kwan AKH, Li LG (2012) Combined effects of water film thickness and paste film thickness on rheology of mortar. Mater Struct Constr 45(9):1359–1374
47. Rodriguez T, Johansson JM, Edeskär JMA (2008) Particle shape determination by two-dimensional image analysis in geotechnical engineering. In: Site investigation and laboratory testing, no. Eurocode 7, pp 1–12
48. I. Standard (2015) Ordinary Portland cement, 53—specification. BIS, no 2015
49. IS 4031-Part6 (1988) Methods of physical tests for hydraulic cement. Bur Indian Stand 4031
50. For S, Cabinets RD (2004) Indian Standard, vol 1979, no Reaffirmed 2001

51. Bureau of Indian Standards (2016) IS 2386 (Part III) Methods of test for aggregates for concrete specific gravity, density, voids, absorption and bulking. Indian Stand 2386(Part, no October 1963):1–19
52. IS:383 (1970) Specification for coarse and fine aggregates from natural sources for concrete. Bur Indian Stand Delhi, pp 1–24
53. Abd Elaty MA, Ghazy MF (2012) Flow properties of fresh concrete by using modified geotechnical Vane shear test. HBRC J 8(3):159–169
54. Bauer E, de Sousa JG, Guimarães EA, Silva FG (2007) Study of the laboratory Vane test on mortars. Build Environ 42(1), 86–92
55. Neville AM, Properties of concrete by A M Neville.pdf, Third Edition
56. For S, Cabinets RD (2004) Methods of test for soils- Part 30 Laboratory Vane Shear Test. BIS 1979(Reaffirmed 2001)

A Comparative Investigation on the Utilization of Marble Dust and Granite Dust in the Cement Mortar Against the Sulphate Resistance

PL. Meyyappan and M. Jemimah Carmichael

Abstract In our country, the marble and granite stone processing is one of the most flourishing industries, in which around 25% of the original stone mass is left out in the form of dust during the cutting and polishing process. Both of these dusts are settled down by sedimentation and then directly disposed as waste materials which will create a serious threat to an environment. This paper highlights the effective utilization of these waste materials in the concrete production, since their composition is most favourable for the replacement of cementitious materials. In this paper, the both waste materials are utilized individually as a replacement for cement in the varying proportions ranging from 0 to 30% to study the sulphate resistance property. For this study, the mortar cube specimens of 70 mm × 70 mm × 70 mm are prepared and immersed in $MgSO_4$ and Na_2SO_4 solution for a period of 28 days. With the detrimental factor of the compressive strength, the optimum replacement of these waste materials on the cement content is arrived individually and the results are compared among each other.

Keywords Cement mortar · Granite dust · Marble dust · Compressive strength

1 Introduction

Marble and granite has been widely used as a building material in the construction industry [1, 2]. During the process of mining, sawing and polishing marble dust and granite dust is observed as a waste material and this is not properly disposed to a safe zone. These waste residual deposits results in serious environmental degradation which poses treat to the human and animal beings. This will also affects the fertility of the agricultural land, if it is dumped in a improper manner [2, 3]. The reuse or

PL. Meyyappan (✉)
Kalasalingam Academy of Research and Education, Krishnankoil, India
e-mail: meyyappan@klu.ac.in

M. J. Carmichael
Vignan's LARA Institute of Technology & Science, Guntur, India

© Springer Nature Switzerland AG 2021

K. Dasgupta et al. (eds.), *Proceedings of SECON 2020*,
Lecture Notes in Civil Engineering 97,
https://doi.org/10.1007/978-3-030-55115-5_48

utilization of these materials can be effectively used as useful alterative materials in construction sector as investigated by many researchers in the past [4–8]. This utilization concept will bring down the cost of cement based products and there by the cost of the entire building components becomes much economical in a financial point of view. Also in environmental side, it is yielding some handsome reliefs in terms of disposing directly into the field [10, 11, 14]. In the various past researches indicating that these utilization improves the mechanical and physical properties in the cement mortar. But in durability point of view needs more valid judgements in accepting these waste materials can be effective replacement materials. Here, an attempt is made to investigate the replacement of cement by marble and granite dust in various proportions such as 0%, 5%, 10%, 15%, 20%, 25% and 30% against the sulphate resistance attack. In order to study the sulphate resistance property for these replacement materials, the cube specimens are casted and allowed to cure under sulphate solutions. This comparative study of replacement of marble dust and granite dust is made against sulphate resistance.

2 Materials Used

(i) ***Cement***

43 Grade Ordinary Portland Cement (OPC) confirms to Indian Standard specification, IS. 8112 code is used in this experimental work. For the entire work, it is assured that the cement is used only from the single point of source.

(ii) ***Marble dust***

The waste marble dust is collected near by the Madurai source during the cutting and dressing process of marble stone. The specific gravity of this marble powder is found to be 2.658.

(iii) ***Granite dust***

The waste granite dust is collected near by the Madurai source during the cutting and dressing process of granite stone. The specific gravity of this granite powder is found to be 2.573.

(iv) ***Fine aggregate***

Locally available natural river sand with 2.36 mm size is used in this experimental work. This source of sand confirms to the Zone 2 of IS 382-2016 having a specific gravity of 2.619.

(v) ***Water***

Potable drinking water is used for mixing the mortar. It ensured that it is free from alkalis and organic matters.

3 Mix Proportions and Investigations

For preparing cement mortar specimens, the mixing ratio adopted is 1 (cement): 3 (sand). Initially, these mortar preparing materials are accurately weighed and mixed thoroughly in the dry state to attain a homogenous mixing. Then the required amount of water is determined on account of the combined weight of cement and sand is to be added to the dry mortar mix. Ensure proper uniform mixing is done before casting the specimens. The replacement of cement by marble dust and granite dust is in the proportions of 0%, 5%, 10%, 15%, 20%, 25% and 30%. A total number of cube specimens of dimensions 70 mm × 70 mm × 70 mm casted for this experimental study are 117 numbers which is to be tested against compressive strength in various curing methods as per Table 1 w.r.t to marble dust and granite replacements. All the specimens are allowed for the various curing of 28 days as mentioned in Table 1. The specimen to be cured by magnesium sulphate solutions are prepared by dissolving magnesium sulphate hydrate content of 5% weight is dissolved in the water.

The same way sodium sulphate solutions are prepared by using sodium sulphate hydrate content of 5% weight in the water. Both the sulphate solutions were replaced every 15 days in each cycle to get efficient sulphate resistance results. Experimental results against sulphate resistance include reduction in compressive strength loss (i.e.) deteriorated factor have to be found out. The compressive strength of the cube specimen under various curing methods is tested from compression testing machine and the loads were applied until the specimens fail. Deterioration factor is nothing but the reduction of strength loss due to the presence of sulphate to the original strength. It is calculated by formula, Where, CS—Compressive Strength

$$Deterioration\ factor = \left(\frac{(CS)_{Water\ Curing} - (CS)_{Sulphate\ Curing}}{(CS)_{Wate\ Curing}} \right) \times 100$$

Table 1 Specimen details

Description	Water curing	Curing under Sulphate solutions	
		Magnesium sulphate	Sodium sulphate
Control specimen	3	3	3
Marble dust replacement	18	18	18
Granite dust replacement	18	18	18
Total	39	39	39
	117 specimens		

4 Results and Discussions

(i) Mable dust replacement

Figure 1a–c shows the specimen under sulphate curing, water curing and the specimen under sulphate attack. Table 2 shows the experimental test results of compressive strength of the specimens having the replacement percentage of marble dust viz. 0%, 5%, 10%, 15%, 20%, 25% and 30% for cement in the volume fraction under various curing such as water, magnesium sulphate and sodium sulphate. It is observed that, for the control specimen (0% replacement) the compressive strength is found as 19.73 N/mm^2, 16.15 N/mm^2 and 15.42 N/mm^2 respectively for the specimens kept under water curing, magnesium sulphate curing and sodium sulphate curing. In comparing magnesium sulphate curing with water curing, the deterioration rate is

(a) (b)

Fig. 1 **a** Specimens under sulphate curing. **b** Specimen under sulphate attack

Table 2 Experimental test results for marble dust replacement

Percentage of cement replaced by Marble dust (%)	Compressive strength of specimens under			Deterioration factor	
	Water curing (N/mm^2)	Magnesium sulphate (N/mm^2)	Sodium sulphate (N/mm^2)	Magnesium sulphate	Sodium sulphate
0	19.73	16.15	15.42	0.1814	0.2184
5%	20.18	16.93	16.17	0.1611	0.1987
10	23.36	20.05	19.57	0.1417	0.1622
15	21.12	17.61	16.95	0.1662	0.1977
2	16.96	13.38	12.68	0.2111	0.2523
25	11.96	8.92	8.19	0.2542	0.3152
30	7.56	5.38	4.91	0.2884	0.3505

18.14% whereas for sodium sulphate curing, it is found as 21.84%. The compressive strength is getting reduced by around 1.27 times due to the effect of sulphate attack which deteriorating the cement content.

Due to the reduction rate of binding materials, the compressive strength is getting continuously affected when the replacement levels goes beyond 15%. The same trend is followed for the specimens kept on sulphate solution curing. It is observed that deterioration rate is more for sodium sulphate solution than the magnesium sulphate solution. Based on the experimental result it is noticed that, deterioration rate on the compressive strength is 18.14% and 21.84% for the control specimens (without marble dust) cured under magnesium sulphate and sodium sulphate solution respectively. When the replacement of marble dust introduced on the specimen upto 5%, it is found that there is decrease in the deterioration factor in the range of 10–12%. When the replacement levels increased to 10%, the deterioration factor is further reduced to 21% to 25%. It is an evident that marble dust of 10% content is effectively enhancing the sulphate resistivity action. If the replacement levels are increased beyond 10%, the deterioration rate seems to be getting increased. For a replacement level of 30% of marble dust the deterioration rate of compressive strength is around 35% (Figs. 2 and 3).

(ii) **Granite dust replacement**

Table 3 shows the experimental test results of compressive strength of the specimens having the replacement percentage of granite dust viz. 0%, 5%, 10%, 15%, 20%, 25% and 30% for cement in the volume fraction under various curing such as water, magnesium sulphate and sodium sulphate. From the graphical representation as in Fig. 4 shows that there is a gradual increase in the compressive strength from 0 to 10% replacement of granite dust. If the replacement percentage level is going beyond 10%, the compressive strength of the specimens is getting continuous decreasing trend. This phenomenon is seen same against irrespective of different curing. For the initial replacement level (5%) of granite dust, it is observed that there

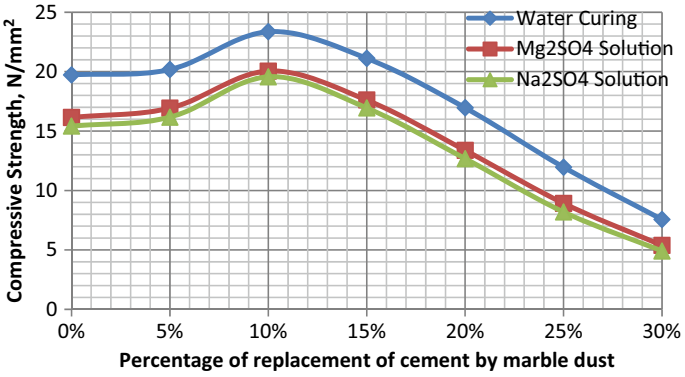

Fig. 2 Graphical representation of marble dust replacement for various curing

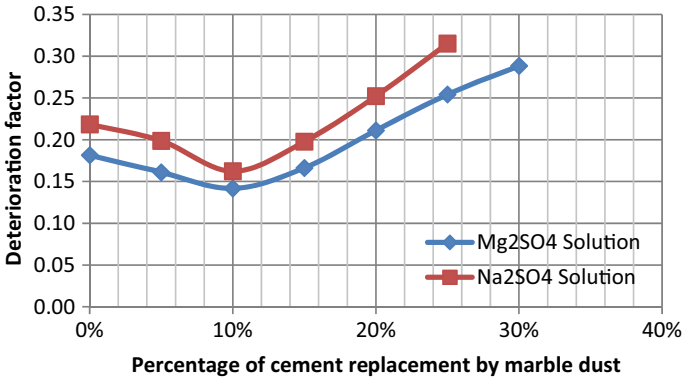

Fig. 3 Graphical representation of deterioration factor under sulphate curing

Table 3 Experimental test results for granite dust replacement

Percentage of cement replaced by Marble dust	Compressive strength of specimens under		Deterioration factor		
	Water curing (N/mm^2)	Magnesium sulphae (N/mm^2)	Sodium sulphate (N/mm^2)	Magnesium sulphate	Sodium sulphate
0%	19.73	16.15	15.42	0.1814	0.2184
5%	20.98	17.7	17.21	0.1563	0.1797
10%	24.6	21.34	20.86	0.1325	0.1520
15%	22.52	19.16	18.64	0.1492	0.1723
20%	18.2	14.63	13.95	0.1962	0.2335
25%	13.45	10.48	9.89	0.2208	0.2647
30%	8.83	6.58	6.03	0.2548	0.3171

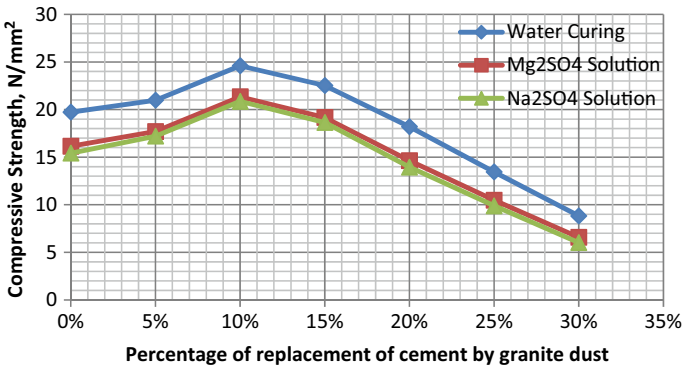

Fig. 4 Graphical representation of granite dust replacement for various curing

is a insignificant increase of around 6% in the compressive strength. But if the replacement is increased from 5 to 10%, the compressive strength is found to be increased by 19.8%, 24.32% and 26.07% for the specimens cured by water, magnesium and sodium sulphate solutions respectively. The compressive strength is found to be a maximum of 24.6 N/mm^2 for the replacement of 10% granite dust due to the arresting of micro pores by the filler elements of fine granite dust. Even though the compressive strength is decreasing from 10 to 15% replacement levels, but it is also identified that, the compressive strength of 15% replacement levels (22.52 N/mm^2) is slightly higher than 0% replacement level (19.73 N/mm^2) of granite dust. If the replacement of granite dust is increased to further of 20%, 25% and 30%, the compressive strength seems to be decreasing continuously due to the reduction rate of cement content and increased content of filler materials. The same trend is seems to applicable for water curing and sulphate solution curing.

In replacement of granite dust also it is observed that deterioration rate is more for sodium sulphate solution than the magnesium sulphate solution. Based on the experimental result it is noticed that, deterioration rate on the compressive strength is 15.63% and 17.97% for the specimens having 5% replacement of granite dust cured under magnesium sulphate and sodium sulphate solutions respectively. When the replacement of granite dust is increased to 10%, the deterioration rate of compressive strength is found to be reduced of 26.95% and 30.40% than the control specimens. It seems that, the deterioration rate of compressive strength can be effectively controlled by the presence of 10% of granite dust replacement. When the replacement level of granite dust is increasing beyond 10%, the deterioration rate of compressive strength is also increasing for the sulphate solution curing conditions. It is observed that, the compressive strength is deteriorated to a maximum level of 25.48% and 31.71% for the replacement of granite dust at 30% (Fig. 5).

(iii) **Comparison of marble dust and granite dust**

It is observed that, the compressive strength is increasing upto 10% for both marble dust and granite dust replacements but if the replacement level goes beyond 10%,

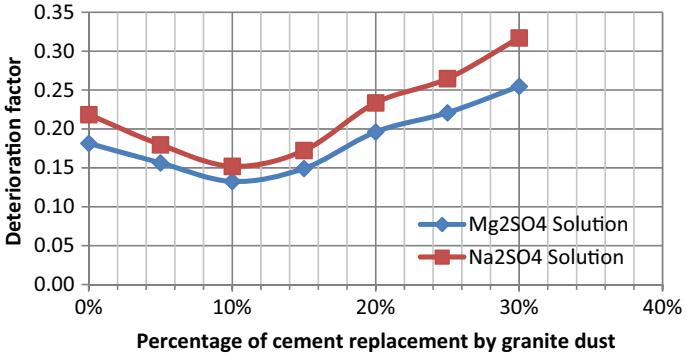

Fig. 5 Graphical representation of deterioration factor under sulphate curing

the compressive strength seems to be decreased as seen in Fig. 6. The decreasing trend is drastic for the replacement levels 15–30%. By comparing with each other, the granite dust seems to be lightly better than the marble dust for all replacement levels. For 5–10% replacement level granite dust is around 6% higher than marble dust. For other replacement levels, the increasing rate will be around 12–15% for granite dust. From that experimental results, it is noticed that, the granite dust is significantly advantageous than the marble dust in terms of strength characteristics because the filler material is well bonded agreement with the binder materials and also with reduction of pores. In Figs. 7 and 8, it is observed that, the deterioration rate of compressive strength is lower for granite dust and marble dust for the specimens under magnesium sulphate and sodium sulphate solution curing conditions. The optimum replacement percentage for both granite dust and marble dust is found as 10–15%. The maximum compressive strength found to be 24.6 N/mm^2 and 23.36 N/mm^2 for granite dust and marble dust respectively.

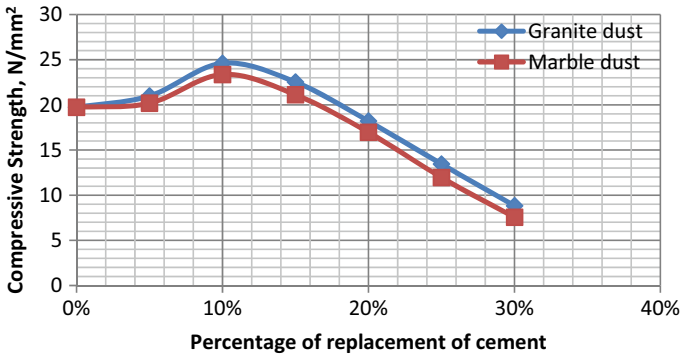

Fig. 6 Graphical representation of compressive strength for granite dust versus marble dust

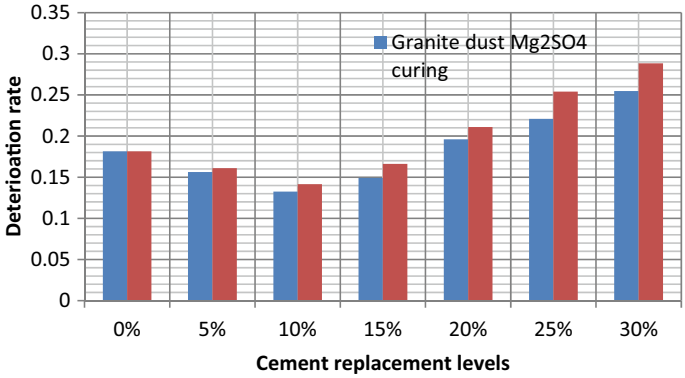

Fig. 7 Graphical representation of deterioration rate for magnesium sulphate solution curing

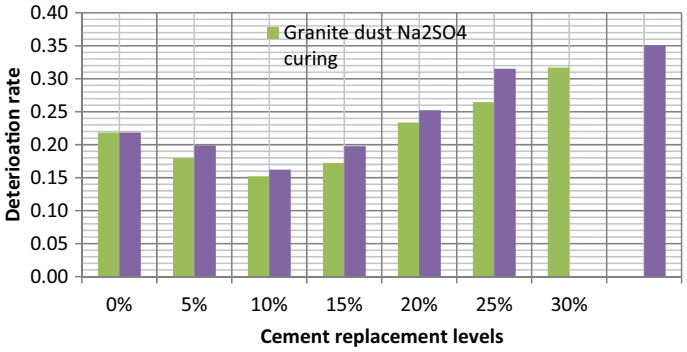

Fig. 8 Graphical representation of deterioration rate for sodium sulphate solution curing

Further replacement levels will affect the performance of strength characteristics. The deterioration rate is found to be lower of 13.25% and 14.17% for a granite dust and marble dust replacement specimens respectively kept under magnesium sulphate solution. For the specimens under sodium sulphate solution, the deterioration rate of compressive strength is 15.20% and 16.22% for a granite dust and marble dust replacements respectively.

5 Conclusions

Based on this experimental study, the following conclusions are derived. They are listed below:

(i) The compressive strength of the control specimen is getting reduced in the range of 18.14% to 21.84% due to the effect of sulphate attack of the magnesium and sodium sulphate solutions.

(ii) For granite dust replacement of 10%, the compressive strength is getting increased by 19.78% whereas the marble dust is getting increased only by 15.53%. In this aspect, the granite dust replacement is seems better than marble dust replacement. Beyond 10% of replacement, the compressive strength is in the declining trend for both granite and marble dusts. This may be due to the reduction of binding cement materials and the improper bonding between the hydrated paste and filler materials.

(iii) Upto 10% replacement of both marble dust and granite dust, the deterioration rate due to the presence of sulphate is found to be less due to arresting of micro pores by these filler elements into the hydrated paste.

(iv) The optimum usage of these waste materials in to the cement manufacturing products is limited to 10% replacement. For 15% replacement is also advantageous than compared to the control specimens. Beyond that replacement proportions, these waste materials affect the compressive strength property.

Reference

1. Udoeyo FF, Inyang H, Young TD, Oparadu EE (2006) Potential of wood waste ash as an additive in Concrete. ASCE-J Mater Civil Eng 18(4)
2. Krishna V, Sabnis GM (2013) Utilization of waste products and By-products in concrete: the key to a sustainable construction. In: International conference on civil and architecture engineering (ICCAE'2013), Malaysia.
3. Aggarwal P, Aggarwal Y, Gupta SM (2007) Effect of bottom ash as replacement of fine aggregates in concrete. Asian J Civil Eng (Build Hous) 8(1)
4. Kesharwani KC, Biswas AK (2017) Experimental study on use of flyash in concrete. Int Res J Eng Technol 4(9)
5. Mageswari M, Vidivelli B (2010) The use of sheet glass powder as fine aggregate replacement in concrete. Open Civil Eng J 4
6. Veera Reddy M (2010) Investigations onstone dust and ceramic scrap as aggregate replacement in concrete. Int J Civil Struct Eng 1(3)
7. Joel M (2010) Use of crushed granite fine as replacement to river sand in concrete production. Leonardo Electron J Pract Technol 9(17)
8. Ahmad SFU (2012) Properties of concrete containing construction and demolition wastes and fly ash. ASCE-J Mater Civil Eng 1
10. Ahirwar SK, Chandraul K, Singh MK (2017) Experimental study on concrete using flyash and coconut coir fibre. Int Res J Eng Technol 4(6)
11. Barbuta M, Serbanoiu AA (2017) Combined effect of flyash and fibers on properties of cement concrete. Procedia 181
14. Hidayawanti R, Legino S, Harjanto D (2018) Optimizing the utilization cement slag and flyash of concrete quality. Int J Adv Mech Civil Eng 5(2)

An Effective Replacement of Granite and Marble Powder on Cement Mortar Subjected to Chloride Ion Penetration Test

PL. Meyyappan and M. Jemimah Carmichael

Abstract Many researches has been carried out regarding the possible reuse of the waste materials like marble and granite powder in a economical and eco-friendly manner. The use of marble and granite products waste is identified as a substitute to cement in mortar mix to an option that come up with concrete products in a cheaper cost in the construction industry. In the sustainable point of view, an experimental study is conducted on the cement mortar with the replacement ratio of 0%, 5%, 10%, 15%, 20%, 25% and 30% of marble powder and granite powder in the cement content to examine the durability properties. For this durability study, the mortar disc specimens of dimensions 80 mm × 50 mm are prepared, cured for a period of 28 days and tested for rapid chloride permeability test. The experimental results are showing that the granite powder replaced mortar is moderately better than marble powder replaced mortar. The optimum replacement is found as 5% for marble dust and 10% for granite powder, since the penetration is low based on the experimental results.

Keywords Cement mortar · Granite powder · Marble powder · Chloride penetration test

1 Introduction

In this century, the concrete is a leading construction material. On its massive demand the global production reaches around 4.4 billion. In the recent years consumption of cement has grasped the attention of construction industry to produce green concrete by consuming alternate and reusable materials [1–3]. The major benefits of utilizing these waste materials into the production of building materials is to limit the usage of

PL. Meyyappan (✉)
Kalasalingam Academy of Research and Education, Krishnankoil, India
e-mail: meyyappan@klu.ac.in

M. J. Carmichael
Vignan's LARA Institute of Technology & Science, Guntur, India

© Springer Nature Switzerland AG 2021

K. Dasgupta et al. (eds.), *Proceedings of SECON 2020*,
Lecture Notes in Civil Engineering 97,
https://doi.org/10.1007/978-3-030-55115-5_49

natural resources, to save energy and to minimize the environmental pollution [4–6]. Among the various industrial wastes generated [7, 8], the marble and granite wastes have potentiality for the utilisation in the replacement of concrete making materials. It is noticed that Granite Stone and Marble stone Industry in India is producing several million tonnes and there by a huge amount of its solid granite waste and marble waste at the time of processing, sawing and polishing processes [9, 10]. If the waste materials are directly leaving will cause a major concern to the environmental problem [11, 12]. These wastes can be used as a filler (substituting sand) to reduce the total voids content in concrete and/or pozzolanic material (substituting cement) in the concrete mix without compromising its physical, mechanical properties and durability properties [12–14]. Hence in this experimental study, an attempt is made to study the durability effect on the cement mortar replaced by both marble and granite dust in various replacement percentages such as 0%, 5%, 10%, 15%, 20%, 25% and 30%.

2 Materials Used

Ordinary Portland Cement (OPC) of 43 grade confirms to Indian Standard specification, IS. 8112 code is used in this experimental work. Consistency of the cement used is 32.25%, Initial setting time and final setting time of the cement is 35 min and 10.25 h. For the entire work, it is assured that the cement is used only from the single point of source. The marble powder and granite powder is collected near by the Madurai source during the cutting and dressing process of marble stone and granite stone respectively. The specific gravity of this marble powder and granite powders is found to be 2.658 and 2.573 respectively. For granite powder, the fineness modulus is 2.432 and the particle size is less than 75 microns sieve. Similarly the marble powder, the fineness modulus is 2.047 and the particle size is less than 75 microns sieve. Locally available natural river sand with less than 2.36 mm size is used in this experimental work as a fine aggregate. This source of this sand confirms to the Zone 2 of IS 382-2016 having a specific gravity of 2.613. Potable drinking water is used for mixing the mortar. The pH and hardness of the water which is used in this study is 7.2 and 152 mg/l respectively. It ensured that it is free from alkalis and organic matters.

3 Mortar Mix Ratio

For preparing cement mortar specimens, the mixing ratio adopted is 1 (cement): 3 (sand). Initially, these mortar preparing materials are accurately weighed and mixed thoroughly in the dry state to attain a homogenous mixing. Then the required amount of water is determined on account of the combined weight of cement and sand is to be added to the dry mortar mix. Ensure proper uniform mixing is done before casting

the specimens. The replacement of cement by marble powder and granite powder is in the fractions of 0%, 5%, 10%, 15%, 20%, 25% and 30%. A total number of specimens (80 mm × 50 mm) casted for this RCPT is 39 out of which 3 numbers is for control specimens, 18 numbers is for marble powder replacement and 18 numbers is for granite powder replacement. These specimens are allowed under water curing for 28 days.

4 Experimental Set up of RCPT

The rapid chloride permeability of cement mortar specimens was determined according to ASTM 1202 standards. This method determines the electrical conductance of cement mortar. The disc size of 80 mm diameter and 50 mm thickness were cast and cured it for 28 days. The experimental setup of rapid chloride penetration test should be done with the help of 4 inch pipe. Then take the two halves of pipe and sealed the pipe ends of two halves with the help of couplers or pipe cap by using araldite mix in proper manner, so that the solution cannot leak in ends. A hole in the two halves of pipe is made and insert with mesh wire to act as cathode and anode. After 28 days curing, the specimen is set to dry and clamped between the pipes with the help of M-seal tightly. In this test, the disc specimen was clamped between two cells and a potential difference of 60 V DC was maintained across them. The upstream cell was filled with 3% sodium chloride (30 g of Nacl per liter) solution and the downstream cell was filled with 0.1 M sodium hydroxide (4 g of NaOH per liter) Solution. The current is recorded at periodic intervals by connecting the power source. The total charge passed, in coulombs is recorded over a six hour period at an interval of 30 min. The whole test has to be performed at room temperature of 20–250 °C. Since 80 mm nominal diameter specimen was used the test results were adjusted according to the standard as mentioned above, i.e. a correction factor was applied the following relationship:

$$Q_s = Q_x * (95/X)^2$$

where

Q_s is the charge passed through the 95 mm diameter specimen,
Q_x is the charge passed through the specimen of X mm diameter.

In which Q_x is calculated by the empirical formula,

$$Q_x = 900\,(_0 + 2I_{30} + 2I_{60} + 2I_{90} + 2I_{120} + 2I_{150} + 2I_{180}$$
$$I + 2I_{210} + 2I_{240} + 2I_{270} + 2I_{300} + 2I_{330} + I_{360})$$

The category of chloride ion permeability is identified based on the Q_x, the charge passed in coulombs as per indication of the ASTM 1202 standards as given Table 1.

Table 1 Category of chloride ion penetration

Charge passed in coulombs	Chloride ion penetration
>4000	High
2000–4000	Moderate
1000–2000	Low
100–1000	Very low
<100	Negligible

5 Results and Discussions

Figure 1 shows the experimental setup of rapid chloride penetration test. In which time interval is noted in the light hand side indication and the amount of charge passing in that particular time interval is noted in the right hand side indication. A pale yellow colour stain is deposited over the specimen, once the amount of chloride passed into it after the time duration of 360 min is as shown in Fig. 2. Tables 2 and 3 shows experimental test results of rapid chloride penetration, in which charges (in coulombs) passing are found out in various time intervals in ranging from 0 to 360 min for various replacements in the range of 0%, 5%, 10%, 20%, 25% and

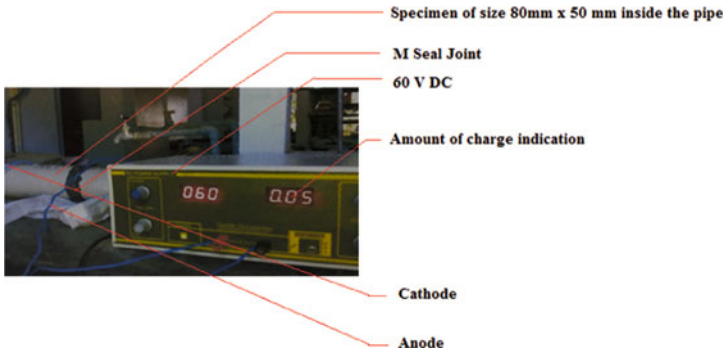

Fig. 1 Experimental Setup of RCPT

Fig. 2 Specimen after RCPT

Table 2 Charge passing in various time intervals for marble powder replacements

Percentage of Marble powder (%)	Charge passing in various time intervals (in coulombs)												
	0 s	30 s	60 s	90 s	120 s	150 s	180 s	210 s	240 s	270 s	300 s	330 s	360 s
0	0.02	0.03	0.03	0.03	0.04	0.04	0.05	0.06	0.07	0.07	0.08	0.09	0.10
5	0.02	0.03	0.04	0.05	0.05	0.06	0.07	0.07	0.08	0.09	0.1	0.11	0.12
10	0.04	0.05	0.06	0.06	0.07	0.07	0.08	0.09	0.10	0.10	0.11	0.12	0.13
15	0.05	0.06	0.08	0.08	0.09	0.10	0.10	0.11	0.12	0.13	0.14	0.15	0.17
20	0.06	0.07	0.09	0.11	0.12	0.13	0.14	0.16	0.18	0.18	0.19	0.19	0.2
25	0.07	0.08	0.11	0.12	0.13	0.15	0.16	0.18	0.2	0.21	0.23	0.25	0.26
30	0.07	0.09	0.11	0.12	0.14	0.16	0.18	0.22	0.23	0.26	0.28	0.3	0.32

Table 3 Charge passing in various time intervals for granite powder replacements

Percentage of Granite powder (%)	Charge passing in various time intervals (in coulombs)												
	0 s	30 s	60 s	90 s	120 s	150 s	180 s	210 s	240 s	270 s	300 s	330 s	360 s
0	0.02	0.03	0.03	0.03	0.04	0.04	0.05	0.06	0.07	0.07	0.08	0.09	0.10
5	0.02	0.03	0.03	0.04	0.05	0.06	0.06	0.07	0.08	0.09	0.10	0.10	0.11
10	0.03	0.03	0.04	0.05	0.06	0.07	0.07	0.08	0.09	0.10	0.10	0.11	0.13
15	0.03	0.05	0.06	0.07	0.08	0.1	0.11	0.12	0.12	0.13	0.13	0.14	0.15
20	0.05	0.07	0.09	0.10	0.11	0.12	0.12	0.13	0.13	0.15	0.15	0.16	0.17
25	0.07	0.09	0.11	0.12	0.13	0.14	0.15	0.17	0.18	0.19	0.2	0.21	0.23
30	0.08	0.09	0.11	0.13	0.14	0.16	0.18	0.2	0.21	0.23	0.25	0.27	0.29

Table 4 Class of penetration of chloride ion permeability for marble and granite powder replacement

Percentage of replacement (%)	Marble powder			Granite powder		
	Charge passed through the specimen of		Penetration of Chloride ion as per ASTM C1202-12.11	Charge passed through the specimen of		Penetration of Chloride ion as per ASTM C1202-12.11
	80 mm diameter (Qx) in coulombs	95 mm diameter (Qs) in coulombs		80 mm diameter (Qx) in coulombs	95 mm diameter (Qs) in coulombs	
0	1170	1461.88	Low	1170	1461.88	Low
5	1422	1776.27	Low	1404	1753.79	Low
10	1791	2237.20	Moderate	1584	1978.63	Low
15	2286	2855.52	Moderate	2160	2368.36	Moderate
20	3042	3799.87	Moderate	2592	3237.76	Moderate
25	3573	4463.16	High	3312	4137.14	High
30	4113	5137.69	High	3879	4845.39	High

30% of marble powder and granite powder respectively. Table 3 shows about, the calculated values of the charge passed through the 80 mm diameter specimen Qx and charge passed through the 95 mm diameter specimen Qs in terms of coulombs for various replacements of marble and granite powder. Category of penetration of Chloride ion as per ASTM C1202-12.11 is also mentioned on this Table 1. For control specimen (without replacement of cement), the Qs value is arrived as 1461.88 coulombs which is categorized as low penetration of chloride ions in to the specimen. Table 4 shows about, the calculated values of the charge passed through the 80 mm diameter specimen Qx and charge passed through the 95 mm diameter specimen Qs in terms of coulombs for various replacements of marble and granite powder.

Category of penetration of Chloride ion as per ASTM C1202-12.11 is also mentioned on this Table 1. For control specimen (without replacement of cement), the Qs value is arrived as 1461.88 coulombs which is categorized as low penetration of chloride ions in to the specimen. This is happened due to the presence of cement content in 100% and thereby the hydrated paste can able to resist the chloride ion penetration. From Fig. 3, it is understood that the penetration of chloride ions is getting increased by the increasing the replacement of granite powder and marble powder. It is a clear evident that, the penetration of chloride ions is directly proportional to the replacement of cement. For 5% replacement, the chloride ion penetration for both marble and granite powder is almost same and the chloride ion penetration is still under low category. In compare with the control specimen, the 5% replacement of both marble and granite powder has around 16.61% of enhancement in the chloride ion penetration. If the replacement is at 10% replacement, granite powder has 11.5% reduction than the marble powder.

In comparing with the control specimen, the chloride ion penetration is 34.68% and 26.13% increment for marble and granite powder replacement respectively. Since

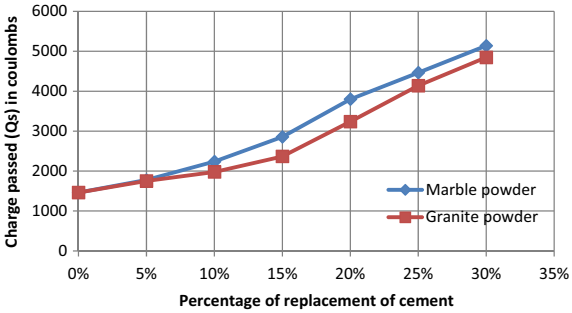

Fig. 3 Charge passed, Qs for replacement of marble powder and granite powder

the Qs is 2237.20 coulombs for marble powder replacement, the category of chloride ion penetration is moderate but for granite powder replacement, Qs is 1978.63 coulombs and thereby its falls within the category of low penetration.

If the replacement is increased to 15%, Qs is 2368.36 coulombs for granite powder but for marble powder Qs is 2855.52 coulombs. So for granite powder, the chloride ion penetration is 17.06% less than the marble powder. Further the replacement is increased to 20%, the Qs of granite powder is 14.79% less than the marble powder. The Qs is 3237.76 coulombs and 3799.87 coulombs for the granite and marble powder replacement respectively. Still if we increase the replacement of cement to 25% and 30%, the Qs is 4137.14 coulombs and 4845.39 coulombs for granite powder respectively. But for marble powder, the chloride ion penetration is increased by 7.31% and 5.68% for replacement of cement by 25% and 30% respectively. For 15% and 20% replacement, both granite and marble powder has the moderate category of chloride ion penetration whereas for 25% and 30%, the category is high. In overall it is found that, the replacement of 10% of granite powder is most optimum than the marble powder and other replacement options. The granite powder seems to be more advantageous than marble powder due to well bonding and performance of the hydrated paste in resistance to the chloride ions penetration.

6 Conclusions

The following conclusions are made based on this experimental study.

(i) The chloride ion penetration is directly proportional to the percentage of replacement of granite and marble powder.
(ii) For control specimen, the chloride ion penetration is in the category of low.
(iii) For the replacement of cement by granite powder is seems to be advantageous than marble powder because for the replacement percentage upto 10% it has fallen under category of low penetration of chloride ions whereas for the same replacement proportion marble powder lying in the medium penetration category. The optimum percentage of granite powder in to the replacement of cement is found to be 10%.

(iv) For replacement percentage more than 10–20%, both granite and marble are under moderate category of chloride ion penetration and if the replacement goes beyond 20%, both materials are under high penetration category.

Reference

1. Aggarwal P, Aggarwal Y, Gupta SM (2007) Effect of bottom ash as replacement of fine aggregates in concrete. Asian J Civil Eng (Build Hous) 8(1)
2. Shahul Hameed M, Sekar ASS (2009) Properties of green concrete containing quarry rock dust and marble sludge powder as fine aggregate. ARPN J Eng Appl Sci 4(4)
3. Krishna V, Sabnis GM (2013) Utilization of waste products and by-products in concrete: the key to a sustainable Construction. In: International conference on civil and architecture engineering (ICCAE'2013), Malaysia
4. Udoeyo FF, Inyang H, Young TD, Oparadu EE (2006) Potential of wood waste ash as an additive in concrete. ASCE-J Mater Civil Eng 18(4)
5. Shi C (2009) Corrosion of glasses and waste mechanism of concrete containing waste glasses as aggregates. ASCE-J Mater Civil Eng 21(10)
6. Mageswari M, Vidivelli B (2010) The use of sheet glass powder as fine aggregate replacement in concrete. Open Civil Eng J 4
7. Ahmad SFU (2012) Properties of concrete containing construction and demolition wastes and fly ash. ASCE-J Mater Civil Eng 1
8. Hidayawanti R, Legino S, Harjanto D (2018) Optimizing the utilization cement slag and flyash of concrete quality. Int J Adv Mech Civil Eng 5(2)
9. Veera Reddy M (2010) Investigations onstone dust and ceramic scrap as aggregate replacement in concrete. Int J Civil Struct Eng 1(3)
10. Joel M (2010) Use of crushed granite fine as replacement to river sand in concrete production. Leonardo Electron J Pract Technol 9(17)
11. Barbuta M, Serbanoiu AA (2017) Combined effect of flyash and fibers on properties of cement concrete. Procedia 181
12. Meyyappan PL, Kumaran K, Gopalakrishnan M, Harikrishnan E (2018) Effect of glass fibers, flyash and quarry dust on strength and durability aspects of concrete—an experimental study. IOP Conf Ser Mater Sci Eng (RAEREST'18), India
13. Ahirwar SK, Chandraul K, Singh MK (2017) Experimental study on concrete using flyash and coconut coir fibre. Int Res J Eng Technol 4(6)
14. Kesharwani KC, Biswas AK (2017) Experimental study on use of flyash in concrete. Int Res J Eng Technol 4(9)

An Experimental and Analytical Investigation on the Characteristics of Light Weight Concrete Using Waste Burnt Ash and Pumice Stones

PL. Meyyappan, M. Pallikonda Rajasekaran, and R. Sathya Soroopan

Abstract Light weight concrete (LWC) has been successfully used since the ancient roman times and it has gained its popularity due to its lower density and superior insulation properties. Compared to the conventional concrete, LWC can significantly reduce the dead load of structural elements, which makes it especially attractive in the construction of multi-storey buildings. The materials used for preparing the light weight concrete is pumice stones, burnt waste material ash and GGBS. The coarse aggregates are partially replaced with pumice stones in the varying fractions of 10%, 20% and 30%. The cement are partially replaced with waste burnt ash in the proportions of 5%, 10% and 15%. Additionally 5% GGBS is introduced into that mix proportions. It is observed that by the optimum presence of light weight aggregates such as 15% of burnt ash and 30% of pumice stone, density of the concrete is reduced upto 2140 kg/m^3. In the same time the compressive strength is achieved around 75% to 81% of the strength of the conventional concrete. Analytical equations models are arrived from LabVIEW software and it has been well correlated the experimental test results with the deviation of ±20%.

Keywords Light weight concrete · Waste burnt ash · GGBS · LabVIEW

1 Introduction

As compared to normal conventional concrete, light weight concrete can significantly reduce the density of structural concrete and low thermal conductivity in indicated in the previous researches [1–3]. Based on the main advantage of reduction of dead load, building constructions can be done in the faster manners as like precast, prefabrication elements etc. and there by cost of the construction will come down drastically as the cross section of the elements is less as compared with the conventional [4–6]. There are many possible ways to reduce the density of the concrete, they are by cellular construction, by entraining large quantities of air, by using no-fines concrete

PL. Meyyappan (✉) · M. P. Rajasekaran · R. S. Soroopan
Kalasalingam Academy of Research and Education, Krishnankoil, India
e-mail: meyyappan@klu.ac.in

© Springer Nature Switzerland AG 2021

K. Dasgupta et al. (eds.), *Proceedings of SECON 2020*,
Lecture Notes in Civil Engineering 97,
https://doi.org/10.1007/978-3-030-55115-5_50

and light weight aggregates. Most economical and feasible method of attaining light weight concrete is by using light weight aggregates. The light weight aggregates are of natural and man-made. The natural light weight aggregates includes pumice stones, volcanic cinders, saw dust, burnt ash and rice husk etc., whereas the artificial light weight aggregate includes artificial cinders, coke breeze, foamed slag, bloated clay, expanded shale and slate, sintered flyash etc. [7, 8]. In most of the educational institutions, paper based waste materials are the major solid wastes which is accumulated and dumped in to a waste land in a daily basis. Then it will be simply burnt until ashes and left out there itself. Generally these left out waste ashes will create a serious environmental threats to the society. In many of the past literatures, it is indicating that, the waste materials of any form can be utilized as filler materials in minimum to maximum extent [8]. So an attempt is made to effectively utilize these waste ashes in a limited proportion in to the concrete. Apart from the specific gravity, the strength is also taken in to the consideration while utilizing these ashes. To maintain the strength aspects in a desired manner, 5% of GGBS content is introduced along with the other constituents. In this manner, in order to achieve the light weight concrete and without comprising much of the strength, an attempt is made to produce that concrete by using pumice stones, GGBS and burnt ashes. In this experimental work, the strength and water absorption property of the produced light weight concrete will be evaluated.

2 Materials Used

(i) *Cement*
43 Grade Ordinary Portland Cement (OPC) confirms to Indian Standard specification, IS. 8112 code is used in this experimental work with a specific gravity of 3.21 and fineness modulus of 2.35%. For plain cement concrete works, the preferred cement is 43 grade and also it is most suitable to make concrete mix M30 in the economical aspects whereas the higher grades of cement are most suitable for RCC type of works.

(ii) *Fine aggregate*
The naturally available river sand which having glossy texture and round in shape is used as fine aggregate for this study conforming to requirements of zone II as per IS:383-1970. The specific gravity of this fine aggregate is 2.685.

(iii) *Coarse aggregate*
The natural rock aggregates which are having angular and irregular texture passing to 20 mm sieve and retained on 4.75 mm sieve is used in this study. The specific gravity of this coarse aggregate is around 2.741.

(iv) *Pumice stones*
The light weight aggregate pumice stone of sizes 12.5 mm having specific gravity 1.15 is taken for this study.

(v) *Burnt ash*
The waste paper and paper cups are burnt into ashes and these ashes are taken in this study. The specific gravity is found to be 2.593.

(vi) *Water*

Potable drinking water is used for mixing the mortar. It ensured that it is free from alkalis and organic matters.

3 Experimental Investigations

The concrete mix was adopted for this experimental investigation is 1:1.54:2.09:0.45 for M30 grade of concrete by using IS 10262. The coarse aggregate has both regular of 20 mm size and pumice stone of 12.5 mm. First the different varieties of coarse aggregates (regular and light aggregate) are to be mixed, then fine aggregate is to be spread out uniformly and finally the cement is dispersed on that aggregate mixture. Care should be taken for the uniform and homogenous mixing on the dry state. Once the dry state of concrete constituents is ready, the calculated quantity of water as per mix design is to be introduced slowly and wet mix required a careful preparation any defects like any slumps, bleeding problems etc. The prepared fresh concrete is filled in to the respective moulds with proper hand compaction in three layers. For both compression and porosity tests, cube specimens of 150 mm × 150 mm × 150 mm were casted for this designed concrete M30 mix. As in total, 120 cube specimens were casted for both the tests in the 28 days of age of curing with 5% GGBS, replacement proportion of 0%, 10%, 20% and 30% of pumices stones and replacement proportion of 0%, 5%, 10% and 15% burnt ash. The compression experimental tests were conducted in the compression testing machine of 200 tonnes capacity. The tests were performed out at a standardized stress rate of 14 N/mm^2/min, once the specimen is kept centered in the machine. Water absorption test were conducted on the cube specimens to arrive its volume of pores. The specimens were kept in the hot air oven on the standard temperature of 120 °C temperature. Before and after placing oven, the dry weights should be noted as W_1 and W^2. The differences in weight of those specimens against the initial dry weight are taken for the calculation of volume of pores. The porosity (volume of pores in percentage) can be calculated by the formula (1) mentioned below:

$$\frac{W_1 - W_2}{W_1} \times 100 \tag{1}$$

where,

W_1 Initial weight of the specimen before placing in oven
W_2 Final weight of the specimen after placing in oven.

The representation of loss of water is an indirect measure of porosity where it has been frequently used in many of the literatures. Actually the porosity of concrete is nothing but the estimation of volume of pores to the total volume of the concrete. Generally the volume of pores is almost equal to the volume of water present in that saturated sample. In that aspect, the volume of water present is calculated from the weight difference of the saturated samples and dry samples. So, this is one of the way the porosity can be calculated.

4 Results and Discussions

(i) ***Experimental studies***

Table 1 shows the experimental test results of compressive strength and water absorption for the specimens with and without light weight aggregates (pumice stones),

Table 1 Experimental test results for marble dust replacement

Mix No.	Replacement %			Average density (kg/m^3)	Average compressive strength (N/mm^2)	Average water absorption test (%)
	Pumice stones	Burnt ash	GGBS			
1	0	0	0	2600	37.83	8.23
2	10	0	0	2550	35.82	8.18
3	20	0	0	2380	33.29	8.06
4	30	0	0	2140	30.64	8.01
5	0	0	5	2600	43.91	7.91
6	10	0	5	2560	41.02	7.62
7	20	0	5	2400	38.12	7.25
8	30	0	5	2150	33.04	6.89
9	0	5	5	2590	43.15	7.59
10	10	5	5	2550	39.78	7.31
11	20	5	5	2390	35.31	6.67
12	30	5	5	2130	29.95	6.06
13	0	10	5	2590	42.04	7.43
14	10	10	5	2530	37.08	7.09
15	20	10	5	2370	30.53	6.4
16	30	10	5	2130	25.76	5.94
17	0	15	5	2560	39.23	7.8
18	10	15	5	2520	34.92	7.39
19	20	15	5	2350	26.86	6.78
20	30	15	5	2100	21.63	6.23

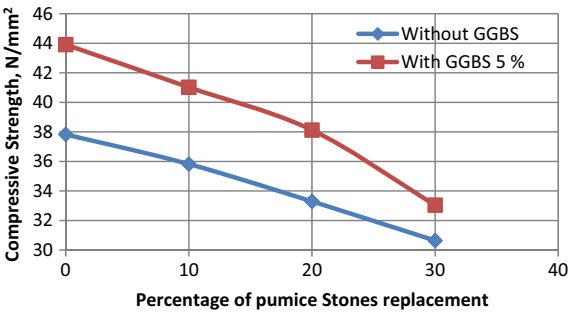

Fig. 1 Compressive strength of specimens with and without GGBS

burnt ash and GGBS. It is observed that the control specimen (conventional concrete) is having the density of 2600 kg/m^3 with a compressive strength of 37.83 N/mm^2 and 8.23% of pores. If the GGBS is introduced into the concrete as 5%, the compressive strength increased by 13.84% and the volume of pores is reduced by 8.7%. This is happened due to the of high cementitious nature and fineness of GGBS. The hydration process is well performed by the cement and GGBS materials. The graph (as shown in Fig. 1) is plotted between the compressive strength and percentage of pumice stones replacement in the range of 0%, 10%, 20% and 30% for the specimens with and without GGBS content of 5%. It is found that, the compressive strength is decreased from 37.83 N/mm^2 to 30.64 N/mm^2 for the specimens having the replacement of pumice stones by 0% to 30%. If GGBS materials introduced the compressive strength is increased more than the non GGBS mixture but the falling trend of compressive strength exists if the pumice stone content is increasing. The same pattern is seen for the water absorption test as shown in Fig. 2. For the specimens having GGBS content the compressive strength is 43.91 N/mm^2, 41.02 N/mm^2, 38.12 N/mm^2 and 34.04 N/mm^2 for the replacement of pumice stones 0%, 10%, 20% and 30% respectively. Due to the presence of GGBS, the compressive strength increased by 12.67%, 11.34% and 9.89% for the replacement of pumice stones 10%, 20% and 30% respectively. From Fig. 2, it is understood that, the reduction of pore volume seems to be increasing, if pumice stone replacement increased. If GGBS is not present, the increasing trend will be very slight; almost graph is looking straight line since the

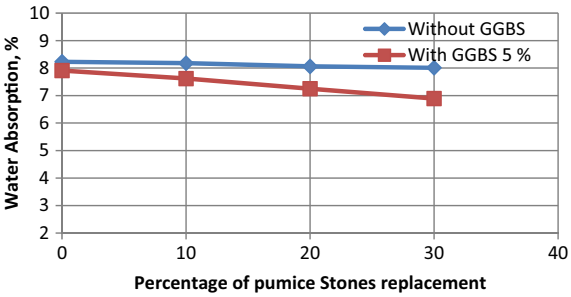

Fig. 2 Water absorption of specimens with and without GGBS

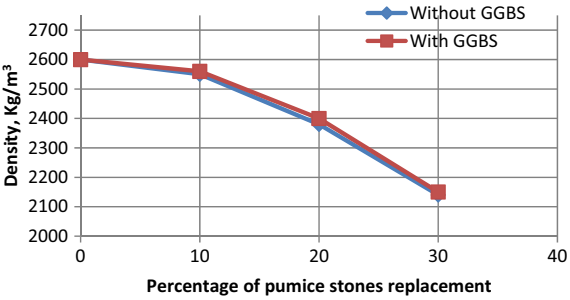

Fig. 3 Density of the specimens with and without GGBS

water absorption is in the range of 8.23% to 8.01%. There is no much difference seen. But if the GGBS is present, the water absorption is found in the range of 7.51% to 6.89%. Some significant amount of volume of pores is reduced (16.29%) due to the presence of finer particles of GGBS and size of coarse aggregate by pumice stones. From Fig. 3, it is found the density of the concrete is reduced by the increasing the replacement of light weight aggregate (pumice stones). The density of the conventional concrete is found to be 2600 kg/m^3. If the coarse aggregate is replaced by 10% pumice stones, the density of the concrete is reduced to 1.92% (2550 kg/m^3).

Further if the pumice stone is increased to 20%, the density of the concrete further reduced to 8.46% (2380 kg/m^3). Then density of the concrete is achieved as 2140 kg/m^3 and there, reduction of 17.69% is seen, if the pumice stone is increased to 30%. If the 5% GGBS is added in to the concrete, the graphical pattern is almost same as previous. There is no much difference is seen in terms of reduction in the density. So it is an evident, that the density reduction is achieved only by the presence of light weight aggregates.

Figure 4, shows that there is a comparison of compressive strength and percentage of pumice stones replacement in the presence of different proportions of burnt ash with 5% GGBS content. In general, the graph showing that the presence of burnt ash and pumice stones bringing down the compressive strength because of the different surface texture among coarse aggregates and pumice stones, bonding effect between the two different coarse particles. Thereby the it is an evident that, the compressive

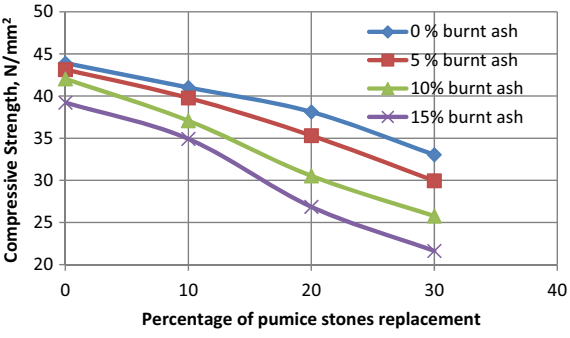

Fig. 4 Compressive strength of the specimens with and with burnt ash

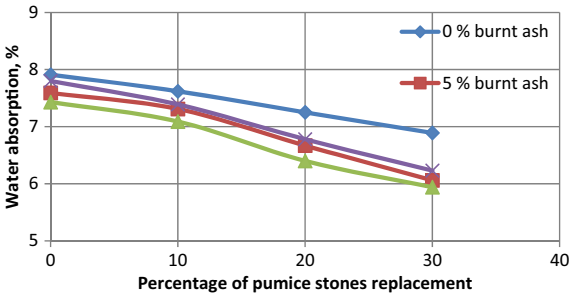

Fig. 5 Water absorption of the specimens with and with burnt ash

strength factor is indirectly proportional to the presence of pumice stones and burnt ash. If the presence of pumice stone and burnt ash is less in content, the compressive strength is affected in low ratio. For 5% addition of burnt ash will affecting the strength by 3.02%, 7.37% and 9.35% for 10%, 20% and 30% of pumice stone replacement respectively. Further if the burnt ash is increased to 10%, the strength is affected from 9.69 to 22.03% for the pumice stone replacement from 10 to 30%. Still if the burnt ash content is increased to a maximum of 15%, the strength is maximally affected from 14.8 to 34.53%. This shows that, the presence of burnt ash of 5 and 10% burnt ash is advantageous and optimum in getting around 90 and 88% of the compressive strength with a density of achieving light weight concrete of around 2130 kg/m^3 in the presence of 30% pumice stones along with the coarse aggregate.

Figure 5 shows that water absorption for various percentages of pumice stones and burnt ash of the specimens with 5% GGBS content. The volume of pores is getting reduced by the presence of pumice stones and burnt ash. For 0% burnt ash, the pores are reduced from 7.91% to 6.89% in the presence of 0% to 30% of pumice stones replacements. For 5% burnt ash content, the water absorption is in the range of 7.59% to 6.06% and for 10% there is an slight reduction in the water absorption in the range of 7.43% to 5.94% but if the burnt ash content is increased to 15%, there is an increase in the water absorption rate as compared to 5% and 10% of burnt ash content. This is may be due to the increase of filler materials, improper hydration and bonding between the aggregate and binder interface.

1. Analytical Studies

In order to verify and validate the experimental test results, analytical studies is carried out to model the studies by using LabVIEW. In LabVIEW, Curve fitting analysis technique is applied for extracting a set of curve parameters or coefficients from the experimental data set to attain a functional account of the data set. The algorithm that works based on the concept of least square method and that fits a curve to a particular data set. The analysis library in the LabVIEW has both linear and non-linear curve fitting algorithms. There will be different types curve fitting formats such as linear fit, exponential fit, polynomial fit and log arithmetic fit. Out of that, the linear fit is chosen in our study since it fits with the experimental data to a straight line in the general format as mentioned in the Eq. (2).

$$y = mx + c \tag{2}$$

In the LabVIEW programming, under the section of library regression.llb controls the noisy data levels on the parameters of the curve that best fits those data points. Then select the type as linear fit in the algorithms selector control. In the last, run the LabVIEW and notice the spread of data points where the curve is fitted. Finally the coefficients of the linear model will be taken for arriving the model Eqs. (3) and (4). Based on the known values of percentage of GGBS, pumice stones and burnt ash, the unknown values such as compressive strength and water absorption of the concern concrete mix can be computed from the Eqs. (3) and (4).

$$\mathrm{CS} = 0.1\mathrm{P_G} - 0.247\mathrm{P_{PS}} + 0.05\mathrm{P_{BA}} + 38.01 \tag{3}$$

$$\mathrm{WA} = 0.1\mathrm{P_G} - 0.034\mathrm{P_{PS}} + 0.012 + \mathrm{P_{BA}} + 7.932 \tag{4}$$

where

CS Compressive strength in N/mm^2
P_G Percentage of GGBS
P_{PS} Percentage of pumice stones
P_{BA} Percentage of burnt ash
WA Water absorption in %.

It has been observed that the, arrived model equations are well correlated with the experimental results since, the difference among them are estimated at around ±20% deviation.

5 Conclusions

The following conclusions are arrived based on this experimental study. They are as follows:

(i) It is found that the control specimen (conventional concrete) is having the compressive strength of 37.83 N/mm^2 and 8.23% volume of pores without GGBS, pumice stone and burnt ash content. If GGBS alone is introduced into the concrete as 5%, the compressive strength increased by 43.91 N/mm^2 and the volume of pores is reduced by 7.91%.
(ii) It is found that the density of the concrete is getting reduced by the increasing the replacement of light weight aggregate (pumice stones) with the normal coarse aggregate. For 30% replacement of pumice stone, the density is reduced from 2600 to 2140 kg/m^3. The reduction in density is upto 17.69%.
(iii) It is observed that by the presence of burnt ash and a pumice stone, around 75–81% of the compressive strength is achieved with the reduction of density around 20%.

(iv) For the 5% replacement of cement by burnt ash will yield around 80% of the compressive strength value of the control specimen and if the replacement percentage is increased to 10%, the achieved compressive strength is only around 70%.
(v) The optimum usage of burnt ash into the concrete is found to be 10% along with GGBS content 5% to achieve 80% of the compressive strength of M30 grade. Also there is reduction in the volume of pores upto 10% of burnt ash content.
(vi) Analytical models are arrived from LabVIEW software to correlate the experimental test results with ±20%.

References

1. Jones MR, McCarthy A (2005) Preliminary views on the potential of foamed concrete as a structural material. Mag Concr Res 57(1):21–31
2. Zulkarnain F, Ramli M (2011) Performance and characteristic foamed concrete mix design with silica fume for housing development. Int J Acad Res 3(2), Part IV
3. Kearsley EEP, Wainwright PJ (2014) Ash content for optimum strength of foamed concrete. Cem Concr Res 32(2):241–246
4. Mydin MAO, Wang YC (2012) Mechanical properties of foamed concrete exposed to high temperatures. Constr Build Mater 26(1):638–654
5. Tan XJ, Chen WZ, Tian HM, Yuan JP (2013) Degradation characteristics of foamed concrete with lightweight aggregate and polypropylene fibre under freeze-thaw cycles. Mag Concr Res 65(12):720–730
6. Alengaram UJ, Al Muhit BA, bin Jumaat MZ, Jing MLY (2013) A comparison of the thermal conductivity of oil palm shell foamed concrete with conventional materials. Mater Des 51:522–529
7. Hunaiti YM (1997) Strength of composite sections with foamed and lightweight aggregate concrete. J Mater Civ Eng 9(2):58–61
8. Meyyappan PL, Kumaran K, Gopalakrishnan M, Harikrishnan E (2018) Effect of glass fibers, flyash and quarry ash on strength and durability aspects of concrete—an experimental study. IOP Conf Ser Mater Sci Eng

Applications of Functionally Graded Materials in Structural Engineering—A Review

S. L. Akshaya, Amar Prakash, and J. Bharati Raj

Abstract Functionally graded materials are an advanced class of composite materials characterized by spatially varying properties and are designed to optimize the performance through the distribution of the desired property. A functionally graded material eliminates the sharp interface between dissimilar materials and possesses a gradual variation from one material to other. The research in this area is still in nascent stage. It has many promising applications in different fields like biomedical, defence, structural engineering etc. As compared to the conventional homogeneous, isotropic materials these are complex in the analysis and design procedures. This paper presents a critical review on the mechanics and behaviour of the functionally graded materials towards their applications in structural engineering, specifically in the design of protective structures. Besides this, a brief description is also provided with suitable formulations regarding the gradation of the properties in a particular direction to achieve the desired functionality.

Keywords Functionally graded materials · Layered composites · Protective structures · Grading laws

1 Introduction

Latest advancements in the field of engineering and processing of materials have led to a new class of composite materials called Functionally Graded Materials (FGMs). These represent a second generation of composite materials and have been

S. L. Akshaya (✉) · J. Bharati Raj
NSS College of Engineering, Palakkad, Kerala 678008, India
e-mail: slakshaya95@gmail.com

J. Bharati Raj
e-mail: bharatiraj83@gmail.com

A. Prakash
CSIR-SERC, Chennai, Tamil Nadu 600113, India
e-mail: amar@serc.res.in

© Springer Nature Switzerland AG 2021

K. Dasgupta et al. (eds.), *Proceedings of SECON 2020*,
Lecture Notes in Civil Engineering 97,
https://doi.org/10.1007/978-3-030-55115-5_51

designed to achieve superior levels of performance [1]. A FGM typically consists of a composite material with a spatially varying property and is designed to optimize performance through the distribution of that property. These materials are characterised by an engineered gradient of composition, structure and/or any specific properties in the preferred direction/orientation and are superior to homogeneous materials composed of similar constituents. In FGMs the mechanical properties such as Young's modulus of elasticity, poisson's ratio, shear modulus of elasticity, and material density, vary smoothly and continuously in preferred directions [2]. Such properties of the materials can be described by material function f(x). The variation of this material function in a homogenous material (constant), in a composite material and in an FGM are depicted in Fig. 1 [3].

FGMs have a graded interface rather than a sharp interface between the two dissimilar materials, thus, an ideal FGM has no sharp interfaces (Fig. 2).These materials exhibit superior mechanical properties when compared to basic (monolithic) and composite materials.

Initially, functionally graded materials were designed as thermal barrier materials for aerospace structures and fusion reactors and, later they were also considered as potential structural materials for future high-speed spacecraft and various other applications [1, 4]. In the mid 1980s, researchers in Japan confronted with a challenge in a hypersonic space plane project requiring a thermal barrier, with outside

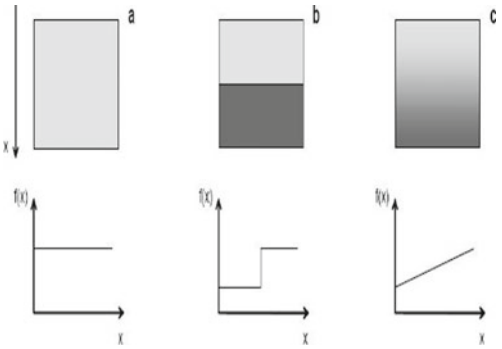

Fig. 1 Schematic representation of material function in different structure; **a** Homogeneous material **b** Composite **c** FGM [3]

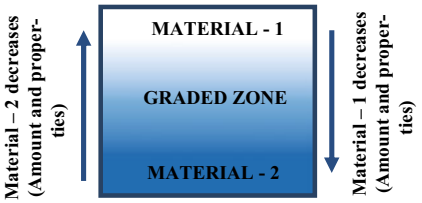

Fig. 2 Concept of FGM

temperature of 2000 K and inside temperature of 1000 K across less than 10 mm thickness [3, 5, 6].Therefore, as a solution to this problem the novel material called Functionally Graded Materials (FGM) were developed.

Functionally graded materials were developed as advancement to composite materials. They provide excellent heat and corrosion resistance capability, and are able to withstand ultra-high temperature gradients. FGM can also act as an interface layer that connects two incompatible materials so as to enhance the bond strength, remove stress concentration, provide multi-functionality namely, ability to control deformation, wear, corrosion, dynamic response etc. [7]. It has been demonstrated by many researchers that FGMs helps to decrease the magnitude of peak thermal stresses, eliminates the stress concentrations at the interface layers and free edges in laminated composites [8, 9].The most commonly available FGMs are ceramic–metal composites, where the ceramic part has good thermal and corrosion resistance capability and the metallic part provides superior fracture toughness and weldability [7]. FGM also improves the fracture toughness of brittle ceramics by introducing a metallic phase that deforms plastically.

2 Homogenization Schemes

Homogenization schemes are used to determine the effective material properties. Most of the FGMs are manufactured by two phases of materials with different properties. The volume fraction of each phase gradually varies in the gradation direction and the effective properties of FGMs viz. elastic moduli, shear moduli, density, etc. change along this direction [10]. Several homogenization schemes or models like rules of mixture (Voigt Scheme) [11–13], Hashin–Shtrikman type bounds, Mori–Tanaka type models [12, 13], self-consistent schemes etc. are available in literature for determination of the bounds of the effective properties. However the most commonly used schemes are the Mori–Tanaka scheme and the Voigt scheme.

3 Gradation Laws

The variation of the desired property of an FGM across any direction (usually thickness direction) can be designed according to the requirement by considering various gradation laws.

3.1 Exponential Law

The exponential law is generally used to deal with problems related to fracture mechanism of FGM. [7, 13] As per this law, for a structure made of FGM with

uniform thickness 'h', the effective material properties P(z) at any point located at a distance 'z' from the reference surface is given by Eq. 1 [2, 7].

$$P(z) = P_t e^{\left(\frac{1}{h}\right)\left(ln\frac{P_b}{P_t}\right)\left(z+\frac{h}{2}\right)} \tag{1}$$

where P_b and P_t represent the material properties at the bottom-most (z = − h/2) and top-most (z = + h/2) surfaces respectively.

3.2 Power Law

The power law is a simple law and is commonly used in the stress analysis of FGM [2]. According to this law, a material property P(z) in a specific direction (along z) of an FGM plate of uniform thickness 'h' can be determined by Eq. 2.

$$P(z) = (P_t - P_b)V_m + P_b \tag{2}$$

It can be seen that the material properties are dependent on the volume fraction V_m of FGM. The volume fraction can be represented by a function of the thickness coordinate Z as given by Eq. 3.

$$V_m = \left(\frac{2Z + h}{2h}\right)^n \tag{3}$$

where, h is the thickness of the structure, and n ($0 \leq n \leq \infty$) is a volume fraction exponent.

It is observed that the young's modulus changes rapidly near the lowest surface for n > 1, and increases quickly near the top surface for n < 1 [14].

3.3 Sigmoid Law

When using power law function and exponential function the stress concentrations appear in one of the interfaces in which the material is continuous but rapidly changing. To overcome this problem Chi and Chung [14] introduced the sigmoid law in which two symmetric FGM layers with power-law distribution is considered. According to this law, the two power law functions are defined by Eqs. (4) and (5), [7].

$$f_1(z) = 1 - (0.5)\left(\frac{\frac{h}{2} - z}{\frac{h}{2}}\right)^p \quad 0 \leq z \leq \frac{h}{2} \tag{4}$$

$$f_2(z) = 1 - (0.5)\left(\frac{\frac{h}{2} + z}{\frac{h}{2}}\right)^p - \frac{h}{2} \leq z \leq 0 \tag{5}$$

where $f_1(z)$ and $f_2(z)$ represent the material property for the particular condition mentioned.

4 Applications

FGMs were initially used in aerospace but with more research and advancements in the field it has expanded its application to various other fields, like industrial materials, optoelectronics, biomaterials, energy materials etc.… They offer great promise in severe operating and loading conditions such as for wear-resistant linings for handling large heavy abrasive ore particles in the mining industry, rocket heat shields, heat engine components, heat exchanger tubes, plasma facings for fusion reactors in nuclear reactor plant, thermo-electric generators, and in the electrical insulating applications [5]. The current areas of applications include aerospace, automobile, defence, electrical/electronic, marine, thermo-electronics etc. [6, 7, 15, 16]. Few FGMs with their properties and applications are provided in Table 1.

4.1 Civil Engineering Field

Application of FGM into civil engineering field is an emerging area of interest. Many researchers have worked on several aspects of FGM related to its structural applications. A lot of research work has been undertaken since the inception of the FGM concept and some of the works include the design of FGM [17], modelling of FGM [18], fabrication and characterization of FGMs and many more. In the last decade analysis of composite structures has become a promising research field since accurate structural and dynamic analyses are required to design various structural components of aerospace, mechanical, naval as well as civil constructions to understand the behavior of the structural response in real time. Numerous studies on stress, deformation, stability, and vibration problems of FGM beams, plates, and shells accounting for various effects, such as geometric and physical nonlinearity and transverse shear deformability are available. Different plate theories have been developed by researchers to analyse composite plates (including FGM plates) and shells which include the classical plate theory [14, 19] and shear deformation theories [20–23]. A brief study of the vibration characteristics and impact response of FGM done by researchers are addressed in the following sections.

Table 1 Few FGMs with their applications Khan et al. [13]

FGM	Property	Application
Al_2O_3 E-glass/Epoxy	Thermal barrier and anti-wear mechanics parts, hardness and damping resistance	Rocket nozzle, wings and engine casting, brake rotors, solar domes, composite piping system, combustion chambers
$BaTiO_3$/Si Carbon/Epoxy	Hardness and Toughness Lightweight and good damping properties	Dielectric motors, Helicopter components i.e. landing gear doors, heat exchanger panels and engine parts
Al alloy	Light weight and high stiffness	Artificial ligaments, MRI scanner spares, eye glass, frames dentistry parts
TiAl/SiC, SiC/C	Temperature and shock resistance Coatings	Heat exchanger panels, rocket nozzle, spacecraft, truss structure, solar panels
Graphite/Epoxy	High strength to stiffness ratio Reduces thermal distortions	Cylindrical pressure hulls, space telescope, cryogenic tanks, satellite antennas
Al/AAl_2O_3, WC/Co, SiCW/Al-Alloy	Heat, wear and tear resistance, thermal resistance, Chemical inertness, and toughness	Machine and forming tools, artificial bones, Storage cylinders, diesel engine pistons, racing bicycle and vehicle frames

4.1.1 Vibration and Dynamic Response of FGM

Ample number of studies have been done on free and forced vibration for FGM plates both with and without initial thermal and/or mechanical in-plane loads. Few journals in this area has been addressed in this section. The study done by some of the authors and their findings have been tabulated in Table 2.

4.1.2 Impact Resistance of FGM

Impact resistance of FGM is a comparatively less addressed area. However, recently many researchers are active in this field. But, it can be observed that many papers mention materials designed according to their function as functionally graded materials. These may be designed according to the function they have to satisfy and hence are graded according to their function, but in these materials the exact definition of FGM where the material property varies continuously may not be absolutely satisfied. Nevertheless even in such material when the difference between the material property is small they may seem to obey the FGM concept. Few journals dealing with impact on FGMs are given in Table 3. The work done by few researchers in

Table 2 Review of vibration and dynamic response of FGM

Author	Study	Main Findings
Cheng and Batra [24]	• Used Reddy's third order plate theory to study the buckling and steady state vibrations of a simply supported FG polygonal plate resting on a Winkler-Pasternak elastic foundation and subjected to uniform in-plane hydrostatic loads • Comparative study of different theories like; Classical plate theory (CLPT), First order shear deformation theories (FSDT) and Higher order shear deformation theories (HSDT)	• They established an exact correspondence between the buckling and vibration eigen values of the third order plate theory, FSDT and CLPT for FG polygonal plates with simply supported rectilinear edges and the vibration eigen value of the corresponding membrane
Yang and Shen [25]	• A semi-analytical approach was used to investigate the free vibration and the dynamic response of functionally graded rectangular plates subjected to impulsive lateral loads combined with initial in-plane actions and under thermal environments	• When thermal effects were included, FG plates with material properties intermediate to those of isotropic ones do not necessarily have intermediate dynamic response • Material composition, temperature rise, in plane and out-of-plane boundary conditions, initial membrane stresses and dynamic load shape has a significant influence on the vibration characteristics and dynamic responses
Vel and Batra [26]	• An analytical solution was presented for the free and forced vibrations of simply supported FG rectangular plates • Exact solutions for an aluminum/zirconia FG plate were compared with those obtained by the CPLT, FSDT and Third order shear deformation theory (TSDT) • A metal–ceramic FG rectangular plates with a power-law variation of the volume fractions of the constituents across the thickness were considered	• For FG thick plates, there was a significant differences between the exact solution and results obtained from the CLPT • FSDT performed better than the TSDT for the FG plates • Results from the FSDT and TSDT compare well with the exact solution
Liu et al. [27]	• Free vibration analysis of a FG isotropic elastic rectangular plate with in-plane material inhomogeneity	• The effect of in-plane material inhomogeneity on the fundamental frequencies were well shown with numerical examples

(continued)

Table 2 (continued)

Author	Study	Main Findings
Lee and Lee [28]	• A unified model to analyze the free vibration and buckling of axially FG Euler-Bernoulli columns subjected to an axial compressive force • Linear variation of material property along the longitudinal direction and linearly tapering column with circular and square cross sections were studied	• Buckling load increased with the modular ratio while the fundamental frequencies exhibited different trends for different end conditions • When the applied compressive load was close to the buckling load, the fundamental frequency dramatically decreased to zero • AFG columns with square cross section had higher fundamental frequency and buckling load than those with circular cross section or a fixed volume of the column

Table 3 Review of impact characteristics of FGM

Author	Study	Main Findings
Apetre et al. [29]	• Study of sandwich panels with a functionally graded core with density, and hence its stiffness, varying through the thickness, subjected to low-speed impact of a one-dimensional sandwich panel by a rigid cylindrical projectile • Poisson's ratio was kept constant while the Young's modulus was varied and was represented by a polynomial in the thickness coordinate	• The contact stiffness of the beam with graded core increased, causing the contact stresses and other stress components in the vicinity of contact to increase • Maximum strain corresponding to the maximum impact load reduced considerably due to grading of the core properties • FG cores can be effectively used to mitigate impact damage in sandwich composites
Quek et al. [30]	• Developed a functionally graded (FG) cementitious panel which consisted of PE-fibrous ferrocement, calcined bauxite aggregates and conventional mortar to resist high-velocity small projectile penetration	• FG-panels displayed superior impact resistance compared to plain mortar targets • Thickening the calcined bauxite aggregate layer was most effective in reducing the penetration depth for all impact velocities • Increasing thickness of the impact and distal face PE-fibrous ferrocement had little influence over the overall impact resistance • It was concluded that FG-panel design can be improved by incorporating thicker high energy absorption materials at the impact face or by adding a layer of PE fibrous ferrocement

(continued)

Table 3 (continued)

Author	Study	Main Findings
Yalamanchili and Sankar [31]	• Studied the problem of contact between a rigid cylindrical indenter and a functionally graded (FG) beam with the elastic modulus of the material varying exponentially across the thickness of the beam • Two types of gradations (soft to hard and hard to soft) and a homogeneous material were studied	• The variation of Young's modulus in FG beams has a significant effect on the contact length • For a particular contact force the contact length in soft contact was found to be about three times that in hard contact and, it reduces the peak contact stress which in turn seems to reduce the stresses in the contact region • The maximum normal and shear strains were in general less in soft impact (when the impact/contact occurred on the softer side) for a given impact energy or maximum contact force
Shariyat and Jafari [32]	• Study of nonlinear low-velocity impact analysis of a two directionally graded circular plate under radial preloads • They considered the property to vary in both radial and transverse direction	• Stated that the distribution of the material properties can significantly affect the impact responses of the two-directionally-graded plates
Gunes et al. [33]	• Experimental and numerical investigation on the responses of FG clamped circular plates composed of ceramic (SiC) and metal (Al) phases varying through the plate thickness subjected to impact by using a drop weight impact test system	• The compositional gradient exponent considerably affected the impact response of the FG circular plates • Hence, the peak contact force increased and the after-impact impressions got narrower with increase in the compositional gradient exponent

(continued)

Table 3 (continued)

Author	Study	Main Findings
Singh et al. [34]	• Studied the low velocity impact response behaviour of aluminium-zirconia FG plates, such as plate displacement, contact force, impactor displacement, and velocity of impactor with respect to time using modified Hertzian contact law and power law • Effects of oblique impact angle and twist angle were studied	• Peak value of contact force intensified as the twist angle increased for a particular material property graded index whereas the peak value of contact force reduced gradually as the angle of oblique impact increased
Lai et al. [35]	• Resistance of a Functionally graded cementitious composite (FGCC),with an anti-penetration layer and crack resistance layer made of ultra high performance coarse aggregate concrete and ultra-high performance steel fiber reinforced concrete respectively, against repeated penetration were done • The FGCC was prepared by varying the distribution of high strength fibers and aggregates	• The penetration depth, crater area and penetration damage decreased greatly due to the synergistic effects of high strength fibers and coarse aggregates
Lai et al. [36]	• Three-layer FGCC consisting of crack resistance layer, spalling resistance layer and anti-penetration layer composed of ultra-high performance hybrid fiber reinforced concrete, ultra high performance steel fiber reinforced concrete and ultra-high performance coarse aggregate concrete respectively, with different content of high strength fibers and coarse aggregates were studied	• Cracking, penetration and spalling of concrete targets were controlled by the synergistic effects of the three different layers • FGCC target with three layers of different concretes had the advantages of both smaller crater area and lower penetration depth

the field of impact on FGM and their findings are tabulated. It would provide a brief summary of the work done in this area.

There is a need for more research into the impact and blast characteristics of FGMs. From the researches considered in this focused review paper, it can be seen that FGMs tend to show better performance than their homogeneous counterparts. FGM specimens have been found to show lower penetration depth, crater area and penetration damage in general. Hence these can be seen as a potential material for impact and blast resistant structures, but more study on this aspect and their potential needs to be exploited.

5 Summary

A brief but focused review of literature on application of FGMs and FG structures for specific purposes has been presented in this paper. In functionally graded materials the mechanical properties such as Young's modulus, poisson's ratio, mass density etc. varies continuously across a preferred direction. Various gradation laws such as power law, exponential law and sigmoid law can be used to define this variation. The diverse fields of application of FGMs were addressed in this paper. FGMs have been beneficially utilized in high temperature application, automobiles, nuclear reactors, biomedical etc. Its application into structural engineering field are scrutinized. Few works on the study of vibration characteristics of FGM were examined. Impact characteristics of FGM is an area which is still not explored much. Research works on the impact characteristics of FGM were reviewed. From the literatures it can be seen that FGMs have better performance than their homogeneous and composite counterparts when subjected to impacts. Studies show that FG-panel design can be improved by the incorporation of thicker high energy absorption materials at the impact face or a layer of PE fibrous ferrocement. Also, FG cores can be effectively used to mitigate impact damage in sandwich composites. Synergetic effects of high strength fibers and coarse aggregates have been reported to provide better impact resistance. But more in-depth and rigorous study of the impact and blast resistant characteristics of FGM are needed to enhance their potential to be used in protective structures.

Acknowledgements This paper is being published with the kind permission of the Director, CSIR-Structural Engineering Research Centre, Chennai.

References

1. Ebrahimi F (2016) Advances in functionally graded materials and structures
2. Jha DK, Kant T, Singh RK (2013) A critical review of recent research on functionally graded plates. Compos Struct 96:833–849

3. Sharma NK, Bhandari M, Ashirvad. Applications of Functionally Graded Materials (FGMs). IJERT 334–339
4. Shen HS (2009) Functionally graded materials-nonlinear analysis of plates and shells. CRC Press
5. Mahamood RM, Akinlabi ET, Shukla M, Pityana S (2012) Functionally graded material : an overview, vol III, pp 1–5
6. EL-Wazery MS, EL-Desouky AR (2015) A review on functionally graded ceramic-metal materials. Mater Environ Sci 6(5):1369–1376
7. Gupta, Talha M (2015) Recent development in modeling and analysis of functionally graded materials and structures. Prog Aerosp Sci 1–14
8. Tanaka K, Tanaka Y, Watanabe H, Poterasu VF, Sugano Y (1993) An improved solution to thermoelastic material design in functionally gradient materials: scheme to reduce thermal stresses. Comput Methods Appl Mech Eng 109:377–389
9. Tanaka K, Tanaka Y, Enomoto K, Poterasu VF, Sugano Y (1993) Design of thermoelastic materials using direct sensitivity and optimization methods. Reduction of thermal stresses in functionally gradient materials. Comput Methods Appl Mech Eng 106:271–284
10. Yin HM, Sun LZ, Paulino GH (2004) Micromechanics-based elastic model for functionally graded materials with particle interactions. Acta Mater 52:3535–3543
11. Shen HS, Wang ZX (2012) Assessment of Voigt and Mori—Tanaka models for vibration analysis of functionally graded plates. Compos Struct 94(7):2197–2208
12. Nguyen TK (2014) Analysis of the effect of the homogenization methods on the shear correction factor of functionally graded beams. IJERT 3(9):1458–1461
13. Khan T, Zhang N, Akram A (2019) State of the art review of functionally graded materials. In: International conference on computing, mathematics and engineering technologies
14. Chi SH, Chung YL (2006) Mechanical behavior of functionally graded material plates under transverse load-Part I: analysis. Int J Solids Struct 43:3657–3674
15. Mahamood RM, Akinlabi ET (2017) Functionally graded materials. Springer, Heidelberg
16. Miyamoto Y, Shiota I (1996) Functionally graded materials. In: Proceedings of the 4th international symposium on functionally graded materials, Japan
17. Zhang Y, Sun M, Zhang D (2012) Designing functionally graded materials with superior load-bearing properties. Acta Biomater 8(3):1101–1108
18. Birman V, Byrd LW (2007) Modeling and analysis of functionally graded materials. ASME 60:195–216
19. Reddy JN (2007) Theory and analysis of elastic plates and shells. CRC Press
20. Reddy JN (2000) Analysis of functionally graded plates. Int J Numerical Methods Eng 47:663–684
21. Reissner E (1942) On the theory of bending of elastic plates. Bull Am Math Soc 48:184–191
22. Zenkour AM (2006) Generalized shear deformation theory for bending analysis of functionally graded plates. Appl Math Model 30:67–84
23. Taj MNAG, Chakrabarti A, Sheikh AH (2013) Analysis of functionally graded plates using higher order shear deformation theory. Appl Math Model 37:8484–8494
24. Cheng ZQ, Batra RC (2000) Exact correspondence between eigenvalues of members and functionally graded simply supported polygonal plates. J Sound Vib 229(4):879–895
25. Yang J, Shen H-S (2002) Vibration characteristics and transient response of shear-deformable functionally graded plates in thermal environments. J Sound Vib 255(3):579–602
26. Vel SS, Batra RC (2004) Three-dimensional exact solution for the vibration of functionally graded rectangular plates. J Sound Vib 272:703–730
27. Liu DY, Wang CY, Chen WQ (2010) Free vibration of FGM plates with in-plane material inhomogeneity. Compos Struct 92: 1047–1051
28. Lee JK, Lee BK (2019) Free vibration and buckling of tapered columns made of axially functionally graded materials. Appl Math Modell 75:73–87
29. Apetre NA, Sankar BV, Ambur DR (2006) Low-velocity impact response of sandwich beams with functionally graded core. Int J Solids Struct 43:2479–2496

30. Quek ST, Lin VWJ, Maalej M (2010) Development of functionally-graded cementitious panel against high-velocity small projectile impact. Int J Impact Eng 37(8):928–941
31. Yalamanchili VK, Sankar BV (2012) Indentation of functionally graded beams and its application to low-velocity impact response. Compos Sci Technol 72(16):1989–1994
32. Shariyat M, Jafari R (2013) Nonlinear low-velocity impact response analysis of a radially preloaded two-directional-functionally graded circular plate: a refined contact stiffness approach. Compos Part B 45:981–994
33. Gunes R, Aydin M, Apalak MK, Reddy JN (2014) Experimental and numerical investigations of low velocity impact on functionally graded circular plates. Compos Part B 59:21–32
34. Singh H, Hazarika B, Dey S (2017) Low velocity impact responses of functionally graded plates. Proc Eng 173:264–270
35. Lai J, Wang H, Yang H, Zheng X, Wang Q (2017) Dynamic properties and SPH simulation of functionally graded cementitious composite subjected to repeated penetration. Constr Build Mater 146:54–65
36. Lai J, Yang H, Wang H, Zheng X, Wang Q (2019) Penetration experiments and simulation of three-layer functionally graded cementitious composite subjected to multiple projectile impacts. Constr Build Mater 196:499–511

Efficient Utilization of Recycled Concrete Aggregates for Structural Applications—An Experimental Study

Jagan Sivamani, T. R. Neelakantan, P. Saravana Kumar, C. Mugesh Kanna, H. Vignesh Harish, and M. R. Akash

Abstract Utilization of recycled concrete aggregates as an alternative material for natural aggregates in concrete have been of greater importance due to its disposal problems followed by the problem on scarcity in construction materials namely aggregates. This paper presents a study on the mechanical properties of concrete manufactured with recycled aggregates collected from a 10 year old demolished building at the institute. Recycled aggregates were immersed in water for 24 h before its utilization in concrete to achieve surface saturated dry density. A total of 8 batches of Recycled Aggregate Concrete and 2 batches of Normal Aggregate Concrete under different replacement levels of 0%, 10%, 20%, 30% and 40% and at two w/c ratios of 0.45 and 0.5 were manufactured. Various parametric tests such as compressive strength, split tensile strength, flexural strength and elastic modulus were performed to study its mechanical properties at the age of 7 days and 28 days. Results indicate that the mechanical properties of RAC was greatly influenced by the w/c ratio as the pre-saturation of recycled aggregates for 24 h prior to manufacturing yielded better strength even at 0.45w/c ratio and at 30% replacement.

Keywords Recycled aggregate concrete · Recycled aggregates · W/c ratio · Mechanical properties · Surface saturated dry · Density

J. Sivamani (✉) · T. R. Neelakantan · C. Mugesh Kanna · H. Vignesh Harish · M. R. Akash
School of Environmental and Construction Technology, Kalasalingam Academy of Research and Education, Anand Nagar, Krishnankoil, Tamilnadu 626126, India
e-mail: s.jagan@klu.ac.in

P. Saravana Kumar
Department of Civil Engineering, Sri Krishna College of Engineering and Technology, Krishnankoil, Coimbatore, Tamilnadu 641008, India

© Springer Nature Switzerland AG 2021

K. Dasgupta et al. (eds.), *Proceedings of SECON 2020*,
Lecture Notes in Civil Engineering 97,
https://doi.org/10.1007/978-3-030-55115-5_52

1 Introduction

Concrete is the most widely used material by the construction industry, which is the mixture of cement, fine aggregate, coarse aggregate and water. Among them, aggregates consume nearly 60–70% of total volume of concrete [1]. Aggregates are inert, granular materials used as a binding medium in the concrete. Current estimates on the global demand for the aggregates in construction industries rose up to 20 billion tons per annum [2, 3]. Construction industries acquire natural resources as their source of raw materials mostly aggregates which leads to depletion of natural resource. Parallely, construction industries generate wastes as a result of retrofitting, rehabilitation and demolition of constructed structures known as Construction & Demolition (C&D) wastes. C&D wastes are being dumped locally nearby the sites of generation or being utilized as materials to fill up the pits near by the roadside. In recent years, owing to increased demand on aggregates, C&D wastes generated as a result of demolition of buildings have been used as alternative material for aggregates in structural applications reducing its environmental impact. Such C&D wastes used as aggregates in concrete either partial/full substitution to Natural Aggregates (NA) ended up in the manufacture of new era of concrete as "Recycled Aggregate Concrete (RAC)". Though RAC has positive environmental benefits, poor quality of Recycled Concrete Aggregates (RCA) imposed limitation on its percentage of utilization in concrete.

Various factors contribute to the poor quality of RCA are adhered mortar content, density, method of recycling, water absorption, gradation, crushing and abrasion resistance and specific gravity [4–12]. From the above mentioned factors, presence of adhered mortar is the important factor responsible for the poor quality of RCA [13–15]. Adhered mortars present on the surface of RA are highly porous with micro-cracks resulting in higher water absorption and weaker Interfacial Transition Zone (ITZ). This in turn reduces the mechanical and durability properties of concrete limiting its structural applications. Also, percentage on replacement of NA with RCA depends on quality and strength of parent concrete as RCA collected from a high strength building results in better quality than those collected from a low strength building [13, 16, 17]. Some studies limit the utilization of RCA to 25% [18], while other limits it till 40% [19]. Apart from the quality of parent concrete, reduction in w/c ratio of concrete can improve the strength of RAC even at higher percentages of replacement [16, 19, 20]. Upon reduction in w/c ratio, highest compressive strength of 83 MPa was achieved at 28 days upon 100% utilization of RCA as NA in concrete [16]. Various studies on RAC summarizes that no predictive equation can be arrived through any correlative analysis for RAC as the strength depends on various factors such as age of concrete, quality of parent concrete, quantity of adhered mortar, recycling techniques etc. But one parameter strengthens the poor quality of RCA for its utilization in concrete is the w/c ratio. Optimal w/c ratio in the manufacture of RAC can result in better mechanical properties even at higher percentages of replacement. The present study involves the behaviour of RAC with variation in w/c ratio under different percentage of replacements of RA. The first phase of the study

involves the mechanical behaviour of RAC at 0.5w/c ratios with 0%, 10%, 20%, 30% and 40% of RA. The second phase involves the mechanical behaviour of RAC at 0.45w/c ratios with 0%, 10%, 20%, 30% and 40% of RA.

2 Experimental Work

Ordinary Portland cement of 43 grade [21], river sand of size 2.36 mm and crushed gravel passing through 20 mm sieve [22, 23] were used to manufacture the concrete. Recycled Aggregates (RA) were collected from a 10 year old demolished building at the institute, crushed to varying size from 10 to 20 mm by series of crushers, and were used by replacing different contents (0%, 10%, 20%, 30% and 40%) of Natural Aggregate (NA). Potable water confirming to IS 456:2000 [24] was also used. Physical properties of crushed RA were tested in accordance with IS 2386:1989 [22] and presented in Table 1. A total of 10 concrete mixtures confirming to IS 10262:2009 [25] were manufactured at 0.45w/c and 0.5w/c ratio and the mechanical properties of concrete like compressive strength, split tensile strength, flexural strength and Elastic modulus were studied at the age of 7 days and 28 days in accordance with IS 516: 1959 [26]. RA were immersed in water for 24 h and dried before its utilization in concrete to achieve Surface Saturated Dry Density (SSD) condition. Mix proportions adopted for the casting of specimens was presented in the Table 2. All the 10 concrete mixes under different levels of replacement and at different w/c ratio were subjected to Normal mixing wherein cement, fine aggregate, NA, RA and water were mixed for 120 s. Process of concrete casting and testing of the casted specimens was presented in the Fig. 1. Prepared concrete mixture were moulded in cubical moulds of size 150 mm × 150 mm × 150 mm, cylindrical moulds of size 150 mm × 300 mm and

Table 1 Physical property on Ingredients of concrete

No	Description of the test	Values	BIS limits
1	Specific Gravity of cement	3.15	3.1–3.16
2	Specific Gravity of fine aggregate	2.64	2.5–3
3	Fineness modulus of fine aggregate	2.31	2–3.5
4	Specific Gravity of NA	2.70	2–3
5	Fineness modulus of NA	6.74	<15
6	Specific Gravity of RA	2.65	2–3
7	Impact value of RA (%)	18.43	<45%
8	Crushing value of RA (%)	14.61	<45%
9	Fineness modulus of RA	7.47	<15
10	Water Absorption of RA (%)	5.32	<3%
11	Abrasion value of NA (%)	26.31	<45%
12	Abrasion value of RA (%)	38.42	<45%

Table 2 Mix proportions

No	Mix ID	Mix Details	Cement (kg/m^3)	F.A (kg/m^3)	C.A (kg/m^3)	Water (kg/m^3)
1	0.5 N	NAC at 0.5w/c	372	829	1015	186
2	0.45 N	NAC at 0.45w/c	372	829	1015	186
3	0.5 R_1	RAC at 0.5w/c (10% RA)	372	829	1015	186
4	0.5 R_2	RAC at 0.5w/c (20% RA)	372	829	1015	186
5	0.5 R_3	RAC at 0.5w/c (30% RA)	372	829	1015	186
6	0.5 R_4	RAC at 0.5w/c (40% RA)	372	829	1015	186
7	0.45 R_1	RAC at 0.45w/c (10% RA)	413	799	1029	186
8	0.45 R_2	RAC at 0.45w/c (20% RA)	413	799	1029	186
9	0.45 R_3	RAC at 0.45w/c (30% RA)	413	799	1029	186
10	0.45 R_4	RAC at 0.45w/c (40% RA)	413	799	1029	186

prism moulds of size 500 mm × 100 mm × 100 mm, allowed drying for 24 h, and cured in water at room temperature for 7 days and 28 days to study its mechanical properties. Results of the mechanical properties of hardened concrete at the age of 7 days and 28 days were presented in the Table 3.

3 Results and Discussions

3.1 Properties of RA

Property test on RA performed in accordance with IS 2386: 1989 satisfied the BIS limits for its utilization in concrete, except the property of water absorption. Other properties of RA falls within the BIS limits but was lesser compared to those of NA. Specific gravity of RA was 1.85% lesser compared to NA and water absorption is 40% more compared to NA. This attribute is due to the adhered mortar on the surface of the RA with micro-cracks which absorbs more water (1–25). Also the property of parent concrete plays a vital in the strength of RAC [4, 16]. Other characteristics like impact strength and crushing strength was found to be 59% and 67% lesser compared to NA but falls within the BIS for its utilization in concrete. This is due to the separation and alluring of adhered mortar on the surface of RA [27]. Conversely,

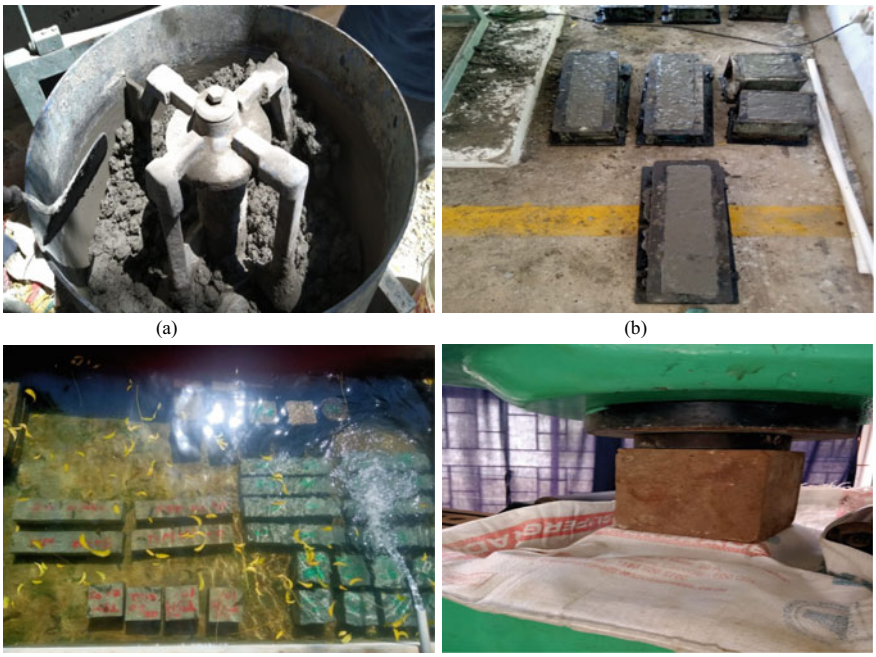

(a) (b)

(c) (d)

Fig. 1 Casting and testing of concrete specimens

Table 3 Mix proportions

No	Mix ID	Compressive strength (N/mm^2)		Split tensile strength (N/mm^2)		Flexural strength (N/mm^2)		Elastic modulus (N/mm^2)28 days
		7 days	28 days	7 days	28 days	7 days	28 days	
1	0.5 N	22.61	33.52	2.42	4.04	2.71	4.05	28948.2
2	0.45 N	26.45	39.26	2.74	4.56	2.94	4.39	31328.9
3	0.5 R_1	23.31	34.79	2.48	4.36	2.75	4.22	29491.6
4	0.5 R_2	23.69	35.59	2.52	4.45	2.79	4.3	29874.3
5	0.5 R_3	24.43	37.26	2.56	4.54	2.84	4.41	30517.5
6	0.5 R_4	23.57	35.18	2.49	4.41	2.77	4.28	29654.4
7	0.45 R_1	27.78	41.34	2.85	4.77	3.06	4.51	32148.5
8	0.45 R_2	28.71	42.13	2.93	4.89	3.08	4.54	32453.1
9	0.45 R_3	30.32	45.93	3.06	5.11	3.11	4.69	33885.8
10	0.45 R_4	28.15	42.01	2.89	4.82	3.03	4.53	32407.1

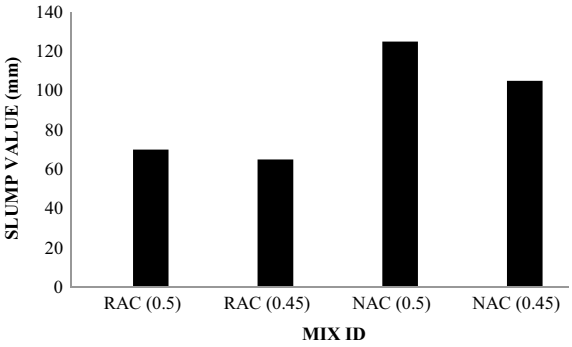

Fig. 2 Slump of concrete mixtures

the property of water absorption was overcome by immersing the RA in water for 24 h and drying it to maintain SSD before its mixing in concrete.

3.2 Fresh Property of Concrete

The workability of fresh concrete mixes for both NAC and RAC under both w/c ratios was performed using slump cone tests and results are presented in Fig. 2. The slump of 125 mm was achieved by the NA approach at 0.5w/c ratio, whereas the slump value by the RAC was found to be 70 mm at 0.5w/c ratio. Similarly, at 0.45w/c ratio, slump value by NAC and RAC was found to be 105 and 65 mm. This attribute is due to the rough texture of RA and its higher water demand compared to NA [28, 29]. Adhered mortar present on the surface of RA is highly porous, increasing the water demand required for achieving the optimal concrete mix.

3.3 Mechanical Properties of RAC

3.3.1 Effect of W/C Ratio on the Mechanical Properties of RAC

Variations in the strength of RAC under both the w/c ratios were presented in Fig. 3. The maximum compressive strength of 45.93 MPa was achieved which is ample for structural applications. Compressive strength of 0.45 N is 14.62% more compared to the strength of 0.5 N. At 10% replacement level, compressive strength of $0.45R_1$ was 15.84% more compared to RAC at $0.5R_1$; at 20% replacement level, compressive strength of RAC at $0.45R_2$ was 15.52% more compared to RAC at $0.5R_2$; at 30% replacement level, compressive strength of RAC at $0.45R_3$ was 18.87% more compared to $0.5R_3$; at 40% replacement level, compressive strength of $0.45R_4$ was 16.25% more compared to $0.5R_4$. Maximum improvement in the strength of RAC was achieved at $0.45R_3$ beyond which it causes the decrease in the strength. This

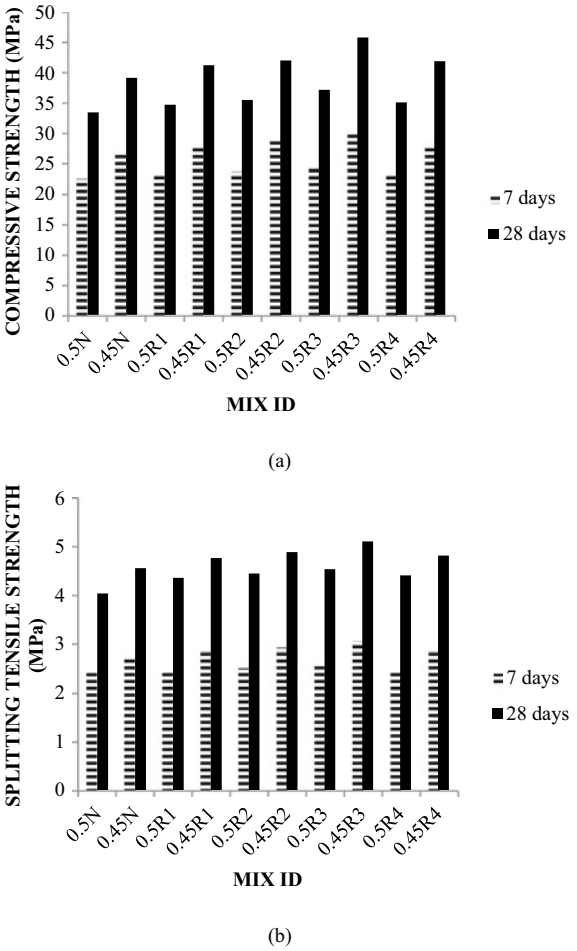

Fig. 3 Variation in mechanical properties upon effect of w/c ratios

may be due to fact that the amount of free water required for cement hydration was absorbed by the adhered mortar on the surface of RA causing decrease in the workability thereby reducing the strength beyond 30% of replacement [19]. Strength of ITZ mainly depends on the effective w/c ratio which decides the strength of RAC. As we know, NAC has only one ITZ, whereas RAC has two ITZ i.e., one between the NA and adhered mortar and other between the adhered mortar and new ITZ. At 0.5w/c, new ITZ which governs the strength of RAC becomes weaker and cracks impound near the surface of new ITZ. At 0.45w/c, new ITZ which governs the strength of RAC becomes stronger compared to old ITZ thereby increasing the strength of RAC compared to 0.5w/c at 30% replacement level [30, 31]. This was also evident through the experimental findings of [32] wherein the strength of mortar as a deciding factor for concrete strength can be achieved through concrete manufactured at lower w/c ratio.

Fig. 3 (continued)

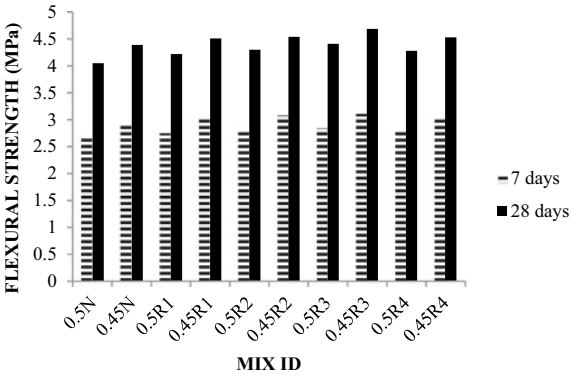

(c)

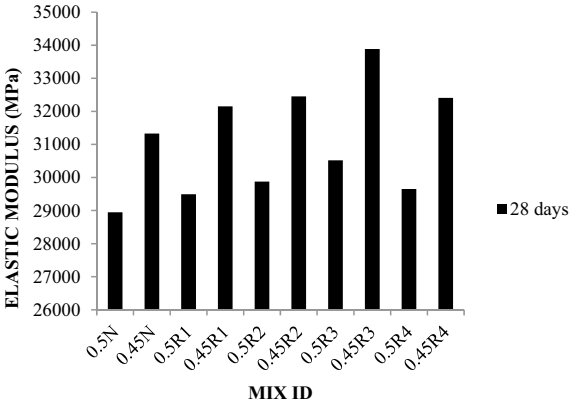

(d)

With respect to the study on the elastic modulus, $0.45M_3$ achieved the higher elastic modulus of 33885.8 MPa at the age of 28 days which is 7.54% more compared to 0.45 N and 14.57% more compared to 0.5 N. Elastic modulus of the concrete depends mainly on the volumetric proportions of cement paste and aggregates. As we know the elastic modulus of aggregates is higher compared to cement paste, reduced level of replacement will tend to increase the volumes of aggregates in concrete. Furthermore, porous nature of such increased RA in concrete tends to reduce its elastic modulus; as a result of which elastic modulus of NA and hardened cement paste will be more compared to the elastic modulus of RA and hardened cement paste [33, 34].

3.3.2 Effect of Replacement on the Mechanical Properties of RAC

Variations in the strength of RAC upon different levels of replacement were presented in Fig. 4. At 0.5w/c, compressive strength of R_3 was 10.37% more compared to 0.5 N, 6.62% more compared to R_2, 4.42% more compared to R_1 and 5.58% more compared to R_4. At 0.45w/c, compressive strength of R_3 was 14.52% more compared to 0.45 N, 10% more compared to R_2, 8.27% more compared to R_1 and 8.53% more compared to R_4. On comparison among w/c ratios, the compressive strength of 0.45 N is 14.62% more compared to 0.5 N. In this study, scenario of reduction in w/c ratio yielding higher strength was intensified by the increase in the level of replacement of RA. Increase in the level of replacement of RA beyond 30% resulted in reduction in the strength of RAC at both 7 days and 28 days for both w/c ratios. This is due to the porous nature of adhered mortar, effectiveness of w/c ratio and weakness of the new

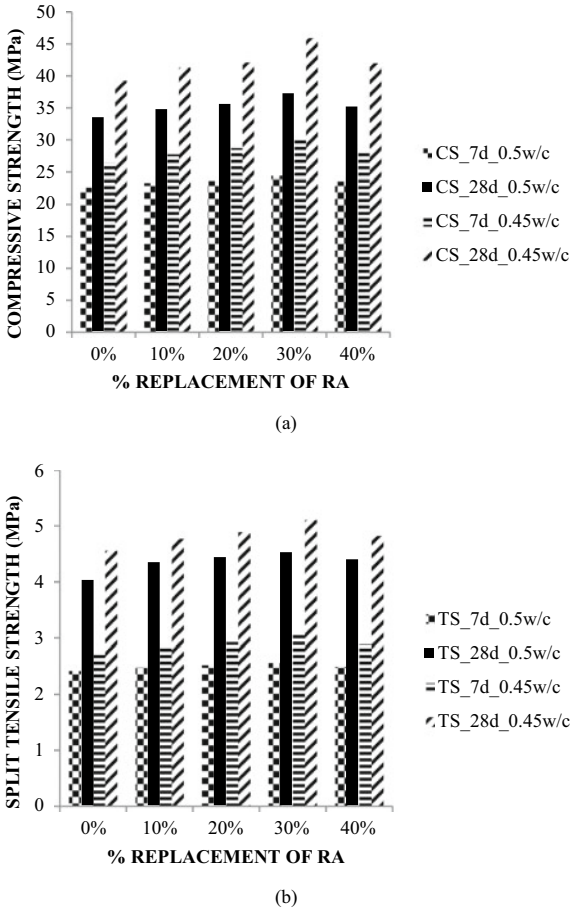

Fig. 4 Variation in mechanical properties of RAC upon effect of replacement levels

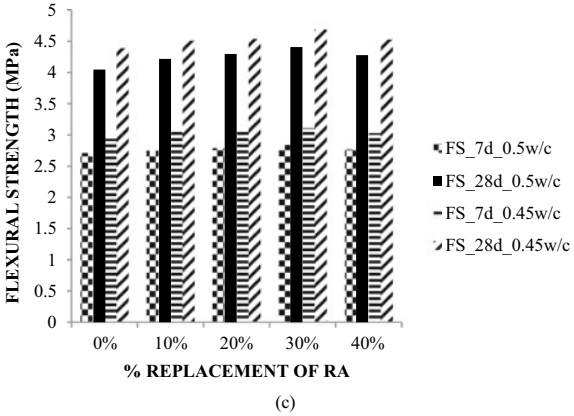

(c)

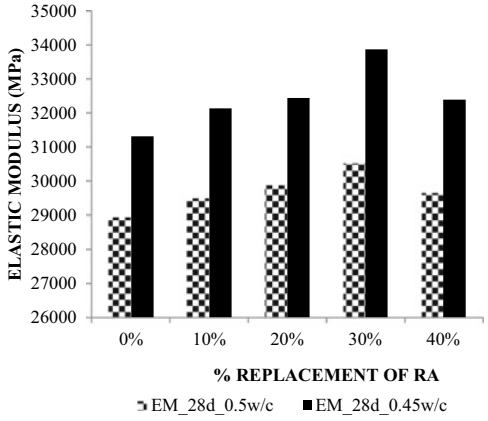

(d)

Fig. 4 (continued)

ITZ formed in RAC [19, 30, 31, 34]. All these factors contribute to the reduction in the strength of RAC upon increase in the level of replacement confining it to 30%. With respect to elastic modulus, upon higher percentage of replacement beyond 30%, percentage of porosity in the volume of aggregates gets increased and thereby the resistivity of the adhered mortar to cracking gets reduced resulting in reduction in the modulus of elasticity of RAC [33, 34].

4 Conclusions

This study involves a realistic approach on the levels of replacement of RA with NA in concrete and the impacts of RA on the mechanical properties of concrete under

different w/c ratios. Inspite of its several drawbacks such as source, quality of parent concrete, adhered mortar, porosity, RA served its intended purpose in achieving the utilization in concrete upon nominal percentages of replacement. Major drawback of higher adsorptive nature of RA, it is immersed in water for 24 h to achieve SSD before its utilization in concrete mix. Mechanical properties were investigated under 0.45w/c and 0.5w/c at 7 days and 28 days to study its level of utilization in structural applications. RA can be replaced up to 30% by weight of NA in concrete under 0.45w/c to achieve the maximum strength of 45.93 MPa at the age of 28 days which is ample for structural applications. Also the elastic modulus of RAC under 30% replacements at 0.45w/c tends to be 14.57% more compared to NAC. Replacement of RA beyond 30% and w/c ratio greater than 0.45 reduces its mechanical properties due to the higher porosity of adhered mortar, weakness of ITZ and the lesser resistivity of adhered mortar to cracking. Also other crucial factors such as quality of parent concrete, stages of recycling, mixing approaches may tend to vary the levels of replacement of RA in concrete [16, 21, 29, 35, 36]. On set of scales as a result of study and previous findings, it could be inferred RA material is a better option of utilization as replacement to NA in concrete overwhelming the problems on scarcity of aggregates and disposal problems of C&D wastes. Further research may be prolonged on treatments to RA to remove the adhered mortar on its surface and by varying the mixing approaches to improve the performance of RAC and to extent its utilization in various structural members.

References

1. Kosmatka SH, Kerkhoff B, Panarese WC (2002) Design and control of concrete mixtures. Portland cement Associations, Washington DC
2. Radonjanin V, Malesev M, Marinkovic SB, Saed Al Malty AE (2013) Green recycled aggregate concrete. Constr Build Mater 47
3. Cakir O (2014) Experimental analysis of properties of recycled coarse aggregate (RCA) concrete with mineral additives. Constr Build Mater 68
4. Hansen TC, Narud H (1983) Strength of recycled concrete made from crushed concrete coarse aggregate. Concr Int 5
5. Xu YZ, Shi JQ (2006) Analyses and evaluation of the behavior of recycled aggregate and recycled concrete. Concrete 7
6. Hansen TC, Boegh E (1985) Elasticity and drying shrinkage concrete of recycled-aggregate. In: Journal Proceedings, vol 82
7. Katz A (2005) Properties of concrete made with recycled aggregate from partially hydrated old concrete. Cement Concr Res 33. https://doi.org/10.1016/S0008-8846(02)01033-5
8. Shayan A, Xu A (2003) Performance and properties of structural concrete made with recycled concrete aggregate. ACI Mater J 100
9. Tavakoli M, Soroushian P (1996) Strengths of aggregate concrete made using field-demolished concrete as aggregate. ACI Mater J 93
10. Prasad MLV, Rathish Kumar P (2007) Strength studies on glass fiber reinforced recycled aggregate concrete. Asian J Civil Eng (Build Housing) 8
11. Juan MS, Gutiérrez PA (2009) Study on the influence of attached mortar content on the properties of recycled concrete aggregate. Constr Build Mater 23. https://doi.org/10.1016/j.conbuildmat.2008.04.012

12. Exteberria M, Vasquez F, Mari AR (2007) Influence of amount of recycled coarse aggregates and production process on properties of recycled aggregate concrete. Cement Concr Res 37. https://doi.org/10.1016/j.cemconres.2007.02.002
13. Abdulla NA (2014) Effect of recycled coarse aggregate type on concrete. J Mater Civil Eng 27. https://doi.org/10.1061/(ASCE)MT.1943-5533.0001247
14. Larrard F (1999) Concrete mixture proportioning: a scientific approach. CRC Press, London, UK
15. Wong VK, Chan W, Kwan AKH (2013) Applying theories of particle packing and rheology to concrete for sustainable development. Organ Technol Manage Constr Int J 5. https://doi.org/10.5592/otmcj.2013.2.3
16. Abrahams M, Rakesh R (2018) Manufacturing concrete with high compressive strength using recycled aggregates. J Mater Civil Eng 30. https://doi.org/10.1061/(ASCE)MT.1943-5533.0002398
17. Huda SB, Alam MS (2014) Mechanical behavior of three generations of 100% repeated recycled coarse aggregate concrete. Constr Build Mater 65. http://dx.doi.org/10.1016/j.conbuildmat.2014.05.010
18. Ozbakkaloglu T, Gholampour A, Xie T (2018) Mechanical and durability properties of recycled aggregate concrete: effect of recycled aggregate properties and content. J Mater Civil Eng 30. https://doi.org/10.1061/(ASCE)MT.1943-5533.0002142
19. Ho NY, Yang PKL, Wee FL, Tarek Z, Keat CC, Giau LL, Seng KT (2013) Efficient utilization of recycled concrete aggregate in structural concrete. J Mater Civil Eng 25. https://doi.org/10.1061/(ASCE)MT.1943-5533.0000587
20. Akcaoglu T, Tokyay M, Celik T (2004) Effect of coarse aggregate size and matrix quality on ITZ and failure behavior of concrete under uniaxial compression. Cement Concr Compos 26. https://doi.org/10.1016/S0958-9465(03)00092-1
21. IS 269 (1989) Specifications for ordinary Portland cement
22. IS 2386 (1989) Methods for test for aggregates for concrete
23. IS 383 (2016) Specifications for coarse and fine Aggregates for concrete
24. IS. 456 (2000) (Reaffirmed 2005)—Plain and reinforced concrete (Fourth Revision) Tenth Reprint Bureau of Indian standards, New Delhi
25. IS 10262 (2009) Guidelines for concrete mix design
26. IS 516 (1959) Methods of test for strength of concrete (Reprint 2006) Bureau of Indian standards, New Delhi
27. Saravanakumar P, Dhinakaran G (2014) Mechanical and durability properties of slag based recycled aggregate concrete. IJST Trans Civil Eng 39. http://dx.doi.org/10.22099/ijstc.2015.3134
28. Revathi P, Amirthavalli RR, Lavanya K (2014) Influence of treatment methods on the strength and performance characteristics of recycled aggregate concrete. J Mater Civil Eng 27. https://doi.org/10.1061/(ASCE)MT.1943-5533.0001128
29. Liang YC, Ye ZM, Vernerey F, Xi Y (2013) Development of processing methods to improve strength of concrete with 100% recycled coarse aggregate. J Mater Civil Eng 27. https://doi.org/10.1061/(ASCE)MT.1943-5533.0000909
30. Ryu JS (2002) Improvement on strength and impermeability of recycled concrete made from crushed concrete coarse aggregate. J Mater Sci Lett 21
31. Otsuki N, Miyazato SI, Yodsudjai W (2003) Influence of recycled aggregate on interfacial transition zone, strength, chloride penetration and carbonation of concrete. J Mater Civil Eng 15. https://doi.org/10.1061/(ASCE)0899-1561(2003)15:5(443)
32. Neville AM (2003) Properties of concrete, 5th edition. Pearson Education Limited, England
33. Young JF, Mindess S, Gray RJ, Bentur A (1998) The science and technology of civil engineering materials. Prentice Hall, Upper Saddle River, NJ
34. Neville AM (1995) Properties of concrete. Prentice Hall, Harlow, UK
35. Zhen-Hua D, Chi-Sun P (2014) Properties of recycled aggregate concrete made with recycled aggregates with different amounts of old adhered mortars. Mater Des 58. https://doi.org/10.1016/j.matdes.2014.01.044

36. Saravanakumar P, Abhiram K, Manoj B (2016) Properties of treated recycled aggregates and its influence on concrete strength characteristics. Constr Build Mater 111. https://doi.org/10.1016/j.conbuildmat.2016.02.064

Evaluation of Strength and Diffusion Capability of High Volume Fly Ash Based Engineered Cementitious Composites Incorporating Powder Scrap Rubber

Abhishank Kumar, Shashi Kant Sharma, and Davinder Singh

Abstract Rigid pavements need overlays for their rehabilitation, which are constituted of fine materials and fibres. The present study is focused on yielding overlays made of engineered cementitious composite containing polypropylene (PP) fibres and high volume fly ash. Scrap rubber has been used as a replacement of fine aggregates @ 10, 20, 30 per cent for improving the straining tendency and bending ability of concrete. The strength of 40 MPa has been targeted. Since the composite is made up of fine materials, therefore the durability has been evaluated in terms of rapid chloride ion penetration and not permeability. This test measures the diffusion capacity of rainwater containing chlorides into the concrete which indicates the corrosion potential of continuous reinforcement. It was found that a composite having fly ash/cement ratio 1.2/1, along with 1.5% polypropylene fibre reinforcement (vol./vol. of concrete) shows a minimal reduction in compressive strength i.e. up to 25 per cent on 30 per cent w/w replacement of fine aggregates with powder scrap rubber but the main aspect is that the diffusion rate shows appreciable decrement with an increase in fine rubber content when compared with the 4 m MPa normal mix which ensures lesser chance of corrosion in reinforcement at joints.

Keywords Engineered cementitious composite · Polypropylene fibres · Rapid chloride ion penetration · Scrap rubber

A. Kumar (✉) · S. K. Sharma · D. Singh
Department of Civil Engineering, NIT Jalandhar, Jalandhar 144001, India
e-mail: abhishank726@gmail.com

S. K. Sharma
e-mail: sharmask@nitj.ac.in

D. Singh
e-mail: singhdj@nitj.ac.in

© Springer Nature Switzerland AG 2021

K. Dasgupta et al. (eds.), *Proceedings of SECON 2020*,
Lecture Notes in Civil Engineering 97,
https://doi.org/10.1007/978-3-030-55115-5_53

1 Introduction

One of the major developments that took place in the concrete industry in early 2000s is composites. One of them is termed as Engineered Cementitious Composites or abbreviated as ECC [1] that has a distinct bending character. An ECC being a fibre reinforced composite shows ductile behaviour when its micromechanics of the fibre-matrix bond are attained by virtue of its mix proportion [2]. Now being a composite, it should have some mechanical properties and durability characteristics that can withstand loading behaviour and environmental actions [3]. The strain capacity of ECC is far more better than the conventional concrete and its crack width generally grows less than 60 μm when the composites are nourished well to counter the tough mechanical and durable conditions [4]. Due to these unique properties of this composite, it has found its application in earthquake resistant frames and in road construction as overlays mainly. One of such features is the diffusion capability of a composite material which should be discussed along with the standard compressive strength test against the normal concrete of strength 40 MPa. Diffusion capability is the ability of the material to sustain penetration of harmful material such as chloride and sulphate etc. into the structures manifold area such as steel bars and other reinforced type structures [5]. The use of high volume fly ash as a secondary cementitious material (SCM) not only shows the reduction in carbon dioxide emission and slowing greenhouse gas emission rate but also helping in increasing the service life of the structures came into existence with ECC under unfavourable conditions [6, 7]. Powder scrap rubber from the rubber industry is found very difficult to be dumped keeping environmental violations in mind. However, the enormous pollution caused by amount of smoke during incineration makes this process so unacceptable that it is prohibited by law in many countries [8]. After the addition of scrap rubber powder, the overall research results indicated a remarkable variation in strength and stiffness behaviour of the concrete. Despite the significant decline in the strength properties, ECC still satisfy the basic requirements of building materials [9].With such tiny voids in ECC, the chloride diffusion properties were found to be nearly the same as that of sound concrete [4, 10]. Further, ECC used in overlays in rigid pavement makes it to bear climatic conditions like rainfall which contains chlorides, sulphates and other chemicals with it. Also in some places where groundwater has chlorine deposits in that region the chance of chlorides to percolate is maximum. In this present study the ECC with high volume pozzolanic cementitious material is being tested in comparison with the Standard normal concrete mix on the basis of strength and chloride penetration rate. Moreover comparison on the basis of strength after the chloride ion penetration of different rubberised ECC (Zhang et al. 2015) is performed in this present study.

2 Materials and Methods

2.1 Materials and Composition

In this study, we have gone with OPC (ordinary Portland cement) grade 43 which follows IS:8112-1989 [11]. The next main component used for substitution of cement on large scale is material with enormous pozzolanic characteristics Fly ash. It has been successfully used on a large scale to limit the use of the cement and also to provide definite flow characteristics to the cementitious composite material. Tables 1 and 2 depicts the necessary compositions of the cementitious powder ingredients used in this study.

Fine river silica sand from river Beas as its source has been taken into use as fine aggregate conforming to zone 3 grading essential as per IS:383-1970 [12]. Scrap tyre rubber of fine size is being as a replacement of fine silica sand in different mixes subsequently. Polypropylene (PP) fibres of micro type have been preferred. The following list of tables gives the idea of chemical and physical composition of different components used in the study (Tables 3 and 4).

Table 1 Chemical compositions of cementitious material

Ingredients	Chemical Compositions %					
	CaO	SiO_2	Al_2O_3	MgO	Fe_2O_3	SO_3
Cement	63.2	21.8	6.8	2.5	3	1.7
Fly ash	5	52.2	22.8	–	11	–

Table 2 Physical Properties of Cementitious material

Constituents	Physical properties					
	Specific surface area(m^2/kg)	Particle size (μm)	Specific gravity	Density(kg/m^3)	Texture	LOI
Cement	372	12	3.15	3200	Light greyish	1.48
Fly ash	389	10	2.17	–	Light greyish	1.05

Table 3 Physical composition of filler materials

Ingredients	Specific gravity	Density (kg/m^3)	Mean particle size (μm)
River sand	2.72	2770	118
Scrap rubber	0.71	722	221

Table 4 Physical properties of PP-fibre

Fibre	Type	Length (mm)	Diameter (μm)	Specific gravity
Polypropylene fibre	Micro	12	150	0.91

Table 5 Mix proportion of ECC

Mix	Cement	Fly ash	Fine Sand/P	Water/P	Rubber %	HRWRA/P (%)	Fibre %
C-40	420	–	2.4	0.3	–	1	–
P-ECC	500	600	0.36	0.3	–	0.6	1.5
R1P-ECC	500	600	0.327	0.3	10	0.55	1.5
R2P-ECC	500	600	0.291	0.3	20	0.5	1.5
R3P-ECC	500	600	0.255	0.3	30	0.5	1.5

P Powder materials (Cement and Fly ash); Units = Kg/m^3

2.2 Mix Proportion

The design mix proportion have been followed eliminating the position of coarse aggregate in the composite and going with fine aggregate alone as suggested by many authors as no code and standard provision is available for this study. In the present study, fine aggregate has been replaced by scrap tyre rubber by following ASTM C 109/C109M standard as shown in Table 5.

2.3 Workability

The workability test of ECC generally gives the idea of its uniqueness, homogeneity and viscosity of the mix. The workability of the ECC gives the idea of not more than one characteristics of the flow that is related to plastic viscosity and yield stress [13]. In the present study we have taken care of yield stress by slump test and plastic viscosity with V-funnel test (Fig. 1). V-funnel test dimension is measured to be 490*65*75 in which all the mixes are filled to its top level and allowed to free flow. Time taken by all the mixes are noted and then compared.

3 Experimental Study

3.1 Chloride Ion Penetration

Chloride ion penetration test is the test conducted to ensure the permeation of chloride ion into the cementitious-mortar interface in the composite sample. The test

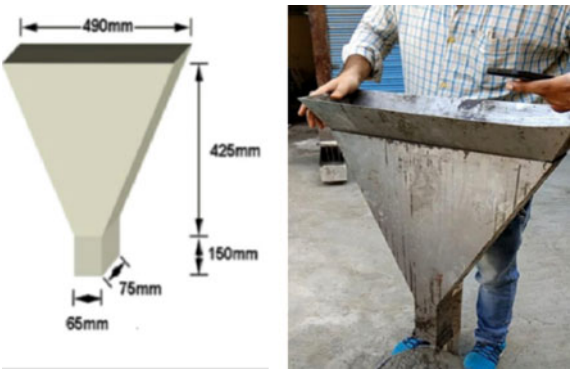

Fig. 1 V-Funnel test (495 mm * 65 mm * 75 mm)

Table 6 Total charge passed (coulombs) against permeability class relationship

Total charge passed (coulombs)	Permeability type
>4000	High
2000–4000	Moderate
1000–2000	Low
100–1000	Very low
<100	Negligible

equipment is known as RCPT (Rapid chloride ion penetration test). It is conducted on a specimen with 100 mm diameter and 50 mm height in a solution of 0.3 NaOH and 3% NaCl at 60 V charge source in compliance with ASTM C 1202 [14]. The results are collected after 6 h of penetration time in accordance with data acquisition system. The mean of two sample results is obtained as the total charge passed for that mix [15]. Table 6 shows relation between total charges passed against the permeability class.

3.2 Compressive Strength Test

Compressive strength is important for any mix proportion to showcase its strength to other alternatives like conventional type of concrete. Compressive testing machine have been used to calculate strength of the different specimen for each mix in accordance with [16]. Figure 2 shows the CTM (compressive testing machine) used in this study.

Fig. 2 Compressive Strength Testing Machine (CTM)

4 Result

Through all the observation and calculations performed in the study we have derived different results for each mix proportion. Different test results for workability test, compressive strength t-est and chloride ion penetration test have been successfully depicted below one by one.

4.1 Workability Test

Workability test are necessary for a concrete mix or composites like ECC to know its flow characteristics and viscous property [17]. The time taken by the each mix is shown in the Table 7. As we can see the time taken to escape out from the funnel decreases with increase in powder rubber percentage because powder rubber has nil water absorption property in Fig. 3 and hence with same w/p ratio flow characteristics improves. R1P:R1P-ECC and so the other two.

Table 7 V-Funnel test results

Mix proportion	Time taken (s)
C 40	44
P-ECC	23
R1P-ECC	21.5
R2P-ECC	20
R3P-ECC	18.5

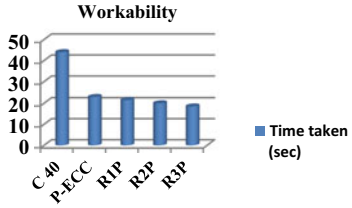

Fig. 3 Flow test

4.2 Compressive Strength

Compressive strength of the ECC has been calculated to compare the different mix on the basis of mechanical ability of the each sample to take load up to its limit. The compressive strength of high volume fly ash based ECC depend on no. of factors like

(a) Conversion of more C-H-S from C_2S or C_3S in the internal micromechanics.
(b) Orientation of fibres (PP) helps in taking the load in definite direction and hence improves strength.
(c) Secondary hydration in case of fly ash based ECC is important as it helps to hydrate in addition with cement very late up to 120 days of curing time.
(d) Curing regimes should be in compliance with IS: 456-2000.
(e) Homogeneous mix with scrap rubber mixed uniformly.

Compressive strength test has been done on the listed mixes and result are studied at 7 days and 28 days of curing condition at controlled temperature at 23 ± 2°C and result observed are P-ECC > R1P-ECC > C 40 > R2P-ECC > R3PECC for both 7 and 28 days shown in Figs. 4 and 5 respectively.

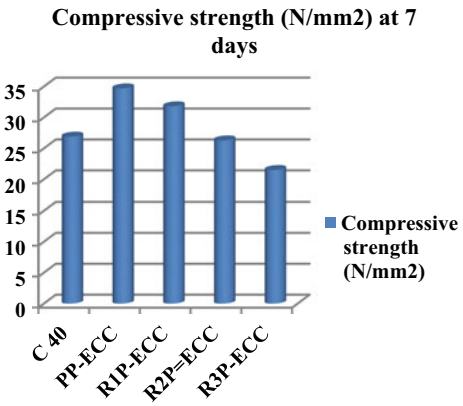

Fig. 4 Compressive strength at 7 days

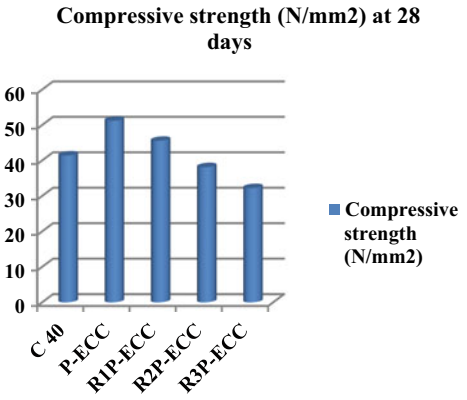

Fig. 5 Compressive strength at 28 days

4.3 Chloride Ion Penetration

Chloride ion penetration is done by rapid chloride ion penetration set up named PROOVEit by germen instrument which gives result in just 6 h than other equipment. Two cylindrical disc of same dimension from two other cylinder where cut by a diamond saw cutter. Both of them were kept in water bath desiccator after being covered with epoxy paint for 18–24 h as per ASTM C 1202. The results are then obtained after 6 h in a report sheet. The RCP test has been performed for each mix after 28 days of curing time and final result is recorded after taking the mean of two results from the same mix. The chloride ion permeability result are shown in terms of total charge (coulombs) passed through a sample mix which is shown in this Table 8.

Chloride ion permeability effect on the ECC mixes with and without rubber shows little increase in chlorine emission with increase in powder scrap rubber volume in Fig. 6. The C 40 normal mix shows high permeability than the ECC mixes which very low chloride ion penetration. The normal PP-ECC shows about 740% less permeability than C 40 concrete samples. Also R1PP-ECC, R2PP-ECC &R3PP-ECC shows 635%, 495% and 400% less chloride ion penetration effects. Among rubberised ECC's for 10%, 20%, 30% replacement of fine silica sand with scrap rubber, the chloride ion permeability increase by 28% and 24% subsequently from R1PP-ECC MIX. However when compared with Normal PP-ECC with 0% rubber content, R1PP-ECC with 10% rubber content in replacement with fine silica sand

Table 8 Chloride ion permeability for ECC mix

Mix proportion	Total charge passed (in coulombs)
C 40	3560
PP-ECC	480
R1P-ECC	560
R2P-ECC	720
R3P-ECC	890

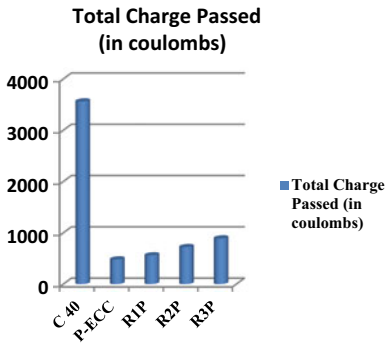

Fig. 6 Chloride ion permeability

shows 16% increment, 50% increase with R2PP-ECC mix with 20% powder scrap rubber content as a replacement for sand and about 86% increment than R3PP-ECC which contains 30% rubber content as replacement of fine sand. The following pattern generated from this result that is C 40 ≫ > R3PP-ECC > R2PP-ECC > R1PP-ECC. One more observation that is observed through this study is that the compressive strength of the composite mixes decreases with increment in rubber content this is because rubber is a material made up of 90% carbon and do not possess any load bearing capacity. Thus, with increase in rubber the compressive strength tends to decrease which can be shown with comparison in the present research as PP-ECC > R1PP-ECC > C40 > R2PP-ECC > R3PP-ECC at 28 curing days. The main result in Fig. 7 shows that the compressive strength after RCPT gets reduced more in case of conventional C 40 concrete by 15% before penetration took place and in case of ECC it is very minimal decrement as compared to compressive strength before the chloride ion penetration test been performed.

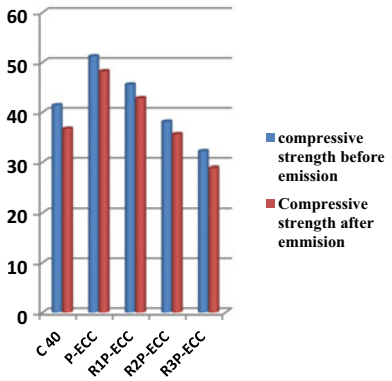

Fig. 7 Effect on compressive strength after RCPT

5 Conclusion

This present study ensures that high volume pozzolanic binder is not only necessary for the development of high strength composites but homogenous mix, uniform particle size and mainly good powder-aggregates interface bond is also very essential. The following conclusion can be drawn going through this present work into this study:

1. The workability of the engineered cementitious composite (ECC) increases with increase in powder scrap tyre rubber content because rubber is a non-absorbent of water but on the other hand coarse aggregate with large surface area has the tendency to absorb water during mixing of ingredients takes place which leads to poor flow character of C 40 concrete mix.
2. The compressive strength of the composite is comparable to the normal C 40 mix due to its fine particles, high packing density, and good compactness. C 40 due to presence of high amount of voids shows less strength in most cases.
3. The compressive strength of ECC decreases with increase in powder rubber content, this is because rubber has non load bearing character due to its chemical composition which has high percentages of carbon amount (about > 90%), it is also a heterogeneous material to concrete ingredients and does not chemically reacts or hydrates during primary and secondary hydration as well to form a substance which can bear load.
4. The chloride emission shows a appreciable decrement for powder scrap rubber content mix from 10 to 30% in this present work, this is because rubber is a material which can allow very little penetration of chlorine inside it due to its small permeable voids present in its micromechanics and thus decreases the depth of penetration to increase permeability but on the other hand C40 mix with coarse aggregate and high percentage of void show penetration on the higher side.
5. The material used in this study is financially viable like scrap rubber and fly ash which is easily available in abundance in rubber industry and thermal power plants.
6. Addition of fly ash and scrap rubber can be done directly into the composite likewise as in other concrete case and can be mixed easily due to absence of coarse aggregate.

References

1. Li VC (2002) Advances in ECC research. ACI Spec Publ Concr 206:373–400
2. Li VC (2003) Engineered Cementitious Composites (ECC)—a review of the material and its applications. J Adv Concr Technol 1(3):215–230
3. Li VC (2007) Engineered Cementitious Composites (ECC)—Material, structural, and durability performance. In: Nawy E (ed) Concrete construction engineering handbook. CRC Press (Chapter 24)

4. Lepech MD, Li VC (2009) Water permeability of engineered cementitious composite. Cement Concr Compos 31:744–753
5. Liu H, Zhang Q, Li V, Su H, Gu C (2017) Durability study on engineered cementitious composites (ECC) under sulfate and chloride environment. Constr Build Mater 133:171–181. https://doi.org/10.1016/j.conbuildmat.2016.12.074
6. Xu G, Shi X (2018) Characteristics and application of fly ash as a sustainable construction material: a state-of-the-art review. Resour Conserv Recycl 136:95–109
7. Tang SW et al (2015) Recent durability studies on concrete structure. Cem Concr Res 78:143–154
8. Siddique R, Naik TR (2004) Properties of concrete containing scrap-tire rubber—an overview. Waste Manage 24(6):563–569
9. Ho AC, Turatsinze A, Vu DC (2008) On the potential of rubber aggregates obtained by grinding v end-of-life tyres to improve the strain capacity of concrete. In: Alexander MG, Beushausen HD, Dehn F, Moyo P (eds) Taylor & Francis Group, London, pp 123–129
10. Sahmaran M, Li M, Li VC (2007) Transport properties of engineered cementitious composites under chloride exposure. ACI Mater J 104(6):604–611
11. IS:8112-1989. Specification for 43 grade ordinary Portland cement. Bureau of Indian Standards, New Delhi, pp 1–17
12. IS:383-1970. Specification for coarse and fine aggregate from natural sources for concrete. Bureau of Indian Standards, New Delhi, pp 1–24
13. Bilici Z, Ozbay E, Erdem TK, Yucel HE, Lachemi M (2013) Composites : Part B improving the workability and rheological properties of engineered cementitious composites using factorial experimental design 45: 356–368. https://doi.org/10.1016/j.compositesb.2012.08.015
14. Drilled T, Cocrete C, Statements B, Speci-CCT, ores TD, Test CC. Standard test method for electrical indication of concrete's ability to resist chloride. 1986; i(95 mm): 1-C6
15. Adesina A, Das S (2020) Influence of glass powder on the durability properties of engineered cementitious composites _ Elsevier Enhanced Reader.pdf. pp. 1–11. Windsor. Construction and Building Materials, Ontario, Canada
16. ASTM C109/C109M-11b (2010) Standard test method for compressive strength of hydraulic cement mortars (using 2-in. or [50-mm] cube specimens)1. Chem Anal 1–9
17. Ferraris CF, Obla K, Hill R (2001) The influence of mineral admixtures on the rheology of cement paste and concrete. Cem Concr Res 31(2):245–255

A Probabilistic Approach for Predicting the Fatigue Life of Concrete

D. R. Renju and Keerthy M. Simon

Abstract The fatigue failure of structural elements subjected to repeated cyclic loading may reduce the life of infrastructures. Heterogeneous nature of concrete and random factors in fatigue testing lead to great variability in fatigue life of concrete. As deterministic approach depends on certain parameters and initial conditions, it is not reliable for the prediction of fatigue life of concrete. In this study, a probabilistic approach using artificial neural network is utilised to predict the fatigue life of plain concrete. An artificial neural network predictive model was developed utilising the data from fatigue tests conducted on plain concrete beams of three different sizes mainly small, medium and large. The model is trained using the available experimental data of small and medium specimen and is validated using available experimental data reported on large specimens. The developed model is able to predict the number of cycles of failure of concrete by considering material and fracture mechanics properties responsible for the softening behavior of concrete as input. This approach is advantageous over other methods as it includes the randomness in the fatigue of concrete and will be able to predict the fatigue life of concrete with reasonable accuracy.

Keywords Artificial neural network (ANN) · Fatigue life · Probabilistic approach

1 Introduction

The phenomenon by which repeated loading cause internal changes in material and triggers crack growth is called fatigue fracture. In ductile materials such as metals and brittle materials like ceramics, extensive fatigue studies were made through different approaches and its fatigue fracture prediction is more reliable due to its homogeneous

D. R. Renju (✉) · K. M. Simon
Department of Civil Engineering, NSS College of Engineering, Palakkad, India
e-mail: renjudr93@gmaill.com

K. M. Simon
e-mail: keerthymsimon@gmail.com

© Springer Nature Switzerland AG 2021

K. Dasgupta et al. (eds.), *Proceedings of SECON 2020*,
Lecture Notes in Civil Engineering 97,
https://doi.org/10.1007/978-3-030-55115-5_54

nature. Despite of this, the heterogeneous nature of concrete and random factors in testing make it more complex for the prediction of fatigue of concrete. Various deterministic approaches were used to predict the fatigue failure of concrete. It includes S-N curve method, fracture mechanics method and continuum damage mechanics method. In this, S-N curve method is more applicable to brittle and ductile material, whereas in quasi-brittle material like concrete it suffers from its discreteness property [1]. The fracture mechanics method is also extended from metals and is proved better in the prediction of crack growth rate and fatigue failure of concrete [2]. But the varying parameters makes it more complex and is not dependable [3]. In fatigue damage mechanics method, the damage in material or energy dissipation due to the damage is made use of to predict the fatigue failure of concrete, but is only applicable for viscoelastic concrete [4, 5] .

In this context, the relevance of probabilistic (stochastic) approach for the prediction of fatigue life of concrete came into importance. This model uses distribution instead of fixed values which includes variation and uncertainty. Some of the generally used stochastic methods were Weibull distribution, Baye's rule, regression analysis etc. But the reliability of these methods remains uncertain. Artificial neural network (ANN) is an effective computational tool which is developed inspired by the biological nervous system. Based on the given input and output data ANN analyse and find the pattern of data and can model complex relationship. ANN is gaining wide acceptance in many engineering problems, especially those which are more complicated [6, 7].

In this paper, the capability of ANN to solve complex problems are utilised to predict the fatigue life of concrete. A novel prediction model of the fatigue life of plain concrete using artificial neural network is developed. The experimental data of plain concrete on three different sizes: small, medium and large are collected and used for training and validation of ANN model. The input data were selected according to the material, geometrical and fracture properties accountable for the fatigue failure of concrete. The model will give the number of cycles of failure of plain concrete in simple and fast approach. This in turn, can help the inclusion of fatigue failure in the design of structures subjected to cyclic loading and thus to ensure its prolonged service life.

2 Artificial Neural Network

Artificial neural network consist of three stages: input, hidden and output layer. The input layer receives the information. Then the hidden layer perceive and analyse the information and finally the output layer gives the output. The number of input nodes and output nodes will be the number of input data and output data respectively. The number of hidden layers and number of neurons will depends on the diversity of input data and is critical for the efficiency of model [8]. There are many rules for the critical selection of number of neurons. However the structure and complexity of the model will decide the number of hidden layers and the neurons in it. The learning

process will be denied if number of neurons is inadequate and excessive number prevents the model from learning the data [9, 10].

2.1 Neural Network Modelling

The neural network model is developed and trained using MATLAB 2017a software. The steps involved for designing neural networks is given in Fig. 1. The data was collected based on the experimental and numerical investigation done earlier by Keerthy et al. [11, 12]. The neural network architecture developed is based on multilayer feed-forward back propagation network or multilayer perceptron network (MLPN). The training algorithm used is Levenberg-Marqaurdt backpropagation algorithm which provide more accuracy with lesser time and is more reliable in complex modelling problems. As stated earlier the three layers (input, output and hidden), their respective neurons and activation function must be selected. As there are 6 inputs and 1 output, the number of neurons in input and output layer had set to be 6 and 1 respectively. In the 6 input neurons, each neuron represents each independent variable and they are: (1) Crack length (2) Fracture energy (3) Energy release rate (4) Brittleness number (5) Tensile stress (6) Stress ratio and the output neuron is number of cycles of failure.

The model is created and trained to predict the number of cycles of failure as a function of the 6 input parameters mentioned above. The details of input parameters is given in Table 1. The ANN model comprises of two stages: training and validation, for this the data are divided into three subsets such as for (i) Training (70% of data set) (ii) validation (15% of data set) (iii) testing (15% of data set). Another set of fresh data set is used for testing and independent validation of the developed model.

A two layer feed-forward backpropagation neural network with tan-sigmoid function in hidden layer and linear function in output layer is used to train the network as this combination of activation function gives the best result for this problem. The selection of number of neurons in hidden layer is crucial for the optimum performance

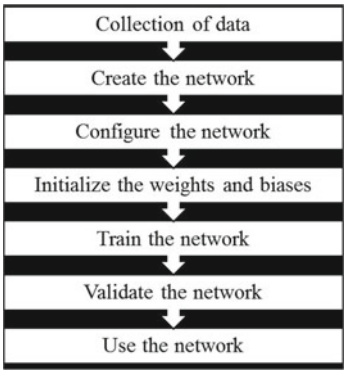

Fig. 1 Steps for designing neural network architecture

Table 1 Details of input parameter

Input neuron no:	Input parameter	Description
1	Crack length (a)	Length of crack with increasing number of cycles
2	Fracture energy (G_f)	Toughness of the material
3	Energy release rate (ΔG)	Energy required by crack to propagate a unit distance
4	Brittleness number (β)	Structural size (D)/transitional size (d0)
5	Tensile stress (σ_t)	Crack occurs only when major principal stress exceed this value
6	Stress ratio (R)	Minimum load/maximum load

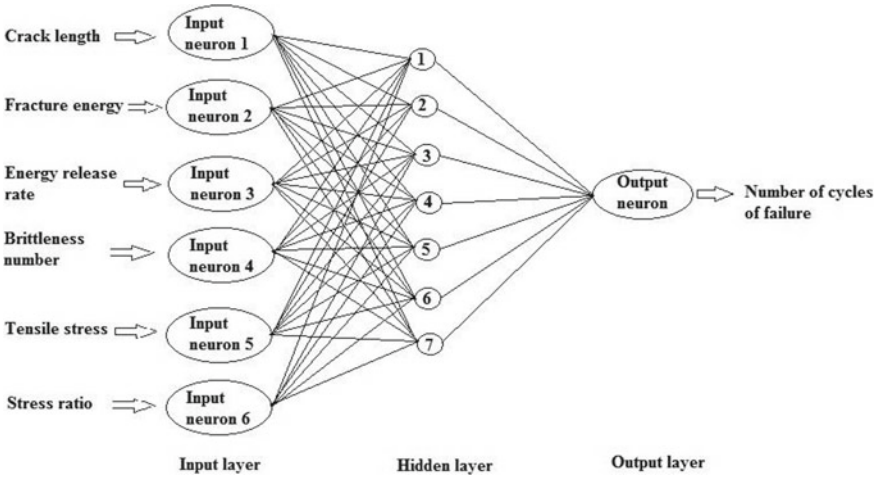

Fig. 2 Neural network architecture model

of the network. The number of hidden neurons were fixed after considering different number of neurons in the hidden layer and calculating the respective prediction error. Also the regression value obtained is taken into consideration for each neuron in the hidden layer. The utilized network architecture with backpropagation neural network model employed is shown in Fig. 2.

2.2 Evaluation of Network Model

The performance of neural network is evaluated by Mean Square Error (MSE) and Regression value (R) to obtain optimum solution. The model with least MSE and R value closer to 1 turn out as the best model. It is necessary to decide the number

Table 2 Training performance of different ANN model

Model	Number of hidden nodes	Performance criteria	
		MSE	R
N 6-9-1	9	2.689	0.985
N 6-10-1	10	1.864	0.991
N 6-11-1	11	1.187	0.999
N 6-12-1	12	2.561	0.987
N 6-13-1	13	3.112	0.979

of neurons in the hidden layer to bring out the optimum network architecture. The number of neurons was varied from 9 to 13 in the hidden layer. The number of neurons below and above this range do not gives satisfactory MSE and R. This may be due to inadequate training and overfitting of data respectively. Table 2 represents the training performance of 5 ANN model and their corresponding MSE and R. It can be noted from Table 2 that increase in number of neurons is not directly related to training process. The neural network model with 11 neurons in the hidden layer showed the best performance. Beyond this value the performance is not acceptable.

N 6-11-1 model exhibited the least error in predicting number of cycles of failure and is in good agreement with the experiment values. N 6-11-1 model is the model with 6 neuron, 11 neuron and 1 neuron in input, hidden and output layer respectively. The MSE and R of the derived model were 1.187 and 0.999 respectively. The least performed model was N 6-13-1. Figure 3 illustrates the potential of the model in the prediction of the number of cycles of failure of concrete for all data sets with R value of 0.99, indicating a high reliability in the model.

3 Results and Discussion

To ensure the reliability of the constructed neural network model Analysis of Variance (ANOVA) in excel is utlised. Analysis of variance for predicted and real values of number of cycles of failure of concrete is shown in Table 3. Thus by making a comparison with the neural network model performance evaluated by MATLAB as shown in Fig. 3 internally and by ANOVA as in Table 3, it can be inferred that the model is valid. R value obtained from ANOVA is same as that of the value from MATLAB. Also the significance F value 0 indicates the statistical validity of model.

4 Conclusions

An artificial neural network model is effectively developed to predict the fatigue life of concrete. The prediction of number of cycles of failure of concrete was carried out by using ANN of back-propagation model with Levenberg-Marquardt training

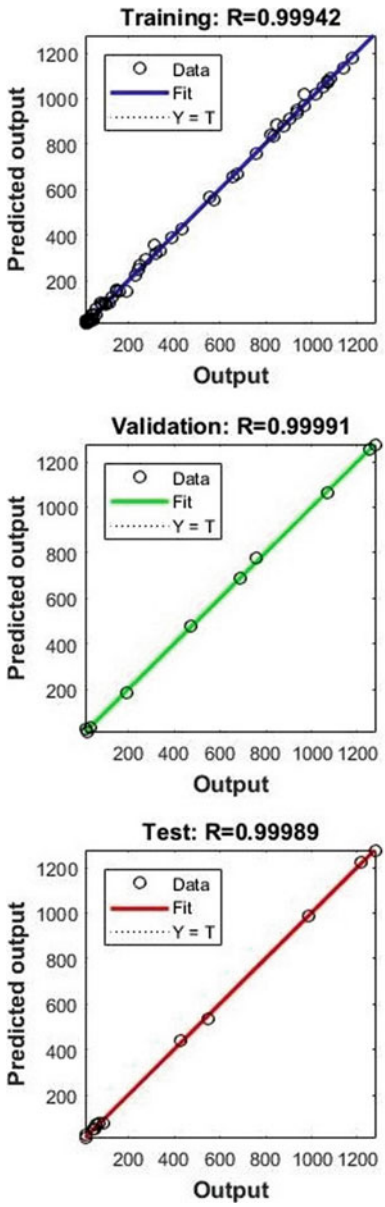

Fig. 3 Regression plot for testing, validation and testing from MATLAB

algorithm. The number of neuron in each layer can be determined by the complexity of the problem and data sets. The R2 and MSE was the selected criterion to evaluate the network with optimum solution. In this study, the main conclusions are:

- The network with 11 neurons in the hidden layer gives good performance result and is in fine agreement with the experimental data.

Table 3 Analysis of variance for predicted versus real output

Summary output					
Regression statistics					
Multiple R	0.999710377				
R Square	0.999420837				
Adjusted R Square	0.999414023				
Standard Error	10.73476536				
Observations	90				
ANOVA					
	df	SS	MS	F	Significance F
Regression	1	16902526.59	16902527	146678.5187	0
Residual	85	9794.990932	115.2352		
Total	86	16912321.58			

- The distribution of data points for neural network model is almost similar and close to the actual experimental data with regression value in range of 0.9–1.0. This indicate that the developed neural network model is capable of making the prediction with reasonable accuracy.
- The comparison of predicted output values using ANOVA also agrees with the reliability of the model.
- The neural network model developed are able to predict the fatigue life of concrete with reasonable accuracy. This shows that artificial neural network is an effective tool to use in complex problems.

References

1. Miner MA (1945) Cumulative damage in fatigue. J Appl Mech 12(3):159–164
2. Slowik V, Plizzari GA, Saouma VE (1996) Fracture of concrete under variable amplitude fatigue loading. ACI Mater J 93(3):272–283
3. Paris P, Erdogan F (1963) A critical analysis of crack propagation laws. J Fluids Eng 85(4):528–533
4. Baluch MH (2003) CDM model for residual strength of concrete under cyclic compression. Cement Concr Compos 25:503–512
5. Lei D (2008) On the energy dissipation in fatigue process and fatigue life prediction. J Exp Mech 5:008
6. Hajela P, Berke L (1991) Neurobiological computational modes in structural analysis and design. Comput Struct 41:657–667
7. Haykin S (1999) Neural networks: a comprehensive foundation, 2nd edn. Prentice Hall, Upper Saddle River, NJ
8. Hagan MT, Demuth HB, Beale M (1996) Neural network design. PWS Publishing Company, Boston, MA
9. Heaton J (2007) Introduction to neural networks with Java [online]. Available from: http://www.heatonresearch.com/articles/5/page2.html

10. Haykin S (1994) Neural networks: a comprehensive foundation. Macmillan Publishing Company, New York, NY
11. Simon KM, Chandra Kishen JM (2107) A multiscale model to describe fatigue behaviour of concrete. Eng Fract Mech 98:1–13
12. Simon KM, Chandra Kishen JM (2016) Influence of aggregate bridging on fatigue behaviour of concrete. Int J Fatigue 90:200–209

Convergence Study of Reinforced Concrete Beam-Column Joints Under Impact Loads

Jhuma Debnath and Hrishikesh Sharma

Abstract Convergence of mesh size is vital in Finite Element Analysis (FEA). It helps the user procure better results and hence enables the user to rely on the FEA model results. FEA models are beneficial in reducing the cost of studies that are otherwise not feasible with experimental models. It allows a faster design of the models in the required studies. However, only after the mesh convergence study, results of the FEA models are considered as fit, accompanied by adequate material models, boundary conditions, loading provided to the model. For validation, experimental literature chosen as such that a steel impactor hits a Reinforced-Concrete (RC) beam-column joint with an absolute velocity at the beam free end. This present model, validated on various parameters like the displacement of the beam and residual velocity of the structure after the impactor has hit the structure. This paper has attempted to converge the mesh size of RC beam-column joint experimental models from the literature, and hence set a mesh size fit to simulate other such models.

Keywords Reinforced concrete · Impact loads · Material model · Finite element software (Ls-DYNA) · Beam-column joints

Introduction

Several terrorist attacks have forced the scientific community to investigate the safety of the existing buildings—most buildings constructed of Reinforced Concrete (RC) materials. In RC building, the joints are the most crucial part in matters of transferring the load of the upper floors to the adjacent bottom floors and hence transferring the loads to the ground. Not making adequate measures for the RC joints makes way for the progressive collapses in the building. The experimental program of such studies makes the study economically more burdensome, and also such programs are generating many wastes. To mitigate these developmental problems, a Finite Element (FE) Software is handy. With a few expert tricks in the software, the studies

J. Debnath (✉) · H. Sharma
Department of Civil Engineering, Indian Institute of Technology Guwahati, Guwahati 781039, India
e-mail: d.jhuma@iitg.ac.in

© Springer Nature Switzerland AG 2021

K. Dasgupta et al. (eds.), *Proceedings of SECON 2020*,
Lecture Notes in Civil Engineering 97,
https://doi.org/10.1007/978-3-030-55115-5_55

could be made with much economic convenience and also creating very marginal to no environmental problems.

For Finite element Analysis (FEA) to yield results, a mesh convergence study is required. Designing of structures predicts deflections, displacements, and stresses. Usually, hand calculation using equations is involved in obtaining solutions. They oversimplify the problem. FEM discretizes the body, keeping the continuity of displacements along the element boundaries and thus becomes more complicated to be solved by hand. The entire mesh model does not need to be refined equally. The local stresses do not affect the entire stresses. Thus, the model is refined in specific regions. Therefore, a transition zone from a coarse to a fine mesh is observed. There are two types of refinements: H-refinement shows a reduction in the size of the element, P-refinement shows increasing order of the element. To measure mesh convergence, analytical and experimental results are to be compared. Errors in displacement, errors in strains, errors in stresses can be defined. These errors could be used for comparison, and they would need to reduce with mesh refinement.

Coarser and finer meshes are analyzed to yield stresses with varying mesh sizes. The coarse meshes result in inaccurateness. However, the fine or very fine meshes converge results of the displacements according to the demand in its accuracy. The converged finer meshes tend to a unique value. However, an increase in the fineness of the meshes increases the cost of computer resources. Curtailing of meshing at some size is to mitigate this resource problem by reducing the computation cost and also render desirable results at the same time. Further refining the mesh sizes results converge with a negligible difference. Mesh size is finally chosen considering the computer resources and also the reliability of the results.

A various experimental study conducted by researchers validates the experimental results with the FEA results. Excellent experimental work was conducted on beam-column joint over impact load [1]. Various other researchers have validated experimental work on columns, joints, and beams using FEA models using Ls-Dyna software, which has obtained a consistent result from the FEA [2–4]. Researches showed that many FEA software gives approximate results [5]. The differences in using size mesh mode and deviation mesh mode was studied on the energy absorption and peak load [6]. The energy absorption value was analyzed using various parameters such as the hourglass control, many through shell thickness integration point, and element formulation in converged mesh mode.

In the current work, mesh convergence is studied. It has also discussed how the material model is generated on the FEA software called Ls-DYNA. The convergence study of an experimental program [1] for further analysis of the RC Beam-Column joint was created by modeling the RC joint in the software, as mentioned earlier. The joint considered in this study is a non-seismically designed joint (with no honeycombs called as the NS-A in the literature). The displacements discussed according to their mesh sizes.

An overall mesh sensitivity analysis has been performed, by modeling for both the concrete and also the reinforcement used in the experimental program, to understand the adequate mesh size suitable for the validation of the experimental program.

1 Finite Element Modeling

1.1 Reinforced Concrete Joint Configuration and Design in Software

The various types of joints that identified in a Special Moment Resisting Frame (SMRF) building consists of the knee joint, exterior joint, and the interior joint. These joints govern the behavior of the structure and failure mechanism under extreme loading. These joints, namely the knee joints, form the top of the edge of a building joint. The exterior and the interior joints of the building form the intermediate stories.

The RC beam-column joint chosen here for validation of the present work is an experimental work [1]. The joint in the experimental work designed according to the Indian standard codes for the Concrete buildings, i.e., the IS 456:2000 and not designed for seismic responses. Fixed end conditions of the columns are considered as the boundary conditions, and the beam has a free end where the impact load is applied. The dimension for the beam-column joint used for the validation work is mentioned as follows. The column is 0.115×0.115 m with clear cover 20 mm, and the beam has dimensions of 0.150×0.115 m with clear cover 15 mm. The reinforcement taken for the design consists of various dimensions for the main longitudinal, transverse, and also a different set of reinforcements bars that have been mentioned in Table 1 below. Configuration of the joint for simulation is taken the same as the experimental model, described in Table 1. Reinforcements are also kept same as the experiment. The study is numerically conducted using Ls-DYNA. The FEA analysis has adequately validated results using the software.

Table 1 Dimensions of beam and column reinforcements used

Reinforcements used	Column	Beam
Longitudinal reinforcements	4 # 16 mm	4 # 12 mm
Transverse reinforcements	6 mm @100 mm c/c	6 mm @110 mm c/c

1.2 Automatic Meshing and User-Generated Meshing

A user has two options for the meshing. The auto-meshing and the selected meshing option. The auto meshing option creates shell meshes on surfaces. The models here are generated as solid elements in a pre-processing software, and hence mesh sizes are selected and not auto-meshed.

1.3 Effect of Element Type Mesh on Mesh Convergence

For 3-Dimensional elements like this RC joint, only tetrahedral or brick elements are used. Finer meshes, along with converging into more approximate results burdens the computer cost and coarser meshes give unacceptable results. A balanced mesh size has to be struck for a desirable result. The various types of formulation used incudes lagrangian, Eulerian formulations mainly. These methods define the node movement analysis. These methods define the node movement and material points. Here, in the Lagrangian analysis, nodes and related materials points get displaced in the deformation domain. The nature of the lagrangian analysis makes it best suited for a process with low deformation. A Eulerian analysis is different from the Lagrangian analysis in terms that the mesh nodes are fixed in space, and the material points are flown through it [7, 8].

2 Preparation of the Reinforced-Concrete Beam-Column Joint Model

The material model for the convergence study, with the help of the FE analysis undertaken with the help of the FE software, Ls-DYNA [9]. The material model prepared for both concrete and reinforcement is used in the RC joint of the experimental program in the FEA model.

MAT WINFRITH CONCRETE (084/085) material model is found suitable for the development of the concrete model for the RC joint. The WINFRITH model is suitable for concrete with high impact. The material model used for the development of the reinforcement is the MAT-PLASTIC KINEMATIC (003). A detailed version of the models given in Sect. 3 below.

2.1 Boundary Conditions

The boundary conditions set for the software model are kept the same as the experimental program. The column ends of the joints are kept fixed. The load is kept

the same as that of the experiment. An impact load is applied with the help of a steel impactor of its mass 1.07 kg. The material for the impactor is developed in the program using the material MAT-PLASTIC KINEMATIC (003) material model. A velocity of 33.39 m/s set for the impactor supposed to hit the beam at a distance of 0.115 m from the free end. The beam end is left free.

Par17

2.2 Mesh Size for the Elements

The mesh sizes utilized in the models for the sensitivity analysis is tabled below in Table 2. The individual results discussed in the result section in Sect. 4.

Figure 1 is the mesh model developed using the FE software (Ls DYNA). This mesh model is selected after the convergence study.

Table 2 Mesh size taken for convergence

Impactor mesh size	Concrete mesh size	Reinforcement mesh size
0.015	0.015	0.010
0.020	0.020	0.015
0.025	0.025	0.020

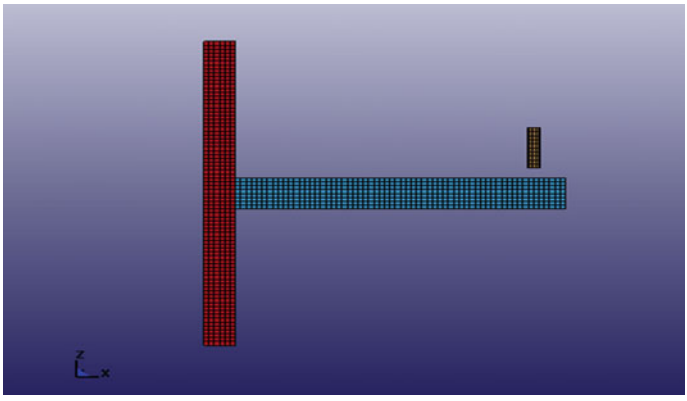

Fig. 1 Mesh modeling RC Beam-column joint

3 Material Model of the Study in FE Software (Ls DYNA)

The materials used in the FE software carefully put together to simulate the displacement response of the RC beam-column joint experimental program. Various materials meticulously used to procure the material behavior of the materials related to the experiment in the software. The Ls DYNA manual is used for the use of the simulation of the material in the software [10]. Here, the concrete model simulated with the help of the MAT_WINFRITH_CONCRETE (085/084) material model card and the reinforcement model is being taken care of with the help of the MAT_PLASTIC_KINEMATIC (003) model card. A contact card is used to stick the beam part of the joint to the column part of the joint, TIED_SURFACE_TO_SURFACE(THERMAL). AUTOMATIC_SURFACE-_TO_SURFACE (THERMAL) card used to make contacts with the concrete beam to the impactor. Fixed-fixed boundary conditions are being used at the column end to simulate similar experimental conditions. The impactor velocity provided with the help of the VELOCITY_GENERATION card. A brief description of all the material models given below.

3.1 Material Model of the Concrete

As stated above, the material model used for the concrete is MAT_WINFRITH (085/084). Input for the material properties is from the experiment conducted or default material properties called from the library for regular strength concrete. Among the two material, 84 and 85, only the former works for rate effects. The Winfrith concrete implemented in the 8-node single integration point continuum element.

3.2 Material Model of Reinforcing Steel

For the material model of the steel, the MAT_PASTIC_KNINEMATIC (003) material is used. This model allows rate effects and is suited to model kinematic and isotropic hardening plasticity. This cost-effective model is working for Hughes-Liu beams, shells, and solid elements. Stress versus strain curve can be defined using this material.

3.3 Contact Card for Sticking Concrete Beam to the Column

The concrete column and the concrete beam were developed separately without continuity of the meshes and then stuck together with the help of the following card. It requires the sticking of the concrete and the reinforcement material of the column and the beam, respectively. The CONTACT_AUTOMATIC_SURFACE_TO_SURFACE(THERMAL) card used to establish the sticking of the concrete elements of both columns and beam together.

3.4 Contact Card to Simulate Bond Between the Steel and the Concrete

Lagrangian coupling method defines the concrete, transverse reinforcement, and the longitudinal reinforcement bond. This method is effective and efficient because matching the concrete and reinforcement nodes is not necessary. The concrete acts as the master element and the reinforcement as the save element. CONSTRAINED _LAGRANE_IN_SOID material card used.

3.5 Velocity of the Impactor

The velocity of the shooting impactor initiated is with the help of the VELOCITY_GENERATION card. The velocity input is to be provided to the card to initiate the velocity of the impactor. This card also defines the contact between the concrete beam and the impactor.

4 Results and Discussion

The mesh convergence displacements results are being discussed in this section. The load applied to the beam joint is an impact load that is applied to the end of the beam end, as mentioned above. The mesh of 0.025 m selected for the validation of the model. This model is found to replicate the experimental joint in the Finite Element software adequately. The mesh size that has appropriately yielded the experimental program is 0.020 m for the reinforcements used in the experiment. The displacement graph of the meshes used, given in Fig. 2. The finer meshes converged with barely much difference in the displacement response

The mesh size is converged, keeping the computer resource as a limitation. The mesh size of the concrete varied from 0.015 to 0.025 m, and the reinforced steel

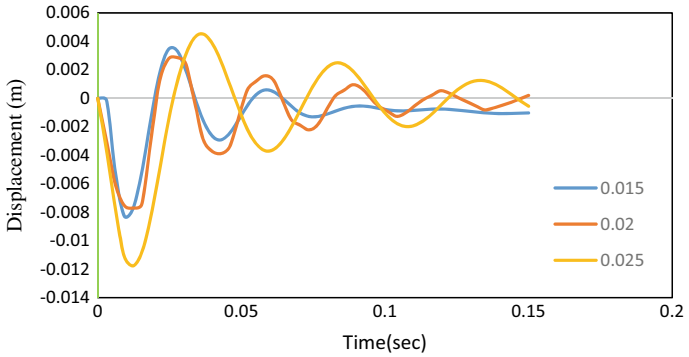

Fig. 2 Displacement response of mesh sizes considered

varies in mesh size from 0.010 to 0.020. The combinations of the meshes for the concrete and the reinforcement of the experimental model is given in Table 2.

The mesh size for the impactor was considered similar to the mesh size of the concrete. A perfect size is not selected for the impactor. It is because the meshing of the impactor is complicated for the meshing of solid cylinders used for creating the impactor.

The displacement for the simulation is 0.01159 m, compared to the experimental displacement result of 0.0126 m. The residual velocity of the model was as validated with the FE simulated model, which matched appropriately at 18.5 m/s for the experimental model and 17.4 m/s for the simulated model.

Conclusion

The mesh size for the models where the loading type is impact loading with lower impact loads has showed similar mesh convergence trends. Therefore, it is to be concluded that the mesh convergence will have similar trend for such impact loads. This FEM model can be used to simulate Reinforced Concrete joints with similar loading types. The mesh size can be either scaled up or scaled down, calibrated to approximate to the desired results.

Another thing that is inferred from the graph in Fig. 3 is that the same phase of displacement response of the simulated and the experimental model denoted the synchrony in the material model developed. Hence, the material model developed here simulates the experimental material behavior adequately.

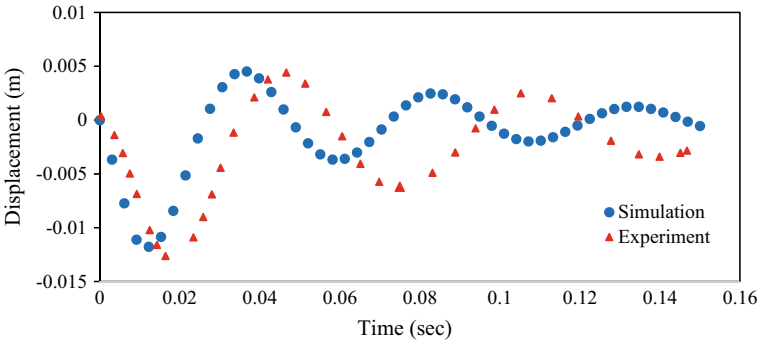

Fig. 3 Displacement graph of the experimental results and the converged mesh simulation

References

1. Rajeev A, Mohotti D, Shelke A (2020) Implications of impact experiments on honeycomb shielded exterior beam-column joint. Eng Struct
2. Kyei C, Braimah A (2010) Effects of transverse reinforcement spacing n the response of reinforced concrete columns subjected to blast loadings. Int J Impact Eng
3. Rajeev A, Parsi SS, Raman SN, Ngo T, Shelke A (2020) Experimental and numerical investigation of an exterior reinforced concrete beam-column joint subjected to shock loading. Int J Impact Eng
4. Yan B, Liu F, Song D, Jiang Z (2015) Numerical study n damage mechanism of RC beams under close-in-blast loading. Eng Failure Anal
5. Fyllingen O, Hopperstad S, Hanssen AG, Langseth M (2010) Modelling tubes subjected to axial crushing. Thin Walled Struct
6. Ahmad M, Ismail KA, Mat F (2013) Convergence of finite element model for crushing of a conical thinwalled tube
7. Priyadarshini A, Pal SK, Samantaray AK (2012) Finite element modelling of chip formation in orthogonal machining. Stat Comput Tech Manuf
8. Jain R, Pal SK, Singh SB (2017) Numerical modelling methodologies for friction stir welding process
9. Ls-DYNA_971 Software. Livermore Software Technology Corporation 7374 as Positas Road, Livermore, CA94551, 01/02/2013
10. Ls-DYNA R Keyword user's manual volume I, 2016

Evaluation of Cementitious Mixes for Printing

M. Vishruthi, S. Raghavendra, Y. Ravi Teja, and K. B. Anand

Abstract To meet the current expeditious work pace, innovative modus like 3D concrete printing will be useful in bridging sustainability in material usage with cost and time efficiency along with overcoming labor constraints. This preliminary study was aimed at partial replacement of 53 grade Ordinary Portland Cement (OPC) with Flyash (FA), Silica Fume (SF) and Ground Granulated Blast Furnace Slag (GGBS) in the preparation of mixes. The replacement percentages were decided based on literature review and preliminary trials. The fine aggregate of particle size in the range 1.18–2.36 mm was used as fillers. The required workability for printing (based on trials) was achieved by using minimal dosages of a PCE based superplasticizer. The extrudability of mixes was tested with a simple mortar grouting applicator. The addition of 0.1% percentage of Polyvinyl Alcohol (PVA) fibre resulted in a better finish of the printed layer. The study is focused on the fresh and hardened state properties of printable cementitious mixes. The test results indicate that the mix containing GGBS, FA and fibre had better printability, good interlayer bonding, reduced gap time, and increased flexural and compressive strengths.

Keywords Printability · Extrudability · Cementitious mix

1 Introduction

The 3D concrete printing gives a new ambit to cement-based construction. The basic technique is building an object by a layer-over-layer process which is facilitated by contour crafting. In comparison with the conventional method of construction process, the flexibility of design, rapid prototyping, savings in materials and labor are few of its advantages. Building without using formwork paves the way to new architectural liberties apart from being cost-effective. Despite the various design constraints and technical issues in production, the walls and columns for buildings are printed on-site. This technology has so far been used to produce single storey

M. Vishruthi · S. Raghavendra · Y. Ravi Teja · K. B. Anand (✉)
Department of Civil Engineering, Amrita School of Engineering, Coimbatore 641112, India
e-mail: kb_anand@amrita.edu

© Springer Nature Switzerland AG 2021

K. Dasgupta et al. (eds.), *Proceedings of SECON 2020*,
Lecture Notes in Civil Engineering 97,
https://doi.org/10.1007/978-3-030-55115-5_56

compact homes, seashore walls, aesthetic structures and some traditional geometrical designs. 3D printing normally reduces the materials utilized and as a result, may have a lesser impact on the environment in comparison with conventionally produced concrete structures.

1.1 Background Literature

In the study conducted by Buswell et al. [1] printability is explained in terms of extrudability, open time and shape stability. Extrudability is the ability for the transportation of fresh printing concrete through pipe and nozzle conforming to the required dimension with good print quality. Workability is the vital material property that influences the extrudability. Open time is the time during which the fresh spray concrete can maintain sufficient workability or it is the time during which a material can be used in 3D printing. In the study conducted by Sanjayan et al. [2], it was observed that as the delay time increased, the adhesion decreased and hence resulted in low interlayer strength.

The primary binding material as observed from the literature survey is Ordinary Portland cement (OPC) conforming to ASTM C-150 [3], the quantity of which adopted in different studies varied from 490 to 670 kg/m^3 [4–6]. Class F fly ash and silica fume (SF) were used as supplementary cementitious materials (SCM). Fly ash is a pozzolan which is added to OPC to reduce the cement content, improve mix cohesiveness without compromising on the strength. Fly ash ranging from 24 to 30% of the mass of cement have been used in the study conducted by Gilson et al. [7]. Silica fume is used to increase the yield stress, reduce the delay in setting and reduce the segregation. 8–15% silica fume relative to the mass of the cement has been adopted in a study by Rahul et al. [8]. River sand of size 1.18 to 2.36 mm was used as filler material to improve the mechanical strength of the cementitious matrix. In the studies [4, 8], the cement sand ratios varied from 0.43 to 0.52. In the reported studies, Superplasticizer is used as an admixture to improve the workability of mixes so that they are extrudable. The usage of Polycarboxylatebased superplasticizer has been reported by Lu et al. [9] from 0.2% to 0.3% by mass of cement, for water-cement ratios of 0.4 to 0.5. In the study conducted by Rubio et al. [6], incorporation of Polyvinyl alcohol (PVA) fibres and Polypropylene (PP) fibres reduced the surface cracks and improved the flexural strength of the mixes. The volume fraction of the Polypropylene fibres varied from 0.2 to 2%.

The fresh state tests to characterize the mix included flow table test and extrudability test [5, 10]. It has been shown [8] that yield stress is a vital property to extrude stable layers without collapsing. Zhang et al. [11] showed that the compressive strength, flexural strength and shrinkage are essential parameters to be evaluated. The hardened state parameters are important for the durability aspects of 3 D printed elements.

1.2 Objectives of the Present Study

This study is aimed at investigating the influence of different materials on the properties of cementitious mixes that can be used for extrusion molding. The objectives of the study are to identify the factors that are needed to be addressed in 3D printing of concrete, arrive at mix proportions suitable for extrusion and to characterize the mixes through fresh and hardened state tests.

2 Experimental Details

Based on the broad understanding of the 3D concrete printing process from the literature review and the procurement convenience, the materials for the present study were identified. The mix proportions for the first few trials were based on reported studies. Later it was modified based on factors such as extrudability with the available equipment, better shape stability of the printed specimen, resource optimization, etc. A mortar grouting gun was used to extrude the cementitious mixes in the study.

2.1 Materials and Methodology

OPC 53 grade (specific gravity 3.15) was used as the binder in the printing mixtures. In the preliminary trials, the binder content was varied from 40 to 50%. But for economy, the OPC content was kept as 40% of the dry materials in the final mixes. Class F flyash (specific gravity 2.5) was taken as 15% in the mixes. River sand (specific gravity 2.65) passing through 2.36 mm sieve and retained on 1.18 mm sieve was taken in the mixes. The sand content was taken as 35% to obtain a suitable mix that could ensure extrusion.

To improve the cohesion and the mechanical properties, Silica fume (specific gravity 2.25) and Ground Granulated Blast Furnace Slag (specific Gravity 2.85) were used as a replacement for cement in different mixes. Glenium, a polycarboxylate based SP was used in the mixes. Since a higher water-cement ratio of 0.5 was adopted, the SP dosage was kept between 0.1 to 0.2%. Polyvinyl alcohol (PVA) fibre was varied between 0.1 and 0.2% of the total volume in the trial mixes. However, trials indicated that the fibre content of 0.1% improved the cohesion of the mixes for the above SP dosage. The mix details are given in Table 1.

Table 1 Mix details

Mix Designation	w/c	OPC%	Sand %	FA %	SF %	GGBS %	SP %	FIBER %
M0	0.5	50	35	15	–	–	–	–
M1	0.5	40	35	15	10	–	0.10	–
M2	0.5	40	35	15	–	10	0.05	–
M3	0.5	40	35	15	10	–	0.20	0.1
M4	0.5	40	35	15	–	10	0.17	0.1

2.2 Fresh State Properties

The solid materials which include OPC, Fly ash, silica fume or GGBS, sand and fibre were dry mixed for five minutes at a slow rate. The mixing is stopped after 5 min and any lumps of solids were crushed. Then, water and superplasticizer were added to the mix and the materials were wet mixed for 15 to 20 min at a faster rate. This is to ensure the reactivity of SP with the mix.

2.2.1 Slump Flow Test

After the preparation of the mix, the slump flow test [12] was performed. The cone-shaped mould of dimensions 100 mm base diameter, 70 mm top diameter, 60 mm height is placed in the center of the flow table. The cementitious mix is filled into the cone in two layers and the table is jolted 25 times in 15 s and the diameter of the spread mortar is measured in four directions. The average of the four readings is taken for the calculation of flow percentage. The typical slump flow is given in Fig. 1.

Fig. 1 Typical slump flow

Fig. 2 Vane shear apparatus

2.2.2 Vane Shear Test

The yield stress of the mix is important for the shape stability of the layers. The vane shear test is performed to find the stress at failure (yield stress) of the mixes. Using the vane shear apparatus (Fig. 2), the initial angle is noted and the final angle at failure is also noted. Torque is given by T = (Initial reading-final reading) x spring constant/180.Torque is converted into yield strength (S) using the equation proposed by Dzuy and Boger [13].

$$S = T/((\pi D^2) * (H/2) + (D/6))$$

where the diameter of the vane D = 12 mm and height of the vane H = 24 mm.

2.2.3 Extrusion

A mortar grouting gun (Fig. 3) of nozzle dimensions 55 mm × 15 mm was adopted for extrusion of the different mixtures (Fig. 4).

Through the preliminary tests, it was found out that the adhesion was maximum for a gap time of 15 min for mixes without fibre and 10 min for mixes with fibre.

Fig. 3 Mortar gun

Fig. 4 Extruding mix

Hence the layers were built up after the specified gap time. The extrudability was evaluated based on the ease of extrusion and layer uniformity. The layers with more cracks failed the extrudability test. Shape stability is the ability of the layers to retain shape and withstand settlement under own weight. The shape stability of layers is related to the deviation of layer dimension with the actual nozzle dimension and also with the layer width getting increased with the addition of upper layers. If the layer settlement was too much or the bottom layer width deviated more, with improper shape retention, the layers would fail in shape stability criteria.

2.3 Hardened State Properties

2.3.1 Compression Test

As the width of the nozzle is 15 mm, the height of one extruded layer will be 15 mm. A long specimen consisting of 4 layers, each of 15 mm height was printed for a length 300 mm. Then cube specimens of size 60 mm each were cut from the long specimen and the edges were trimmed. To obtain the material strength of the mix, the cementitious mix was cast into cubes of dimensions 50 × 50 mm and tested according to BS EN 12390-3 [14]. The compressive strength (7 day and 28 day) was found for both the cast and printed specimen to find the differences between material and layer strength. For the printed specimen the compressive strength values were taken in two directions, viz., in axial as well as transverse directions as shown in Fig. 5a, b. The Compressive strength values in the transverse direction give the maximum load-bearing capacity of the specimen and this value is compared with the material strength [10]. The compressive strength in the axial direction is indicative of the bonding strength between the layers of the specimen.

2.3.2 Flexure Test

The beam specimens of length 120 mm with 3 layers were extruded. The 7 day and 28 day flexure strength of the printed beam specimens was tested using a universal

(a) (b)

Fig. 5 Compression test **a** Axial **b** Transverse

Fig. 6 Flexure test arrangement

testing machine. The 120 mm long specimen was supported on two metal blocks at a distance of 25 mm from both the ends and a central point load was applied on the specimen (Fig. 6).

2.3.3 Drying Shrinkage Test

The shrinkage test is significant in understanding the dimensional stability of the specimen and to understand how modifications are effected by the incorporation of fibres. Drying shrinkage of the different mixes adopted for extrusion was done based on ASTM C157 [15]. The drying shrinkage specimens of size 160 mm × 40 mm × 40 mm were cast. The shrinkage values were measured using length comparator as shown in Fig. 7. The drying shrinkage values for 1, 3, 7, 14 and 28 days of the mixes were calculated.

Fig. 7 Shrinkage test

3 Results and Discussion

3.1 Fresh State Properties

3.1.1 Slump Flow

The average diameter of the spread in four directions after jolting was taken to calculate the percentage flow of various mixes. The flow values corresponding to the different mixes are shown in Fig. 8.

As shown the obtained flow values varied from 70 to 110%. The Mixes with GGBS showed lesser flow values when compared to the mix with SF. The reduction in flow values of mixes M1 through M4 when compared to control mix M0 is primarily due to the addition of fine mineral admixtures. The mixes with fibres showed a stiffening tendency and resulted in a marginally reduced flow. Mix M0 (control mix) showed

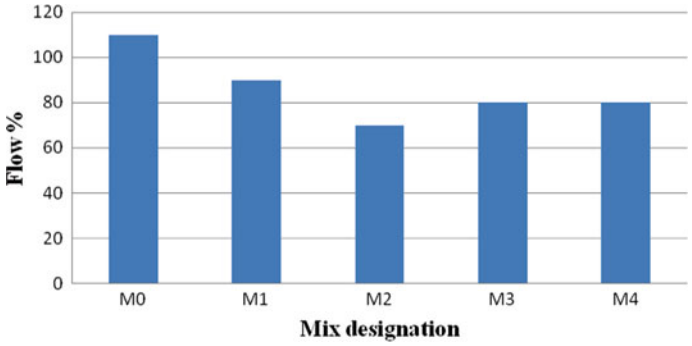

Fig. 8 Percentage flow of various mixes

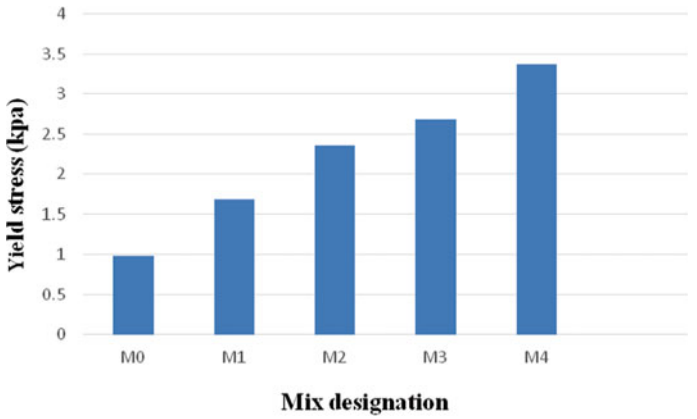

Fig. 9 Yield stresses of various mixes

a higher flow value due to bleeding. The addition of silica fume reduced segregation and bleeding tendencies of the mix as seen from the relatively lower flow value of M1 mix compared to M0. The mixes M2, M3 and M4 showed even lower flow values due to the addition of GGBS and PVA fibres, because of their stiffening tendency.

3.1.2 Yield Stress

The yield stress values of the mixes are presented in Fig. 9. It can be noted that there is an increase in yield stress in ascending order from mix M0 to mix M4. It can be inferred that the Yield stress of the mix containing GGBS was more than the mix with SF. The mixes containing fibre showed higher yield stress when compared to mixes without fibre. The mix M4 has the highest yield stress compared to the other 4 mixes. It can be inferred that the addition of both fibre and GGBS contributes to the increase in yield stress. The yield stress has a direct bearing on the shape stability of mixes during the extrusion process.

3.1.3 Extrudability

The ease of extrusion is related to the workability of the particular mix. The mixes were extruded through a rectangular nozzle of dimensions 55 mm $\times$ 15 mm. The extrusion properties are related to the workability (percentage flow) and yield stress of the mix.

The control mix M0 had the maximum flow value so it was very easy to extrude when compared to other mixes. The extrusion pressure required to be applied manually was minimum. The mix M4 (with GGBS and fibre) which had the least flow value was difficult to extrude than the other mixes. Therefore as flow decreased, the

ease of extrusion also decreased. Mixes with fibre contributed to a more even and smooth surface finish than the other mixes. Considering the aspects of printability and shape stability, the stability of the control mix (M0) was not satisfactory. For M0 the deviation (increase) of layer width after extrusion was 12.7% in relation to the width of the nozzle. But for GGBS with fibre mix (M4), the deviation in width was only 4.5%. This indicates that the layer settlement was more for M0 mix. The extruded layers of control mix and GGBS mix are shown in Fig. 10a, b.

The shape stability of the extruded layers can be interpreted from the yield stress of the mixes. The yield stress of M4 (GGBS mix) was found to be greater than M0 (control mix). Hence the shape stability of mix M4 layers was found to be better than mix M0 layers as seen in Fig. 11a, b.

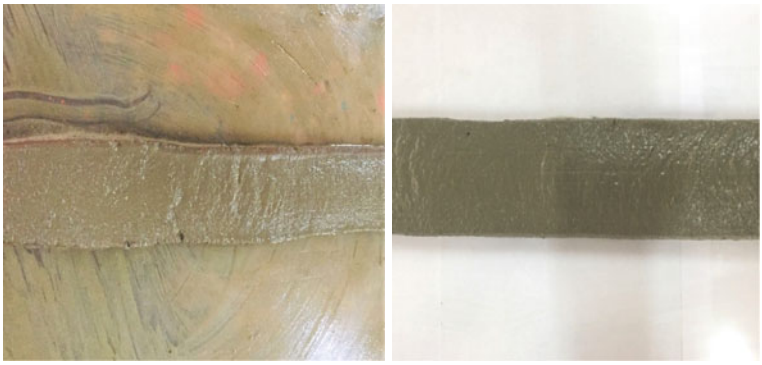

(a) (b)

Fig. 10 **a** Extruded control mix **b** Extruded GGBS mix

(a) (b)

Fig. 11 **a** M0 cube layers **b** M4 cube layers

3.2 Hardened State Properties

3.2.1 Compressive Strength

Compressive strength is one of the most important hardened state properties of any concrete specimen. The hardened state image of the extruded specimens is given in Fig. 12. The 7 and 28 day compressive strength values of the specimens of different mixes are given in Table 2.

The compressive strengths of the cast cubes are more than that of printed cubes by 20% to 63%. The lower strengths of extruded samples are primarily due to the lower density of samples. The compressive strength value of cast specimens of mixes M0, M1, M2, M3 and M4 are 63%, 37%, 20%, 36% and 29% more than that of their extruded specimens. The compressive strength of the GGBS mix (M2) accounts for the highest value in comparison to other mixes.

The compressive test in axial direction yielded values that were 35–67% lower than that of the compressive strength values in the transverse direction. The compressive strength values tested in axial direction improved with the incorporation of GGBS and deteriorated with the addition of fibres.

Fig. 12 Hardened specimen

Table 2 Compressive and Flexural Strengths

Mix designation	Compressive strength (MPa)						Flexural load (kN)	
	Cast cube		Printed cube-Transverse		Printed cube-axial			
	7 days	28 days	7 days	28 days	7 days	28 days	7 days	28 days
M0	12.1	18.4	3.7	5.5	2.4	3.6	3.2	4.1
M1	21.0	23.1	8.1	12.3	7.3	11.1	3.2	4.6
M2	16.0	24.8	11.1	16.1	9.7	15.0	6.3	8.9
M3	14.0	27.2	5.7	14.4	2.5	6.4	4.7	6.0
M4	15.3	23.4	8.9	13.6	3.4	5.2	10.0	14.2

3.2.2 Flexure Test

The flexure strength values of the printed beam specimens of different mixes are given in the Table 2. It can be observed that there is an increase in flexural strength from mix M0 to mix M4 in ascending order. The mix M0 and M1 are found to have the same flexural load capacity. It is also observed that the mix with GGBS has more flexure strength compared to the mix with silica fume.

The usage of fibres in GGBS mix (M4) has proven to be effective in increasing the flexural strength almost twice compared to mix containing only GGBS (M2). Comparing M1 and M3, it is found that the use of fibre has sufficiently increased the flexural strength of silica fume mix.

3.2.3 Drying Shrinkage

ASTM C157 [15] is the method used to measure the drying shrinkage of the mixes. The drying shrinkage values for 1, 3, 7, 14, 28 days of the mixes were calculated based on the shrinkage readings obtained from the length compactor and the results are given in Fig. 13.

The mix with silica fume (M1) showed the highest shrinkage. The addition of fibres resulted in the reduction of shrinkage by 67% for silica fume mix (M3) and 42% for the GGBS mix (M4). In the study conducted by Zhang et al. [16], the shrinkage of 3D printable concrete varied between 807 and 840 micro-strain. This low value of shrinkage might be due to the high sand/cement ratio of 1.5 in that study. Since a lower sand/cement ratio of 0.8 was adopted (for ease in the manual extrusion of mixes) in the current experiments, the shrinkage was found to be in the higher range.

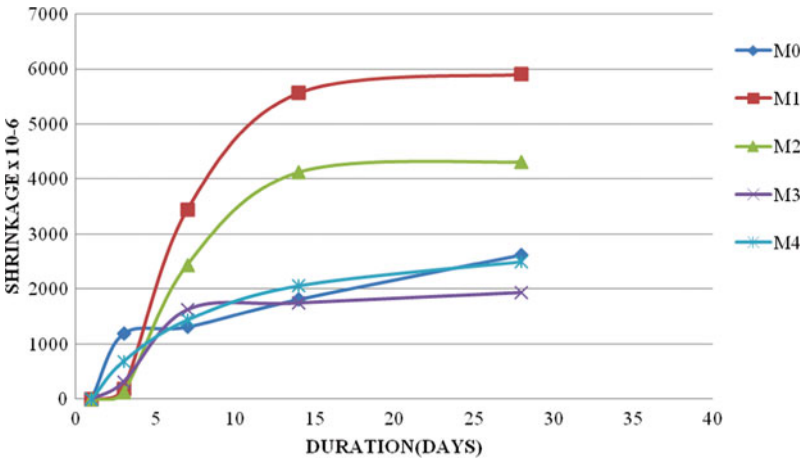

Fig. 13 Drying shrinkage-time relationship

4 Conclusion

Compared to the mix with silica fume, the mix with GGBS had lower workability (flow) and hence could have a negative influence on ease of extrusion. The yield stress and hence shape stability of the mixes incorporating GGBS and fibre enhanced the yield stress and hence the shape stability which is a vital property to extrude layers without collapsing. The compressive strength values tested in the axial direction and flexural strength improved with the incorporation of GGBS. Besides enhancement in flexural strength, fibre incorporation resulted in the smoother surface finish of extruded layers. As there is no formwork covering the surface of the freshly printed element, lower shrinkage is preferred. The addition of fibre resulted in the reduction of shrinkage by 67% for silica fume mix and 42% for the GGBS mix

References

1. Buswell RA, Leal de Silva WR, Jones SZ, Dirrenberger J (2018) 3D printing using concrete extrusion: a roadmap for research. Cement Concr Res 112:37–49
2. Sanjayan JG, Nematollahi B, Xia M, Marchment T (2018) Effect of surface moisture on inter-layer strength of 3D printed concrete. Constr Build Mater 172:468–475
3. ASTM C-150. Standard specification for Portland cement
4. Kazemian A, Yuan X, Cochran E, Khoshnevis B (2017) Cementitious materials for construction-scale 3D printing: laboratory testing of fresh printing mixture. Constr Build Mater 145:639–647
5. Papachristoforou, Mitsopoulos V, Stefanidou M (2018) Evaluation of workability parameters in 3D printing concrete. In: 1st international conference of the Greek society of experimental mechanics, Thessaloniki, Greece, May 2018
6. Rubio M, Sonebi M, Amziane S (2017) 3D Printing of fibre cement-based material fresh and rheological performances. HALId:hal-01576184 https://hal.archives-ouvertes.fr/hal-01576184
7. Lomboy GR, Wang X, Wang K (2014) Rheological behavior and formwork pressure of SCC, SFSCC, and NC mixtures. Cement Concr Compos 54:110–116
8. Rahul, MS, Meena H, Ghani Z (2019) 3D printable concrete: mixture design and test methods. Cement Concr Compos 97:13–23
9. Lu B, Yiweiweng, Li M, Qian Y, Leong KF, Tan MJ (2019) A systematic review of 3D printable cementitious materials. Constr Build Mater 207:477–490
10. Le TT, Austin SA, Lim S, Buswell RA, Law R, Gibb AGF, Thrope T (2012) Hardened properties of high-performance printing concrete. Cement Concr Res 42:558–566
11. Zhang Y, Zhang Y, Liu G, Yang Y, Meng W, Pang B (2018) Fresh properties of a novel 3D printing concrete ink. Constr Build Mater 174:263–271
12. ASTM C1437-15-Standard test methods for the flow of hydraulic cement mortar
13. Dzuy NQ, Boger DV (1983) Yield stress measurement for concentrated suspensions. J Rheology 27:321–349
14. BS EN 12390-3:2009-Testing hardened concrete-compressive strength of test specimen
15. ASTM C157-Standard test method for length change of hardened hydraulic-cement mortar and concrete
16. Zhang Y, Zhang Y, She W, Yang L, Liu G, Yang Y (2019) Rheological and harden properties of the high-thixotropy 3D printing concrete. Constr Build Mater 201:278–285

Review of Performance of Existing Vertical Irregularity Indicators for Steel Framed Buildings

Brij M. Shah, Robin Davis, C. G. Nandakumar, and Pradip Sarkar

Abstract Due to architectural compulsions, buildings invite various types of irregularities due to which seismic performance of them is highly affected. With increase in such type of buildings, it is important to know the extent to which an irregularity could be introduced without causing any major damage to the structure. Different kinds of Irregularity indices are used by many previous studies for quantifying the vertical irregularities in buildings. This study discusses about the previous irregularity indicators and an attempt is made to evaluate their effectiveness to predict the seismic risk of irregular buildings. Steel buildings having various kinds of vertical irregularities such as mass, stiffness and/or strength are considered in this study and their seismic risks is evaluated. Pearson r correlation methodology is considered for correlating the irregularity indicators and the associated seismic risks and conclusions are drawn from them.

Keywords Irregularity index · Seismic risk · Correlation coefficient

1 Introduction

Multi-storey buildings are being generally constructed with unequal distribution of mass, stiffness, and strength due to functional and architectural reasons. The buildings having unequal distribution of irregularity of mass/stiffness/strength individually or

B. M. Shah (✉) · R. Davis · C. G. Nandakumar
National Institute of Technology Calicut, Calicut, India
e-mail: brij.shah35@gmail.com

R. Davis
e-mail: robin@nitc.ac.in

C. G. Nandakumar
e-mail: nandagopalan27@gmail.com

P. Sarkar
National Institute of Technology Rourkela, Rourkela, India
e-mail: sarkarp@nitrkl.ac.in

© Springer Nature Switzerland AG 2021

K. Dasgupta et al. (eds.), *Proceedings of SECON 2020*,
Lecture Notes in Civil Engineering 97,
https://doi.org/10.1007/978-3-030-55115-5_57

in combination across the height are called vertically irregular buildings. It has been reported by many previous studies [1–5] that the performance of these types of buildings is poor as compared to that of regular buildings.

Seismic design criteria have been provided for vertically irregular buildings in various inter-national codes. However, many studies report the parameters mentioned in the codes for the quantification of irregularity exists in a building needs improvement. Previous studies [4–7] have proposed the regularity indices for quantifying the vertical irregularity based on the modal parameters or geometric parameters. It is to be noted that all the previous studies on the parameters used for quantification of irregularity in buildings were focused on the seismic performance of vertical irregular RC buildings.

The purpose of this paper is to check whether the existing irregularity indices can capture the vertical irregularities in the steel framed buildings. This research focusses on the performance of existing vertical irregularity indices by checking the correlation of them with the seismic risk of the selected vertically irregular buildings. The seismic risk is evaluated by following the procedure proposed by Allin Cornell et al. [8].

2 Detailing of the Building Considered

A seven storey steel framed building having uniform distribution of mass and stiffness considered as a regular building is taken for reference. The steel framed building is assumed to be situated in a location of seismic zone with PGA = 0.16 g (Zone-III). Plan and elevation of the selected buildings are shown in Fig. 1. The sections of beams and columns are design according to [9, 10] and details of those sections are mentioned in Table 1. Thickness of the floor slab is assumed to be concrete of 120 mm [11] which is resting on the steel beams.

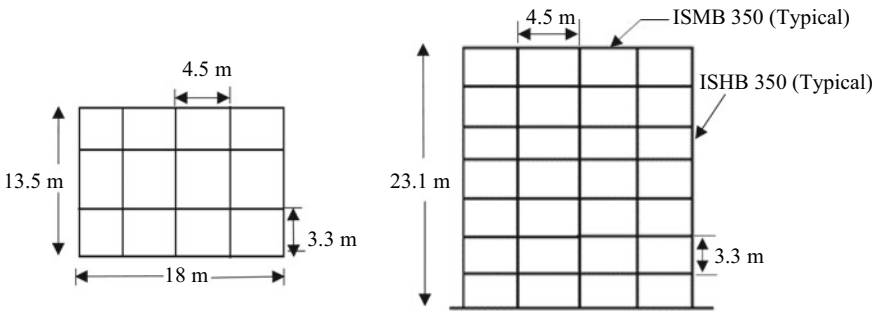

Fig. 1 **a** Plan of building considered **b** Elevation of building considered

Table 1 Different type of sections

Frame	Column section	Beam section
M-R	ISHB 350	ISMB 350
M7-7	ISHB 400	ISMB 300
M4-7	ISHB 400	ISMB 300
SI-R	ISHB 350	ISMB 350
SI-I-O	ISHB 250	ISMB 300
SI-7-O	ISHB 350	ISMB 350
SI-4-O	ISHB 250	ISMB 300
SI-1-O	ISHB 300	ISMB 300

Typical buildings with mass and a stiffness/strength irregularity are considered in this study. Mass irregular buildings are modelled by considering a swimming pool or a storage place at the top and intermediate storeys. The seismic weight of the additional mass at a selected floor in a building is taken to be in the range of 500%–700% of the seismic weight of a typical floor. A mass irregular building with a mass of 5 times of mass of typical floor level, at 4th floor level is denoted as M5-4. Similarly, M7-4 frame indicates a mass irregular frame having 7 times of the typical mass at 4th (intermediate) floor level. The performance of mass irregular buildings is evaluated with reference to a regular building (M-R) having uniform masses in all storeys.

For studying the behavior of stiffness/strength irregular buildings, a regular reference building (SI-R) is taken in which the lateral stiffness/strength at each storey (cross bracings are provided on each storey) is equal (uniform in all storeys). Stiffness/strength irregularity or discontinuity in vertical direction is introduced by considering a bays without any bracings in a particular storey. SI-1-O represents a stiffness/strength irregular building frame having ground storey (index '1' stands for first storey) as an open ground storey (index 'O' for open storey). SI-M-O depicts the frame with no bracings at 3rd and 4th storeys, SI-4-O depicts frame with no bracings at 4th storey and SI-7-O depicts the frame with no bracings at 7th storey. Figure 2 shows detailing of all the vertical irregular buildings.

3 Regularity Index

Various regularity indices have been proposed by many previous studies to quantify the irregularity of a building as shown in Table 2. Out of selected approaches, [4] proposed the index which was focused on steel setback framed buildings. Indices proposed by Pradip et al. [5, 6] was based on modal participation factor and the frequency of the building, respectively. Bhosale et al. [7] proposed the regularity index based on the ratio of maximum inter-storey drift of an irregular and regular building from elastic analysis. The regularity index proposed by Karavasilis et al. [4]

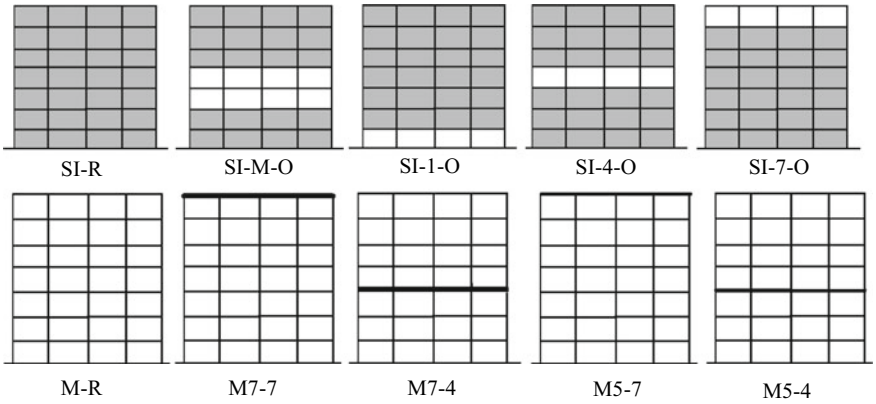

Fig. 2 Selected stiffness and mass irregular steel framed buildings

Table 2 Proposed irregularity indicators from previous studies

References	Building type	Proposed regularity indices
[5]	RC stepped frame	$\eta = \frac{\Gamma_1}{\Gamma_{ref}}$
[6]	RC setback frame	$\lambda_r = \sum_{k=1}^{N} \frac{\omega_{k,ir}}{\omega_{k,r}}$
[7]	RC framed building	$\text{SVI} = \frac{Max(ISD_{IR})}{Max(ISD_R)}$

Note Γ, Γ1 is the first mode participation factor for an irregular and regular building, respectively. ω,, ω, = *k*-th mode frequency of irregular and regular building. ISDIR, ISDR = inter-storey drift of irregular and regular building

is not included in this study as it deals with only geometric irregular buildings. It can be noted that regularity index of a regular frame will be unity and as the irregularity increases the regularity index decreases.

4 Probabilistic Seismic Risk Assessment Methodology and Modelling for Non-linear Dynamic Analysis

The current study evaluates the vulnerability of the selected vertically irregular frames by following an accepted methodology proposed by Allin Cornell et al.[8]. It uses a Probabilistic seismic demand model (PSDM), which is a relationship between PGA and median of the maximum inter-storey drifts (ISD) recorded from the nonlinear dynamic time history analysis. The slope of PSDM curve infers about the inter storey drift of the frames. The building having highest slope could be taken as most vulnerable compared to other buildings.

Table 3 Random variables considered

Material	Mean	COV (%)	Source
Yield strength of steel	250 MPa	10	Ranganathan (1999)
Global damping ratio	5%	40	Davenport and Carroll (1986)

The beams and columns of all the selected frames were modelled in OPENSEES laboratory tool [12] using the fiber element modelling approach for performing nonlinear time history analysis. An ensemble of 44 ground motions whose PGA ranging from 0.1 to 1.0 g was used for the time history analysis. The parameters, yield strength of steel and global damping ratio, were taken as random variables. Values of mean and coefficient of variation of the random variables are shown in Table 3. Latin hypercube sampling method (LHS) was used to generate 44 samples of random variables and accordingly computational models are developed using these realizations of the random samples representing the building frames. Nonlinear dynamic time history analyses of the computational models are done to record the maximum inter-storey drift from each of the building models. A graph between the parameters, PGA and ISD is plotted to obtain the PSDM model as shown in Fig. 3. It can be seen that SI-1-O shows the highest inter-storey drift whereas the SI-R is having the lowest one. The PSDM obtained from all the models is shown in Table 4.

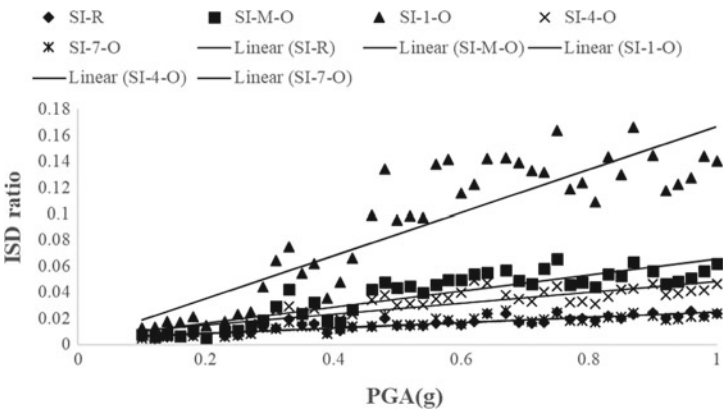

Fig. 3 PSDMs for all models

Table 4 PSDM model and measure of dispersion

Frame	PSDM	R2	βD|PGA
SI-R	0.0248(PGA)0.7336	0.7854	0.1996
SI-M-O	0.0715(PGA)1.1148	0.7788	0.2894
SI-1-O	0.1857(PGA)1.2386	0.7882	0.2833
SI-4-O	0.0508(PGA)0.8959	0.7597	0.2357
SI-7-O	0.025(PGA)0.7519	0.7471	0.2014

5 Correlation of Proposed Regularity Indicators and Probability of Unacceptable Performance

As the vertical irregularity in a frame increases the irregular frame is more likely to perform poorly. In other words, probability of unacceptable performance (failure) of irregular frames also increases with amount of irregularity. This section refers to the correlation between the proposed regularity indices with the probability of failure. Previous studies [5–7] have proposed indices which could be used in measuring irregularity which states how much a frame is irregular. In order to study the performance of the existing irregularity indicators, correlation of the existing indicators with the probability of unacceptable seismic performance (P_{PL} at various performance levels, IO, LS and CP) of the vertically irregular buildings has been calculated as shown in Tables 5 and 6. It can be noted that the order the frames in the increasing value of PPL respectively for stiffness irregular and mass irregular frames are SI-7-O < SI-R < SI-M-O < SI-4-O < SI-1-O and M-R < M7-4 < M5-4 < M5-7 < M7-7.

In case of stiffness irregular frames, the vertical irregularity increases in the order SI-1-O < SI-R < SI- 7-O < SI-4-O < SI-M-O for [5], SI-R-O < SI-7-O < SI-4-O < SI-M-O < SI-1-O for [6] and SI-R < SI-7-O < SI-4-O < SI-M-O < SI-1-O for [7].

In case of mass irregularity, the vertical irregularity increases in the order M-R = M5-4 < M7-7 < M7- 4 < M5-7 for [5], M-R = M5-7 < M7-7 < M5-4 < M7-4 for [6] and M7-4 < M5-4 < M7-7 < M5-7 < M-R for [7].

Figures 4 and 5 show the correlation between the probability of failure and irregularity index for stiffness and mass irregular frames, respectively. In case of stiffness

Table 5 Comparison of existing irregularity indices with annual Probability of unacceptable performance, P_{PL} for stiffness irregular buildings

		Existing Irregularity Index as per			Annual Probability of collapse P_{PL} ($\times 10^{-3}$)	
Frame	[5]	[6]	[7]	IO	LS	CP
SI-R	1	1	1	6.16	1.52	0.97
SI-M-O	1.10	1.47	2.6	12.41	4.94	3.67
SI-1-O	0.925	1.85	6.6	29.14	12.72	9.74
SI-4-O	1.041	1.204	1.92	13.79	4.38	3.03
SI-7-O	1.01	1.030	1.04	5.93	1.51	0.97

Table 6 Comparison of existing irregularity index with annual Probability of collapse P_{PL} for mass irregular buildings

		Existing Irregularity Index as per			Annual Probability of collapse P_{PL} ($\times 10^{-3}$)	
Frame	[5]	[6]	[7]	IO	LS	CP
M-R	1	1	1	2.3	1.13	0.9
M7-4	1.063	1.069	0.935	2.36	1.12	0.88
M7-7	1.010	1.02	0.979	6.94	2.53	1.83
M5-4	1	1.03	0.963	2.42	1.15	0.9
M5-7	1.123	1	0.98	3.14	1.4	1.08

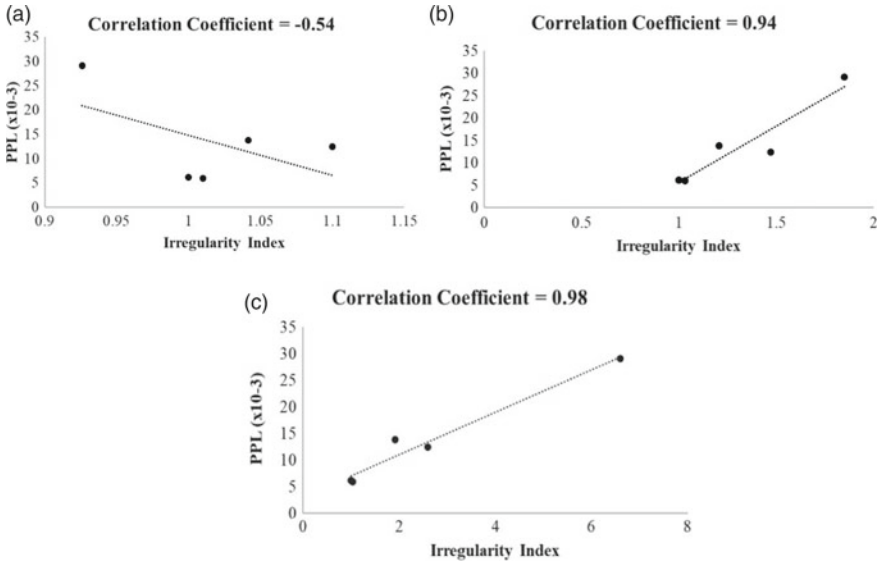

Fig. 4 Correlation between Irregularity Index and P_{PL} for: **a** [5]; **b** [6]; and **c** [7] at IO level

irregular frames, it can be observed that correlation coefficient is positive for the indices proposed by Varadharajan [6, 7] whereas it is negative for the index proposed by [5]. In case of mass irregular frames, correlation coefficient is negative for both [5, 6] but positive for [7].

6 Conclusions

Various indicators are used in existing literature to quantify the vertical irregularities in buildings. Focus of the present study is to evaluate the adequacy of the existing

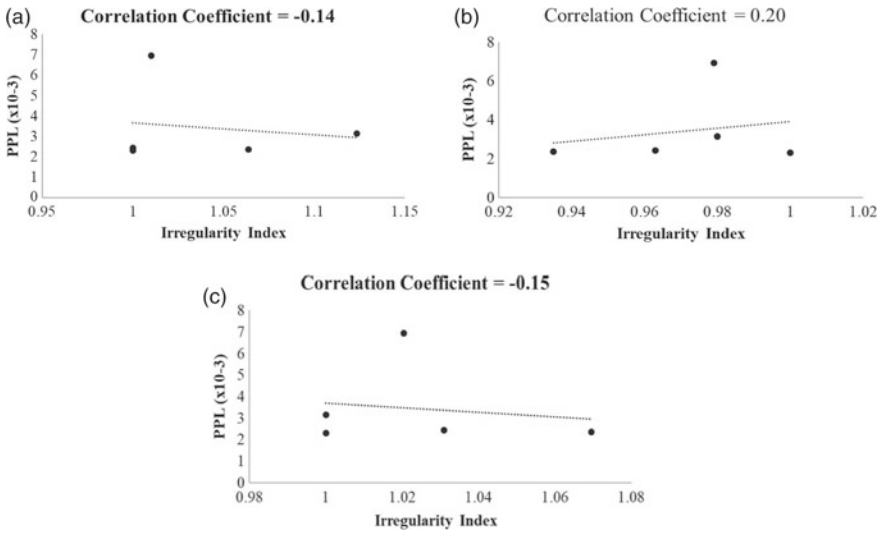

Fig. 5 Correlation between Irregularity Index and P_{PL} for: **a** [5]; **b** [6]; and **c** [7] at IO level

irregularity indicators to quantify the irregularity in selected vertically irregular steel framed buildings. Correlation between the existing indicators with the seismic risk of the selected buildings are considered and the following conclusions are made.

- Regarding seismic risk, the frames SI-1-O and M7-7 are found to be the most vulnerable when compared to respective regular buildings.
- In case of stiffness irregular framed buildings, it has been observed that the behavior of SI-7-O is very much similar to that of a regular building and hence irregularity caused by reducing the stiffness of a top storey is not much harmful during earthquake. In case of mass irregular building frame, it has been observed that the seismic risk is reduced to a far extent when swimming pool is provided at an intermediate storey rather than at top storey. The behavior of this frame is similar to that of a regular building.
- It is found that existing irregularity indicators proposed by Varadharajan [6, 7] perfectly correlates with the seismic risk.
- In case of mass irregular framed buildings, the indicators proposed by Bhosale et al. [7] is correlating well with the seismic risk.

References

1. Kien L, Kihak L, Jaehong L, Do HL (2012) Evaluation of seismic behaviour of steel special moment frame buildings with vertical irregularities. Struct Design Tall Spec Build 21:215–232

2. Zohreh B, Mehdi P (2016) Seismic evaluation of geometrically irregular steel moment resisting frames with setbacks considering their dynamic characteristics. Bull Earthquake Eng 14:2757–2777
3. Bhosale AS, Robin D, Pradip S (2017) Vertical irregularity of buildings: regularity index versus seismic risk. J Risk Uncertainty Eng Syst Part A: Civ Eng. https://doi.org/10.1061/arjua6.0000900
4. Karavasilis TL, Bazeaos N, Beskos DE (2008) Seismic response of plane steel MRF with setbacks: estimation of inelastic deformation demands. J Constr Steel Res 64(2008):644–654
5. Pradip S, Meher AP, Devdas M (2010) Vertical geometric irregularity in stepped building frames. Eng Struct 32:2175–2182
6. Varadharajan S, Seghal VK, Babita S (2013) Determination of inelastic seismic demands of RC moment resisting frames. Arch Civil Mech Eng I3:370–393
7. Bhosale AS, Robin D, Pradip S (2018)New seismic vulnerability index for vertically irregular buildings. J Risk Uncertainty Eng Syst Part A: Civ Eng 4(3):04018022
8. Allin Cornell C, Fatemeh J, Ronald OH, Douglas AF (2002) Probabilistic basis for 2000 SAC federal emergency management agency steel moment frame guidelines. J Struct Eng 128(4):526–533
9. IS 800: 2007. General construction in steel-code of practice
10. IS 1893 (Part-1). 2016 Criteria for earthquake resistant design of structures
11. IS 456: 2000. Plain and Reinforced Concrete- code of practice
12. McKenna F, McGann C, Arduino P, Harmon JA (2014) Opensees laboratory. Accessed 15 Jan 2016. https://nees.org/resources/openseeslab

Modelling the Rheological Properties of Fly Ash Incorporated Superplasticized Cement Paste at Different Temperature Using Multilayer Perceptrons in Tensorflow

Rogin C. Robert, Nelvin Mani Kuriakose, K. Gopikrishnan, Dhanya Sathyan, and C. B. Rajesh

Abstract The rheology deals with flow of matter. It changes with respect to the material composition and test condition. This work investigate the influence of dosage and family of superplasticizer and dosage of mineral admixture and effect of temperature on the rheological properties of cement paste. For this purpose cement pastes were prepared at a water cement ratio of 0.37 using OPC cement, different percentage of fly ash(15, 25, 35) and different dosages of superplasticizer (one from each family). Rheological tests were carried out using co axial cylinder viscometer at three different temperature (15, 27, 35 °C). Rheological parameters like yield stress and plastic viscosities were calculated using Bingham and Herschel bulkley model. Rheological performance were modeled using Multilayer Perceptrons in Tensorflow. Out of 252 data generated, 204 data is used for training the model. The input parameters consists of variables like dosage of cement, fly ash, water, four families of super plasticizers and three different temperatures. The output consists of the measured value of yield stress and plastic viscosity of cement paste. Accuracy of the model is tested using 48 data set. From the predicted data it is clear that the python can be used effectively to predict the rheological properties (yield stress and plastic viscosity) of cement paste.

Keywords Rheology · Fly ash · Modeling · Superplasticizer · Temperature

R. C. Robert · N. M. Kuriakose · D. Sathyan (✉)
Department of Civil Engineering, Amrita School of Engineering, Amrita VishwaVidyapeetham, Coimbatore, India
e-mail: s_dhanya@cb.amrita.edu

K. Gopikrishnan · C. B. Rajesh
Department of Electronics and Communication Engineering, Amrita School of Engineering, Amrita VishwaVidyapeetham, Coimbatore, India
e-mail: cb_rajesh@cb.amrita.edu

© Springer Nature Switzerland AG 2021

K. Dasgupta et al. (eds.), *Proceedings of SECON 2020*,
Lecture Notes in Civil Engineering 97,
https://doi.org/10.1007/978-3-030-55115-5_58

1 Introduction

Chemical and mineral admixtures are added to concrete to improve its fresh and hardened stage properties. Mainly mineral admixtures like fly ash is added to the concrete to improve workability, reduce heat of hydration, and reduce porosity by microfiller effect. Chemical admixtures like superplasticizers are added to improve the workability of concrete. Fresh stage property of concrete is mainly governed by paste phase.

The study carried out by Sathyan et al. [1] dealt with the rheological properties of Portland pozzolana cement paste (PPC) at different temperatures with different dosages of superplasticizers (SPs). In this study, cement pastes were prepared using four brands of PPC and SPs. The rheological parameters were obtained using temperature-controlled coaxial cylinder viscometer (Brookfield DV-II) with the mixes subjected to stepwise loading pattern with the shear rate ranging from 30-65 S^{-1} at three different temperatures (15, 27 and 35 °C). From the study, it is observed that the yield stress and the plastic viscosity decreased with an increase in superplasticizer dosage and increased with an increase in temperature. Rheological performance of the cement paste was also studied by other researchers [2, 3].

Authors has already studied the effectiveness of soft computing techniques like RKS and ANN in Modeling the flow behavior of cement paste [1, 4] and flow and hardened stage properties of SCC [5, 6].

The paper written by Yijin et al. [7] discussed the effect of fly ash on various phases of cement in terms of its setting time, workability and flowing property. The study showed that the spherical and smooth surface of the fly ash revealed an increased water reduction effect with increasing fineness. The setting time of the cement paste and slump increased with the addition of Ultra fine fly ash and the water demand reduced with an increase in fineness.

The research done by Sathyan and Anand [8] dealt with the durability of concrete by the combined effect of superplasticizer and pozzolanic materials. Sulphate attack, chloride penetration, acid attack were considered as the major durability problems. The reduction of permeability of concrete increased the durability of concrete which was achieved through proper compaction. The addition of superplasticizer reduced the porosity and the workability was found to be increasing.

Dispersing effectiveness of commercial plasticizers were studied by Ng and Justnes [9]. In this study Ordinary Portland Cement (OPC) was replaced by fly ash and plasticizers from different groups (LS, NSF, PCEs) were also added in this study. Fly ash replacement was done up to 60%. At lower concentration, fly ash acts as a filler and does not affect the plasticizer significantly. When 40% fly ash was used, it was found that PCEs showed reduced performance when compared with NSF and LS in the OPC system because of the greater affinity of the polymer.

Wallevik and Wallevik [10] examined how rheology can influence the optimization of concrete with the help of rheograph and workability boxes. The change in the rheological behavior of the cement-based mixture was revealed by the rheograph in a symmetrical way. Using this method, the behavioral change in different types

of concrete with the change in the quantities of its constituents and the effects of different admixtures was studied.

The research work carried out by Sonebi et al. [11] investigated the effects of metakaolin, viscosity-modifying agent and superplasticizer (SP) on optimizing the rheological parameters, hardening properties(3, 7, 28 days) and setting times of added cement grouts. The results from the study showed that the increase in SP led to an increase in flow property, setting times and decrease in cohesion, flow time, rheological study parameters.

In the research work carried out by Wu et al. [12], the development of a mathematical model to predict and analyse the rheological parameters of CPB (a mixture of binders, water, and tailings) under the effects of both temperature and hydration was studied with the help of COMSOL Multiphysics software. The predicted values obtained from the software on CPB were compared with the data obtained from various rheological or flowability tests (rheometer, slump test, and vane shear) to check the prediction ability of the software. The result showed a positive relationship between the predicted and measured rheological properties.

Python is a high-level and general-purpose programming language that comes under the category of Free and Open Source Softwares (FOSS). It finds applications in many domains such as Machine Learning, Artificial Intelligence, Blockchain, Competitive Coding, Web Development, Software development and Software testing. Multiple regression is an extension of simple linear regression, which is one of the classes that comes under Machine Learning. Multiple regression is used when the value of a variable is to be predicted based on two or more external features that are provided as inputs. The variable that is predicted is called the dependent variable, also known as the target or the criterion, and the variables that are fed as inputs are called the independent variables or the features. Multiple regression also helps in determining the model's overall fit and the relative contribution of each predictor to the total variance obtained.

2 Significance and Objectives of This Study

The effectiveness of chemical admixtures mainly depends up on the various physical and chemical factors. Compatibility checks need to be performed before selecting any binders and chemical admixtures [13, 14]. So in order to reduce the time and money required to conduct the experiments to find the compatible combinations and its required property, it is better to have a mathematical model which can predict the required property if material quantity and, test parameters are given as the input parameters

So the objectives of this work is to study the effect of test temperature on the rheology of cement paste and model the rheological property using python.

Table 1 Properties of Cement

Ordinary Portland Cement (53 Grade)	
Fineness (%)	0.5
Specific Gravity	2.86
Standard Consistency (%)	33
Initial setting time (minutes)	85
Final setting time (minutes)	305

Table 2 Properties of Fly Ash

Fly ash-Class F	
Specific gravity	2.11
Fineness %	1.2

Table 3 Properties of Superplasticizers

Superplasticizer	Solid content (%)	Density (g/cc)
LS 1	40	1.158
LS 2	17.07	1.072
PCE 1	38.095	1.225
PCE 2	37	1.079
SMF	31.665	1.227
SNF 1	37.5	1.217
SNF 2	39.13	1.225

3 Details of Materials and Sample Preparation

One brand of ordinary portland cement, superplasticizer from four different families and class F fly ash at different ratios (15, 25 and 35%) were used to prepare the cement paste. Properties of materials tested according to the codal provisions of IS4031 [15, 16, 17, 18] and IS 9103 [19] are given in the Tables 1, 2 and 3.

4 Determination of Saturation Dosage

Marsh cone [20] and mini slump tests [21] were carried out to find the saturation dosages of superplasticizer. For rheological study, the mix with superplasticizer dosage above, equal and below saturation dosage were used.

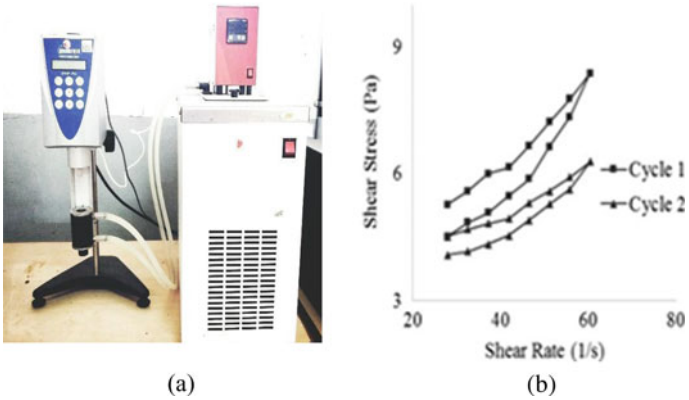

Fig. 1 **a** Viscometer; **b** Flow curve

5 Rheological Studies with Viscometer

5.1 Experimental Setup

Coaxial cylinder viscometer was used in this study (Fig. 1a). Tests were done at 15, 27, and 35 °C temperature. Loading was done in two cycles. Step wise shear rate increment (starting from 30 s^{-1} ending with 65 s^{-1}) were applied to the mix. Yield stress and plastic viscosity was determined by fitting second cycle downward curve (Fig. 1b). Bingham model and Herschel–Bulkley flow model were used to fit the data.

5.2 Effect of Temperature on Rheological Properties

Variation of rheological properties with temperature for some representative samples are shown in Figs. 2 and 3.

From the experimental result it is observed that the yield stress and plastic viscosity of cement paste decreases with superplasticizer dosage up to saturation dosage and increases with increase in temperature.

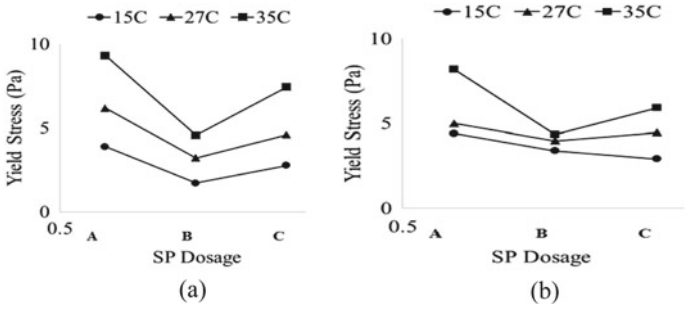

Fig. 2 Variation of yield stress with temperature for control mix having no fly ash **a** LS1 (Lignosulphate 1), **b** LS2 (Lignosulphate 2)

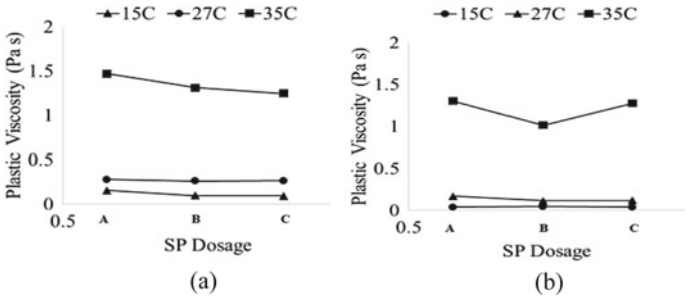

Fig. 3 Variation of Plastic Viscosity with temperature for mix having 25% fly ash and superplasticizer **a** SMF (sulfonated melamine formaldehyde condensates), **b** SNF1 (sulfonated naphthalene formaldehyde condensates)

6 Modeling of Rheological Properties

6.1 Python

To create the model, the Keras library, which is built on Tensor flow is used. To preprocess the data, the scikit-learn library in Python has been used.

A Fully Connected Dense Layer model has been implemented here. The proposed model consists of a Fully Connected Dense layer consisting of 128 nodes that takes in the input parameters, which is passed on to a dropout layer of 20% to prevent overfitting. This finally culminates in a single node that predicts the value of the output parameter.

6.2 Normalisation of Data

Normalization of data can be done in many ways. The most commonly used methods are the norm method and the standard deviation method. The method used for this modelling is the norm method. The actual values of input parameters of the test data (Selected Samples) are given in Table 4. The normalized values of out put parameters of test data are given in Table 5 (Selected values).

Table 4 Input values of test data (Selected sample)

Sample No.	C (g)	FA (g)	W (ml)	LS1 (ml)	LS2 (ml)	PCE 1 (ml)	PCE 2 (ml)	SMF (ml)	SNF 1 (ml)	SNF 2 (ml)	T (^{O}C)
1.	2000	0	724.4	25.9	0	0	0	0	0	0	15
2.	2000	0	729.3	0	0	17.1	0	0	0	0	15
5.	1700	300	694.6	0	54.6	0	0	0	0	0	15
6.	1700	300	724.2	0	0	0	25.0	0	0	0	15
9.	1500	500	721.8	30.2	0	0	0	0	0	0	15
10.	1500	500	726.7	0	0	21.4	0	0	0	0	15
13.	1300	700	694.6	0	54.6	0	0	0	0	0	15
14.	1300	700	724.2	0	0	0	25.0	0	0	0	15
19.	2000	0	718.7	0	0	0	0	31.0	0	0	27
20.	2000	0	720.0	0	0	0	0	0	31.9	0	27
23.	1700	300	728.6	0	0	0	0	0	18.2	0	27
24.	1700	300	729.8	0	0	0	0	0	0	16.6	27
27.	1500	500	722.3	0	0	0	0	25.8	0	0	27
28.	1500	500	725.7	0	0	0	0	0	22.7	0	27
29.	1300	700	694.6	0	54.6	0	0	0	0	0	27
30.	1300	700	724.2	0	0	0	25.0	0	0	0	27
31.	1300	700	722.3	0	0	0	0	25.8	0	0	27
39.	1700	300	728.6	0	0	0	0	0	18.2	0	35
40.	1700	300	729.8	0	0	0	0	0	0	16.6	35
41.	1500	500	721.8	30.2	0	0	0	0	0	0	35
42.	1500	500	726.7	0	0	21.4	0	0	0	0	35
43.	1500	500	722.3	0	0	0	0	25.8	0	0	35
44.	1500	500	725.7	0	0	0	0	0	22.7	0	35
45.	1300	700	694.6	0	54.6	0	0	0	0	0	35
46.	1300	700	724.2	0	0	0	25.0	0	0	0	35
47.	1300	700	722.3	0	0	0	0	25.8	0	0	35
48.	1300	700	729.8	0	0	0	0	0	0	16.6	35

Table 5 Normalized values of test data output (Selected values)

Sample No:	Plastic Viscosity	Yield stress
1.	0.017321	0.020176
2.	0.002473	0.004177
5.	0.078385	0.040118
6.	0.001372	0.014128
9.	0.13062	0.053887
10.	0.004414	0.03758
13.	0.057008	0.03174
14.	0.002671	0.014905
19.	0.032454	0.054612
20.	0.022576	0.042307
23.	0.162234	0.058152
24.	0.125143	0.0261
27.	0.011473	0.061176
28.	0.006763	0.020805
29.	0.103124	0.050614
30.	0.005638	0.015959
31.	0.039724	0.06425
39.	0.013489	0.073752
40.	0.010954	0.032332
41.	0.124636	0.054154
42.	0.006788	0.016937
43.	0.060643	0.076049
44.	0.041245	0.05062
45.	0.204801	0.070302
46.	0.044323	0.064538
47.	0.234202	0.081949
48.	0.197111	0.041267

6.3 Prediction Using the Model

The accuracy of prediction of rhelogical parameters of cement paste mixtures largely depend on accuracy of the training data. If data point is more accuracy will be also more. The trials were performed by changing the quantity of ingredients and test conditions. The model was trained using 204 training data sets. The input parameters are quantities of cement, fly ash, water, superplasticizers and three different temperatures.

The output is yield stress and plastic viscosity of cement paste. To check the accuracy of the model 48 set of testing data was used for predictions. Normalised

test data set are given in Tables 4 and 5. The measured and predicted values of yield stress and plastic viscosity of test data are shown in the Table 6. Root Mean Square Error (RMSE) which is the standard deviation of the residuals is used to measure the accuracy of prediction.

Table 6 Measured and predicted value of plastic viscosity and yield stress for test data

No	Plastic viscosity		Yield stress	
	Measured	Predicted	Measured	Predicted
1	0.01732	0.01698	0.02018	0.02005
2	0.00247	0.00242	0.00418	0.00415
3	0.13165	0.12903	0.04011	0.03986
4	0.00466	0.00457	0.01484	0.01475
5	0.07839	0.07683	0.04012	0.03986
6	0.00137	0.00134	0.01413	0.01404
7	0.01543	0.01512	0.04474	0.04445
8	0.00982	0.00962	0.03443	0.03421
9	0.13062	0.12802	0.05389	0.05354
10	0.00441	0.00433	0.03758	0.03734
11	0.11391	0.11164	0.0471	0.0468
12	0.06445	0.06317	0.02288	0.02273
13	0.05701	0.05587	0.03174	0.03154
14	0.00267	0.00262	0.01491	0.01481
15	0.01074	0.01053	0.04589	0.0456
16	0.00547	0.00536	0.02048	0.02035
17	0.08805	0.0863	0.04964	0.04932
18	0.00387	0.00379	0.01417	0.01408
19	0.03245	0.03181	0.05461	0.05426
20	0.02258	0.02213	0.04231	0.04204
21	0.16211	0.15888	0.05911	0.05873
22	0.01674	0.01641	0.03844	0.0382
23	0.16223	0.15901	0.05815	0.05778
24	0.12514	0.12265	0.0261	0.02593
25	0.10317	0.10112	0.03508	0.03486

(continued)

Table 6 (continued)

No	Plastic viscosity		Yield stress	
	Measured	Predicted	Measured	Predicted
26	0.00443	0.00434	0.06454	0.06413
27	0.01147	0.01124	0.06118	0.06078
28	0.00676	0.00663	0.02081	0.02067
29	0.10312	0.10107	0.05061	0.05029
30	0.00564	0.00553	0.01596	0.01586
31	0.03972	0.03893	0.06425	0.06384
32	0.02697	0.02643	0.04283	0.04255
33	0.17402	0.17055	0.06695	0.06652
34	0.03043	0.02982	0.04019	0.03993
35	0.21304	0.2088	0.07015	0.0697
36	0.1522	0.14917	0.03424	0.03402
37	0.13391	0.13124	0.03651	0.03627
38	0.00696	0.00682	0.02964	0.02945
39	0.01349	0.01322	0.07375	0.07328
40	0.01095	0.01074	0.03233	0.03213
41	0.12464	0.12216	0.05415	0.05381
42	0.00679	0.00665	0.01694	0.01683
43	0.06064	0.05944	0.07605	0.07556
44	0.04125	0.04042	0.05062	0.0503
45	0.2048	0.20073	0.0703	0.06985
46	0.04432	0.04344	0.06454	0.06413
47	0.2342	0.22954	0.08195	0.08143
48	0.19711	0.19319	0.04127	0.041

From the results of analysis, it can be observed that the model could predict the yield stress and plastic viscosity of testing data with a RMSE value of 0.04% and 0.19% respectively.

7 Conclusions

- For all the mixes, increase in yield stress and plastic viscosity is observed with increase in temperature.
- PCE (Polycarboxylate Ether) based mixes has displayed effective dispersing ability in all three test temperature range investigated.
- The model predicted the training and testing data values of yield stress and plastic viscosity. Their root mean square error is 0.029 and 0.04% for training and testing data of yield stress values and 0.134 and 0.19% for training and testing values of plastic viscosity.
- The proposed model has some limitation in prediction due to limited amount of training data. If more datas are available the accuracy can be improved.

References

1. Sathyan D, Balakrishnan AK, Mohandas SM (2018) Temperature influence on rheology of superplasticized pozzolana cement and modeling using RKS algorithm. J Mater Civil Eng 30(9):04018221
2. Sindhu Menon M, Dhanya Sathyan, Anand KB (2017) Studies on rheological properties of superplasticised PPC paste. Int J Civil Eng Technol 8(10):939–947
3. Robert RC, Dhanya Sathyan, Anand KB (2018) Effect of superplasticizers on the rheological properties of fly ash incorporated cement paste. In: Material today proceeding, pp 23955–23963
4. Sathyan D, Anand KB, Jose C, Aravind NR (2018) Modelling the mini slump spread of superplasticized PPC paste using RLS with the application of random kitchen sink. IOP conference series, vol 310. https://doi.org/10.1088/1757-899x/310/1/012035
5. Sathyan D, Anand KB, Prakash AJ, Premjith B (2018) Modeling the fresh and hardened stage properties of self-compacting concrete using random kitchen sink algorithm. Int J Concr Struct Mater 12(1):24
6. Prakash AJ, Dhanya Sathyan, Anand KB, Aravind NR (2018) Comparison of ANN and RKS approaches to model SCC strength. In: IOP conference series, vol 310. https://doi.org/10.1088/1757-899x/310/1/012037
7. Yijin L, Shiqiong Z, Jian Y, Yingli G (2004) The effect of fly ash on the fluidity of cement paste, mortar, and concrete. In: Proceedings of the international workshop on sustainable development and concrete technology, Beijing, pp 339–345
8. Sathyan D, Anand KB (2019) Influence of superplasticizer family on the durability characteristics of fly ash incorporated cement concrete. Constr Build Mater 204:864–874
9. Ng S, Justnes H (2016) Influence of plasticizers on the rheology and early heat of hydration of blended cements with high content of fly ash. Cement Concr Compos 65:41–54
10. Wallevik OH, Wallevik JE (2011) Rheology as a tool in concrete science: the use of rheographs and workability boxes. Cement Concr Res 41(12):1279–1288
11. Sonebi M, Lachemi M, Hossain KMA (2013) Optimisation of rheological parameters and mechanical properties of superplasticised cement grouts containing metakaolin and viscosity modifying admixture. Constr Build Mater 38:126–138
12. Wu D, Fall M, Cai SJ (2013) Coupling temperature, cement hydration and rheological behaviour of fresh cemented paste backfill. Minerals Eng 42:76–87
13. Sathyan D, Anand KB, Mini KM (2016) Experimental study on Portland pozzolana cement-superplasticiser compatibility in mortar. Int J Earth Sci Eng 9(2):539–544

14. Jayasree C, Gettu R (2008) Experimental study of the flow behaviour of superplasticized cement paste. Mater Struct 41(9):1581–1593
15. IS 4031, Part 5 (2005) Method for determination of initial and final setting time of cement. Bureau of Indian standards, New Delhi, India
16. IS: 4031, Part 1 (2005) Indian standard specification for method of physical tests for hydraulic cement, determination of fineness by dry sieving. Bureau of Indian standards, New Delhi
17. IS: 4031, Part 11 (2005) Indian standard specification for method of physical tests for hydraulic cement, determination of density. Bureau of Indian standards, New Delhi
18. IS: 4031, Part 4 (2005) Indian standard specification for method of physical tests for hydraulic cement, determination of consistency of standard cement paste. Bureau of Indian standards, New Delhi
19. IS 9103 (2004) Concrete admixture-specification. Bureau of Indian standards, New Delhi, India
20. EN B (2007) 445, Grout for Prestressing tendons-test methods. British Standards Institution
21. Kantro DL (1980) Influence of water reducing admixture on properties of cement paste—a miniature slump test. Cement Concr Aggregates 2(2):95–102
22. IS 1727 (2013) Methods of test for pozzolanic materials. Bureau of Indian standards, New Delhi, India

Study on Shear Strength of Corrugated Webs with Artificial Corrosion Pits

M. V. Rahul and V. I. Beena

Abstract Steel bridge girders are very common in marine or offshore structures. In such salty conditions chance of formation of pitting corrosion is high and the failure due to pitting is observed to be catastrophic. Steel girders with corrugated web can be widely used as bridge girders due to its out of plane buckling strength and also the number of stiffeners can be minimised compared to plane web. Since the failure due to pitting corrosion mainly occurs at supports, assessment of shear buckling strength is very much important. In this study shear strength of corrugated web with artificial corrosion pits numerically computed by varying corrosion volume and position. Failure patterns and the behaviour was investigated. The critical buckling load was found to be decreased while increasing the volume ratio. In the case of specimens with same volume ratio corrosion position has a significant role in assessment of shear strength of the specimen.

Keywords Corrugated web · Pitting corrosion · Shear strength etc

1 Introduction

Corrugated web I girders is one of the advancements in steel structures especially in thin steel structures. The corrugated web boosts the buckling stability of I girders and provides adequate stiffness. The corrugated steel plates are widely used in plenty of structures as structural elements. Corrugated web girders have been substantially used in many steel structures like bridges, beams, roofs etc. Many researchers have pointed out that trapezoidal corrugated webs are most efficient and economical sections in many aspects. Corrugations produces numerous corners in the web configuration. Due to such corners corrugated webs force to catch moisture, sediment and other

M. V. Rahul (✉) · V. I. Beena
Government College of Engineering, Kannur, India
e-mail: rahulmvcpnr@gmail.com

V. I. Beena
e-mail: drvibeena@gmail.com

© Springer Nature Switzerland AG 2021

K. Dasgupta et al. (eds.), *Proceedings of SECON 2020*,
Lecture Notes in Civil Engineering 97,
https://doi.org/10.1007/978-3-030-55115-5_59

impurities. Thus, corrugated steel plates are more prone to corrosion and disintegration than flat plates. Exposure of a steel girders, especially in the case of bridges, to the marine conditions and scarce maintenance will cause corrosion and leads to deterioration of its operation. Corrosion becomes one of the major causes of deterioration of steel girder bridges which reduce their load carrying capacities, structural performances and ultimately leads to catastrophic collapses.

Pitting corrosion is the localised corrosion of a metal surface, concentrated to a point or small area that results in the form of cavities or holes. Distinct areas of a material undergo accelerated attack while most of the other surface remains practically unaffected.

The attack leads to characteristic forms of cavity, such as pits or crevices in the metal surface which also run in depth of plate. In this study artificial pitting corrosion was considered in which environmental effects on corrosion or chemical products of corrosion neglected.

The aim of this study is to do further research on the shear behaviour of corrugated web beams with artificially created corrosion pits. Influence of corrosion volume and position effects the shear buckling load is investigated.

2 Literature Review

In order to increase the out-of-plane stiffness and buckling strength without the use of vertical stiffeners, corrugated webs has been used many years before, first in aircraft design and later for civil engineering applications in buildings and bridges. Several researches were conducted by researchers on corrugated web structures. Extensive and wide research has been done on the behaviour of beams with corrugated webs. It is almost accepted that the strength of the web is less affected by flexure. Thus the primary aim of a web is to prevent shear forces in a corrugated web beam.

Tests were done on beams with corrugated webs to failure under shear and observed that the cause of the failure was buckling of web. The test specimens could be using finite element programs to perform nonlinear analysis [1]. Corrugated web fails under different buckling modes. Slenderness of individual folds found to be controlling the local buckling and slenderness of the unified web was noticed to be controlling the global buckling [2]. By analyzing the post-buckling behaviour as well as the shear buckling behaviour, the shear buckling failure modes of web panels with corrosion can be evaluated. Modifying the geometrical conditions and corrosion conditions of the web panels their shear buckling values were evaluated from non-linear analysis. In the uncertainty of the corrosion problem of web the reduction factor can be used to evaluate the residual strength. [3].

A non-linear FE analysis method is the right way to obtain the shear stress distribution in a flat and corrugated web, since there was limitations to find out stress distribution through experimental investigations. There are three types of shear buckling: local, global, and interactive in models [4]. Local shear buckling behaviour can be done by eigen value buckling analysis. In the local shear buckling behaviour of

beams with trapezoidal corrugated webs web thickness, width of panel and height of web on the local shear buckling coefficient had significant influence [5].

The effective thickness of corroded girder determines the remaining strength of girder depending up on the different corrosion conditions [6]. In the case of pitting corrosion stress concentration would occur near the corrosion pits. In order to assess stress concentrating effects of pitting corrosions like fatigue life reduction caused by the state of a corroded specimen. And it was done particularly by the study of stress concentrations considering the geometrical inconsistency introduced to a surface [7]. Different corrosion height, depth and pit diameter are the parameters that influence the ultimate shear strength of corroded corrugated girders. The bearing capacity decreased by nearly half compared with no corrosion through 8% corrosion volume decrease. The curve of vertical displacements and load was linear before reaching the ultimate strength and corrosion affects the slope of the curve. Yielding, local buckling, global buckling or interactive buckling are the major failure modes under shear load [8].

3 Structural Model and Material Properties

The specimen I-girder had a height of 624 mm with web height (h) 600 mm. and of length 2.66 m. The corrosion length is limited to half of the girder length and was kept same for all specimens. The corrosion height was set to one-quarter of the web height. Corrosion depth is made 100% (complete perforation). The corrosion depth, volume and classification of specimen are shown in Table 1. Ratio of the uncorroded volume to the total volume of the corrugated web is represented as volume ratio.

High quality cold-rolled steel plates (Q235) which is chinese standard of steel used in bridges which is equivalent to E250 BR of Indian standard steel. Stress-strain data of colled rolled Q235 steel was used [9]. The values of poisson's ratio and Young's modulus were taken as 0.3 and 200 GPa respectively. Dimensions and support condition of specimen are as shown in Fig. 1. Load is provided statically on top of the specimen at its mid-span.

Table 1 Specimen dimensions and details

Name	Artificial pit diameter (mm)	Depth	Extend	Volume ratio (%)	Position
CW0P0D	Uncorroded			100	
CW5P2DT	5	Perforation	¼ h	95	Top
CW5P2DM	5	Perforation	¼ h	95	Middle
CW5P2DB	5	Perforation	¼ h	95	Bottom
CW10P2DT	10	perforation	¼ h	92	Top
CW10P2DM	10	Perforation	¼ h	92	Middle
CW10P2DB	10	Perforation	¼ h	92	Bottom

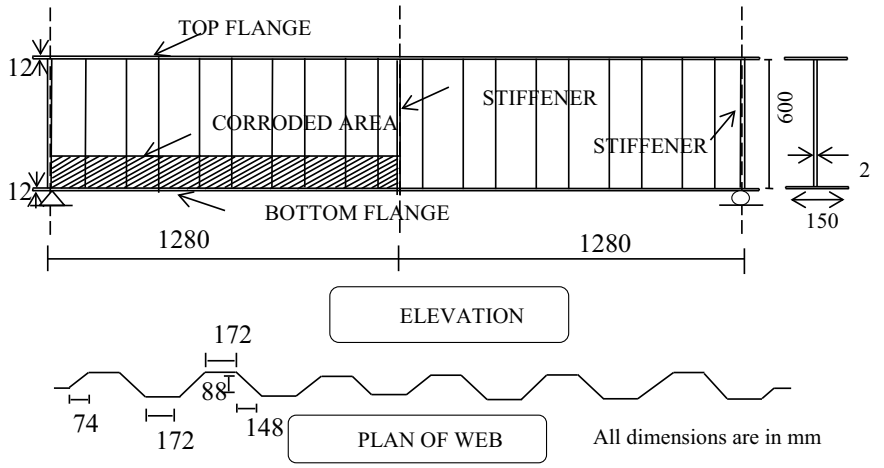

Fig. 1 Dimensions of specimen with corroded web panel (Zongyi Wen et al.)

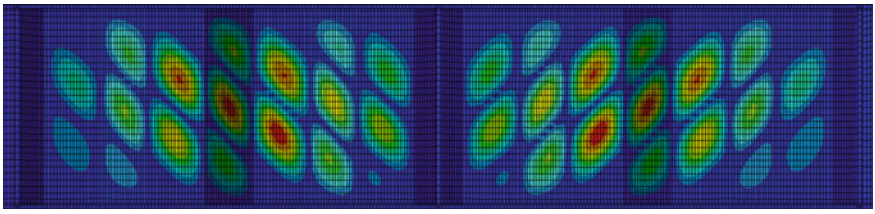

Fig. 2 Total deformation of CW0P0D specimen

4 Finite Element Analysis and Modelling

Evaluation of shear buckling behaviour of corrugated webs with corrosion pits experimentally was very difficult. Assessment of shear stress was much difficult in experiment since shear failures are catastrophic. So finite element analysis was done using ANSYS 19.1 on various corrugated webs with artificial corrosion pits. Also analysis was done by changing the position and volume of corrosion.

The steel girder with corrugations were modelled using SHELL181 elements. SHELL181 is suitable for analysing thin to moderately-thick shell structures. It is a four-noded element.At each node it has six degrees of freedom which includes translations in the x, y, and z directions, and rotations about the x, y, and z-axes. Corrosions were created by removing material from corrugated web forming holes of 5 and 10 mm diameter.

5 Validation

The purpose of the validation of models was to check the veracity of nonlinear FE analysis results with experimental results. Validation was done on the specimen used in the experiment conducted by Wen et al. [8]. Displacements were applied to the ends to simulate boundary conditions. In the I-girder test is done under constant shear stress by applying a one point load at its mid-span of the specimens. In non-linear analysis of corrugated webs in order to track the exact behaviour it was necessary to perform eigen value buckling and post buckling analysis. The post buckling behaviour is a non-linear behaviour which takes place in a very short time. The specimens were loaded using force control. An initial imperfection of 1 kN in eigen value buckling and Post buckling was done by providing 10 kN in each step. After eigen value buckling a multiplier value is obtained, which on multiplying with initial imperfection load results in buckling load of specimen in that mode shape. In practical cases. imperfections were present in corrugated webs like material and geometrical imperfections which affects the buckling behaviour of specimen.

Figure 3 depicts the relation between load and lateral deformation of corrugated web. The specimen CW0P0D with no corrosion had critical load of 200 kN from experiment while FEM analysis gave 191.30 kN as critical buckling load. It may be due to variation of properties or error experimental setup. The specimen failed by local shear buckling. exhibited local shear buckling failure. Figure 2 shows the total deformation of uncorroded corrugated web specimen. It exhibited that diagonal out of plane displacements were confined to within the panel boundary (Fig. 4).

Figure 4 shows the failure mode and strip formation in the specimen with 5 mm pit corrosion at bottom of the web both in experiment and in FEM analysis. It was found to be multiple failure strips extend at a constant angle, in the range 40°–50° and the angle increases when it continue beyond the perforated or corroded area.

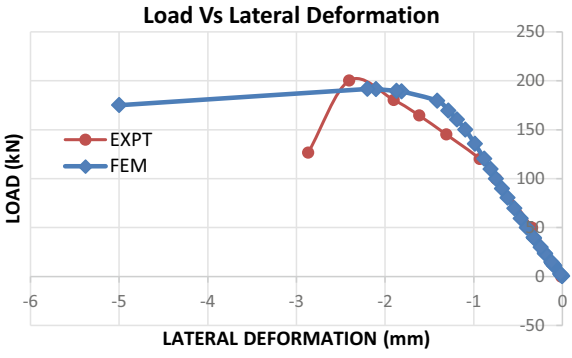

Fig. 3 Load versus lateral deformation graph of specimen CW0P0D specimen

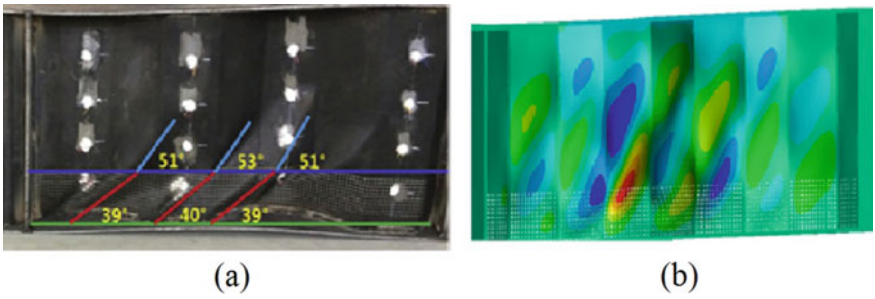

Fig. 4 Failure mode with 5 mm corrosion pits **a** Specimen by Wen et al. (2019), **b** CW5P2DB

6 Results and Discussion

The specimens were loaded using force control, with the force applied at the top centre of the beam. The boundary conditions were taken as simply supported condition. The specimens CW5P2DT, CW5P2DM, CW5P2DB had 5 mm diameter corrosion pits extended up to one-fourth of the height at different positions top, middle, bottom respectively of the web. And the specimens CW10P2DT, CW10P2DM, CW10P2DB had 10 mm diameter corrosion pits extended up to one-fourth of the height at different positions top, middle, bottom respectively of the web.

The critical load and ultimate shear strength were analysed from the displacement diagrams and stress-strain plots. The first bifurcation point in the stress-strain curve is found to be critical buckling load. And the maximum load was represented as the ultimate strength. The ultimate shear strength sometimes equivalent to their critical buckling load. Also by drawing the load-principal strain relationships and load-shear stress relationships the critical buckling load and shear strength can be clearly identified. Shear stress distribution in various specimen with 5 mm pit corrosion at different position showed in Fig. 5.

Figure 5a, b exhibited global buckling and 5c showed local or interactive buckling. From the shear stress distribution of each model, it could be inferred that the maximum shear stress concentrated along the diagonal line of the web plate subjected to the shear load.

In order to obtain the critical buckling load and shear strength the relation between load and shear stress, load and principal strain were drawn and depicted in Fig. 6a, b. Critical buckling load and ultimate shear strength, maximum load in the curve, were equal and it was around 120 kN. There was no noticeable change according to the position of corrosion. But in the case of specimens with 10 mm diameter pits at middle portion had a critical load less than the other two. The relation between load, shear stress and principal strain of specimens with 10 mm diameter pits shown in Fig. 7a, b to find out the critical buckling load and shear strength.

The critical buckling load of CW10P2DB is slightly higher than the other two specimens with 10 mm diameter and it is about 115 kN. Maximum principal strain of three specimen showed similar trends and maximum value was around 1100.

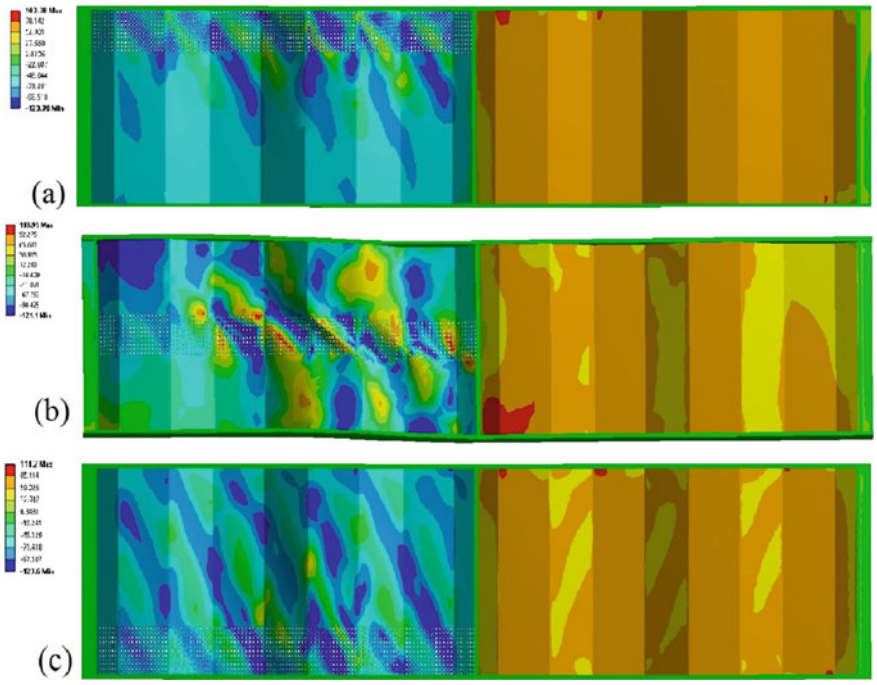

Fig. 5 Shear stress distribution of specimen **a** CW5P2DT, **b** CW5P2DM, **c** CW5P2DB

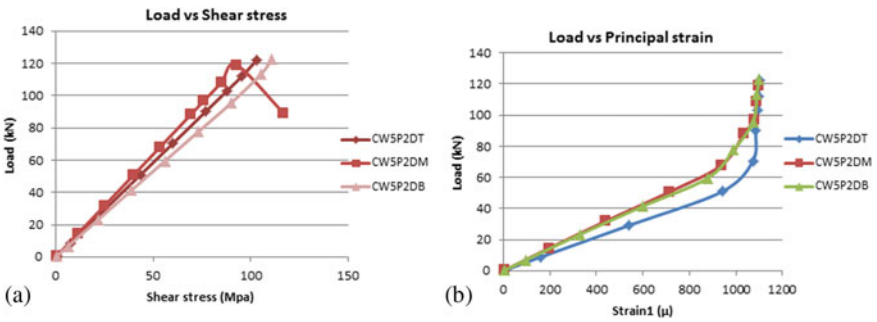

Fig. 6 Load–shear stress/principal stain relationships of specimen with pits of 5 mm diameter

7 Conclusion

The behaviour of corrugated webs with artificial corrosion pits were studied numerically by changing volume ratio and corrosion position.

- Specimens with volume ratio 95% showed larger critical buckling load than specimen with 92% volume ratio.

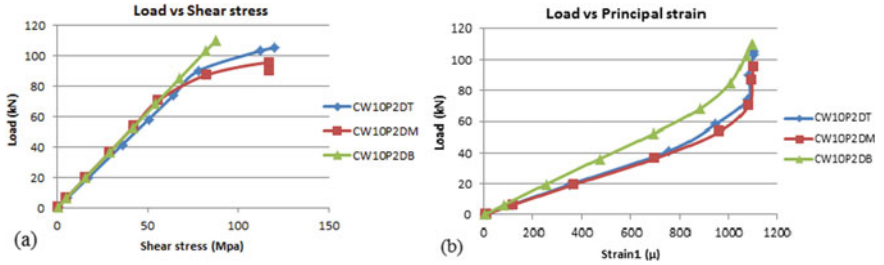

Fig. 7 Load–shear stress/principal stain relationships of specimen with pits of 10 mm diameter

- Specimens with volume ratio 92% or with 10 mm diameter pits, the specimen with corrosion positioned at bottom failed in minimum shear stress compared to other specimens.
- Corrosion volume is a crucial factor that affects the behaviour of corrugated web. As the corrosion volume increased, buckling load decreased.
- In case of specimens with volume ratio 95%, specimen corrosion at middle buckles with minimum shear stress.
- Specimens with corrosion at middle had taken shear stress even after buckling to certain extent, may be due to some fold formation at middle.
- Corrosion position has a significance in the case of specimens with larger corrosion volume. Corrosion position affect the failure modes and formation of failure strips. More study is needed to predict its influence in shear strength.

Appropriate design guide lines have to be added in design of corrugated web girders in order to reduce the risk due to corrosion by doing further research.

References

1. Elgaaly M, Hamilton RW, Seshadri A (1996) Shear strength of beams with corrugated webs. J Struct Eng 122(4):390–398
2. Sause R, Braxtan TN (2011) Shear strength of trapezoidal corrugated steel webs. J Constr Steel Res 67(2):223–236
3. Ahn JH, Kim IT, Kainuma S, Lee MJ (2013) Residual shear strength of steel plate girder due to web local corrosion. J Constr Steel Res 89:198–212
4. Riahi F, Behravesh A, Fard MY, Armaghani A (2018) Shear buckling analysis of steel flat and corrugated web I-girders. KSCE J Civil Eng 22(12):5058–5073
5. Aggarwal K, Wu S, Papangelis J (2018) Finite element analysis of local shear buckling in corrugated web beams. Eng Struct 162:37–50
6. Appuhamy JRS, Ohga M, Chun PJ, Dissanayake PR (2013) Enhanced effective thickness for remaining strength estimation of corroded steel bridge members
7. Kolios A, Srikanth S, Salonitis K (2014) Numerical simulation of material strength deterioration due to pitting corrosion. Proc CIRP 13:230–236

8. Wen Z, Wei X, Xiao L, He K (2019) Experimental evaluation of the shear buckling behaviors of corrugated webs with artificial corrosion pits. Thin-Walled Struct 141:251–259
9. Xu G, Liu Y, Xu N (2015) Constitutive relation research of Q235 Steel based on support vector machine. In: International conference on architectural, civil and hydraulics engineering. Atlantis Press

Collapse and Buckling Behavior of Octagonal Concrete Filled Steel Column Connected to a Beam Under Cyclic Loading

Silia Mary Silbi and Sajan Jose

Abstract The Octagonal concrete filled steel tubular (CFST) sections offer greater efficiency than square and rectangular tubular sections because of their better local-buckling resistance and flat surfaces that allow easier connection construction compared with circular tubular sections. This paper presents analytical studies on the seismic behavior of steel I-beam to octagonal CFST column assemblies with external diaphragms. Different stiffeners, slenderness ratios and moment capacities were introduced in the external and corner octagonal column-beam model and studied analytically using the software ANSYS 16.1. In the analytical study finite element models are developed to predict the hysteretic behavior and the stress distribution. Steel to concrete interfaces are modelled by hard contact with friction. The loading condition is displacement controlled and the axial load is applied on the top of the column and lateral load is applied on the column by cyclic vertical load on the beam ends. The stress distribution of model components, including steel beams, steel tubes, stiffeners and concrete cores are illustrated. The results indicate that failure modes have significant effects on the characteristic of stress distribution.

Keywords Concrete filled steel tube (CFST) · Finite element analysis · Hysteretic behavior · Stress distribution

1 Introduction

A column or a pillar in architecture and structural engineering is the structural element that transmits, through compression, the weight of the structure above to other structural elements below. In other words, the column is a compression member. For the purpose of wind or earthquake engineering, the columns may be designed to resist lateral forces. Other compression members are often termed columns because of similar stress conditions. Columns are frequently used to support the beams or the arches on which the upper parts of walls or ceilings rest. In the architecture, column

S. M. Silbi (✉) · S. Jose
Department of Civil Engineering, Universal Engineering College, Thrissur, India
e-mail: siliamarysilbi@gmail.com

© Springer Nature Switzerland AG 2021

K. Dasgupta et al. (eds.), *Proceedings of SECON 2020*,
Lecture Notes in Civil Engineering 97,
https://doi.org/10.1007/978-3-030-55115-5_60

refers to such a structural element that also has certain proportional and decorative features. A column might also be a decorative element not needed for the structural purposes. Column is a vertical member in building whose primary function is to support structural load and transfer it through the beams. Upper columns transfers the load to the lower columns and finally to the ground through the footings.

Concrete-filled steel tubular (CFST) columns are among the most economical and structurally efficient among reinforced and composite members in terms of resistance to high compressive loads. In addition to the steel tube being used as a load-carrying component. It also provides the confinement to concrete core, thereby increases the compressive strength and improves ductility of the concrete. Further, the steel sections can be used as temporary works for fresh concrete so the cost of fabricating formworks can be saved. The load capacities and stress-strain relationships of octagonal steel tube confined concrete (STCC) stub columns are very close to those of circular STCC, and the reduction of confinement effectiveness due to the change in the cross section shapes from circular to octagonal shape is small in terms of the load capacity. The confinement effectiveness in square STCC is much lower than that in circular and octagonal STCC [1]. In stub column tests, it was observed that the compact octagonal cross-section showed a similar cross-sectional behaviour in compression comparing with that for circular cross section and showed a better performance compared to the square cross-section with the same equivalent width [2].

The objectives of the topics are to improve the buckling strength and axial load performance of octagonal CFST column, to study the effective octagonal column under seismic performance by applying cyclic load and using stiffeners to improve the buckling capacity by different shapes, positions and arrangement.

2 Proposed Methodology

Literature survey is to be done by referring and going through articles and journals published in the related area of the studies to get detail subject knowledge. Model selection and related data collection that will aid in completing the work has to be done, such as validation model detail collection, earth quake data collection etc. Software study is an important step in this project; one should do a software study to get used to the software tools. This helps to eliminate all possible errors that could creep up during modeling and analysis. Then the modeling of validation model. Octagonal column with axial load is modeled for validating. Validation process is an important process which ensures correctness of the end product, this process helps to check product quality obtained from the software. Validation should be done using same software in which project study is being planned. Analysis of the octagonal columns beam connection with varying parameters (type of stiffeners, arrangement of stiffeners, various slenderness ratios, and moment capacities) helps to understand the cyclic performance. Result and discussion is a key step in the project. After conducting analysis, results obtained are carefully studied and reasons

for such outputs have to be discussed in detail to understand the obtained output. Conclusions have to be drawn from the obtained result. This should consist of a brief account of the entire project including procedure adopted and result.

3 Validation

The column selected for validating the software is 1500 mm height 197 mm edge length of octagon section 5.88 mm thickness of the steel tube [3]. The corner to corner length of the section is 475 mm. Pushover analysis was performed. Modelling and Analysis were done using ANSYS 16.1.

The column exhibit local buckling. Pushover analysis of the octagonal column modeled in ANSYS 16.1 gives a load carrying capacity of 13,491 kN against the one obtained in the validating journal as 12,992 kN (as shown in Fig. 1).

The result obtained from ANSYS is close to the result in the validating journal. There is only 3.69% error in the result. By validating the results through Finite

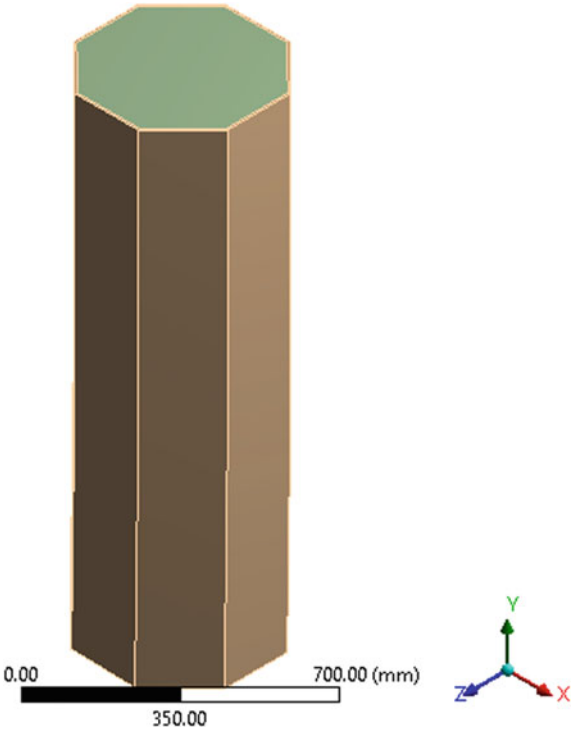

Fig. 1 Isometric view

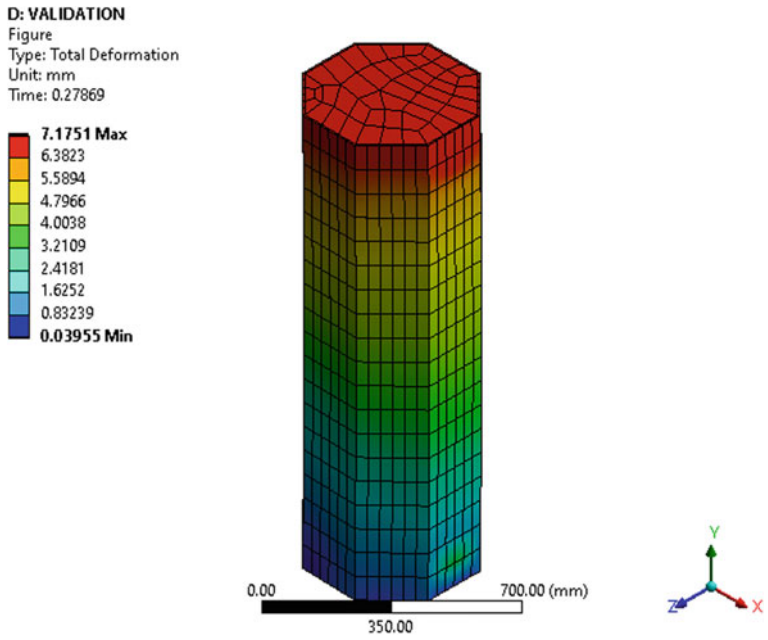

Fig. 2 Total deformation

element analysis it can be concluded that structure modeling is correct and results obtained are closer to original value. Further analysis can done (as shown in Fig. 2).

4 Modelling and Analysis

The column size is selected as 1500 mm height 197 mm edge length of octagon section and 5.88 mm thickness of the steel tube. The corner to corner length of the section is 475 mm. The column is analysed on the basis of different stiffeners, different slenderness ratios and different moment capacities in interior and corner columns. The column subjected to axial and cyclic loading. First the axial load is only applied and then the lateral load is applied on the beam in the column. By applying the axial load the stiffness of the column can calculated and then the column is under the lateral load. The material properties of concrete and steel are given in Table 1 [4, 5]. The FE modeling uses the element type 20 noded solid 186. It is a nonlinear analysis. The concrete has multilinear property. Steel have bilinear property.

Table 1 Material properties

Properties	Concrete	Steel
Young's modulus (MPa)	37,881	2×10^5
Yield strength(MPa)	–	345
Poisson's ratio	0.15	0.256

4.1 Axial Strengthening of Column by Stiffeners

From the old papers it is seen that the column under axial load will deformed as local buckling as bulging of the member. The column is under axial loading only. To reduce these effect different type of stiffeners are provided. The adopted stiffeners based on shapes are

- Rectangular stiffeners—continuous
- U-shaped stiffeners—continuous
- L-shaped stiffeners—continuous.

From the above three models the more load carrying capacity is for rectangular stiffeners. Hence this model is taken for further analysis. The arrangement of the stiffeners in the column was changed as below

- Rectangle single row 4 sides
- Rectangle single row 8 sides
- Rectangle double row 4 sides.

The result as shown in Table 2. The arrangement of rectangular stiffeners does not give any significance in the load carrying capacity of the column. The most effective model is concluded as rectangular- continuous stiffeners and it is taken for the further analysis (as shown in Fig. 3).

Table 2 Result of different stiffeners in column

		Load (kN)	Deformation (mm)
Shape of stiffeners	Rectangle	13,602	8.69
	U-shape	13,409	11.09
	L-shape	13,413	9.875
Arrangement of stiffeners	Rectangle single row 4 sides	13,215	16.74
	Rectangle single row 8 sides	13,130	14.19
	Rectangle double row 4 sides	13,161	14.75

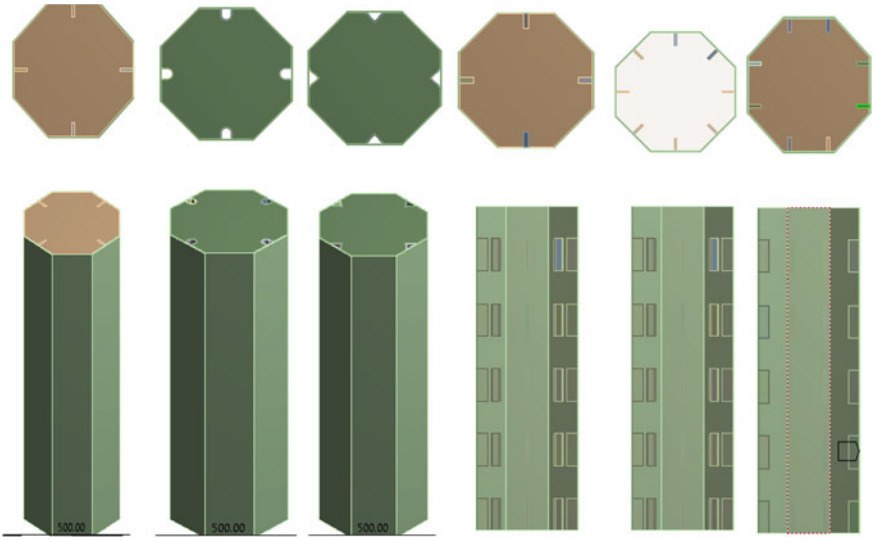

Fig. 3 Arrangement of stiffeners

4.2 Columns Under Cyclic Loading

To study the cyclic behaviour of column an ISLB 300@ 0.377 kN/m beam were connected on the octagonal column. Lateral load is applied as displacement controlled method up to 4% of drift. From FEMA (Federal Emergency Management Agency) drift percentage values are 0.3750, 0.5000, 0.7500, 1.000, 1.500, 2.000…etc. According to AISC seismic provisions for the special moment frames, the beam column connection shall be capable of sustaining an inter story drift angle of at least 0.04 radians (AISC-2005). From the values 4.000 is taken as drift percentage for the project (given in Table 3) [3, 5, 6].

$$\text{For } 4.000\% \text{ radian} = \frac{4}{100} \text{ radian}$$
$$= 0.04 \text{ radian}$$

$$\text{Drift angle, } \theta = 0.04 \times \frac{180}{\pi} = 2.2918^{\circ}$$

Table 3 Geometrical and material properties of specimens

Model		Section (mm)	Yield strength (MPa)
I- beam	Flange Web	150 × 9.4 281.2 × 6.7	257 285
Diaphragm		300 × 6	332

Table 4 Load deformations (slenderness ratios)

Slenderness ratios	Ultimate load (kN)	Displacement (mm)
7.82	165.85	40.456
9.116	172.03	41.662

$$\begin{aligned}\text{Drift displacement, x} &= \text{beam length} \times \tan(2.2918)\\ &= 1.3022 \times \tan(2.2918)\\ &= 0.052115\ \text{m}\\ &= 52.115\ \text{mm}\end{aligned}$$

4.2.1 Slenderness Ratios in Exterior Column

The effect of slenderness ratios in column beam joint were illustrated in Table 4. The length of the column is taken as 3.3 m and the width of the octagonal column were changed.

4.3 Failure Modes

For the exterior joints, the failure mode of severe beam flange buckling and moderate web buckling, shown in Fig. 4 in the finite element analysis (as shown in Fig. 5).

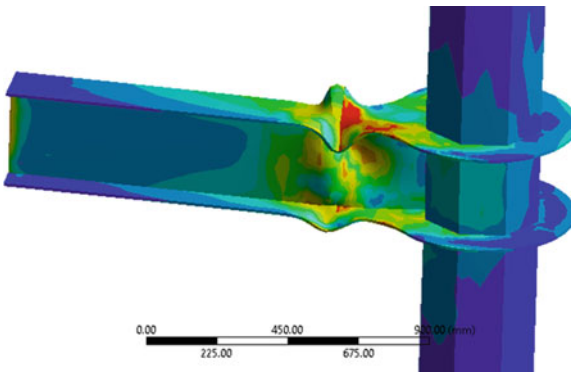

Fig. 4 Stress distribution

Fig. 5 Failure behavior of column

4.4 Hysteretic Behavior

Figure 6 show the predicted load–displacement hysteretic curves. For the exterior joints the initial stiffness, yield load, hardening stiffness, peak load, and unloading slope of the predicted curves are in good agreement.

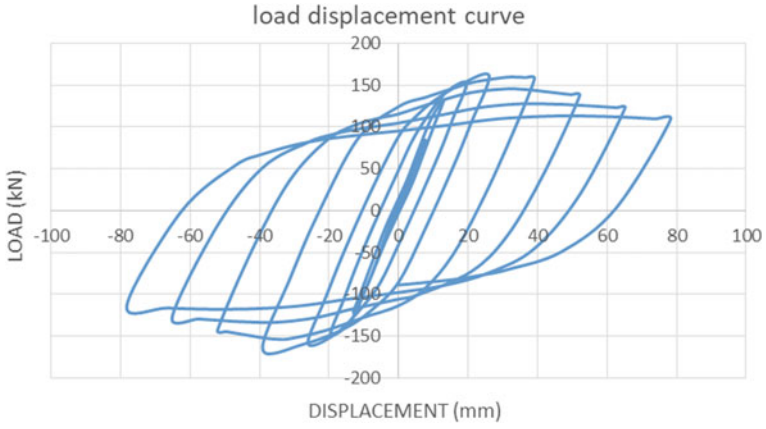

Fig. 6 Load deflection curve

4.5 Stress Distribution

The stress distributions of the exterior joint models are shown in Fig. 4

Steel beam

Figure 4 shows the stresses of the steel beam in the x direction. It can be seen that the upper flange is under tension and the lower flange is under compression. As the development of local buckling stresses are redistributed from the flange to the web.

Steel tube.

Figure 4 shows the stresses of the steel tube in the longitudinal direction. The effect of beam buckling on is demonstrated by its great non-uniform distribution.

Concrete core.

Figure 4 shows the distribution of minimum principal stresses of concrete core. It can be seen that the stress distributions along the column are very similar. Due to the confinement of the steel tube, the largest concrete's minimum principal stress reaches −78.5 MPa, which is higher than the concrete's cube compressive strength.

5 Conclusions

- The octagonal CFST column with rectangular continuous stiffener gives the better efficiency compare to L-shape and U-shape stiffeners
- The load carrying capacity of rectangular continuous stiffener is 13,602 kN and deformation is 8.69 mm while the load carrying capacity of L-shape and U-shape stiffeners gives 13,409 kN and 13,413 kN respectively and deformations are 11.09 and 9.875 mm
- The arrangement of rectangular stiffeners does not give any significance in the load carrying capacity of the column.
- For the exterior joints, the failure mode of severe beam flange buckling and moderate web buckling
- The diaphragm is fail under the lateral loading.

References

1. Zhu J-Y, Chan T-M (2019) Experimental investigation on steel-tube-confined-concrete stub column with different cross-section shapes under uniaxial-compression. J Struct Eng © Elsevier Science Ltd. https://doi.org/10.1016/s0263-8231(03)00046-6
2. Zhua J-Y, Chana T-M, Youngb B (2019) Cross-sectional capacity of octagonal tubular steel stub columns under uniaxial compression. J Struct Eng © Elsevier Science Ltd. https://doi.org/10.1016/s0263-8231(03)00046-6

3. IS SP:6 Code for steel sections
4. IS 456:2000 code for RCC structures
5. IS 800:2007 Code for steel sections
6. IS 1730:1989 steel plates strip and flats for general purpose sizes
7. Ding F, Li Z, Cheng S, Yu Z (2016) Composite action of octagonal concrete-filled steel tubular stub columns under axial loading. J Struct Eng © Elsevier Science Ltd. https://doi.org/10.1016/s0263-8231(03)00046-6

Comparative Study on Effect of Different Mineral Admixtures on Plastic Fiber Reinforced Concrete

K. S. Somiya and Vidya Jose

Abstract Fiber reinforce concrete (FRC) has been in use for more than 50 years now. The conventional concrete is generally weak in tension, has low tensile strain capacity, and is brittle in nature, whereas, fiber reinforced concrete containing fibrous materials enrich the tensile and bending performance of concrete. Here concrete is prepared by adding PET bottle strips as fiber which may help to reuse the plastics and to reduce environmental pollution. Incorporating plastic fiber in concrete increases both the tensile strength as well as durability. The strength requirement of plastic fiber reinforced concrete (at 0.5%, 1%, 1.5% by weight of binder content) can be improved by adding supplementary cementitious materials at 10%, 20%, 30% and 40% by weight of cement. A comparative study of fiber reinforced concrete with different mineral admixtures such as Rice Husk Ash (RHA), Ground Granulated Blast-furnace slag (GGBS)and Metakaolin (MK) in optimum percentage was considered. In this work the physical and mechanical behaviour of PET fiber reinforced concrete with various mineral admixture were studied.

Keywords Polyethylene terephthalate (PET) · Fiber reinforced concrete (FRC) · Mineral admixtures · Physical and mechanical behaviour

1 Introduction

Fiber reinforced concrete (FRC) is a concrete that contains fibrous material which increases the integrity of its structures. It comprises small discrete fibers, which are distributed uniformly and oriented randomly. Fiber is a small piece of reinforcement material that has other properties such as rigidity, torsional strength, ductility etc. A parameter called “aspect ratio” also defines the fibre. The varying fiber aspect ratio is the ratio of its length to its diameter. Typical aspect ratios vary from 30 to 150 for different fibres. Plastic waste is a non-biodegradable substance so it does not degenerate or degrade in water or soil. Plastic waste disposal contributes to environmental

K. S. Somiya (✉) · V. Jose
Civil Engineering Department, Toc H Institute of Science and Technology, Kerala, India
e-mail: kssomiya30@gmail.com

© Springer Nature Switzerland AG 2021

K. Dasgupta et al. (eds.), *Proceedings of SECON 2020*,
Lecture Notes in Civil Engineering 97,
https://doi.org/10.1007/978-3-030-55115-5_61

emissions. The possibility of using fibers from polyethylene terephthalate (PET) bottles helps to increase concrete ductility and cost can be dramatically regulated if we can reduce the amount of cement needed.

In other words, a portion of cement could be substituted with some material other than cement which could be used with cement to produce similar cementitious properties. These are called minerals admixtures. Examples of mineral admixtures include Ground Granulated Blast Furnace Slag (GGBS), Metakaolin (MK), Rice Husk Ash (RHA) etc. MK is a calcined anhydrous type of the mineral clay kaolinite. Kaolinite-rich minerals are known as china clay, or kaolin, commonly used in porcelain manufacturing. MK is smaller in particle size than cement particles. Highly reactive MK was available in concrete as a reactive pozzolanic material. Ground granulated blast furnace slag is obtained by quenching the molten iron slag in water or steam from blast furnace. It is primarily glassy and granulated material that is in fine powder later on the sheet. Its chemical composition varies according to the raw materials used to produce iron. It is pozzolanic in nature, and can be used as a partial replacement for concrete cement. RHA is collected from commercial rice milling. Since these industries produce a lot of rice husk during rice processing, this is used as a fuel in the boilers and when burnt, it transforms into pozzolanic ash which can be used in concrete as other mineral admixtures.

2 Materials Used

To carry out this study, normal Portland cement of 53 grade was hand-picked. Testing of cement was done as per IS: 12269–1987. varied tests results conducted on the cement is reportable in Table 1. Coarse aggregates having a maximum size of 20 mm were employed. Testing on coarse aggregates was done as per IS: 383–1970. the particular gravity of coarse and fine combination was 2.68 and 2.72. The sand used for the experimental program was conformed to grading zone II as per IS: 383–1970. Super plasticizers(SP) used is Master Glenium B233. The superplasticizer indefinite quantity is adjusted to provide concrete with an equivalent slump of 120 ± 10 mm and don't show visual signs of segregation throughout the traditional casting of concrete within the moulds. Physical properties of Master Glenium B233 is given in Table 2. The plastic fibers employed in this study is obtained from synthetic

Table 1 Physical properties of cement

Sl. No.	Characteristics	Values obtained	Standard values
1	Specific gravity of cement	3.15	3.1–3.25
2	Standard consistency of cement	32%	22–32%
3	Initial setting time of cement	55 min	Varies for different grade of cement
4	Fineness of cement	5%	Not exceeding 10%

Table 2 Physical properties of Master Glenium B233

Sl.no	Physical properties	Values obtained
1	Aspect	Dark brown free flowing liquid
2	Relative Density	1.24 ± 0.02 at 25 °C
3	pH	>6
4	Chloride ion content	<0.2%

Table 3 Physical properties of PET fibers

SI. No	Characteristics	Values obtained
1	Type of fiber	PET fiber
2	Length	20–30 mm
3	Diameter	0.5 mm
4	Aspect ratio	50
5	Tensile strength	55–75 MPa
6	Density	1380 kg/m^3
7	Young's modulus	2800–3100 MPa

Table 4 Properties of cement

Table	Characteristics Values Obtained
1	Specific Gravity of Cement 3.15
2	Standard Consistency of Cement 32%
3	Initial Setting Time of Cement 70 min
4	Fineness of Cement 5%
5	Specific Gravity of GGBS 2.91
6	Specific Gravity of MK 2.6
7	Specific Gravity of RHA 2.11

resin terephthalate (PET) bottles that are take terribly tiny strips is taken. Physical properties of PET fibre are shown in Table 3. Also, normal Portland cement is partly replaced by mineral admixtures like MK, Ground granulated blast furnace slag, and RHA is given in Table 4.

3 Mix Design of Concrete and Procedure

Mix design can be defined as the process of selecting suitable ingredients of concrete such as cement, aggregates, water and determining their relative proportions with the object of producing concrete of required minimum strength, workability and

Table 5 Mix proportion of M40 grade concrete for 1 cubic meter

Material	Cement (kg/m^3)	Fine aggregate (kg/m^3)	Coarse aggregate (kg/m^3)	Water (kg/m^3)
Quantity of concrete	376	695	1227	158
Mix ratio	1	1.84	2.36	0.48

durability as economically as possible. The mix proportions were carried out using IS: 10262–2019. The proportions of concrete batches were tabulated in Table 5.

Mixing of concrete components was done on a concrete mixer machine. All the dry constituents were mixed for 2 min to ensure uniformity of the mix. During mixing of concrete, initially only half of the water was used for mixing and then remaining water was used with SP during mixing. Mixing of all ingredients was continued for a period of 2 min. The amount of SP was adjusted for each mix to achieve the required workability without segregation. And for FRC, fiber was added during dry mixing for 2 min then the SP and water was added accordingly. After the moulds had been filled with concrete it is then compacted and the surface of concrete were levelled, and were kept in laboratory conditions for 24 h and the surfaces of moulds were covered by plastic sheets. After demoulding, the samples were kept for water curing.

An M40 grade of fiber reinforced concrete was used. Varying percentage of mineral mineral admixtures like MK (MK), GGBS and RHA at 10%, 20%, 30%, 40% were added to the optimum percentage of PET FRC and test results were obtained. Then a comparative study of these mineral mineral admixtures on PET FRC were conducted.

4 Results and Discussion

The discussion on results of the material testing done in the laboratory is given below:

4.1 Workability of Concrete

Slump test was used to determine the workability of fresh concrete. Slump test as per IS: 1919–1959 was followed. The slump value of FRC was 75 mm. Workability decreases with the increase in addition of PET fiber. The concrete slump depends on fibre concentration in the concrete mix. It is clear that the slump of the concrete mix significantly decreases with growing content of PET fibers. The results indicate that the workability of the mix decreases with addition of PET fibres. With increase of PET fibre in concrete the slump value starts decreasing, this may be due smooth surface of PET fiber causing a weak bond between cement matrix and aggregates The fibers content above 1% causes serious problems concerning homogeneity and

workability of the concrete mix. The workability decreased to 65 mm, 58 mm and 49 mm with 0.5%, 1% and 1.5% of PET fibre content.

4.2 Effect of Fiber and Mineral Admixtures on Mechanical Properties

The results of strength parameter of specimen with fibres added are shown in Figs. 4, 5 and 6. Fibres are mainly used to improve the toughness, impact resistance and flexural properties, they can improve compressive strength by preventing the propagation of cracks [3]. The crushing of concrete particles helps in achieving better strength. A substantial amount of fibers incorporated into concrete can achieve the absolute maximum load (fiber yielding) [2]. The most important constituents for any mineral admixture are silica and alumina oxides. In comparison with OPC, the mineral admixtures have higher quantity of silica oxide in their constituent [4]. The concrete mixtures having higher MK replacement levels gained high strengths. FRC with 30% MK showed higher strength at all ages [1]. Based on test conducted, the reactivity of mineral admixtures is of the order: MK > GGBS > RHA. Smaller particle size and higher specific surface area of mineral admixtures are favourable to produce highly dense and impermeable concrete and they cause low workability and more water demand which may be offset by adding effective superplasticizer.

Figures 1, 2 and 3 shows specimen of prism, cube and cylinder being tested.

Fig. 1 A specimen of a prism being tested

Fig. 2 A specimen of cube being tested

4.2.1 Compressive Strength

The compressive strength of concrete was done on Compression testing machine according to IS 516:1959 (Reaffirmed 2004). Cubes of 150 mm size were used for the testing. Figure 4 shows the change in compressive strength with different ratios of PET fibers. The compressive strength of FRC with 0.5% PET fiber was 45.56 N/mm^2 at 28 days. On addition of 1% PET fiber, the compressive strength increases to 46.11 N/mm^2. Again with addition of PET fiber at 1.5% the strength got decreases 44.12 N/mm^2 28 days. Thus it indicates that the PET fiber at 1% provides the optimum value. Table 6 gives the FRC with different percentage of MK in 7 days and 28 days' compressive strength results. Addition of 10% of MK to the optimum content of FRC the compressive strength is 46.9 N/mm^2 in 28 days. With the addition of 20% of MK, compressive strength increased to 48.95 N/mm^2. With 30% MK the strength increased to 51.12 N/mm^2 in 28 days respectively. It then decreases 48.13 N/mm^2 with 40% MK. It indicates that 30% MK gives the optimum value of compressive strength in FRC. The increase of compressive strength with the use of MK is attributed to extremely high surface area of MK Similarly, for, 30% of GGBS (Table 6) gives the optimum value for compressive strength, i.e. 48.89 N/mm^2 at 28 days. The increase in strength and slump value is due to small particle size of GGBS causing better cohesive and adhesive bonding And addition of 20% of RHA gives the optimum value for compressive strength i.e. 46.67 N/mm^2 in 28 days.

Fig. 3 A specimen of a cylinder being tested

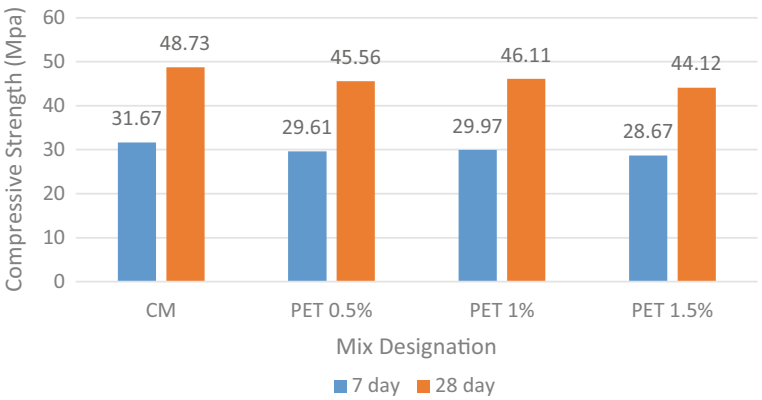

Fig. 4 Effect of PET fiber on compressive strength of concrete

Table 6 Compressive, Split tensile and Flexural strength of mineral mineral admixtures with 1% PET

Sl.no	Mineral admixtures	PET fiber (%)	Mineral admixture sadded (%)	Compressive strength (N/mm^2)		Split tensile strength (N/mm^2)		Flexural strength (N/mm^2)	
				7 days	28 days	7 days	28 days	7 days	28 days
1	MK	1	10	30.48	46.9	3	4.25	4	5.07
			20	31.81	48.95	3.3	4.65	4.18	5.21
			30	33.22	51.12	3.85	4.86	4.81	5.78
			40	31.27	48.12	3.45	4.35	4.43	5.3
2	GGBS	1	10	28.92	44.5	3.5	4.11	4.01	5.09
			20	30.29	46.61	3.11	4.29	4.07	5.23
			30	31.7	48.89	3.58	4.65	4.65	5.66
			40	29.96	46.12	3.23	4.01	4.23	5.10
3	RHA	1	10	26.65	41	2.9	4.04	4.03	5.1
			20	30.3	46.67	3.23	4.25	4.23	5.21
			30	27.3	42.67	3.12	4.07	4.17	5.10
			40	26	40.78	2.78	3.95	3.86	4.95

With addition of RHA the slump value shows a steady decrease, this is because the specific surface of RHA is significantly larger than the cement. Therefore, the concrete performance is drastically reduced and more water is needed to fix it.

4.2.2 Split Tensile Strength

Splitting tensile strength test on the concrete cylinder is a method to determine the tensile strength of concrete as per IS 5816: 1999 (Reaffirmed 2004). Cylindrical specimens of diameter 150 mm and height 300 mm were used for this test. Figure 5 shows the change in split tensile strength with different ratios of PET fibers The tensile strength of fiber reinforced concrete with PET fiber at 0.5% was 4.19 N/mm^2 at 28 days. With addition 1% of PET fiber, the strength increases 4.30 N/mm^2. Then again on addition of PET fiber at 1.5% the value decreases to 4.19. With addition of PET fiber at 1.5% it was concluded that the split tensile strength got decreased from 4.30 N/mm^2 to 4.19 N/mm^2 at 28 days. Which indicates that addition of 1% of PET fiber in concrete gives the optimum value for split tensile strength.

Table 6, gives the FRC with different percentage of MK in 7 days and 28 days' split tensile strength results. Addition of 10% of MK to the optimum content of FRC the split tensile strength is 4.25 in 28 days. With the addition of 20% of MK, split tensile strength increased to 4.62 N/mm^2 in 28 days. With 30% MK the strength increased to 4.86 N/mm^2 in 28 days respectively. On addition of 40% of MK the value decreases to 4.35 N/mm^2. It indicates that 30% MK gives the optimum value for split tensile strength in FRC. Similarly, (Table 6) 30% of GGBS gives the optimum value for split tensile strength, i.e. 4.65 N/mm^2 in 28 days. And addition of 20% of RHA gives the optimum value for split tensile strength i.e. 4.25 N/mm^2 in 28 days respectively.

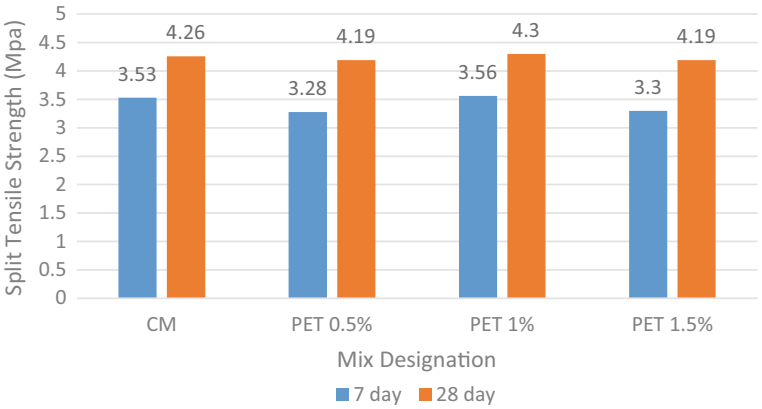

Fig. 5 Effect of PET fiber on split tensile strength of concrete

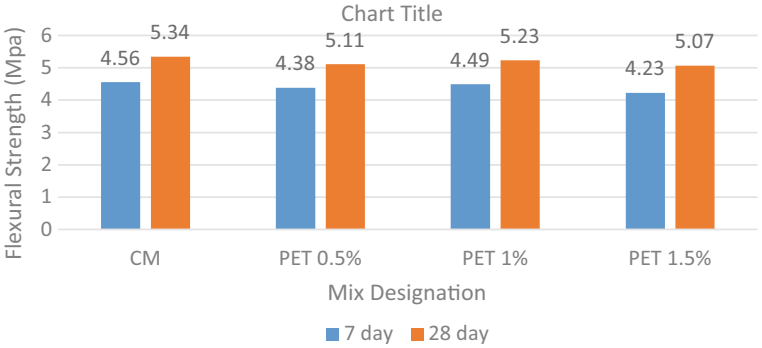

Fig. 6 Effect of PET fiber in flexural strength of concrete

4.2.3 Flexural Strength

The flexural test was carried out in accordance with IS 516:1959 (reaffirmed on 2004) on reinforced beams 700 mm long and 150 × 150 mm in cross section. The testing was conducted on Universal Testing Machine (UTM) with two-point loading setup. Figure 6 shows change in flexural strength with different percentage of PET fiber. The flexural strength of FRC at 0.5% of PET fiber was 5.11 N/mm^2 at 28 days. PET fiber at 1% the strength increases to 5.23 N/mm^2 in 28 days. Again when the pet fiber was added at 1.5% the flexural strength value decreased to 5.07 N/mm^2. It was noted that with the addition of PET fiber 1.5% the flexural strength value got decreasing from 5.23 to 5.07 N/mm^2 at 28 days, which indicates that the 1% PET gives the optimum value for flexural strength.

Table 6 gives the FRC with different percentage of MK in 7 days and 28 days' flexural strength results. On addition of MK at 20% to the optimum value of PET FRC the value is 5.21 N/mm^2. Again on further addition of MK at 30% the value got increased to 5.78 N/mm^2. Again on addition of MK at 40% the value got decreased from 5.3 N/mm^2 at 28 days. Which indicates that on addition of MK 30% to the FRC gives the optimum value for flexural strength. Similarly, (Table 6) 30% of GGBS gives the optimum value for flexural strength, i.e. 5.66 N/mm^2 in 28 days. And for addition of 20% of RHA gives the optimum value for split tensile strength. i.e. 5.21 N/mm^2 in 28 days respectively.

5 Conclusion

Based on the experimental investigation conducted in this work, the following conclusions were found out.

- Use of PET bottle strips as fiber in Fiber reinforced concrete has a slump in the range of 75–104 mm. Addition of PET fiber at 0.5%,1%, and 1.5% shows a

steady decrease from 65 mm to 49 mm. Workability decreases with the increase in addition of PET fiber.

- The test result shows that FRC with 1% PET fiber has the optimum value among the various values examined (0.5%, 1%, and 1.5%).
- M40 Grade of concrete has strength value of 48.73 N/mm^2, 4.26 N/mm^2, 5.34 N/mm^2 at 28 compressive strength, split tensile strength and flexural strength.
- For 1% of PET FRC an optimum value of 46.11 N/mm^2, 4.26 N/mm^2 and 5.34 N/mm^2 at 28 days compressive, split tensile and flexural strength were obtained respectively.
- When comparing the control mix values with that of PET FRC the strength parameters are higher for control mix values this may be due to the smooth surface of PET fiber causing a weak bond between cement matrix and aggregates which results in reduction in strength.
- The use of different mineral admixtures such as GGBS, MK and RHA in concrete mixes improved the mechanical properties of concrete.
- All the strength parameters i.e. compressive, split tensile and flexural strength have been increased by replacement of cement with these admixtures.
- Replacement of cement with MK gave the higher strength values as compared to other two mineral admixtures.
- FRC with MK at 30% gave the highest compressive strength from 33.22 N/mm^2 at 7 days to 51.12 N/mm^2 at 28 days followed by GGBS and RHA.
- The strength values of GGBS in FRC is slightly less as compared to MK with PET fiber, similarly the RHA with FRC has the lowest strength as compared to the other two admixtures. ○ Use of fiber in concrete increases tensile strength. Here PET fiber in concrete proves to have a better tensile strength especially with MK, 3.85 N/mm^2 at 7 days to 4.86 N/mm^2 in 28 days as compared to the other two admixtures.
- The FRC with MK as admixture has percentage increase of 6.25%, 4.51% and 10.94% for compressive, split tensile and flexural strength respectively.

References

1. Wei C, Chi LF, Junjie W, Jianhe X (2019) Coupling effects of recycled aggregate and GGBS/MK on physicochemical properties of geopolymer concrete. J Constr Build Mater 226:345–359
2. Filip G, Mychal M, Tomasz T (2019) Mechanical properties of fibre reinforced concrete with recycled fibres. J Constr Build Mater 198:323–331
3. Karthikeya B, Dhinakaran G (2018) Influence of ultrafine TiO_2 and silica fume on performance of unreinforced and fiber reinforced concrete. J Constr Build Mater 161:570–576
4. Pradeep KM, Mini KM, Murali R (2018) Ultrafine GGBS and calcium nitrate as concrete mineral admixtures for improved mechanical properties and corrosion resistance. J Constr Build Mater 182:249–257

Shear Behavior of Joints in Precast Prestressed Concrete Segments-A Finite Element Study

Sheela J. George, A. K. Farvaze Ahmed, S. Maheswaran, and Mathews M. Paul

Abstract The behavior of segmental structures depends mainly on the behavior of the joints between the segments. Even though joints forms a discontinuity; they should have the capacity to transmit compressive and shear stresses. Shear behavior of the joints is greatly influenced by the confining pressure and the surface properties. According to shear friction approach, shear capacity of joints can be improved by varying the surface properties of joints. It is observed that limited studies were done on the factors affecting the friction at joints and only few Finite Element studies on joints were done. In this study, a three-dimensional Finite Element study using ABAQUS has being carried out on joints with various surface properties. The Finite Element Analysis model consisted of two parts in surface to surface contact. The C3D8R element and B31 element with a refined mesh size of 10 mm is used for modelling concrete and reinforcement respectively. The material properties considered were modulus of elasticity of 27.38 GPa and Poisson's ratio of 0.2 for concrete and for reinforcement steel were Young's Modulus 210 GPa and poisson's ratio 0.3. Material nonlinearity is introduced by Concrete Damage Plasticity model. Parameters studied are prestressing force and coefficient of friction at joints. The shear resistance of joints under different surface properties were evaluated using FE study and compared with experimental results available from a reported literature (Jiang et al in Mech Comput 19(1):1–16 2015, [1]).

Keywords Segmental joints · Prestress · Shear strength · ABAQUS

S. J. George (✉) · M. M. Paul
Department of Civil Engineering, Mar Athanasius College of Engineering, Kothamangalam, Kerala, India
e-mail: sheelajgeorge21@gmail.com

M. M. Paul
e-mail: mmp_mace@rediffmail.com

A. K. Farvaze Ahmed · S. Maheswaran
CSIR-Structural Engineering Research Centre, Chennai, Tamil Nadu, India
e-mail: farvaze@serc.res.in

S. Maheswaran
e-mail: smahes@serc.res.in

© Springer Nature Switzerland AG 2021

K. Dasgupta et al. (eds.), *Proceedings of SECON 2020*,
Lecture Notes in Civil Engineering 97,
https://doi.org/10.1007/978-3-030-55115-5_62

1 Introduction

Now a days, precast concrete segmental construction is becoming more popular due to better quality control, increased speed in erection, and its applicability to variety of span lengths. The behavior of joints between segments are the prominent factors affecting the overall behavior of segmental structures. The shear resistance at the joint section is always lesser when compared with section without joints within the member. The joints can be provided as flat or keyed joints, dry (no fill) or epoxy type. Even though precast concrete segmental structures with dry joints are popular for their rapid-construction advantages, the problems such as deficient shear capacity compared with epoxy joints and corrosion of prestressed tendons exists. Significant variation in the shear capacity of flat dry joints was observed due to the variation in coefficient of friction at joints which can be explained by the differences in concrete surface properties [2]. Epoxied joint have strength more that of dry joints, but its failure is brittle and sudden without much warnings, which is undesirable.

The push-off test is used to determine interface shear transfer in concrete. For a push-off specimen with flat dry joint, when a normal load is applied on it, shear stresses are transferred from one part of the specimen to another through the small undulation in the surfaces of the shear plane. These unevenness made of cement paste starts to deform when loaded and shows a linear behavior. When its strength is reached, the load-deformation behavior becomes nonlinear and the two surfaces starts sliding past each other when most of the undulations gets sheared off [2]. When the segments are loaded in shear, slip will occur along the shear plane. The faces of shear plane even if carefully polished are actually rough, therefore when the slip occurs, the faces are forced to separate or get dilated. But when a prestressing force is provided connecting the segments, a compressive force is induced which produces a frictional resistance to sliding between segments, thus providing the shear resistance to the applied load and improves shear carrying capacity of joints [3].The shear strength of keyed joint is due to a combination of supporting effect of the shear keys and the frictional resistance between the flat contact surfaces. The shear keys behave like small plain concrete corbels when they are in contact [4]. When the tensile strength of concrete is reached, crack starts forming at the bottom corner of the shear key and propagates away from the shear plane at 45° with respect to horizontal. Then several short diagonal cracks initiates at root of the key and gets interconnected when the load is increased. The formation of crack is accompanied with dilation in the specimen. At maximum load, key shear off from rest of the specimen and a sudden slip occurs. The load was then carried mainly through frictional forces by aggregate interlock [5]. The shear strength of multiple keyed joints are less than that of single keyed dry joints due to imperfection in the fitting of keys. As the number of keys increased, average shear strength transferred across joint seems to decrease, but this can be solved by increasing the prestressing force.

Several shear design formulas were proposed to estimate the shear capacity of key joints which are aimed to prevent shear failures initiated by diagonal cracking. The design formulas suggested in AASHTO 2003 and that proposed by Rombach

and Specker tend to underestimate the shear capacity of single keyed joints but overestimates the shear capacity of multiple-keyed dry joints. Hence it could be unsafe for multiple keyed joints. Hence a shear strength reduction factor has to be introduced to those formulas inorder to estimate shear capacity of multiple-keyed joints [6].

1.1 Research Significance

Previous studies shows that the main parameters affecting shear resistance of joints are pre-compression, geometry of the key, characteristic compressive strength of concrete and surface characteristics of concrete. In this study, the influence of these parameters are investigated by numerical analysis. From the previous experimental studies it can be seen that the coefficient of friction depends on the pre-compression and surface characteristics of concrete. A wide variation is observed in coefficient of friction for flat dry joints which needs to be investigated. The strength and stiffness of flat dry joints increases with increase in prestress. When an externally applied normal compressive stress acts on the specimen, the shear resistance due to friction increases. The crack in the shear plane locks up and behavior and ultimate strength becomes same as that of uncracked specimen. In such cases, the shear strength depends upon the concrete strength [3]. Also in this study, the shear resistance of joints under different surface properties were evaluated using finite element analysis and compared with experimental results available from previous studies.

1.2 Numerical Model Validation Using Experimental Data

The experimental test results obtained from reported literature [1] has been used for numerical validation. Push-off specimens were used to study shear transfer and aggregate interlock behavior of flat, monolithic and single keyed dry joints in concrete segments. The dimensions of the test specimens are depicted in Fig. 1.

All the specimens had shear plane area of 200 mm $\times$ 100 mm,where 100 mm is the thickness of the specimen. Inorder to avoid premature failure of concrete by bending or crushing due to loading, prior to the failure in shear plane, the specimens were reinforced with 16 mm diameter bars and 12 mm stirrups. This reinforcement is known as skin reinforcement. The concrete mix was designed for a grade of C40 according to Chinese code and specimens with flat and keyed joints were match cast.

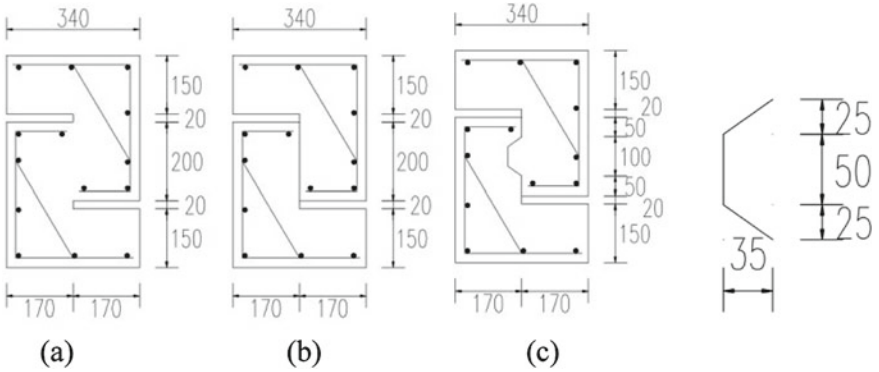

Fig. 1 Specimen dimensions for **a** Monolithic, **b** Flat Dry and **c** Single Keyed Joints

1.2.1 Numerical Model

The numerical modelling of the specimens to study the shear capacity of joints and validation of the experimental results from the literature was done using the finite–element analysis package ABAQUS as shown in Fig. 2. The Finite Element Analysis model consisted of two parts in surface to surface contact. The C3D8R element with a refined mesh size of 20 mm was used for modelling. The skin reinforcement with 16 mm diameter bars was modeled using beam element B31. The bond between reinforcing steel and concrete is simulated using embedded interaction. The material properties considered for concrete were modulus of elasticity of 31.6 GPa and Poisson's coefficient of 0.2. The elastic-plastic behavior of concrete was simulated by Concrete Damage Plasticity (CDP) Model as shown in Fig. 3 [7].

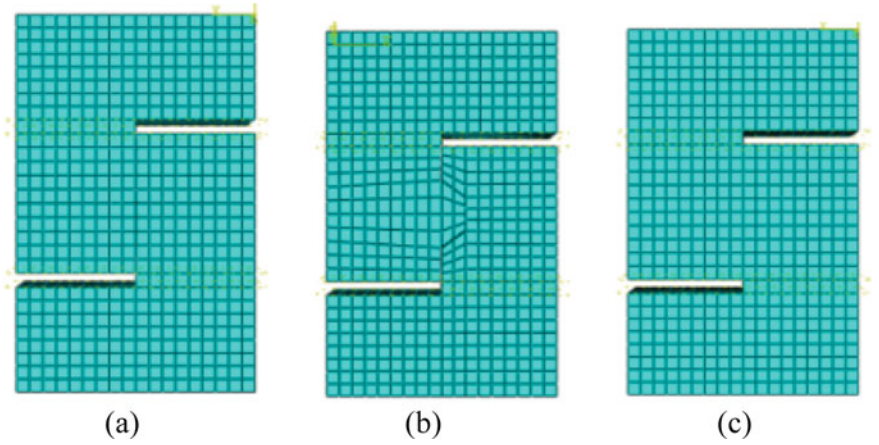

Fig. 2 Meshed three-dimensional finite element model of **a** Flat joint **b** Single Keyed Dry Joint and **c** Monolithic Joint

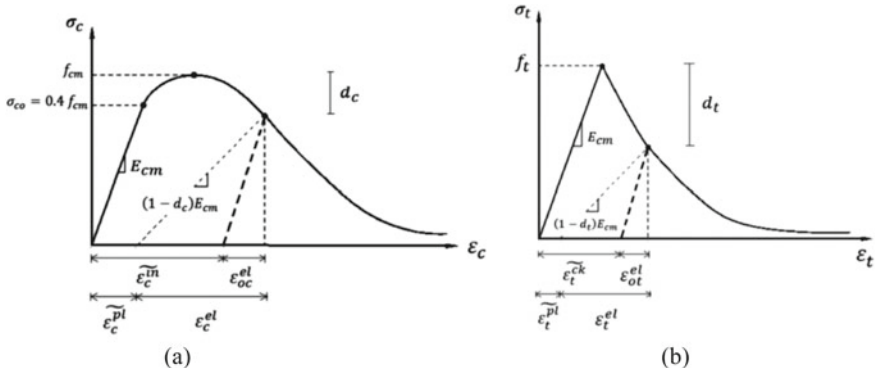

Fig. 3 Concrete damage parameters **a** Compressive and **b** Tensile

The CDP model defines the inelastic behavior of concrete including its damage characteristics in both compression and tension. It is based on compressive crushing and tensile cracking of concrete and requires concrete compressive and tensile constitutive relationship, cracking and crushing damage parameters, special parameters such as dilation angle, eccentricity, biaxial to uniaxial compressive stress ratio $\left(\frac{f_{b0}}{f_{c0}}\right)$, second stress invariant ratio(K) and viscosity parameter [8] as given in Table 1.

The prestress and normal load was applied as pressure loads on both sides across the shear plane and on top surface respectively. The bottom surface of model was hinged. The load was applied in two steps, in which the prestress of a given magnitude was applied in the first step and normal load in next step. Hard Contact model was used to model surface to surface interaction in normal direction and the tangential behavior was provided by a frictional coefficient of 0.6. The analysis results is shown in Table 2.

1.3 Results and Discussions

The analysis results are in close agreement with the experimental data and hence validated. The maximum deviation of 3.13%, 4.29% and 5.35% was found in flat, single keyed and monolithic joint.

Normalized shear stress-Vertical Displacement graph is plotted for flat joint subjected to a prestress of 1 MPa as shown in Fig. 4. Normalized shear stress ($\tau_c^{'}$) includes the effect of the variation of cylinder concrete strength in same type of specimens and can be found out as shown in Eq. (1).

$$\tau_c^{'} = \frac{\tau_c}{\sqrt{f_c^{'}}} \tag{1}$$

Table 1 Material Properties of M 40 Concrete with CDP Model

Material parameters			
Grade	M40	Concrete plasticity parameters	
Concrete Elasticity Parameters		Dilation angle	31
Young's Modulus E (GPa)	31.6	Eccentricity	0.1
		fb0/fc0	1.16
Poisson's Ratio μ	0.2	K	0.67
		Viscosity parameter	0
Concrete compressive behavior		Concrete compression damage	
Yield stress (MPa)	Inelastic strain	Damage parameter C	Inelastic strain
20.4	0	0	0
25.6	2.66667E-05	0	2.66667E-05
30	0.00008	0	0.00008
33.6	0.00016	0	0.00016
36.4	0.000266667	0	0.000266667
38.4	0.0004	0	0.0004
39.6	0.00056	0	0.00056
40	0.000746667	0	0.000746667
39.6	0.00096	0.01	0.00096
38.4	0.0012	0.04	0.0012
36.4	0.001466667	0.09	0.001466667
33.6	0.00176	0.16	0.00176
30	0.00208	0.25	0.00208
25.6	0.002426667	0.36	0.002426667
20.4	0.0028	0.49	0.0028
14.4	0.0032	0.64	0.0032
7.6	0.003626667	0.81	0.003626667
Concrete tensile behavior		Concrete tension damage	
Yield stress (MPa)	Cracking strain	Damage parameter T	Cracking strain
4	0	0	0
0.04	0.001333333	0.99	0.001333333

where, τ_c and $f_c^{'}$ indicate shear stress of joint and characteristic compressive strength of concrete respectively, obtained from Table 2.

Table 2 Validation Results of Experimental and Numerical Values

Type	Prestress (MPa)	Experimental values Jiang et al. [1]			Numerical Values		% variation in load
		Concrete Cylinder Strength $f_c^{'}$(MPa)	Load (kN)	Shear Stress τ_c (MPa)	Load (kN)	Shear Stress (MPa)	
Flat Joint	1	40.49	12.38	0.619	11.99	0.599	3.13
	2	40.49	23.4	1.17	23.99	1.19	2.52
Single Keyed Joint	1	41.51	89.69	4.485	93.54	4.677	4.29
	2	41.51	113.87	5.694	117.83	5.89	3.477
Monolithic	1	40.72	137.59	6.88	130.22	6.511	5.35
	2	40.72	163.55	8.178	156.09	7.804	4.55

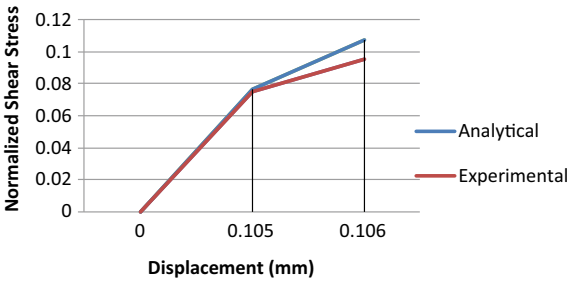

Fig. 4 Comparison of experimental and analytical results of flat joint

2 Shear Capacity of Joints

The frictional shear resistance of flat dry joints along the shear plane is equal to prestress force multiplied by the coefficient of friction for concrete. The frictional coefficient recommended by ACI Code and AASHTO is 0.6. Shear capacity of keyed joints is taken as algebraic sum of shear contributions of keys and the contacting flat portion between segments. The design formula for estimating the shear capacity of joints are shown in table below. Also the experimental results were checked with those formulas as shown in Table 3.

2.1 Parametric Study

The effect of confining pressure or prestress and characteristic compressive strength of concrete (f_{ck}) on shear capacity of joints was studied as shown in Fig. 6. The material properties of concrete were modulus of elasticity of 27.38 GPa and Poisson's coefficient of 0.2 with a refined mesh size of 10 mm. The reinforcing steel has Young's

Table 3 Design formulas for shear capacity of joints

Type of Joint	Author	Formula	Prestress (MPa)	Load (kN)	Shear stress (MPa)	%load variation
Flat Joint	Mohr Columb Equation	$V_{dryjoint} = \mu A_{joint} \sigma_n$	1	12	0.6	3.06
			2	24	1.2	2.56
Keyed Joint	AASHTO [9]	$V_j = A_k \sqrt{f_c'}[0.9961 + 0.2048\sigma_n] + 0.6 A_{sm} \sigma_n$	1	83.371	4.16	7.04
			2	102.56	5.128	9.93
	Rombach and Specker [10]	$V_j = 0.14\ f_c A_k + 0.65\ \sigma_n A_{joint}$	1	71.114	3.555	20.71
			2	84.114	4.205	26.13
	Turmo [11]	$V_j = A_k \sqrt{f_c'}[0.9064 + 0.1863\sigma_n] + 0.45 A_{sm} \sigma_n$	1	74.9	3.745	16.49
			2	91.403	4.57	19.73

Where , A_{joint} = total area of the shear plane (mm^2), A_k = base areas of all keys in the shear plane (mm^2),A_{sm} = area of smooth surface without keys in the shear plane (mm^2), σ_n = applied prestress (MPa),μ = coefficient of friction, f_c' = characteristic compressive strength of concrete (MPa).

modulus 210 GPa and Poisson's ratio 0.3. The shear capacity of joints increases with an increase in confining pressure irrespective of the type of joint. The shear capacity of monolithic and keyed joint was found to depend on f_{ck} and shows a positive correlation, whereas not much effect was seen in case of flat joints.

Inorder to study the effect of surface properties on the ultimate shear strength of joints, different type of undulations were made on shear plane as shown in Fig. 5. The material used for modeling undulations was cement mortar with Young's Modulus 3600 MPa and Poisson's ratio 0.17. The size of the undulation used was 10 mm × 5 mm. The size of the undulation was assumed to be less than the size of aggregate in concrete, therefore cement mortar was used for modeling. From Table 4, it can be noted that, the shear carrying capacity of joints increases with variation in the surface properties of joints, when compared with that of flat joints.

2.2 Finite Element Analysis Results

The results obtained from the analysis are shown in Figs. 6 and 7.

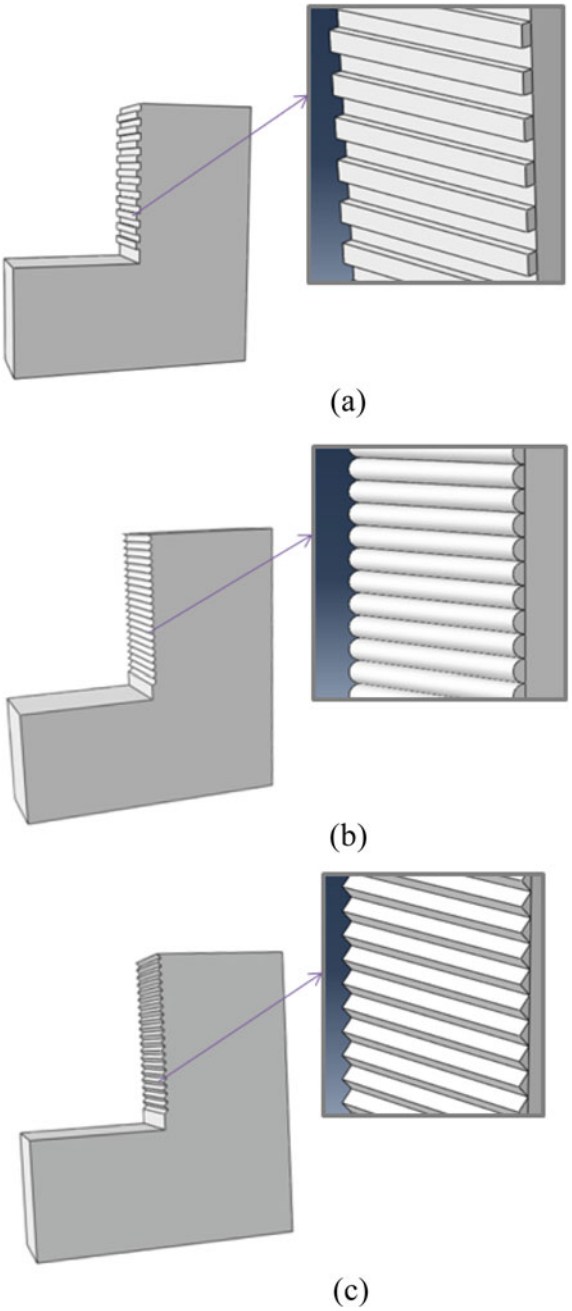

Fig. 5 Specimen model of joint with **a** Rectangular, **b** Curved and **c** V shaped undulations

Table 4 Ultimate shear stress for various surface properties

Type of Undulation	Prestress(MPa)	Ultimate Load (kN)	Ultimate Shear stress (MPa)
Rectangular	1	57.900	2.895
Curved	1	30.082	1.504
V shaped	1	26.834	1.341

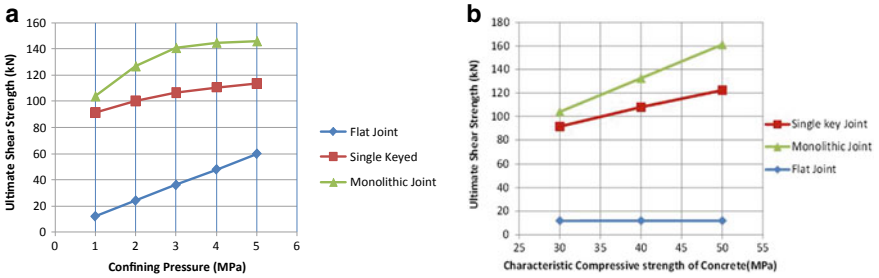

Fig. 6 Ultimate shear strength of flat, single keyed and monolithic joint **a** Under different values of confining pressure **b** For M30, M40 and M50 Concrete for 1 MPa confining pressure

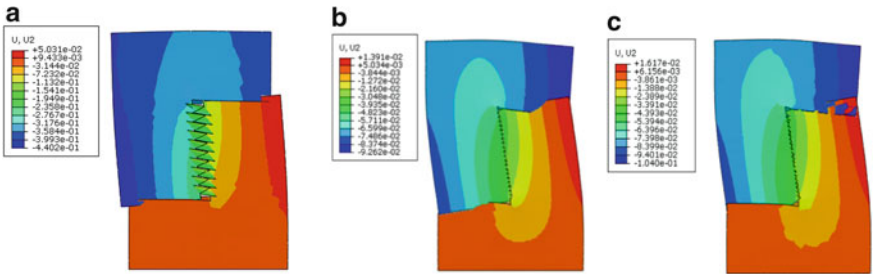

Fig. 7 Vertical displacement diagram of **a** Rectangular, **b** Curved and **c** V shaped undulations

3 Conclusions

This study was aimed to understand the effect of parameters such as confining pressure or pre-compression, characteristic compressive strength of concrete and surface characteristics of joint on the shear strength of joint. From the validation results, it was found that the finite element model can be used to simulate the shear capacity of joints. Based on the simulation results, the following conclusions can be made:

1. The Mohr-Columb equation for flat joints and AASHTO 2003 design formula for shear capacity of keyed joints are in close agreement with experimental results.
2. The AASHTO formula tends to underestimate the shear capacity of single keyed joints.
3. As the confining pressure increases, the shear carrying capacity also increases.

4. The influence of characteristic compressive strength of concrete on ultimate shear strength of joint was seen predominantly in keyed and monolithic joints whereas in flat joints, the effect is negligible.
5. The ultimate shear strength of joint can be improved by varying the surface properties of joint, which means that the coefficient of friction has to be changed accordingly.
6. The rectangular undulations gives higher shear capacity compared to curved and V shaped undulations due to its better interlocking property.

Acknowledgements This research has been done at CSIR-Structural Engineering Research Centre(CSIR-SERC), Chennai, India.The support provided by the organisation and scientists for carrying out the research is greatly appreciated. This paper is being published with the kind permission of the Director of CSIR-SERC.

References

1. Jiang H, Li C, Ma ZJ, Feng W (2015) Shear behavior of dry joints with castellated keys in precast concrete segmental bridges. Mech Comput 19(1):1–16
2. Buyukozturk O, Bakhoum MM, Michael Beattie S (1990) Shear behavior of joints in precast concrete segmental bridges. J Struct Eng 30(1):656–667
3. Mattock AH, Hawkins NM (1972) Shear transfer in reinforced concrete-recent research. PCI J 19(1):55–75
4. Jiang H, Feng J, Liu A, Liang W, Tan Y, Liang H (2019) Effect of specimen thickness and coarse aggregate size on shear strength of single-keyed dry joints in precast concrete segmental bridges. Struct Concr 32(2):634–693
5. Jiang H, Fang Z, Ma Z, Fang X, Jiang Z (2016) Shear strength of steel fiber-reinforced concrete dry joints in precast segmental bridges. Autom Constr 32(2):430–456
6. Zhou X, Mickleborough N, Li Z (2005) Shear strength of joints in precast concrete segmental bridges. Int Conf High Performance Mater Bridges 21(2):150–161
7. Shamass R, Zhou X, Alfano G (2015) Finite-element analysis of shear-off failure of keyed dry joints in precast concrete segmental bridges. J Bridge Eng 20(6):1–12
8. Chen G, Fang Z, Wang S, Jiang H, Liang H (2019) Numerical analysis on shear behavior of joints under low confining and eccentric loads. In: Advances in civil engineering, pp 1–16
9. AASHTO (2003) Guide specifications for design and construction of segmental concrete bridges, 2003 interim revision, 2nd edn. AASHTO, Washington, DC
10. Rombach GA, Specker A (2004) Segmentalbrucken, vol. 1 of Betonkalender. Verlag Ernst & Sohn, Berlin, pp 177–212
11. Turmo J, Ramos G, Aparicio AC (2006) Shear strength of dry joints of concrete panels with and without steel fibres: application to precast segmental bridges. Eng Struct 28(1):23–33

Structural Performance of Innovative Lean Duplex Stainless Steel Built-Up Columns Under Various Loading

M. S. Hima and Samithamol Salim

Abstract The use of cold-formed steel structures has increased in recent years, and some built-up section members are also widely used for their excellent structural behaviors. The stainless steel is not a single material but it is a family of corrosion resistant steel. The Lean Duplex Stainless Steel (LDSS), which is a category of stainless steel is becoming popular as a structural member because of its increased corrosion resistance and durability compared with that of steel. When compared to other construction materials, the LDSS has many unique properties that are advantageous not only from a corrosion view point, but from a strength and safety viewpoint as well. These LDSS may be used as primary structures for compression members of trusses or built-up columns due to varieties of advantages such as high strength to weight ratio, ease of fabrication, no need of protective coatings and they can be fully recycled after a useful life. This study presents an investigation on the LDSS built-up columns of rectangular, I, T and Z shaped sections under the axial loading and eccentric loading for various eccentricities. The finite element models of LDSS built-up columns are developed using ANSYS 16.1 WORKBENCH in order to investigate the behavior of various built-up columns at axial loading and eccentric loading. This study considers the eccentric loadings at 25, 50 and 75% eccentricities of the rectangular, I, T and Z shaped LDSS built-up columns.

Keyword Built-up columns · Axial loading · Eccentric loading

1 Introduction

Cold formed steel (CFS) built-up members have a traditional application in civil engineering for compressed structural elements, mostly as columns and members of lattice structures to carry heavier loads and over longer spans when a single individual section is insufficient. Built-up of normal CFS into new member with

M. S. Hima (✉) · S. Salim
Sree Narayana Gurukulam College of Engineering, Kadayiruppu, Kolenchery, Ernakulam, Kerala, India
e-mail: himams3333@gmail.com

© Springer Nature Switzerland AG 2021

K. Dasgupta et al. (eds.), *Proceedings of SECON 2020*,
Lecture Notes in Civil Engineering 97,
https://doi.org/10.1007/978-3-030-55115-5_63

higher strength can be produced efficiently by attaching the steel. The section is connected by using bolt, screw, or weld. By using cold-formed Lean Duplex Stainless Steel (LDSS) structures in the building construction industry it can provide more potential benefits including high strength to weight ratio, rapid constructability and ease of transportability and more over resistance to corrosion. So there is a scope for using the LDSS as built-up columns to improve the structural stability of buildings.

Huang and Young [3] conducted an experimental study on pin-ended cold-formed LDSS columns compressed between pinned ends to determine the axial load carrying capacity of different column specimens. Rossi [4] presented a discussion on the use of stainless steel in constructions in view of sustainability. In this paper, attention is first paid to the advantages associated with the use of stainless steel in recent construction projects in view of sustainability. Dabaon et al. [1] presents an experimental investigation on behavior and design of built-up cold-formed steel section battened columns. Two modes of failure were observed in the tests which are flexural buckling (F) and local buckling (L). Dobric et al. [2] conducted an experimental study on the Resistance of cold-formed built-up stainless steel columns and addresses their flexural buckling capacity about the minor principal axis.

In this study built-up models of LDSS such as rectangular, I, T and Z sections have been modeled using ANSYS 16.1 WORKBENCH to compare its load carrying capacity. The objectives of this study include: (1) To investigate the axial loading performance of various LDSS built-up sections such as rectangular, I, T and Z section; (2) To analyze the eccentric loading for various eccentricities in various LDSS built-up sections such as rectangular, I, T and Z section in X and Z directions at eccentricities such as 25, 50 and 75%.

2 Numerical Study on Various LDSS Built-Up Sections

A column of length 900 mm, width 50 mm and depth 70 mm with thickness 2.5 mm is used to construct the various LDSS built-up columns. Three numbers of columns with same dimensions are used to model the various LDSS built-up columns. Built-up columns of four different shapes such as are rectangular section, I section, T section and Z sections are proposed in this study. The bolted interconnections were designed with steel bolts M5, class 5.8. The spacing between the bolt centres is 95 mm. LDSS built-up columns of various shapes were analyzed using finite element analysis in ANSYS 16.1 WORKBENCH. S4R shell element which allow each node to have three degrees freedom both along translational and rotational directions were used to model the various LDSS built-up column. Across the length and width of the column, a mesh size of 5 mm x 5 mm was used. The LDSS built-up columns were compressed between the pinned ends. Pinned boundary condition was modeled by applying rotations and displacements to both the ends of columns through a reference point. Geometrical details and material properties of the column specimen used in the study are given in Table 1. Figures 1, 2, 3 and 4 shows the model of the various LDSS built-up specimens used in the study.

Table 1 Measured specimen dimensions for CL900

Specimen	Depth (mm)	Width (mm)	Thickness (mm)	Outer-radius (mm)	Inner-radius (mm)	σ 0.2 (MPa)	σu (MPa)	Eo (GPa)
CL900	70	50	2.5	4.2	1	635	756	198

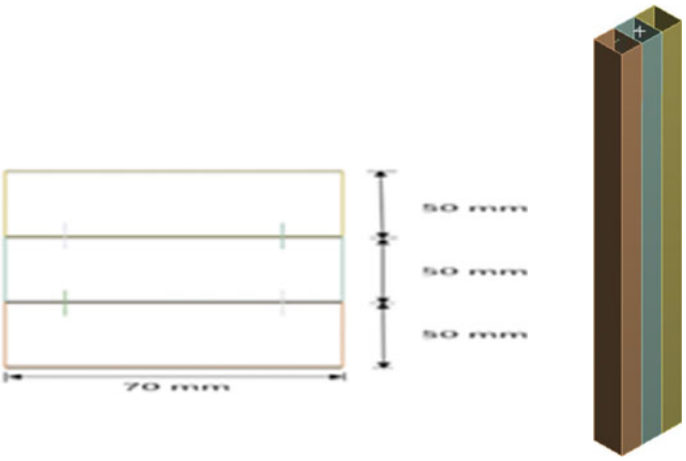

Fig. 1 Rectangular shaped LDSS column

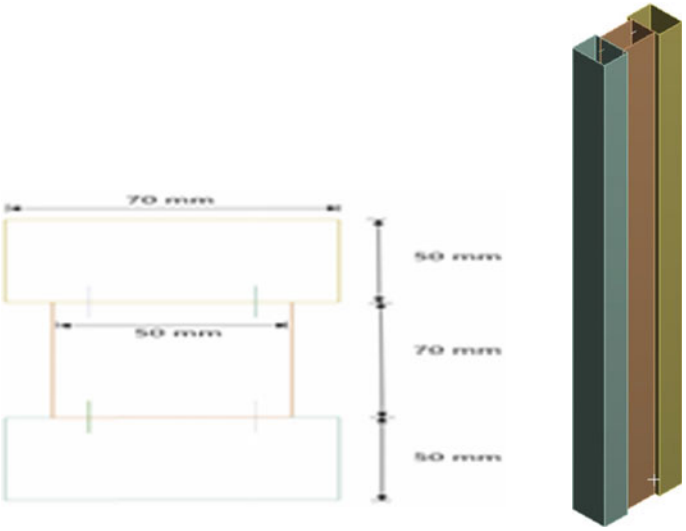

Fig. 2 I shaped LDSS built-up column

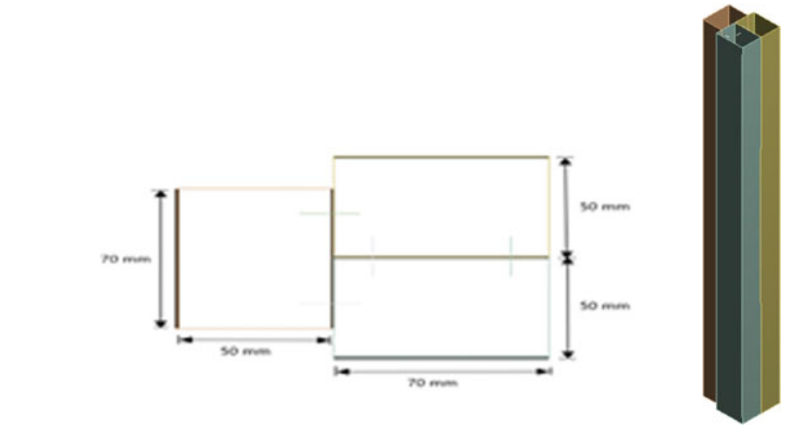

Fig. 3 T shaped LDSS built-up column

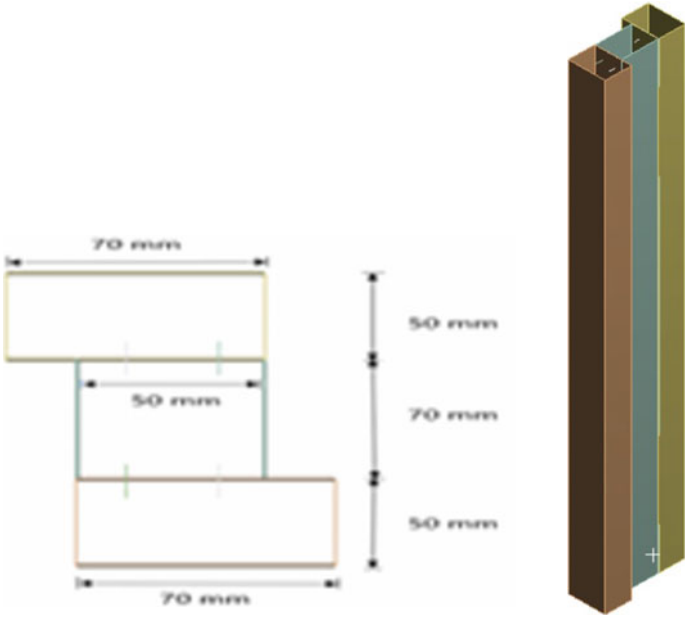

Fig. 4 Z shaped LDSS column

3 Results and Discussion

3.1 Axial Loading and Eccentric Loading Performance of Various Built-Up Sections

The axial and eccentric loading capacity of LDSS built-up columns was determined from FE analysis. The eccentricities are provided at 25, 50 and 75% in both Z and X directions. Table 2 shows the maximum load and deflection of axially and eccentrically loaded various LDSS built-up columns. Figures 5, 6, 7, 8, 9, 10 and 11 shows the comparison of axial and eccentric loading performed in various built-up columns.

From Fig. 5, the axial load carrying capacity of the LDSS T section increased up to 26.7% with LDSS rectangular section, 30.6% with LDSS I section and 19.6% with that of LDSS Z section.

From Fig. 6, the load carrying capacity at an eccentricity of 25% in Z direction of the LDSS T-section increased up to 26.7% with LDSS rectangular section, 30.77% with LDSS I-section and 19.6% with that of LDSS Z-section.

From Fig. 7, the load carrying capacity at an eccentricity of 25% in X direction of the LDSS T-section increased up to 3.4% with LDSS rectangular section, 18.7% with LDSS I-section and 6.5% with that of LDSS Z-section.

From Fig. 8, the load carrying capacity at an eccentricity of 50% in Z direction of the LDSS T-section increased up to 28% with LDSS rectangular section, 30% with LDSS I-section and 20% with that of LDSS Z-section.

From Fig. 9, the load carrying capacity at an eccentricity of 50% in X direction of the LDSS T-section increased up to 1% with the LDSS rectangular section, 11% with LDSS I-section and 10% with that of LDSS Z-section.

From Fig. 10, The load carrying capacity at an eccentricity of 75% in Z direction of the LDSS T section increased up to 26.4% with LDSS rectangular section, 31.5% with LDSS I-section and 19.4% with that of LDSS Z-section.

From Fig. 11, The load carrying capacity at an eccentricity of 75% in X direction of the LDSS T-section increased up to 4% with LDSS rectangular section, 16.6% with LDSS I-section and 9.2% with that of LDSS Z-section.

The maximum load on which a single LDSS column can carry was 270 kN. When it is used as LDSS built-up column in this present study, the load carrying capacity of various shaped LDSS built-up sections is found to be increased.

4 Conclusions

The finite element analysis of Lean Duplex Stainless Steel in various built-up section was carried out for studying the structural performance of various LDSS built up sections. Based on the objectives of the project following conclusions were obtained:

Table 2 Maximum load and deflection of axially loaded rectangular, I, T and Z section

Built-up columns	Results obtained	Axially loaded	In Z direction			In X direction		
			Eccentric load at 25%	Eccentric load at 50%	Eccentric load at 75%	Eccentric load at 25%	Eccentric load at 50%	Eccentric load at 75%
Rectangular built-up column	Deflection (mm)	3.94	3.9407	2.94	3.19	3.28	6.03	8.76
	Load (kN)	889	889.08	888.13	889.29	866.65	739.5	677.72
I built-up column	Deflection (mm)	3.43	3.2677	3.67	4.97	5.87	6.46	9.33
	Load (kN)	862	861.45	862.28	855.23	754.78	671.31	603.88
T built-up column	Deflection (mm)	2.891	2.8913	2.95	2.96	4.98	5.49	5.61
	Load (kN)	1126	1126.6	1128.1	1124.8	896.29	745.3	704.34
Z built-up column	Deflection (mm)	2.86	2.8694	2.95	2.86	4.20	12.76	7.19
	Load (kN)	941	941.87	943.41	941.87	813.89	672.45	645.07

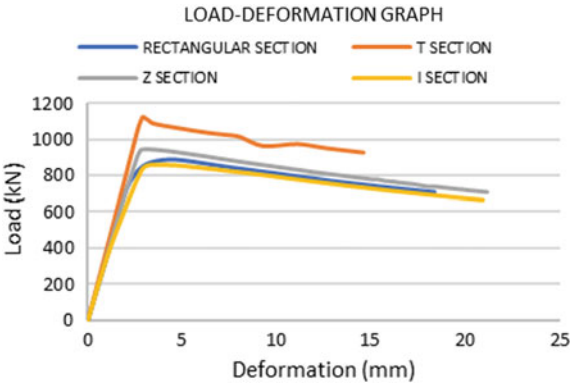

Fig. 5 Comparison of load-deflection graph of various LDSS built-up columns loaded axially

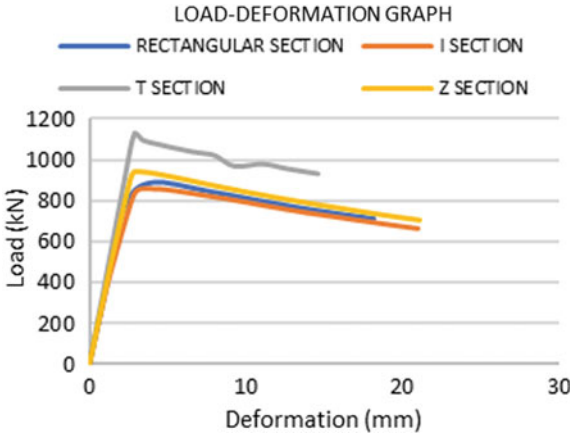

Fig. 6 Comparison of load-deflection graph of various LDSS built-up loaded eccentrically at 25% in Z direction

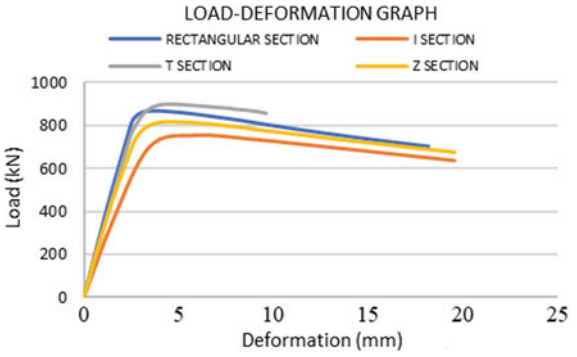

Fig. 7 Comparison of load-deflection graph of various LDSS built-up column loaded eccentrically ath 25% in X direction

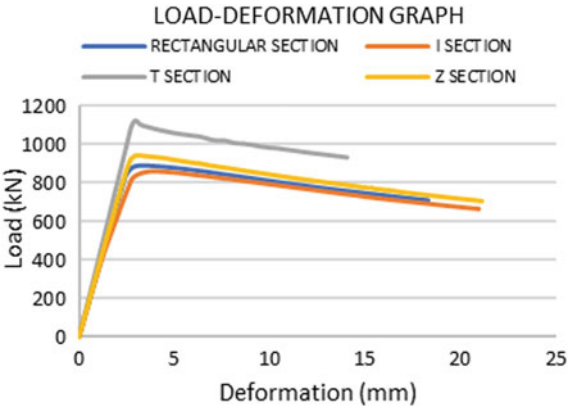

Fig. 8 Comparison of load-deflection graph of various LDSS built-up column loaded eccentrically ath 50% in Z direction

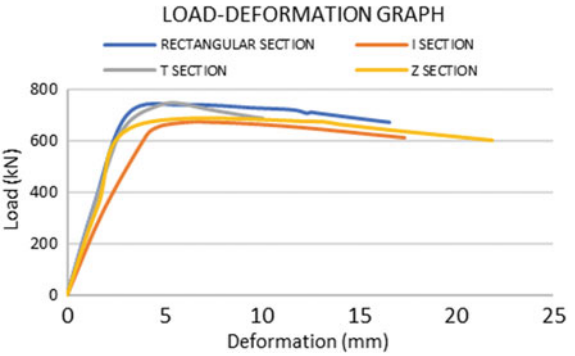

Fig. 9 Comparison of load-deflection graph of various LDSS built-up column loaded eccentrically ath 50% in X direction

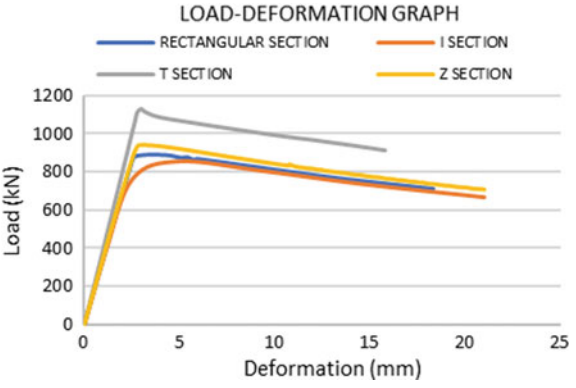

Fig. 10 Comparison of load-deflection graph of various LDSS built-up column loaded eccentrically ath 75% in Z direction

- All the LDSS built-up sections considered in the study perform the load carrying capacity in both axial and eccentric loading conditions quite well.

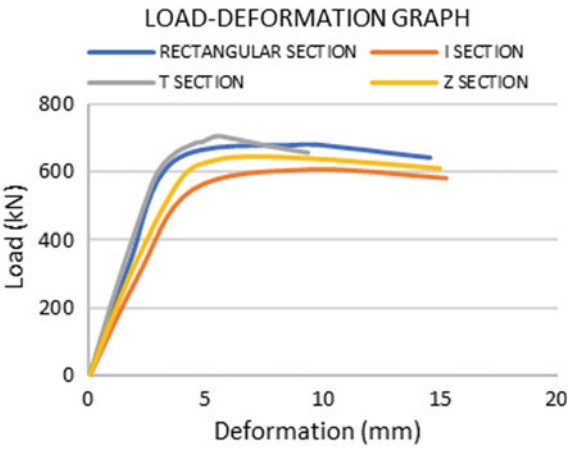

Fig. 11 Comparison of load-deflection graph of various LDSS built-up column loaded eccentrically ath 75% in X direction

- The behavior of all LDSS built-up sections are similar to each other and there is only a slight variation in the load carrying capacity when compared with each other and failure is represented by local buckling.
- Among them, the T shaped LDSS built-up section has the maximum axial and eccentric loading compared to other various built-up columns proposed in this study even though it has an unsymmetrical shape with respect to X axis.
- Therefore the use of various shaped LDSS built-up sections is recommended as it is able to carry the load for which it is designed.

References

1. Dabaon M et al (2015) Experimental investigation of built-up cold-formed steel section battened columns. Thin-Walled Struct 92:137–145
2. Dobrić J et al (2018) Resistance of cold-formed built-up stainless steel columns–part I: experiment. J Constr Steel Res 145:552–572
3. Huang Y, Young B (2013) Tests of pin-ended cold-formed lean duplex stainless steel columns. J Constr Steel Res 82:203–215
4. Rossi B (2014) Discussion on the use of stainless steel in constructions in view of sustainability. Thin-Walled Struct 83:182–189

Blended Cement Using Calcined Clay and Limestone for Sustainable Development—A Review

Ranjan Abraham, T. R. Neelakantan, Ramesh Babu Chokkalingam, and Elson John

Abstract In the cement industry, the use of pozzolanic materials is attaining paramount interest due to their beneficial effect on various properties of cement. Many type of cement have been developed in the last two decades to meet specific requirements. Ternary cement is one such type of modern cement, which consists of two pozzolanic materials with ordinary clinker. Blending reduces overall clinker content in cement. Ternary cement saves cost, resources and energy. Further, they reduce emissions & wastage of raw materials. Partially replacing clinker by calcined clay combined with limestone can be adopted to achieve blended cement with good performance. Higher levels of clinker substitution up to 50% are possible with 30% calcined clay, 15% lime stone and 5% gypsum, which contribute to reduction of CO_2 emission associated with cement production. Previous studies on such replacements and how they were beneficial for sustainable development are summarized in this review paper.

Keywords Blended cement · Supplementary cementitious materials · Sustainability · Calcined clay · Limestone · CO_2 emission

R. Abraham (✉) · T. R. Neelakantan · R. B. Chokkalingam
Department of Civil Engineering, School of Environmental and Construction Technology, Kalasalingam Academy of Research and Education, Krishnankoil, Srivilliputhur, Tamil Nadu 626126, India
e-mail: ranjan@klu.ac.in

T. R. Neelakantan
e-mail: neelakantan@klu.ac.in

R. B. Chokkalingam
e-mail: babussr@gmail.com

E. John
Department of Civil Engineering, Mar Athanasius College of Engineering, Kothamangalam, Ernakulam, Kerala 686666, India
e-mail: elson78@gmail.com

© Springer Nature Switzerland AG 2021

K. Dasgupta et al. (eds.), *Proceedings of SECON 2020*,
Lecture Notes in Civil Engineering 97,
https://doi.org/10.1007/978-3-030-55115-5_64

1 Introduction

The use of Supplementary Cementitious Materials (SCM) has a large potential to reduce the emission of carbon and saving the consumption of raw materials used for cement production. This is highly beneficial, especially for developing countries like India. But the wider use of SCMs is not supported due to a limited supply of them in many countries. More than 80% of SCMs used to reduce clinker fraction in cement are limestone, fly ash or slag. Calcined clay in combination with limestone has immense potential to be used as supplementary cementitious material, in partial replacement of clinker [1].

This paper concentrates mainly on the studies on Limestone Calcined Clay Cement (LC3), which focuses on reactive kaolinitic clays. Amount of slag available worldwide is around 5–10% of the amount of cement produced, which is not likely to change, as demand for steel is increasing less rapidly than demand for cement and more steel is being recycled, due to environmental aspects. Amount of fly ash available is somewhat high, but quality is very much variable, with less than one third suitable for blending in cement [2]. Long term availability of fly ash cannot be ascertained, as burning of coal to produce electricity is not entertained in most countries, to reduce environmental emissions.

Even though limestone is available in abundance, addition of more than 10% of limestone alone to cement results in increased porosity and poorer properties [3]. To extend the strategy of reducing clinker content, identification of new types and sources of SCMs have become essential. Even though Rice husk ash, sugar cane bagasse ash and ashes of other agricultural wastes are pozzolanic, scattered distribution leads to economic viability of their use.

Clays are abundantly available worldwide. Clays having significant portion of kaolinite and calcined between 700 and 850 °C are highly pozzolanic [4]. Metakaolin, a very reactive mineral addition, has been produced by calcining high purity kaolinitic clays. Metakaolin is around 3 times costlier than cement, which makes it not feasible for production of general purpose cement.

Studies conducted at Ecole Polytechnique Fédérale de Lausanne (EPFL) [5, 6] proved that a kaolinite content of about 40% in a mixture of LC3-50 (50% ground clinker, 30% calcined clay, 15% limestone, 5% gypsum) could produce mechanical properties similar to reference plain Portland cement sample in 7 days. Clays are widely available in most developing countries where cement demand going to increase in future. The requirement of calcination makes clay costlier than slag or fly ash. But unavailability of slag and fly ash in many places makes it viable and high level of clinker substitution is possible by combination of calcined clay and limestone and exhibit similar mechanical properties of pure Portland cement [7]. Low cost of limestone balance the cost of calcination of clay. Industrial production of cement having 50% clinker, combined with a blend of calcined clay and limestone has proven successful through industrial trials carried out in Cuba and India. Cements produced had mechanical performance similar to Portland cement, with clinker content above 90% [8–10].

2 Technology

Clay is calcined by heating to around 700–850 °C. No sophisticated equipment is necessary to produce calcined clays, since calcination temperature is low, compared to clinker production. Coupled addition of calcined clay and limestone is used to substitute part of clinker in blended cement and are designated LC3—X, where X refers to the clinker content of blend in percent. Calcination of clay containing kaolinite leads to formation of metakaolin, which is an amorphous alumino silicate ($Al_2Si_2O_7$). It can react with calcium hydroxide as a conventional pozzolan to give C–(A)–S–H and aluminate hydrates. In addition, alumina can react with limestone to produce carbo-aluminate hydrates [7]. All these products fill space and contribute to development of strength and durability properties. Clays containing 40% or above kaolin give strengths comparable to plain Portland cement when used in LC3-50 (50% clinker, 30% calcined clay, 15% limestone and 5% gypsum). The coupled substitution of two materials leads to good mechanical performance than other pozzolan at early ages even under higher levels of substitution. Clay, which is a finely divided product, reacts faster and to a higher degree.

Trial production runs of LC3 have been made in Cuba and India [8–10] where cement could be substituted one for one in standard applications by untrained workers, with similar water cement ratios and super plasticizers. In India it was used for preparation of roof tiles, which showed higher breaking strengths than tiles made with the usual Portland fly ash cement. In Cuba, the cement was used in blocks and pre-cast concrete culverts. The technology proved to be robust under situations like usage in poor and remote regions, by unskilled workers, lack of control of aggregate quality, poor control of water content, use without admixtures, usage under hot climate and precast constructions where high early strength is required. Studies are yet to be done in areas of stability of workability at high temperature and sensitivity to common contamination.

Calcined clay has high fineness, which is worsened if it is inter ground with clinker, which may cause higher water demand, or require higher levels of super plasticizer. Ideally the clinker should be ground first and then blended with calcined clay and limestone. As calcined clay contains reactive alumina, it is also important that blends are properly sulfated by checking level of sulfate addition needed using isothermal calorimetry [7].

3 Strength of LC3 Blends Prepared from Low Grade Clays

Potential of blends based on limestone, calcined clay, and clinker (LC3), incorporating calcined clay from several countries (India, Brazil, Thailand and Cuba) were analyzed [1] and strengths obtained are shown in Fig. 1. Plotting these results against the kaolinite content of clays, it was seen that kaolinite content is the main parameter determining strength development and is shown in Fig. 2. In these experiments

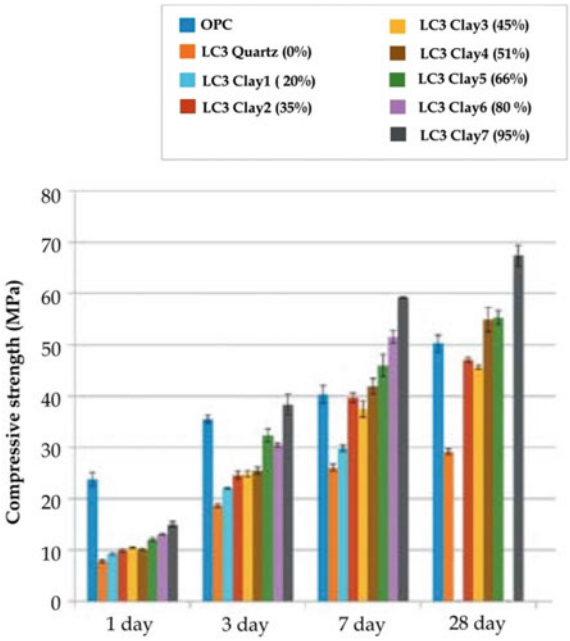

Fig. 1 Strength development for a range of blends all containing 50% clinker, 5% gypsum, 15% limestone and 30% calcined clay. (Clays originated from India, Brazil, Thailand and Cuba) [1]

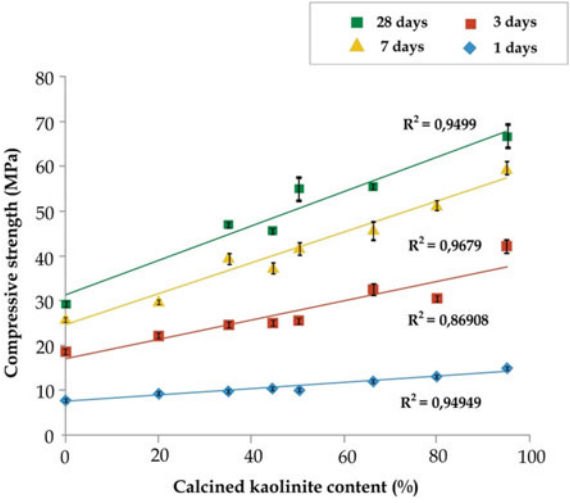

Fig. 2 Relationship between kaolinite content of calcined clay and strength [1]

cements were prepared by intermixing based on the same ground clinker. It could be seen that one day strengths are still rather low, but, for a kaolinite content of 50% or more, higher strengths than the reference were achieved by 7 days after testing Mortar cubes. One day strength could be improved by inter-grinding as is currently done for fly ash blended cements.

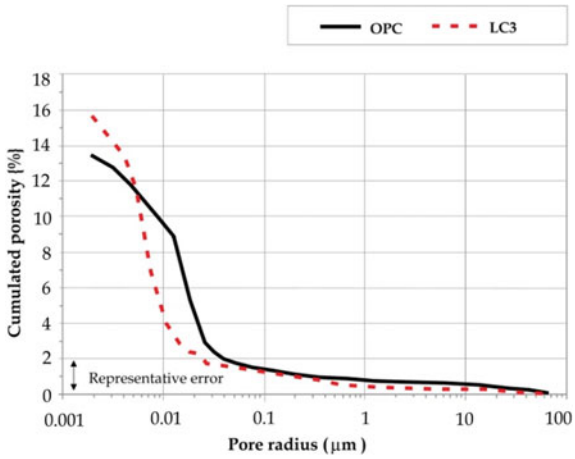

Fig. 3 Mercury intrusion porosity of results for LC3 blend and reference Portland cement [1]

4 Durability of LC3 Blends Prepared from Low Grade Clays

While considering a new cement formulation, question of durability is of prime importance. A wide-ranging and detailed study of durability of LC3 was done in Switzerland, India and Cuba. Mercury intrusion porosimetry and Chloride penetration tests were done to assess durability. Those studies looked at underlying scientific mechanisms as well as full scale exposure conditions. The material is expected to have good durability due to following reasons.

Firstly, the phase composition of materials was very similar to existing Portland and blended cements. The principal hydrate was calcium silicate hydrate, C–S–H, whose long-term behaviour is well known and understood. Other aluminate containing phases, mono and hemi carbonate and ettringite were also formed in limestone cements, widely used in Europe for many years.

Secondly, analysis of pore structure shown in Fig. 3 revealed that, pores were smaller, even though overall porosity was be slightly higher [1].

Thirdly, preliminary results on resistance to penetration of chloride ions are extremely good. Figure 4 shows chloride profiles after two years ponding in 0.5 M NaCl solution [1].

5 Environmental and Economic Potential

Developing countries demand increased need of infrastructures and production of more quantity of cement. Use of SCM is a promising solution to increase cement production without increasing negative environmental impact.

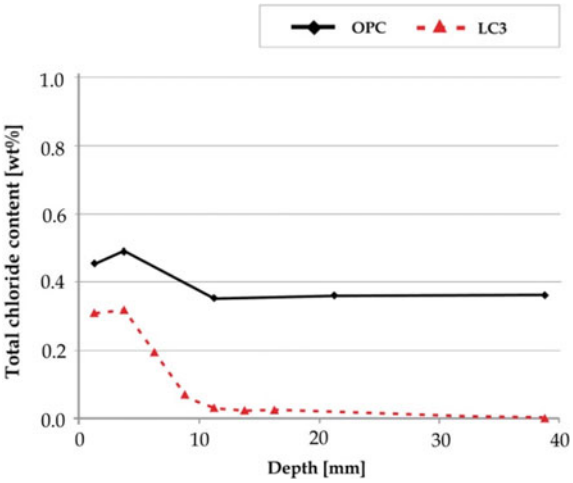

Fig. 4 Chloride profiles after 2 years ponding in 0.5 M NaCl solution [1]

A method was developed to assess details of economic and environmental potential of LC3 technology in Cuban context, in which a comparison of OPC and PPC was done. Study included a sensitivity analysis where different types of technology as well as alternative fuel types have been tested. Sensitivity of green house gas emissions savings for LC3 production was evaluated depending on level of technology, fuel and transport type [11]. Results, shown in percentages saved and tabulated in Table 1, provided data for development of LC3 technology in the Cuban market, which can be further extended to markets in other developing countries.

Technology changes induce variations from 6 to 10% depending on type of fuel used. Changes in fuel types do not provide great changes in Global Warming Potential (GWP) except when a flash calciner was used for LC3 and a preheater + pecalciner kiln was used for clinker production. Similar results were found when comparison of LC3 was made over OPC or PPC. Savings compared to OPC were around 35% while savings compared to PPC were around 25%.

Availability of suitable clay source was also a key aspect in LC3 production process. When clays were transported by truck over 350 km, economic benefits of LC3 against OPC were less. Figure 5 shows results of sensitivity of raw materials transport of LC3 compared to current OPC production costs in Cuba. If raw material transport was done by train, contribution to overall negative environmental impact of LC3 was negligible.

Comparison of environmental impact for OPC, blended cement PPC and LC3 for three different technical levels: Pilot, Industrial and Best Available Technology (BAT) are shown in Fig. 6. LC3 cement always produced 30% savings approximately. Worst LC3 cement made in pilot industrial trial was better than best OPC produced with BAT. Major emission reductions were related to energy savings and clinker substitution, although there reported a significant decrease in electricity consumption during grinding process, due to softness of LC3 in comparison with OPC.

Table 1 Economic impact sensitivity to fuels & technology [11]

GWP savings comparing PPC-LC3 (%)					GWP savings comparing OPC-LC3 (%)				
Fuels/techno	Wet (%)	Dry (%)	BAT (%)	BBAT (%)	Fuels/techno	Wet (%)	Dry (%)	BAT (%)	BBAT (%)
Crude	26	24	24	34	Crude	36	35	35	42
Petcoke	24	25	23	33	Petcoke	36	36	32	40
Gas+ Waste	26	26	25	20	Gas+ Waste	37	36	33	27

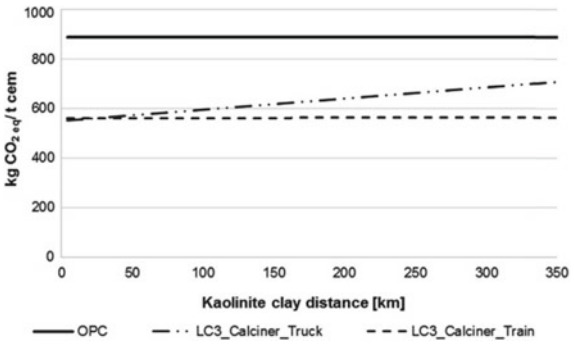

Fig. 5 GWP Comparison per transported tonne of cement [11]

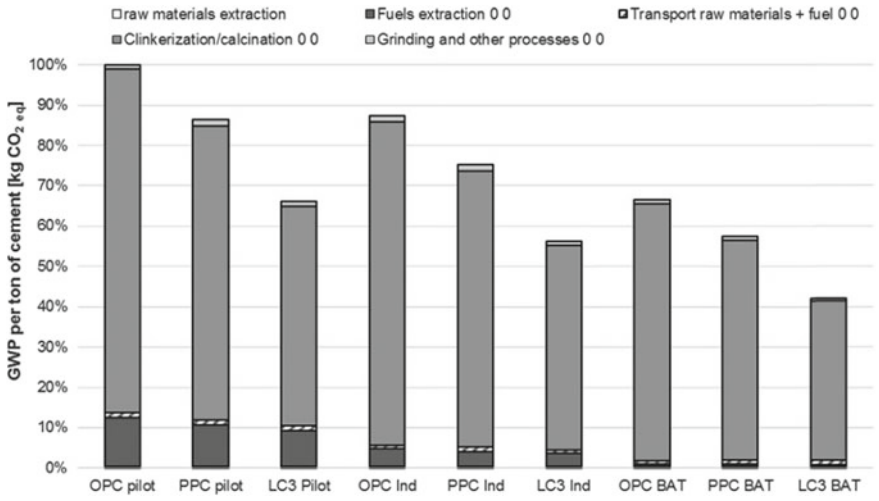

Fig. 6 Relative GWP impact of cement production in Cuba—all scenarios [11]

Concerning economic feasibility of LC3 production, an analysis was carried out and cost savings referred to OPC and PPC are presented in Fig. 7.

Sensitivity to fuel and technology showed a different pattern than environmental sensitivity. Variation in term of production costs was higher than for GWP when differences in technology were considered. It varied from 10 to 30% depending on technology and type of fuel used. Using BAT technology for clinker production as well as clay calcination (BBAT Technology) could induce higher production cost for LC3 when secondary fuels were used in the clinkerization process.

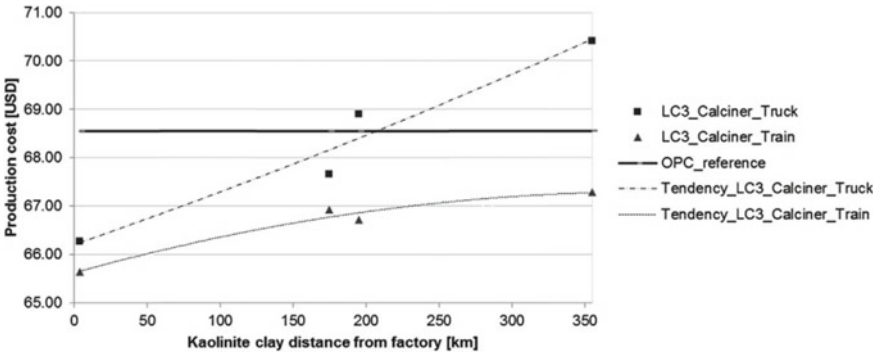

Fig. 7 Comparison depending on transport distance and cost of alternate materials [11]

6 Conclusions

- Blends with 50% clinker, 30% calcined clay, 15% unburned limestone and 5% gypsum is a promising option to achieve energy efficiency, cost efficiency and lower CO_2 emission
- Kaolinite content in clay is the main parameter determining strength development.
- The phase composition of materials was very similar to OPC and PPC.
- The size of pores was smaller compared to PPC, when LC3 was used.
- LC3 offered extremely good resistance to penetration of chloride ions.
- LC3 technology leads to reduced greenhouse gas emissions and lower global warming potential compared to OPC and PPC.

References

1. Scrivener KL (2014) Options for the future of cement. Indian Concr J 88(7):11–19
2. Snellings R (2016) Assessing understanding and unlocking supplementary cementitious materials. RILEM Tech Lett [S.l.] 1:50–55
3. Matschei T, Lothenbach B, Glasser FP (2007) The role of calcium carbonate in cement hydration. Cem Concr Res 37(4):551–558
4. Fernandez R, Martirena F, Scrivener KL (2011) The origin of pozzolanic activity of calcined clay minerals: a comparison between kaolinite, illite and montmorillonite. Cem Concr Res 41(1):113–122
5. Alujas A, Fernández R, Quintana R, Scrivener KL, Martirena F (2015) Pozzolanic reactivity of low grade kaolinitic clays: influence of calcination temperature and impact of calcination products on OPC hydration. Appl Clay Sci 108:94–101
6. Avet F, Snellings R, Alujas Diaz A, Ben Haha M, Scrivener K (2016) Development of a new rapid, relevant and reliable (R3) test method to evaluate the pozzolanic reactivity of calcined kaolinitic clays. Cem Concr Res 85:1–11
7. Antoni M, Rossen J, Martirena F, Scrivener K (2012) Cement substitution by a combination of metakaolin and limestone. Cem Concr Res 42:1579–1589

8. Vizcaíno-Andrés L, Sánchez-Berriel S, Damas-Carrera S, Pérez-Hernández A, Scrivener K, Martirena Hernandez JF (2015) Industrial trial to produce a low clinker, low carbon cement. Mater Constr 65:(317)
9. Bishnoi S, Maity S, Mallik A, Joseph S, Krisnnan S (2014) Pilot scale manufacture of limestone calcined clay cement: the Indian experience. Indian Concr J 88(7):22–28
10. Emmanuel A, Halder P, Maity S, Bishnoi S (2016) Second pilot production of limestone calcined clay cement in India: the experience. Indian Concr J 90:57–64
11. Sanchez Berriel S, Favier A, Rosa Domínguez E, Sanchez Machado IR, Heierli U, Scrivener K, Martirena Hernandez F, Habert G (2016) Assessing the environmental and economic potential of Limestone Calcined Clay Cement in Cuba. J Clean Prod 124:361–369

Seismic Performance Improvement Techniques for Infill Frames—A Review

A. Athira Nair and Keerthy M. Simon

Abstract Masonry infill walls are commonly used as external walls and partition walls in RC frame buildings. RC frames in earthquake regions are usually designed with higher ductility and hence undergo large displacements under horizontal loading which lead to a rapid activation of the significantly stiffer infills. This activation generates an undesired interaction between the frame and the infill resulting in the participation of the masonry infills for load transfer. The seismic performance of masonry infill walls under earthquake loading have been studied experimentally and analytically. Damages under in-plane loading are found to escalate the out-of plane response. Over the years the studies have been extended from steel frames to RC frames and the infill materials have been varied from masonry infill to concrete panels. However, the studies are particularly focused on masonry infill units. With the rising concern for environmental pollution control, alternative green materials are also being recommended as infills. This paper presents a review on the techniques that have been developed to improve the seismic performance of infilled frames. It can be achieved by providing a rigid connection between the infill and the frame or by completely isolating the infill walls from the surrounding frame and by using seismic isolation elements.

Keywords Masonry infill · RC frame · Seismic isolation

1 Introduction

Masonry infill panels can be found as interior and exterior walls in reinforced concrete (RC) and steel frame structures. The term infilled frame is used to denote a composite structure formed by the combination of moment resisting plane frames and filler

A. Athira Nair (✉) · K. M. Simon
Department of Civil Engineering, NSS College of Engineering, Palakkad, India
e-mail: athiranair31195@gmail.com

K. M. Simon
e-mail: keerthymsimon@gmail.com

© Springer Nature Switzerland AG 2021

K. Dasgupta et al. (eds.), *Proceedings of SECON 2020*,
Lecture Notes in Civil Engineering 97,
https://doi.org/10.1007/978-3-030-55115-5_65

walls. Infills are generally built integral with the RC frame, but it is considered as non-structural elements and their presence is often ignored by structural engineers. The entire lateral force on the building is carried by the bare frame alone. However, unless they are separated from the frames by adequate movement joints along the ends and top, they will interact with the surrounding frame when the structure is subjected to wind or earthquake loads.

Infills interfere with the lateral deformations of the RC frame and improve the stiffness of the building. Under seismic loading the non-structural components such as partition walls helps in load transfer and it takes place along the diagonal of the infill. Compression strut forms along one diagonal and the separation of frame and infill takes place along the other. The structural load transfer is converted into truss action rather than the frame action which is usually observed.

Energy dissipation is observed to be better in the case of infill frames than bare frames as the inelastic effects in infills is also considered in addition to the inelastic effects in the frame members and joints. Hence, the masonry infill wall increases strength, stiffness, overall ductility and energy dissipation of the building. More importantly, they help in drastically reducing the deformation and ductility demand on RC frame members [1, 2].

2 Seismic Safety of Masonry Infills

Infill walls can have a beneficial effect on the structural response provided that they are placed regularly throughout the structure. Damage to infill walls is a seismic hazard hence it is essential to preserve its integrity. The damages caused can hamper the safe movement of occupants evacuating buildings or of rescue workers entering buildings. It affects the performance level of the building even if the structural components are safe to offer an immediate occupancy level. Major facilities crucial in a seismic event such as rescue operations and medical facilities would be adversely affected. Hence various solution strategies were developed to increase the seismic safety of masonry infilled RC frames and to reduce the detrimental effect of the masonry infill [3].

Multiple failure mechanisms have been observed in Unreinforced Masonry walls (URM) under earthquake action, including both in-plane mechanisms and out-of-plane collapse. By increasing the lateral stiffness of the structure, the infills shift the natural period of the structure on the earthquake response spectrum in the direction of a higher seismic shear and story shears and direct earthquake forces to non-structural elements. During an earthquake, these infill walls increases the earthquake lateral load significantly and are often damaged prematurely due to diagonal tension and compression or out-of-plane failure. Various solution strategies were developed to increase the seismic safety of masonry infilled RC frames and to reduce the detrimental effect of the masonry infill [3].

2.1 Rigid Connection and Strengthening

The seismic safety of the infill wall can be improved either by improving the load bearing capacity of a masonry infill-wall by providing a rigid connection to the frame or by completely isolating the infill walls from the surrounding frame by intentionally creating a construction gap. This however had to compromise with the original function of the partition walls such as acoustic insulation and protection from environmental phenomena. Another shortcoming of the isolation option is that the beneficial effects of the masonry infill in stiffening and strengthening the structural frame system will not be employed. Deformation capacity of the masonry infill wall can be increased by means of special construction measures like sliding surfaces in the wall. Strengthening of the walls, though a retrofitting technique can also be employed during the construction phase especially for buildings in the seismic prone areas.

Column-isolated infill condition effectively preserves the integrity of infill panel. It avoids out-of-plane failure of masonry wall by keeping infill panel tightly fitted with bounding beam by utilizing the steel connectors between columns and infill panel. It exhibits the improved seismic performance than the completely infilled frame in terms of ductility, degradation of stiffness and strength, and energy dissipation capability [4].

The techniques to prevent soft storey mechanisms like base insulations, shear walls, bracings, or strengthening the columns are expensive. A viable option available is to soften the upper stories by adding slit separated features at the edges of infill walls. RC infill wall is separated from the moment frame by two vertical silts at the edges of the wall and one horizontal gap on the top of the wall. The slits can be designed with different widths to absorb the inter-story drift in each story. Slit-separated wall can be isolated to be free from damage under small lateral story drifts. It eliminates the soft-story problem caused by vertically irregular configuration of RC infill and improves the drift capacity. It increases the lateral resistance without inhibiting the ductility of the steel moment frame under large earthquake attack [5]. Analytical studies have shown that by a combined use of proper sliding joints inserted in the masonry and deformable joints at the wall-frame interface out-of-plane stability can be ensured. It helps in limiting the level of damage at different seismic intensities, providing a prominent reduction of the cost of reparability after seismic events and a wide margin towards the life safety requirements [6].

RC frames infilled with weak masonry panels can be provided with light reinforcement, in the mortar layers or in the external plaster. The external meshes improve the response enormously, in terms of strength, stiffness and energy dissipation capacity. The economic benefit of such simple measures of protection is extraordinarily important, particularly when compared with the relatively low additional construction cost [7].

Strengthening of the masonry infills to achieve a better performance during seismic loading is a rational solution. The conventional strengthening technique of masonry infills comprises of application of external steel-mesh reinforcement in

combination with shotcrete or plaster on the face of the infill, application of sprayable ductile-fiber reinforced cementitious composites, steel fiber reinforced mortar and Fiber-Reinforced Polymer (FRP) sheets [8].

The external application of special plasters or Textile Reinforced Mortars (TRM) strengthening systems reduces the infill damage, change the crack pattern and can influence the out-of-plane response of the infill wall which is of the utmost importance during earthquakes. Reinforcing meshes are still very effective when applied to gypsum based plasters with low mechanical characteristics. TRM embedded with anchorages reduces the displacements at maximum load, allowing a highly controlled failure mode to develop after the peak load [9].

Brick infill wall can be strengthened by using expanded metal which can be well bonded with mortar plastering. The effects of ferrocement enhances the compressive strength, stiffness, and ductility of masonry panels. The expanded metal with fine mesh type is recommended for overlaying on the infill panel for better bond strength. It helps in a significant increase of strength for the infill panel. Strengthened infilled frame develops greater strength than the brick infilled frame due to the effect of ferrocement which enhances the diagonal compressive strength and sliding shear strength of the infill panel. When the infill panel is sufficiently strong in these diagonal and sliding modes, the corner compression will result in crushing and consequently lead to shear failure of the column. It prevents the sliding failure mode and changes it to the corner crushing mode [10].

Fiber reinforced Engineered Cementitious Composites (ECC) layers can be employed to strengthen the URM infills. ECC overlays are attached onto the surface of masonry infill only by their cohesion and mechanical anchorage is not provided between the strengthening layers and the RC frame. ECC-strengthening technique can effectively increase the lateral strength and energy absorption capacity of the infilled frame and prevent brittle failure modes in the infill wall [11].

Strengthening of infill walls by Carbon Fiber Reinforced Polymer (CFRP) is effective on increasing lateral load carrying capacity and initial stiffness of infilled RC frame specimens. CFRP which is pasted on the infill wall by epoxy take part in carrying compressive stresses by keeping the masonry in place under compression and by spreading the compressive stress over a larger area. Providing diagonal CFRP on the infill wall helps in transferring the diagonal tensile stress to the frame elements until failure [12]. CFRP sheets attached to the masonry wall faces and anchored to the concrete frame carries the diagonal tension. The CFRP laminate maintain the structural integrity of the fully infilled frame and prevents collapse and debris fallout. It further contains and localizes the damage of the URM walls even after ultimate failure. This reduces the possibility of the external walls or partitions spalling, which, in itself is a major source of hazard during earthquakes even if the whole structure remains safe and functioning. Energy dissipation capacity is better when CFRP is wrapped around the column to prevent the shear failure [13].

Strengthening and reinforcement measures significantly improve the load-bearing and deformation capacities of the masonry infills but can no longer be regarded as a non-load-bearing wall and must be designed for seismic forces. In addition, the acceptance of these measures in practice is rather low as they quickly become

unattractive and uneconomical in comparison to a reinforced concrete solution due to the amount of required manual construction work.

2.2 Seismic Isolation

The isolation option had to be replaced with a better solution which not only improves the seismic response but also prevents the failure of non-structural components. In general, since the masonry infill walls are heavy it greatly increases the effective seismic weight of the building, and hence it would be logical to engage them also in lateral load resistance. Hence, a rigid connection between the frame and infill is essential. The concept of fuse systems similar to the electrical fuses which get damaged when the loads are high and thereby prevent the structure is an intermediate option. The fuse material helps to maintain the rigidity of the frame and decouples when the structure is weak to support the load and thus can prevent the damages to an extent.

Seismic behaviour of masonry infilled RC frames could be enhanced by decoupling the frame and the masonry infill so that deformations of the frame do not generate any stresses in the masonry infill. This idea developed from the desirability of employing beneficial effects of strength and stiffness of infill walls to reduce story drifts during seismic events up to certain controlled levels and to isolate the infill wall from the frame in order to avoid damage to the wall or the frame under strong shaking [14, 15].

Pilot studies included the concept of Seismic Infill Wall Isolator Subframe (SIWIS) system. It consists of two vertical and one horizontal sandwiched light-gauge steel studs with rigid-brittle elements in the vertical members. It acts as a sacrificial element just like a fuse to save the infill wall and frame from failure by disengaging under damaging events by allowing brittle failure. Concrete disks of 69 mm diameter and varying thickness 22.2, 25 and 28.6 mm and a compressive strength of 24 MPa was used for the study. The system was found effective in considerably increasing the initial stiffness of the frame analytically [16]. Alternative materials such as steel and lumber disks were later implemented in the SIWIS system and the experimental results showed that the flexible frames benefitted more compared to stiffer frames [17]. Providing vertical tie-down elements helps in maximizing the in-plane strength and stiffness of the masonry wall.

To prevent the soft storey mechanism appropriate capacity arrangements of the fuses in elevation and in bays facilitates a sequential crushing of the fuses and hence provide adequate structural performance. For frames with higher ultimate load capacity fuse elements of larger capacity should be used. At lower positions of the fuse, the initial stiffness of the entire system will be reduced and the fuse breaks at larger deflection whereas at higher positions the fuse element improves performance efficiency. The stiffness of the frame members affects the design of the fuse capacity and for a given frame stiffness, the overall behavior is sensitive to the fuse capacity.

Existing finite element modelling software is effective to model the complex use of masonry walls [14, 18].

Thin layers of foamed polyethylene characterized by extremely high deformation capacity, was used to isolate infill panels from the surrounding RC frame for low and moderate storey drifts. The isolated system preserves the integrity of infill panels at moderate storey drifts and increases shear strength and lateral stiffness of the infilled frames at higher deformations. Partially infilled frames confirmed that cellular material joints at the sides of infills decreases the adverse effects of the infill-frame interaction [19, 20].

Under the European research project INSYSME a special decoupling element; Innovative Decoupled Infill System (INODIS) was developed. It consisted of an elastomeric cellular material with hyper elastic behaviour provided along the columns and the top beam which are glued to the outer bricks and move onto plastic profiles that are connected to the RC frames by nailing or screwing. The system delays the in-plane activation of the infill. It allowed interstory drifts of more than 3% and prevented the stress concentrations in the contact areas to the frame. The viscoelastic behaviour of the elastomeric cellular materials resulted in the higher energy dissipation and is compatible with different types of bricks [15].

3 Conclusions

This paper presents a review on the methods to improve the seismic behaviour of unreinforced masonry infills. RC frame are often not even formally designed for seismic loading even in severe seismic zones. Such buildings are commonly used as residential or office buildings which typically have a fairly large number of infills placed more or less uniformly and in such situations, the infills could be relied upon to ensure good seismic performance. Masonry infill wall panels increase strength, stiffness, overall ductility and energy dissipation of the building. The techniques are mainly aimed at reducing the damages caused to the masonry infill walls but at the same time to draw maximum advantage of these non-structural components under seismic loading.

Implementation of retrofitting measures such as reinforcement meshes and strengthening techniques can be easily employed to ensure better energy dissipation. Isolating the infills from the frame ensures seismic safety of infills but it affects the purpose of infills, such as insulation and protection. However the seismic isolation technique using cellular materials overcomes the problem by ensuring the infill-frame system to act as a unit and thus ensures seismic safety. Studies concerning the SIWIS system reveal that with capacity arrangement of the fuses it is possible to deal with major issues like soft storey mechanism. The techniques discussed in this paper have proved to be efficient as per the analytical and experimental studies. Further optimization of the models and full scale studies are required to make it suitable for implementing in normal construction.

References

1. El-dakhakhni WW, Drysdale RG (2004) 3-D finite element modelling of masonry-infilled frames with and without openings, pp 1–10
2. Murty CVR, Jain SK (2000) Beneficial influence of masonry infill walls on seismic performance of Rc frame buildings. In: Twelfth world conference on earthquake engineering, pp 1–6
3. Filiatrault A, Sullivan T (2014) Performance-based seismic design of nonstructural building components: the next frontier of earthquake engineering 13:17–46
4. Kuang JS Cyclic load tests of RC frame with column-isolated masonry infills
5. Ju RS, Lee HJ, Chen CC, Tao CC (2012) Experimental study on separating reinforced concrete infill walls from steel moment frames. J Constr Steel Res 71:119–128
6. Morandi P, Milanesi R, Magenes G (2018) Innovative solution for seismic-resistant masonry infills with sliding joints: in-plane experimental performance
7. Taylor P, Calvi GM, Bolognini D, Strutturale M, Pavia U, Ferrate V (2008) Seismic response of reinforced concrete frames infilled with weakly reinforced masonry panels. pp. 37–41
8. Koutas L, Pitytzogia A, Triantafillou TC, Asce M, Bousias SN, Asce M (2014) Strengthening of infilled reinforced concrete frames with TRM : study on the development and testing of textile-based anchors 18(3):1–12
9. Porto F, Modena C (2015) Effectiveness of plasters and textile reinforced mortars for strengthening clay masonry infill walls subjected to combined in-plane/out-of-plane actions Wirksamkeit von Putz und textilbewehrtem Mörtel bei der Verstärkung von Ausfachungswänden aus Ziege 19:334–354
10. Leeanansaksiri A, Panyakapo P, Ruangrassamee A (2018) Seismic capacity of masonry in filled RC frame strengthening with expanded metal ferrocement. Eng Struct 159:110–127
11. Dehghani A, Nateghi-Alahi F, Fischer G (2015) Engineered cementitious composites for strengthening masonry infilled reinforced concrete frames. Eng Struct 105:197–208
12. Erol G, Karadogan HF, Cili F (2008) Seismic strengthening of infilled Rc frames by CFRP 1981
13. Dehghani A (2008) Experimental behavior of brick-infilled concrete frames strenthed by CFRP with improved attachig technique
14. Drahansky M et al (2016) We are IntechOpen, the world' s leading publisher of open access books built by scientists, for scientists TOP 1%. Intech i:13
15. Marinković M, Butenweg C (2019) Innovative decoupling system for the seismic protection of masonry infill walls in reinforced concrete frames. Eng Struct 197:109435
16. Aliaari M, Memari AM (2005) Analysis of masonry infilled steel frames with seismic isolator subframes 27:487–500
17. Aliaari M, Ph D, Memari AM, Ph D, Asce M (2007) Experimental evaluation of a sacrificial seismic fuse device for masonry infill walls, pp 111–125
18. Aliaari M, Memari AM (2012) Development of a seismic design approach for infill walls equipped with structural fuse, pp 249–263
19. Tsantilis AV, Trianta TC (2018) Innovative seismic isolation of masonry in fills using cellular materials at the interface with the surrounding RC frames 155:279–297
20. Tsantilis AV, Triantafillou TC (2018) Innovative seismic isolation of masonry infills in steel frames using cellular materials at the frame- infill interface innovative seismic isolation of masonry in fills in steel frames using cellular materials at the frame-in fill interface. J Earthq Eng 00(00):1–18

Analysis of the Concrete Filled Steel Tubes with Diagonal Ribs

K. P. Ansa and S. Keerthi

Abstract Nowadays high-rise buildings and multi-storey buildings are more common and popular, they require highly strong and efficient structural system. Concrete Filled Steel Tube [CFST] are capable of providing the same. Many innovative ideas are being put forward in the improvement of the CFST section, which resulted in better improvisation of their column behaviors. Diagonal rib stiffened square concrete filled steel tube can increase the confinement, load-carrying capacity and ductility compared with the CFST specimens without stiffeners. By introducing the diagonal rib fitting, the composite effect of the square concrete filled steel can be improved, which is proved from the previously conducted experiments by several researchers on CFST sections. By analyzing the test results from experiments, a cost effective, robust and safe designed cross section is developed. The development of an analytical model for the CFST with diagonal ribs for predicting their axial load carrying capacities was done by finite element analysis method. It helps in predicting the results of combinations made by using various parameters.

Keywords Diagonal ribs · Axial load capacity · Concrete filled steel tube

1 Introduction

Concrete filled steel tubes (CFST) are the mainly used in the modern constructions for more efficient and strong system. They are mainly used in high rise buildings and multi storey buildings as columns and beams in low rise industrial buildings due to their superior structural performance. Concrete filled steel tubes combines the advantages of both steel and concrete. Steel offers high tensile capacity and ductility which can confine the concrete and delay its buckling. Whereas the concrete is

K. P. Ansa (✉)
Master of Technology NSS College of Engineering, Palakkad, India
e-mail: ansakp42@gmail.com

S. Keerthi
Department of Civil Engineering, NSS College of Engineering, Palakkad, India
e-mail: keerthis93@gmail.com

© Springer Nature Switzerland AG 2021

K. Dasgupta et al. (eds.), *Proceedings of SECON 2020*,
Lecture Notes in Civil Engineering 97,
https://doi.org/10.1007/978-3-030-55115-5_66

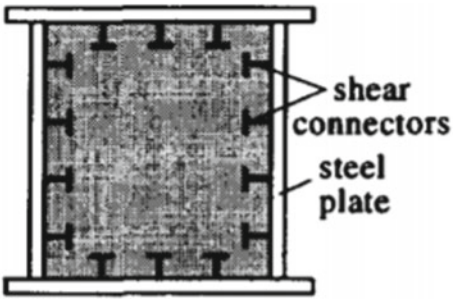

Fig. 1 Composite section with studs [2]

strong in compression and stiffness. CFST altogether has improved strength, high seismic performance and cost effective nature. Many innovative ideas are being introduced in the CFST for the improved composite effect of steel and concrete. They include the infills like timber, Carbon fibre reinforced polymer layers, stiffeners like studs, longitudinal stiffeners, and diagonal ribs etc. These items further increase the composite effect of CFST. They can be used as mega columns which can take up large vertical loads, in spite of complex fabrication. Among various improvisation methods the diagonal rib stiffened CFST has more efficiency. Experimental as well as analytical studies are in progress in this area.

2 Methods of Improvisation

There are various methods that can improve the composite effect of CFST. Like point confinement, line confinement and lateral closed confinement [1].

2.1 Usage of Studs

The usage of studs that provide confinement for the concrete at the point of the each stud and enhance the interface shear capacity. Studs are also called as shear connectors which are used to ensure reliable stiffness of the composite cross-section even in the region of elastic behaviour as shown in Figs. 1 and 2.

2.2 Usage of Longitudinal Stiffeners

Longitudinal stiffeners provides line confinement throughout the column axially. It confines the steel tube along the portion where it's welded. It provides more confinement than point confinement provided by the studs. Another benefits are

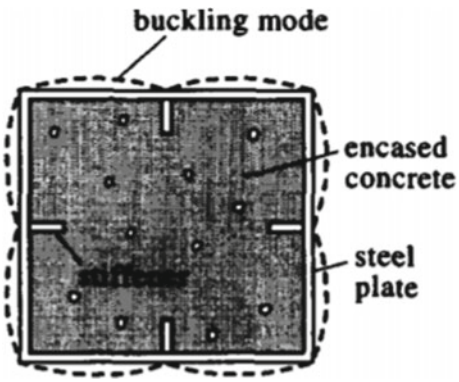

Fig. 2 Buckling mode of CFST with Studs [2]

increased local buckling strength and interface shear capacity [3] as shown in Figs. 3 and 4.

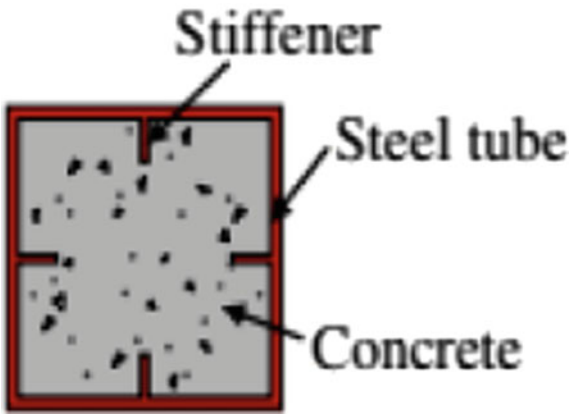

Fig. 3 Longitudinal stiffened CFST [4]

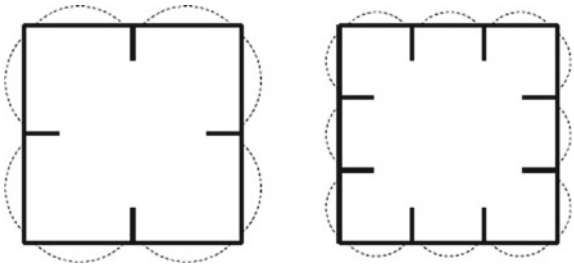

Fig. 4 Buckling mode [3]

2.3 Usage of Binding Bars

Binding bars provide lateral closed confinement. It increases the confinement from the steel tube to the infilled concrete more than the longitudinal stiffeners and studs, because it yielded quickly after the specimen reached the ultimate strength. Local buckling of the steel tube is delayed much more resulting in the yielding of the binding bar before reaching the ultimate strength. The confinement was increased at the corner region and centre region. As well as the ductility was improved [5] as shown in Figs. 5 and 6.

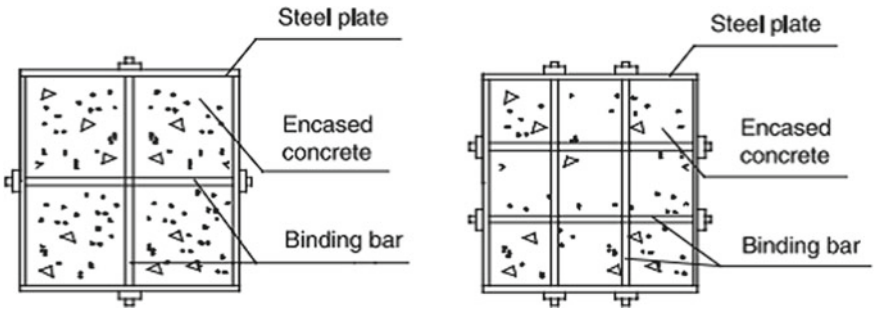

Fig. 5 Square cross-section of CFST columns with binding bars [5]

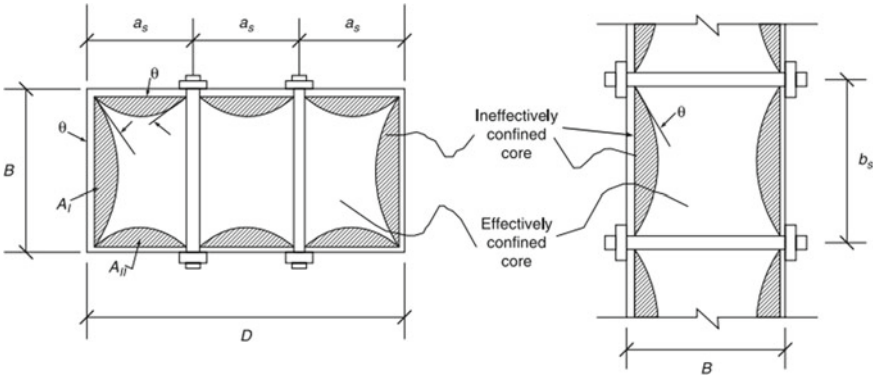

Fig. 6 Effectively confined concrete core for rectangular CFT with binding bars [5]

3 Diagonal Rib Stiffened CFST

Combining the merits of the point, line and lateral closed confinement the idea of introducing a diagonal ribs stiffener was evolved. They have furthermore advantages like

- Continuous strong confinement
- Can relax width to thickness ratio
- Enhanced fire resistance
- Openings in ribs act as shear connectors
- Increased ultimate strength and ductility
- Cost effective
- Take up large vertical loads, therefore its used as mega columns.

3.1 Construction and Details of Specimens

By fillet welding the diagonal rib to the U shaped cold formed steel plates and then butt welding two such U shaped cold formed steel plates we can form the specimen as shown in Figs. 7 and 8.

After completing the steel portion the concrete is filled in the column, through the openings in the ribs concrete will easily fill the triangular portions (Fig. 8).

The width of 300 mm and length of 900 mm was used. The width to thickness ratio was 150, 100, 50 for steel thickness of 2 mm, 3 mm, 6 mm respectively as shown in Fig. 9.

The other conventional specimens which were used for comparing the result were

- CFST without stiffeners in Fig. 10
- CFST with longitudinal stiffeners shown in Fig. 11
- Octagonal CFST shown in Fig. 12.

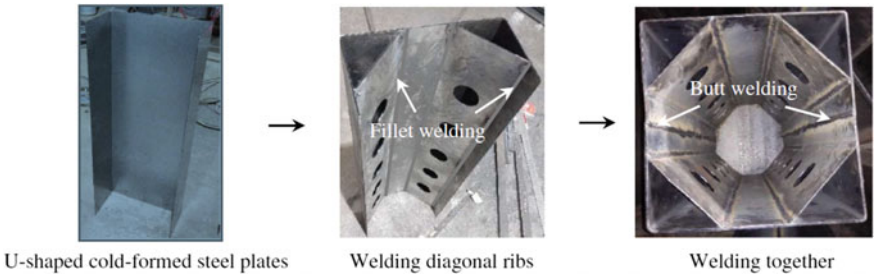

Fig. 7 Fabrication process of diagonal rib–stiffened square steel tube [1]

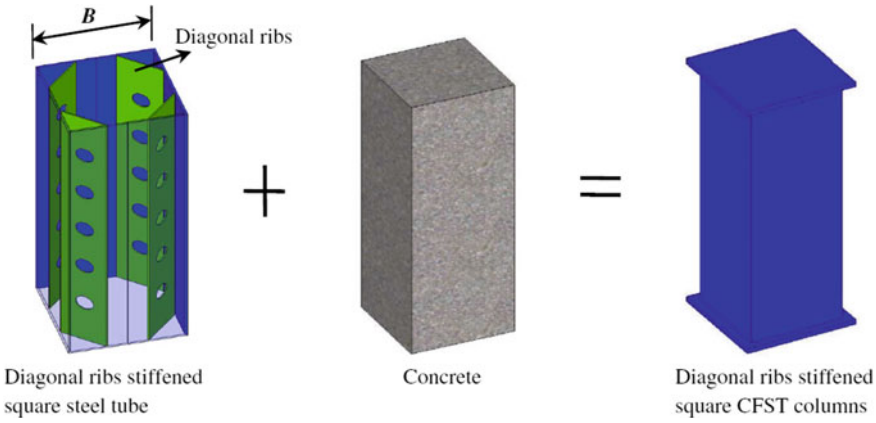

Fig. 8 Diagonal rib–stiffened square CFST column [1]

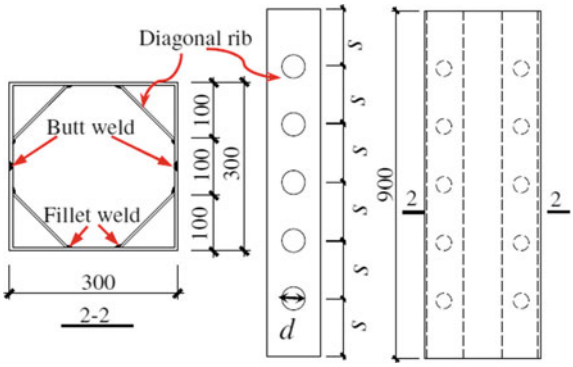

Fig. 9 Dimensions of specimen [1]

3.2 Test Results

3.2.1 Details of the Previously Conducted Experiments

Different specimen groups were constructed of breadth 300 mm and length 900 mm. The specimens were square CFST specimen without stiffeners (Fig. 10), CFST with longitudinal stiffeners (Fig. 11), Octagonal CFST (Fig. 12), CFST with diagonal ribs (Fig. 9) [1].

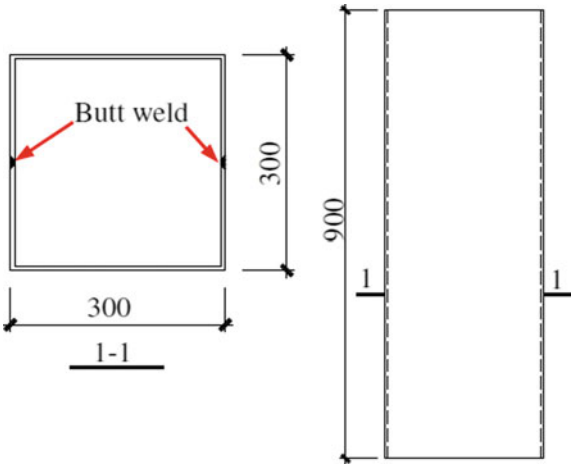

Fig. 10 CFST without stiffeners [1]

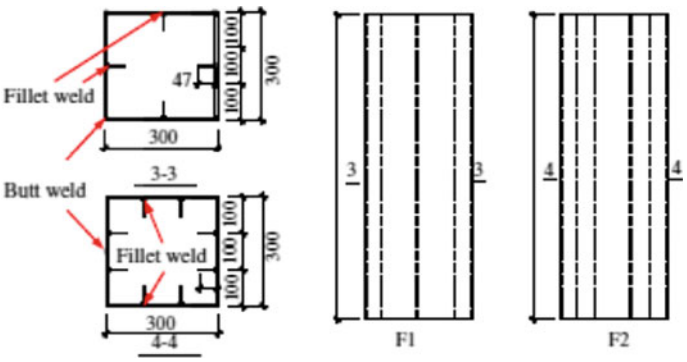

Fig. 11 CFST with longitudinal stiffeners [1]

3.2.2 Analysis of Results

Under compression load with LVDT (Linear Variable Differential Transformer) Load given at a rate of 200 kN/min. Different test results were observed as follows

- Tube buckling
  For the specimens without stiffeners the buckling occurred in prepeak stage and buckling was delayed when width to thickness ratio was decreased meaning when thickness was increased.
  For the stiffened specimens both with the diagonal rib ones and longitudinal ones the buckling at or after reaching the ultimate load, therefore we can understand that the buckling was delayed to a post peak stage.

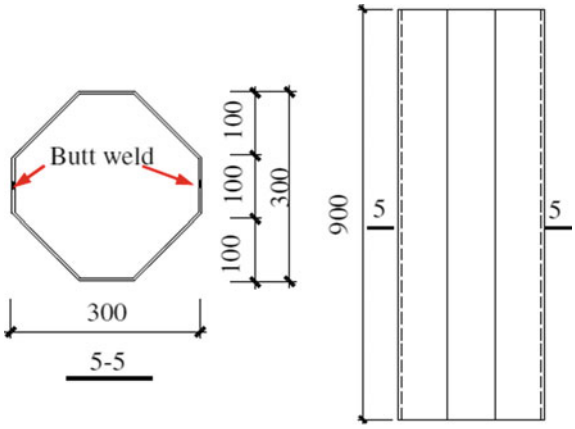

Fig. 12 Octagonal CFST [1]

For the octagonal specimens the buckling was near the ultimate load, which concludes that octagonal CFST is better than square CFST.

- Failure modes

  For unstiffened specimen they were failed under shear failure.
  For stiffened ones the failure mode was when concrete crushed where the tube buckled.
  For octagonal specimens failure mode changed shear failure to squashed failure when the thickness was increased from 2 to 3 mm.

- Indices
  Strength Index, I_s

$$I_s = N_u/N_n$$

N_u Experimental Ultimate Strength
N_n Superposed strength

$$N_n = f_c A_c + f_{yt} A_t + f_{ys} A_s$$

A_c, A_t, A_s are the area corresponding to concrete, steel tube and diagonal rib respectively.
The superposed strength corresponds to the weakest cross-section, i.e. the areas of opening in the rib is subtracted from the A_s.
Ductility Coefficient, μ

$$\mu = \varepsilon_{85\%}/\varepsilon_y$$

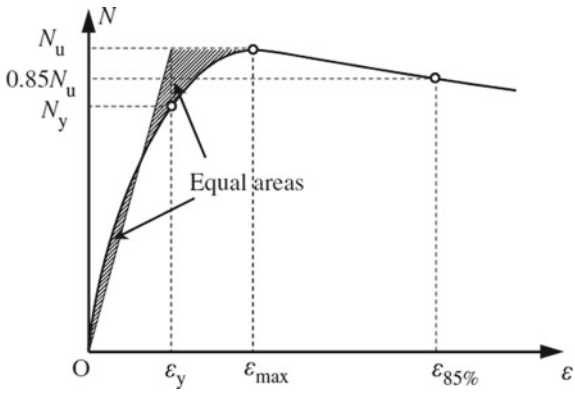

Fig. 13 Load versus strain graph [1]

$\varepsilon_{85\%}$ = Axial strain when the load falls to 85% of the ultimate load and ε_y, yield strain as shown in Fig. 13.

From Load verses Strain graph of various combinations certain results were analysed.

For instance comparing a 3 mm thick steel tube specimens as shown in Fig. 14.

- Comparing the results of unstiffened specimen and stiffened specimen with a 2 mm thick diagonal bar (both specimen of 3 mm thick steel tube) the ductility coefficient increased by 73.4%, ultimate load increased by 9.2%, strength index increased by 8.7%.

  Concluding various results.

  Thickness of diagonal rib improves the ductility in a higher rate but not much influence in the ultimate strength.
- When the details of the openings of rib was taken into account like opening shape, dimension of opening, spacing; load verses strain graph was plotted by varying the above parameters.

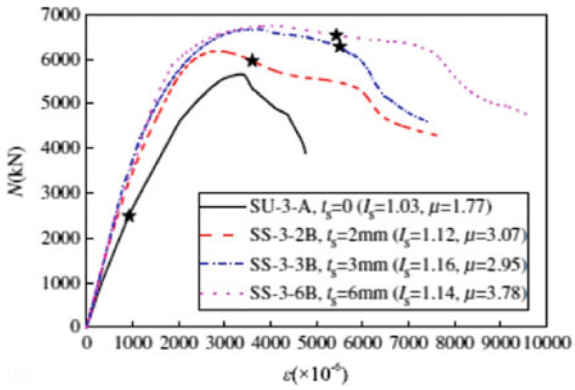

Fig. 14 Load versus strain graph of 3 mm thick steel tube (rib thickness) [1]

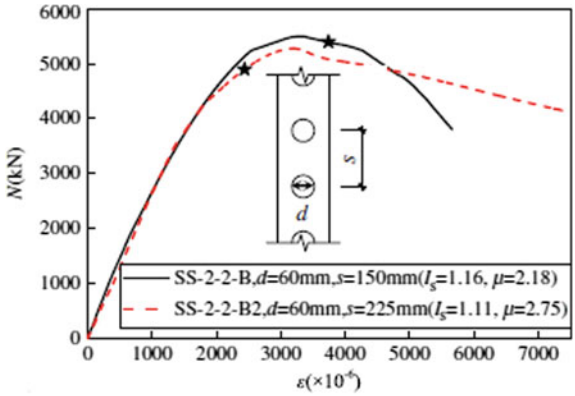

Fig. 15 Load versus strain graph of 2 mm thick steel tube (opening spacing) [1]

For instance comparing the graph Fig. 15, Specimens both stiffened with 2 mm thick rib, 2 mm steel tube and of an opening diameter 60 mm but with varying spacing of 150 and 225 mm.

When the spacing was increased ductility increased by 26% whereas the strength was decreased but in a small rate of 6% in average.

Concluding various results.

The ultimate strengths and ductility capacities differ little when the opening diameter is about 0.4–0.6 times the diagonal rib width or the opening spacing is about 2.5–3.8 times the opening diameter.

- When the opening shape is taken under consideration shown in Fig. 16.
  Comparing results square openings has more strength but less ductility compared to circular openings. The strength was more because net cross sectional area of steel is more for square than for circle. The ductility was reduced due to stress concentration. The ductility had a greater change of 37.5% while strength only

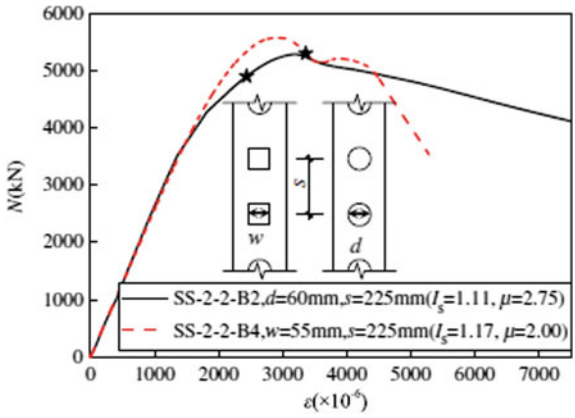

Fig. 16 Load versus strain graph of 2 mm thick steel tube (opening shape) [1]

a slight difference of 6% was found. Hence by giving more credit to ductility circular openings were finalised.

- Comparing the section efficiency
  The octagonal CFST can be seen as diagonal rib stiffened without four triangular corners. Due to presence of four triangular corner, the increase in ultimate strength was about 35%. Therefore it's noted that four corner triangular prisms provide more axial performance.
  Confinement of diagonal ribbed specimens is more than that of octagonal ones. Octagonal specimens has more confinement than square CFST. The buckling mode various specimens is shown in Figs. 17 and 18.
- Strain Development
  Before the ultimate load the strain development of steel tube and diagonal ribs were the same, linear and the experimental results were consistent. While approaching ultimate load the steel tube buckled before the diagonal rib, but both yielded before the ultimate load.
  The $\varepsilon_h/\varepsilon_v$ of the diagonal ribs and steel tube was 0.25 which is equal to poisons ratio. The strain development shows that the diagonal ribs and the steel tube carried load together, and the diagonal ribs played a similar role as the steel tube,

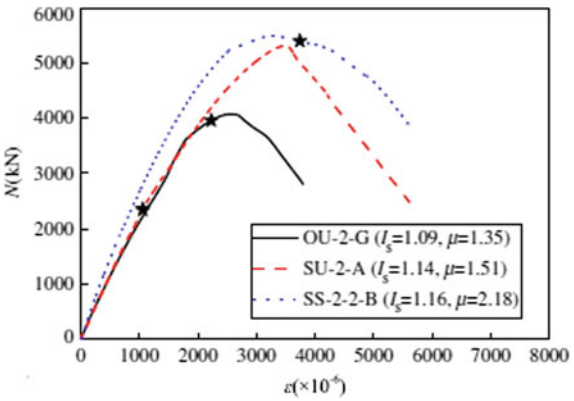

Fig. 17 Load versus strain graph of 2 mm thick steel tube (cross-section) [1]

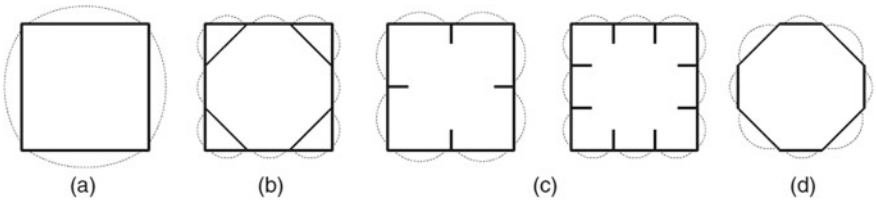

Fig. 18 Buckling mode of various specimens [1]

i.e., the diagonal ribs improved the axial performance by co-carrying the axial compressive force with the steel tube and confining the steel tube and concrete.
When the strain data was analysed, strains before ultimate load was similar which shows that the section was under uniform compression and thereby concrete was under uniform confinement.
From all these results it is concluded that the diagonal rib stiffened CFST has the more structural performance compared to all the other sections [1].

- Welding positions
  The confinement effectiveness coefficient was calculated

$$K_e = \left(B^2 - 0.75b^2 - 0.66(B - 2b)^2\right)/\left(B^2\right)$$

To get its maximum it is differentiated with respect to rib width, b.
We get

$$b = B/3$$

B = steel tube width [6].

3.3 Analytical Studies

3.3.1 Results from ANSYS Software

A finite element model was developed using ANSYS software. One end fixed and at the other end displacement in z direction was allowed. Load is given at the latter end. As shown in Fig. 19.

After modelling the model was validated with the experimental results until similar values were obtained. The failure model as well as axial load strain curves were same as the experimental results.

- Opening diameter
  By varying the diameter from 0 to 50% of steel tube width (B). The ultimate strength was reduced by 5%. Therefore increase in the diameter leads to strength decrease. But provision of openings helps in concreting, increased anchorage and avoid disengagement with concrete and steel.
  Providing an average diameter opening will give an optimum strength. Therefore circular diameter in a range of 20–25% of steel tube width is suitable. Smaller diameter for wider ribs and larger for narrower can be provided in order to facilitate the concreting.
- Opening spacing
  By varying the spacing from 1 to 7 times the opening diameter, there was a total increase of strength by 2%. If the spacing is reduced, it will result in highly stressed region making it weak in strength. By observation, providing a spacing of 1–2 times the opening diameter had an abrupt increase in the ultimate strength.

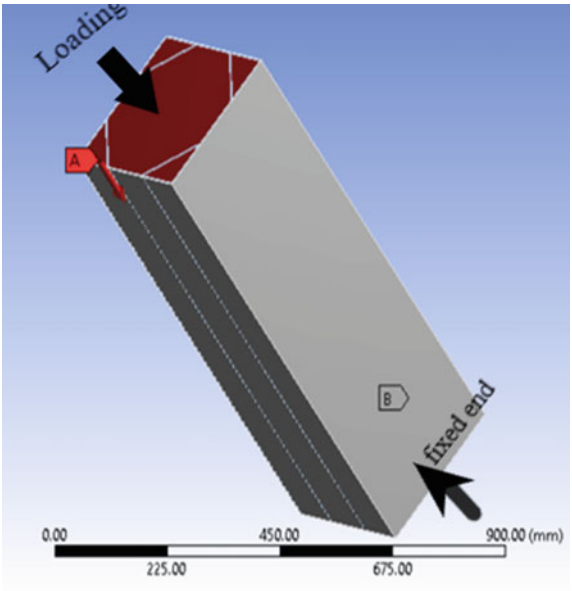

Fig. 19 Finite element model

Hence opening spacing should be at least 2 times opening diameter.

- Concrete and Steel strength
  By using high strength concrete from 50 to 70 MPa the ultimate strength was increased by 35%.
  By using high strength steel for steel tube the increase in ultimate strength was 12% but for diagonal rib it was about 2%. Therefore provide high strength steel for the tube for more axial capacity.
- Slenderness
  Increasing the slenderness ratio by means of increased length, the ultimate strength firstly decreased and reached a constant state.
  Increasing the slenderness ratio by means of decreased lateral dimension, the ultimate strength decreased abruptly. When lateral dimension was changed from 500 to 300 mm the ultimate strength dropped by 60%.

3.3.2 Results from MATLAB

A program function was developed using MATLAB. It was validated with the experimental results. By varying the parameters the ultimate strength and Euler's critical buckling load of diagonal rib stiffened CFST can be obtained. The function developed predicted the ultimate strength with minimum standard deviation from experimental results.

The parameters that can be varied for predicting the ultimate strength are

- Breadth of the square steel tube

- Thickness of steel tube
- Length of steel tube
- Thickness of diagonal rib
- Diameter of the openings in diagonal rib
- Spacing of the openings in diagonal rib
- Yield stress of steel tube and diagonal rib
- Compressive strength of concrete used.

The program for ultimate strength and critical buckling load was developed based on the following concept. The strength capacity of a section can be analysed from the basic equation of stress multiplied by the force acting normal cross-sectional area. Thereby applying the same method over here, the ultimate strength will be the sum of strength from steel tube, concrete core and diagonal rib.

$$Np = A_c\sigma_{cc} + A_t\sigma_{tv} + A_s\sigma_{sv}$$

Np is the predicted ultimate strength; A_c, A_t, A_s are the effective cross-sectional areas of concrete, steel tube, and diagonal ribs, respectively. $\sigma_{cc,}$ σ_{tv}, σ_{sv} are the compressive strength of confined concrete, vertical stresses of steel tube and diagonal ribs, respectively. According to Mander et al. [7]

$$\sigma_{cc} = f_c\left(-1.254 + 2.254\sqrt{\left(1 + 7.94f_r'/f_c\right)} - 2f_r'/f_c\right)$$

$$f_r' = k_e f_r$$

f_r', f_r is the effective confining stress and confining stress respectively. k_e is the confinement effectiveness coefficient.

$$k_e = A_{ce}/A_c$$

A_{ce} cross-sectional area of effectively confined concrete.

Critical buckling load,

$$P_{cr} = 9.86 * (EI)_{eff}/L_{eff}^2$$

$(EI)_{eff}$ Effective flexural stiffness.

4 Conclusions

The diagonal rib stiffened CFST is more improved version in the evolution of CFST, it's used as mega columns, high rise buildings and multi-storey buildings. The observations and results of this specimen is as follows

- It combines the advantages of point, line and lateral closed confinement.

As well as it has got continuous strong confinement and can relax width to thickness ratio.

- Enhanced fire resistance, Cost effective and increased ultimate strength and ductility.
- The tube buckling was delayed even after the ultimate load, which makes it more structurally good in the case of columns.
- The failure mode of this specimen was when concrete crushed where the tube buckled.
- Thickness of diagonal rib improves the ductility in a higher rate but not much influence in the ultimate strength.
- Ultimate strengths and ductility capacities differ little when the opening diameter is about 0.4–0.6 times the diagonal rib width or the opening spacing is about 2.5–3.8 times the opening diameter. The shape optimised was circular shape than square.
- Comparing the sectional efficiency the diagonal rib stiffened specimen performed greater than the octagonal specimen due to the presence of four extra corner triangular prisms. And the octagonal CFST is better than square CFST.
- By strain analysis it was found that the strain development of steel tube and diagonal ribs were the same, which implies both co carries the axial load. And the compression was uniform thereby the confinement was uniform.
- Theoretical ultimate strength could evaluate the strength in an approximate way. From analytical studies, opening diameter in a range of range of 20–25% of steel tube width is suitable. Opening spacing should be at least 2 times opening diameter.
- The best welding position is when the rib thickness equals 1/3 of tube width and use of high strength steel and concrete enhances the properties.
- High strength concrete can increase the axial capacity by 35%. If high strength steel is used as steel tube it provides better result.
- Increased slenderness ratio can decrease the ultimate strength by 60%.
- MATLAB function program is developed which can well predict the ultimate strength of diagonal rib stiffened CFST and critical buckling load.

References

1. Zhou Z, Gan D, Zhou X (2019) Improved composite effect of square concrete-filled steel tubes with diagonal binding ribs. J Struct Eng 145(10):04019112
2. Kitada T (1998) Ultimate strength and ductility of state-of-the-art concrete-filled steel bridge piers in Japan. Eng Struct 20(4–6):347–354
3. Yang Y, Wang Y, Fu F (2014) Effect of reinforcement stiffeners on square concrete-filled steel tubular columns subjected to axial compressive load. Thin-Walled Struct 82:132–144
4. Zhang JG, Liu YJ, Yang J, Xu KL (2011) Experimental research and finite element analysis of concrete-filled steel box columns with longitudinal stiffeners. Adv Mater Res 287:1037–1042

5. Tao Z, Han LH, Wang ZB (2005) Experimental behaviour of stiffened concrete-filled thin-walled hollow steel structural (HSS) stub columns. J Constr Steel Res 61(7):962–983
6. Zhou X, Zhou Z, Gan D (2019) Analysis and design of axially loaded square CFST columns with diagonal ribs. J Constr Steel Res, p 105848
7. Mander JB, Priestley MJN, Park R (1988) Theoretical stress strain model for confined concrete. J Struct Eng 114(8)

Seismic Pounding Between Adjacent RC Buildings with Asymmetric Alignment

P. Ambili, V. N. Krishnachandran, and Katta Venkataramana

Abstract During earthquakes, adjacent structures may collide with each other due to different dynamic characteristics. When buildings vibrate out-of-phase and the separation gap provided between buildings is not sufficient to accommodate their relative motions, collisions can cause severe damage or even complete collapse of structures, and is known as seismic pounding. In metropolitan cities, due to increased population and land values, buildings have been constructed with inadequate separation distance between them. The seismic oscillations induced in a structure in a block of buildings will be partly restrained in lateral displacements and hence torsional movements are introduced (asymmetric pounding). Two different types of impacts may occur during pounding including floor-to-floor and floor-to-column (inter-storey) collisions. In this paper, the effects of asymmetric (contact asymmetry) pounding on the seismic response of adjacent buildings with symmetric plan and unequal building heights are studied. Time history analysis of adjacent buildings with different pounding cases involving 1, 2 and 3 column pounding is carried out using the software ETABS and the corresponding torsional response is evaluated. The influence of separation gap and floor heights between the adjacent structures on the torsion effect is investigated and the results are compared with no pounding case.

Keywords Separation gap · Inter-storey pounding · Contact asymmetry · Time history analysis · Torsion

P. Ambili (✉) · V. N. Krishnachandran
Department of Civil Engineering, NSS College of Engineering, Palakkad, Kerala, India
e-mail: ambiligopinath308@gmail.com

V. N. Krishnachandran
e-mail: vnkrishnachandran@gmail.com

K. Venkataramana
Department of Civil Engineering, NITK, Surathkal, Mangalore, India
e-mail: katta@nitk.edu.in

© Springer Nature Switzerland AG 2021

K. Dasgupta et al. (eds.), *Proceedings of SECON 2020*,
Lecture Notes in Civil Engineering 97,
https://doi.org/10.1007/978-3-030-55115-5_67

1 Introduction

Damage assessment of buildings from past earthquakes has revealed that excessive torsional response is one of the most important factors, which produces severe damage or even complete collapse of structures. Such torsional effects occurs due to different reasons such as the non-uniform distribution of mass, stiffness and strength, the presence of rotational components in ground motions, etc. Generally torsion is caused by the distance (eccentricity) between Centre of mass and Centre of rigidity of the structure. In addition, the pounding of adjacent structures may also produce torsion in buildings due to the restriction in lateral displacements between them.

The rise of population and limited availability of land in urban areas have led to the construction of elevated structures with less or no separation distance between them. In such areas, pounding can happen between the closely spaced buildings during large earthquakes [1]. Seismic pounding refers to the hammering or collision of adjacent structures or buildings resulting in the generation of high impact force and short duration acceleration pulses, developing both local and global damages. These collisions are enhanced when the adjacent structures vibrate out of phase due to difference in their natural periods, as most of the buildings are of different dynamic properties [2].

The two types of interactions that may occur during pounding include floor-to-floor collisions and floor-to-column collisions as shown in Fig. 1. The first type occurs when the adjacent structures have same floor heights, while the second type takes place when they have different floor heights [3]. Apart from these, pounding of heavier building with adjacent lighter building, pounding of taller building with adjacent shorter building, torsional pounding and end building pounding are also observed during seismic ground motions.

Majority of the studies so far have focused on the symmetric (i.e., translational) pounding while the asymmetric (i.e., torsional) pounding is ignored. The asymmetric pounding occurs as any of the following two cases:

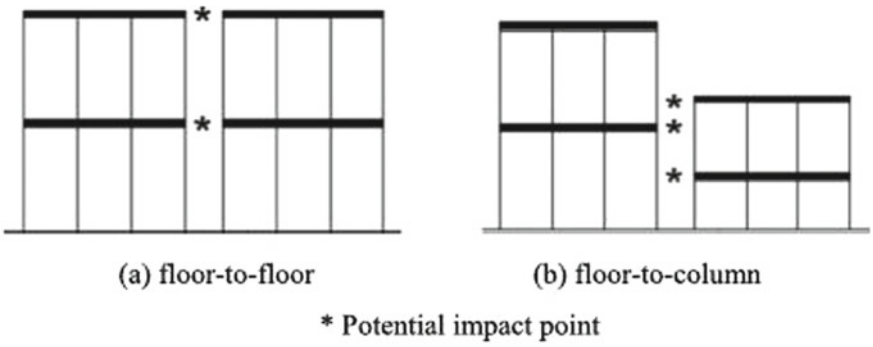

Fig. 1 Types of pounding [3]

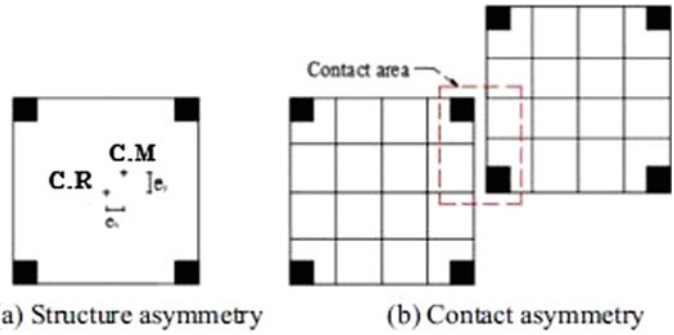

Fig. 2 Two cases of asymmetric pounding [4]

1. Structure asymmetry: In this case, one of the two colliding structures is asymmetric, that is there will be eccentricity (e_x or e_y) between the Centre of Mass (C.M) and the Centre of Rigidity (C.G). This type of asymmetric pounding is also termed as eccentric pounding (Fig. 2a).
2. Contact asymmetry: In this case, the contact area is asymmetric, that is the colliding buildings may not be on the same row (Fig. 2b).

The asymmetric pounding may induce torque in colliding buildings. The torsional effects due to this type of pounding has not been studied effectively yet. In metropolitan cities, the seismic oscillations induced in a structure in a block of buildings will be partly restrained in lateral displacements and hence torsional movements are introduced [4].

This paper aims to study the torsional effects induced due to asymmetric (contact asymmetry) floor-to-floor pounding between adjacent reinforced concrete buildings of different heights by considering different separation distances between them.

2 Pounding Cases

In order to evaluate the torsional effects due to pounding between adjacent buildings that are partly in contact to each other in an asymmetric way, the following pounding cases are considered (Fig. 3):

Case 1: 3-column pounding
Case 2: 2-column pounding
Case 3: 1-column pounding.

It is assumed that the seismic induced oscillations of the tall building is laterally partly restrained by the other structure and therefore torsional behavior is introduced during earthquake excitation. Therefore in the examined cases, pounding between adjacent structures introduces significant plan symmetry in the building in terms of

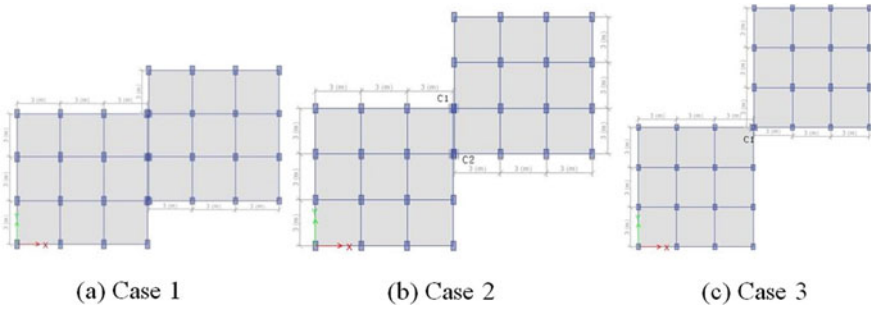

Fig. 3 Various pounding cases

lateral stiffness distribution. All the above said cases include asymmetric pounding between a 6 storey and an adjacent building having n_s storey levels, where $n_s = 1, 2, 3, 4, 5$ and 6. Each one of the pounding cases is examined, considering the structures having an initial separation gap of 80 mm between them; further each pounding case is examined considering that there is no gap ($d_g = 0$) and the results are compared with no pounding case.

3 Gap Element

To model the collision between buildings, gap element is used. It is an element that connects two adjacent nodes to model the contact. In ETABS 2016, gap has been defined as a link element. It is a compression-only element required to assess the pounding force and simulate the effect of pounding. This becomes activated when the corresponding nodes come into contact and gets deactivated when they go far away [5]. The stiffness of gap element is taken as 477600 kN/m [6].

The response of the contact element is shown in Fig. 4. The negative direction of the X-axis represents the condition that the buildings move away from each other. In the positive direction of X-axis, there are two parts in order to simulate the actual behavior of structures in case there is an initial small gap distance (d_g) between them. The first part represents that the structures move one towards the other but the displacements are small and the existing gap is not covered. In this case, the contact element remains non-active and the buildings continue to vibrate independently. The second inclined part represents that the structures move towards each other and the sum of displacements of adjacent buildings bridge the existing gap or the structures are in contact from beginning ($d_g = 0$). In this case, the contact element responds as a spring with large stiffness [7].

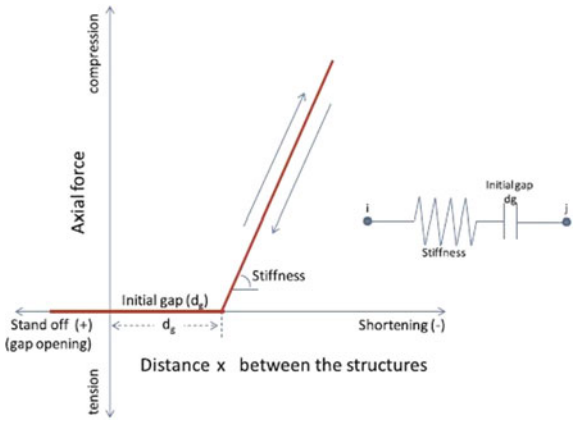

Fig. 4 Response of the contact elements [8]

4 Structural Modeling

In this paper, two adjacent buildings having different floor heights with gap elements are considered to represent pounding. These consists of two typical moment resisting RC framed buildings A and B of three bays in each direction, located in high seismicity region of India. Building A is a 6-storey structure and the number of floors (n_s) of building B is varied from 1 to 6. These buildings are designed according to IS 456:2000 considering both gravity and seismic loads.

Plan dimension of both buildings A and B are 9 m × 9 m and floor height is 3.0 m. An accidental eccentricity equals to ±5% of the relevant plan dimension of the building as per IS 1893:2016 (Part1) [9] is considered. Material properties are assumed to be M25 grade for beams and M30 grade for columns and Fe415 grade steel for reinforcement. The slab thickness is taken as 120 mm and all beams are 300 mm × 400 mm. The column size is taken as 300 mm × 600 mm for Ground and first floors and 300 mm × 400 mm for remaining floors. The live load considered is 3 kN/m^2 on the floors and 1.5 kN/m^2 on the roof. Floor finish on the floors is taken as 1 kN/m^2.

5 Non-linear Analysis of Pounding

The structural modeling and analysis of different pounding cases are carried out using ETABS software. The beam and column elements of the buildings are modeled as non-linear frame elements connected at nodes with lumped mass at the center of each floor. Each structure responds dynamically and vibrates independently. Collision occurs when the lateral displacements of the structure at floor levels exceed the pre-defined gap distance (d_g) between the two structures.

In this study, time history analysis is carried out to evaluate the dynamic response of the structure. Both the buildings are subjected to El-Centro ground motion (Imperial Valley, 1940) in the longitudinal direction.

6 Results and Discussions

6.1 Torsional Behavior

The time history of torsional moment at the base floor of the 6-storey building, due asymmetric pounding that occur between it and an adjacent 3 storey building, for the 3 pounding cases are presented in Fig. 5. It is observed that case 3 (1-column pounding) induced more peak torsional moments at the base floor than the other cases due to high asymmetry.

The influence of number of stories (total height) of the adjacent structure on the torsional response developed at the base of building A due to asymmetric pounding cases 2 and 3 is shown in Figs. 6 and 7. The results of pounding between the 6 storey building A (6RC) and a single storey (1RC), a three storey (3RC), a five storey (5RC) and a 6 storey (6RC) buildings are shown.

From the analysis, it is clear that the torsion developed in 6 storey building depends on the height of the adjacent building. In general, it is observed that the developing torsion increases as the height (number of storeys) of the adjacent building increases.

Figure 8 presents the torsional response due to asymmetric pounding cases 2 and 3 for separation distance 80 mm and no gap between the 6 storey and 2 storey buildings. It is found that as the separation distance is increased, the developing torsional moments in the building are reduced. From the figures, it can be found that asymmetric type of pounding results in significant torsional response and high value

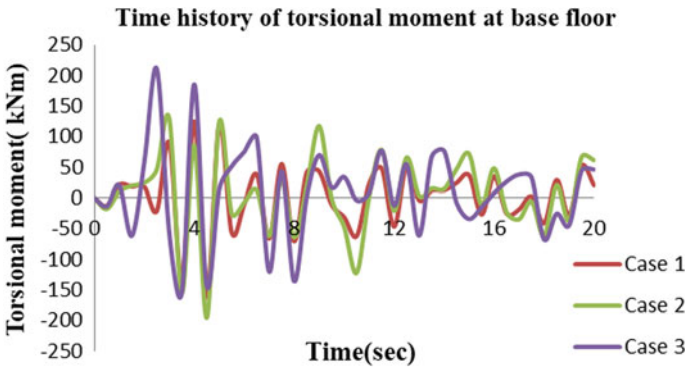

Fig. 5 Time history of torsional moment at base floor due to asymmetric pounding between 6 storey and 3 storey buildings for various pounding cases

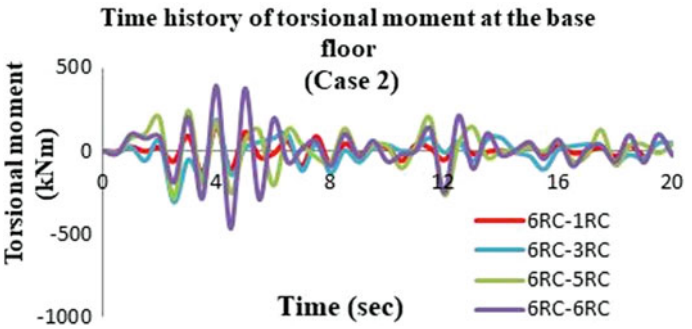

Fig. 6 Torsional moment at the base of building A (6RC) due to case 2 (2-column) pounding

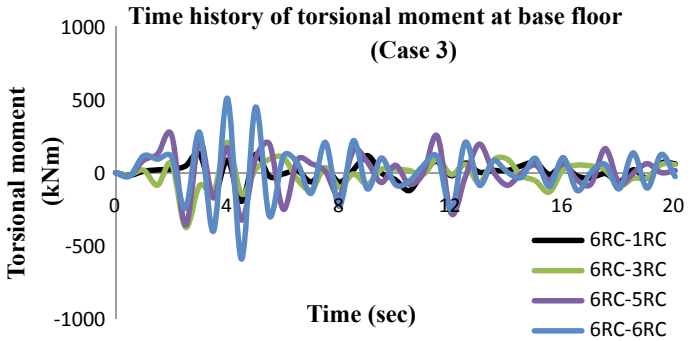

Fig. 7 Torsional moment at the base floor of building A (6RC) due to case 3 (1-column) pounding

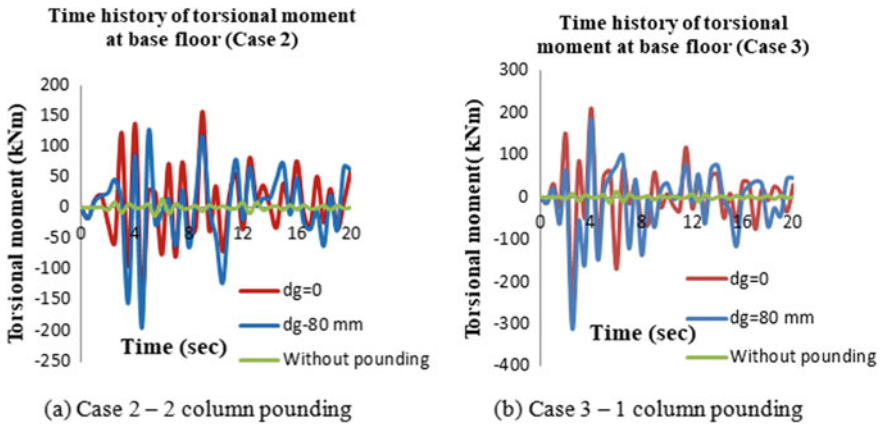

Fig. 8 Time history of torsional moment due to asymmetric floor-to-floor pounding between 6-storey and 2-storey buildings for various cases

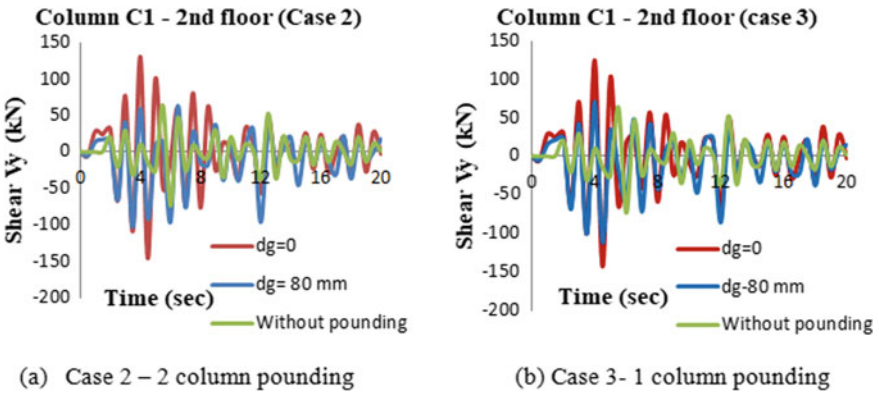

Fig. 9 Shear time history for column C1 of second floor due to torsional movement induced by asymmetric pounding cases between 6-storey and 2-storey buildings

torsional moments in the building although the plan view is symmetric. In the case of building without pounding, it is found that no torsional moments are developed and consequently no torsional movement (Fig. 8).

6.2 Column Shear Forces

As expected, the developed torsional moments in the considered building significantly influences the distribution of shear forces in the columns. It is seen that the shear forces developed in column C1 of building A decrease in the direction of earthquake excitation (x-direction) due to movement restraint provided by adjacent 2-storey building, whereas significant shear forces are developed in the normal direction (Y-direction). Figure 9 presents the time history of developed shear forces in the peripheral column C1 of the second floor of building A, for asymmetric pounding cases 2 and 3 between 6-storey and 2-storey buildings. Results indicate that peak shear forces are induced in case 3 pounding as compared to case 2 pounding.

7 Conclusions

- Seismic induced oscillations between adjacent buildings that are asymmetric in contact introduces significant torsional movements.
- The developed torsional moment at the base increases as the number of storeys (or total height) of the adjacent building increases.
- The cases with buildings that were in contact developed more torsional response than buildings with a separation distance of 80 mm. In the case of buildings without

pounding, it is found that no torsional moments are developed and consequently no torsional movement.

- The torsional moments developed due to asymmetric pounding significantly affects the shear force developed in the peripheral column of the floor undergoing pounding.
- High shear forces are developed in the columns, in the direction normal to the direction of earthquake excitation, although the plan view is symmetric in both directions.
- Results indicate that the peak torsional moments and shear forces are developed in case of 1-column pounding than 2-column pounding, due to high asymmetry.

References

1. Anagnostopoulos SA (1988) Pounding of buildings in series during earthquakes. Earthq Eng Struct Dyn, 16:443–456
2. Anagnostopoulos SA, Spiliopoulost V (1992) An investigation of earthquake induced pounding between adjacent structures. Earthq Eng Struct Dyn 21:289–302
3. Papadrakakis M, Apostolopoulou C, Zacharopoulos A, Bitzarakis S (1996) Three-dimensional simulation of structural pounding during earthquakes. J Eng Mech 122:423–431
4. Miari M, Choong KK, Jankowski R (2018) Seismic pounding between adjacent buildings: identification of parameters, soil interaction issues and mitigation measures. Soil Dyn Earthq Eng 121:135–150
5. Favvata MJ, Mochla SE, Naoum MC, Karayannis CG (2015) Assessment of multistorey RC buildings suffering inter-storey pounding. In: 5th ECCOMAS thematic conference on computational methods in structural dynamics and earthquake engineering, May, 2015
6. Rajaram C, Ramancharla PK (2014) Three dimensional analysis of pounding between adjacent buildings. J Struct Eng 41(2):1–11
7. Karayannis CG, Naoum MC (2018) Torsional behavior of multistorey RC frame structures due to asymmetric interaction. Earthq Eng Struct 163:93–111
8. Favatta MJ (2017) Minimum required separation gap for adjacent RC frames with potential inter-story seismic pounding. Eng Struct 152:643–659
9. IS 1893 (Part 1) (2016) Criteria for earthquake resistant design of structures

Performance Characteristics of Self-cured Recycled Aggregate Concrete with SCM's

Lakshmi Thotakura, Sankar Kumar Reddy Pullalacheruvu, Ganesh Babu Kodeboyina, and V. Krishna Rao Mupparisetty

Abstract Self-cured recycled aggregate concrete with shrinkage reducing admixtures is one of the pioneering researches in the construction industry. There is a possibility of depletion of natural resources due to prolonged consumption over a period of time in our modern civilization. In this research, characteristics of recycled aggregate concrete with supplementary cementitious materials (SCM) like powdered limestone and fly ash with self-curing agent PEG6000 were investigated along with the conventional concrete. Hydration plays a predominant role in the properties of hardened concrete. Particularly in high strength concretes, micro cracking occurs due to the absence of pore water and lack of relative humidity thus causes self-desiccation. The experimental studies exhibit the performance of concrete mixes with 35% limestone powder in LP60 and 35% fly ash in SC60 and RA60. The mechanical and durability properties of M60 concretes with SCM's and PEG6000 were investigated. The results indicated that concretes with 1% self-curing compound shows improved results than the mixes with 0%. All the concretes mixes achieve the properties at the range of self-compacting concrete in the green state.

Keywords Concrete · Curing-internal curing · Self-curing · Supplementary cementitious materials-limestone powder · Fly ash · Recycled aggregate · PEG6000

L. Thotakura (✉) · S. K. R. Pullalacheruvu
Mahatma Gandhi Institute of Technology, Gandipet, Hyderabad, India
e-mail: amaraswini12@gmail.com

G. B. Kodeboyina
Mahindra Ecole Centrale, Jeedimetla, Hyderabad, India

V. K. R. Mupparisetty
Chaitanya Bharathi Institute of Technology, Gandipet, Hyderabad, India

© Springer Nature Switzerland AG 2021

K. Dasgupta et al. (eds.), *Proceedings of SECON 2020*,
Lecture Notes in Civil Engineering 97,
https://doi.org/10.1007/978-3-030-55115-5_68

1 Introduction

Concrete is the most consumed material in the construction industry because of its versatility. Curing of concrete plays an essential role in the process of cement hydration in the early stages to maintain optimal conditions in the concrete after casting. The better hydration of cement results the requisite fresh and hardened properties of concrete as well as increases the performance of the structure [1]. Concrete mixes with low water-cement ratios (w/c) having inadequate amount of water to promote the hydration thus results the cracks and shrinkage in concrete. To conquer these complications by incorporating supplementary cementitious materials (SCM) for effective hydration of cement. Due to low w/c approximately 0.4, the water might not be obtainable for the SCMs to react with calcium hydroxide.

The self-curing or internal curing technique (IC) was proposed to enhance the properties of external curing to overcome the issues regarding hydration and shrinkage properties. Internal curing (IC) is described from the American Concrete Institute (ACI), as: "supplying water throughout a freshly placed cementitious mixture using reservoirs, via pre-wetted lightweight aggregates, that readily release water as needed for hydration or to replace moisture lost through evaporation or self–desiccation" (ACI 2010). This practice includes the supply of water internally with in the concrete during casting which promotes better hydration as well as maintaining of relative humidity [2].

Internal curing creates a revolution in the construction industry and enhance the properties of pore and micro structure. However, the consequences of internal curing were examined on the mixes contains SCMs like natural pozzolans (NP) of fly ash, GGBS, ferrosilicon etc. The substitution of ordinary Portland cement (OPC) with natural pozzolan might enlarge the autogenous and drying shrinkage of concrete. Self-curing (IC) might be of great advantage by the addition of NP because it can promote the pozzolanic reactions and reduce shrinkage properties of concrete [3]. The main function poly ethylene glycol (PEG) is to reduce the surface tension of water and reduce water evaporation from concrete and also it is easily soluble in water with because of its high molecular weight than water [4]. PEG is a hydroxyl compound and helps to retain water in the concrete.

On the other hand, utilization of recycled aggregate as a replacement of coarse aggregate in concrete for the sustainable development of the society and minimize the depletion of natural resources in the construction industry and manage the demolition waste. Recycled aggregate (RA) is a new alternative to natural aggregate which preserves the environment [5]. The efficacy of self-curing of high-strength self-consolidating concrete (SCC) using saturated recycled-concrete aggregates shows superior results on shear strength of concrete [6]. 100% utilization of Recycle aggregates meet the higher strength and durability properties when compared with the control concrete. Addition of crushed returned concrete aggregate (CCA) with light weight fine aggregate (LWFA) significantly reduces the autogenous shrinkage [7]. Incorporation of Lime powder in concrete as a replacement of cement enhance the properties of microstructure properties [8]. The carbonation behavior of hydraulic

and nonhydraulic calcium silicate phases was subjected to carbonation reaction at different concentration of CO_2 and temperatures. The hydraulic and non-hydraulic calcium silicates demonstrated increased reaction rate in case of carbonation reaction rather than the hydration [9].

2 Experimental Approach

2.1 Materials

The main aim of this research were investigated to quantify the behavior of materials for better sustainability. The following materials were used in this investigation to examine the performance characteristics of self-curing concrete. Ordinary Portland cement of 53 grade conforming to S12269:1987, with a fineness of cement less than 90 μ and specific gravity of cement is 3.15. Initial and final Setting time of cement were found to be 40 and 550 min respectively. The limestone powder (LP) were used as replacement of cement having particle sizes are very much finer than the cement ranging in diameter less than 1 microns to not more than 90 μm. Class F fly ash were used in this investigation with a specific gravity of 2.2.

Locally available fine aggregate were used in this research with a Specific gravity of 2.62 and Fineness Modulus of 3.02 respectively. The Sand were conforming to zone II as per IS 383:1970. Saturated surface dry recycled concrete aggregate were used as a replacement of coarse aggregate and they were brought from the crushed concrete blocks used in the laboratory and crushed in a mini crusher with a maximum size of 20 mm shown in Fig. 1. The shrinkage reducing admixture, Polyethylene

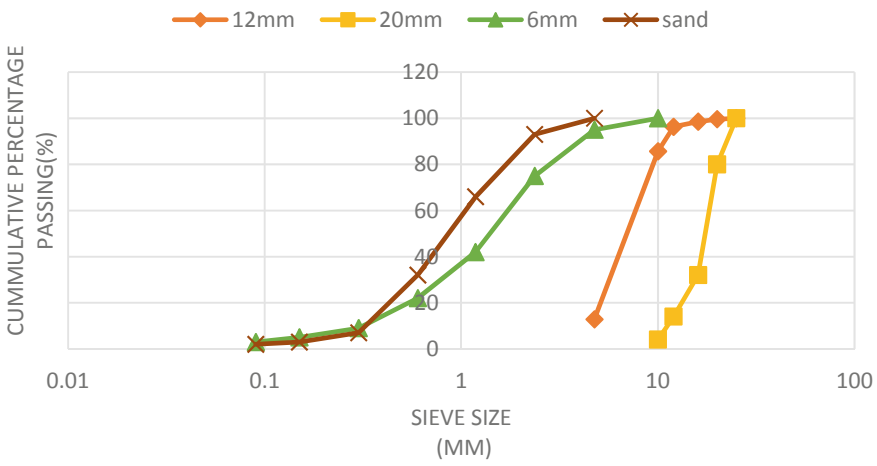

Fig. 1 Gradation curves of recycled aggregates and fine aggregates

glycol (PEG) was used as a self-curing agent having hydrophilic polymer in nature and available in the form of white flakes. The specific gravity of PEG 6000 is 1.08 and PH values lies between 5 and 7. Polycarboxylate based super plasticizer with little amount of VMA were used in this investigation to accelerates and increase the strength at initial stages and eventually reduces the demand of water. The water used for mixing and curing of concrete is fresh portable water available in the laboratory.

2.2 Mix Details

To investigate the effect of Polyethylene glycol 6000 with limestone powder and fly ash on the properties of self-cured recycle aggregate concrete, M60 grade of concrete mixes were designed as per ACI and IS standard specifications and modified according to EFNARC specifications and GNS Rao [10] et al. based on efficiency of fly ash in SCC. In this research, four types of mixes were designed with different material proportions. The first mix is of replacing cement with 35% limestone powder (LP), the second mix contains replacement of cement with 35% fly ash and the third mix contains replacement of cement with 35% fly ash by the addition of 1% PEG6000 as self-curing (SC) agent in concrete with 100% recycled aggregate (RA). NA60 is control mix of concrete. From Table 1, There are 4 mixes of LP60, RA60, SC60 and NA60 concretes and 3 types of curing regimes: Fully Cured (FC), Partially Cured (PC), Internal-cured or self-cured (IC), were carried out. To examine the performance parameters of concrete with 26 cube specimens of size 15 cm × 15 cm × 15 cm and 27 cylinders of size 15 cm dia. and 30 cm height were prepared.

As said earlier, there are 3 types of curing regimes in which the specimens were placed in water just after demolding the specimens and continued for 28 days for fully cured. Whereas in Partially cured, the specimens were placed in water for 3 h on 3rd day after casting and no further curing were done. For internal-cured, the specimens were uncured and left over in a room at nominal room temperature.

Table 1 Mix design of M60 concrete for supplementary cementitious materials along with control concrete in different proportions

Mix	Cementitious materials (kg)			Recycled aggregates (kg)			Water (kg)	PEG (%)	SP (%)
	Cement	LP	FA	20 mm	12 mm	Sand			
LP60	325	175	0	497	497	663	160	0	1.5
RA60	325	0	175	497	497	663	160	0	1.5
SC60	325	0	175	497	497	663	160	1	1.5
NA60	325	0	0	497	497	663	160	0	1.5

Table 2 Workability of M60 concrete mixes with slump flow and J-ring

Mix	Slump flow (mm)	J-ring (mm)
LP60	240	650
RA60	200	580
SC60	230	680
NA60	210	600

2.3 Testing Methodology

The following testing methods were conducted in this research to determine the properties of concrete. Fresh properties of workability were examined by slump flow and J-ring parameters as per EFNARC, ACI and IS code guidelines. The hardened properties such as compressive strength was carried out at 3, 7 and 28 days according to IS 516 (BIS, 1956). Similarly, the Rebound hammer test was conducted as per the IS: 13311(2)-1992. The split tensile strength was carried out for 7 and 28 days as per IS 5816 (1999). The sorpitivity test were conducted according to ASTM C1585-13.

3 Results and Analysis

3.1 Green State Characteristics of M60 Concrete Mixes

From the above observations the workability properties of J-ring, for LP60 mix, the slump flow was found to be around 240 mm and the J-ring flow is in the range of 650 mm which also resembles the highly fluidic nature of concrete compared with RA60 and NA60 provided in Table 2. For SC60 mix contains PEG6000, the slump flow was found to be around 230 mm and J-ring flow is 680 mm with high fluidic nature. These concretes attain the workability in the range of self-compacting concrete with EFNARC specifications.

3.2 Hardened State Characteristics of M60 Concrete Mixes

3.2.1 Variation of Weights Loss in M60 Concrete Mixes with Age

From Table 3 it is clearly shown that the results of variation of weights with time. In the above mixes the % weight loss for LP60 Fully cured specimens were increased from 0.81% to 4.49 for 1 day and 7 days and suddenly reduced 3.05% at 7 days and 2.55% at 28 days. Similarly, for RA60, SC60 mixes also shows similar variation of weight loss results whereas in NA60 Specimens weights increased at 28 days.

Table 3 % Variation of weight loss with age in M60 concrete mixes

% Variation of weight loss with age				
Mix	Day 1	Day 3	Day 7	Day 28
LP60FC	0.81	4.49	3.05	2.55
LP60PC	0.93	3.56	4.63	5.05
LP60IC	1.32	3.77	4.51	4.85
RA60FC	3.72	4.42	2.29	1.91
RA60PC	2.11	2.96	3.07	3.33
RA60IC	1.99	2.91	3.43	3.64
SC60FC	2.47	3.69	1.78	1.30
SC60PC	2.04	2.96	3.46	4.25
SC60IC	1.87	3.81	4.11	4.80
NA60FC	1.75	2.79	0.19	−0.75
NA60PC	1.77	2.77	2.77	2.95
NA60IC	1.53	2.58	3.16	3.20

For Partially cured (PC) specimens, the variation of weights for all mixes were shows similar effect and the loss will be goes on increasing along with the age. For Internal cured (IC) specimens also shows the similar effect along with the age.

3.2.2 Compressive Strength and Rebound Number of M60 Concrete Mixes

The compressive strength and rebound number of 4 mixes were given in Table 4. LP60 mixes gain early strength due to higher hydration where as in RA60, SC60 and NA60 shows better results. From Fig. 2 it can be clearly observed that, in fully cured specimens, control concrete attains 62.6 MPa strength slightly higher values than the remaining mixes for 28 days.

For partially cured (PC) specimens, less strength was attained for LP60 is 54.7 MPa for 28 days when compared with remaining mixes. For Internally cured (IC) specimens, SC60 gain good amount of high strength of 56.2 MPa for 28 days when compared with other mixes. Coming to Rebounder Number, the results shows higher values for RA60 and NA60 when compared with LP60 and SC60.

3.2.3 Split Tensile Strength of M60 Concrete Mixes with Age

The split tensile strength for 4 mixes were given in Table 5 and shown in Fig. 3. It is clearly observed that the fully cured specimens of LP60 and NA60 got 6.9 MPa and as 7.1 MPa strengths slightly higher than the RA60 and SC60 for 28 days. For partially cured (PC) specimens, attained strength was shows similar results for

Table 4 Compressive strength (MPa) and rebound number of M60 concrete along with age

Mix	Compressive strength			Rebound number		
	Day 3	Day 7	Day 28	Day 3	Day 7	Day 28
LP60FC	27.2	40.1	60.6	1	45	64
LP60PC	23.8	34.4	54.7	34	38	60
LP60IC	21.2	32.3	51.4	33	35	54
RA60FC	24.3	39.2	60.8	34	42	66
RA60PC	23.5	38.5	57.1	33	40	63
RA60IC	20.3	36.3	54.8	32	39	58
SC60FC	25.6	38.4	60.9	34	43	67
SC60PC	24.3	36.2	58.1	33	39	61
SC60IC	24.1	34.6	56.2	32	38	57
NA60FC	29.2	42.7	62.6	35	45	68
NA60PC	25.4	35.9	57.8	33	39	62
NA60IC	22.1	34.8	54.3	32	39	55

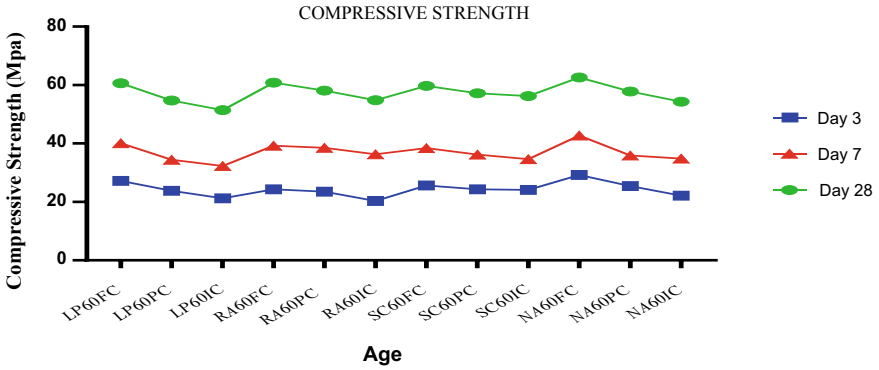

Fig. 2 Compressive strength of M60 concrete with different mix proportions

all mixes. Even for Internally cured (IC) specimens also achieves the good amount strength both for 7 and 28 days.

3.2.4 Sorpitivity Studies of M60 Concrete Mixes with Absorption and Desorption

Figure 4 shows the results of sorpitivity studies after conducting absorption and desorption. First, the absorption was done in hot air oven at 110 °C and observed initial and final weights of specimens and calculated evaporable pore water after that desorption was conducted to measure permeable pore space in the concrete. The

Table 5 Split Tensile Strength of M60 concrete for 7 and 28 days

Mix	Split tensile strength	
	Day 7	Day 28
LP60FC	4.50	6.90
LP60PC	3.80	5.70
LP60IC	3.10	5.10
RA60FC	4.01	6.23
RA60PC	3.93	5.90
RA60IC	3.54	5.32
SC60FC	4.31	6.41
SC60PC	3.95	5.92
SC60IC	3.76	5.63
NA60FC	4.72	7.10
NA60PC	3.80	5.82
NA60IC	3.50	5.27

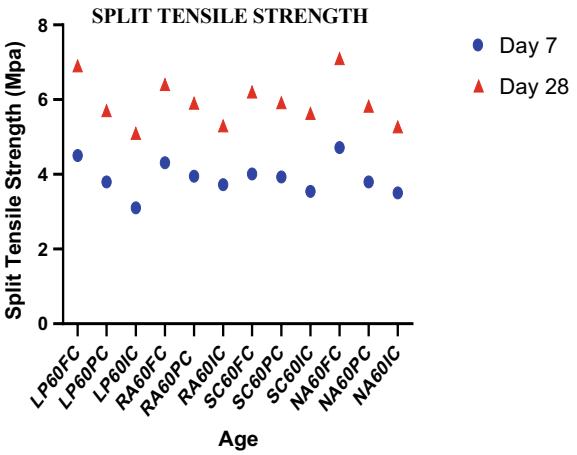

Fig. 3 Split tensile strength of M60 concrete mixes with different curing regimes

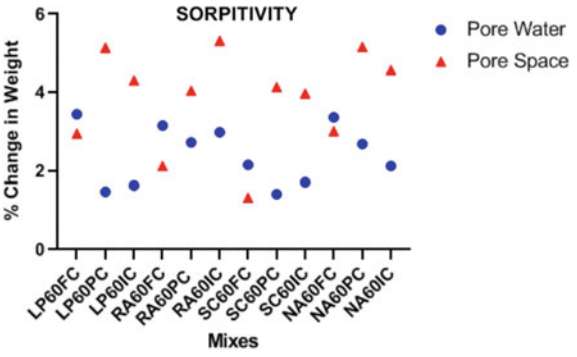

Fig. 4 Sorpitivity results of M60 concrete mixes

observed pore water for fully cured specimens as 3.44% for LP60, 3.15% for RA60 and 2.15 and 3.36% for SC60 and NA60.similarly the pore space was observed as 2.95% for LP60, 2.12% for RA60, 1.32 and 3.01% for SC60 and NA60. For partially cured specimens pore water is found as 1.47, 2.72, 1.41 and 2.68% where as in pore space was it was found to be 5.14, 4.04, 4.14 and 5.16%. Even for Internally cured specimens also pore water is observed as 1.63, 2.98, 1.71 and 2.12% whereas pore space was observed as 4.31, 5.32, 3.97 and 4.57%.

4 Conclusions

This research clearly shows the performance characteristics of supplementary cementitious materials such as limestone powder, fly ash and shrinkage reducing admixture PEG6000 as self-curing agent in recycled aggregate concrete. The following observation were concluded and those are listed below:

1. The workability, slump flow ang J-ring values of the four mixes achieved the properties up to the mark of EFNARC specifications.
2. The concretes containing self-curing agent PEG 6000 and fly ash increases the workability and also fly ash in concrete enhances later strengths.
3. The variation of weights for the mixes with and without self-curing agent indicates the slight variation due to the aging and it is more in partially cured specimens. The weights were increased by replacing normal aggregates with recycled concrete aggregates (SSD).
4. For different curing regimes like fully cured, partially cured and internally cured specimens, the compressive strength and rebound number of LP60 mixes achieved early strength due to higher hydration where as in RA60, SC60 mixes were having fly ash, it will give later strengths and also the split tensile strength was observed as slightly higher for fully cured specimens whereas similar results were found to be in partial and internal cured specimens for all mixes.
5. Evaporable pore water is more in fully cured specimens rather than the partial and internal curing. Permeable pore spaces are less in fully cured concretes when compared with partial and internal curing.
6. Utilization of constructional demolition waste products like Recycled concrete aggregate and fly ash from Thermal power stations etc., helps in minimizing the waste and also provides a clean and green environment.

References

1. Mehta PK, Monteiro PJM (2006) Concrete: microstructure, properties, and materials, 3rd edn. McGraw-Hill, New York
2. Philleo RE (1991) Concrete science and reality. In: Skalny J, Mindess S (eds) Materials science of concrete II. American Ceramic Society, Westerville, OH, pp 1–8

3. Espinoza-Hijazin G, Paul Á, Lopez M (2012) Concrete containing natural pozzolans: new challenges for internal curing. https://doi.org/10.1061/(ASCE)MT.1943-5533.0000421
4. Mousa MI, Manhdy MG, Abdel-Reheem AH, Yehia AZ (2014) Mechanical properties of self-curing concrete (SCUC). Housing and Building National Research Center
5. Yehia S, Helal K, Abusharkh A, Zaher A, Istaitiyeh H (2015) Strength and durability evaluation of recycled aggregate concrete. Int J Concr Struct Mater 219–239
6. Fakitsas CG, Papakonstantinou PEA, Kiousis PD, ASCE AM, Savva A (2012) Effects of recycled concrete aggregates on the compressive and shear strength of high-strength self-consolidating concrete 356–361
7. Kim H, Bentz D (2008) Internal curing with crushed returned concrete aggregates for high performance concrete. In: NRMCA concrete technology forum: focus on sustainable development
8. Jung S-H, Saraswathy V, Karthick S, Kathirvel P, Kwon S-J (2018) Microstructure characteristics of fly ash concrete with rice husk ash and lime stone powder. Int J Concr Struct Mater
9. Ashraf W, Olek J (2016) Carbonation behavior of hydraulic and non-hydraulic calcium silicates: potential of utilizing low-lime calcium silicates in cement-based materials. J Mater Sci 51:6173–6191
10. Ganesh Babu K, Siva Nageswara Rao K (1996) Efficiency of fly ash in concrete with age. Cem Concr Res 26(3):465–474

Experimental Investigation on Hydrophobic Concrete

Ahallya Raveendran and Jiji Antony

Abstract The people of Kerala state experienced extreme hardship and unmitigated misery in the year 2018 and 2019 during the month of August. The fury nature of rainfall caused floods and various negative impacts on structures, thereby truncating durability of structures. Some of them were completely destroyed and some required proper maintenance. This paper depicts the strength and hydrophobic characteristics of concrete, developed by partial replacement of cement with stearic acid treated metakaolin. The results showed better properties than normal concrete.

Keywords Stearic acid · Metakaolin · Strength · Hydrophobic concrete · Normal concrete

1 Introduction

Concrete is one of the most commonly used building material in construction. The materials deployed in its fabrication constantly interacts with the environment around it, as a result temperature and humidity affect the moisture levels within it. 2018 and 2019 Kerala flood created huge damages in case of concrete structures, due to corrosion of reinforcing steel and leakages in the structures. Similar situations are accelerated by water penetration through tiny capillary pores formed during hydration process. Aforesaid scenario due to hydrophilic nature (due to capillary pores) of normal concrete, reflects the need to develop concrete structures that can tolerate adverse climatic conditions with minimal maintenance. Hydrophilic nature of concrete affect concrete's strength and durability characteristics.

Hydrophobic concrete repels water and is developed using hydrophobic crystals, integral waterproofing additives, surface coatings, chemical admixtures and

A. Raveendran (✉) · J. Antony
Department of Civil Engineering, Federal Institute of Science and Technology (FISAT), Ernakulam 683577, India
e-mail: ahallyaraveendran@gmail.com

J. Antony
e-mail: jijiantony13@gmail.com

© Springer Nature Switzerland AG 2021

K. Dasgupta et al. (eds.), *Proceedings of SECON 2020*,
Lecture Notes in Civil Engineering 97,
https://doi.org/10.1007/978-3-030-55115-5_69

mineral admixtures. According to the studies conducted by Mazen et al. [1], aqueous hydrophobic materials showed higher compressive strength than cementitious admixture. Surface coatings highly reduces water penetration according to the findings of Vanessa et al. [2]. Studies by Marcelo et al. (2008) proved that, surface hydrophobic agents (alkilalkoxisiloxanes) effectively reduces penetration by capillary suction [3]. Low cost mineral admixture treated with fatty acid, stearic acid, animal oil etc. can produce hydrophobic materials. Waste marble powder, can be made hydrophobic using a modification agent Perflurooctlyethoxysilane. By increasing the amount of modifying agent, resistance against water penetration can be increased according to the studies of Wong et al. (2016) [4]. Also waste paper sludge ash and ground granulated blast furnace slag (GGBS) treated with stearic acid shows improved performance [5, 6]. The hydrophobic nature of nanomaterials based superhydrophobic coatings, stearic acid treated GGBS and Ultra high performance concrete were determined using water contact angle test [7–10]. Contact angle smaller than 90° is considered to be hydrophilic, larger than 90° is hydrophobic and one which is equal to or higher than 150° is superhydrophobic.

Various studies have verified the improved performance of GGBS [6, 9]. This paper focuses on comparative study between GGBS and metakaolin. Metakaolin was chosen due to its higher specific surface area than GGBS and contains higher percentage of silica. Silica has great physical properties that can enhance the strength characteristics. The optimized sample will be extended to concrete for further studies.

2 Basic Mechanism

A material can be made hydrophobic in nature by reducing polarity of interparticle molecules. Water molecules being polar, simply attract to partial positive or negative charges. Whereas on neutral surface, they bunch up to form a spherical water droplet.

Chemical admixtures (stearic acid) are active chemicals comprising of long-chain organic molecules, having a polar hydrophilic cluster (–COO–) connected to a non-polar hydrophobic organic chain with some polar groups (–OH). The polar groups within the chain get adsorbate on the surface of cement grains, and therefore the hydrophobic side chain with polar hydrophilic groups at the tip, purpose outwards keeps cement particles apart by electrostatic repulsion. With the progress of hydration, electric charge diminishes and natural action of hydrating product occurs.

3 Materials

The materials used for the study were ordinary portland cement, M-sand, coarse aggregate, metakaolin, Ground Granulated Blast Furnace Slag (GGBS) and stearic acid ($CH_3(CH_2)_{16}COOH$).

Table 1 Properties of cement

Physical properties	Results
Specific gravity	3.17
Fineness	5.89%
Standard consistency	31%
Initial setting time	83 min
Final setting time	264 min

Table 2 Properties of M-sand

Physical properties	Results
Specific gravity	2.7
Water absorption (%)	1.27
Fineness modulus	2.79

3.1 Cement

Ordinary portland cement of grade 53 with commercial name "Sharjah cement" were collected and its physical properties was tested according to IS 4031:1991—part 2. The results were tabulated as shown in Table 1.

3.2 M-Sand

M-Sand were collected and its material characterization were done according to IS 2386:2016—part 3. As per IS 383:1970 the tested sample belongs to zone 2. The results of test conducted on the collected sample are shown in Table 2.

3.3 Mineral Admixtures

GGBS and metakaolin are the mineral admixtures used for the study and their material characterization are depicted in Table 3.

Table 3 Properties of mineral admixture

Mineral admixture	Physical properties	Results
GGBS	Specific gravity	2.85
	Specific surface area (m^2/kg)	420
Metakaolin	Specific gravity	2.6
	Specific surface area (m^2/kg)	41,940

Table 4 Properties of coarse aggregate

Constituents	Values
Assay	99%
Melting range	54–56 °C
Iodine number	0.5%
Sulphated ash	0.05%
Heavy metals (Pb)	0.001%

Table 5 Properties of stearic acid

Physical properties	Results
Spdsdsecific gravity	2.8
Water absorption	0.60%

3.4 Coarse Aggregate

The 10 mm coarse aggregate used in the study were collected and tested according to IS 2386:2016—part 3 and the results are shown in Table 4.

3.5 Stearic Acid ($CH_3(CH_2)_{16}COOH$)

Stearic acid is a long chain of saturated fatty acid that comes from animal and vegetable fats and oils and are most commonly used material to produce hydrophobic materials [11, 12]. The characterization of stearic acid are shown in Table 5.

4 Experimental Programme

Strength properties and water absorption of normal and modified mortar samples are tested. Optimized samples were extended to concrete specimen. Thereafter, hydrophobic properties of the optimized sample are examined.

4.1 Mix Design for Optimization

Mortar cube (1:5 ratio by weight) of size 70.5 × 70.5 × 70.5 mm were casted with 5, 10, 15 and 20% of replacement of cement with 1% stearic acid treated metakaolin and GGBS. The samples were designated as MK5, MK10, MK15, MK20, GG5, GG10, GG15 and GG20 respectively. Stearic acid amount is fixed since researches have proven 1% shows better performance [9]. Mineral admixtures such as metakaolin

Table 6 Mix proportion

Trial mix	Cement (kg/m^3)	Fine aggregate (kg/m^3)	Coarse aggregate (kg/m^3)	Water (l)	Super plasticizer (%)	Slump value (mm)	Mix proportion
W/C—0.38	408	1005	957	170	1	140	1:2.46:2.34
W/C—0.40	386	1179	1105	174	1	106	1:3.05:2.86
W/C—0.45	324	1169	867	146	1	0	1:3.61:2.68

and GGBS are thoroughly blended with stearic acid to make them hydrophobic, before the actual mixing of mortar is done. Mortar specimens are cured for 24 h at 100% RH and were air dried at room temperature for rest of the curing period (28 days of curing). The mortar specimen with better performance is extended to concrete blocks, with cube dimension 150 mm × 150 mm × 150 mm under same curing condition. M20 grade concrete as per IS 10262:2009 [8], using trial and error method was adopted. Table 6 shows the concrete mix proportion and W/C ratio 0.40 was selected and target strength of 26.6 N/mm^2 was attained.

4.2 Tests on Mortar and Concrete

The compressive strength and water absorption tests were conducted for mortar and concrete cube specimens. Hydrophobicity test were carried out for optimized sample using mortar cubes.

4.3 Compressive Strength and Water Absorption Test

Compressive strength test was carried out according to IS 516-2016 (concrete specimen) and IS 4031 part 6 (mortar specimen). Water absorption test was conducted according to IS: 2185 (PART4).

4.4 Hydrophobicity Test

Water contact angle test was used to determine hydrophobicity of the optimized sample. Contact angle are determined using Canon EOS 6D camera and ImageJ software [13]. For conducting the test, water droplet were allowed to fall on the surface of optimized mortar and normal mortar specimen using a syringe. The photographs of droplet after 10 s (stabilization time) was captured and analyzed.

5 Results and Discussion

5.1 Compressive Strength

28th day compressive strength of mortar were determined as per IS 4031 part 6. The results obtained for modified and normal mortar cube specimen (average of 3 samples) are shown in Fig. 1a. The compressive strength value of 1:5 mortar mix with 53 grade cement is found to be less than 53 N/mm^2 due to reduced cement content in it. Also various parameters such as w/c ratio, specific gravity etc. affects the compressive strength value of mortar specimen. Test results showed an increase in compressive strength for MK5 and GG5 sample, thereafter decreasing. Modified mortar showed higher value compared to normal mortar which is due to the dense packing introduced by metakaolin and GGBS. Comparing MK5 and GG5, MK5 showed higher value. This is due to higher surface area of metakaolin than GGBS. The decrease in strength at higher replacement level is due to decrease in workability thereby lowering the performance. 28th day compressive strength (average of 3 samples) obtained for normal and optimized concrete sample (MK5) are shown in Fig. 1b. In case of concrete specimen the estimated target strength was achieved in the 28th day.

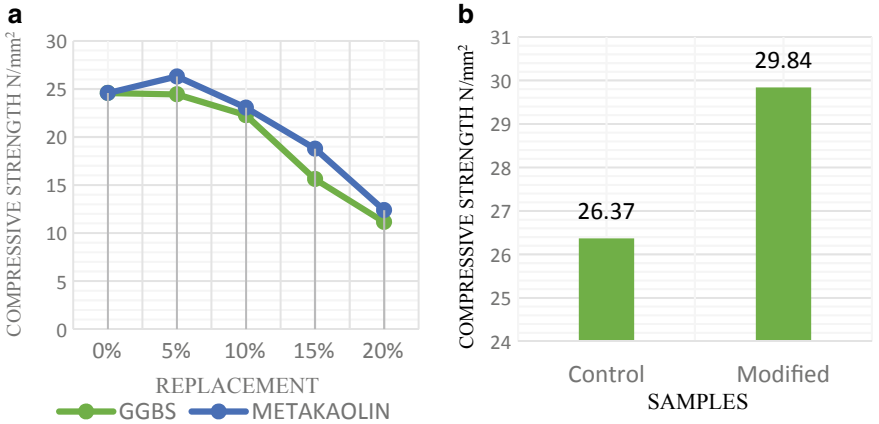

Fig. 1 **a** 28th day compressive strength, **b** compressive strength of control and optimized sample at 28th day

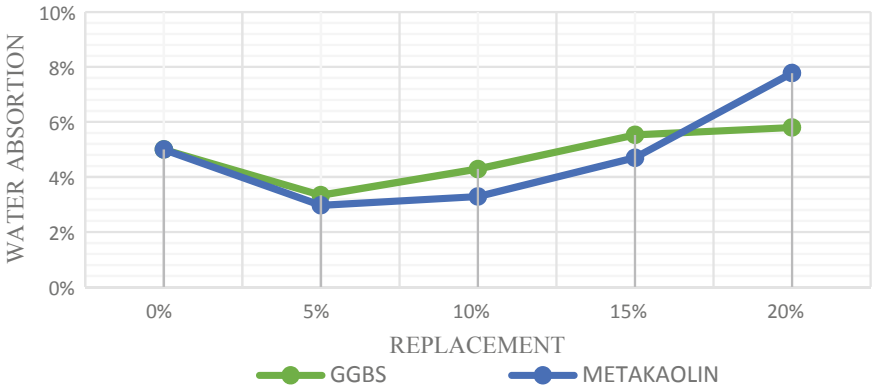

Fig. 2 Water absorption after replacing with GGBS and metakaolin

Table 7 Water absorption of optimized concrete specimen

Sample	Results (%)
Normal	1.77
Hydrophobic	0.59

5.2 Water Absorption Test

Results of water absorption test (average of 3 samples) conducted on modified and normal samples are graphically represented in Fig. 2. The percentage of water absorption increases with increase in percentage replacement. GG5 and MK5 samples showed least water absorption than normal specimen. This is because optimum blending occurs at 5% replacement leading to the formation of crystalline products in the pore created during the hydration period [1]. Comparing GG5 and MK5, MK5 showed better results due to higher surface area of metakaolin. The increase in water absorption at higher replacement is due to reduced crystalline formation as a result of reduced workability. Results of the optimized concrete specimen are shown in Table 7.

5.3 Hydrophobicity Test

The test has been conducted on 4 MK5 samples and 4 normal samples. Figure 3a–d shows water droplets on modified specimen and Fig. 3e shows water droplet on normal mortar specimen. From Fig. 3 we can see that in case of modified specimen the droplet attains a spherical shape. This shape is lost as the water gets penetrated through any of the pore lacking crystalline formation or as it slips off the surface. But in case of normal specimen due to the presence of number of tiny pores, the water

a) Sample 1 b) Sample 2 c) Sample 3

d) Sample 4 e) Normal specimen

Fig. 3 **a** Sample 1, **b** Sample 2, **c** Sample 3, **d** Sample 4, **e** normal specimen

Table 8 Results of contact angle test

Samples	Contact angle (°)
1	176.987
2	179.409
3	174.427
4	176.286

droplet gets easily penetrated into it as shown in Fig. 3e. Analyzing the water droplet using contact angle jar plugin of ImageJ software, average contact angle obtained was 177.52° indicating that the sample belongs to superhydrophobic category. Table 8 shows results of contact angle test.

6 Conclusion

The present study focuses on hydrophobic nature of concrete using metakaolin, GGBS and stearic acid.

1. Compressive strength of hydrophobic sample (MK5) increased by 13.16% due to dense matrix formation resulting from its higher specific surface area
2. Water absorption decreased by 66.67% in case of MK5 sample than normal sample due to dense crystalline formation in capillary pores

3. Modified sample has an average contact angle of 177.52° indicating the superhydrophobic nature of tested sample.

References

1. Al-Kheetan MJ, Rahman MM, Chamberlain DA (2018) Development of hydrophobic concrete by adding dual-crystalline admixture at mixing stage. Struct Concr 19(2018):1504–1511
2. Cappellesso VG, dos Santos Petry N, Dal Molin DCC, Masuero AB (2016) Use of crystalline waterproofing to reduce capillary porosity in concrete. Build Rehabil 9:3–12
3. de Medeiros MHF, Helene P (2008) Efficacy of surface hydrophobic agents in reducing water and chloride ion penetration in concrete. Mater Struct 41:59–71
4. Wong Y, Tong L, Hu Y, Wu P (2016) A self-assembly and high-robustness super-hydrophobic coating based on waste marble powder. Mater Trans 57(12):2127–2131
5. Wong HS, Barakat R, Alhilali A, Saleh M, Cheeseman CR (2015) Hydrophobic concrete using waste paper sludge ash. Cem Concr Res 70:9–20
6. She W, Wang X, Miao C, Zhang Q, Zhang Y, Yang J, Hong J (2018) Biomimetic superhydrophobic surface of concrete: Topographic and chemical modification assembly by direct spray. Constr Build Mater 181:347–357
7. Weisheit S, Unterberger SH, Bader T, Lackner R (2016) Assessment of test methods for characterizing the hydrophobic nature of surface-treated high performance concrete. Constr Build Mater 110:145–153
8. Arabzadeh A, Ceylan H, Kim S, Gopalakrishnan K, Sassani A, Sundararajan S, Taylor PC (2017) Superhydrophobic coatings on Portland cement concrete surfaces. Constr Build Mater 141:393–401
9. Qu ZY, Yu QL (2018) Synthesizing super-hydrophobic ground granulated blast furnace slag to enhance the transport property of lightweight aggregate concrete. Constr Build Mater 191:176–186
10. Horgines M, Chen JJ (2014) Superhydrophobic concrete surfaces with integrated microtexture. Cem Concr Compos 52:81–90
11. Dashairya L, Sahu A, Saha P (2019) Stearic acid treated polypyrrole-encapsulated melamine formaldehyde superhydrophobic sponge for oil recovery. Adv Compos Hybrid Mater 2:70–82
12. Zhu SG, Wu CX, Luo YL (2010) Effect of stearic acid on synthesis of nanocomposite WC-MgO powders by mechanical alloying. J Mater Sci 45:1817–1822
13. Williams DL, Kuhn AT, Amann MA, Hausinger MB (2010) Computerized measurement of contact angles. Galvanotechnik 101:2502–2512

Study of the Behavior of Air Entrained Concrete Containing Mineral Admixtures with the Addition of Coal Bottom Ash

Shashi Kant Sharma, Kanish Kapoor, Sandeep Singh, and K. P. Marisala Chaitanya

Abstract With the addition of different pozzolanic cementitious materials, an air entrained concrete shows different behavior in terms of durability and compressive strength. The amount of entrapped air is reduced when fly Ash is used in air entrained concrete. The resulting volume of air decreased appreciably with increasing silica-fume content in air entrained concrete. This paper has focused on the effect of replacement of coal bottom ash (CBA) as a fine aggregate in the air entrained concrete in the presence of different pozzolanic cementitious materials and it compares the different properties with the normal concrete. Experimental work shows that CBA causes a reduction in 7 days compressive strength appreciably @ 50% natural fine aggregate (NFA) replacement in comparison to that at 25%. Beyond 7 days curing CBA starts acting as a Pozzolan and there is not much strength decrement in mixes with 50% NFA replacement. Also, this replacement level mitigate the effect of reduction in air entrainment caused by fine mineral admixtures in wet state thereby increasing the air entrainment capacity of concrete. Hence it was concluded that if we increase the content of Coal Bottom Ash up to 50% then it will be beneficial for air entrained concrete production.

Keywords Air entrained concrete · Natural fine aggregates · Coal bottom ash · Pozzolans · Silica fume · Compressive strength · Superplasticizers, air entraining agent

S. K. Sharma · K. Kapoor · S. Singh (✉) · K. P. Marisala Chaitanya
Department of Civil Engineering, NIT Jalandhar, Jalandhar, Punjab 144001, India
e-mail: sandeeps.ce.19@nitj.ac.in

S. K. Sharma
e-mail: shashi.pec@gmail.com

K. Kapoor
e-mail: kapoork@nith.ac.in

K. P. Marisala Chaitanya
e-mail: atpocivilkcet@gmail.com

© Springer Nature Switzerland AG 2021

K. Dasgupta et al. (eds.), *Proceedings of SECON 2020*,
Lecture Notes in Civil Engineering 97,
https://doi.org/10.1007/978-3-030-55115-5_70

1 Introduction

Air Entrained Concrete is made either by using air entraining cement or by mixing a small quantity of AEA. These airs entraining agent produce millions of micro air bubbles inside the concrete mix acting as flexible ball bearings. The micro air bubbles of size ranging from 5 to 80 μm distribute in the entire mass of concrete resulting in modification of the properties of it regarding workability, segregation, bleeding and finishing quality [1]. Entrained air has major impact on water-cement ratio. AEC can have lower water cement ratios than non-air-entrained concrete; this minimizes the reductions in strength that generally accompany and related to air entrainment [2]. Two of the revolutionary developments in concrete technology in the last century have been produced by AEAs and superplasticizers (SP) [3]. SPs or high range water reducing admixtures (HRWRAs) are concrete admixtures which can be mainly used either to increase the workability of fresh concrete at a given mix composition or to reduce the amount of mixing water and water/cement (w/c) ratio for a given workability in order to increase strength and durability [4, 5]. For instance to compensate for the loss of workability in mixes like those containing pozzolanic materials such as condensed Silica Fume (SF) and Metakaolin or even increase the water reduction effect of pulverized fuel ash and ground granulated blast furnace slag we normally use SPs [6]. Due to addition of SPs the slump increase at a given mix composition can be 150–200 mm and the reduction of mixing water at a given slump can be up to 30%, both depending on the method of addition, dosage and type of admixture used. Presently the most important HRWRAs available are based on condensed Melamine Sulfonated Formaldehyde (MSF) or Naphtalene Sulfonated Formaldehyde (NSF) in the form of 40% aqueous solution to facilitate an accurate, reliable and automatic dispensing at the batching plant. The optimum dosage of commercial SPs is in general in the range 1–2% by mass of cement. The main action of the molecules of such SPs is to wrap themselves around the cement particles and give them a highly negative charge so that they repel each other [7, 8] . This results in deflocculation and dispersion of cement particles with the resulting improvement in workability. Coal Bottom Ash (CBA) is formed in coal furnaces. It is made from agglomerated ash particles that are too large to be carried in the flue gases and fall through open grates to an ash hopper at the bottom of the furnace [9–11]. CBA is mainly comprised of fused coarser ash particles. These particles are quite porous and look like volcanic lava. CBA forms up to 25% of the total ash while the FA forms the remaining 75%. Literature has shown that there is a strongly possibility of CBA being used as substitute/replacement of NFA (NFA). Its use in concrete becomes more significant and important in view of the fact that sources of NFAs are getting depleted gradually, and it is of prime importance that substitute of NFA be explored . The present study is totally based on the behavior of air entrained concrete when we replace natural fine aggregates with the coal bottom ash in the presence of different pozzolans. Then final results have been compared with the normal concrete on the basis of compressive strength and flexural strength of the concrete.

2 Materials and Methodology

2.1 Materials and Theory of Mixing

Cement is a fine, grey powder. It is mixed with water and materials such as NFA, gravel, and crushed stone to make concrete. The cement and water form a paste that binds the other materials together. The ordinary cement contains two basic ingredients namely argillaceous and calcareous. In argillaceous materials clay predominates and in calcareous materials, calcium carbonate predominates. Portland pozzolana cement was used for casting of cubes and cylinders for all concrete mixes. The cement was of uniform color. The physical properties of the cement as determined from various test conforming to IS: 1489-1991. The NFA used for the experimental programme was locally procured and conformed to Indian Standard Specifications IS: 383-1970. The NFA was first sieved through 4.75 mm sieve to remove any particles greater than 4.75 mm and then was washed to remove the dust. The NFAs belonged to grading zone II. Coal Bottom Ash used in this study was collected from coal fired thermal power plant at Bathinda, Punjab (India). Specific gravity and water absorption of CBA was determined as per Indian standard BIS: 2389-1963 (Part III) an equivalent to ASTM C 128-93. The material which is retained on IS sieve no. 4.75 is termed as a coarse aggregate. The nature of work decides the maximum size of the coarse aggregate. Locally available coarse aggregate having the maximum size of 10 mm and 20 mm was used in a ratio of 50 and 50%. The aggregates were washed to remove dust and dirt and were dried to surface dry condition. The aggregates were tested as per IS: 383-1970. Supplementary Cementitious Materials (SCMs) used in the investigation included FA (Class F) and SF. Amongst these, FA was procured from Ambuja Cement Plant, Ropar, India and it was ensured that the material complies with the requirements as per IS: 1727-1967. SF was purchased from Elkem Materials. Hydrogen peroxide was used in different dosages by weight of binder to achieve desirable properties of AEC. H_2O_2 was used having the relative density of 1.1. H_2O_2 was preferred over all air entrained agents because it is giving the good compressive strength test results over olive oil (widely used) and vinsol resin.

2.2 Mix Proportions

Twenty seven mixture proportions were made. First was control mix (without CBA and cement replacement), Second and third are cement replaced by FA 20% and 40% respectively, Fourth and Fifth are cement replaced by SF 5% and 10% respectively. Sixth and seventh both are having 20% FA, 5% and 10% SF replacement of cement respectively. Eighth and ninth both are having 40% FA, 5 and 10% SF replacement of cement respectively. Mixes from ten to eighteen follow same trend as one to nine but here NFA was replaced with CBA by 25% weight. Mixes from nineteen to twenty seven follow same trend as one to nine but here NFA (NFA) was replaced with CBA

by 50% weight. Mix notations and details of mixes are given in Table 1. Mix proportions are given in Table 2. The controls mix without CBA was proportioned as per Indian standard Specifications IS: 10262-1982, to obtain a 28-days cube compressive strength of 48.25 MPa. Hand mixing was done for the concrete mixes. In all mixes 0.4 w/c ratio is maintained.

The casting of the specimens was done under laboratory conditions using standard equipment. Each batch consists 6 standard cubes of 100 mm × 100 mm × 100 mm

Table 1 Mix notations and details of mixes

Mix id	Mix designation	Mix description
M1	C	100%C + 0%SF + 0%FA + 100%NFA + 0%CBA + 100%NCA
M2	CF1	80%C + 0%SF + 20%FA + 100%NFA + 0%CBA + 100%NCA
M3	CF2	60%C + 0%SF + 40%FA + 100%NFA + 0%CBA + 100%NCA
M4	CS1	95%C + 5%SF + 0%FA + 100%NFA + 0%CBA + 100%NCA
M5	CS2	90%C + 10%SF + 0%FA + 100%NFA + 0%CBA + 100%NCA
M6	CF1S1	75%C + 5%SF + 20%FA + 100%NFA + 0%CBA + 100%NCA
M7	CF1S2	70%C + 10%SF + 20%FA + 100%NFA + 0%CBA + 100%NCA
M8	CF2S1	55%C + 5%SF + 40%FA + 100%NFA + 0%CBA + 100%NCA
M9	CF2S2	50%C + 10%SF + 40%FA + 100%NFA + 0%CBA + 100%NCA
M10	C[a]	100%C + 0%SF + 0%FA + 75%NFA + 25%CBA + 100%NCA
M11	CF1[a]	80%C + 0%SF + 20%FA + 75%NFA + 25%CBA + 100%NCA
M12	CF2[a]	60%C + 0%SF + 40%FA + 75%NFA + 25%CBA + 100%NCA
M13	CS1[a]	95%C + 5%SF + 0%FA + 75%NFA + 25%CBA + 100%NCA
M14	CS2[a]	90%C + 10%SF + 0%FA + 75%NFA + 25%CBA + 100%NCA
M15	CF1S1[a]	75%C + 5%SF + 20%FA + 75%NFA + 25%CBA + 100%NCA
M16	CF1S2[a]	70%C + 10%SF + 20%FA + 75%NFA + 25%CBA + 100%NCA
M17	CF2S1[a]	55%C + 5%SF + 40%FA + 75%NFA + 25%CBA + 100%NCA
M18	CF2S2[a]	50%C + 10%SF + 40%FA + 75%NFA + 25%CBA + 100%NCA
M19	C[b]	100%C + 0%SF + 0%FA + 50%NFA + 50%CBA + 100%NCA
M20	CF1[b]	80%C + 0%SF + 20%FA + 50%NFA + 50%CBA + 100%NCA
M21	CF2[b]	60%C + 0%SF + 40%FA + 50%NFA + 50%CBA + 100%NCA
M22	CS1[b]	95%C + 5%SF + 0%FA + 50%NFA + 50%CBA + 100%NCA
M23	CS2[b]	90%C + 10%SF + 0%FA + 50%NFA + 50%CBA + 100%NCA
M24	CF1S1[b]	75%C + 5%SF + 20%FA + 50%NFA + 50%CBA + 100%NCA
M25	CF1S2[b]	70%C + 10%SF + 20%FA + 50%NFA + 50%CBA + 100%NCA
M26	CF2S1[b]	55%C + 5%SF + 40%FA + 50%NFA + 50%CBA + 100%NCA
M27	CF2S2[b]	50%C + 10%SF + 40%FA + 50%NFA + 50%CBA + 100%NCA

C—cement, FA—FA, SF—SF, NFA—natural NFAs, CBA—CBA, CA—coarse aggregates, SP—SP, AEA—air entrained agent

[a]25% CBA, [b]50% CBA as natural NFA replacement

Table 2 Mix proportions

Mix id	Mix designation	Cement [kg/m^3]	SF %	SF [kg/m^3]	FA %	FA [kg/m^3]	NFA [kg/m^3]	CBA %	CBA [kg/m^3]	NCA [kg/m^3]	SP %	AEA %
M1	C	491.9	0	0	0	0	546.3	0	0	971.9	0.5	1
M2	CF1	393.7	0	0	20	98.24	533.6	0	0	949.25	0.5	1
M3	CF2	295.1	0	0	40	196.8	519.5	0	0	924.25	0.5	1
M4	CS1	467.3	5	24.6	0	0	543.5	0	0	966.88	0.5	1
M5	CS2	442.7	10	49.19	0	0	540.3	0	0	961.77	0.5	1
M6	CF1S1	368.9	5	24.6	20	98.38	529.7	0	0	942.55	0.5	1
M7	CF1S2	343.3	10	49.2	20	98.38	526.8	0	0	936.84	0.5	1
M8	CF2S1	276	5	24.56	40	196.8	516.2	0	0	918.38	0.5	1
M9	CF2S2	246	10	49.19	40	196.8	513.1	0	0	912.84	0.5	1
M10	C[a]	491.9	0	0	0	0	409.7	25	110.6	971.9	1	1.5
M11	CF1[a]	393.7	0	0	20	98.24	400.2	25	108	949.25	1	1.5
M12	CF2[a]	295.1	0	0	40	196.8	389.6	25	105.2	924.25	1	1.5
M13	CS1[a]	467.3	5	24.6	0	0	407.6	25	110	966.88	1	1.5
M14	CS2[a]	442.7	10	49.19	0	0	405.2	25	109.4	961.77	1	1.5
M15	CF1S1[a]	368.9	5	24.6	20	98.38	397.3	25	107.2	942.55	1	1.5
M16	CF1S2[a]	343.3	10	49.2	20	98.38	395	25	106.6	936.84	1	1.5
M17	CF2S1[a]	27.6	5	24.56	40	196.8	387.2	25	104.5	918.38	1	1.5
M18	CF2S2[a]	246	10	49.19	40	196.8	384.8	25	103.9	912.84	1	1.5
M19	C[b]	491.9	0	0	0	0	273.2	50	221.2	971.9	1.5	2
M20	CF1[b]	393.7	0	0	20	98.24	266.8	50	216	949.25	1.5	2
M21	CF2[b]	295.1	0	0	40	196.8	259.7	50	210.3	924.25	1.5	2

(continued)

Table 2 (continued)

Mix id	Mix designation	Cement [kg/m^3]	SF %	SF [kg/m^3]	FA %	FA [kg/m^3]	NFA [kg/m^3]	CBA %	CBA [kg/m^3]	NCA [kg/m^3]	SP %	AEA %
M22	CS1[b]	467.3	5	24.6	0	0	271.7	50	220.2	966.88	1.5	2
M23	CS2[b]	442.7	10	49.19	0	0	270.2	50	218.7	961.77	1.5	2
M24	CF1S1[b]	368.9	5	24.6	20	98.38	264.9	50	214.5	942.55	1.5	2
M25	CF1S2[b]	343.3	10	49.2	20	98.38	263.3	50	213.2	936.84	1.5	2
M26	CF2S1[b]	27.6	5	24.56	40	196.8	258.1	50	209	918.38	1.5	2
M27	CF2S2[b]	246	10	49.19	40	196.8	256.6	50	207.7	912.84	1.5	2

(Fig. 1) for determination of 7 and 28 days compressive strength. For every mix, the quantity of various ingredients cementations content, NFAs, CBA, coarse aggregates, water were kept ready in the required amount. The required amount of the NFA and cement were initially mixed thoroughly in dry condition and no concentration of either material was visible. After that, coarse aggregate was added to the previous mix of NFA and cement in dry condition and was mixed thoroughly by turning twice or thrice in the same dry state in a tilting type rotary drum for one minute. Then SF and FA are mixed in required quantity into the mix. After that amount of water mixed with SP and AEA was added into the mix to get a uniform mix of a required slump and mixing process in the drum was continue for about one minute to get a better mix. For casting the specimens moulds were cleaned, brushed and oiled and placed on the ground. After filling the concrete in the moulds, the surface was leveled and finished clearly by trowel. After three hours of setting, specimens were marked accordingly and were left for setting in the mould for 24 h. After 24 h specimens were demoulded and immersed in water for curing in curing tank. Potable water was filled in the curing tank and after regular intervals water of curing tank was changed.

Fig. 1 Casted cubes

Fig. 2 Compressive strength test

2.3 Parameters Studied

2.3.1 Compressive Strength Test

This test is based on IS 516-1959. The test was conducted on cubes of size 100 mm × 100 mm × 100 mm. Specimens were cured for 7, 28 and 90 days in the curing tank. After the curing, specimens were taken out from the curing tank and left in the air to drip down the surface water. Specimens were then tested on 200 tones capacity Compression Testing Machine (CTM) (Fig. 2). The specimen was kept at side other than the casting side while testing for the compressive strength. Centre of the thrust of the spherically seated plates of CTM and the axis of specimens was carefully aligned. The application of load on specimen was gradual without any shock and it was increased at a constant rate of 2.5 N/mm^2/min until failure of specimen take place. The representative value of compressive strength for each batch of concrete was taken as the average of two cubes. The calculation of compressive strength was done by dividing the maximum compressive load by the cross-sectional area of the cube specimens. Hence through this process, the compressive strength of different specimens was obtained (Table 3).

3 Results

In order to study the effect on compressive strength, AEC obtained after cement replacement and natural NFA replacement with different proportions of SF & FA,

Table 3 Compressive strength

Mix id	Mix designation	Compressive strength (MPa)	
		7 Day	28 Day
M1	C	33.36	41.8
M2	CF1	28.51	42.38
M3	CF2	18.7	26.4
M4	CS1	37.53	46.17
M5	CS2	29.19	37
M6	CF1S1	23.3	36.6
M7	CF1S2	24.7	37.64
M8	CF2S1	19.6	24.34
M9	CF2S2	20.5	28.6
M10	C[a]	21.95	28.8
M11	CF1[a]	19.22	29.2
M12	CF2[a]	12.3	18.19
M13	CS1[a]	24.69	31.81
M14	CS2[a]	19.2	25.49
M15	CF1S1[a]	15.33	25.21
M16	CF1S2[a]	16.25	25.93
M17	CF2S1[a]	12.89	16.77
M18	CF2S2[a]	13.49	20.89
M19	C[b]	19.35	25.31
M20	CF1[b]	16.54	25.66
M21	CF2[b]	10.84	15.98
M22	CS1[b]	21.76	27.94
M23	CS2[b]	16.93	22.39
M24	CF1S1[b]	12.12	19.15
M25	CF1S2[b]	11.54	20.77
M26	CF2S1[b]	9.15	14.72
M27	CF2S2[b]	9.57	17.3

and CBA respectively, were prepared and kept for curing for a duration of 7 and 28 days. The intention was apparent, i.e. to study the initial foundation effect of air entrainment combined with pore size refinement of pozzolans in bringing a change in the compressive strength of concrete. During the process of air entrainment air is also entrapped to create other voids like capillary voids (smaller) and air entrapped voids (bigger). Air entrainment in the initial stage of hydration is effective in reducing plastic and drying shrinkage as it insulates the concrete against temperature gradient. The bigger size voids reduce the strength of concrete which should be mitigated. As a compensating material the pozzolans are supposed to hydrate at later stages to

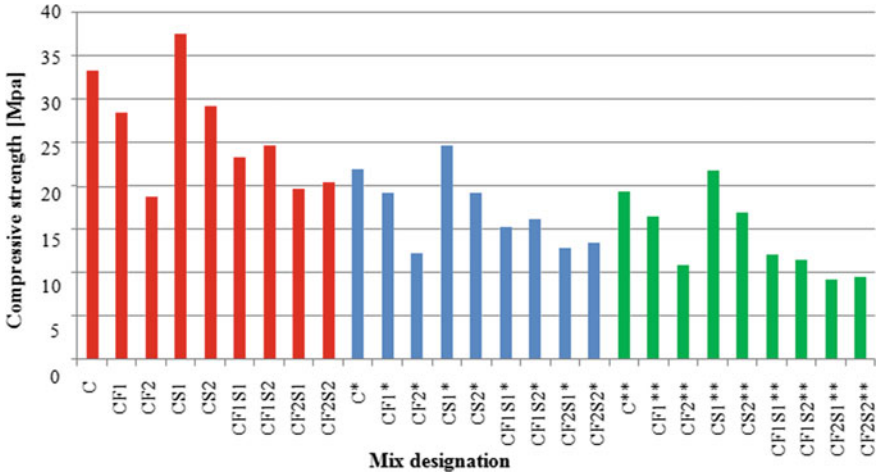

Fig. 3 Compressive strength of air entrained concrete mixes at 7 days curing

reduce the pore size so that the air entrapped voids are converted into air entrained voids and capillary voids [12–15].

Figure 3 shows the 7 day variation of compressive strength values of different concrete mixes wherein red bars, blue bars and green bars represent the strength values of corresponding mixes having 0, 25 and 50% NFA replacement with CBA. The strength variation depicts coherently that in comparison to normal AEC (33 MPa) all mixes but CS1 show lower strength. It was observed that with FA introduction there is a decrease in strength value abruptly. The rate of decrease was quite steep for FA variation from 20 to 40%. CS1 containing 5% SF show higher compressive strength (36.5 MPa) than normal AEC. As the content of SF increase further a decrease in compressive strength value has been observed, whose rate of decrease is comparatively lower than that of FA. The strength value of CF1S1 is surprisingly lesser than that of either CF1 or CS1. With an increment in SF content from 5% in CF1S1 to 10% in CF1S2 the strength increases minutely. The strength of mix CF2S1 is apparently higher than that of mix CF2 but lower than CS2 which justifies the effect of strength enhancement by SF in comparison to FA. Also with an increment in SF from 5% in mix CF2S1 to 10% in mix CF2S2 a very small increment in strength has been observed. The mix CF2 has shown least compressive strength (18.7 MPa).

SF also releases air from voids [16, 17] but it adsorbs all air which leads to higher value of air entrainment (5.17%) in this mix leading to lesser strength. Strength increased on addition of further 5% SF in mix CF1S2 and CF2S2 in comparison to CF1S1 and CF2S1 because SF consumes more CH when present in higher amounts to produce CSH, rather than the decrease in strength caused by its air consumption. Very small increment in compressive

strength value from mix CF1S1 to CF1S2 and from mix CF2S1 to CF2S2 has been observed which could have been larger had the mixes were normal (because

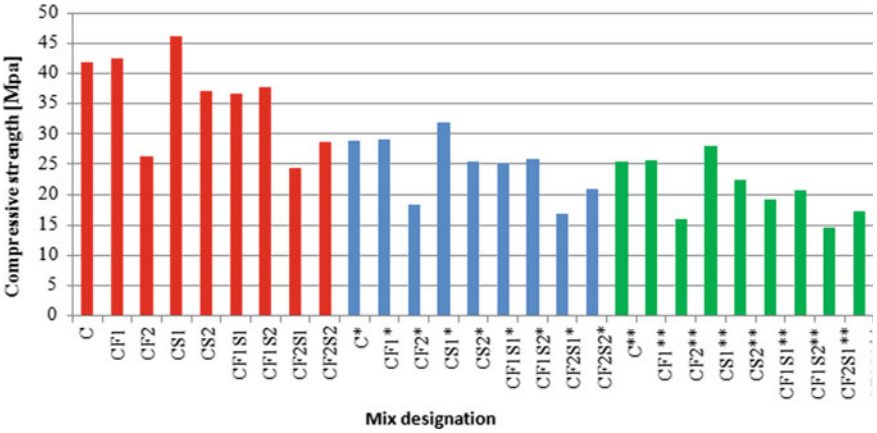

Fig. 4 Compressive strength of air entrained concrete mixes at 28 days curing

of higher reactivity of SF) and not air entrained. In mix CF1S1, 20% FA competes with 5% SF for reaction with CH, whereas in case of CF2S2, 40% FA is competing with 10% SF. Since SF is more reactive it consumes more CH liberated by primary hydration [18–20], leaving excess FA in mix CF2S2 as non-reacted which tries to decrease the strength. CBA causes a reduction in 7 day compressive strength. This could be seen for mixes containing 25% CBA and 50% CBA. There is a significant decrease in strength when 50%

NFA is replaced with CBA with respect to 25% CBA. This shows that like FA, CBA is also a weak pozzolan and increasing its content jeopardize the strength of concrete in initial stage.

The strength behavior of mixes after 28 days was quite satisfactory with respect to normal AEC if NFA is not replaced with CBA. The strength variation trend of the mixes remains same in this case also (Fig. 4), but the strength values of some mixes are noteworthy; i.e. mix CF1 (42.38 MPa) having higher value than normal AEC (41.8 MPa). It was also observed that mix CF2S2 shows higher increment in compressive strength than mix CF2S1, and mix CF1S2 shows relatively lower increment in strength than mix CF1S1 at 28 days with respect to 7 days. This converse behavior could be explained on basis of pozzolanic reactivity of FA and SF and their competition for CH. When FA is mere 20%, it starts reacting with the consumption of SF after 7 days. Hence a significant increment in strength has been observed for mix CF1S1 at 28 days. The strength value of mix CF1S2 does not show any variation from strength increment rate with respect to 7 days since SF has been mostly utilized during the said period. As a result the strength increment rate remains constant.

4 Conclusions

The study was aimed to determine the effect of using high volume mineral admixtures like FA and SF (cement substitutes) and CBA (NFA substitute) on the compressive strength of AEC.

The strength of the mixes has been found directly from compressive strength test. Compressive strength test mainly depends upon strength of mortar. Strength of interface depends upon the composition of paste around the aggregates. Paste having the higher binding tendency to aggregate results in higher compressive strength.

- The behaviour of both FA and SF in smaller volumes i.e. 20% FA and 5% SF improves after 7 days of curing in imparting strength of concrete. At this stage initial air entrainment levels start increasing or decreasing depending upon the combination of FA & SF. Higher volumes of FA greatly reduces the strength, whereas higher volumes of SF brought very minute improvement in strength of concrete.
- CBA starts showing pozzolonic effect after 7 days and it is beneficial to use 50% CBA in comparison to 25% CBA curing is allowed for this duration.

References

1. Lausten S (2011) Engineered air-entrainment for concrete, Doctoral thesis., Technical University of Denmark, Lyngby, Denmark
2. Cordon WA (1946) Entrained Air-A factor in the design of concrete mixes. Materials Laboratories Report No C-310, Research and Geology Division, Bureau of Reclamation, Denver, March 15, 1946
3. Collepardi M (1994) SPs and AEAs: state of the art and future needs. In: Concrete technology past present and future, proceedings of V. Mohan Malhotra symposium, ACI SP-144, pp 399–416
4. Dodson V (1990) Concrete admixtures. Ed. Van Nostrand Reinhold
5. Powers TC (1968) The properties of fresh concrete. Wiley, New York
6. Virtanen J Freeze-Thaw resistance of concrete containing blast furnace slag, FA or condensed SF. ACI Special Publication SP-79, vol II, Aug
7. Shang Y, Miao C, Lui J, Ran Q (2010) Influencing factors of air void characteristics in hardened concrete. In: 2nd international symposium of service life design for infrastructure, pp 817–824
8. Dodson VH (1990) Concrete admixture. Van Nostrand Reinhold, New York
9. "Pozzolanic and Cementitious materials" (1996) In: Malhotra VM, Mehta,PK (eds) Gordon and Preach Publishers
10. Bouzoubaâ G, Zhang A, Bilodeau MH, Malhotra VM (1997) The effect of grinding on the physical properties of FAes and a Portland cement clinker, pp 1861–1874
11. Sturrup VR, Hooton RD, Clendenning TG (1983) Durability of FA concrete. ACI SP-79, vol I, pp 47–69
12. Larson TD (1964) Air entrainment and durability aspects of FA concrete. Proc ASTM 64:866–886
13. Samarin A, Munn RL, Ashby JB (1983) The use of FA in concrete-Australian experience. ACI SP-79, vol I, pp 143–172

14. Gebler S, Klieger P () Effect of FA on the air void stability of concrete. In: Malhotra VM (ed) Proceedings, first international conference on the use of FA, SF, slag and other mineral by-products in concrete, Montebello, Canada, July 31–August 5, 1983, ACI SP-79, pp 103–142
15. Carette G.G. and Malhotra VM (1984) Characterization of Canadian Flyashes and their performance in concrete. Division Report, MRP/MSL 84-137 (OP&J),CANMET, Energy, Mines and Resources Canada
16. Dhir RK, McCarthy MJ, Limbachiya MC, El Sayad HI, Zhang DS (1999) Pulverized fuel ash concrete: air entrainment and freeze/thaw durability. Mag Concr Res 51(1):53–64
17. Carette GG, Malhotra VM (1983) SF concrete-properties, applications and limitations. Concr Int: Des Constr, 5(5):40–46
18. Carette GG, Malhotra VM (1983) "Mechanical properties, durability and drying shrinkage of Portland cement concrete incorporating SF. ASTM J Cem, Concr Aggreg 5(1):3–13
19. Toutanji HA (1998) The influence of air entrainment on the properties of SFconcrete. Adv Cem Res 10(4):135–139
20. Sabir BB, Kouyiali K (1991) Freeze-Thaw durability of air-entrained SF concrete. Cem Concr Compos 13:203–208

Investigation on the Effect of Steel Fibers in Self Curing Concrete

Annamol Sunny and Elba Helen George

Abstract Concrete curing is one of the most critical process to obtain the desired concrete properties. The traditional method of curing is achieved by wetting the exposed surface and preventing concrete from losing moisture. However when the mineral admixtures are applied to concrete, the demand for curing water will be much greater than that in a ordinary Portland cement concrete. If this water is not readily available, it can result in significant autogenous deformation and cracking. In order to overcome these draw back the attention is focused on advanced technology in curing i.e., self-cuing concrete. Self-curing or internal curing is a technique in which no additional water is required to enhance the rate of hydration. These self-curing concretes are also weak in resisting tensile forces, but by incorporating fibers on self-curing concrete both the tensile strength as well as the durability can be increased. In this study, self-curing concrete is achieved by incorporating Polyethylene Glycol (PEG-400) at different dosage (0.5, 1, 1.5 and 2%) by weight of binder content of M40 grade of concrete. To its optimum dosage the hooked end steel fibres are added to this self-curing concrete at different percentage (0.5, 1, 1.5, and 2%) by volume of concrete. The optimum steel fibre content is then determined with respect to strength parameters. The strength properties of self-curing concrete with steel fibers is then compared to that of conventional concrete and self curing concrete.

Keywords Self curing concrete · Polyethylene glycol · Steel fibers

A. Sunny (✉) · E. H. George
Toc H Institute of Science and Technology, Arakkunnam, India
e-mail: annamols1996@gmail.com

E. H. George
e-mail: elbaheleng@tistcochin.edu.in

© Springer Nature Switzerland AG 2021

K. Dasgupta et al. (eds.), *Proceedings of SECON 2020*,
Lecture Notes in Civil Engineering 97,
https://doi.org/10.1007/978-3-030-55115-5_71

1 Introduction

Efficient curing improves strength and durability of concrete. Curing of concrete is a major challenge in the construction industry, especially in areas, which suffer from shortages of water. Even when meticulously performed only water evaporation can be minimized, but the water supply on the surface of vertical structural elements is still a technical problem. The time allocated for curing is a stagnation of building time increasing costs and efforts [1]. Thus the idea of self curing of concrete has gained popularity and is steadily progressing from laboratory to field of practice. Internal curing or self curing refers to mechanism whereby cement hydrates due to the availability of additional internal water that is not part of the mixing water [2, 3]. The internal curing for concrete can be performed using several materials but the use of shrinkage-reducing admixture like propylene glycol type and polyethylene glycol products in the concrete mixtures, has been recently advised to reduce the cracks in concrete construction caused by drying shrinkage [4]. The mechanism of this admixture based on the reduction of the surface tension of the mixing water as a physical change rather than on a reduction of water evaporation. When using polyethylene type of curing agent, the polyethylene glycol with average molecular weight 400 is more preferred rather than any other molecular weight [5].

Some manufacturing properties of concrete can also be extend by the use of fibers as an additional material within the concrete mixture. The foremost beneficial characteristics of fiber-reinforced systems are those of inflated flexural capability, toughness, post-failure ductility and crack management. The type of fiber and its volume fraction contains a marked impact on the properties of fiber reinforced concrete [6]. Hooked-end fibers had the highest compressive and flexural strengths, compared with straight fibers and corrugated fibres. This is because hooked-end steel fibers provide better mechanical interlock compared with other shaped fibers [7]. Workability of reinforced concrete mixture is dramatically decreased for fibers with aspect ratio of 80 and volume of fiber of 1.0 and 1.5%. Usage of steel fiber in concrete significantly increases the split tensile and flexural strength of concrete and ultrasonic pulse velocity of SRFCs decreased with fiber content [8].

An effort has been made in this research to investigate the effect of different percentage of self curing agent on mechanical properties of fly ash based M40 concrete where cement is replaced by 20% of fly ash. M40 concrete was chosen since it has been recently advised for creating external walls and slabs as well as for structural pilings etc. The self-curing agent used is polyethylene glycol 400 (PEG), varied by 0.5, 1, 1.5 and 2% by weight of binder content and the effect of hooked end steel fibres with different ratios on mechanical properties are determined. The different percentages of steel fiber taken are 0.5, 1, 1.5 and 2% by volume of concrete.

Table 1 Physical properties of cement

Sl. No.	Characteristics	Values obtained
1	Specific gravity of cement	3.15
2	Standard consistency of cement	32%
3	Initial setting time of cement	55 min
4	Fineness of cement	5%

Table 2 Physical properties of Master Glenium B233

Aspect	Dark brown free flowing liquid
Relative density	1.24 ± 0.02 at 25 °C
PH	>6
Chloride ion content	<0.2%

2 Materials

To carry out this study, ordinary Portland cement of 53 grade and fly ah of class F were selected. Tests on cement was conducted as per IS: 12269-1987 and the results are reported in Table 1. The 20% of cement is replaced by fly ash of specific gravity 2.3. Coarse aggregates with a maximum size of 20 mm were used. Coarse aggregates was tested as per IS: 383-1970. The specific gravity of coarse and fine aggregate were 2.68 and 2.72. The sand used for the experimental program was conformed to grading zone II according to IS: 383-1970. The self curing agent taken for the study was of chemical type PEG 400.

Super plasticizer used is Master Glenium. The superplasticizer dosage is adjusted to produce concretes with the same slump of 120 ± 10 mm and do not show visual signs of segregation during the normal casting of concrete in the moulds. Physical properties of Master Glenium B233 is given in Table 2. Water content can be a reduced by 20% by using superplasticizer. As the water cement ratio decreases strength of concrete increases. Hooked end steel fibres of length 25 mm, 0.5 mm dia (aspect ratio −50), tensile strength of 500 MPa, density of 7900 kg/m^3 and youngs modulus of 2×10^5 N/m^2 was taken for the study.

3 Mix Design and Procedure

Mix design can be defined as the method of selecting suitable concrete materials and deciding their relative proportions as economically as possible with the object of producing concrete of required minimum strength, workability and durability. The mix proportions were carried out using IS: 10262-2019. The proportions of concrete batches were tabulated in Table 3.

All of the dry constituents were blended for 2 min to ensure the blend was consistent. During mixing, half of the mixing water was gradually added and then the

Table 3 Mix proportion of M40 grade concrete for 1 cubic meter

Cement (kg)	Fine aggregate (kg)	Coarse aggregate (kg)	Water (kg)	Fly ash (kg)
331	672	1187	158	82.8

remaining water with SP was added. However in the case of self curing concrete, polyethylene-glycol was added gradually during mixing. Mixing of all constituents continued for a period of 2 min. For each mix the SP content was balanced to achieve the necessary workability without segregation. For steel fiber reinforced self-curing concrete steel fibres are added during dry mixing for 2 min then the self-curing agent, SP and water were added accordingly. After the moulds were filled with concrete and compacted, the concrete surface was levelled and kept for 24 h in laboratory conditions while plastic sheets covered the surfaces of the moulds. Then demoulded normal concrete was water cured while the self-curing concrete and the steel fiber reinforced self-curing concrete were kept in dry air (25 °C) during the experiment in a laboratory.

SCUC 0, SCUC 0.5, SCUC 1, SCUC 1.5 and SCUC 2 represents the fly ash based M40 concrete with 0%, 0.5, 1, 1.5 and 2% of PEG respectively and SCUC SF 0.5, SCUC SF 1, SCUC SF 1.5 and SCUC SF 2 represents the fly ash based fiber reinforced self curing concrete.

4 Results and Discussion

4.1 Workability of Concrete

The workability of fresh concrete was determined using slump test as per IS: 1919-1959. The slump value of reference concrete was 78 mm. The slump values of SCUC 0.5, SCUC 1, SCUC 1.5 and SCUC 2 were 83 mm, 91 mm, 98 mm and 108 mm respectively, Workability increases with the increase in addition of PEG, this may be due to the availability of sufficient moisture content. It can be seen that hooked-end steel fiber incorporated into the concrete affects the flowability compared with the self curing concrete. The workability decreased to 77, 69, 58 and 46 mm for 0.5, 1, 1.5 and 2% of steel fibre content. This might be due to that the dispersion of the steel fiber in fresh concrete will form a fiber-cement matrix network in which the cement mortar wraps around the fiber to form a fiber–matrix interfacial bonding. The network restricts the flowability of fresh concrete.

4.2 Compressive Strength of Concrete

The compressive strength of concrete was assessed by crushing to the destruction of the test cubes by means of compression testing machine according to IS 516:1959 (Reaffirmed 2004). Figures 1 and 2 shows the change in compressive strength with different ratios of PEG and steel fibres in 7 day and 28 day from the results obtained from the test.

The compressive strength of reference concrete was 32.57 and 48.4 in 7 day and 28 day respectively. And it is seen that with addition of PEG at 0.5% the compressive strength decreases to 31.67 in 7 days and 47.49 in 28 day respectively. With 1% of PEG the strength increases to 33.97 in 7 day and 49.02 in 28 day respectively. It then decreases to 32.73 and 31.86 in 7 day and 48.35 and 47.23 in 28 day with 1.5% and 2% addition of PEG respectively. Thus it indicate that the 1% PEG is the optimum ratio. Again with the addition of steel fiber it is noted than the compressive strength

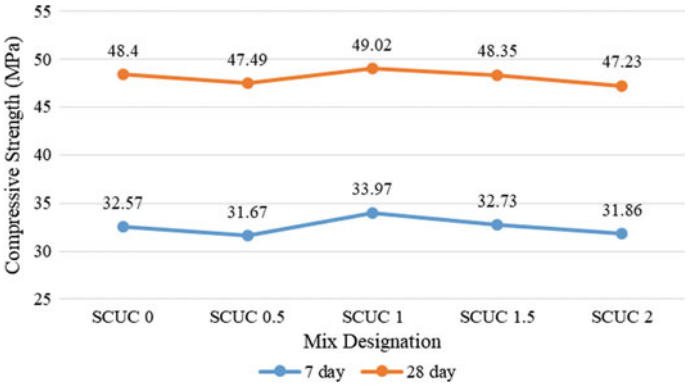

Fig. 1 Effect of PEG in compressive strength of concrete

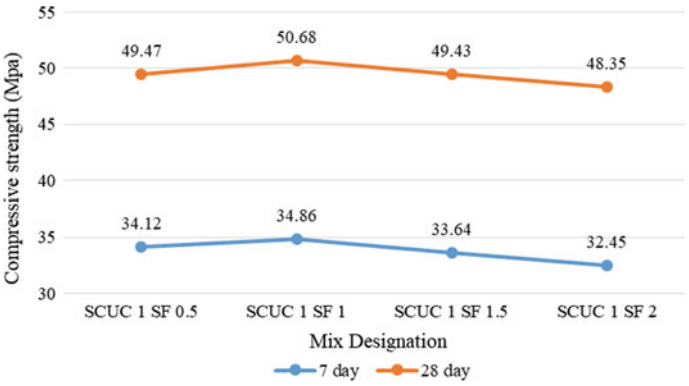

Fig. 2 Effect of steel fibres in compressive strength of self curing concrete

increases to 34.12 and 34.86 in 7 day and 49.47 and 50.68 in 28 days with the addition of 0.5%, 1% steel fibres and then decreases to 33.64 and 32.45 in 7 day and 49.43 and 48.35 in 28 day with 1.5% and 2% of steel fibres respectively. This that indicates that 1% steel fiber is the optimum percentage with respect to compressive strength.

4.3 Split Tensile Strength

Splitting tensile strength test on the concrete cylinder is a method to determine the tensile strength of concrete as per IS 5816: 1999 (Reaffirmed 2004). Figures 3 and 4 shows the changes in split tensile strength with different ratios of PEG and steel fibres in 7 day and 28 day from the results obtained from the test. The tensile strength of conventional concrete was 3.16 at 7 day and 4.37 at 28 day. When PEG was added at 0.5% the strength decreased to 3.02 at 7 day and 4.25 in 28 day. It then increases to 3.42 at 7 day and 4.68 at 28 day. But with increase in percentage of PEG i.e., for 1.5% and 2% the strength decreases to 3.31 and 3.12 in 7 day and 4.52 and 4.39 in

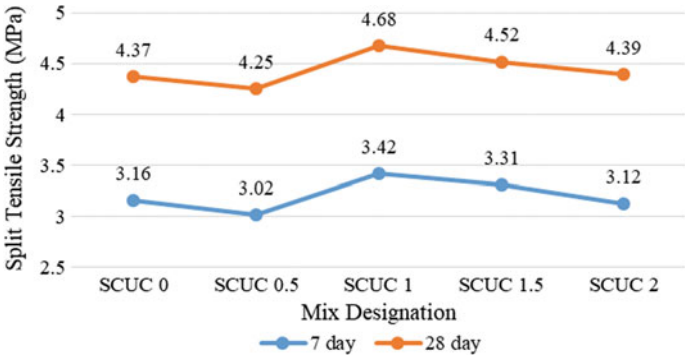

Fig. 3 Effect of PEG in split tensile strength of concrete

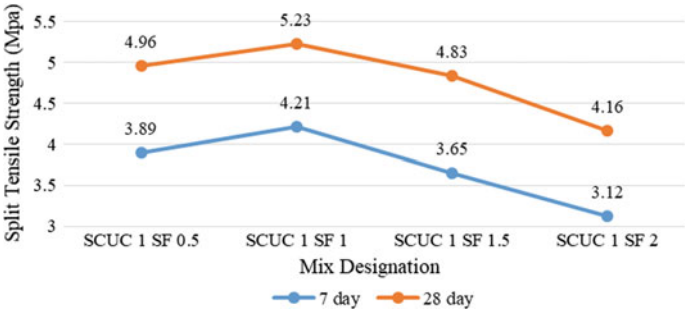

Fig. 4 Effect of steel fibres in split tensile strength of self curing concrete

28 day respectively. Again with the addition of steel fiber it is noted than the tensile strength increases to 3.89 and 4.21 in 7 day and 4.96 and 5.23 in 28 days with the addition of 0.5%, 1% steel fibres and then decreases to 3.65 and 3.12 in 7 day and 4.83 and 4.16 in 28 day with 1.5% and 2% of steel fibres respectively. Indicates that the 1% steel fiber is the optimum percentage with respect to split tensile strength.

4.4 Flexural Strength

The flexural test was conducted as per IS 516:1959 (reaffirmed on 2004). Figures 5 and 6 shows that, concrete with self curing agent and steel fibres exhibited a higher flexural strength at early ages compared with concretes without PEG and steel fibres. The flexural strength of reference concrete was 4.43 at 7 day and 5.56 at 28 day. As

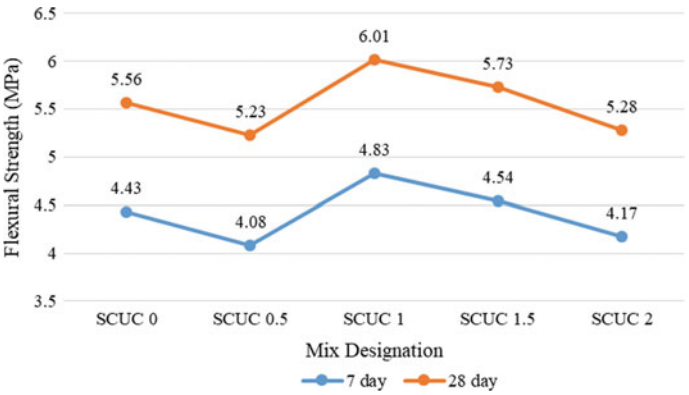

Fig. 5 Effect of PEG in flexural strength of concrete

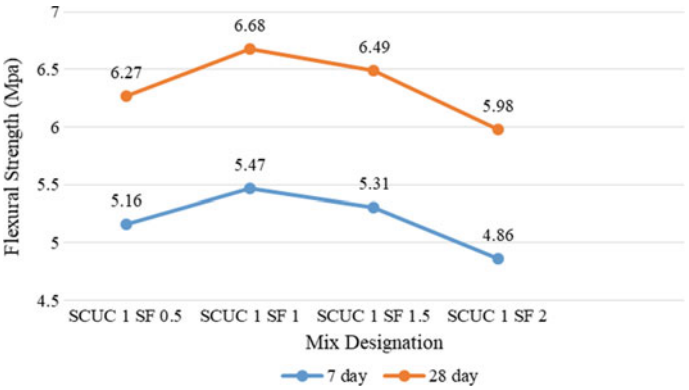

Fig. 6 Effect of steel fibres in flexural strength of self curing concrete

self curing agent PEG was added at 0.5% the strength decreased to 4.08 at 7 day and 5.23 in 28 day. It then increases to 4.83 at 7 day and 6.01 at 28 day. But with increase in percentage of PEG i.e., for 1.5% and 2% the strength decreases to 4.54 and 4.17 in 7 day and 5.73 and 5.28 in 28 day respectively. Again with the addition of steel fiber it is noted than the strength increases to 5.16 and 6.27 in 7 day and 6.27 and 6.68 in 28 days with the addition of 0.5%, 1% steel fibres and then decreases to 5.31 and 4.86 in 7 day and 6.49 and 5.98 in 28 day with 1.5% and 2% of steel fibres respectively. Indicates that the 1% steel fiber is the optimum percentage.

5 Conclusions

Based on the experimental investigation conducted in this work, the following conclusions were drawn.

- Self curing concrete with PEG as self-curing agent and fly ash as partial replacement of cement has a slump in the range of 83-08 mm. Workability increases with the increase in addition of PEG, due to the availability of sufficient moisture content. But the workability of fiber reinforced self curing concrete decreases with increase in fiber content. Fiber content of 1, 1.5 and 2% shows dramatically decreased by 77–46 mm.
- The use of self curing agent in concrete mixes improved the mechanical properties of concrete under air regime. The test result shows that the PEG with 1% has the optimum content among the values examined (0.5, 1, 1.5 and 2%).
- The self curing agent with 1% PEG has higher compressive, flexural and tensile strength about 1.2%, 6.7% and 7.5% than the reference concrete respectively.
- The use of steel fibres in self curing concrete mixes also improved the mechanical properties of concrete under air regime. The test result shows that the steel fibres with 1% has the optimum content among the values examined (0.5, 1, 1.5 and 2%).
- The steel fiber with 1% by volume of concrete has higher compressive, flexural and tensile strength about 4.4%, 16.4% and 16.8% respectively.

References

1. Chaitanya CVK, Prasad P, Neeraja D, Ravitheja A (2015) Effect of LECA on mechanical properties of self-curing concrete. Proc Mater Today
2. Mousa MI, Mahdy MG, Abdel-Reheem AH, Yehia AZ (2015) Mechanical properties of self-curing concrete. Hous Build Natl Res Cent J 11:311–320
3. Mousa MI, Mahdy MG, Abdel-Reheem AH, Yehia AZ (2015) Physical properties of self-curing concrete. Hous Build Natl Res Cent J 11:167–175
4. Mousa MI, Mahdy MG, Abdel-Reheem AH, Yehia AZ (2015) Self curing concrete types; Water retention and durability. Alex Eng J 54:565–575

5. Kamal MM, Safan MA, Bashandy AA, Khalil AM (2018) Experimental investigation on the behaviour of normal strength and high strength self-curing self-comparing concrete. J Build Eng 16:79–93
6. Kalpana M, Tayu A (2019) Light weight steel fibres reinforced concrete: a review. Proc Mater Today
7. Wu Z, Shi C, He W, Wu L (2016) Effects of steel fiber content and shape on mechanical properties of ultra high performance concrete. Constr Build Mater 103:8–14
8. Yazici S, Inan G, Tabak V (2007) Effect of aspect ratio and volume fraction of steel fiber on the mechanical properties of SFRC. Constr Build Mater 21:1250–1253

Effect of Communication Patterns in Safety Performance of Construction Workers

Reshma Geordy, M. B. Sridhar, and J. Sudhakumar

Abstract Safety in construction is crucial to avoid fatal accidents. To enhance safety in construction sites it is necessary to recognize the causes of accidents and take proper measures. It is necessary to make workers aware of such hazards which is possible through trainings, meetings, toolbox talks, communication among workers etc. Indian construction sites which have a diverse language speaking work force will have difficulty in communicating efficiently. This paper tries to identify the major causes of accidents in construction sites and to analyse the communication patterns of the workforce using Social Network Analysis (SNA) in the construction sites of Chennai. The study also measures the safety performance of the workforce and compare it with the network characteristics identified through SNA. The study would thus help to recognize all the safety issues and to measure the current safety condition of the Indian construction Industry

Keywords Safety performance · Construction · Hazard recognition · Safety communication

1 Introduction

Indian construction industry is the second largest employment sector with an employment rate of 51.5% in the year 2016 [1]. The reports show that construction industry contributes to an increased GDP rate of 2379 INR billion in the year 2018 from 2198 INR billion in 2017 [2]. Even though there is a tremendous growth in the construction

R. Geordy (✉) · J. Sudhakumar
Department of Civil Engineering, NIT Calicut, Kozhikode, India
e-mail: reshmageordy5@gmail.com

J. Sudhakumar
e-mail: skumar@nitc.ac.in

M. B. Sridhar
Department of Civil Engineering, SRM Institute of Science and Technology, Kattankulathur, India
e-mail: m.bsridhar@yahoo.co.in

© Springer Nature Switzerland AG 2021

K. Dasgupta et al. (eds.), *Proceedings of SECON 2020*,
Lecture Notes in Civil Engineering 97,
https://doi.org/10.1007/978-3-030-55115-5_72

industry, work space safety is given least importance. Reports show that in the year 2016, 2302 fatal and non-fatal accidents had occurred in Indian construction sites. This statistical report shows only the number of accidents which are recorded, as in a country like India construction companies maintain little or no official records of accident statistics on occupational health and illness []. In this context attempts were made by [3] to collect data regarding occupational accidents from state and government agencies but found that some of the data were underestimated. Whereas Statistics show that other developed countries like USA and UK which follows standards like OSHA have very high accident rates with a fatality of 4693 for private industry in the year 2016 [4]. Therefore, Safety in the construction sites of India must be looked at different perspective. Considering the importance of safety on construction sites Government, Clients, Consultants have spent a great deal of time and effort attempting to evolve legislation, rules and regulations to help to reduce the loss of life and high number of lost work days which include Building and other construction workers act 1996, Building and other construction workers central rules 1998, Building and other construction workers welfare cess act 1996 and many more. The recent researches show that construction industry has very high accident rates across the world; as a result, every construction industry needs to employ stringent measures to minimize the number of incidents [5].

The legislation alone cannot reduce the accidents rate unless operational and management team take some positive actions to integrate these rules into their everyday activities by implementing safety management programme. To avoid such accidents safety professionals recommend conducting safety meetings, toolbox meetings, training to identify safety hazards prior to starting of an activity and incentives for best safety performance [6, 7]. The studies showed that safety performance was affected by the actual safety programs [8]. Improper safety measures can affect the construction workers as well as the management because it can lead to injuries and cause financial loss to management. Moreover, proper safety and health management can improve employee retention [9]. Safety management plays a major role in the success of the projects in order to minimize additional costs and delays [5]. In order to reduce workplace accidents, safety professionals have identified various factors affecting safety in construction sites, among them Hazard recognition was identified as the most effective method [10]. Studies reveal that construction site accidents occur due to lack of hazard recognition performance by management, workers, and supervisors [6, 7, 11]. Moreover, studies revealed that workers who identify hazards and communicate effectively have high safety performance [12]. However, site safety meetings and communication can be difficult in a country like India where language and cultural differences exist among workers.

1.1 Safety Communication

The identification of factors affecting safety along with communication of hazards are effective in improving the safety management [13]. Even though the workers

identify the factors affecting safety, they do not communicate the hazards effectively. Therefore, Effective communication among workers is essential to prevent accidents in construction sites [14, 15]. As per US Department of Labour, safety communication gap due to language barriers, and cultural differences among workers lead to high rate of accidents in construction sites.

In India, construction site workers are mostly illiterates and unskilled who migrate from different part of the country in search of job. The workers employed in a project are from different culture and speak different languages. Therefore, it is necessary to identify the views of these diverse workers as well as management in Indian construction industry towards safety and its effect on safety performance. This helps to identify and analyse the critical factors and causes that affect the occurrence of accidents in the construction industry of India. Along with this, SNA is used to study the safety communication patterns among members in construction sites of Chennai. It also aims to study and visualize the network pattern and measure safety communication and safety performance.

2 Literature Review

2.1 Social Network Analysis (SNA)

Social Network Analysis (SNA) is the most effective method adopted by professionals to measure the safety communication within crew members of a site [7, 14]. Social Network Analysis was first developed by Jacob Moreno in 1934 to study the social interactions of groups. Moreno (1960) defined SNA as, "A quantitative analytic tool used to study the exchange of resources among different groups." It is also defined by Haythornthwaite (1996) as "An approach and set of techniques used to study the exchange of resources among actors." The main advantage of SNA is to identify social network patterns among members [16]. In addition, SNA analyses the structure of these patterns and identifies their effects on individual behaviour. SNA is being used as a research method in many fields of sciences to develop the relationships among different members within organizations. The relationships can be an information exchange, safety knowledge or work-related communication, strength or weakness of members [17]. In addition, SNA is a useful technique for researchers to visualize the network patterns among members.

Social network data consists of actors, relationships among members, and characteristics of each member in the network. In order to analyse a social network, it is essential to draw a network diagram with relationships between each member. The social network data can be visualized by sociograms, which illustrate the connections among participants of interest [16]. Social network model contains nodes representing members and the links between members represent the relationship between them.

3 Research Methodology

3.1 Factors Affecting Safety in Construction Sites

The research is started with a proper review of relevant papers based on safety in construction sites. The study identified the factors affecting construction site accidents. The questionnaire consisted of 37 questions related to causes of accidents in construction sites which were grouped into 8 main factors. The factors considered were (1) demographic factors, (2) workers behavioral factors, (3) site-related factors, (4) protective gear and equipment factors, (5) communication factors, (6) organizational factors, (7) awareness factors and (8) environmental factors. The survey is conducted among engineers, safety professionals, contractors and workers in construction sites of Chennai. The respondents were approached personally and the details were collected and they took 20 min to fill each form. The collection of survey started by enquiring the demographic details of each respondent including name, age, experience, and position in the company. Among 200 questionnaires circulated, 65% (N = 130) responses were returned which were used for analysis. A total of 54.61% responses were obtained from management and 45.3% were received from workers. Different category of responses was collected to check the difference in opinion regarding each statement.

The responses are collected on a Likert scale with 5 = "Strongly agree", 4 = "Agree", 3 = "Moderate, 2 = "Disagree" and 1 = "Strongly Disagree". A Likert scale response was collected to check how strongly each respondent agree or disagree a statement. The respondents were asked to indicate the types of safety measures taken in each construction sites where they work. The data were then coded and analyzed using the software package SPSS. The data collected from the questionnaire are analyzed using the tools like descriptive statistics, independent sample t test, and relative importance index.

The social network analysis is done using UCINET 6 is the software package used for the analysis. It helps to analyze as well as visualize the networks with the help of NetDraw [18, 19]. Once the data for analysis is obtained it can be entered into the software either by importing the excel file containing data or through spreadsheets available within the software. Usually square matrix is used the data in the matrix is coded as binary numbers (0^s and 1^s). The NetDraw feature in UCINET helps to visualize the network.

3.2 Frequency Rate

One of the aim of the project is to measure the Frequency rate of accidents of the workers and compare it with network characteristics. It helps to differentiate between low performing and high performing groups. The Frequency Rate can be obtained from the recordable injury rate and total man hours worked by each crew of the company.

$$\text{Frequency Rate} = \frac{Total\ Number\ of\ recordable\ accidents}{Total\ Man\ hours\ worked} \times 10^6 \quad (1)$$

4 Results and Discussion

The factors affecting safety in construction sites were evaluated and ranked using Relative Importance Index (RII). The relative importance index is a most popular measure to identify the importance of factors among the group of factors. RII finds the extent of the contribution of the various factors identified as factors affecting safety on construction sites. RII can be measured by calculating the ratio weighted sum each response to the maximum possible score i.e., (5 in this case) The formula for calculating RII was given by Fagbenle et al. (2004), which is shown below:

$$RII = \frac{\sum W_i U_i}{N(n)} \quad (2)$$

where,

RII relative importance index;
Wi Rating of the respondent's;
Ui number of respondents placing identical weighting;
N sample size; and n = the maximum possible score.

In the analysis, the relative importance index was calculated for all the factors affecting safety in construction sites. Workers behavioral factor (0.87) have the highest RII value. The maximum value of RII was 0.93 obtained for "Workers under influence of drugs and alcohol" are more prone to accidents. The Negligence to safety rules with RII 0.92, Irresponsible attitude of the workers while handling machines and Carelessness of workers while working at height have very high with RII value 0.91. Risk of injuries increase with age was the lowest rated factor with RII of 0.67. Hence, the results reveal that construction sites should monitor the workers behavior towards safety, provide safety training before every activity so that workers do no neglect the rules and helps to generate a positive attitude towards safety practices. Top three factors and its implications are described below. The RII results are shown in Fig. 1.

Workers behavioral factor and Safety

The study revealed that worker under the influence of drugs and alcohol have high risk of injuries in construction sites. At the same time, negligence to safety rules, carelessness and irresponsible attitude also have high risk rates. Health and safety authority say that "causes of accidents depends on how we do it and not on what we did". Hence the study highlights that's that workers perception towards safety is to be improved to reduce risk rates. Workers behavior can be improved by behavior-based

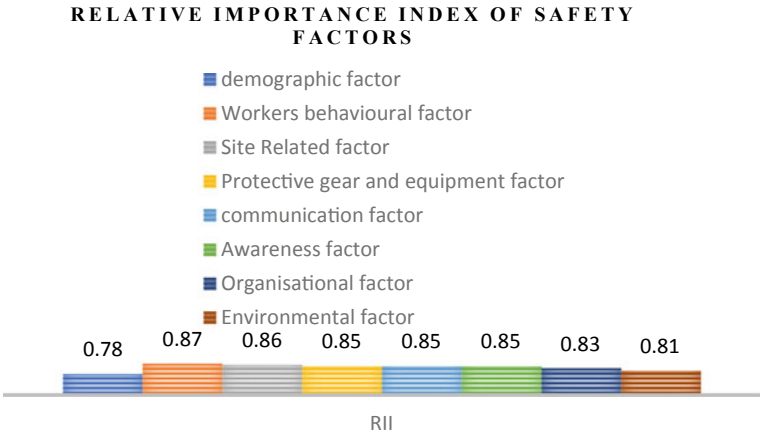

Fig. 1 RII of factors affecting safety

safety and an approach based on culture. Studies are conducted based on behavior-based safety and ergonomics of workers to identify actions or behaviors which lead to accidents.

Site Related factors and safety

Site related factors have considerable effect on causing accidents in construction sites. The study concede that construction practices have considerable effect on safety, as well as improper use of tools and machines. 91% of respondents indicated that Improper use of tools and machines can lead to accidents. The interaction with workers indicated that many construction sites do not provide enough training prior to use of tools and machines. Use of ladders and safety nets are not available in most of the sites. The study suggests to provide proper training and establishment of health and safety associations for every work site.

Communication factor and Safety

Indian construction sites consist of diverse work forces. Most of the construction sites in study area employee workers from northern part of India. The supervisors and other local workers find it difficult to communicate properly and convey appropriate messages. 76% of responses indicate that language barriers among workers can lead to accidents and 82% responded that they do not receive proper communication on safety practices from safety managers. Researches recommends that frequent and open communication about safety shall be conveyed to workers to improve work site safety (CPWR 2014).

From the test results we can infer that at 5% level of significance, the p value is greater than 0.05 in all cases, thus the null hypothesis is accepted (Table 1). There is no significant difference between category of employees and demographic

Table 1 t test for significant difference between category of employees and factors affecting safety in construction

	Management	Workers	T value	*p*
	Mean	Mean		
Demographic factors	3.94	3.78	1.967	0.051
Workers behavioural factors	4.35	4.32	0.292	0.770
Site related factors	4.36	4.36	−0.020	0.984
Protective gear and equipment factors	4.23	4.21	0.233	0.816
Communication factors	4.28	4.22	0.653	0.515
Organisational factors	4.19	4.06	1.323	0.188
Awareness factors	4.32	4.19	1.270	0.206
Environmental factors	4.08	3.95	1.520	0.131

factors, workers behavioural factors, site related factors, protective gear and equipment factors, communication factors, organisational factors, awareness factors and environmental factors. Hence it can be concluded that there is no difference in opinion regarding factors affecting safety in construction sites by employees at management level and workers level. The test result reveals that the factors considered in this study is relevant and both categories of employees equally suggest that these factors can lead to accidents in sites.

Investigating the factors affecting safety in construction sites helps to identify all the major causes of accidents and help in improving safety performance. The result reveals that Communication factor have high impact on safety performance with a RII value of 0.85.

4.1 Social Network Analysis

The study was focused on calculating the network characteristics and to calculate safety performance of each the crews. Previous studies revealed that Crew with high network density outperforms other crews with lower network density [7]. The results of this study show that the top performing crews have higher network density. The work type and No. of workers in each crew are shown in Table 2.

4.2 Network Density

The network density of each crew represents the relationship and how well each member are connected [18]. The network densities for each of the crew members were analysed. The network density values can range from 0 to 1. The crew in which all the members have two-way communication are said to be well connected and

Table 2 Crew demographics

Crew No.	Work type	No. of workers
1	Concrete work	12
2	Carpenter	12
3	Concrete work	10
4	Helper	10
5	Equipment operators	7
6	Fitter	8
7	Steel work	14
8	Shuttering work	11
9	Electrical work	10
10	Plumbing	9

the network density will be 1. On the other hand, crew members with no communication have network density of 0 representing no ties or relationship. In the study, Fig. 2 represents crew 7 with highest network density value of 0.841, whereas Fig. 3 represents crew 8 with lowest network density of 0.091. Crew 7 have the highest density because the crew have a greater number of site supervisors who are the main communicators. Previous studies have revealed that supervisors play more central role in communicating safety related information's [14]. The network density and the accident frequency rate of the crews is shown in Table 3.

Using the network density and the accident frequency rate a linear regression analysis was done to test the hypothesis that network density and accident frequency rate have a significant relationship. The results of the hypothesis testing are shown in Table 4. It reveals that the network density and accident frequency rate are statistically significant indicating that the crews with highest density have least accident frequency.

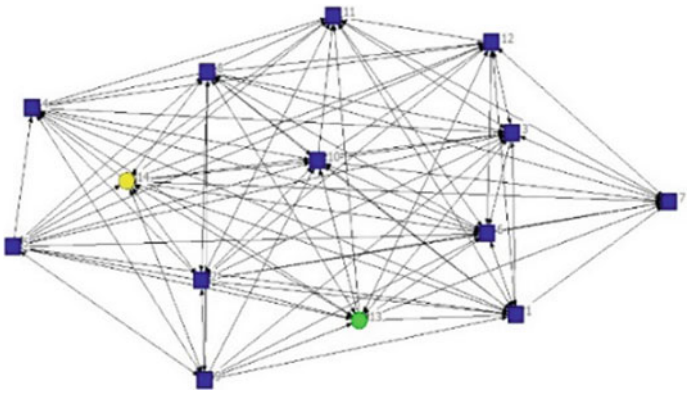

Fig. 2 Network diagram of crew 7

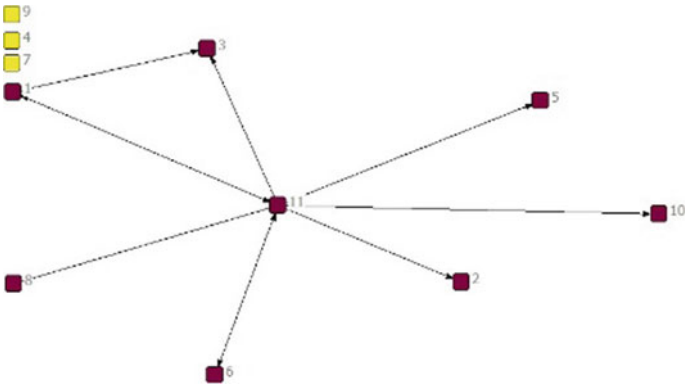

Fig. 3 Network diagram of crew 8

Table 3 Network density and accident frequency rate

Crew No.	Network density	Frequency rate
1	0.667	22.26
2	0.212	44.52
3	0.211	53.42
4	0.778	26.71
5	0.262	38.15
6	0.482	33.39
7	0.841	19.08
8	0.091	48.56
9	0.289	26.71
10	0.431	29.68

Table 4 Linear regression analysis of network density and accident frequency rate

Model	Regression Coefficient	Standard Error	T value	*P* value	r^2
Constant	50.1	4.20	11.846	<0.01	0.66
Network density	−37.3	8.60	−4.336	<0.05	

4.3 Degree Centrality of Crews

Centrality represents the total number of relationships an actor has with other actors in the network. The actors who have higher relationships with other actors play more central role in the crew [20]. The Outdegree centrality represents the flow of information from an actor and In-centrality represents the information received by an actor. The degree centrality values and Accident frequency rate of each actor is depicted in Table 5. A crew with high percentage of centralization show that there

Table 5 Centrality and accident frequency rate

Crew No.	Indegree centralization	Outdegree centralization	Frequency rate
1	0.3636	0.3636	22.26
2	0.7603	0.4628	44.52
3	0.7531	0.1358	53.42
4	0.2469	0.1235	26.71
5	0.2778	0.0833	38.15
6	0.2653	0.4286	33.39
7	0.1716	0.0888	19.08
8	0.6700	0.1200	48.56
9	0.4198	0.4198	26.71
10	0.2188	0.3594	29.68

Table 6 Linear regression analysis of centrality and accident frequency rate

Model	Regression Coefficient	Standard Error	T value	*P* value	r^2
Constant	16.8	4.7	3.59	<0.01	0.65
In centrality	42.1	10	4.21	<0.05	
Constant	37.0	7.6	4.87	<0.01	−0.10
Out centrality	−10.5	25.3	−41.5	0.68	

is less percentage of actors with high number of relationships with other actors. On the other hand, crew with less percentage of centralization have equally distributed percentage of actors with high percentage of relationship with others [14, 19].

The relationship between degree centrality and accident frequency rate is tested using Linear Regression analysis with the hypothesis that a significant relationship exists between Degree Centrality and Accident Frequency Rate. The centrality values reveal that the amount of information provided by the crew members are less compared to the information received by each crew member as most of the crew members are unilingual. The results also reveal that In-centrality and Accident frequency rate have statistically significant relationship ($p < 0.05$), whereas out-centrality and Accident frequency rate have no significant relationship (Table 6).

4.4 Betweenness

Betweenness is the measure of data that must flow from a particular actor who lies between two other actors. In another word, this metric shows the aggregate number of events when a particular actor is required to associate two unique actors in a system [19]. Actors having high betweenness centrality when they connect with other actors in shortest path [20]. The betweenness centrality and accident frequency rate of each

Table 7 Betweenness and accident frequency rate

Crew No.	Betweenness	Frequency rate
1	12.15	22.26
2	12.23	44.52
3	40.59	53.42
4	1.82	26.71
5	14.44	38.15
6	12.93	33.39
7	0.62	19.08
8	14.78	48.56
9	1.70	26.71
10	38.17	29.68

Table 8 Linear regression analysis of betweenness and accident frequency rate

Model	Regression Coefficient	Standard Error	T value	*P* value	r^2
Constant	27.5	4.9	5.64	<0.01	0.22
Betweenness	45.5	24.3	1.87	0.09	

crew is represented in Table 7. The significant relationship between betweenness and accident frequency rate is tested using linear regression analysis. The results are represented in Table 8 which reveals that betweenness and accident frequency rate does not have significant statistical relationship and is not an indicator of safety performance.

Relevant studies reveal that bilingual work crews play more central role in communicating and removes barrier in communication. A statistical test was conducted to test whether bilingual workers play more central role in a crew. To test the hypothesis, all the actors in the crews were divided into bilingual and unilingual workers. As all the site supervisors are bilingual workers, they are not considered for the study. The sample considered for the study are unequal (74 unilingual workers and 20 bilingual workers) therefore, Mann Whitney 2 sample t test is used to test the hypothesis. The results are represented in Table 9. The test reveals that average out centrality is 1.88 times greater than unilingual and average in centrality is 1.78 times greater than unilingual workers. This show that bilingual workers provide more amount of safety information than they receive such information.

Table 9 Mann Whitney 2 sample test

SNA metric	Unilingual	Bilingual	Difference	*P* value
Avg. out centrality	0.422	0.797	0.375	0.000
Avg. in centrality	0.445	0.795	0.320	0.000
Betweenness	0.029	0.045	0.016	0.243

5 Conclusion

The aim of the study was to identify all the factors affecting safety in construction sites, most commonly used safety measures and to measure the communication patterns among workers and their effect on safety performance. The findings suggest that the employee's perception towards factors affecting safety do not change based on their position in work environment. Both the categories believe that the factors considered in the study are of significant importance.

The relative importance index analysis results revealed that workers under the influence of drugs and those who neglect safety rules are prone to accidents. Therefore, concluded that workers behavioural factors have more importance in affecting safety in construction industry. So more detailed study is required in monitoring workers attitude towards safety practices. The SNA results reveal that the crews with highest network density (0.841) have least accident frequency rate. This shows that crews with good tie strength can identify hazards and thereby reduce accident frequency. Whereas, crews with least network density have high accident frequency. In-centrality of crews show that the amount of information provided by the crew members are less compared to the information received by each crew member as most of the crew members are unilingual. Mann Whitney t test result reveals that bilingual workers provide more amount of safety information than they receive such information. Betweenness and accident frequency rate does not have significant statistical relationship and is not an indicator of safety performance.

This study was an effective effort to identify the opinion of management towards factors affecting safety in construction sites, the frequency of safety practices followed in firms and analyse and visualize the safety communication patterns of crews. The study also measured the accident frequency rate of the crews and tested its significance with network characteristics. This study reveals SNA can be an effective tool to be implemented in construction industries of India to evaluate the safety knowledge transfer among workers and how effectively they implement safety in working environment. Further this tool can be used significantly to measure the safety communication patterns among unilingual and bilingual workers and it can be also used at the earlier stages of a project to make preconstruction decisions.

References

1. Ima-india.com (2019) IMA India—IMA India's Published reports. [online] Available at: http://ima-india.com/index.php?option=com_content&view=article&id=650&Itemid=365
2. Ibpsguide.com (2019) India GDP growth rate projection by different financial organizations. [online] Available at: https://www.ibpsguide.com/india-gdp-growth-rate-projection-different-financial-organizations
3. Patel DA, Jha KN Neural network model for the prediction of safe work behavior in construction projects, pp 1–13
4. Anon (2019) [online] Available at: https://www.coursehero.com/file/p53nc44/United-States-Department-of-Labor-2016-maintains-that-the-annual-rate-of/

5. Gunduz M, Laitinen H (2018) Construction safety risk assessment with introduced control levels. J Civ Eng Manag 24(1):11–18
6. Albert A, Hallowell MR, Kleiner BM (2014) Experimental field testing of a real-time construction hazard identification and transmission technique. Constr Manag Econ 32(10):1000–1016
7. Albert A, Hallowell MR (2017) Modeling the role of social networks on hazard recognition and communication. Pract Period Struct Des Constr 22(4):04017016
8. Aksorn T, Hadikusumo BHW (2008) Measuring effectiveness of safety programmes in the Thai construction industry. Constr Manag Econ 26(4):409–421
9. Wilkins JR (2011) Construction workers' perceptions of health and safety training programmes. Constr Manag Econ 29(10):1017–1026
10. Carter G, Smith SD (2006) Safety hazard identification on construction projects. J Constr Eng Manag 132(2):197–205
11. Perlman A, Sacks R, Barak R (2014) Hazard recognition and risk perception in construction. Saf Sci 64:13–21
12. Jaselskis EJ, Asce AM (2016) Improving hazard-recognition performance and safety training outcomes: integrating strategies for training transfer 142(10):1–11
13. Hale A, Borys D, Adams M (2015) Safety regulation: the lessons of workplace safety rule management for managing the regulatory burden. Saf Sci 71(PB):112–122
14. Alsamadani R et al (2013) Relationships among language proficiency, communication patterns, and safety performance in small work crews in the United States 139:1125–1134
15. Törner M, Pousette A (2009) Safety in construction—a comprehensive description of the characteristics of high safety standards in construction work, from the combined perspective of supervisors and experienced workers. J Saf Res 40(6):399–409
16. Eteifa SO, El-adaway IH (2018) Using social network analysis to model the interaction between root causes of fatalities in the construction industry. J Manag Eng 34(1):04017045
17. Comu S, Unsal HI (2011) Dual impact of cultural and linguistic diversity on project network performance. J Manag Eng, pp 179–187
18. Borgatti SP, Everett MG (2006) A graph-theoretic perspective on centrality. Soc Netw 28(4):466–484
19. Borgatti SP, Everett M, Freeman LC (2002) UCINET 6.0 for windows: software for social network analysis, user's guide. Anal Technol Inc., p 47
20. "From G. Scott & R. Garner (2013)," pp 111–124
21. Indiastat.com (2019) growth statistics details figures. [online] Available at: https://www.indiastat.com/faqs/faqs.aspx
22. Moreno JL, Jennings HH (1960) The sociometry reader. Free Press, Glencoe, IL
23. Haythornthwaite C (1996) Social network analysis: An approach and technique for the study of information exchange. Libr Inf Sci Res 18(4):323–342
24. CPWR (2013) The construction chart book: the US construction industry and its workers
25. Fagbenle O, Adeyemi A, Adesanya D (2004) The impact of non-financial incentives on bricklayers' productivity in Nigeria. Constr Build Mater 22:899–911

Development of Pavement Quality SCC Having High Early Strength Under Site Conditions

Shashi Kant Sharma, Kanish Kapoor, Dadi Rambabu, and Mohit Kumar

Abstract Pavement quality self-compacting concrete (PQSCC) incorporating ground granulated blast furnace slag (GGBS), flyash and silica fume has been investigated for early strength development, for various curing conditions. After being tested for workability befitting that of a SCC, the concrete mixes were tested for strength. Three different curing regimes considered are: normal water curing (23 °C), hot water curing at 40 °C, and steam curing at 60 °C. For making the curing procedure possible at site, least possible curing duration was chosen i.e. 8 h per day (2 h after each 4-hour cycle). $CaCl_2$ was also added in permissible limits (1.5% by weight of binding material) to compare the strength gain. Test results indicate that amongst the three curing regimes, steam curing performs well even without $CaCl_2$ incorporation whereas hot water curing must be complemented with $CaCl_2$ to achieve high strength. Both GGBS and flyash based composites perform better with special curing measures but flyash based composites performed much better in presence of $CaCl_2$ accelerator whereas flyash composites need steam curing. These improvements are attributed to two main factors: mix design of pavement quality SCC on basis of combination of high packing density theory and Okamura and Ozawa method, and application of special curing procedure which is subjective to different pozzolans.

Keywords Curing regime · Pavement quality concrete · Self-compacting concrete · Pozzolans · $CaCl_2$

S. K. Sharma (✉) · K. Kapoor · D. Rambabu · M. Kumar
Department of Civil Engineering, NIT Jalandhar, Jalandhar 144001, India
e-mail: sharmask@nitj.ac.in

K. Kapoor
e-mail: kapoork@nitj.ac.in

D. Rambabu
e-mail: dadir.ce.19@nitj.ac.in

M. Kumar
e-mail: mohitmoral@gmail.com

© Springer Nature Switzerland AG 2021

K. Dasgupta et al. (eds.), *Proceedings of SECON 2020*,
Lecture Notes in Civil Engineering 97,
https://doi.org/10.1007/978-3-030-55115-5_73

1 Introduction

There has always been a demand of having a pavement quality concrete which satisfy three major requirements; tensile strength of 4.5 MPa or Compressive Strength of 40 MPa [1], abrasion resistance and smooth surface, and high shrinkage resistance. Use of heavy dose of accelerators promise required strength but it compromises the chloride ion resistance and shrinkage resistance of concrete [2]. The durability properties of the concrete mainly depend on its curing age among the other factors. Porosity and chloride ion penetration of concrete decreases with increase in the curing age [3]. Therefore the literature suggests the use of curing methods which could influence the hydration rate of concrete in such a manner that a high early strength could be obtained with minimal loss of durability [4]. Autoclave curing, hot air curing and electrical curing are a few examples which have been found to increase the early strength of concrete though it was also found that these methods of curing led to the reduction in the fatigue strength and residual strength, and an increase in the porosity of concrete [5]. Steam curing and hot water bath curing have been suggested in the literature to produce a concrete having early strength, high fatigue strength and less porosity [6]. These studies mostly dealt with nano silica or silica fume and minimal amount of flyash or GGBS as their purpose was to achieve high early strength. Low performance mineral admixtures could not be relied for getting high early strength, hence micro/nano silica were used. Also, these studies were focused on drying shrinkage of concrete, which has special significance in rigid pavements. Present study aims to obtain a high early strength SCC made by substituting cement in high amount with mineral admixtures by utilizing the steam/hot water curing at laboratory, and by relying more upon the chemical composition of the mixes (containing high volumes of low performing mineral admixtures) for their reactivity and simultaneously using medium amounts of silica fume to ensure an increase in strength [7]. The SCC in present study has been designed partially after ensuring high bulk density of the aggregate mix and the remaining on the basis of Okamura and Ozawa method [8], which suggests paste volumes for different aggregate mixes to obtain high flow. Properties of mixes passing self-compaction criteria were compared with those of normal pavement quality concrete's, designed as per IRC. The early strength gain has been relied upon the mix design procedure and special curing of different chemical compositions of the trial concrete mixes.

2 Materials and Methodology

2.1 Materials and Theory of Mixing

In the present study Ordinary Portland Cement (43 Grade) has been taken which complies with IS: 8112-1989. Flyash and GGBS are the next important pozzolanic materials used for substituting cement on large scale. Flyash has been chosen to

Table 1 Chemical composition of concrete mixes

Constituents	Chemical Compositions %					
	CaO	SiO_2	Al_2O_3	MgO	Fe_2O_3	SO_3
Cement	63.2	21.8	6.8	2.5	3	1.7
Flyash	5	52.5	22.5	–	11	–
GGBS	39.7	35	12.3	–	1	–
Silica fume	<1	91	<0.5	–	–	–

Table 2 Physical properties of concrete mixes' ingredients

Constituents	Physical properties					
	Specific surface area (m^2/kg)	Particle size (μm)	Specific gravity	Density (kg/m^3)	Colour	LOI
Cement	373	12	3.15	3200	Light grey	1.48
Flyash	390	10	2.17	–	Light grey	1.06
GGBS	455	21	2.90	–	*Dark grey*	*0.98*
Silica fume	19380	0.09	2.24	310	*Dark grey*	*1.14*

enhance the flow ability of concrete whereas GGBS has been chosen because of its sticky nature which serves the purpose of viscosity modifying admixture [6]. Undensified silica fume has been used in the present study which complies with ASTM C 1240-95a and IS: 15388-2003. It has been chosen as it is known to provide high early strength to concrete [9]. The chemical and physical compositions of these materials are present in Tables 1 and 2, respectively.

River bed sand has been used as fine aggregate, conforming to zone IV grading requirement as per IS: 383-1970. For normal pavement quality concrete mix, coarse aggregates of sizes 20 and 12.5 mm have been taken in the ratio 70:30 as per IS: 383:1970 to yield a nominal maximum size of 16 mm and fineness modulus of 7.5. For pavement quality SCC, coarse aggregates of sizes 20, 12.5, 10 and 4.75 mm have been combined with the fine aggregates to obtain a maximum packing density.

2.2 Mix Design

Firstly, maximum bulk density has been obtained for set of coarse aggregates and fine aggregates separately [10]. Afterwards fractions of coarse aggregates and fine aggregates have been combined to obtain a maximum resultant bulk density [11]. In the present study, after conducting trials, it was found that coarse aggregate to fine aggregate ratio of 44:56 yields maximum flowing ability& appropriate bulk density of 1.93 g/cm^3. As aggregates are good in reducing the shrinkage strains in concrete and since their coefficient of thermal expansion is much lower than hydrated cement

pastes, therefore it was decided to enhance the packing density of aggregate mix [12]. This measure reduces the paste demand to induce flow on basis of reduction in voids' volume, in comparison to the mixes containing only open graded aggregate mix. The mix design by present approach does not rely upon using single sized aggregates and therefore distributes the paste equally in between the voids of aggregates which should reduce the shrinkage cracking in concrete [13]. This approach differs from Ozawa and Okamura approach on the basis that it fixes the aggregate content first to obtain benefits related to pavement quality concrete whereas latter's approach improves flow of any kind of aggregate mix by proposing paste volumes to improve packing factor of concrete [14]. The mix design parameters in Table 3 prove that the total aggregate to paste ratio (w/w) does not demand appreciable reduction for yielding PQSCC through this approach. The resulting concrete is tight, cohesive and homogeneous which induces flow.

(i) This approach follows packing density method which has been specified [15] for yielding a low cement normal concrete [16].
(ii) Constant paste volume: After fixing the packing density of combined aggregates, the volume of paste is obtained as unity minus packing density of aggregates. Minimum paste content is calculated as the sum of the void content in combined aggregates and the excess paste over and above the voids to coat the aggregate particle. The water to cement ratio in the paste is chosen on basis of strength, and it decides the amount of cement in the mix. Any possible increment in water demand to meet the workability standards of SCC should be satisfied via use of super plasticizer [17].

2.2.1 Mix Proportions

Normal concrete mix of high strength (M70) has been attempted in the present study to achieve a flexural strength of at least 4.5 MPa after 7 days of curing. A very high cement content of 642.19 kg/m^3 is required in such mix which is much higher than the cement content (450 kg/m^3) required in producing a concrete with flexural strength of 4.5 MPa after 28 days curing as per IRC 44 [18]. If the upper limit of cement content (based on shrinkage resistance criteria) in rigid pavements is neglected then about 575 kg/m^3 of cement would be required to impart 4.5 MPa strength at 7 days as per IRC 44. Therefore it was decided to bring down the cement content much below 575 kg/m^3, even lower than 450 kg/m^3 so that the purpose of obtaining a cheap high strength self compacting concrete could be realized. After finding out the cement content per cum of normal concrete, workability trails were performed on mixes substituting cement primarily with flyash and GGBS @ 10%(up to 20% each) and secondarily with silica fume @ 5% (up to 15%). Hence cement substitution has been done on large scale (maximum up to 55%). GGBS has been coded as G1, G2 and G3 for 10, 20 and 30% substitution levels. Similarly, flyash has been coded as F1, F2 and F3. Silica fume has been coded as S1, S2 and S3 for 5, 10 and 15% substitution levels. Though 10% silica fume levels have been suggested in the literature for medium strength concretes, but the trials have been performed with

Table 3 Mix volumes of NPQC (M70) and trial PQSCC mixes

Mix	W_{pm} (kg/m^3)	W/C	Cement (kg/m^3)	GGBS (kg/m^3)	FA (kg/m^3)	SF (kg/m^3)	W (kg/m^3)	SP (kg/m^3)
C(100)	642.19	0.26	642.19	0.00	0.00	0.00	164.19	12.84
CG3S1 (65, 30, 5)	621.42	0.26	403.92	186.43	0.00	31.07	159.08	12.43
CG3S2 (60, 30, 10)	612.28	0.26	367.37	183.68	0.00	61.23	157.97	12.25
CG3S3 (55, 30, 15)	603.45	0.26	331.90	181.04	0.00	90.52	156.90	12.07
CG2F1S1 (65, 20, 10,5)	600.95	0.26	390.62	120.19	60.10	30.05	159.37	12.02
CG2F1S2 (60, 20, 10, 10)	592.45	0.26	355.47	118.49	59.25	59.25	158.30	11.85
CG2F1S3 (55, 20, 10, 15)	584.19	0.26	321.30	116.84	58.42	87.63	156.56	11.68
CG1F2S1 (65, 10, 20, 5)	581.85	0.26	378.20	58.18	116.37	29.09	158.96	11.64
CG1F2S2 (60, 10, 20, 10)	573.87	0.26	344.32	57.39	114.77	57.39	157.93	11.48
CG1F2S3 (55, 10, 20, 15)	566.12	0.26	311.36	56.61	113.22	84.92	156.93	11.32
CG2F2S1 (55, 20, 20, 5)	578.67	0.26	318.27	115.73	115.73	28.93	158.67	11.57
CG2F2S2 (50, 20, 20, 10)	570.78	0.26	285.39	114.16	114.16	57.08	157.65	11.42
CG2F2S3 (45, 20, 20, 15)	563.11	0.26	253.40	112.62	112.62	84.47	156.66	11.26
CF3S1 (65, 30, 5)	563.92	0.26	366.55	0.00	169.17	28.20	156.88	11.28
CF3S2 (60, 30, 10)	556.42	0.26	333.85	0.00	166.93	55.64	155.91	11.13
CF3S3 (55, 30, 15)	549.13	0.26	302.02	0.00	164.74	82.37	154.96	10.98

15% because GGBS introduces extra lime in the mixture which could be utilized by additional contents of silica fume. The mix volumes of normal pavement quality concrete (NPQC) and trial concretes have been presented in Table 3. The volume of fine & coarse aggregates and binder volume has been kept at 710 and 1060 kg/m^{3,} and 0.21 m^3 in NPQC. In trial mixes, the volume of fine &coarse aggregates has been kept at 965.82 and 758.86 kg/m^3, whereas the binder volume has been decided on basis of void theory and binder requirement for coating of aggregates. Cement substitution with mineral admixtures gives high volume per unit weight thus facilitating higher cement substitution as could be seen in Table 3 for trial mix CF3S3; with a binder weight of 549.13 kg/m^3 and a cement substitution of 340 kg/m^3.

2.2.2 Parameters Studied

Workability

These tests were conducted on fresh concrete mixes as per the guidelines suggested by EFNARC [19]. Flowing ability, passing ability and segregation resistance of trial mixes were checked through Abrams cone flow diameter test, and L Box test respectively. Slump cone test has been performed as per ASTM C 143(2002) in which the "spread" or "flow" of the concrete sample is measured once the cone is lifted. Results have been recorded as T50 time in seconds which is the amount of time the concrete takes to flow to a diameter of 50 cm. Typically, slump flow values of approximately 24–30 in. (600–750 mm) are within the acceptable range; acceptable T50 times range from 2 to 5 s. The L-box value is the ratio of levels of concrete at each end of the box after the test is complete. The L-box consists of a "chimney "section and a "trough "section. After the test is complete, the level of concrete in the chimney has been recorded as H_1; the level of concrete in the trough has been recorded as H_2. The L-box value is simply H_2/H_1. Typical acceptable values for the L-box value are in the range of 0.8–1.0.

Destructive Testing

Since the early strength development of a pavement quality SCC incorporating large volumes of mineral admixtures has not been extensively researched. therefore present study focuses on early strength development of PQSCC under normal (23 °C), hot water bath curing (40 °C) and steam curing (60 °C) with and without the use of accelerator $CaCl_2$ for selected durations of 7 days. It was decided to compare the best curing method out of steam and hot water bath curing (based on 7 days curing results) Normal curing was provided by covering the samples with water (23 °C) soaked jute bags only. Steam curing was performed on otherwise normally cured samples for 8 h in a day i.e. steam curing for two hours after every four hours of normal bur lapped curing. Though, many studies have been performed in the literature with a high frequency of curing intervals, for e.g. 4 h performed curing alternatively

for total 12 h in a day, but in the present study the frequency has been reduced to make the curing conditions possible even at the site.

3 Result

In order to avoid exhaustive exercise of writing various mixes in a given category it has been decided to name the mix categories as C, CG3SX, CG2F1SX, CG1F2SX, CG2F2SX and CF3SX for mixes C, (CG3S1, CG3S2, CG3S3), (CG2F1S1, CG2F1S2, CG2F1S3), (CG1F2S1, CG1F2S2, CG1F2S3), (CG2F2S1, CG2F2S2, CG2F2S3), (CF3S1, CF3S2 and CF3S3), respectively in the results.

3.1 Effect of Mineral Admixture Proportions on Workability of Concrete

3.1.1 Flow Ability

The results of flowing ability tests have been shown in Figs. 1 and 2. It has been observed that almost all types of mix combinations except mixes CG3SX show flowing ability of a SCC. It is quite apparent from the results that GGBS reduces the flowing ability of concrete and it needs flyash or silica fume to increase the flow. Addition of flyash liberates water in the mix due to negative charge carried by its particles which cause repulsion between cement particles when it gets adsorbed over their surfaces. Also flyash has ball bearing effect because of its smooth round shape. Similarly silica fume also has ball bearing effect in the concrete, but it also adsorbs large amount of water over its surface due to its higher surface area and also makes the concrete sticky [20]. Therefore silica fume decreases the flowing ability of

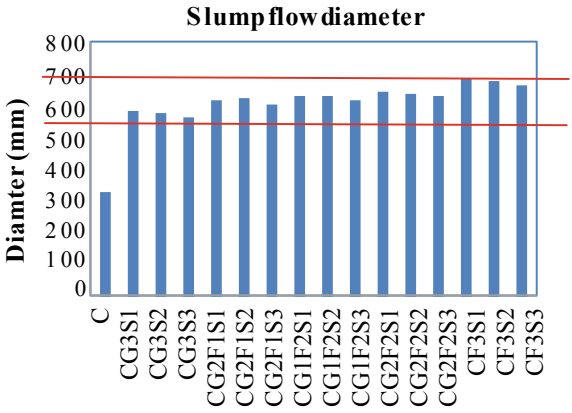

Fig. 1 Result of Slump flow diameter

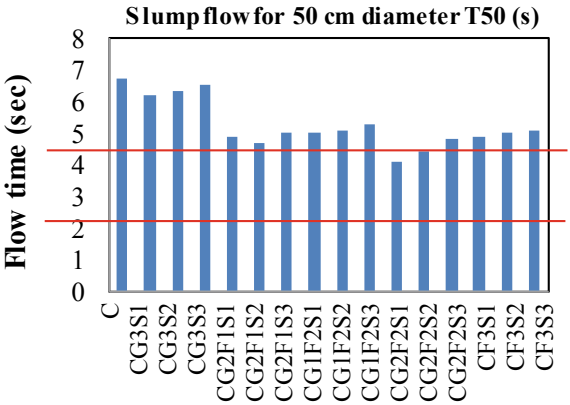

Fig. 2 Result of Slump flow for 50 cm diameter T50 (s)

concrete. The flowing ability of mixes as per flow diameter test varies in the following sequence:

$$\text{CG3SX} < \text{CG2F1SX} < \text{CG1F2SX} < \text{CGF2SX} < \text{CF3SX}$$

This variation clearly shows that flowing ability of mixes increases with flyash content. Mixes CG2F2SX have higher flowing ability than CG1F2SX which indicates that 20% of GGBS and 20% of flyash make tight and homogeneous concrete mixes which increase the flow irrespective of the sticky nature of GGBS [21]. The flowing ability test based on time taken to achieve flow diameter of 500 mm gives quite similar results as normal flow diameter test. In this test also, silica fume was found increasing the flow time of mixes which shows its tendency to reduce the flowing ability of mixes. The flowing ability of mixes as per this test varies in the following sequence:

CG3SX < CG1F2SX < CF3SX < CG2F1SX < CG2F2SX. The unsimilarity in these results from the flow diameter test is based on the reason that the spread rate of concrete is different from the final spread diameter. It was observed that tight/homogeneous mixes with lesser viscosity gave higher flow rate. Mixes CG3SX are not homogeneous as there is a huge particle size gap between GGBS and silica fume. Apart from this GGBS introduce high viscosity in the concrete. Hence mixes CG3SX have least flow rate. Flyash reduce the viscosity of concrete mix which explains the higher flow rate of mixes CG1F2X and CF3SX than mixes CG3SX. Mixes CG2F1SX and mixes CG2F2SX have still higher flow rates as these mixes are very homogeneous. It was observed during the test that these mixes spread uniformly in all directions with equal rates smoothly. Mixes CG2F2SX have highest flow rate owing to higher homogeneity and lesser viscosity than mixes CG2F1SX.

3.1.2 Passing Ability

All of the trial combinations were able to pass the passing ability test which indicates that fine light weight mineral admixtures significantly improve the passing ability of concrete mixes [22]. Amongst these mineral admixtures GGBS is heaviest. Both silica fume and flyash have nearly two third specific gravity values of GGBS. It is very difficult to comment on the variation of passing ability of mixes containing both GGBS and flyash, but since the passing ability of mixes containing 30% GGBS (CG3SX) is lesser than those containing 30% flyash (CF3SX), it would be candid to say that flyash promotes passing ability in comparison to GGBS. L box height ratio H2/H1 value close to 1 indicates better passing ability as concrete has same elevation before and after the obstruction. Looking over this way it could be said that mixes CG2F2SX have the best passing ability followed by CG1F2SX and CG2F1SX. It is conspicuous that mixes CG1F2SX being rich in flyash than mixes CG2F1SX, show correspondingly better passing ability, but CG2F2SX has highest passing ability. This seriously indicates that apart from light weight characteristics of concrete the cohesiveness of concrete is also a major factor which allows the concrete to pass the obstruction altogether. Equal proportions of GGBS and flyash make the concrete just that much light weight and cohesive which promotes best flowing ability, whereas either if GGBS content is increased or flyash content is increased, that would only result in the loss of one or the other property. Silica fume has been found to reduce the height ratio because of its viscous nature which reduces the flow of concrete when it confronts the obstruction. Since mixes have shown just passing value of height ratio upto15% silica fume contents, therefore it is not recommended to use silica fume above 15% (Fig. 3).

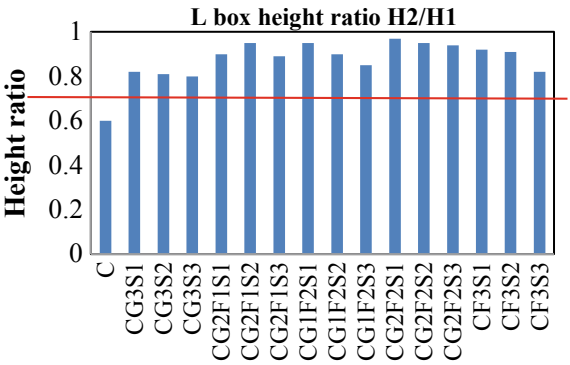

Fig. 3 Result of L box height ratio

3.2 *Effect of Mineral Admixture Proportions on Compressive Strength of Concrete*

3.2.1 Compressive Strength at 7 Days for Normal and Hot Water Curing

The compressive strength variation of different mixes after 7 days of curing (normal and hot water) has been shown in Fig. 3.6. Normal curing with and without $CaCl_2$ led to the following strength variation trends amongst mixes:

CG2F1SX > CG1F2SX > **CG3SX** > CF3SX > **CG2F2SX**
and **CG3SX** > **CG2F1SX** > CF3SX > CG1F2SX > **CG2F2SX**

In case of hot water curing, the strength variation follows this pattern:

CF3SX > CG1F2SX > CG2F1SX > **CG2F2SX** > **CG3SX**

Hence GGBS is best for normal curing whereas flyash is best for steam curing. These patterns are irrespective of $CaCl_2$ which seems to complement the strength equally in both types of curing. All of the mixes except CG3SX mixes showed an early strength of 40 MPa with hot water curing without $CaCl_2$. With $CaCl_2$ and hot water curing all mixes exhibited 40 MPa strength.

These results could be analyzed further in four ways: firstly comparison on basis of difference in normal and hot water curing without $CaCl_2$, secondly comparison on basis of difference in normal and hot water curing with $CaCl_2$, thirdly comparison on basis of difference in normal curing with and without $CaCl_2$, and lastly comparison on basis of difference in hot water curing with and without $CaCl_2$. Following results were obtained from compressive strength analysis at 7 days of curing:

(i) Hot water curing gives high early strength with respect to normal curing in all mixes. Generally, there is a steep rise in early strength values between normal curing without $CaCl_2$ and hot water curing without $CaCl_2$, except in mixes containing higher proportions of GGBS. Flyash and silica fume have complemented each other in giving high early strengths to the mixes when cured with hot water.
(ii) Like the latter case, there is also a steep rise between normal curing with $CaCl_2$ and hot water curing with $CaCl_2$ except in mixes containing higher proportions of GGBS.
(iii) The presence of $CaCl_2$ does not bring much rise in early strength values in case of normal curing. It was observed that in all mixes there was an almost equal improvement in strength values (shown by the blue and green stripes in Fig. 4).
(iv) The presence of $CaCl_2$ brings significant changes in the early strength values in case of hot water curing. In some mixes it increases it a lot, whereas in other mixes it keeps the values equal (shown by the red and purple stripes in

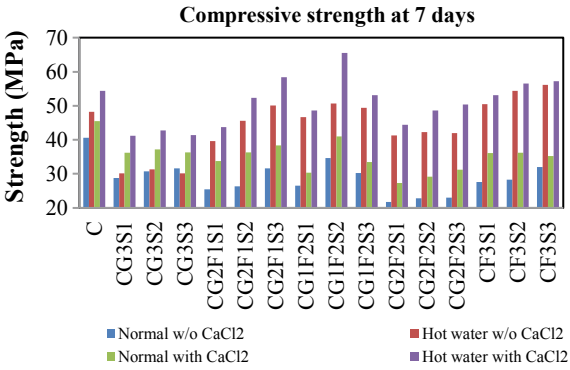

Fig. 4 Compressive strength at 7 days for normal and hot water curing

Fig. 4). Except from few cases, it could be pointed out that the mixes containing higher content of GGBS showed lower early strength with respect to mixes containing higher contents of flyash. Silica fume does not seem to complement GGBS significantly in the early strength gain. Hot water curing with $CaCl_2$ is favorable for obtaining high early strength in generally all mixes. Mixes CF3SX give similar strengths with and without $CaCl_2$.

3.2.2 Compressive Strength at 7 Days for Normal and Steam Curing

All mixes gave a minimum strength of 40 MPa with steam curing and without $CaCl_2$. If $CaCl_2$ is added then the minimum strength further scales upwards to a value of 50 MPa for all mixes after 7 days of curing. Normal PQC with normal curing gave a strength value of 45.5 and 40.6 MPa at this stage with and without $CaCl_2$. Steam curing further improved its strength to 57.5 and 54.8 MPa with and without $CaCl_2$. Most of the mixes except CG3SX gave steam cured strength greater than that of normal concrete with addition of $CaCl_2$ accelerator, whereas most of the mixes except CG3SX and CG2F2SX gave without $CaCl_2$.

Following results were obtained from the comparative compressive strength analysis at 7 days of curing:

(i) Steam curing is more advantageous than normal curing for flyash dominant mixes without $CaCl_2$ i.e. mixes CG3SX are poor towards this curing.
(ii) Like the latter case, CG3SX mixes are poor performer in case of steam curing with $CaCl_2$.
(iii) Steam curing with and without $CaCl_2$ led to the following strength variation trends amongst mixes (Fig. 5):

CG2F1SX > **CG1F2SX** > **CF3SX** > CG2F2SX > **CG3SX**
and **CF3SX** > **CG1F2SX** > CG2F1SX > CG2F2SX > **CG3SX**

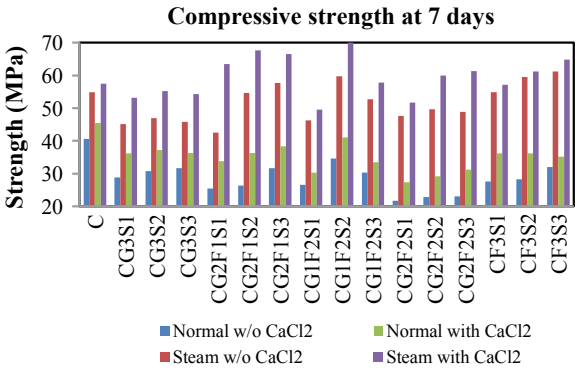

Fig. 5 Compressive strength at 7 days for normal and steam curing

4 Conclusion

The study makes it apparent that high volume of mineral admixtures could also be beneficially used under steam curing for obtaining a high early strength pavement quality self compacting concrete with or without the use of accelerators, provided a high packing density is achieved and proper combinations of mineral admixtures are used. Following main conclusions could be drawn out from this study:

1. High volume of binder is not necessary for attaining high strength SCC. Infect requisite binder could be introduced to fill the voids formed after ensuring high density of combined aggregate mix. This brings the mortar: aggregate ratio as well as fine aggregate: coarse aggregate ratio in the range which promotes workability for attaining self compaction also.
2. SCC mixes containing flyash (20%) and GGBS (10%) along with 10% silica fume have higher strength than other concrete samples but mixes containing flyash at 30% and silica fume at 15% also perform better. This signifies the possibility of using high volume of flyash for getting high strength SCC.
3. Higher volumes of silica fume are a must when the amount of weak pozzolans like flyash or GGBS is high. Though under normal curing they may not increase the strength sufficiently but under steam curing they could bring miracles.

Appendix

Mix design calculations

The mix design is based on assuring workability and strength simultaneously [15]. In the present study a packing density of 0.703 gm/cm^3 was found for the combined aggregates. Voids content $= 1 - 0.7033 = 0.2967$.

Assuming paste content as 25% in excess of void content, which has also been adopted in [23]; detailed calculations to obtain all the ingredients of concrete is given below.

Paste content 25% in excess of void content

(i) Paste content $= 0.2967 + 0.25 \times 0.2967 = 0.3709\ \text{cm}^3$.

(ii) Volume of aggregates $= 1 - 0.3709 = 0.6291\ \text{cm}^3$. From this value, the weight of aggregates of different sizes has been calculated.
For M70 grade concrete keeping in mind the target mean strength suitable water-cement ratio is fixed as per trial mixes.

(iii) W/C ratio $= 0.26$; then $W = 0.26C$

(iv) Total Paste $= C+W = C/3.15 + 0.26C/1 = 0.5775C$
Cement content $= 0.3709/0.5775 \times 1000 = 642.3\ \text{kg/m}^3$
Water content $= 0.26 \times 642.3 = 166.998$ kg/cum.

(v) Determination of flyash (FA), GGBS and silica fume (SF) contents.
According to the flow table tests (ASTM C230) with standard sand and the same dosage of SP, the W/S ratio of GGBS mortar is 0.27, and the W/SF ratio of SF mortar is 0.30; W/F ratio of FA mortar is 0.35 for obtaining the same consistency of cement mortar with W/C ratio = 0.26. Since FA: GGBS: SF:C (by weight) = A:B:C:D, the total volume of FA, GGBS, SF and Cement paste can be obtained using the following equation:

$$V_{PF} + V_{PGB} + V_{PSF} + V_C + V_W = 0.3709$$
$$= \frac{(A \times Wpm)}{2150} + \frac{(0.32 \times A)}{1000} + \frac{(B \times Wpm)}{2920} + \frac{(0.27 \times B)}{1000}$$
$$+ \frac{(C \times Wpm)}{2200} + \frac{(0.3 \times C)}{1000} + \frac{(D \times Wpm)}{3150} + \frac{(0.26 \times D)}{1000}$$

i.e. A, B, C, D, are 10%, 20%, 5%, 65%, then $W_{pm} = 600.95$ kg.
Where, A, B, C, D are % of each mineral admixture and cement in paste by weight. Amount of FA, GGBS and SF (Wpm) needed when A, B, C and D are 10%, 20%, 5%, 65%,

I. FA content $W_F = A \times W_{pm} = 60.10\ \text{kg/m}^3$
II. GGBS content $W = B \times W_{pm} = 120.19\ \text{kg/m}^3$
III. SF content $WSF = C \times W_{pm} = 30.05\ \text{kg/m}^3$
IV. Cement content $W_c = D \times W_{pm} = 390.62\ \text{kg/m}^3$.

(vi) Determination of mixing water content required for FA, GGBS SF, & C.

I. Water content for FA $W_{wf} = 0.35 \times 60.10 = 21.04\ \text{kg/m}^3$
II. Water content for GGBS $W_{wS} = 0.27 \times 120.19 = 32.45\ \text{kg/m}^3$
III. Water content for SF $W_{wSF} = 0.30 \times 30.05 = 9.02\ \text{kg/m}^3$
IV. Water content for Cement $W_{wc} = 0.26 \times 390.62 = 101.56\ \text{kg/m}^3$

(vii) Determination of the SP dosage.

The solid content of SP is 40%. According to previous engineering experience, the dosage of SP is 2% of the content of binders for meeting the SCC requirements Dosage of SP (Master Glenium @51, a second generation based modified polycarboxylic ether):

$$W_{SP} = 0.02 \times (W_F + W_{GB} + W_{SF} + W_C) = 12.02\,\text{kg/m}^3$$

Adjustment of mixing water content needed in SCC Amount of water in SP; $W_{wSP} = (1\text{-}0.40) \times WSP = 7.21\ \text{kg/m}^3$.
Amount of mixing water needed for SCC

$$W = W_{wf} + W_{wB} + W_{wSF} + W_{wc} - Ww_{SP} = 156.85\,\text{kg/m}^3$$

It was also decided to add $CaCl_2$ accelerator in the mixes to understand the behavior of early strength development of a PQSCC with and without steam curing.

References

1. Panchal S, Pradesh H, Pradesh H, Pradesh H, Sharma A, Pradesh H, Pradesh H (2017) Effect of glass reinforcement and glass powder on the characteristics 8(3):648–653
2. Sharma SK, Ransinchung GD, Praveen K (2016) Rigid pavements constructed with WMF reinforced SCC in rural roads. In: A National conference on fifteen years of PMGSY(FYPMGSY), Roorkee, India
3. Ramezanianpour AA, Malhotra VM (1995) Effect of curing on the compressive strength, resistance to chloride-ion penetration and porosity of concretes incorporating slag, fly ash or silica fume. Cem Concr Compos 17:125–133
4. Zhao Q, Liu X, Jiang J (2015) "Effect of curing temperature on creep behavior of fly ash concrete. Constr Build Mater 96:326–333
5. Pai BHV, Bhat K, Prashanth S (2016) Influence of properties of coarse aggregates on self compacting concrete mixes. Int J Adv Struct Geotech Eng ISSN
6. Zhang Z, Li M, Wang Q (2017) Influence of high-volume mineral mixtures and the steam-curing temperatures on the properties of precast concrete. Indian J Eng Mater Sci, Natl Inst Sci Commun Inf Resour (NISCAIR) 24(5):397–405
7. Güneyisi E, Gesoğlu M, Algin Z (2013). Performance of self-compacting concrete (SCC) with high-volume supplementary cementitious materials (SCMs). Eco-Efficient Concrete, Elsevier Ltd., pp 198–217
8. Kwan AKHK, Wong HHC (2008) Packing density of cementitious materials: part 2—packing and flow of OPC + PFA + CSF. 773–784
9. Yu XW, Gao YH, Hao D, Li SZ, Wang LY (2009) The research and application of self-compacting concrete. Key Eng Mater
10. Ahmadi M, Alidoust O, Sadrinejad I, Nayeri M (2007) Development of mechanical properties of self compacting concrete contain rice husk ash. Int J Comput, Inf, Syst Sci, Eng 1(4):259–262
11. Sohail MG, Wang B, Jain A, Kahraman R, Ozerkan NG, Gencturk B, Dawood M, Belarbi A (2017) Advancements in concrete mix designs: high-performance and ultrahigh-performance concretes from 1970 to 2016. J Mater Civ Eng 30(3):04017310

12. Ju Y, Wang L, Liu H (2015) An experimental investigation of the thermal spalling of polypropylene-fibered reactive powder concrete exposed to elevated temperatures, vol 60. Elsevier B.V. and Science China Press, pp 2022–2040
13. Liu F, Wang J, Qian X, Hollingsworth J (2017) Cement and Concrete Research Internal curing of high performance concrete using cenospheres. Ceme Concre Res 95:39–46
14. Concrete G (2007) Chapter 3: Materials and Methods, pp 59–95
15. Raj N, Patil SG, Bhattacharjee B (2014). Concrete mix design by packing density method 11(2):34–46
16. Sharobim KG, Mohammedin H, Mohamed A, Fattouh MS, Sharobim KG (2017) Predicting the compressive strength and the optimum water to binder ratios by packing density theory for high strength self-compacting concrete. IOSR J Mech Civ Eng 14(5):2278–1684
17. Nanak PJ, Darshana BR (2013) Comparision between Mechanical Properties of M30 grade self compacting concrete for conventional water immersion and few non-waterbased curing techniques. Int J Eng Adv Technol
18. IRC (Indian Roads Congress) (1996) Tentative Guidelines for Cement Concrete Mix Design for pavements "IRC-44;1996, NewDelhi."IRC(IndianRoadsCongress). (2017)."TentativGuidelines for Cement Concrete Mix Design for pavements" IRC-44;2017, New Delhi
19. Yugandhar B, Lakshmi MS (2017) Experimental study of self compacting concrete with fly ash, GGBS and broken tiles as partial replacement to cement, Fine 17157–17163
20. Juenger MCG, Siddique R (2015) Cement and concrete research recent advances in understanding the role of supplementary cementitious materials in concrete. Cement and Concrete Research, Elsevier Ltd
21. Jung MS, Shin MC, Ann KY (2012) Fingerprinting of a concrete mix proportion using the acid neutralisation capacity of concrete matrices. Constr Build Mater 26(1):65–71
22. Mengxiao S, Qiang W, Zhikai Z (2015) Comparison of the properties between high-volume fly ash concrete and high-volume steel slag concrete under temperature matching curing condition. Constr Build Mater 98:649–655
23. Su N, Hsu KC, Chai HW (2001) A simple mix design method for self-compacting concrete. Cem Concr Res 31(12):1799–1807

Hybrid Model Based on PPP and EPC Contracts

Rahul Rajasekharan and Shibi Varghese

Abstract Public Private Partnership (PPP) was introduced in India as a viable project implementation mechanism to meet the growing demand for new and better infrastructure services. Rise of non-performing assets accompanied by high risk at various stages of PPP made government adopt Engineering, procurement, and construction (EPC) contracts. Based on poor performance and failing to meet the deliverables of EPC projects, a Hybrid model based on PPP and EPC is necessary. In this study failure factors in PPP and EPC projects is identified, analyzed and ranked using multivariate factor analysis and Delphi technique. To develop a Hybrid model, a systematic research approach (literature review and interviews with experts and experienced practitioners) has been taken to understand infrastructure projects. The findings can be used to create a Hybrid model obtained by eliminating highly occurring failure factors in EPC and PPP projects in India.

Keywords Public private partnership · Engineering procurement construction · Delphi · Infrastructure · Hybrid model

1 Introduction

Public-Private Partnership (PPP) has been accepted as an important policy instrument for central and state governments in the implementation of commercially viable projects. The Department of Economic Affairs (DEA), Ministry of Finance, with support from the erstwhile Planning Commission of India, has been overseeing the development of public infrastructure through the PPP model across the country. The portfolio of project under PPPs in India for infrastructure surpasses all other countries today. According to the Economic Survey of India 2014–15, in the private sector, the number of stalled projects was rising at an alarming rate. Report also

R. Rajasekharan (✉) · S. Varghese
MACE, Kothamangalam, India
e-mail: mr.rahulrajasekharan@gmail.com

Kerala Technological University, Thiruvananthapuram, India

© Springer Nature Switzerland AG 2021

K. Dasgupta et al. (eds.), *Proceedings of SECON 2020*,
Lecture Notes in Civil Engineering 97,
https://doi.org/10.1007/978-3-030-55115-5_74

pointed out that for every 100 rupees of projects under implementation, 10.3 rupees' worth of projects were stalled, while for the private sector the number stood at 16. Thus it the significant role played by PPPs in infrastructure was limited as either it did not elicit any bids from private parties as their cost was too high or a few that were terminated by the government due to lack of interest shown by the developers. And it is here that the failure of PPP is becoming apparent almost all the projects in under the "private" category are public-private partnerships, which affects the public sector directly. After understanding this, for projects estimate totalling above 5 crores, the government shifted from conventional PPPs to the alternate project delivery mechanism of Engineering Procurement Construction (EPC).

In Engineering, Procurement and Construction (EPC) project the contractor is responsible for engineering and design of the project, procurement of all resources such as labour, material and equipment, and construction of the project. Complex long-lasting processes and varying organisational structures incorporate various risk in EPC projects. Recently the famous failure of Palarivattom flyover in Kerala was EPC mode. The administrative sanction was granted by the government to construct a four-lane bridge at Palarivattom under the BOT (build, operate and transfer) scheme. It included the acquisition of land with an estimated amount of 72.6 crores. It was not envisaged as an engineering, procurement and construction (EPC) project. However, while tenders were invited at some level, it was decided to invite tenders by EPC without informing the government. Based on the EPC, the contractor was given the freedom to design the flyover and was one of the part that led to failure. This highlights that, it is imperative to study the failure factors both of EPC and PPP projects in Kerala and to develop a Hybrid model which can overcome the current adversities in these infrastructure projects.

2 Literature Review

Analysis of project success varies according to different contextual factors of a project, for example, the type of sector, type of project, type of contract, different funding and finance arrangements, project characteristics and stakeholder involvement. According to the Champika et al. success of public private partnership(PPP) project can be done by assessing critical success factors (CSFs), use of Key Performance Indicators (KPIs) and assessing value for money aspect [1]. This paper follows the analysis of critical success factors with multivariate factors. Ajith et al. studied dispute mechanism in PPP projects and argued that projects have suffered cost and time delays due to disputes over land acquisition, grants for environmental and forest clearance, and other approvals [2].

Ramakrishna et al. used a questionnaire survey were to identify the critical success/failure factors during all four major project stages. According to the results, it can be clearly understood that the most responsible factor for project failure of road PPP projects in project preparation stage is Public protest & opposition, in

procurement stage is the Influence of higher authorities & political parties, in development stage is Force majeure, and in construction, operation and maintenance stage is Maintenance cost overruns [3]. With cases of examples, Lakshya et al. investigated financial risk associated with highway infrastructure projects by creating a model of risk by analysing real-world PPP infrastructure projects in India [4].

Ashwin Mahalingam studies five key barriers that PPP projects face in the urban Indian context using a combination of archival sources, case studies, and insights from discussions on PPPs. According to him the included distrust between the public and private sector, a lack of political will to develop PPPs, the absence of an enabling institutional environment for PPPs, a lack of project preparation capacity on the part of the public sector, and poorly designed and structured PPP project [5]. Mohsin et al. Analyzed the project delivery mechanism with respect to many problems where both the public and private sectors suffered huge losses and ultimately led to project failures, By evaluating 35 failed transportation PPPs around the world, they investigated the actions and decisions of private-sector partners [6]. Also identified and discussed the casual relationship between a set of drivers responsible for the failures of transportation PPPs, and finally evaluates a set of failure mechanisms initiated by the private-sector partners.

With a lack of papers on addressing issues of EPC project delivery system in Indian perspective, a major review of the literature was done on international projects. Wenxin et al. studies the causes of contractors' claims in international EPC projects and are empirically modelled and tested with Delphi technique, structural equation modelling and case studies were taken from the perspective of Chinese contractors. The created model was used to measure the causes of contractors' claims (socio-political risks, economic risks, and natural hazards), clients' organizational behaviour (untimely payment, change orders, and inefficient processing), and project definition in the contract (unclear scope of works, and unclear technical specification) as an external risk [7]. A comprehensive review of the literature was conducted by Benyamin et al. to identify the risks in EPC projects. 26 identified risks were categorized into eight groups. It was found that among the above recurring risks; "inflation or sudden fluctuation of prices and foreign currency", "inadequate conceptual design", "financial deficiency and delayed progress payments ", and "easing quality of work" are found to be the most prominent [8]. Sadi et al. identified and assessed the main causes of contractors' failure in industrial projects in Saudi Arabia. 24 causes were identified from the literature for assessment by owners, contractors and subcontractors. The report concluded that lack of experience in the business field, inadequate project management, bad cost estimation, unavailability of the project leader stationed at the site, neglect and type of the contract are the most severe causes behind failure in construction projects under private partnerships [9].

The hybrid model was based on extensive literature review. Venkateswararao et al. suggested that capital intensive innovative projects can be done under Swiss challenge method [10]. Love et al. studied the cost overrun in road construction projects. He analysed the traditional lump contract and a contingency plan is developed using probability distribution function [11]. Ajit Kumar and Kumar Neeraj studied judicial overreach on construction projects and suggested some application

of future purposes [12]. This can be coupled with quasi-judicial body. According to Xianhai [13] establishing owner's payment guarantee system has the same importance as the contractor's performance. Ferzon et al. discusses an organisational level frame work to measure performance in construction based on information management. Digitalizing of construction methodology based on information management shows 92% agreement is validated by key performance indicators [14]. Osei-Kyei et al. recommended seven key strategies for managing unsolicited PPP proposals. Existence of well-structured and clear policy guidelines for unsolicited proposals; thorough assessment of value for money, innovation, cost, and risks of proposals; employment of highly skilled and competent staff during evaluations of proposals; competitive, fair, and transparent tendering process; extensive public consultation and stakeholder engagement; comprehensive evaluation of the impact of unsolicited proposals on sector/national policy; and adequate protection of intellectual property rights of the original proponent [15].

Application of Delphi technique is in construction management research is illustrated by Matthew R. Hallowell and John A. Gambatese. Bias in judgment is important to consider in Delphi technique and five methods were introduced to avoid bias was given in this literature. Bias counter measures include (1) controlled feedback, (2) Randomised order of questions, (3) independent risk recording, (4) ensure anonymity. (5) ratings as median [16].

3 Methodology

The methodology for this research consist of a five-stage process:

1. Identify the factors affecting PPP and EPC projects on the basis of an extensive literature survey.
   Based on literature review an extensive set of factors which affect the construction process is determined. This factors are exclusively selected such that it concession agreements have direct impact on such factors. So that studies involving concession agreement were only selected.
2. Categorize the factors stage-wise through solicitation of expert opinions.
   From expert opinion obtained factors were divided according to the stages of construction. Each factor was studied for best suitable stage which has high impact on the project and classified accordingly.
3. Design questionnaire and collect data based on a Likert-type scale.
   Questionnaire were designed such a way as to collect data based on Likert scale. For that each factor were listed and respondents were asked to rate according to importance scale given in questionnaire.
4. Analysis the data on SPSS for mean and Relative Important Index (RII) and
   From responses the data were checked for mean values based on ranking score and then a relative important index for each factor were created. From RII critical failure factor for each stage was calculated.

5. Develop a hybrid model eliminating the critical failure factors.
   An extensive literature review and based on expert opinions, various techniques were selected to remove critical failure factors. These techniques were analysed systematically and incorporated together to form a hybrid model.

3.1 Delphi Technique

The Delphi method was created by Olaf Helmer and Norman Dalkey of the Rand Corporation in 1950s. In Delphi method a circulating series of questionnaires being sent experts to comment based on their personal opinion, experience, or previous research. In this study, experts are carefully chosen by such a way that they have at least 3-year direct experience in handing a project on PPP or EPC projects or currently working on an elite project in the category. Delphi technique is a qualitative approach based on perceptions of experts. It's the best approach when dealing with factors for establishing a model which cannot be done by qualitatively. Factors and their frequency can be obtained quantitatively by case studies and other similar techniques but model cannot be prepared systematically. By taking the perceptions of experts increases the coherence of the model as the data is obtained collectively, and increases the adeptness of model as the experts have right experiences.

In order to remove bias a controlled feedback mechanism and ensured anonymity of expert were taken care. Controlled feedback involved asking for specific feedback from respondents for their responses in a random manner. Anonymity of respondents ensured the absence of dominance bias. As each of the factors given independent importance neglect of probability bias is eliminated [16].

3.2 Details of the Questionnaire

Set 1 It comprised questions on the profile of the respondent. Four basic questions included were—the name of the respondent, his/her organization, the designation of the respondent and email id. These questions framed to understand the level of experience and capability of the respondent to answer these questions in his/her relevant field.

Set 2 It consisted of the various factors which affect a EPC and PPP projects. The factors were categorized in three stages project preparation stage, procurement stage and operation and maintenance stage.

3.3 Questionnaire Survey and Interview

Most of the respondents were interviewed and asked to them to give response to the questionnaire and some of the respondents were answered through email. The

Table 1 Likert scale and details of questionnaire

Order shown in questionnaire	Description	Metrics used in analysis
1	Not important	1
2	Slightly important	2
3	Moderately important	3
4	Important	5
5	Highly important	5

respondents were asked to rank the failure factors on a Likert Scale. A 5-point scale was chosen. Table 1 shows the description, metrics and scale used in the questionnaire given to respondents.

Likert assumed there are infinite number of points between two attitudes in a person to consider responses [17]. To attribute a central normalizing tendency an odd scale should be prepared, between which two extremities can be established. Usually a 7 point or 5 point scale is chosen. When dispersion is responses increases 7 point and compactness of responses is measure 5 point scale is selected. Here undertakes a ranking of factors and respondents should select a well-defined point a 5-point scale is optimal [18].

4 Failure Factors in PPP and EPC Projects

Through the literature survey various factors associated with project failure were identified. Shortlisted the factors that affect PPP and EPC project failure over project life cycle after consultation with assistant executive engineers who had several years' experience in the field.

The question categorized into different project cycle stages. The different project life cycle stages that are considered in our research study are:

1. Planning stage; This includes determining needs, goals and objectives, taking feasibility studies, design development and contract documents development,
2. Procurement stage; This includes securing and purchasing of labor, materials and equipment, determining everything from construction site setup and beginning of work and
3. Construction, operation and maintenance stage; This includes measuring project progression and performance ensuring everything happening aligns with the plan (Tables 2, 3 and 4).

Table 2 Factors affecting planning stage

Factors	Description
Amendments in laws and policy	Rules and regulations pertaining to the project
Bid process/criteria	Fairness, transparency and duration of subbing contract
Financial attraction of project	Perceived benefits for the stakeholders
Incompleteness of concession/contract	Missing clauses in the contract like termination clause etc.
Influence of political groups	Influence by political parties which have direct impact on project
Market analysis	Potential available for project in the market
Public protest and opposition	Support or reaction from people for the project

Table 3 Factors affecting procurement stage

Factors	Description
Approval and clearances	Environmental, Forest clearances etc.
Delayed decision making	Delay in making decisions due to various reasons
Force majeure	Unforeseen conditions
Infusion of capital into the project	The amount of money that can be inputted into the project
Interest and inflation rates	Prevailing market conditions or changes in government rules pertaining to interest exchange rates
Land acquisition	Difficulties in obtaining the land for the project
Material/drawing/approval unavailability	Support or reaction from people for the project
Organization and coordination among stakeholders	Communication and relationship among each stake holder
Procurement of equipment, material and labour	Availability of resources
Safety violations	The violation of a particular safety standard, regulation, policy, or rule

5 Data Analysis

Based on the responses received in the questionnaire survey, the mean scores of the responses to various factors calculated. The means scores are used to rank the factors so as to assess failure factors EPC and PPP projects. Two methods are used for data analysis, which include: (1) Ranking of Factors based on Mean Scores (Average Ranking) (2) Ranking based on Relative Importance Index (RII).

Table 4 Factors affecting construction stage

Factors	Description
Cost overruns	Cost overruns in construction due to problems like sanctions accidents etc.
Delay in payment	Time lost in getting the money for the work by the contractor
Financial Closure	Completing all project related financial transactions and accounts of the project
Lack of public support	Protest by public and local authority which have direct impact on project
Maintenance related issues	Lack of maintenance and problems due to inadequate maintenance
Operating environment	Difficulties encountered due to weather, noise, dust, temperature etc.
Problems with dispute resolution	Disputes leading to arbitration, time and cost overruns
Technical closure	Completing all project related specification and the requirements of the project
Time delays	A delay in construction due to various reasons

$$\text{Relative Importance Index(RII)} = \frac{\sum \text{iSi} \times \text{N i}}{(\text{A} \times \text{N})} \tag{1}$$

where Si is the scores on the Likert scale used (here, it ranges from (0 to 5), Ni is the number of responses to the Likert scale score, A is the highest score (here 5) and N is the total number of respondents (here, 21). Essentially, the RII uses the weightage of responses to each score and normalizes it using the highest possible score that can be assigned by all the respondents (Tables 5, 6, 7, 8, 9 and 10).

Table 5 EPC ranking of factors planning stage

Factors	1	2	3	4	5	Mean	RII	Rank
Amendments in laws and policy	0	0	4	14	3	3.952	0.790	2
Bid process/criteria	0	0	1	15	5	4.190	0.838	1
Financial attraction of project	0	4	7	10	0	3.285	0.657	5
Incompleteness of concession/contract	0	0	9	12	0	3.571	0.714	4
Influence of political groups	0	2	15	3	1	3.142	0.628	6
Market analysis	0	1	18	2		3.047	0.609	7
Public protest and opposition	0	0	8	10	3	3.761	0.752	3

Table 6 EPC ranking of factors for procurement stage

Factors	1	2	3	4	5	Mean	RII	Rank
Approval and clearances	0	0	3	18	0	3.85	0.77	3
Delayed decision making	0	0	0	18	3	4.14	0.82	1
Force majeure	0	1	15	5	0	3.19	0.63	7
Infusion of capital to project	0	0	8	13	0	3.61	0.72	6
Interest and inflation rates	0	2	15	4	0	3.09	0.61	9
Land acquisition	0	0	5	15	1	3.80	0.76	4
Material/unavailability	1	5	15	0	0	2.66	0.53	10
Organization and coordination among stakeholders	0	0	6	15	0	3.71	0.74	5
Procurement of equipment, material and labour	0		4	15	2	3.90	0.78	2
Safety violations	0	2	15	3	1	3.14	0.62	8

Table 7 EPC ranking of factors for construction stage

Factors	1	2	3	4	5	Mean	RII	Rank
Cost overruns	0	0	14	4	2	3.23	0.64	6
capabilities of contractor	0	1	13	2	3	3.04	0.60	8
Financial closure	0	3	10	4	4	3.42	0.68	5
lack of public support	0	0	14	4	3	3.47	0.69	4
Operating environment	0	0	16	4	1	3.28	0.65	7
problems with dispute resolution	0	0	11	6	4	3.66	0.73	2
Time delays	0	0	12	7	2	3.52	0.70	3
Technical closure	0	0	9	9	3	3.71	0.74	1
Cost overruns	0	0	14	4	2	3.23	0.64	6

Table 8 PPP ranking of factors for planning stage

Factors	1	2	3	4	5	Mean	RII	Rank
Amendments in laws	0	0	4	14	3	3.952	0.790	2
Bid process/criteria	0	0	5	13	3	3.904	0.780	3
Financial attraction of project	0	0	0	18	3	4.142	0.828	1
Incompleteness of concession/	0	0	9	12		3.571	0.714	7
Influence of political groups	0	1	3	16	1	3.809	0.761	4
Market analysis	0	1	5	15		3.666	0.733	5
Public protest and opposition	0	3	5	10	3	3.619	0.723	6

Table 9 PPP ranking of factors for procurement stage

Factors	1	2	3	4	5	Mean	RII	Rank
Approval and clearances	0	0	1	13	7	4.285	0.857	2
Land acquisition	0	0	3	8	10	4.333	0.866	1
Force majeure	0	0	14	5	2	3.428	0.685	9
Infusion of capital into the project	0	0	4	9	8	4.190	0.838	4
Interest and inflation rates	0	2	15	4	0	3.095	0.619	10
Delayed decision making	0	0	4	15	2	3.904	0.780	6
Material/drawing/approval unavailability	0	0	2	15	4	4.095	0.819	5
Organization and coordination among stakeholders	0	0	5	16	0	3.761	0.752	7
Procurement of equipment, material and labour	0		4	8	9	4.238	0.847	3
Safety violations	0	0	10	8	3	3.666	0.733	8

Table 10 PPP ranking of factors for construction stage

Factors	1	2	3	4	5	Mean	RII	Rank
Cost overruns	0	1	15	3	2	3.285	0.657	6
Delay in payment	0	1	15	2	3	3.334	0.667	5
Financial closure	0	4	12	3	2	3.142	0.628	9
Maintenance related issues	0	0	11	6	4	3.667	0.734	2
Lack of public support	0	2	14	4	1	3.190	0.638	8
Operating environment	0	1	15	4	1	3.238	0.647	7
Problems with dispute resolution	0	0	11	5	5	3.714	0.742	1
Technical closure	0	0	9	9	2	3.476	0.695	4
Time delays	0	0	10	9	2	3.619	0.723	3

6 Hybrid Model

Hybrid model was needed in the planning stage to overcome bidding criteria discrepancies and to attract investors to come and take up the project. A lump sum contract mixed with a unit price contract, adding contingency items and special incentives for project acceleration can be effective to tackle these issues [11]. Since unit price of every item is specified which gives overall goal of the project and clear cut objectives. Thus this establishment can reduce bid discrepancy while special incentives and contingency allowance can attract more investors. But the provisions regarding failure to comply with any requirements which will result in the contractor incurring monetary liabilities should also be stressed. In order to attract investors another method is to create a Hybrid Annuity Model (HAM) clause in planning stage such as the government will contribute to 40% of the project cost in the first five years through annual payments (annuity) [19]. The remaining payment will be made on the basis of

the assets created and the performance of the developer. This has been tested successfully in India power projects. In procurement stage delay in decision makings should be reduced and effective land acquisition be made. In EPC mode, handing over 90 percent required before commencing of work. Such EPC provisions ensures that no hindrance will occur to work once it commences. This is one very effective method to tackle land acquisition problem and it can also be used at an earlier stage for effectively checking feasibility regarding land availability. Currently the work progress and submission of reports which uses online platform centered around government departments. Since in EPC mode decision are made upon request from contactor, there end also should be made to be digital and be accountable for daily works. Digitalizing can bring more coordination and transparency among stakeholders which can reduce delay in decision making [14]. For better coordination among stake holders the consultancy services should also be periodically reviewed. Subcontracting of work should also be effectively monitored and selection of such contractors also be made with same scrutiny as main contractors. Swiss challenge model can be effectively used for subcontractor selection [15]. Swiss Challenge Method is a project delivery mechanism an unsolicited bid for a government project is proposed and original proposal is challenged through an open bidding by third party, and then lets the original proponent counter match most competitive offer [10] (Fig. 1).

EPC contracts include a guaranteed completion date that is either a fixed date or a fixed period after the commencement of the EPC contract [13]. If this date is not met the contractor is liable for delay liquidated damages. Bringing clarity to these liquidated damages can ensure low turnout of disputes [12]. Like liquidated damages clauses and performance guarantee clauses, adding technical testing and its procedure and requirements after completion should ensure technical closure to the project. Similar to the estimate is done at the beginning of the project a similar approach is should be done after completion to ensure technical closure to the project. An institutionalized mechanism can ensure time bound and periodic review of technical testing, like quality cell, during implementation of projects. The need for a quick, efficient and enforceable dispute resolution mechanism for PPP projects is undeniable [12].

7 Results

Analysis based on mean score and RII score reveal the following:

- Bidding process or criteria was the main reason for failure of EPC contracts at planning stage. Amendments in laws and policy and Public protest and opposition also causes major problems.
- Undervaluation of profits for stakeholders was the main reason for failure of PPP contracts at planning stage. Amendments in laws and policy, transparency and duration of subbing contract were causes project failures at planning stage.

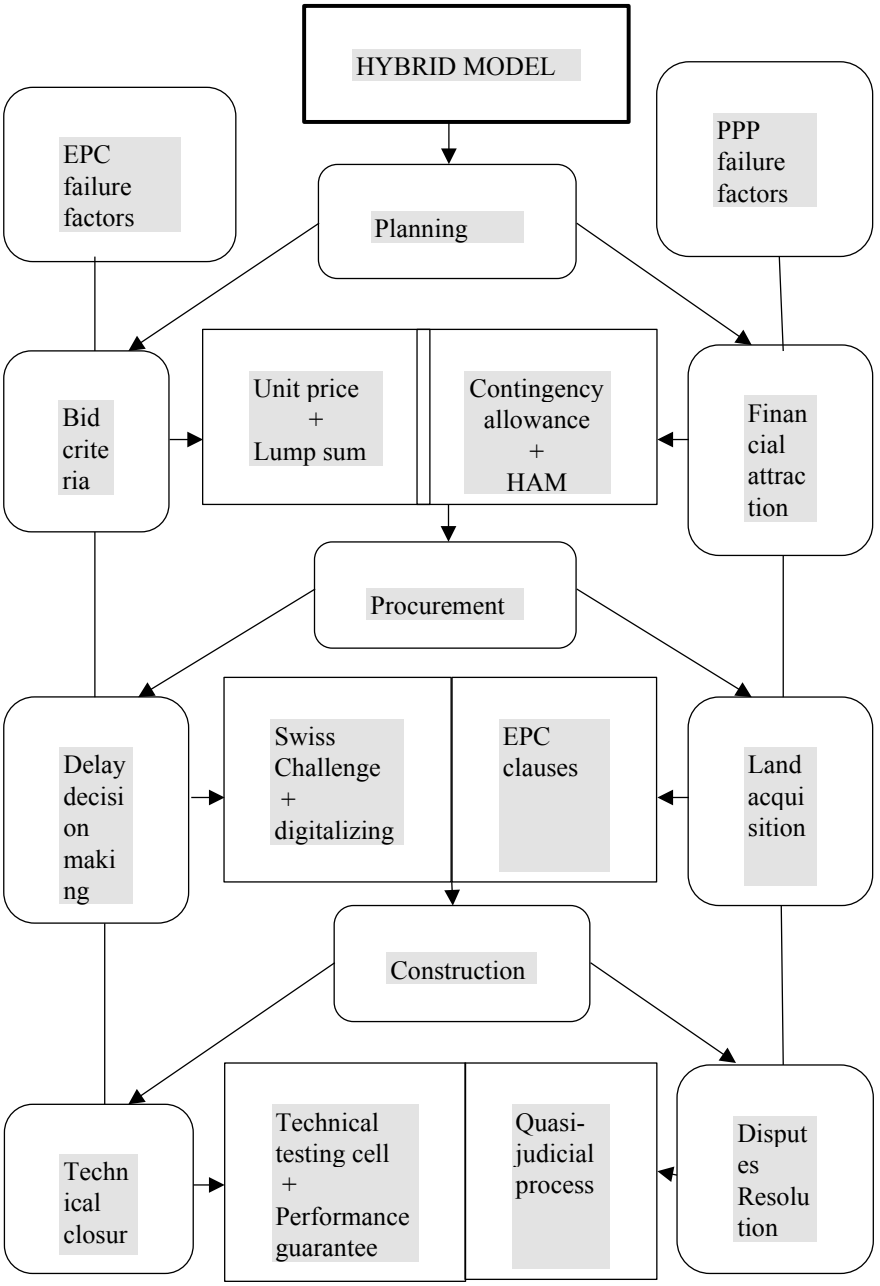

Fig. 1 Hybrid model

- During construction stage, delayed decision making was most responsible factor leading to failure of EPC while land acquisition was for PPP contracts leading to failure. Notably, 'Approval and clearances' and 'Procurement of equipment, material and labour' were also crucial factors.
- Ability to obtain technical closure was the prominent factor for project failure for EPC projects at construction stage. 'Problems with dispute resolution' and "Time delays' were also causes EPC project to fail.
- Problems associated with dispute resolution was the main reason for PPP contract failure at construction stage. 'Maintenance related issues' and 'Time delays' were another major factor causes PPP failure.

On upon closer analysis and interpretation with the help of expert interview, certain conclusion can be obtained for the failure of EPC model.

Planning stage: Bidding process is a single stage two-part system for selection of the bidder for award of the Project. Eligibility and qualification of the bidder will be first examined based on the details submitted under technical bid with respect to eligibility and qualifications criteria prescribed. The financial bid under the second part shall be opened of only those bidders whose technical bids are responsive to eligibility and qualifications. Since the bidding is done online there is adequate transparency, fairness and minimum delay in the process but the criteria for the bids are often ambiguous. Number or per meter length is most accepted method of quoting the bids which diminishes the importance of specification. For example: 30 km of road construction or 1 flyover etc. are often expressed.

Procurement stage: Weak coordination between parties, long time spent on contract reviews, lack of control on subcontractors, contractor's lack of motivation and delay in material delivery by suppliers where leads to delayed decision making.

Construction Stage: Ideally technical specification for competition of project is stated under concession agreement, but after construction the performance evaluation techniques are not given importance. The technical testing procedures are not set out in the EPC contract, which leads to opportunist behaviour from contractor to omit minute but necessary items.

On upon closer analysis and interpretation with the help of expert interview certain conclusion can be obtained for the failure of PPP model.

Planning stage: The low amount of profit of about 10 percent based on scheduled rates that revises very abnormally, are not attracting huge investment. From the experience investors are reluctant to enter into concession agreement which involves complex infrastructure projects.

Procurement Stage: Normally in PPP contracts the land acquisition starts from planning stage and continue even after starting of the work. Acquiring right land at right time is the most difficult task in procurement stage. Hefty fees, delay in acquiring land or even not acquiring the land leads to partial or total abandonment of the project.

Construction stage: Available dispute resolution mechanism of PPP contracts include mediation or conciliation are not binding on stakeholders. Escalation of disputes to decision of domain experts also in large numbers creates less difference.

After attempting various dispute resolution mechanism, the PPP model calls for litigation. Thus moving to judiciary system becomes necessary. Indian judiciary system of dispute resolution is very length and time consuming which leads to delay or even abandonment of project.

The provisions and clauses in a contract agreement need to be flexible in terms of the sharing of risks by the public and private authorities, and this concession agreement needs to be ensured specific, simply worded, and unambiguous, leaving no space for alternative interpretations. A mechanism required to reach quick settlement of claims through a quasi-judicial process is essential with binding powers on stakeholders. In case the dispute relates to both project proponent and the claims must be settled proportionally.

8 Conclusion

Infrastructure development in India is coupled with effective utilization of private resources and its capability. PPP and EPC are used as most important project delivery instruments to bring together private parties to undertake huge projects. Both of this project delivery mechanism failed to provide its high quality results that expected and obtained internationally. The projects in India require a Hybrid model that can reap the advantages of both system or eliminate the factors causing failures. Through this study at various stages the failure factors are identified for both EPC and PPP.

A Hybrid model involves incorporating lump sum and unit price at planning stage is recommended to eliminate bid criteria and incentive scheme together with hybrid annuity mix model which can attract more investors. Ensuring land acquisition clauses as such as in EPC mixed with digitalizing entire platform of work and more systematic selection of contractors such as Swiss challenge is recommended in procurement stage [15]. Current dispute resolution mechanisms are slow and not very well developed, often shifting the project timelines and freezing investments. By providing simplified concession agreements, appointment of a quasi-judicial and bringing clarity to testing and measurement can enhance more coordination among stakeholders, thereby reduce delay in dispute resolution and enforce technical closure.

Perceptions play an important part in Delphi technique and expert interview, as a result, learnings from this study can only be utilized for similar geopolitical zones. But with necessary customisation this study can be extended to more sectors and can have wider applications.

References

1. Liyanage C, Villalba-Romero F (2015) Measuring success of PPP transport projects: a cross-case analysis of toll roads. Transp Rev: A Trans Transdiscipl J 35(2):140–161
2. Ajit Kumar Sinha and Kumar Neeraj Jha (2020) Dispute resolution and litigation in PPP road projects: evidence from select cases. J Leg Aff Disput Resolut Eng Constr 12
3. Nallathiga R, Shaikh HD, Shaikh TF, Sheik FA (2017) Factors affecting the success/failure of road infrastructure projects under PPP in India. KICEM J Constr Eng Proj Manag 7
4. Kumar L, Jindala A, Velaga NR (2018) Financial risk assessment and modelling of PPP based Indian highway infrastructure projects. Transp Policy 62:2–11
5. Mahalingam Ashwin (2010) PPP experiences in Indian cities: barriers, enablers, and the way forward. J Constr Eng Manag 136:419–429
6. Soomro MA, Zhang X (2013) Roles of private-sector partners in transportation public-private partnership failures. J Manag Eng 34
7. Shen W, Tang W, Yu W, Duffield CF, Hui FKP, Wei Y, Fang Jun (2017) Causes of contractors' claims in international engineering-procurement-construction projects. J Civ Eng Manag 23:727–729
8. Sadeghi B, Mortaheb MM, Kashani, H (2016) Identification of recurring EPC contract risks and mitigation Strategies'. In: 52nd ASC annual international conference proceedings, Tehran, 2016
9. Assaf S, Hassanain MA, Al-Zahrani S (2015) Causes of contractors' failure in industrial projects in Saudi Arabia. Res J Appl Sci, Eng Technol 9:158–164
10. Podile V, Janardana Rao N (2017) Swiss challenge method—an innovative public private partnership model in India. Asian J Res Bus Econ Manag 7(7):384–390
11. Love PED, Sing C-P, Carey B, Kim JT (2015) Estimating construction contingency: accommodating the potential for cost overruns in road construction projects. J Infrastructure Syst 21, 2
12. Sinha AK, Jha KN (2020) Impact of judicial overreach on PPP construction projects. J Leg Aff Disput Resolut Eng Constr 12
13. Menga X (2002) Guarantees for contractor's performance and owner's payment in China. J Constr Eng Manag 128:3
14. Aziz F, Rankin JH, Waugh LM (2016) Construction organizational level information management framework. J Manag Eng 32:2
15. Osei-Kyei R, Chan APC, Dansoh A, Joseph K (2018) Strategies for effective management of unsolicited public–private partnership proposals. J Manag Eng 34:3
16. Hallowell MR, Gambatese JA (2010) Qualitative research: application of the Delphi method to CEM research. J Constr Eng Manag 136:1
17. Likert R (1932) A technique for the measurement of attitudes. Arch Psychol 22:140
18. Joshi A, Kale S, Chandel S, Pal DK (2015) Likert scale: explored and explained. Bri J Appl Sci Technol 7(4):396–403
19. Garg S, Mahapatra D (2019) Hybrid annuity model: hamming risk allocations in Indian highway public–private partnership. J Public Aff

AHP Model for Performance Improvement in LSGD Projects

Ammu David and Shibi Varghese

Abstract With an increased demand for public works projects, there is a need to focus attention on the efficient delivery of construction project services in the public sector and in particular municipal project delivery. This includes a broad category of infrastructure projects financed and constructed by the local self-government for uses in the greater community. These type of projects have special challenges that may differ from other construction projects. A decision—making process known as AHP (analytical hierarchy process) was used to identify and prioritize the various parameters affecting performance in LSGD projects. A comparison—based survey is conducted to quantify relative priorities for a given set of alternatives on a ratio scale based on the judgment of the construction professional's experience. Through the AHP model, various parameters, as well as improved techniques, are identified to reach the optimum goal of performance improvement.

Keywords Performance improvement · AHP · LSGD

1 Introduction

The construction industry plays an indispensable role in the Indian economy, and is a significant contributor to economic growth. Planning, designing, construction of buildings and other works, their demolition and maintenance are the main responsibility of construction industry. It is essentially a service industry, obtaining its inputs and outputs from various sectors of the economy with which it is interrelated and interlinked, often in quite complex ways. Construction projects are always complex, risky and time-consuming. Due to the unique features of construction activities it is the industry which has more risks. Major risks include long period, complicated

A. David (✉)
MACE, Kothamangalam, India
e-mail: ammudavid68@gmail.com

S. Varghese
Kerala Technological University, Thiruvananthapuram, India

© Springer Nature Switzerland AG 2021

K. Dasgupta et al. (eds.), *Proceedings of SECON 2020*,
Lecture Notes in Civil Engineering 97,
https://doi.org/10.1007/978-3-030-55115-5_75

processes, obnoxious environment, financial instability and complex organization structures.

Poor information and communication systems in the construction industry lead to rework, ineffective constructability, cost overruns, changes in the order and delays, it can be considered as the biggest causes of waste, especially in the public sector. The LSGD projects are one of the sectors where improvement is very much needed due to the frequent incompatibility and discrepancy between the design information provided and the actual site conditions. Diversity in projects is the main peculiarity of local self-government works. LSGD projects include public buildings such as schools, hospitals, convention centers etc., transport infrastructures such as roads, culverts, bridges, irrigation pipelines, canals, bunds, public spaces such as public squares, parks, public services like water supply, sewage lines, river training works and other, usually short and long-term, physical assets and facilities.

This study uses a research methodology technique known as Analytic Hierarchy Process (AHP) is adopted. AHP is a method for the mathematical treatment of decision problems, and it is recommended for stakeholder's decision-makers. This research approach is utilized to prioritize improvement techniques look for continuous construction improvement. One of the greatest advantage of AHP is the ability to use it for group decisions where participants evaluate the alternatives and thus arriving at an optimum solution [1]. Here each and every criteria and alternatives are checked with one another in order to making rational decisions regarding the problem.

2 Literature Review

According to the Odeh et al. productivity level on a construction site cannot be viewed in isolation and it depends upon a number of factors that comes throughout the project life cycle. Improving site conditions, management and supervision, proper payment procedures on completed works, avoiding labour density and improved scheduling are some of the important factors when attempting to limit productivity losses on site [2]. According to Bullinger et al. the short-lived construction project life cycle and project-based management hinder progressive improvements in work conditions and management. The practice quickly gets lost if the contractors move to another site where the same conditions and requirements are not strictly enforced [3].

Allmon et al. revealed four primary ways of increasing productivity through management, namely planning, resource supply and control, supply of information and feedback and selection of the right people to control certain factors. An essential requirement towards improvement is a clear understanding and knowledge of the severity of each factor on site. Productivity improvement is a function of management as changes for improvement can only be implemented at management level [4].

According to Aziz et al. the controllable waste that mainly affects the productivity can be divided into three different activities as follows:

1. Controllable causes associated with flows which includes resources (materials, equipment, labor) Information
2. Controllable causes associated with conversions which include method, planning, quality
3. Controllable causes associated with management activities such as decision-making, ineffective supervision/control [5].

According to Doloi poor productivity of construction workers is one of the major causes of cost overruns and schedule slippages in construction projects [1]. Use of statistical analysis in identifying critical attributes in construction engineering practice is quite widespread Statistical analysis mainly relies on the documented evidence of past practices, which requires significant population data from reliable and valid sources. However, one of the major limitations of the statistical analysis is that it cannot be used decisively for resolving conflicting objectives.

According to Enshassi et al. multi-objective decision-making approaches provide a convenient set of mathematical tools to identify an optimal alternative given a set of competing objectives [6]. Saaty introduced one such multi-objective decision making technique known as AHP (Analytical hierarchy process) The Analytical Hierarchy Process (AHP) is a decision aiding method aimed at quantifying relative priorities for a given set of alternatives on a ratio scale, based on the judgment of the decision-maker, and stresses the importance of the intuitive judgments of a decision-maker as well as the consistency of the comparison of alternatives in the decision-making process. AHP is effective even if without a significant sample size. Here in order to assess the relative importance of each criteria number of pairwise comparisons between quantitative or qualitative criteria are done. These criteria can be arranged in a hierarchical manner known as a 'value tree' for sets of attributes, and qualities (levels) within these attributes. The AHP method can be done even with a single respondent in case of an extreme case and can be used efficiently instead of complex surveys. The core of AHP is the comparison of pairs instead of sorting (ranking), voting (assigning points), or the free assignment of priorities [7].

According to Schot et al. as the input data in AHP analysis are based on an expert's perceived judgment, a single input usually represents a group of representatives in the sample data. Other similar techniques such as choice experiments do not realize statistically reliable results even if there are a large number of consistent survey responses. Most conjoint analyses place quite a high 'cognitive burden' on respondents in that they are asked to make comparisons across options that have a large bundle of attributes and levels of these attributes. In contrast, under AHP, respondents are not asked to make choices between all criteria and thus respondents are less likely to adopt mental short cuts by concentrating disproportionately on one attribute or level [8].

Waris et al. used AHP for sustainable procurement of construction equipment [9]. One of the applications of AHP was included by Subramanian et al. who have classified the AHP into five broad areas of operation research which include operation strategy, process, product design, planning and scheduling resources, and project management and managing the supply chain process as prominent decision areas

[10]. Another application of AHP in Qureshi et al. is to obtain preference weights of environmental, social and economic objectives which have been used in ranking riparian revegetation policy in Australia [11].

3 Methodology

The Analytic Hierarchy Process (AHP) approach of the research methodology was applied. AHP is a method for the mathematical treatment of decision problems, and it is recommended for stakeholder's decision-makers. This research approach is utilized to prioritize improvement techniques and to look for continuous construction improvement. The methodology of the paper is given through the following steps:

1. Identify the factors that affect the performance in LSGD projects
2. Conduct initial survey to identify the top factors
3. Structure the decision factors and improvement techniques in a hierarchy
4. Conduct survey of industry professionals
5. Analyze the data and discuss the results.

The AHP solution is as follows

1. A complex problem is made simple by decomposing it in to hierarchy by including all elements to reflect the aim of the decision maker
2. Elements are compared pairwise using a scale to measure their relative importance
3. Using the same scale, the relative importance of each alternative is evaluated with respect to each criterion element in the hierarchy
4. Aggregate to overall score of each alternative is arrived [12].

A general flowchart of AHP model is shown in Fig. 1.

An optimal method to understand people's behaviour with integrating all factors such as social, economic, political, environmental and cultural does not exist. This is the main reason why AHP treats people separately from conditions in which they find themselves. The AHP is an instrument used to construct a complete order through which optimum choice is derived [13]. Contrary to other conjoint analysis, AHP asks the respondents to compare the criteria pairwise instead of making decisions between all criteria at once. Here different attributes are not directly compared. Thus respondents are less likely to adopt mental short cuts by concentrating disproportionately on one attribute or level thus controlling the human element [1]. AHP enables people to make more effective decisions by assisting them in organizing their thoughts and judgments. Its structures are based on observations of how influences are transmitted and its arithmetic is derived from psychologists' observations of how people function in attempting to understand their behaviour [13].

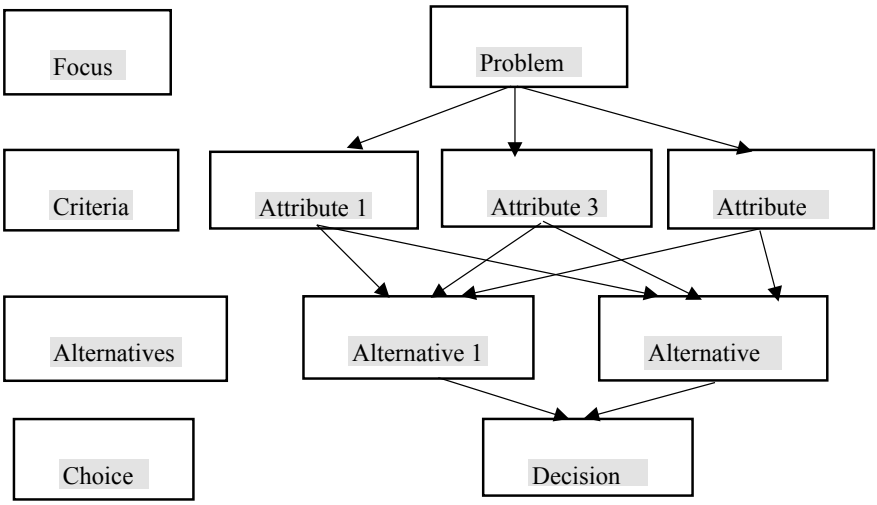

Fig. 1 The AHP model

4 Decision Making Process for Performance Improvement

4.1 Selection of Attributes and Alternatives

The factors that affects performance in LSGD were identified from literature and are categorized through simple questionnaire survey among engineers and contractors in LSGD sector in and around Ernakulam. Commonly 5-point or 7-point Likert scale are used. When the number of points increases random tendency to answer also increase. So instead of simple yes or no 2 points for positive 2 points for negative and a point for neutral is given and thus adopting a 5 point Likert scale. The response rating of experts on a Likert 5 point scale are statistically analyzed to identify the relevance. After collecting opinion from 40 experts the summary of the analysis is shown in Table 1.

These factors are shortlisted and categorized into 8 criteria

1. Resources
2. Method
3. Design
4. Planning
5. Quality
6. Safety
7. Cost
8. Public support.

Table 1 Analysis of criteria

Criteria	Mean
Availability of equipment and its failure	3.5
Quality and shortage of materials	3.91
Shortage of labor and technical personnel	3.75
Improper communication	3.33
Poor information quality	2.91
Improper designing	3.58
Construction methods	3.58
Complexity of project	3.14
Improper planning	4.16
Unforeseen site conditions	3.66
Weather condition	3.58
Quality assurance	3.83
Construction mistakes and defectives works	3.16
Decision making	3.66
Ineffective supervision	3.75
Site management	3.83
Safety	3.58
Finance and payment	4.25
Lack of public support	3.66

Though many alternatives that is improvement techniques are reported in the literature, many of them are not suitable/common to Indian construction industry. The alternatives considered for the analysis are

1. Proper project planning and scheduling
2. Effective communication
3. Adoption of modern construction methods and technologies
4. Proper resource management
5. Adherence to standards and specifications.

4.2 Measurement Scale

The analytical hierarchy process requires the comparison of criteria based on a measurement scale. The expert is asked to give his/her preference of importance among the attributes depending on the project data on a 9-point scale. The scale item and the corresponding values are shown in Table 2.

The second scale was used to compare the alternatives on the basis of the extent to which a category possess a particular attribute in comparison with another alternative and is shown in Table 3.

Table 2 9-point scale for comparing attributes

Scale items	Measures
Same importance	1
Slightly more importance	3
Considerably more important	5
Significantly more important	7
Absolutely more important	9

Table 3 9-point scale for comparing alternatives

Scale items	Measures
Equally preferred	1
Moderately preferred	3
Strongly preferred	5
Very strongly preferred	7
Extremely preferred	9

4.3 Pairwise Comparison

The comparison are made pairwise. A square matrix is setup by listing the criterion to be compared on the left and on top. Then one begins with a criteria on the left and asks how much more important it is than a criteria listed on top. When compared with itself, the ratio is 1. When compared with another element, either it is more important than that element, then an integer value from the scale is used or it's reciprocal in the opposite case. Similarly pairwise comparison can be done for alternatives with respect to each criterion using the scale.

5 Analysis and Results

According to Saaty [12] an important aspect of the AHP is the idea of consistency. If one has a scale for a property and the property of an object is measured with that scale then, there is no judgmental inconsistency. Although if one has a physical scale and applies it to objects in pairs and then derives the relative standing of the objects on the scale from the pairwise comparison matrix, it is likely that inaccuracies will have occurred in the act of applying the physical scale and again there would be inconsistency.

The priority of consistency to obtain a coherent explanation of a set of facts must differ by an order of magnitude from the priority of inconsistency which is an error in the measurement of consistency. Thus, on a scale from O-1, inconsistency should not exceed 0.10 by very much. Note that the requirement of 10% should not be made much smaller such as 1 or 0.1%. The reason is that inconsistency itself is

important, for without it new knowledge which changes preference order cannot be admitted. When experiences continued adjustment in understanding it contradicts the assumption that all knowledge to be consistent. Thus the objective of developing a wide-ranging consistent framework depends on admitting some inconsistency.

This also accounts for why the number of elements compared should be small. Distortion of priorities can occur considerably when a number of elements are large as a large number of elements attribute to small relative priorities. On the other hand if the number of items is small then the priorities are comparable. The relative priorities would be about the same as a small error does not affect the order of magnitude of the answers. For example, when the number of items is less than 10 so that their values would be greater than 10% each and therefore they remain relatively unaffected by 1% error [12].

Following steps are involved in the application of analytical hierarchy process (AHP)

A comparison matrix for attributes is constructed.
Comparison matrices for each attribute based on different alternatives are constructed and these are evaluated by experts.
Normalized vector is found out by adding each column elements.
Priority vector/Eigen vector is found out by dividing the respective row elements corresponding to its normalized vectors to find the average of row elements.
Largest Eigen Value (LEV) is calculated by adding the product of each column normalized vector with the priority vector of the corresponding criteria.

$$\text{Consistency index (CI)}, \text{CI} = \frac{\text{LEV} - \text{n}}{\text{n} - 1}, \tag{1}$$

where n is the size of matrix. The value of random consistency is shown in Table 4 for the size of the matrix. The values of RI for different sizes of judgement matrices are found in Saaty [7].

$$\text{Consistency ratio (CR)}, \text{CR} = \frac{\text{CI}}{\text{RI}}, \tag{2}$$

where RI is the random consistency given in Table 4.

The consistency is checked by taking the consistency ratio of the CI with appropriate one of the following set of numbers to see if it is about 10% or less, otherwise study the problem and revise the judgements.

Table 4 Random consistency values

N	1	2	3	4	5	6	7	8
RI	0	0	0.58	0.9	1.12	1.24	1.32	1.41

Composite priority is obtained by multiplying each column vector with the priority of the corresponding criterion and added across each row.

Final decision is taken by finding the geometric mean of individual responses for each alternatives.

The analytical hierarchy was programmed into an Excel spreadsheet for implementation of the AHP process.

5.1 A Sample Analysis

To facilitate this a matrix is provided with various criteria as the rows and columns. For comparing the criteria in the rows with those in the columns, the following scale can be used.

Scale:

Same importance = 1;
Slightly more important = 3;
Considerably more important = 5;
Significantly more important = 7;
Absolutely more important = 9 (Table 5).

For comparing the alternative in the rows with those in the columns, the following scale can be used.

Scale:

Equally preferred = 1;
Moderately preferred = 3;
Strongly preferred = 5;
Very strongly preferred = 7;
Extremely preferred = 9 (Table 6).

Here 1 represent project planning and scheduling.

2 represent effective communication.

3 represent adoption of modern construction methods and technologies.

4 represent proper resource management.

5 represent adherence to standards and specifications (Tables 7, 8, 9, 10, 11, 12 and 13).

The survey technique involves obtaining essential data from a representative sample selected from target population selected. The targeted participants were from management levels of LSGD as they are usually responsible for facilitating change within the system. A total of 25 experts including assistant executive engineers, assistant engineers, and other technical assistants from different LSGDs such as block panchayat municipality and corporation in Ernakulam region were interviewed. The research questionnaires asked respondents to reflect on the way they believe the different issues impinge upon performance and to rate in differing degrees

Table 5 Comparison of attributes

Matrix		Planning	Resources	Quality	Design	Method	Safety	Cost	Public support	Normalized principal Eigen vector (%)
		1	2	3	4	5	6	7	8	
Planning	1	1	3	3	3	5	9	9	9	36.12
Resources	2	1/3	1	1	3	3	7	7	7	20.42
Quality	3	1/3	1	1	3	1	3	5	3	13.67
Design	4	1/3	1/3	1/3	1	1	3	3	3	8.51
Method	5	1/5	1/3	1	1	1	5	5	5	11.33
Safety	6	1/9	1/7	1/3	1/3	1/5	1	3	3	4.39
Cost	7	1/9	1/7	1/5	1/3	1/5	1/3	1	1/3	2.28
Public support	8	1/9	1/7	1/3	1/3	1/5	1/3	3	1	3.28

LEV = 8.588 CI = 0.22 CR = 6%

Table 6 Comparison of alternatives based on planning as criterion

	1	2	3	4	5	Normalized principal Eigen vector (%)
1	1	3	7	7	7	51.38
2	1/3	1	5	5	5	27.42
3	1/7	1/5	1	3	1	8.78
4	1/7	1/5	1/3	1	3	7.08
5	1/7	1/5	1	1/3	1	5.34

LEV = 5.488 CI = 0.39 CR = 6%

Table 7 Comparison of alternatives based on resource as criterion

	1	2	3	4	5	Normalized principal Eigen vector (%)
1	1	1	1/3	1/5	3	11.93
2	1	1	1/5	1/9	1/3	5.68
3	3	5	1	1/3	3	24.56
4	5	9	3	1	3	47.79
5	1/3	3	1/3	1/3	1	10.05

LEV = 5.49 CI = 0.39 CR = 7%

Table 8 Comparison of alternatives based on quality as criterion

	1	2	3	4	5	Normalized principal Eigen vector (%)
1	1	1/3	1	1	1/5	8.44
2	3	1	3	3	1/5	21.33
3	1	1/3	1	1	1/3	9.76
4	1	1/3	1	1	1/5	8.44
5	5	5	3	5	1	52.04

LEV = 5.234 CI = 0.19 CR = 8%

Table 9 Comparison of alternatives based on design as criterion

	1	2	3	4	5	Normalized principal Eigen vector (%)
1	1	5	5	5	1	38.95
2	1/5	1	1	3	1/5	10.29
3	1/5	1	1	1	1/3	8.71
4	1/5	1/3	1	1	1/5	6.47
5	1	5	3	5	1	35.59

LEV = 5.182 CI = 0.15 CR = 4%

Table 10 Comparison of alternatives based on method as criterion

	1	2	3	4	5	Normalized principal Eigen vector (%)
1	1	1	1/5	1/3	1/3	6.98
2	1	1	1/5	1/3	1/3	6.98
3	5	5	1	5	3	50.71
4	3	3	1/5	1	1	17.00
5	3	3	1/3	1	1	18.32

LEV = 5.138 CI = 0.11 CR = 4%

Table 11 Comparison of alternatives based on safety as criterion

	1	2	3	4	5	Normalized principal Eigen vector (%)
1	1	1/5	1/3	1	1/5	6.24
2	5	1	3	3	1/3	26.59
3	3	1/3	1	3	1/3	15.04
4	1	1/3	1/3	1	1/5	6.92
5	5	3	3	5	1	45.22

LEV = 5.216 CI = 0.18 CR = 6%

Table 12 Comparison of alternatives based on cost as criterion

	1	2	3	4	5	Normalized principal Eigen vector (%)
1	1	1/5	1	1/3	1/3	8.18
2	5	1	3	3	3	44.32
3	1	1/3	1	1	1	13.71
4	3	1/3	1	1	1	16.90
5	3	1/3	1	1	1	16.90

LEV = 5.138 CI = 0.11 CR = 3.1%

Table 13 Comparison of alternatives based on public support as criterion

	1	2	3	4	5	Normalized principal Eigen vector (%)
1	1	5	1	1	3	29.82
2	1/5	1	1/3	1/3	1	8.08
3	1	3	1	1	3	26.61
4	1	3	1	1	3	26.61
5	1/3	1	1/3	1/3	1	8.87

LEV = 5.032 CI = 0.03 CR = 1%

Table 14 Summary of AHP analysis for performance improvement in LSGD

	Planning 34.5%	Resources 21%	Quality 13.4%	Design 8.23%	Method 12.5%	Safety 4.6%	Cost 2%	Public support 3.77%
Proper project planning and scheduling	51.7%	12%	8.33%	39%	6.8%	6.5%	8.3%	28.9%
Effective communication	26.9%	5.5%	22%	10.4%	6.4%	25.9%	43.8%	8.56%
Adoption of modern construction methods and technologies	8.8%	24.6%	9.34%	8.7%	51.5%	15%	12.9%	26.54%
Proper resource management	7%	47.5%	8.33%	6%	16.9%	7.02%	17.09%	26.86%
Adherence to standards and specification	5.6%	10.4%	52%	35.9%	18.4%	45.58%	17.91%	9.14%

of importance, the major implicating factors that limit the level of ongoing attainable performance.

As per Saaty [7] a consistency ratio of 0.1 or less is considered acceptable. Only 20 responses out of 25 falls under this. Even with one respondent AHP can be applied. AHP is applied to each response individually and analysis is done independently. Following the reasoning, the Chebyshev's theorem statistical test was suggested by Saaty [7] based on which at least 75% of the dataset must lie within the range of average 2 standard deviations to accept the dataset. From the dataset, over 80% of the obtained data were found to be within the above range. Furthermore, the resulting inconsistency ratio of the pairwise comparison matrix are less than 0.1 represents an additional indication of reliability of the obtained responses in the analysis. According to Doloi [1] the small sample size is not an issue from the AHP methodology point of view. Salman et al. [14] used only 12 respondents' input in validating a BOT viability model for large-scale infrastructure projects. In Dias and Ioannou [15], only 12 and 8 respondents had respectively accepted the invitation and completed the questionnaires. A single input represents a group of sample [16]. Therefore, the reliability of the sample size taken is acceptable.

Pairs of criteria are compared in order to systematically determine the relative influence of the criteria on the attributes positioned one level higher in the hierarchy. Reference to the response to a leading question was used to compare the performance separately for each set in the hierarchy. The responses from each of the survey participants were used to develop the judgment matrices to calculate the relative importance of the criteria. Based on the relative importance given by individual participants, the mean values of relative importance for the criteria were computed and are shown in Table 14.

6 Conclusions

This study was aimed to determine the optimum solution to achieving improved performance in LSGD projects focusing on a number of selected LSGDs in Ernakulam. The findings of the research have provided substantial evidence on the current understanding and perception of performance in the industry and have provided clear pathways for LSGDs to address the current productivity problems. The responses drawn in this research from the professionals of LSGD sectors in Ernakulam have given an insight into the current issues surrounding LSGD projects.

The results provide a solid basis for increased focus and participation of the construction management sector in achieving higher productivity in the industry.

The research suggests planning and resource as the most critical factors to improving performance in LSGD projects with priorities 34.5 and 21% respectively. It can be inferred that most of the issues that LSGD projects facing are related to inadequate planning and lack of resource management. So it is clear that over all planning and resource management for a project through all phases such as the work scheduling, activity programming, site coordination and construction must be given

primary focus by LSGD organization, if they are to improve upon current levels of performance. This result demonstrates the necessity for giving priority to activities associated with planning and resource management. Application of improvement techniques should have more consideration and importance in these activities in order to improve performance and productivity.

The result shown in Table 14 provides a set of priorities demonstrating the importance of alternatives for reaching the superior goal of performance and productivity improvement in LSGD projects. Proper project planning and scheduling is the most important technique in reducing problems related to planning designing and lack of public support with priorities of 51.7%, 31% and 28.9% respectively. Proper resource management is the most important technique while dealing with problems related to resources with priority of 47.5%. Adherence to standards and specifications has significant effect in improving productivity and performance considering quality design and safety aspects with priorities of 52%, 35.9%, 45.58% respectively. Adoption of modern construction methods and technologies is the most important technique in reducing problems related to method with priority of 51.5%. While adopting proper project planning and scheduling problems related to planning can be rectified. Even though proper resource management has a low priority of 7% in dealing with problems related to planning but considering issues with resources, proper resource management is the best method. As the study already pointed out that improvement techniques for planning and resource management should be given prime importance, it can be concluded that adopting proper project planning and scheduling and proper resource management can improve the performance in LSGD projects significantly.

References

1. Doloi H (2008) Application of AHP in improving construction productivity from a management perspective. Constr Manage Econ 26(8):841–854
2. Odeh AM, Battaineh HT (2002) Causes of construction delay: traditional contracts. Int J Project Manage 20(1):67–73
3. Bullinger H-J, Menrad W (2002) Changes in remuneration practice in production: success factors of sustainable remuneration systems for innovative concepts of work organization. Int J Prod Res 40(15):3955–3971
4. Allmon E, Hass C, Borcherding JD (2000) US construction labour productivity trends 1970–1998. J Constr Eng Manage 126(2):97–104
5. Aziz RF, Hafez SM (2003) Applying lean thinking in construction and performance improvement. Alexandria Eng J 52(4):679–695
6. Enshassi A, Mohamed S, Mustafa ZA, Mayer PE (2007) Factors affecting labour productivity in building projects in Gaza Strip. J Civ Eng Manage 13(4):245–254
7. Saaty TL (1980) The analytical hierarchy process. McGraw Hill, New York
8. Schot J, Fischer K (1993) Introduction: the greening of the industrial firm. In: Environmental strategies for industry. Island Press, Washington, pp 3–33
9. Waris M, Panigrahi S, Mengal A, Soomro MI, Mirjat NH, Ullah M, Azlan ZS, Khan A (2019) An application of analytic hierarchy process (AHP) for sustainable procurement of construction equipment: multicriteria-based decision framework for Malaysia. Hindawi Math Probl Eng 2019:20, Article ID 6391431

10. Subramanian N, Ramanathan R (2012) A review of applications of analytic hierarchy process in operations management. Int J Prod Econ 138(2):215–241
11. Qureshi ME, Harrison SR (2003) Application of the analytic hierarchy process to riparian revegetation policy options. Small-Scale For Econ Manage Policy 2(3):441–458
12. Saaty RW (1987) The analytical hierarchy process—what it is and how it is used. Math Model 9(3–5):161–176
13. Saaty TL, Vargas LG (2012) Models, methods, concepts & applications of the analytic hierarchy process. International series in operations research and management science (2 edn). Springer, Berlin, 978-1-4614-3597-6
14. Salman AFM, Skibniewski MJ, Basha I (2007) BOT viability model for large scale infrastructure projects. J Constr Eng Manage 133(1):5–63
15. Dias A Jr, Ioannou PG (1996) Company and project evaluation model for privately promoted infrastructure projects. J Constr Eng Manage 122(1):71–82
16. Golden Bruce L, Wasil Edward A, Harker Patrick T (1989) The analytical hierarchy process: applications and studies. Springer, New York

Prevention of Flutter Instability in Control Surface of a Test Vehicle Through Parametric Studies

Bilpriya, S. Rajendran, P. Ashok Gandhi, and Manju George

Abstract This paper mainly deals with the prevention of flutter instability in fin with shroud of a typical Rocket body through parametric studies. Flutter is an aeroelastic instability which occurs when aerodynamic loads cause deformation of the body which in turn initiates an oscillation in the body and further interacts with aerodynamics. The crew escape system is an emergency escape structure designed to swiftly pull the crew module along with the astronauts to a secure distance from the launch vehicle during launch abort. For the control of crew escape system during the ascent phase of trajectory, sweep back fins are used at the bottom of the vehicle. Finite element modelling of the fin was done using MSC/PATRAN software. Flutter analysis is carried out in MSC/NASTRAN using in-built aerodynamics. MSC/NASTRAN uses plate theories such as Doublet Lattice Method for subsonic Mach number, ZONA51 for transonic and low supersonic Mach numbers and Piston theory for high supersonic Mach numbers to generate the aerodynamic force within NASTRAN. MSC/PATRAN is a software developed to provide a systematic approach towards making finite element modeling fast and accurate; MSC/NASTRAN is a general purpose finite element analysis computer program that addresses a wide range of engineering problem and is also capable to focus on particular types of analysis. In this work, initially normal mode analysis was carried out for the modeled fin and flutter analysis was performed. It was observed that flutter instability occurred in most of the Mach numbers. In order to prevent flutter, the method of mass redistribution is adopted. Mass addition is carried out on leading edge and trailing edge to see the effect of movement of C.G with respect to the shaft axis. By carrying out various mass redistribution studies, the flutter instability in the fin is alleviated. This effort will be helpful for flutter prevention in control surfaces of upcoming vehicles also.

Bilpriya (✉) · M. George
Department of Civil Engineering, Mar Baselios Institute of Technology and Science, Nellimattom, India
e-mail: elizabethpriyabijoy@gmail.com

S. Rajendran · P. A. Gandhi
Vikram Sarabhai Space Centre, Thiruvananthapuram, India

© Springer Nature Switzerland AG 2021

K. Dasgupta et al. (eds.), *Proceedings of SECON 2020*,
Lecture Notes in Civil Engineering 97,
https://doi.org/10.1007/978-3-030-55115-5_76

Keywords Aeroelasticity · Flutter · Control surface · Finite element model · Parametric · MSC/PATRAN · MSC/NASTRAN

1 Introduction

The branch of physics and engineering that deals with the interaction between inertial, elastic and aerodynamic forces is called aeroelasticity. Flutter testing and Prevention of flutter instability has become an integral part in the design of aerospace vehicles in order to ensure survivability. Flutter and divergence are two important dynamic and static aeroelastic phenomena which must be considered in the preliminary design phase of the air vehicle structural design. Flutter is a self excited dynamic instability of an elastic structure in a fluid flow, caused by positive feedback between the body's deflection and the force exerted by the fluid flow. It happens when an aerodynamic force is applied to an object causing it to oscillate and as the force increases the oscillations also increase, until the object fails by means of fracture. This catastrophic event must be avoided at any cost. Real flight testing and wind tunnel testing are two ways to clear a vehicle for flutter, but both are expensive and occur at the later stage of the design process. Therefore engineers rely on the computational methods to assess the aeroelastic characteristics of flight vehicles. The unsteady aerodynamic loads are calculated and the flutter equation is solved using P-K method embedded in MSC/NASTRAN Flutter analysis by means of simple harmonic motion. Accordingly, frequency and damping curves of the typical fin are estimated. MSC/NASTRAN has the ability to execute aeroelastic analyses since the early 1970s. This paper mostly deals with the prevention of flutter instability in fin with shroud of a typical rocket body through parametric studies.

2 Literature Review

For theoretical analysis of active flutter suppression Paek and Lee [1] discussed about the root locus and iterative V-g method to analyze the flutter for a control surface of a launch vehicle with control actuators. Karadal and Librescu [2] presented the control of the flutter instability and the conversion of the dangerous character of the flutter instability boundary into not dangerous one for a cross-sectional wing in a supersonic/hypersonic flow field. In order to study the flutter suppression in fins Karadal and Şahin [3] conducted the theoretical analysis of an active flutter suppression methodology applied on a smart fin where the fin consisted of a cantilever aluminum plate-like structure with surface bonded piezoelectric (PZT, Lead-Zirconate-Titanate) patches. Njuguna [4] addressed the flutter phenomenon and effectual means of flutter prevention and reviews some of the most recent theoretical and experimental developments in flutter analyses. The theoretical, computational

and experimental flutter for composite structures is pursued. Zhao et al. [5] did dedicated study on the flutter characteristics of control rudder of high speed flight vehicle They proposed a novel parameter-tuning method for the flutter characteristics parametric of control rudder at the beginning design stage of flight vehicle by combining parameterized dynamic modeling technology, aerodynamic and aeroelastic flutter analysis methodology. Vikhorev and Goman [6] found that flutter of the nonlinear aeroelastic wing section system with actuator constraints can be effectively stabilized under action of large external disturbances using only the trailing-edge flap.

3 Modeling

The finite element model of the fin is created and meshed in MSC/PATRAN. The skeletal structure is completed with assembly of one, two, three-dimensional elements such as bar elements, beam elements, and plate elements providing a cantilever boundary condition at the nodes where the fin will be attached to the shroud. For modeling beam, CBEAM elements are used. In order to define membrane, bending, transverse, shear and coupling parameters of thin shell, PSHELL elements are used. For this purpose, quadrilateral plate element connection CQUAD4 and triangular plate element connection CTRIA3 are used. The finite element model is shown in Fig. 1. The fin is modeled in two parts mainly fixed part and movable part. The fixed part of the fin is attached to the L-bracket using multi point constraints and it is also provided with fixed support at points where the fin is attached to the shroud. The typical rocket body in which the fins are used is shown in Fig. 2 and typical trajectory profile is shown in Fig. 3.

4 Analysis

The method adopted for the flutter analysis is explained as follows. It involves four steps viz., the first one is the creation of the Finite Element model, then the second is structural dynamic analysis to identify the flexible mode shapes and its frequencies, and the third is generation of aerodynamic mesh and coupling of aerodynamic and structural mesh, and then finally the fourth is solving the flutter problem using P-K method. The finite element model of the fin is made using MSC/PATRAN software and the analysis is carried out for flutter using MSC/NASTRAN. The aerodynamic mesh and structural mesh are different and hence splining function in-built in NASTRAN is used, which takes care of the transfer of forces from aero mesh to structure mesh. The aerodynamic mesh of the fin modeled is as shown in Fig. 4.

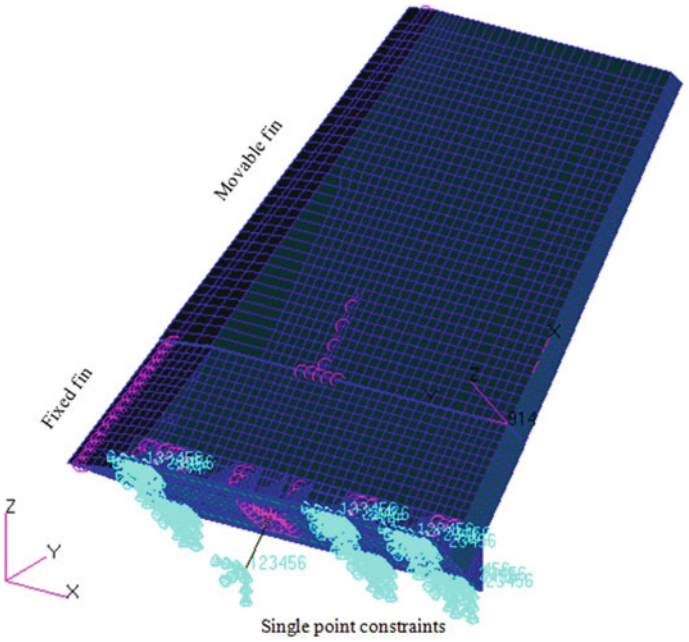

Fig. 1 Fin modelled in MSC/PATRAN

4.1 Modal Analysis

A modal analysis calculates the frequency modes or natural frequencies of a given system. The natural frequency (ω) of a system is dependent only on the stiffness of the structure and the mass which participates with the structure. It is useful to know the modal frequencies of a structure as it allows you to ensure that the frequency of the applied periodic loading will not coincide with a modal frequency and hence cause resonance, which leads to large oscillations. Table 1 shows the frequencies at different modes of the fin. Generally, here bending, torsion and in-plane modes are taken and mode shapes are also plotted in Fig. 5.

4.2 Flutter Analysis

Flutter speed is an essential performance index in aircraft design. The flutter speed of the fin is obtained from the flutter analysis performed in NASTRAN. To NASTRAN, we provide an input file which contains the structural model, aerodynamic model, splining definition and the flight conditions such as Mach number, dynamic pressure and air density for which flutter analysis has to be carried out. The flight trajectory parameters are shown in Fig. 3. From the output of NASTRAN, we find the flutter

Fig. 2 Typical Rocket body

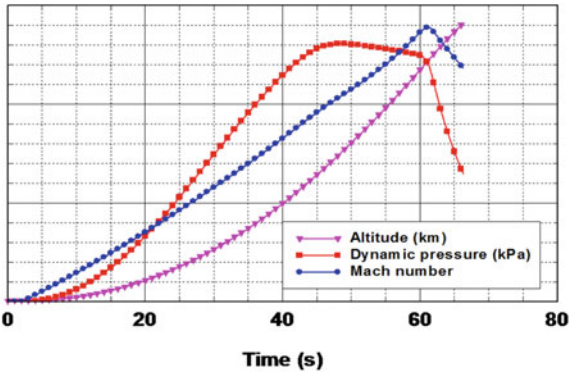

Fig. 3 Trajectory of typical Rocket body

Fig. 4 Aero mesh of fin

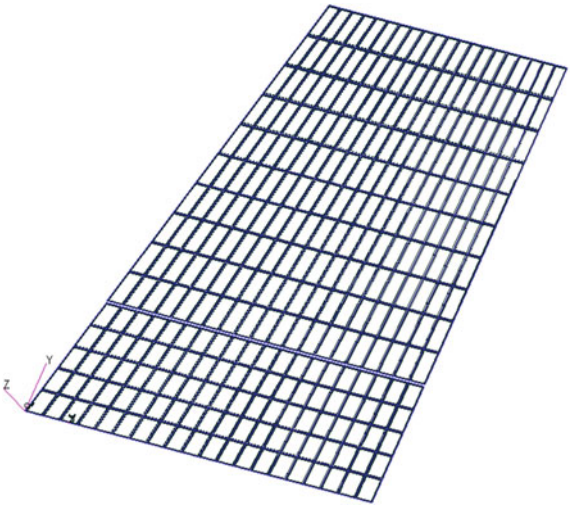

Table 1 Frequencies of the original fin design

Modes	1	2	3
Frequency (Hz)	22.1	28.1	28.6

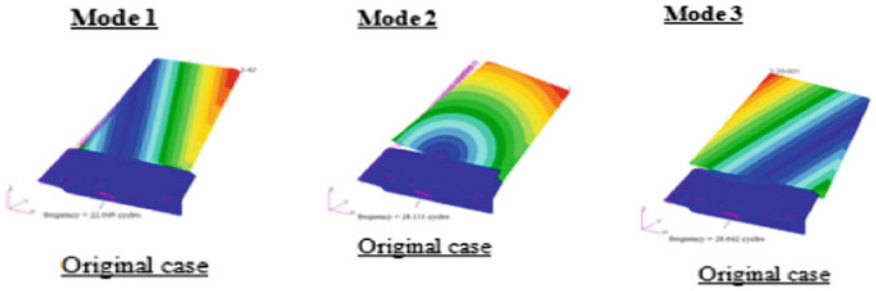

Fig. 5 Mode shape of original fin design

velocity. The lowest velocity value where the system damping changes the sign (negative to positive in NASTRAN output) for the modes we consider is termed as the flutter velocity of the respective system. Two very important numbers that appear repeatedly in flutter analysis are the Mach no. and reduced frequency (k). Mach no. is the ratio of free stream air speed over the speed of sound. From the flutter analysis it was revealed that the original fin was susceptible to flutter, since it had a negative flutter margin. To prevent the fin from flutter instability, various parametric studies are done. One technique of reducing flutter is by setting a maximum air speed using a ratio of energies such as energy input to energy output. But this won't work in the current case as the flutter margin are negative, meaning the flight would experience

flutter before it reaches the desired vehicle velocity itself, so setting up the maximum air speed is ruled out for this case. Another method is to adjust the distribution of the mass load by bringing the centre of gravity closer to the centre of twist. This causes natural damping thus reducing the oscillations within the structure and cancelling out the flutter. Alternative way is to use a ratio between the stiffness and mass. By increasing this ratio we can get better stability in the wing and a more rigid outcome. This is the hardest to achieve, because when the mass of material is reduced, it leads to a reduction in rigidity. So to get past this, a new material has to be used. Hence in the present work, the technique of mass distribution is used to alleviate the flutter situation.

4.3 Parametric Studies Carried Out

The method of parametric is done by redistributing the mass in leading edge and trailing edge of the movable fin. The leading edge had an initial mass of 5 kg and an addition of mass of 3, 5 and 11 kg are done sequentially. At 11 kg mass addition on leading edge it is found that positive margin is obtained and addition of this mass is effective in preventing flutter. In the alternate approach, while the initial mass of trailing edge was about 3 kg, an addition of 3, 5 and 11 kg is done sequentially. In all these cases it is found to be effective and no flutter is observed at higher Mach numbers. But adding 11 kg in the leading edge had more effect of increasing the Flutter margin above 3.0 when compared to trailing edge mass addition giving a value of 1.0.

4.4 Methodology

The flutter analysis is carried out for all the lifting structures of the rocket body are done to ensure the safety of the rocket body while flying through the atmosphere. The unsteady aerodynamics for the flutter analysis is generated from NASTRAN inbuilt aerodynamic theory namely Doublet lattice method for subsonic regime of Mach numbers (0.5–0.8) and ZONA51 method for transonic and supersonic regime of Mach numbers (0.8–2.0). In transonic regime, ZONA51 gives fairly decent results up to M = 0.9 and above M = 1.1. Out of the three types of flutter solutions i.e., p-method, k-method and p-k method, the p-k method is found to be more appropriate for the present analysis. The flutter can be observed from the frequency-damping-velocity plot called as flutter plots or ν-g-ω plot.

Table 2 Frequencies for leading edge and trailing edge mass addition case

Frequencies for different mass addition case (Hz)							
Modes	Original	On leading edge mass addition			On trailing edge mass addition		
		3 kg	5 kg	11 kg	3 kg	5 kg	11 kg
1	22.1	21.8	21.6	20.5	19.8	18.6	16.0
2	28.1	26.5	25.3	23.1	26.7	25.8	23.6
3	28.6	27.1	26.5	24.7	28.4	28.2	27.8

5 Results and Discussions

5.1 Modal Analysis of Fin

Table 2 and Fig. 6 show the comparison of modal analysis of fin after addition of the mass in leading edge of the fin. From the figure it can be seen that the mass addition of 11 kg makes the fin modes decoupled (bending and torsion modes are pure, visible from the fringe pattern). Table 3 and Fig. 7 show the comparison of mode shapes of original case and trailing edge mass addition case. It can be seen from Fig. 7 that the modes are still coupled. The grid independence study was carried out and the mesh giving converged results are used.

5.2 Flutter Analysis of Fin

5.2.1 Leading Edge Mass Redistribution Case

From the studies conducted, it is observed that flutter instability can be prevented by adding sufficient mass at leading edge or trailing edge. But mass redistribution in leading edge is effective for the reason that, by adding 11 kg in leading edge gives flutter margin above 1.0 for all Mach numbers than adding the same mass in trailing edge. The graphs and table given below show the flutter margin for different cases. Table 3 shows the original case of fin which had a negative flutter margin. Figure 8 also shows the actual flutter margin versus Mach no. Minimum flutter margin is found to be −0.04. As per NASA criteria, minimum flutter margin required is above 0.15, meaning flutter velocity should be minimum 15% more than the vehicle velocity.

$$FlutterMargin = \frac{flutter\ velocity}{vehicle\ velocity} - 1.0$$

In leading edge, the mass additions are 3, 5 and 11 kg. The flutter margin for all the cases are given in Table 4. The comparison of flutter margin for all these options along with original design case is depicted in Fig. 9. As seen from the figure

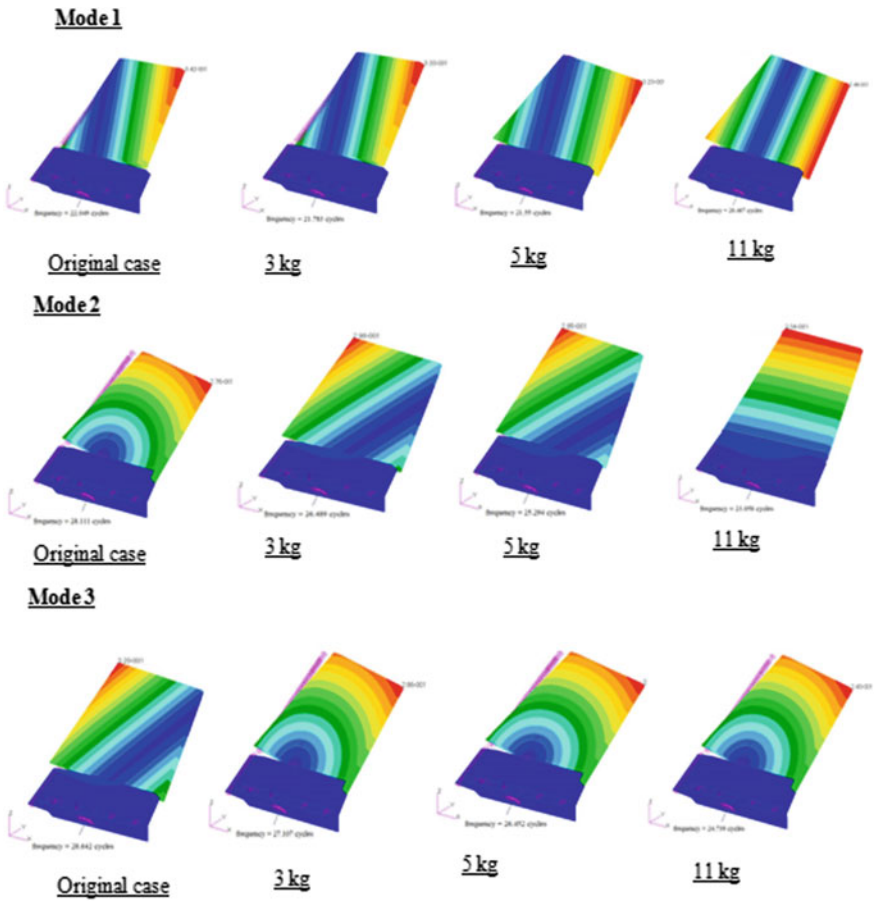

Fig. 6 Mode shapes of original and leading edge mass distribution case

and table, adding 3 and 5 kg at the leading edge gives lower flutter margin than the original case, the reason being, when we try to move the C.G towards leading edge, initial cases of 3 and 5 kg, the modes become more coupled hence reduces the flutter margin further. But for the last case of 11 kg addition, the modes become decoupled, flutter is avoided, and hence gives higher margin.

The intention of mass addition is to move the C.G so that the coupled modes which existed in the original fin become uncoupled. There are two ways to do that; either move the C.G above the shaft axis by adding more mass in the leading edge, or by adding the mass on the trailing edge. Mass redistribution can also be attempted on the middle portion of the fin, but that does not give a drastic movement in the C.G. Initially the case of adding mass in leading edge is studied. By adding 11 kg to the leading edge the C.G has moved about 24 mm towards the leading edge. From Fig. 9, it is seen that 11 kg mass addition has the positive margin throughout for

Table 3 Flutter margin for original case

Mach no. (M)	Air density (kg/m^3)	Vehicle velocity, V_v (m/s)	Flutter velocity, V_f (m/s)	Flutter ratio (V_f/V_v)	Flutter margin ($V_f/V_v - 1.0$)
0.5	0.9638	170.63	184.8	1.08	0.08
0.6	0.8883	203.33	206.1	1.01	0.01
0.7	0.811	235.03	234.3	1.00	0.00
0.8	0.7338	265.78	255.6	0.96	-0.04
0.9	0.6569	295.82	290.9	0.98	-0.02
1.1	0.493	350.57	389.9	1.11	0.11
1.2	0.4258	374.46	453.5	1.21	0.21
1.5	0.2905	441.15	559.6	1.27	0.27
1.8	0.2045	506.38	708.1	1.40	0.40
2.0	0.1383	569.12	No flutter velocity upto 800 m/s		

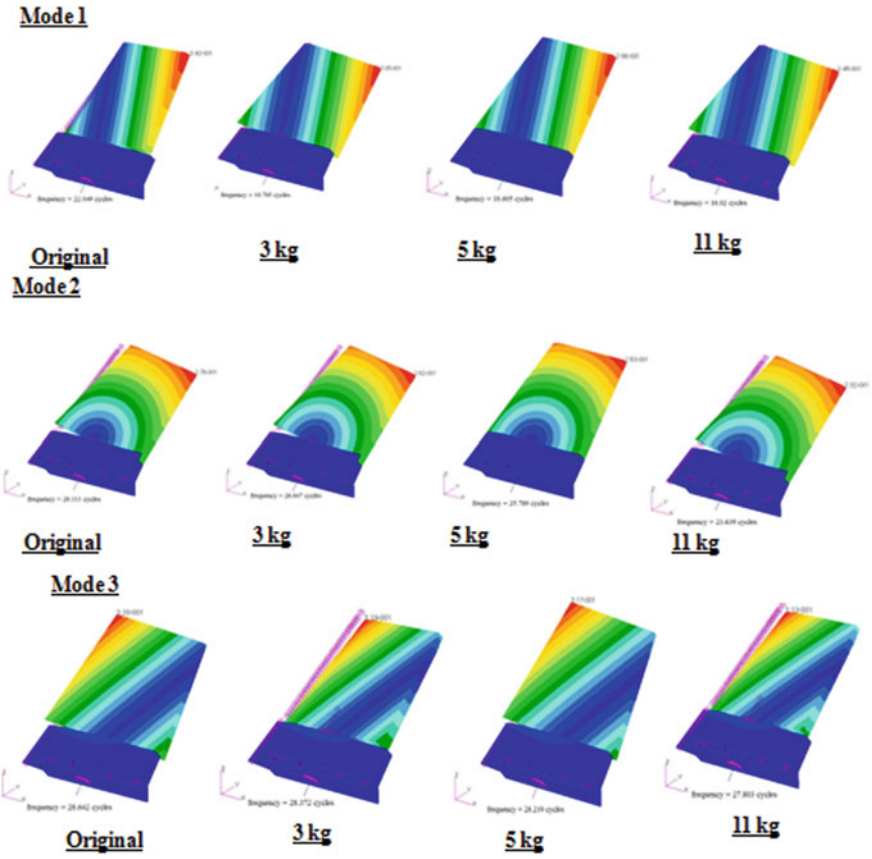

Fig. 7 Mode shapes of original and trailing edge mass distribution case

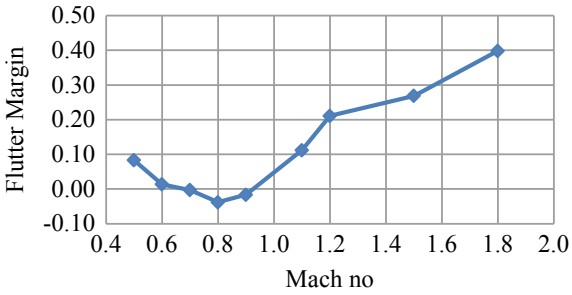

Fig. 8 Flutter margin of original case

Table 4 Flutter margin for different mass addition in leading edge

Mach no.	Density (kg/m^3)	Vehicle velocity, V_v (m/s)	Flutter velocity, V_f (m/s)			Flutter margin ($V_f/V_v - 1.0$)		
			3 kg	5 kg	11 kg	3 kg	5 kg	11 kg
0.5	0.9638	170.6	170.7	191.9	715.2	0.00	0.12	3.19
0.6	0.8883	203.3	184.8	199.0	729.3	−0.09	−0.02	2.59
0.7	0.811	235.0	206.1	213.1	743.4	−0.12	−0.09	2.16
0.8	0.7338	265.8	220.2	220.2	750.5	−0.17	−0.17	1.82
0.9	0.6569	295.8	248.5	234.3	754.5	−0.16	−0.21	1.55
1.1	0.493	350.6	326.3	290.9	827.3	−0.07	−0.17	1.36
1.2	0.4258	374.5	404.0	375.8	No flutter velocity upto 1100 m/s	0.08	0.00	Flutter margin >1.0
1.5	0.2905	441.2	503.0	488.9		0.14	0.11	
1.8	0.2045	506.4	630.3	602.0		0.24	0.19	
2.0	0.1383	569.1	792.9	757.6		0.39	0.33	

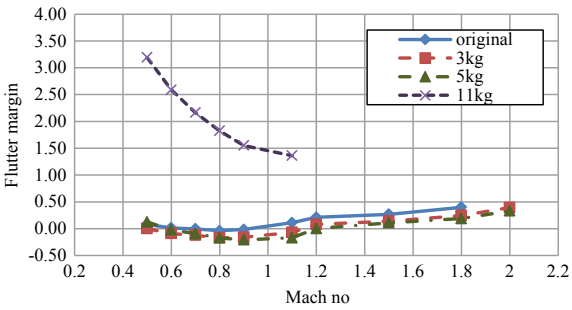

Fig. 9 Comparison of flutter margin for leading edge mass addition with original design

all the Mach numbers, i.e., well above 1.0, which is a better margin considering the scenario of the original fin. Though 0.15 margin is sufficient as per NASA criteria, still enough margins are built in to take care of uncertainties in the theory in transonic regime and actual damping values. Also during transonic Mach number, between M = 0.9–1.1, there is a chance for transonic bucket or dip type behavior to occur in the

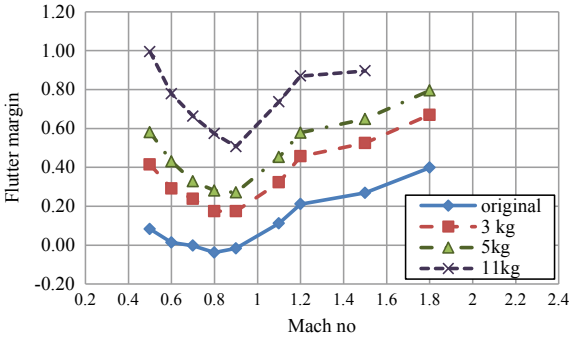

Fig. 10 Comparison of flutter margin for trailing edge mass addition with original design

flutter margin curve. So considering all these, addition of 11 kg mass is the preferred solution, with minimum penalty in weight.

5.2.2 Trailing Edge Mass Redistribution Case

Mass at the trailing edge is added in the similar way as the leading edge, and the flutter analysis is repeated for all the cases of 3, 5 and 11 kg. The flutter margin for all the cases are given in Tables 8, 9 and 10 respectively. The comparison of flutter margin for all these options along with original design case is depicted in Fig. 10. It is seen that the flutter margin improves when the mass is added at the trailing edge too. With mass addition of 11 kg at the trailing edge the flutter margin is above 0.5 for all the Mach numbers. A gradual increase from negative flutter margin to positive flutter margin is seen for each mass addition case. Still these are not as advantageous as the leading edge case, which gives much better flutter margin. By adding 11 kg of trailing edge mass, the C.G is moved about 89 mm below the original C.G position (Table 5).

Though the flutter margins are positive, the advantage what we get by adding 11 kg mass in leading edge is not seen in the trailing edge mass addition option. The answer to this lies in the decoupling of bending and torsion mode. When we add 11 kg to the leading edge the coupled mode of bending and torsion becomes decoupled and pure which is evident from Fig. 6, but adding 11 kg in trailing edge doesn't make the modes decoupled as seen from Fig. 7.

6 Conclusions

Flutter analysis and testing has become an integral part of the design process to ensure survivability. Flutter can cause vehicle structures to fail, and is an important element of the flight envelope to investigate. In this paper, aeroelasticity with regard to flutter analysis is covered. Through analysis, it was found that the original fin design was

Table 5 Flutter margin for different mass addition in trailing edge

Mach no.	Density (kg/m^3)	Veh. velocity, V_v (m/s)	Flutter velocity, V_f (m/s)			Flutter margin ($V_f/V_v - 1.0$)		
			3 kg	5 kg	11 kg	3 kg	5 kg	11 kg
0.5	0.9638	170.6	241.4	269.7	340.4	0.41	0.58	0.99
0.6	0.8883	203.3	262.6	290.9	361.6	0.29	0.43	0.78
0.7	0.811	235.0	290.9	312.1	390.9	0.24	0.33	0.66
0.8	0.7338	265.8	312.1	340.4	418.2	0.17	0.28	0.57
0.9	0.6569	295.8	347.5	375.8	445.5	0.17	0.27	0.51
1.1	0.493	350.6	463.6	509.1	609.1	0.32	0.45	0.74
1.2	0.4258	374.5	545.5	590.9	700	0.46	0.58	0.87
1.5	0.2905	441.2	672.7	727.3	836.4	0.52	0.65	0.90
1.8	0.2045	506.4	845.5	909.1	>1100	0.67	0.80	>1.0
2.0	0.1383	569.1	No V_f obtained up to 1100 m/s			Flutter margin >1.0		

susceptible to flutter, so parametric studies were carried out in order to avoid flutter. Through various parametric studies, it is concluded that mass addition in leading edge of the fin could successfully produce a positive margin to greater extent when compared to adding same mass to the trailing edge. The reason is understood to be the extent of decoupling the bending-torsion coupled modes is more effectively done by adding higher mass to the leading edge than to the trailing edge; but for lesser mass addition, it works out to be other way. The addition of 5 kg in trailing edge would give the flutter margin above 0.15, but in order to build sufficient margin to take care of uncertainties in the theoretical computation, damping values and to take care of the transonic dip in the flutter curves, 11 kg mass addition in leading edge is considered to be the preferred solution.

Acknowledgements The authors would like to acknowledge, the scientists from VSSC, ISRO who have initially guided us in successfully carrying out the dynamic and aeroelastic analysis of sounding rockets and reusable launch vehicle type rockets. We would also like to acknowledge MSC/NASTRAN technical support people for guiding us in the software side.

References

1. Paek S-K, Lee I (1996) Flutter analysis for control surface of launch vehicle with dynamic stiffness. Comput Struct 60:593–599
2. Marzocca P, Librescu L (2010) About the effect of control on flutter and post-flutter of a supersonic/hypersonic cross-sectional wing 3:1–25
3. Karadal FM, Şahin M (2008) Active flutter control of a smart fin. In: International conference on adaptive structures and technologies, vol 19, pp 1–12, Department of Aerospace Engineering

4. Njuguna J (2007) Flutter prediction, suppression and control in aircraft composite wings as a design prerequisite. Struct Control Health Monit 14:715–758
5. Zhao X, Cao C, Guo P (2018) Simulation analysis study on the flutter characteristics of control rudder in high speed flight vehicle. J Phys Conf Ser 1:1–8
6. Vikhorev KS, Goman M (2010) Effect of control constraints on active stabilization of flutter, vol 3. The University of Nottingham, Nottingham, pp 1–9
7. Petyt M (2003) Introduction to finite element vibration analysis, vol 7. Institute of Sound and Vibration Research, pp 1–27
8. Fung YC (2003) An introduction to the theory of aero elasticity, vol 3. University of California, pp 160–186

Experimental Investigations on Using Distributed Fiber Sensing for Monitoring Pipelines

Shika George, B. Arun Sundaram, and Mathews M. Paul

Abstract Pipeline networks are responsible for transporting vital materials such as water, oil and gas. Complicated loads, material aging, environmental corrosion, and vibration fatigue are the factors which may cause structural deteriorations of pipelines during the life cycle service because of which leaks may arises. Any leakage in the pipeline system can cause major financial losses and possible environmental damages. Currently, buried pipelines are only monitored at key points, which can be spaced several kilometers apart. The use of these discrete sensors for large pipelines is simply impracticable and not cost effective. Distributed fiber optic sensing offers the ability to measure temperatures and strains at thousands of points along a single fiber. DSTS-BOTDA (Distributed Strain and Temperature Sensor-Brillouin Optical Time Domain Analysis) utilizes "stimulated" Brillouin scattering while a DSTS-BOTDR (Distributed Strain and Temperature Sensor-Brillouin Optical Time Domain Reflectometer) utilizes "spontaneous" Brillouin scattering. In this paper, experimental investigations carried out using distributed fiber optic sensing for leakage identification in pipelines is presented. Two different kinds of sensors were used for monitoring strain and temperature variations during leakage. The methodology adopted for instrumentation and the results obtained are presented in detail in this paper.

Keywords Distributed fiber optic sensor · PVC pipelines · Brillouin optical time domain analysis

S. George (✉) · M. M. Paul
Department of Civil Engineering, Mar Athanasius College of Engineering, Kothamangalam, Kerala, India
e-mail: shikageorge9098@gmail.com

B. A. Sundaram
CSIR-Structural Engineering Research Centre, Chennai, India

© Springer Nature Switzerland AG 2021

K. Dasgupta et al. (eds.), *Proceedings of SECON 2020*,
Lecture Notes in Civil Engineering 97,
https://doi.org/10.1007/978-3-030-55115-5_77

1 Introduction

Pipeline network constitute one of the most important ways to transport large amounts of oil and gas through long distances. Leakages in pipelines are very dangerous since they may induce severe environmental problem and economic losses [1]. Factors such as corrosion, vibration, and external impacts may cause pipeline leakages [2]. A major issue of monitoring existing pipelines is that normally the pipelines are very long and is often buried underground or underwater, so it is not easy to get access to retrofit monitoring sensors.

In many structural applications, it is often desirable that strain and temperature are monitored at multiple locations at the same time [3]. Moreover, the use of these multi-point localized sensors for large civil structures is simply impracticable and not cost effective. Distributed fiber optic sensors allows the monitoring of local strain, temperature, and corrosion rate, etc. at thousands of locations distributed along a single mono-mode optical fiber. These sensors can be distributed along the length of pipe network via the guiding of lightwaves along the fiber optic lines. Leakage in pipeline may cause a temperature rise around the leakage point.

Feng et al. studied the feasibility of leakage monitoring of oil pipeline by using BOTDR. Four kinds of sensing cables with different structures are evaluated in the experiments by comparing their effectiveness in the leakage monitoring and three kinds of laying styles such as straight line, tri-fold, and spiral styles are used. Sensing cable provided with loose tube structure is better for the temperature monitoring. Straight line and spiral are suitable for the leakage monitoring, which can detect the leakage of 1.1 m^3/h [4]. Wong et al. studied experimentally the ability of distributed optical fibre strain sensor to monitor the fatigue crack growth along the cast iron pipeline having a diameter of 660 mm and 18 mm remaining wall thickness which was used for the fatigue testing. Distributed optical fibre sensor was instrumented on the pipe in order to monitor the condition of the pipe. Fatigue test is carried out using a newly developed large scale cyclic pressure loading facility which vicinity to typical water pressure loading experienced in the field. Distributed optical fibre sensor can only detect the change due to the presence of the crack when the distance between the sensor and the damage was less than 40 mm [5].

Brillouin Optical Time Domain Analysis (BOTDA) uses the optical fiber to sense the change of environment and can measure the temperature at every position of fiber. In this paper the experimental investigations were carried out using distributed fiber optic sensors for identification of leakage in pipeline and is presented in detail. The studies were carried out using a PVC pipeline model in the laboratory and controlled leakages were made and the leakage was identified using BOTDA.

2 Brillouin Scattering Principle

Brillouin scattering occurs due to the interaction between optical and probe light-wave and the acoustic wave in fiber. The Brillouin wavelength shift is proportional to the acoustic velocity in the fiber which in turn is related to its density. However, density depends on the strain and the temperature of the optical fibre [6]. Brillouin shift can be used to measure those parameters. DSTS-BOTDA (Distributed Strain and Temperature Sensor-Brillouin Optical Time Domain Analysis) utilizes "stimulated" Brillouin scattering while a DSTS-BOTDR (Distributed Strain and Temperature Sensor-Brillouin Optical Time Domain Reflectometer) utilizes "spontaneous" Brillouin scattering. These are two types of distributed sensor systems which are explained in the following sections.

2.1 DSTS-BOTDA

Brillouin Optical Time Domain Analysis (BOTDA) utilizes "stimulated" Brillouin scattering to measure strain and temperature. In a BOTDA system, two laser beams are injected into opposite ends of the fiber. A continuous wave (CW) beam is injected into one end of the fiber, while a pulse is injected into the other. Energy transfer occurs from one beam to the other, and it is actually the loss in the CW beam that is monitored.

Although a BOTDA requires access to both ends of the fiber, it is popular because of its sensitivity, which is significantly better than that of a BOTDR. The improved sensitivity allows spatial resolution as fine as 10 cm, and shorter measurement times compared to a BOTDR.

2.2 DSTS-BOTDR

In a BOTDR, a single laser beam is pulsed into one end of the fiber. A very small percentage of the light is scattered back to the source by means of spontaneous Brillouin scattering, which takes place along the entire length of the fiber. Spectral analysis of the light from the Brillouin scattering reveals the change in strain and/or temperature, while the time of arrival of the scattered pulse determines the position of the measurement along the length of the fiber.

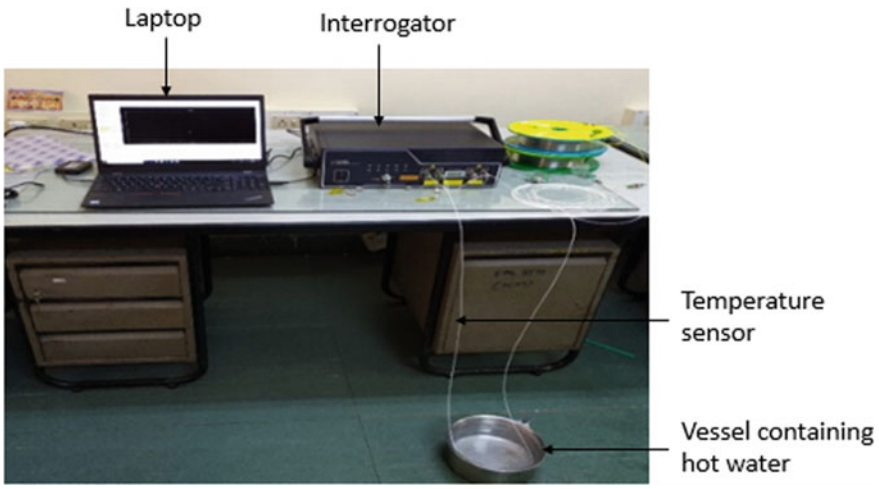

Fig. 1 Calibration test set-up

3 Calibration Test

The calibration studies were carried out to understand the response of the distributed fiber sensor to known temperature variations. The calibration test setup is as shown in Fig. 1. A vessel was filled with hot water having a temperature of around 70 °C. The optical fiber was connected to the interrogator in BOTDA mode (both the ends were connected to interrogator). Baseline frequency of the optical fiber was measured at room temperature prior to the experimental program. A small portion of the optical fiber was placed in the vessel with hot water. The temperature of the hot water was also monitored using a thermometer for validation with the distributed sensor. The Brillouin frequency was measured at frequent intervals during the experimental program. The measured frequency shift is converted into temperature using the fiber temperature coefficient 0.9765 MHz/°C.

4 Experimental Investigations in Pipeline by Simulating Leakage

Experimental investigations were carried out using a PVC pipeline model of length 3000 mm and diameter 50 mm. The PVC pipeline model was made with elbow joints at both ends to facilitate filling of water during the experimental investigations. The schematic of the experimental setup is as shown in Fig. 2. A wooden box of dimensions 2.5 × 0.65 × 0.63 m was made and partially filled with sand upto a depth of around 200 mm. The model pipeline with the elbows was placed inside box with two supports at the ends. Small holes were drilled in the pipeline at intervals

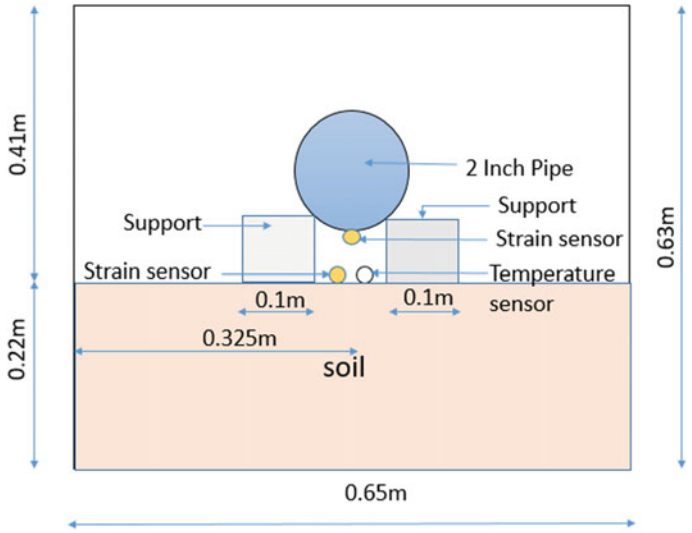

Fig. 2 Schematic representation of instrumentation on the pipe specimen

of 450 mm to simulate leakage. Two optical fibers one for strain and another for temperature measurement was placed at a depth of around 10 mm below the pipeline in the soil. Another fiber optic sensor was bonded to the bottom of the pipeline for measuring the strain response as shown in Fig. 3. The instrumented fiber optic sensors were connected to the interrogator in BOTDA mode (Fig. 4). Both ends of each optical fiber was connected to the interrogator. The baseline Brillouin frequency for both the fibers was measured prior to the start of the experimental program. Additionally a small portion of the optical fiber was kept in a beaker to be used for

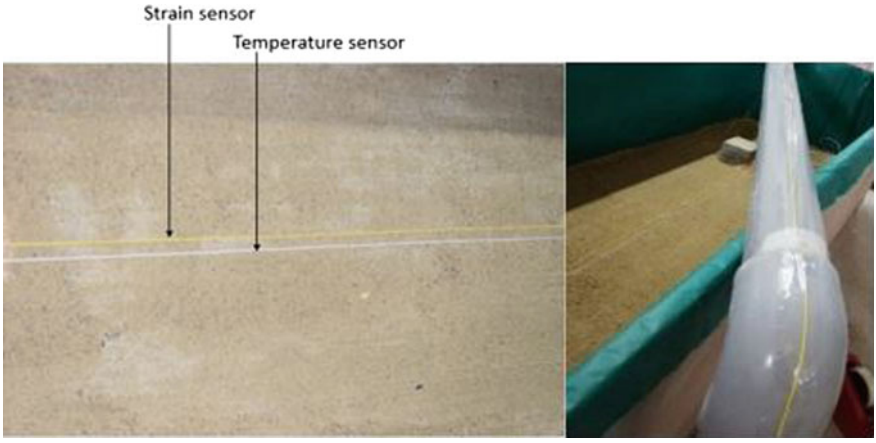

Fig. 3 Instrumentation of strain and temperature sensor

Fig. 4 DSTS connected to interrogator

measuring the shift in the wavelength of the optical fiber when immersed in hot water. Fiber strain coefficient and fiber temperature coefficient is about 18.9150 MHz/με and 0.9765 MHz/°C respectively. These coefficients will be used for converting the measured frequency shifts to temperature and strain. The experimental setup along with the data acquisition system is as shown in Fig. 5. The pipeline was filled with hot boiling water. The beaker was also filled with hot water to see the response of the optical fiber. Due to the holes present in the pipeline, the hot water was leaking from the pipeline. The shift in frequency in the optical fiber was measured in regular intervals.

Fig. 5 Experimental set-up for pipeline monitoring

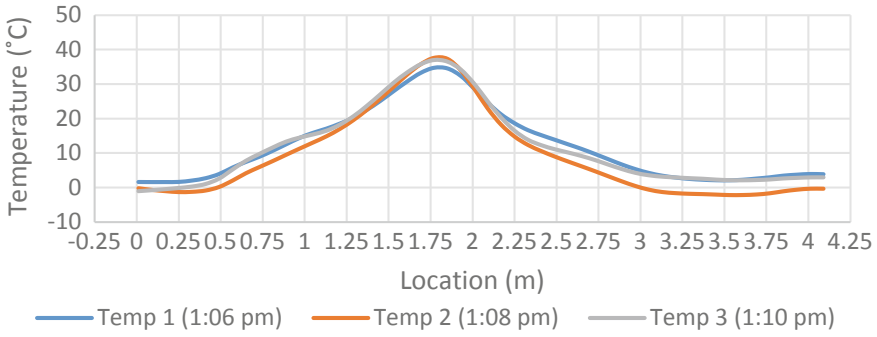

Fig. 6 Calibration curve obtained by dipping temperature fiber in hot water

5 Results and Discussions

5.1 Calibration Study

The Brillouin frequency was measured at regular intervals after pouring the hot water in the vessel. The absolute temperature of the water was also measured using a thermometer which was around 70 °C. The difference between the baseline frequency and the measured frequency is plotted in Fig. 6. From the plot it can be seen that the measured temperature was around 38 °C. The room temperature during the measurement of baseline frequency was around 30 °C. Hence the absolute temperature measured was 68 °C. Thus the optical fiber sensor is sensitive to temperature variations and also gives variation of temperature profile along the length of the fiber.

5.2 Leakage Study

The baseline frequency measured prior to the experimental program is plotted along with the frequency measured after filling the pipeline with hot water is shown in Fig. 7. The baseline frequency was obtained as 10798.60 MHz. The Brillouin frequency shift is obtained as 10840 MHz at 1.71 m of fibre length. Fiber temperature coefficient is about 0.9765 MHz/°C. Therefore the temperature rise is obtained as 42.39 °C. Therefore the total temperature of hot water in beaker is obtained as 69.39 °C as the ambient temperature was around 27 °C. The baseline frequency for 3rd leakage point was obtained as 10,806.565 MHz at 4.73 m. The Brillouin frequency shift is obtained as 10,833.1081 MHz at 4.73 m of fibre length. Therefore the temperature rise is obtained as 27 °C. Therefore the total temperature gradient at the 3rd leakage point is obtained as 54 °C. It can be seen from the plot that, the Brillouin frequency shift has been seen only at those three points where leakage has been simulated and also in the portion of the fiber in the beaker. Due to leakage in the pipelines, there

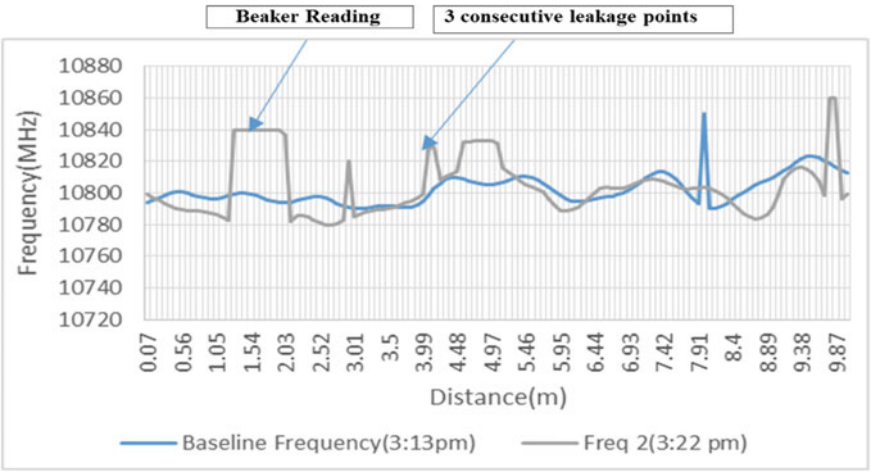

Fig. 7 Response measured during leakage testing

will be change in the temperature of the surrounding soil. Hence by using these distributed optical fiber sensors, the leakage can be identified along with the location of leakage.

6 Conclusions

Experimental investigations have been carried out by simulating leakage in a PVC pipeline model and monitoring the change in temperature of the surrounding soil through distributed fiber sensing. Two sensors were laid in the soil near to the pipeline for measuring strain and temperature. Hot water was filled in the pipeline. Leakage has been simulated at three different locations and from the responses measured, the leakage locations were identified. The temperature measured during calibration studies was around 68 °C as against the actual temperature of 70 °C. The baseline frequency for 3rd leakage point was obtained as 10,806.565 MHz at 4.73 m. The Brillouin frequency shift is obtained as 10,833.1081 MHz at 4.73 m of fibre length. Therefore the temperature rise is obtained as 27 °C. Therefore the total temperature gradient at the 3rd leakage point is obtained as 54 °C. Due to leakage in the pipelines, there will be change in the temperature of the surrounding soil. Hence by using these distributed optical fiber sensors, the leakage can be identified along with the location of leakage. There was no variation in strain and hence it is not presented.

Acknowledgements Authors would like to thank Structural Health Monitoring Laboratory, CSIR-Structural Engineering Research Centre, Chennai for the facilities provided for carrying out the experimental investigations.

References

1. Ren L, Jiang T, Jia Z-G, Li D-S, Yuan C-L, Li H-N (2018) Pipeline corrosion and leakage monitoring based on the distributed optical fiber sensing technology. Measurement 115(5):57–58
2. Fidanboylu E (2009) Fiber optic sensors and their applications. In: 5th International advanced technologies symposium (IATS'09), May 13–15, Karabuk, Turkey
3. Rajeev P, Kodikara J, Chiu WK, Kuen T (2013) Distributed optical fibre sensors and their applications in pipeline monitoring. Key Eng Mater 558:424–434
4. Wang F, Sun Z, Zhu F, Zhu C, Pan Y, Dong J, Zhang X, Gao L (2016) Research on the leakage monitoring of oil pipeline using BOTDR. In: Progress in electromagnetic research symposium, Aug 2016, pp 8–11
5. Wong L, Rathnayaka S, Chiu WK, Kodikara J (2017) Fatigue damage monitoring of a cast iron pipeline using distributed optical fibre sensors. Procedia Eng 188:293–300
6. Glisic B, Inaudi D (2007) Fibre optic methods for structural health monitoring. Wiley, Hoboken

Performance Assesment of GGBS and Rice Husk Ash Based Geopolymer Concrete

Maria Eldho, V. Srinivasan, and Sarah Anil

Abstract Geopolymer concrete technology is a promising technology for the construction industry. Replacing the conventional resource consuming Portland cement with supplementary cementitious material can reduce the carbondioxide emission as well as energy consumption. It serves as an effective way of disposing industrial wastes that found difficult to be handled in past. Rice husk ash, an agricultural biomass which is rich in silica can be used as an effective source material. In the present study M30 grade GGBS and rice husk ash based geopolymer concrete is developed. Rice husk ash of varying percentage of 5 and 15% is considered to study its effect on mechanical and durability properties. 6 M sodium hydroxide is used. Ratio of sodium hydroxide to sodium silicate used is 1:2. Ambient curing of 28 days is done. The result is compared with OPC concrete specimen to evaluate the performance of geopolymer concrete.

Keywords Geopolymer concrete · Supplementary cementitious materials · GGBS · Rice husk ash · Durability · Ambient curing

1 Introduction

Concrete is the major construction material used all over the world, and its use is second to water [1]. Construction industry has now become the largest consumer of the global natural resources. The production of cement consumes large amount of natural resources [2, 3]. And it can be said that production of cement means production of pollution due to production of carbondioxide. The cement industry contributes to about 5–7% of the global carbondioxide emission [4]. Moreover there is an ever-increasing need for cement in the world so that about three tons of concrete

M. Eldho (✉) · S. Anil
Department of Civil Engineering, Mar Athanasius College of Engineering, Kothamangalam, Kerala, India
e-mail: mariyaaeldho@gmail.com

V. Srinivasan
CSIR-Structural Engineering Research Centre, Chennai, India

© Springer Nature Switzerland AG 2021

K. Dasgupta et al. (eds.), *Proceedings of SECON 2020*,
Lecture Notes in Civil Engineering 97,
https://doi.org/10.1007/978-3-030-55115-5_78

would be consumed annually per one human living on the earth [5]. Therefore, to produce environmentally friendly concrete, it is inevitable to use alternative materials to replace traditional Portland cement that consumes resources. The use of industrial byproducts as source material can reduce the CO_2 emmission and problem of disposing the waste to atmosphere.

In this respect geopolymer concrete is a promising technique. The term geopolymer concrete was first introduced by Joseph Davidovits in 1978. Geopolymers are chains of mineral molecules linked with covalent bonds. Geopolymers are produced by the alkaline activation of source materials such as fly ash, GGBS, rice husk ash, metakaolin.

Fly ash is popular due to amorphous alumina silica content inside and it is abundantly available. The total amount of fly ash produced in the world has now reached 480 million tons annually, while the total OPC production is reaching 3.3 billion. There is a gap between fly ash and OPC production. Therefore additional source material is imperative, which will reduce these gap to lower value.

Rice husk ash is generated from the combustion of rice husk. Rice husk is an issue for environment due to its abundance and capability to resist natural degradation. The annual world production of rice husk ash is about 130 million tons. The current available disposal method of rice husk ash by burning and dumping create environmental pollutions. Rice husk when subjected to control burning of 500–700 °C produces Micronized Biomass Silica (MBS) which contains very high amount of silica content and is amorphous in nature. The amorphous silica contained in RHA can react with cementitious binders to perform pozzolanic activity. Thus it can be effectively used as a source material [6].

2 Experimental Program

2.1 Materials

GGBS and rice husk ash has been used as the source material. Natural sand as fine aggregate and crushed stone aggregate with size 20 and 12 mm in the ratio 40:60 were used. The aggregates confirms to IS 383–1970 [7]. The alkaline activators used were NaOH and Na_2SiO_3 in the ratio 1:2. The molarity of NaOH used is 6 M. Ordinary potable water is used. The oxide composition of GGBS and rice husk ash by XRF analysis is listed in Table 1. The physical properties of the materials are given in Table 2.

Table 1 Oxide composition of GGBS and rice husk ash

Oxide	GGBS (%)	RHA (%)
SiO_2	43.40	88.18
Al_2O_3	12.50	1.61
Fe_2O_3	–	0.56
CaO	40.30	1.59
MgO	1.50	1.63
Na_2O	0.90	–
K_2O	0.60	1.67
TiO_2	–	–
Mn_2O_3	–	–
SO_3	–	–
Carbon	–	2.67
Others	–	2.09
Moisture	–	0.79

Table 2 Physical properties

Physical properties	GGBS	RHA	Sand	Aggregate
Specific gravity	2.87	2.19	2.63	2.7
Water absorption	–	–	0.4	0.5
Bulk density	–	–	1520	1630

2.2 Mix Proportion

As no standard mix design is available for geopolymer concrete, the mixes were designed by trials. The concrete was designed for a grade of M30. 5 and 15% replacement of GGBS with rice husk ash is made. Ordinary Portland cement concrete was used for control specimen with w/c of 0.45. The mix proportions are given in Table 3.

2.3 Specimen Preparation

For casting, source materials and aggregates were dry mixed in the mixer for about 2–3 min. Then it is mixed with alkaline solution for another 3–4 min to form a uniform mix. The fresh concrete was cast into cubes of 100 mm, cylinders of 100 mm diameter and 200 mm height and prism of 100 mm × 100 mm × 500 mm. After casting the specimens were left for 24 h before removing mould. Then samples were cured under ambient condition for 28 days.

Table 3 Mix details in m^3

Materials	Quantity		
	5%	15%	OPC
Cement	–	–	430 kg
w/c	–	–	0.45
GGBS	409 kg	366 kg	–
Rice husk ash	21 kg	65 kg	–
Fine aggregate	683 kg	683 kg	683 kg
12 mm coarse aggregate	650 kg	650 kg	650 kg
20 mm coarse aggregate	434 kg	434 kg	434 kg
Molarity of NaOH	6 M	6 M	–
AAS	360 kg	360 kg	–

2.4 Experimental Set Up

2.4.1 Mechanical Property Testing

The hardened geopolymer concrete specimen were tested for destructive tests. Compressive strength, split tensile strength, flexural strength were conducted for 3 samples after 28 days of curing and the average of three was taken.

2.4.2 Water Absorption Test

ASTM C642 [8] determines the rate of water absorption by two saturation methods. In the present study, oven dry mass of the specimen is obtained by placing concrete discs of diameter 100 mm and thickness 50 mm in an oven at a temperature of 100 ± 5 °C for 24 h. The specimens are the cooled down to room temperature. Later, the saturated mass of samples is determined by immersing them in water for 24 h. The water absorption is calculated by Eq. 1.

$$\text{Water absorption} = \frac{W_2 - W_1}{W_1} \times 100 \tag{1}$$

W_1 Oven dry mass in kg
W_2 Saturated mass in kg.

2.4.3 Rapid Chloride Penetration Test

Rapid Chloride Penetration Test (RCPT) is commonly used to evaluate the resistance of concrete to chloride ion ingress through electrical conductivity measurements. The RCPT test was conducted as per the guidelines of ASTM C1202 [9]. The test consists

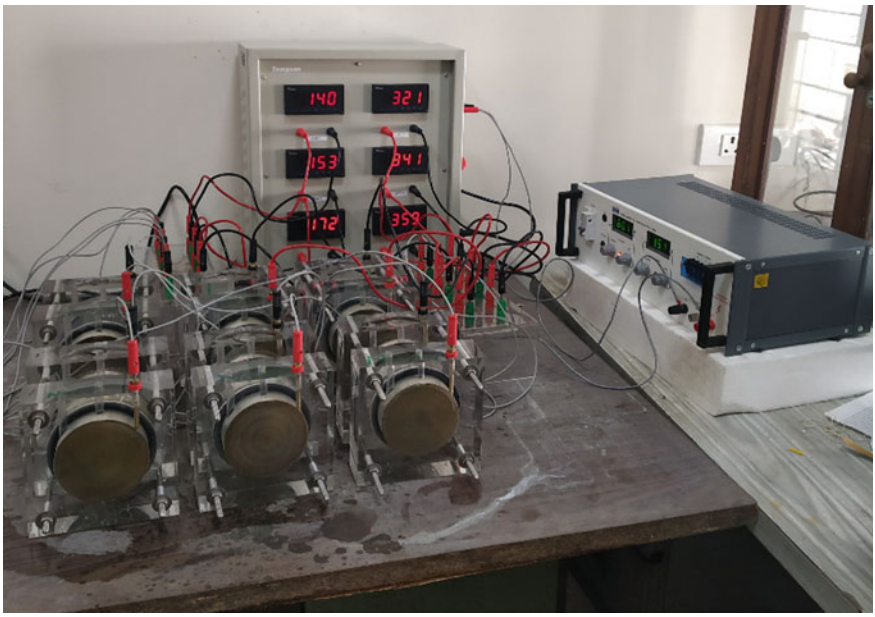

Fig. 1 RCPT set up

of cutting a 50 mm thick disc from cylinder of 100 mm diameter and 200 mm height. The slices were immersed in water for 24 h. It is then placed in the RCPT cell. The −ve side of test cell is filled with 3% NaCl solution and +ve side with 0.3 M NaOH solution. The system is then connected and a 60 V potential is applied for a period of 6 h. Readings are taken at every 30 min. At the end of the test the amount of current passed through the specimen in coulombs is calculated. Figure 1 shows the RCPT set up.

3 Results

3.1 Mechanical Properties

The 28 days compressive strength, split tensile strength and flexural strength properties are listed in Tables 4, 5 and 6 respectively.

The 28 days compressive strength of geopolymer concrete is well above the target mean strength. The increase in strength is due to high silica to alumina ratio (silica content >80%) and higher fineness of RHA compared to GGBS which increases the specific surface and thereby reactivity. The split tensile and flexural strength of

Table 4 Compressive strength results

Mix	Compressive strength (N/mm^2)
GPC-5	58.03
GPC-15	64.10
OPC	47.08

Table 5 Split tensile strength results

Specimen	Split tensile strength (N/mm^2)
GPC-5	3.4
GPC-15	3.64
OPC	4.55

Table 6 Flexural strength results

Specimen	Flexural strength (N/mm^2)
GPC-5	3.953
GPC-15	4.393
OPC	5.268

Table 7 Water absorption results

Specimen	Water absorption (%)
GPC-5	4.322
GPC-15	4.8
OPC	5.016

geopolymer concrete is slightly lower than that of OPC concrete. As per IS 456—2000, flexural strength is given by $0.7\sqrt{fck} = 3.8$ N/mm^2. The experimental results is well within the limit.

3.2 Water Absorption

The water absorption results is listed in Table 7.

The geopolymer concrete specimens performs better in water absorption when compared to that of OPC concrete specimen. This may be due to the improved microstructure of geopolymer concrete.

3.3 Rapid Chloride Penetration Test

The RCPT results is listed in Table 8.

Table 8 RCPT results

Specimen	Current (coulombs)
GPC-5	3680
GPC-15	3223
OPC	3980

Based on ASTM C1202, the chloride penetrability of all three specimen is classified as moderate. The chloride ion penetrability of geopolymer concrete is lower than that of control specimen. The decrease in chloride ion permeability is due to the fine particle size of RHA which produce micro filler effect. The micro filler effect results in dense and compact microstructure thereby reducing the penetration of chloride ions.

4 Conclusions

In the present study, ambient cured geopolymer concrete with GGBS as the source material and partial replacement of it by rice husk ash was developed. GGBS was partially replaced by RHA by 5 and 15%. The performance of geopolymer concrete in mechanical and durability properties was studied. On the basis of the experimental results obtained, it is evident that geopolymer concrete performs better than OPC concrete. Following are the conclusions made from the study:

- The compressive strength of geopolymer concrete is higher than OPC concrete.
- The indirect tensile strength of geopolymer concrete is marginally lower than OPC.
- The mechanical properties improves by increasing the percentage of replacement of RHA from 5 to 15%.
- The durability properties such as water absorption and rapid chloride penetration test results shows better performance of geopolymer concrete over OPC concrete.
- The chloride ion penetrability of the specimens falls under moderate class as per ASTM C1202.
- This improvement may be attributed to the improved dense and compact microstructure of geopolymer concrete due to the inclusion of RHA [2].
- Utilization of GGBS and RHA for concrete production proved as a solution for the disposal of these industrial and agricultural byproducts.
- The geopolymer concrete reduces the emission of carbondioxide that are released during the manufacture of cement.

Acknowledgements Authors acknowledge the assistance rendered by the staffs of Advanced Material Laboratory, CSIR–SERC. This paper is published with the kind permission of the Director, CSIR–SERC, Chennai, India.

References

1. Zabihi SM et al (2018) Engineering and microstructural properties of fiber-reinforced rice husk–ash based geopolymer concrete. J Mater Civ Eng 30
2. Mohseni E et al (2019) Evaluation of mechanical and durability properties of fiber-reinforced lightweight geopolymer composites based on rice husk ash and nanoalumina. Constr Build Mater 240:532–540
3. Sturm P et al (2016) Synthesizing one-part geopolymers from rice husk ash. Constr Build Mater 146:961–966
4. Sangoju B et al (2011) Studies on chloride-induced corrosion of steel in cracked concretes: experimental study. J Mater Civ Eng 23:1057–1066
5. Sangoju B et al (2011) Chloride-induced corrosion of steel in cracked OPC and PPC concretes: experimental study. J Mater Civ Eng 23(7):231–251
6. Kusbiantoro A et al (2012) The effect of microwave incinerated rice husk ash on the compressive and bond strength of fly ash based geopolymer concrete. Constr Build Mater 36:695–703
7. IS 383 (1970) Specification for coarse and fine aggregates from natural source for concrete. Bureau of Indian Standards, New Delhi, India
8. ASTM C642-06, Standard test for density, absorption and voids in hardened concrete
9. ASTM C1202, Standard test method for electrical indication of concrete's ability to resist chloride ion penetration
10. IS 456 (2000) Plain and reinforced concrete—code for practice. Bureau of Indian Standards, New Delhi, India

Analysis of Strains in Brick Masonry Prism Using ABAQUS

Agnus A. Mathew, S. Saibabu, Vimal Mohan, and Deepa Varkey

Abstract In this study, the response of brick masonry specimen subjected to vertical load is analytically calculated using existing formulas and numerically investigated using a popular software ABAQUS. The brick masonry specimen is a small part of the old building which was constructed with brick masonry was taken for analytical and numerical investigation purpose. It consists of three layers of brick and two layers of mortar. The height, width and thickness of the specimen is 245 mm, 220 mm, and 100 mm respectively. Macro and micro model of the specimen was developed using ABAQUS software. The material model used is elastic plastic model C3D8R. Vertical load from 0 to 30.0 kN at interval of 3.0 kN was applied on the specimen. It is very difficult to study the behaviour of brick and mortar together and separately of brick masonry considering the effect of continuity of materials at the joints between brick and mortar. To study the behaviour, macro and micro models are developed and tested upto design load. From the macro and micro models, deflections and strains of brick and mortar upto design load were predicted and these values were compared with analytical calculations. It was found from the investigation, that the increase in strains and deflections are almost proportional to the applied loads.

Keywords Brick masonry · Macro and micro model · ABAQUS

1 Introduction

The masonry is one of the oldest and most widespread structural materials and is still used for various construction purposes. The major constituents of masonry are units and mortar and therefore classified as a heterogeneous anisotropic material whose analysis, understanding and capture of the structural behaviour is complex.

A. A. Mathew (✉) · D. Varkey
Department of Civil Engineering, Mar Athanasius College of Engineering, Kothamangalam, Kerala, India
e-mail: agnusamathew7@gmail.com

S. Saibabu · V. Mohan
CSIR-Structural Engineering Research Centre, Chennai, India

© Springer Nature Switzerland AG 2021

K. Dasgupta et al. (eds.), *Proceedings of SECON 2020*,
Lecture Notes in Civil Engineering 97,
https://doi.org/10.1007/978-3-030-55115-5_79

The development of computer and the computer software made simpler to predict the behavior of the structures. In numerical analysis selection of a mathematical model is important. The FEM involves dividing a structure into a discrete number of elements from which the approximate numerical solution is obtained. Several researchers have reported valuable results on simulating masonry wall behaviour using a simplified micro-model approach, finite element modelling of structural clay brick masonry subjected to axial compression, stress-strain characteristics of clay brick masonry under uniaxial compression [1–3]. Some scientists have invested using equivalent elastic moduli for analysis of brick masonry structures and also using bond strength and compressive stress-strain characteristics of brick masonry [4, 5]. Similarly using finite element analysis many researchers also studied on behaviour and strength assessment of masonry prisms, numerical simulation of masonry prism test using ANSYS and ABAQUS, numerical simulation of masonry structures based on ANSYS contact analysis, a stress-strain model for brick prism under uniaxial compression [6–9].

The numerical study is conducted using ABAQUS 6.14 which includes micro and macro modeling approach. Finite Element Method (FEM) for masonry is mainly depended on two modeling approaches namely micro and macro modeling. In macro model the units and mortar are modelled as a single element in which the combined or expanded properties of brick and mortar units are provided. In the micro model approach the units and mortar are modelled as continuum elements and unit mortar interfaces are modelled as discontinuum elements. The numerical simulation is being used due to the difficulties in experimental study of existing masonry structures. Numerical simulation of the masonry structures will help in determining the weaker sections and to understand the stress strain distributions. The masonry unit and the mortar will be under multi-axial state of stress when masonry is under compression. Hence, the present investigation is an attempt to develop a finite element model using ABAQUS to predict the masonry prism compressive strain and deflection subjected to concentric compressive loading. Distribution of strain and deflection when the Young's modulus of brick units greater than that of mortar joints and when the Young's modulus of brick units lesser than that of mortar joints are also studied. The numerical values obtained from the finite element model is validated by comparing with those obtained from the analytical results. The present research included a numerical study on the behaviour of brick masonry triplex prism under compressive loading which is small piece of building as shown in Fig. 1.

2 Description of Triplex

The three brick stack bonded clay brick masonry prism is considered to determine the masonry strength. The clay brick masonry prism of size 220 mm × 245 mm × 100 mm is considered. The size of each masonry unit is 220 × 100 × 75 mm. The size of each mortar joint is 220 × 100 × 75 mm and it is shown in Fig. 2. The finite element model was used to understand the results of the compression tests

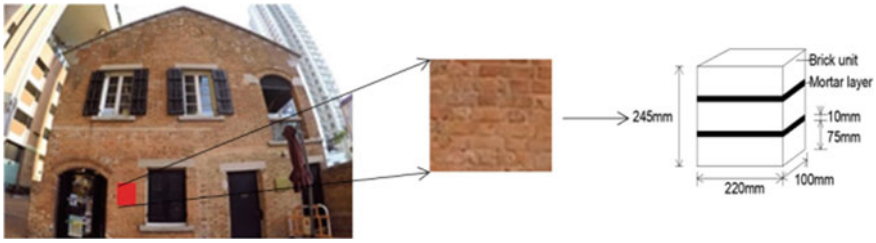

Fig. 1 Small section of old building taken for analysis

Fig. 2 Three stack brick masonry prism

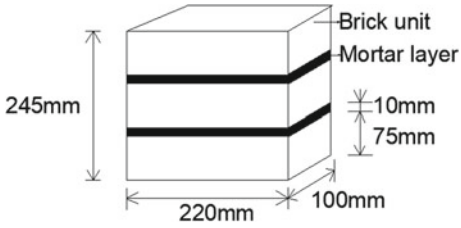

on masonry wall panel. Micro and macro modelling are done and the results are validated.

2.1 Material Properties

ABAQUS has a set of material library in the engineering data section. Either we can select a material from the library or we can manually enter the properties of material in ABAQUS/CAE. The C3D8R element is used which requires linear isotropic and multi-linear isotropic material properties to properly model brick masonry. The elastic properties for micro modelling are shown in the Tables 1 and 2.

Table 1 Material properties for type-1 micro modelling when $E_b < E_m$

Modulus of elasticity (E_b) of brick in MPa	3070
Poisson's ratio (μ) of brick	0.20
Modulus of elasticity (E_m) of mortar in MPa	5385
Poisson's ratio (μ) of mortar	0.15

Table 2 Material properties for type-2 micro modelling when $E_b > E_m$

Modulus of elasticity (E_b) of brick in MPa	5385
Poisson's ratio (μ) of brick	0.15
Modulus of elasticity (E_m) of mortar in MPa	3070
Poisson's ratio (μ) of mortar	0.20

3 Theoretical Predictions

Strain in the macro and micro model of triplex is found using the following equations for validation of results obtained from the ABAQUS models.

3.1 Macro Model

Macro-modelling is probably the most popular and common approach due to its reduced calculation demands. On large structural members or full structures, a detailed description of the interaction between units and mortar may not be necessary. In these cases, macro-modeling is used which does not make any distinction between units and joints. The macro-modeling strategy regards the material as a fictitious homogeneous orthotropic continuum.

In macro modelling the equation for the elastic properties of the equivalent material is derived in terms of elastic properties of the brick and mortar, together with the relative thickness. Uniform Building Code (UBC) recommends that the modulus of elasticity of masonry (E_m) in compression can be calculated using the following equation:

$$E_m = \left(\frac{1 + \gamma_t}{1 + \frac{\gamma_t}{\gamma_m}} \right) E_b \tag{1}$$

where

$\gamma_t = \frac{t_j}{t_b}$
$\gamma_m = \frac{E_j}{E_b}$
t_j = thickness of mortar = 10 mmm
t_b = thickness of masonry = 75 mm
E_j = modulus of elasticity of mortar joints = 5385 MPa
E_b = modulus of elasticity of bricks = 3070 MPa
E_m = Equivalent modulus of elasticity of masonry = 5113 MPa.

The stress in the brick masonry of macro model triplex (f_{ma}) subjected to vertical load is given by Eq. (2).

$$f_{ma} = \frac{P}{A_p} \tag{2}$$

where

P = loading in N
A_p = area of cross section of brick prism = 22,000 mm^2.

In macro modeling the deflection is calculated theoretically using the Eq. (3).

$$\delta = \frac{P d_p}{A \times E} \tag{3}$$

where

d_p = depth of triplex prism.

3.2 Micro Model

The so-called detailed micro-models describe the units and the mortar at joints using continuum finite elements whereas the unit-mortar interface is represented by discontinuous elements accounting for potential crack or slip planes. Detailed micro-modeling is probably the more accurate tool available to simulate the real behavior of masonry. It is particularly adequate to describe the local response of the material. Elastic and inelastic properties of both unit and mortar can be realistically taken into account. The micro-modeling approaches are suitable for small structural elements with particular interest in strongly heterogeneous states of stress and strain.

For Type-1 and Type-2 micro models, the analytical strain in brick (ϵ_b) and strain in the mortar (ϵ_m) of the triplex was calculated separately and it is explained from Eqs. (4) to (10).

$$\epsilon = \frac{\beta \times p}{E_m} \tag{4}$$

$$\beta_1 = \frac{E_b}{E_m} = 0.57 \tag{5}$$

$$\beta_2 = \frac{m}{E_b} = 1.75 \tag{6}$$

E_b = Modulus of elasticity of brick
E_m = Modulus of elasticity of mortar.

Type-1 When $E_b < E_m$

$$E_b = 3070 \text{ MPa}$$
$$E_m = 5385 \text{ MPa}$$

$$\epsilon_b = \frac{\beta_2 \times P}{E_m} \tag{7}$$

$$\epsilon_m = \frac{\beta_1 \times P}{E_m} \tag{8}$$

Type-2 When $E_b > m$

$$E_{\mathrm{b}} = 5385 \text{ MPa}$$
$$E_{\mathrm{m}} = 3070 \text{ MPa}$$

$$\epsilon_{\mathrm{b}} = \frac{P}{E_m} \tag{9}$$

$$\epsilon_{\mathrm{m}} = \frac{\beta_2 \times P}{E_m} \tag{10}$$

3.3 ABAQUS Modeling

ABAQUS 6.14 was selected for the simulation of brick masonry prism since its interface is very easy to use and supports parametric modelling.

3.4 Element Types

Element type used for brick units and mortar in this study is continuum element in three dimension with eight nodes and reduced integration (C3D8R) which is an 8 node linear brick element with hour glass control which gives more stable results. In order to develop brick units and mortar units, 8-node continuum solid element was utilized. The element is having has eight nodes with three degrees of freedom at each node. For uniform distribution of load on top of the prism a steel plate is provided.

3.5 Loading and Boundary Conditions

Vertical load varied from 0 to 30.0 kN at interval of 3.0 kN was applied on the specimen to predict linear elastic stresses. Uniform pressure loading is provided on the top. For that a steel plate is provided on the top. The boundary condition is such that the bottom of the prism is fixed is depicted in Fig. 3.

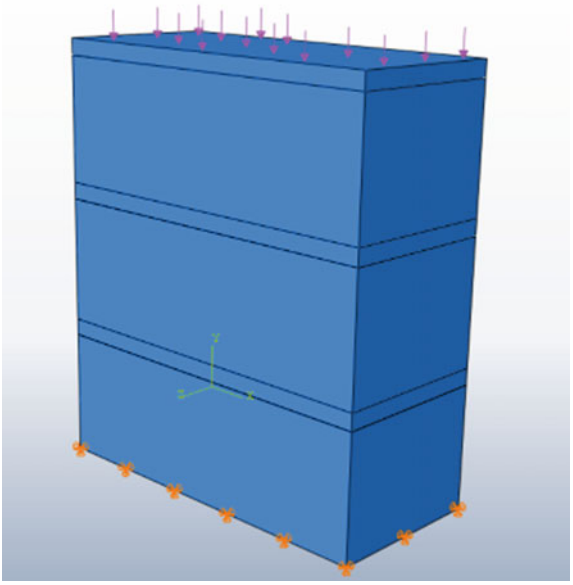

Fig. 3 Loading and boundary conditions

3.6 Interface Between Brick Units and Mortar Units

The cohesive interaction is provided between the brick and mortar layers and defined as a function of displacement separation between the edges of potential cracks. Furthermore, Coulomb frictional contact behaviour was applied to the current models by introducing a coefficient of friction which prevents component's penetration after forming the contact especially for the normal behaviour of contacts. For this study, surface-to-surface contact was chosen and the contacting properties for the tangential and normal behaviour were specified. This type of contact is generally used to describe the behaviour of two deformable surfaces connecting together. In the interaction properties the coefficient of friction is given as 0.7.

4 Contour Plots

The contour plots gives the variation in stress, strains and deflections with respect to the loading and material properties. The stress concentrated areas, regions with more compressive strength, regions with more tensile strength etc. can be identified with the help of contour plots.

4.1 Stress, Strains and Deflection Contours of Macro Model

The variation of stress, strains and deflection in the macro model of the masonry prism under vertical compressive loading is shown from Figs. 4, 5 and 6.

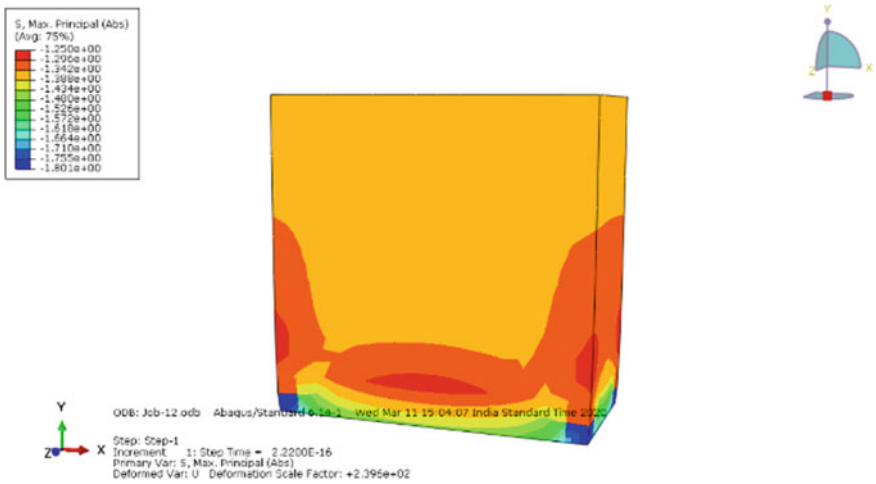

Fig. 4 Stress contour of macro model

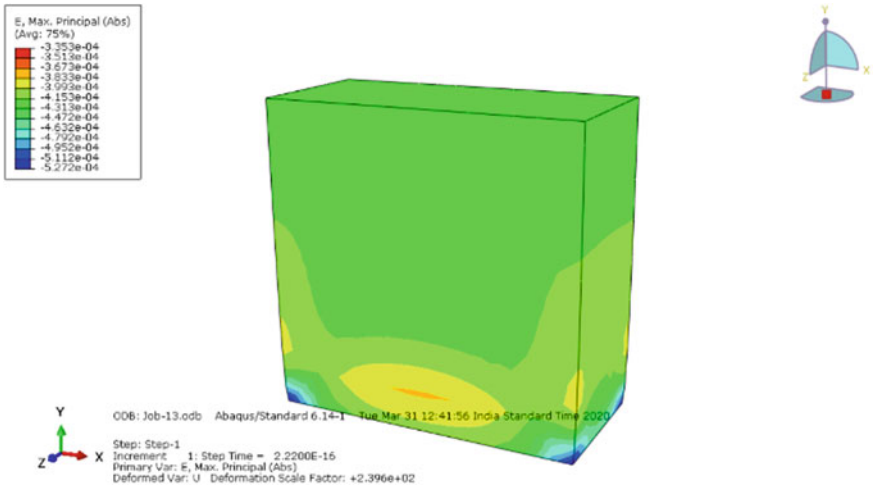

Fig. 5 Strain contour of macro model

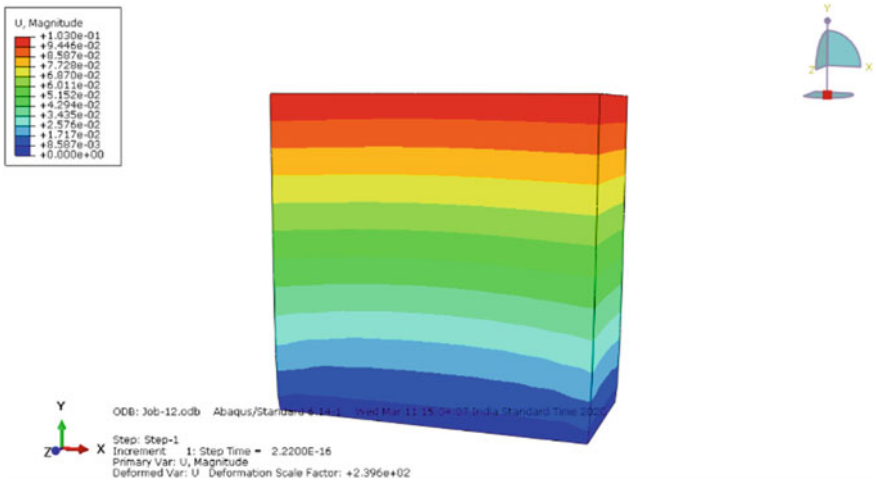

Fig. 6 Deflection contour of macro model

4.1.1 Stress, Strain and Deflection Contours of Type-1 Micro Model

The modulus of elasticity values affects the distribution of stress and strains in the brick units and mortar layer. The change in the stress, strain and deflection values due to the effect of Young's modulus when $E_b < E_m$ in micro model is shown from Figs. 7, 8 and 9.

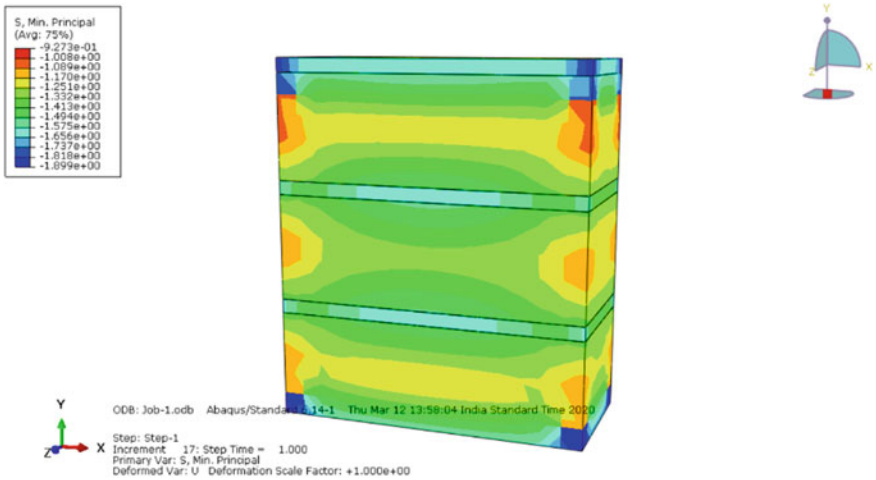

Fig. 7 Stress contours of type-1 micro model

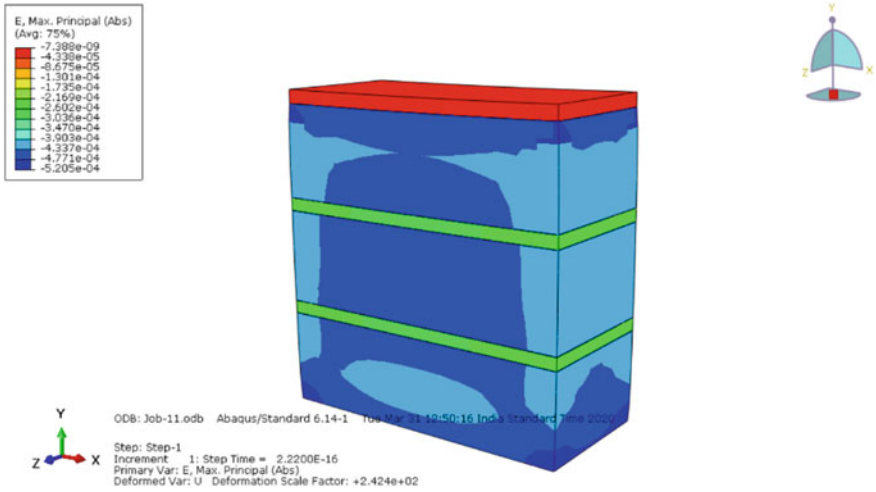

Fig. 8 Strain contours of type-1 micro model

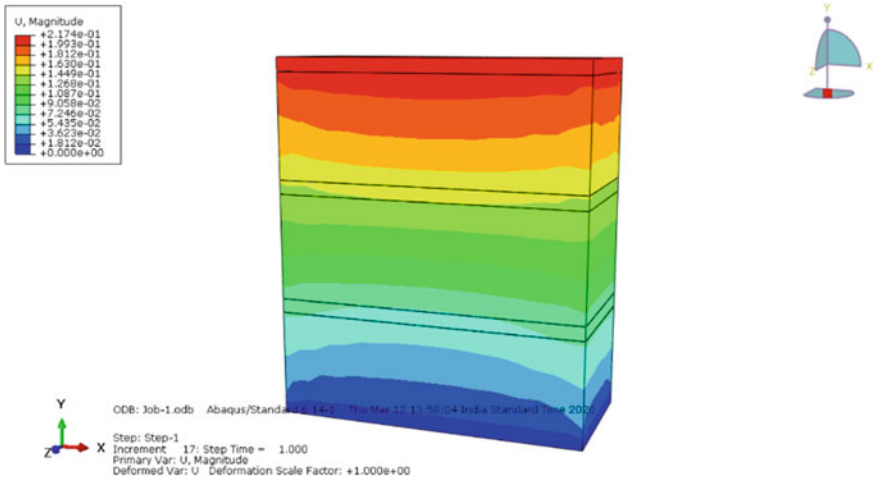

Fig. 9 Deflection contours of type-1 micro model

4.1.2 Stress, Strain and Deflection Contours of Type-2 Micro Model

The change in the stress, strain and deflection values due to the effect of Young's modulus when $E_b > E_m$ in micro model is shown from Figs. 10, 11 and 12.

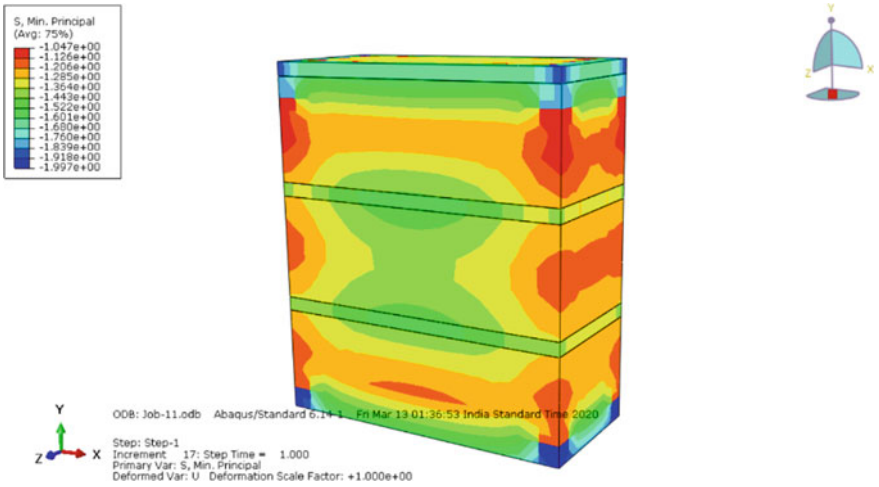

Fig. 10 Stress contours of type-2 micro model

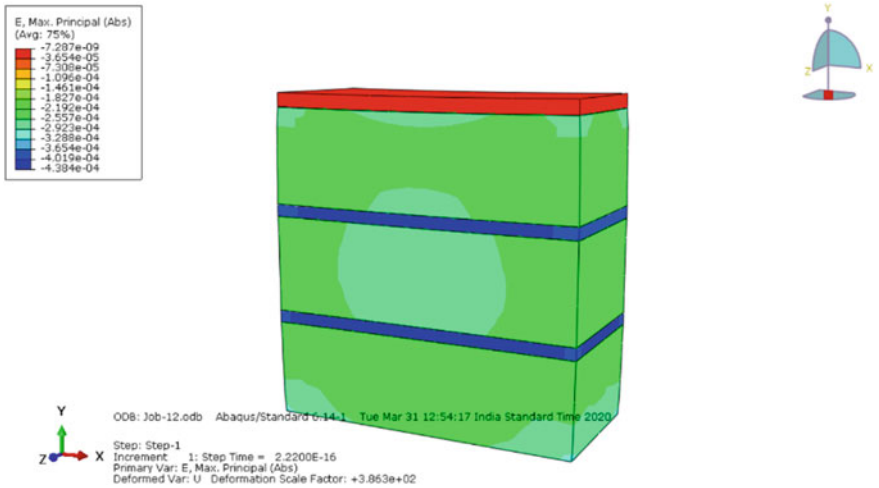

Fig. 11 Strain contours of type-2 micro model

5 Comparison of Results

The graph showing the plot between calculated values and numerical results for strain and deflection from the macro model of specimen is given in Figs. 13 and 14.

The strain values of mortar and brick against applied stress for type-1 micro model, which are obtained from the analytical and numerical analysis are presented from Figs. 15, 16, 17 and 18.

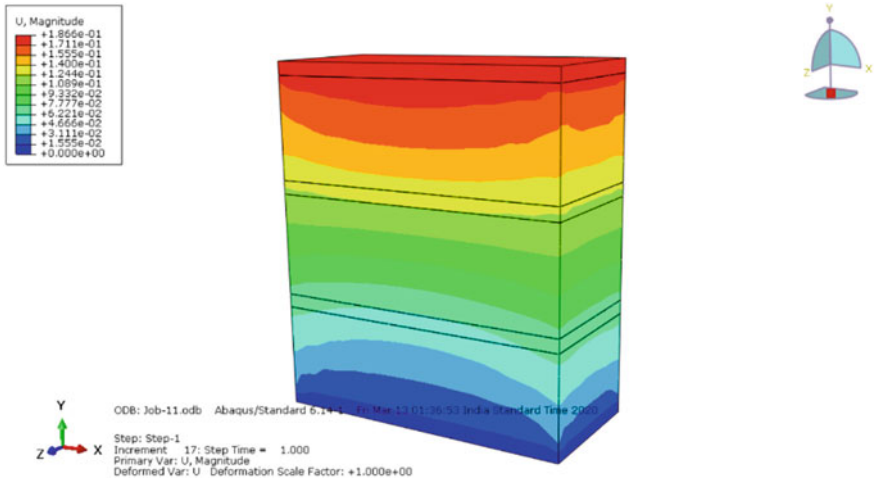

Fig. 12 Deflection contours of type-2 micro model

Fig. 13 Comparison of strains-macro model

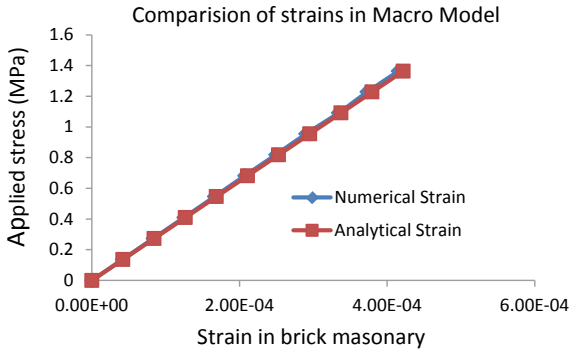

Fig. 14 Comparison of deflection-macro model

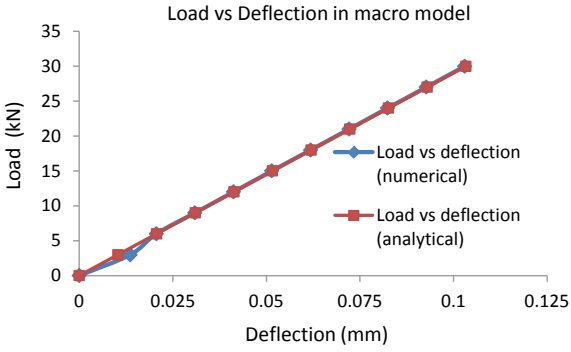

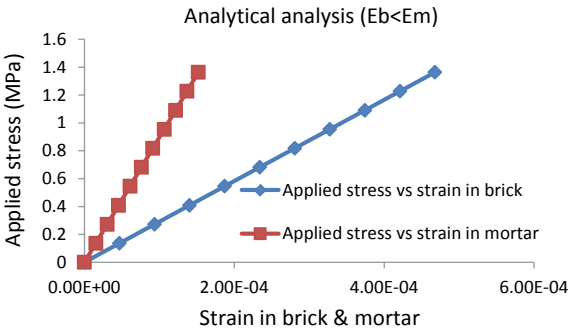

Fig. 15 Comparison of analytical strain data of type-1 micro model

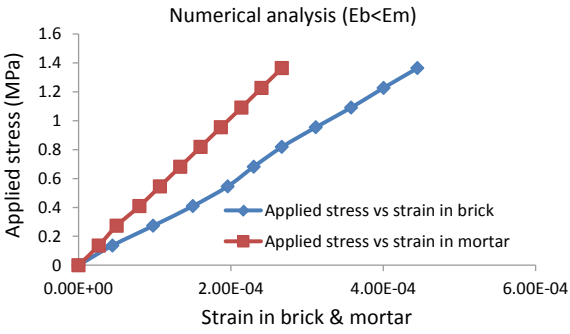

Fig. 16 Comparison of numerical strain data of type-1 micro model

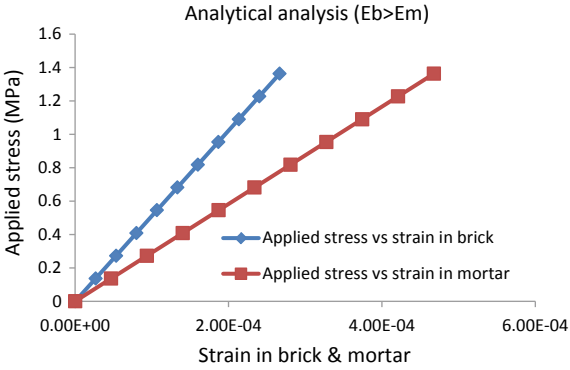

Fig. 17 Comparison of analytical strain data of type-2 micro model

Comparison of strain in mortar and brick when $E_b < E_m$ and $E_b > E_m$ was made and it is shown in the bar charts of Figs. 19 and 20 respectively.

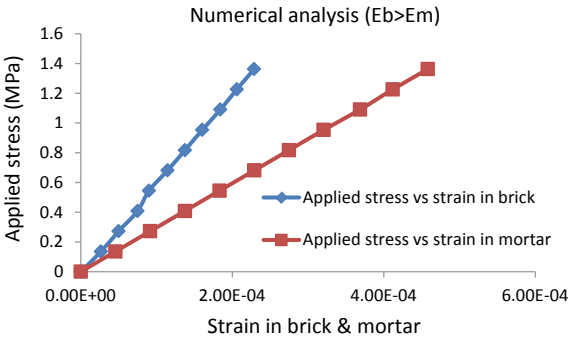

Fig. 18 Comparison of numerical strain data of type-2 micro model

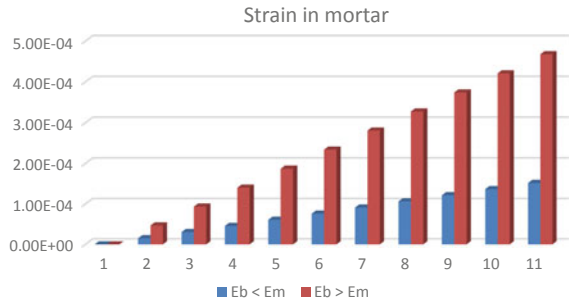

Fig. 19 Comparison of strain in mortar when $E_b < E_m$ and $E_b > E_m$

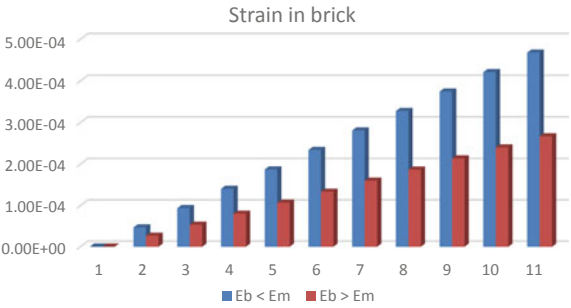

Fig. 20 Comparison of strain in brick when $E_b < E_m$ and $E_b > E_m$

6 Conclusions

Linear FE analyses of the brick masonry triplex under simple vertical load was carried out and compared the results obtained from the macro and micro models with the theoretical predictions for validation. The results show that the FE analysis are in very good agreement with those of the theoretical predictions. The FE analyses of micro model predicted strains correctly compared with macro model. The strain value varies linearly with increase in stress. From this investigation it is found that the strain values of brick and mortar are depended on strength of modulus of elasticity of the material.

Cracks in brick masonry structures occurs due to either strain in brick or strain in mortar exceed their corresponding permissible strain of the materials and also it is depended on the values of material modulus of elasticity. To validate this statement, macro and micro numerical simulation using abacus model was developed for brick masonry prims. The strains and deflection values obtained from the models are compared with the analytically computed values and it was shown good agreement. It is found that the strain and deflections of prism are proportional to the applied load.

Acknowledgements This paper is published with the permission of the Director, CSIR-Structural Engineering Research Centre, Chennai, India

References

1. Abdulla KF, Cunningham LS, Gillie M (2017) Simulating masonry wall behaviour using a simplified micro-model approach. Eng Struct 151:349–365
2. Bakhteri J, Makhtar AM, Sambasivam S (2004) Finite element modelling of structural clay brick masonry subjected to axial compression. J Teknol 41(1):57–68
3. Kaushik HB, Rai DC, Jain SK (2007) Stress-strain characteristics of clay brick masonry under uniaxial compression. J Mater Civ Eng 19(9):728–739
4. Pande GN, Liang JX, Middleton J (1989) Equivalent elastic moduli for brick masonry. Comput Geotech 8(3):243–265
5. Singh SB, Munjal P (2017) Bond strength and compressive stress-strain characteristics of brick masonry. J Build Eng 9:10–16
6. Thaickavil NN, Thomas J (2018) Behaviour and strength assessment of masonry prisms. Case Stud Constr Mater 8:23–38
7. Vindhyashree HS, Rahamath A, Kumar WP, Kumar MT (2015) Numerical simulation of masonry prism test using ANSYS and ABAQUS. Int J Eng Res Technol 4(7):1019–1027
8. Wang J (2014) Numerical simulation of masonry structures based on ANSYS contact analysis. Ind Technol Innov 1:19
9. Yang KH, Lee Y, Hwang YH (2019) A stress-strain model for brick prism under uniaxial compression. Adv Civ Eng

Machine Learning Approach to Failure Mode Prediction of Reinforced Concrete Infilled Frames

J. Ashish Manoj, A. Asiya, Dasari Navya, G. Ganesh Kumar, and P. Robin Davis

Abstract Earthquake damage assessment studies conducted throughout the world have already established the importance of considering the contribution of reinforced concrete infilled frames in the response of structures subjected to sudden lateral loads. Still, much clarity needs to be made on the behaviour, and failure mechanisms of RC infilled frames when subjected to such large and sudden earthquake loads. A data-driven machine learning approach to the prediction of failure modes of RC infilled frames is suggested in this paper. An exhaustive database consisting of experimental results done throughout the world was gathered. A failure mode classification system consisting of three predominant failure modes is proposed. Suitable parameters are identified for the purpose of machine learning modelling. Machine learning algorithms like AdaBoost, CatBoost, KNN, Decision Trees were used to predict the failure modes. An open-source dynamic model is created, which could be updated once new data is available from experiments. Google provides a free TensorFlow enabled Jupyter notebook for machine learning (Google Colabs). The same was used in this study as it supports remote access from different locations, and the model would always remain in the cloud, making it instantly accessible. Three performance measures were used in this study to evaluate the performance of the various machine learning models: accuracy, precision, and recall. The results obtained indicate that for complex structural interaction problems having (a number of dependent parameters) machine learning modelling techniques, in which the dataset is allowed to speak for itself, can be successfully employed.

Keywords Machine learning · RC infilled frame · Earthquake · Lateral loads · Data-driven modelling

J. Ashish Manoj (✉) · A. Asiya · D. Navya · G. Ganesh Kumar · P. Robin Davis
Department of Civil Engineering, National Institute of Technology Calicut, Kozhikode, India
e-mail: ashishmanoj@outlook.com

© Springer Nature Switzerland AG 2021

K. Dasgupta et al. (eds.), *Proceedings of SECON 2020*,
Lecture Notes in Civil Engineering 97,
https://doi.org/10.1007/978-3-030-55115-5_80

1 Introduction

As per the National Disaster Management Authority of India (NDMA) official vulnerability profile [1], India is vulnerable, in varying degrees, to a large number of disasters. Some of the major disasters which are likely to affect Indian subcontinent are—earthquakes, floods, droughts and tsunamis. About 59% of the total landmass of India is prone to moderate to very high-intensity earthquakes (NDMA). Earthquakes are widely regarded as being the most severe and deadly among naturally occurring disasters. This may be chiefly due to the fact that only the probability of a significant earthquake happening within a specified time period at a specific location can be ascertained. Even with all the advents in geological sciences and remote sensing, it is still not possible to accurately predict the occurrence of an earthquake.

The high mortality rate of past major earthquakes in India can be attributed to the poor construction and maintenance practices rather than the earthquake itself. Many studies were conducted after the Jabalpur and Bhuj earthquakes, which shed light on this fact. One of the critical components which could play a significant role in better seismic preparedness was identified as the presence of masonry infilled frames.

In reinforced concrete framed structures, exterior walls and many interior partition walls are made up of masonry. These members are usually considered as non-load bearing, and their interaction not taken into account in the calculation of final limit state stresses in design. The general consensus was that not accounting for them would lead to more conservative strength values, and thus the design ending up on the safe side. However, further studies found out that this was not particularly true when subjected to sudden huge lateral loads as in the case of earthquakes. Despite the extensive experimental efforts over the last few decades using a variety of analytical and experimental tools, the behaviour of RC infilled frame, and its subsequent failure modes remain an unsolved mystery. In this paper, data-driven machine learning models are suggested for the proper evaluation and identification of RC infilled frame failure modes.

1.1 Research Significance

Numerous researchers in the field of structural as well as earthquake response engineering have established the fact that the presence of RC infilled frame will affect the seismic load-carrying capacity of the structure. Thus, sufficient research should be carried out to negate the undesirable effects as well as to benefit from the positive side effects of having an infilled member in structures subjected to sudden earthquake loads. In the limit state of design, the corresponding failure modes of the structure has to be known, and the failure loads for different modes of failure have to be computed in order to determine the ultimate capacity of the structure. Thus, it is essential to predict the type of failure mode of a given infilled structure. After the prediction of failure mode, suitable retrofitting or maintenance techniques could be employed for

existing structures and sufficient factor of safety can be given in the design of new structures. Previously finite element and analytical models were created, but none of them could predict the complex phenomenon of failure of an infilled frame to a desired level of accuracy.

Many of the finite element models could only be used for specific cases involving a large number of fixed parameters. Machine learning is ideally suitable for such complex interaction problems; it can efficiently find the underlying hidden relationships between input data. In machine learning modelling, the dataset is allowed to speak for itself, with no inherent bias to any particular outcome.

Mangalathu and Jeon [2, 3] suggested a few machine learning models to identify the failure mode of beam-column joints and circular bridge columns. They have successfully shown that the machine learning model is about 10% more accurate than the contemporary finite element based models. Aguilar et al. [4] have proposed a neural network-based model for prediction of shear strength of reinforced masonry walls. Huang and Burton [5] have attempted to classify the failure mode of RC infilled frames using machine learning modelling. In the current study, the same is being attempted by using more advanced machine learning algorithms and also a broader database with some considerable view on including experimental data on RC infilled frame from India also. The results so obtained could aid structural engineers working in this field make more informed decisions regarding the seismic response of buildings.

2 Failure Modes of RC Infilled Frame

Wood [6] was one of the first to propose a relative lateral strength parameter, based on the relative strength relationship between the infill and frame. This dimensionless parameter could explain the relative occurrence of the various failure modes.

$$m = \frac{8M_P}{f_w l_w t_w} \tag{1}$$

where M_p is the plastic moment capacity of the corners of the frame, f_w is the compressive strength of the infill, t_w is the thickness of the infill and l_w the length of the infill panel. The infill shows a variety of failure modes depending on geometric and material properties [7]. Failure of the infill can also be classified as

- Corner Compression: Due to the high-stress concentrations at each corner of the compression diagonal. Similar to the corner crushing failure mode proposed by Asteris et al. [8]. For concrete frames, involves very extensive damage which usually extends to the frame itself.
- Diagonal Cracking: Usually occurs when the tensile strain due the applied loads exceed the limiting cracking strain of the infill panel material. Begins typically

from the centre of the infill and extends from one corner to another in a direction parallel to the compression diagonal.

- Shear Cracking: This type of failure is mainly dependent on the shear strength of mortar joints, which in turn depends on the coefficient of friction and bond strength. This failure mode involves cracking in the masonry panel due to shear stresses. Shear cracks can be seen as either stepped cracks or horizontal sliding cracks along the mortar joints.

The current study would be focusing on the three modes of failure, as proposed by Irshad Abdul Azeez [7]. For ease of representation, they are shown as (**Y**):

- Corner Compression (**CC**)—Class 0
- Diagonal Cracking (**DC**)—Class 1
- Shear Cracking (**SC**)—Class 2.

3 Input Parameters

In any data-driven modelling studies, the selected parameters play a massive role in accurately predicting the response (in our case, the failure mode of RC infilled frames). For this study, we have identified a total of 10 parameters, which is assumed to affect the performance leading to failure of a reinforced concrete infilled frame subjected to lateral loads. They have been selected to include all relevant material, geometric and other physical properties of the frame under consideration.

Many previous experimental, analytical and modelling studies [7, 9, 10, 6] have established that both the properties of the infill as well as the frame material would have an impact on the potential mode of failure of the frame. For including the strength properties of infill material, compressive strength and modulus of elasticity obtained from tests conducted on masonry prisms were selected. As per ASCI code 41-17 [11], stiffness of infill is given by:

$$k_{infill} = \frac{3E_{prism}I_{infill}}{h^3} \tag{2}$$

The effective moment of inertia on infill panel, I_{infill}, is further given by [11]:

$$I_{infill} = \frac{lt^3}{12} \tag{3}$$

Therefore, to account for all these factors, height of the infill panel (h), length of the infill panel (l) and thickness of masonry in the panel (t) were selected. The load at which the frame underwent failure (P) was also considered.

The final input parameters were:

1. Compressive strength of masonry prisms, f_{cprism} (MPa)—$\mathbf{X}_1$
2. Modulus of elasticity of masonry prisms, E_{prism} (MPa)—$\mathbf{X}_2$

3. Compressive strength of the material of the frame, f_{cframe} (MPa)—$\mathbf{X}_3$
4. Tensile strength of the material of the frame, f_{tframe} (MPa)—$\mathbf{X}_4$
5. Modulus of elasticity of the material of the frame, E_{frame} (MPa)—$\mathbf{X}_5$
6. Tensile strength of main reinforcement of the frame, f_y (MPa)—$\mathbf{X}_6$
7. Failure load, P (kN)—$\mathbf{X}_7$
8. Height of the infill panel, h (m)—$\mathbf{X}_8$
9. Length of the infill panel, l (m)—$\mathbf{X}_9$
10. Thickness of masonry in the panel, t (m)—$\mathbf{X}_{10}$.

4 Machine Learning Modelling and Results

A correlation analysis was conducted on the input parameters to identify potentially strongly correlated features. Since some of the chosen parameters exhibited high correlation within themselves, it was realised that in a statistical sense they were not linearly separable and that highly complex, non-linear classification techniques would be needed to predict the failure mode correctly. Such a complex, non-linear problem in which several features are seen to be correlated with each other can be efficiently handled with machine learning modelling. The collected database consisted of 132 data points with corner crushing accounting for 50 failures, diagonal cracks accounting for 49 failures and shear cracks for the failure of 33 infill frames. Initial modelling with few datapoints was done using the classification learner application available in MATLAB using two different ML techniques, and sufficient confidence was gained to proceed to more rigorous modelling using Python.

Google provides a free TensorFlow enabled Jupyter notebook for machine learning (Google Colabs). The same was used in this study as it supports remote access from different locations, and the model would always remain in the cloud, making it instantly accessible. Modelling was done in Google Colabs using ten machine learning techniques. To get an estimate of the accuracy of the prediction made by each model the collected database was divided into two the training dataset (which is feed into the system during the training phase and the model parameters are estimated) and the test dataset (which is hidden from the model during the training phase). Once training is done using the train dataset, the test set is feed into the system, and various performance measures relating to the accuracy of predictions is estimated. Since the model is made to predict on previously unseen data, the accuracy would be a best estimate, and the model can be expected to have a satisfactory level of generalisation capabilities.

Three performance measures are being introduced in the current paper to assess the relative suitability of each machine learning algorithm to the classification problem at hand: accuracy, precision, and recall. The accuracy represents the fraction of predictions the model predicted correctly, i.e., the accuracy is the ratio of the number of correct failure mode predictions to the total failure mode predictions. At the same time, recall expresses the ability of our model to find all relevant instances in a dataset; precision expresses the proportion of the data points our model says was relevant

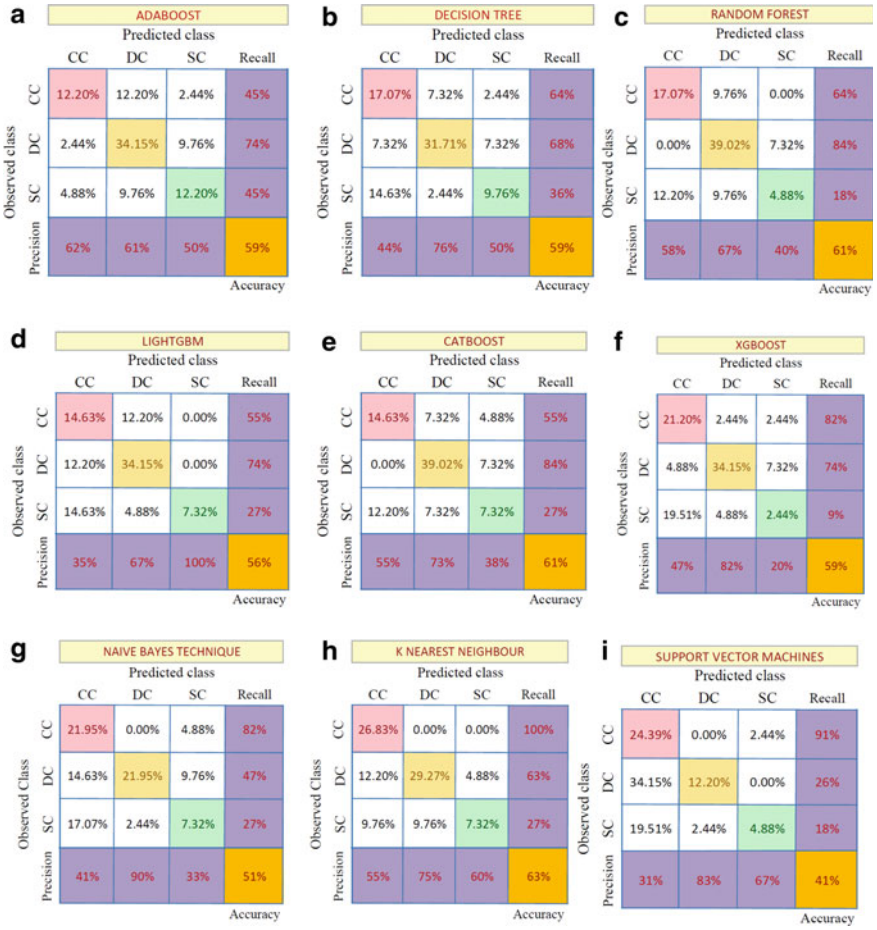

Fig. 1 a–i Confusion matrices obtained for various ML algorithms—AdaBoost, Decision Trees, Random Forest, LightGBM, CatBoost, XGBoost, Naïve Bayes, KNN, SVM

actually were relevant. Now accuracy can be considered to be a global measure of the performance of the machine learning method. At the same time, precision and recall are particular to each failure mode (local in nature) [12]. High values for accuracy, precision, and recall for a model indicates that it can correctly predict the failure mode. A train-test split of 70–30% was used for the current study. The purpose of our modelling is to establish a non-linear relationship between the input parameters and the occurrence of failure modes of RC infilled frame.

$$Failure\,Mode,(Y) = f\left([X_1, X_2, X_3, X_4, X_5, X_6, X_7, X_8, X_9, X_{10},]^{\mathrm{T}}\right) \quad (4)$$

Confusion matrices are obtained for each model shown in Fig. 1, which shows the performance measures. It can be seen from Fig. 1 that the highest accuracy obtained for any model is about 63%. The best performing model was KNN, followed by Random Forest and CatBoost. The schematic representation of the neural network used for modelling is shown in Fig. 2. It has ten input layers for the ten selected input features. Figure 3 shows the plot of accuracy shown by the model with an increasing number of trials (epochs). As is expected, the final accuracy is very high when the model is evaluated on the train dataset compared to the unseen test dataset. This can be attributed to the fact that the train dataset was previously encountered during training, and when the model is made to evaluate on it again, the accuracy obtained is very high.

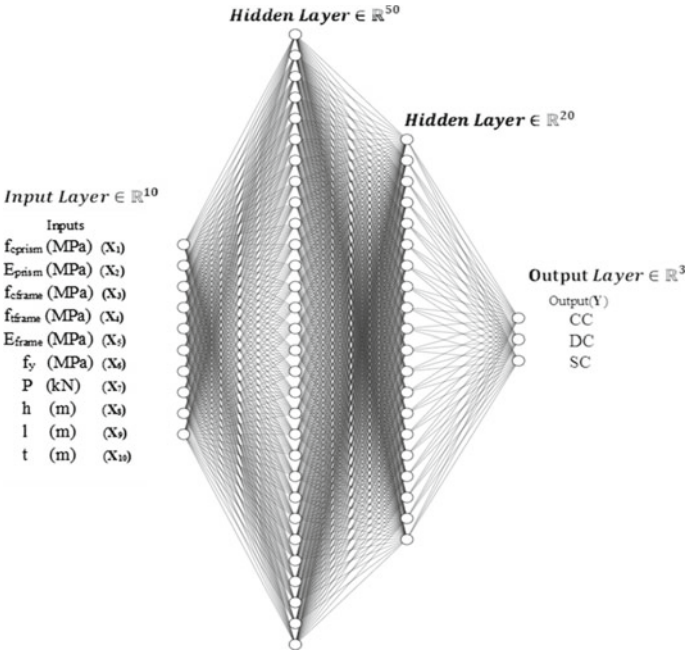

Fig. 2 Neural network architecture used for modelling

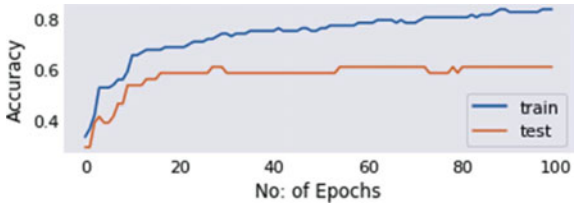

Fig. 3 Plot of accuracy versus number of epochs for neural network

5 Conclusions

Infill frames form an integral part of any framed load-carrying structures. Even though in the past the contribution of infilled frames was usually neglected in the design phase, recent studies conducted in the field of Earthquake engineering shows that infilled frames play a very vital role in the response of a structure to lateral loads. An exhaustive open-source experimental database consisting of about 130 RC infilled frames is collected as part of the study, which can be used by other researchers also for future failure modes classification. Around 30 research papers from a number of leading journals were reviewed, and data collected from.

The entire collected dataset was divided into two—training set used to establish the predictive models and testing set used for end evaluation of the models so obtained. Ten machine learning algorithms were used for modelling—Naïve Bayes, K-Nearest Neighbors, Decision Tree, Random Forest, AdaBoost, XGBoost, LightGBM, CatBoost, Artificial Neural Networks and Support Vector Machines. The performance of the model was evaluated using three metrics: global accuracy, precision, and recall. The results of the study showed that K-Nearest Neighbours, Random Forest and CatBoost have the highest accuracy.

The results obtained also highlighted the need for a train-test split as almost all the algorithms had accuracy above 90% for the train data. The proposed open-source model could be used by structural engineers throughout the world and would help immensely in the design of earthquake-resistant structures. The model obtained is dynamic in the sense that, if and when new experimental data becomes available, it can be conveniently added to the existing database to get more reliable and accurate results.

More research has to be done on such interdisciplinary fields to have efficient ways of formulating and solving complex problems encountered by civil engineers. Any new advancement techniques have seldom failed to make the life of an analyst/designer easier.

References

1. National Disaster Management Authority (2020) Vulnerability profile of India. Accessed online from https://ndma.gov.in/en/vulnerability-profile.html. Last accessed 2020/03/10
2. Mangalathu S, Jeon J-S (2018) Classification of failure mode and prediction of shear strength for reinforced concrete beam-column joints using machine learning techniques. Eng Struct 160:85–94
3. Mangalathu S, Jeon J-S (2019) Machine learning-based failure mode recognition of circular reinforced concrete bridge columns: a comparative study. J Struct Eng 145:04019104
4. Aguilar V, Sandoval C, Adam JM, Garzón-Roca J, Valdebenito G (2016) Prediction of the shear strength of reinforced masonry walls using a large experimental database and artificial neural networks. Struct Infrastruct Eng 12:1663–1676
5. Huang H, Burton HV (2019) Classification of in-plane failure modes for reinforced concrete frames with infills using machine learning. J Build Eng 25:100767

6. Wood RH (1978) Plasticity, composite action and collapse design of unreinforced shear wall panels in frames. Proc Inst Civ Eng 65:381–411
7. Irshad Abdul Azeez P (2019) Studies on infilled RCC frames with and without openings. PhD thesis, NIT Calicut
8. Asteris PG, Kakaletsis DJ, Chrysostomou CZ, Smyrou EE (2011) Failure modes of in-filled frames. Electron J Struct Eng 11:11–20
9. Ghosh AK, Amde AM (2002) Finite element analysis of infilled frames. J Struct Eng 128:881–889
10. Mehrabi AB, Benson SP, Schuller MP, Noland JL (1996) Experimental evaluation of masonry-infilled RC frames. J Struct Eng 122:228–237
11. American Society of Civil Engineers (2017) ASCE standard ASCE/SEI 41-17: seismic evaluation and retrofit of existing buildings
12. Mangalathu S, Jang Hansol H, Jeon J-S (2020) Data-driven machine-learning-based seismic failure mode identification of reinforced concrete shear walls. Eng Struct 208:110331

Punching Shear Strengthening of Flat Slabs with External Bonded CFRP on Grooves (EBROG)

Jijo P. George and Roshini T. Mohan

Abstract The main objective of this study is the strengthening of flat slabs against punching shear with an experimental model. The flat slab strengthens by a newly introduced method, named as grooving method (GM), was utilized in the present study. The groove provided in two orthogonal directions (x and y axes) of slab plan and then mounting the external FRP bar in one direction and FRP strip on another direction in EBROG (externally bonded reinforcement on groove) method. For this purpose, 700 × 700 × 100 mm dimensions slab was tested under concentrated loading. The slabs were tested for ultimate load and deformation after curing for 28 days. The experimental results showed that the EBROG method with FRP enhanced the strength of flat slab against punching shear with great efficiency, and punching shear capacity of strengthened samples increased between 28 and 58% compared to control one. Hence this is a highly innovative practice that can be implemented in the construction industry as the method is high efficiency and the environment-friendly

Keywords Punching shear · CFRP · EBROG

1 Introduction

Flat slab is one of the most widely used structural forms of a roof and floor system. And they have many advantages like reduced building height, shorter construction time, easier formwork, large clear ceiling height, easier reinforcement placement, Creating relatively large spans, and the ease of implementation of this type of roof in different work conditions. In Flat slabs, the loads are directly transferred to columns without beams. Due to the absence of a strong member such as the beam, the most of failure occurs in the flat slab under punching shear. The punching shear failure mechanism in a structural member under the action of concentrated load on a smaller

J. P. George (✉) · R. T. Mohan
Department of Civil Engineering, Sreepathy Institute of Management and Technology, Vavanoor, Palakkad 679533, India
e-mail: jijopgeorge09@gmail.com

© Springer Nature Switzerland AG 2021

K. Dasgupta et al. (eds.), *Proceedings of SECON 2020*,
Lecture Notes in Civil Engineering 97,
https://doi.org/10.1007/978-3-030-55115-5_81

area. To ensure that there is no punching failure is an important option that should be considered in the course of design.

There are several methods to strengthen the punching shear slab studied by researchers including installing the beam at the tensile side of the slab near the column, putting the stud in the direction perpendicular to the slab plane to deal with shear, the use of metal sheets at the sides of the slab and the use of various FRP composites strengthening. Externally bonded reinforcement is the most common method to mount FRP sheets onto a concrete [1]. FRP debonding is the main problem that affects the efficiency of this technique. To avoid the debonding of FRP material to introduce a new grooving method is called "externally bonded reinforcement on grooves" (EBROG) [2–6]. In the EBROG technique, the concrete on which FRP sheet to be installed is prepared by cutting a groove on the concrete surface, and epoxy is filled in the groove and surface before the FRP is installed.

In this study use external bonded CFRP on the groove at the tension side of the slab. The CFRPs are commonly used as a high strength-to-weight ratio that is required, such as aerospace, automotive, civil engineering, sports, and other technical applications. CFRPs are composite materials of two parts: a matrix and reinforcement. In CFRP the reinforcement material is carbon fiber, which provides the strength of the material, and the matrix is usually a polymer resin, to bind the reinforcements (carbon fiber) together. The CFRP consists of two different elements, the material properties depend on these two elements.

The present study aims to investigate the possibility of flat slab strengthening against punching shear by horizontal FRP bars inside the grooves and CFRP strip in the EBROG technique in the orthogonal direction.

2 Materials Used

2.1 Cement

Ordinary Portland cement of 53 grades was used in this work. The physical properties of the cement are given in Table 1.

Table 1 Properties of cement

Physical properties	Results
Fineness	1.61
Standard consistency	34%
Initial setting time	50 min
Specific gravity	3.15
Soundness	1 mm
Compressive strength of cement for 7 days	40.67 Mpa

Table 2 Properties of aggregates

Physical properties	Results	
	Coarse aggregate	Fine aggregate
Bulk density	1.69	1.78
Specific gravity	2.78	2.65
Void ratio	0.71	0.49
Fineness modulus	7.279	3.42
Uniformity coefficient	1.761	3.55
Coefficient of curvature	0.87	0.76

2.2 Aggregates

The coarse aggregates used are crushed stone those retaining in 4.75 mm sieve. The maximum size of the coarse aggregate used is 20 mm.fine sand used as M sand or manufactured sand. The fine aggregates used are those passing through 4.75 mm sieve. The tests are conducted according to IS 2386; 1963. From the gradation curve, it was found that the fine aggregate is of zone 2. The obtained values are given in Table 2.

2.3 CFRP

The CFRP IS used as "Cera CFR W 100 laminate" with size 700 × 50 × 1 mm (Fig. 1), and FRP rod of size 8 mm diameter.

Fig. 1 CFRP strips

2.4 Epoxy Resin

The "Cera bond EP CFR" is used as adhesive material for bonding FRP and concrete.

2.5 Water

In the concrete mix portable water that is free from oils and other impurities is used. The water used has no acidic or alkaline content in it.

3 Experimental Investigations

The slab samples were of size 0.7 × 0.7 × 0.1 m. 8 mm diameter Fe 500 steel reinforcement bars was used. The reinforcement bars were provided at 150 mm spacing. The mix design for M25 grade concrete is done according to IS 10262: 2009. The slabs are denoted by S1, S2, S3, S4 (Table 3) and one slab used as control slab the remains slabs are strengthened by FRP. The concrete specimens were removed from the mould just one day after casting and cured in a water bath at a fixed temperature for 28 days. After the curing, the slab is externally bounded by FRP in two orthogonal directions. One direction FRP rod is used and another direction CFRP strip is used. The rod & strip is implemented in the tension side of the slab. And in one direction the bar inside the grooves (EBRIG) and in the other orthogonal direction FRP using EBROG was used for strengthening. The FRP rods have 8 mm diameter and CFRP strip in 50 mm width, 700 mm length, and 1 mm thickness. Epoxy resin was used as adhesive material to bond FRP's into the slab. Specimens strengthened with 1 or 2 or 3 stacked bars at each face of the loading point in one direction and 1 or 2 or 3 EBROG-FRP strip(s) at each side of the loading point in another orthogonal direction (Fig. 2). All the strengthened slabs were cured for at least five days before testing. The tests were carried out under a loading frame (Fig. 3). The load is applied by handily operated hydraulic jack with the capacity of 100 T and two linear variable differential transducers (LVDTs), mounted at the mid-span, were installed and connected to a data logger to obtain an accurate force and deflection reading. Crack initiation and propagation were also monitored by visual inspection during the tests.

Table 3 Specimen denominations

S1	Control slab
S2	Slab with 1 bar and 1 strip at each side of the loading
S3	Slab with 2 bars and 2 strips at each side of the loading
S4	Slab with 3 bars and 3 strips at each side of the loading

Fig. 2 Specimens—S2, S3, S4

Fig. 3 Experimental setup

4 Results and Discussions

The four samples are tested, and to find out the maximum load and deflection of the samples. The failure pattern of the S2 slab is given below (Fig. 4). The graph between failure load and deflection is plotted (Fig. 5). The ultimate loads of samples are given in the graph (Fig. 6) and also the percentage of increasing loads from the control specimen is plotted (Fig. 7).

The punching shear load-carrying capacity of the slab without CFRP S1 and slab with CFRP S2 are observed and there is a 28.4% increase in the load-carrying capacity of S2 in comparison with S1. S3 and S4 have 46.6% and 58% increased in comparison with the ultimate load of S1. The percentage of increase in load 28.4% in comparison with S1 and S2, 18.2% compared with S2 and S3, and 11.4% compared with S3 and S4. It was observed that punching shear load carrying capacity is an increase from 1 bar and 1 strip at each side of loading to 3 bars and 3 strips at each side of loading, but the percentage of increasing load is reduced.

Fig. 4 Failure pattern of S2 slab

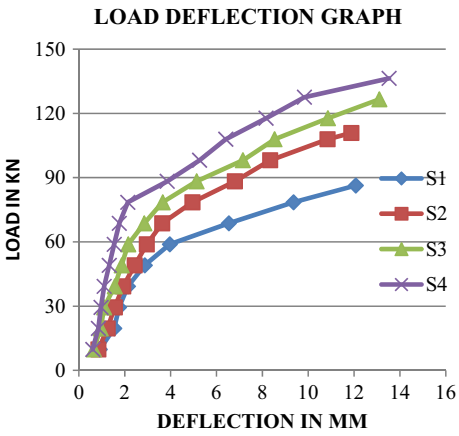

Fig. 5 Load deflection graph

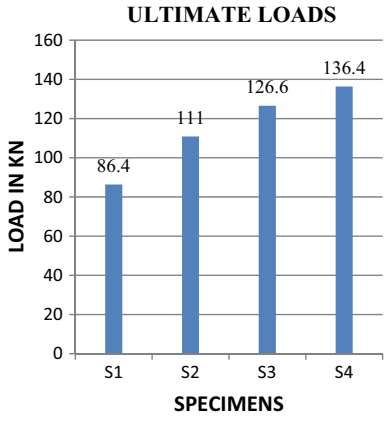

Fig. 6 Ultimate loads

Fig. 7 % of increasing loads

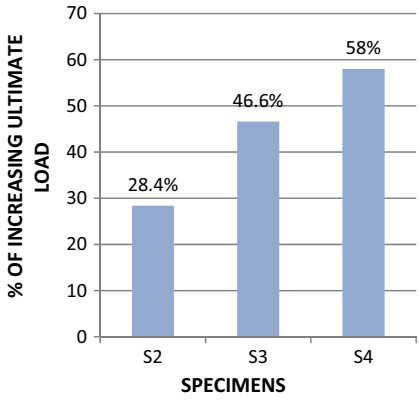

5 Conclusions

In this study to strengthen flat slabs against the punching shear, the EBRIG method is used for the bar and the EBROG methods are applied for the FRP sheets without any shear reinforcement against punching shear. According to research slabs reinforced with the bar inside the groove in one direction and CFRP sheet in the other direction by EBROG, an increase in shear capacity 28.4–58% was observed. The cracking pattern of the tested slab to understand the crack is first initiated at the bottom side of the centre of the slab, and crack propagated in the sides of the slab. The failure pattern to conclude the slab is failed in punching shear. The FRP is placed most as possible at the shear zone if away from loading the percentage of increasing load reduced. The EBROG shearing method is a more efficient method to strengthen the flat slab against punching shear.

References

1. Banijamali SM (2015) Reviewing the FRP strengthening systems. Am J Civ Eng
2. Moghaddas A, Mostofinejad D (2018) Empirical FRP-concrete bond strength model for externally bonded reinforcement on grooves (ASCE) CC.1943-5614.0000924. © 2018
3. Hosseinia A, Mostofinejada D, Shamelia SM (2014) EBROG and EBRIG methods for strengthening of RC beams by FRP sheets. Eur J Environ Civ Eng
4. Mostofinejad D, Shameli SM (2012) Externally bonded reinforcement in grooves (EBRIG) technique to postponed bonding of FRP sheets in strengthened concrete beams. Science Direct, 2012 Elsevier Ltd.
5. Moshiri N (2014) Compressive strength of CFRP composites used for strengthening of RC columns: comparative evaluation of EBR and grooving methods. ASCECC.1943-5614.0000545. © 2014 American Society of Civil Engineers
6. Azizi R, Talaeitaba SB (2019) Punching shear strengthening of flat slabs with CFRP on grooves (EBROG) and external rebars sticking in grooves. Int J Adv Struct Eng

Study on Performance of Concrete Made with Copper Slag and Mineral Admixtures

E. Lalith Prakash, Prakash Chinnayan, K. Siva Kavinesh, Ambrish Adithiya, G. Sarath Sanjeev, Sriram Gnanaprakasam, and Gautham Sukumar

Abstract Copper slag is one of the discarded material that is found to be having a better scope in concrete technology as an alternate for the river sand. Studies show that substituting copper slag partially for the sand leads to the bleeding which further affects the performance of the concrete. In this paper the mineral admixtures such as fly ash and Ground Granulated Blast furnace Slag (GGBS) were added to the concrete containing fine aggregates which is partially substituted with copper slag. An attempt is made to bring down the concrete bleeding and enhance the performance of the Copper slag incorporated concrete. Fly ash and GGBS were chosen mainly based on their global environmental sustainability, cost and durability qualities. Test experiments were designed using Response Surface Method (RSM) to obtain the various trial proportions. Three factors such as Copper Slag, GGBS, and Fly Ash are considered. Three levels of partial replacement are considered for each factor. The levels were 20, 30, and 40% for copper slag; 20, 35, and 50% for GGBS; and 15, 25, and 35% for Fly ash. Test were performed on each trial proportion to study the compressive strength, split tensile strength, chloride penetration and sorptivity properties. The results show that there is considerable improvement in the performance of the copper slag concrete at the optimum dosage of GGBS and fly ash.

Keywords Ground Granulated Blast furnace Slag (GGBS) · Copper slag · Fly ash · Response Surface Methodology (RSM) · Concret bleeding

1 Introduction

Copper slag is a refuse of copper refining and matte smelting processes. For each tonne of copper production around 1.8–2.2 tonnes of slag comprising calcium

E. Lalith Prakash (✉) · P. Chinnayan · K. Siva Kavinesh · A. Adithiya · G. Sarath Sanjeev · S. Gnanaprakasam · G. Sukumar
Department of Civil Engineering, Amrita School of Engineering, Amrita Vishwa Vidyapeetham, Coimbatore 641112, India
e-mail: e_lalithprakash@cb.amrita.edu

© Springer Nature Switzerland AG 2021

K. Dasgupta et al. (eds.), *Proceedings of SECON 2020*,
Lecture Notes in Civil Engineering 97,
https://doi.org/10.1007/978-3-030-55115-5_82

oxide, alumina, silica, and iron is generated [1]. Annually, around 4 billion tonnes of solid wastes is produced by Asia alone, and metal solid waste accounts to 790 million tonnes in which six percentage (48 million tonnes) of it is generated in India [2]. Approximately 6.5 million tonnes of slag is produced in Indian copper industry every year [3]. Currently copper slag is used as a sand replacement in concrete. It is widely recognized and used in the government road projects and ready mix concrete production [4]. Even though the copper slag concrete performs equally as standard concrete, the settling time of the copper slag concrete mainly depends on the particle size of the copper slag. The bleeding rate in the concrete is increased due copper slag as the fine aggregate, which is directly dependent on the water cement ratio, volume fraction of air content and slag [5]. This aspect provides scope in further research on the copper slag concrete.

Over 22 million tonnes of fly ash per year, is used in a varied range of engineering applications. The fly ash comprises silica, aluminium, calcium, and iron in oxide forms [6]. Fly ash is a fine refuse which is acquired from the pulverized coal combustion; it is captured by mechanical separators, electrostatic precipitators or bag fillers [7]. The inclusion of the fly ash in the concrete improves its durability. It also improves the workability and provides chemical resistance to the concrete. Usage of Fly ash in concrete reduces the degree and rate of bleeding primarily due to the reduced water demand which counters the disadvantage of copper slag. The settling time of concrete is not only dependent on the quantity and composition of the fly ash used but also on the type of cement, quantity of cement, quantity of water, temperature, and the quantity of chemical admixtures [8]. The permeability of concrete is reduces by percentage replacement of the binding material with fly-ash.

GGBS is obtained when the molten ash from the furnace is cooled at a faster rate [9]. In this process, the GGBS slag changes into pozzolanic powder and meets the requirement of IS 12089:1987. The disposal of GGBS requires higher energy. On the other hand, partially replaced GGBS concrete showed better resistance to sulphate attack and corrosion [10]. The specific gravity of GGBS is found to be 2.85. GGBS can be incorporated in the concrete as a replacement for Portland cement up to 80% by its mass [11]. When hydration takes place in Portland cement, alkalis and sulphates are released, which serve as activators for the GGBS [11]. The compressive strength of the concrete improves as the quantity of the GGBS in the concrete as a replacement for cement upto 55% replacement [12].

The key focus of the study is to determine whether the addition of the admixtures such as GGBS and fly ash to the partially replaced copper slag concrete can positively influence its performance. Also, the study focuses on determining the optimum percentage replacements of the fine aggregates with copper slag (CS) and the binding material with Fly ash (FA) and Ground Granulated Blast furnace Slag (GGBS) showing better performance.

2 Materials and Design

2.1 Materials

2.1.1 Cement

Grade 53 Ordinary Portland cement (OPC) was used. IS 2720-Part 3 was followed for testing the cement properties. The specific gravity of the cement used is 2.98.

2.1.2 Aggregates

The natural fine aggregate used was with a maximum nominal size of 4.75 mm. IS 383 was followed in order to determine various properties of both fine and coarse aggregates. The obtained results are shown in Table 1. Crushed coarse aggregates available locally having a maximum nominal size of 20 mm was used.

2.1.3 Preliminary Tests for Mix Design

2.1.4 Copper Slag and Mineral Admixtures

Copper slag (Table 2) was used to partially replace the fine aggregates in the concrete by weight. The mineral admixture used as partial replacement for cement were Ground Granulated Blast furnace Slag (GGBS) and Class F Fly Ash (Table 2).

2.2 Mix Design

Using the preliminary test results (Table 1), a control design mix was designed as per IS 456-2000 and IS 10262-2009. The control mix ratio is 1:1.47:2.77.

2.3 Design of Experiments

Past researches show that the sand replacement with copper slag up to 50% enhances the compressive strength of concrete [13], and the concrete shows upward trend in compressive strength values only up to 50% GGBS replacement [14]. Concrete performed better with the addition of Fly ash up to 50% cement replacement when the early-age strength requirement is met in other suitable ways, while the optimum Fly Ash content in concrete is considered to be ranging between 15 and 25% historically. The design of experiments is an effective tool to reduce the number of trial mixes when

Table 1 Preliminary test results considered for mix design

	Cement	Sand	Coarse aggregates	Partial replacement of FA by copper slag				GGBS	Fly ash
				100%	20%	30%	40%		
Specific gravity	2.98	2.61	2.77	3.61	2.73	2.75	2.94	2.81	2.10
Fineness modulus	–	2.57	6.96	3.29	–	–	–	–	–
Water absorption (%)	–	1	0.75	0.4	0.68	0.52	0.45	–	–

Table 2 Chemical properties of copper slag, fly ash and GGBS

Chemical compounds	Copper slag	GGBS	Fly ash
CaO (%)	2.64	35.67	2.91
SiO_2 (%)	37.8	33.02	61.21
Al_2O_3 (%)	4.34	19.61	28.24
Fe_2O_3 (%)	47.92	0.95	3.89
MgO (%)	–	8.56	0.92
SO_3 (%)	2.90	0.18	0.74
Na_2O (%)	0.94	0.16	0.01
K_2O (%)	2.96	0.91	1.35
TiO_2 (%)	0.48	0.94	–
Loss on ignition (%)	–	–	0.73

two or more factors are involved in addition to the primary concrete components. Three factors such as Copper Slag, Fly-ash, and GGBS were considered for the design of experiments using Response Surface Methodology (RSM). Based on literature study, three levels were considered for each of the factors, such as Copper Slag (20, 30, and 40%), GGBS (20, 35, and 50%), and Fly-ash (15, 25, and 35%). Face centred central composite design was adopted using Minitab software for generating the number of trails and the mix proportions (Table 3).

3 Results and Discussions

3.1 Compressive Strength

Test result show that the compressive strength of the control mix is 35 MPa at 7 days and 44.5 MPa at 56 days (Fig. 1). The control mix has reached higher compressive strength at the early stage whereas the other trials had an increase in strength progressively. At 56 days, run order R1 and R4 are 50.5 MPa and 47 Mpa respectively which are greater than the strength of the control mix at 56 days (Fig. 1). The run orders R2, R5, R7, R10, R12, R14, R16, R17, R19 achieved 56 days compressive strength values similar and nearer to the control mix strength value (Fig. 1 and Table 4).

3.2 Split Tensile Strength

The split tensile strength of the control mix was observed to be higher than all the trials at 28 days curing. The change of strength between 28 and 56 days of the control mix was determined to be 4.2% increment which is very low compared to the run orders (Fig. 2). The split tensile strength of almost all the run orders is greater than

Table 3 Response surface methodology—run order

Run order	Copper slag (%)	GGBS (%)	Fly ash (%)
R1	20	50	15
R2	30	35	25
R3	30	50	25
R4	40	20	15
R5	20	35	25
R6	20	50	35
R7	30	35	25
R8	40	50	35
R9	20	20	35
R10	30	35	25
R11	40	20	35
R12	30	20	25
R13	40	50	15
R14	30	35	25
R15	30	35	15
R16	30	35	25
R17	30	35	25
R18	40	35	25
R19	20	20	15
R20	30	35	35

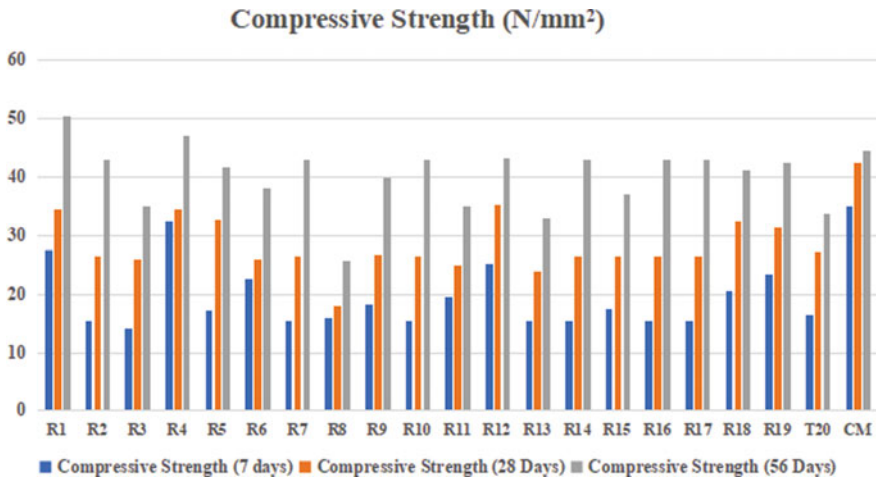

Fig. 1 Compressive strength comparison based on duration

Table 4 Test result—compressive strength (7, 28, and 56 days)

Run order	Compressive strength (7 days) (N/mm^2)	Compressive strength (28 days) (N/mm^2)	Compressive strength (56 days) (N/mm^2)
R1	27.5	34.5	50.5
R2	15.5	26.5	43
R3	14	26	35
R4	32.5	34.5	47
R5	17.2	32.75	41.75
R6	22.5	26	38
R7	15.5	26.5	43
R8	16	18	25.75
R9	18.2	26.75	39.75
R10	15.5	26.5	43
R11	19.5	25	35
R12	25.2	35.25	43.25
R13	15.5	24	33
R14	15.5	26.5	43
R15	17.5	26.5	37
R16	15.5	26.5	43
R17	15.5	26.5	43
R18	20.5	32.5	41.25
R19	23.5	31.25	42.5
R20	16.5	27.25	33.75
CM	35	42.5	44.5

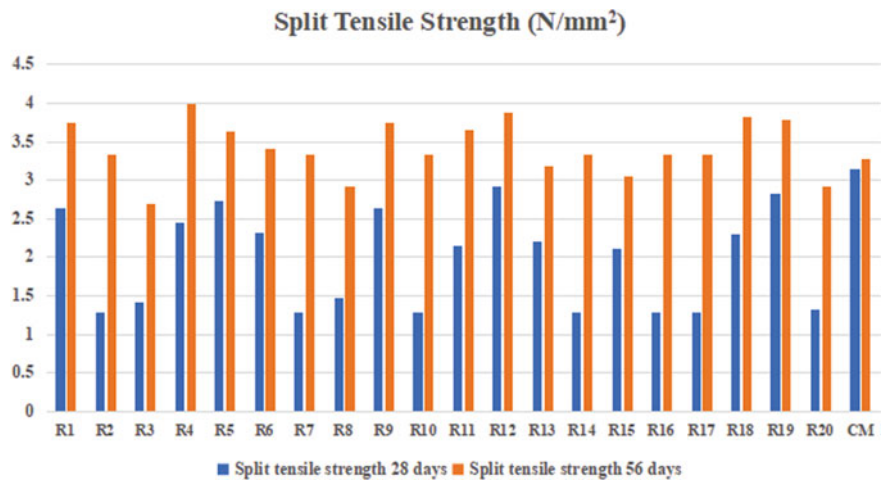

Fig. 2 Split tensile strength comparison based on duration

Table 5 Test result—split tensile strength (28 and 56 days)

Run order	Split tensile strength (N/mm^2) 28 days	Split tensile strength (N/mm^2) 56 days
R1	2.64	3.75
R2	1.28	3.34
R3	1.41	2.7
R4	2.45	3.98
R5	2.73	3.63
R6	2.32	3.4
R7	1.28	3.34
R8	1.47	2.92
R9	2.64	3.75
R10	1.28	3.34
R11	2.14	3.66
R12	2.92	3.88
R13	2.2	3.18
R14	1.28	3.34
R15	2.12	3.05
R16	1.28	3.34
R17	1.28	3.34
R18	2.3	3.82
R19	2.83	3.78
R20	1.32	2.92
CM	3.14	3.28

the control mix at 56 days, among which R4 had the highest split tensile strength value (Fig. 2 and Table 5).

3.3 Sorptivity

The sorptivity value at 2 hours' time period was found to be 1.86×10^{-7} for the mix (Fig. 3). The rate of absorption for R1, R2, R5, R7, R11, R14, R16, and R17 was observed to be less compared to mix demonstrating more durable characteristics among which R1 had the lowest absorption rate (Fig. 3 and Table 6).

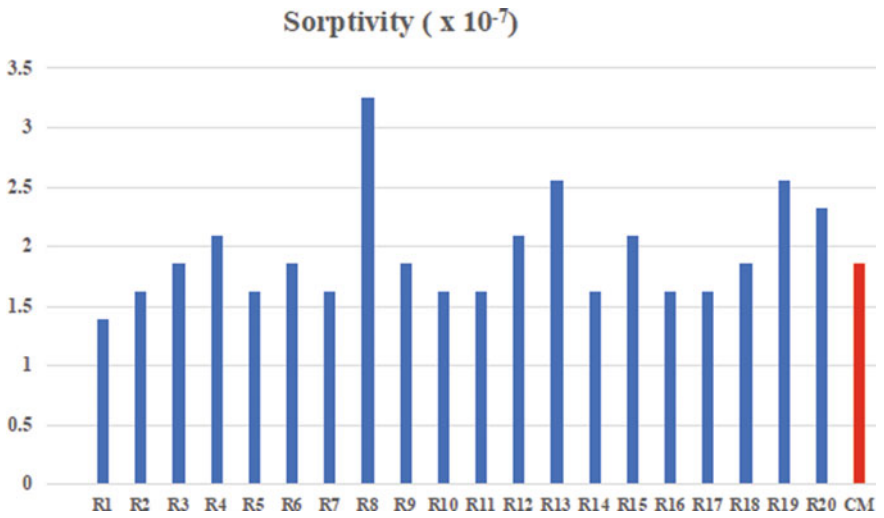

Fig. 3 Sorptivity ($\times 10^{-7}$ (m/$\sqrt{}$min)) test result—comparison

3.4 Rapid Chlorine Penetration Test (RCPT)

The charge passed through the test specimen for the test period of 6 h for the mix was observed to be 1854 C which is greater than all the run orders. Among the run orders, R3, R20 and R1 have passed charge of 243, 297 and 306 C respectively which was found to be the lowest inferring better durability characteristics (Fig. 4 and Table 7).

4 Conclusion

The key focus of this study is on the performance of the concrete with partial replacement of copper slag and mineral admixtures. The following inferences have been obtained from the test outcomes. The mineral admixture concrete showed lesser compressive strength at 28 days curing period when compared to the control mix, but there was an improvement at 56 days curing period. Run orders R1 (20% CS, 50% GGBS and 15% FA) and R4 (40% CS, 20% GGBS and 15% FA) show greater compressive strength value than the control mix at 56 days of curing. This may be attributed due to the mineral admixtures which is known for its improved pozzolanic reaction over a longer period in concrete. But the run orders with Fly Ash content more than 25% showed lesser compressive strength. Split tensile strength of all the mineral admixture concrete was less compared to that of the control mix at 28 days curing period. A total of fifteen among the twenty run orders showed higher split tensile strength when compared to the control mix split tensile strength value at after 56 days of curing. Among the fifteen run orders, R4 recorded the highest 56 days split tensile

Table 6 Sorptivity test result

Run order	Initial weight (kg)	Weight after 30 min	Weight after 60 min	Weight after 90 min	Weight after 120 min	Sorptivity $\times 10^{-7}$ (m/$\sqrt{}$min)
R1	0.942	0.948	0.948	0.95	0.954	1.39
R2	1.008	1.014	1.016	1.018	1.022	1.63
R3	0.994	1.002	1.004	1.006	1.01	1.86
R4	0.994	1.004	1.006	1.008	1.012	2.09
R5	0.95	0.958	0.958	0.96	0.964	1.63
R6	0.908	0.918	0.92	0.922	0.924	1.86
R7	1.008	1.014	1.016	1.018	1.022	1.63
R8	0.992	1.008	1.012	1.014	1.02	3.25
R9	0.95	0.956	0.96	0.964	0.966	1.86
R10	1.008	1.014	1.016	1.018	1.022	1.63
R11	1.038	1.044	1.046	1.048	1.052	1.63
R12	0.96	0.97	0.974	0.976	0.978	2.09
R13	1.028	1.04	1.044	1.046	1.05	2.56
R14	1.008	1.014	1.016	1.018	1.022	1.63
R15	1.016	1.026	1.03	1.032	1.034	2.09
R16	1.008	1.014	1.016	1.018	1.022	1.63
R17	1.008	1.014	1.016	1.018	1.022	1.63
R18	1.032	1.04	1.042	1.044	1.048	1.86
R19	0.956	0.966	0.97	0.972	0.978	2.55
R20	0.972	0.98	0.984	0.986	0.992	2.32
CM	0.992	1	1.002	1.004	1.008	1.86

strength value (3.98 N/mm^2) and R1 recorded almost closer value (3.75 N/mm^2). Sorptivity test revealed that nine among twenty run orders possess less water absorption than the control mix. Among the nine-run orders, R1 recorded the least value. All run orders having copper slag content lesser than 30% performed well in terms of sorptivity. Based on a rapid chlorine penetration test, all the run orders obtained lower value than the control mix. This may be attributed due to the presence of the mineral admixtures even though copper slag accounting to higher permeability is present. R3 (30% CS, 50% GGBS and 25% FA), R1 (20% CS, 50% GGBS and 15% FA), and R20 (30% CS, 35% GGBS and 35% FA) recorded the least RCPT values. This may be due to the presence of copper slag below 30% partial replacement, as higher copper slag content affects the permeability of the concrete. The run orders R5, R6, R8, R9, R12, R13, and R19 showed higher RCPT values closer to that of the control mix. These mixes either had higher copper slag content (40%) or higher Fly ash content (25% and above). Summarizing the above inferences, the concrete with either higher copper slag content (40%) or higher Fly ash content (more than

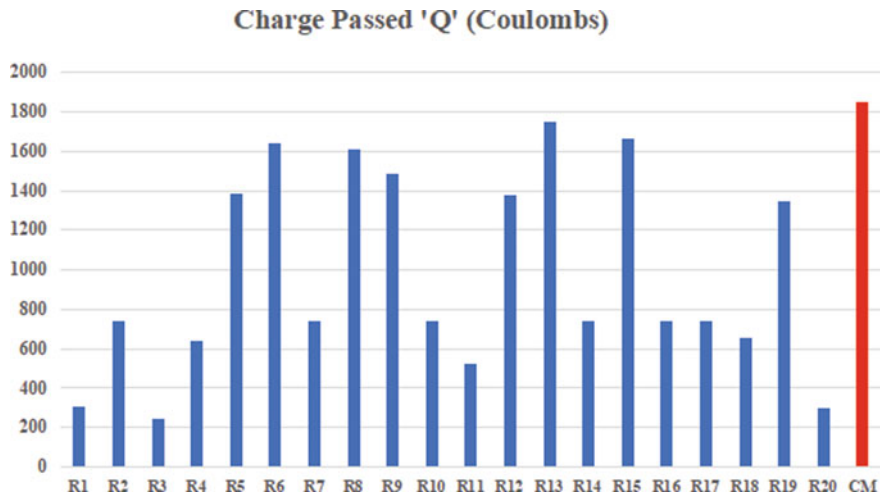

Fig. 4 Rapid chlorine penetration test result—comparison

Table 7 RCPT result

Run order	Charge passed 'Q' (C)	Chloride ion penetrability
R1	306	Very low
R2	738	Very low
R3	243	Very low
R4	639	Very low
R5	1386	Low
R6	1638	Low
R7	738	Very low
R8	1611	Low
R9	1485	Low
R10	738	Very low
R11	522	Very low
R12	1377	Low
R13	1746	Low
R14	738	Very low
R15	1665	Low
R16	738	Very low
R17	738	Very low
R18	657	Very low
R19	1350	Low
R20	297	Very low
CM	1854	Low

15%) showed lower performance at least in one of the tested characteristics. It was found that the concrete mix in which the river sand is replaced with 20% of copper slag and cement replaced with GGBS and Fly Ash by 50% and 15% respectively, perform better in the strength, permeability, and porosity characteristics. Thus, the results prove that the controlled partial substitution of copper slag for fine aggregate along with the controlled partial substitution of GGBS and Fly Ash for cement, has significantly improved the performance in terms of permeability, porosity and strength of concrete than that of control mix.

References

1. Gorai B, Jana RK (2003) Characteristics and utilization of copper slag—a review. Resour Conserv Recycl 39(4):299–313
2. Murari K, Siddique R, Jain KK (2015) Use of waste copper slag, a sustainable material. J Mater Cycles Waste Manage 17(1):13–26
3. Dash MK, Patro SK, Rath AK (2016) Sustainable use of industrial-waste as partial replacement of fine aggregate for preparation of concrete—a review. Int J Sust Built Environ 5(2):484–516
4. BIS, IS 383-2016 (2016) Coarse aggregate and fine aggregate for concrete—specification. Bureau of Indian Standards, New Delhi
5. Shoya M, Nagataki S, Tomosawa F, Sugita S, Tsukinaga Y (1997) Freezing and thawing resistance of concrete with excessive bleeding and its improvement, vol 170. Special Publication, pp 879–898
6. Joshi RC, Lohita RP (1997) Fly ash in concrete: production, properties and uses, vol 2. CRC Press
7. ASTM C618, Annual bool of ASTM standard volume 4.02. ASTM International
8. Thomas MDA (2007) Optimizing the use of fly ash in concrete, vol 5420. Portland Cement Association, Skokie, IL, pp 1–10
9. Arivalagan S (2014) Sustainable studies on concrete with GGBS as a replacement material in cement. Jordan J Civ Eng 159(3147):1–8
10. Statistic Data Report (2005) Environmental Protection Administration. Executive Yuan, Taipei, Taiwan
11. Pavía SARA, Condren E (2008) Study of the durability of OPC versus GGBS concrete on exposure to silage effluent. J Mater Civ Eng 20(4):313–320
12. Oner A, Akyuz S (2007) An experimental study on optimum usage of GGBS for the compressive strength of concrete. Cement Concr Compos 29(6):505–514
13. Al-Jabri KS, Hisada M, Al-Oraimi SK, Al-Saidy AH (2009) Copper slag as sand replacement for high performance concrete. Cement Concr Compos 31(7):483–488
14. Hawileh RA, Abdalla JA, Fardmanesh F, Shahsana P, Khalili A (2017) Performance of reinforced concrete beams cast with different percentages of GGBS replacement to cement. Arch Civ Mech Eng 17(3):511–519

Effect of Size and Shape of Concrete Column Elements Exposed to High Temperature

Y. K. Guruprasad

Abstract Reinforced concrete (RC) structures and the structural elements (beams, columns, slabs) undergo degradation in strength and stiffness, when exposed to high temperature in the event of a fire breaking out in such structures. The concrete column elements tend to support the compressive loads transferred onto it from the floors and maintain the stability of the structure. The degradation in the compressive strength of concrete and degradation of yield strength of reinforcing steel present in the RC columns that get exposed to high temperature, in the event of a fire causes instability or collapse of the entire structure. In this work the variation of temperature across the cross section of reinforced concrete (RC) columns having various sizes and shapes (square and rectangular) exposed to different high temperatures (475 and 625 °C) and time of exposure (1 and 3 h) has been studied by carrying out a heat transfer analysis in Abaqus. The heat transfer analysis is carried out using heat transfer elements that possess the thermal properties of the materials (concrete and steel) that are temperature dependent. The depth of variation of a particular temperature for a particular time of exposure from the outer surface of the RC column upto the core having a particular size and shape is assessed. It is inferred from the analysis results, the time taken for a particular temperature to reach upto the core of the RC column is related to the size and shape of the concrete column. It is also learnt from the results, apart from increasing the concrete cover, a particular optimum size of a concrete column in cross section is necessarily to be provided while designing the column from thermal resistance point of view. As this optimum size of the column would delay the temperature reaching the core for a particular time of temperature exposure and would maintain a certain portion of concrete around the core portion to retain its original strength without causing failure of the column before the fire is put off.

Keywords Concrete column · High temperature · Exposure time · Size · Shape

Y. K. Guruprasad (✉)
Department of Civil Engineering, Ramaiah Institute of Technology, Bengaluru 560054, India
e-mail: guruprasad.civil.iisc@gmail.com

© Springer Nature Switzerland AG 2021

K. Dasgupta et al. (eds.), *Proceedings of SECON 2020*,
Lecture Notes in Civil Engineering 97,
https://doi.org/10.1007/978-3-030-55115-5_83

1 Introduction

Most of the present day reinforced concrete (RC) structures are vulnerable to undergo damage when they are subjected earthquakes [1], exposure to high temperature in the event of a fire [2], due to ageing and erroneous design or over loading. For the stability of a reinforced concrete structure, the strength and stiffness of reinforced concrete (RC) columns to be retained is of outmost importance. Damage is assessed in the distressed RC structural elements adopting non destructive testing techniques [3]. The repair or retrofit of such damaged structural elements is possible when the damage is within a certain repairable limit. In the case of an event of a fire in a structure, heat generated from the fire causes a rise in the temperature. Due to high temperature exposure there is strength and stiffness reduction in concrete due to the physiochemical changes that is taking place in concrete, at different temperatures of exposure. The reduction in strength and stiffness due to high temperature exposure, causes a reduction in the load carrying capacity of the structural members in the RC structure. Especially, when there is degradation of the strength and stiffness of RC columns in a RC structure that is exposed to high temperature in the event of a fire, the whole structure would collapse due to instability. The strength and stiffness degradation of the concrete in the RC column, especially in the core portion when exposed to high temperature [4], causes the column to collapse causing instability in the structure partially or completely. Li et al. [5] carried out compressive tests on concrete cylinder and cube test specimens to study the compressive strength variation due to different shapes and sizes of the test specimens. Li et al. developed empirical relations that co related the static and dynamic compressive strengths of concrete obtained from the test specimens that were having different shapes and sizes. Fládr and Bílý [6] studied the effect of specimen size on the compressive and flexural strength of high strength fibre reinforced concrete having coarse aggregates. It was learnt from the test results of Fládr and Bílý's work that, there was an influence of the size of the test samples on the compressive and flexural strength of concrete. Their results showed that, the size dependence of compressive strength reduces when the strength of the concrete increases and conversion factors were put forth with respect to compressive and flexural strengths of members. Baalbaki et al. [7] have determined the elastic modulus of concrete based on strains measured from concrete cylinders having two sizes subjected to uniaxial compression. The two cylinder sizes adopted for the study had the same mix proportion and their test results showed that the larger test specimens had a lower compressive strength and a higher elastic modulus. Kodur et al. [8] developed a numerical model for assessing resistance to fire of columns made up of high performance concrete. The numerical model developed by Kodur et al. was able to assess the high performance concrete column's fire resistance for various parameters, such as applied load, cross sectional dimensions, strength of concrete, column height, fiber content, and type of aggregates used. Emberley [9] developed numerical calculations in excel to determine the performance of concrete columns with varying loading, various types of aggregates and different dimensions of column for different time temperature curves. The model thus developed helped engineers

and students to assess and design of RC columns exposed to fire. Lie et al. [10] worked on reinforced concrete columns and assessed the residual strength of these columns that were exposed to high temperature and different exposure time corresponding to standard fire cases. Lie et al. adopted a mathematical model, utilized non destructive test namely, ultrasonic pulse technique and adopted load testing as modalities for their assessment. Lie et al. determined the residual strength of columns and compared it with the values determined through the mathematic model, non destructive test and determined by the load test. Their results indicated there was a good agreement with the results obtained through the modalities and the experimental values.

It is understood from the study of the literature that has been carried out that, there is a necessity of a better understanding of the influence of size and shape of the concrete structural element on the strength and the load carrying capacity when exposed to a particular temperature. **Objective of the present work**: The present work has been taken up to study the effect of the size and shape of RC columns cross sections adopted in structural designs, that get exposed to different higher temperatures (475 and 625 °C for exposure durations of 1 and 3 h [11]) in the event of a fire. In this work, an optimum size of the column cross section from fire resistance perspective is arrived at, based on the temperatures developed across the cross section of the column exposed to fire, that has an influence on the load carrying capacity and stability of the RC column. The optimum size of the column cross section arrived at, helps in delaying the temperature developed around the core of the column which in turn, delays the failure of the column before the fire is put off. Temperatures higher than 625 °C has not been considered in the present work as concrete looses upto 50–80% of its compressive strength when exposed to temperatures ranging from 550 to 700 °C respectively. Therefore, a value of temperature less than 550 °C and a value less than 700 °C has been adopted in this work.

2 Assessing the Influence of Shape and Size of RC Columns Exposed to Higher Temperatures on Its Load Carrying Capacity

In this section the details of the finite element analysis that was carried out on RC column cross sections that were having square and rectangular shapes and having different sizes exposed to different temperatures has been explained.

2.1 Finite Element Analysis of Various RC Column Cross Sections that Were Exposed to Different Temperatures

Square and rectangular column cross sectional shapes having different sizes have been adopted for the analysis. The sizes of the cross sections selected are having

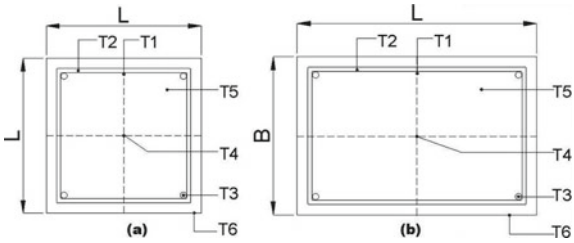

Fig. 1 Sizes of RC columns having different shapes of cross sections **a** square cross section; **b** rectangular cross section

standard sizes that are usually adopted in actual construction and design practice as per IS 456 [12]. The sizes of the square cross sections adopted in the present work are: 300 mm × 300 mm and 450 mm × 450 mm. The sizes of the rectangular cross sections adopted are 230 mm × 450 mm and 300 mm × 450 mm. Each cross section of the RC column in the analysis is provided with 4 numbers of 12 mm diameter rebars and 8 mm diameter lateral ties spaced at 300 mm centre to centre. The reinforcing steel adopted is having a yield strength of 500 MPa and the concrete adopted is having a compressive strength of 25 MPa. The RC column cross sections were modeled in two dimensions in the finite element model adopting quadrilateral heat transfer elements. A structured mesh was considered for meshing the cross section. The density of concrete and reinforcing steel considered in the finite element analysis are 2400 and 7850 kg/m^3. Thermal properties such as thermal conductivity and specific heat values of concrete and reinforcing steel, that vary with different temperatures of exposure has been adopted from EN 1994-1-2:2005 [13] as an input into the finite element analysis. The details of the locations where the temperatures are recorded in different locations in the cross section of RC columns that are obtained when the finite element analysis is carried out for, square and rectangular RC column cross sections are shown in Fig. 1. In Fig. 1, L = 300 mm/450 mm and B = 230 mm/300 mm/450 mm corresponding to the square and rectangular cross sections. In Fig. 1, T1 refers to the temperature measured close to the lateral tie (close to the centre of one side dimension (L) of the cross section). T2 refers to the temperature measured on the lateral tie. T3 refers to the temperature measured on the longitudinal rebar. T4 refers to the temperature measured at the central core or the centre point of the cross section. T5 refers to the temperature measured at a point in concrete that is located at (L/8, B/8). T6 refers to the temperature measured on the surface of the cross section where the external temperature (475 and 625 °C) is applied. Heat transfer analysis is carried out for different temperatures (475 and 625 °C), that are applied on all the outer external surfaces (T6) of the RC column cross section for exposure time of 1 and 3 h respectively. The time considered in this study upto 3 h is based on an average realistic fire condition [14]. The magnitude of the external temperature (475 and 625 °C) applied is kept constant over a particular exposure time (1 or 3 h) in the finite element analysis.

3 Results and Discussions

In this section the results and discussion of the finite element analysis carried out on RC columns, exposed to different temperature and exposure time has been presented.

3.1 Results of Finite Element Analysis of RC Column Cross Sections Exposed to Different Temperatures

The temperature distribution across square and rectangular cross sectional shapes of RC columns having various sizes (300 mm × 300 mm, 450 mm × 450 mm, 230 mm × 450 mm and 300 mm × 450 mm) exposed to different temperatures and exposure time, namely, 475 and 625 °C for exposure durations of 1 and 3 h, have been shown in Fig. 3a–p. Table 1 shows the temperatures measured at different locations in the RC columns having square and rectangular cross sections in reference to Fig. 1. It can be observed from Fig. 3a–p and the results in Table 1 that, larger the size of the RC column exposed to a particular temperature and time of exposure, the temperature developed around the core portion of the RC column was lower when compared to the temperature developed around the core portion of the RC column that was having a smaller cross sectional size. The reason being, the amount of heat required to raise the temperature in a RC column cross section having a larger size was larger, as this is due to a larger volume of concrete present in the cross section. Whereas, in the case of RC column having smaller cross sectional dimensions and exposed to high temperature, there is lesser volume of concrete present that causes the temperature to rise faster for the same amount of heat supplied. It is learnt from the results (in Table 1), for RC columns having the least cross sectional dimension less than 300 mm, a higher value of temperature develops around the core portion (at points T4 and T5 indicated in Fig. 2 and Table 1), which in turn causes a larger amount of degradation of strength and stiffness of concrete in that portion due to physiochemical changes taking place for a particular exposure temperature. The effect of shape is not predominantly seen in all the cases. Degradation of concrete around the core portion leads to a reduced volume of concrete to exist in intact condition to carry the axial load, thereby causing instability of the column further leading to its failure. It can be observed from Table 1 that, the cross section 450 mm × 450 mm has lower temperatures developed in its cross section for different external exposure temperatures when compared to other cross sections. It is learnt from the analysis results (Table 1) of the present work that, the optimum least cross sectional dimension in RC columns from fire resistance point of view is identified as 300 mm. This value of 300 mm is arrived based on the observation of lower temperatures developed around the core portion (T4 and T5) and across the cross section, in various cross sections of columns considered in this study that has 300 mm as the least dimension in the cross section(seen in Table 1). This optimum least cross sectional dimension of 300 mm that is arrived at may be considered in design of the cross section so that, there is an optimum

volume of concrete existing in the cross section. In such an optimum cross section, the temperature developed around the core portion (T4 and T5) for a particular time of exposure is lower, as this causes a delay in the rise of temperature. Such an optimum sectional dimension that is used to design an optimum cross section, helps in restoring the stability of the column by the time the fire is put off, from fire resistance point of view. It is also observed from Table 1, the cross section having a least dimension of 230 mm has higher values of temperature developed in the cross section (T1–T6 seen in Table 1). It is observed from Table 1, based on the values of the temperatures developed (T1–T6) across the cross sections having various sizes and shapes, a rectangular column having a size of 300 mm × 450 mm has comparatively lower temperatures developed across its cross section for different external exposure temperatures and time durations. Therefore, this rectangular RC column having a size 300 mm × 450 mm is considered as an optimum cross section dimension from fire resistance point of view. It has to be noted that, providing very large cross sectional areas of RC columns from fire resistance point of view in design after taking into consideration the design due to all types of loads, will make the design uneconomical and non-aesthetical (Fig. 3).

It can be observed from Table 1, the experimental (Ex) results of Lin et al. [15] (*Ex For section C1B: 400 mm × 400 mm, in the paper) is in close correlation with the FE analysis results, (**FEM) of the same RC column that was analysed for an external exposure temperature of 670 °C for 1 h exposure duration. The FE analysis of Lin et al.'s RC column was carried out to validate the FE model used in this study.

4 Conclusion

1. It is inferred from the results of this work, an RC column cross section having a particular shape and comparatively having a larger cross sectional dimension tends to possess a larger volume of concrete. A larger volume of concrete requires a higher quantity of heat to be supplied to raise its temperature to a particular value in a certain time of exposure. An RC column comparatively having smaller cross sectional dimensions tends to have lesser volume of concrete in it. Such an RC cross section with lesser volume of concrete would have a higher value of temperature rise for a particular time of exposure for the same quantity of heat supplied.
2. It is understood from the analysis results, RC columns that have one of its least cross sectional dimension less than 300 mm, tend to develop a higher value of temperature around the core portion (points T4 and T5). Higher temperature developed around the core causes a larger amount of degradation of strength and stiffness of concrete, leading to a lesser volume of concrete remaining in intact condition around the core portion to participate in carrying the loads. Such an RC column has a very high probability of failure. It is understood from this study the effect of shape is not much predominant.

Table 1 Temperatures measured at different locations in RC columns having square and rectangular cross sections as per Fig. 1 exposed to different temperatures and time of exposure

Section mm × mm	External exposure temp (°C)	Exposure time (h)	T1 (°C)	T2 (°C)	T3 (°C)	T4 (°C)	T5 (°C)	T6 (°C)
300 × 300	475	3 h	323	325	311	117	247	475
300 × 300	475	1 h	200	132	127	24	92	475
450 × 450	475	3 h	302	416	410	36	219	475
450 × 450	475	1 h	186	430	421	20	79	475
300 × 450	475	3 h	385	389	376	81	244	475
300 × 450	475	1 h	187	130	119	21	84	475
230 × 450	475	3 h	334	366	342	145	263	475
230 × 450	475	1 h	207	310	298	30	102	475
300 × 300	625	3 h	392	485	471	124	290	625
300 × 300	625	1 h	201	132	127	24	105	625
450 × 450	625	3 h	369	520	510	37	280	625
450 × 450	625	1 h	200	430	420	21	89	625
300 × 450	625	3 h	385	470	456	86	288	625
300 × 450	625	1 h	224	163	130	22	89	625
230 × 450	625	3 h	424	585	570	157	360	625
230 × 450	625	1 h	331	362	402	31	124	625
400 × 400 [15] *Ex	670	1 h	281	493	493	30	96	670
400 × 400 **FEM	670	1 h	236	450	453	21	93	670

*Experimental (Ex) result: 400 mm × 400 mm, section C1B in reference [15]; Material properties: $f_y = 354.60$ N/mm^2 (3616 kg/cm^2); $f_c = 20.59$ N/mm^2 (210 kg/cm^2)
**FEM validation of Ex result

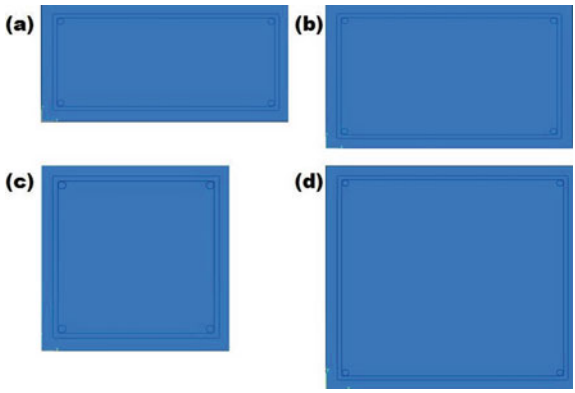

Fig. 2 Finite element model of RC columns having different shapes and sizes exposed to different temperature exposed to different temperatures and time of exposure
a 230 mm × 450 mm,
b 300 mm × 450 mm,
c 300 mm × 300 mm and
d 450 mm × 450 mm

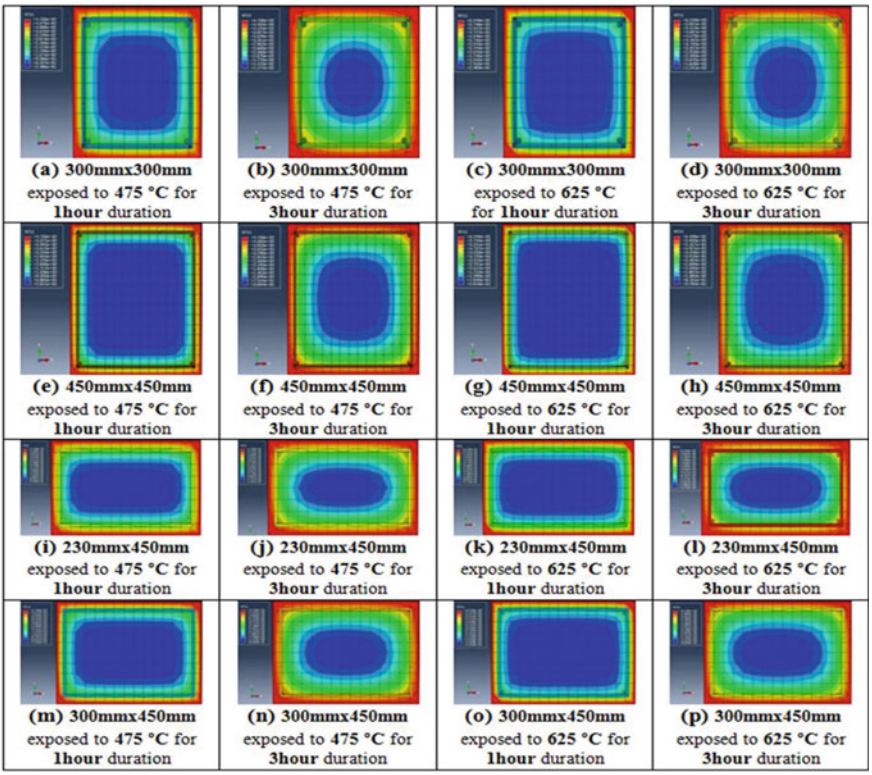

Fig. 3 a–p Temperature distribution across RC columns having square and rectangular cross sections exposed to different temperatures and exposure time

3. A value of 300 mm is identified to be the least optimum dimension in the column cross section. This value of 300 mm is arrived at after examining the analysis results (Table 1) and with respect to different time of exposure [14], based on the observation of lower temperatures developed around the core portion (T4 and T5) and across the cross section, in various cross sections of columns considered in this study that has 300 mm as the least dimension.
4. It is observed from the results (Table 1), the cross section 450 mm × 450 mm has lower temperatures developed in its cross section for different external exposure temperatures when compared to other cross sections adopted in this work. Therefore, an optimum minimum cross section dimensions should be arrived at from load carrying capacity and fire resistance points of view. It means, from design calculations, if the cross section dimension of the RC column from load carrying capacity point of view is smaller than the optimum minimum cross section dimensions required for fire resistance, then, an optimum minimum cross section is provided for the RC column which will satisfy both the load carrying capacity and fire resistance criterions. At the same time it has to be kept in mind

that, providing very large cross section dimensions of RC columns larger than the cross section dimensions required for load carrying capacity from fire resistance point of view, will make the design uneconomical.

5. It is learnt from the results of this study (Table 1), based on the values of the temperatures developed across the cross section (T1–T6), a rectangular RC column having a size of 300 mm × 450 mm is seen to be an optimum minimum cross section from fire resistance and design point of view.

References

1. Ates S, Kahya V, Yurdakul M, Adanura S (2013) Damages on reinforced concrete buildings due to consecutive earthquakes in Van. Soil Dyn Earthq Eng 53:109–118
2. Ada M, Sevim B, Yüzer N, Ayvaz Y (2018) Assessment of damages on a RC building after a big fire. Adv Concr Constr 6(2):177–197
3. Helal J, Sofi M, Mendis P (2015) Non-destructive testing of concrete: a review of methods. Electron J Struct Eng 14(1):97–105
4. Bikhiet M, El-Shafey NF, El-Hashimy HM (2014) Behavior of reinforced concrete short columns exposed to fire. Alexandria Eng J 53:643–653
5. Li M, Hao H, Shi Y, Hao Y (2018) Specimen shape and size effects on the concrete compressive strength under static and dynamic tests. Constr Build Mater 161(10):84–93
6. Fládr J, Bílý P (2018) Specimen size effect on compressive and flexural strength of high-strength fibre-reinforced concrete containing coarse aggregate. Compos B Eng 138:77–86
7. Baalbaki W, Baalbaki M, Benmokrane B, Aitcin PC (1992) Influence of specimen size on compressive strength and elastic modulus of high-performance concrete. Cem Concr 14(2):113–117
8. Kodur VKR, Wang TC, Cheng FP, Sultan MA (2003) A model for evaluating the fire resistance of high performance concrete columns. In: Fire safety science—Proceedings of the seventh international symposium, pp 1013–1024
9. Emberley RL (2013) A study into the behavior of reinforced-concrete columns under fire exposures using a spreadsheet-based numerical model. Masters thesis, Department of Civil Engineering, Worcester Polytechnic Institute
10. Lie TT, Rowe TJ, Lin TD (1986) Residual strength of fire-exposed reinforced concrete columns. In: ACI symposium, vol 92, pp 153–174
11. IS: 3809-1979, Indian Standard fire resistance test of structures (1st rev), Reaff
12. IS 456 (2000) Indian Standard plain and reinforced concrete—code of practice (4th rev), Reaff
13. EN 1994-1-2: 2005 (E), Eurocode 4—Design of composite steel and concrete structures. Part 1–2: General rules—structural fire design
14. IS: 1642-1989, Code of practice for fire safety of buildings (general): details of construction, Reaff
15. Lin C-H, Chen S-T, Hwang T-L (1989) Residual strength of reinforced concrete columns exposed to fire. J Chin Inst Eng 12(5):557–565

Diagrid Structural System for Tilted Steel Buildings

Archana Joy Eluvathingal and G. Unni Kartha

Abstract The rapid growth of urban population and the limitation of available land, taller structures are preferred for sustainability. When the height of the structure increases, the consideration of lateral load becomes critical and the lateral load resisting system becomes more important than the structural system that resists the gravitational loads. Diagrid structural system is widely used for tall buildings due to its structural efficiency and aesthetic potential provided by the unique geometric configuration of the system. In this paper, the impacts of variation of the angle of tilting on steel diagrid structures are presented. Modal and time history analysis of three, six and nine-storey buildings with a base dimension of 36 m × 36 m is performed using ETABS 2016. The results in terms of the time period, undamped natural frequency, maximum storey displacement, maximum storey drift, storey shear and overturning moment are compared. Tilted 3 storey diagrid building was found to have lateral stiffness very much similar to that of a prismatic diagrid. While the lateral stiffness of 6 storeys and 9 storey tilted buildings up to 2° was found to be similar to that of prismatic diagrid building.

Keywords Diagrid structures · Tilted building · Modal analysis · Time history analysis

1 Introduction

The rapid growth of urban population and consequent pressure on limited space have considerably influenced the residential development of the city. The high cost of land, the desire to avoid a continuous urban sprawl, and the need to preserve important agricultural production have all contributed to driving residential buildings upward.

A. J. Eluvathingal (✉) · G. Unni Kartha
Federal Institute of Science and Technology, Angamaly, Ernakulam, India
e-mail: archanajoy96@gmail.com

G. Unni Kartha
e-mail: unnikartha@gmail.com

© Springer Nature Switzerland AG 2021

K. Dasgupta et al. (eds.), *Proceedings of SECON 2020*,
Lecture Notes in Civil Engineering 97,
https://doi.org/10.1007/978-3-030-55115-5_84

As the height of the building increases, the lateral load resisting system becomes more important than the structural system that resists the gravitational loads. The lateral load resisting systems that are widely used are the rigid frame, shear wall, wall-frame, braced tube system, outrigger system, and tubular system [1].

Recently, the diagrid—Diagonal Grid—the structural system is becoming popular due to its structural efficiency and aesthetic potential provided by the unique geometric configuration of the system [2]. Compared to conventional exterior-braced frame structures, in diagrid structures, almost all the conventional vertical columns are eliminated. This is possible since the diagonal members in diagrid structural systems can carry gravity loads as well as lateral forces owing to their triangulated configuration [1].

Diagrid is formed by intersecting the diagonal and horizontal components [3]. The famous examples of diagrid structures all around the world are the Swiss Re in London, Hearst Tower in New York, and Cyclone Tower in Asan (Korea) [4]. The configuration and efficiency of a diagrid system reduce the number of structural elements required on the facade of the building and there will be less obstruction to the outside view. The structural efficiency of the diagrid system also helps in avoiding interior and corner columns allowing significant flexibility with the floor plan. Perimeter "diagrid" systems save approximately 20% of the structural steel weight when compared to a conventional moment-frame structure [4].

2 Previous Studies

Studies about diagrid systems have been conducted by researchers worldwide and is proven to be a better solution for lateral load resisting systems [1, 2, 5]. These studies have indicated that structures with diagrid systems can give better efficiency, expressiveness and sustainability. Diagrid structures have comparatively less deflection to that of conventional buildings and up to 28% less weight [6]. Due to inclined columns, lateral loads are resisted by axial action of the diagonal compared to bending of vertical columns in a framed tube structure and diagonal structures generally do not require a core because lateral shear can be carried by diagonals on the periphery of the building. Diagrid structural systems are more effective in resisting the lateral load due to wind or earthquake due increase in the lever arm of peripheral diagonal columns [1]. The major parameters that researchers study for comparison are time period, maximum top storey lateral displacement, maximum base shear, maximum storey displacement, and maximum storey drift [5]. Changes in the geometrical pattern of diagrid have a great influence on its performance. The detailed study by Montuori et al. [7] have brought out the behaviour of diagrid structures with the angle of diagonals (variable-angle i.e. VA) and the number of diagonals (variable-density i.e. VD) along with the height of the building. Studies using hexagrid systems [5], Isotruss grid [8] have indicated that diagrid buildings perform better than normal buildings. These studies are mainly conducted on buildings with simple plans using software like SAP and ETABS. Architects who try intriguing designs like tilted buildings pose

big challenges in its analysis and design. Due to its inherent advantages, diagrid structures can be a good choice for such systems. Buildings with a tilt like the Capital Gate Tower in Abu Dhabi and the Gate of Europe Towers in Madrid have been constructed using diagrid systems. These designs have employed diagrid systems and have better performance compared to conventional designs. More studies into using diagrids for tilted structures are required for a better understanding of the behaviour and limitations.

3 Analysis of Diagrid Buildings with Tilt

To study the effect of tilted on diagrid buildings, 3, 6 and 9 storied structures were modelled using etabs software. The analysis structure had plan dimensions 36 m × 36 m and storey height 3. 6 m. The inclined columns were provided at six-meter spacing along the perimeter. All structural members were designed using Indian standard code IS 800:2007. The design dead load and lived load on the floor slab were 3.75 kN/m^2 and 2.5 kN/m^2 respectively. The design earthquake load was computed based on the zone factor of 0, 16, medium soil, importance factor of 1 and the response reduction factor of 5 [9]. The support conditions of columns were assumed as hinged. The yield strength of steel was considered as 250 N/mm^2. The diagrid provided for all the buildings was 450 mm pipe sections with 25 mm thickness. They were provided at a 6 m interval all around the periphery of the buildings. The angle of inclination of the diagrid was kept uniform throughout the height. The diagrid building without any tilting had an angle of inclination 64°.

The effect of four different angles, 1°, 2°, 3°, and 4° tilted were investigated in this study. Figure 1 shows the elevation of the 3 storeys tilted diagrid building with the angle of tilted 1°, 2°, 3°, and 4° respectively. Similar modes were used for 6 storey and 9 buildings. The buildings were tilted only in the x-direction.

3.1 Modal Analysis

Tables 1, 2 and 3 show the undamped natural frequency of the first six modes of vibration obtained from the modal analysis.

It was observed that as the angle of tilt increases from 1° to 4°, the value of undamped natural frequency decreases, but the change is less than 1%. A decrease in natural frequency indicates that the stiffness of the building has decreased. This points to the fact that tilted diagrid buildings will be more susceptible to deformation than the diagrid building without tilt.

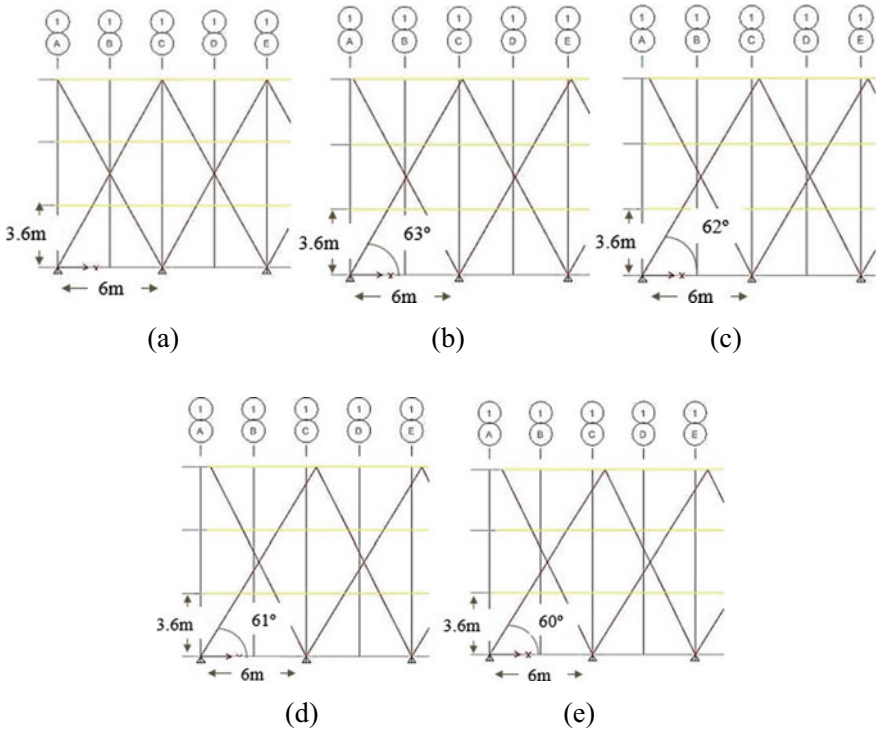

Fig. 1 Three storey tilted diagrid building **a** without tilt **b** with 1° tilt **c** 2° tilt **d** 3° tilt and **e** 4° tilt

Table 1 Natural frequency of diagrid and tilted 3 storey diagrid buildings

Mode of vibration	Frequency of diagrid building in Hz	Frequency of tilted diagrid building in Hz			
		1°	2°	3°	4°
1	5.51	5.469	5.453	5.448	5.451
2	5.524	5.496	5.483	5.477	5.471
3	11.633	11.576	11.921	11.908	11.57
4	12.315	12.071	12.342	12.301	12.046
5	19.047	18.939	18.954	18.761	18.548
6	19.613	19.019	19.514	19.477	18.95

3.2 Time History Analysis

The time-history analysis provides for a linear or nonlinear evaluation of dynamic structural response under loading which may vary according to the specified time function. The time history of the El Centro Earthquake (Imperial Valley earthquake) which occurred in 1940 in southern California is used for studying the performance

Table 2 Natural frequency of diagrid and tilted 6 storey diagrid buildings

Mode of vibration	Frequency of diagrid building in Hz	Frequency of tilted diagrid building in Hz			
		1°	2°	3°	4°
1	3.095	3.061	3.058	3.056	3.06
2	3.098	3.079	3.071	3.075	3.076
3	7.568	5.558	5.559	5.554	5.559
4	7.733	7.542	7.534	7.516	7.515
5	10.895	7.608	7.619	7.592	7.597
6	11.506	10.829	10.811	10.797	10.795

Table 3 Natural frequency of diagrid and tilted 9 storey diagrid buildings

Mode of vibration	Frequency of diagrid building in Hz	Frequency of tilted diagrid building in Hz			
		1°	2°	3°	4°
1	2.069	2.043	2.043	2.041	2.044
2	2.07	2.056	2.057	2.055	2.056
3	3.921	3.878	3.873	3.87	3.874
4	5.566	5.547	5.53	5.525	5.527
5	5.617	5.555	5.531	5.527	5.531
6	8.441	8.512	8.385	8.379	8.378

of diagrid buildings with tilt. This earthquake had a moment magnitude of 6.9 and a maximum perceived intensity of X (Extreme) on the Mercalli intensity scale.

3.2.1 Storey Displacement

Figure 2a–c shows the maximum storey displacements in the x-direction versus storey for diagrid building without any tilt and with 1°, 2°, 3° and 4° tilts respectively for 3 storey, 6 storey and 9 storey building. It is observed that the overall displacement values of tilted diagrid buildings decrease by 5% when compared to the diagrid building without any tilt in the case of three storey buildings. In the case of six storey buildings, the value first increases by 32% then a drop of 8% occurs after which the value again increases by 8% then finally reduces to almost the same values of 1° tilted building. In the nine storey building, there is an increase in values by 30% upto 3° tilted building after which the values drop back to almost the same as that of non tilted diagrid building. This variation in the values maybe be the result of change in optimum angle of 64° in diagrid building without any tilt.

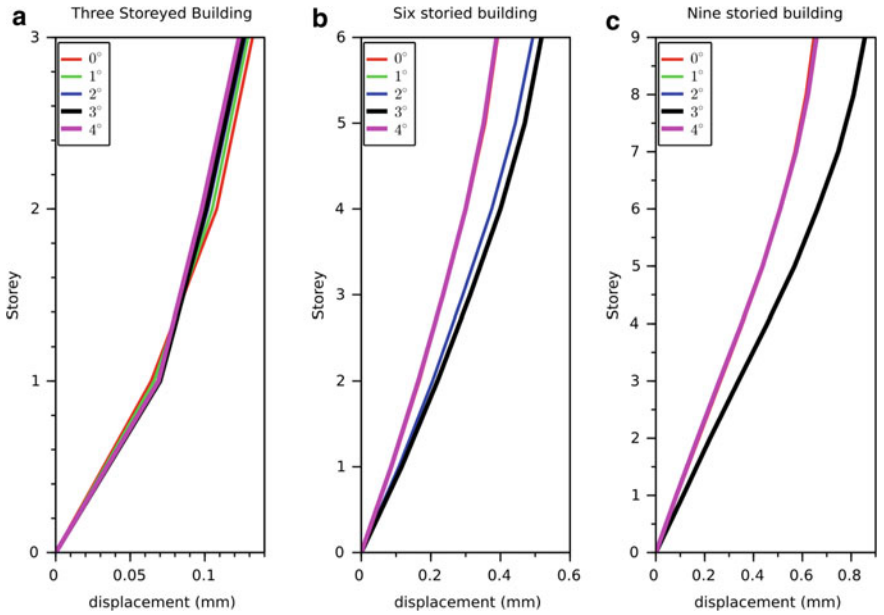

Fig. 2 **a** Maximum storey displacement of 3 storey building, **b** maximum storey displacement of 6 storey building, **c** maximum storey displacement of 9 storey building

3.2.2 Storey Drift

Figure 3a–c shows the maximum storey drift observed in the analyses conducted. It is observed that the overall drift values of tilted diagrid buildings decreases by 1% when compared to the diagrid building without any tilt in the case of three storey buildings. In the case of six storey buildings, the value first increases by 33% then a drop of 2% occurs after which the value again increases by 2% then finally reduces to almost the same values of 1° tilted building. In the nine storey building, there is an increase in values by 32% upto 3° tilted building after which the values drop back to almost the same as that of non tilted diagrid building. This pattern is similar to the observed values of maximum displacements.

3.2.3 Storey Shear

Figure 4a–c shows the maximum storey shear observed in the analyses conducted. It is observed that the overall shear values of tilted diagrid buildings decreases by 3% when compared to the diagrid building without any tilt in the case of three storey buildings. In the case of six storey buildings, the value first increases by 34% then a drop of 12% occurs after which the value again increases by 12% then finally reduces to almost the same values of 1° tilted building. In the nine storey building, there is

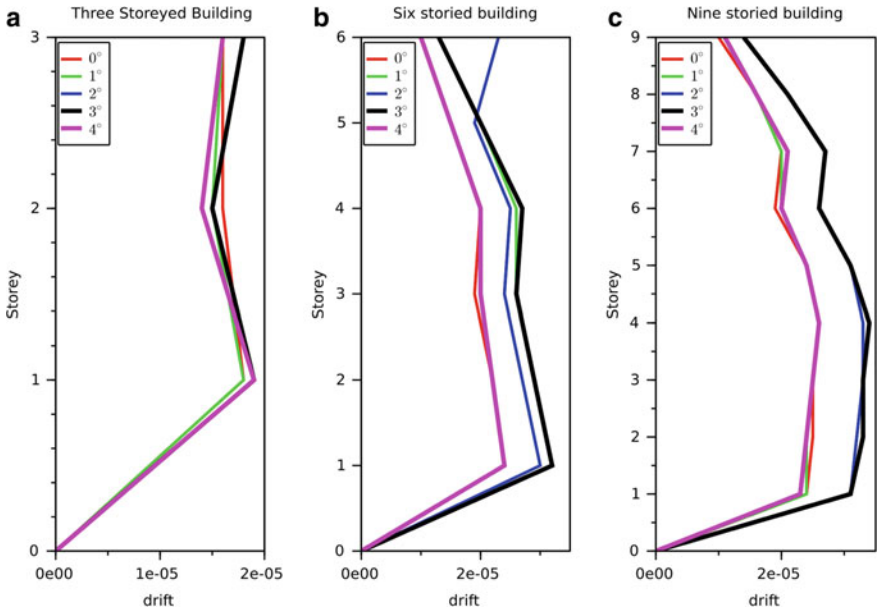

Fig. 3 **a** Maximum storey drift of 3 storey building, **b** maximum storey drift of 6 storey building, **c** maximum storey drift of 9 storey building

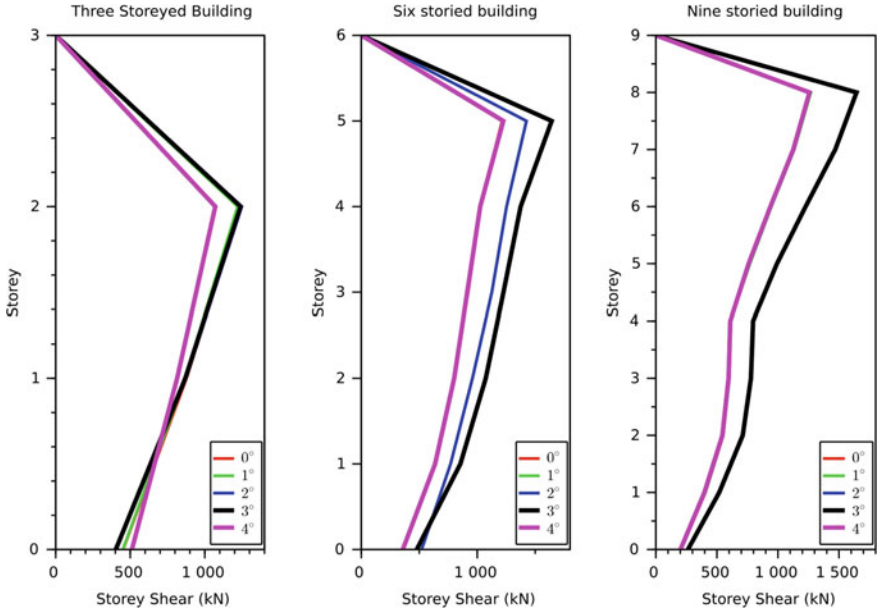

Fig. 4 **a** Maximum story shear of 3 storey building, **b** maximum storey shear of 6 storey building, **c** maximum storey shear of 9 storey building

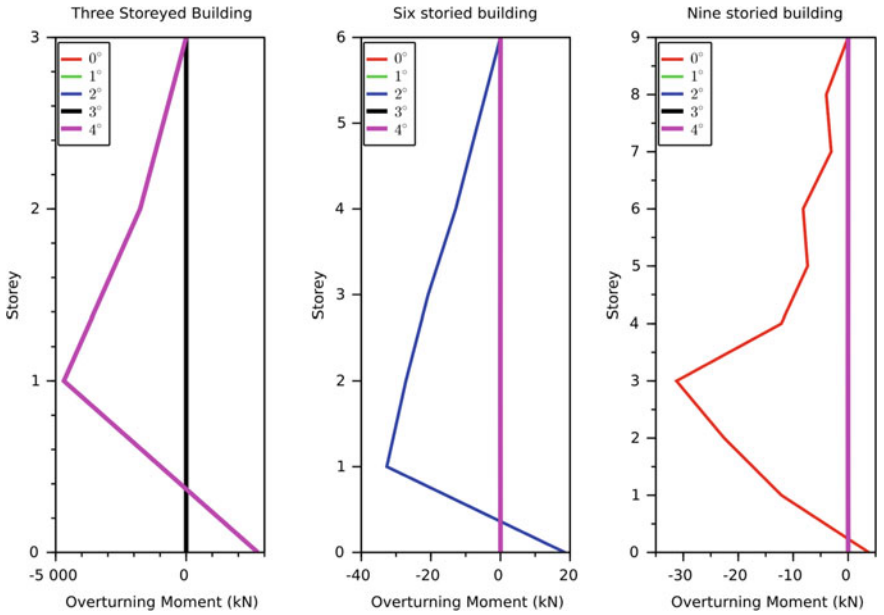

Fig. 5 **a** Maximum overturning moment of 3 storey building, **b** maximum overturning moment of 6 storey building, **c** maximum overturning moment of 9 storey building

an increase in values by 30% upto 3° tilted building after which the values drop back to almost the same as that of non tilted diagrid building.

3.2.4 Overturning Moment

Figure 5a–c shows the maximum storey overturning moment observed in the analyses conducted. It can be observed that the storey overturning moment of non tilted diagrid building, 1°, 2° and 3° overlap each other while 4° tilted building has much higher values in the case of three storey buildings. In the case of six storey buildings, the storey overturning moment of non tilted diagrid building, 1°, 3° and 4° overlap each other while 2° tilted building has much higher values. In the nine storey building, there is an overlap of curves from 1° to 4° while the values of non tilted diagrid building is much higher.

4 Results and Discussions

The effect of tilt in three buildings, with 3, 6 and 9 storey buildings studied in this study. The buildings were tilted in the x-direction at an angle of 1°, 2°, 3° and 4°

Table 4 Results of modal analysis and time history analysis

	3 storey building	6 storey building	9 storey building
Undamped natural frequency	Decrease by 0.07%	Decrease by 1%	Decrease by 1%
Maximum storey displacement	Decrease by less than 10%	First increases when titled up to 3° then decreases	First increases when titled up to 3° then decreases
Storey drift	Decrease by less than 10%	First increases when titled up to 3° then decreases	First increases when titled up to 3° then decreases
Storey shear	Decrease by less than 10%	First increases when titled up to 3° then decreases	First increases when titled up to 3° then decreases
Storey overturning moment	Decrease by less than 10%	First increases when titled by 1° then it goes on decreasing	First increases when titled by 1° then it goes on decreasing

respectively. Modal analysis and time history analysis were conducted and the results are summarised in Table 4. The views on the various results obtained are discussed in the conclusions.

5 Conclusions

The unique compositional characteristics of diagrid structure provide lateral stiffness very efficiently and at the same time produce distinguished architecture as aesthetics in any existing cityscapes. Diagrid systems can be adopted for better designs of buildings with tilt. The following conclusions may be arrived at based on the results of the study conducted. Lateral stiffness of the tilted diagrids is very much similar to that of a prismatic diagrid for 3 storey building, and up to 2° in the case of 6 storeys and 9 storey building. Hence it is possible to tilt a 3 storey diagrid building up to 4° without compromising the performance of the building. In the case of 6 and 9 storey tilted diagrid buildings, diagrid buildings can be tilted up to 2° safely without compromising the performance of the building.

Today's complex-shaped tall buildings require more detailed system design, analysis and construction. Not only architectural but also structural and other related performance issues should be considered holistically to produce better performing and the higher quality built environment.

References

1. Jani K, Patel PV (2013) Design of diagrid structural system for high rise buildings as per Indian Standards. Structures congress 2013, ASCE
2. Kim J, Jun Y, Lee YH (2010) Seismic performance evaluation of diagrid system buildings. In: 2nd Specialty conference on disaster mitigation
3. Joshi RS, Dhyani DJ (2017) A review on novel structural development in tall building: diagrid structure. Int J Adv Eng Res Dev
4. Jani K, Patel PV (2013) Analysis and design of diagrid structural system for high rise steel buildings. Procedia Eng 51:92–100
5. Lee H-U, Kim Y-C (2017) Preliminary design of tall building structures with a hexagrid system. Procedia Eng 171:1085–1091
6. Shah MI, Mevada SV, Patel VB (2016) Comparative study of diagrid structures with conventional frame structures. Int J Eng Res Appl 6(5), (Par-2). ISSN: 2248-9622
7. Montuori GM et al (2014) Geometrical patterns for diagrid buildings: exploring alternative design strategies from the structural point of view. Eng Struct 71(2014):112–127
8. Kim T-H, Lee H-U, Kim Y-C (2017) Development of a building structural system using an IsoTruss® grid. Procedia Eng 171:1077–1084
9. IS:1893 (Part-I)-2002 (2002) Criteria for earthquake resistant design of structures. Bureau of Indian Standard, New Delhi

Investigation on the Suitability of Jarofix as a Fine Aggregate Replacement in Concrete Building Blocks

Robert V. Thomas and Deepa G. Nair

Abstract Excessive utilization of natural resources and dumping of waste materials aggravates environmental degradation. Utilization of a locally available industrial waste facing disposal issues—Jarofix as fine aggregate replacement in concrete building blocks is investigated through this research. Test results justify the potential of jarofix for replacement of fine aggregate up to 30% in concrete building blocks with improved strength characteristics. Test on structural masonry verify the suitability of these blocks over conventional concrete blocks.

Keywords Jarofix · Fine aggregate · Construction building blocks · Structural masonry

1 Introduction

Concrete building blocks are most popular these days due to its easy availability and economic viability compared with other conventional alternatives. But usually the strength and durability of these blocks are found far below building standards due to competition among the local manufacturers in reducing the cost compromising to quality. Utilization of alternative materials replacing cement and natural aggregates needs attention at this juncture. Environmental issues arising due to excessive sand mining urges the need for alternative materials to replace conventionally used fine aggregate (river sand).

Jarosite produced during the extraction of Zinc ore concentrate is a locally available industrial waste in Cochin facing disposal issues. Jarosite is disposed by combining it with cement and lime to form a composite namely jarofix. Chen et al. [1] and Seyer et al. [2] carried out mineralogical study of Jarofix and reported

R. V. Thomas (✉) · D. G. Nair
School of Engineering, Cochin University of Science and Technology, Cochin, Kerala 682022, India
e-mail: robertmodiyil@yahoo.com

D. G. Nair
e-mail: deepagnair@cusat.ac.in

© Springer Nature Switzerland AG 2021

K. Dasgupta et al. (eds.), *Proceedings of SECON 2020*,
Lecture Notes in Civil Engineering 97,
https://doi.org/10.1007/978-3-030-55115-5_85

better mechanical strength and durability characteristics over jarosite. Pappu et al. [3, 4] studied the utilization potential of jarosite in soil stabilization for reducing the shrinkage of clay. He also observed that the compressive strength and durability characteristics of jarofix are compactable to that of any construction material confirming standards. Havanagi et al. [5] and Vsevolod et al. [6] also suggested different applications of jarofix in general civil engineering applications. Sharma [7] reported that the physico-chemical characterization of jarosite has applications in building blocks, tiles, cement and other composites. According to Arora et al. [8] jarofix has positive effects on compressive and flexural strength of hardened concrete. This paper investigates the feasibility of using jarofix as an alternative source of fine aggregate to partially replace river sand in solid concrete blocks suitable for structural masonry.

2 Experimental Programme

Experimental programme includes the characterization of the materials, mix optimization for building blocks, block making and tests on structural masonry. Details of experiments and results are presented.

2.1 Material Characterization

Cement, river sand (fine aggregate), 6 mm broken stone (coarse aggregate) and jarofix are the materials used for this study.

- Cement: Cement used was ordinary portland cement satisfying the requirements of IS 4031–1988 [9] and IS 8112–1989 [10] under the commercial name Malabar cement.
- Fine aggregates: River sand passing through 4.75 mm IS sieve and retained at 150 micron sieve satisfying the requirements of IS: 383–1970 [11] are used in this study. Figure 1 shows the particle size distribution of river sand. It indicate a uniform distribution of particles lying under Zone II.
- Jarofix: Jarofix samples collected from Binani Zinc Ltd., Kochi, Kerala were subjected to different tests as per IS 383-1970. Jarofix include Sodium Jarosite ($NaFe_3(SO_4)_2(OH)_6$)—80%, Hydrated lime ($Ca(OH)_2$)—5% and Portland Cement—15%. Table 1 shows the physical properties and chemical composition of jarofix. Figure 2 shows the particle size distribution of jarofix. It indicates the presence of very fine particles lying between 0.0016 and 0.352 mm.
- X-ray diffraction analysis of jarofix was conducted using Bruker AXS D8 Advance X-ray diffraction system operating with a 50 kV, 50 mA Cu radiation source. The diffraction pattern of the sample shows the presence of gypsum, bassanite, anhydrite, natrojarosite, quartz and magnetite (Fig. 3).

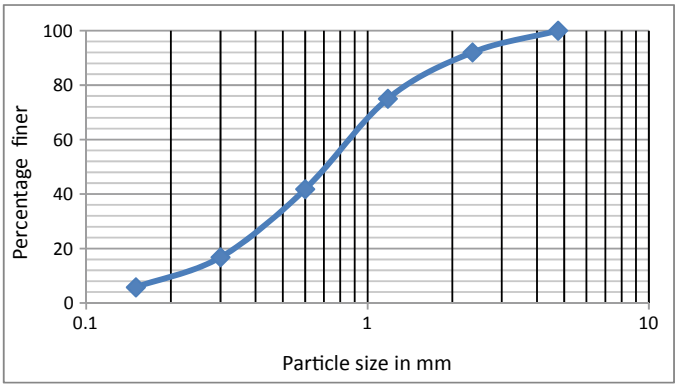

Fig. 1 Particle size distribution of fine aggregate (river sand)

Table 1 Properties of jarofix

Physical properties	
Moisture content	35%
Bulk density	1.26
Specific gravity	2.86
Chemical composition	
Component	%
Fe	15.0–20.0
Ca	7.5–9.0
SiO_2	10–12
Zn	2.0–3.0
Pb	3.0–5.0
pH	8.0–9.0

- Coarse aggregate: 6 mm nominal size broken stone satisfying the requirements of IS 383-1970 was used as the coarse aggregate for this study. Figure 4 indicates the particle size distribution.

2.2 Mix Optimization and Casting of Blocks

Concrete mixes (1:4:8) were prepared with river sand and jarofix as fine aggregates. Mixes are designated as JC0, JC1, JC2, JC3 and JC4 based on the replacement levels of fine aggregate with jarofix varying from 0%, 10%, 20%, 30% and 40% respectively. Cube specimens of size 150 mm × 150 mm × 150mm were cast and compressive strength test was conducted after 28 days as per IS: 2185 part I-2005 [12]. Trial mixes are done for different mixes with water cement ratios 0.40, 0.42,

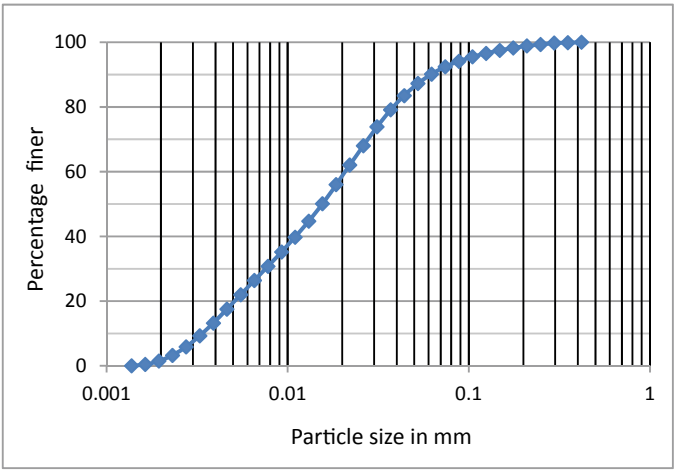

Fig. 2 Particle size distribution of jarofix

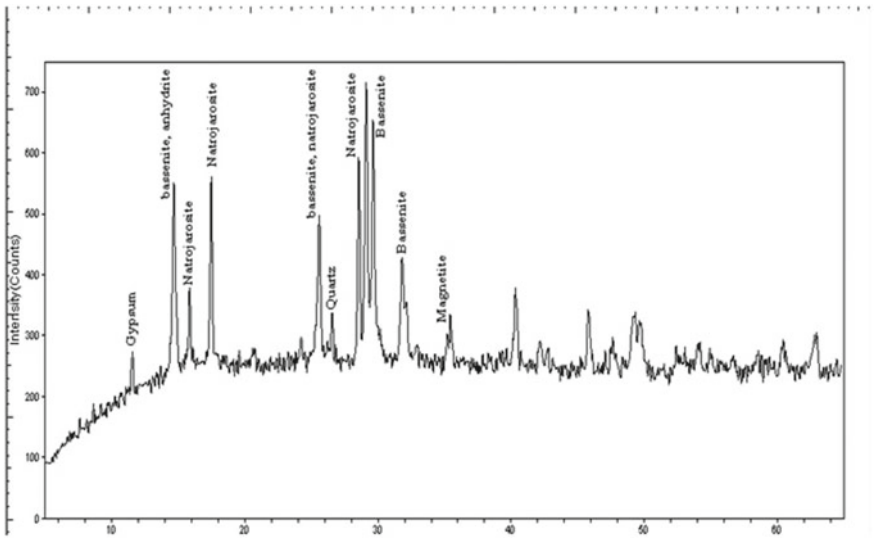

Fig. 3 X-ray diffraction pattern of jarofix

0.45 and 0.50. Mixes with low water binder ratios (0.40 to 0.45) were found less workable owing to the higher water requirement of jarofix. Hence further studies were done with water binder ratio 0.50 for all mixes. Tests on density (ASTM C 140–03 [13]) and water absorption (IS 1237 [14]) were also conducted. Results are shown in Table 2.

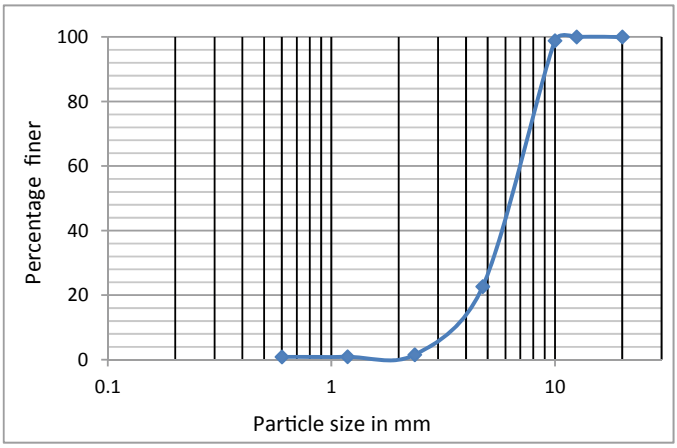

Fig. 4 Particle size distribution of coarse aggregates

Table 2 Test results—mix optimization—1:4:8 mix

S. No.	Mix designation	w/c ratio	Fine aggregate replacement with jarofix	Average COMPRESSIVE strength (N/mm^2)	Average density (kg/m^3)	Water absorption (%)
			% Jarofix	28 days	28 days	
1	JC0	0.50	0	5.48	2089	7.58
2	JC1	0.50	10	9.00	2113	9.12
3	JC2	0.50	20	10.05	2128	9.35
4	JC3	0.50	30	11.00	2153	9.70
5	JC4	0.50	40	10.18	2105	9.98

All the mix proportions were found satisfying the strength characteristics and hence blocks were cast by using all proportions. Solid concrete blocks (40 cm × 20 cm x 15 cm) were cast using hydraulic block making machine (H800 from Nova engineering company) and kept as such for 24 h in the production yard. Blocks were then kept immersed in a water tank for 28 days. After curing, blocks were taken out, wiped off and subjected to different tests. Blocks were designated as JB0, JB1, JB2, JB3 and JB4 similar to the mix designations for optimization.

2.3 Tests on Building Blocks

Determination of compressive strength, density and water absorption were conducted as per standards. Building blocks after curing were subjected to compressive strength test according to IS:2185 Part 3 (1984) [15] using a compressive strength testing

Table 3 Test results on concrete building blocks

S. No.	Mix designation	w/c ratio	Fine aggregate replacement with Jarofix (%)	28th day average compressive strength (N/mm^2)	Average density (Kg/m^3)	Average water absorption (%)
1	JB0	0.50	0	5.18	2168	7.81
2	JB1	0.50	10	5.66	2177	8.57
3	JB2	0.50	20	6.41	2189	8.81
4	JB3	0.50	30	7.19	2243	9.23
5	JB4	0.50	40	5.63	2099	9.65

machine of maximum capacity 2000 kN. Density of the blocks were determined as per ASTM C 140-03 and water absorption test was conducted as per IS: 1237. Results of the above tests are presented in Table 3.

2.4 Test on Structural Masonry

Prisms were constructed with control block (JB0) and JB3 blocks having maximum strength using cement mortar 1:6 (16 N/mm^2). Capping was also done with the same mortar according to IS: 1905-1983 [16]. A height to thickness (h/t) ratio of 3.25 was maintained for prism. Mortar thickness was limited to 1 cm. Figure 5a, b shows the dimensions of prism and test setup.

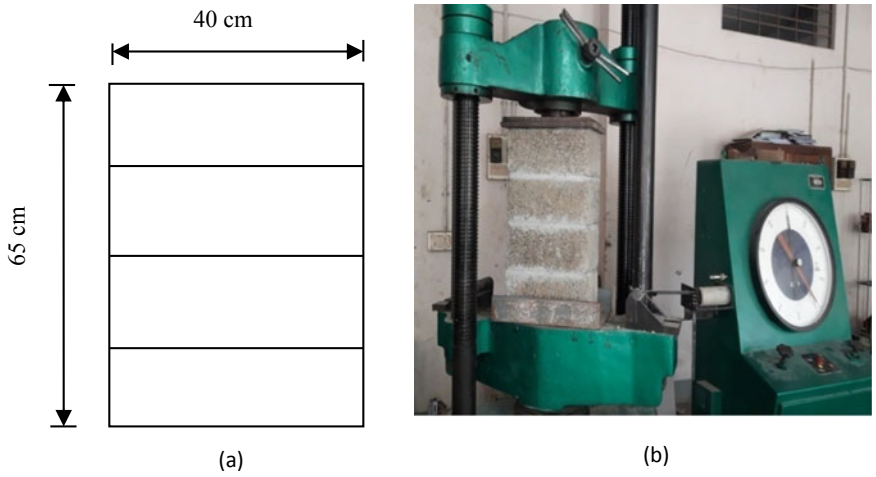

Fig. 5 **a** Dimensions of prism. **b** Test set up of prism

Table 4 Strength characteristics of structural masonry

Block masonry	Size (mm)			Masonry strength (N/mm^2)	Correction factor	Normalized strength (N/mm^2)	Block strength (N/mm^2)	Masonry efficiency (%)
	L	B	D					
Control block masonry	400	200	650	3.88	1.09	4.23	5.18	81.62
Jarofix block masonry	400	200	650	5.38	1.09	5.86	7.19	81.45

These samples were cured for 28 days and subjected to compressive strength test in universal testing machine as per ASTM C 1314-12 [17]. Gradually increasing axial compressive load at a rate of 5 kN was applied to the specimens till failure and ultimate load was noted. The strain was measured using Demec-guage of 200 mm guage length. Stress and Strain were noted for regular intervals of 25 kN and graph is plotted as shown in Fig. 10. Normalized compressive strength of masonry with correction factor 1.09 (ASTM C 1314-12) and masonry efficiency (ratio between masonry strength and block strength) were also found out. Results are presented in Table 4.

3 Results and Discussions

Discussion on the variations in compressive strength, water absorption, density with respect to different levels of replacements and characteristics of structural masonry are presented below.

3.1 Compressive Strength

In concurrence with the test results for mix optimization, similar variations were observed in the compressive strength of concrete building blocks (Fig. 6).

Strength was found increasing on increasing the replacement of fine aggregate up to 30% and decreasing thereafter. Finer jarofix particles get packed up between the interface of fine aggregates and coarse aggregates, reducing the entrapped air, densifying the mix and resulting in improved compressive strength. Presence of gypsum, cement and lime in the jarofix also imparts additional strength. Homogeneity of the mix was found reducing on further increasing the replacements due to the formation of boulders and resulted in the reduction in strength.

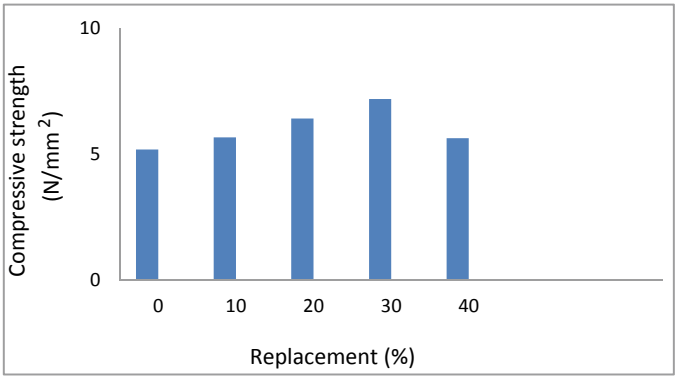

Fig. 6 Variation in the 28th day compressive strength

3.2 Water Absorption

Water absorption of jarofix concrete blocks were found increasing on increasing the percentage of jarofix as shown in Fig. 7. Fineness nature of jarofix and presence of gypsum in jarofix can be considered for the increased rates of water absorption. Even though the water absorption was higher, the results were found within the specified limits.

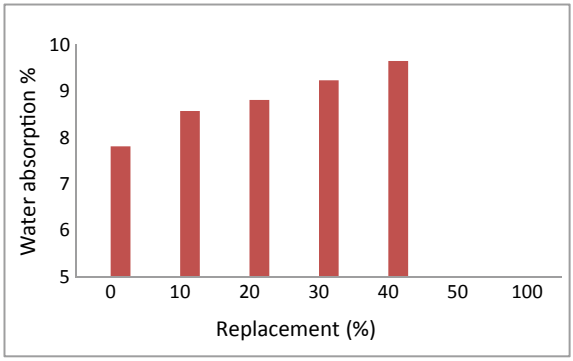

Fig. 7 Comparison of water absorption

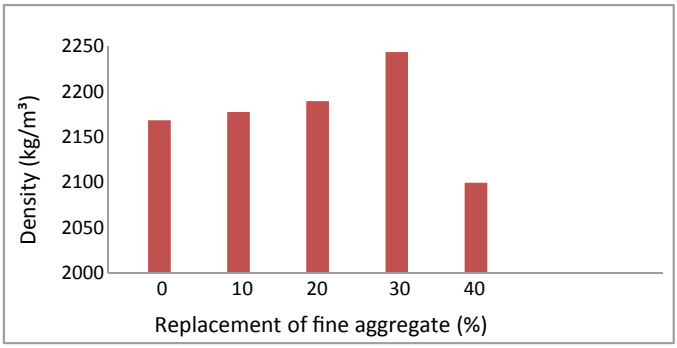

Fig. 8 Variation in density with respect to % of replacement

3.3 Density

Density of concrete blocks showed a similar variation as that of compressive strength (Fig. 8). This can be due to the presence of denser matrix resulted from the filler effect of finer jarofix particles. Above 30%, reduction in the density occurs due to the non-homogeneity of the mix resulted from the boulder formation.

3.4 Tests on Structural Masonry

Masonry efficiency of the prisms showed similar variations with respect to corresponding block strength and masonry strength. Figure 9a, b shows the pictures of the failure patterns of prisms made with control block masonry (JB0) and proposed jarofix masonry (JB3). Compression failures in both the units were found similar as seen in the figure. Since both the masonry units were made by blocks having strength lower than that of mortar, failures were visible through the surface of the blocks. On applying the load, cracks were found gradually progressing towards the top from the bottom. Scattered cracks were observed in both the specimens on increasing the load showing the ductile nature of failure. Prisms were able to withstand higher loads even after initial cracks, confirming this nature. Figure 10 shows the comparison of the stress–strain characteristics of prisms. Relatively higher E values were observed for JB3 specimens compared to control specimens. Thus verifying the ductile nature of cracks for JB3 masonry over control block masonry.

Fig. 9 **a** JB0 Prism failure pattern. **b** JB3 Prism failure pattern

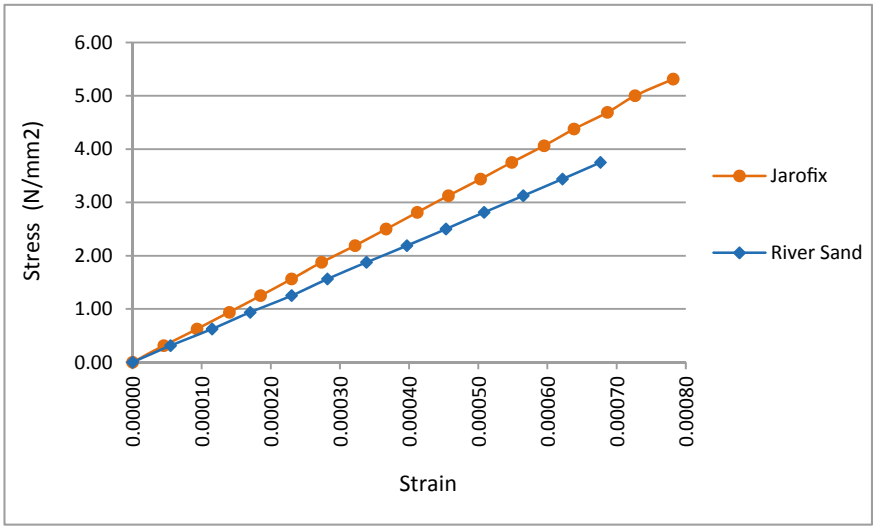

Fig. 10 Stress–strain relationship—JB0 and JB3 prism

4 Conclusions

This research recommends a fine aggregate replacement of 30% with jarofix in the production of concrete building blocks suitable for load bearing structural masonry.

Improvements in the surface texture of proposed blocks, reduction in cost and comparable durability characteristics are positive features of these blocks. Utilization of a waste material to replacing river sand, a depleting natural resource also add to the sustainability of these blocks.

References

1. Chen TT, Dutrizac JE (2000) A mineralogical study of jarofix products for the stabilisation of jarosite disposal. The Minerals, Metals and Materials Society (TMS), pp 917–933
2. Seyer S, Chen TT, Dutrizec JE (2001) Jarofix: addressing iron disposal in the zinc industry. J Mineral 53(12):32–35
3. Pappu A (2004) Application of coal combustion residues for hazardous waste management. Ph.D. thesis, Indian Institute of Technology, Mumbai, India
4. Pappu A, Saxena M, Asolekar SR (2005) Coal combustion residues—environmental implications and recycling potentials. Resour Conserv Recycl 43(4):239–252
5. Havanagi VG, Sinha AK, Arora VK, Mathur S (2012) Waste materials for construction of road embankment and pavement layers. Int J Environ Eng Res 1:51–59
6. Vsevolod AM, Haroldo AP, Patricio RI (2005) Potential application of acid Jarosite wastes as the main component of construction materials. J Constr Build Mater 19:141–146
7. Sharma P (2016) Feasibility study of industrial jarosite waste as vital material for construction: positive and negative aspects. Malays J Civil Eng 28(1):139–154
8. Arora V, Sachdeva SN, Aggarwal P (2015) Effect of use of Jarosite on workability and early age strength of concrete. Int J Comput Math Sci IJCMS 4(Special Issue). ISSN 2347-8527
9. IS 4031-1988, Methods of physical tests for hydraulic cement, Bureau of Indian standards, New Delhi, India
10. IS 8112-1989, Specification for 43 grade ordinary Portland cement
11. IS:383-1970, Specification for coarse and fine aggregate. Bureau of Indian standards, New Delhi, India
12. IS 2185-2005: Concrete masonry units, part 1: Hollow and solid concrete blocks, Bureau of Indian standards, New Delhi, India
13. ASTM C 140-03, Standard test methods for sampling and testing concrete masonry units and related units. ASTM International
14. IS: 1237 Standard test method for rate of water absorption
15. IS:2185 Part 3 (1984)
16. IS: 1905-1983, Indian standard code of practice for structural use of unreinforced masonry. Bureau of Indian standards, New Delhi, India
17. ASTM C 1314-12, Standard test method for compressive strength of masonry prisms, ASTM International